A RC Slab to CFT Column Connection for Improved Seismic Behavior of Multi-Story Buildings

Alec S. Yeutter

A thesis

submitted in partial fulfillment of the

requirements for the degree of

Master of Science in Civil Engineering

University of Washington

2020

Reading Committee:

Dawn E. Lehman

Charles W. Roeder

Michael R. Motley

Program Authorized to Offer Degree:

Civil and Environmental Engineering

University of Washington

Abstract

A RC Slab to CFT Column Connection for Improved Seismic Behavior of Multi-Story Buildings

Alec S. Yeutter

Co-Chair of the Supervisory Committee:
Dawn E. Lehman
Civil and Environmental Engineering
Charles W. Roeder
Civil and Environmental Engineering

Slab-column systems are commonly used as the gravity system of reinforced concrete buildings in high seismic regions. These systems are economical and typically constructed using stud rails at the reinforcement for the slab-column connection. However, prior work indicates that these connections are susceptible to damage and may lose load-carrying capacity at drift demands between 2% and 4%. A research program was undertaken to investigate a new slab-column system which: (i) is economical, (ii) mitigates damage and (iii) can sustain large drifts without loss in strength. The system is novel in that it uses concrete filled steel tubes (CFSTs) as the columns; prior work has demonstrated that these components are ductile, with high flexural, axial and shear capacities. In addition, the tube eliminates the need for longitudinal and transverse internal reinforcement as well as column formwork, thereby reducing construction

time. The connection replaces a traditional drop panel with sandwiched steel rings. The rings are connected to the slab with post-tensioned bolts, eliminating the need for stud-rail reinforcement. The steel tubes are prefabricated with the rings and the lower column has longitudinal reinforcement welded to it; this is the only reinforcement in the column and extends through the slab reinforcement into the upper tube of the upper CFST column. This longitudinal reinforcement facilitates load transfer as does the ring-bolt connection assembly. This new connection was investigated experimentally using full-scale tests. Four specimens were tested with the primary study parameters as follows: (i) ring dimension, (ii) bolt pattern. The results indicate that the connection can sustain 6% drift with minimal damage.

TABLE OF CONTENTS

LIST OF FIGURES

LIST OF TABLES

ACKNOWLEDGEMENTS

I would like to thank my advisors, Professor Dawn Lehman and Professor Charles Roeder for their guidance and support throughout this research project. I would especially like to recognize the hours they committed to answering my questions (at all hours of the day), the wealth of knowledge and experience they brought to this project, and the abundance of patience they showed through the construction of the test setup. I would also like to thank Professor Michael Motley for serving on my committee.

I would like to recognize and thank the numerous people who helped with construction and testing in the Structural Research Lab at the University of Washington. I especially want to thank Vongsant (Vince) Chaijaroen. I could not have accomplished what I did without the extensive knowledge and experience in constructing, moving, and testing large scale research experiments along with everything that needs to happen in between. I would also like to give special thanks to Tasha Tardieu, Sam Turner, Austin Anderson, Taneum Luciani, Chris Pyke, and Ken Sulivan for their help on casting and test days, I couldn't have done it without the support of each of them along with numerous others.

The project was funded by the National Science Foundation and their support is greatly appreciated. I would also like to thank Skyline steel for donating the steel tubes used for constructing specimen columns and JSW Stud Rails for donating the transverse reinforcement used in the reference specimen.

I would not be receiving my degree without the support of my fellow graduate students at the University of Washington. Thank you for your time and friendship. A special thanks to my officemates Sarah Bergquist, Anne Magnus, and Gloria de Zamacona for their constant encouragement when things weren't going according to plan.

Most importantly, thank you to my family and friends, I'm where I am today because of their love and support.

Chapter 1. INTRODUCTION

1.1 RESEARCH IMPETUS

Concrete filled steel tubes (CFSTs) are well suited for use as column. CFSTs are strong in shear, approximately 2.5 times the shear strength of a similarly sized RC column. CFSTs also have more axial and flexural strength than similarly sized RC columns (Stephens 2016) and can sustain forces greater than yield without loss of strength, stiffness or deformability. Concrete in a CFST is completely confined and is able to reach higher compressive stresses than concrete in traditional columns, allowing smaller columns to be detailed when designed using CFSTs. These characteristics make the particularly well suited for use as columns in high seismic regions.

Circular CFSTs have additional characteristics that make them well suited as columns in Vertical Evacuation Structures (VES). Tsunami loading cause large lateral loads. As such, the vertical components of the gravity system must be able resist large shear forces. As mentioned, CFSTs are strong in shear. Additionally, the circular section reduces the shear demands from the tsunami loading (ASCE 7-16). Using CFSTs as the primary vertical component in a VES will enable the engineer to achieve a more efficient design when resisting the base shear induced by lateral loads. The steel tube of a CFST also shields the column from impact loads. If used in a VES, the tube could shield the column from debris carried into the structure by a tsunami.

The limitation with using CFST columns is the connection. Although prior work has developed ductile connections for using CFST columns in bridges, few studies have focused on using these columns for slab-column systems in RC buildings. There are advantages to developing such a connection. From a construction standpoint, CFSTs enable an accelerated construction schedule and reduce reinforcing bar cage detailing and requirements. The tube acts as permanent formwork, eliminating the time needed to assemble and disassemble column formwork. The column and slab can also be cast simultaneously (if the tube is discontinuous from one floor to the next) compacting the typical construction sequencing of casting columns and slabs at separate times. If the tube is designed to resist construction loads, loads could be applied to the columns before the concrete reaches its full strength. Most importantly, using the tube to resist flexural and shear loading eliminates the need for almost all of the internal reinforcement. This is particularly advantageous for seismic regions, where the transverse detailing requirements for columns in slab-

column systems in RC buildings are onerous and splices of the longitudinal steel are not permitted at the end of the columns. In addition, removing stud-rail reinforcement, which has been shown by prior studies to only moderately improve the seismic response of slab-column connections, would also improve their constructability; this is also an objective of this connection. These detailing requirements increase the cost of construction and their elimination will be beneficial to construction timeline and labor requirements. Development of this type of connection is the primary objective of this research.

1.2 PROPOSED CONNECTION

The connection must be designed to meet the strength requirements, ductility and to prevent unwanted failure modes, which for slab-column connections includes one-way and two-way shear. Shear failure is particularly problematic due to the brittle nature of the failure mode and that it can induce progressive collapse. Additionally, shear stresses can be exacerbated under lateral loads as the stresses due to the slab flexural response can compound the stresses due to gravity loading as described in the commentary on section 8.4.4.2.3 of ACI 318-19.

The proposed connection investigated in this report seeks to provide an efficient connection with structural integrity, sufficient strength to prevent unwanted failure modes and high drift capacity prior to strength degradation. The concept of the connection is shown in Figure 1-1. The primary components are as follows:

- CFST columns above and below the flat slab
- Longitudinal continuity reinforcement welded to the bottom column and extending through the slab to the top column
- A ring flange on the top and bottom of each tube for each column, with pre-drilled holes to accommodate post-tensioned bolts. These bolts act to prestress the concrete under the ring as well as outside of the ring (in bolts outside of the ring are included) to ensure adequate shear strength and replace the stud rails typically used to enhance the shear strength of the slab-column connection.

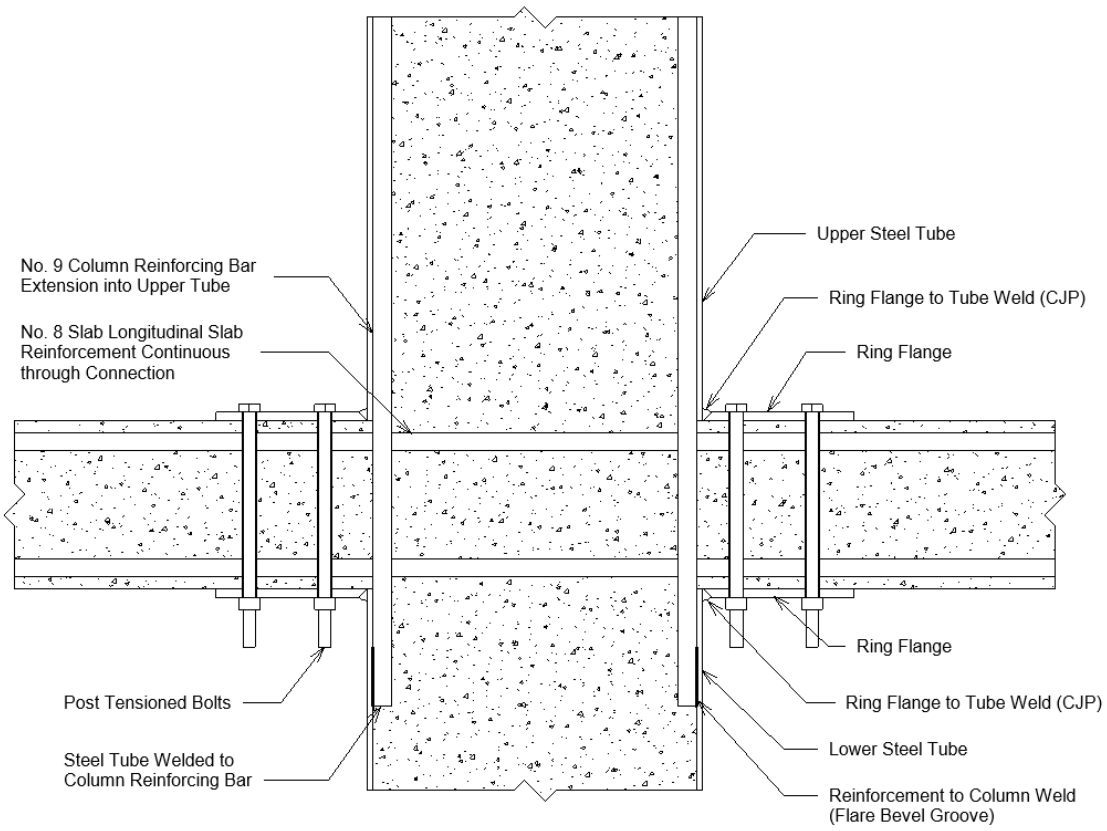

Figure 1-1: Proposed Connection Detail

The study investigated four different connections. The first was a reference specimen designed using stud-rail reinforcement. For the remaining three specimens, two design variables were investigated, the size of a ring flange (shown in Figure 1-1) and the number of bolts beyond the ring flange. The test matrix is shown in Figure 1-2 and is further discussed in Chapter 3. The proposed connection reinforces the critical area around the column with the ring flanges and bolts; this assembly confines the concrete in the joint region and increase the critical shear perimeter around the column. In one connection, additional bolts are prestressed through the slab beyond the ring flange.

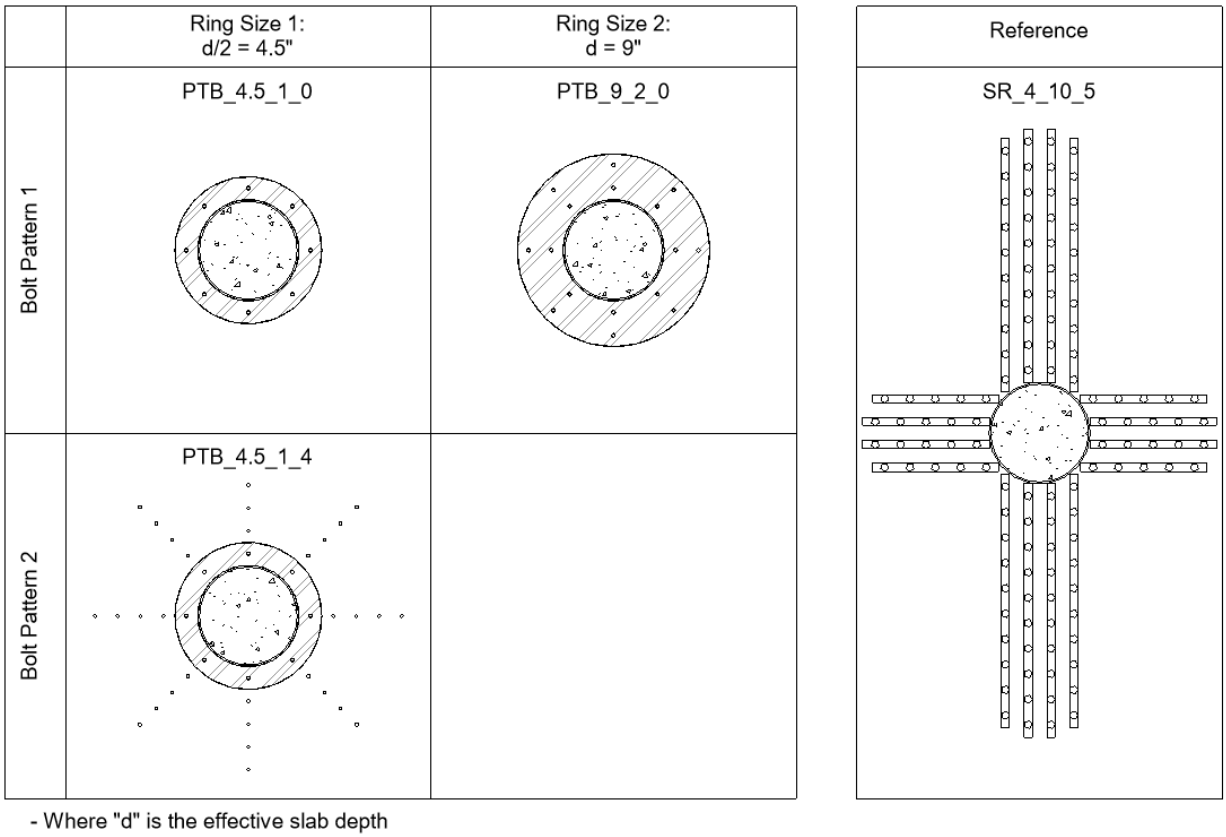

Figure 1-2: Test Matrix for Experimental Program

The proposed connection is designed to mitigate the possibility of shear failure under combined gravity and lateral loading. It is designed to enable accelerated construction through prefabrication of the steel components, eliminating most of the internal reinforcement, eliminating the stud-rail reinforcement; this will both accelerating the construction schedule and reduce the labor requirements.

1.3 RESEARCH OBJECTIVES

This experimental investigation was undertaken to characterize the behavior of the proposed connection and that of a typical slab-column connection detail under seismic style loading. To achieve this goal, the following objectives were established:

- Experimentally investigate the seismic response of connections using typical stud-rail shear reinforcement.

- Experimentally investigate the seismic response of design variants of the proposed connection concept shown in Figure 1-1.
- Compare the seismic response, including performance, of a baseline connection and the proposed connection variations.
- Proposed design recommendations for a robust seismic connection between reinforced concrete flat plate slabs and concrete filled steel tube columns.
- Determine a simple nonlinear model for the proposed slab-column connection.

1.4 ORGANIZATION OF THESIS

To address the objectives outlined in Section 1.3, this thesis is divided into an additional six chapters:

- **Chapter 2: Literature Review**, provides an overview of existing research on flat-plate slab-column connection tests and the approach to experimental testing.
- **Chapter 3: Experimental Test Program**, provides a description of the proposed connection and an overview of specimen design, construction, and instrumentation.
- **Chapter 4: Experimental Observations**, provides a description the measured and observed response of each test specimen including the damage progression observed during tests.
- **Chapter 5: Data Analysis**, provides a comparison of the global and local behavior measured during testing.
- **Chapter 6: Evaluation of Results Using Design Expressions and Analytical Modeling**, provides a discussion of various design documents and their predictions of test specimen strength, and presents calibrated rotational springs for the slab-column connection.
- **Chapter 7: Summary, Conclusions, and Future Work**, presents the main findings of the experimental program and provides recommendations for future work

Chapter 2. LITERATURE REVIEW

This chapter provides a summary of the previous experimental research performed on slab-column connections subjected to cyclic lateral loading. The objectives of the chapter are to:

- familiarize readers with the body of experimental research performed on slab-column connections.
- provide an understanding of primary design parameters effecting response
- evaluate test setups to be adapted for use at the University of Washington

This chapter contains an overview of pertinent experimental tests and a description of pertinent test programs. The overview of experimental tests includes a summary specimen designs and geometry, and a summary of test methods. The description of test programs includes:

- Research Objectives
- Test Program
- Test Setup
- Test Results
- Research Conclusions

2.1 OVERVIEW

Data were collected from test programs that met the following criteria:

- Specimens with slabs at least 4 in. thick
- Specimens that had continuous bottom reinforcement through the joint region
- Research programs that did not explore the effects of prestressed slabs or fiber reinforced concrete

Table 2.1 summarizes the specimen geometry and reinforcement. Tests varied from full scale to half scale as testing facilities allowed and as a result varied widely in length and width. Additionally, a wide variety of longitudinal reinforcement ratios were studied. The majority of test use reinforcement ratios between 0.5% and 1.5% though some (especially more recent tests) have used lower reinforcing ratios.

Additionally, the older body of research placed a focus on exploring the effects of stirrups placed in the slab that extend from the faces of the column (often referred to as integral beams). However, more recent research has explored shear studs (also called stud rails) and shear capitals. Even more recent works have explored the effects of fiber reinforced concrete on the strength of the connection region, though this work is not included here as it is not pertinent to the experimental program conducted.

Table 2.1: Specimen Details

Year	Authors	No. of Tests	Slab Dim. (in.)			Column Dim. (in.)	Longitudinal Reinforcement Ratio (%)		Transverse (shear) Reinforcement
			Length	Width	Height		Top	Bot.	
1974	Hawkins, Mitchell, & Sheu	6	156	84	6	12x12	0.57 to 1.29	0.26 to 0.56	None, Stirrups
1975	Hawkins, Mitchell, & Hanna	5	156	84	6	12x12	0.90 to 1.29	0.49 to 0.56	Stirrups
1976	Symonds	6	156	84	6	12x12	0.57 to 1.10	0.40 to 0.56	None, Stirrups
1976	Ghali, Elmasri, & Dilger	6	72	72	6	12x12	0.5 to 1.5	0.17 to 0.5	None
1987	Elgabry & Ghali	5	71	71	5.9	10x10	1.0 to 1.1	0.4	Stud Rails
1990	Robertson	9	238 114 62	78	4.5	10x10	0.44	0.37	None, Closed hoop stirrups
1992	Pan & Moehle	4	144	144	4.8	10.8x10.8	0.44	0.33	None
1992	Wey & Durrani	4	114	78	4.5	10x10	0.48	0.41	Shear Capitals
2002	Robertson, Kawai, Lee, & Enomoto	4	118	108	4.5	9.8x9.8	0.41	0.35	None, closed hoop and single leg stirrups, Headed studs

Table 2.2 summarizes the loading of test specimens. All experimental programs considered in this literature review tested specimens under combined loading. Combined loading involves

applying gravity loads across the slab column interface and subsequently applying an unbalanced moment to the slab column interface (simulating lateral loading). In test conducted by Hawkins, Michell, and Sheu (1974), Hawkins, Mitchell, and Hanna (1975), and Symonds (1976) the gravity loads were applied to the slab while lateral loading was simulated by applying loads in opposite direction at the ends of the slabs. The method adopted in more recent research is to apply gravity loads to the slab and then apply lateral loads to the top of the column while pining the bottom of the column.

The applied gravity loads are also included in Table 2.2. As the same gravity load applied during testing can have very different effects on a slab column connection depending on the column dimensions and slab depth, the approximate gravity shear stress has also been included (calculated on a perimeter half the effective depth of longitudinal reinforcement away from the column). The gravity shear stress is calculated on the critical perimeter around the column and beyond shear capitals if present.

Table 2.2: Test Details

Year	Author	Gravity Load (Kip)	Gravity Shear (psi)	Loading Type
1974	Hawkins, Mitchell, & Sheu	28.2 to 33.7	94.9 to 107.7	Pseudo
1975	Hawkins, Mitchell, & Hanna	28.3 to 29.9	95.3 to 100.7	Pseudo
1976	Symonds	53 to 61	178.5 to 205.4	Pseudo
1976	Ghali, Elmasri, & Dilger	29	91.1	Pseudo and dynamic
1987	Elgabry & Ghali	33.7 to 101.2	128.3 to 385.3	Pseudo
1990	Robertson	18.0 to 54.1	34.8 to 134.6	Pseudo
1992	Pan & Moehle	14.0 to 22.8	61.1 to 97.2	Pseudo (biaxial and uniaxial)
1992	Wey & Durrani	9	13.5 to 42.8	Pseudo
2002	Robertson, Kawai, Lee, & Enomoto	11.5 to 11.7	53.6 to 54.7	Pseudo

The majority of tests included in this literature review are performed pseudo-static and uniaxial loading during testing. Two exceptions to this include Ghali, Elmasri, and Dilger (1976) who compared the effects of dynamic loading against pseudo-static loading and Pan and Moehle (1992) who compared the effects of biaxial loading to uniaxial loading.

The variation in loading, data presentation, and the changes in design documents (mainly ACI 318) over the decades makes it difficult to numerically compare tests without doing extensive

calculations. As a result, general observations are listed while discussing results, comparing the specimens within an experimental program as best as possible.

2.2 TEST PROGRAMS

2.2.1 *Hawkins, Mitchell, and Sheu (1974)*

Hawkins, Mitchell, and Sheu (1974) conducted six tests on reinforced concrete flat plate slab-column connections to investigate the effects of cyclic loading on strength, ductility, and energy absorption/dissipation. The longitudinal reinforcement ratio for the slab and the presence and type of shear reinforcement were varied from test to test to explore the effects of these parameters on the previously stated characteristic behaviors of the connection.

All specimens were nominally identical other than test variables mentioned above. The research discussed in Hawkins, Mitchell, and Sheu (1974) was continued in Hawkins, Mitchell, and Hanna (1975) and in Symonds (1976). The clearest figures describing the setup of the larger experimental program and the layout of test specimens are provided by Symonds (1976) and these figures will be used for the discussion of Hawkins, Mitchell, and Sheu (1974).

Figure 2-1 shows the overall layout of the specimen and the setup used for testing. Slabs were 156 x 84 in. (length and width, respectively) and 6 in. thick with 12x12 in. columns that extended 42 in. above and below the slab (due to the test setup, the pivot point was 48 in. above and below the slab). Specimen variations were tabulated by Hawkins, Mitchell, and Sheu and the table is replicated in Table 2.3. When describing the shear reinforcement, the spacing is the spacing between subsequent legs of reinforcement and the reinforced length is the distance from the face of the column to the termination of shear reinforcement.

Table 2.3: Hawkins, Mitchell, and Sheu (1974) Specimen Details

Specimen	Top Bars			Bottom Bars			Shear Reinforcement		
	Bar Size (No.)	Bar Spacing (in.)	Reinf. Ratio (%)	Bar Size (No.)	Bar Spacing (in.)	Reinf. Ratio (%)	Bar Size (No.)	Spacing (in.)	Reinforced Length (in.)
S1	6	7.5	1.29	4	7.5	0.56	-	None	-
S2	5	7.5	0.90	4	9.0	0.49	-	None	-
S3	4	7.5	0.57	3	9.0	0.26	-	None	-
S4	6	7.5	1.29	4	7.5	0.56	-	None	-
SS1	6	7.5	1.29	4	7.5	0.56	3	1.5	14.25
SS2	5	7.5	0.90	4	9.0	0.49	2	1.5	9.75

In all specimens, the reinforcement ratio of top steel was approximately double the ratio for bottom reinforcement. Specimens SS1 and SS2 were nominally identical to S1 and S2, respectively, other than the addition of shear reinforcement in the form of stirrups (two legged hoops). Material strengths and gravity loading are summarized in Table 2.4.

Table 2.4: Hawkins, Mitchell, and Sheu (1974) Materials and Loading

Specimen	f'_c (psi)	f_y Longitudinal (ksi)	f_y Transverse (ksi)	Gravity load (kip)	Gravity Shear (psi)
S1	5050	65.8	-	28.8	100.0
S2	3400	68.0	-	32.0	107.7
S3	3200	66.0	-	31.2	105.1
S4	4690	67.1	-	33.7	113.5
SS1	4000	66.6	68.0	28.2	94.9
SS2	3730	75.0	65.8	29.0	97.6

All specimens were tested using the setup shown in Figure 2-1 (shown in section 2.2.3). The bottom column was supported on a pin assembly and the top column was fixed in place with tie rods (also creating a pin condition). Two systems of jacks were used to load the slab. One system applied a constant gravity load (constant shear) to the slab throughout the test. The other

system applied equal but opposite loads to the end of the slab to replicate the unbalance moment placed on a slab-column connection during lateral loading. Additionally, before testing began, the column was prestressed with 50 kips to simulate axial loading. After lateral loading tests were complete, gravity loads were increased monotonically (to test the residual capacity of the slab) until failure or until the slab had deflected 4 in.

A brief description of the results of each test are provided below:

- Specimen S1 was cycled twice before the final loading to failure. Failure was by punching shear on the side of the column where the effects of moment and shear compounded one another. The ductility of the connection and its ability to transfer moment after the punching failure were negligible.
- Specimen S2 was cycled once before the final loading to failure. Failure was by punching shear on the side of the column where the effects of moment and shear compounded one another. The ductility of the connection and its ability to transfer moment after the punching failure were negligible.
- Specimen S3 was cycled four times before the final loading to failure. Failure was by punching shear on the side of the column where the effects of moment and shear compounded one another as well as to the two sides of the column, extending further than for S1 or S2. The ductility of the connection and its ability to transfer moment after the punching failure were negligible.
- Specimen S4 was cycled five before the load was increase. The same pattern was followed with the load increased four times before failure occurred during the second cycle of the fourth load increment. Failure was by punching shear on the side of the column where the effects of moment and shear compounded one another. The ductility of the connection and its ability to transfer moment after the punching failure were negligible.
- Specimen SS1 was loaded through seven sets of five cycles before peak capacity was reached. Crushing occurred around the column during the eighth set of five cycles, however the crushing did not cause an immediate decrease in capacity. Testing was discontinued after completion of the tenth set of cycles while the specimen still maintained the capacity for energy absorption.

- Specimen SS2 was loaded through the first set of five cycles and the first two cycles of the second set a malfunction occurred leading to a punching shear on the side of the column where the effects of moment and shear compounded one another. The second set of cycles was then completed and a third set was run demonstrating a low capacity on the failed side of the slab.
- After testing the residual capacity (post punching shear failure) of Specimens S3, S4, and SS2 it was found could achieve a load 35% larger than the dead load that would theoretically be acting on the connection while SS2 could achieve a load 70% greater.

The research conducted by Hawkins, Mitchell, and Sheu in 1974 produced the following conclusions:

- High intensity reversed cyclic loadings can result in connections having maximum capacities as much as 20 percent less than those of similar connections loaded monotonically to failure. (p. 44)
- The critical factors determining the response of connections with shear reinforcement are the amount, extent and spacing of the shear reinforcement, the load for first yielding of the top bars of the slab passing through the column and the load for crushing of the concrete on the compression face of the slab at the slab-column interface. (p. 47)
- After punching failure occurs or there is crushing of the concrete on the compression surface of the slab, the lateral load capacity of a connection with shear reinforcement decreases with cycling. The rate of decrease is faster when punching failure has occurred. (p. 48)

2.2.2 *Hawkins, Mitchell, and Hanna (1975)*

Hawkins, Mitchell, and Hanna (1975) conducted five concrete flat plate slab to concrete column connection tests to investigate how effective detailing of transverse slab reinforcement can improve the shear strength and deformability of slabs. Different stirrup details were studied. Results of tests using integral beam stirrup reinforcement were then compared with previous tests that utilized headed shear and integral beam reinforcement. Specimens SS1 and SS2 discussed in Hawkins, Mitchell, and Hanna (1975) are also discussed in Hawkins, Mitchell, and Sheu (1974).

All specimens were nominally identical other than test variables mentioned above. The research discussed in Hawkins, Mitchell, and Hanna (1975) is a continuation of Hawkins, Mitchell, and Sheu (1974) and is continued in Symonds (1976). The clearest figures describing the setup of the larger experimental program and the layout of test specimens are provided by Symonds (1976) and these figures will be used for the discussion of Hawkins, Mitchell, and Hanna (1975).

Figure 2-1 (shown in section 2.2.3) shows the overall layout of the specimen and the setup used for testing. Slabs were 156 x 84 in. (length and width, respectively) and 6 in. thick with 12x12 in. columns that extended 42 in. above and below the slab (due to the test setup, the pivot point was 48 in. above and below the slab). Specimen variations were tabulated by Hawkins, Mitchell, and Hanna and portions the table is replicated in Table 2.5. When describing the shear reinforcement, the spacing is the spacing between subsequent legs of reinforcement and the reinforced length is the distance from the face of the column to the termination of shear reinforcement.

Table 2.5: Hawkins, Mitchell, and Hanna (1975) Specimen Details

Specimen	Top Bars			Bottom Bars			Shear Reinforcement		
	Bar Size (No.)	Bar Spacing (in.)	Reinf. Ratio (%)	Bar Size (No.)	Bar Spacing (in.)	Reinf. Ratio (%)	Bar Size (No.)	Spacing (in.)	Reinforced Length (in.)
SS1	6	7.5	1.29	4	7.5	0.56	3	1.5	15.75
SS2	5	7.5	0.90	4	9.0	0.49	2	1.5	11.25
SS3	6&4	5&8	1.1	4&3	5&8	0.56	3	1.5	14.25
SS4	6&4	5&8	1.1	4&3	5&8	0.56	3	1.5	14.25
SS5	5	7.5	0.90	4	9.0	0.49	2	1.5	12.75

In all specimens, the reinforcement ratio of top steel was approximately double the ratio for bottom reinforcement. Specimens SS4 and SS5 were nominally identical to SS3 and SS2, respectively, other than the change in the shear reinforcement detailing which took the form of stirrup (two legged hoops) for all specimens. Specimens SS3 and SS4 had a different concentration of longitudinal reinforcement in the central 36 in. having a different reinforcement spacing and reinforcing ratio. Material strengths and gravity loading are summarized in Table 2.4.

Table 2.6: Hawkins, Mitchell, and Sheu (1974) Materials and Loading

Specimen	f'_c (psi)	f_y Longitudinal (ksi)	f_y Transverse (ksi)	Gravity load (kip)	Gravity Shear (psi)
SS1	4000	66.6	68.0	29.9	100.7
SS2	3730	67.1	65.8	28.4	95.6
SS3	3750	66 & 66.0	68.0	28.5	100.0
SS4	4000	66 & 66.0	68.0	28.7	96.6
SS5	4670	67.1	65.8	28.3	95.3

All specimens were tested using the setup shown in Figure 2-1. The same setup was used for tests recorded in Hawkins, Mitchell, and Sheu (1974) and is described in section 2.2.1.

A brief description of the results of testing is provided below:

- The inclusion of shear reinforcement improved the ductility, energy absorption, and strength of specimens with comparable longitudinal reinforcement and the lower the reinforcement ratio, the greater the improvement.
- The increased length of transverse reinforcement in SS5 allowed longitudinal reinforcement to yield across the width of the slab as opposed to SS2 which failed in punching shear before all longitudinal reinforcement could yield.
- By comparing the residual capacity of SS3 (found by monotonically increasing gravity loads to failure after cyclic lateral testing) to previous experimental programs, it was found that transverse reinforcement significantly increased the residual capacity of the test specimen.

The research conducted by Hawkins, Mitchell, and Hanna in 1975 produced the following conclusions:

- A flat plate column connection will behave in a ductile manner and have adequate residual shear strength if properly designed and detailed integral beam stirrup reinforcement is provided in the slab. (p. 581)

- The beneficial effects of providing properly designed and detailed integral beam stirrup reinforcement in the slab are (a) an increase in the ductility of the connection at ultimate load, (b) an increase in the energy absorption of the connection along with a decrease in stiffness with cycling, (c) a change in the hysteretic behavior of connections with low reinforcement ratios from a shear to a moment type of energy dissipation mechanism, (d) an increase in the strength particularly for low reinforcement ratios, and (e) an increase in the residual shear capacity. (p. 581)
- In order for the stirrups to be fully effective they must be detailed so that: (a) they are closed hoops with a longitudinal reinforcing bar in each corner, (b) they are anchored by 135° standard bends around one or more longitudinal bars, and (c) they extend far enough out from the column face into each column strip that the wide beam shear force V_u on the shear periphery…does not result in a shear stress V_u/bd exceeding $2\sqrt{f'_c}$ …and that perimeter does not approach closer than *1.5h* to the column perimeter. (p. 581-582)
- The behavior of the connection, especially for low reinforcement ratios [of longitudinal reinforcement], is likely to be improved if the flexural reinforcement is concentrated around the immediate column region. (p. 582)

2.2.3 *Symonds (1976)*

Symonds (1976) conducted a five tests on reinforced flat plate slab-column connections to investigate the effects of cyclic loading on strength, ductility, and energy absorption/dissipation. The amount of longitudinal reinforcement and its distribution as well as the detailing of integral beam shear reinforcement were varied to explore the effects of these parameters on the previously stated characteristic behaviors of the connection.

Figure 2-1 shows the overall layout of the specimen and the setup used for testing. Slabs were 156 x 84 in. (length and width, respectively) and 6 in. thick with 12x12 in. columns that extended 42 in. above and below the slab (due to the test setup, the pivot point was 48 in. above and below the slab). Specimen variations were tabulated by Symonds and portions the table is replicated in Table 2.5. When describing the shear reinforcement, the spacing is the spacing between subsequent legs of reinforcement and the reinforced length is the distance from the face of the column to the termination of shear reinforcement.

Table 2.7: Symonds (1976) Specimen Details

Specimen	Top Bars			Bottom Bars			Shear Reinforcement		
	Bar Size (No.)	Bar Spacing (in.)	Reinf. Ratio (%)	Bar Size (No.)	Bar Spacing (in.)	Reinf. Ratio (%)	Bar Size (No.)	Spacing (in.)	Reinforced Length (in.)
S-6	6&4	5&8	1.1	4&3	5&8	0.56	-	None	-
S-7	5	7.5	0.90	4	9	0.49	-	None	-
S-8	4	7.5	0.57	3	9	0.40	-	None	-
SS-6	5	7.5	0.57	4	9	0.49	2	1.5	12.75
SS-7	6&4	5&8	1.1	4&3	5&8	0.56	3	1.5	20.25

In all specimens, the reinforcement ratio of top steel was approximately double the ratio for bottom reinforcement. Specimens SS-6 and SS-7 were nominally identical to S-7 and S-6, respectively, other than the addition of shear reinforcement in the form of stirrups (two legged hoops). Specimens S-6 and SS-7 had a different concentration of longitudinal reinforcement in the central 36 in. having a different reinforcement spacing and reinforcing ratio. Material strengths and gravity loading are summarized in Table 2.8.

Table 2.8: Symonds (1976) Materials and Loading

Specimen	f'_c (psi)	f_y Longitudinal (ksi)	f_y Transverse (ksi)	Gravity load (kip)	Gravity Shear (ksi)
S-6	3360	66 & 66.0	-	61	205.4
S-7	3840	67.1	-	61	205.4
S-8	4470	66.0	-	53	178.5
SS-6	3510	67.1	65.8	61	205.4
SS-7	3900	66 & 66.0	68.0	61	205.4

All specimens were tested using the setup shown in Figure 2-1. The same setup was used in tests recorded in Hawkins, Mitchell, and Sheu (1974) and is described in section 2.2.1.

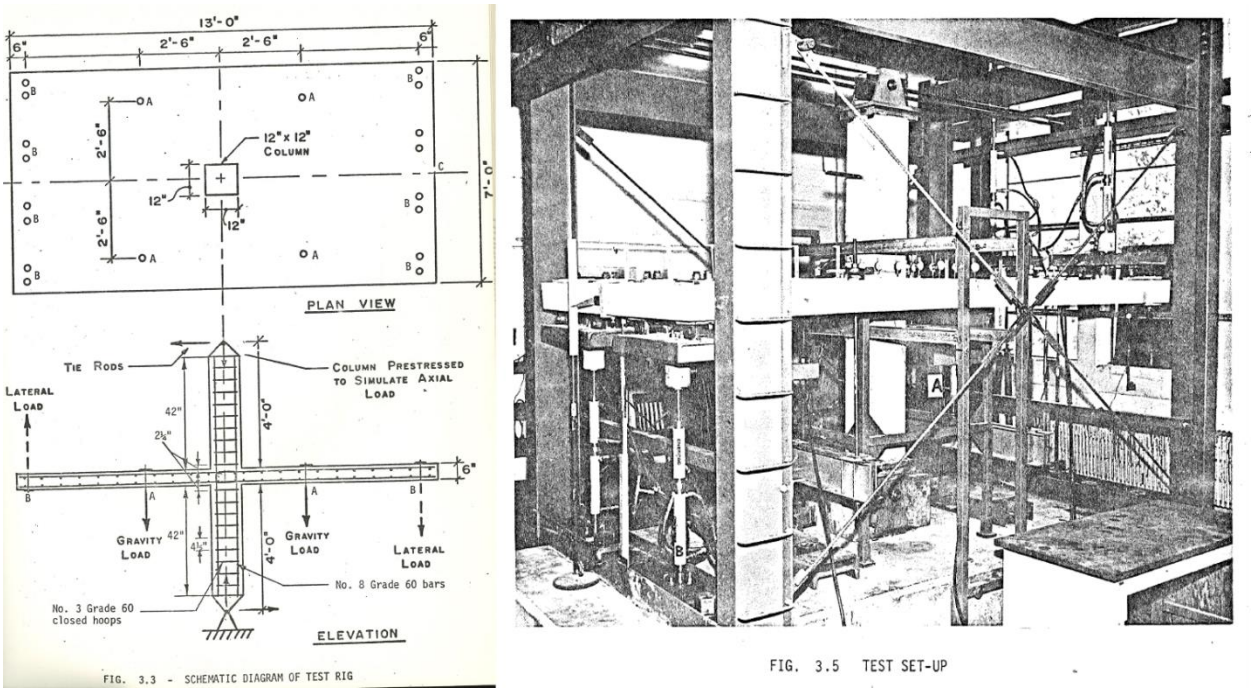

Figure 2-1: Symonds (1976) Test Setup

A brief description of the results of each test are provided below:

- Specimen S-6 failed in punching shear which initiated near the corner of the column after seventh cycle and third load increment. Reinforcement passing through the column yielded during the second displacement increment but complete yielding of reinforcement did not occur before failure.
- During gravity loading of Specimen S-7, reinforcement passing through the column yielded. Specimen S-7 failed during the seventh cycle and third displacement increment. By this point, all reinforcement except that at the very edge had yielded. S-7 failed in punching on all sides of the column.
- During gravity loading of Specimen S-8, full yielding occurred across the width of the whole specimen. S-8 failed during the sixth cycle and second displacement increment and the punching failure occurred simultaneously at all column faces.
- During gravity loading of Specimen SS-6, reinforcement passing through the column yielded. Specimen SS-6 failed during the ninth cycle and the fourth displacement increment. When failure occurred, reinforcement had yielded across the entire slab width.

The punching shear failure occurred outside the transverse reinforcement, not at the column face.

- Specimen SS-7 failed in punching beyond the transverse reinforcement during the eleventh cycle and the fourth displacement increment. Yielding had not occurred across the full slab by failure.
- S-6, S-7, SS-6, and SS-7 had residual shear capacities under gravity loading larger than the maximum gravity loading applied during testing. This residual capacity appeared to be largely due to dowel action of the bottom reinforcement.

The research conducted by Symonds in 1976 produced the following conclusions:

- Considerable ductility can be achieved with properly detailed stirrup reinforcement even for connections in which the flexural steel is stressed inelastically by the gravity loading prior to the application of the lateral loading. (p. 49)
- The provision of properly detailed integral beam stirrups results in larger and wider hysteresis loops than for companion specimens without stirrups. The concentration of flexural reinforcement in the column region results in higher capacity, little increase in ductility and a decrease in the damping ratio. (p. 49)
- The provision of stirrups ensures a marked residual shear capacity for a connection even after failure under cyclic loading. The residual capacity of connections without stirrups is less than one half that with stirrups. (p. 50)
- The width of the slab considered effective for an equivalent frame analysis for lateral loadings should not be greater than the column width plus d within a distance equal to the slab thickness from the column face. Outside of that region, the effective width can be taken as the panel width. (p. 51)

2.2.4 *Ghali, Elmasri, and Dilger (1976)*

Ghali, Elmasri, and Dilger (1976) explored the dynamic response of flat plate slab-column connections under combined shear and moment loading with loading applied using different loading rates. A total of six specimens were tested. The specimens were paired with one of each

pair tested pseudo-statically and the other tested dynamically. In addition to the loading rate, the flexural reinforcement was varied. No transverse reinforcement was placed in the specimens.

Specimens were 72 in. square with 6 in. thick slabs. Columns were 12x12 in. in cross section and 46 in. tall with the slab at mid-height. Specimen details are summarized in Table 2.9.

Table 2.9: Ghali, Elmasri, and Dilger (1976) Specimen Details

Specimen	Top Bars			Bottom Bars			Shear Reinforcement		
	Bar Size (No.)	Bar Spacing (in.)	Reinf. Ratio (%)	Bar Size (No.)	Bar Spacing (in.)	Reinf. Ratio (%)	Bar Size (No.)	Spacing (in.)	Reinforced Length (in.)
SM 0.5	4	8	0.5	4	24	0.17	-	None	-
DM 0.5	4	8	0.5	4	24	0.17	-	None	-
SM 1.0	4	4	1.0	4	12	0.33	-	None	-
DM 1.0	4	4	1.0	4	12	0.33	-	None	-
SM 1.5	4	2.67	1.5	4	8	0.5	-	None	-
DM 1.5	4	2.67	1.5	4	8	0.5	-	None	-

Specimens were tested with the slab in a vertical position resulting in the column being horizontal. To produce the effects of gravity loading on the slab, an axial load was applied to the column while the edges of the slab were simply supported. After the application of gravity loads, equal and opposite forces were applied to each end of the column to replicate the effects of lateral loading. For static tests, the top and bottom of the column was displaced 2.5 in. over the course of 6 minutes (0.00694 in/sec) while for the dynamic tests 2.5 in was reached in approximately 0.1 seconds (25 in/sec). The loading as well as the material strengths from testing are summarized in Table 2.10.

Table 2.10: Ghali, Elmasri, and Dilger (1976) Materials and Loading

Specimen	f'_c (psi)	f_y Longitudinal (ksi)	f_y Transverse (ksi)	Gravity load (kip)	Gravity Shear (psi)	Lateral Load Type
SM 0.5	5329	69.0	-	29	91.1	Pseudo
DM 0.5	6399	69.0	-	29	91.1	Dynamic
SM 1.0	4835	69.0	-	29	91.1	Pseudo
DM 1.0	4740	69.0	-	29	91.1	Dynamic
SM 1.5	5794	69.0	-	29	91.1	Pseudo
DM 1.5	6158	69.0	-	29	91.1	Dynamic

A brief description of the results are provided below:

- All test ultimately failed in punching, though the specimens with the smallest reinforcement ratio first exhibited a flexural response.
- Specimens loaded dynamically failed at larger moments/higher strengths than tests performed pseudo-statically and also had higher energy absorption.
- Increasing the reinforcement ratio increased the strength but decreased the energy absorption capacity.
- The increase in strength from 0.5% to 1.0% longitudinal reinforcement resulted in a larger increase in strength than when longitudinal reinforcement was increased from 1.0% to 1.5%, indicating that failure occurs due to shear before all reinforcement could be mobilized

The researchers provided the following conclusions:

- Within a wide range of flexural reinforcement (ρ = 0.5 to 1.5 percent), the increase of [moment] produces sudden punching failure following plastic rotation. The amount of rotation immediately before punching is smaller with the higher reinforcement ratios. (p. 572)
- Increase in the flexural reinforcement ratio increases the ultimate moment transferred M_u up to a limit (1 percent [reinforcement]). With higher flexural steel ratios, failure occurs due to shear before mobilization of the full flexural strength. The available methods to

predict the ultimate strength need improvement to correctly incorporate the effect of reinforcement. (p. 572)

- Failure occurs at higher M_u compared to static loading when applied at a high rate, and the increase corresponds to the expected strength of the materials concrete and steel due to rapid straining. (p. 572)

2.2.5 *Elgabry and Ghali (1987)*

Elgabry and Ghali (1987) conducted five tests on flat plate slab-column connections to explore the effectiveness of shear-stud (stud rail) reinforcement in increasing strength and ductility of the connections. Shear stud spacing and longitudinal reinforcement ratio within a strip of slab the width of the column and 1.5 times the depth of the slab on either side of the column were the main parameters varied in the study.

All specimens had slabs that were 71x71 in and 5.9 in. thick. Columns were 9.8x9.8 in. in cross section and 61 in. tall with the slab at mid height. The details of longitudinal reinforcement are summarized in Table 2.11 while the details of the transverse reinforcement are summarized in Table 2.12. Reinforcement ratios presented in parenthesis are the increased ratios in the area through the column.

Table 2.11: Elgabry and Ghali (1987) Specimen Details

Specimen	Top Bars			Bottom Bars		
	Bar Size (No.)	Bar Spacing (in.)	Reinf. Ratio (%)	Bar Size (No.)	Bar Spacing (in.)	Reinf. Ratio (%)
1	5	5.8&6.7	1.0 (1.1)	3	7.9	0.4
2	5	5.8&6.7	1.0 (1.1)	3	7.9	0.4
3	5	5.2&6.7	1.0 (1.23)	3	7.9	0.4
4	5	4.6&6.7	1.1 (1.39)	3	7.9	0.4
5	5	4.6&6.7	1.1 (1.39)	3	7.9	0.4

Table 2.12: Elgabry and Ghali (1987) Shear Stud Details

Specimen	Stud Diameter (mm)	Distance from column face to		Spacing between rows of studs	Number of studs per rows	Total number of studs
		first row of studs	last row of studs			
1	-	-	-	-	-	None
2	0.5	0.5*d*	2.75*d*	0.75*d*	4	32
3	0.5	0.5*d*	4.25*d*	0.75*d*	6	48
4	0.37	0.35*d*	2.75*d*	0.5*d* up to distance of 0.85*d* then spacing is increased to 0.95*d*	4	32
5	0.37	0.35*d*	4.25*d*	0.5*d* up to distance of 1.35*d* then spacing is increased to 0.97*d*	6	48

Specimens were tested with the slab in a vertical position resulting in the column being horizontal. To produce the effects of gravity loading on the slab, an axial load was applied to the column while the edges of the slab were simply supported. The load applied to the column varied from test to test and is shown in Table 2.13 along with material strengths from testing. After the application of gravity loads, equal and opposite forces were applied to each end of the column to replicate the effects of lateral loading.

Table 2.13: Elgabry and Ghali (1987) Materials and Loading

Specimen	f'_c (psi)	f_y Longitudinal (ksi)	f_y Transverse (ksi)	Gravity load (kip)	Gravity Shear (psi)
1	55076	65.5	-	33.7	128.3
2	4887	65.5	40	33.7	128.3
3	5655	65.5	40	67.4	256.6
4	5916	64.7	54	67.4	256.6
5	6612	64.7	54	101.2	385.3

A brief description of the results are provided below:

- Specimen 1 failed in punching shear.
- Specimen 2 failed in punching within the transverse reinforced zone and a compression failure on the bottom of the slab occurred simultaneously. The punching failure was

accompanied by a compression failure on the bottom face of the slab. Specimen 2 had more transverse reinforcement than was necessary and as a result, the transverse reinforcement did not yield.

- Specimen 3 failed in punching shear within the transverse reinforced zone. Specimen 3 was had more transverse reinforcement than was necessary and as a result, the transverse reinforcement did not yield.
- Specimen 4 failed in punching shear within the transverse reinforced zone. The studs in specimen 4 reached or were close to yielding when failure occurred.
- Specimen 5 failed in punching shear within the transverse reinforced zone. The studs in specimen 5 reached or were close to yielding when failure occurred.
- Top anchor plates with area 10 times that of the stud cross section provided sufficient anchorage up to yielding of the studs
- The inclusion of transverse reinforcement increase the amount of shear and/or moment at ultimate and increased deflection when compared to the reference test, Test 1. The larger deflections observed in Tests 3 to 5 were accompanied by yielding of slab reinforcement within the effective width (width of the column plus 1.5 time the depth of the slab to either side of the column).

The research conducted by Egabry and Ghali concluded that the research program proved the effectiveness of well-anchored stud-shear reinforcement in increasing the shear strength and ductility of slab-column connections subjected to shear force and unbalanced moment. (p. 441). Where well anchored shear reinforcement is able to reach its yield stress in the shank.

2.2.6 *Robertson (1990)*

Robertson (1990) conducted nine tests on flat slab-column subassemblies to investigate the impact of level of gravity load demand, shear reinforcement, stiff edge beams at exterior connections on the drift capacity of the connections. Seven of the tests included slab column connections (two exterior and one interior), called combined specimens, while the remaining two tests were on isolated interior and exterior connections, called individual or isolated specimens.

The slabs of all specimens were 78 in wide and 4.5 in thick. The slabs of the seven multi connection tests 238 in. long, the slab of the interior connection was 114 in. long, and the slab of the exterior connection was 62 in. long. All columns were 10x10 in. During testing there was an issue (electronic failure of the actuator control system) with specimen 1, so a second control specimen was constructed, and its results were used for comparisons to other tests. As a result, the first test is excluded from the discussion below. The flexural reinforcement ratios were the same for all specimens. Reinforcement was concentrated over the supports and the smaller bar spacing shown in Table 2.14 while the larger spacing was used outside this region (equal to the column width plus 1.5 times the depth of the slab to both sides of the column)

Table 2.14: Robertson (1990) Specimen Details

Specimen	Top Bars			Bottom Bars			Shear Reinforcement		
	Bar Size (No.)	Bar Spacing (in.)	Reinf. Ratio (%)	Bar Size (No.)	Bar Spacing (in.)	Reinf. Ratio (%)	Bar Size (No.)	Spacing (in.)	Reinforced Length (in.)
2C	3	9&3	0.44	3	5&3	0.37	-	None	-
3SE	3	9&3	0.44	3	5&3	0.37	-	None	-
4S	3	9&3	0.44	3	5&3	0.37	2	2.5	full
5SO	3	9&3	0.44	3	5&3	0.37	-	None	-
6LL	3	9&3	0.44	3	5&3	0.37	-	None	-
7L	3	9&3	0.44	3	5&3	0.37	-	None	-
8I	3	9&3	0.44	3	5&3	0.37	-	None	-
9E	3	9&3	0.44	3	5&3	0.37	-	None	-

The main variables explored using each test are:

- 2C: Control
- 3SE: Stiff exterior edge beams
- 4S: Closed hoop stirrups as shear reinforcement
- 5SO: Slab overhang at exterior connections
- 6LL: Additional gravity load (heavy)
- 7L: Additional gravity load (intermediate)

- 8I: Interior connection
- 9E: Exterior connection

All specimens were subjected to the same cyclic displacement history with no axial load applied to the columns. A summary of the gravity load applied to the slab and the material properties of each specimen is shown in Table 2.15

Table 2.15: Robertson (1990) Materials and Loading

Specimen	f'_c (psi)	f_y Longitudinal (ksi)	f_y Transverse (ksi)	Gravity load (psf)	Gravity load (kip)	Gravity Shear (psi)
2C	4790	72.55	-	140	18.0	44.8
3SE	6380	72.55	-	140	18.0	44.8
4S	6360	72.55	46.67	140	18.0	44.8
5SO	5506	72.55	-	140	18.0	44.8
6LL	4670	76.13	-	420	54.1	134.6
7L	4460	76.13	-	285	36.7	91.3
8I	5700	76.13	-	140	8.6	42.8
9E	5700	76.13	-	140	4.7	34.8

All specimens were tested in the reaction frame shown in Figure 2-2. Two-bay specimens were attached via load cells at the tops of the columns to an independently supported distributor beams. The bottoms of the exterior columns were placed on rollers with load cells restraining lateral movement and measuring the base shear while the middle column was supported by a load cell on a pin connection. Lateral load was applied to the top of the distribution beam, imposing equal displacements to the tops of all columns. Gravity loads were applied by hanging weights. Additional weights were placed on the top of the slab for tests 6LL and 7L to achieve the desired increase in gravity loads. Weights were placed to simulate a uniform load on the slab. For specimens 8I and 9E, the slab edges were supported by a rigid arm which restricted vertical displacements but allowed for rotations and horizontal displacement.

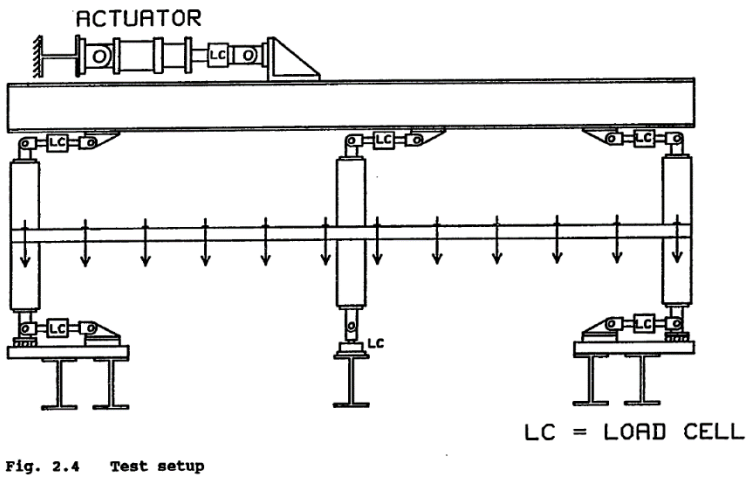

Figure 2-2: Robertson (1990) Test Setup

A brief description of the results are provided below:

- Specimens 5SO, 6LL, and 7L failed in punching shear at peak lateral resistance and never recovered a comparable level of lateral resistance. Other specimens gradually lost lateral resistance until failure of a connection or termination of testing.
- Specimen 3SE sustained the highest lateral load 24% greater than 2C before a punching failure occurred at the interior connection resulting in a loss of 70% of the peak lateral load
- Specimen 4S carried comparable lateral loads to 2C and lost lateral load resistance at the slowest rate of all specimens. The transvers reinforcement prevented a punching shear failure and allowed the specimen to deteriorate in a flexural response.
- Specimen 5SO reached a peak lateral resistance 16% greater than 2C. At peak load, the middle connection failed in punching shear resulting in further lateral load resistance never exceeding 70% of the former peak lateral resistance.
- Specimen 6LL failed in punching shear at the interior connection at a relatively low drift, achieving only 48% the lateral load resistance of 2C. The exterior connection subsequently failed during further testing.
- Specimen 7L failed in punching at the interior connection at a relatively low drift, though at a higher drift than 6LL. 7L only reached 65% of the peak lateral resistance of 2C.
- Specimen 8I reached peak lateral resistance at the same drift as 2C but failed in punching shear where 2C showed no signs of punching shear failure through the completion of testing.

- Specimen 9E reached peak lateral resistance at a similar drift to 2C and failed similarly in a combination of torsion and flexure.
- At low drifts (<1.5% drift), the lateral force resistance of isolated specimens behaved similarly to the larger tests though saw lower lateral resistances at higher drifts.

The research conducted by Robertson in 1990 produced the following conclusions:

- For low drift levels, the summation of individual connection lateral loads is identical to that of the combined specimen. Beyond 1.5 percent drift, the combined specimen supports up to 20 percent more lateral load than the individual connection specimens. This is the result of the slab axial force caused by the slab elongation, and the ability of the combined specimen to redistribute load away from a weak connection. (p. 151)
- The assumption that the point of contraflexure in the slab is stationary at midspan is invalid for almost all practical situations. Estimation of the change in the point of contraflexure is essential for the correct interpretation of results obtained from individual connection tests which make this assumption. (p. 151)
- Slab moments at the face of the supports, both interior and exterior, were affected by the movement of the point of contraflexure. Negative slab moments were lower at the same drift levels. (p. 151)
- When subjected to lateral load, the total stiffness of three individual connections was almost identical to the stiffness of the combined specimen which they represent. (p. 151)

2.2.7 *Pan and Moehle (1992)*

Pan and Moehle (1992) conducted five tests on flat plate slab-column connection assemblies to investigate the effects of different types of loading as well as the viability of connection repair (using a combination of epoxy and grout). Specimens were loaded uniaxially or biaxially with varying gravity loads. At the end of the investigation, one specimen was repaired and retested. The repaired specimen is not included in this discussion as repairing a connection is outside the scope of this report.

All specimens were identical with 144x144 in. slabs that were 4.8 in. thick and had 10.8x10.8 in. columns. Top reinforcement was concentrated over the column (resulting in the

smallest spacing) and was reduced away from the column. This lead to a higher reinforcement ratio over the column and a lower one away from the column as shown in Table 2.16. Bottom reinforcement was uniformly spaced across the slab but 50% of the bars were discontinues when passing parallel to the column (all bars passing within 18 in of the column were continued). This lead to a higher reinforcement ratio away from the column and a lower over the column as shown in Table 2.16.

Table 2.16: Pan and Moehle (1992) Specimen Details

Specimen	Top Bars			Bottom Bars		
	Bar Size (No.)	Bar Spacing (in.)	Reinf. Ratio (%)	Bar Size (No.)	Bar Spacing (in.)	Reinf. Ratio (%)
1	3	9 & 4.5 & 3	0.44 & 0.21	3	9 & 18	0.33 & 0.21
2	3	9 & 4.5 & 3	0.44 & 0.21	3	9 & 18	0.33 & 0.21
3	3	9 & 4.5 & 3	0.44 & 0.21	3	9 & 18	0.33 & 0.21
4	3	9 & 4.5 & 3	0.44 & 0.21	3	9 & 18	0.33 & 0.21

For Tests 1 and 2 a gravity shear of $1.4\sqrt{f'_c}$ was targeted while for Tests 3 and 4 a gravity shear of $0.88\sqrt{f'_c}$ was targeted. These targets as well as the material properties shown in Table 2.17 were used to calculate the approximate loading which is also shown in Table 2.17. Test 1 and 3 were performed using uniaxial loading while Tests 2 and 4 were performed using biaxial loading.

Table 2.17: Pan and Moehle (1992) Materials and Loading

Specimen	f'_c (psi)	f_y Longitudinal (ksi)	Gravity load (kip)	Gravity Shear (psi)
1	4825	68.4	22.8	97.2
2	4825	68.4	22.8	97.2
3	4550	68.4	14.0	61.1
4	4550	68.4	14.0	61.1

All specimens were tested using the setup shown in Figure 2-3. Lateral loads were applied by two actuators attached to the top of the column. Gravity loads were applied using a combination of 100 lb. lead blocks and a hydraulic jack under the column that was continuously adjusted to maintain the proper load on the column. Slab corners were restrained by struts that acted as roller supports. Both ends of all struts and the ends of the columns were fitted with universal bearings, allowing rotations in any direction. A frame was also constructed to prevent rigid body twisting.

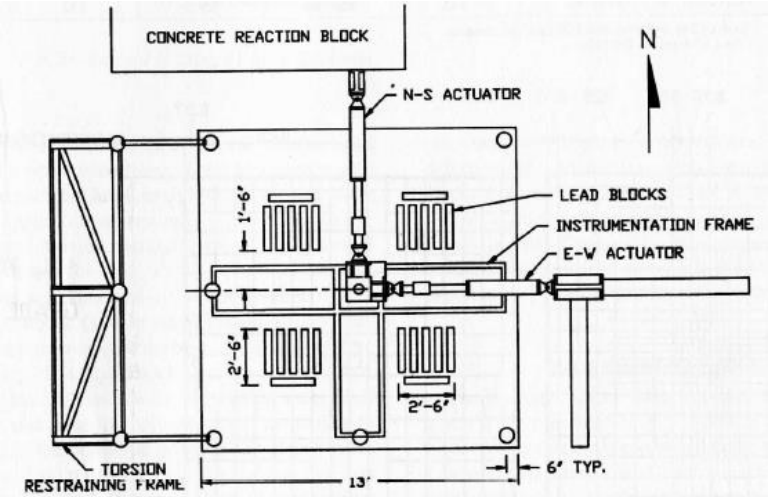

Fig. 1(a)—Test setup: Plan (1 in. = 25.4 mm)

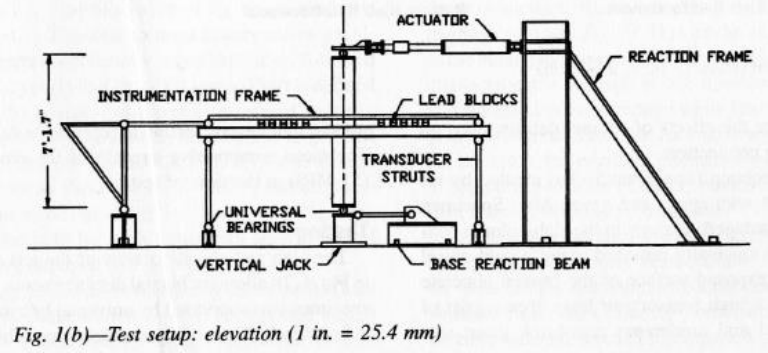

Fig. 1(b)—Test setup: elevation (1 in. = 25.4 mm)

Figure 2-3: Pan and Moehle (1992) Test Setup

A brief description of the results are provided below:

- Specimens 1 through 4 failed in punching shear and initiated on the side of the column where the effects of gravity loading and lateral loading compound one another. Further lateral loading to full punching of the slab.
- Specimen 2 (biaxially loaded) experienced a 21% reduction in lateral strength comparing the east-west loading to Specimen 1 (uniaxially loaded) and a 36% reduction when comparing the north-south.
- Specimen 4 (biaxially loaded) experienced a 4% reduction in lateral strength comparing the east-west loading to Specimen 3 (uniaxially loaded) and a 21% reduction when comparing the north-south.

- Greater damage was present around the column of specimens loaded biaxially than specimens loaded uniaxially
- Reducing gravity loading from Specimen 1 to 3 resulted in a 200% increase in the maximum drift. A similar increase was observed amongst the biaxially loaded specimens

The research conducted by Pan and Moehle in 1992 produced the following conclusions:

- Biaxial lateral loading reduces the lateral stiffness, strength, and drift capacity of reinforced concrete slab-column connections. (p. 636)
- The magnitude of the gravity load shear carried by the slab is a primary variable affecting the lateral behavior of reinforced concrete flat plates. Significant increases in strength, stiffness, and displacement capacities were observed in the test specimens when gravity shear stresses on the slab critical section was reduced from $1.4\sqrt{f'_c}$ to $0.88\sqrt{f'_c}$ psi. (p. 636-637)
- The magnitude of gravity load and lateral inter-story drift should be controlled to ensure that the integrity of slab-column connections is maintained under seismic loading. (p. 637)
- Continuous bottom slab reinforcement should be placed directly over the columns of flat plates to prevent progressive collapse in the event in the event of connection shear failure. (p. 637)

2.2.8 *Wey and Durrani (1992)*

Wey and Durrani (1992) performed four tests on slab-column connections to investigate the influence of shear capitals on strength, stiffness, and failure mechanism. The size of shear capitals was the main variable in this investigation and specimens were constructed to be half scale.

Slab dimensions were 114x78 in. (length and width, respectively) and the slab was 4.5 in. and all shear capitals extended 3.5 in from the bottom of the slab and were equal lengths to a side. Columns were 10x10 in. All specimens had the same flexural reinforcement, with a slightly greater concentration of bars through the column. Reinforcement details for the slab and the shear capitals is shown in Table 2.18.

Table 2.18: Wey and Durrani (1992) Specimen Details

Specimen	Top Bars			Bottom Bars			Shear Capital			
	Bar Size (No.)	Bar Spacing (in.)	Reinf. Ratio (%)	Bar Size (No.)	Bar Spacing (in.)	Reinf. Ratio (%)	Bar Size (No.)	Bar Spacing (in.)	Reinf. Ratio (%)	Size
SC0	3	9 & 3.5	0.48	3	9 & 3.6	0.41	-	-	-	None
SC6	3	9 & 3.5	0.48	3	9 & 3.6	0.41	3	7.5 & 7	0.25	24
SC4	3	9 & 3.5	0.48	3	9 & 3.6	0.41	3	5.75 & 7	0.28	32
SC2	3	9 & 3.5	0.48	3	9 & 3.6	0.41	3	5.25 & 7	0.30	40

A uniform gravity load was applied to all specimens. The applied gravity load and the resulting gravity shear stress on a critical perimeter around the column and beyond the shear capital are shown with the specimen material strengths in Table 2.19.

Table 2.19: Wey and Durrani (1992) Materials and Loading

Specimen	f'_c (psi)	f_y Longitudinal (ksi)	Gravity load (kip)	Gravity Shear (psi)
SC0	5700	76.1	9	42.8
SC6	5020	82.4	9	17.8 & 21.2
SC4	5340	82.4	9	17.8 & 16.5
SC2	5650	82.4	9	17.8 & 13.5

All specimens were tested using the setup shown in Figure 2-4. Displacements were applied to the top of the column using an actuator while the bottom of the column was supported on a pin connection. The ends of the slab were stiffened with channels running the width of the slab which were attached to reaction links, simulating a roller support. Applied loads were measured at the top of the column and reaction forces were measured at the base of the column and in the reaction links at the ends of the slab. Gravity loads were applied by hanging twenty 450 lb. weights (anchored at the top of the slab) from the slab as shown.

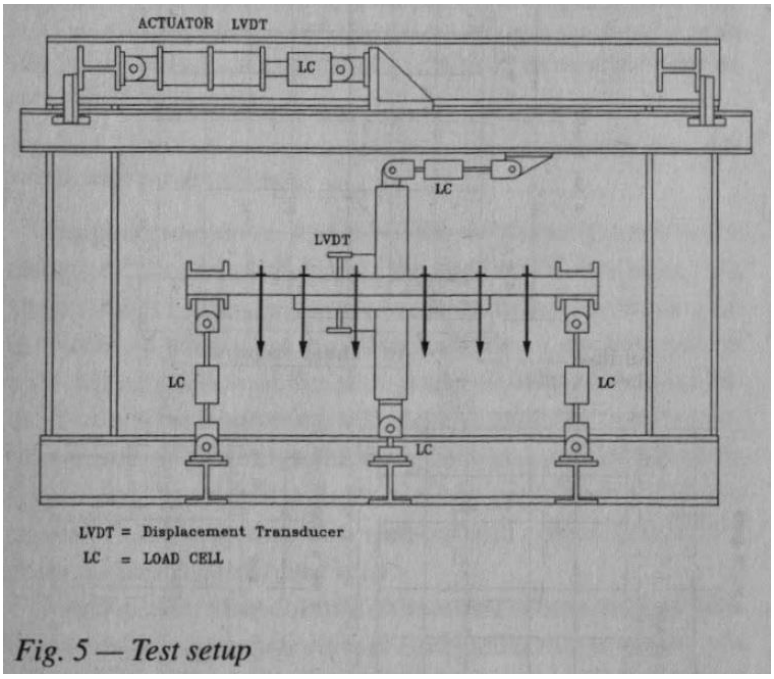

Figure 2-4: Wey and Durrani (1992) Test Setup

A brief description of the results are provided below:

- Specimens SC0 and SC6 failed in punching shear while Specimens SC4 and SC2 failed in flexure. Specimen SC6 had an unusual failure surface than extended from the outer edge of the shear capital on the bottom of the slab *toward* the column instead of away as expected.
- The presence of shear capitals resulted in an increased strength, especially above 3% drift and resisted roughly 90% (SC6), 100% (SC4), 130% (SC2) higher loads than the reference, Specimen SC0, when comparing peak loading.
- Specimens with shear capitals had an increased initial stiffness that was roughly the same for all specimens regardless of the size of the capital. The rate of stiffness degradation at drifts below 2% was not largely effected by the presence of shear capitals. However, at drifts higher than 2% the stiffness degradation was reduced by 15% when the shear capital increased in size by 30%.

The research conducted by Wey and Durrani in 1992 produced the following conclusions:

- When lateral loads are expected to produce net positive moment at the connection, the length of the shear capital should not be less than four times the height of the main slab plus the largest column dimension. (p. 690)
- The presence of a properly detailed shear capital in a slab-column connection subjected to lateral as well as gravity loads will increase the strength, stiffness, and energy dissipation of that connection. Improvement of the response of the connection by an increase in size of the shear capital is more evident at drifts larger than 2 percent. (p. 691)
- When investigating the critical section near the face of the shear capital, the width of the slab effective in transferring a portion of the unbalanced moment to the column by flexure should be increased from c2+3H to L_{sc}+3h, where L_{sc} is the length of the shear capital transverse to the direction of lateral loading. (p. 691)
- Moment transfer from the slab to the shear capital occurs predominantly by flexure. (p. 691)
- For shear capitals to be effective, they should by properly reinforced. Vertical reinforcement near the shear capital edge should be anchored into the slab, and horizontal reinforcement should be provided for flexural resistance against load reversals. (p. 691)

2.2.9 *Robertson, Kawai, Lee, and Enomoto (2002)*

Robertson, Kawai, Lee, and Enomoto (2002) performed four tests on half-scale flat plate slab-column connections to compare the effectiveness of various types of shear reinforcement at increasing the ductility of the connection. Types of shear reinforcement tested included: closed hoop stirrups, single leg stirrups, and headed studs (stud rails).

Specimens were nominally identical other than the variation in shear reinforcement. Slabs were 118x108 in. (length and width, respectively) and were 4.5 in. thick. The columns were 9.8x9.8 in. on the cross section and extended 28 in above and below the slab. A summary of the longitudinal and transverse reinforcement detailing is provided in Table 2.20. Reinforcement was concentrated over the columns leading to a tighter spacing in this region, reinforcement ratios represent the total across the entire specimen. Additionally, all transverse reinforcement was constructed from No. 2 smooth reinforcing bars (including the shear studs).

Table 2.20: Robertson, Kawai, Lee, and Enomoto (2002) Specimen Details

Specimen	Top Bars			Bottom Bars			Shear Reinforcement		
	Bar Size (No.)	Bar Spacing (in.)	Reinf. Ratio (%)	Bar Size (No.)	Bar Spacing (in.)	Reinf. Ratio (%)	Bar Size (No.)	Spacing (in.)	Reinforced Length (in.)
1C	3	8.9&3.9	0.41	3	8.9&3.9	0.35	-	None	-
2CS	3	8.9&3.9	0.41	3	8.9&3.9	0.35	2	2.6	65
3SL	3	8.9&3.9	0.41	3	8.9&3.9	0.35	2	2.6	65
4HS	3	8.9&3.9	0.41	3	8.9&3.9	0.35	2	2.6	65

Transverse reinforcement was placed in test specimens as follows:

- Specimen 1C: no transverse reinforcement
- Specimen 2CS: closed hoop transverse reinforcement extending from the face of the column
- Specimen 3SL: single leg stirrups extending from the face of the column
- Specimen 4HS: headed transverse reinforcement in a cruciform patter around the column

During testing, a gravity load was applied to the slab to replicate the effects of the full dead load and 30% of the live load on the joint. The resulting gravity shear ratio was reported by Robertson, Kawai, Lee, and Enomoto and from material strengths and the provided equations, the gravity shear and gravity loading were calculated. The gravity loading and the material properties are included in Table 2.21.

Table 2.21: Robertson, Kawai, Lee, and Enomoto (2002) Materials and Loading

Specimen	f'_c (psi)	f_y Longitudinal (ksi)	f_y Transverse (ksi)	Gravity load (kip)	Gravity Shear (psi)
1C	5134	60.9	-	11.5	53.7
2CS	4554	60.9	67.4	11.7	54.7
3SL	6295	60.9	67.4	11.7	54.7
4HS	5540	60.9	67.4	11.5	53.6

The setup is shown in Figure 2-5. Additional gravity load was first applied using concrete weights suspended under the slab. After gravity loads were applied, three pin ended rods were attached to each end of the slab, providing a roller condition, restricting vertical displacement but not lateral displacement or rotation. Lateral loads were then applied to the top of the column using an actuator attached to a pin at the top of the column. The base of the column was attached to a pin that was supported by a load cell with another pin between the load cell and the laboratory floor.

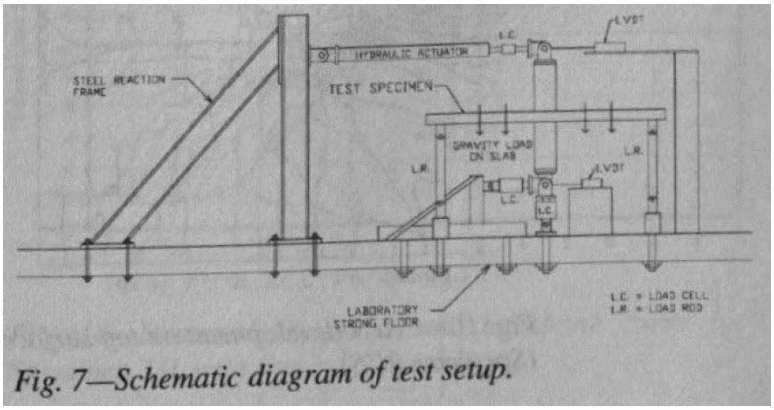

Figure 2-5: Robertson, Kawai, Lee, and Enomoto (2002) Test Setup

A brief description of the results are provided below:

- The control specimen experienced a punching shear failure at 3.5% drift while all of the other specimens were pushed to 8% drift without a punching shear failure.
- Specimens pushed to 8% drift show no more than a 15% reduction below peak lateral force resistance.
- No gauges placed on transverse reinforcement indicated yielding though strains of up to 75% of the yield strain were recorded with the relatively low gravity load applied during testing. This indicates that heavier gravity loading may have caused the transverse reinforcement to fail.

The following conclusions were made:

- The control specimen without shear reinforcement failed as a result of punching shear failure around the slab-column connection during the 305% drift cycle….None of the

specimens with slab shear reinforcement experienced punching failure although they were tested to 8% lateral drift. (p. 612)

- The load-drift envelopes…indicate that the specimens with slab shear reinforcement experienced peak lateral loads up to 22% greater than that of the control specimen with increased drift capacity. These connections failed in flexure without reaching the full capacity of the shear reinforcement. (p. 612)
- All three types of slab shear reinforcement proved equally effective in resisting punching shear failure of the slab-column connections under relatively low levels of gravity shear. (P. 612-613)

Chapter 3. EXPERIMENTAL TEST PROGRAM

An experimental program was developed to explore the behavior of three specimens designed using variations of the proposed connection under lateral loading and to compare the behavior to a reference specimen detailed with traditional transverse reinforcement. Specimen design and test design implementation were informed by the body of literature presented in Chapter 2. In accordance with the body of literature, interior slab-column subassemblies were designed for testing assuming points of contraflexure at the top and bottom of the column and at the end of the slab. This chapter seeks to provide sufficient information on specimen design and construction, and test implementation that the test results presented in later chapters can be understood and compared to other experimental programs. To convey this information, this chapter presents an overview of:

- Prototype structure design
- Specimen design and test matrix
- Specimen construction
- Materials used in construction
- Test setup
- Specimen Installation
- Specimen Instrumentation

3.1 DESIGN OF PROTOTYPE STRUCTURE

A prototype structure, shown in Figure 3-1, was designed to inform the construction of slab-column subassemblies for testing. Additionally, this experimental research program is part of a larger program exploring Vertical Evacuation Structures (VES). As a result, a structure with a large column spacing was considered desirable to minimize the loads on the structure during Tsunami loading. A column spacing of 30 ft. OC in both directions was chosen in conjunction with 10 in. thick mildly-reinforced (i.e., not post-tensioned) concrete flat slabs. The structure is unique in that it represents a new structural system utilizing CFST columns and a new slab-column

connection which is the focus of the research presented here. The important structural characteristics are:

- Column
- Connection
- Connection to foundation (either direct or pile cap or footing).
- LFRS in addition to the slab-column connections

Though the prototype structure was nominally designed as a VES, the connection detail explored in this experimental program is not limited to VES.

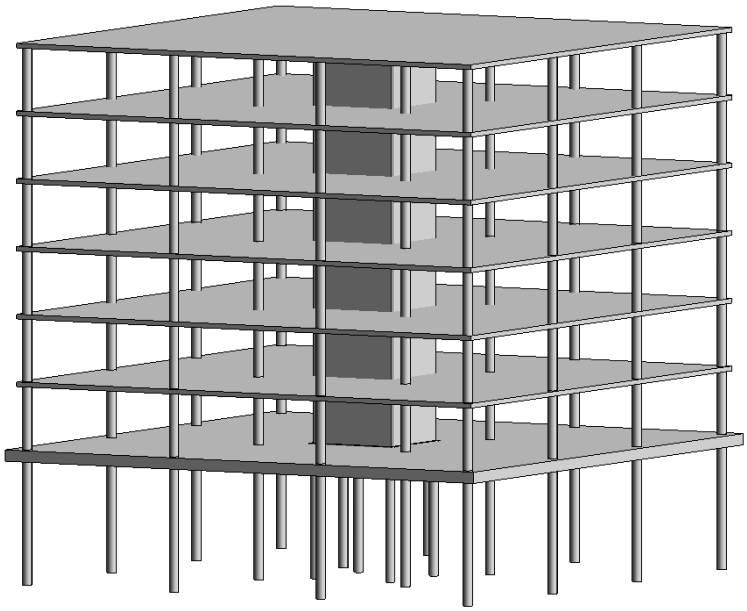

Figure 3-1: Prototype Structure

The design live loads were as follows. For design of the evacuation floors, a floor live load of 80 psf was selected and a super imposed dead load of 25 psf, which included 10 psf for partitions, was used. The primary use of this type of structure would not typically require a live load of 80 psf but rather 40 psf throughout. However, in the case of a tsunami, evacuation floors would see higher live loads while sheltering members of the public and so the live load was increased.

The slab was designed using the direct design method detailed in Section 8.10 of ACI 318-14. 4000 psi concrete was selected as this strength is commonly used for two-way slabs.

Reinforcing bar was designated as ASTM A615 Grade 60. Concrete cover was ¾ in. Calculations for the design of the slab of the prototype structure are shown in Appendix A. The design for shear was neglected while designing the prototype structure as the method used to resist shear failures was the object of the experimental program.

The slab reinforcement was increased to (1) increase the shear stress demands (for testing purposes) and (2) increase the flexural capacity of the slab column connection to provide increased resistance to lateral loading from a tsunami or earthquake or both. Following best practices for seismic design, equal top and bottom reinforcement bar sizes and spacing were used, and were continuous through the column, No. 8 bars spaced at 9 in. OC in both directions, top and bottom for the final design (an equivalent longitudinal reinforcement ratio of 1%).

The columns were designed using the plastic stress distribution method (PSDM) in accordance with Part 16 Chapter I Section 2a of the 14th edition of the AISC Steel Construction Manual. A 20 in. OD pipe with 3/8 in. thick walls was selected because it meets the local slenderness limits. Four (4) ksi concrete was used in the column to facilitate construction (the slab and supporting columns were cast monolithically). The column was designed as an RC columns with an effective concrete stress reaching $0.95f'_c$ (instead of $0.85f'_c$) which has been demonstrated by prior research and adopted by AISC in the steel construction manual.

The slab to CFST column connection design was the focus of this research study. The new connection offers the following advantages: (1) CFST columns have large shear, axial and flexural capacities, (2) no need for formwork or transverse reinforcement for the column, (3) simple connection to the slab without the need for stud rails. Stud rails are commonly used in RC slab column connections, but the CFST columns with ring flanges eliminates the need for stud rails; in addition, this connection offers construction speed and improved seismic performance.

Figure 3-2 illustrates the components of the connection. The connection was designed to: (1) have continuous slab longitudinal reinforcement, (2) minimize the length of the column longitudinal reinforcement, (3) eliminate the need for column splices, (4) eliminate the need for column transverse reinforcement (this reinforcement is needed to transfer the load to and from the slab but the column axial, shear and flexural demands are sustained by the CFST columns), and (5) eliminate the need for stud rails. The ring flanges were welded to the end of the steel tube prior to construction. Holes are placed in the ring flange to accommodate the bolts. In some connections, additional holes are placed in the slab for connection designs using bolts outside of the ring. The

top and bottom rings were joined by high strength bolts, prestressed to approximately 65 ksi (if using A325 bolts) to clamp the RC slab. This clamping action provided confinement to the concrete and was expected to improve the inelastic performance of the connection.

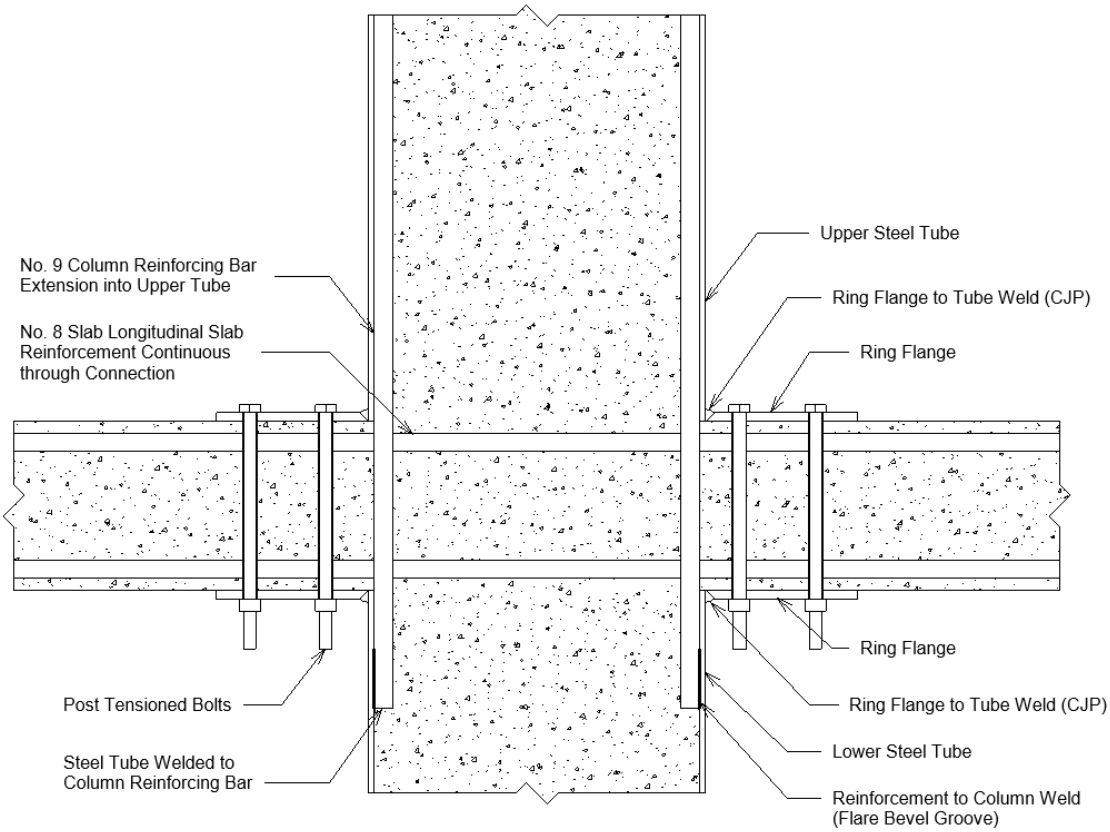

Figure 3-2: CFST Column with Ring Flange to RC Slab Connection (connection shown only has bolts in the ring)

The discontinuous tubes can be manufactured off site in a fabrication shop and shipped to site in their final configuration, saving construction time and costs. As mentioned previously, a discontinuous tube permits the slab longitudinal reinforcement to pass through the connection which provides residual strength to prevent progressive collapse after initial failure of the connection. If the tube was continuous through the slab, slab reinforcement would need to be welded to the tube resulting in more onsite work and higher construction costs. Also, most seismic

design discourages welding of yielding elements. As designed, the primary yielding elements (the slab longitudinal reinforcement) was not welded in this design.

Column longitudinal reinforcement was welded to the lower column and extended into the upper column through the joint as shown in Figure 3-2. Reinforcement extending from a lower column through the slab into an upper column was designed to transfer a significant portion of the axial and flexural capacity of the steel tube from the lower column to the upper column. Complete transfer of the column resistance through internal reinforcement welded to the tube is impractical due to constructability issues (prohibitively tight reinforcement spacing) and unnecessary with the slab-column system (bolts through the slab and ring flanges provide additional path for transfer of axial and flexural effects in the column). No. 9 ASTM A706 Grade 60 reinforcing bars were used. The penetration distance of the reinforcing bar into the lower column as well as the weld size and length were detailed to enable the full yield force of the bar to be transferred into tube of the lower column. The bar length was detailed such that it would extend out of the lower tube by 150% of the development length (Section 25.4 of ACI 318-14). An example shop drawing for the tubes used with the proposed connection is shown in Figure 3-3. All units are those used for the tests conducted as part of this experimental program.

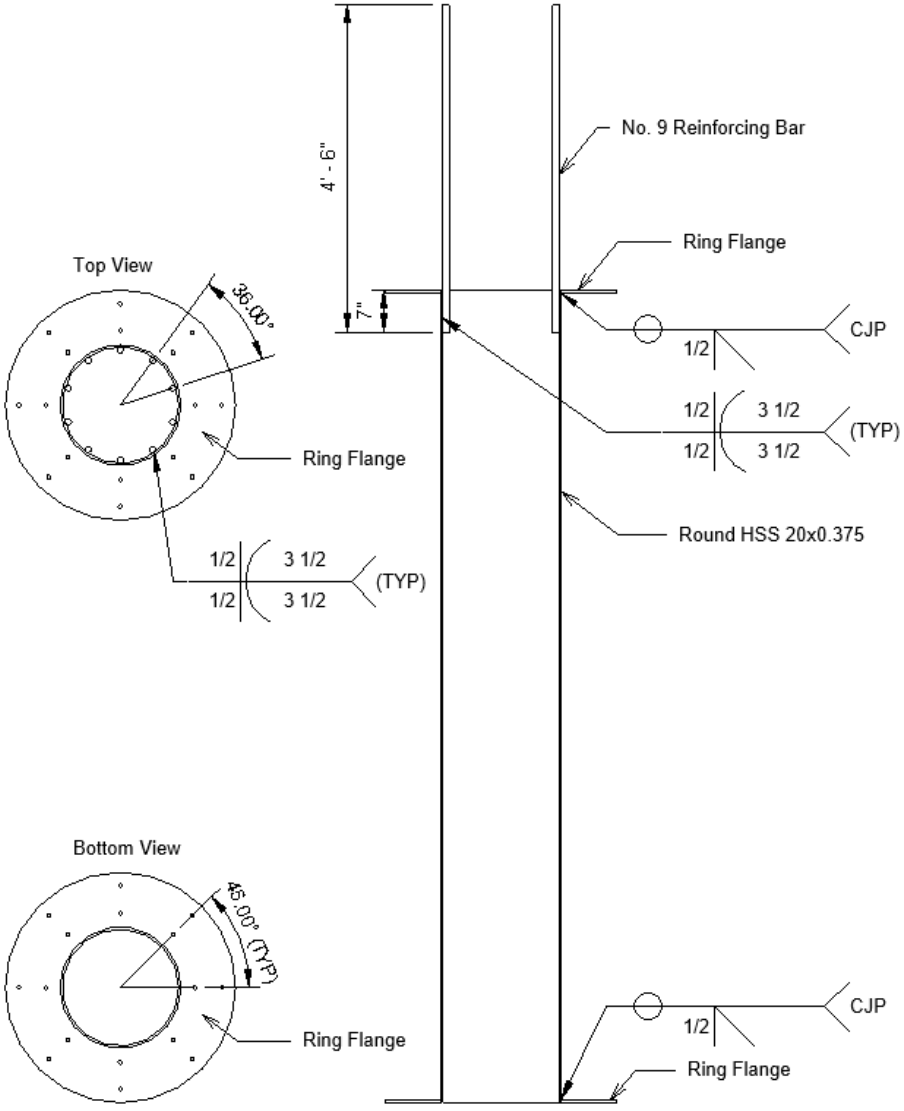

Figure 3-3: Example Tube Shop Drawing

3.2 TEST SPECIMENS AND MATRIX

All test specimens had the same geometry and longitudinal reinforcement. The only parameters that were varied were the dimension of the ring and the number of bolts for specimens designed with variations of the proposed connection. For a complete set of plans detailing specimen design, see Appendix B.

Figure 3-4 shows the test matrix that was developed for this experimental program. One specimen was a baseline with stud rails in a cruciform pattern. The other three tests varied the size of ring flange welded to the column above and below the slab as well as the number of prestressed bolts used both on and off the ring flange.

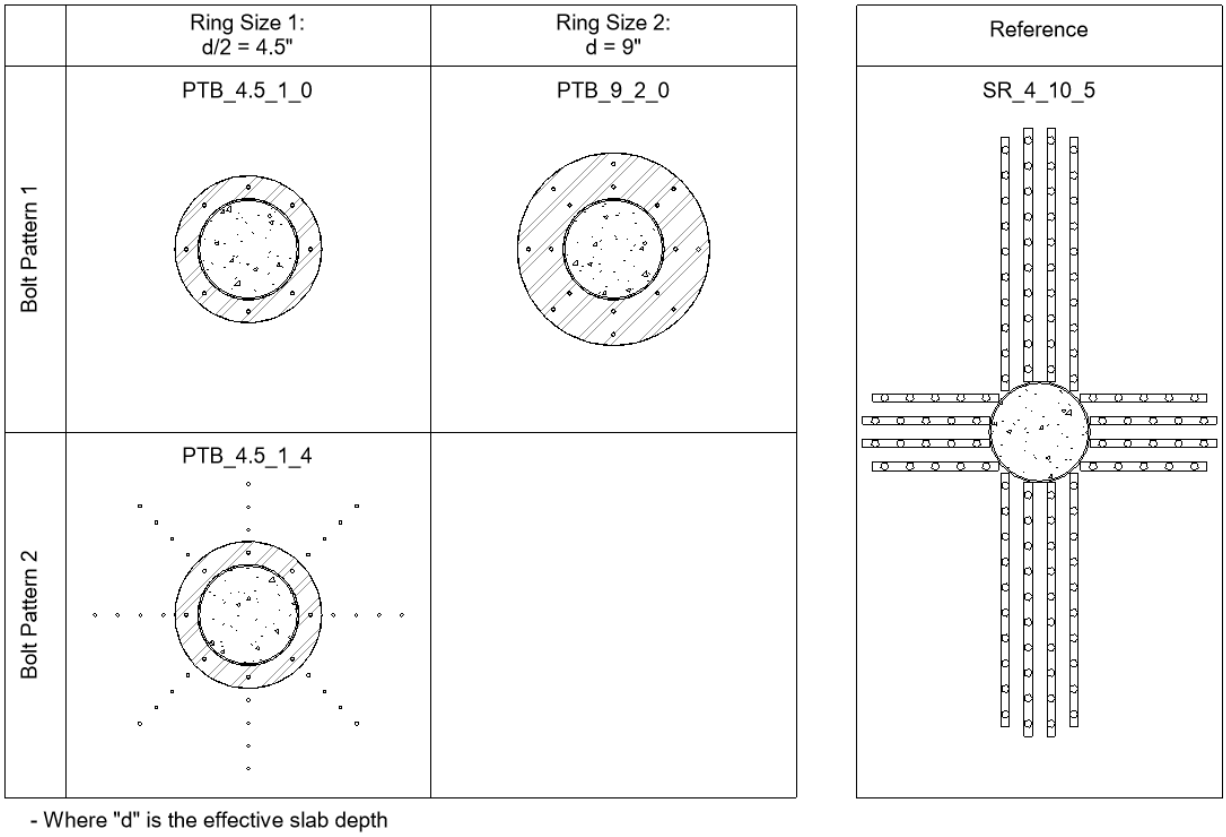

Figure 3-4: Test Matrix for Experimental Program

The specimen naming has four parts and is explained in Table 3.1 and Table 3.2. The naming convention was chosen to convey critical information about the style and spacing of transverse reinforcement. Critical information included in the naming of the stud rail specimen included the number of rails to a column face, the number of studs per rail and the spacing of studs. Critical information for the specimen design with variations of the proposed connection included ring size, number of bolts on the ring, and number of bolts off the ring.

Table 3.1: Naming-Reference Specimen

Specimen ID	Type of Shear Reinforcement	No. of Rails per Column Face	No. of Studs per Rail	Stud Spacing (in)
SR_4_10_5	Stud Rails	4	10	5

Table 3.2: Naming - Proposed Connection

Specimen ID	Type of Shear Reinforcement	Ring Size (in)	No. of Bolts on Ring	No. of Bolts off Ring
PTB_4.5_1_0	Post Tensioned Bolts	4.5	1	0
PTB_4.5_1_4	Post Tensioned Bolts	4.5	1	4
PTB_9_2_0	Post Tensioned Bolts	9	2	0

The first (reference) specimen simulated current practice and, as such, stud rails were chosen as shear reinforcement. A cruciform pattern was selected to minimize conflicts of studs with flexural reinforcing bars. The stud spacing and rail length were chosen (to meet or extend beyond the critical section). Design checks made to ensure this specimen was ACI 318-19 compliant included:

- Checking a critical perimeter d/2 away from the column face under
    - Gravity loading
    - Combined gravity and lateral loading (lateral loads result in an increase in stress due to unbalanced moments)
- Checking a critical perimeter d/2 beyond the termination of transverse reinforcement under gravity loading

The primary study parameters for the remainder of the specimens (note this is just the first phase of a two-phase study) included: (a) the size (diameter) of the ring, (b) the number of bolts within the ring and (3) the number of bolts outside of the ring. These parameters were established as follows:

1. The ring diameter was used to confine the concrete. Ring size was increased in increments of 4.5 in. (approximately 0.5d where d is the effective depth of the slab).
2. The bolts provide a confining force on the concrete under the ring and under the local concrete if they are located off the ring. The bolts would be spaced 4.5 in. apart (again 0.5d), half of the effective slab depth. The first bolts were placed 2.25 in. from the column, half the typical spacing as prescribed for shear reinforcement by ACI 318-19.

The test specimens were 13 ft. in length and 6 wide. (These dimensions were chosen based on the constraints of the testing equipment). The height of the columns above and below the slab were roughly half the height of a full-scale column between floors. The columns were terminated at mid-height of the full-scale column because this is where the point of contraflexure is assumed to be located. To accommodate the MTS Actuator the upper column needed to be taller than the lower, though this increase in height did not change the geometry of the loading. The lower column was 5 ft. 3 7/8 in. and the upper column was 5 ft. 10 7/8 in. for the first two tests and 6 ft. 10 7/8 in. for the last two tests. Upper column's height was increased from the first set of tests to the second set of tests to provide more clearance for the MTS Actuator at the request of the lab manager. The increase in column height resulted in a small increase in P-Δ effects which were controlled for while analyzing test results. The test geometry for the fourth test is shown in Figure 3-5. The point of lateral load application and the location of reactions were the same for all tests.

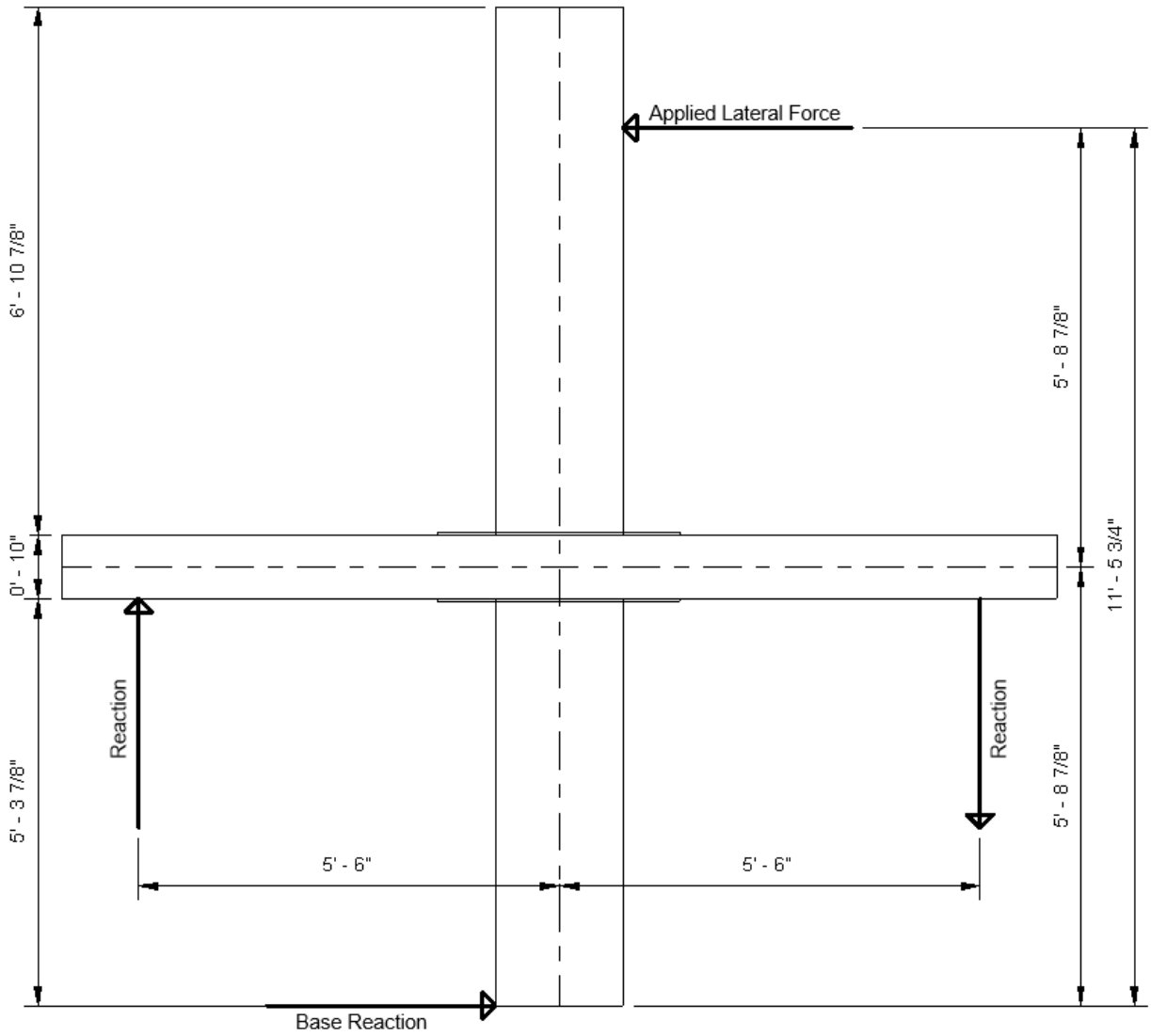

Figure 3-5: Test Geometry

Figure 3-6 shows specimen slab dimensions and the layout of flexural reinforcement used for all tests and depicts a specimen with a 9 in. ring flange on the column. Flexural reinforcement in the direction of loading is referred to as "longitudinal" x-direction reinforcement while flexural reinforcement perpendicular to the direction of lateral loading is referred to as longitudinal y-direction reinforcement. It was decided that longitudinal reinforcement in the x direction would be placed at the cover which was ¾ in. for all test specimens. This was done because the reinforcement in the x-direction direction resists the majority of lateral loads during testing. To help ensure proper anchorage, 180° hooks were detailed on the longitudinal reinforcement and 90° bends were placed

on the transverse reinforcement. 180° hooks could not be placed on the transverse reinforcement because the minimum bend diameter was too large to avoid clashing with the longitudinal bars. This is reasonable because the maximum stress in the longitudinal reinforcement in the y-direction was expected to be negligible.

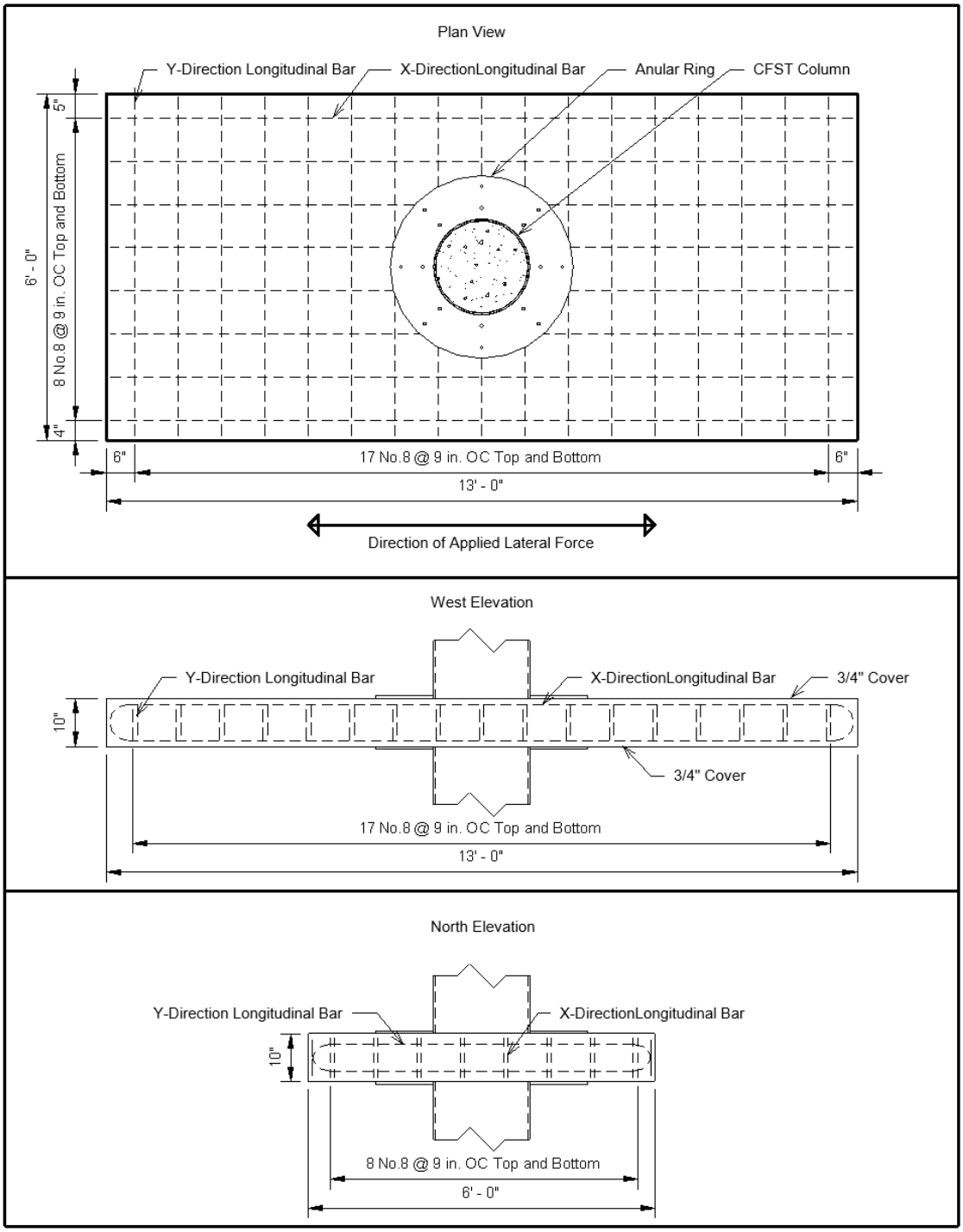

Figure 3-6: Slab Longitudinal Reinforcement Overview

3.3 SPECIMEN CONSTRUCTION

The test specimens were constructed in two phases, with two specimens being built simultaneously. Phased construction was chosen to mitigate the impact of curing time on the test schedule. The first two specimens constructed were PTB_4.5_1_0 and PTB_4.5_1_4; PTB_9_2_0 and SR_4_10_5 were constructed next.

3.3.1 *Formwork*

Formwork was built in the University of Washington Structural Engineering Laboratory to support the construction of test specimens. A 3D view of the formwork used to construct formwork is shown in Figure 3-7. For complete formwork plans, see Appendix C.

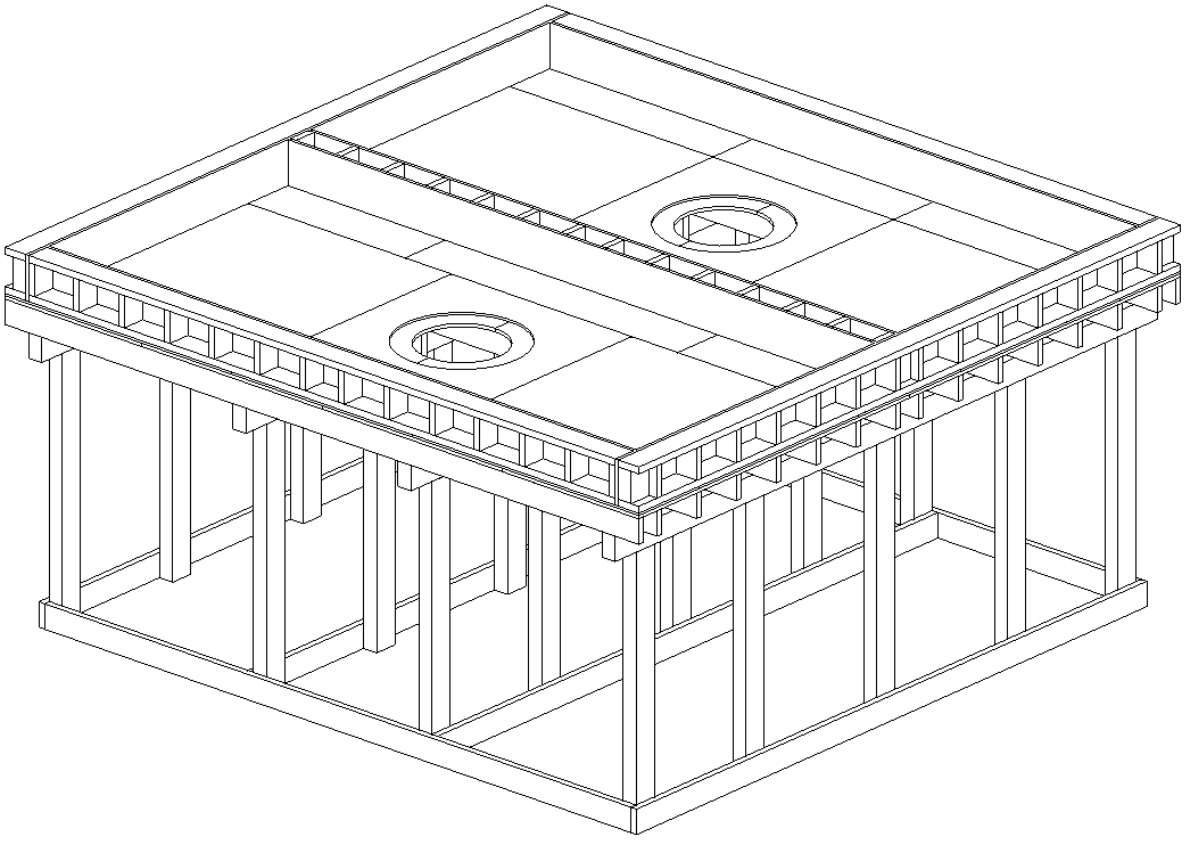

Figure 3-7: Test Specimen Formwork

Specimen dimensions required that the slab be cast approximately 6 ft. above the laboratory floor. The formwork for the two specimens was integral, and therefore needed to support the full weight of two specimens. Formwork was designed to meet the required loading and then members were increased to minimize deflections. Two layers of plywood were used under the bottom of the slab to minimize the risk of forms leaking during casting.

Holes were cut in the bottom slab forms to accommodate the 20-inch diameter columns and the top layer of plywood was cut to ensure that the ring welded to the bottom of the column sat flush with the formwork as shown in Figure 3-8.

3.3.2 *Column Fabrication*

The steel tube sections were cut on site from single piece of tube using a specialized oxy-acetylene torch. The rings for the first two specimens were fabricated on site using an oxy-acetylene torch and drill press. However, due to difficulty in meeting required precision, the ring for PTB_9_2_0 was manufactured at a professional fabrication shop. The edge of the rings were prepared for a CJP weld and welded to the tube by a certified welder. The ring was welded around the entire perimeter of the tube and the weld was backgouged and filled with weld. The longitudinal reinforcing bars extending from the lower column through the slab were welded to the lower tube using 0.5 in. thick, 3.5 in. long, double sided flare bevel groove welds. All welds were E70-Txx electrode. Once fully welded, the lower column tube was placed in the formwork as shown in Figure 3-8.

Figure 3-8: Welded Ring-Tube-Reinforcing Bar Placed in Slab Forms

3.3.3 *Slab Fabrication*

A set of completed reinforcement cages are shown in Figure 3-9. Longitudinal reinforcement was placed (after the application strain gauges), at approximately 9 in. on center. PVC pipe were placed in pre-drilled holes in the formwork and caulked in place to accommodate placement bolts or threaded rods (for the setup). Flexural reinforcement was moved a minimal distance such that PVC and reinforcing bars did not interfere.

Four lifting anchors were placed in the formwork in locations such that moments resulting from lifting would be minimized. Strain gauge wires were then labeled and carefully guided out of the specimens in a way that they were shielded by the longitudinal reinforcement but still at the

mid height of the slab. These precautions were taken with the strain gauge wires to maximize the chance that gauges would survive casting. Changes were made in how wires were shielded from one cast to the next due to the loss of more strain gauges than deemed acceptable.

Figure 3-9: Completed Rebar Cage for Specimens PTB_4.5_1_0 and PTB_4.5_1_4

3.3.4 *Casting*

A concrete mix design for interior structural applications was cast using a concrete boom pump truck. Both lower columns were filled. Concrete from the middle of the batch was used to cast cylinders (36 during casting of the lower column and slab and six during casting of the upper column) for material testing. The slabs were then cast and the concrete surface finished. Due to workability issues during the first casting, a retarder was added for casting the subsequent test specimens. Wet burlap was placed on the surface of the slabs to optimize curing. After a minimum

of three days, the upper column tubes were placed and secured. Then, one to two weeks after casting the slabs and lower columns, the upper columns were filled. Concrete was then allowed to reach the specified design strength (at a minimum) before moving of specimens. Specimens cured for a minimum of 28 days after casting before they were tested.

3.4 SPECIMEN MATERIALS

Concrete used for the slab and as fill for the tubes was sourced from two suppliers across four distinct casts. All longitudinal reinforcing bars were sourced from a single supplier and was received in one shipment while steel used as transverse reinforcement and steel used to construct the tube came from four other suppliers.

3.4.1 *Concrete*

A total of four casts were done. Specimens were cast in pairs, with the slab and lower columns of two specimens cast at once. A few weeks later, a second, smaller cast was made to fill the upper columns.

Concrete was ordered from two different ready-mix plants in the Seattle area. A 4000 psi mix was specified with ¾ in. aggregate passing. A retarder was added to the concrete mix when casting the lower columns and slabs of Specimens PTB_9_2_0 and SR_4_10_5 to enhance and maintain workability for a prolonged period so proper finishing could be performed.

While casting specimens, 4 in. diameter by 8 in. tall cylinders were made for material testing according with the number of cylinders made and their use described in Table 3.3. As two test specimens were built simultaneously, Table 3.3 details the number of cylinders needed for two slab-column connection tests. As minimal concrete damage was expected in the column, only cylinders used to find test day compressive strengths were made while casting the upper column.

Table 3.3: Cylinders for Concrete Material Tests

Components Cast	Cylinder Use	Number Made
Slab and Lower Column	7 Day Strength	3
	14 Day Strength	3
	21 Day Strength	3
	28 Day Strength	3
	Test Day Compressive Test	6
	Test Day Splitting Tensile Test	6
	Test Day Elastic Modulus Test	6
	Extra Cylinders in case of poor consolidation	6
Upper Column	Test Day Compressive Strength	6

Cylinders for specimens PTB_4.5_1_0 and PTB_4.5_1_4 were stored in a fog room until tests were performed. Due to building maintenance, a bath was used for cylinders from specimens PTB_9_2_0 and SR_4_10_5. Unfortunately, hydrated lime was not added to the bath until after cylinders for specimen SR_4_10_5 were tested, but before cylinders for Specimen PTB_9_2_0 were tested. As a result, material tests may not be representative (with the concrete cylinder indicating lower strengths that were actually in the specimen) for Specimen SR_4_10_5.

Cylinders used for compressive tests and elastic modulus tests were sulfur capped to ensure parallel loading surfaces. Compressive tests and splitting tensile tests were performed in accordance with appropriate ASTM standards. Results of compression and splitting tensile test are summarized in Table 3.4.

Table 3.4 Test Day Concrete Properties

Specimen ID	Compressive Test: (psi)				Splitting Tensile Test (psi)	
	Slab and Lower Column		Upper Column			
	Mean	St. Dev.	Mean	St. Dev.	Mean	St. Dev.
SR_4_10_5	5786.3	431.2	5496.4	457.4	473.5	52.2
PTB_4.5_1_0	8085.6	260.6	NA	NA	513.3	11.3
PTB_4.5_1_4	7082.7	595.1	8816.8	215.2	553.06	39.2
PTB_9_2_0	6978.4	227.0	6462.0	334.2	563.7	65.7

Elastic modulus (Emod) tests used and went beyond the ASTM standards because the entire stress-strain curve was needed for modeling purposes (modeling was performed in parallel with this experimental program). Emod cylinders were fitted with a compressometer and displacement readings were gathered using an extensometer. Cylinders were loaded at the displacement rate listed in ASTM C469 / C469M – 14 *Standard Test Method for Static Modulus of Elasticity and Poisson's Ratio of Concrete in Compression*. The loading continued uninterrupted until compressive failure was reached. Stress was then calculated from loading data and strain was calculated from the displacement measured by the extensometer using the equation described in ASTM C469 / C469M – 14.

3.4.2 *Reinforcing Bars*

Reinforcing bars were purchased from Addison Construction Supply in Tacoma Washington and were all delivered at one time. Flexural reinforcing bars for the slab were A615 Gr. 60 and column reinforcement was A706 Gr. 60. When ordering, it was requested that all reinforcement of the same size and grade be from the same heat.

Yielding of the reinforcement was expected under lateral loading. To appropriately predict and analyze results, the stress strain relationship of the reinforcement was characterized using:

- Yield stress (f_y)
- Yield Strain (ε_y)

- Ultimate Stress (f_u)
- Ultimate Strain (ε_u)
- Failure Stress (f_r)
- Failure Strain (ε_r)

The specified and measured properties of the longitudinal reinforcement are shown in Table 3.5. The measured stress-strain relationship for the slab reinforcement and the column reinforcement are shown in Figure 3-10 and Figure 3-11, respectively. All material test specimens failed outside the gauge length and strains measured at the end of the tests do not capture the "necking" behavior. Failure strain was calculated from the final deformed length of the tests measured after failure.

Table 3.5: Reinforcing Bar Material Properteis

	Reinforcing Bar			
	Slab		**Column**	
	Average	**St. Dev.**	**Average**	**St. Dev.**
Steel Grade	A615 Gr. 60	NA	A706 Gr. 60	NA
Specified Yield Stress (ksi)	60	NA	60	NA
Measured f_y (ksi)	72.3	0.98	75.3	6.49
Measured ε_y	0.0046	$2.8*10^{-5}$	0.0046	$1.9*10^{-4}$
Measured f_u (ksi)	108.5	0.91	111.1	6.53
Measured ε_u	0.1054	0.0045	0.1169	0.027
Measured f_r (ksi)	39.5	0.82	43.8	9.23
Measured ε_r	0.1311	$8.4*10^{-4}$	0.1498	0.014

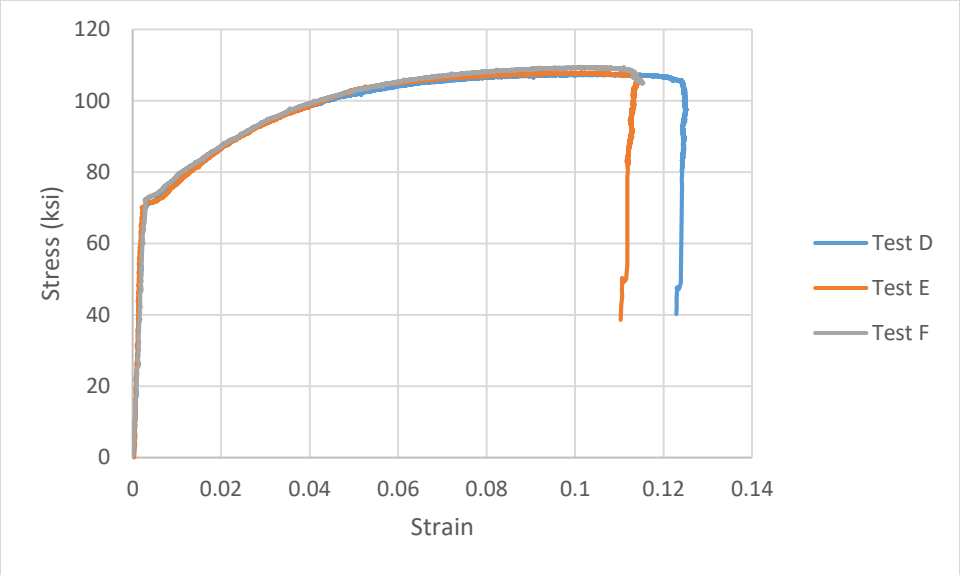

Figure 3-10: Stress vs. Strain #8 Reinforcing Bars

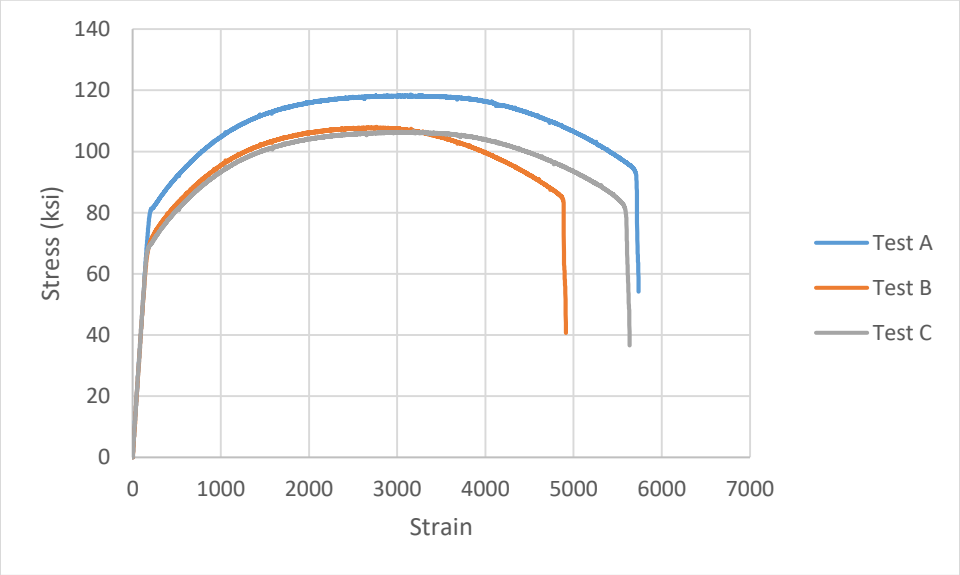

Figure 3-11: Stress vs. Strain #9 Reinforcing Bars

3.4.3 *Steel Tubes*

The steel tubes are ASTM A252 Gr. 3 with a 60 ksi minimum yield. Tubes were donated by Skyline Steel in Fife, Washington. Material properties were reported by the manufacturer and certificates provided. Reported yield and ultimate stresses are summarized in Table 3.6.

Table 3.6: Column, Ring, and Stud Rail Material Properties

	Tube	Ring Plates	Stud Rails	
			Rail	Stud
Steel Grade	A252 Gr. 3	A572 Gr. 50	NA	C1010
Specified Yield Stress (ksi)	60	50	NA	44.2
Reported Yield Stress (ksi)	62.0	NA	54.7	51.3
Reported Ultimate Stress	68.9	NA	77.7	70.6

3.4.4 *Column Ring Plates*

The rings for Specimens PTB_4.5_1_0 and PTB_4.5_1_4 were cut from ½ in. thick A572 Gr. 50 plate steel. The plate thickness was sized to meet or exceed the tube wall thickness (3/8 in.). Due to the difficulty in fabricating the rings for PTB_4.5_1_0 and PTB_4.5_1_4, the rings for Specimen PTB_9_2_0 were manufactured by a local vendor and were also A572 Gr. 50 steel.

Ring plates were welded to the columns using 5/64 in diameter Coreshield 8 E70 welding electrode. All structural welding was performed by an appropriately certified welder. Ring Plate material properties are summarized in Table 3.6.

3.4.5 *Shear Studs*

Shear studs were donated by JSW Stud Rails in Lake Stevens. Material properties were reported by the manufacturer and certificates provided. The material properties for the rails and studs are reported in Table 3.6.

3.5 EXPERIMENTAL TEST SET UP

To characterize the response of the test specimens a setup was developed that could

1. Apply lateral loads to the top of the column
2. Apply vertical/axial loads to the column
3. Appropriately support the column and slab ends in a way that replicates the conditions in a structure under lateral loading

Figure 3-12 shows the components developed to meet the requirements stated above using Specimen PTB_9_2_0. Lateral loads were applied using a combination of an MTS Actuator and a Self-Reacting Test Frame and vertical/axial loads were applied using the Baldwin Universal Testing Machine via a spherical bearing.

To appropriately replicate the conditions, present in a structure under lateral loading, the supports needed to simulate the points of contraflexure in the column and in the slab. These conditions were simulated using three roller supports (at the ends of the slab and top of the column) and one pin support (at the base of the column). Lateral and vertical/axial loads may then be applied to the top of the column to simulate the gravity and lateral loading of a slab-column connection.

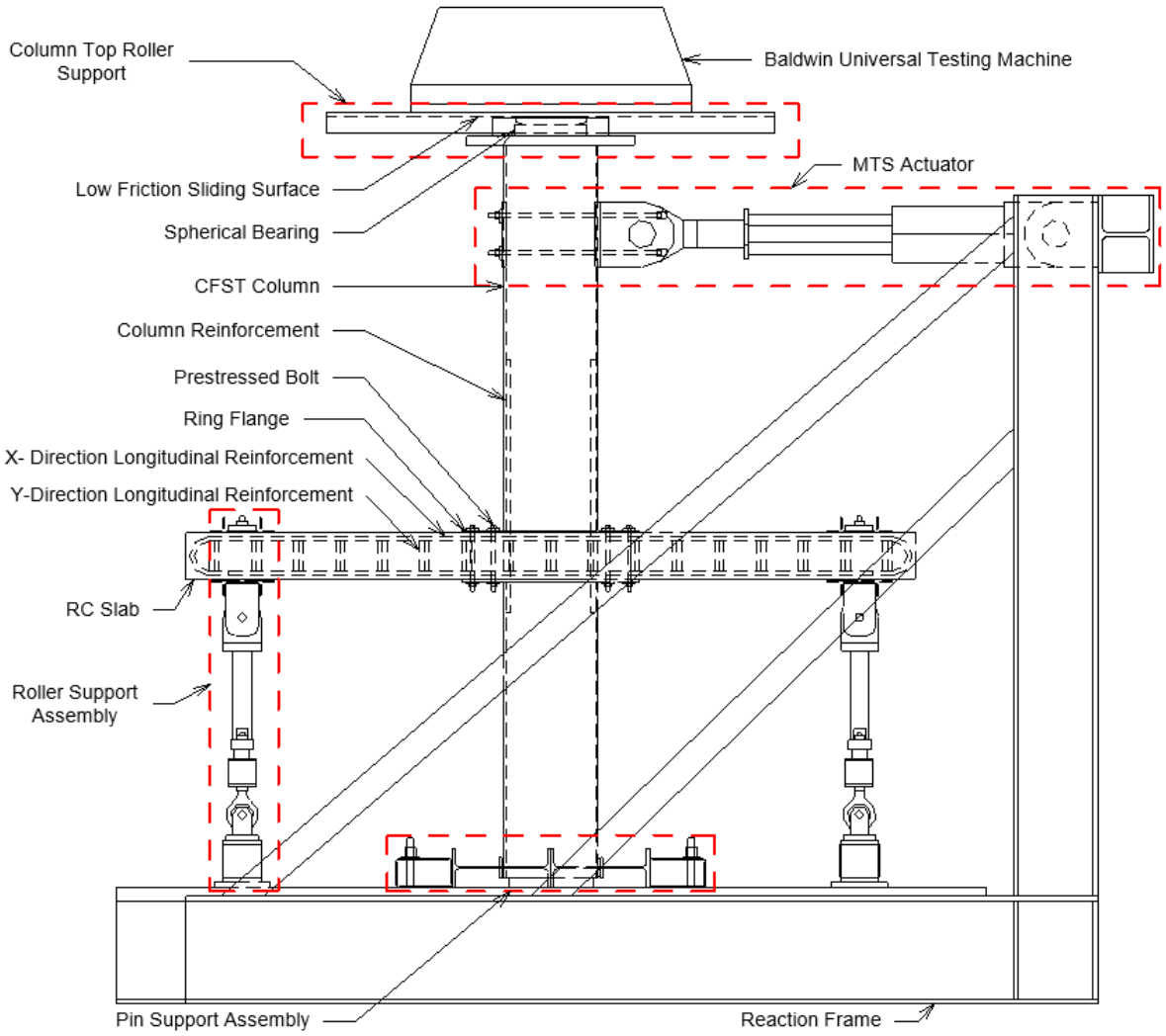

Figure 3-12: Experimental Setup Overview

3.5.1 *Lateral Load Application*

Lateral loads were applied using an MTS Actuator in conjunction with a Self-Reacting Test Frame shown in Figure 3-12.

The MTS Actuator has a capacity of 220 kips and a maximum stroke of ±10 in. The actuator applied a lateral load at the top of the column, simulating increasing story drifts and was operated under displacement control. For each test, the actuator was attached to the column using four 1 in. high strength rods, spreader plates, and rubber pads. The high strength rods were prestressed to

ensure the actuator head was in contact with the column throughout the test. The spreader plates and rubber pads distributed the applied force over an appropriate area to prevent localized damage.

The Self-Reacting Test Frame is used in conjunction with the MTS Actuator to apply lateral loads to the specimen. The frame is also a strong floor that test equipment and specimens can be tied down to. The Column Base Pin Support and Slab End Roller support are both prestressed to the frame. Before placing the specimen, the Self-Reacting Test Frame is moved under the Baldwin and tied down to the laboratory floor.

3.5.2 *Vertical/Axial Load Application*

Axial loads were applied to the column using the Baldwin Universal testing machine. The Baldwin Universal Testing Machine (Baldwin) is capable of applying a 3400 kips load. For the purposes of these tests, the Baldwin applied a constant 330 kip load to the top of the column, simulating loading due to upper stories and the resultant P-Δ force.

To enable the top of the column to displace while maintaining axial loading, an assembly was constructed to act as a roller support at the top of the column (Column Top Roller Support) and is shown in Figure 3-13. The critical components of this assembly were a spherical bearing and a low friction sliding surface though additional components were included to restrict out of plane movements and evenly transfer the vertical loads from the spherical bearing to the column.

The spherical bearing allows the top of the column to be displaced by the MTS Actuator while maintaining the Baldwin load. As shown, a piece of greased PTFE is embedded in the top of the spherical bearing. The greased PTFE provides low friction sliding surface between the bearing and the channel, minimizing friction effects.

The spreader plate is used to apply the axial force from the Baldwin evenly across the top of the column. The plate is also modified with HSS and more greased PTFE, as shown in Figure 3-13, to provide a track for the channel which together prevent transverse displacement during testing.

The large steel channel is bolted to the head of the Baldwin and acts as a guiding track. The interior web of the channel is lined with stainless steel providing a smooth surface on which the greased PTFE slides.

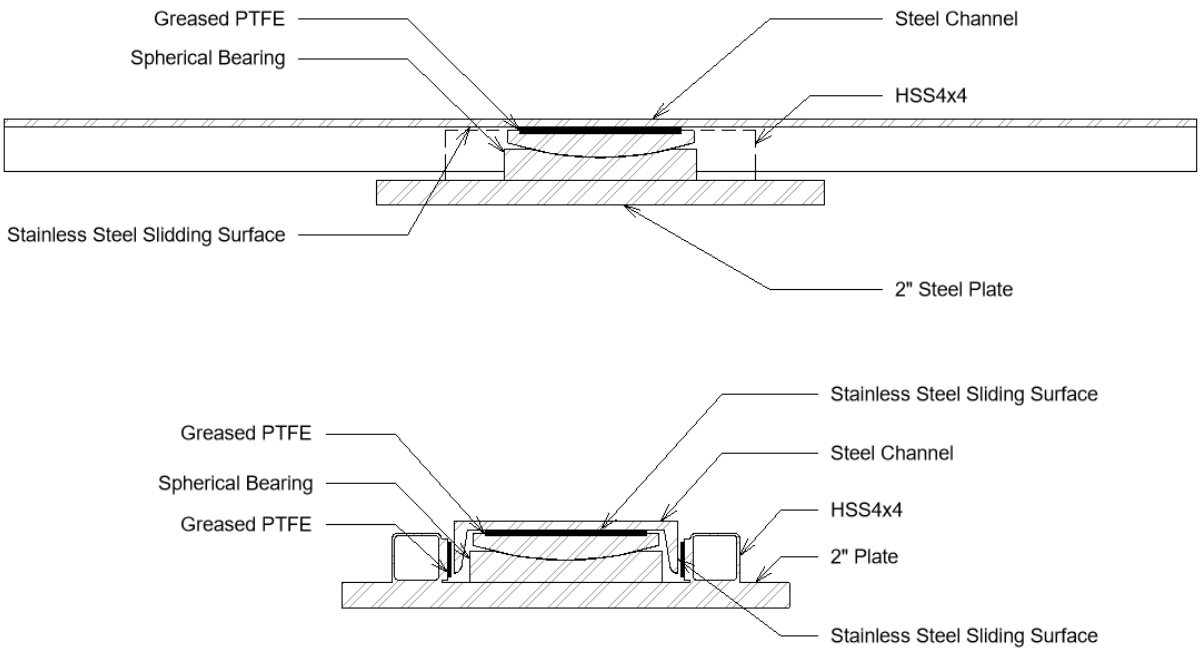

Figure 3-13: Column Top Roller Support

3.5.3 *Slab and Column Supports*

The specimen is supported by a pin assembly at the base of the column and roller supports at the ends of the slab. The pin assembly is referred to as the "Column Base Pin Support" and the roller supports are referred to as the "Slab End Roller Support". These supports provided points of contraflexure at the end of the slab wile restraining displacements as in a building.

The Column Base Pin Support has a cotton duck bearing pad to support axial load and permit end rotation and a shear collar to provide translational restraint. The column Base Pin Support is shown below in Figure 3-14. The shear collar is constructed of two identical pieces that bolt together around the column and are prestressed to the Self-Reacting Frame. Each piece is a modified W-section laid on its side with one flange welded to a rectangular HSS. As shown in Figure 3-14, the W-sections have sections cut away to accommodate the circular column. The HSS is welded to the W-section and extends the collar to reach prestressing points embedded in the Self-Reacting Frame. ½ in. thick strips of cotton duck bearing pad are placed between the collar and the column to ensure free rotation.

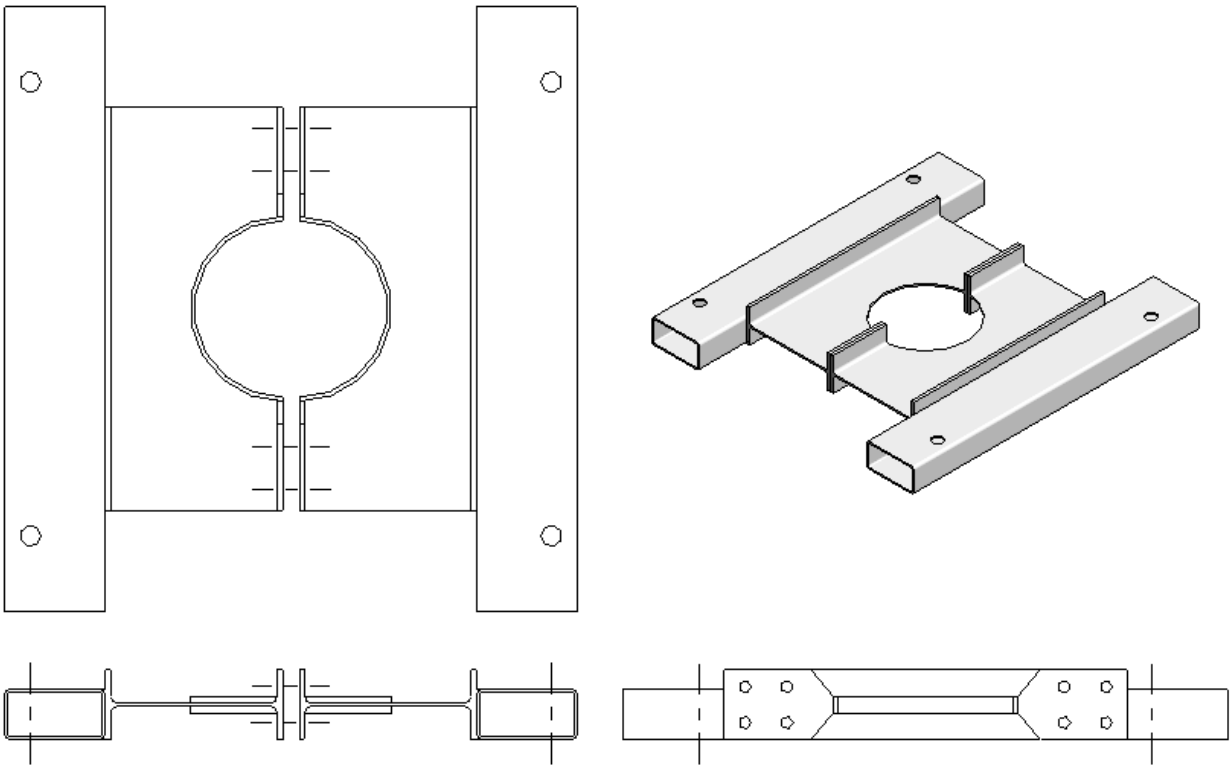

Figure 3-14: Column Base Pin Support

The Slab End Roller Supports are four one-directional truss members (two per slab end) with clevises at either end and load cells in the middle and are depicted below in Figure 3-15. The truss members provide vertical (shear) constraint but leave the slab free to rotate and displace in the north/south direction. The clevises at the base of each truss member is bolted to an adaptor that is prestressed down to the Self-Reacting Test Frame. The clevis at the top of the truss member is prestressed to the slab and bears on T-beams that span the width of the slab, distributing the reaction force in the truss member. A load cell was included in the truss member to monitor the hysteretic response of the slab during testing.

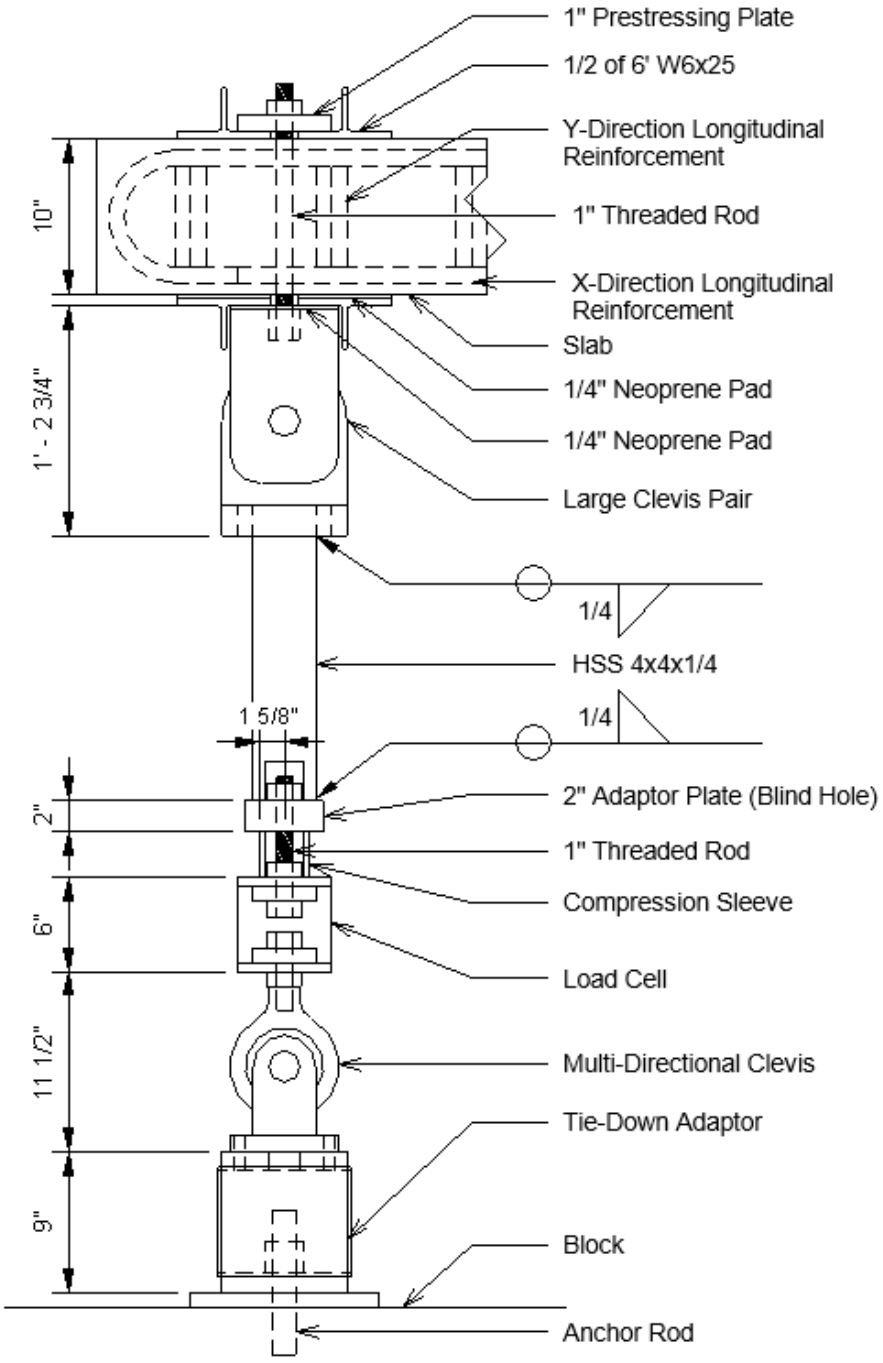

Figure 3-15: Slab End Roller Support

3.6 SPECIMEN INSTALLATION

When concrete had achieved sufficient strength, specimens were moved into the Self-Reacting Test frame. Specimens were moved using a combination of cranes, forklifts, and the Baldwin Universal Testing Machine. Specimens were then secured to the Baldwin while supports were attached. Supports were usually attached in the following order:

1. Column Base Pin Support
2. Column Top Roller Support
3. MTS Actuator
4. Slab End Roller Supports

Supports were removed in reverse order after testing was complete.

The southern half of the Column Base Pin Support was placed before specimens were moved into the Self-Reacting Test Frame and prestressed down with two rods tensioned to approximately 60 kips each. This was done to ensure that the base of the column would be properly placed for testing. After the specimen was place, the north half of the Column Base Pin Support was bolted to the south half and then prestressed down to the block with two rods also prestressed to approximately 60 kips each.

The column top roller support was attached to the Baldwin head before the specimens were moved into the Self-Reacting Test Frame. Once the Column Base Pin Support was attached, the spherical bearing and spreader plate were lowered from the Baldwin head onto the column and fixed in place using angles bolted to the bottom of the spreader plate. Fresh grease was then applied to the spherical bearing to minimize friction.

The MTS actuator was then attached to the column using four 1 in. diameter A354 Gr. BD threaded rods. High strength rods were selected to ensure that rods would not yield under high prestressing forces and would not fracture under cyclic loading. Once the MTS actuator was attached, the specimen was considered stable and the chains attaching the specimen to the Baldwin were removed.

Slab End Roller Supports were then assembled piece by piece. Tie down adaptors and the female half of the large clevis pair were, respectively, tensioned to the Self-Reacting Test Frame and specimen with approximately 60 kips. The remaining parts of the slab end roller support were then assembled.

The slab end roller supports were left loose until axial load from the Baldwin was applied. This was done for prevent any of the axial load from transferring to the Slab End Roller Supports due to deformation in the cotton duct bearing pad at the base of the column.

The pretensioning force was determined by calculating the maximum force expected in the truss members. This force was found by calculating the maximum shear the slab would carry when the slab formed a plastic hinge at the column. The maximum expected force in the slab end roller supports was then multiplied by a factor of two, resulting in a pretensioning force of 60 kips

Once all parts of the test setup were in place, instrumentation was connected to the specimen and the data acquisition system. Load cells, strain gauges, and various potentiometers were used as well as an Optotrak camera and targets. The load cells, strain gauges, potentiometers were all routed to a single data acquisition system while the Optotrak system was routed to a separate system. Instrumentation is discussed in more detail in Section 3.8.

3.7 TESTING IMPLEMENTATION

Testing was carried out for all specimens in accordance with test procedures written below. Before testing, an experimental checklist was completed. Once the checklist was completed and the lab manager verified test equipment was prepared the following procedure was performed:

Initializing:

1. Data acquisition systems were initialized
2. Axial load was applied to the column using the Baldwin Universal Testing Machine
3. Hex nuts integral in the Slab End Roller Supports were tightened to restrict vertical displacements (vertical displacements at roller supports were not restricted while axial loads were applied to the column to prevent column loading from transfer into the slab)

For Each Target Displacement:

4. 1 full cycle at target displacement was performed
5. A second cycle at the same target displacement was initiated and stopped at the first peak
6. Cracks were marked in red, crack sizes were recorded, crack maps were updated to record cracking, spalling and crushing, and pictures were taken to record spalling, crushing, and bar buckling
7. The cycle was continued and halted when the MTS actuator read zero force

8. Residual displacement was recorded, and crack sizes were recorded
9. The cycle was continued and halted at the second peak
10. Cracks were marked in blue, crack sizes were recorded, crack maps were updated to record cracking, spalling and crushing, and pictures were taken to record spalling, crushing, and bar buckling
11. The cycle was continued and halted when the MTS actuator read "0" force
12. Residual displacement was recorded, and crack sizes were recorded
13. The cycle was completed
14. Steps 4 – 13 were repeated at increasing displacements until specimen failure was achieved or equipment limits were reached

Test Conclusion:

15. Slab End Roller Supports are loosened
16. Axial load was removed from the column
17. Data acquisition systems were halted, and data was saved
18. Spalling was removed and more pictures were taken showing the specimen after testing concluded

3.8 INSTRUMENTATION

To fully characterize the response of test specimens to lateral loading, imposed displacements, lateral load resistance, support reactions, local displacements, and strains were recorded. The imposed displacements and lateral load response were used in conjunction to characterize and compare the force drift response of each specimen. The local displacements and strains were used to determine failure modes and characterize the local behavior of the slab.

3.8.1 *Lateral Load Response*

A critical property of structural systems in seismic regions is their lateral force resistance response. Lateral force resistance of connections is often neglected when designing structures for lateral loads. However, a connections response to lateral loading can indicate the connections ability to maintain its integrity at under large lateral displacements. A brittle connection may

suddenly lose lateral force resistance while a more ductile connection will maintain lateral resistance at large drifts.

Lateral loads were recorded using a load cell integral with the MTS Actuator. The loads measured by this load cell are used for the main discussion of connection lateral resistances. At large drifts, P-Δ effects also become significant. The Baldwin Universal Testing machine also contains an integral load cell and the loads recorded were used to remove P-Δ effects during analysis, enabling a clearer understanding of connection response.

3.8.2 *Support Reactions*

Support reactions at the end of the slab are also important, indicating the shear and moment transferred by the connection from the column into the slab. Load cells were integrated into the slab end roller support to monitor these reactions.

3.8.3 *Displacements*

To characterize the deformations of the test specimens under lateral loading, displacements at level of lateral load application and displacements along the slab were measured. Displacement at the point of lateral loading is used to develop the force-drift response of the connection. The force drift response is used to compare performance of connections and indicates which connection details provide a more robust response under lateral loads. The deformed shape of the slab can indicate the type of failure occurring in the slab. Potential slab failures associated with slab deformations are:

- A flexural response may be indicated by a sudden change in slope of the deformed shape of the slab. The sudden change in slope indicates the formation of a plastic hinge.
- A shear failure may be indicated by a sudden change (vertical discontinuity) in the deformed shape while the slope of the deformed shape changes little. This would indicate a breakaway of the slab from the column or of the slab from itself.

To monitor displacements at critical locations, string potentiometers were attached to test specimens.

To monitor the displacement at the level of lateral force application, a reference tower was placed to the north of the specimen and a string potentiometer attached between the tower and the column. Though the MTS Actuator has an internal LVDT for measuring displacements, these displacements were not used in analysis because the deformation of the setup made them unreliable. Instead the string potentiometer attached to the reference column was used to characterize the force-drift response.

Slab vertical displacements were monitored using additional string potentiometers attached to the bottom of the slab according to the plan shown in Figure 3-16. A smaller spacing between potentiometers was detailed in the joint region because most deformations were expected to occur in this area. Locations were also chosen to correspond to the placement of strain gauges on longitudinal reinforcement as discussed in Section 3.8.4. String potentiometers were attached to rods threaded into anchors that were embedded in the bottom of the slab during casting. Additional potentiometers were attached to the south end of the slab and measured the horizontal displacement of the slab. These potentiometers were used to monitor rigid body rotations of the specimen.

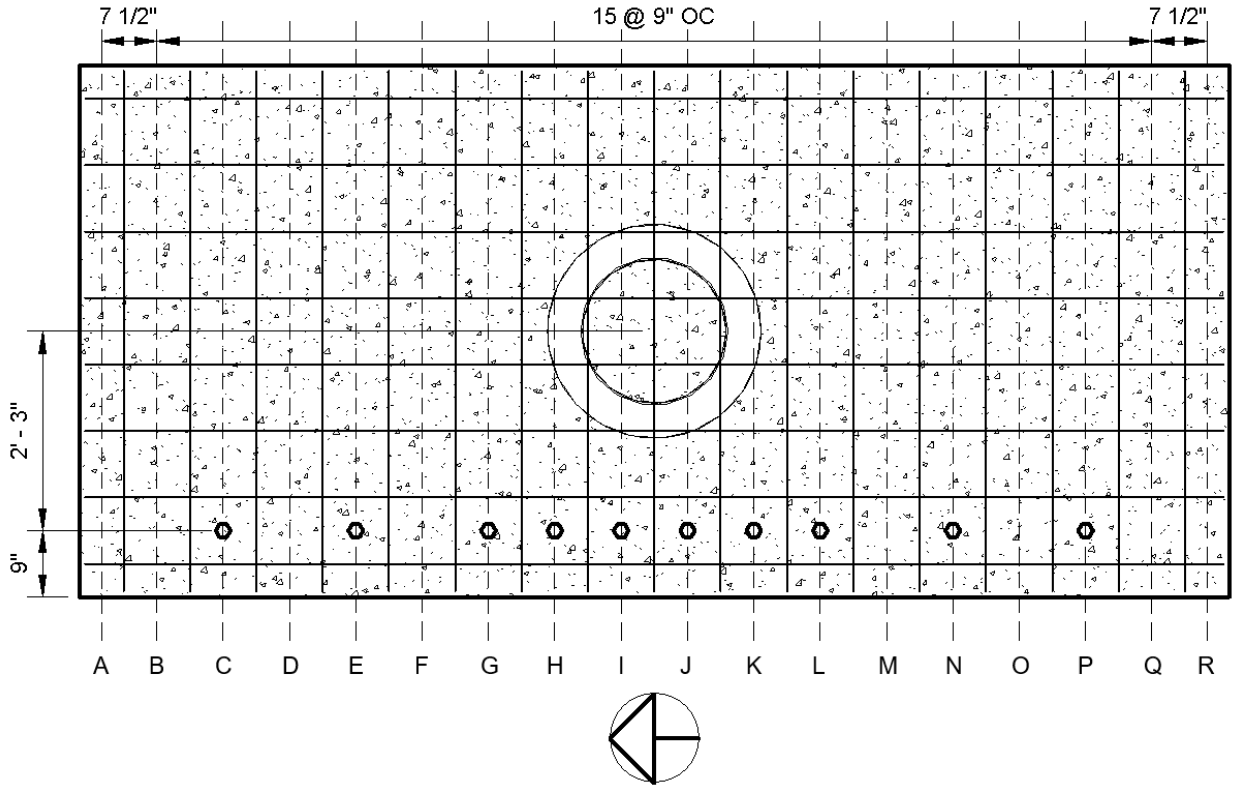

Figure 3-16: Slab String Potentiometer and Optotrak Layout

Additional string potentiometers were placed to monitor deformations of the setup so that these deformations could be controlled for when analyzing results. Of primary concern were the deformations of the slab end roller supports as the stiffness of these supports is different in compression and tension and any vertical deformation of the supports results in the supports not acting as true roller supports. Deformations of the slab end roller supports were monitored with string potentiometers the deformations were removed in analysis.

In addition to displacement measurements taken using potentiometers, an Optotrak system was used to capture displacement information for the slab and upper column as a backup. No targets could be placed on the lower column due to visibility constraints. Optotrak targets were placed on the top of the slab in locations corresponding to locations of string potentiometers (see Figure 3-16 for locations). On the top column, Optotrak targets were placed at the level where lateral forces were applied, the same point where the reference column string potentiometer was attached. Additional Optotrak targets were placed at a spacing of 12 in. down the column. Figure 3-17 shows the planned locations for placement of Optotrak targets, though targets were only placed at locations “F” through “K” for reasons previously mentioned.

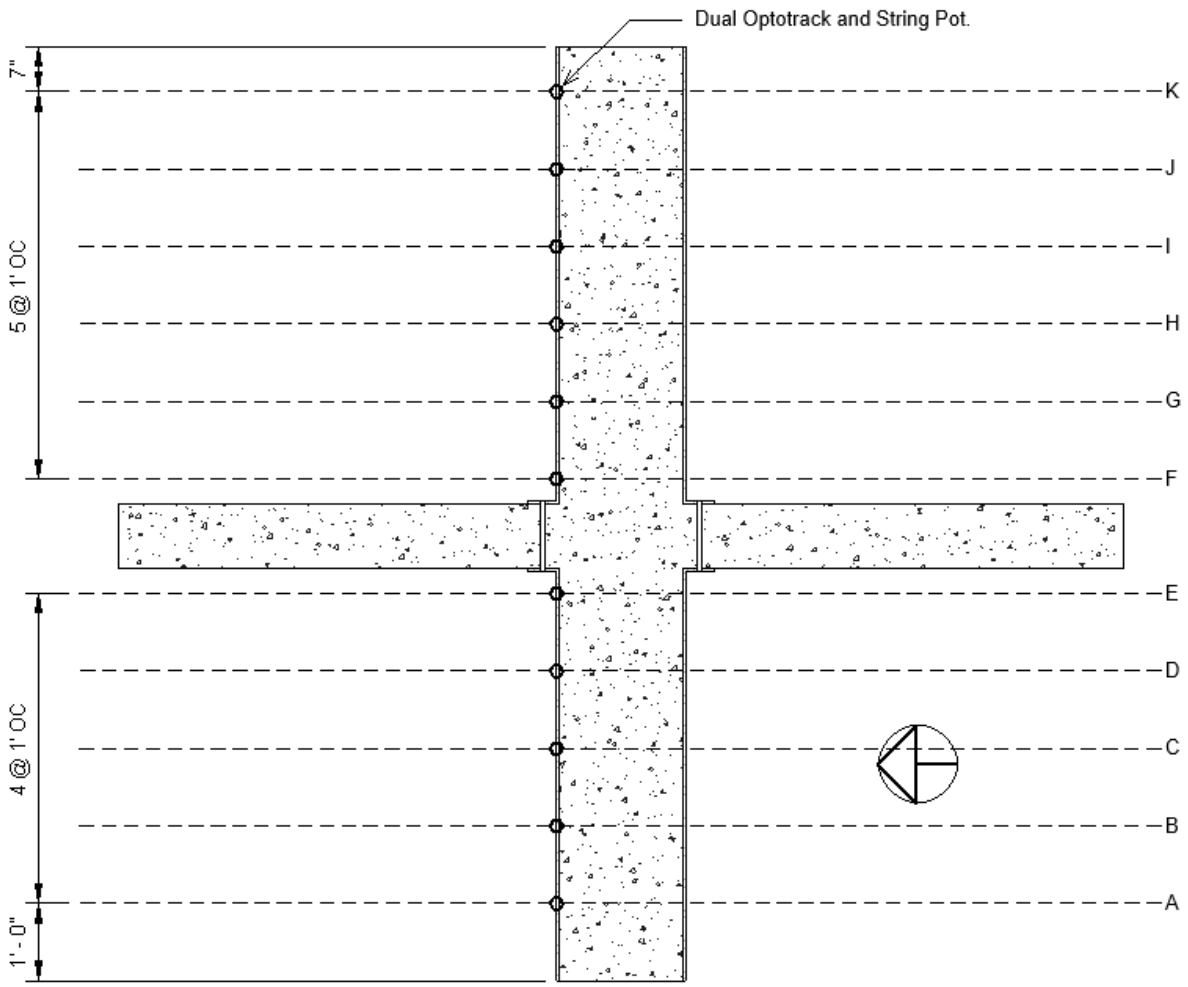

Figure 3-17: Column Optotrak Layout

3.8.4 *Strains*

Knowing the yield behavior of reinforcement as it related to lateral loading was an important metric for the evaluation of specimen performance as the location of yielding can indicate the failure mode. Potential failure modes and the associated yield behavior are as follows:

- A flexural response is indicated by yielding of longitudinal reinforcement across the width of the slab.
- A shear failure in the reinforced region is indicated by yielding of transverse reinforcement.
- A shear failure outside the reinforced region is indicated by no yielding of either longitudinal or transverse reinforcement before failure.

- A weak column relative to the slab would be indicated by yielding of column reinforcement.

To monitor these potential failure modes, strain gauges (TML YFLA strain gauges) were placed on a portion of flexural reinforcement, transverse reinforcement, and column reinforcement. As strain gauge readings are sometimes considered to be unreliable, it was intended that strain gauge readings would be used to characterize the yield behavior and compare the results from various tests.

To monitor the flexural response of the slab, strain gauges were placed according to the plan shown in Figure 3-18. Gauges were applied to only longitudinal flexural reinforcement in the direction of loading because the stresses in longitudinal reinforcement in the orthogonal direction were not expected to be significant. To decrease build time, symmetry was assumed, and gauges were only placed in the east half of test specimens. To characterize the extent of yielding in longitudinal reinforcement across the length and width of test specimens, a greater number of gauges were placed on reinforcement passing through the column while fewer gauges were placed on reinforcement at the edge of the specimen. Fewer gauges were placed towards the edge of the specimen for two reasons (1) because it was expected that the connection would mostly activate reinforcement closer to the column and (2) because once all longitudinal reinforcement had yielded a flexural response would be established. Gauges were placed on both top and bottom reinforcement to check for any asymmetry in the response.

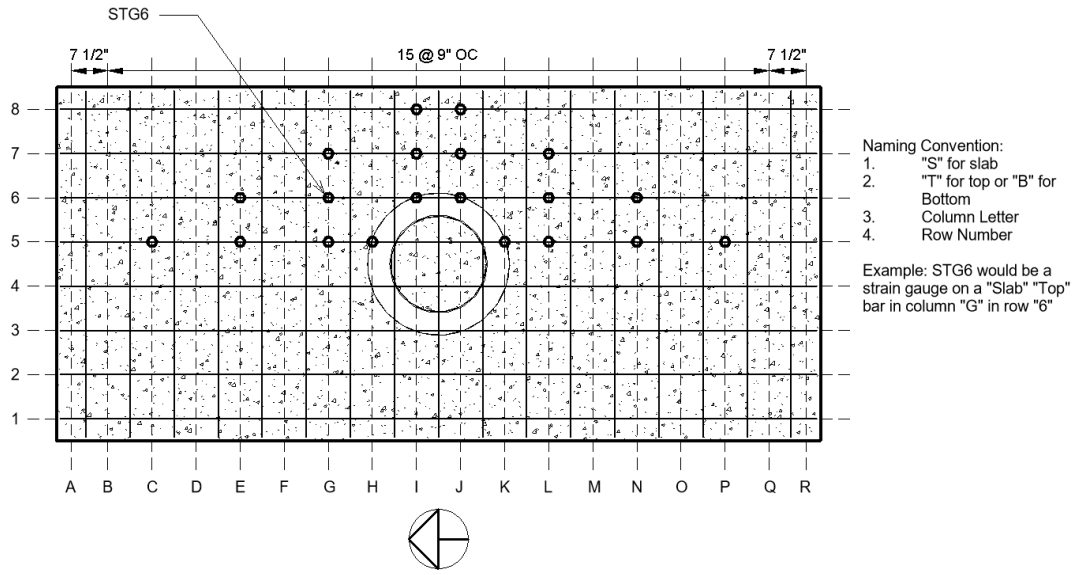

Figure 3-18: Slab Strain Gauge Layout

To monitor potential weakness in the column relative to the slab, strain gauges were placed on four reinforcing bars extending from the lower column to the upper column as shown in Figure 3-19 for Specimens PTB_4.5_1_0 and PTB_4.5_1_4 and in for Specimens SR_4_10_5 and PTB_9_2_0. Gauges were placed on the most northern and southern bars because if yielding occurred in column reinforcement, it would first occur in the reinforcement furthest from the neutral axis if the column. Additionally, bars were gauged at one location bellow and three locations above to monitor the starting location and extent of any potential yielding. No gauges were placed in the joint as it was believed gauges in this region would be break shortly after testing was started. For specimens SR_4_10_5 and PTB_9_2_0, gauges were only placed on column bars C and I as the results from the first two tests showed there was no need for gauges on bars D and H.

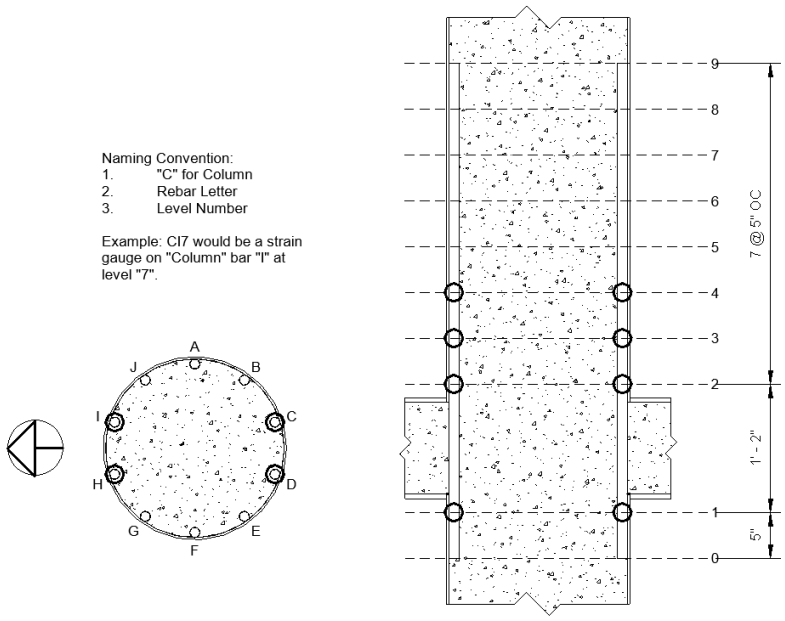

Figure 3-19: Strain Gauge Layout on Column Longitudinal Reinforcement

To monitor a potential shear failure in the transverse reinforced region of Specimen SR_4_10_5, strain gauges were placed on shear studs as shown in Figure 3-20. To decrease build time, symmetry was assumed, and gauges were only placed in the NE quadrant of the specimen.

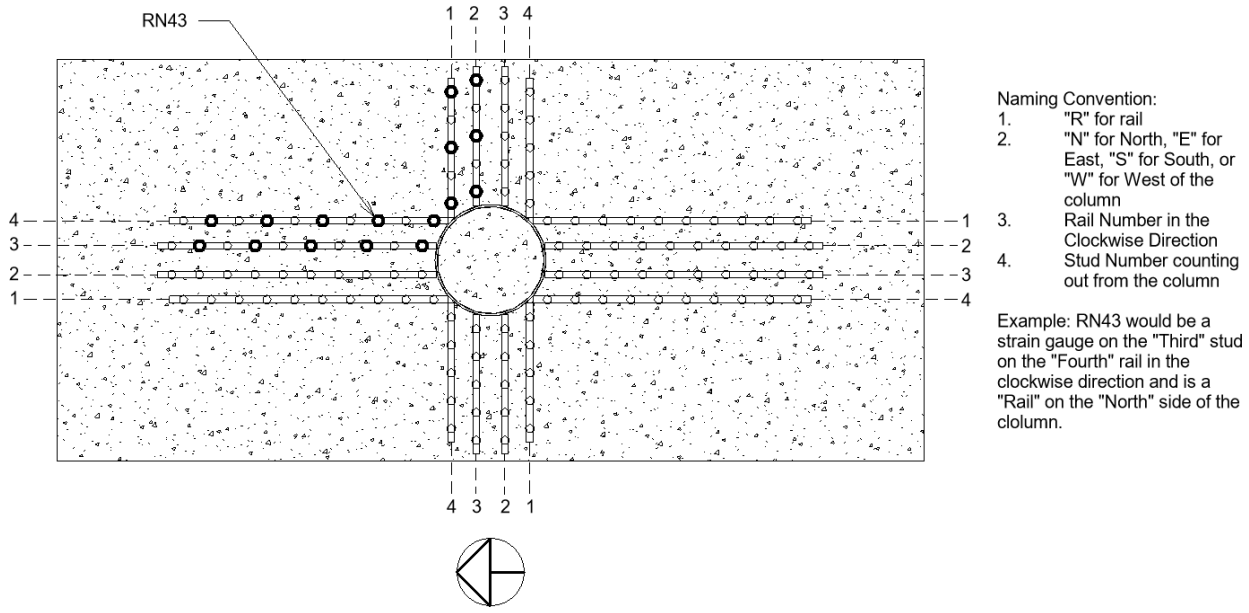

Figure 3-20: Stud Rail Strain Gauge Layout

As mentioned in Section 3.3, after bars were placed, gauge wires were labeled and guided out of the specimen. Wires were suspended at mid height between bars and exited Specimens PTB_4.5_1_0 and PTB_4.5_1_4 as a single bundle. After it was realized many gauges did not survive casting, changes were made to how gauges were secured to bars and how wires were guided out of specimens. After the procedures for placing a gauge were complete, the gauge site was wrapped in electrical tape to protect the gauge and secure the gauge wire. Gauge wires were also suspended beneath bars as they exited the test specimens instead of being suspended between bars. Additionally, wires exited the specimens in four separate bundles to minimize the opportunity for concrete to impact wires during placing. These precautions proved to significantly increase the likelihood of gauges surviving casting and a minimal number of gauges were broken prior to testing specimens PTB_9_2_0 and SR_4_10_5.

Chapter 4. EXPERIMENTAL OBSERVATIONS

This chapter contains descriptions of each specimen including damage observations, crack patterns, and global force-drift response. Each section begins with a description of the specimen, an overview of the displacement and loading histories, a presentation of the global response, and a performance summary. The damage and crack patterns are described for different levels of drift, as follows:

- Low Drift Cycles: Test specimen has cracked and there is minimal (if any) yielding of slab flexural reinforcement. (Approximately 0-1.5% drift)
- Moderate Drift Cycles: Test specimen has yielded reached peak lateral force resistance but lateral force resistance has not begun to degrade. (Approximately 1.5-3.6%)
- High Drift Cycles: Test specimen lateral force resistance has begun to degrade and specimen failure occurs or test equipment reaches its deflection limit. Specimen failure is defined as a sudden loss of lateral force resistance or loss of 50% peak lateral force.

The specimens were cycled under displacement control using the displacement history described in subsequent sections. The target displacement included flexibility of the test setup (including the reaction frame and actuator). The actual drift was measured using an independent string pot attached to an instrumentation column. As such, the actual drift was nearly always less than the target. At small drifts, the controller for the MTS actuator sometimes overshoots the target drift, resulting in actual drifts higher than those targeted. Target and actual drifts for each specimen are provided Table 4.1.

Table 4.1: Displacements/Target Drifts and Measured Drifts

Series	Target Disp. (in.)	Target Drift (%)	Measured Drift (%)							
			SR_4_10_5		PTB_4.5_1_0		PTB_4.5_1_4		PTB_9_2_0	
			South	North	South	North	South	North	South	North
1	0.5	0.36	0.21	- 0.34	N/A	N/A	0.34	- 0.49	0.30	- 0.31
2	1.0	0.73	0.56	- 0.68	N/A	N/A	0.56	- 0.71	0.63	- 0.64
3	1.5	1.1	0.91	- 1.0	N/A	N/A	0.91	- 1.1	0.96	- 0.97
4	2.0	1.5	1.3	- 1.4	1.3	- 1.3	1.2	- 1.4	1.3	- 1.3
5	3.0	2.2	2.0	- 2.1	2.0	- 2.0	1.9	- 2.0	2.0	- 2.0
6	4.0	2.9	2.7	- 2.8	2.6	- 2.6	2.6	- 2.8	2.7	- 2.7
7	5.0	3.6	3.4	- 3.5	3.4	- 3.3	3.4	- 3.5	3.4	- 3.4
8	6.0	4.4	4.2	- 4.2	4.1	- 4.0	4.1	- 4.2	4.1	- 4.1
9	7.0	5.1	4.9	- 4.9	4.8	- 4.8	4.8	- 4.9	4.9	- 4.8
10	8.0	5.8	5.6	- 5.7	N/A	N/A	5.5	- 5.6	5.6	- 5.5
11	9.0	6.5	6.4	- 6.4	N/A	N/A	6.3	- 6.3	6.4	- 6.2
12	9.5	6.9	N/A	N/A	N/A	N/A	6.7	- 6.7	N/A	N/A

To facilitate comparison, target drifts are used in chapter headings while measured drifts are used in the discussion.

4.1 Overview of Damage States

The following section provides an overview of various damage states and describes the method used to present observations. Damage states are as follows:

Table 4.2: Damage States

Damage State	Description
Cracking	Flexural and torsional cracks develop
Yielding	Flexural reinforcement yields
Spalling	Concrete cover separates from surrounding concrete
Crushing/Exposure of Reinforcement	Cover concrete is completely removed and reinforcement is exposed
Bar Buckling	Exposed reinforcement buckles in compression

The coordinate system will utilize cardinal directions. North is the direction corresponding to MTS Actuator in compression. Directions are noted on the crack maps. The sides of the slab are referred to as an "edge" and are paired with a direction.

On crack maps, cracks and spalling marked on pauses at peak southern deflection (MTS Actuator in tension) are in red. Cracks and spalling marked on during peak northern deflection (MTS Actuator in compression) are in blue. Cracks are marked after the completion of one full cycle of a target drift, therefore cracks formed at any point during the first cycle that are visible may marked in red though some judgement was used to determine if cracks formed during northern drifts or southern drifts.

For the purpose of this discussion, crushing is differentiated from spalling by the severity of damage. Crushing is the removal of concrete cover while spalling is damage to/delamination of cover without complete removal.

4.1.1 *Cracking*

A crack map from the testing of Specimen PTB_4.5_1_4 is shown in Figure 4-1. Crack maps are shown for the drift where flexural cracks first spanned the entire width (west to east) of the specimen (stage 1 cracking), at the last drift where there was a significant increase in cracking (stage 2 cracking), and at an intermediary target drift of 2.2%. These benchmarks were selected to best characterize the progression of cracking from the elastic portion testing into the inelastic portion. Crack maps from cycles before full flexural cracking are not included as it is believed that earlier cracking is mostly due to temperature and shrinkage cracks that were temporarily covered

with primer. Crack maps from drifts after cracks have reached their full extent are not included in the discussion as the majority of damage after this point is due to spalling and crushing of concrete.

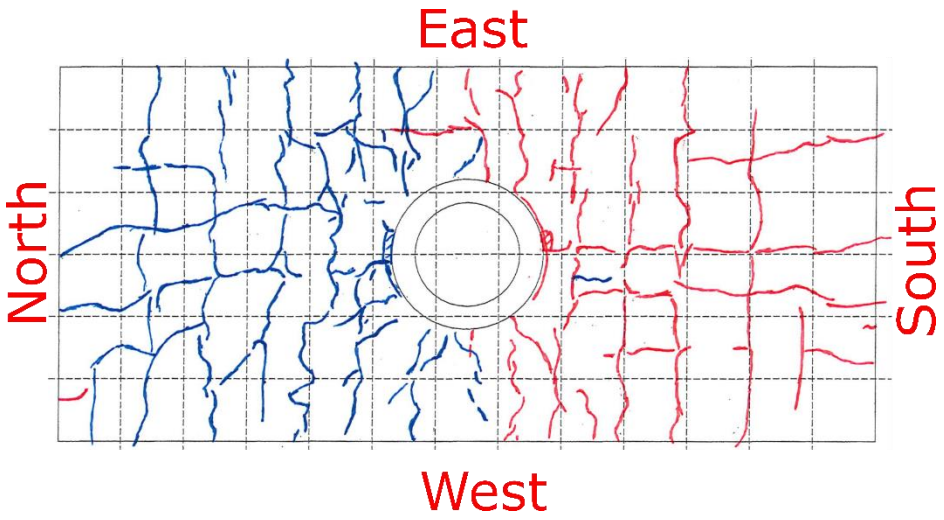

Figure 4-1: Example of Crack Map

The grid spacing on all crack maps is 1ft. x 1ft. This grid served as a guide but was not strictly adhered to for all tests. After a crack map was completed for a target drift level, it was copied and cracks formed during the next drift level were added to the copy. A complete set of crack maps are provided in Appendix D.

Throughout the chapter crack widths are reported in two ways. The maximum crack widths measured during test pauses (at peak drifts) are reported when discussing observations. Typical crack sizes are reported in tables summarizing cracking during low, moderate, and high drift cycle. Both measures of crack sizes are given because maximum crack sizes are not necessarily representative of typical cracking throughout the majority of the slab.

4.1.2 *Yielding*

Yielding of reinforcement was determined using strain gauges placed on longitudinal reinforcement before concrete was cast. Figure 4-2 shows an example of a diagram summarizing the level of strain in gauges placed on flexural reinforcement in the slab. Diagrams show the perimeter of the specimen, the outline of the column and the outline of the ring flange using solid

black lines. Dashed lines are used to denote longitudinal reinforcement in the slab. As shown in the legend, symbols signify the following:

- Black Circle: measured strain is in the elastic range
- Red Circle: measured strain indicates the bar has yielded
- Red Diamond: measured strain indicates the bar has reached the strain corresponding to the ultimate strength
- Red X: measured strain indicates the bar has reached the fracture/rupture strain
- Black X: strain gauge was broken at the start of testing

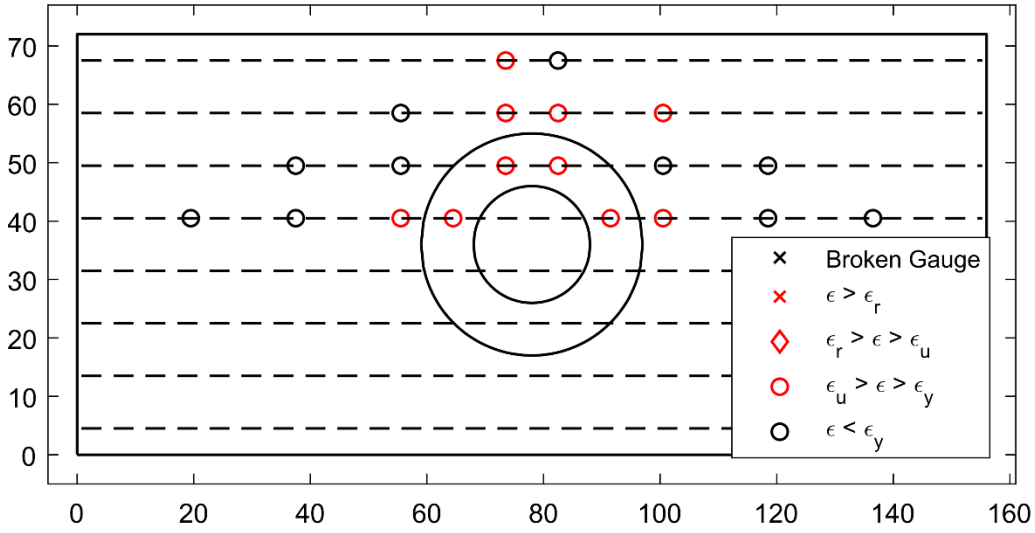

Figure 4-2: Example Reinforcement Strain Summary

Two limit states were used to describe the yielding of specimens: (1) the onset of yielding and (2) full yielding. The onset of yielding was determined by noting when one strain gauge indicated yielding of the slab flexural reinforcement and full yielding was determined by noting when at least one strain gauge indicated yielding of each slab flexural reinforcing bar.

Strain measurements are taken at the peak drifts of a given drift range. The peak strains typically occurred during the first cycle of a drift range. A complete set of strain summary plots are provided in Appendix E.

4.1.3 *Spalling*

Concrete spalling mostly occurred around the slab-column joint and tends to precede concrete crushing/exposure of reinforcement. An example image showing spalling around the ring flange of Specimen PTB_4.5_1_0 is shown in Figure 4-3. To provide context for photos showing damaged regions of test specimens, graphics indicating the part of a specimen depicted are included to the right of photos taken during tests which the area depicted outlined on the graphic in red.

Figure 4-3: Example Spalling around Bottom Joint

4.1.4 *Crushing*

For the purpose of the discussion included in this chapter, crushing is used to describe regions where concrete has both crushed and fallen away or where cyclic tensile yielding and compression loading of reinforcement has caused cover concrete to be completely removed, exposing longitudinal reinforcement. Figure 4-4 shows the bottom joint of Specimen SR_4_10_5 north of the column where crushing has exposed the longitudinal reinforcement as well as the base rail of the transverse reinforcement.

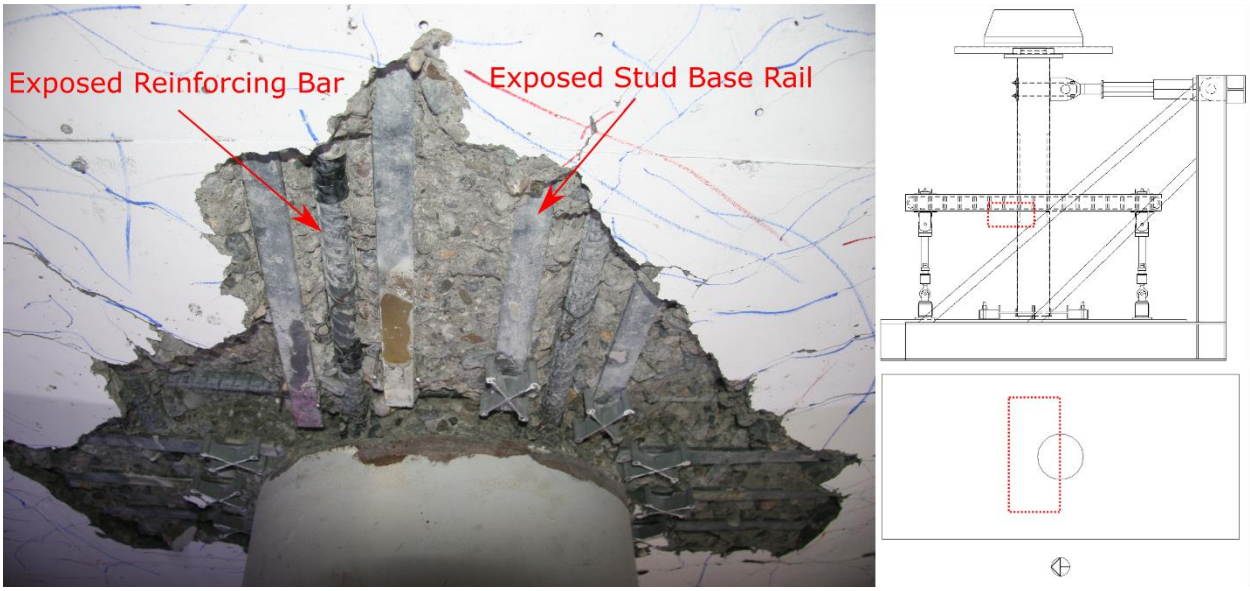

Figure 4-4: Example Crushing around Bottom Joint

4.1.5 *Bar Buckling*

After multiple cycles where flexural reinforcement is yielded in tension followed by reverse loading in compression, bars running through the slab-column joint had a tendency to buckle directly north or south of the connection. Figure 4-5 shows reinforcement buckling in the region directly south of the bottom joint of Specimen PTB_4.5_1_4.

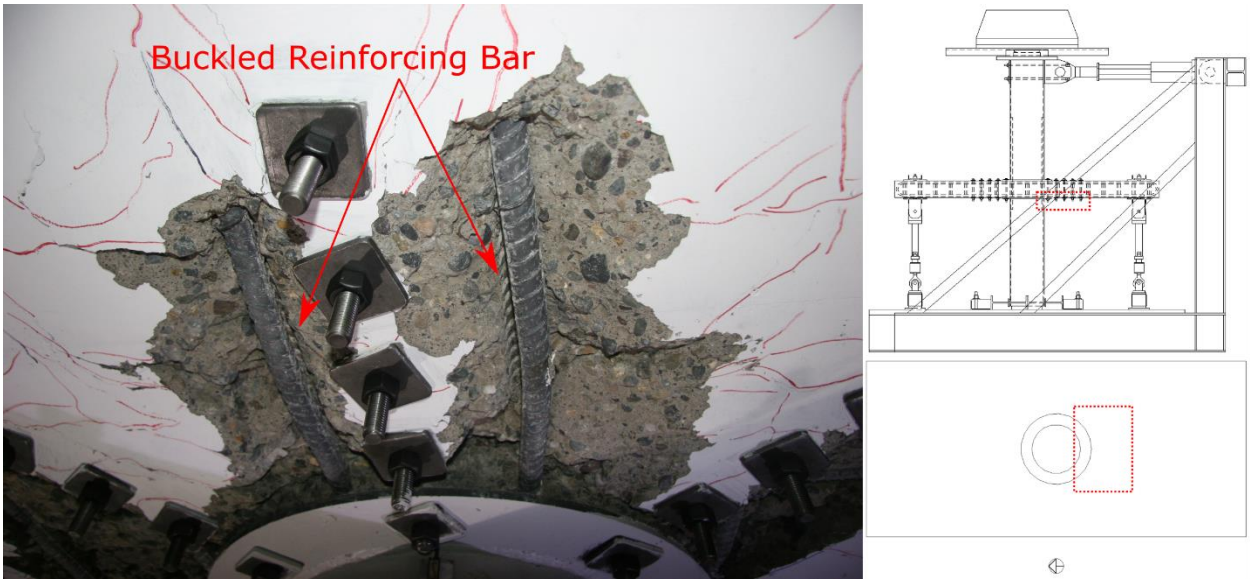

Figure 4-5: Example Reinforcement Buckling

4.2 SPECIMEN SR_4_10_5

Specimen SR_4_10_5, the reference specimen, was tested on August 7th, 2019 in the Structural Research Laboratory at the University of Washington. The test was performed 55 days after casting the slab and lower column and 35 days after casting the upper column.

4.2.1 *Specimen Overview*

A description of the test specimen can be seen in Chapter 3. The test went smoothly and there were no interruptions throughout the test other than those planned (for marking cracks or initializing the next cycle). The induced drift and applied lateral loads can be seen in Figure 4-6 and Figure 4-7, respectively.

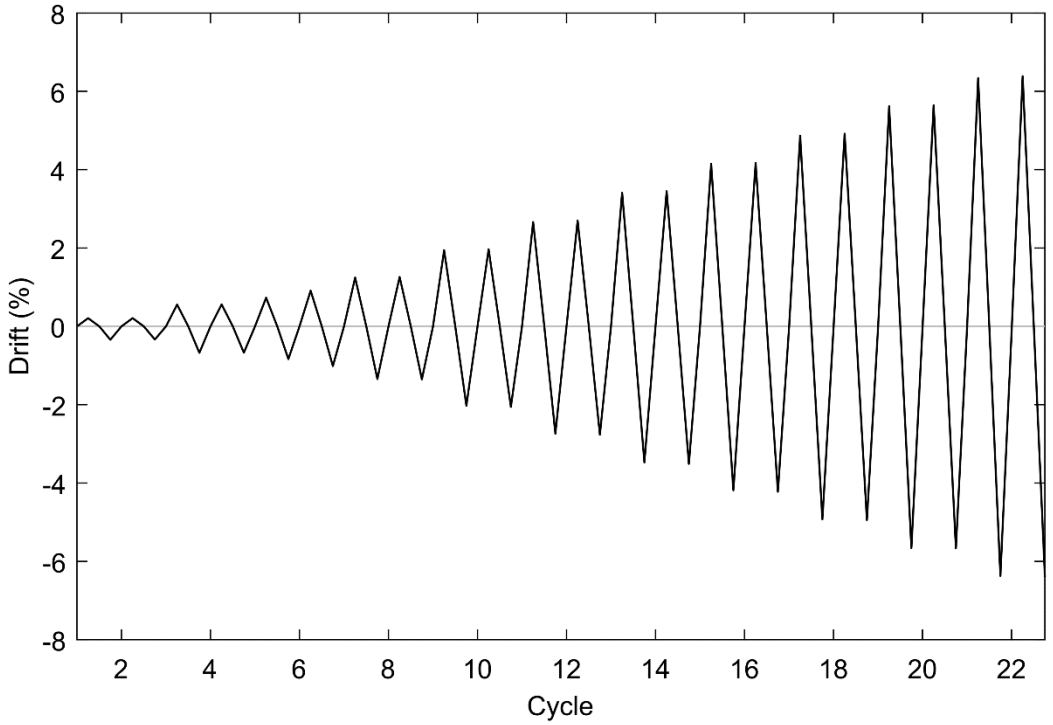

Figure 4-6: Induced Drift (SR_4_10_5)

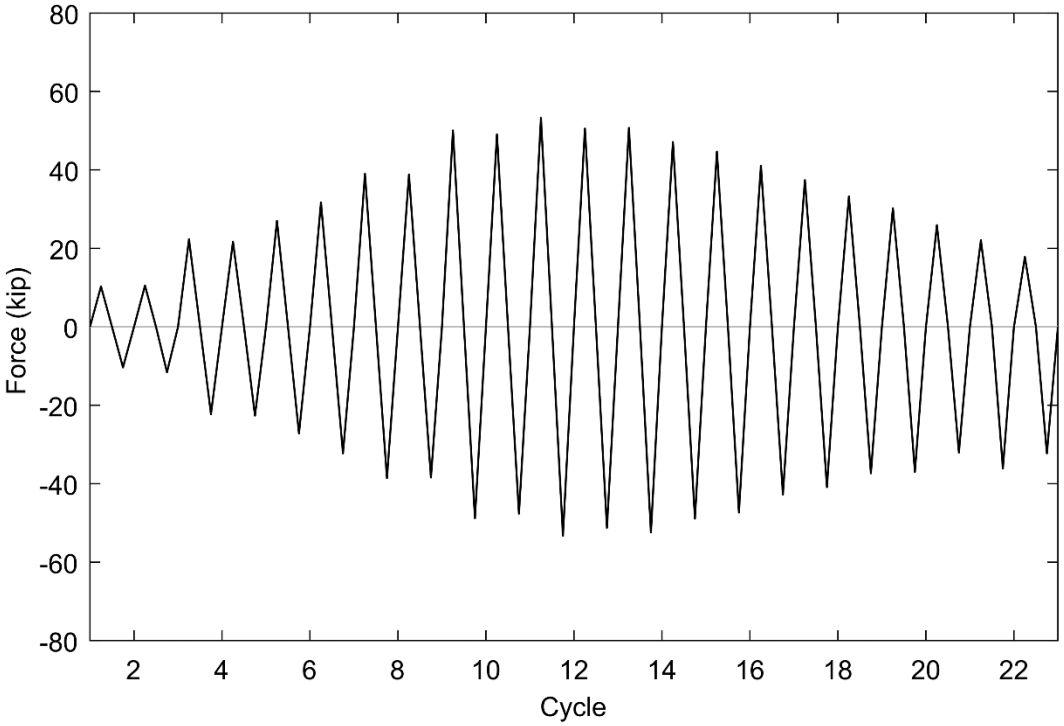

Figure 4-7: Applied Lateral Load (SR_4_10_5)

It can be seen from Figure 4-7 that SR_4_10_5 had a maximum resistance of 53.2 kip. The specimen completed 22 full cycles before the test was terminated due to reaching the limits of the MTS Actuator stroke. The connection's lateral force resistance increased until it reached a maximum resistance in cycle 11 at which point the connection began to lose strength. At the termination of testing, 66.5% of lateral force resisting capacity had been lost. The maximum lateral force resistances and drifts recorded during each cycle can be seen in Table 4.3. Table 4.3 and Figure 4-7 show a drop in resistance during the second cycle of a target drift, possibly indicating irrecoverable damage occurred during the previous cycle.

Table 4.3: Maximum Resistances and Drifts in Each Cycle (SR_4_10_5)

Cycle	Maximum Measured Resistance (kips)		Maximum Drift (%)	
	Tension	Compression	Tension	Compression
1	10.3	- 10.3	0.21	- 0.34
2	10.5	- 11.6	0.21	- 0.34
3	22.3	- 22.2	0.56	- 0.68
4	21.6	- 22.7	0.56	- 0.68
5	27.0	- 27.2	0.72	- 0.84
6	31.7	- 32.3	0.91	- 1.0
7	39.0	- 38.6	1.2	- 1.3
8	38.8	- 38.4	1.3	- 1.4
9	50.1	- 48.8	1.9	- 2.0
10	49.1	- 47.6	2.0	- 2.1
11	53.2	- 53.2	2.7	- 2.7
12	50.5	- 51.2	2.7	- 2.8
13	50.8	- 52.4	3.4	- 3.5
14	47.1	- 48.9	3.4	- 3.5
15	44.7	- 47.3	4.1	- 4.2
16	41.0	- 42.7	4.2	- 4.2
17	37.5	- 41.0	4.9	- 4.9
18	33.2	- 37.3	4.9	- 4.9
19	30.2	- 37.0	5.6	- 5.7
20	25.9	- 32.1	5.6	- 5.7
21	22.1	- 36.1	6.3	- 6.4
22	17.8	- 32.3	6.4	-6.4

Table 4.3 shows that the maximum drift achieved was 6.4% story drift. It is thought that the failure was ultimately punching/two-way shear after first undergoing a flexural response. The following section will present the progression of damage through the testing of SR_4_10_5. The force-drift hysteresis curve of the slab column connection is shown in Figure 4-8 and a modified force-drift hysteresis curve with P-Δ effects from the column axial load removed is shown in Figure 4-9. Force has been normalized against the nominal moment capacity of the slab predicted by ACI 318-14.

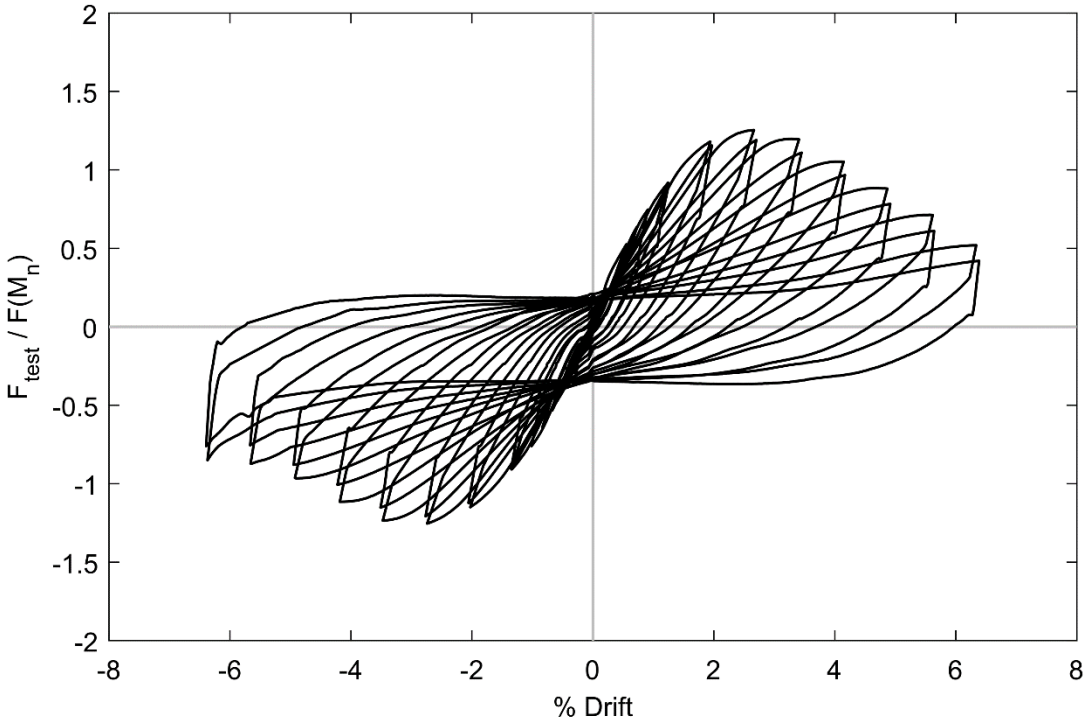

Figure 4-8: Normalized Drift Response (SR_4_10_5)

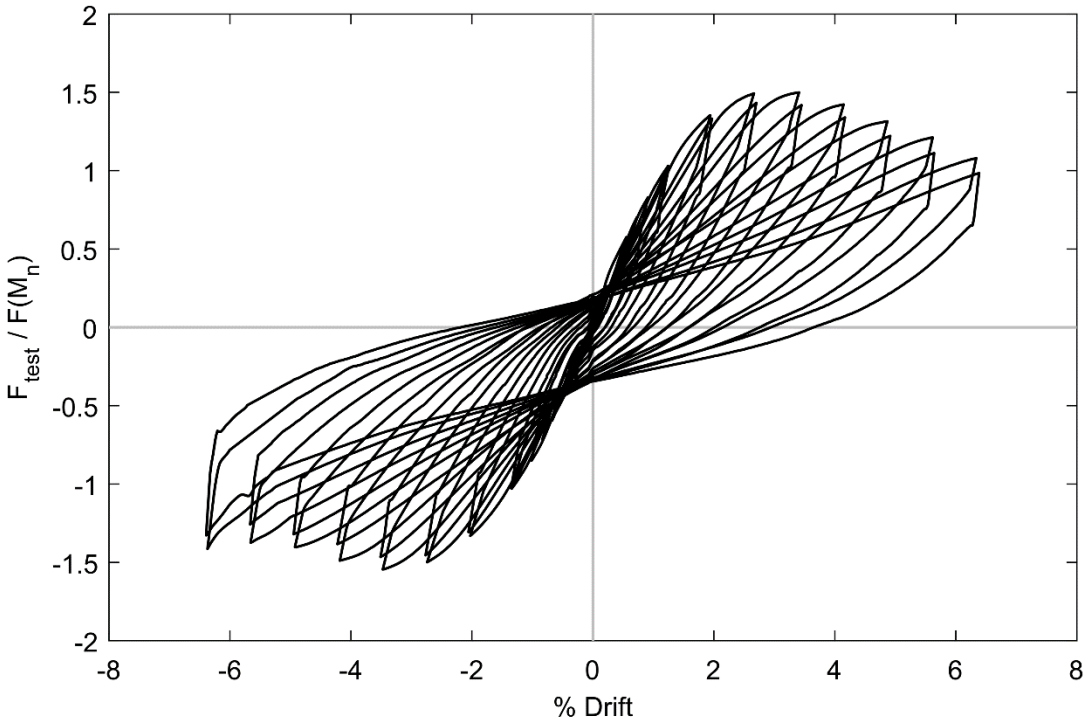

Figure 4-9: Normalized Drift Response with P-Δ Effects Removed (SR_4_10_5)

4.2.2 *Specimen Performance State Summary*

The progression of damage states throughout the test is very important. The level of damage a connection experiences may determine if a connection can be repaired or retrofitted after a seismic event or if it must be replaced. The performance state summary for SR_4_10_5 can be seen in Table 4.4.

Table 4.4: Summary of Damage (SR_4_10_5)

Damage state	**Drift (%)**
Cracking	0.73 - 2.9
Yielding	2.2 - NA
Spalling	2.9
Crushing	4.4
Bar Buckling	NA

4.2.3 *Low Drift Cycles (0.0% - 1.5% Target Drift)*

Cycle 1 (+0.21/-0.34% drift) was run without interruption and a small amount of cracking was first observed when the test was paused at peak displacements during cycle 2 (+0.21/-0.34% drift) though cracking was not extensive enough to meet the requirements of stage 1 cracking. Cracks patterns and typical crack sizes were recorded and the next drift levels was initiated. The largest crack noted while pausing at the peak southern drift of cycle 2 opened 0.05 mm and was located on the top of the slab north of the column. The largest crack noted while pausing at the peak northern drift of cycle 2 opened 0.1 mm and was located on the top of the slab south of the column. Typical crack sizes recorded during pauses at peak drifts throughout low drift cycles are recorded in Table 4.5.

Table 4.5: Low Drift Cycle Typical Crack Opening at Peaks (SR_4_10_5)

Cycle	Drift (%)		Bottom (mm)		Top (mm)		Side (mm)	
	South	North	South	North	South	North	South	North
2	0.21	- 0.34	0.5	0.1	0.01	0.1	0.1	0.1
4	0.56	- 0.68	0.1	0.1	0.1	0.1	0.1	0.1
6	0.91	- 1.0	0.25	0.3	0.25	0.3	0.25	0.3
8	1.3	- 1.4	0.3	0.3	0.3	0.4	0.3	0.3

Cycle 3 (+0.56/-0.68% drift) was then run and stage 1 cracking occurred during cycle 4 (+0.56/-0.68% drift). Cracking initially began near the edge of column and propagated outward across the slab. Crack patterns are shown in Figure 4-10 and Figure 4-11. The largest cracks noted while pausing at the peak southern drift of cycle 4 opened 0.2 mm and were located on the top of the slab north and northwest of the column. The largest crack noted while pausing at the peak northern drift of cycle 4 opened 0.2 mm and was located on the top of the slab south of the column.

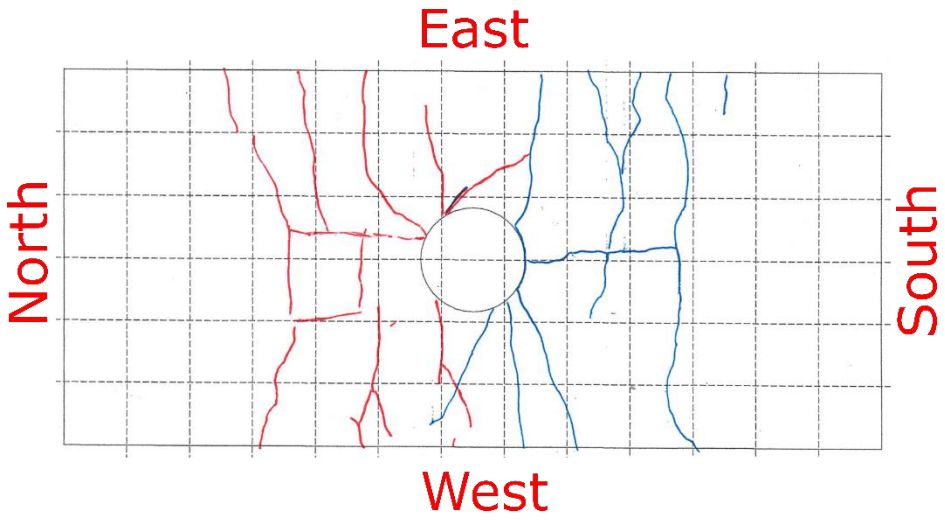

Figure 4-10: Top of Slab Crack Map – 0.68% Drift (SR_4_10_5)

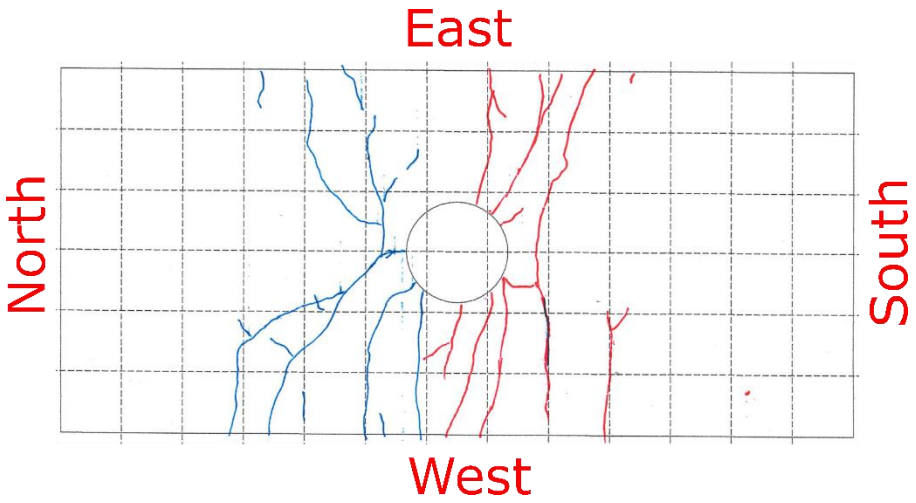

Figure 4-11: Bottom of Slab Crack Map – 0.68% Drift (SR_4_10_5)

Cycle 5 (+0.72/-0.84% drift) was then run before continuing to cycle 6 (+0.91/-1.0% drift). Cycle 6 was paused at peak drifts, crack sizes were recorded and crack maps updated. The largest cracks noted while pausing at the peak southern drift of cycle 6 opened 0.2 mm and were located on the top of the slab north and northwest of the column. The largest crack noted while pausing at the peak northern drift of cycle 6 opened 0.3 mm and was located on the top of the slab southwest of the column.

Cycle 7 (+1.2/-1.3% drift) was then run and was completed uninterrupted. Cycle 8 (+1.3/-1.4% drift) was then performed with pauses at peak drifts to update crack maps and measure cracks. The largest crack noted while pausing at the peak southern drift of cycle 8 opened 0.4 mm and was located on the top of the slab northwest of the column. The largest crack noted while pausing at the peak northern drift of cycle 8 opened 0.4 mm and was located on the top of the slab southwest of the column.

4.2.4 *Moderate Drift Cycles (1.5% - 3.6% Target Drift)*

Moderate drift cycles initiated with cycle 9 (+1.9/-2.0% drift) which was completed uninterrupted. Once strain gauge data was analyzed, it was discovered that a gauge indicated yielding of longitudinal reinforcement in the bottom of the slab at the peak drifts of cycle 9. As shown in Figure 4-13, yielding occurred just north of the column. Figure 4-12 indicates that longitudinal reinforcement in the top of the slab remained elastic during this cycle.

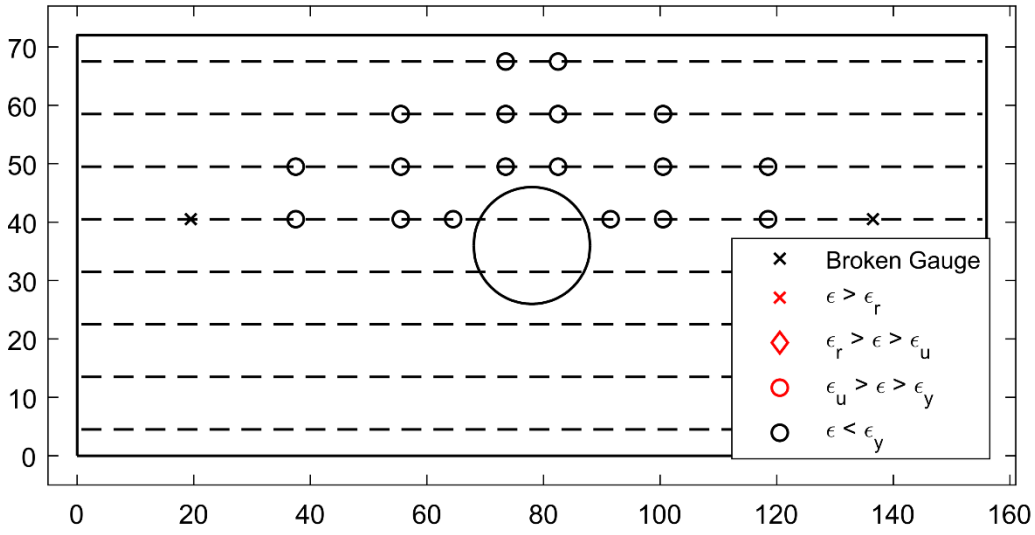

Figure 4-12: Top Reinforcement Strain Summary – 2.0% Drift (SR_4_10_5)

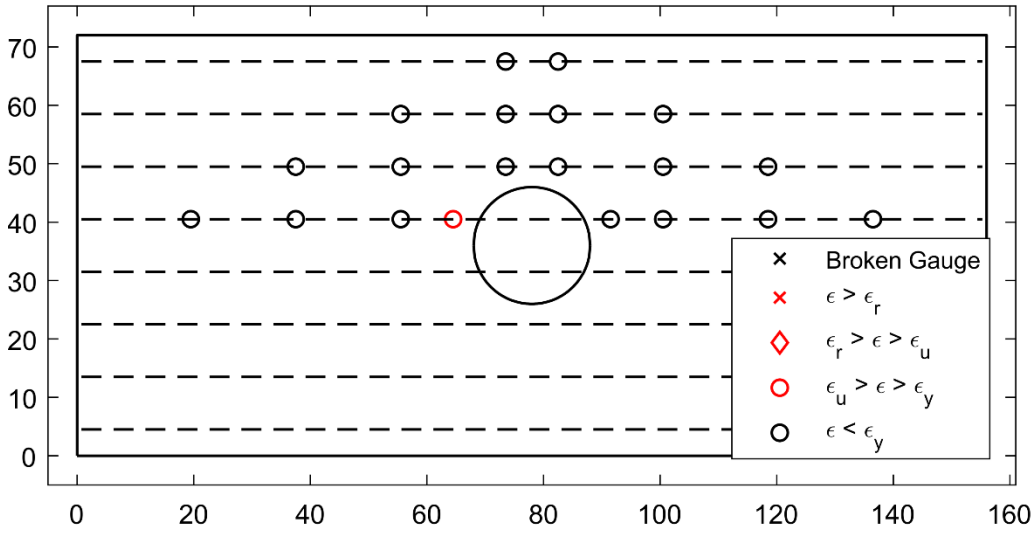

Figure 4-13: Bottom Reinforcement Strain Summary – 2.0% Drift (SR_4_10_5)

Cycle 10 (+2.0/-2.1% drift) was paused at peak drifts, crack sizes were recorded and crack maps updated. The largest cracks noted while pausing at the peak southern drift of cycle 10 opened 0.5 mm and were located on the top of the slab northwest and northeast of the column. The largest crack noted while pausing at the peak northern drift of cycle 10 opened 0.6 mm and was located

on the top of the slab south of the column. Typical crack sizes recorded during moderate drift cycles are listed in Table 4.6.

Table 4.6: Moderate Drift Cycle Typical Crack Opening at Peaks (SR_4_10_5)

Cycle	Drift (%)		Bottom (mm)		Top (mm)		Side (mm)	
	South	North	South	North	South	North	South	North
10	2.0	- 2.1	0.4	0.4	0.6	0.5	0.5	0.4
12	2.7	- 2.8	0.5	NA	0.5	0.5	-	-
14	3.4	- 3.5	0.6	0.6	0.75	0.25	0.6	0.6

By the completion of cycle 10, cracks had grown to cover the majority of both the top and bottom of SR_4_10_5 as shown in Figure 4-14 and Figure 4-15.

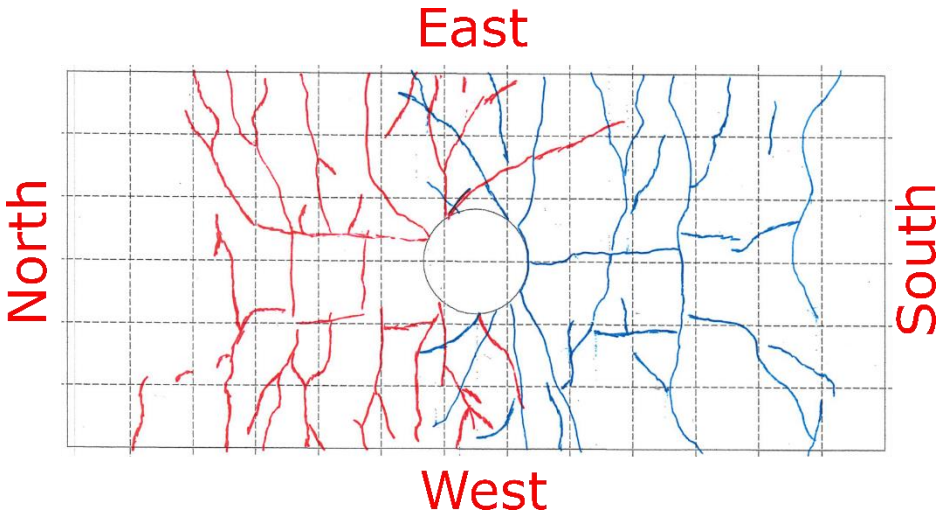

Figure 4-14: Top of Slab Crack Map – 2.0% Drift (SR_4_10_5)

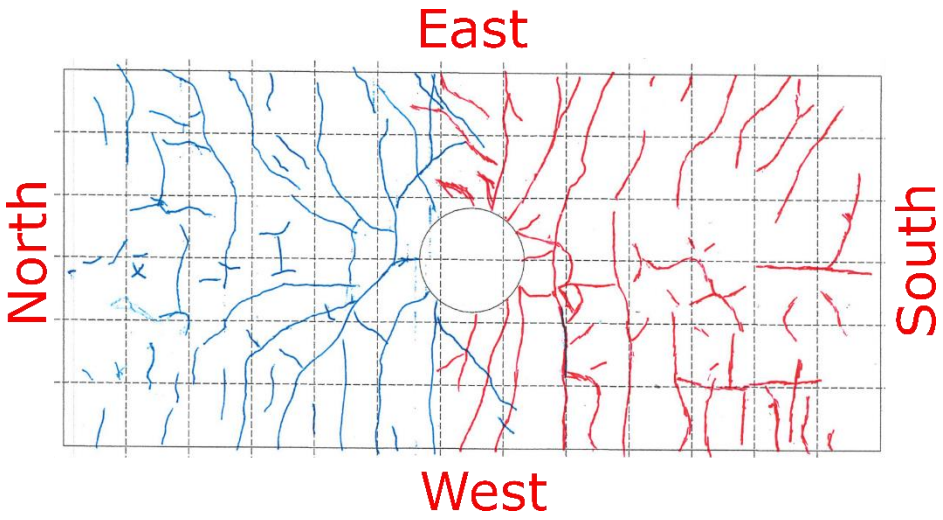

Figure 4-15: Bottom of Slab Crack Map – 2.0% Drift (SR_4_10_5)

Cycle 11 (+2.7/-2.7% drift) was then run. Strain gauge data indicates that at the peak drifts of cycle 11, yielding of longitudinal reinforcement in the slab had only occurred in the bar passing through the column. As shown in Figure 4-16 and Figure 4-17, yielding is indicated to the north and south of the column in the top and bottom reinforcement.

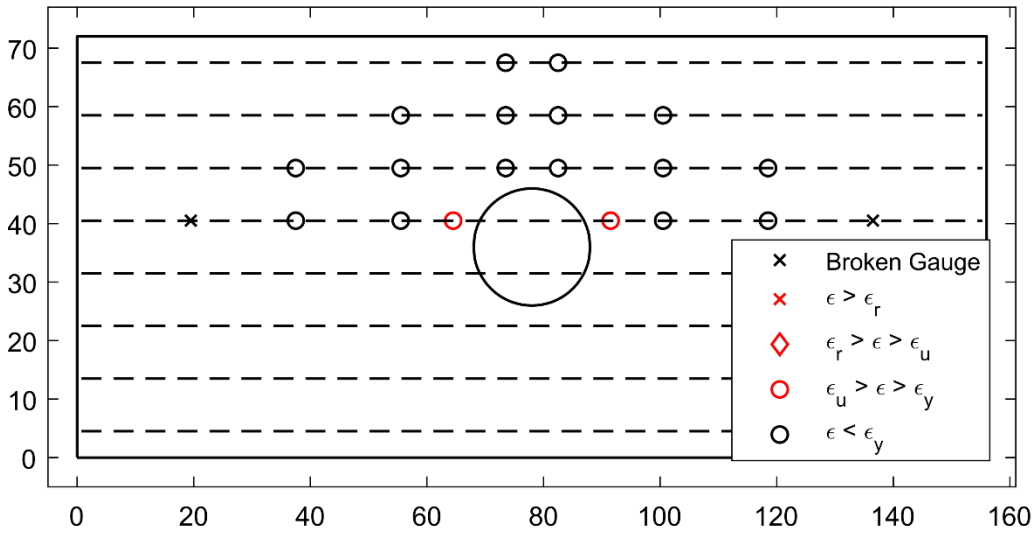

Figure 4-16: Top Reinforcement Strain Summary – 2.7% Drift (SR_4_10_5)

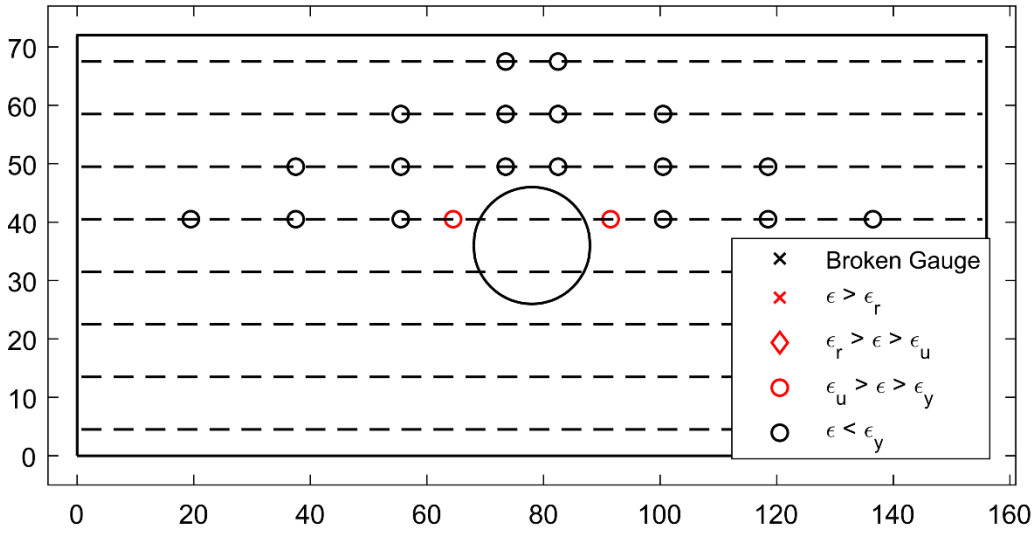

Figure 4-17: Bottom Reinforcement Strain Summary – 2.7% Drift (SR_4_10_5)

Cycle 12 (+2.7/-2.8% drift) was then performed with pauses at peak drifts to update crack maps and measure cracks. The largest cracks noted while pausing at the peak southern drift of cycle 12 opened 0.75 mm and were located on the top of the slab north and northwest of the column. The largest cracks noted while pausing at the peak northern drift of cycle 12 opened 0.75 mm and were located on the top of the slab southwest and southeast of the column. After comparing the crack patterns recorded during cycle 12 to those recorded throughout the remainder of the test, it was determined that stage 2 cracking occurred in cycle 12. Crack maps for cycle 12 are shown in Figure 4-18 and Figure 4-19.

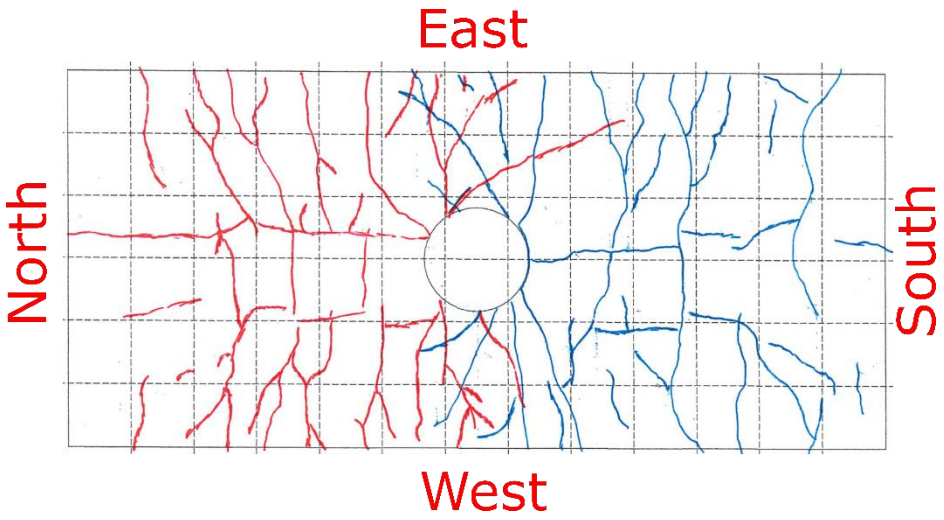

Figure 4-18: Top of Slab Crack Map – 2.7% Drift (SR_4_10_5)

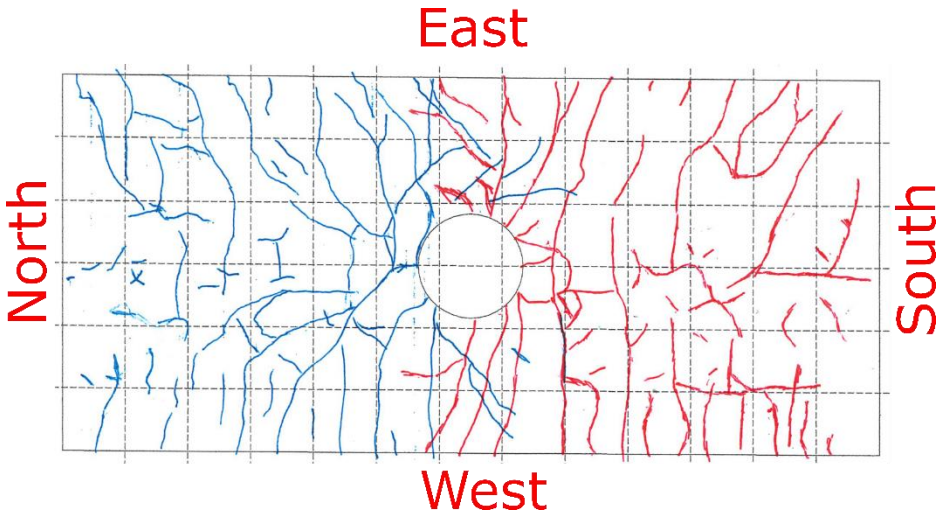

Figure 4-19: Bottom of Slab Crack Map – 2.7% Drift (SR_4_10_5)

The onset of spalling was also noted during the norther pause in cycle 12. The first spalling occurred on the bottom of the slab on the north side of the slab-column joint as shown in Figure 4-20.

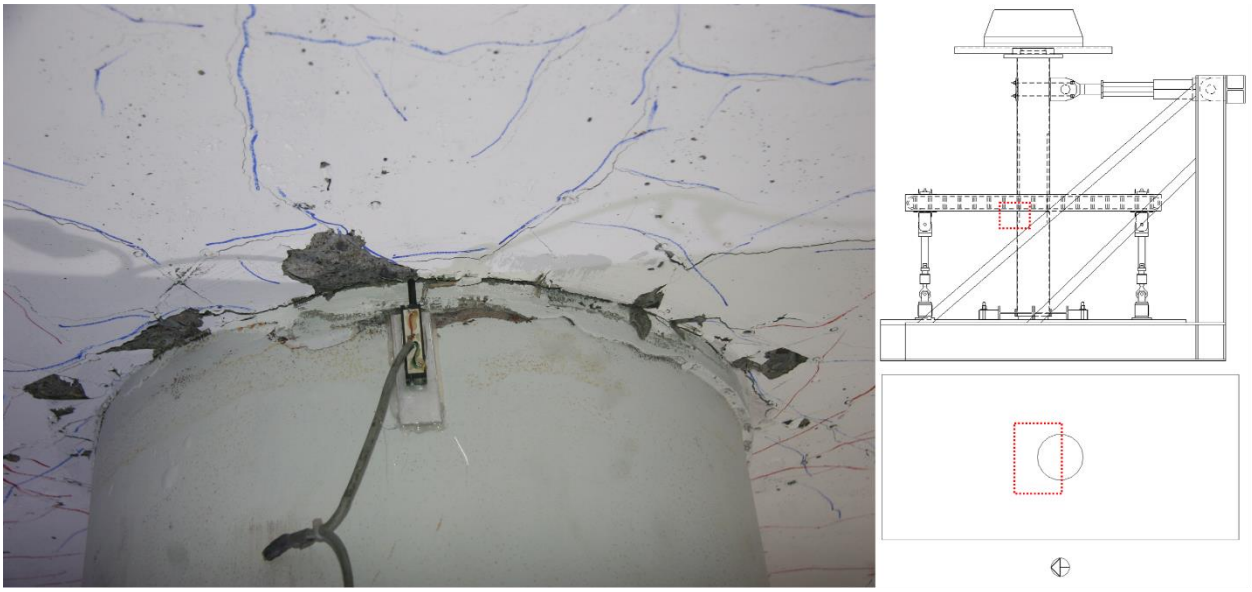

Figure 4-20: Bottom Joint North Side Spalling - 2.8% Drift (SR_4_10_5)

Cycle 13 (+3.4/-3.5% drift) was then run without interruption. Cycle 14 (+3.4/-3.5% drift) was then performed with pauses at peak drifts to update crack maps and measure cracks. The largest cracks noted while pausing at the peak southern drift of cycle 14 opened 1.25 mm and were located on the top of the slab north and northwest of the column. The largest crack noted while pausing at the peak northern drift of cycle 14 opened 1.5 mm and was located on the top of the slab southwest of the column.

4.2.5 *High Drift Cycles (Greater than 3.6% Target Drift)*

High drift cycles initiated with cycle 15 (+4.1/-4.2% drift) which was completed uninterrupted before continuing to cycle 16 (+4.2/-4.2% drift). Cycle 16 was paused at peak drifts, crack sizes were recorded and crack maps updated. The largest cracks noted while pausing at the peak southern drift of cycle 16 opened 1.5 mm and were located on the top of the slab north, northwest, and northeast of the column. The largest crack noted while pausing at the peak northern drift of cycle 16 opened 2 mm and was located on the top of the slab southwest of the column. Typical crack sizes recorded during high drift cycles are listed in Table 4.7.

Table 4.7: High Drift Cycle Typical Crack Opening at Peaks (SR_4_10_5)

Cycle	Drift (%)		Bottom (mm)		Top (mm)		Side (mm)	
	South	North	South	North	South	North	South	North
16	4.2	- 4.2	0.75	0.75	0.75	0.75	0.5	0.5
18	4.9	- 4.9	0.75	0.75	0.75	0.75	0.5	0.5
20	5.6	- 5.7	1.0	1.0	1.5	1.0	0.75	0.75
22	6.4	-6.4	NA	NA	NA	NA	NA	NA

The onset of crushing was noted during the pauses in cycle 16. The first crushing occurred on the bottom of the slab around the perimeter of the slab-column joint. Figure 4-21 shows the northern side of the connection while Figure 4-22 shows the southern side of the connection. Exposed longitudinal reinforcement and base plate of transverse reinforcement are visible in Figure 4-21.

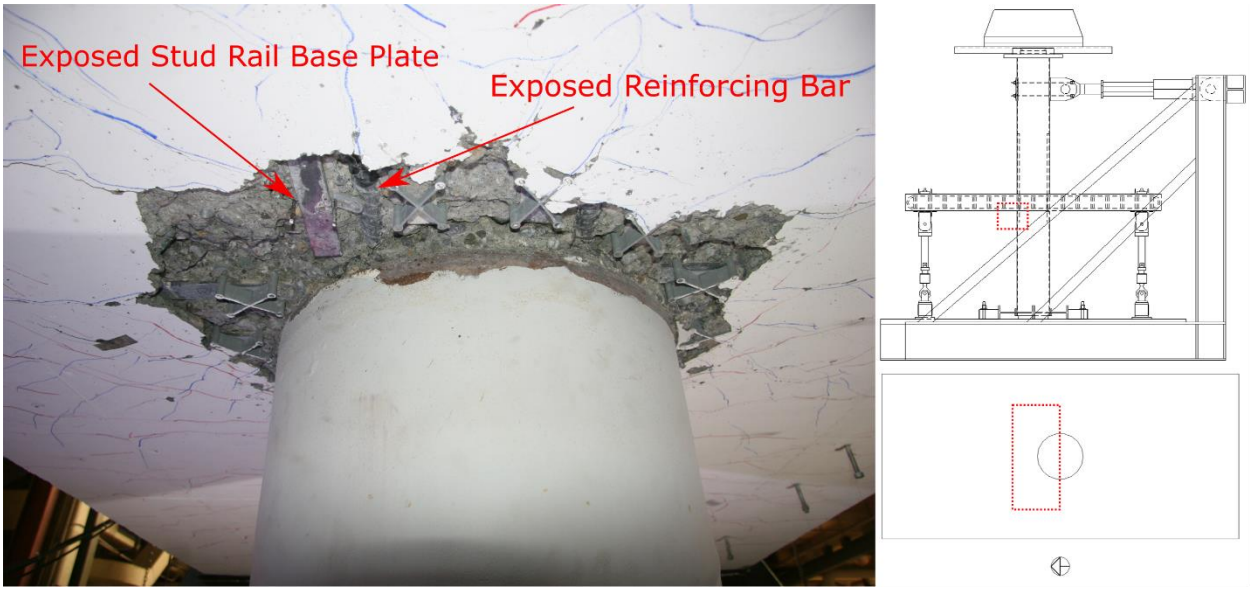

Figure 4-21: Bottom Joint North Side Crushing – 4.2% Drift (SR_4_10_5)

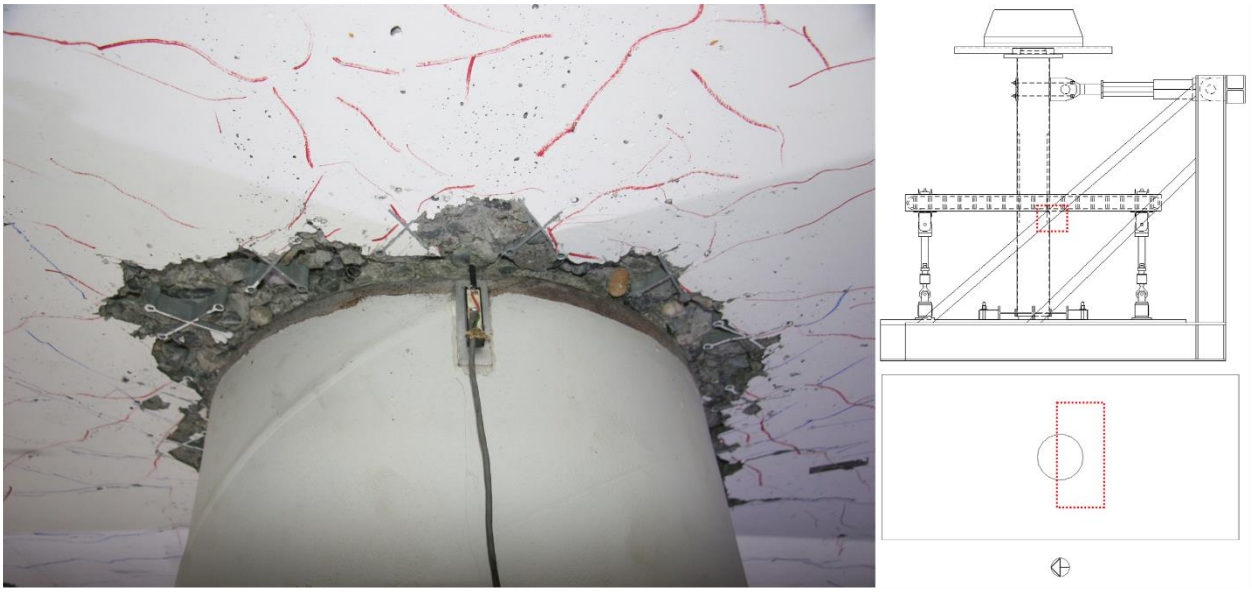

Figure 4-22: Bottom Joint South Side Crushing – 4.2% Drift (SR_4_10_5)

Cycle 17 (+4.9/-4.9% drift) was then run before continuing to cycle 18 (+4.9/-4.9% drift). Cycle 18 was paused at peak drifts, crack sizes were recorded and crack maps updated. The largest cracks noted while pausing at the peak southern drift of cycle 18 opened 2 mm and were located on the top of the slab north, northwest, and northeast of the column. The largest crack noted while pausing at the peak northern drift of cycle 18 opened 3 mm and was located on the top of the slab southwest of the column. The crushed region on the bottom of the slab around the column did not significantly grow during cycles 17 and 18, but crushing became apparent on the top of the slab around the slab-column joint.

Cycle 19 (+5.6/-5.7% drift) was then run before continuing to cycle 20 (+5.6/-5.7% drift). Cycle 20 was paused at peak drifts, crack sizes were recorded and crack maps updated. The largest crack noted while pausing at the peak southern drift of cycle 20 opened 3 mm and was located on the top of the slab northeast of the column. The largest crack noted while pausing at the peak northern drift of cycle 20 opened 4 mm and was located on the top of the slab southwest of the column. The crushed region around the column did not significantly grow during cycles 19 and 20.

Cycle 21 (+6.3/-6.4% drift) was then run before continuing to cycle 22 (+6.4/-6.4% drift). Cycle 22 was paused at peak drifts and crack maps updated. The crushed region grew significantly on the top and bottom of the slab around the column joint during cycles 21 and 22. As a result,

recording crack sizes became impractical. At the completion of cycle 22, crushing extended at least 1 ft. from the column on all sides. Testing was halted after cycle 22 due to equipment displacement limits being reached. After completion of testing, crushing was further explored and measured.

4.2.6 *Post Test*

After the completion of testing, loose concrete around the slab-column joint was removed to explore the extent of damage. Figure 4-23 shows that crushing around the slab-column joint on the top of the slab extended 1 – 2 ft. north of the joint and roughly 1 ft. to the east and west of the joint. Figure 4-24 shows crushing extending roughly 1.5 ft. south of the joint. Longitudinal reinforcement is visible in Figure 4-23 and Figure 4-24 to the east and west of the column and headed transverse reinforcement is visible on all sides of the column.

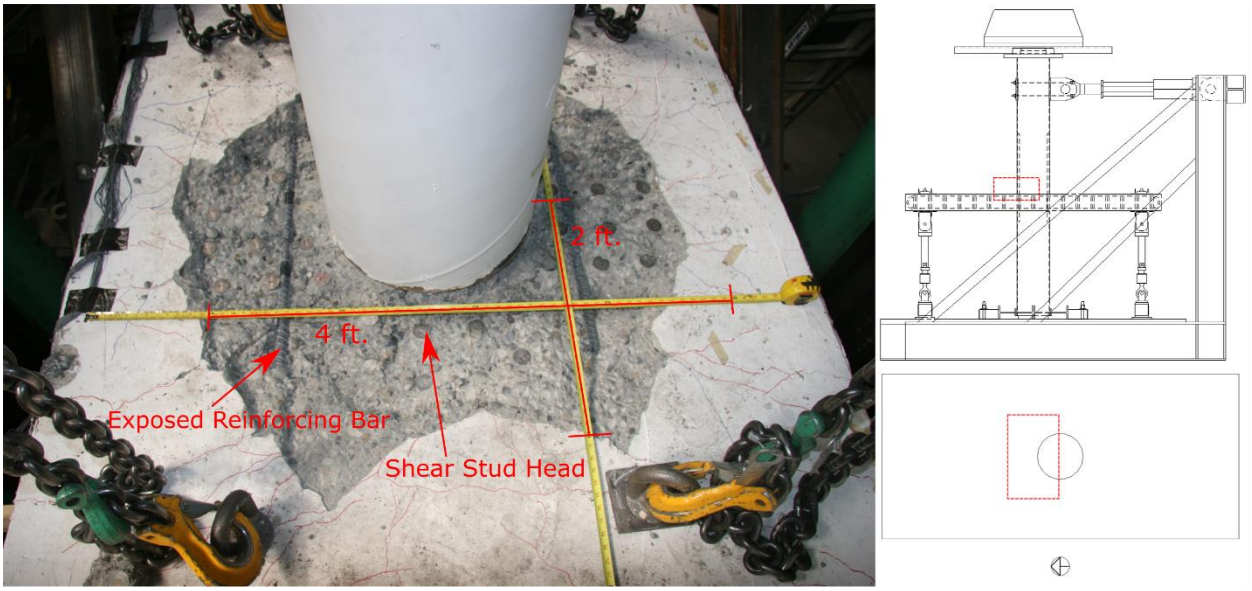

Figure 4-23: Top Joint North Side Crushing – 6.4% Drift (SR_4_10_5)

Figure 4-24: Top Joint South Side Crushing – 6.4% Drift (SR_4_10_5)

Figure 4-25 shows that crushing extended roughly 1 ft. to the north, south, and east of the column. The base rail of the transverse reinforcement (stud rails) is visible on all sides of the column. Longitudinal reinforcement passing the column is visible to the north and south of the column and more reinforcement is exposed to the east and west of the column.

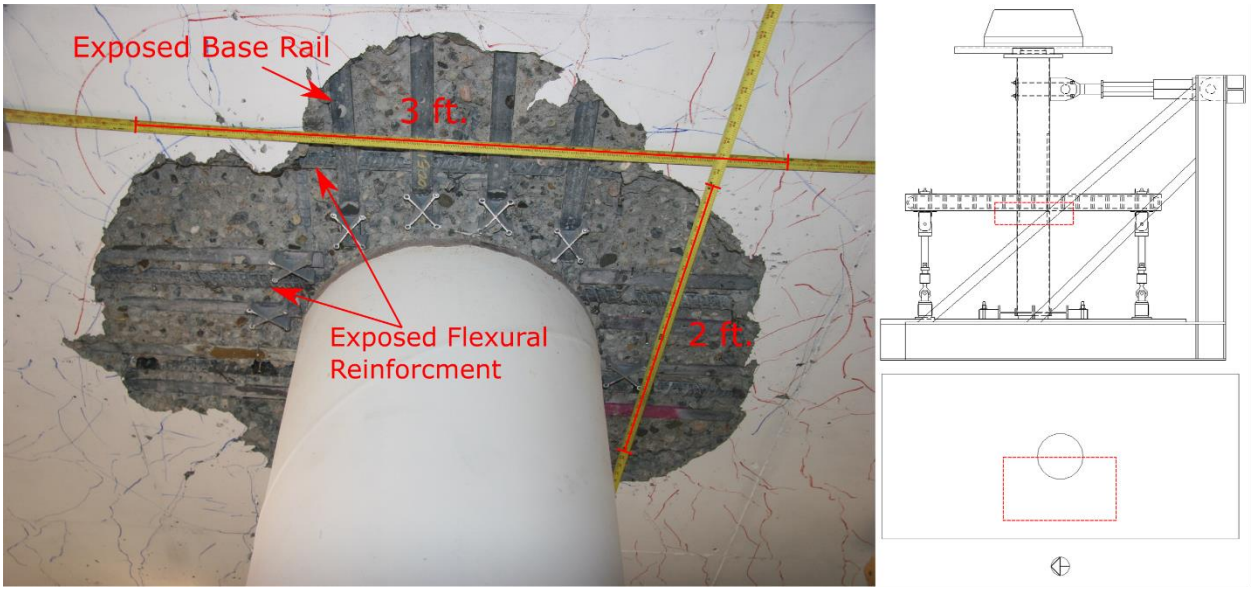

Figure 4-25: Bottom Joint West Side Crushing – 6.4% Drift (SR_4_10_5)

Figure 4-26 shows a closer view of the bottom of the slab on the north side of the slab-column joint. Exposed column reinforcement is visible and a large crack can also be seen. This large crack was found to be visible around the entire perimeter of the column from both the top and bottom of the slab. It is thought that this large crack propagated completely through the slab, resulting in the slab being supported by only the slab longitudinal reinforcement passing through the slab-column joint.

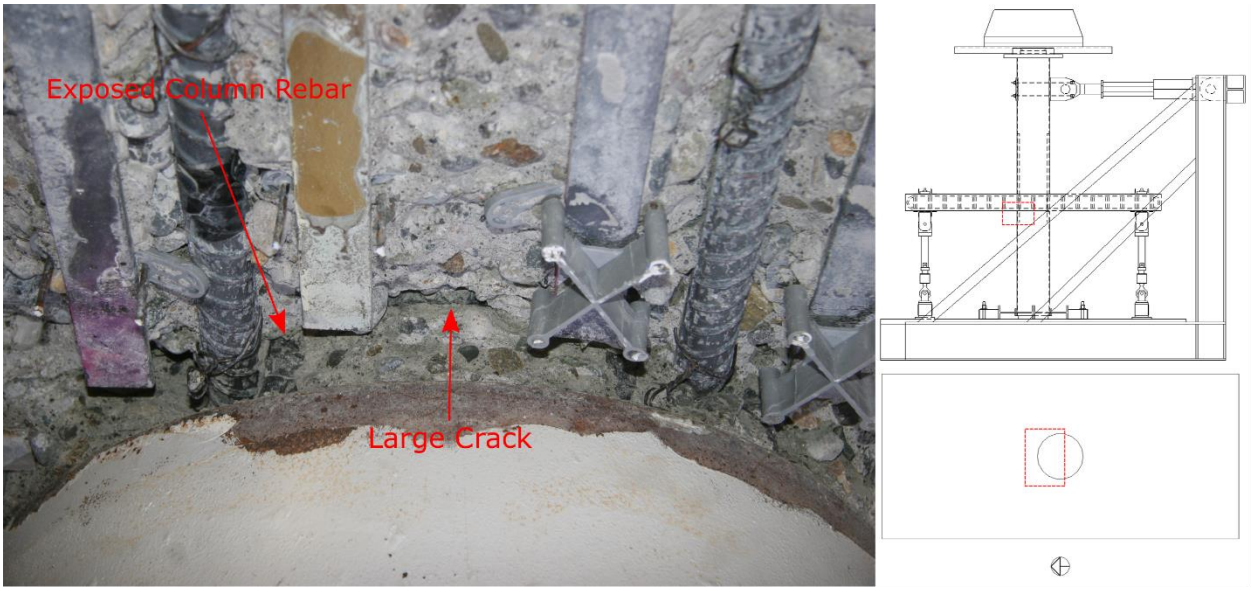

Figure 4-26: Bottom Joint North Side Damage – 6.4% Drift (SR_4_10_5)

4.2.7 *Test Summary*

SR_4_10_5 reached a drift range of 12.8% (-6.4% to 6.4%). Cracking occurred shortly after the beginning of testing, with some cracking observed during the first two cycles (+0.21/-0.34% drift) followed by cracking across the width of the specimen by the third and fourth cycles (+0.56/-0.68% drift). Yielding first occurred in the longitudinal reinforcement passing through the slab-column joint at 2.0% drift. Maximum lateral force resistance occurred at a drift of 2.7%. Minimal damage was visible until 2.8% drift when the first spalling was observed around the column. Spalling was followed by crushing at 4.2% and a loss of more than 50% lateral force

resistance by 5.6% drift. Reinforcement at the edge of the slab was not indicated to have yielded by the completion of testing.

4.3 SPECIMEN PTB_4.5_1_0

Specimen PTB_4.5_1_0 was tested March 25th, 2019 in the Structural Research Laboratory at the University of Washington. The test was performed 168 days after casting the slab and lower column and 157 days after casting the upper column.

4.3.1 *Specimen Overview*

A description of the test specimen can be seen in Chapter 3. Two prior attempts were made to test PTB_4.5_1_0 but were unsuccessful due to failure of the setup. For the first attempt, the setup was designed with the Slab End Roller Support extending from the end of the slab. This design resulted in the end of the slab breaking off outside the rebar cage when lateral loads were applied. For the second attempt, the Slab End Roller Support was relocated under the end of the slab and testing recommenced. However, a component of the Slab End Roller support (1 in. threaded rod) buckled under loading. For the third attempt, a compression sleeve specific to each strut was machined before each test to prevent buckling and testing proceeded. The test went smoothly and there were no interruptions throughout the test other than those planned (for marking cracks or initializing the next cycle). Qualitative observations from the first two test attempts are briefly discussed, but the main discussion focuses on the successful test. The induced drift and applied lateral loads can be seen in Figure 4-27 and Figure 4-28, respectively.

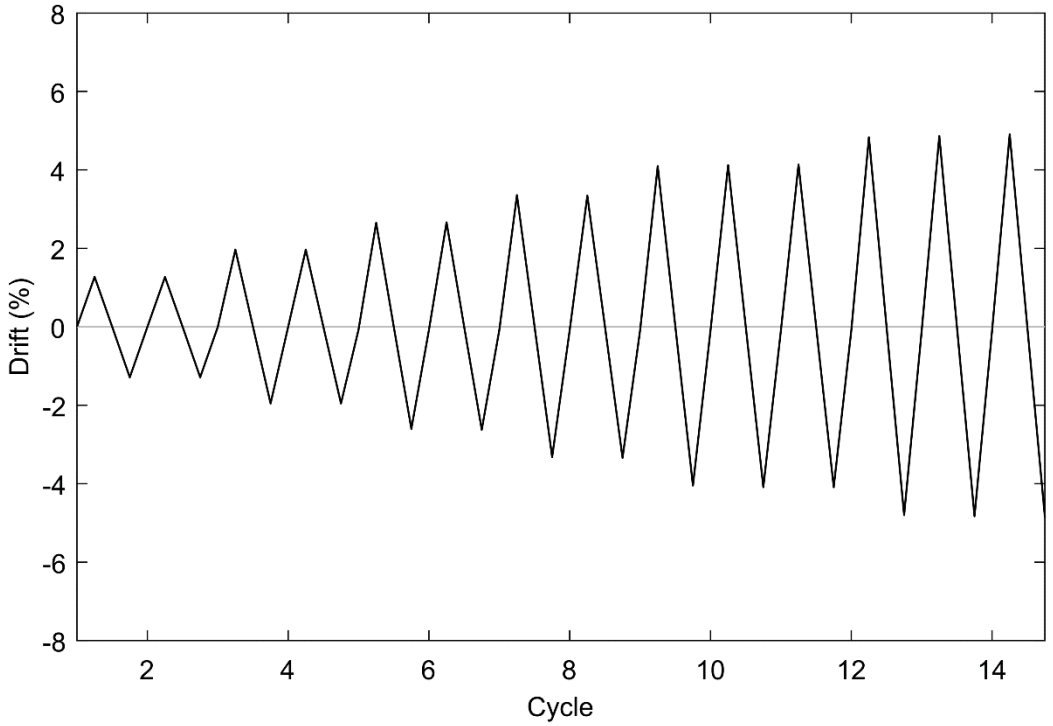

Figure 4-27: Induced Drift (PTB_4.5_1_0)

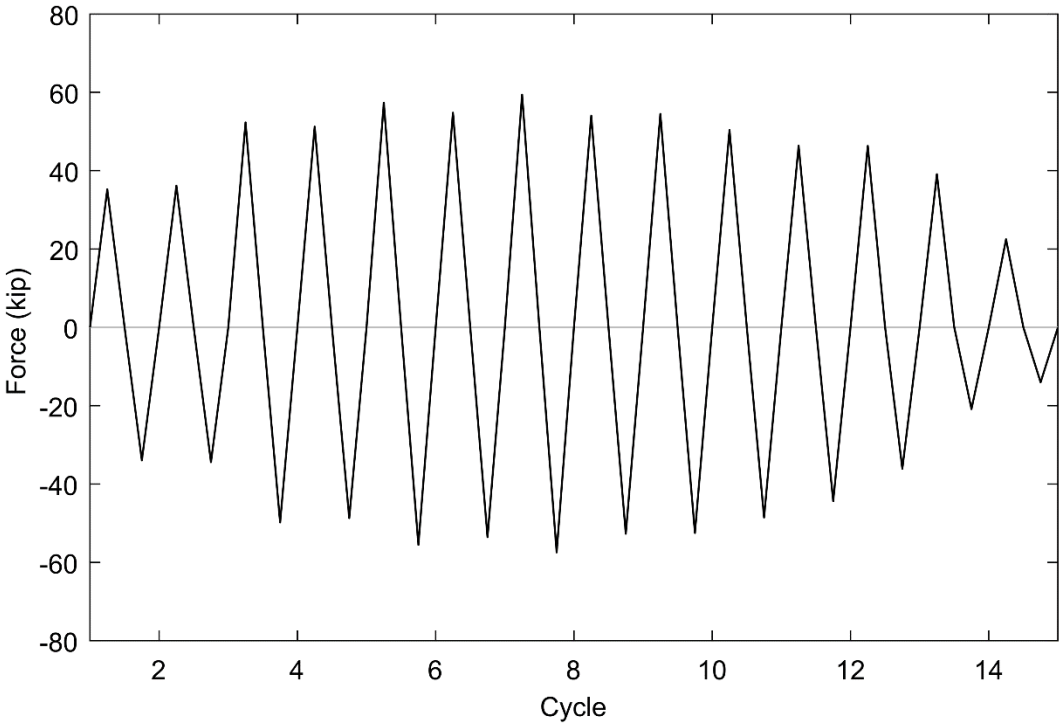

Figure 4-28: Applied Lateral Load (PTB_4.5_1_0)

It can be seen from Figure 4-27 that PTB_4.5_1_0 had a maximum resistance of 59.4 kip. The specimen completed 14 full cycles before the test was terminated due to a large drop in lateral force resistance during the 14th cycle. The connection's lateral force resistance increased until it reached a maximum resistance in cycle 7 at which point the connection began to lose strength. At the termination of testing, 74.2% of lateral force resisting capacity had been lost. The maximum lateral force resistances and drifts recorded during each cycle can be seen in Table 4.8. Table 4.8 and Figure 4-28 show a drop in resistance during the second cycle of a target drift, possibly indicating irrecoverable damage occurred during the previous cycle.

Table 4.8: Maximum Resistances and Drifts in Each Cycle (PTB_4.5_1_0)

Cycle	Maximum Measured Resistance (kips)		Maximum Drift (%)	
	Tension	Compression	Tension	Compression
1	35.2	- 33.9	1.3	-1.3
2	36.2	- 34.4	1.3	-1.3
3	52.3	- 49.8	2.0	-2.0
4	51.2	- 48.7	2.0	-2.0
5	57.4	- 55.5	2.6	-2.6
6	54.8	- 53.6	2.7	-2.6
7	59.4	- 57.6	3.4	-3.3
8	54.0	- 52.7	3.3	-3.3
9	54.5	- 52.5	4.1	-4.0
10	50.4	- 48.5	4.1	-4.1
11	46.3	- 44.3	4.1	-4.1
12	46.4	- 42.5	4.8	-4.8
13	39.1	- 24.3	4.9	-4.8
14	24.6	- 15.3	4.9	-4.9

It can be seen from Table 4.8 that the maximum drift achieved was 4.9%. It is thought that the failure was ultimately one-way shear after first undergoing a flexural response. The following section will present the progression of damage through the testing of PTB_4.5_1_0. The force-drift hysteresis curve of the slab column connection is shown in Figure 4-29 and a modified force-drift hysteresis curve with P-Δ effects from the column axial load removed is shown in Figure 4-

30. Force has been normalized against the nominal moment capacity of the slab predicted by ACI 318-14.

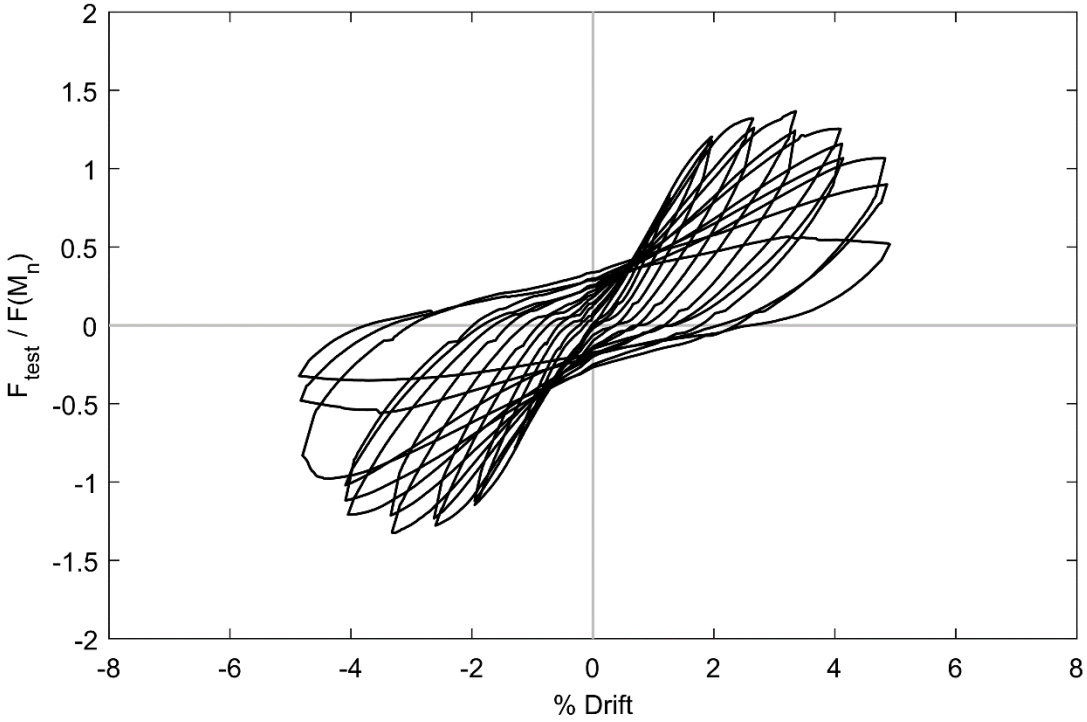

Figure 4-29: Normalized Drift Response (PTB_4.5_1_0)

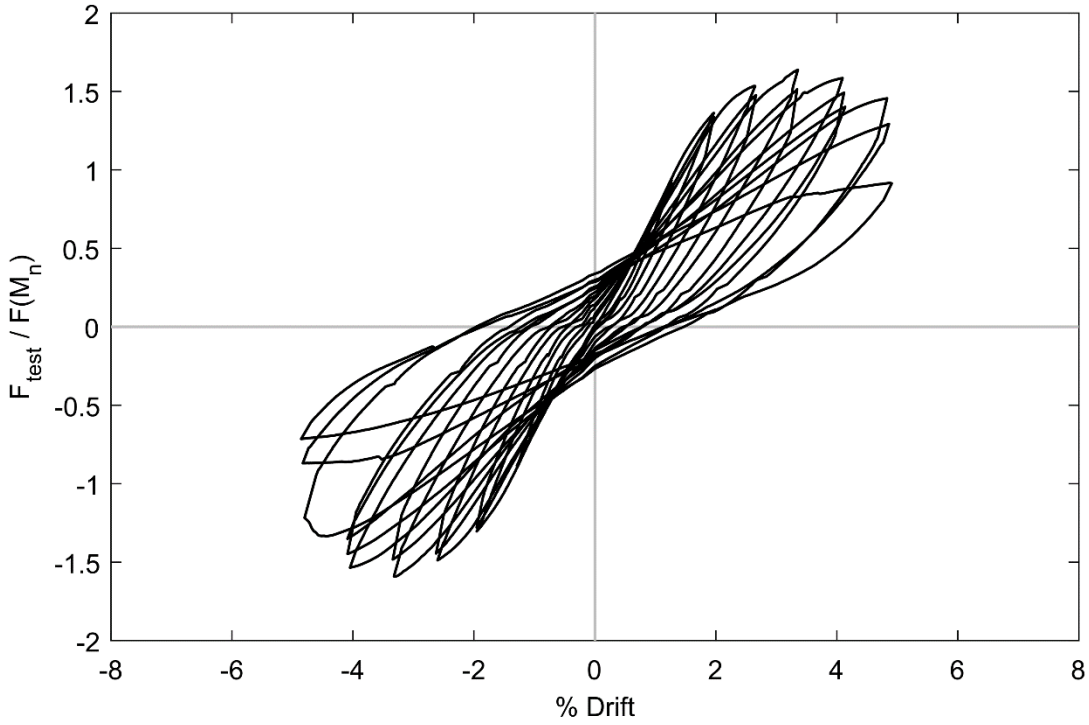

Figure 4-30: Normalized Drift Response with P-Δ Effects Removed (PTB_4.5_1_0)

4.3.2 *Specimen Performance State Summary*

The performance state summary for PTB_4.5_1_0 can be seen in Table 4.9.

Table 4.9: Summary of Damage (PTB_4.5_4_0)

Damage state	**Drift (%)**
Cracking	0.73 – 3.6
Yielding	2.2 – 5.1
Spalling	1.5
Crushing	4.4
Bar Buckling	5.1

4.3.3 *Low Drift Cycles (0.0% - 1.5% Target Drift)*

Due to two previous attempts at testing PTB_4.5_1_0, the slab was cracked when testing began. Additionally, due to the initial setup design, part of the axial load placed on the column was transferred into the slab causing the bottom of the slab to crack. The crack pattern shown in Figure 4-31 was recorded during initial testing attempts during a target 0.73% drift cycle. This crack pattern meets the standard of stage 1 cracking.

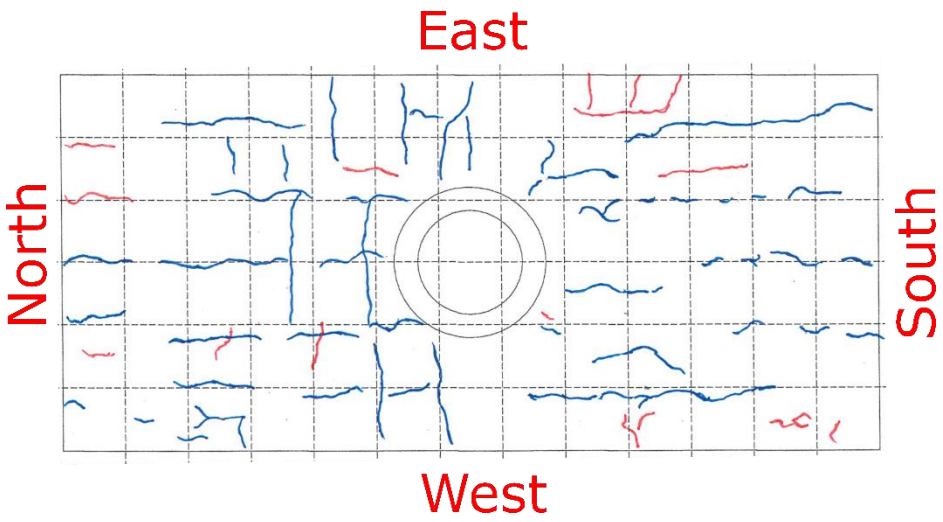

Figure 4-31: Bottom of Slab Crack Map – 0.73% Drift (PTB_4.5_1_0)

After the setup was changed, testing continued starting with a target drift of 1.5%. Cycle 1 (+1.3/-1.3% drift) was then run before continuing to cycle 2 (+1.3/-1.3% drift). Cycle 2 was paused at peak drifts and crack maps updated. The largest crack noted while pausing at the peak southern drift of cycle 2 opened 0.5 mm and was located on the top of the slab north of the column. The largest crack noted while pausing at the peak northern drift of cycle 2 opened 0.3 mm and was located on the top of the slab southeast of the column. Typical crack sizes recorded during pauses at peak drifts through low drift cycles are recorded in Table 4.10.

Table 4.10: Low Drift Cycle Typical Crack Opening at Peaks (PTB_4.5_1_0)

Cycle	Drift (%)		Bottom (mm)		Top (mm)		Side (mm)	
	South	North	South	North	South	North	South	North
2	1.3	-1.3	0.3	0.2	0.4	0.2	0.25	0.2

The onset of spalling was noted during the pause at the southern peak drift in cycle 2. The first spalling occurred on the bottom of the slab on the north side of the slab-column joint at the edge of the ring flange as shown in Figure 4-32.

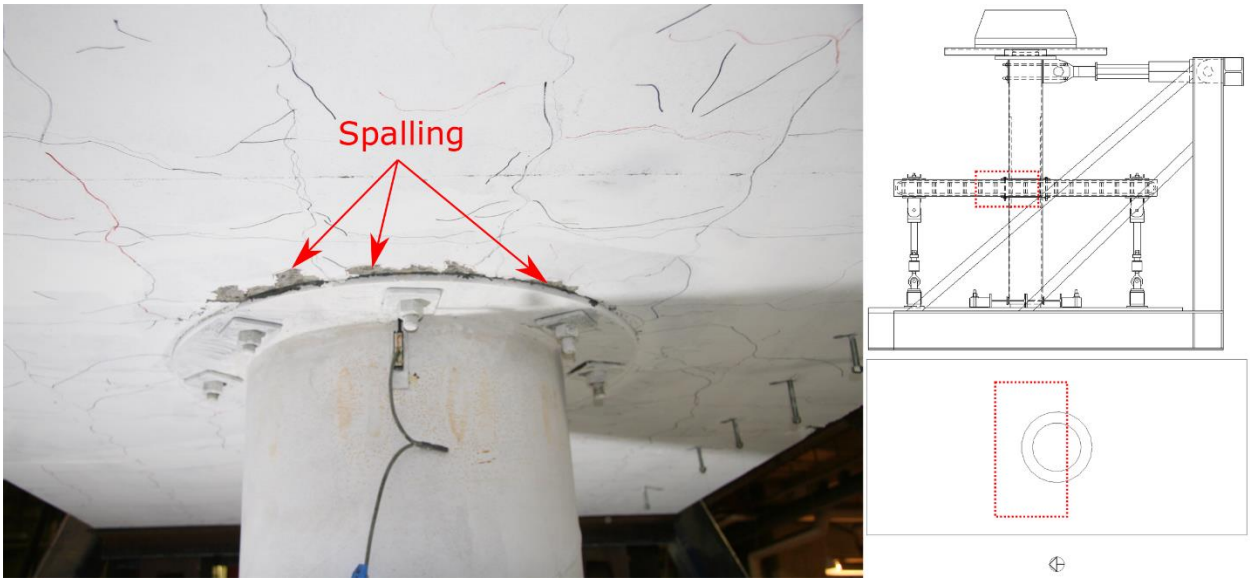

Figure 4-32: Bottom Joint North Side Spalling – 1.3% Drift (PTB_4.5_1_0)

4.3.4 *Moderate Drift Cycles (1.5% - 3.6% Target Drift)*

Moderate drift cycles initiated with cycle 3 (+2.0/-2.0% drift) which was completed uninterrupted. Once strain gauge data was analyzed, it was discovered that gauges indicated yielding of flexural reinforcement in the bottom of the slab at the peak drifts of cycle 3. As shown in Figure 4-33, yielding occurred just north and south of the column.

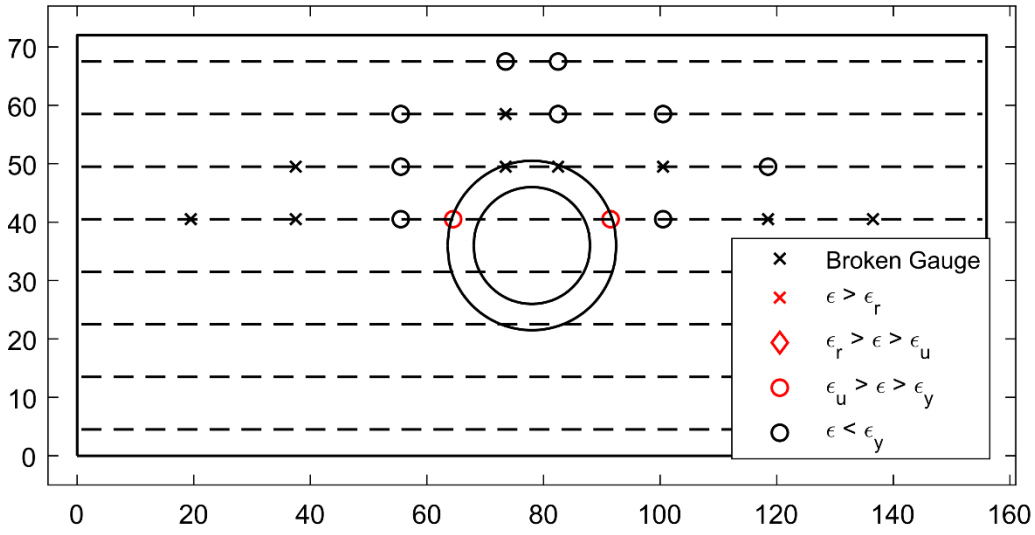

Figure 4-33: Bottom Reinforcement Strain Summary – 2.0% Drift (PTB_4.5_1_0)

Cycle 4 (+2.0/-2.0% drift) was paused at peak drifts, crack sizes were recorded and crack maps updated. The largest crack noted while pausing at the peak southern drift of cycle 4 opened 0.7 mm and was located on the top of the slab north of the column just beyond the ring flange. The largest crack noted while pausing at the peak northern drift of cycle 4 opened 0.7 mm and was located on the top of the slab west of the column. Typical crack sizes recorded during moderate drift cycles are listed in Table 4.11.

Table 4.11: Moderate Drift Cycle Typical Crack Opening at Peaks (PTB_4.5_1_0)

Cycle	Drift (%)		Bottom (mm)		Top (mm)		Side (mm)	
	South	North	South	North	South	North	South	North
4	2.0	-2.0	0.3	0.2	0.4	0.3	0.2	0.2
6	2.7	-2.6	0.4	0.4	0.4	0.3	0.2	0.2
8	3.3	-3.3	0.4	NA	0.4	NA	0.3	NA

By the completion of cycle 4, cracking had grown to cover the top and bottom of the slab and had become denser around the ring flange as shown in Figure 4-34 and Figure 4-35.

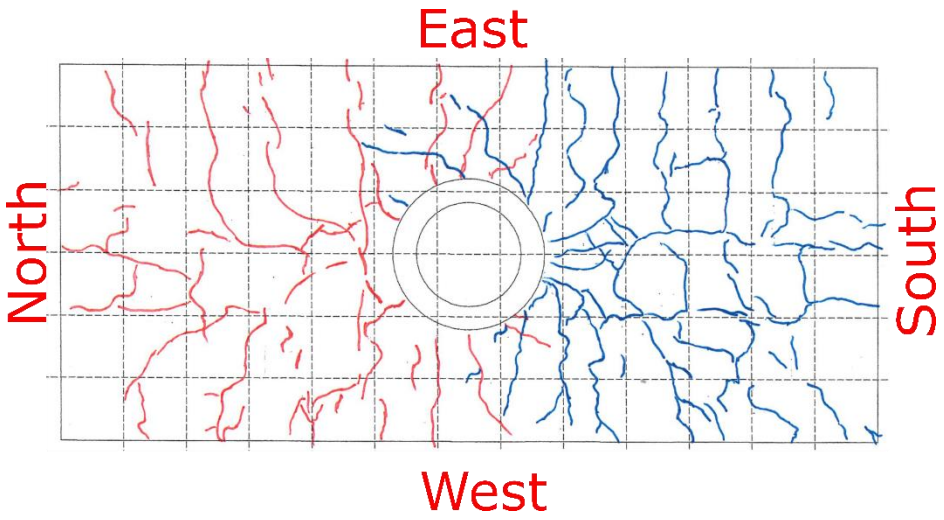

Figure 4-34: Top of Slab Crack Map – 2.0% Drift (PTB_4.5_1_0)

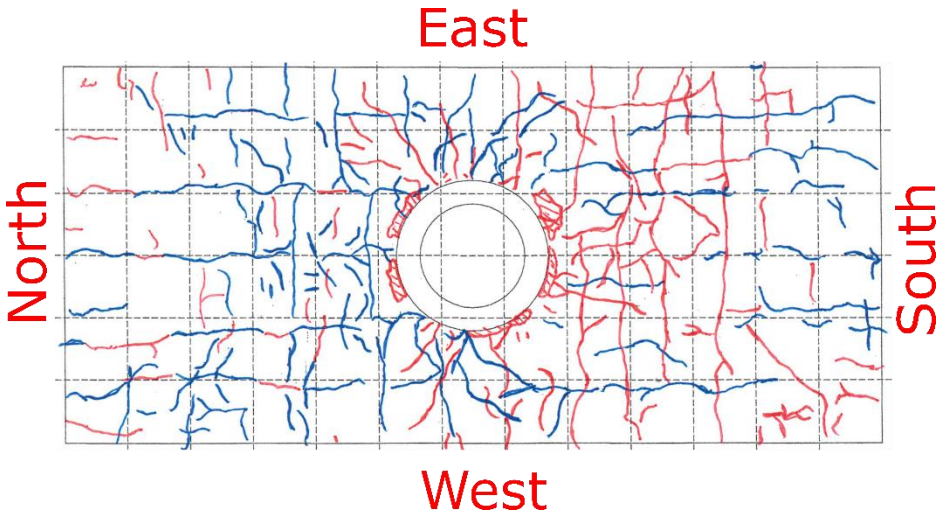

Figure 4-35: Bottom of Slab Crack Map – 2.0% Drift (PTB_4.5_1_0)

Cycle 5 (+2.6/-2.6% drift) was then run. Strain gauge data indicates that at the peak southern drift of cycle 5, yielding of flexural reinforcement in the slab had only occurred in the bar passing through the column. As shown in Figure 4-36, yielding has occurred just north and south of the column.

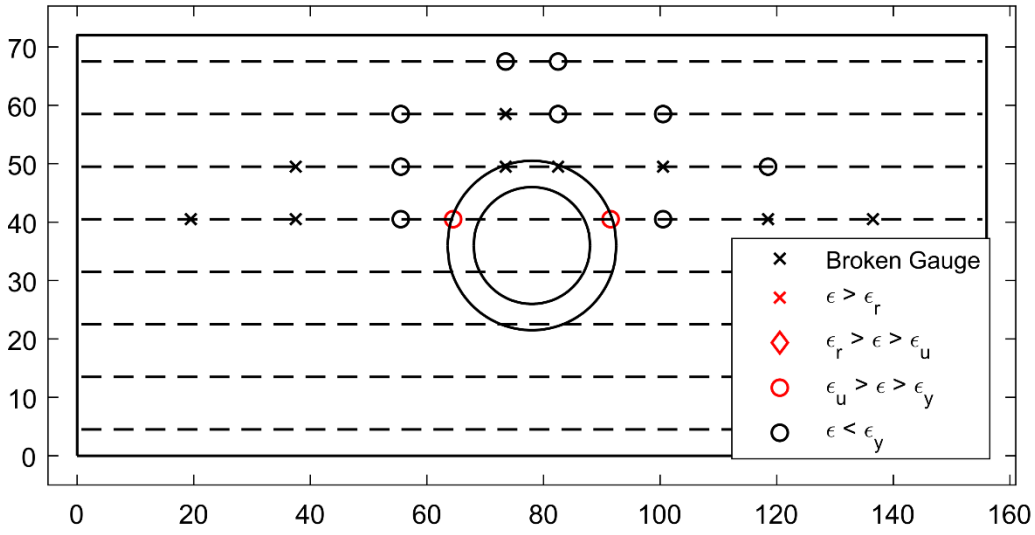

Figure 4-36: Bottom Reinforcement Strain Summary – 2.6% Drift (PTB_4.5_1_0)

Cycle 6 (+2.6/-2.6% drift) was then performed with pauses at peak drifts to update crack maps and measure cracks. The largest cracks noted while pausing at the peak southern drift of cycle 6 opened 1 mm and was located on the bottom of the slab south of the column. The largest cracks noted while pausing at the peak northern drift of cycle 6 opened 1.5 mm and were located on the top of the slab southeast of the column and on the bottom of the slab north of the column, just beyond the ring flange.

Cycle 7 (+3.4/-3.3% drift) was then run before continuing to cycle 8 (+3.3/-3.3% drift). Cycle 8 was paused at peak drifts, crack sizes were recorded and crack maps updated. The largest crack noted while pausing at the peak southern drift of cycle 8 opened 2.5 mm and was located to the west of the column on the edge of the slab. The largest crack noted while pausing at the peak northern drift of cycle 8 opened 2.5 mm and was located on the top of the slab southwest of the column. After comparing the crack patterns recorded during cycle 8 to those recorded throughout the remainder of the test, it was determined that stage 2 cracking occurred in cycle 8. Crack maps for cycle 8 are shown in Figure 4-37 and Figure 4-38.

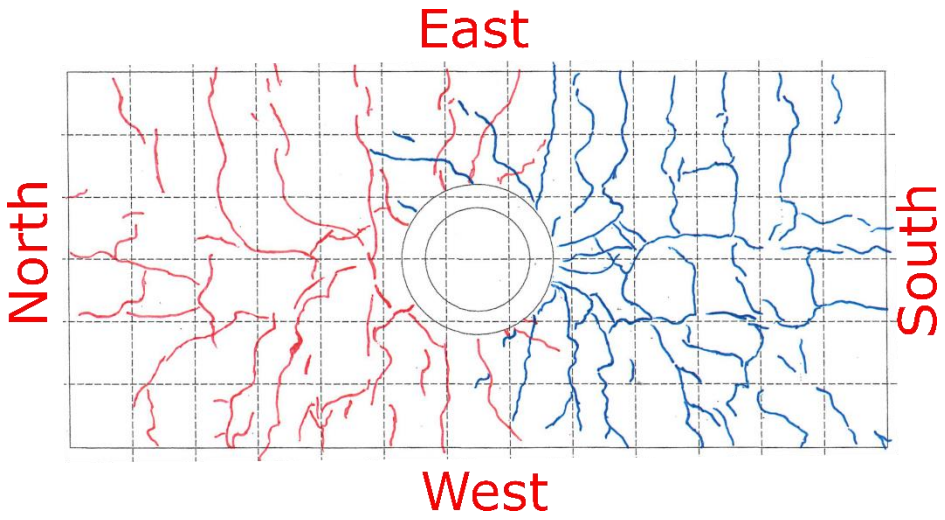

Figure 4-37: Top of Slab Crack Map – 3.4% Drift (PTB_4.5_1_0)

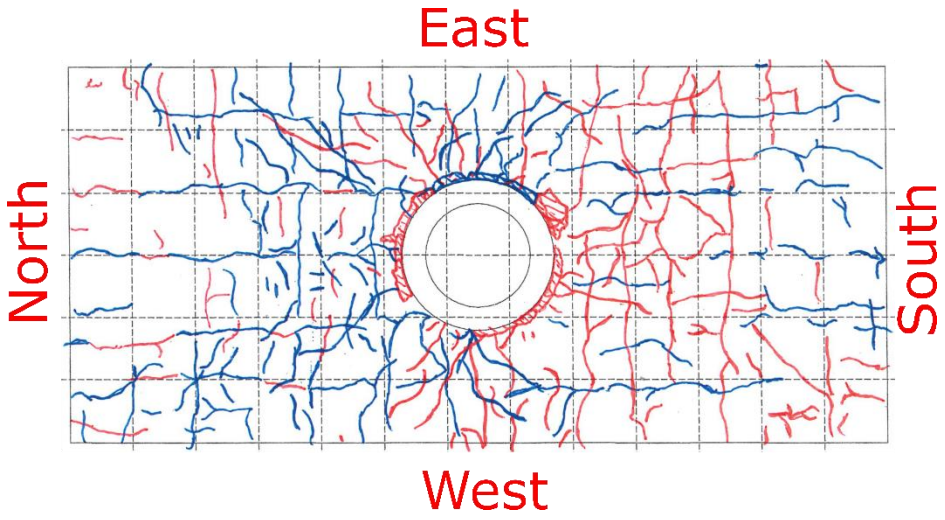

Figure 4-38: Bottom of Slab Crack Map – 3.4% Drift (PTB_4.5_1_0)

4.3.5 *High Drift Cycles (Greater than 3.6% Target Drift)*

High drift cycles initiated with cycle 9 (+4.1/-4.0% drift) which was completed without interruption. Cycle 10 (+4.1/-4.1% drift) was then performed with pauses at peak drifts to update crack maps and measure cracks. The largest crack noted while pausing at the peak southern drift of cycle 6 opened 3.5 mm and was located to east of the column on the edge of the slab. The largest crack noted while pausing at the peak northern drift of cycle 6 opened 2 mm and was located on

the top of the slab southeast of the column. A large diagonal crack directly to the west of the column on the edge of the specimen was noted during cycle 10 and is shown in Figure 4-39.

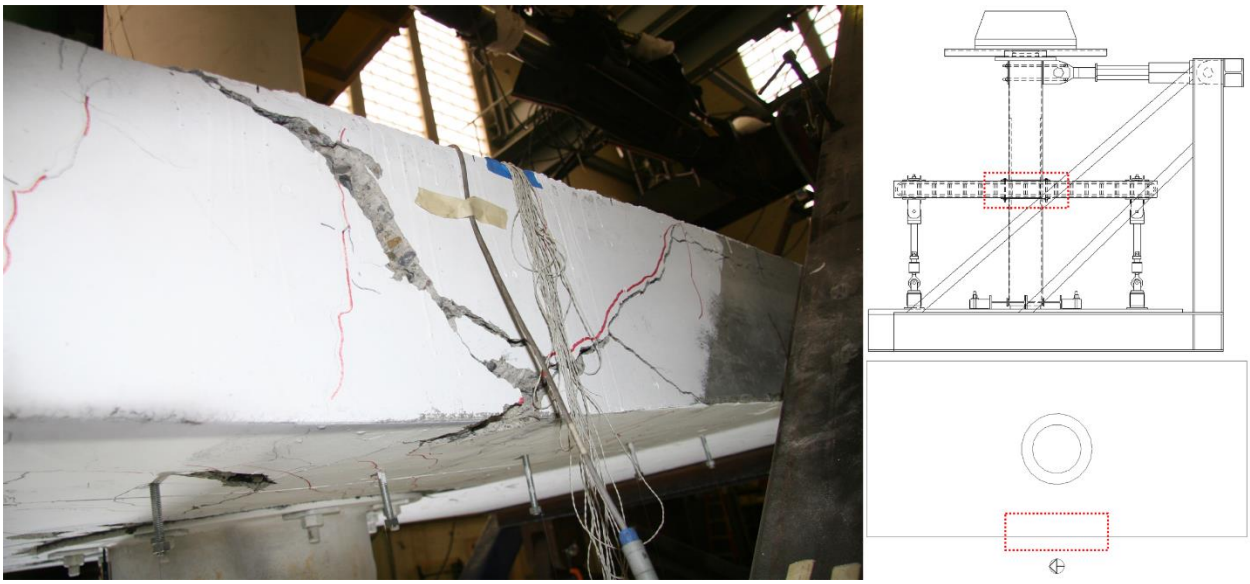

Figure 4-39: West Edge Shear Cracking – 4.1% Drift (PTB_4.5_1_0)

The onset of crushing was noted during the pauses in cycle 10. The first crushing occurred on the bottom of the slab to the east of the slab-column joint. Figure 4-40 shows the eastern side of the connection. Reinforcement had not been exposed at this time but the damage was severe enough that it was judged to represent crushing.

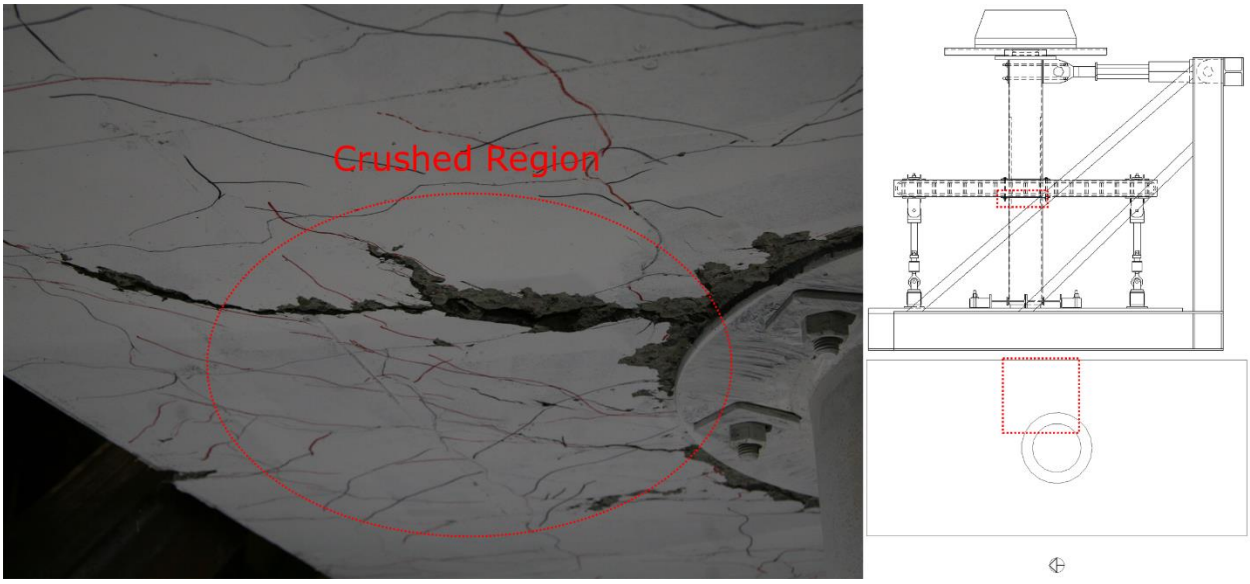

Figure 4-40: Bottom Joint East Side Crushing – 4.1% Drift (PTB_4.5_1_0)

Following the completion of cycle 10, an additional cycle at a target drift of 4.4% was performed and cycle 11 (+4.1/-4.1% drift) was completed without interruption.

Cycle 12 (+4.8/-4.8% drift) was then run. Strain gauge data indicates that at the peak southern drift of cycle 12, yielding of flexural reinforcement in the slab had likely occurred in all bars that were gauged. As shown in Figure 4-41, yielding is indicated to the south and east of the column in the bottom reinforcement and in one bar to the north of the column.

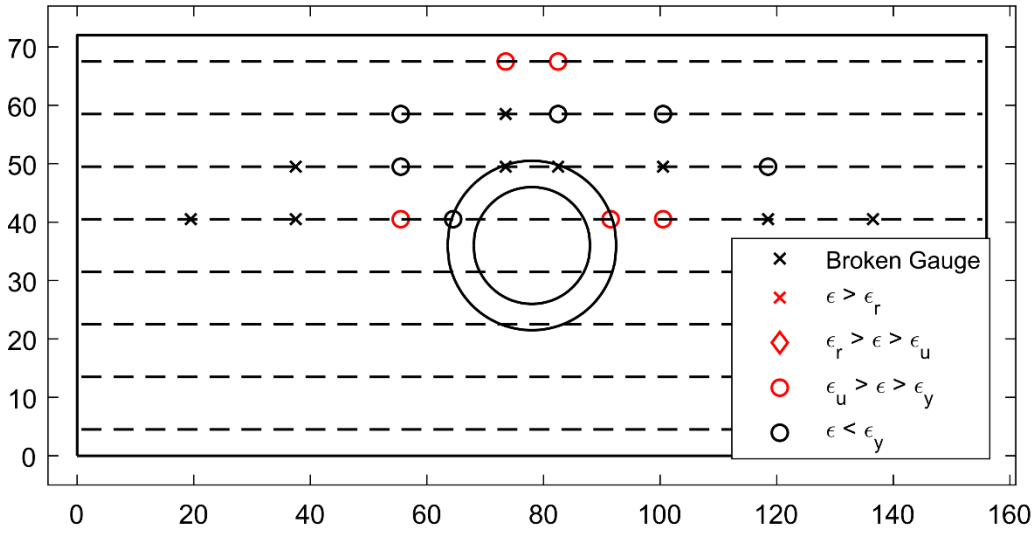

Figure 4-41: Bottom Reinforcement Strain Summary – 4.8% Drift (PTB_4.5_1_0)

Cycle 13 (+4.9/-4.8% drift) was then run and paused at peak drifts, crack sizes were recorded and crack maps updated. The largest crack noted while pausing at the peak southern drift of cycle 13 opened 3/4 in. and was located to the west of the column on the edge of the slab. The largest crack noted while pausing at the peak northern drift of cycle 13 opened 3/8 in. and was located to the west of the column on the edge of the slab. The crushed region around the column grew during cycle 13. Cycle 14 (+4.9/-4.9% drift) was then run until large pieces of concrete fell from the bottom of the specimen exposing flexural reinforcement across the width of the specimen. Testing was halted after cycle 14 due to a large single cycle loss of lateral resistance resulting in measured lateral loads less than 50% of peak lateral loads. After completion of testing, crushing was further explored and measured.

4.3.6 *Post-Test*

After the completion of testing, loose concrete around the slab-column joint was removed to explore the extent of damage. During post-test exploration, it was noted that bars passing through the connection were buckled directly to the south of the connection. Buckled bars are pointed out in Figure 4-42.

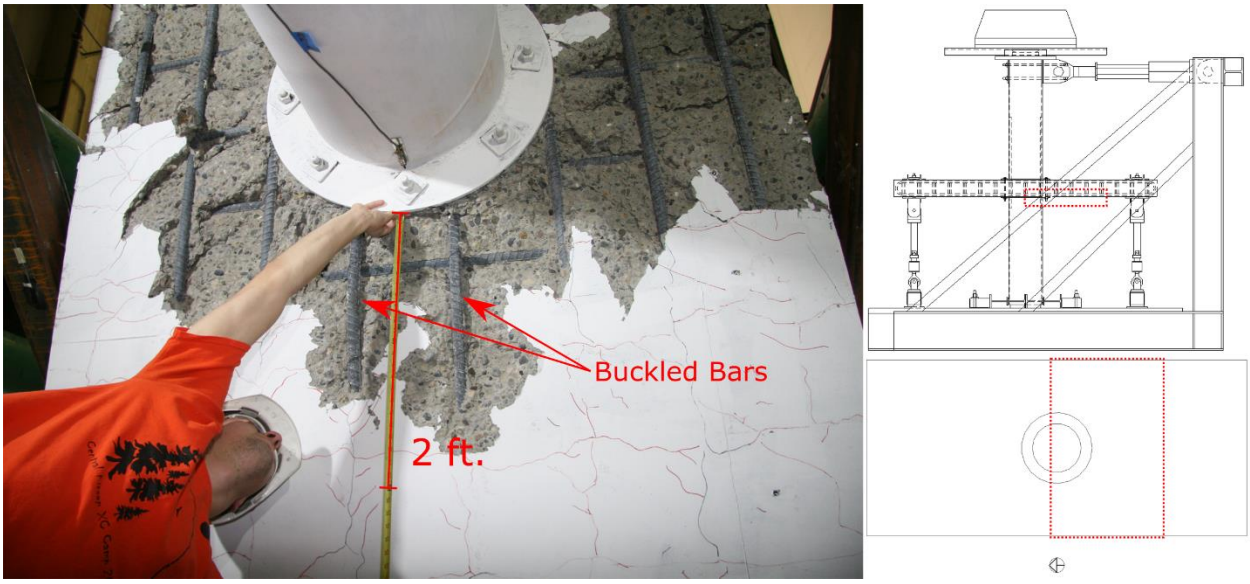

Figure 4-42: Bottom Bar South Side Bar Buckling – 4.8% Drift (PTB_4.5_1_0)

Figure 4-43 shows that crushing around the slab-column joint on the bottom of the slab extended approximately 3 ft. through the connection region west of the column and spanned the 21.5 in. from the edge of the ring plate to the edge of the specimen slab.

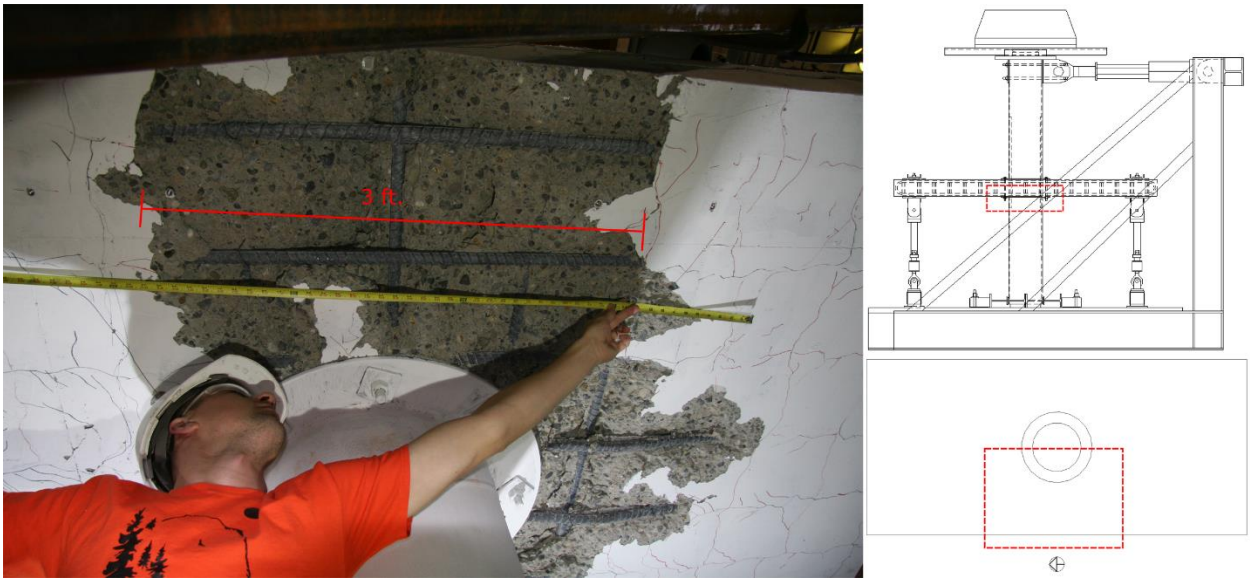

Figure 4-43: Bottom West Side Concrete Crushing – 4.8% Drift (PTB_4.5_1_0)

Figure 4-44 shows that crushing around the slab-column joint on the bottom of the slab extended approximately 3 ft. through the connection region east of the column and spanned the

21.5 in. from the edge of the ring plate to the edge of the specimen slab but was somewhat less extensive closer to the edge of the slab.

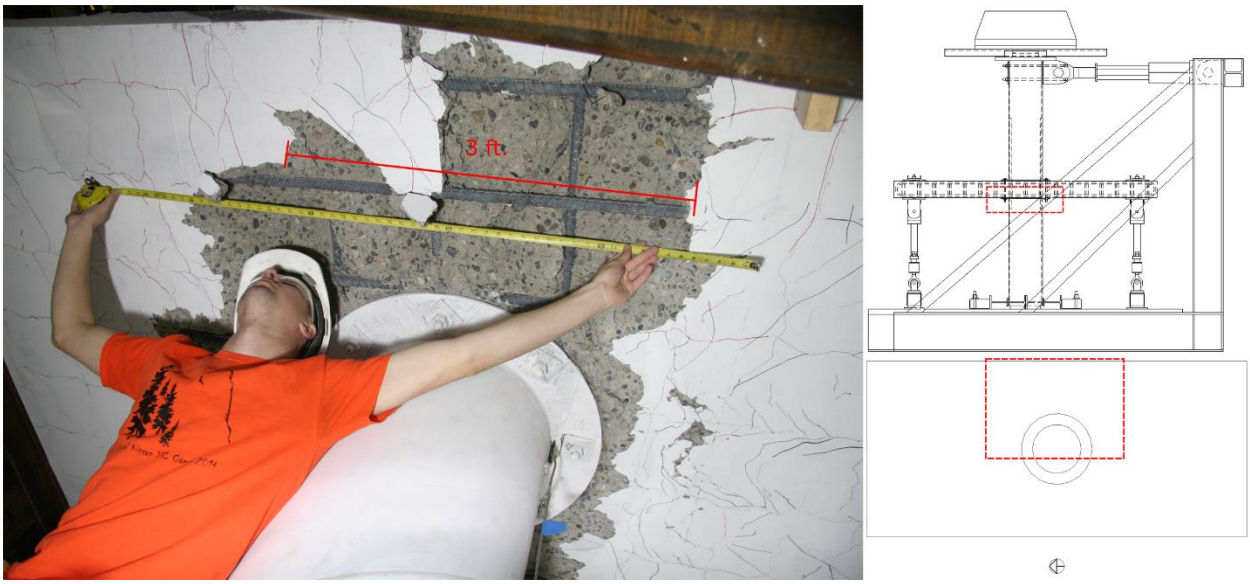

Figure 4-44: Bottom East Side Concrete Crushing – 4.8% Drift (PTB_4.5_1_0)

Figure 4-45 shows the large diagonal cracks west of the column on the edge of the slab that expanded from cycle 10 through the end of the test. Figure 4-46 shows similar diagonal cracks east of the column on the edge of the slab. The diagonal cracks on the edge of the specimen are why PTB_4.5_1_0 is thought to have ultimately failed in one-way shear after first undergoing a flexural response.

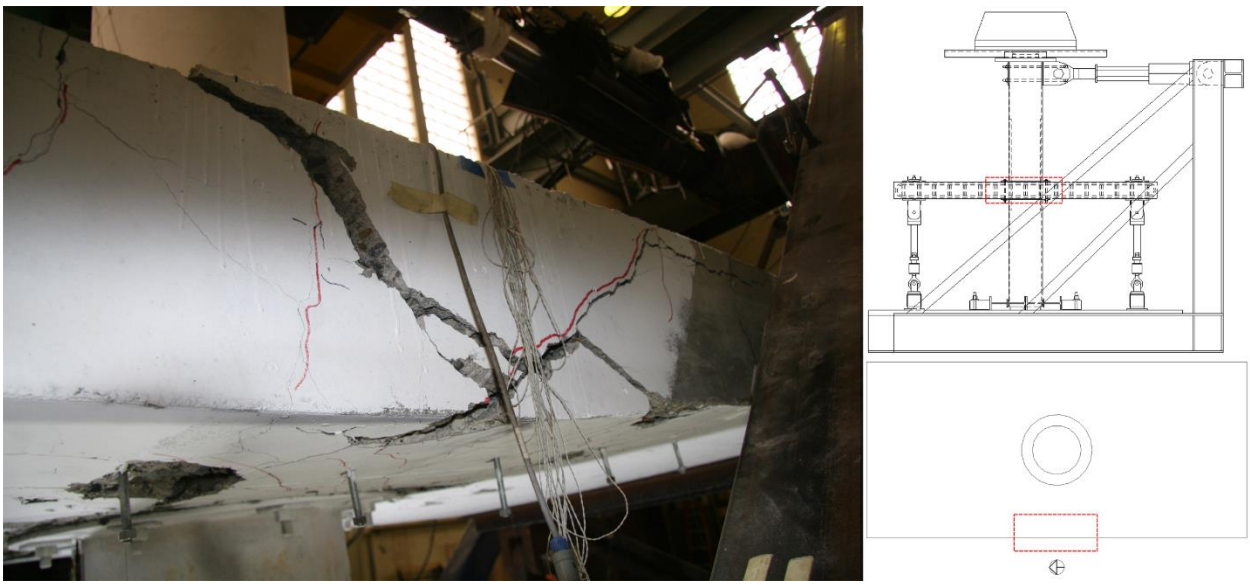

Figure 4-45: West Edge Shear Cracks – 4.8% Drift (PTB_4.5_1_0)

Figure 4-46: East Edge Shear Cracks – 4.8% Drift (PTB_4.5_1_0)

4.3.7 *Test Summary*

PTB_4.5_1_0 reached a drift range of 9.8% (-4.9% to 4.9%). Cracking occurred at the beginning of the first testing attempt. Spalling was first observed around the ring at 1.3% drift. Yielding first occurred in the longitudinal reinforcement passing through the slab-column joint at 2.0% drift. Maximum lateral force resistance occurred at a drift of 3.4%. Crushing began at 4.1%

drift. All longitudinal bars yielded by 4.8% drift. Failure occurred 4.9% drift when pieces of concrete spalled from the connection region and there was a loss of more than 50% lateral force resistance.

4.4 SPECIMEN PTB_4.5_1_4

Specimen PTB_4.5_1_4 was tested April 11th, 2019 in the Structural Research Laboratory at the University of Washington. The test was performed 185 days after casting the slab and lower column and 174 days after casting the upper column.

4.4.1 *Specimen Overview*

The test went smoothly and there were no interruptions throughout the test other than those planned (for marking cracks or initializing the next cycle). The induced drift and applied lateral loads can be seen in Figure 4-47 and Figure 4-48, respectively.

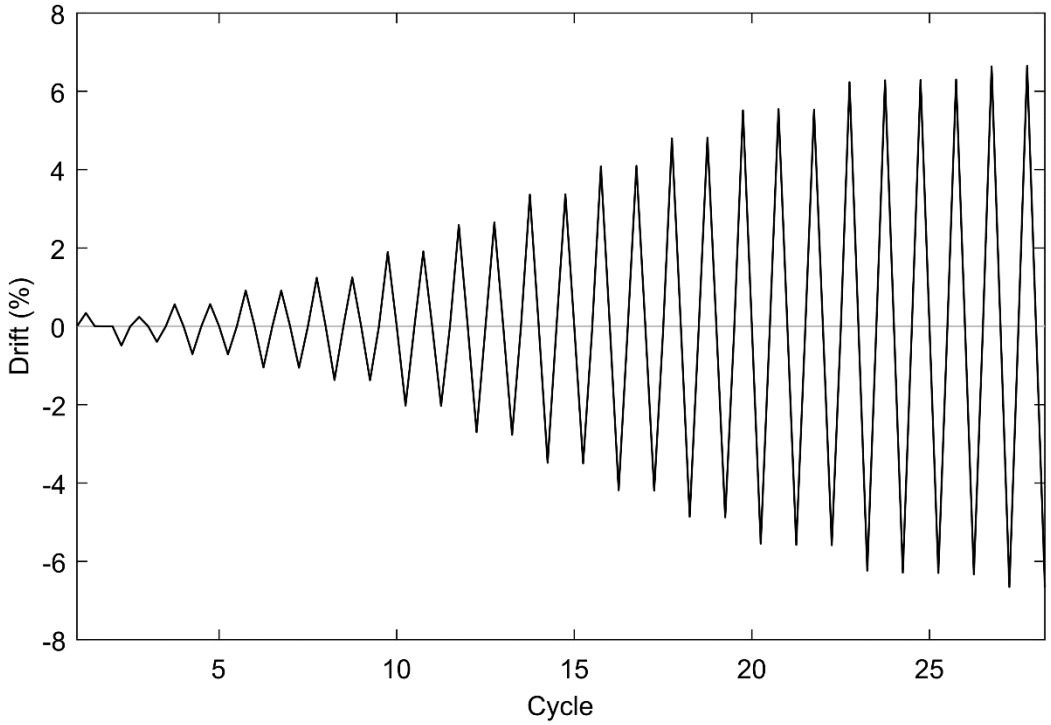

Figure 4-47: Induced Drift (PTB_4.5_1_4)

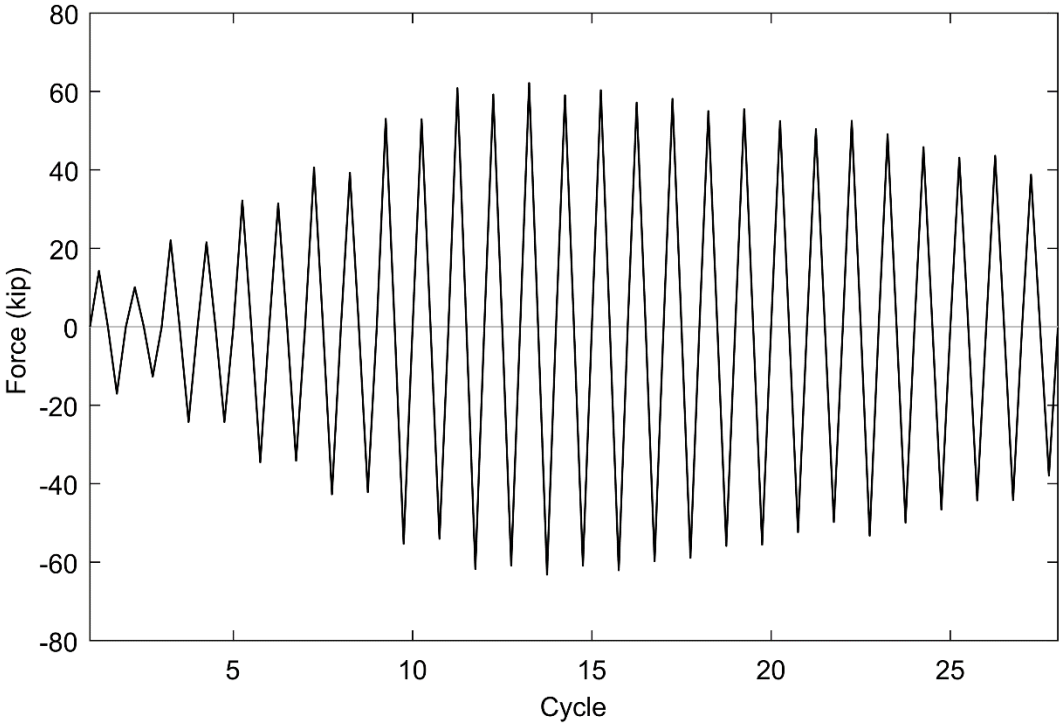

Figure 4-48: Applied Lateral Load (PTB_4.5_1_4)

It can be seen from Figure 4-48 that SR_4_10_5 had a maximum resistance of 63.2 kip. The specimen completed 27 full cycles before the test was terminated due to reaching the limits of the MTS Actuator stroke. The connection's lateral force resistance increased until it reached a maximum resistance in cycle 13 at which point the connection began to lose strength. At the termination of testing, 38.6% of lateral force resisting capacity had been lost. The maximum lateral force resistances and drifts recorded during each cycle can be seen in Table 4.12. Table 4.12 and Figure 4-48 show a drop in resistance during second cycle of a target drift, possibly indicating irrecoverable damage occurred during the previous cycle.

Table 4.12: Maximum Resistances and Drifts in Each Cycle (PTB_4.5_1_4)

Cycle	Maximum Measured Resistance (kips)		Maximum Drift (%)	
	Tension	Compression	Tension	Compression
1	14.2	- 17.0	0.34	- 0.49
2	10.1	- 12.7	0.24	- 0.39
3	22.0	- 24.3	0.56	- 0.71
4	21.6	- 24.4	0.56	- 0.71
5	32.2	- 34.5	0.91	- 1.0
6	31.4	- 34.1	0.91	- 1.1
7	40.6	- 42.7	1.2	- 1.4
8	39.6	- 42.1	1.2	- 1.4
9	53.0	- 55.3	1.9	- 2.0
10	52.9	- 54.0	1.9	- 2.0
11	60.8	- 61.8	2.6	- 2.7
12	59.2	- 60.8	2.6	- 2.8
13	62.1	- 63.2	3.4	- 3.5
14	59.0	- 60.9	3.4	- 3.5
15	60.3	- 62.1	4.1	- 4.2
16	57.1	- 59.7	4.1	- 4.2
17	58.1	- 58.9	4.8	- 4.9
18	55.0	- 55.8	4.8	- 4.9
19	55.5	- 55.5	5.5	- 5.5
20	52.4	- 52.3	5.5	- 5.6
21	50.4	- 59.8	5.5	- 5.6
22	52.5	- 53.2	6.2	- 6.2
23	49.1	- 49.9	6.3	- 6.3
24	45.8	- 46.6	6.3	- 6.3
25	43.1	- 44.2	6.3	- 6.3
26	43.6	- 45.5	6.6	- 6.7
27	38.8	- 40.8	6.7	- 6.7

It can be seen from Table 4.12 that the maximum drift achieved was 6.7%. It is thought that a flexural response was maintained throughout the test. The following section will present the progression of damage through the testing of PTB_4.5_1_0. The force-drift hysteresis curve of the

slab column connection is shown in Figure 4-49 and a modified force-drift hysteresis curve with P-Δ effects from the column axial load removed is shown in Figure 4-50. Force has been normalized against the nominal moment capacity of the slab predicted by ACI 318-14. Figure 4-50 shows that after reaching what appeared to be peak lateral force resistance according to Figure 4-49 at 3.5% drift, PTB_4.5_1_4 maintains a nearly consistent level of lateral force resistance until beginning to lose strength 6.6% drift.

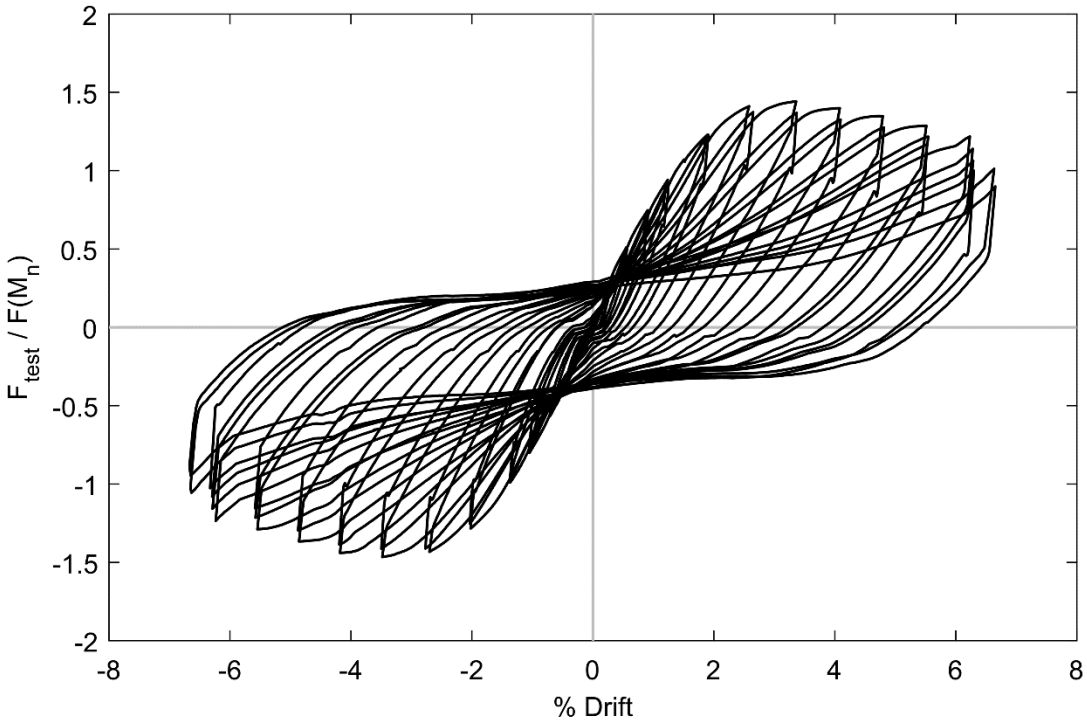

Figure 4-49: Normalized Drift Response (PTB_4.5_1_4)

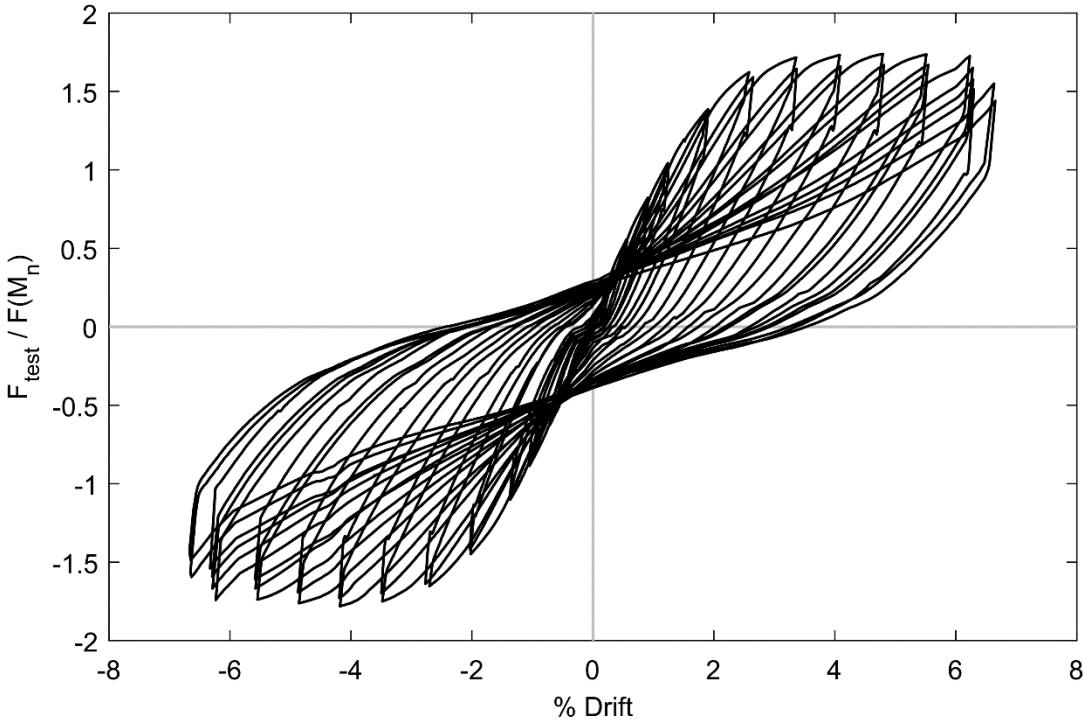

Figure 4-50: Normalized Drift Response with P-Δ Effects Removed (PTB_4.5_1_4)

4.4.2 *Specimen Performance State Summary*

The performance state summary for PTB_4.5_1_5 can be seen in Table 4.13.

Table 4.13: Summary of Damage (PTB_4.5_1_4)

Damage state	Drift (%)
Cracking	0.73 – 3.6
Yielding	2.2– 4.4
Spalling	2.2
Crushing	5.1
Bar Buckling	6.5

4.4.3 *Low Drift Cycles (0.0% - 1.5% Target Drift)*

Cycle 1 (+0.34/-0.49% drift) was run without interruption and a small amount of cracking was first observed when the test was paused at peak displacements during cycle 2 (+0.24/-0.39% drift). Cracks patterns and typical crack sizes were recorded and the next drift levels was initiated. The largest cracks noted while pausing at the peak southern drift of cycle 2 opened 0.1 mm and were located on the top of the slab north of the column and on the bottom of the slab southwest and southeast of the column. Typical crack sizes recorded during pauses at peak drifts throughout low drift cycles are recorded in Table 4.14.

Table 4.14: Low Drift Cycle Typical Crack Opening at Peaks (PTB_4.5_1_0)

Cycle	Drift (%)		Bottom (mm)		Top (mm)		Side (mm)	
	South	North	South	North	South	North	South	North
2	0.24	- 0.39	0.1	0.1	0.1	0.1	0	0.1
4	0.56	- 0.71	0.1	0.1	0.1	0.15	0.1	0.1
6	0.91	- 1.1	0.2	0.15	0.15	0.15	0.1	0.15
8	1.2	- 1.4	0.2	0.2	0.2	0.2	0.2	0.2

Cycle 3 (+0.56/-0.71% drift) was then run and stage 1 cracking occurred during cycle 4 (+0.56/-0.71% drift). Cracking initially began near the edge of the ring flange and propagated outward across the slab. Crack patterns are shown in Figure 4-51 and Figure 4-52. The largest cracks noted while pausing at the peak southern drift of cycle 4 opened 0.15 mm and were located on the bottom of the slab to the south and southwest of the column. The largest crack noted while

pausing at the peak northern drift of cycle 4 opened 0.3 mm and was located on the top of the slab southeast of the column.

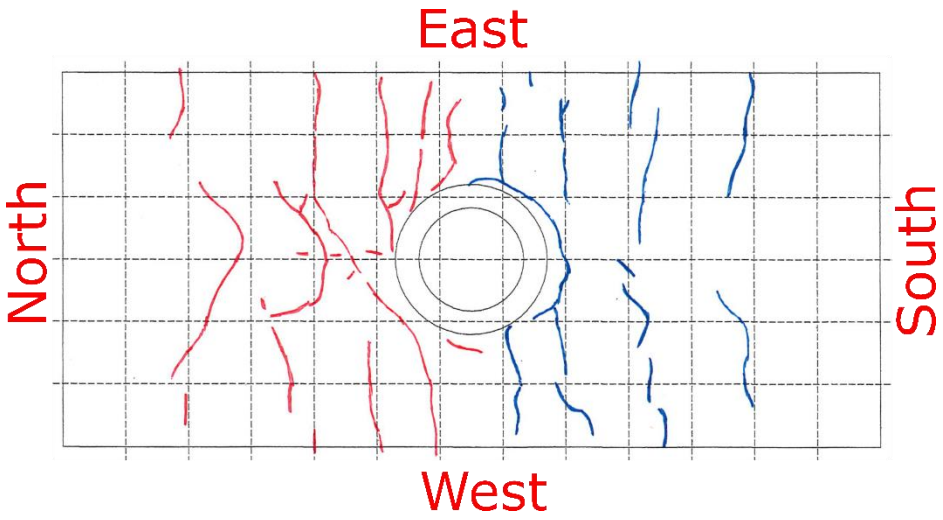

Figure 4-51: Top of Slab Crack Map – 0.71% Drift (PTB_4.5_1_4)

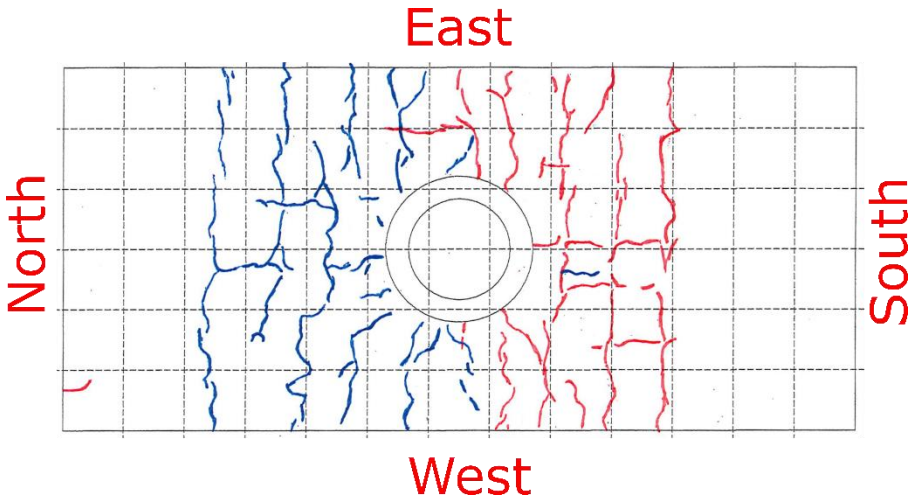

Figure 4-52: Bottom of Slab Crack Map – 0.71% Drift (PTB_4.5_1_4)

Cycle 5 (+0.91/-1.0% drift) was then run before continuing to cycle 6 (+0.91/-1.1% drift). Cycle 6 was paused at peak drifts and crack sizes were recorded and crack maps updated. The largest cracks noted while pausing at the peak southern drift of cycle 6 opened 0.3 mm and were located on the top of the slab north and northeast of the column. The largest crack noted while pausing at the peak northern drift of cycle 6 opened 0.4 mm and was located on the top of the slab southeast of the column.

Cycle 7 (+1.2/-1.4% drift) was then run before continuing to cycle 8 (+1.2/-1.4% drift). Cycle 8 was paused at peak drifts and crack sizes were recorded and crack maps updated. The largest cracks noted while pausing at the peak southern drift of cycle 8 opened 0.35 mm and were located on the top of the slab north and northeast of the column. The largest crack noted while pausing at the peak northern drift of cycle 6 opened 0.5 mm and was located on the top of the slab east of the column.

4.4.4 *Moderate Drift Cycles (1.5% - 3.6% Target Drift)*

Moderate drift cycles initiated with cycle 9 (+1.9/-2.0% drift) which was completed uninterrupted. Once strain gauge data was analyzed, it was discovered that a gauge indicated yielding of flexural reinforcement in the bottom of the slab at the peak drifts of cycle 9. As shown in Figure 4-53 and Figure 4-54, yielding did not occur in the top longitudinal reinforcement but did occur just north, south, and east of the column in the bottom longitudinal reinforcement.

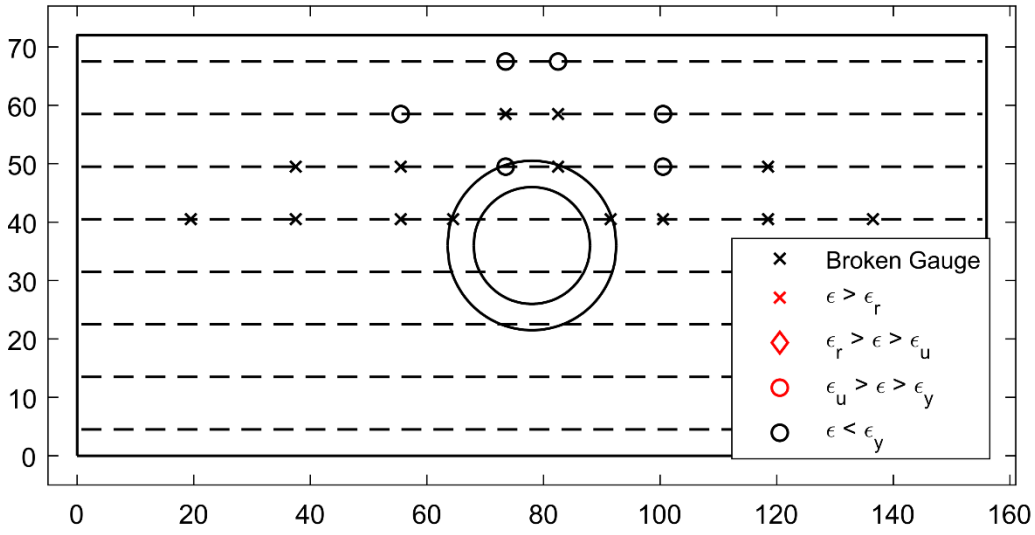

Figure 4-53: Top Reinforcement Strain Summary – 1.9% Drift (PTB_4.5_1_4)

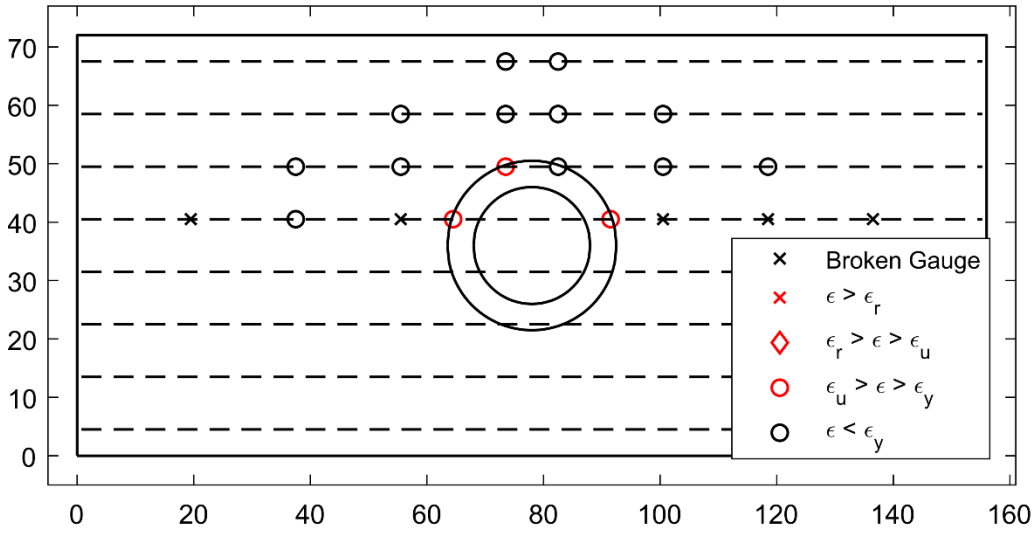

Figure 4-54: Bottom Reinforcement Strain Summary – 1.9% Drift (PTB_4.5_1_4)

Cycle 10 (+1.9/-2.0% drift) was paused at peak drifts, crack sizes were recorded and crack maps updated. The largest crack noted while pausing at the peak southern drift of cycle 10 opened 0.8 mm and was located on the top of the slab northeast of the column extending from the ring flange. The largest crack noted while pausing at the peak northern drift of cycle 10 opened 1.0 mm and was located on the top of the slab southeast of the column near the ring flange. Typical crack sizes recorded during moderate drift cycles are listed in Table 4.15.

Table 4.15: Moderate Drift Cycle Typical Crack Opening at Peaks (PTB_4.5_1_4)

Cycle	Drift (%)		Bottom (mm)		Top (mm)		Side (mm)	
	South	North	South	North	South	North	South	North
10	1.9	- 2.0	0.3	0.2	0.3	0.3	0.2	0.2
12	2.6	- 2.8	0.3	0.3	0.3	0.4	0.2	0.2
14	3.4	- 3.5	0.4	0.4	0.4	0.5	0.3	0.4

By the completion of cycle 10, cracking had grown to cover the top and bottom of the slab as shown in Figure 4-55 and Figure 4-56.

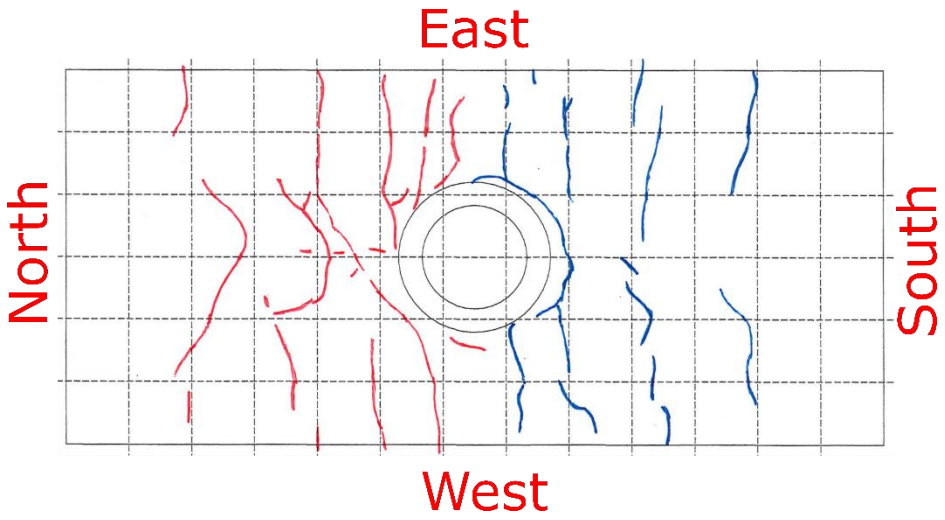

Figure 4-55: Top of Slab Crack Map – 2.0% Drift (PTB_4.5_1_4)

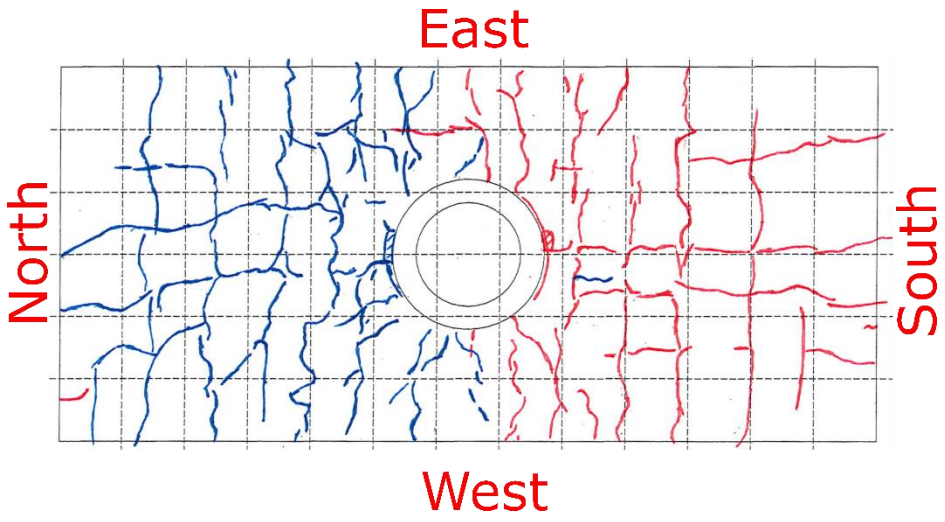

Figure 4-56: Bottom of Slab Crack Map – 2.0% Drift (PTB_4.5_1_4)

The onset of spalling was also noted during the pause at the northern peak drift in cycle 10. The first spalling occurred on the bottom of the slab on the north side of the slab-column joint as shown in Figure 4-20.

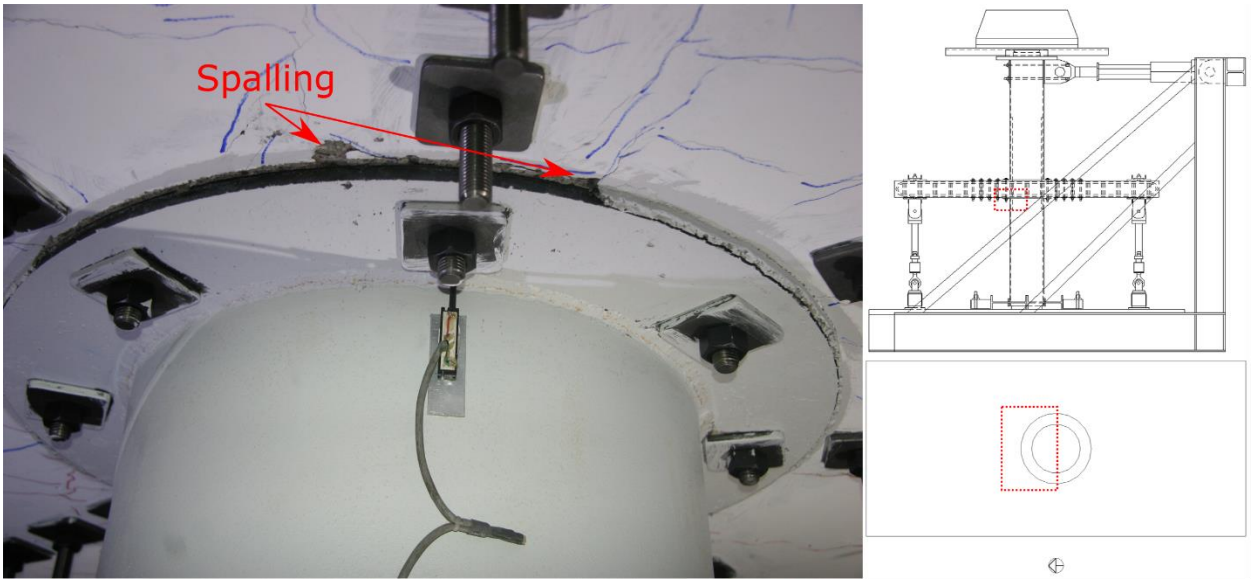

Figure 4-57: Bottom Joint North Side Spalling – 2.0% Drift (PTB_4.5_1_4)

Cycle 11 (+2.6/-2.7% drift) was then run. Strain gauge data indicates that at the peak southern drift of cycle 11, yielding of flexural reinforcement in the slab had occurred in three of eight bars that were gauged. As shown in Figure 4-58 yielding is indicated to the east of the column in the top reinforcement while Figure 4-59 indicates yielding to the north, south and east of the column.

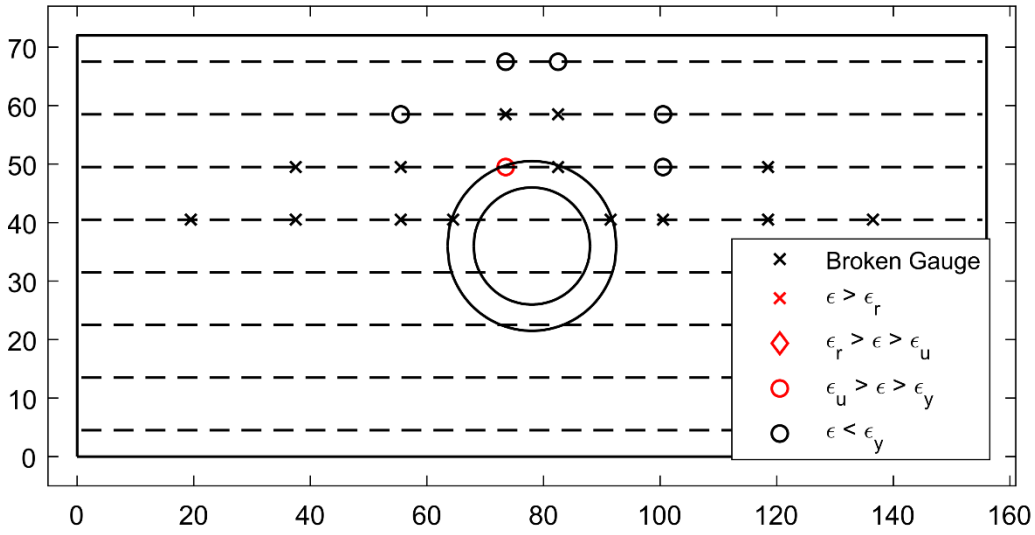

Figure 4-58: Top Reinforcement Strain Summary – 2.6% Drift (PTB_4.5_1_4)

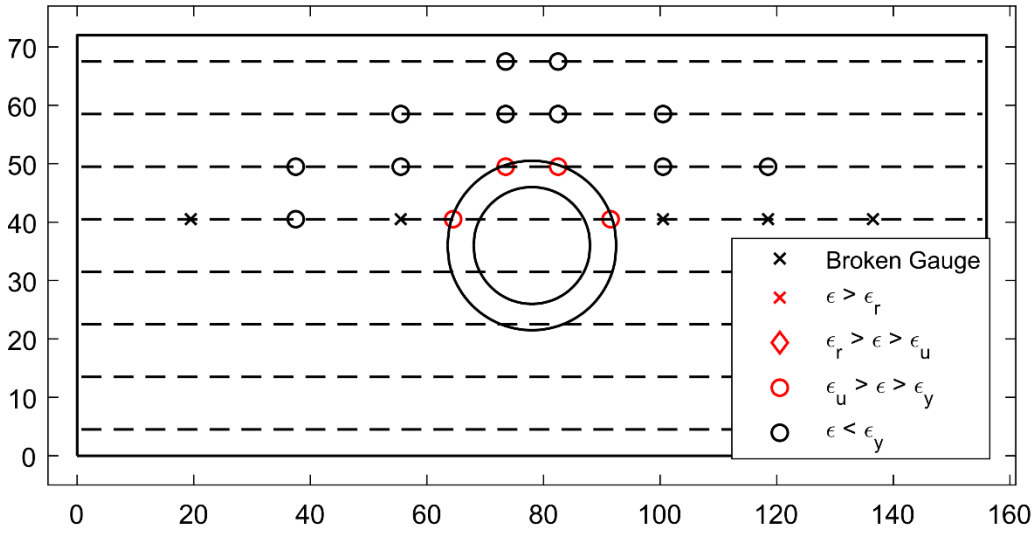

Figure 4-59: Bottom Reinforcement Strain Summary – 2.6% Drift (PTB_4.5_1_4)

Cycle 12 (+2.6/-2.8% drift) was then performed with pauses at peak drifts to update crack maps and measure cracks. The largest crack noted while pausing at the peak southern drift of cycle 12 opened 0.9 mm and was located on the top of the slab north of the column. The largest crack noted while pausing at the peak northern drift of cycle 12 opened 1.5 mm and was located on the top of the slab southeast of the column.

Cycle 13 (+3.4/-3.5% drift) was then run without interruption. Cycle 14 (+3.4/-3.5% drift) was then performed with pauses at peak drifts to update crack maps and measure cracks. The largest crack noted while pausing at the peak southern drift of cycle 14 opened 2.5 mm and was located on the top of the slab northeast of the column extending from the ring flange. The largest cracks noted while pausing at the peak northern drift of cycle 14 opened 2.5 mm and was located on the top of the slab southeast of the column extending from the ring flange. After comparing the crack patterns recorded during cycle 14 to those recorded throughout the remainder of the test, it was determined that cracking had reach its full extent in cycle 14. Crack maps for cycle 14 are shown in Figure 4-60 and Figure 4-61.

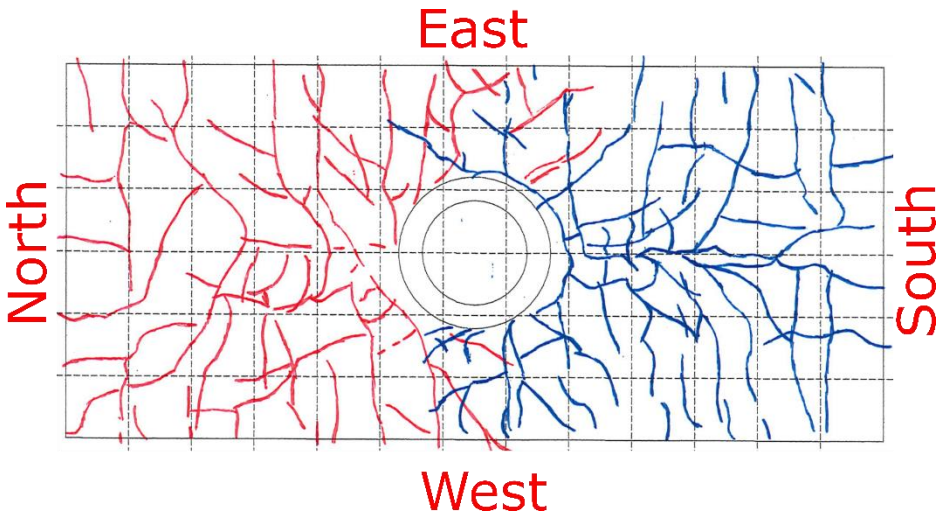

Figure 4-60: Top of Slab Crack Map – 3.5% Drift (PTB_4.5_1_4)

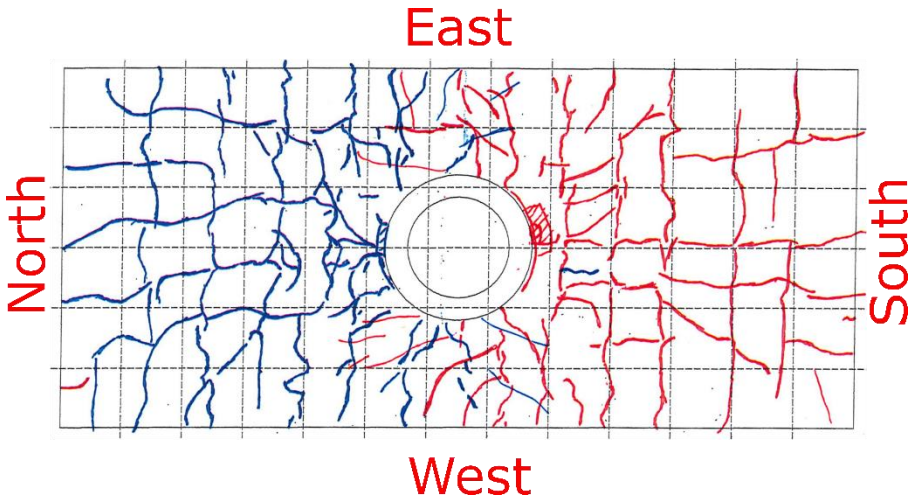

Figure 4-61: Bottom of Slab Crack Map – 3.5% Drift (PTB_4.5_1_4)

4.4.5 *High Drift Cycles (Greater than 3.6% Target Drift)*

High drift cycles initiated with cycle 15 (+4.1/-4.2% drift) which was completed. Strain gauge data indicates that at the peak drifts of cycle 15, yielding of flexural reinforcement in the slab had occurred in all bottom bars that were gauged. As shown in Figure 4-62, yielding is indicated to the south and east of the column in the top reinforcement while Figure 4-63 indicates yielding to the north, south and east of the column.

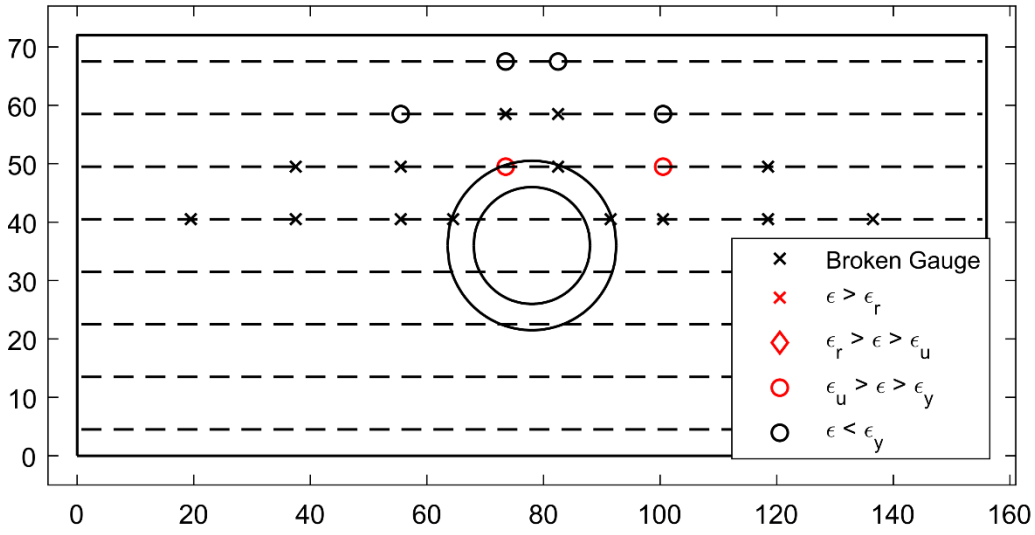

Figure 4-62: Top Reinforcement Strain Summary – 4.1% Drift (PTB_4.5_1_4)

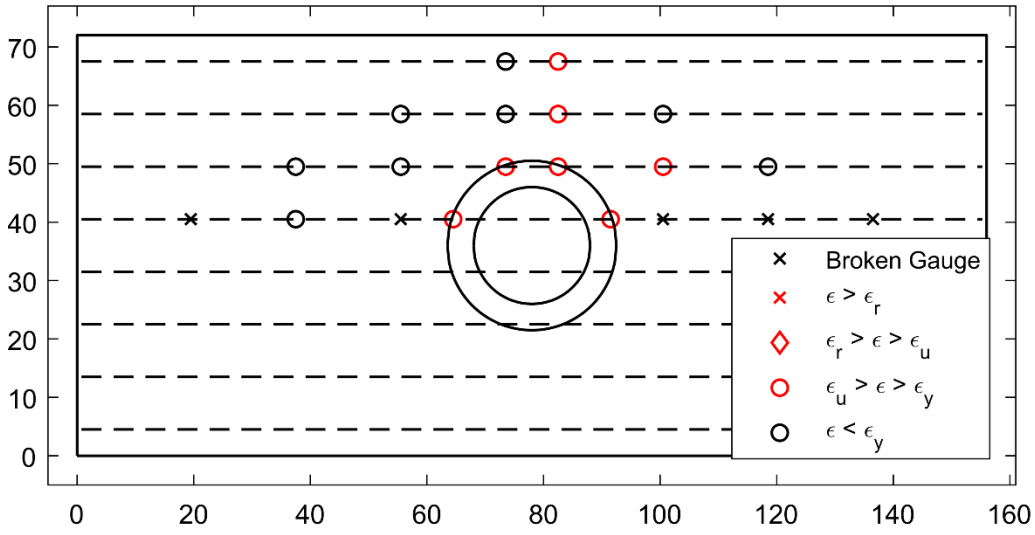

Figure 4-63: Bottom Reinforcement Strain Summary – 4.1% Drift (PTB_4.5_1_4)

Cycle 16 (+4.1/-4.2% drift) was run and paused at peak drifts, crack sizes were recorded and crack maps updated. The largest cracks noted while pausing at the peak southern drift of cycle 16 opened 1.5 mm and were located on the top of the slab northwest and northeast of the column. The largest crack noted while pausing at the peak northern drift of cycle 16 opened 2.5 mm and

was located on the top of the slab southeast of the column. Typical crack sizes recorded during high drift cycles are listed in Table 4.7.

Table 4.16: High Drift Cycle Typical Crack Opening at Peaks (PTB_4.5_1_4)

Cycle	Drift (%)		Bottom (mm)		Top (mm)		Side (mm)	
	South	North	South	North	South	North	South	North
16	4.1	- 4.2	0.6	0.6	0.8	0.8	0.6	0.6
18	4.8	- 4.9	0.8	0.8	0.8	0.8	0.7	0.8
20	5.5	- 5.6	0.8	0.75	0.8	0.75	0.8	0.75
22	6.2	- 6.2	NA	NA	NA	NA	1.0	NA

Cycle 17 (+4.8/-4.9% drift) was then run before continuing to cycle 18 (+4.8/-4.9% drift). Cycle 18 was paused at peak drifts, crack sizes were recorded and crack maps updated. The largest crack noted while pausing at the peak southern drift of cycle 18 opened 2.5 mm and was located on the top of the slab north of the column. The largest crack noted while pausing at the peak northern drift of cycle 18 opened 2.5 mm and was located on the top of the slab southwest of the column. The onset of crushing was noted during the pauses in cycle 18. The first crushing occurred on the bottom of the slab to the north and south of the slab-column joint. Figure 4-64 shows the northern side of the connection while Figure 4-65 shows the southern side of the connection. Exposed longitudinal reinforcement is visible in Figure 4-64 and Figure 4-65.

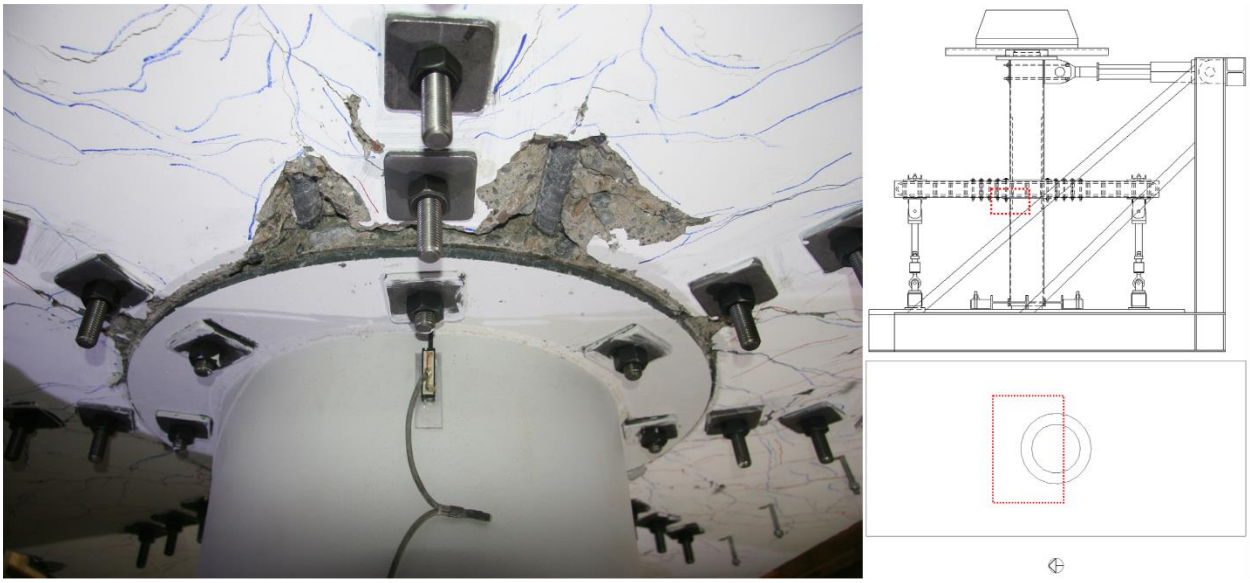

Figure 4-64: Bottom Joint North Side Crushing – 4.9% Drift (PTB_4.5_1_4)

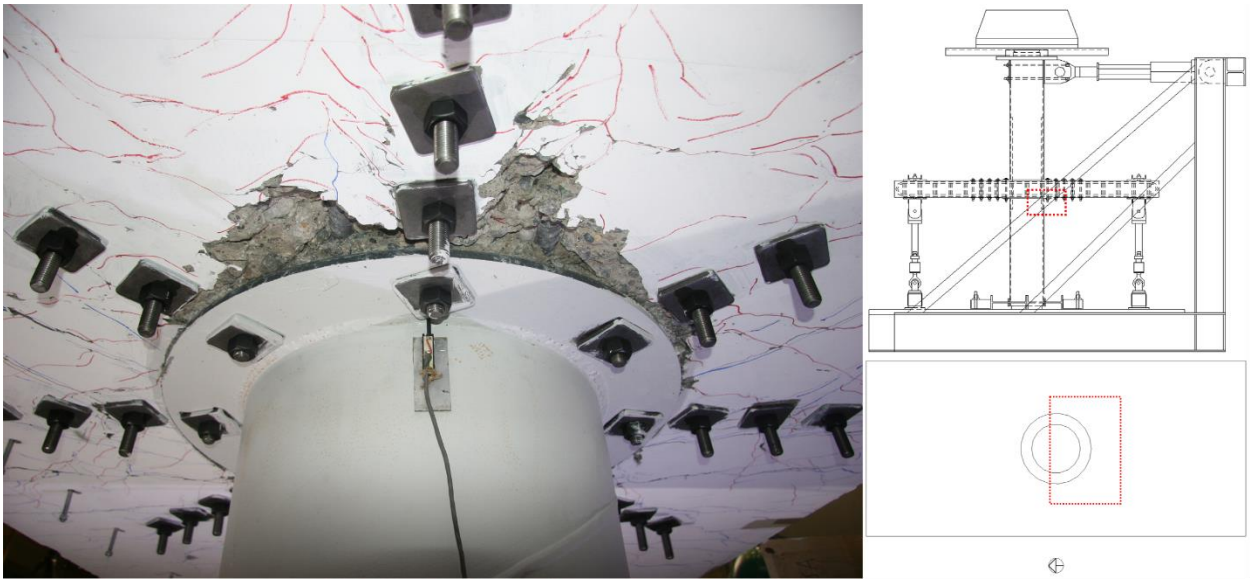

Figure 4-65: Bottom Joint South Side Crushing – 4.9% Drift (PTB_4.5_1_4)

Cycles 19 (+5.5/-5.5% drift) and 20 (+5.5/-5.6% drift) were then run before continuing to cycle 21 (+5.5/-5.6% drift). Cycle 21 was paused at peak drifts, crack sizes were recorded and crack maps updated. The largest crack noted while pausing at the peak southern drift of cycle 20 opened 2.5 mm and was located on the top of the slab northwest of the column. The largest crack noted while pausing at the peak northern drift of cycle 21 opened 3.5 mm and was located to the west column on the edge of the slab. The crushed region to the north and south of the ring extended

during cycles 19, 20 and 21 with the majority of crushing occurring along longitudinal reinforcement while other parts of the slab remained relatively undamaged. A diagonal crack to the west of the column on the edge of the specimen was noted during cycle 21 and is shown in Figure 4-66.

Figure 4-66: West Edge Shear Cracking – 5.5% Drift (PTB_4.5_1_4)

Cycle 22 (+6.2/-6.2% drift) 23 (+6.3/-6.3% drift), and 24 (+6.3/-6.3% drift) were then run before continuing to cycle 25 (+6.3/-6.3% drift). Cycle 25 was paused at peak drifts and crack maps updated. The largest crack noted while pausing at the peak southern drift of cycle 25 opened 3 mm and was located on the west of the column on the edge of the slab. The largest crack noted while pausing at the peak northern drift of cycle 25 opened 4 mm and was located to the west column on the edge of the slab. The crushed region grew significantly on the top and bottom of the slab around the column joint during cycles 22 through 25 and extended out from the column in all directions between lines of prestressed bolts. During pauses of cycle 25, it was noticed that bottom longitudinal reinforcement to the south of the column had buckled. Buckled reinforcement is pointed out in Figure 4-67.

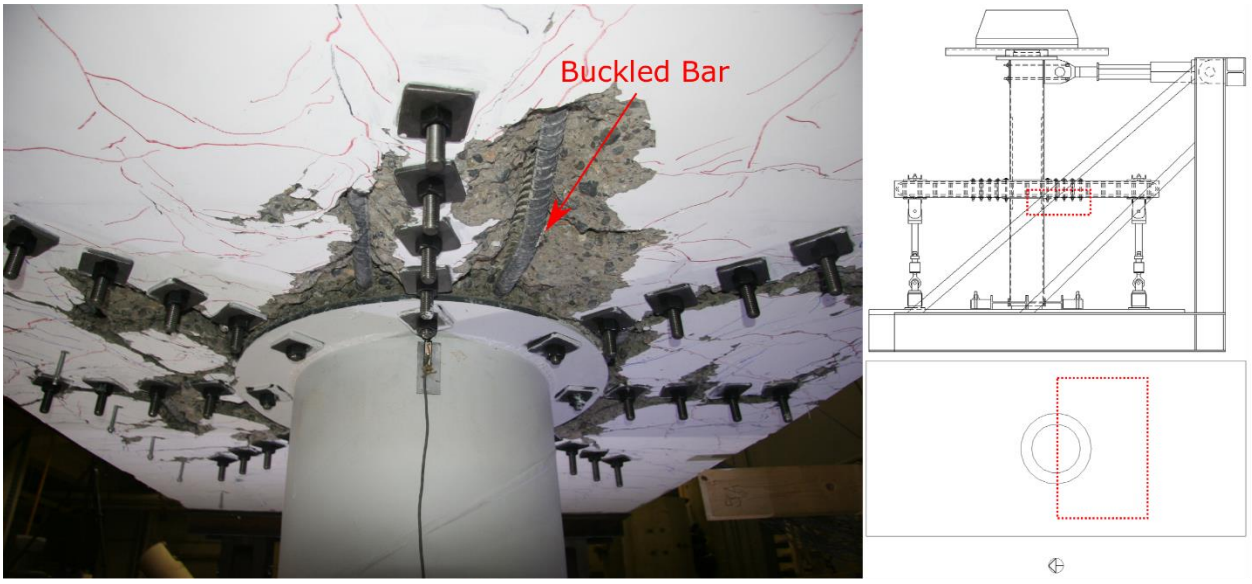

Figure 4-67: Bottom South Side Bar Buckling – 6.2% Drift (PTB_4.5_1_4)

Cycle 26 (+6.6/-6.7% drift) was then run before continuing to cycle 27 (+6.7/-6.7% drift). Cycle 27 was paused at peak drifts and crack maps updated. The crushed region grew significantly on the top and bottom of the slab around the column joint during cycles 26 and 27. As a result, recording crack sizes became impractical. At the completion of cycle 27, crushing extended east and west from the ring flange to the edge of the slab and north and south along longitudinal reinforcement. Testing was halted after cycle 27 because deformation limits of the equipment were reached. After completion of testing, crushing was further explored and measured.

4.4.6 *Post-Test*

After the completion of testing, loose concrete around the slab-column joint was removed to explore the extent of damage. Damage was mostly confined to areas bordered by post-tensioned bolts. The concrete under post-tensioned bolts remained largely undamaged throughout the tests, while crushing occurred in the areas between bolts. Crushing to the southeast of the column on top of the slab is shown in Figure 4-68 and extends from the ring flange to the edge of the slab. Crushing to the bottom of the slab north and south of the column is shown in Figure 4-69 and Figure 4-70. Crushing extends north and south of the ring flange to where post tensioned bolts terminate and east and west of the column to the edges of the slab.

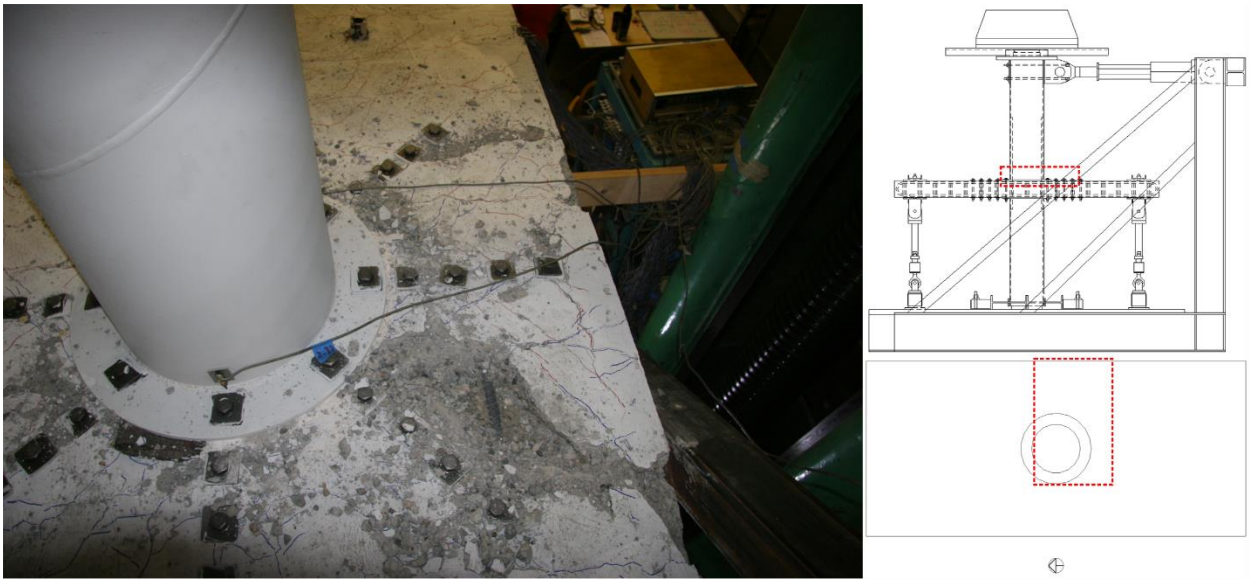

Figure 4-68: Top Southeast Side Joint Crushing – 6.7% Drift (PTB_4.5_1_4)

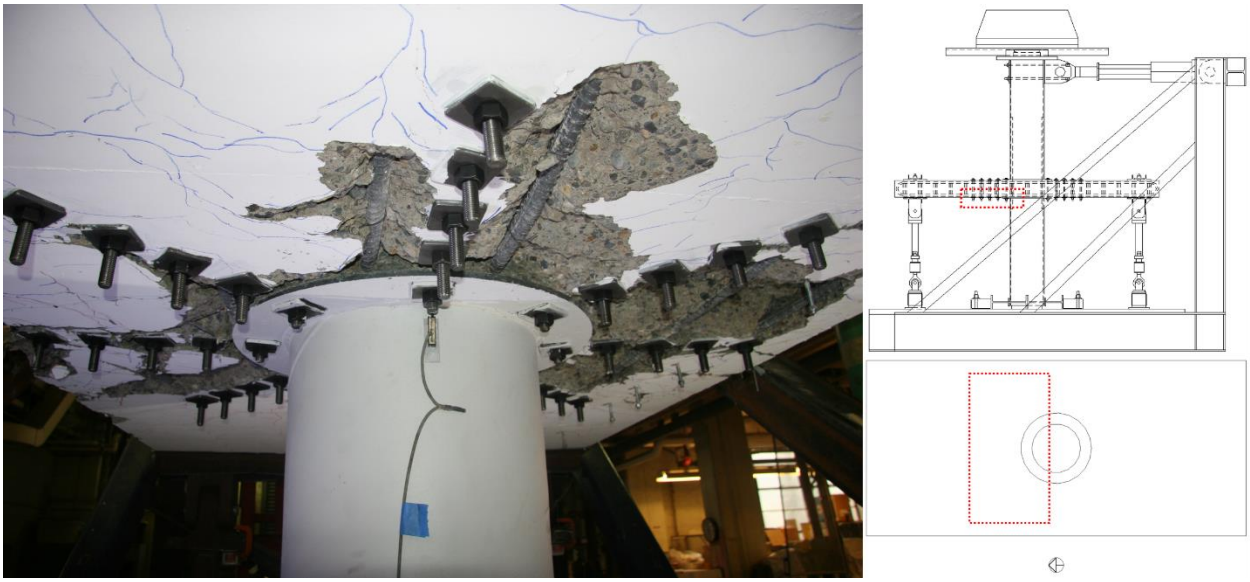

Figure 4-69: Bottom North Side Joint Crushing – 6.7% Drift (PTB_4.5_1_4)

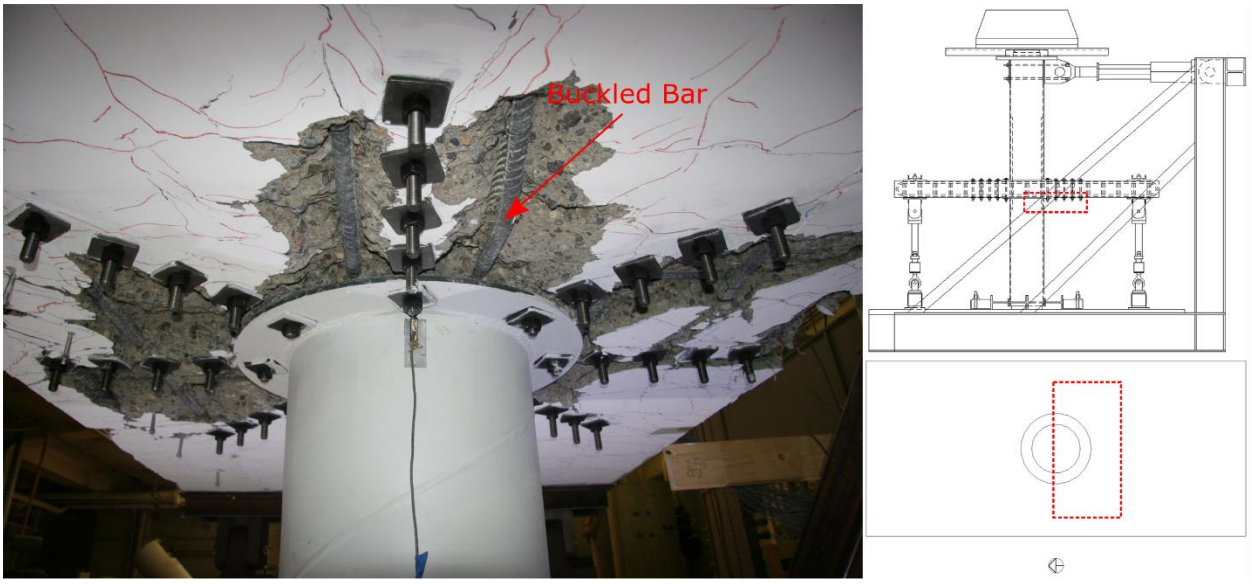

Figure 4-70: Bottom South Side Joint Crushing – 6.7% Drift (PTB_4.5_1_4)

4.4.7 *Test Summary*

PTB_4.5_1_4 reached a drift range of 13.4% (-6.7% to 6.7%). Cracking occurred shortly after the beginning of testing, with some cracking observed during the first two cycles (+0.34/-0.49% drift) followed by cracking across the width of the specimen by the third and fourth cycles (+0.56/-0.71% drift). Yielding first occurred in the longitudinal reinforcement passing through the slab-column joint at 1.9% drift. There was minimal visible damage until spalling began around the ring at 2.0% drift. The maximum lateral force resistance occurred at a drift of -3.5%. All longitudinal bars had yielded by 4.1% drift. Crushing began at 4.9% and the crushed region grew until the test was terminated at 6.7% drift due to equipment limits being reached.

4.5 SPECIMEN PTB_9_2_0

Specimen PTB_9_2_0 was tested August 28th, 2019 in the Structural Research Laboratory at the University of Washington. The test was performed 76 days after casting the slab and lower column and 56 days after casting the upper column.

4.5.1 *Specimen Overview*

The test went smoothly for the most part, however there was one interruption other than those planned (for marking cracks or initializing the next cycle). Halfway through cycle 10, the second cycle with a target drift of 2.2%, the hydraulic pump running the MTS Actuator overheated and needed to cool down. This pause had no significant impact on the test and any associated effects have been removed from the data. The induced drift and applied lateral loads can be seen in Figure 4-71 and Figure 4-72, respectively.

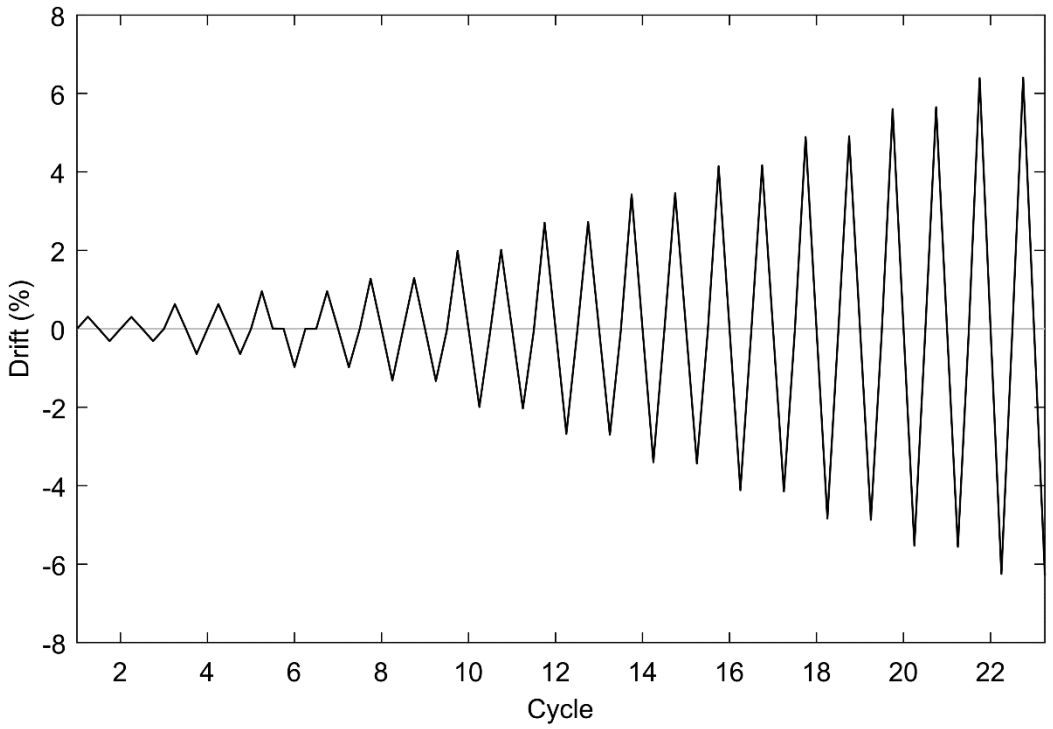

Figure 4-71: Induced Drift (PTB_9_2_0)

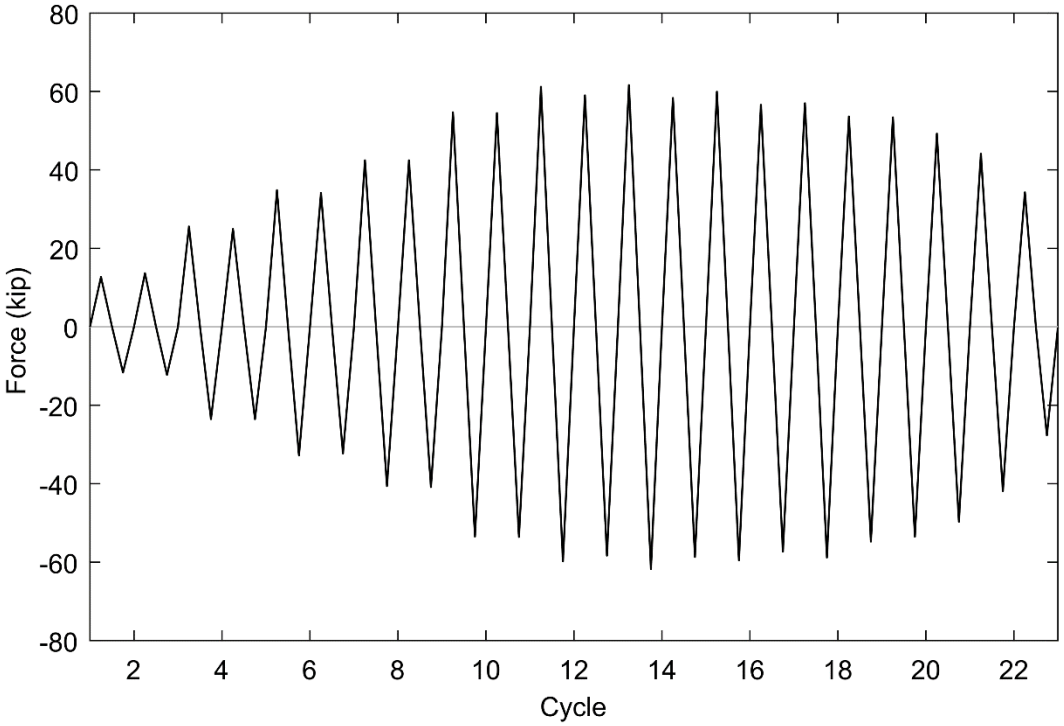

Figure 4-72: Applied Lateral Load (PTB_9_2_0)

It can be seen from Figure 4-72 that PTB_9_2_0 had a maximum resistance of 62.2 kip. The specimen completed 22 full cycles before the test was terminated due to reaching the limits of the MTS Actuator stroke. The connection's lateral force resistance increased until it reached a maximum resistance in cycle 13 at which point the connection began to lose strength. At the termination of testing, 52.9% of lateral force resisting capacity had been lost. The maximum lateral force resistances and drifts recorded during each cycle can be seen in Table 4.17. Table 4.17 and Figure 4-72 show a drop in resistance during second cycle of a target drift, possibly indicating irrecoverable damage occurred during the previous cycle.

Table 4.17: Maximum Resistances and Drifts in Each Cycle (PTB_9_2_0)

Cycle	Maximum Measured Resistance (kips)		Maximum Drift (%)	
	Tension	Compression	Tension	Compression
1	12.7	- 11.6	0.31	- 0.31
2	13.6	- 12.3	0.30	- 0.31
3	25.5	- 23.5	0.63	- 0.64
4	24.9	- 23.5	0.63	- 0.64
5	34.8	- 32.8	0.96	- 0.97
6	34.1	- 32.6	0.95	- 0.98
7	42.4	- 40.3	1.3	- 1.3
8	42.4	- 40.9	1.3	- 1.3
9	54.7	- 53.5	2.0	- 2.0
10	54.5	- 53.6	2.0	- 2.0
11	61.2	- 59.8	2.7	- 2.7
12	59.0	- 58.3	2.7	- 2.7
13	61.6	- 62.2	3.4	- 3.4
14	58.3	- 58.7	3.5	- 3.4
15	59.9	- 59.5	4.1	- 4.1
16	56.6	- 57.3	4.2	- 4.1
17	57.0	- 58.8	4.9	- 4.8
18	53.6	- 54.7	4.9	- 4.9
19	53.4	- 53.7	5.6	- 5.5
20	49.2	- 49.7	5.6	- 5.6
21	45.4	- 43.3	6.4	- 6.2
22	34.4	- 29.3	6.4	- 6.3

It can be seen from Table 4.17 that the maximum drift achieved was 6.3%. It is thought that the failure was ultimately one-way shear after first undergoing a flexural response. The following section will present the progression of damage through the testing of PTB_9_2_0. The force-drift hysteresis curve of the slab column connection is shown Figure 4-73 and a modified force-drift hysteresis curve with P-Δ effects from the column axial load removed is shown in Figure 4-74. Force has been normalized against the nominal moment capacity of the slab predicted by ACI 318-14 Figure 4-74 shows that after reaching peak lateral force resistance at 3.5% drift,

PTB_4.5_1_4 maintains a nearly consistent level of lateral force resistance until beginning to lose strength 6.3% drift.

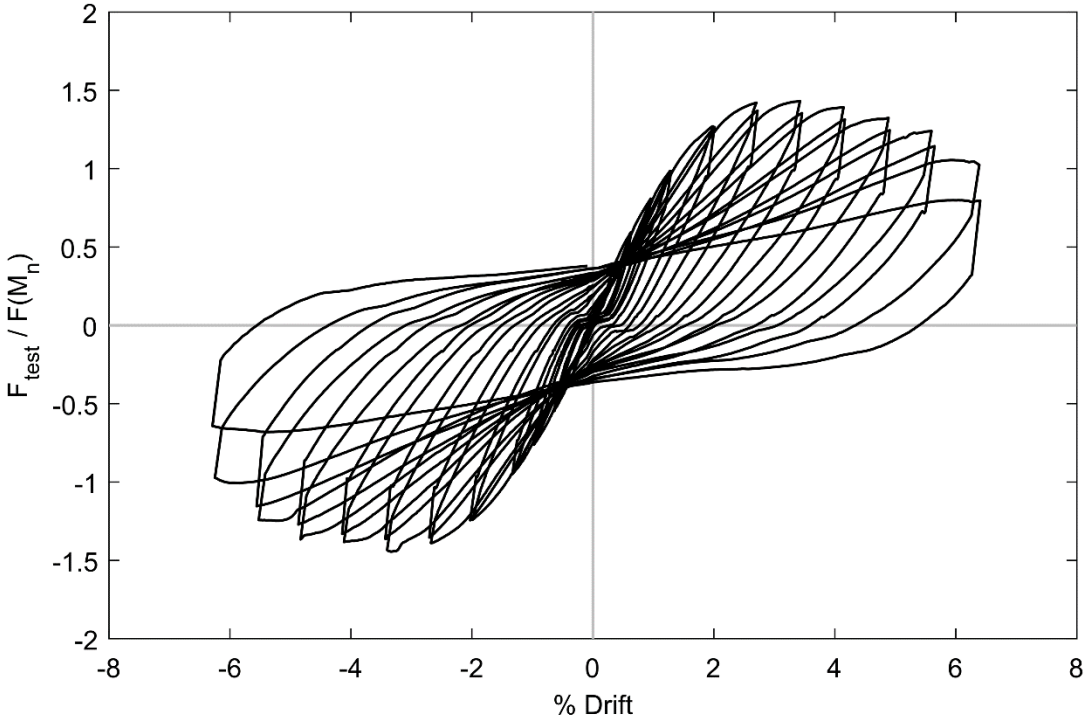

Figure 4-73: Normalized Drift Response (PTB_9_2_0)

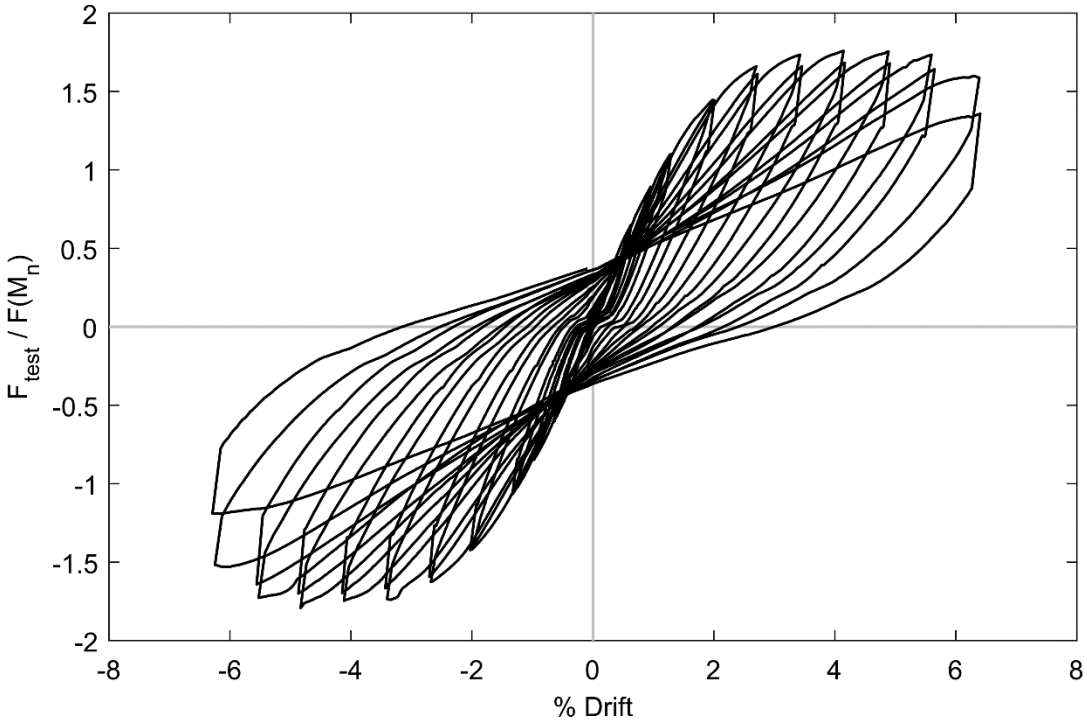

Figure 4-74: Normalized Drift Response with P-Δ Effects Removed (PTB_9_2_0)

4.5.2 *Specimen Performance State Summary*

The performance state summary for PTB_9_2_0 can be seen in Table 4.18.

Table 4.18: Summary of Damage (PTB_9_2_0)

Damage state	Drift (%)
Cracking	0.73 - 3.6
Yielding	2.2 – 4.4
Spalling	3.6
Crushing	5.1
Bar Buckling	6.5

4.5.3 *Low Drift Cycles (0.0% - 1.5% Target Drift)*

Cycle 1 (+0.31/-0.31% drift) was run without interruption and a small amount of cracking was first observed when the test was paused at peak displacements during cycle 2 (+0.30/-0.31% drift). Cracks patterns and typical crack sizes were recorded and the next drift levels was initiated. The largest cracks noted while pausing at the peak southern drift of cycle 2 opened 0.1 mm and were located on the top of the slab to the northwest and northeast of the column. The largest cracks noted while pausing at the peak northern drift opened 0.1 mm and were located on the top of the slab to the southwest and southeast of the column. Typical crack sizes recorded during pauses at peak drifts throughout low drift cycles are recorded in Table 4.19.

Table 4.19: Low Drift Cycle Typical Crack Opening at Peaks (PTB_9_2_0)

Cycle	Drift (%)		Bottom (mm)		Top (mm)		Side (mm)	
	South	North	South	North	South	North	South	North
2	0.30	- 0.31	0.05	0.1	0.01	0.1	0.1	0.1
4	0.63	- 0.64	0.1	0.1	0.1	0.1	0.1	0.1
6	0.95	- 0.98	0.25	0.3	0.25	0.3	0.25	0.3
8	1.3	- 1.3	0.3	0.3	0.3	0.4	0.3	0.3

Cycle 3 (+0.63/-0.64% drift) was then run and stage 1 cracking occurred during cycle 4 (+0.63/-0.64% drift). Cracking initially began near the edge of the ring flange and propagated outward across the slab. Crack patterns are shown in Figure 4-75 and Figure 4-76. The largest cracks noted while pausing at the peak southern drift of cycle 4 opened 0.3 mm and were located on the top of the slab to the northwest and northeast of the column. The largest cracks noted while pausing at the peak northern drift of cycle 4 opened 0.3 mm and were located on the top of the slab southwest and southeast of the column.

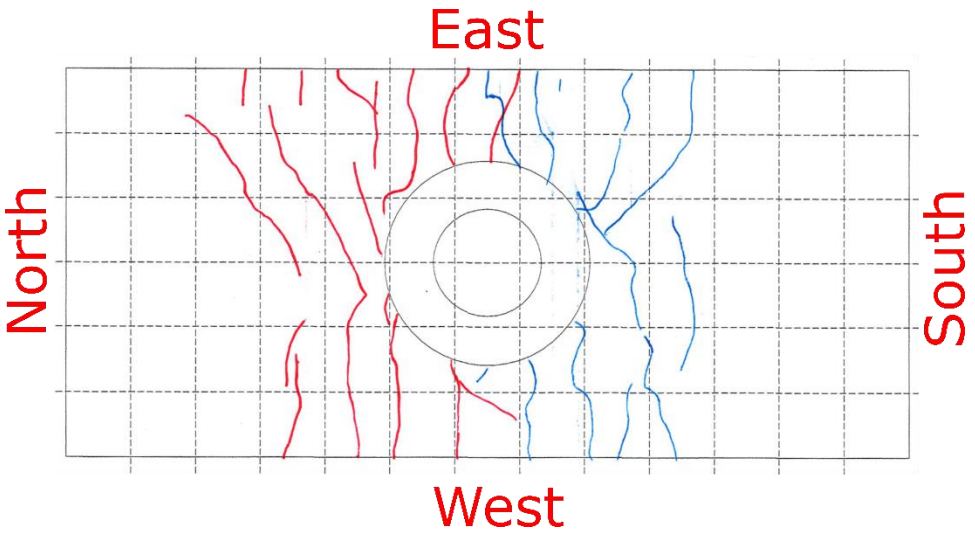

Figure 4-75: Top of Slab Crack Map – 0.64% Drift (PTB_9_2_0)

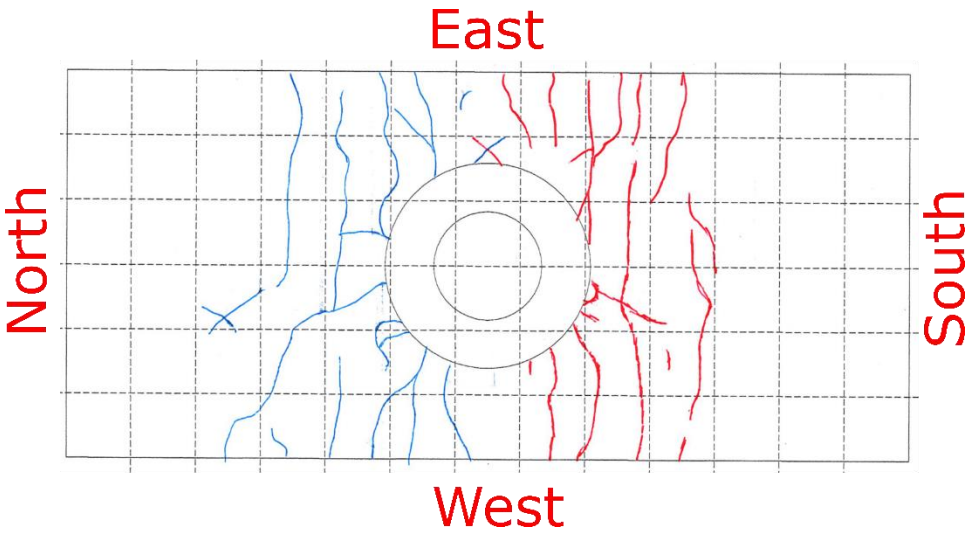

Figure 4-76: Bottom of Slab Crack Map – 0.64% Drift (PTB_9_2_0)

Cycle 5 (+0.96/-0.97% drift) was run before continuing to cycle 6 (+0.95/-0.98% drift). Cycle 6 was paused at peak drifts, crack sizes were recorded and crack maps updated. The largest cracks noted while pausing at the peak southern drift of cycle 6 opened 0.5 mm and were located on the top of the slab northeast and southeast of the column. The largest crack noted while pausing at the peak northern drift of cycle 6 opened 0.5 mm and was located on the top of the slab south of the column.

Cycle 7 (+1.3/-1.3% drift) was then run without pauses. Cycle 8 (+1.3/-1.3% drift) was then performed with pauses at peak drifts to update crack maps and measure cracks. The largest crack noted while pausing at the peak southern drift of cycle 8 opened 0.75 mm and was located on the top of the slab northeast of the column. The largest crack noted while pausing at the peak northern drift of cycle 8 opened 0.6 mm and was located on the top of the slab southeast of the column.

4.5.4 *Moderate Drift Cycles (1.5% - 3.6% Target Drift)*

Moderate drift cycles initiated with cycle 9 (+2.0/-2.0% drift) which was completed uninterrupted. Once strain gauge data was analyzed, it was discovered that a gauge indicated yielding of flexural reinforcement in the top and bottom of the slab at the peak southern drift of cycle 9. As shown in Figure 4-77 and Figure 4-78, yielding occurred north and south of the column in top and bottom longitudinal reinforcement and south of the column, under the ring flange in bottom longitudinal reinforcement.

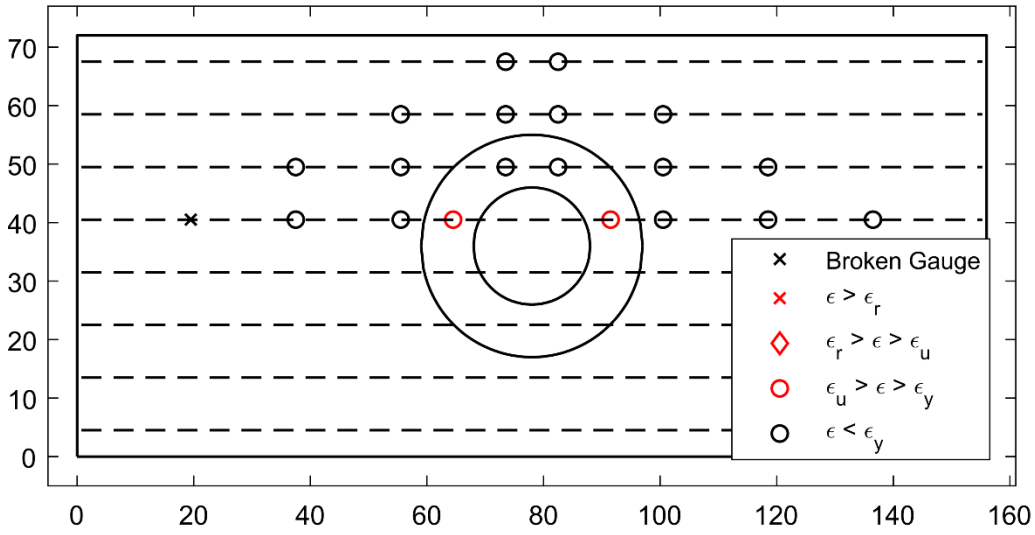

Figure 4-77: Top Reinforcement Strain Summary – 2.0% Drift (PTB_9_2_0)

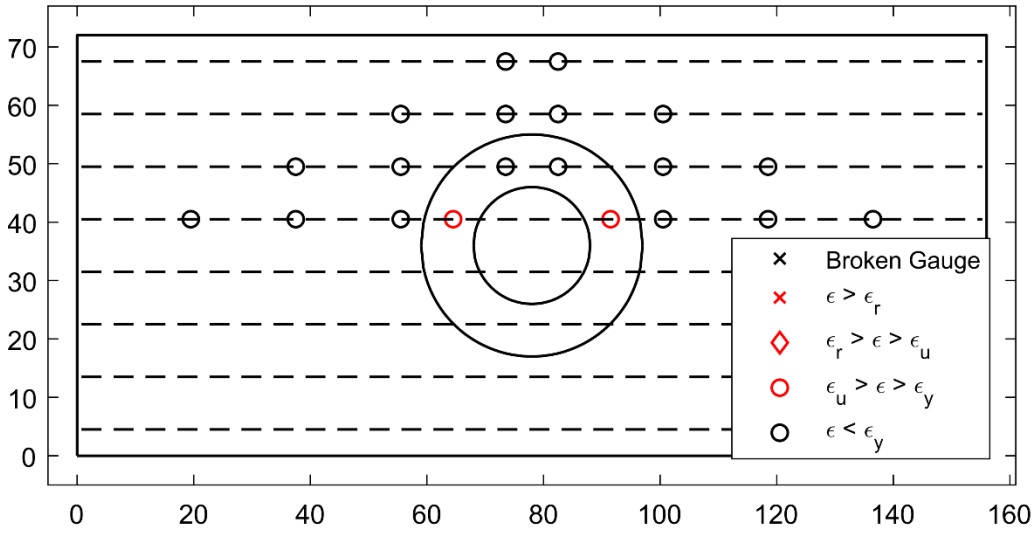

Figure 4-78: Bottom Reinforcement Strain Summary – 2.0% Drift (PTB_9_2_0)

Cycle 10 (+2.0/-2.0% drift) was paused at peak drifts, crack sizes were recorded and crack maps updated. The largest crack noted while pausing at the peak southern drift of cycle 10 opened 1.25 mm and was located on the top of the slab northwest of the column. The largest cracks noted while pausing at the peak northern drift of cycle 10 opened 0.75 mm and were located on the top of the slab southeast and southwest of the column. Typical crack sizes recorded during moderate drift cycles are listed in Table 4.20.

Table 4.20: Moderate Drift Cycle Typical Crack Opening at Peaks (PTB_9_2_0)

Cycle	Drift (%)		Bottom (mm)		Top (mm)		Side (mm)	
	South	North	South	North	South	North	South	North
10	2.0	- 2.0	0.4	0.4	0.6	0.5	0.5	0.4
12	2.7	- 2.7	0.5	NA	0.5	0.5	NA	NA
14	3.5	- 3.4	0.6	0.6	0.75	0.25	0.6	0.6

By the completion of cycle 10, cracking had grown to cover the top and bottom of the slab as shown in Figure 4-79 and Figure 4-80.

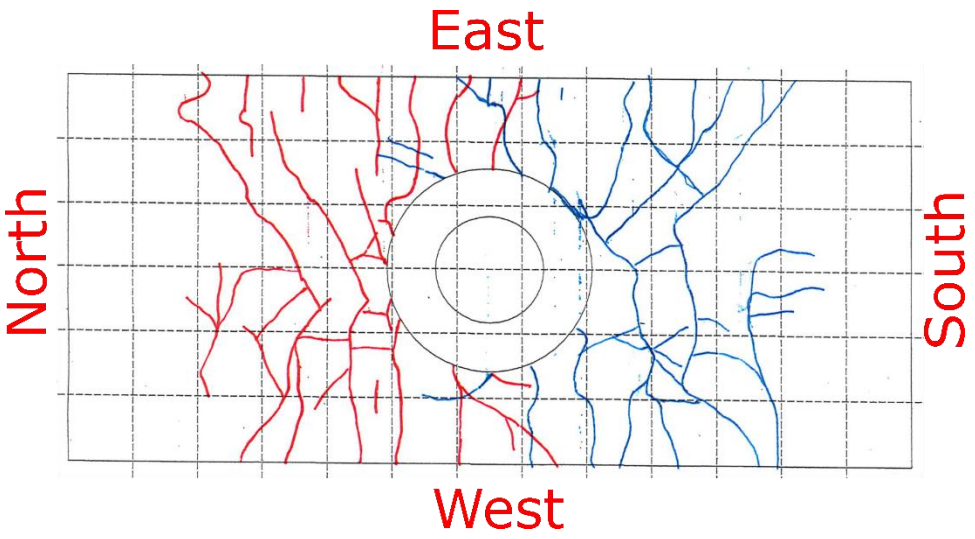

Figure 4-79: Top of Slab Crack Map – 2.0% Drift (PTB_9_2_0)

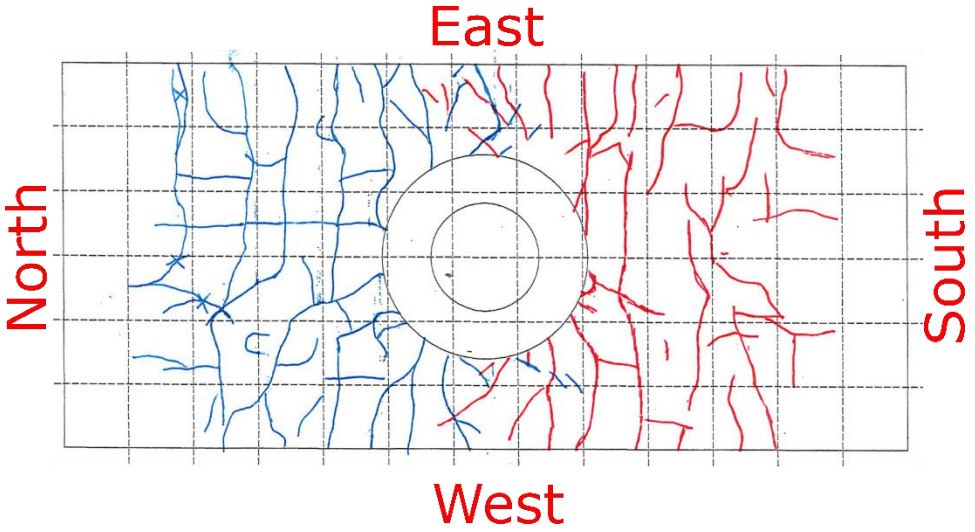

Figure 4-80: Bottom of Slab Crack Map – 2.0% Drift (PTB_9_2_0)

Cycle 11 (+2.7/-2.7% drift) was then run. Strain gauge data indicates that at the peak southern drift of cycle 11, yielding of flexural reinforcement in the slab had occurred in four of eight bars that were gauged. As shown in Figure 4-81 and Figure 4-82, yielding is indicated under the ring flange and to the north, south and east of the column in the top and bottom reinforcement.

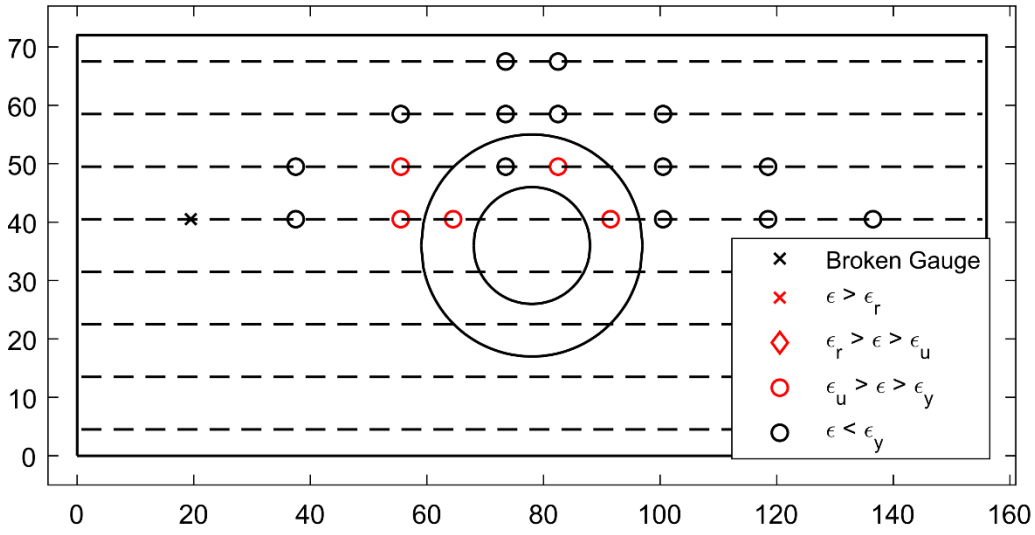

Figure 4-81: Top Reinforcement Strain Summary – 2.7% Drift (PTB_9_2_0)

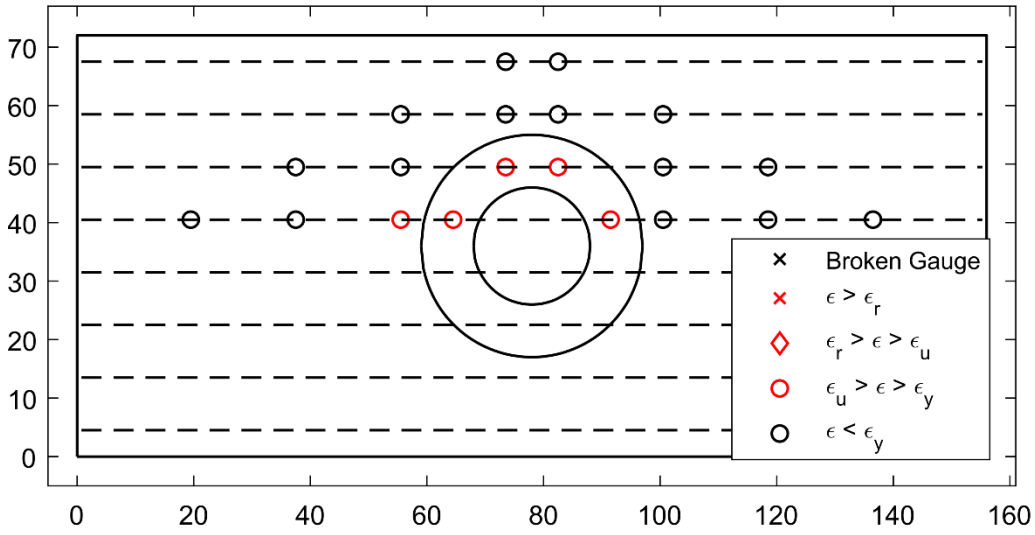

Figure 4-82: Bottom Reinforcement Strain Summary – 2.7% Drift (PTB_9_2_0)

Cycle 12 (+2.7/-2.7% drift) was then performed with pauses at peak drifts to update crack maps and measure cracks. The largest cracks noted while pausing at the peak southern drift of cycle 12 opened 2 mm and were located on the top of the slab north and northeast of the column.

The largest cracks noted while pausing at the peak northern drift of cycle 12 opened 1.25 mm and were located on the top of the slab southwest and southeast of the column.

Cycle 13 (+3.4/-3.4% drift) was then run without interruption. Cycle 14 (+3.5/-3.4% drift) was then performed with pauses at peak drifts to update crack maps and measure cracks. The largest cracks noted while pausing at the peak southern drift of cycle 14 opened 1.25 mm and were located on the top of the slab northwest and northeast of the column. The largest crack noted while pausing at the peak northern drift of cycle 14 opened 3.0 mm and was located on the top of the slab south of the column. After comparing the crack patterns recorded during cycle 14 to those recorded throughout the remainder of the test, it was determined that stage 2 cracking was occurred in cycle 14. Crack maps for cycle 14 are shown in Figure 4-83 and Figure 4-84.

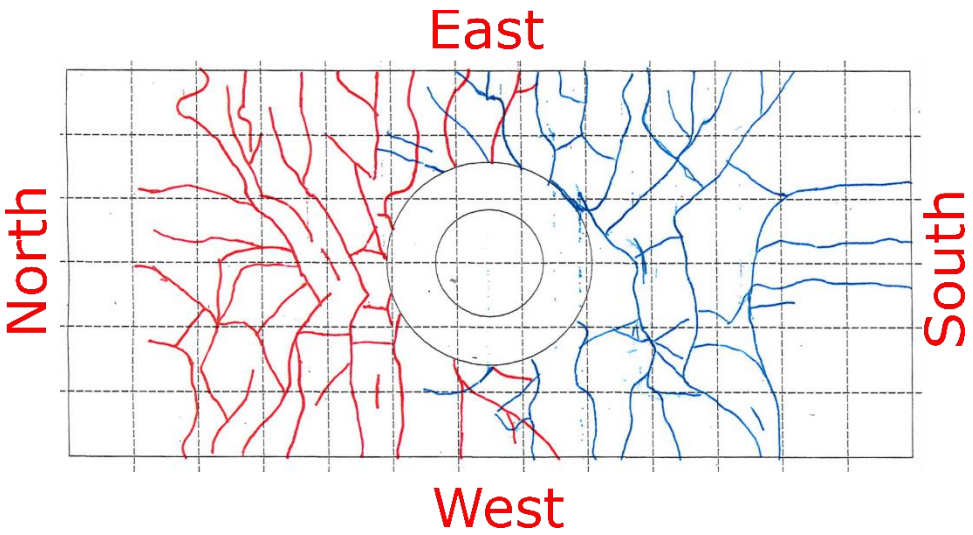

Figure 4-83: Top of Slab Crack Map – 3.4% Drift (PTB_9_2_0)

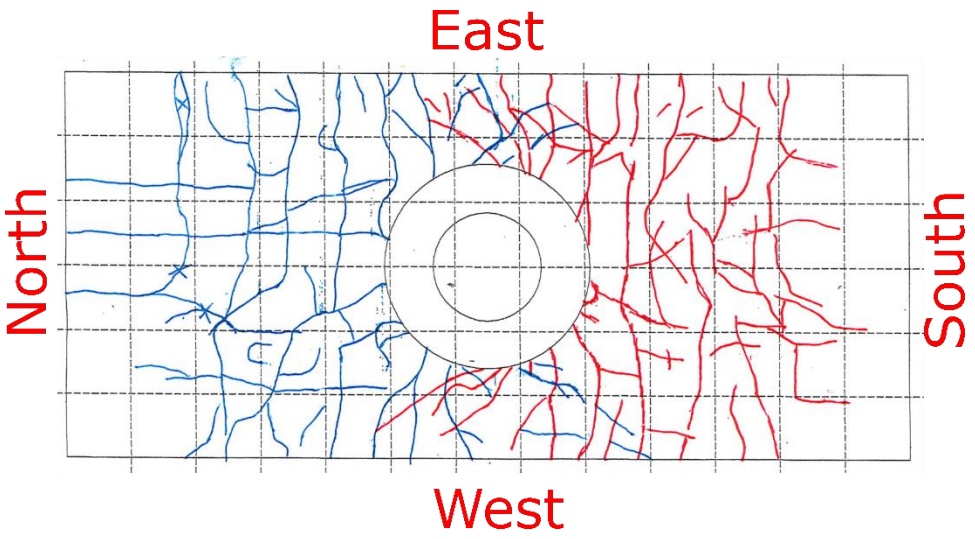

Figure 4-84: Bottom of Slab Crack Map – 3.4% Drift (PTB_9_2_0)

The onset of spalling was also noted during the pause at the northern peak drift in cycle 14. The first spalling occurred on the bottom of the slab on the north side of the slab-column joint as shown in Figure 4-85.

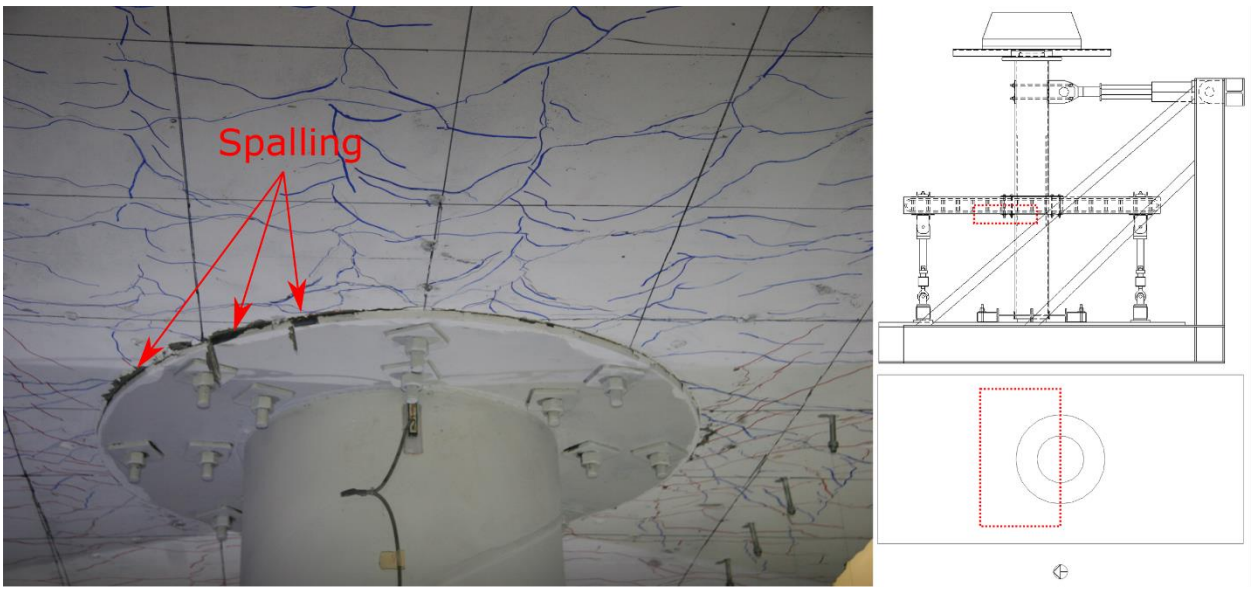

Figure 4-85: Bottom Joint North Side Spalling – 3.4% Drift (PTB_9_2_0)

4.5.5 *High Drift Cycles (Greater than 3.6% Target Drift)*

High drift cycles initiated with cycle 15 (+4.1/-4.1% drift) which was completed uninterrupted. Strain gauge data indicates that at the peak southern drift of cycle 15, yielding of flexural reinforcement in the slab had occurred in all bottom bars that were gauged. As shown in Figure 4-86 and Figure 4-87, yielding is indicated under the ring flange and to the north, south, and east of the column in the top and bottom reinforcement.

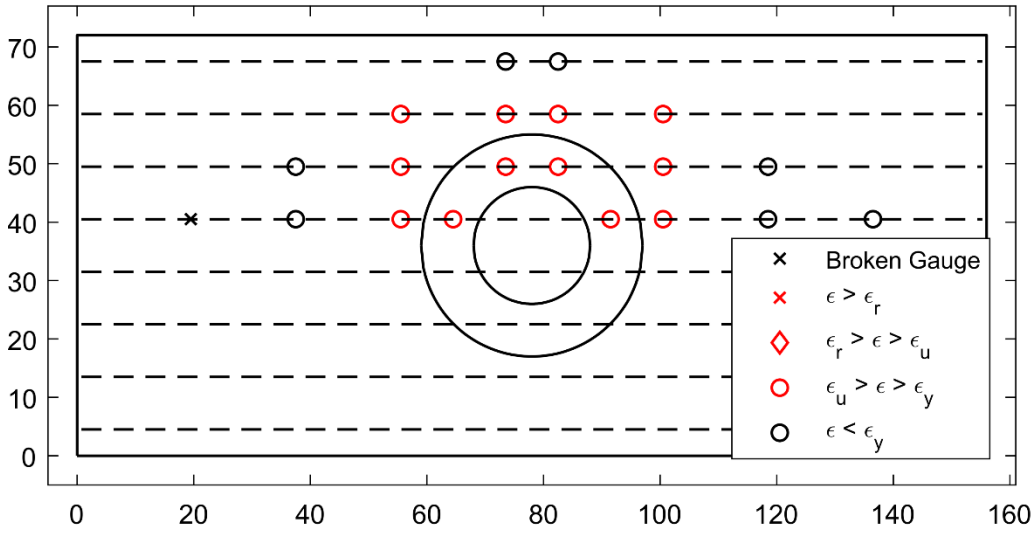

Figure 4-86: Top Reinforcement Strain Summary – 4.1% Drift (PTB_9_2_0)

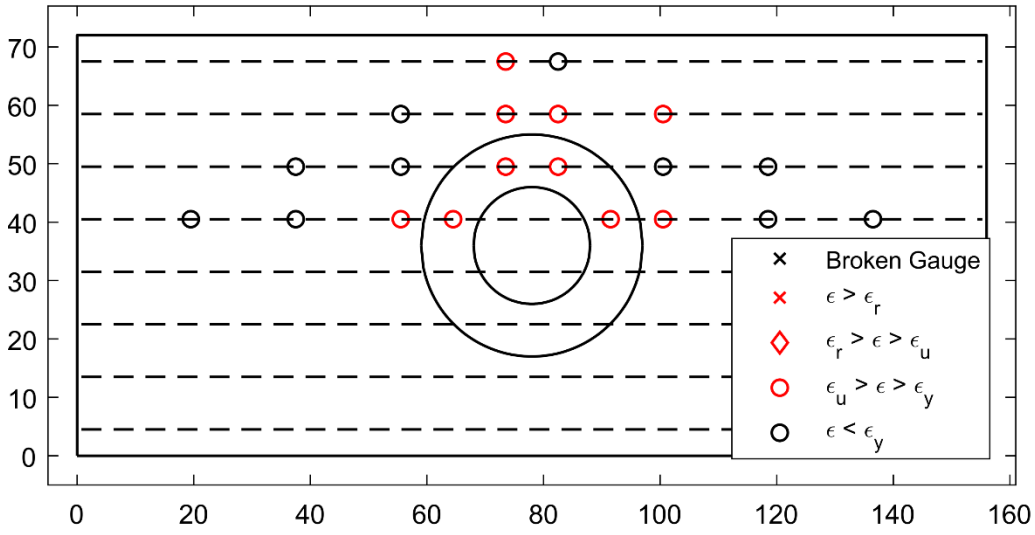

Figure 4-87: Bottom Reinforcement Strain Summary – 4.1% Drift (PTB_9_2_0)

Cycle 16 (+4.2/-4.1% drift) was paused at peak drifts, crack sizes were recorded and crack maps updated. The largest cracks noted while pausing at the peak southern drift of cycle 16 opened 2 mm and were located on the top of the slab northwest and northeast of the column. The largest cracks noted while pausing at the peak northern drift of cycle 16 opened 1.5 mm and were located on the top of the slab southwest and southeast of the column. Typical crack sizes recorded during high drift cycles are listed in Table 4.21.

Table 4.21: High Drift Cycle Typical Crack Opening at Peaks (PTB_9_2_0)

Cycle	Drift (%)		Bottom (mm)		Top (mm)		Side (mm)	
	South	North	South	North	South	North	South	North
16	4.2	- 4.1	0.75	0.75	0.75	0.75	0.5	0.5
18	4.9	- 4.9	0.75	0.75	0.75	0.75	0.5	0.5
20	5.6	- 5.6	1.0	1.0	1.5	1.0	0.75	0.75

Additional spalling was also noted during the norther pause in cycle 16. The spalling occurred to the west of the slab column joints as shown in Figure 4-88.

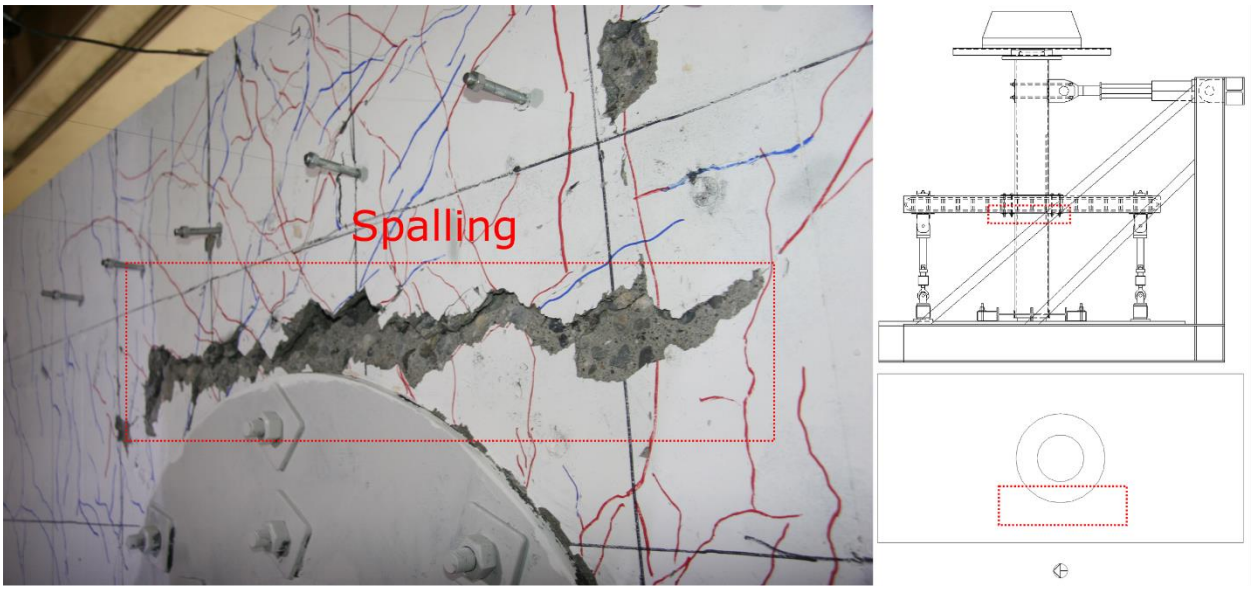

Figure 4-88: Bottom Joint West Side Spalling – 4.1% Drift (PTB_9_2_0)

Cycle 17 (+4.9/-4.8% drift) was then run before continuing to cycle 18 (+4.9/-4.9% drift). Cycle 18 was paused at peak drifts, crack sizes were recorded and crack maps updated. The largest crack noted while pausing at the peak southern drift of cycle 18 opened 3 mm and was located on the top of the slab northwest of the column. The largest crack noted while pausing at the peak northern drift of cycle 18 opened 3 mm and was located on the top of the slab southeast of the column. The onset of crushing was noted during the pauses in cycle 18. The first crushing occurred on the bottom of the slab to the north and west of the slab-column joint. Figure 4-89 shows the northern side of the connection while Figure 4-90 shows the western side of the connection. Exposed longitudinal reinforcement is visible in Figure 4-89 and Figure 4-90.

Figure 4-89: Bottom Joint North Side Crushing – 4.9% Drift (PTB_9_2_0)

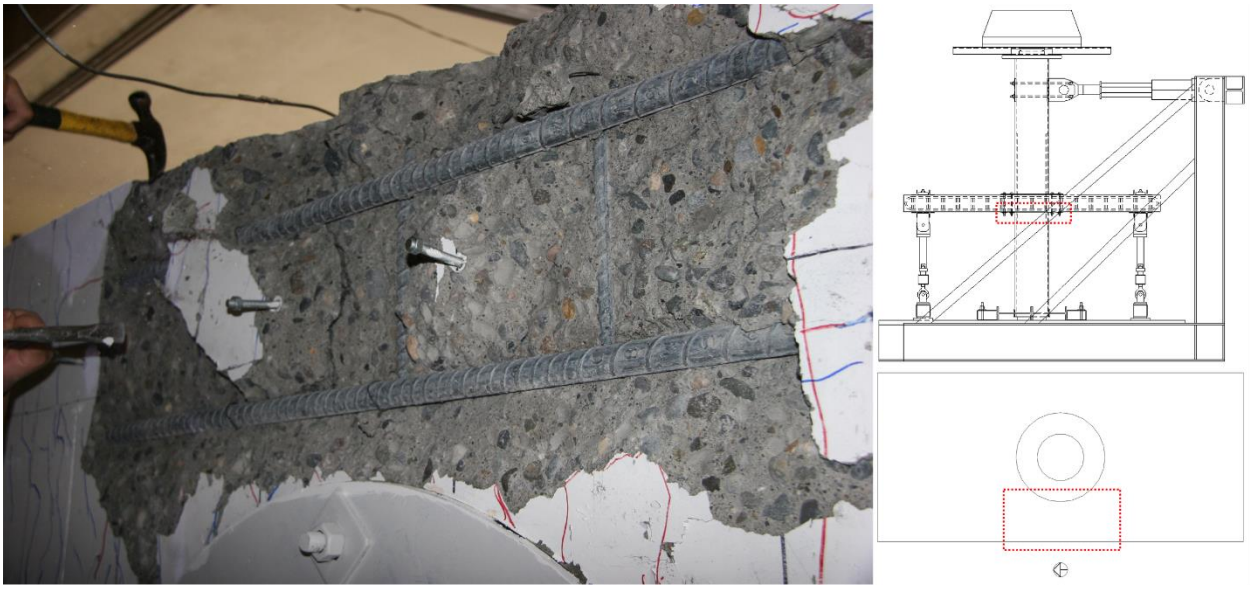

Figure 4-90: Bottom Joint West Side Crushing – 4.9% Drift (PTB_9_2_0)

Cycle 19 (+5.6/-5.5% drift) was then run before continuing to cycle 20 (+5.6/-5.6% drift). Cycle 20 was paused at peak drifts, crack sizes were recorded and crack maps updated. The largest crack noted while pausing at the peak southern drift of cycle 20 opened 3 mm and was located on the top of the slab northwest of the column. The largest crack noted while pausing at the peak northern drift of cycle 20 opened 4 mm and was located on the top of the slab southwest of the

column. A large diagonal crack to the east of the column on the edge of the specimen was noted during cycle 10 and is shown in Figure 4-91.

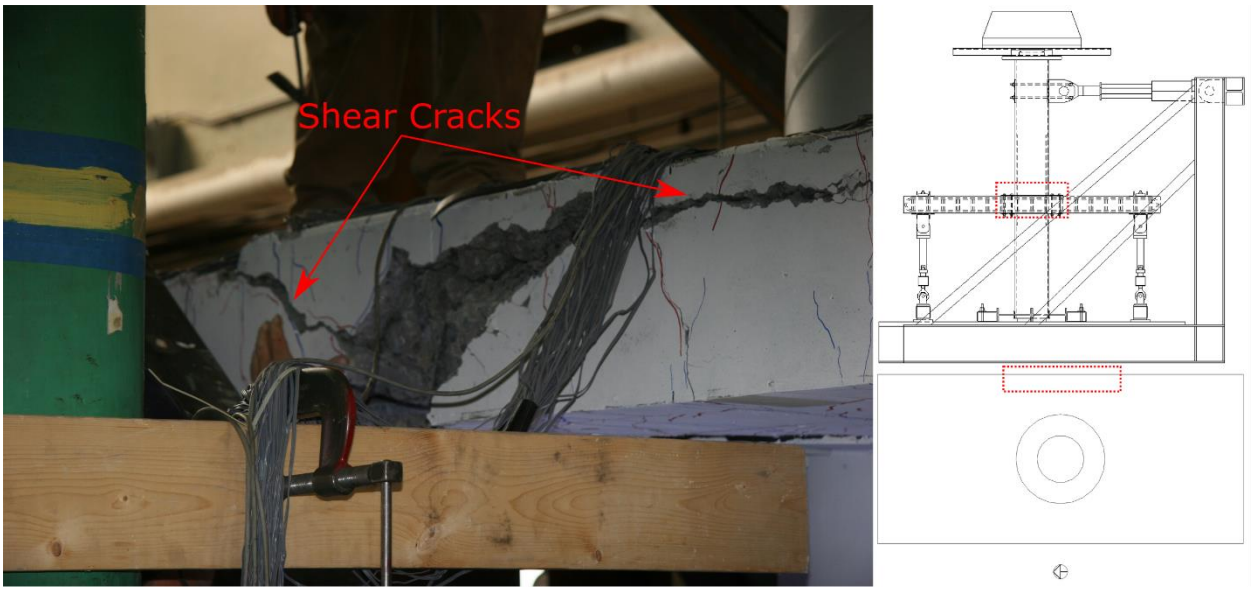

Figure 4-91: East Edge Shear Cracks – 5.6% Drift (PTB_9_2_0)

Cycle 21 (+6.4/-6.2% drift) was then run before continuing to cycle 22 (+6.4/-6.3% drift). Cycle 22 was paused at peak drifts and crack maps updated. The crushed region grew significantly on the top and bottom of the slab around the column joint during cycles 21 and 22. As a result, recording crack sizes became impractical. During pauses of cycle 22, it was noticed that bottom longitudinal reinforcement to the south of the column had buckled over a short length. Buckled reinforcement is pointed out in Figure 4-92. Testing was stopped after cycle 22 because equipment deformation limits had been reached. After completion of testing, crushing was further explored and measured.

Figure 4-92: Bottom South Side Bar Buckling – 6.4% Drift (PTB_9_2_0)

4.5.6 *Post-Test*

After the completion of testing, loose concrete around the slab-column joint was removed to explore the extent of damage. Figure 4-93 shows the crushing on the top of the slab to the north of the slab column joints. Crushing extends approximately 2 ft. north from the edge of the ring flange.

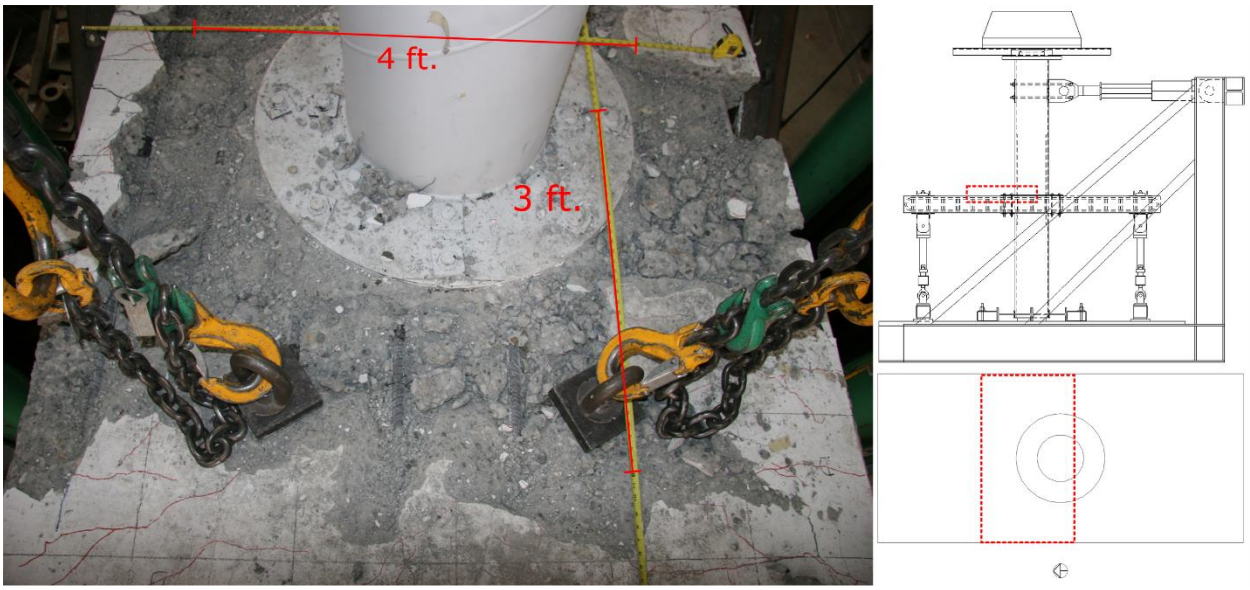

Figure 4-93: Top Joint North Side Crushing – 6.4% Drift (PTB_9_2_0)

Figure 4-94 shows crushing on the top of the slab to the south of the slab column joint. There is significantly less crushing the south of the column than north of the column.

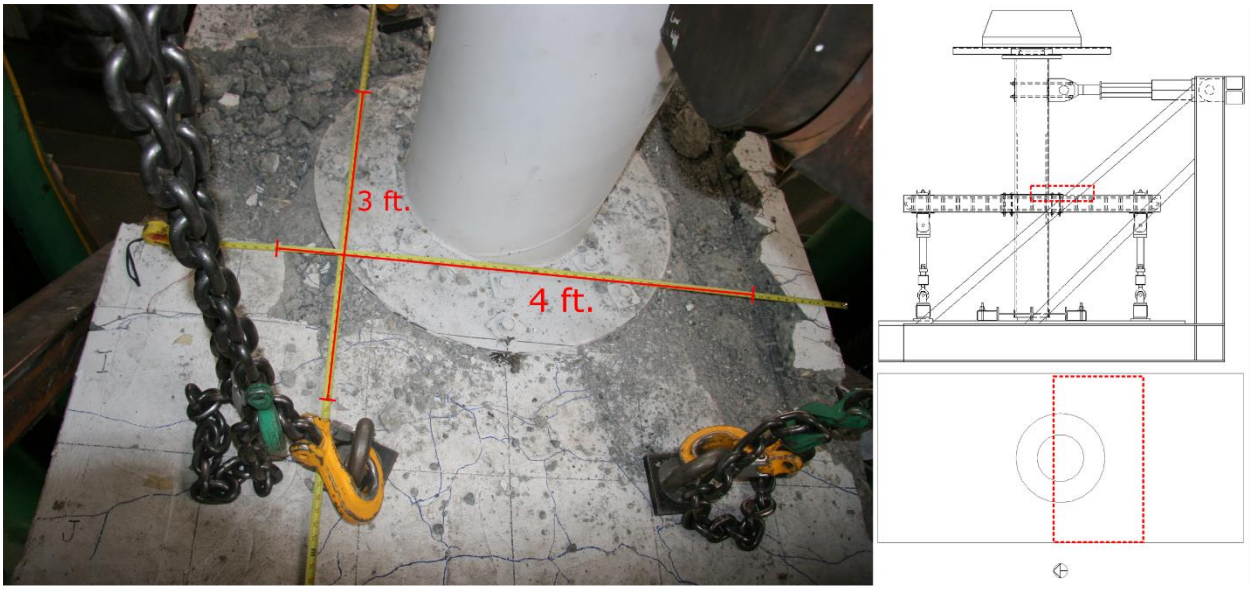

Figure 4-94: Top Joint South Side Crushing – 6.4% Drift (PTB_9_2_0)

Figure 4-95 and Figure 4-96 show crushing on the top of the slab to the west and east of the slab-column connection, respectively. Crushing extends from the edges of the ring flange to the edges of the specimen.

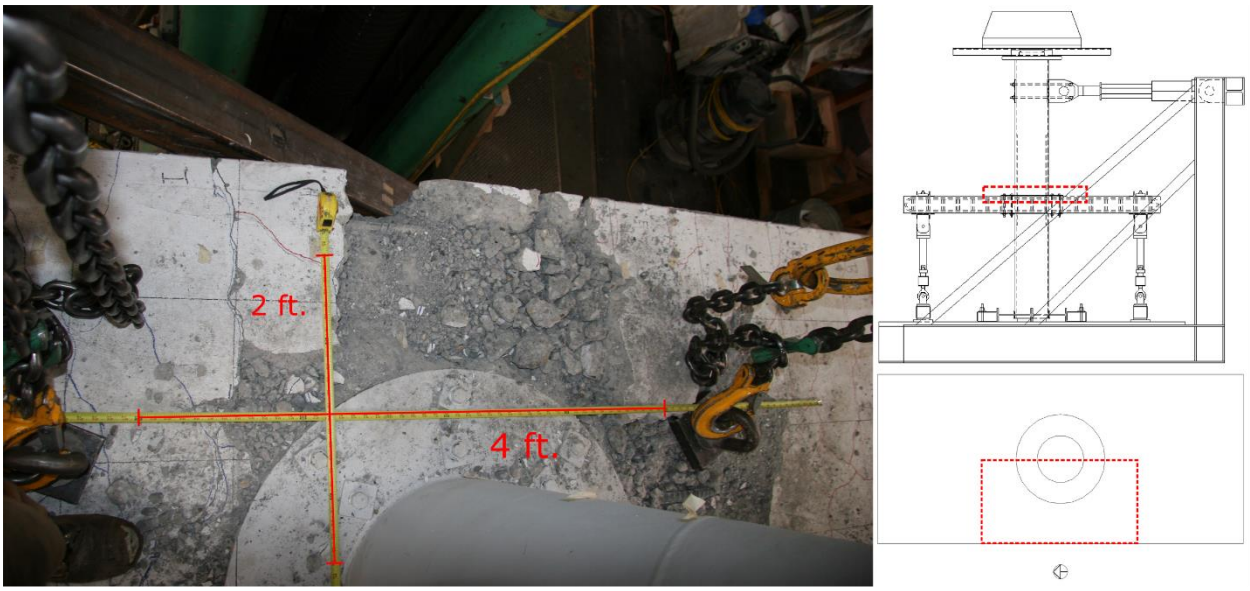

Figure 4-95: Top Joint West Side Crushing – 6.4% Drift (PTB_9_2_0)

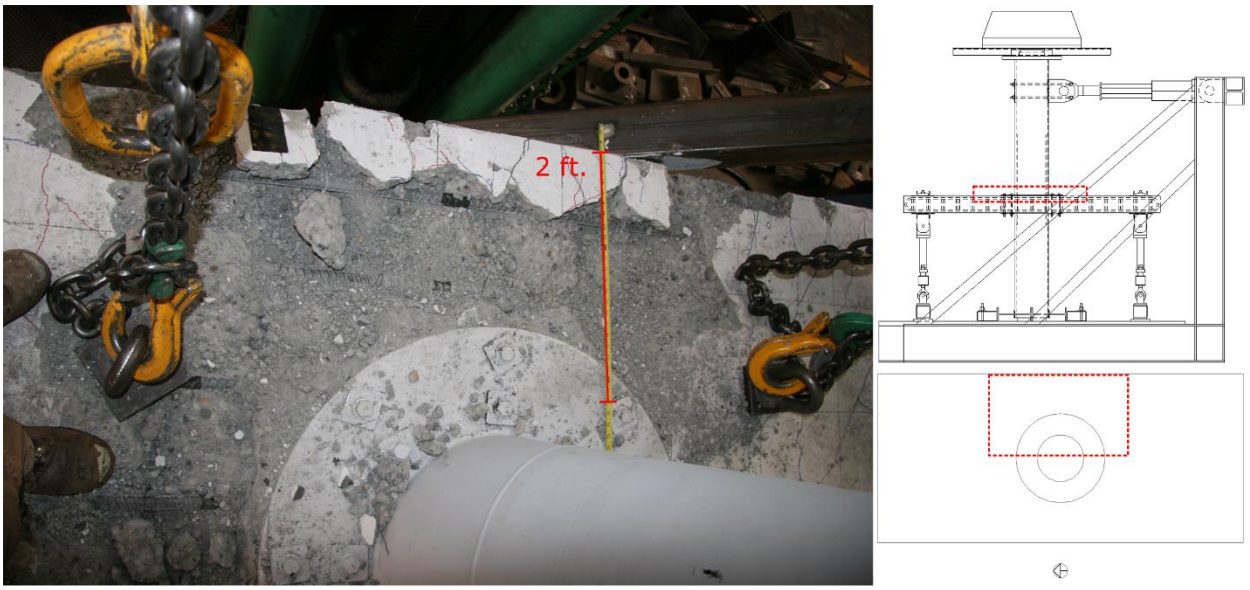

Figure 4-96: Top Joint East Side Crushing – 6.4% Drift (PTB_9_2_0)

Figure 4-97 shows crushing on the bottom of the slab to the north of the slab-column joint. Crushing extends north roughly 1.5 - 2 ft. from the edge of the ring flange.

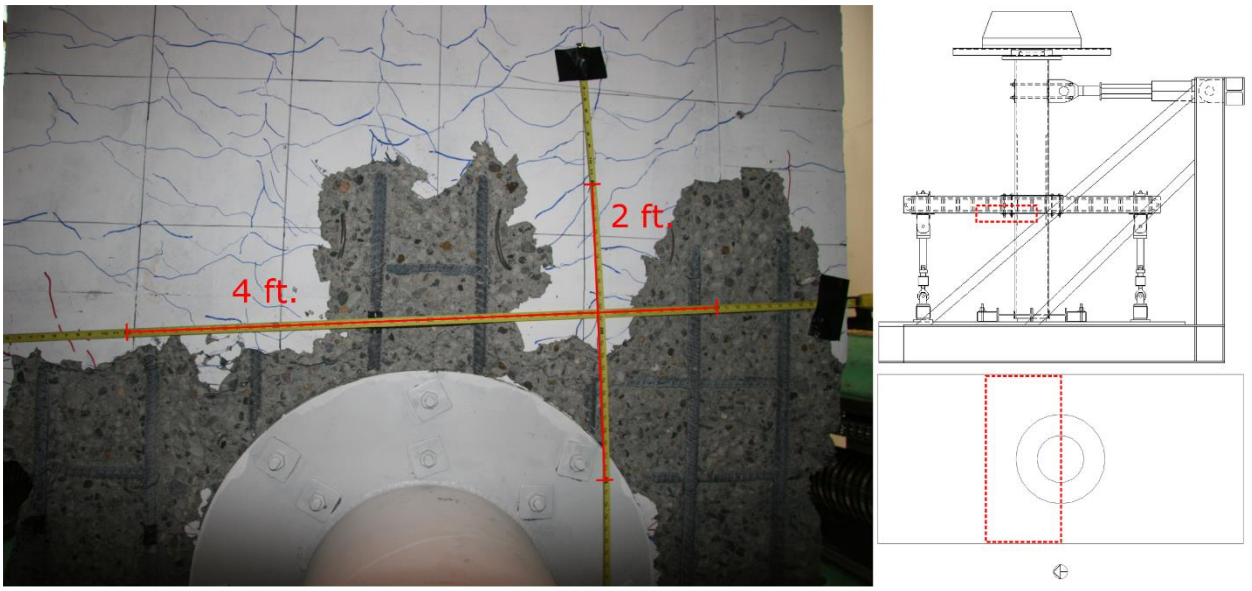

Figure 4-97: Bottom Joint North Side Crushing – 6.4% Drift (PTB_9_2_0)

Figure 4-98 shows crushing on the bottom of the slab to the south of the slab-column joint. There is less crushing on the south side of the connection than the north with damage extending only about 6 in. from the edge of the ring flange.

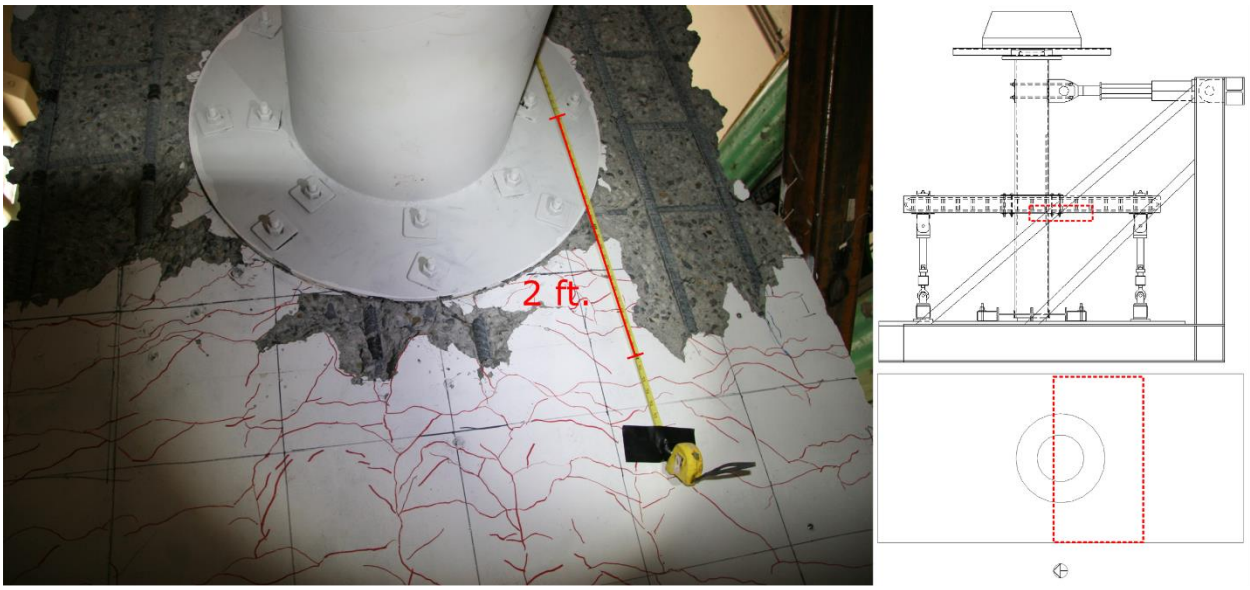

Figure 4-98: Bottom Joint South Side Crushing – 6.4% Drift (PTB_9_2_0)

Figure 4-99 and Figure 4-100 show crushing on the bottom of the slab to the west and east of the slab-column joint, respectively. Crushing extends from the edges of the ring flange to the edges of the specimen.

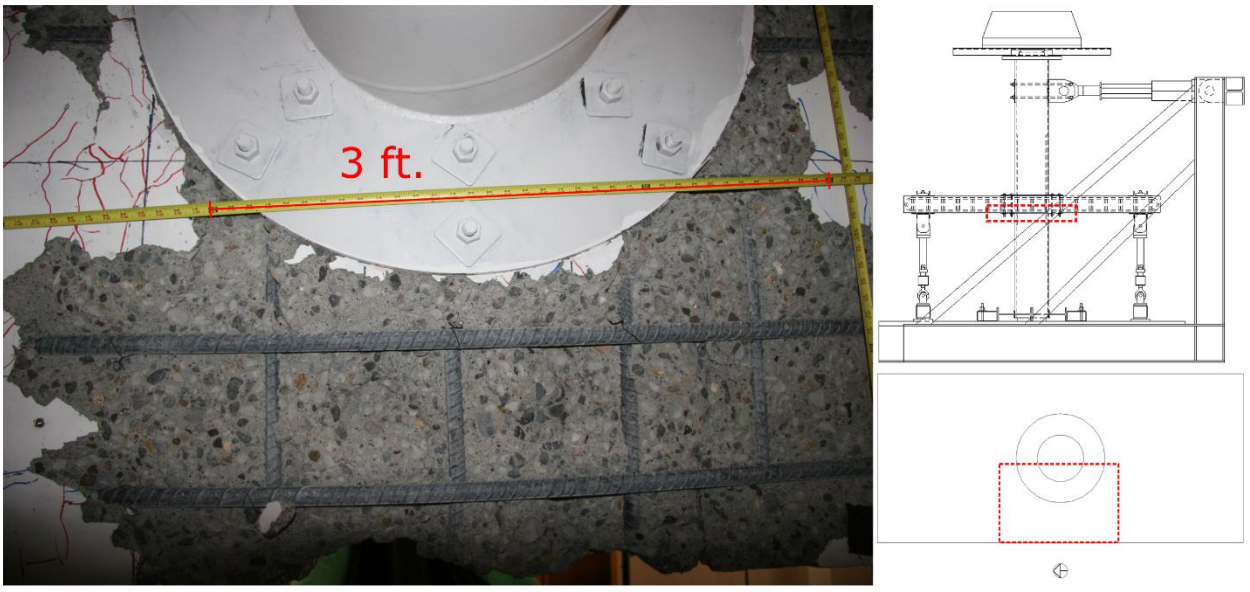

Figure 4-99: Bottom Joint West Side Crushing – 6.4% Drift (PTB_9_2_0)

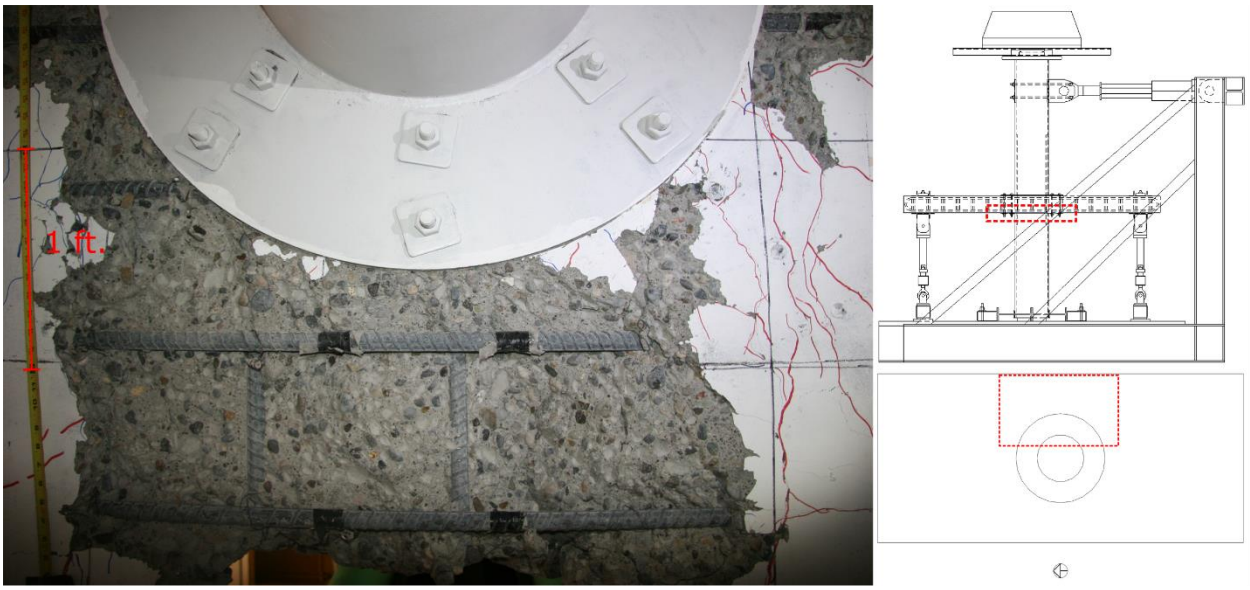

Figure 4-100: Bottom Joint East Side Crushing – 6.4% Drift (PTB_9_2_0)

Figure 4-101 and Figure 4-102 show the west and east edges of the slab, respectively. Large pieces of concrete have spalled off of both the west and east edges of the specimen as shown. The diagonal cracking and loss of concrete on the west and east edges are why it is thought PTB_9_2_0 ultimately failed in one-way shear after first undergoing a flexural response.

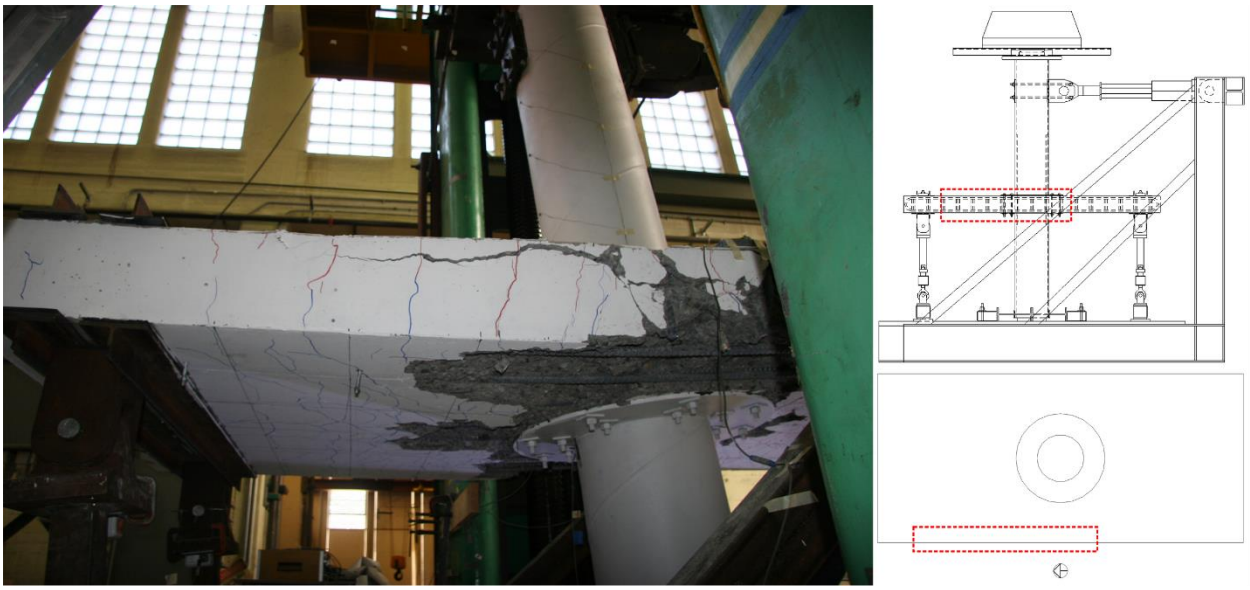

Figure 4-101: West Edge Joint Crushing – 6.4% Drift (PTB_9_2_0)

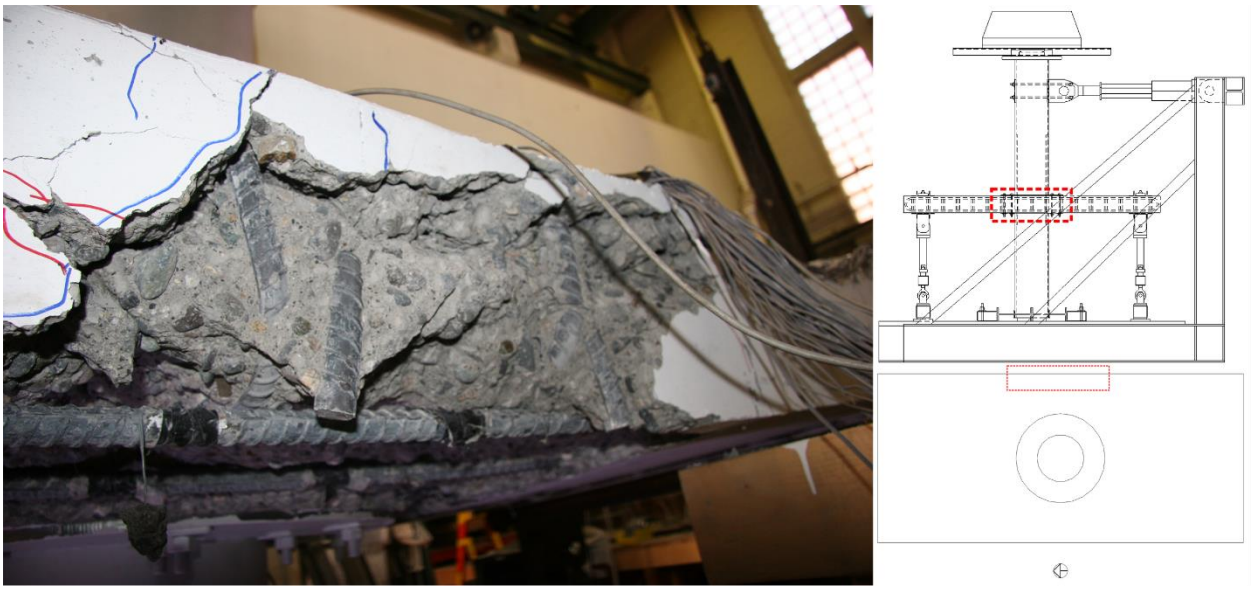

Figure 4-102: East Edge Joint Crushing – 6.4% Drift (PTB_9_2_0)

4.5.7 *Test Summary*

PTB_9_2_0 reached a drift range of 12.7% (-6.3% to 6.4%). Cracking occurred shortly after the beginning of testing, with some cracking observed during the first two cycles (+0.31/-0.31% drift) followed by cracking across the width of the specimen by the third and fourth cycles (+0.63/-0.64% drift). Yielding first occurred in the longitudinal reinforcement passing through the slab-column joint at 2.0% drift. Minimal damage was visible until 3.4% drift when maximum lateral force resistance was reached and the first spalling was observed around the ring flange. Yielding across the width of the slab occurred at 4.1% drift. Crushing began at 4.9% and the crushed region grew until the test was terminated at 6.4% drift due to equipment limits being reached and the 50% of lateral force resistance had been lost.

Chapter 5. DATA ANALYSIS

This chapter compares the measured response of the test specimens, including observed damage, system behavior, and local behavior. Damage levels are compared as a function of drifts using the damage states discussed in Chapter 4. The system behavior comparison is based on the (1) force-displacement response and (2) energy dissipation. Comparisons of the local behavior includes: (1) displaced shapes of the slab, and (2) strain distributions in the slab.

In all cases, Specimen SR_4_10_5 is considered the reference, since it simulates current design. Next, Specimen PTB_4.5_1_0 is compared; this specimen uses the smallest ring and the fewest PTBs. Following this, Specimen PTB_4.5_1_4 is compared to both of the prior specimens; this specimen uses more PTBs, which extend beyond the ACI 318 (ACI 2019) critical section. Finally, Specimen PTB_9_2_0 is compared with the three prior specimens; this specimen has the largest ring (twice the dimension of the other two specimens) with PTBs only on the ring.

5.1 DAMAGE

This section compares of the damage states discussed in Chapter 4. Specimens are compared based on the drift at which damage states were reached.

The cracking damage states occur at similar drifts for all specimens, as shown in Figure 5-1. Cracking spanned the width of the slab (Cracking Stage 1) during the 0.73% target drift cycles. Cracking stabilized (i.e. no additional cracks or crack extensions) during the 3.6% target drift cycles for Specimens PTB_4.5_1_0, PTB_4.5_1_4, and PTB_9_2_0. Cracking stabilized during the 2.9% target drift cycles for Specimen SR_4_10_5. Cracking is likely similar because most cracking initiates while the specimens are elastic or in early stages of the plastic range where the specimens have similar global behaviors (shown in Section 5.2).

The occurrence of initial yielding of reinforcement is shown in Figure 5-1. Initial yielding (Yielding Stage 1) was measured for all specimens during the 2.2% target drift cycles. It is though initial yielding was similar for all tests because all specimens respond similarly before the concrete begins to degrade.

Full yielding of the longitudinal reinforcement across the width of the slab (Yielding Stage 2) occurred during the 4.4% target drift cycles for Specimens PTB_4.5_1_4, and PTB_9_2_0; Specimen PTB_4.5_1_0 reached Yielding Stage 2 during the 5.1% target drift cycles. Specimen SR_4_10_5 did not reach Yielding Stage 2. It is though the specimens designed with variations of the proposed connection provide a more robust connection through which forces can be transferred from the slab to the column. Conversely, the connection of the reference specimen degraded before enough force to yield all reinforcement could be transferred between the slab and the column.

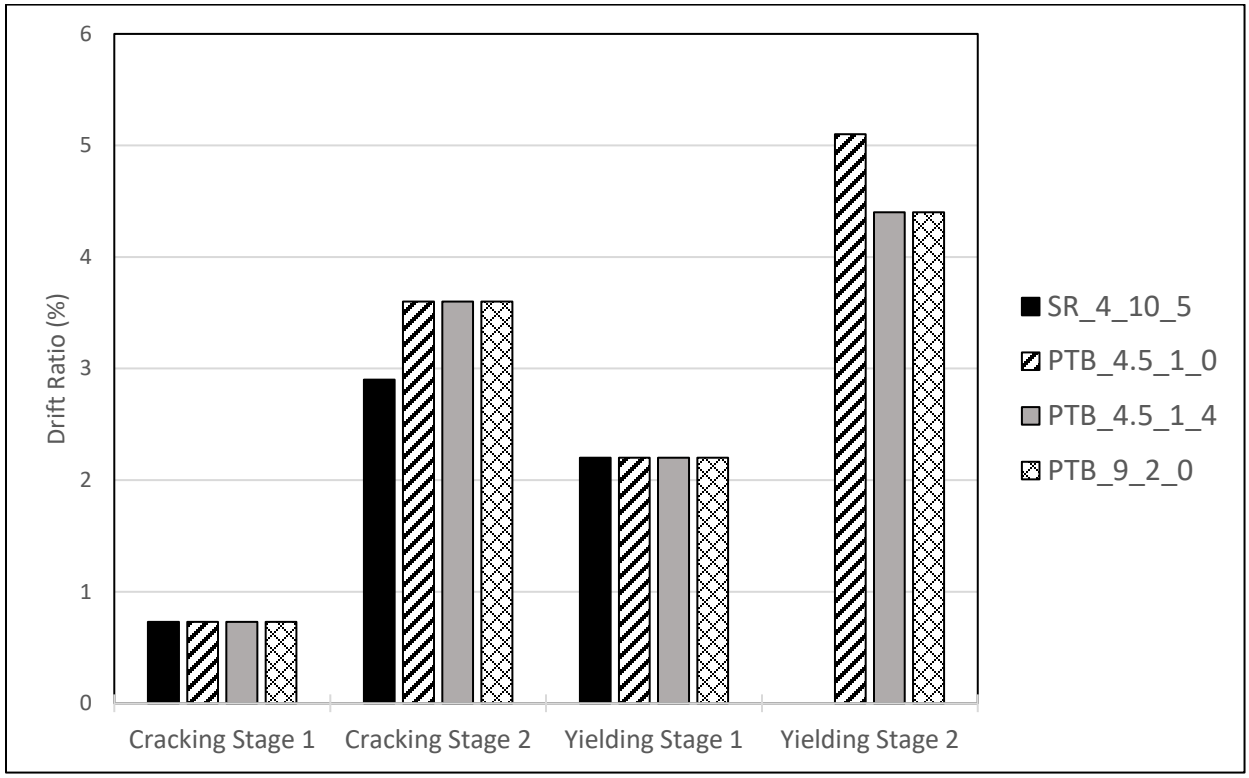

Figure 5-1: Damage Summary (1/2)

Figure 5-2 compares the Spalling, Crushing, and (observed) Bar Buckling damage states. For definitions of Spalling, Crushing and Bar Buckling, see Chapter 4.

Specimen PTB_4.5_1_0 sustained initial spalling at 1.5% drift, Specimen PTB_4.5_1_4 at 2.2%, SR_4_10_5 at 2.9%, and Specimen PTB_9_2_0 at 3.6% drift. The start of spalling began near the column for the reference specimen and around the ring for the other specimens. It is thought spalling likely occurred at a higher drift for Specimen SR_4_10_5 because the lack of posttensioning force on the joint, which allowed the stress transferring from the connection to the

slab to be distributed more gradually than in the connections with the 4.5 in. ring. Specimens PTB_9_2_0 likely began spalling at a higher drift because the larger ring provided a larger perimeter for stress to be transferred from the connection to the slab. Specimen PTB_4.5_1_0 and Specimen PTB_4.5_1_4 likely began spalling earlier due to the combination a small perimeter to transfer stress from the connection to the slab and the prestressing of the joint forcing a sudden change in stress at the edge of the ring.

Crushing (damage of concrete to the point that reinforcement is visible) was noted at 4.4% drift for Specimens SR_4_10_5 and PTB_4.5_1_0; the crushing damage state occurred at a slightly larger drift of 5.1% for Specimens PTB_4.5_1_4 and PTB_9_2_0. It is thought crushing potentially occurred earlier in Specimen SR_4_10_0 due to the lack of confinement of the slab reinforcement, allowing the longitudinal reinforcement to de-bond from the surrounding concrete to the point where the cover broke away from the slab. Crushing likely occurred earlier in Specimen PTB_4.5_1_0 due to the complete lack of transverse reinforcement outside the ring, which also allowed the longitudinal reinforcement to de-bond from the surrounding concrete. Specimen PTB_4.5_1_4 and Specimen PTB_9_2_0 likely delayed crushing the longest because the connection details more effectively distributed the forces transferring from the slab to the column over a larger area.

Bar Buckling was not observed in Specimen SR_4_10_5. Bar buckling was observed at 5.1% drift for Specimen PTB_4.5_1_0 and 6.5% drift for Specimens PTB_4.5_1_4 and PTB_9_2_0. Bar buckling was observed but not quantified as bar buckling may occur before it is visible and it would be misleading to try and quantify buckling only once it became visible. It is thought bar buckling likely only occurred in specimens designed with variations of the proposed connection due to the prestressing effects on the joint. The prestressing on the ring effectively confined the concrete and reinforcement in the joint region restricting deformations in the joint leading to a large deformation requirement in the reinforcement once beyond the region effected by the PTBs on the ring. The large deformation in the reinforcement caused large plastic deformation in the reinforcement just beyond the ring which lead to bar buckling on the reverse cycle.

Specimens PTB_4.5_1_4 and PTB_9_2_0 sustained higher drifts for the more severe damage states, crushing and bar buckling. By delaying crushing and bar buckling, Specimens PTB_5.4_1_0 and PTB_9_2_0 prolonged their lateral force resistance and maintained their

structural integrity to higher drifts. The lack bar buckling observed in Specimen SR_4_10_5 does not indicate a better connection response, but rather a different failure mode which is more closely tied to the degradation of the reinforcement bond with the concrete.

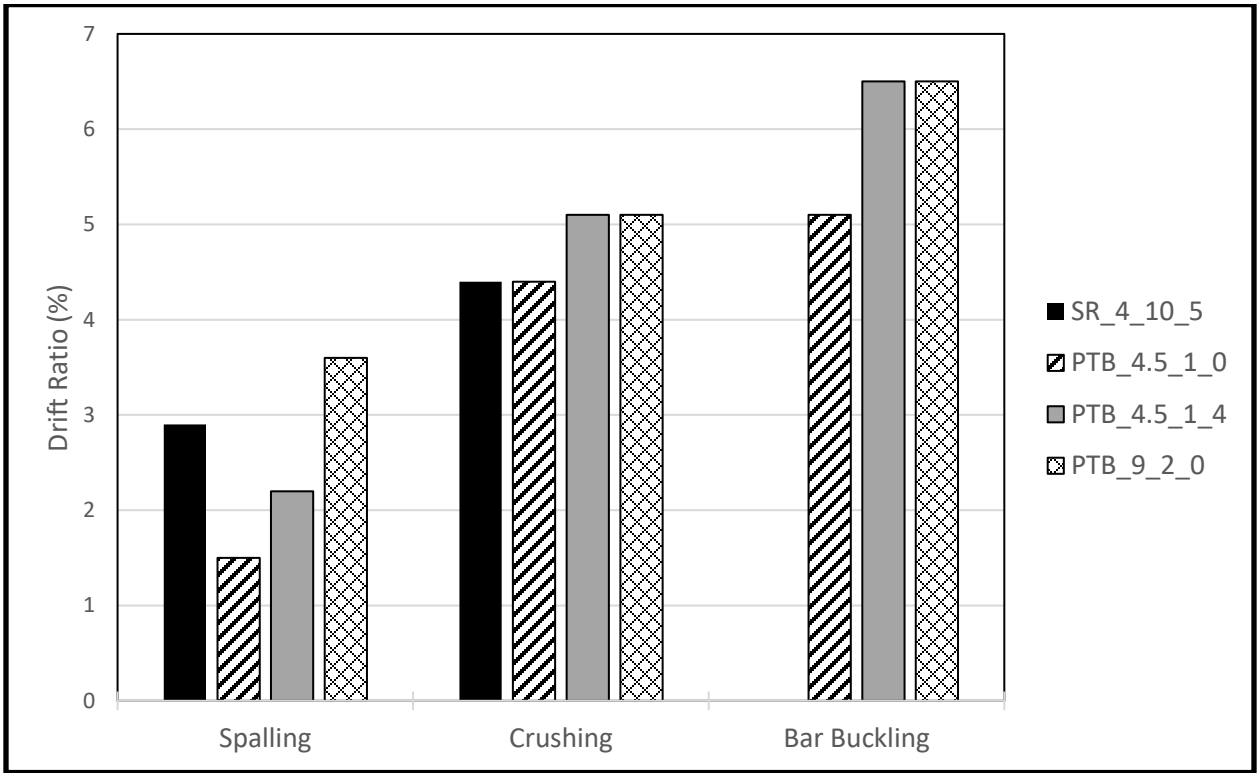

Figure 5-2: Damage Summary (2/2)

5.2 System Behavior

System behavior was quantified using the force-drift response and energy dissipation capabilities of the test specimens. For the force-drift response, the full hysteretic response were compared, the envelopes were compared, the elastic stiffnesses were compared, and the peak and ultimate drift values were compared.

5.2.1 *Hysteretic Response Including Energy Dissipation*

Figure 5-3, Figure 5-4, Figure 5-5, and Figure 5-6 show the hysteretic curves from Specimens SR_4_10_5, PTB_4.5_1_0, PTB_4.5_1_4, and PTB_9_2_0 (respectively) after P-Δ effects have been removed and the lateral force resistances have been normalized by the MTS Actuator forces required to reach the nominal moment capacities (as prescribed by ACI 318-19) of the connections. Nominal moment capacities were calculated using measured material strengths. All hysteresis show "pinching" of the hysteretic curve which is characteristic cyclic testing of concrete and indicates the damage to the concrete around the slab column joint. The reference specimen is the only specimen to show a prolonged degradation of lateral force resistance after reaching the peak lateral force. Specimens designed with variations of the proposed connection tended to maintain significant lateral force resistance until failure (Specimen PTB_4.5_1_0) or until the termination of testing at large drifts (Specimens PTB_4.5_1_0 and PTB_9_2_0).

The response in both the north and south direction were largely similar as expected (due to symmetry of design) though at large drifts there was an increase in stiffness visible in the northern displacements of the last two target drifts of Specimen SR_4_10_5 and in both the north and south displacements of the last two target drifts of Specimen PTB_4.5_1_4. This unexpected increase in stiffness was attributed to the behavior of the MTS Actuator's electronic instrumentation as it approaches its maximum stroke by the laboratory technician, not to an actual change in the response of the connections being tested.

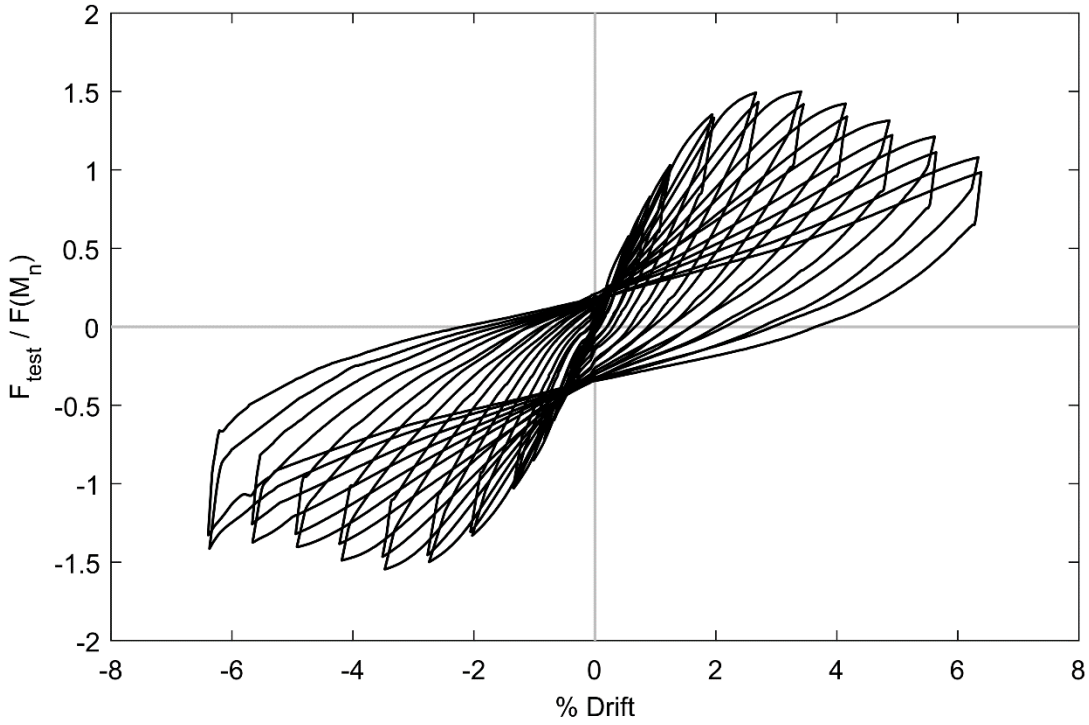

Figure 5-3: Normalized Drift Response with P-Δ Effects Removed (SR_4_10_5)

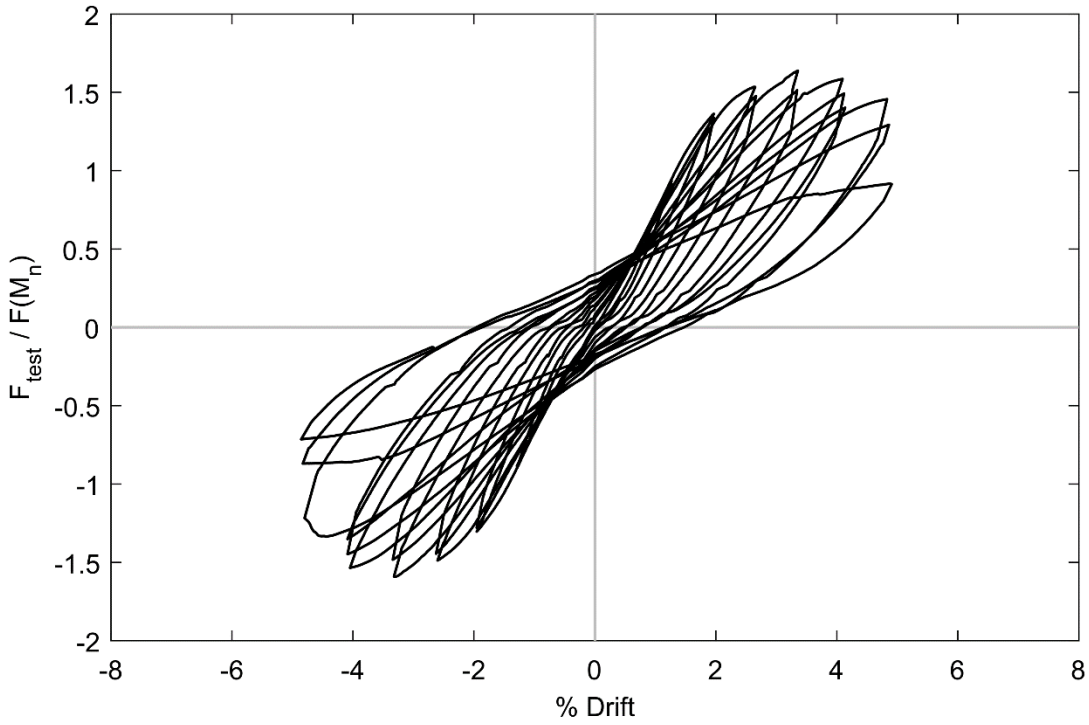

Figure 5-4: Normalized Drift Response with P-Δ Effects Removed (PTB_4.5_1_0)

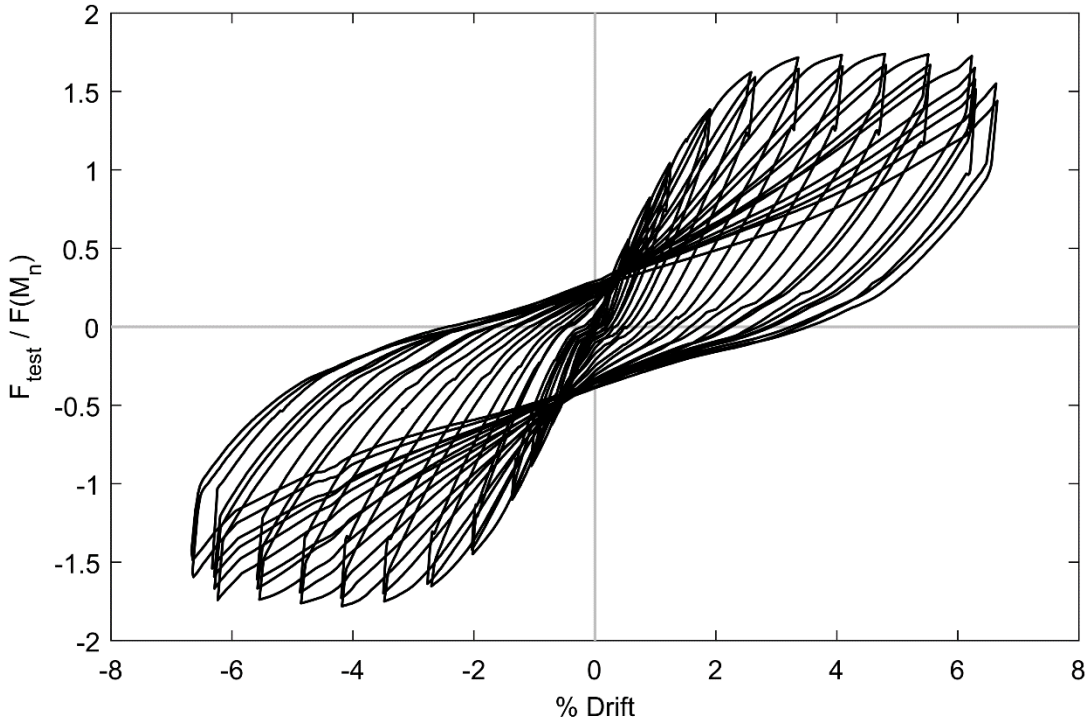

Figure 5-5: Normalized Drift Response with P-Δ Effects Removed (PTB_4.5_1_4)

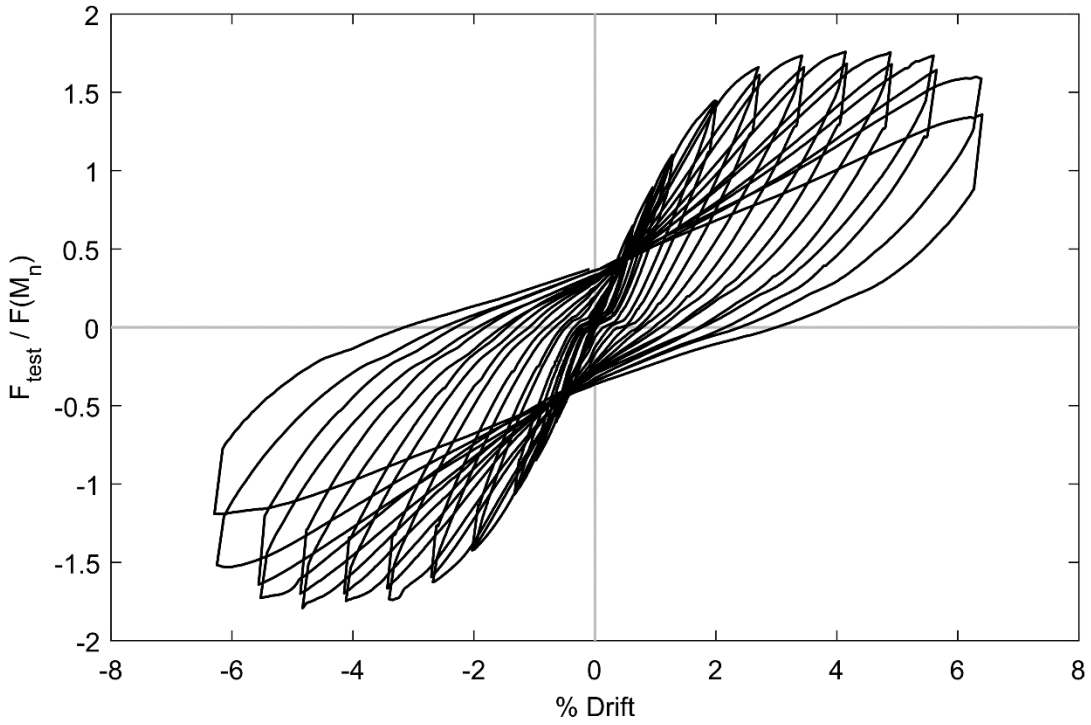

Figure 5-6: Normalized Drift Response with P-Δ Effects Removed (PTB_9_2_0)

Energy dissipated during testing was calculated by finding the area under the hysteretic curve. Figure 5-7 and Figure 5-8 show the energy dissipated plotted against the target displacement. Only the energy dissipated during the first cycle of each target drift has been included in Figure 5-7, because, as indicated in Chapter 4, the displacement histories for Specimen PTB_4.5_1_0 and Specimen PTB_4.5_1_4 are different than the displacement histories for Specimen SR_4_5_10 and Specimen PTB_9_2_0. Energy dissipation was calculated through the maximum drift cycle each specimen was tested to.

As shown in Figure 5-7, Specimen PTB_4.5_1_0 dissipated a similar amount of energy to the reference specimen until failure. Specimens PTB_4.5_1_4 and PTB_9_2_0 dissipated similar amounts of energy and dissipated more energy than either of the other specimens. Specimen PTB_4.5_1_4 dissipated the most energy, as expected, because it was tested to the highest drift.

Figure 5-8 shows that when the energy dissipated during the entire test is considered, Specimen PTB_4.5_1_4 dissipates much more energy than other specimens. This is partially because Specimen PTB_4.5_1_4 was tested through many more cycles than other specimens. Figure 5-8 also demonstrates that Specimen PTB_4.5_1_0 did not fail early because it absorbed a greater amount of energy at lower drifts.

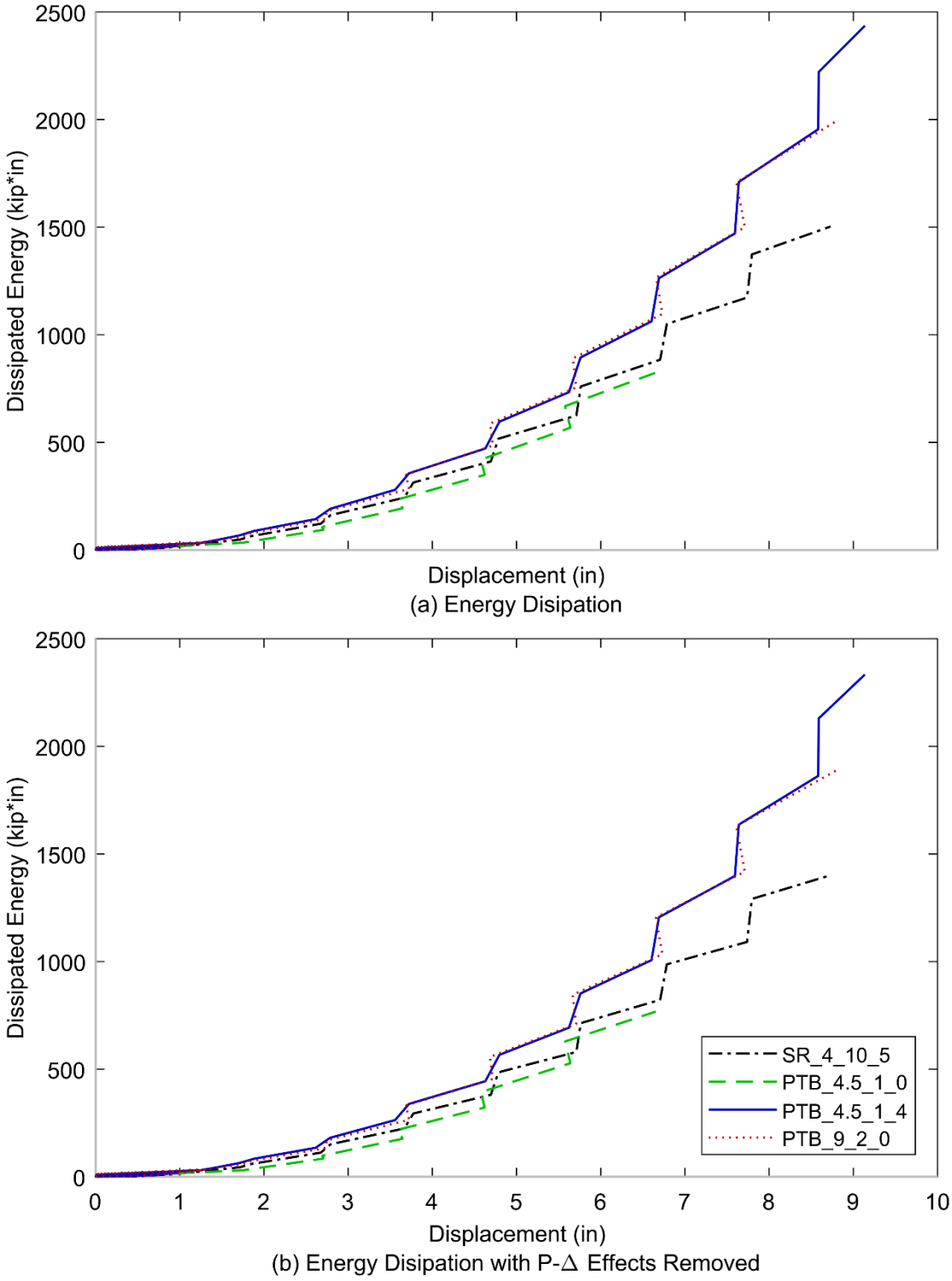

Figure 5-7: Single Cycle Energy Dissipation vs. Displacement

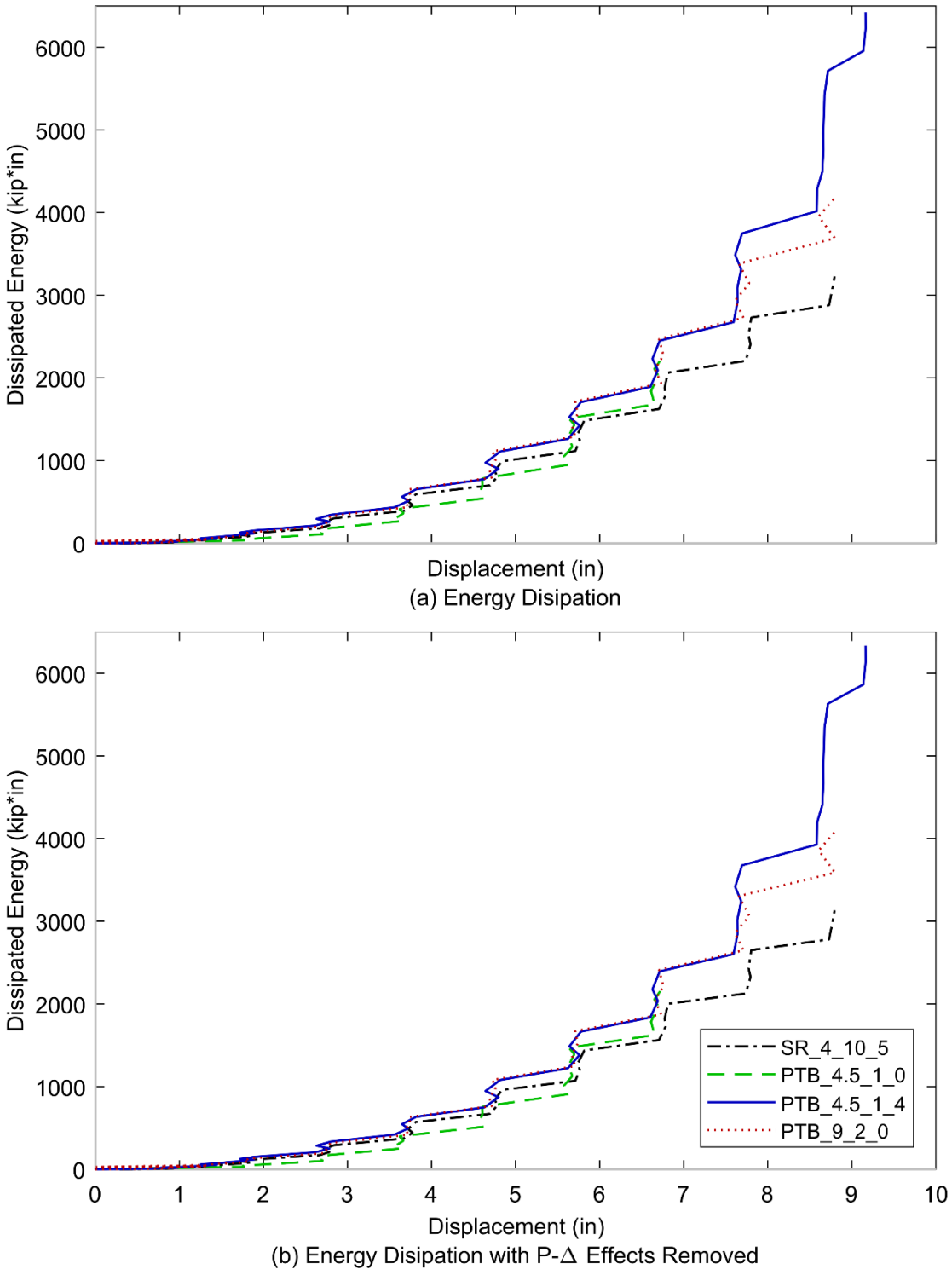

Figure 5-8: Total Energy Dissipation vs. Displacement

5.2.2 *First Drift Cycle Envelopes*

The hysteretic envelopes were obtained from the peak forces for the first cycle of the force-drift hysteretic response. The envelopes are shown for the measured response and the response with P-Δ effects removed in Figure 5-9. Figure 5-10, respectively. Three distinct regions of behavior can be observed: the (approximately) elastic region, the inelastic and hardening region, and the inelastic and deteriorating region.

The elastic region occurs in the early drift ranges when the response of the connection is approximately linear because slab reinforcement has not yielded. Although cracking does results in nonlinearity, it is not significant and neglected in this discussion.

The primary design variable that is of interest in the elastic region is the secant stiffness. Using the nominal moment strength (see Chapter 4) to compute the story shear force (F_{Mn}). The effective stiffness was calculated to using the force and displacement correspond to 80% of F_{Mn}, as given in Eq. 5.1.

$$K_{elastic} = \frac{0.8 * F_{M_n}}{\Delta(0.8 * F_{M_n})} \qquad 5.1$$

Table 5.1: Connection Elastic Stifness

Specimen	Measured			P-Δ Removed		
	kip / in.	kN / m	% Change	kip / in.	kN / m	% Change
SR_4_10_5	24.1	4229.1	-	28.3	4956.1	-
PTB_4.5_1_0	20.7	3623.9	-14.1	23.2	4070.9	-18.0
PTB_4.5_1_4	24.5	4290.5	1.7	28.3	4954.1	0.0
PTB_9_2_0	26.5	4647.3	10.0	30.1	5270.9	6.4

Specimen PTB_4.5_1_0 had the lowest elastic stiffness of any connection tested while PTB_4.5_1_4 had the highest.

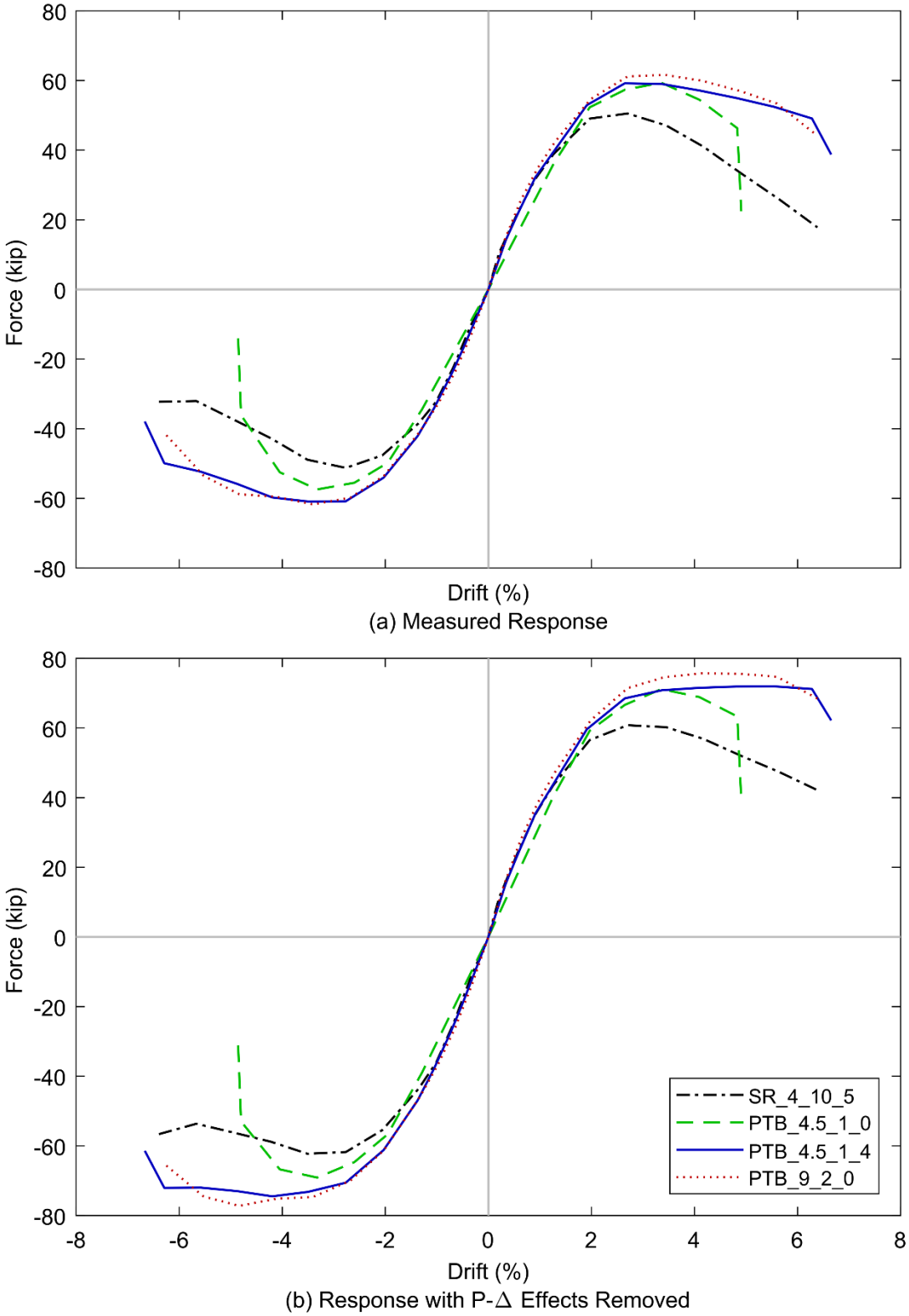

Figure 5-9: Envelopes

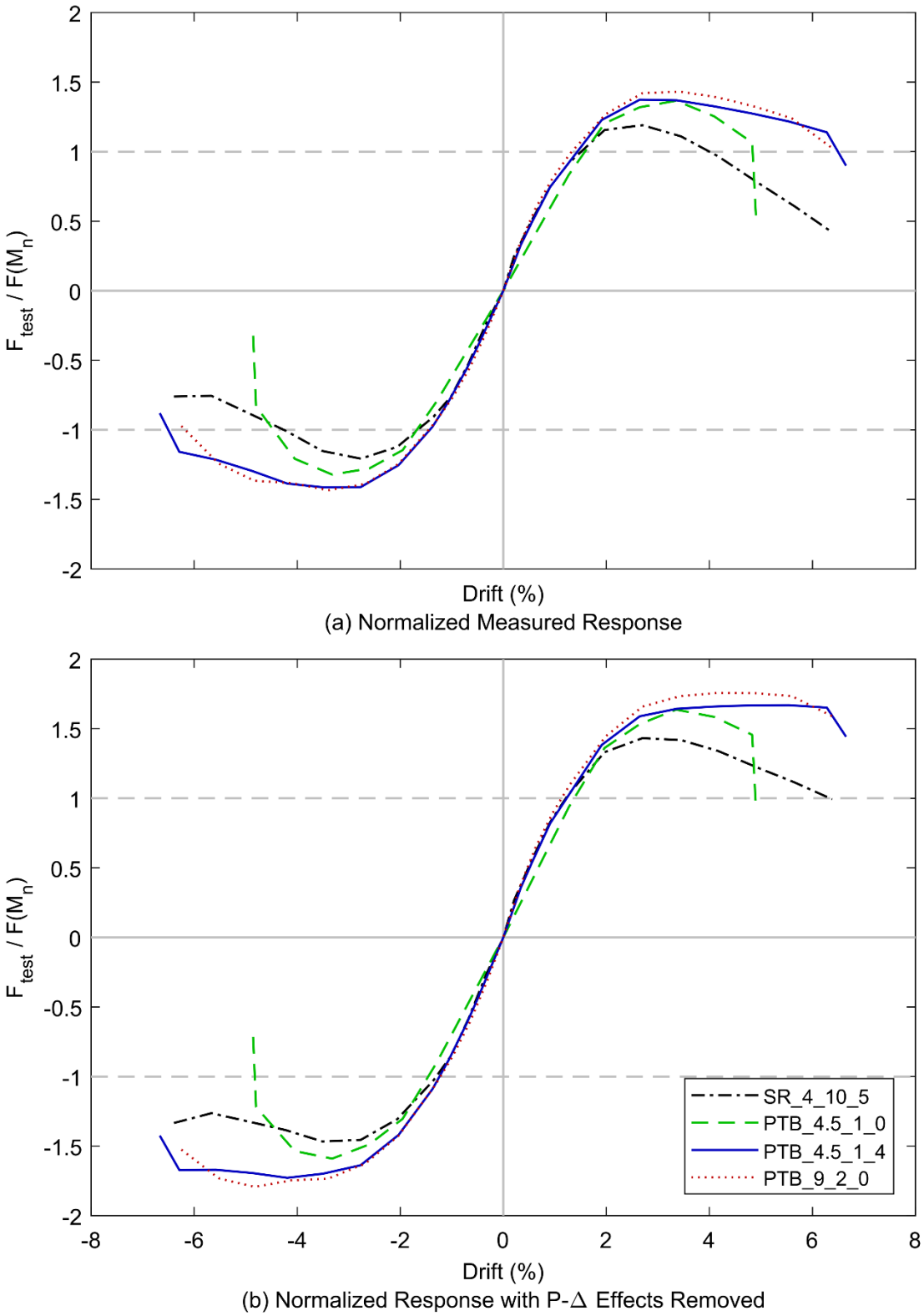

Figure 5-10: Normalized Envelopes

The plastic region occurs after initial yielding of the slab reinforcement. All of the connections yielded at similar drifts. The response of Specimens including P-Δ effects deteriorates beyond 3% drift. However, when P-Δ effects were removed, lateral force resistance is shown to not degrade for Specimens PTB_4.5_1_4 and PTB_9_2_0. The following discussion references the response with P-Δ effects removed.

Specimen SR_4_10_5 reached the peak resistance at 2.7% drift before immediately beginning to lose lateral force resistance. Specimen PTB_4.5_1_0 reached a similar peak resistance to PTB_4.5_1_4 and PTB_9_2_0. However, the strength of Specimen PTB_4.5_1_0 degraded shortly after reaching peak resistance at 3.4% drift before suddenly failing at 4.9% drift. Specimens PTB_4.5_1_4 and PTB_9_2_0 had a well-defined yield plateau and did not lose strength until approximately 6% drift. All tests seem to suggest that the method for calculating the flexural strength of slab column connections detailed in ACI 318 is conservative.

5.2.3 *Peak and Ultimate Resistance and Drift Values*

The yield and peak strengths are shown in Table 5.2 and Table 5.3. These values are also presented normalized using the nominal moment capacity (M_n) of the slab in Table 5.2 and using the plastic moment capacity of the slab (M_P) in Table 5.3. M_n corresponds to the capacity predicted by ACI 318 (ACI 19) as previously discussed while M_P corresponds to the moment required to yield all of the slab tensile reinforcement in a test specimen. The percent change of the normalized yield and peak strengths is also shown, where the percent change is based on the reference specimen (Specimen SR_4_10_5).

Specimen PTB_4.5_1_4 had the largest yield strength. However, in the inelastic region, Specimen PTB_9_2_0 had the largest resistance after P-Δ effects were removed. Specimens PTB_9_2_0 and PTB_4.5_1_4 had a strengths approximately 20% and 24% (respectively) larger than the reference specimen.

M_n appears to result in an underestimate of the peak resistance. The peak resistance of the reference specimen exceeds M_n by 47%. The specimens designed with variations of the proposed connection exceed M_n by 64% to 79% as shown in Table 5.2.

M_P appears to result in a better prediction of the peak resistance than the nominal moment capacity predicted by ACI 318, especially for Specimen SR_4_10_5, exceeding M_P by 9% after

P-Δ effects are removed. The specimens designed with variations of the proposed connection exceeded M_P by 22% to 33% with Specimens PTB_4.5_1_4 and PTB_9_2_0 performing similarly (exceeding M_P by 29% and 33% respectively) as shown in Table 5.3.

Table 5.2: Peak Measured Resistance with P-Δ Effects Removed (Normalized by M_n)

Specimen	Initial Yield Resistance			Maximum Inelastic Resistance		
	kip	F/F(M_n)	% Change	kip	F/F(M_n)	% Change
SR_4_10_5	43.6	1.03	-	62.2	1.47	-
PTB_4.5_1_0	59.2	1.36	32.6	71.2	1.64	11.6
PTB_4.5_1_4	61.2	1.42	38.2	74.5	1.73	17.8
PTB_9_2_0	47.4	1.10	7.2	77.2	1.79	22.2

Table 5.3: Peak Measured Resistance with P-Δ Effects Removed (Normalized by M_P)

Specimen	Initial Yield Resistance			Maximum Inelastic Resistance		
	kip	F/(M_P)	% Change	kip	F/F(M_P)	% Change
SR_4_10_5	43.6	0.76	-	62.2	1.09	-
PTB_4.5_1_0	59.2	1.01	33.0	71.2	1.22	12.0
PTB_4.5_1_4	61.2	1.06	38.5	74.5	1.29	18.0
PTB_9_2_0	47.4	0.82	7.4	77.2	1.33	22.4

Peak drift is defined as drift at the peak resistance; ultimate drift is the drift corresponding to 20% loss of the peak measured lateral resistance (where measured lateral resistance is the resistance that includes P-Δ effects) on the envelope. The drift values are summarized in Table 5.4. Specimen SR_4_10_5 sustained a peak drift at (+2.70/-2.77 %) and an ultimate drift of (+4.23/-4.45 %). Specimen PTB_4.5_1_0 had sustained slightly larger values: peak drifts of (+3.36/-2.77 %) and ultimate drifts of (+4.72/-4.35 %). Specimen PTB_4.5_1_4 reached its peak at (2.65/-3.50%); these values are slightly lower than the prior two specimens, but it reached and ultimate drift of (6.34/-6.33%), the largest ultimate drift of the four specimens studied. Specimen PTB_9_2_0 reached the following: peak drifts (3.42/-3.40%) and ultimate drift (5.95/-5.78%). This specimen had better response than SR_4_10_5 and PTB_4.5_1_0, with similar response to PTB_4.5_1_4 although slightly lower values (however PTB_9_2_0 had constructability advantages, as discussed in the conclusions.

Table 5.4: Peak and Ultimate Measured Drifts

Specimen	Drift (%)					
	Maximum			Ultimate		
	Positive	Negative	Range	Tension	Compression	Range
SR_4_10_5	2.70	-2.77	5.47	4.23	-4.45	8.68
PTB_4.5_1_0	3.36	-3.32	6.68	4.72	-4.35	9.07
PTB_4.5_1_4	2.65	-3.50	6.15	6.34	-6.33	12.67
PTB_9_2_0	3.42	-3.40	6.83	5.95	-5.78	11.73

5.3 LOCAL BEHAVIOR

Local responses used to compare specimens included: displaced shape of the slab at peak drifts, and peak strains and strain distribution (particularly a focus on elastic and post yield strains) of the slab reinforcement. Displacements and strains were used to compare the inelastic behavior in the slab as larger drifts were imposed and to compare the behavior of the slabs designed with variations of the proposed connection to the behavior of the slab of Specimen SR_4_10_5, the reference specimen. When discussing the location of an instrument/the location a reading was taken, the location is relative to the column centerline. A negative distance indicates the instrument is north of the column centerline while a positive distance indicates the instrument is south of the column centerline.

5.3.1 *Slab Displacements*

In this section, slab displacements are presented for the initial drift cycle of target drift ranges. Plots comparing displacements at approximately 1.3%, 2.0%, and 4.1% are included and the maximum displacement and the location where they were recorded during each initial cycle is tabulated.

Vertical displacement at specified location in the slab were recorded using string potentiometers. Figure 5-11 shows a plan view of the location of string potentiometer. During higher drift cycles, the anchors in the critical region were lost due to concrete damage and as a

result, displacements measured during higher drift cycles become unreliable. A comprehensive set of plots detailing displacements is provided in Appendix F, but this section will use a limited number of plots to discuss the general trends.

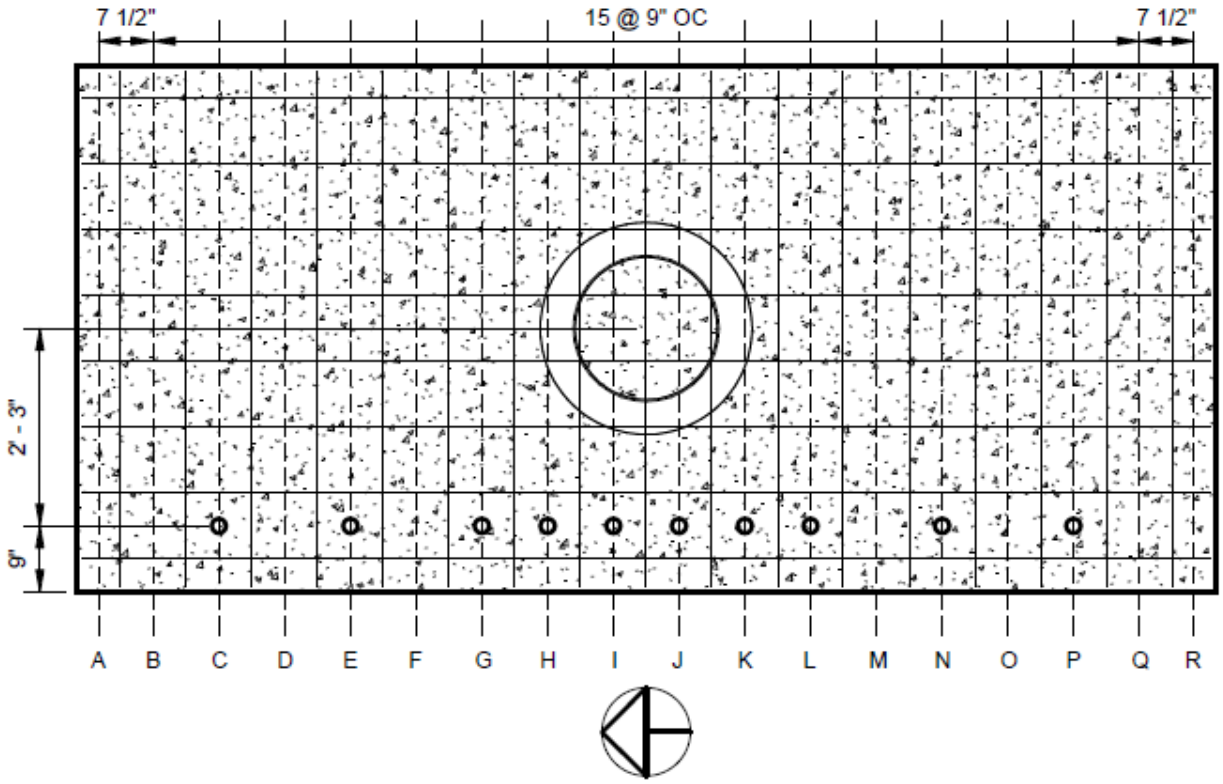

Figure 5-11: Location of Vertical Potentiometers on Slab (Indicated with circles)

Figure 5-12 shows the measured vertical displacements of the slab of Specimen SR_4_10_5 recorded during low drift cycles. Due to deformation of the slab end roller support and slop in the pin connections, the north and south ends of the slab were able to displace vertically under little load. The deformation in the slab end roller support was recorded during testing and they were removed. Plots of the corrected slab displacement are used for discussion in this section. For the plots of measured slab displacement, see Appendix F. All plots of the deformed shape of the slab show both peak southern drift (top subplot) and the reversal peak northern drift (bottom subplot). Rotations were found using the displaced shape and are included in Appendix G.

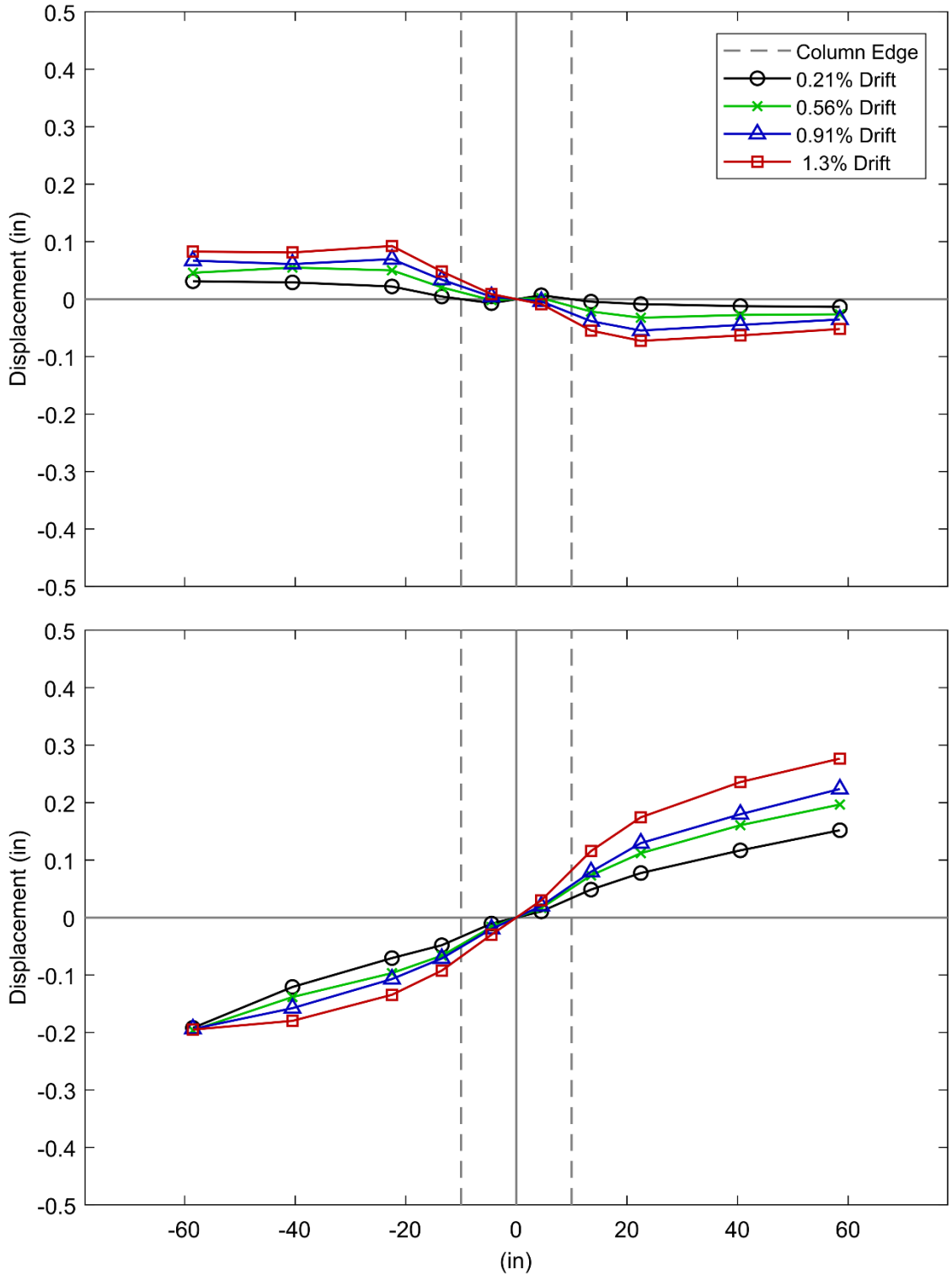

Figure 5-12: Low Drift Cycles Measured Slab Displaced Shape (SR_4_10_5)

Table 5.5 shows the maximum corrected slab displacement measured during the initial cycle of each target drift and the location where the displacement was measured. Entries marked with and asterisk show values taken after concrete degradation damaged anchor locations.

Table 5.5: Maximum Corrected Displacement by Target Drift Cycle

Specimen			SR_4_10_5	PTB_4.5_1_0	PTB_4.5_1_4	PTB_9_2_0
Target Drift (%)	0.36	Disp. (in.)	0.031	NR	0.0034	0.027
		Loc. (in.)	-58.5	NR	-40.5	58.5
	0.73	Disp. (in.)	0.044	NR	0.055	0.077
		Loc. (in.)	22.5	NR	22.5	-13.5
	1.1	Disp. (in.)	0.620	NR	0.083	0.095
		Loc. (in.)	22.5	NR	-40.5	40.5
	1.5	Disp. (in.)	0.010	0.125	0.105	0.120
		Loc. (in.)	22.5	40.5	-40.5	40.5
	2.2	Disp. (in.)	0.131	0.150	0.156	0.140
		Loc. (in.)	-22.5	22.5	-40.5	22.5
	2.9	Disp. (in.)	0.171	0.200	0.204	0.220
		Loc. (in.)	-22.5	22.5	-22.5	22.5
	3.6	Disp. (in.)	0.203	0.259	0.27	0.313
		Loc. (in.)	-13.5	22.5	-22.5	22.5
	4.4	Disp. (in.)	0.221	0.781	0.337	0.367
		Loc. (in.)	-22.5	22.5	-22.5	22.5
	5.1	Disp. (in.)	0.246	1.1.8*	1.173*	2.777*
		Loc. (in.)	-22.5	-22.5*	58.5*	4.5*
	5.8	Disp. (in.)	0.280	NR	1.142*	2.728*
		Loc. (in.)	-22.5	NR	58.5*	22.5*
	6.5	Disp. (in.)	0.314	NR	1.162*	4.353*
		Loc. (in.)	-22.5	NR	58.5*	4.5*
	6.9	Disp. (in.)	NR	NR	4.036*	NR
		Loc. (in.)	NR	NR	-13.5*	NR

Figure 5-13: Corrected Slab Displaced Shape (1.3% Drift) shows the slab deformation of all test specimens at approximately 1.3% drift. At this drift, slab deformations are similar across

all specimens and there are no obvious indications of plastic hinges forming in the slab around the column. Deformations are especially similar within ±22.5 in. of the column centerline. This similarity is likely due to the influence of the column and rings which force the slab to deform in somewhat of a rigid body fashion in that region. If there was greater torsional stiffness to the sides of the column, the slope of the deformation in this region may be more uniform. Outside the column/ring region the slab is freer to deform according to the detailing of the connection and according to the strengths and stiffnesses of the concrete and reinforcing steel.

Figure 5-14 shows the slab deformation of all test specimens at approximately 2.0% drift. At 2.0% drift, plastic hinges can be seen forming in all specimens. Plastic hinging is denoted by a sudden change in the slope of the displaced shape. Plastic hinges appear to be forming in most specimens between 13.5 in. and 22.5 in. to the north and/or south of the column centerline. This area is beyond the edge of the column for Specimen SR_4_10_5 and beyond the edge of the rings of the specimens designed with variations of the proposed connection. The displaced shapes are still similar in the region within 13.5 to 22.5 in of the column centerline, indicating that the column rotation and relative stiffness of the joint controls much of the rotation in this region.

Figure 5-15 shows the slab deformation of all test specimens at approximately 4.1% drift. At this point plastic hinging is evident in all specimens and appears to be occurring in the area between 13.5 in. and 22.5 in. north and/or south of the column centerline. While specimen deformations still take the same general shape, they are no longer that similar, even in the joint region. The slope of the deformation through the joint is still fairly uniform for each specimens individually though is less uniform than in previous drift cycles. The relative uniformity of slope indicates the rotation of the column still significantly influences the displacements of the slab on either side of the column. The slight decrease in the uniformity of the slope in the column region is likely due to local damage of the concrete, which is especially true for the deformed shape of PTB_4.5_1_0 during the peak southern drift where the reading recorded 4.5 in. to the south of the column centerline indicates the anchor for the string potentiometer had been lost.

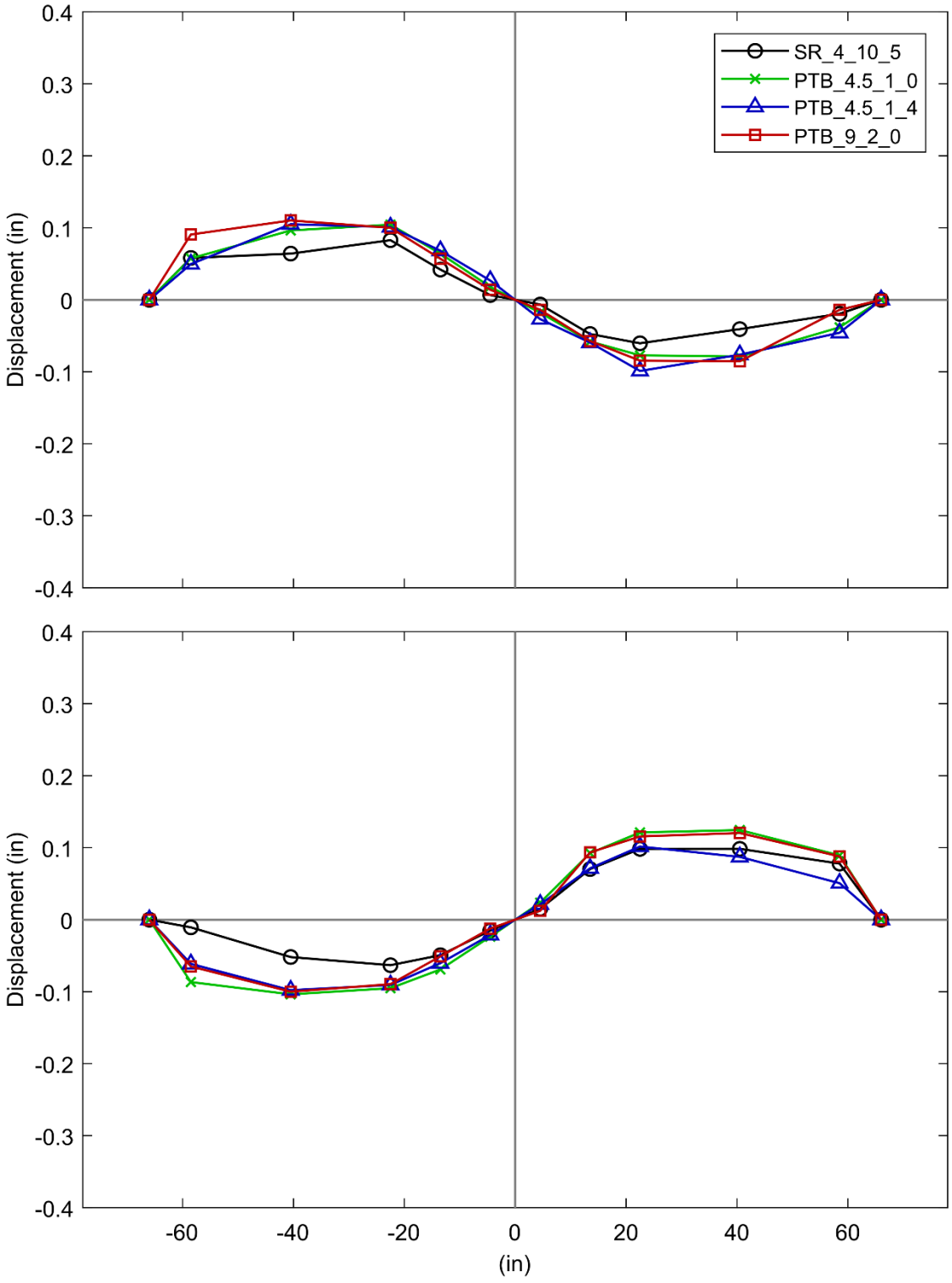

Figure 5-13: Corrected Slab Displaced Shape (1.3% Drift)

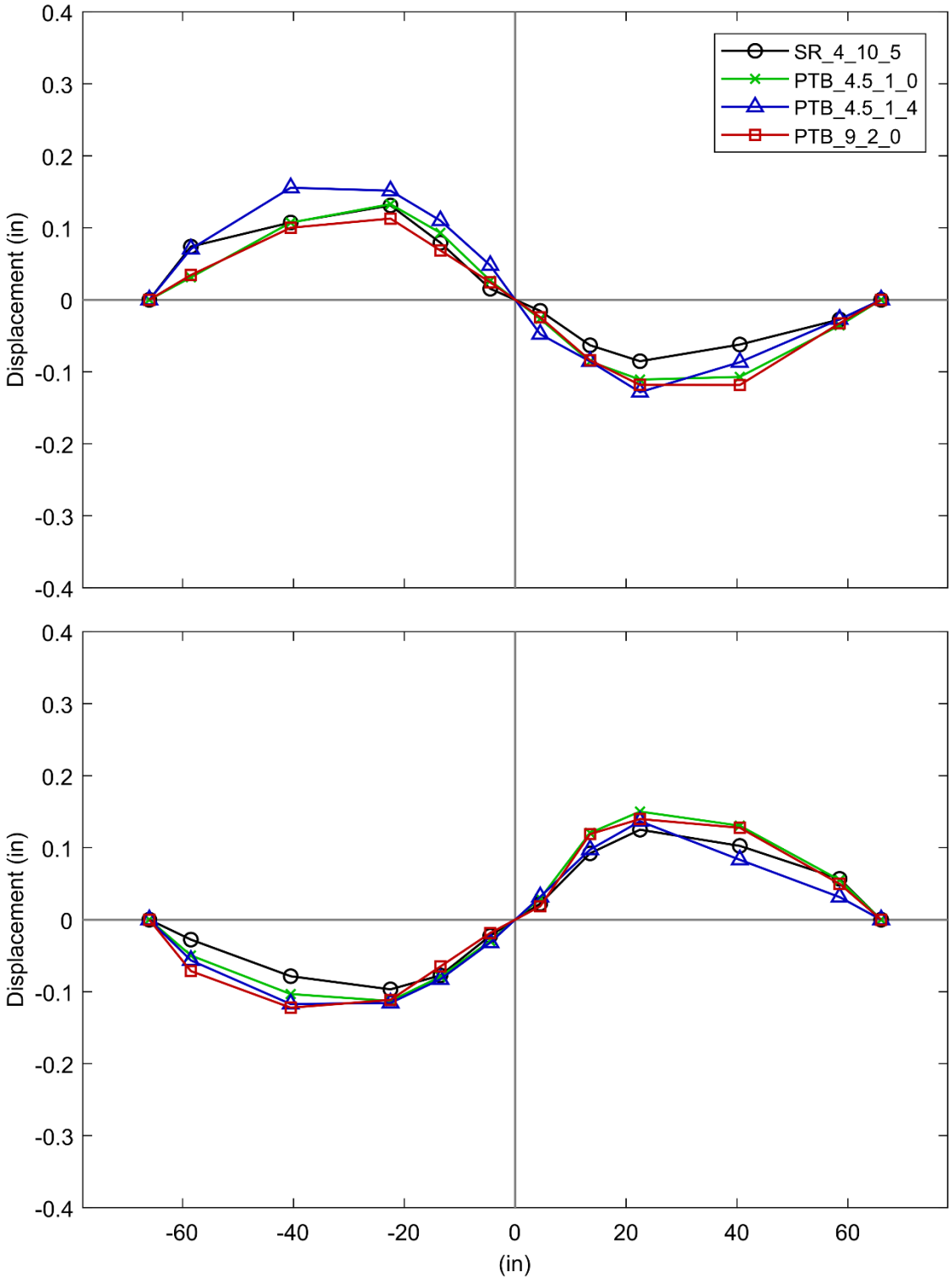

Figure 5-14: Corrected Slab Displaced Shape (2.0% Drift)

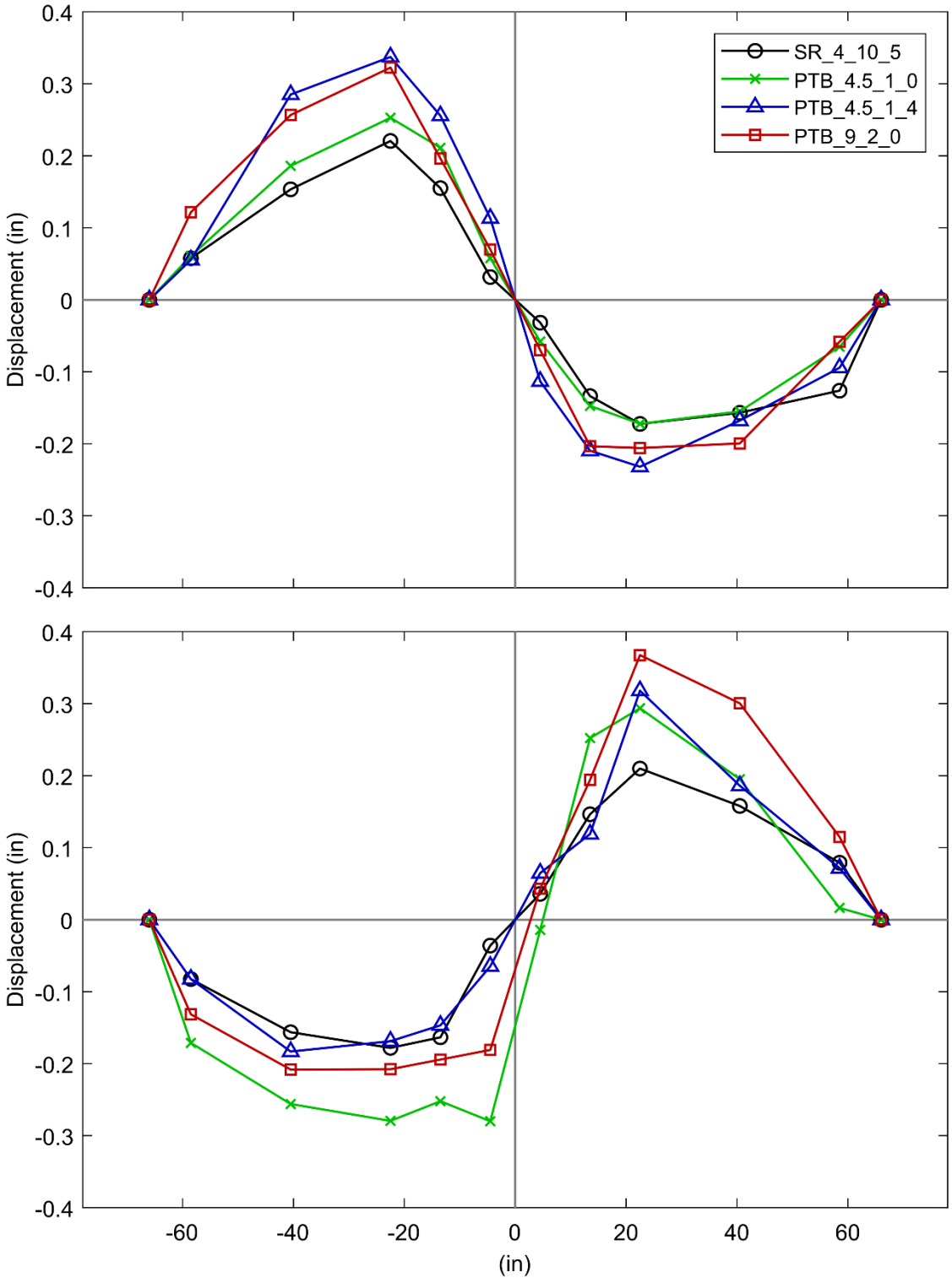

Figure 5-15: Corrected Slab Displaced Shape (4.1% Drift)

5.3.2 *Reinforcement Strain Profile*

The following sections presents strain distributions along the length of slab reinforcement for the bottom reinforcement. The largest values corresponding to the peak drift in either the north or south direction (direction corresponding to the largest tensile strain demands on the reinforcement) during the first cycle of a target drift (repeated cycles at the same drift were not studied) are used in this discussion. Table 5.6 shows a breakdown of the maximum strain according to the target drift. For the corresponding measured drifts, see Chapter 4.

Figure 5-16 shows the location of strain gauges on the longitudinal slab reinforcement. To identify the bars, a column-type indicator system was used with the bars in the long direction numbered and the bars in the short direction indicated with letters. The top and bottom bars were laid out the same and so they were differentiated using the letter T for top or B for bottom. (More information about the strain gauge nomenclature in given in Figure 5-16). Strains were assumed to be zero at the end of the reinforcement and are assumed to be distributed linearly between the strain gauges.

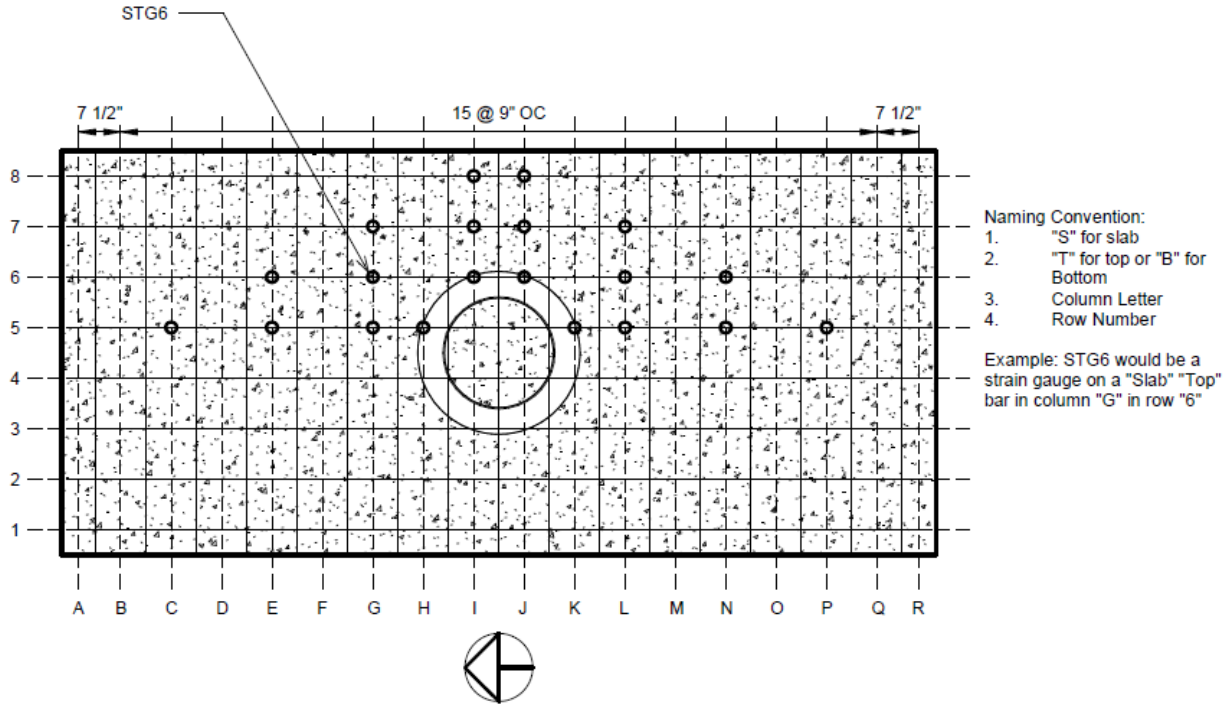

Figure 5-16: Slab Strain Gauge Layout

Table 5.6 shows the maximum recorded tensile strain measured during the initial cycle of each target drift and the location where the strain was measured. Entries marked with and asterisk show values that did not change from one cycle to the next and likely indicate a broken gauge.

Table 5.6: Strain Summary Bottom Reinforcement

Specimen			SR_4_10_5	PTB_4.5_1_0	PTB_4.5_1_4	PTB_9_2_0
Target Drift (%)	0.4	Max Strain ($\varepsilon*10^{-3}$)	0.38	NR	0.6	0.3
		Bar No.	5	NR	5	5
	0.7	Max Strain ($\varepsilon*10^{-3}$)	1.4	NR	1.2	1.2
		Bar No.	5	NR	5	5
	1.1	Max Strain ($\varepsilon*10^{-3}$)	2.0	NR	1.9	1.9
		Bar No.	5	NR	5	5
	1.4	Max Strain ($\varepsilon*10^{-3}$)	2.6	2.1	2.5	2.5
		Bar No.	5	5	5	5
	2.2	Max Strain ($\varepsilon*10^{-3}$)	4.7	10.4	54.6	8.3
		Bar No.	5	5	5	5
	2.9	Max Strain ($\varepsilon*10^{-3}$)	11.2	72.7*	54.6	13.7
		Bar No.	5	5*	5	5
	3.6	Max Strain ($\varepsilon*10^{-3}$)	13.4	72.7*	74.5*	61.9
		Bar No.	5	5*	5*	6
	4.4	Max Strain ($\varepsilon*10^{-3}$)	15.2	72.7*	74.5*	64.5*
		Bar No.	5	5*	5*	7*
	5.1	Max Strain ($\varepsilon*10^{-3}$)	14.8	72.7*	74.5*	64.5*
		Bar No.	5	5*	5*	7*
	5.8	Max Strain ($\varepsilon*10^{-3}$)	13.6	NR	74.5*	64.5*
		Bar No.	5	NR	5*	7*
	6.5	Max Strain ($\varepsilon*10^{-3}$)	12.6	NR	74.5*	64.5*
		Bar No.	5	NR	5*	7*
	6.9	Max Strain ($\varepsilon*10^{-3}$)	NR	NR	74.5*	NR
		Bar No.	NR	NR	5*	NR

The peak strains from the first cycle at each drift level were plotted as a distribution. Some of the strain gages were not working from the start of the test. Others stopped working during

testing. Data from gauges that were readily identifiable as broken is not presented here. For plots of strain vs. drift, see Appendix H.

Figure 5-17 shows the strain in the reinforcement of all test specimens at approximately 1.3% drift. As expected strains are largest towards the center of the reinforcement, where the greatest moment demand is placed on the slab. Also as expected, strains are largest at the middle of the specimens (Bar 5) and smallest toward the edge of the specimens (Bar 6) as bars closer to the column are more directly influenced by the rotation of the slab-column joint. At 1.3% drift, yielding is not indicated in any reinforcement. Strains in Bar 7 and Bar 8 are relatively similar across all specimens. Some of the variability from one specimen to another that can be observed in Bar 5 and Bar 6 may be due to the elimination of broken strain gauges on these bars creating the appearance of different behavior (especially on Bar 6 of Specimen PTB_4.5_1_0).

Figure 5-18 shows the strain in the reinforcement of all test specimens at approximately 2.0% drift. The strains towards the center of the reinforcement are higher and the largest in Bar 5. At 2.0% drift, Bar 5 for Specimen PTB_4.5_1_4 is indicated as having a very large strain 13.5 in. to the north of the column centerline and the gauge at this location may have broken. Bar 5 in all specimens has yielded. Strains in Bar 6 and 7 for all specimens is near the yield strain but Bar 6 and 7 have yielded only in some of the test specimens. Bar 8 has not yielded in any of the test specimens.

Figure 5-19 shows the strain in the reinforcement of all test specimens at approximately 4.1% drift. Overall, strains are still higher toward the center of the reinforcement and largest in bar 5 though bars other than Bar 5 are indicating strains above the hardening strain by 4.1% drift. Bar 5 has continued to yield in all specimens. Additionally, Bars 6, 7, and 8 have yielded in Specimens PTB 4.5_1_4 and PTB_9_2_0.

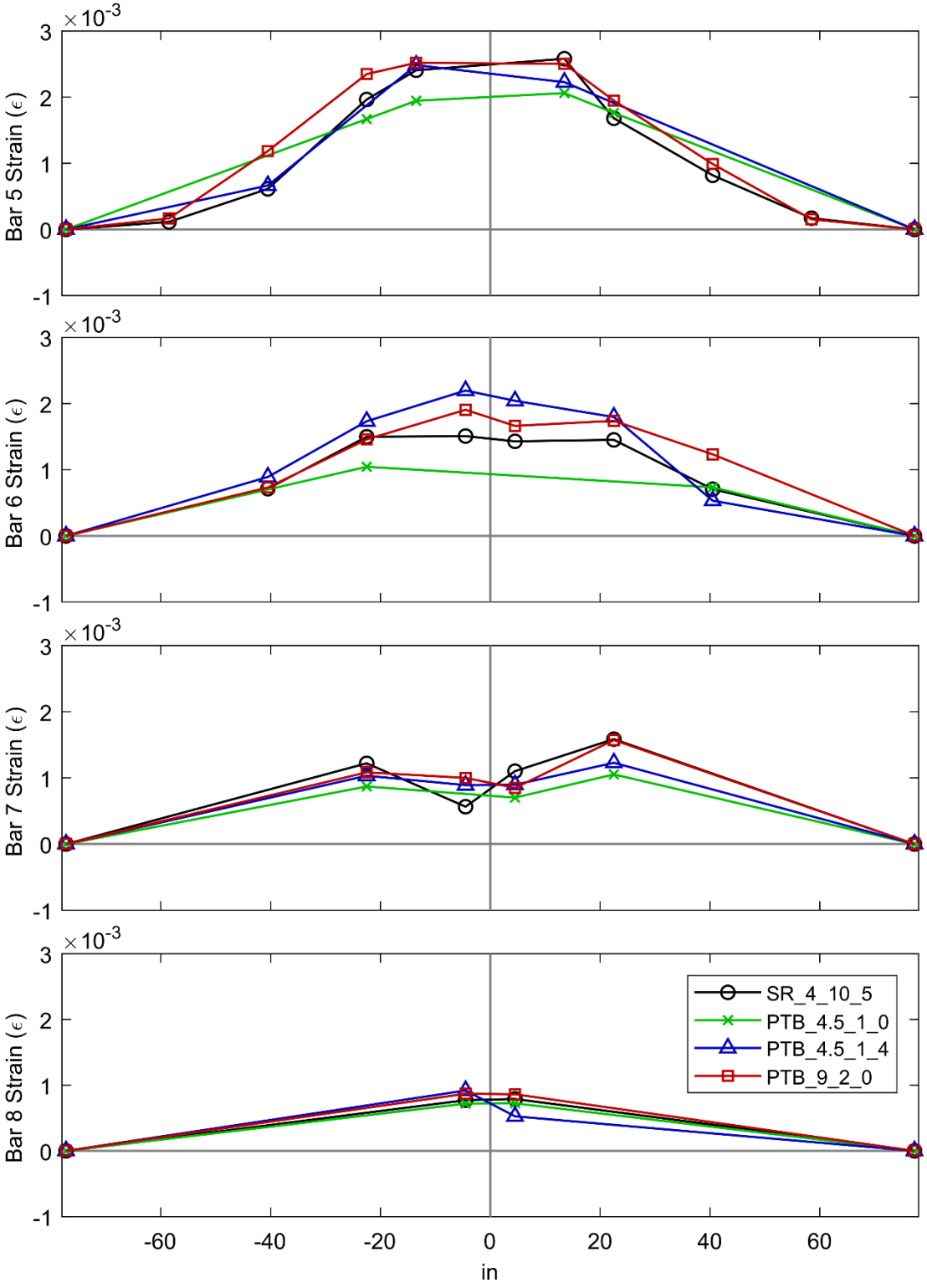

Figure 5-17: Reinforcement Strain Profile (1.3% Drift)

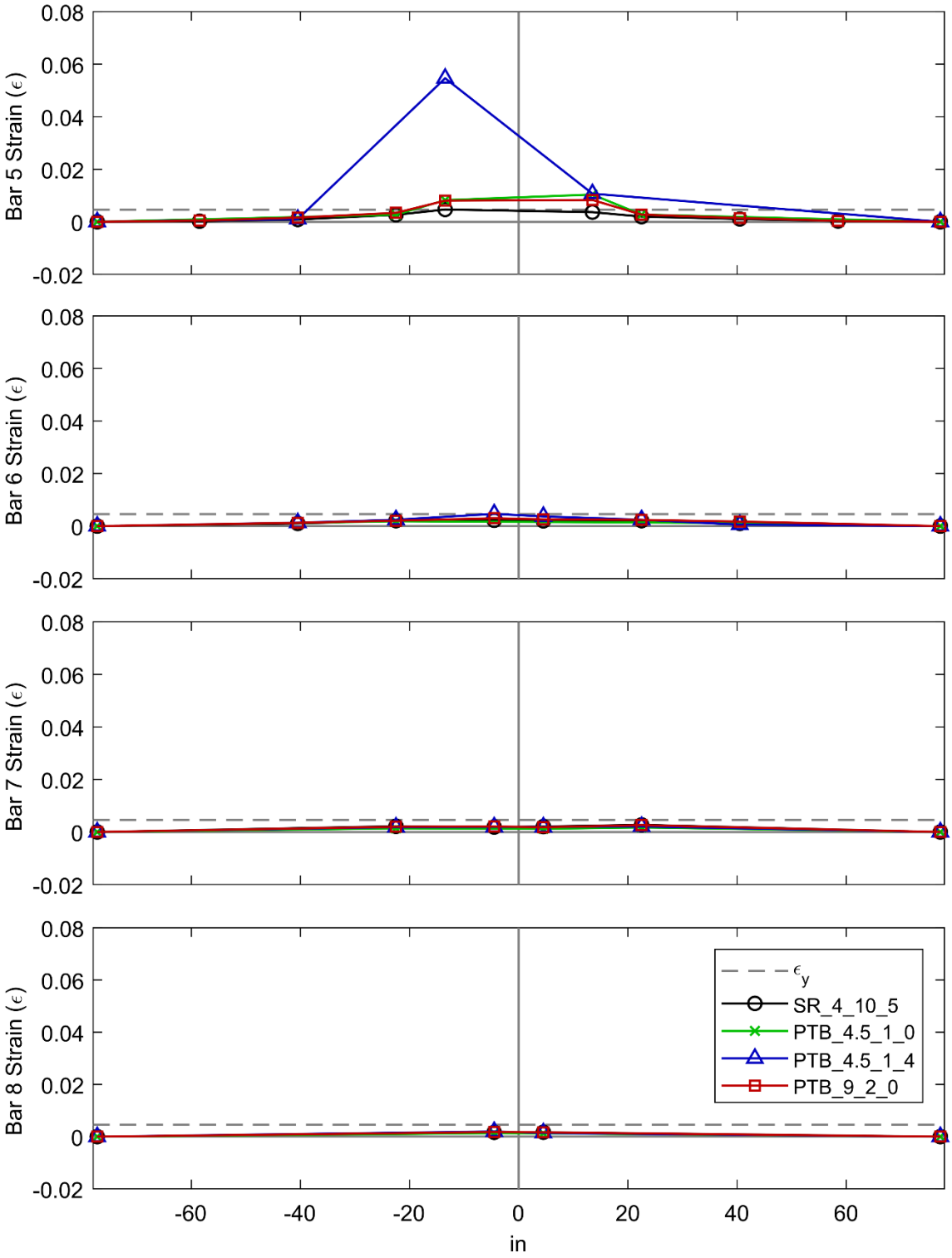

Figure 5-18: Reinforcement Strain Profile (2.0% Drift)

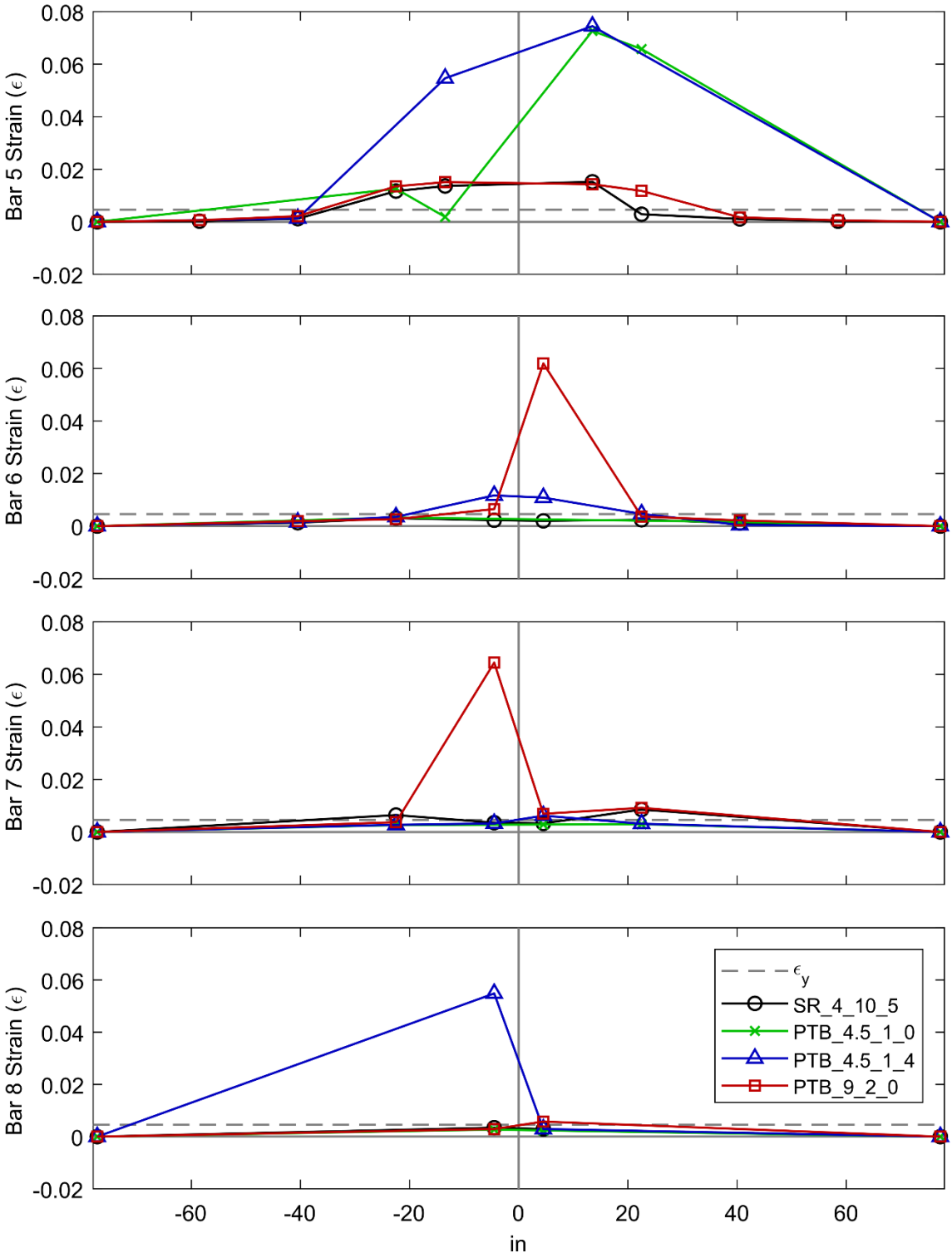

Figure 5-19: Reinforcement Strain Profile (4.1% Drift)

Chapter 6. EVALUATION OF RESULTS USING DESIGN EXPRESSIONS AND ANALYTICAL MODELING

This chapter presents code prediction from five design codes for the strength of test specimens, along with calibrated rotational springs for the slab column connection. Prediction for the flexure, one-way shear, and two-way shear strength are presented in Section 6.1 and compared to check the predicted failure mode. Nonlinear rotational springs were calibrated for the slab-column connection for each specimen in accordance with procedures presented in ASCE 41-17 and are presented in Section 6.2. Advanced Finite Element Modeling (FEM) was also done by another student in parallel with this experimental program. Information on the FEM and its results are presented in Appendix I.

6.1 CODE PREDICTIONS

Several design codes were used to calculate the nominal design strengths of test specimens corresponding to flexural, one-way shear, and two-way shear response. The predicted strengths are compared across design codes and from specimen to specimen. Calculations are performed using the predominant system of units used when writing each document. Results are then converted into both imperial and metric units and also normalized by the measured strength of each test specimen for comparison. The following codes are used:

- Building Code Requirements for Structural Concrete (ACI 318-19) published by the American Concrete Institute
- Eurocode 2: Design of concrete structures – Part 1-1: General rules and rules for buildings (EN 1992-1-1 2004) published by the European Committee for Standardization
- Standard Specifications For Concrete Structures – 2007 (JSCE-SPCS-2007) published by the Japan Society of Civil Engineers
- Design of Concrete Structures (CSA-A23.3-04) published by the Canadian Standards Association
- Concrete Structures Standard (NZS 3101.1:2006) published by Standards New Zealand

All strengths are calculated using the measured strengths of materials used in testing. The geometry used in calculations is shown in Figure 6-1

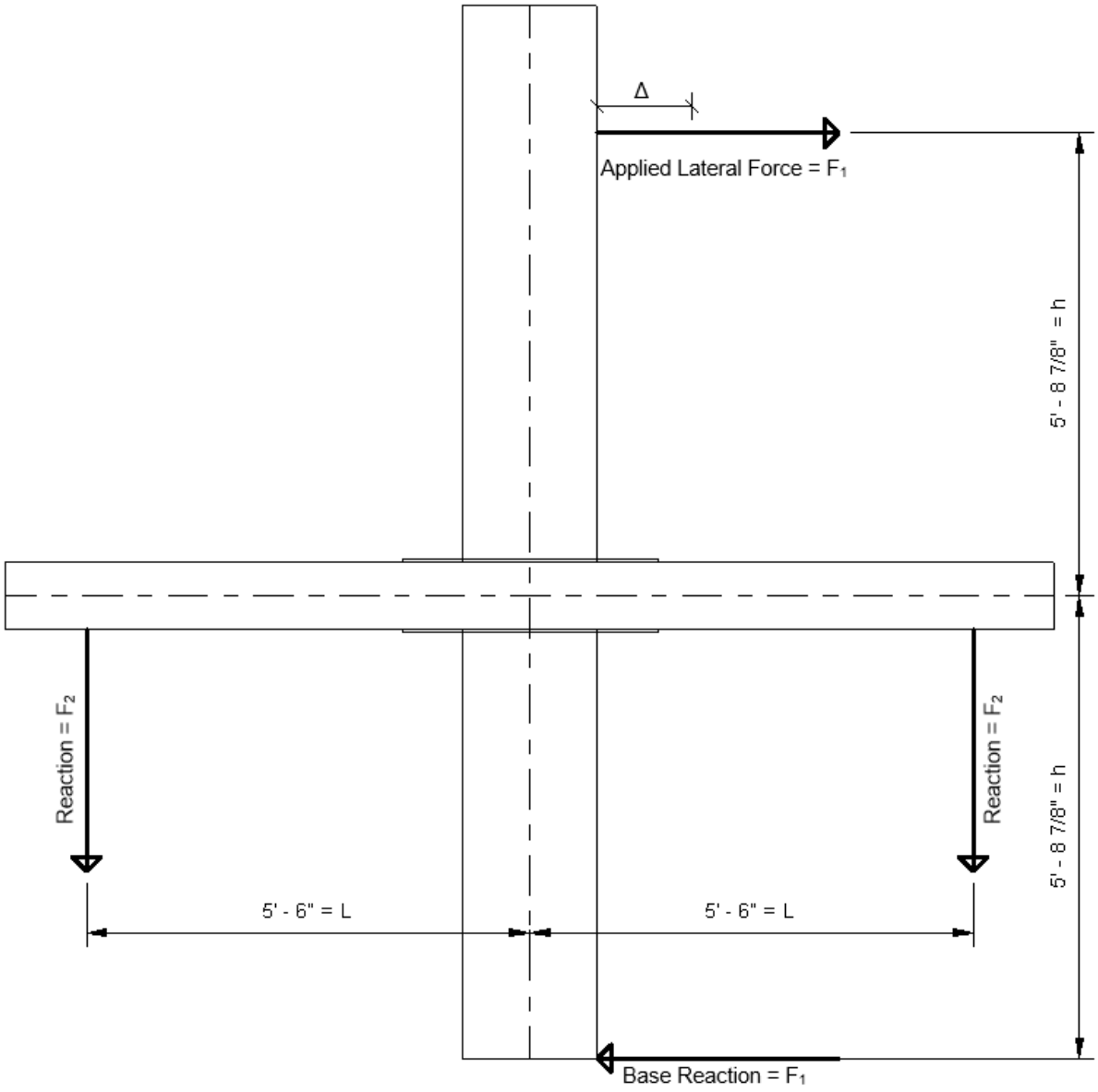

Figure 6-1: Test Geometry

6.1.1 *Flexural Strength*

The flexural capacity of the test specimens was determined using an equivalent stress block as prescribed in Section 22.2 of ACI 318-19, Section 3.1.7 of EN 1992-1-1 2004, Section 9.2.2 of JSCE-SPCS-2007, Section 10.1 of CSA-A23.3-04, and Section 7.4 of NZS 3101.1:2006. When

determining the width considered to contribute to the flexural strength, ACI 318-19, CSA-A23.3-04, and NZS 3101.1:2006 prescribe an effective width to calculate the moment transfer capacity from a slab to an interior column. When an effective width is defined, the nominal flexural capacity was determined using it; where no effective width was prescribed, the nominal flexural capacity was calculated using the entire width of the specimen.

To determine the measured force corresponding to development of the nominal moment capacity of the slab, it was assumed flexural hinges would form in the slab at the edges of the column. The corresponding force applied by the MTS Actuator was then calculated using Equation 6.1 using the nominal moment capacity, M_n, and a corresponding shear, V_{Mn}. V_{Mn} was calculated according to Equation 6.2. The MTS Actuator force needed to cause the slab to reach the nominal moment capacity of each specimen is recorded in Table 6.1. Figure 6-2 shows the force needed to cause the slab to reach the nominal moment capacity normalized by the measured capacity of each specimen. The codes EN 1992-1-1 2004 and JSCE-SPCS-2007 did not provide an effective width for moment transfer from slabs to columns for interior connections resulting in a higher predicted nominal moment capacity than other design codes.

$$P_n = \frac{M_n}{h} + \frac{c1 * V_{Mn}}{2h} \tag{6.1}$$

$$V_{Mn} = \frac{M_n}{L - c1} \tag{6.2}$$

Where,

P_n = the MTS Actuator force to cause the desired failure

M_n = nominal moment capacity of the slab

V_{Mn} = shear caused by a moment equal to the slab nominal moment capacity located at the face of the column

h = the height from the slab centerline to the level of the applied force (F_1)

L = the distance from the column centerline to the reaction force (F_2)

$c1$ = the dimension of the column in the direction of lateral loading

Table 6.1: Nominal Flexural Capacity

Design Code	SR_4_10_5			PTB_4.5_1_0			PTB_4.5_1_4			PTB_9_2_0		
	kip	kN	%	kip	kN	%	kip	kN	%	kip	kN	%
Measured	51.2	228	-	59.4	264	-	60.9	271	-	61.7	274	-
ACI 318-19	46.1	205	111	47.3	210	126	46.9	209	130	46.8	208	132
EN 1992-1-1 2004	64.2	286	80	65.3	291	91	64.9	289	94	64.9	289	95
JSCE-SPCS-2007	63.4	282	81	64.8	288	92	64.3	286	95	64.3	286	96
CSA-A23.3-04	46.9	209	109	48.1	214	124	47.7	212	128	47.6	212	130
NZS 3101.1:2006	47.0	209	109	48.3	215	123	47.8	213	127	47.8	213	129

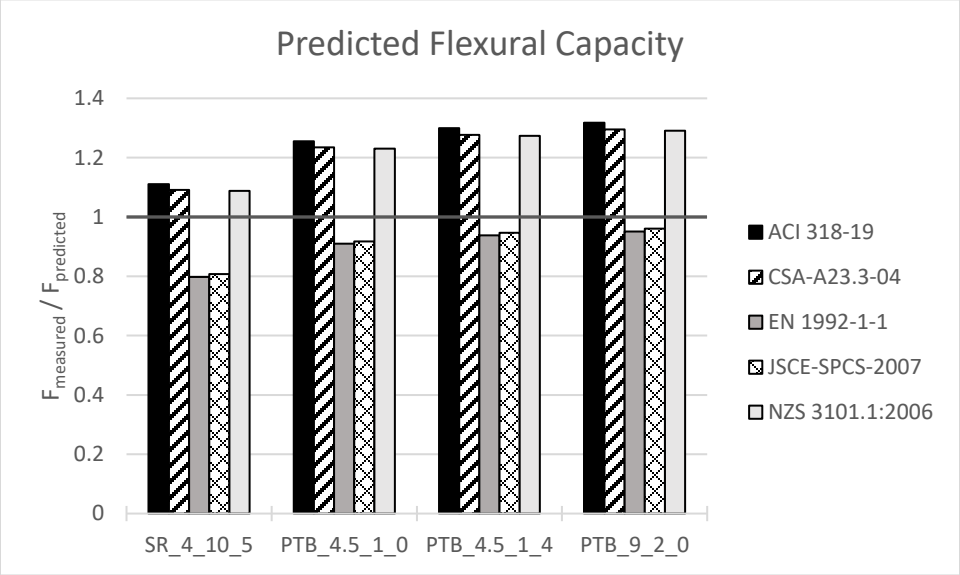

Figure 6-2: Normalized Predicted Flexural Capacity

6.1.2 *One-Way Shear*

One-way shear strength was calculated assuming a shear plane across the width of the slab developing at the edge of the column for Specimen SR_4_10_5 or at the edge of the ring for specimens with ring plates. The nominal one-way shear capacity was then used to calculate the force that needed to be applied by the MTS actuator to reach the nominal one-way shear capacity of the slab.

6.1.2.1 ACI 318-19 One-Way Shear Resistance

Nominal one-way shear strength is calculated using Section 22.5 of ACI 318-19. The nominal shear capacity is calculated according to Equation 5.1

$$V_n = V_c + V_s \tag{6.3}$$

Where,

V_n = nominal shear strength (lbs.)

V_c = nominal shear strength provided by the concrete (lbs.)

V_s = nominal shear strength provided by shear reinforcement (lbs.)

If $A_v \geq A_{v,min}$, V_c is calculated using either Equation 6.4 or Equation 6.5.

$$(a) V_c = \left[2\lambda\sqrt{f'_c} + \frac{N_u}{6A_g}\right] b_w d \tag{6.4}$$

$$(b) V_c = \left[8\lambda(\rho_w)^{\frac{1}{3}}\sqrt{f'_c} + \frac{N_u}{6A_g}\right] b_w d \tag{6.5}$$

If $A_v \leq A_{v,min}$, V_c is calculated using either Equation 6.6.

$$(c) V_c = \left[8\lambda_s\lambda(\rho_w)^{1/3}\sqrt{f'_c} + \frac{N_u}{6A_g}\right] b_w d \tag{6.6}$$

Where,

λ_s = factor used to modify shear strength based on the effects of member depth

λ = modification factor to reflect the reduced mechanical properties of lightweight concrete relative to normal-weight concrete of the same compressive strength

ρ_w = ratio of A_s to $b_w d$

f'_c = specified compressive strength of concrete (psi)

N_u = factored axial force normal to cross section occurring simultaneously with V_u or T_u (lbs.)

A_g = gross area of concrete section (in.)

b_w = web width or diameter of circular section (in.)

d = distance from extreme compression fiber to centroid of longitudinal compression reinforcement (in.)

When shear reinforcement is present, V_s is calculated using Equation 6.7.

$$V_s = \frac{A_v f_{yt} d}{s} \qquad 6.7$$

Where,

A_v = area of shear reinforcement within spacing s (in.^{2})

f_{yt} = specified yield strength of transverse reinforcement (psi)

s = center-to-center spacing of items (in.)

The values used to calculate the nominal one-way shear resistance, V_n, are tabulated in Table 6.2.

Table 6.2: ACI 318-19 One-Way Shear Calculation

	SR_4_10_5	PTB_4.5_1_0	PTB_4.5_1_4	PTB_9_2_0
V_n (kip)	183.2	94.0	233.7	87.3
V_c (kip)	79.5	94.0	88.0	87.3
V_s (kip)	103.7	0	145.8	0
f'_c (psi)	5786	8085	7082	6978
b_w (in.)	72	72	72	72
d (in.)	8.25	8.25	8.25	8.25
λ	1	1	1	1
λ_s	1	1	1	1
N_u (kip)	0	0	0	0
A_g (in.^{2})	720	720	720	720
ρ_w	0.01	0.01	0.01	0.01
A_v (in.^{2})	1.23	0	1.33	0
f_{yt} (ksi)	51.2	NA	60.0	NA
s (in.)	5	NA	4.5	NA

6.1.2.2 EN 1992-1-1 2004 One-Way Shear Resistance

Nominal one-way shear resistance is calculated using Section 6.2 of EN 1992-1-1 2004. The nominal shear capacity when no transverse reinforcement is present is calculated according to Equation 6.8.

$$V_{Rd,c} = \left[C_{Rd,c}k(100\rho_1 f_{ck})^{1/3} + k_1\sigma_{cp}\right]b_w d \qquad 6.8$$

Where,

$V_{Rd,c}$ = the design shear resistance of the member without shear reinforcement (N)

$C_{Rd,c}$ = factor considering the resistance factor γ_c for concrete

k = factor related to the depth of the member

ρ_1 = reinforcing ratio for longitudinal tension reinforcement

f_{ck} = characteristic compressive cylinder strength of concrete (MPa)

k_1 = factor accounting for effects of axial force on the cross section

σ_{cp} = compressive stress in the concrete from axial load or prestressing (MPa)

b_w = the smallest width of the cross-section in the tensile area (mm)

d = effective depth of a cross-section (mm)

The nominal shear resistance when transverse reinforcement is present is calculated according to Equation 6.9 and Equation 6.10.

$$V_{Rd} = V_{Rd,s} + V_{ccd} + V_{td} \quad 6.9$$

$$V_{Rd,s} = \frac{A_{sw}}{s} z\, f_{ywd}\ \cot\theta \quad 6.10$$

Where,

V_{Rd} = design value of the shear force which can be sustained by the member (N)

$V_{Rd,s}$ = design value of the shear force which can be sustained by yielding shear reinforcement (N)

V_{ccd} = design value of the shear component of the force in the compression area, in the case of an inclined compression chord (N)

V_{td} = design value of the shear component of the force in the tensile reinforcement, in the case of an inclined tensile chord (N)

A_{sw} = cross-sectional area of the shear reinforcement (mm^2)

s = spacing of the shear reinforcement (mm)

z = inner lever arm, for a member with constant depth, corresponding to the bending moment in the element under consideration (mm)

f_{ywd} = design yield strength of the shear reinforcement (MPa)

θ = angle between concrete compression strut and the beam axis perpendicular to the shear force

The values used to calculate the one-way shear resistance, V, are tabulated in Table 6.3. The shear capacity was taken as the larger of $V_{Rd,c}$ and V_{Rd}.

Table 6.3: EN 1992-1-1 2004 One-Way Shear Calculation

	SR_4_10_5	PTB_4.5_1_0	PTB_4.5_1_4	PTB_9_2_0
V (kN)	475.7	531.8	508.8	506.3
$V_{Rd,c}$ (kN)	475.7	531.8	508.8	506.3
V_{Rd} (kN)	332.0	0	466.9	0
$V_{Rd,s}$ (kN)	332.0	0	466.9	0
V_{ccd} (kN)	0	0	0	0
V_{td} (kN)	0	0	0	0
f_{ck} (MPa)	39.9	55.7	48.8	48.1
d (mm)	209.6	209.6	209.6	209.6
b_w (mm)	1828.8	1828.8	1828.8	1828.8
$C_{Rd,c}$	0.18	0.18	0.18	0.18
k	1.98	1.98	1.98	1.98
k_1	0.15	0.15	0.15	0.15
ρ_1	0.01	0.01	0.01	0.01
σ_{cp} (MPa)	0	0	0	0
A_{sw} (mm^2)	791.7	0	855.1	0
f_{ywd} (MPa)	282,4	NA	330.9	NA
s (mm)	127	NA	114.3	NA
z (mm)	188.6	188.6	188.6	188.6
θ (°)	45	45	45	45

6.1.2.3 JSCE-SPCS-2007 One-Way Shear Resistance

Nominal one-way shear resistance is calculated using Section 9.2.2.2 of JSCE-SPCS-2007. The nominal shear capacity is calculated according to Equation 6.11.

$$V_{yd} = V_{cd} + V_{sd} + V_{ped} \tag{6.11}$$

Where,

V_{yd} = design shear capacity of a member (N)

V_{cd} = design shear capacity of linear members without shear reinforcing steel (N)

V_{sd} = design shear capacity of shear reinforcement (N)

V_{ped} = component of effective tensile force in longitudinal tendon parallel to the shear force (N)

The nominal shear resistance provided by the concrete is calculated according to Equation 6.12.

$$V_{cd} = \beta_d * \beta_p * \beta_n * f_{vcd} * b_w * d \,/\, \gamma_b \qquad 6.12$$

Where,

β_d = factor for the depth of the cross section

β_p = factor for the longitudinal reinforcing ratio

β_n = factor for the moment on the cross section

f_{vcd} = design compressive strength of the concrete (MPa)

b_w = web width (mm)

d = effective depth (mm)

γ_b = resistance factor

The nominal shear resistance provided by shear reinforcement is calculated according to Equation 6.13.

$$V_{sd} = \left[A_w f_{wyd}(\sin\alpha_s + \cos\alpha_s)/S_s + A_{pw}\sigma_{pw}\left(\sin\alpha_p + \cos\alpha_p\right)/S_p\right]z \,/\, \gamma_b \qquad 6.13$$

Where,

A_w = total area of shear reinforcement placed in S_s (mm^2)

f_{wyd} = design yield strength of shear reinforcement (MPa)

α_s = angle between shear reinforcement and member axis

S_s = spacing of shear reinforcement (mm)

A_{pw} = total area of prestressing steel expected to act as shear reinforcement placed in S_p (mm)

σ_{pw} = prestressing stress plus design yield stress of prestressing steel expected to act as shear reinforcement (MPa)

α_p = angle between prestressing steel acting as shear reinforcement and member axis

S_p = spacing of prestressing steel expected to act as shear reinforcement (mm)

z = distance from location of compressive stress resultant to centroid of tension steel (mm)

γ_b = resistance factor

The nominal shear resistance provided by inclined longitudinal prestressing steel is calculated according to Equation 6.14.

$$V_{ped} = P_{ed} * \sin \alpha_p \ / \gamma_b \qquad 6.14$$

Where,

P_{ed} = effective tensile force in longitudinal prestressing steel (N)

α_p = able between extreme compression fiber and member axis

γ_b = resistance factor

The values used to calculate the one-way shear resistance, V_{yd}, are tabulated in Table 6.4.

Table 6.4: JSCE-SPCS-2007 One-Way Shear Calculation

	SR_4_10_5	PTB_4.5_1_0	PTB_4.5_1_4	PTB_9_2_0
V_{yd} (kN)	822.9	416.3	1006.2	416.3
V_{cd} (kN)	395.1	416.3	416.3	416.3
V_{sd} (kN)	427.7	0	589.9	0
V_{ped} (kN)	0	0	0	0
f_{ved} (MPa)	0.68	0.72	0.72	0.72
d (mm)	209.6	209.6	209.6	209.6
b_w (mm)	1828.8	1828.8	1828.8	1828.8
β_d	1.48	1.48	1.48	1.48
β_p	1.02	1.02	1.02	1.02
β_n	1	1	1	1
γ_b	1	1	1	1
f_{ywd} (MPa)	353.0	NA	NA	NA
A_w (mm^2)	791.7	0	0	0
α_s (°)	90	NA	NA	NA
S_s (mm)	127	NA	NA	NA
σ_{pw} (MPa)	NA	NA	400	NA
A_{pw} (mm^2)	0	0	855.1	0
α_p (°)	NA	NA	90	NA
s_p (mm)	NA	NA	114.3	NA
z (mm)	194.4	NA	197.1	NA
P_{ed} (N)	0	0	0	0
α_p (°)	NA	NA	NA	NA

6.1.2.4 CSA-A23.3-04 One-Way Shear Resistance

Nominal one-way shear resistance is calculated using Section 11.3.3 of CSA-A23.3-04. The nominal shear capacity is calculated according to Equation 6.15. V_p is taken as zero as the test specimens were not prestressed.

$$V_r = V_c + V_s + V_p \quad 6.15$$

Where,

V_r = factored shear resistance (N)

V_c = shear resistance attributed to the concrete factored by φ_c (N)

V_s = shear resistance provided by shear reinforcement factored by φ_s (N)

V_p = component in the direction of the applied shear of the effective prestressing force factored by φ_p (N)

The nominal shear resistance provided by the concrete is calculated according to Equation 6.16. φ_c is taken as 1.0 for the purpose of these calculations.

$$V_c = \varphi_c \, \lambda \, \beta \, \sqrt{f'_c} \, b_w \, d_v \quad 6.16$$

Where,

φ_c = resistance factor for concrete

λ = factor to account for low-density concrete

β = factor accounting for shear resistance of cracked concrete

f'_c = specified compressive strength of concrete (MPa)

b_w = width of web (mm)

d_v = effective shear depth, taken as the greater of $0.9d$ or $0.72h$ (mm)

The nominal shear resistance provided by the transverse reinforcement is calculated according to Equation 6.17. φ_s is taken as 1.0 for the purpose of these calculations.

$$V_s = \frac{\varphi_s A_v f_y d_v \cot\theta}{s} \quad 6.17$$

Where,

φ_s = resistance factor for non-prestressed reinforcing bars

A_v = area of shear reinforcement within a distance s (mm^2)

f_y = specified yield strength of non-prestressed reinforcement or anchor steel (MPa)

θ = angle of inclination of diagonal compressive stresses to the longitudinal axis of the member

s = spacing of shear or torsion reinforcement measured parallel to the longitudinal axis of the member (mm)

The values used to calculate the one-way shear resistance, V_r, are tabulated in Table 6.5.

Table 6.5: CSA-A23.3-04 One-Way Shear Calculation

	SR_4_10_5	PTB_4.5_1_0	PTB_4.5_1_4	PTB_9_2_0
V_r (kN)	984.8	498.3	1267.3	462.9
V_c (kN)	392.1	498.3	433.8	462.9
V_s (kN)	592.7	0	833.5	0
V_p (kN)	0	0	0	0
f'_c (MPa)	39.9	55.7	48.8	48.1
d_v (mm)	188.6	188.6	188.6	188.6
b_w (mm)	1828.8	1828.8	1828.8	1828.8
λ	1	1	1	1
β	0.18	0.19	0.18	0.19
φ_c	1	1	1	1
f_y (MPa)	353.0	NA	413.7	NA
A_v (mm^2)	791.7	0	855.1	0
s (mm)	127	NA	114.3	NA
θ (°)	35	35	35	35
φ_s	1	1	1	1

6.1.2.5 NZS 3101.1:2006 One-Way Shear Resistance

Nominal one-way shear resistance is calculated using Section 7.5 of NZS 3101.1:2006. The nominal shear capacity is calculated according to Equation 6.18.

6.18

$$V_n = V_s + V_c$$

Where,

V_n = total nominal shear strength of section (N)

V_s = nominal shear strength provided by the shear reinforcement (N)

V_c = nominal shear strength provided by concrete (N)

The nominal shear resistance provided by the concrete is calculated according to Equation 6.19 and Equation 6.20.

$$V_c = v_c A_{cv} \quad 6.19$$

Where,

v_c = nominal shear stress (MPa)

A_{cv} = the effective shear area (mm^2)

$$v_c = k_d k_a v_b \quad 6.20$$

Where,

k_d = factor allowing for the influence of member depth on shear strength

k_a = factor allowing for the influence of aggregate size on shear strength

v_b = basic shear stress (MPa)

The nominal shear resistance provided by the transverse reinforcement is calculated according to Equation 6.21.

$$V_s = A_v f_{yt} \frac{d}{s} \quad 6.21$$

Where,

A_v = area of shear reinforcement perpendicular to the span within a distance s (mm)

f_{yt} = design yield strength of transverse reinforcement provided for shear and/or torsion (MPa)

d = distance from extreme compression fiber to centroid of tension reinforcement (mm)

s = center-to-center spacing of shear or torsional reinforcement measured in the direction parallel to the longitudinal reinforcement (mm)

The values used to calculate the one-way shear resistance, V_n, are tabulated in Table 6.6.

Table 6.6: NZS 3101.1:2006 One-Way Shear Calculation

	SR_4_10_5	PTB_4.5_1_0	PTB_4.5_1_4	PTB_9_2_0
V_n (kN)	945.2	541.9	1184.1	531.6
V_c (kN)	484.1	541.9	535.6	531.6
V_s (kN)	461.1	0	648.5	0
v_c (MPa)	1.26	1.41	1.40	1.39
A_{cv} (mm^2)	383225	383225	383225	383225
k_d	1	1	1	1
k_a	1	1	1	1
v_b (MPa)	1.26	1.41	1.40	1.39
A_v (mm^2)	791.7	0	855.1	0
f_{yt} (MPa)	353.0	NA	413.7	NA
d (mm)	209.6	209.6	209.6	209.6
s (mm)	127	NA	114.3	NA

6.1.2.6 Predicted One-Way Shear Strength

To calculate the force needed to be applied by the MTS Actuator to reach the nominal one-way shear capacity, Equation 6.22 was used. The MTS Actuator force needed to cause the slab to reach the nominal one-way capacity of each specimen is recorded in Table 6.7. Figure 6-3 shows the force needed to cause the slab to reach the nominal one-way capacity normalized by the measured capacity of each specimen.

$$P_n = \frac{L * V_n}{h} \qquad 6.22$$

Where,

P_n = the MTS Actuator force to cause the desired failure

V_n = the nominal one-way shear capacity of the slab

h = the height from the slab centerline to the level of the applied force (F_1)

L = the distance from the column centerline to the reaction force (F_2)

Table 6.7: Nominal One-Way Shear Capacity

Design code	SR_4_10_5			PTB_4.5_1_0			PTB_4.5_1_4			PTB_9_2_0		
	kip	kN	%	kip	kN	%	kip	kN	%	kip	kN	%
Experimental	51.2	228	-	59.4	264	-	60.9	271	-	61.7	275	-
ACI 318-19	175.5	781	29	90.1	401	66	224.0	996	27	83.7	372	74
EN 1992-1-1 2004	102.5	456	50	114.6	510	52	109.6	488	56	109.1	485	57
JSCE-SPCS-2007	176.7	786	29	89.7	399	66	216.1	961	28	89.7	399	69
CSA-A23.3-04	212.2	944	24	107.4	478	55	273.0	1214	22	99.7	443	62
NZS 3101.1:2006	203.6	906	25	116.8	520	51	255.1	1135	24	114.5	509	54

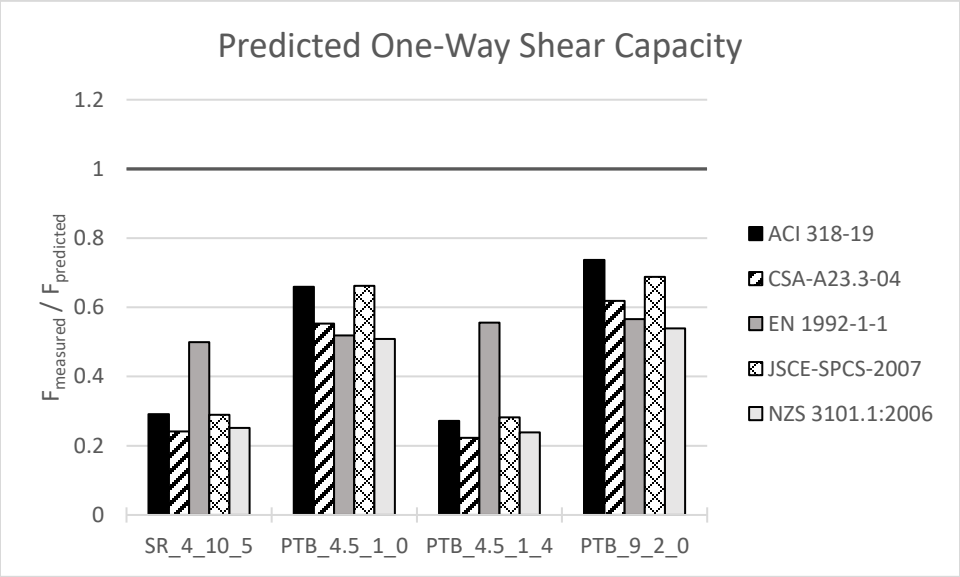

Figure 6-3: Normalized Nominal One-Way Shear Capacity

6.1.3 *Two-Way Shear*

Two-way shear strength was calculated assuming a critical perimeter prescribed by each design code that develops the prescribed distance from the column for Specimen SR_4_10_5 or the prescribed distance from the edge of the ring for specimens with ring plates. The nominal two-way shear capacity was then used to calculate the force that needed to be applied by the MTS actuator to reach the nominal two-way shear capacity of the slab.

6.1.3.1 ACI 318-19 Two-Way Shear Resistance

Nominal two-way shear strength on the critical section is calculated using Section 22.6 of ACI 318-19. The nominal shear resistance when no transverse reinforcement is present is calculated according to Equation 6.23.

$$v_n = v_c \tag{6.23}$$

Where,

v_n= equivalent concrete stress corresponding to nominal two-way shear strength of slab or footings (psi)

v_c= stress corresponding to nominal two-way shear strength provided by concrete (psi)

When transverse reinforcement is not present, v_c is calculated as the lesser of Equation 6.24, Equation 6.25, and Equation 6.26.

$$(a) v_c = 4\lambda_s\lambda\sqrt{f'_c} \tag{6.24}$$

$$(b) v_c = \left(2 + \frac{4}{\beta}\right)\lambda_s\lambda\sqrt{f'_c} \tag{6.25}$$

6.26

$$(c) v_c = \left(2 + \frac{\alpha_s d}{b_o}\right) \lambda_s \lambda \sqrt{f'_c}$$

Where,

λ_s= factor used to modify shear strength based on the effects of member depth

λ= modification factor to reflect the reduced mechanical properties of lightweight concrete relative to normal-weight concrete of the same compressive strength

f'_c= specified compressive strength of concrete in psi

β= ratio of long to short dimensions of sides of column

α_s= 40 for interior columns, 30 for edge columns, and 20 for corner columns

d= distance from extreme compression fiber to centroid of longitudinal compression reinforcement (in.)

b_o= perimeter of critical section for two-way shear in slabs and footings (in.)

The nominal shear resistance when transverse reinforcement is present is calculated according to Equation 6.27.

$$v_n = v_c + v_s \qquad 6.27$$

When transverse reinforcement is present, v_c is calculated as the lesser of Equation 6.28, Equation 6.29, and Equation 6.30 and v_s is calculated using Equation 6.31.

$$(a) v_c = 3\lambda_s \lambda \sqrt{f'_c} \qquad 6.28$$

$$(b) v_c = \left(2 + \frac{4}{\beta}\right) \lambda_s \lambda \sqrt{f'_c} \qquad 6.29$$

$$(c) v_c = \left(2 + \frac{\alpha_s d}{b_o}\right) \lambda_s \lambda \sqrt{f'_c} \qquad 6.30$$

$$v_s = \frac{A_v f_{yt}}{b_o s} \quad 6.31$$

Where,

A_v= area of shear reinforcement within spacing s (in.)

f_{yt}= specified yield strength of transverse reinforcement (psi)

s= center-to-center spacing of items (in)

The values used to calculate v_n are tabulated in Table 6.8.

Table 6.8: ACI 318-19 Two-Way Shear Calculation

	SR_4_10_5	PTB_4.5_1_0	PTB_4.5_1_4	PTB_9_2_0
v_n (psi)	712.0	359.7	599.5	334.1
v_c (psi)	388.2	359.7	252.5	334.1
v_s (psi)	483.8	0	147.0	0
f'_c (psi)	5786	8085	7082	6978
d (in.)	8.25	8.25	8.25	8.25
b_o (in.)	103.9	135.8	135.8	167.7
λ	1	1	1	1
λ_s	1	1	1	1
β	1	1	1	1
α_s	40	40	40	40
A_v (in.^{2})	4.91	0	3.53	0
f_{yt} (ksi)	51.2	NA	60.0	NA
s (in.)	5	NA	4.5	NA

In the commentary on Section 8.4.4.2.3 in ACI 318-19, Equation 6.32 is given to account for the effects moment transfer from the slab to the column due to unbalanced moments.

$$v_{u,AB} = v_{uv} + \frac{\gamma_v M_{sc} c_{AB}}{J_c} \quad 6.32$$

Where,

$v_{u,AB}$= the stress at the extreme fiber of the critical section due to the superposition of gravity loads and unbalanced moments (psi)

v_{uv}= factored shear stress on the slab critical section for two-way action (psi)

γ_v= factor used to determine the fraction of M_{sc} transferred by eccentricity of shear at slab-column connections

M_{sc}= factored slab moment resisted by the column at a joint (in.-lbs.)

c_{AB}= distance from the centroidal axis of the critical section to the extreme fiber of the critical section (in.)

J_c= property of assumed critical section analogous to polar moment of inertia (in^4)

The unbalanced moment the slab is capable of carrying can be calculated by taking $v_n = v_{u,AB}$ and assuming the shear from gravity loading is negligible due to redistribution of the slab dead load to the slab end roller supports during testing. The values used to calculate M_{sc} are tabulated in Table 6.9.

Table 6.9: ACI 318-19 Unbalanced Moment Shear Calculation

	SR_4_10_5	PTB_4.5_1_0	PTB_4.5_1_4	PTB_9_2_0
M_{sc} (kip-in.)	11009.9	12255.3	20426.9	21265.3
$v_{u,AB}$ (psi)	712.0	359.7	599.5	334.1
v_{uv} (psi)	0	0	0	0
γ_v	0.4	0.4	0.4	0.4
c_{AB} (in.)	13.2	17.2	17.2	21.2
J_c (in^4)	81877	234765	234765	540011

6.1.3.2 EN 1992-1-1 2004 Two-Way Shear Resistance

Nominal two-way shear strength on the critical section is calculated using Section 6.4 of EN 1992-1-1 2004. The nominal shear resistance when no shear reinforcement is present is calculated according to Equation 6.33.

$$v_{Rd,c} = C_{Rd,c}k(100\rho_1 f_{ck})^{1/3} + k_1\sigma_{cp} \geq (v_{min} + k_1\sigma_{cp}) \quad 6.33$$

Where,

$v_{Rd,c}$ = the design punching shear resistance of the slab without shear reinforcement (MPa)

$C_{Rd,c}$ = factor considering the resistance factor γ_c for concrete

k = factor related to the depth of the member

ρ_1 = reinforcing ratio for longitudinal reinforcement

f_{ck} = characteristic compressive cylinder strength of concrete at 28 days (MPa)

k_1 = factor accounting for effects of axial force on the cross section

σ_{cp} = compressive stress in the concrete from axial load or prestressing (MPa)

v_{min} = minimum shear stress (MPa)

The nominal shear resistance when shear reinforcement is present is calculated according to Equation 6.33.

$$v_{Rd,cs} = 0.75\, v_{Rd,c} + 1.5\, (d/s_r)\, A_{sw}\, f_{ywd,ef}\, \left(1/(u_1 d)\right) \sin\alpha \qquad 6.34$$

Where,

$v_{Rd,cs}$ = the design punching shear resistance of the slab with shear reinforcement (MPa)

d = mean of the effective depths in the orthogonal directions (mm)

s_r = radial spacing of perimeters of shear reinforcement (mm)

A_{sw} = area of one perimeter of shear reinforcement around the column (mm^2)

$f_{ywd,ef}$ = effective design strength of the punching shear reinforcement (MPa)

u_1 = the length of the basic control perimeter 2d away from the column (mm)

α = angle between the shear reinforcement and the plane of the slab

The values used to calculate $v_{Rd,c}$ and $v_{Rd,cs}$ are tabulated in Table 6.10.

Table 6.10: EN 1992-1-1 2004 Two-Way Shear Calculation

	SR_4_10_5	PTB_4.5_1_0	PTB_4.5_1_4	PTB_9_2_0
$v_{Rd,c}$ (MPa)	1.24	1.39	1.33	1.32
v_{min} (MPa)	0.61	0.73	0.68	0.67
$v_{Rd,cs}$ (MPa)	3.43	NA	2.82	NA
f_{ck} (MPa)	39.9	55.7	48.8	48.1
d (mm)	209.6	209.6	209.6	209.6
u_1 (mm)	4229.2	4947.4	4947.4	5665.5
$C_{Rd,c}$	0.18	0.18	0.18	0.18
k	1.98	1.98	1.98	1.98
k_1	0.15	0.15	0.15	0.15
ρ_1	0.01	0.01	0.01	0.01
σ_{cp} (MPa)	0	0	0	0
A_{sw} (mm^2)	3166.9	0	2280.2	0
$f_{ywd,ef}$ (MPa)	282.4	NA	302.4	NA
s_r (mm)	127	NA	114.3	NA
α (°)	90	90	90	90

In Section 6.4.3 in EN 1992-1-1 2004, Equation 6.35 and Equation 6.36 are given to account for the effects moment transfer from the slab to the column due to unbalanced moments. Combining these equations and assuming the shear from gravity loading can be neglected because it was redistributed from the slab dead load to the slab end roller supports during testing results in Equation 6.37.

$$v_{Ed} = \beta \frac{V_{Ed}}{u_i d} \tag{6.35}$$

$$\beta = 1 + 0.6\pi \frac{M_{Ed}}{V_{Ed}(D + 4d)} \tag{6.36}$$

$$v_{Ed} = \frac{V_{Ed}}{u_i d} + 0.6\pi \frac{M_{Ed}}{u_i d(D + 4d)} \tag{6.37}$$

Where,

v_{Ed} = maximum shear stress on the perimeter (MPa)

V_{Ed} = shear force acting on the perimeter (N)

u_i = the length of the control perimeter being considered (mm)

M_{Ed} = unbalanced moment being transferred from the slab to the column (N-mm)

D = the diameter of the circular column (mm)

The unbalanced moment the slab is capable of carrying can be calculated by taking $Max(v_{Rd,c}, v_{Rd,cs}) = v_{Ed}$. The values used to calculate M_{Ed} are tabulated in Table 6.11.

Table 6.11: EN 1992-1-1 2004 Unbalanced Moment Shear Calculation

	SR_4_10_5	PTB_4.5_1_0	PTB_4.5_1_4	PTB_9_2_0
M_{Ed} (kN-m)	2170.1	1202.0	2446.7	1500.8
V_{Ed} (kN)	0	0	0	0
v_{Ed} (MPa)	3.43	1.39	2.82	1.32
u_i (mm)	4229.2	4947.4	4947.4	5665.5
d_{eff} (mm)	209.6	209.6	209.6	209.6
D (mm)	508	736.6	736.6	965.2

6.1.3.3 JSCE-SPCS-2007 Two-Way Shear Resistance

Nominal two-way shear strength on the critical section is calculated using Section 9.2.2.3 of JSCE-SPCS-2007. The nominal shear resistance is calculated according to Equation 6.38.

$$V_{pcd} = \beta_d * \beta_p * \beta_r * f_{ped} * u_p * d/\gamma_b \quad 6.38$$

Where, (units)

V_{pcd} = design punching shear capacity (N)

β_d = factor for the depth of the cross section

β_p = factor for the reinforcing ratio in both directions

β_r = factor for the critical perimeter and the effective depth

f_{pcd} = design strength of the concrete (MPa)

u_p = peripheral length of the design cross section located at a distance $d/2$ from the loaded area (mm)

d = average effective depth in both directions (mm)

γ_b = member resistance factor

The two-way shear design expressions included in JSCE-SPCS-2007 does not account for additional strength due to shear reinforcement nor do the design expressions include a direct way of calculating the effects of moment transfer to the column. Due to these factors, two-way shear strength was not calculated using JSCE-SPCS-2007.

6.1.3.4 CSA-A23.3-04 Two-Way Shear Resistance

Nominal two-way shear strength on the critical section is calculated using Section 13.3 of CSA-A23.3-04. The nominal shear resistance when no shear reinforcement is present is calculated according to Equation 6.33.

$$v_r = v_c \tag{6.39}$$

Where, (units)

v_r = factored shear stress resistance (MPa)

v_c = factored shear stress resistance provided by the concrete (MPa)

When no transverse reinforcement is present, v_c is calculated as the least of Equation 6.40, Equation 6.41, or Equation 6.42.

$$(a) v_c = \left(1 + \frac{2}{\beta_c}\right) 0.19 \lambda \varphi_c \sqrt{f'_c} \quad 6.40$$

$$(b) v_c = \left(\frac{\alpha_s d}{b_o} + 0.19\right) \lambda \varphi_c \sqrt{f'_c} \quad 6.41$$

$$(c) v_c = 0.28 \lambda \varphi_c \sqrt{f'_c} \quad 6.42$$

Where,

β_c = ratio of long side to short side of concentrated load or reaction area

λ = factor to account for low-density concrete

φ_c = resistance factor for concrete

f'_c = specified compressive strength of concrete (MPa)

α_s = factor that adjusts v_c for support dimensions

d = distance from extreme compression fiber to centroid of longitudinal tension reinforcement (mm)

b_o = perimeter of critical section for shear in slabs and footings (MM)

The nominal shear resistance when transverse reinforcement is present is calculated according to Equation 6.43.

$$v_r = v_c + v_s \quad 6.43$$

Where,

v_s = factored shear stress resistance provided by shear reinforcement (MPa)

When transverse reinforcement is present, v_c is calculated using Equation 6.44 and v_s is calculated using Equation 6.45.

$$v_c = 0.28\lambda\varphi_c\sqrt{f'_c} \quad 6.44$$

$$v_s = \frac{\varphi_s A_{vs} f_{yv}}{b_o s} \quad 6.45$$

Where,

φ_s = resistance factor for non-prestressed reinforcing bars

A_{vs} = cross-sectional area of headed shear reinforcement on a line parallel to the perimeter of the column (mm^2)

f_{yv} = specified yield strength of headed shear reinforcement (MPa)

s = spacing of headed shear reinforcement or stirrups measured perpendicular to b_o (mm)

The values used to calculate v_r are tabulated in Table 6.12.

Table 6.12: CSA-A23.3-04 Two-Way Shear Calculation

	SR_4_10_5	PTB_4.5_1_0	PTB_4.5_1_4	PTB_9_2_0
v_r (MPa)	5.67	2.84	4.73	2.64
v_c (MPa)	1.78	2.84	1.96	2.64
v_s (MPa)	3.90	0	2.78	0
f'_c (MPa)	39.9	55.7	48.8	48.1
d (mm)	209.6	209.6	209.6	209.6
b_o (mm)	2254.2	2972.4	2972.4	3690.6
λ	1	1	1	1
β_c	1	1	1	1
α_s	4	4	4	4
φ_c	1	1	1	1
f_{yv} (MPa)	353.0	NA	413.7	NA
A_{vs} (mm^2)	3166.9	0	2280.1	0
s (mm)	127	NA	114.3	NA
φ_s	1	1	1	1

In Section 13.3.5.5 in CSA-A23.3-04, Equation 6.46 accounts for the effect of moment transfer from the slab to the column due to unbalanced moments.

$$v_f = \frac{V_f}{b_o d} + \left(\frac{\gamma_v M_f e}{J}\right)_x + \left(\frac{\gamma_v M_f e}{J}\right)_y \quad 6.46$$

Where,

v_f = factored shear stress (MPa)

V_f = factored shear force (N)

γ_v = fraction of unbalanced moment transferred by eccentricity of shear at slab-column connections

M_f = factored moment at interior support resisted by elements above and below the slab (N-m)

e = distance from the centroid of section for critical shear to point where shear stress is being calculated (mm)

J = property of the critical shear section analogous to the polar moment of inertia (mm^4)

The unbalanced moment the slab is capable of carrying can be calculated by taking $v_r = v_f$ and assuming the shear from gravity loading is negligible due to redistribution of the slab dead load to the slab end roller supports during testing. The values used to calculate M_f are tabulated in Table 6.13. The moment is assumed to be only in the x-direction.

Table 6.13: CSA-A23.3-04 Unbalanced Moment Shear Calculation

	SR_4_10_5	PTB_4.5_1_0	PTB_4.5_1_4	PTB_9_2_0
M_f (kN-m)	1028.9	1179.6	1967.9	2097.6
v_f (MPa)	5.67	2.84	4.73	2.64
V_f (kN)	0	0	0	0
d (mm)	209.6	209.6	209.6	209.6
b_o (mm)	2254.2	2972.4	2972.4	3690.6
γ_v	0.4	0.4	0.4	0.4
e (mm)	358.8	473.1	473.1	587.4
J (mm^4)	$2.60*10^{10}$	$7.87*10^{10}$	$7.87*10^{10}$	$18.70*10^{10}$

6.1.3.5 NZS 3101.1:2006 Two-Way Shear Resistance

Nominal two-way shear strength on the critical section is calculated using Section 12.7.3 of NZS 3101.1:2006. The nominal shear resistance is calculated according to Equation 6.47.

$$V_n = V_s + V_c \tag{6.47}$$

Where,

V_n = nominal shear strength of section (N)

V_s = nominal shear strength provided by the shear reinforcement (N)

V_c = nominal shear strength provided by the concrete mechanisms (N)

The contribution of the concrete to the shear strength is calculated using Equation 6.48.

$$V_c = v_c b_o d \tag{6.48}$$

Where (units),

v_c = shear stress resisted by concrete (MPa)

b_o = perimeter of critical section for slabs and foundations (mm)

d = distance from extreme compression fiber to centroid of tension reinforcement (mm)

The shear stress resisted by the concrete is calculated as the least of Equation 6.49, Equation 6.50, and Equation 6.51.

$$(a) v_c = \frac{1}{6} k_{ds} \left(1 + \frac{2}{\beta_c}\right) \sqrt{f'_c} \tag{6.49}$$

$$(b) \quad v_c = \frac{1}{6} k_{ds} \left(\frac{\alpha_s d}{b_o} + 1\right) \sqrt{f'_c} \tag{6.50}$$

6.51

$$(c) v_c = \frac{1}{3} k_{ds} \sqrt{f'_c}$$

Where,

k_{ds} = allows for the influence of size on v_c

β_c = ratio of long side to short side of concentrated load or reaction area

f'_c = specified compressive strength of concrete (MPa)

α_s = factor accounting for columns

The contribution of the shear reinforcement to the shear strength is calculated using Equation 6.52.

$$V_s = A_v f_{yv} \frac{d}{s} \qquad 6.52$$

Where,

A_v = area of shear reinforcement within a distance s (mm^2)

f_{yv} = design yield strength of transverse reinforcement provided for shear and/or torsion (MPa)

s = center-to-center spacing of shear or torsional reinforcement measured in the direction parallel to the longitudinal reinforcement (mm)

The values used to calculate V_n are tabulated in Table 6.14.

Table 6.14: NZS 3101.1:2006 Two-Way Shear Calculation

	SR_4_10_5	PTB_4.5_1_0	PTB_4.5_1_4	PTB_9_2_0
V_n (kN)	2462.0	1864.0	2622.2	2121.2
V_c (kN)	617.4	1864.0	892.8	2121.2
V_s (kN)	1844.6	0	1729.3	0
v_c (MPa)	1.05	2.43	1.16	2.24
b_o (mm)	2639	3449	3449	4260
d (mm)	209.6	209.6	209.6	209.6
f'_c (MPa)	39.9	55.7	48.8	48.1
k_{ds}	0.98	0.98	0.98	0.98
β_c	1	1	1	1
α_s	20	20	20	20
f_{yv} (MPa)	353.0	NA	413.7	NA
A_v (mm^2)	3167	0	2280	0
s (mm)	127	NA	114.3	NA

In Section 12.7.7 of the commentary in NZS 3101.2:2006, Equation 6.53 is given to account for the effects moment transfer from the slab to the column due to unbalanced moments.

$$v_{AB} = \frac{V^*}{A_c} + \frac{\gamma_v M^* c_{AB}}{J_c} \qquad 6.53$$

Where,

v_{AB} = maximum design shear stress on section AB (MPa)

V^* = design shear force (N)

A_c = area of concrete section resisting shear transfer (mm^2)

γ_v = fraction of unbalanced moment considered to be transferred by eccentricity of shear

M^* = unbalanced moment (N-m)

c_{AB} = distance from the centroid of the critical section to the extreme fiber of the critical section (mm)

J_c = property of assumed critical section analogous to polar moment of inertia (mm^4)

The unbalanced moment the slab is capable of carrying can be calculated by taking $V_n/(b_o d) = v_f$ and assuming the shear from gravity loading, V^*, is negligible due to redistribution

of the slab dead load to the slab end roller supports during testing. The values used to calculate M^* are tabulated in Table 6.15.

Table 6.15: NZS 3101.1:2006 Unbalanced Moment Shear Calculation

	SR_4_10_5	PTB_4.5_1_0	PTB_4.5_1_4	PTB_9_2_0
M^* (kN-m)	1107.6	1820.5	2466.6	2977.7
v_{AB} (MPa)	3.16	2.58	3.49	2.38
V^* (kN)	0	0	0	0
A_c (mm^2)	553005	722817	722817	892629
γ_v	0.4	0.4	0.4	0.4
c_{AB} (mm)	225.1	326.4	326.4	427.7
J_c (mm^4)	$3.16*10^{10}$	$9.22*10^{10}$	$9.22*10^{10}$	$21.45*10^{10}$

6.1.3.6 Predicted Strength

To calculate the force needed to be applied by the MTS Actuator to reach the nominal two-way shear capacity, Equation 6.22 was used. The MTS Actuator force needed to cause the slab to reach the nominal two-way capacity for each specimen is recorded in Table 6.16. Figure 6-4 shows the force needed to cause the slab to reach the nominal two-way capacity for each specimen. Normalized by the measured capacity of each specimen. EN 1992-1-1 2004 tended to predict lower two-way shear strength than other design codes, especially in the specimens without shear reinforcement beyond the ring plate.

$$P_n = \frac{0.5 * M_{unbalanced}}{h} \qquad 6.54$$

Where,

P_n = the MTS Actuator force to cause the desired failure

$M_{unbalanced}$ = the unbalanced moment that will cause a two-way shear failure in the slab

h = the height from the slab centerline to the level of the applied force (F_1)

Table 6.16: Nominal Two-Way Shear Capacity

Design code	SR_4_10_5			PTB_4.5_1_0			PTB_4.5_1_4			PTB_9_2_0		
	kip	kN	%	kip	kN	%	kip	kN	%	kip	kN	%
Measured	51.2	228	-	59.4	264	-	60.9	271	-	61.7	275	-
ACI 318-19	79.9	355	64	89.0	396	67	148.3	660	41	154.4	687	40
EN 1992-1-1 2004	69.7	310	73	38.6	172	154	78.6	350	77	48.2	214	128
JSCE-SPCS-2007	NA	NA	NA	NA	NA	NA	NA	NA	NA	NA	NA	NA
CSA-A23.3-04	66.1	294	77	75.8	337	78	126.4	562	48	134.8	600	46
NZS 3101.1:2006	71.2	317	72	117.0	520	51	158.5	705	38	191.3	851	32

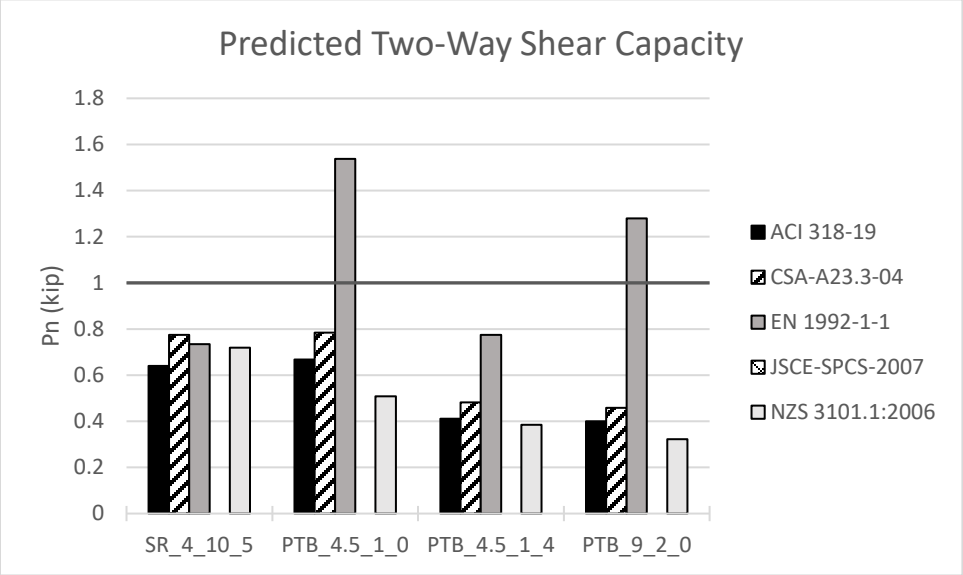

Figure 6-4: Normalized Nominal Two-Way Shear Capacity

6.1.4 *Predicted Failure Mode*

Figure 6-5 shows the predicted strength of Specimen SR_4_10_5 for flexural, one-way shear, and two-way shear failure mode. All design codes considered predict a flexural failure in the slab and predict that the specimen is weaker in two-way shear than in one-way shear.

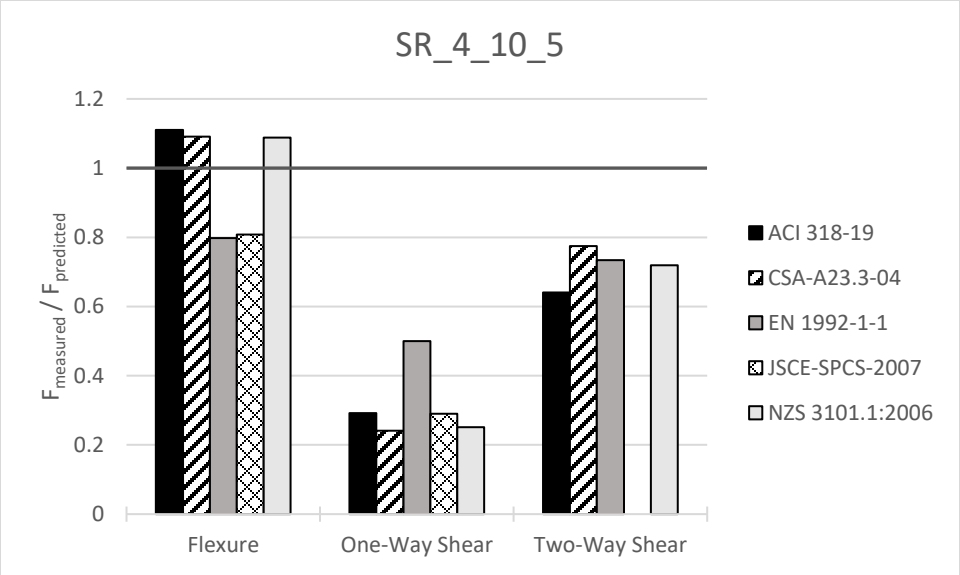

Figure 6-5: Specimen SR_4_10_5 Normalized Predicted Capacity

Figure 6-6 shows the predicted strength of Specimen PTB_4.5_1_0 for flexural, one-way shear, and two-way shear failure mode. Four of the five design codes considered predict a flexural failure in the slab and all codes predict the specimen is weaker in two-way shear than in one-way shear. However, EN 1992-1-1 2004 predicts a two-way shear capacity is lower than the flexural capacity.

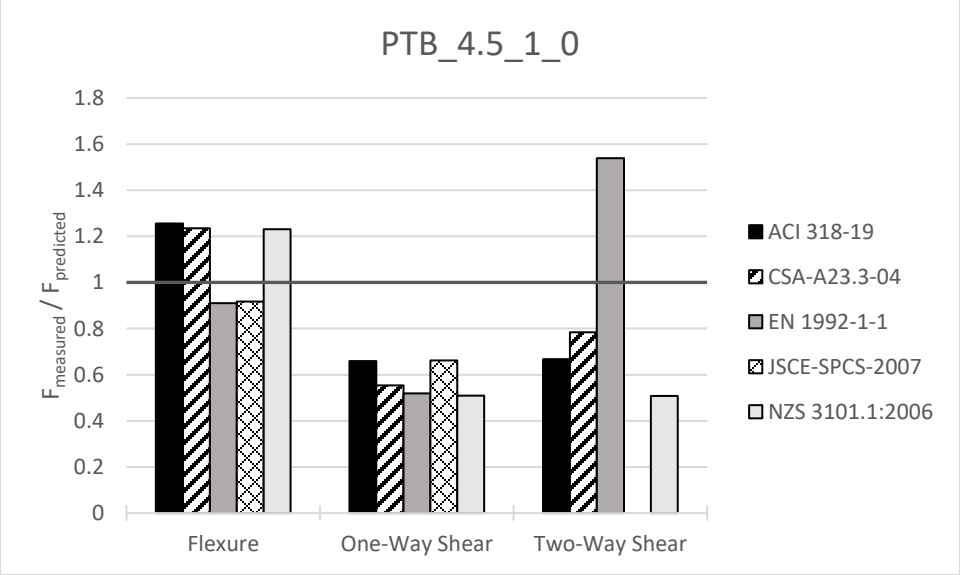

Figure 6-6: Specimen PTB_4.5_1_0 Normalized Predicted Capacity

Figure 6-7 shows the predicted strength of Specimen PTB_4.5_1_4 for flexural, one-way shear, and two-way shear failure mode. All design codes considered predict a flexural failure in the slab and predict that the specimen is weaker in two-way shear than in one-way shear.

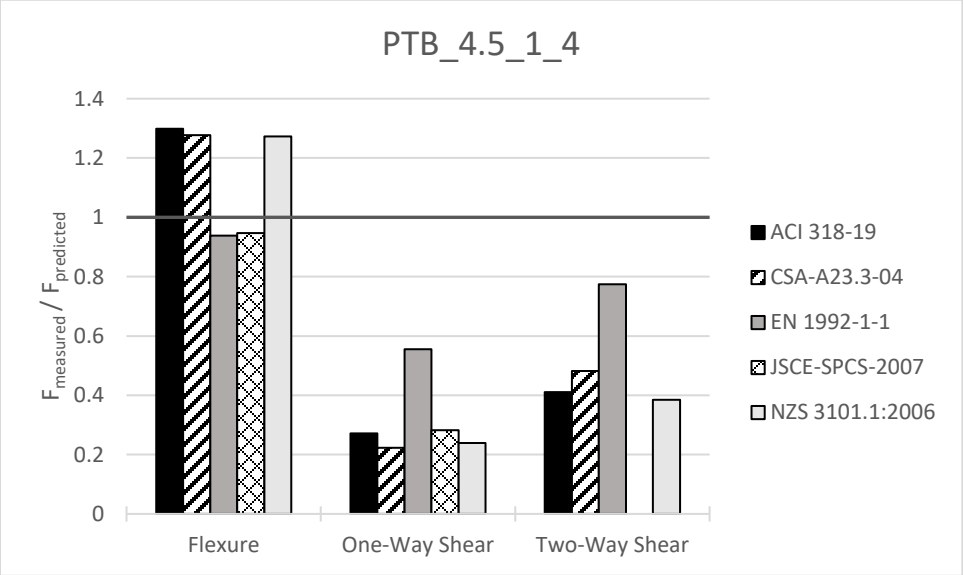

Figure 6-7: Specimen PTB_4.5_1_4 Normalized Predicted Capacity

Figure 6-8 shows the predicted strength of Specimen PTB_9_2_0 for flexural, one-way shear, and two-way shear failure mode. Four of the five design codes considered predict a flexural failure in the slab. However, EN 1992-1-1 2004 predicts a two-way shear capacity is lower than the flexural capacity. ACI318-19, CSA-A23.3-04, and NZS 3103.1:2006 predict that the one-way shear capacity of the specimen is lower than the two-way shear capacity.

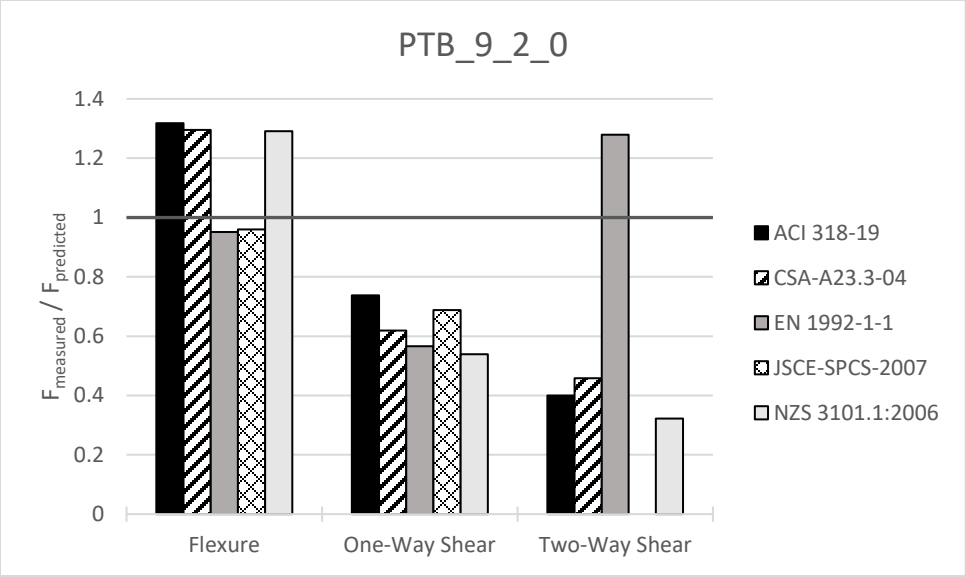

Figure 6-8: Specimen PTB_9_2_0 Normalized Predicted Capacity

6.2 CALIBRATED ROTATION SPRING

Rotational springs for the slab-column connection were calibrated in accordance with ASCE 41-17 using the results from testing. The idealized curve presented in ASCE41-17 (p. 148) is shown below in Figure 6-9. These calibrated springs can be used in a line-element type nonlinear analysis and relate deformation (displacement or rotation) to a normalized resistance (force or moment).

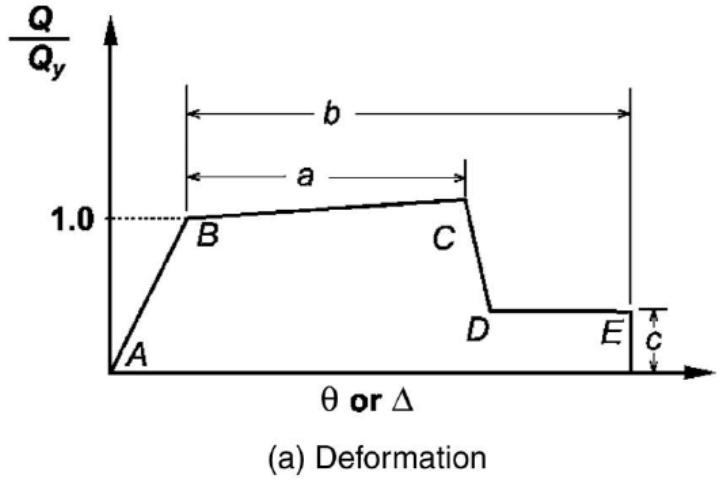

Figure 6-9: ASCE 41-17 Generalized Force-Deformation Relation for Concrete Elemetns or Components (p.148)

Using the force applied to the column by the MTS Actuator (F_1) and the displacement (Δ) measured at the level of the MTS Actuator, the force applied to the end of the slab (F_2) by the slab end roller support was calculated by enforcing equilibrium. The structure can be represented as shown in Figure 6-10 with the rotational spring located where the slab and column centerline meet with the spring attached each half of the slab to the column centerline.

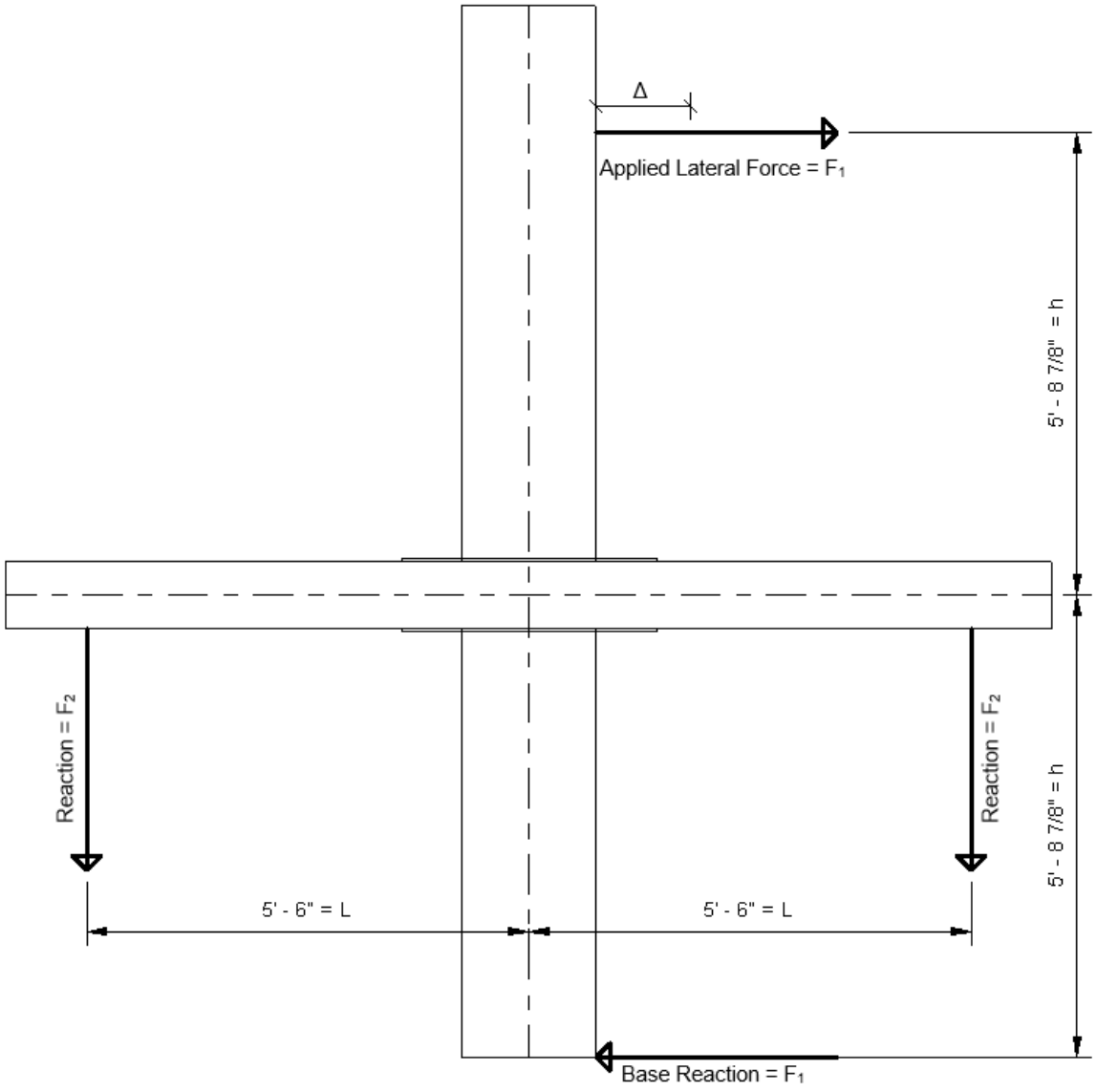

Figure 6-10: Test Geometry

Equation 6.55 describes the rotation of the column (along the centerline) from the MTS actuator to the centerline of the slab.

$$\theta = \frac{F_1}{2EI_{eff}}(x)^2 - \left(\frac{F_1 * (h)^2}{6EI_{eff}} + \frac{\Delta}{2 * (h)}\right) \qquad 6.55$$

Where,

θ= the angle of rotation in radians

EI_{eff} = the effective stiffness of the column

x = distance from the MTS actuator to the point of interest

F_1 = column shear force (force applied by MTS Actuator with P-Δ removed)

Δ = the displacement of the column at the effective height of the column (Figure 6-10)

h = the height from the slab centerline to the level of the applied force (F_1)

According to Roeder, Lehman, and Bishop (2010), the effective stiffness of the column can be calculated using Equation 6.56 and 6.57.

$$EI_{eff} = E_s I_s + C' E_c I_c \tag{6.56}$$

$$C' = 0.15 + \frac{P}{P_0} + 2\frac{A_s}{A_s + A_c} < 0.9 \tag{6.57}$$

Where,

E_s= elastic modulus of the steel tube

I_s = moment of inertia of the steel tube

E_c= elastic modulus of the concrete

I_c = moment of inertia of the concrete

P = axial load on the column

P_0 = axial capacity (squash load) of the column

A_s = area of the steel

A_c = area of concrete

Equation 6.58 describes the rotation of the slab (along the centerline) from the slab end roller support to the centerline of the column.

$$\theta = \frac{-F_2}{2EI_{eff}}(x)^2 + \frac{F_2 * (L)^2}{6EI_{eff}} \quad 6.58$$

Where,

θ= the angle of rotation in radians

F = the force applied by the MTS Actuator to the column

EI_{eff} = the effective stiffness of the slab

x = distance from the MTS actuator to the point of interest

L = the length from the column centerline to the reaction force (F_2)

According to Table 6.6.3.1.1 from ACI 319-19, the effective moment of inertia can be taken as $0.25I_g$, resulting in an effective stiffness of the slab described by Equation 6.59.

$$EI_{eff} = E_c * 0.25I_g \quad 6.59$$

Where,

EI_{eff}= effective stiffness of the slab

E_c= elastic modulus of the concrete

I_g = moment of inertia of the concrete

Using the loads measured from the MTS actuator and the displacements measured at the top of the column and the equations shown above, the rotation of the column and slab at the slab column joint can be calculated and the difference in rotation found. Using Table 10-15 from ASCE 41-17, values for "a", "b" and "c" (visible in Figure 6-9) are chosen according to the gravity shear ratio on the connection (zero during testing due to redistribution of the slab dead load). Selected values are shown in Table 6.17.

Table 6.17: ASCE 41-17 Slab-Column Connection Modeling Parameters

a (rad)	b (rad)	c (M/M_n)
0.035	0.05	0.2

A comparison of the calibrated rotational springs is shown in Figure 6-11.

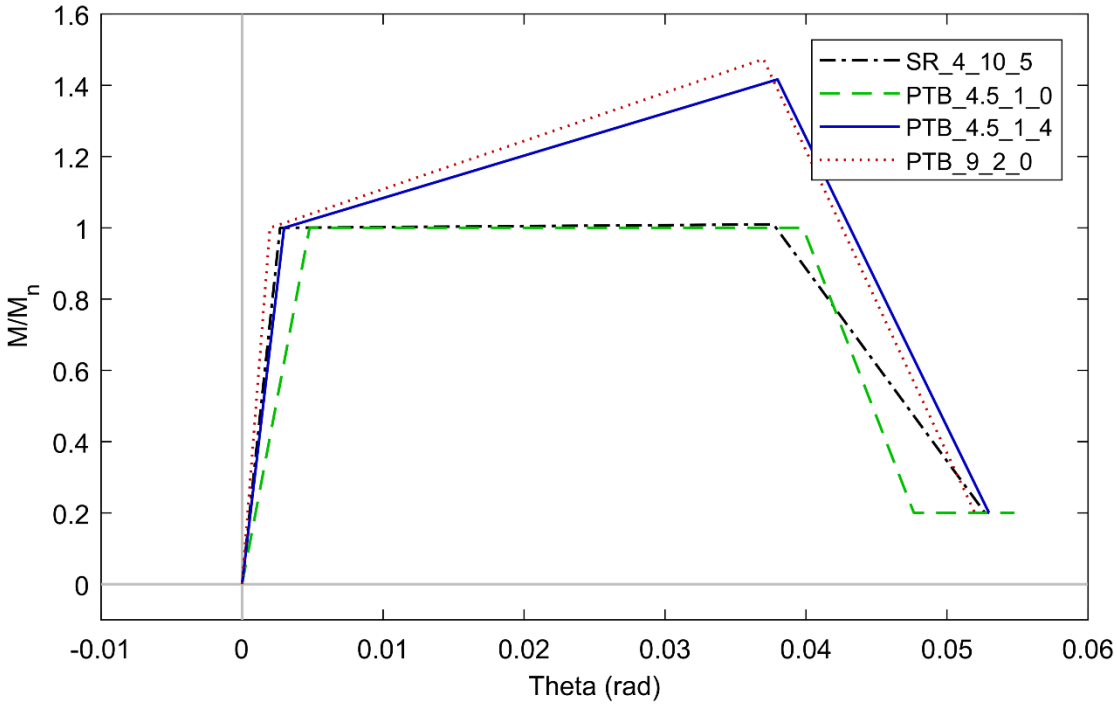

Figure 6-11: ASCE 41-17 Rotational Spring (Summary)

Rotational springs are calibrated for each specimen using the response curves shown in Figure 6-12 to find point "B" from which the x-values points "C" and "E" can be found. The y-value for point "C" is found by setting the slop between "B" and "C" between zero and 10% of the slope from "A" to "B". The y-value for "D" was the same as for "E" while the x-value was found utilizing the slope of the response curve if possible, otherwise point "D" is set equal to point "E". The coordinates of the indices for the rotational springs calibrated in accordance with ASCE 41-17 are shown in Table 6.18.

Table 6.18: ASCE 41-17 Calibrated Rotational Spring Backbone

	SR_4_10_5			PTB_4.5_1_0			PTB_4.5_1_4			PTB_9_2_0		
	θ	Moment		θ	Moment		θ	Moment		θ	Moment	
	(rad.)	kip*in	kN*m	(rad.)	kip*in	kN*m	(rad.)	kip*in	kN*m	(rad.)	kip*in	kN*m
A	0	0	0	0	0	0	0	0	0	0	0	0
B	0.00270	1	0.11	0.00479	1	0.11	0.00298	1	0.11	0.00198	1	0.11
C	0.03770	1.01	0.11	0.03979	1	0.09	0.03798	1.42	0.16	0.03698	1.47	0.19
D	0.05270	0.2	0.02	0.04765	0.2	0.02	0.05298	0.2	0.02	0.05198	0.2	0.02
E	0.05270	0.2	0.02	0.05479	0.2	0.02	0.05298	0.2	0.02	0.05198	0.2	0.02

The springs calibrated using ASCE 41-17 show a fairly good match for the behavior of the reference specimen, but over predict the deformation capacity of Specimen PTB_4.5_1_0 and under predict the deformation capacity of Specimens PTB_4.5_1_4 and PTB_9_2_0. For PTB_4.5_1_4 and PTB_9_2_0, the values for "a" and "b" should be much higher based on what was observed in the tests. Modified ASCE 41-17 springs were calibrated using the tests by changing the value of "a" to match the curve for Specimens SR_4_10_5 and PTB_4.5_1_0 while the end slop of the M-θ response from testing was used to extrapolate values for Specimen PTB_4.5_1_4 and PTB_9_2_0. Calculated values for "a" are shown in Table 6.19. Values for "b" could not be changed because testing was terminated before high enough deformations could be reached.

Table 6.19: ASCE 41-17 Modified Modeling Parameters

	ASCE 41-17	SR_4_10_5	PTB_4.5_1_0	PTB_4.5_1_4	PTB_9_2_0
a (rad)	0.035	0.034	0.032	0.056	0.072
% of ASCE 41-17	-	97	91	160	206

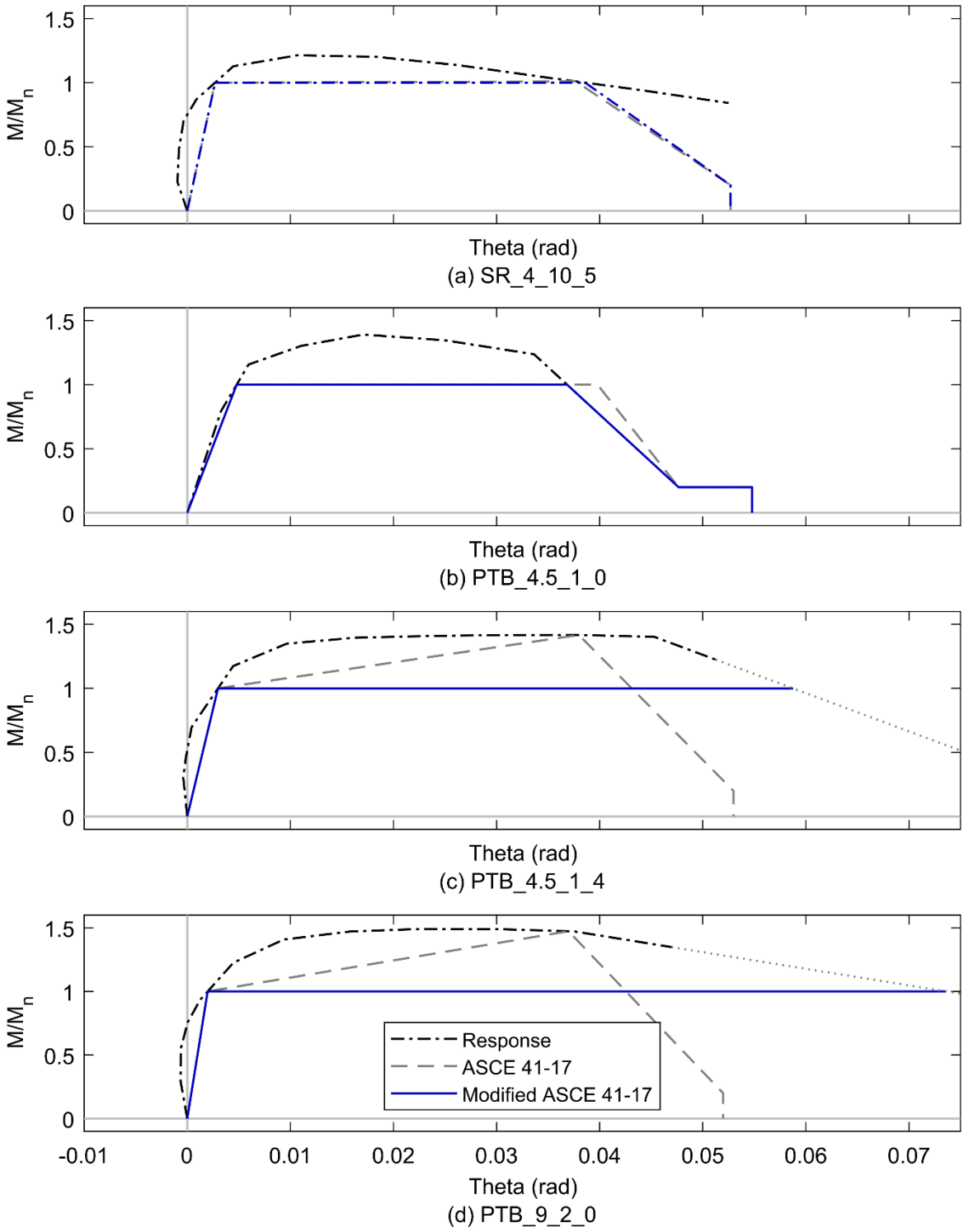

Figure 6-12: Rotational Spring Calibration

Chapter 7. SUMMARY, CONCLUSIONS, AND FUTURE WORK

The experimental research program was conducted to investigate the behavior of variations of the proposed connection compared to a control specimen constructed using a more traditional connection detail. The following sections contain a summary of the tests performed and the behavior observed, lists conclusions, and suggests topics for future research.

7.1 SUMMARY OF RESEARCH

Vertical evacuation structures and structures expected to remain serviceable after an earthquake need new structural systems that can resist large forces with minimal damage. The experimental program detailed in this report examines a proposed connection for CFST columns to RC slabs that can sustain large lateral forces without damage and sustain large drift demands with minimal decrease in lateral-force resistance. A new connection is proposed for this system. The connection components are as follows:

- CFST columns above and below the flat slab
- Longitudinal continuity reinforcement welded to the bottom column and extending through the slab to the top column
- A ring flange on the top and bottom of each tube for each column, with pre-drilled holes to accommodate post-tensioned bolts. These bolts act to prestress the concrete under the ring as well as outside of the ring (in bolts outside of the ring are included) to ensure adequate shear strength and replace the stud rails typically used to enhance the shear strength of the slab-column connection.

A total of four, full-scale slab-column connections were tested. One connection utilized traditional stud-rail shear reinforcement to provide a baseline for comparison while three connections were constructed using design variant of the proposed connection. The transverse reinforcement of the reference specimen is as follows:

- SR_4_10_5
    - Four stud rails to each column face for a total of 16 stud rails
    - In the direction of loading, rails had 10 studs each

    - Perpendicular to the direction of loading, rails had 5 studs each
    - Studs were placed at a spacing of 5 in. OC

Two parameters were varied across the three versions of the proposed connection, size of the ring flange and the number of prestressed bolts on and off the ring. The specimens were as follows:

- Specimen PTB_4.5_1_0
    - Ring flanges extending 4.5 in. (0.5d and 0.225D) beyond the column circumference
    - One set of eight bolts on the ring at a radius of 12.25 in.
    - No bolts beyond the ring
- Specimen PTB_4.5_1_4
    - Ring flanges extending 4.5 in. (0.5d and 0.225D) beyond the column circumference
    - One set of eight bolts on the ring at a radius of 12.25 in.
    - four sets of eight bolts beyond the ring (again, need to indicate the dimensions)
- Specimen PTB_9_2_0
    - Ring flanges extending 4.5 in. (1.0d and 0.45D) beyond the column circumference
    - Two sets of eight bolts on the ring at a radius of 12.25 in. and 15.75 in.
    - No bolts extending beyond the ring

The four specimens were tested under combined axial and lateral loading of the column. Axial loads were applied using a 2.4 million pound Universal Testing Machine and the lateral loads were applied using an MTS Actuator attached to a self-reacting test frame. The ends of the slab and top of the column were restricted using simulated roller supports and the bottom of the column was restrained using a pin support. These supports conditions were chosen to replicate points of contraflexure present in buildings under lateral loading.

While testing, damage states were monitored for later comparison after testing. It was found that:

- All reinforcement (four bars monitored with strain gauges) in specimens designed with variations of the proposed connections yielded in the slab while only three bars yielded in the reference specimen

- Initiation of spalling varied greatly from one test to another (1.5% - 3.6% drift) potentially due to the presence and size of a ring flange and the amount of prestressing in the joint region
- The onset of crushing was relatively consistent (4.4% - 5.1% drift) with the variation potentially due to prestressing effects on the joint region
- In all cases loss of strength resulted from flexural damage including spalling and bar buckling (although the bars did not buckle for the reference stud-rail specimen)

When the normalized measured response of specimens was compared (P-Δ effects removed), it was found that Specimen SR_4_10_5 had the lowest lateral resistance (all specimens were built with a reinforcing ratio of approximately 1% both top and bottom) while all variations of the proposed connection reached similar peak resistances. Additionally:

- Specimen SR_4_10_5 sustained degradation of lateral force resistance after reaching peak resistance at +2.70/-2.77% drift.
- Specimen PTB_4.5_1_0 reached peak resistance at +3.36/-3.32% drift and maintained lateral force resistance until suddenly losing lateral-force resistance at +4.72/-4.35% drift
- Specimen PTB_4.5_1_4 and Specimen PTB_9_2_0 had similar responses to lateral loads and retained lateral load resistance capacities at high drifts

Five design codes were used to compare predicted strengths assuming either a flexural, one-way shear, or two way shear response. All codes predicted a flexural response for the reference specimen and Specimen PTB_4.5_1_4. Four of five codes predicted a flexural response for Specimens PTB_4.5_1_0 and PTB_9_2_0 while one code (EN 1992-1-1) predicted a two-way shear response for theses specimens.

ASCE 41-17 was used to calibrate moment-rotation spring for simplified analysis of the slab column connections. The ASCE 41 springs were then compared to the measured response. The ASCE 41 springs matched the behavior of the reference specimen and Specimen PTB_4.5_1_0 relatively well while ASCE 41 under predicted the deformation capacity of Specimens PTB_4.5_1_4 and PTB_9_2_0.

7.2 RESEARCH RESULTS AND CONCLUSIONS

The following conclusions were reached based on interpretation of experimental observations, measured response, damage state characterizations, and comparisons to design codes:

- The proposed connection provides a viable alternative to traditional connections for slab-column gravity systems in reinforced concrete construction as shown by high drift capacity and lack of degradation of lateral force resistance to high drifts.
- The proposed connection has the potential when appropriately detailed to provide a greater drift capacity than a slab-column connection using traditional stud rail shear reinforcement as shown by the drift capacities and lateral force resistance of Specimens PTB_4.5_1_4 and PTB_9_2_0.
- Either a sufficiently large ring flange or a small ring with additional prestressed shear bolts is needed for a ductile, high drift capacity slab-column connection.
- The proposed connection reduces congestion in the slab around the column, increasing constructability by reducing the amount of required transverse reinforcement.
- By using CRST columns, the proposed connection has the potential to enable accelerated construction by reducing the amount of formwork and internal reinforcement required while also reducing the number of concrete placements needed to cast the gravity load resisting system.
- A flexural response was predicted by most of the design codes examined and was observed as the primary response during testing.
- Rotational springs detailed according to ASCE 41-17 matched the measured response of the reference specimen but under predicted the deformation capacity of Specimens PTB_4.5_1_4 and PTB_9_2_0.

7.3 RECOMMENDATIONS FOR FUTURE WORK

Several recommendations for future work were determined while testing and analyzing the results of the experimental program. The recommendations include:

- Experimental investigation using thinner slabs to determine whether the ring flange diameter should be a function of the effective slab depth or the diameter of the column or both.
- Experimental investigation using prestressed slabs to determine the effects of prestressing on the behavior of the proposed connection.
- Experimental investigation using slabs with additional gravity load to determine the effects of an increased gravity shear ratio on the behavior of the connection.
- Experimental investigation using the proposed connection in pure punching shear to better characterize its behavior under gravity loads.
- Experimental investigation using square CFST columns for use in buildings that are not intended to be used as VES.
- Perform a parametric study of the proposed connection using modeling software to further characterize the behavior of the proposed connection

REFERENCES

[1] ACI Committee 318. (2014). *Building Code Requirements for Structural Concrete (ACI 318-14) [and] Commentary on Building Code Requirements for Structural Concrete (ACI 318R-14).*

[2] ACI Committee 318. (2019). Building Code Requirements for Structural Concrete (ACI 318-19): An ACI Standard: Commentary on Building Code Requirements for Structural Concrete (ACI 318R-19). American Concrete Institute.

[3] American Institute of Steel Construction. (2011). *Steel construction manual.* (Fourteenth ed.). Chicago, Illinoi]: American Institute of Steel Construction

[4] ASCE/SEI 7-16. (2017). Minimum design loads and associated criteria for buildings and other structures. Reston, VA: American Society of Civil Engineers.

[5] ASCE-41-17. (2017). ASCE Standard, ASCE/SEI, 41-17: Seismic Evaluation and Retrofit of Existing Buildings. Reston, VA: American Society of Civil Engineers.

[6] ASTM. (2014). ASTM C469: Standard test method for static modulus of elasticity and poisson's ratio of concrete in compression. West Conshohocken, PA: American Society for Testing and Materials.

[7] Bu, W., & Polak, M. A. (2011). Effect of opening and shear bolt pattern in seismic retrofit of reinforced concrete slab-column connections. *Engineering* structures, 33(12), 3329-3340.

[8] Canadian Standards Association. (2004). Design of concrete structures. Mississauga, Ont.: Canadian Standards Association.

[9] Elgabry, A. A., & Ghali, A. (1987). Tests on concrete slab-column connections with stud-shear reinforcement subjected to shear-moment transfer. *Structural* Journal, 84(5), 433-442.

[10] Ghali, A., Elmarsri, M. Z., & Dislger, W. (1976, October). Punching of flat plates under static and dynamic horizontal forces. In *Journal* Proceedings (vol. 73, No. 10, pp. 566-572).

[11] Hawkins, N. M., Mitchell, D., & Hanna, S. N. (1975). The effects of shear reinforcement on the reversed cyclic loading behavior of flat plate structures. *Canadian Journal of Civil* Engineering, 2(4), 572-582.

[12] Hawkins, N. M., Mitchell, D., & Sheu, M. S. (1974). *Cyclic behavior of six reinforced concrete slab-column specimens transferring moment and shear*. Division of Structures and Mechanics, Department of Civil Engineering, University of Washington.

[13] JSCE. (2007). Standard specifications for concrete structures-2007, Design. Tokyo (Japan): Japan Society of Civil Engineers.

[14] Pan, A. D., & Moehle, J. P. (1992). An experimental study of slab-column connections. *Structural Journal*, 89(6), 626-638.

[15] Robertson, I. N. (1990). *Seismic response of connections in indeterminate flat-slab subassemblies* (Doctoral dissertations, Rice University, 1990).

[16] Robertson, I. N., Kawai, T., Lee, J., & Enomoto, B. (2002). Cyclic testing of slab-column connections with shear reinforcement. *Structural Journal*, 99(5), 605-613.

[17] Standard, B. (2004). Eurocode 2: Design of concrete structures-. Part 1-1: *General rules and rules for buildings*, 230.

[18] Standard, New Zealand. (2006). NZS3101 Concrete Structures Standard.

[19] Stephens, M. T. (2016). *Design Expressions and Dynamic Evaluation of CFST Bridges Subjected to Seismic Hazards* (Doctoral dissertation).

[20] Symonds, D. W. (1976). *Slab-column connections subjected to high intensity shears and transferring reversed moments* (Doctoral dissertation, Division of Structures and Mechanics, Department of Civil Engineering, University of Washington).

[21] Wey, E. H., & Durrani, A. J. (1992). Seismic response of interior slab-column connections with shear capitals. *Structural Journal*, 89(6), 682-691.

APPENDIX A: PROTOTYPE SLAB DESIGN

The direct design method detailed in ACI 318-14 section 8.10 was used to design the reinforcement in the prototype slab. This section contains the calculations for this design.

Loads:

$LL = 80\ psf, DL = 150\ psf (self\ weight\ of\ 125\ psf\ and\ SIDL\ of\ 25\ psf)$

$1.6LL + 1.2DL = 308\ psf$

Materials:

Concrete:

$f_c' = 7{,}000\ psi$

Reinforcing Bars:

$f_y = 60\ ksi$

Geometry:

Bay Dimensions:

$\ell_1 = 30\ ft., \ell_2 = 30\ ft.$

Column Strip:

Width to either side of the column:

$0.25 * \min(\ell_1, \ell_2) = 7.5\ ft. \rightarrow 15\ ft. total$

Total Moment: (ACI 318-14 Section 8.10.3.2)

$$M_o = \frac{w_u \ell_2 {\ell_1}^2}{8} = \frac{308psf * 30ft. * (30ft.)^2}{8} = 1039.5\ k * ft.$$

Apportion Moment: (ACI318-14 Table 8.10.4.1)

Assume: Interior slab with no beams anywhere

Negative Moment:

$0.65 * M_o = -675.675\ k * ft.$

Positive Moment:

$0.35 * M_o = 363.825\ k * ft.$

Moment in the Column Strip: (ACI 318-14 Section 8.10.5)

$\frac{\alpha_{f1} * \ell_2}{\ell_1} = 0$ and $\frac{\ell_2}{\ell_1} = 1$

Portion of interior negative M_u in column Strip: (ACI 318-14 Table 8.10.5.1)

$M_u^- = 0.75 * (-675.675\ k * ft.) = -506.76\ k * ft$

Portion of interior negative M_u in middle Strip:

$M_u^- = (-675.675\ k * ft.) - (-506.76\ k * ft.) = -168.91\ k * ft.$

Portion of interior positive M_u in column strip: (ACI 318-14 Table 8.10.5.5)

$M_u^+ = 0.6 * (363.825\ k * ft.) = 218.295\ k * ft$

Portion of interior positive M_u in middle strip:

$M_u^+ = (363.825\ k * ft.) - (218.295\ k * ft.) = 145.53\ k * ft$

Slab Design: Column Strip

Slab Dimension:

$h = 10\ in., d = h - cover = 9.75\ in., b = 15\ ft.$

Find minimum area of bottom steel required

$M_u^+ = 218.295\ k * ft \leq \phi M_n$

$\mu_n = \frac{M_{n,req.}}{b * d^2 * 0.85 * f_c' * \phi} = 0.0318$

$\omega_d = 1 - \sqrt{1 - 2 * \mu_n} = 0.0323$

$$\rho = \frac{\omega_d * 0.85 * f_c'}{f_y} = 0.0032$$

$$A_s \geq \rho * b * d = 5.33\ in.^2 \rightarrow \#5@9\ in.\ OC = 6.2\ in.^2$$

Find minimum area of top steel required

$M_u^- = -506.76\ k * ft. \leq \phi M_n$

$\mu_n = 0.0737$

$\omega_d = 0.0767$

$\rho = 0.0076$

$A_s \geq 12.66\ in.^2 \rightarrow \#8@9in.\ OC = 15.8\ in^2$

Slab Design: Middle Strip

Find minimum area of bottom steel required

$M_u^+ = 145.53\ k * ft \leq \phi M_n$

$\mu_n = 0.0212$

$\omega_d = 0.0214$

$\rho = 0.002$

$A_s \geq 3.33\ in.^2 \rightarrow \#4@9in.\ OC = 4\ in^2$

Find minimum area of top steel required

$M_u^- = -168.92\ k * ft. \leq \phi M_n$

$\mu_n = 0.025$

$\omega_d = 0.025$

$\rho = 0.0025$

$A_s \geq 4.16\ in.^2 \rightarrow \#5@9in.\ OC = 6.2\ in^2$

APPENDIX B: SPECIMEN PLANS

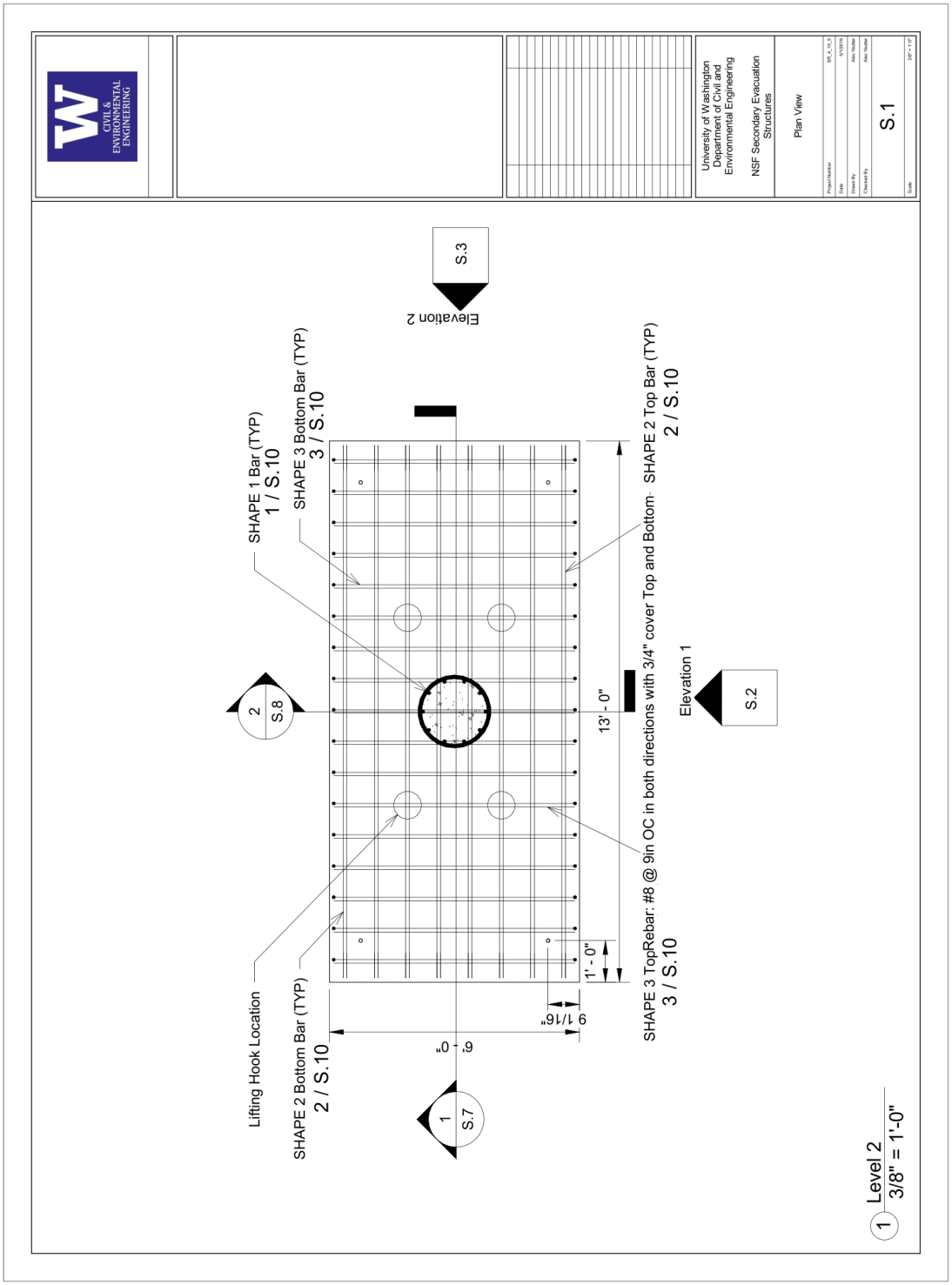

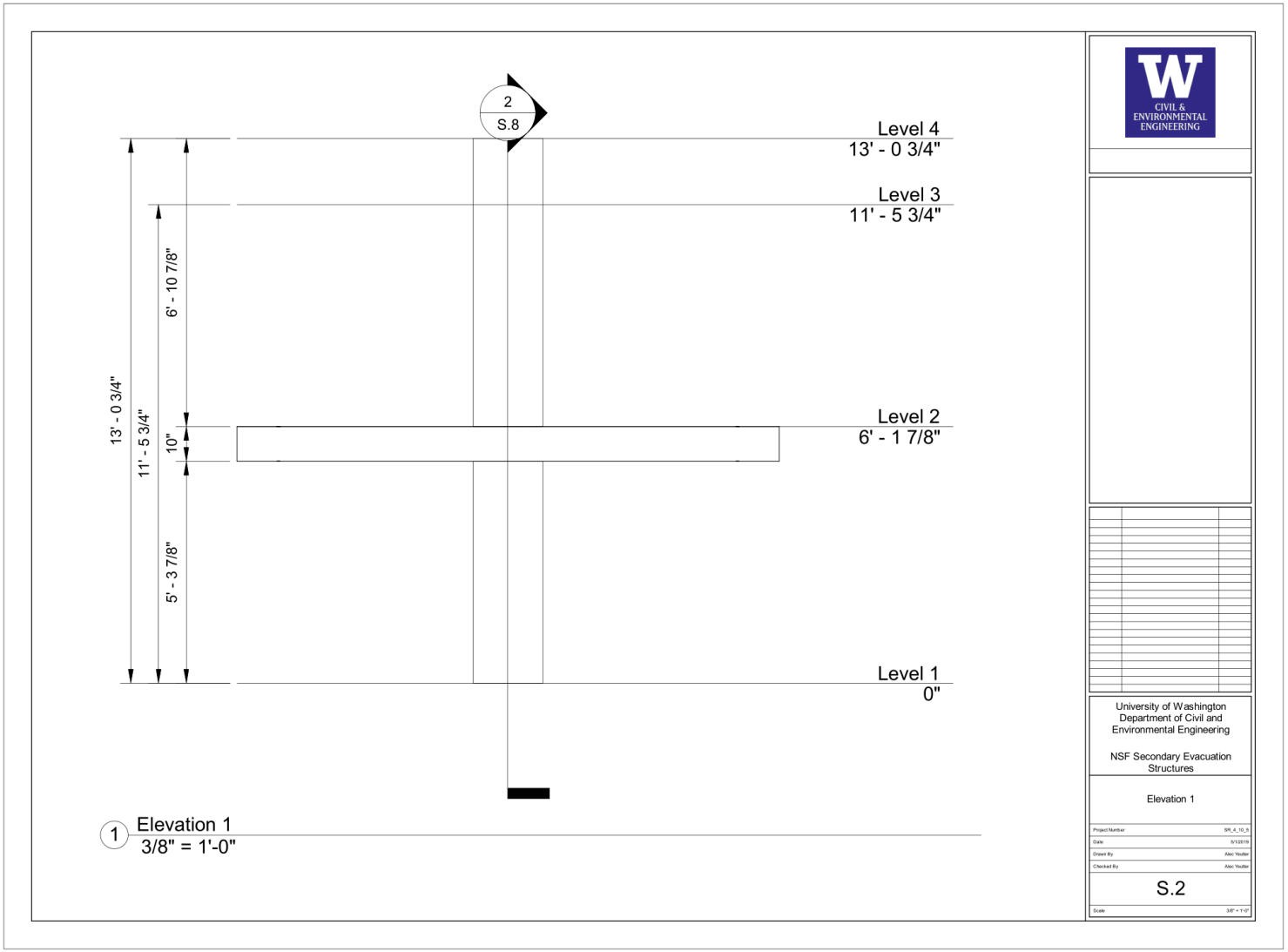

CIVIL & ENVIRONMENTAL ENGINEERING

University of Washington
Department of Civil and Environmental Engineering

NSF Secondary Evacuation Structures

Elevation 1

Project Number	SR_4_10_5
Date	5/1/2015
Drawn By	Alec Youtter
Checked By	Alec Youtter

S.2

Scale 3/8" = 1'-0"

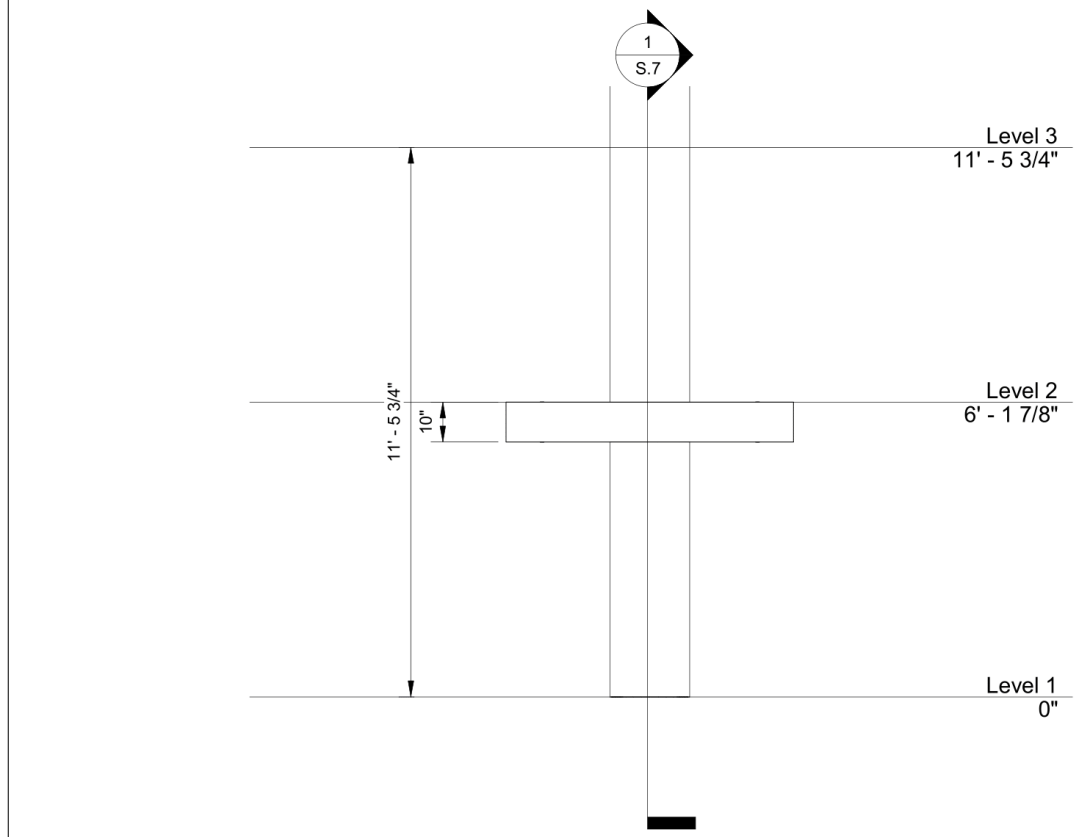

1 Elevation 2
3/8" = 1'-0"

CIVIL & ENVIRONMENTAL ENGINEERING

University of Washington
Department of Civil and Environmental Engineering

NSF Secondary Evacuation Structures

Elevation 2

Project Number	SR_4_10_5
Date	5/1/2015
Drawn By	Alec Youtter
Checked By	Alec Youtter

S.3

Scale 3/8" = 1'-0"

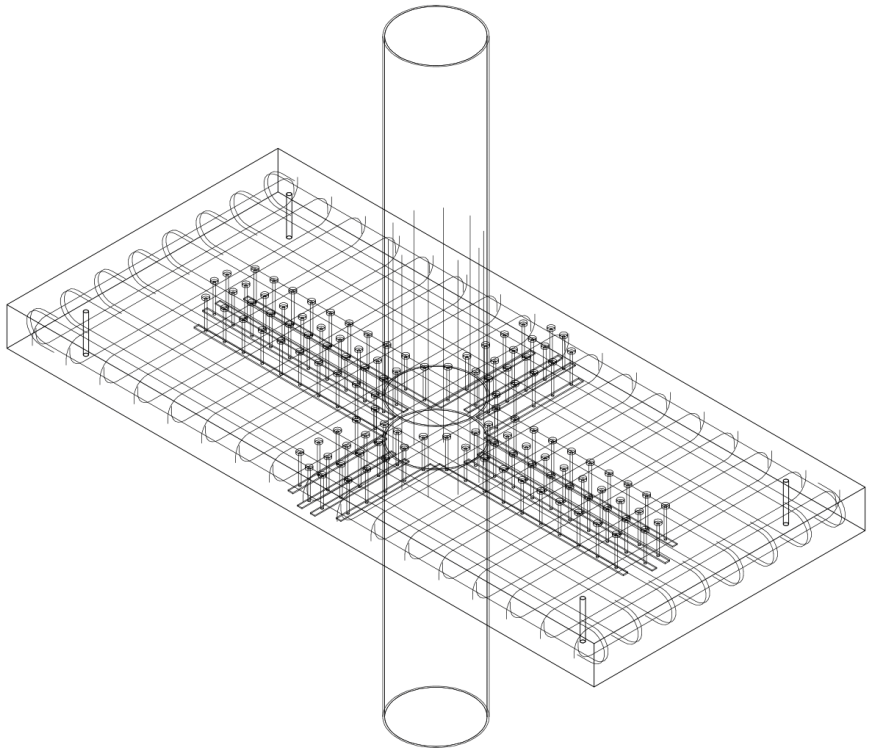

1 3D Isometric Wire Frame

CIVIL & ENVIRONMENTAL ENGINEERING

University of Washington
Department of Civil and Environmental Engineering

NSF Secondary Evacuation Structures

3D Isometric Wire Frame

Project Number	SR_4_10_5
Date	5/1/2015
Drawn By	Alec Youtter
Checked By	Alec Youtter

S.4

Scale

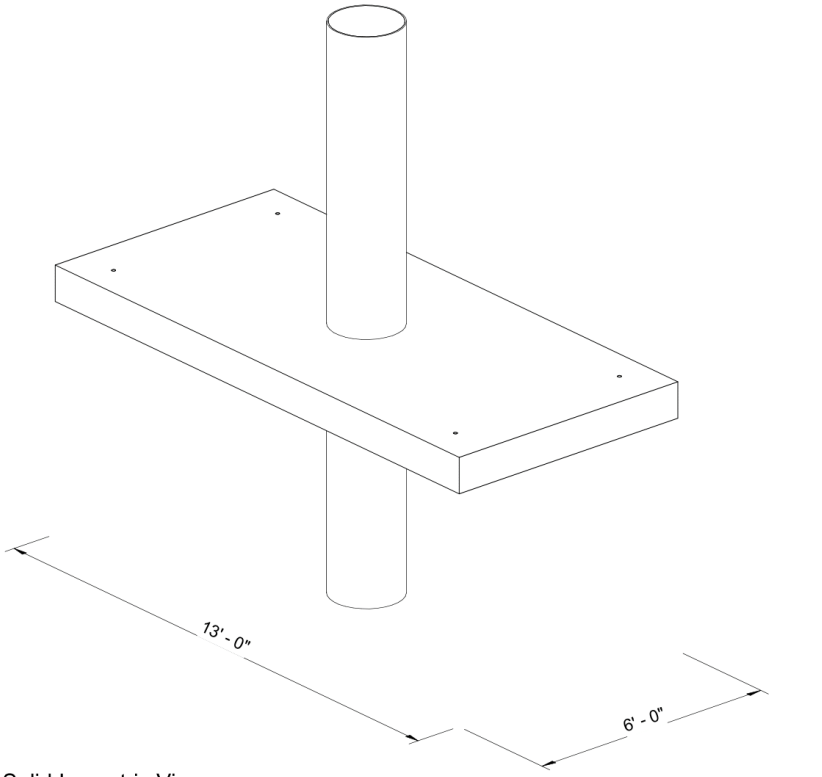

1 3D Solid Isometric View

CIVIL & ENVIRONMENTAL ENGINEERING

University of Washington
Department of Civil and Environmental Engineering

NSF Secondary Evacuation Structures

3D Solid Isometric View

Project Number	SR_4_10_5
Date	5/1/2015
Drawn By	Alec Youtter
Checked By	Alec Youtter

S.5

Scale

1 3D Semi-Transparent Render

CIVIL & ENVIRONMENTAL ENGINEERING

University of Washington
Department of Civil and Environmental Engineering

NSF Secondary Evacuation Structures

3D Semi-Transparent Render

Project Number	SR_4_10_5
Date	5/1/2015
Drawn By	Alec Youtter
Checked By	Alec Youtter

S.6

Scale

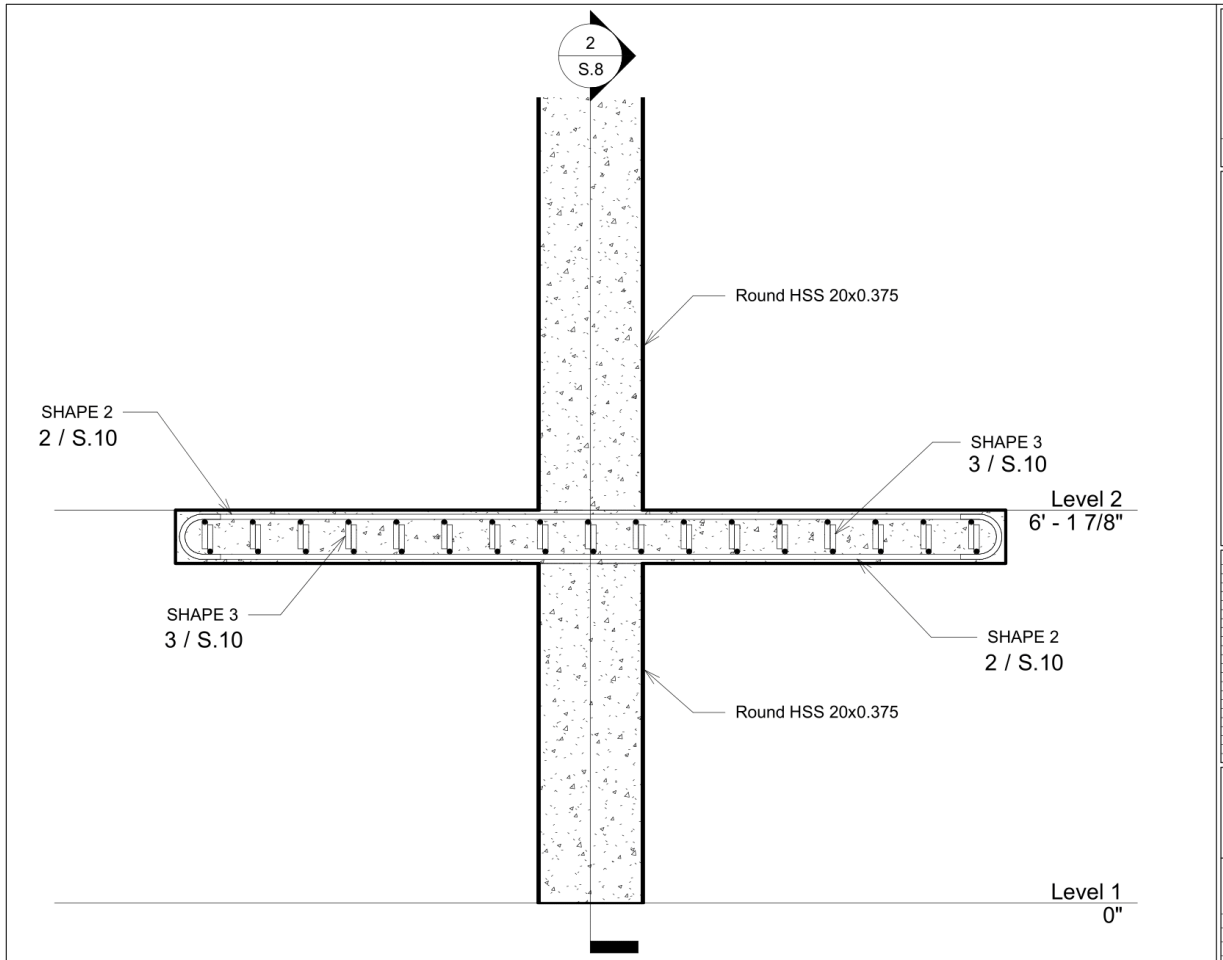

1 Section 1
1/2" = 1'-0"

CIVIL & ENVIRONMENTAL ENGINEERING

University of Washington
Department of Civil and Environmental Engineering

NSF Secondary Evacuation Structures

Section 1

Project Number	SR_4_10_5
Date	5/1/2015
Drawn By	Alec Youtter
Checked By	Alec Youtter

S.7

Scale 1/2" = 1'-0"

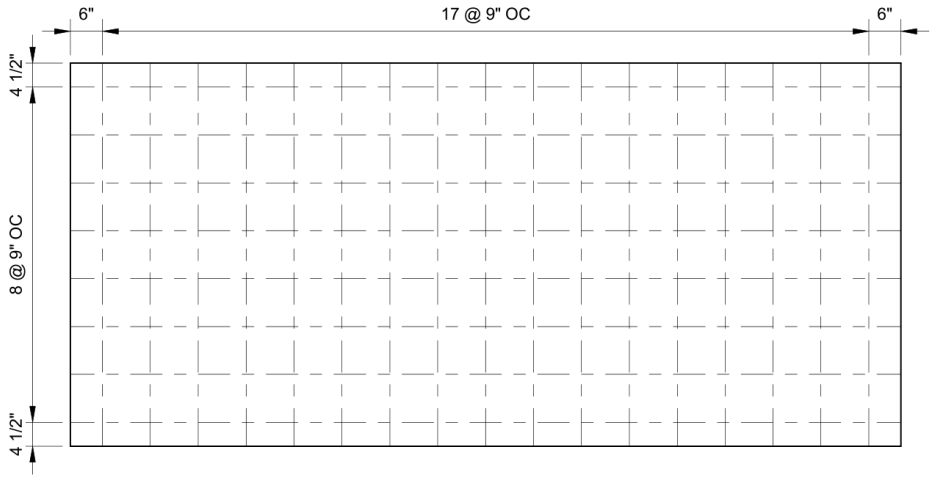

1 Slab Rebar Layout Top and Bottom
1/2" = 1'-0"

CIVIL & ENVIRONMENTAL ENGINEERING

University of Washington
Department of Civil and Environmental Engineering

NSF Secondary Evacuation Structures

Slab Rebar Layout Top and Bottom

Project Number	SR_4_10_5
Date	5/1/2015
Drawn By	Author
Checked By	Checker

S.9

Scale 1/2" = 1'-0"

SHAPE 1: #9 Bar

1 Rebar SHAPE 1
1/2" = 1'-0"

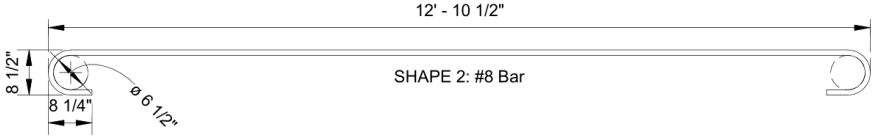

SHAPE 2: #8 Bar

2 Rebar SHAPE 2
1/2" = 1'-0"

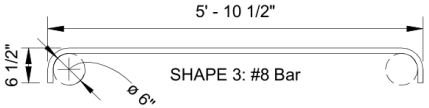

SHAPE 3: #8 Bar

3 Rebar SHAPE 3
1/2" = 1'-0"

CIVIL & ENVIRONMENTAL ENGINEERING

University of Washington
Department of Civil and Environmental Engineering

NSF Secondary Evacuation Structures

Rebar Details

Project Number	SR_4_10_5
Date	5/1/2015
Drawn By	Author
Checked By	Checker

S.10

Scale 1/2" = 1'-0"

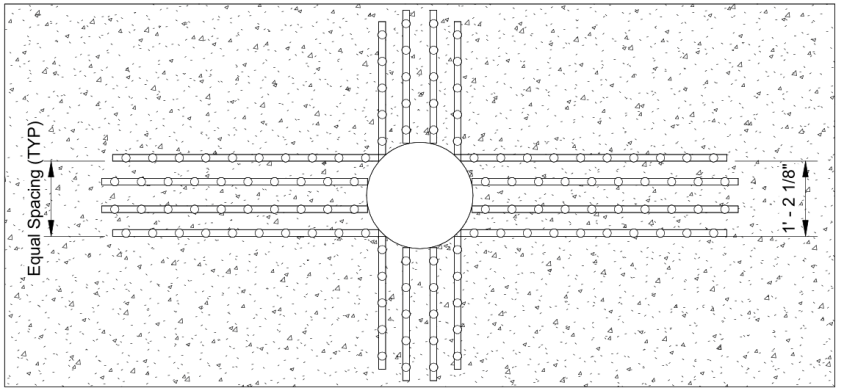

1 Stud Rail Layout
1/2" = 1'-0"

CIVIL & ENVIRONMENTAL ENGINEERING

University of Washington
Department of Civil and Environmental Engineering

NSF Secondary Evacuation Structures

Stud Rail Layout

Project Number	SR_4_10_5
Date	5/1/2015
Drawn By	Alec Youtter
Checked By	Alec Youtter

S.11

Scale 1/2" = 1'-0"

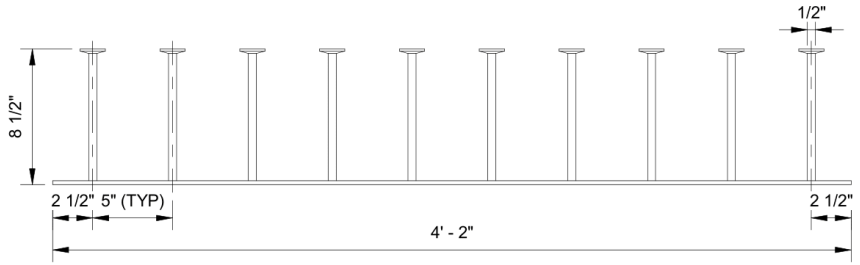

1. Studrail assembly shall conform to ASTM A1044

1 Stud Rail Detail
1 1/2" = 1'-0"

CIVIL & ENVIRONMENTAL ENGINEERING

University of Washington
Department of Civil and Environmental Engineering

NSF Secondary Evacuation Structures

Stud Rail Detail

Project Number	SR_4_10_5
Date	5/1/2015
Drawn By	Alec Youtter
Checked By	Alec Youtter

S.12

Scale 1 1/2" = 1'-0"

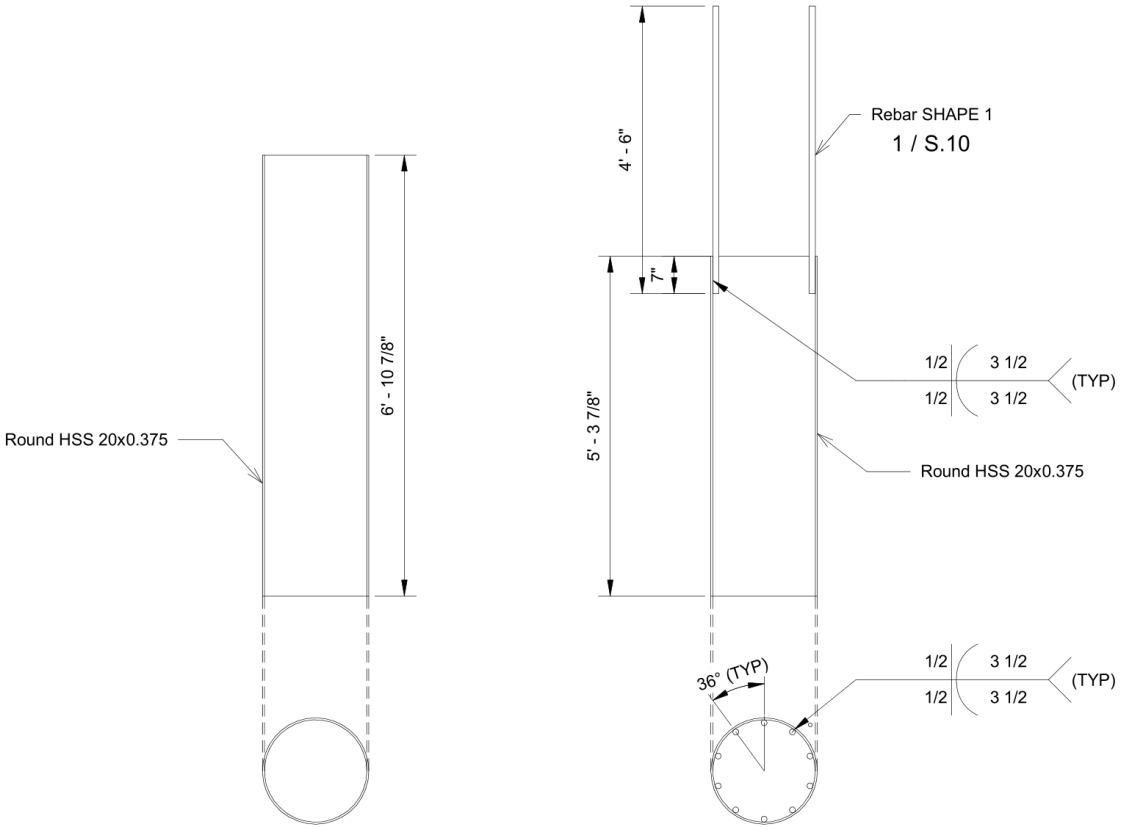

1 Collumn Fabrication Details
1/2" = 1'-0"

CIVIL & ENVIRONMENTAL ENGINEERING

University of Washington
Department of Civil and Environmental Engineering

NSF Secondary Evacuation Structures

Column Fabrication Details

Project Number	SR_4_10_5
Date	5/1/2015
Drawn By	Alec Youtter
Checked By	Charles Roeder

S.13

Scale 1/2" = 1'-0"

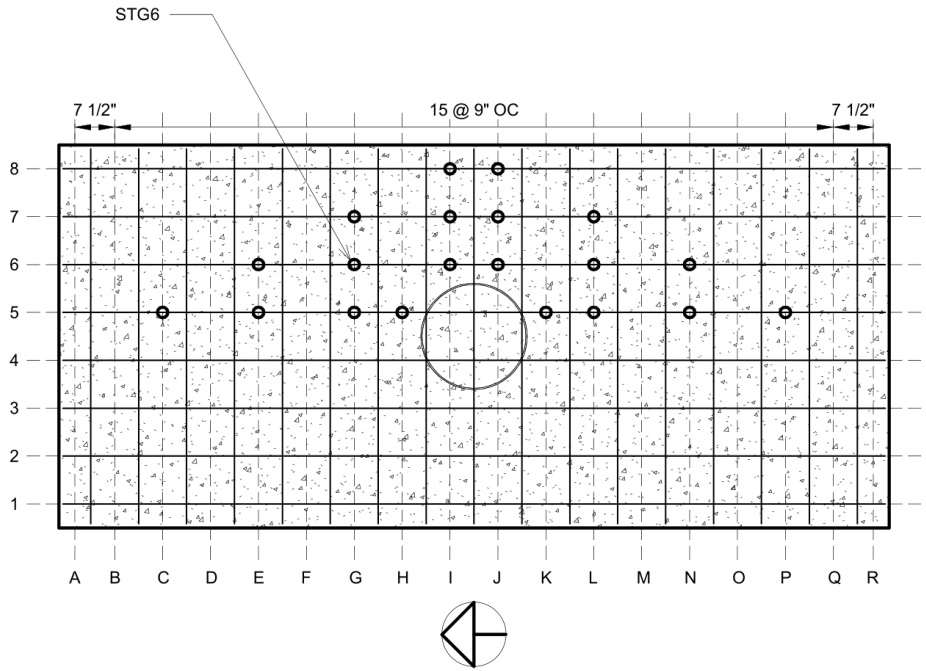

Naming Convention:
1. "S" for slab
2. "T" for top or "B" for Bottom
3. Column Letter
4. Row Number

Example: STG6 would be a strain gauge on a "Slab" "Top" bar in column "G" in row "6"

1 Slab Strain Gague Layout
1/2" = 1'-0"

CIVIL & ENVIRONMENTAL ENGINEERING

University of Washington
Department of Civil and Environmental Engineering

NSF Secondary Evacuation Structures

Slab Strain Gauge Layout Top and Bottom

Project Number	SR_4_10_5
Date	5/1/2015
Drawn By	Author
Checked By	Checker

S.14

Scale 1/2" = 1'-0"

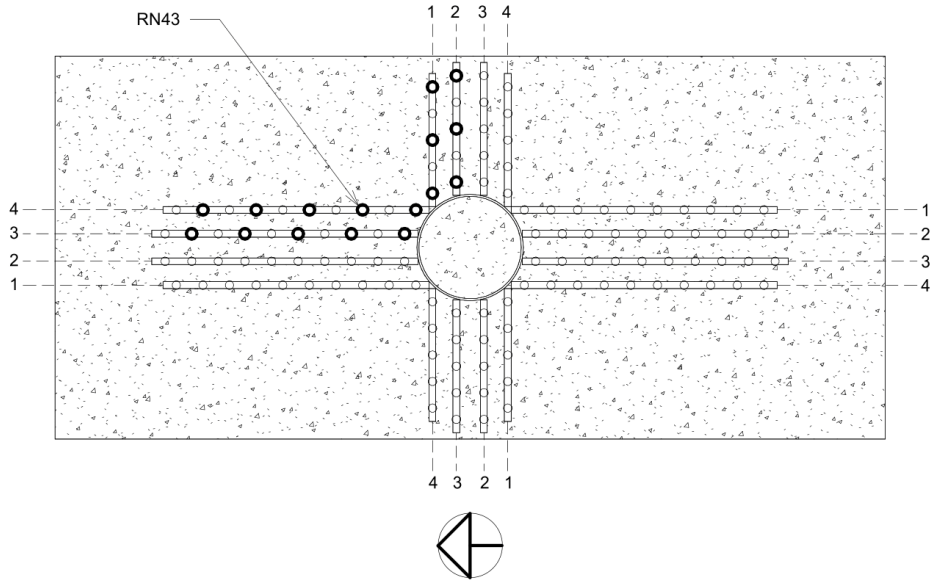

Naming Convention:

1. "R" for rail
2. "N" for North, "E" for East, "S" for South, or "W" for West of the column
3. Rail Number in the Clockwise Direction
4. Stud Number counting out from the column

Example: RN43 would be a strain gauge on the "Third" stud on the "Fourth" rail in the clockwise direction and is a "Rail" on the "North" side of the clolumn.

1 Stud Rail Strain Gauge Layout
1/2" = 1'-0"

CIVIL & ENVIRONMENTAL ENGINEERING

University of Washington
Department of Civil and Environmental Engineering

NSF Secondary Evacuation Structures

Stud Rail Strain Gauge Layout

Project Number	SR_4_10_5
Date	5/1/2015
Drawn By	Author
Checked By	Checker

S.15

Scale 1/2" = 1'-0"

Naming Convention:
1. "C" for Column
2. Rebar Letter
3. Level Number

Example: CI7 would be a strain gauge on "Column" bar "I" at level "7".

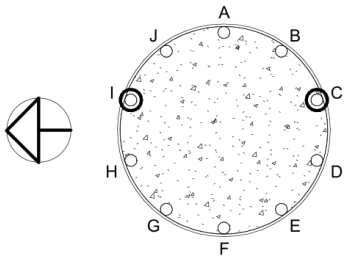

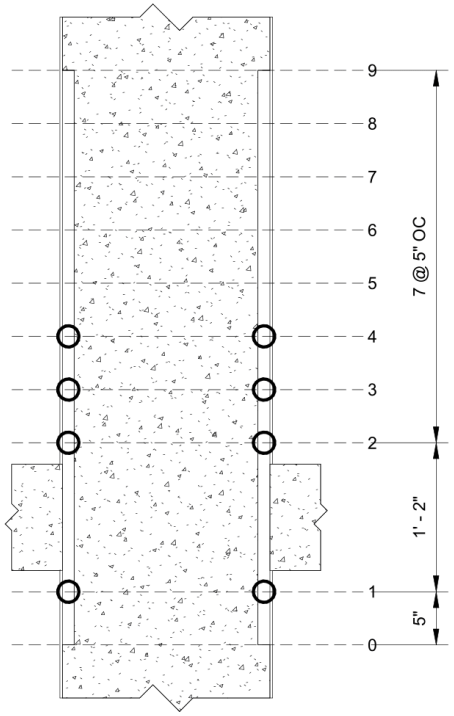

1 Column Strain Gauge Layout
1" = 1'-0"

CIVIL & ENVIRONMENTAL ENGINEERING

University of Washington
Department of Civil and Environmental Engineering

NSF Secondary Evacuation Structures

Column Strain Gauge Layout

Project Number	SR_4_10_5
Date	5/1/2015
Drawn By	Author
Checked By	Checker

S.16

Scale 1" = 1'-0"

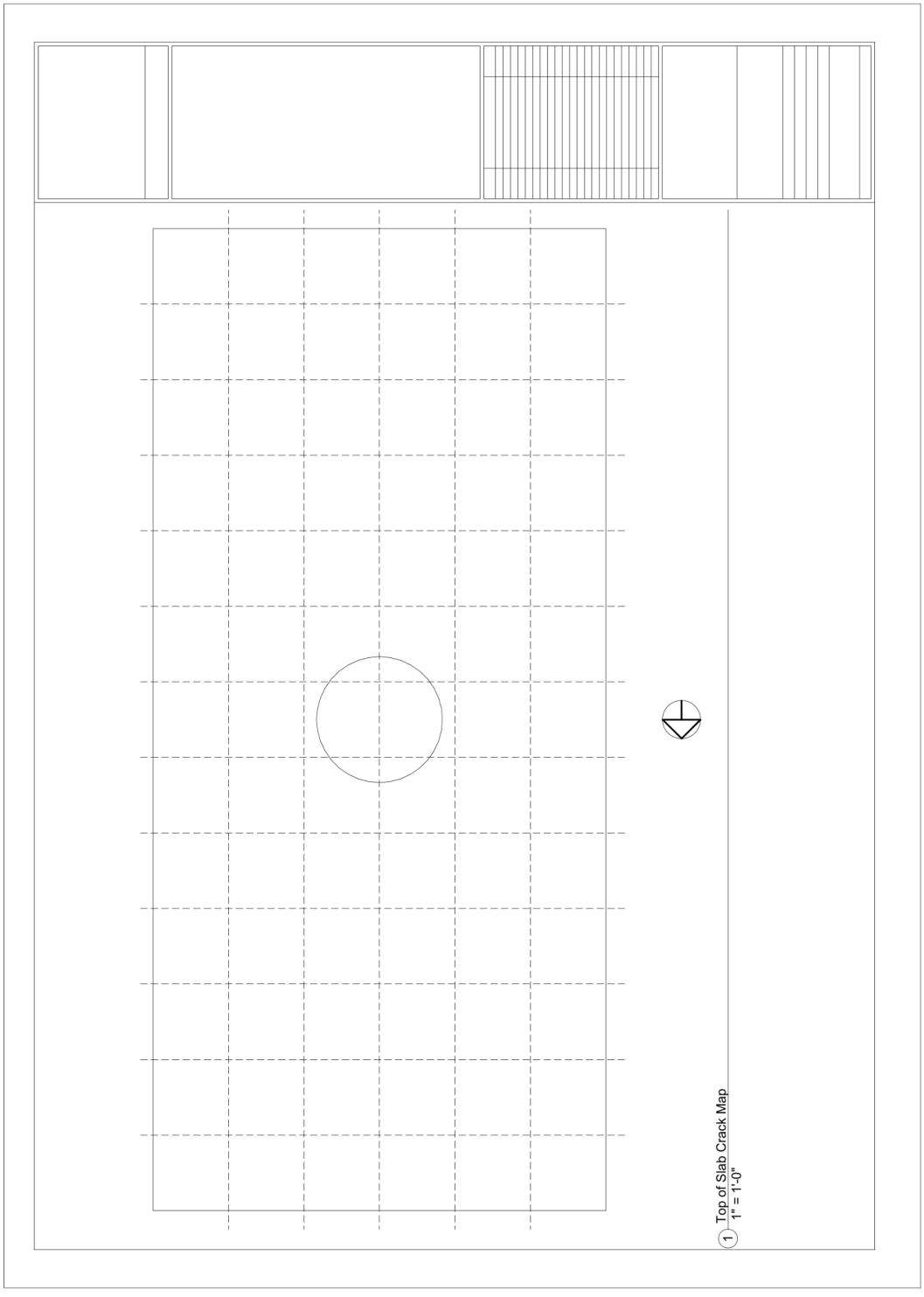
1 Top of Slab Crack Map
1" = 1'-0"

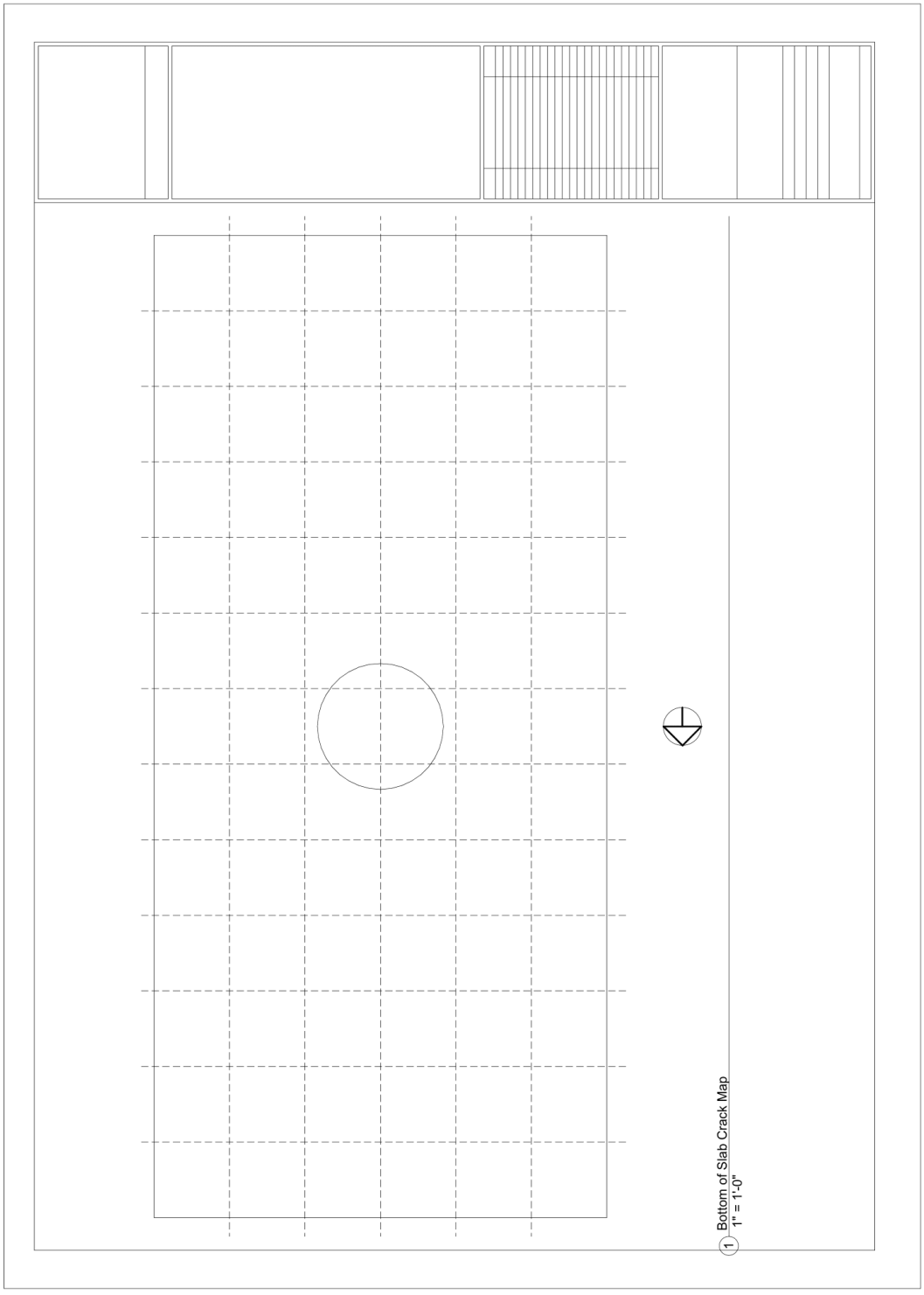
1
Bottom of Slab Crack Map
1" = 1'-0"

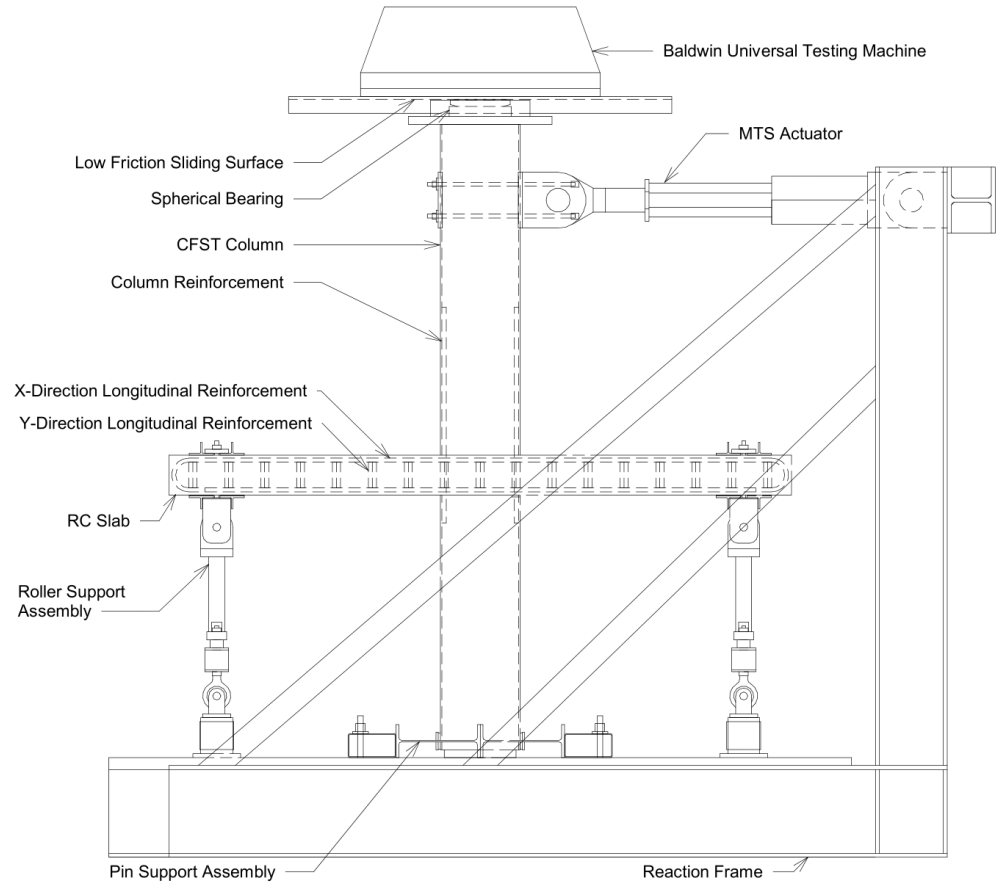

1 Setup Overview
3/8" = 1'-0"

CIVIL & ENVIRONMENTAL ENGINEERING

University of Washington
Department of Civil and Environmental Engineering

NSF Secondary Evacuation Structures

Setup Overview

Project Number	SR_4_10_5
Date	5/1/2015
Drawn By	Alec Youtter
Checked By	Alec Youtter
Scale	3/8" = 1'-0"

S.19

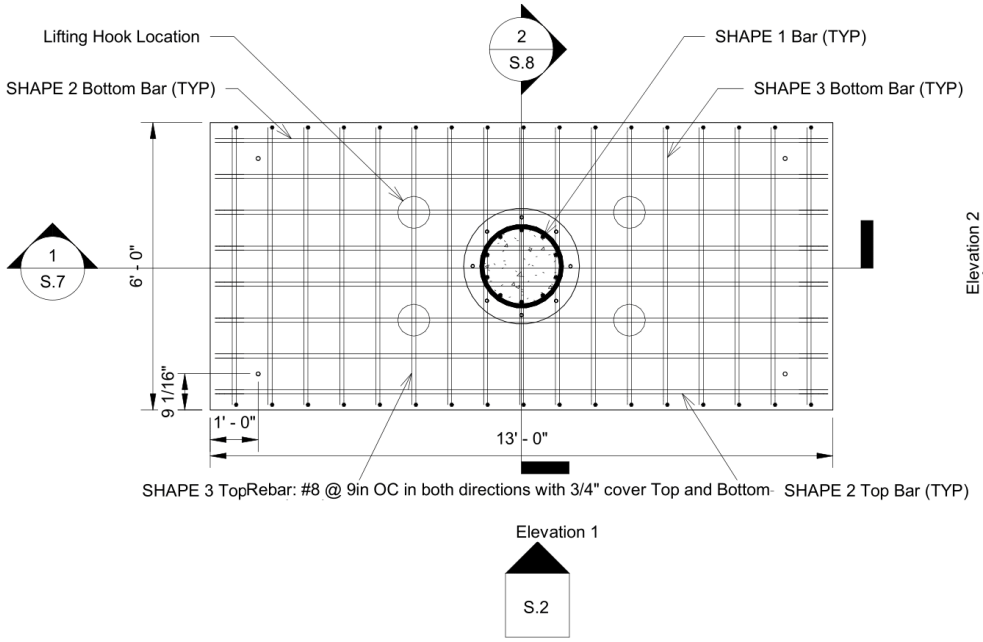

1 Level 2
3/8" = 1'-0"

CIVIL & ENVIRONMENTAL ENGINEERING

University of Washington
Department of Civil and Environmental Engineering

NSF Secondary Evacuation Structures

Plan View

Project Number	PTB_4.6_1_0
Date	5/1/2015
Drawn By	Alec Youtter
Checked By	Alec Youtter

S.1

Scale 3/8" = 1'-0"

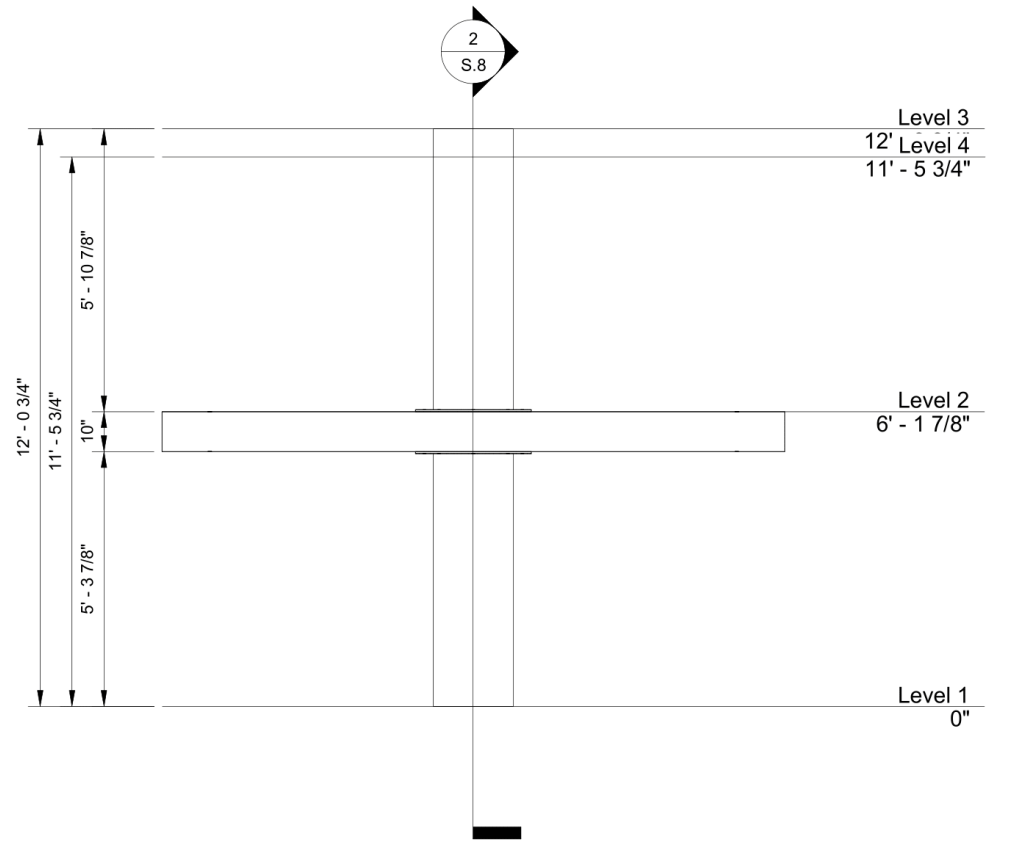

1 Elevation 1
3/8" = 1'-0"

CIVIL & ENVIRONMENTAL ENGINEERING

University of Washington
Department of Civil and Environmental Engineering

NSF Secondary Evacuation Structures

Elevation 1

Project Number	PTB_4.8_1_0
Date	5/1/2015
Drawn By	Alec Youtter
Checked By	Alec Youtter

S.2

Scale 3/8" = 1'-0"

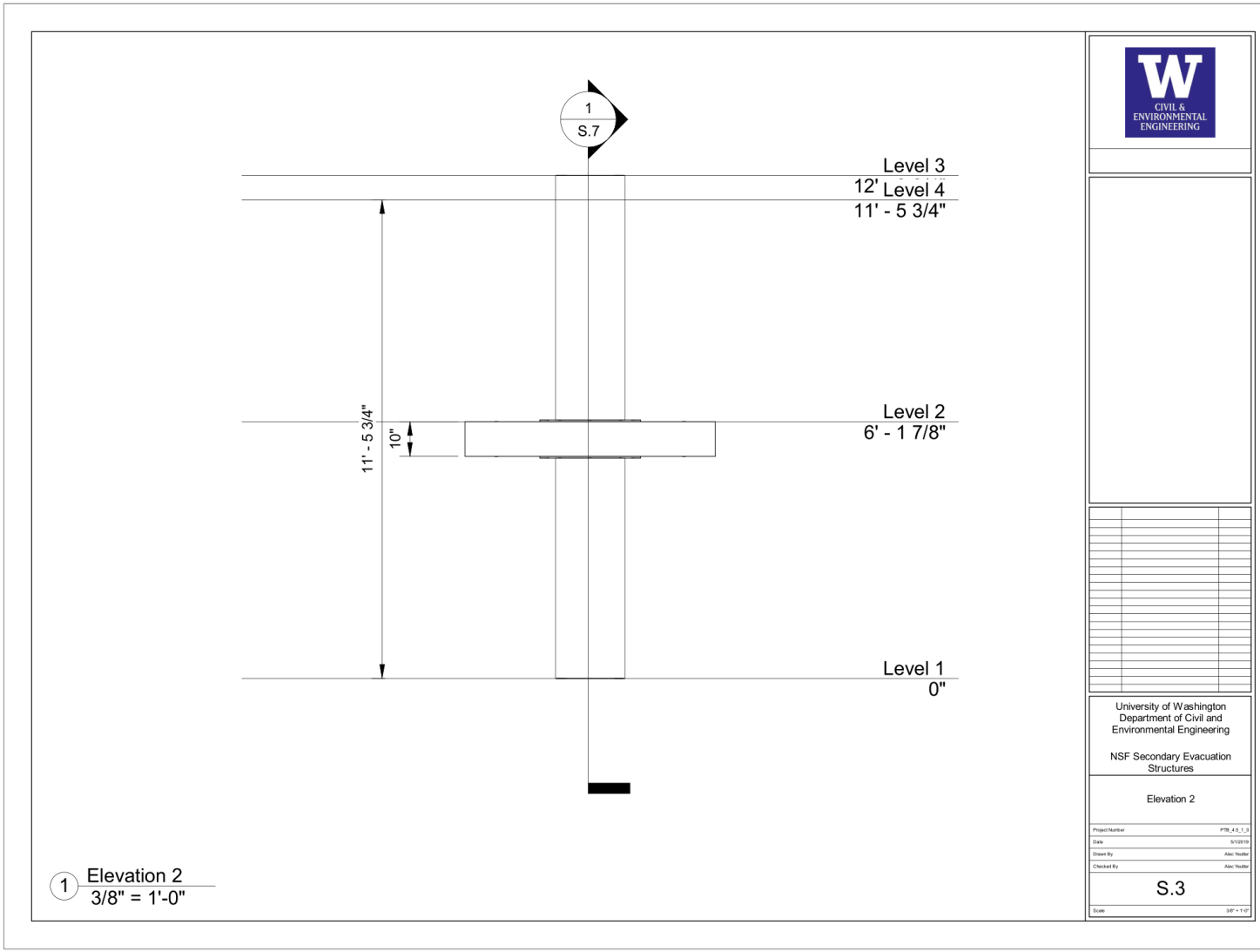
1
S.7
Level 3
12' Level 4
11' - 5 3/4"
Level 2
6' - 1 7/8"
Level 1
0"
11' - 5 3/4"
10"
1 Elevation 2
3/8" = 1'-0"
CIVIL & ENVIRONMENTAL ENGINEERING
University of Washington
Department of Civil and Environmental Engineering
NSF Secondary Evacuation Structures
Elevation 2
Project Number PTB_4.6_1_0
Date 5/1/2015
Drawn By Alec Youtter
Checked By Alec Youtter
S.3
Scale 3/8" = 1'-0"

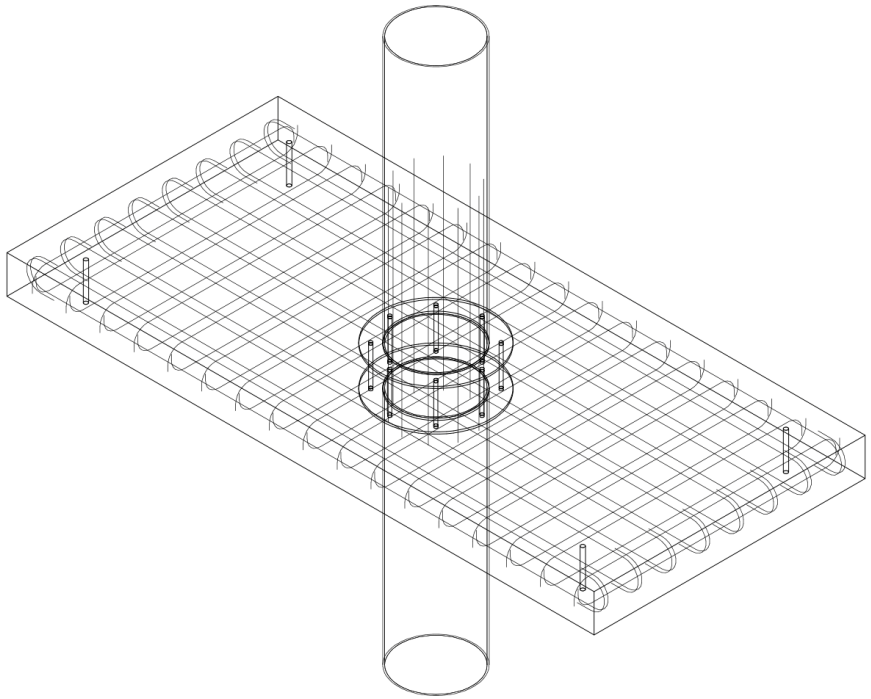

1 3D Isometric Wire Frame

CIVIL & ENVIRONMENTAL ENGINEERING

University of Washington
Department of Civil and Environmental Engineering

NSF Secondary Evacuation Structures

3D Isometric Wire Frame

Project Number	PTB_4.6_1_0
Date	5/1/2015
Drawn By	Alec Youtter
Checked By	Alec Youtter

S.4

Scale

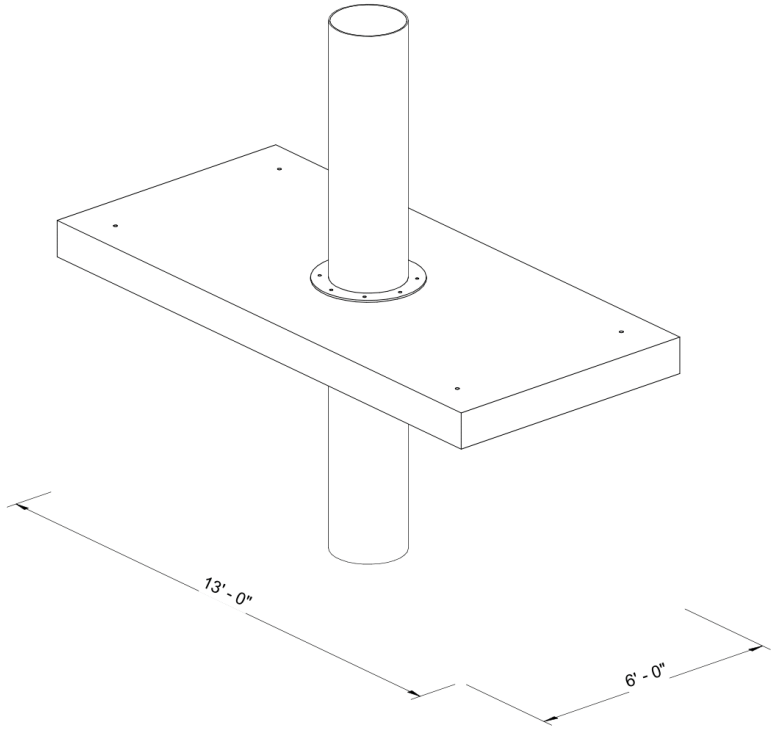

1 3D Solid Isometric View

CIVIL & ENVIRONMENTAL ENGINEERING

University of Washington
Department of Civil and Environmental Engineering

NSF Secondary Evacuation Structures

3D Solid Isometric View

Project Number	PTB_4.6_1_0
Date	5/1/2015
Drawn By	Alec Youtter
Checked By	Alec Youtter

S.5

Scale

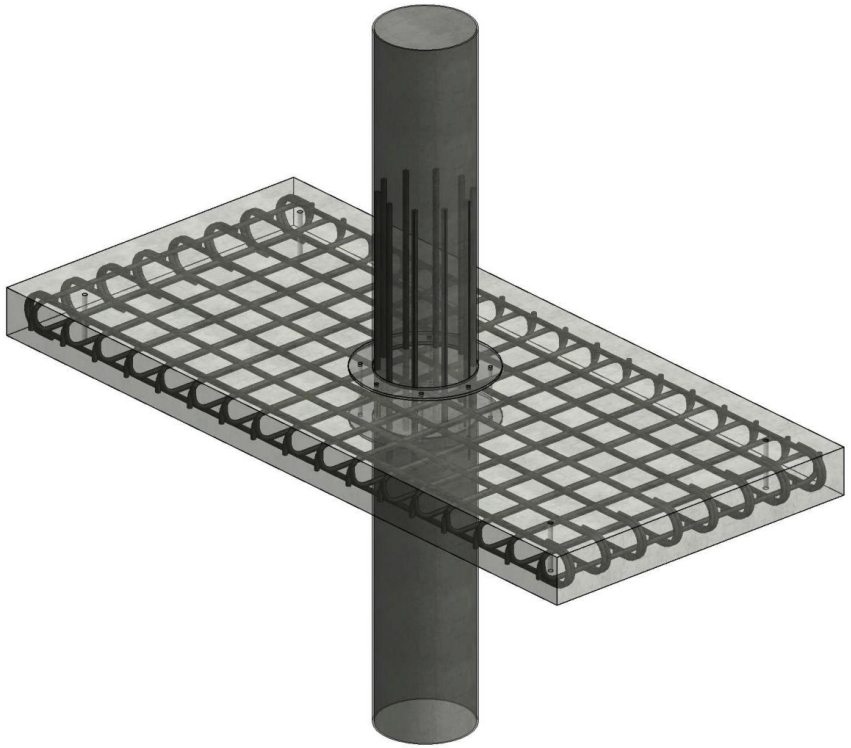

1 3D Semi-Transparent Render

CIVIL & ENVIRONMENTAL ENGINEERING

University of Washington
Department of Civil and Environmental Engineering

NSF Secondary Evacuation Structures

3D Semi-Transparent Render

Project Number	PTB_4.6_1_0
Date	5/1/2015
Drawn By	Alec Youtter
Checked By	Alec Youtter

S.6

Scale

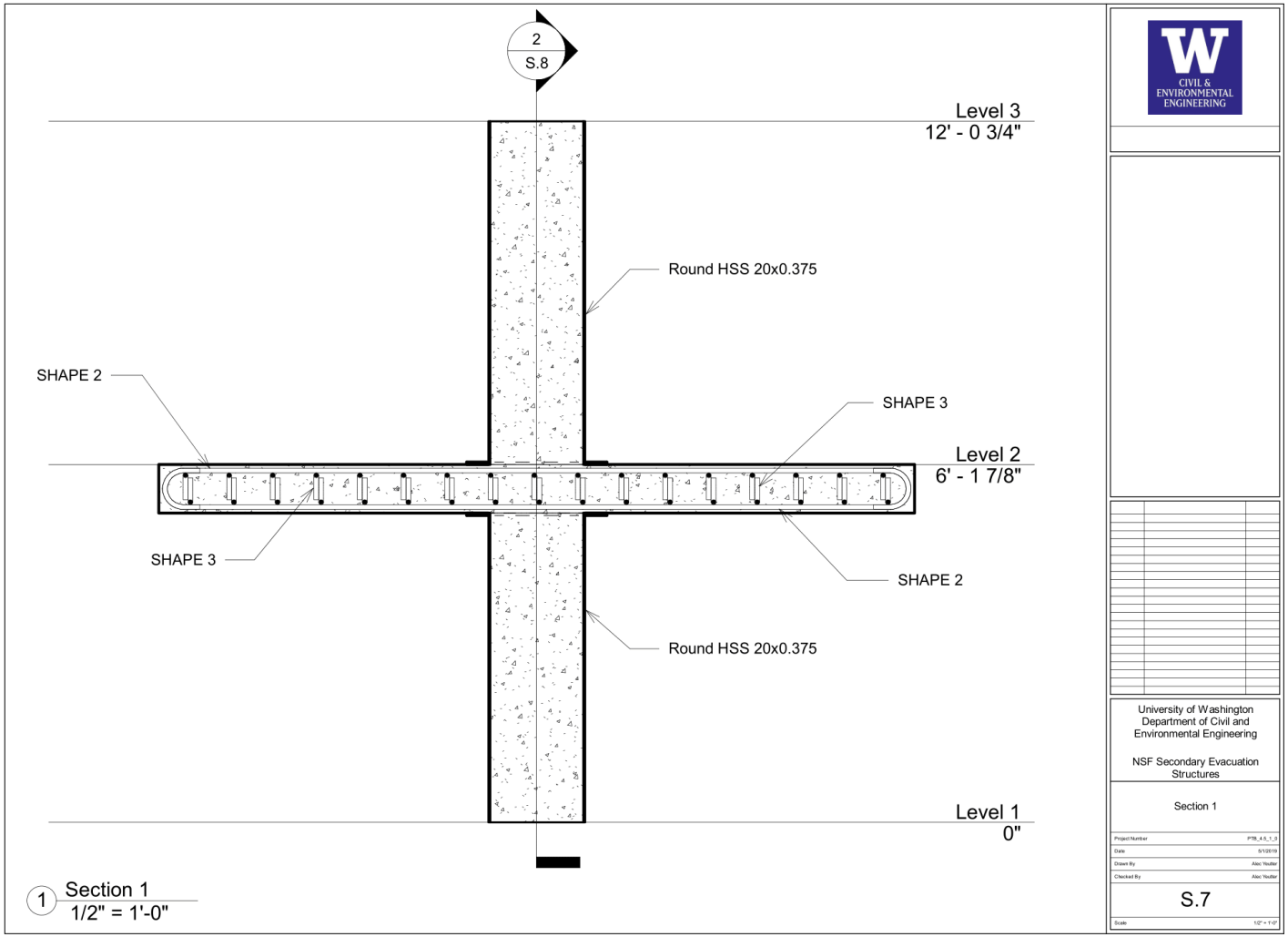
2
S.8
Level 3
12' - 0 3/4"
Round HSS 20x0.375
SHAPE 2
SHAPE 3
Level 2
6' - 1 7/8"
SHAPE 3
SHAPE 2
Round HSS 20x0.375
Level 1
0"
1
Section 1
1/2" = 1'-0"
CIVIL & ENVIRONMENTAL ENGINEERING
University of Washington
Department of Civil and Environmental Engineering
NSF Secondary Evacuation Structures
Section 1
Project Number
PTB_4.8_1_0
Date
5/1/2015
Drawn By
Alec Youtter
Checked By
Alec Youtter
S.7
Scale
1/2" = 1'-0"

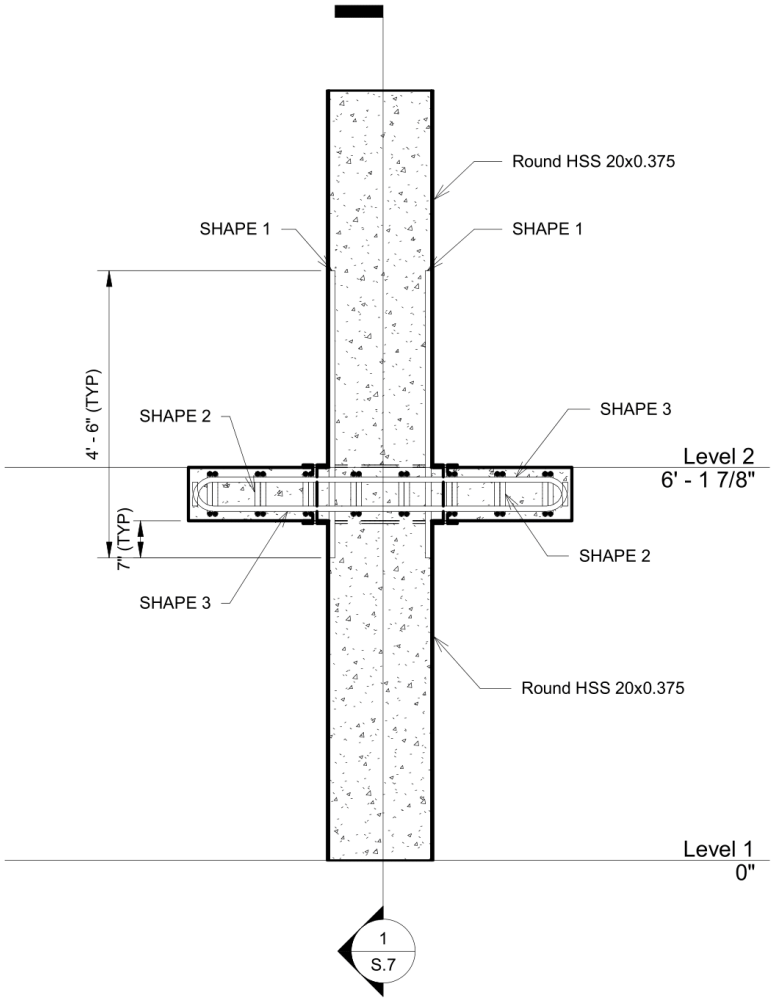

2 Section 2
1/2" = 1'-0"

CIVIL & ENVIRONMENTAL ENGINEERING

University of Washington
Department of Civil and Environmental Engineering

NSF Secondary Evacuation Structures

Section 2

Project Number	PTB_4.8_1_0
Date	5/1/2015
Drawn By	Alec Youtter
Checked By	Alec Youtter

S.8

Scale 1/2" = 1'-0"

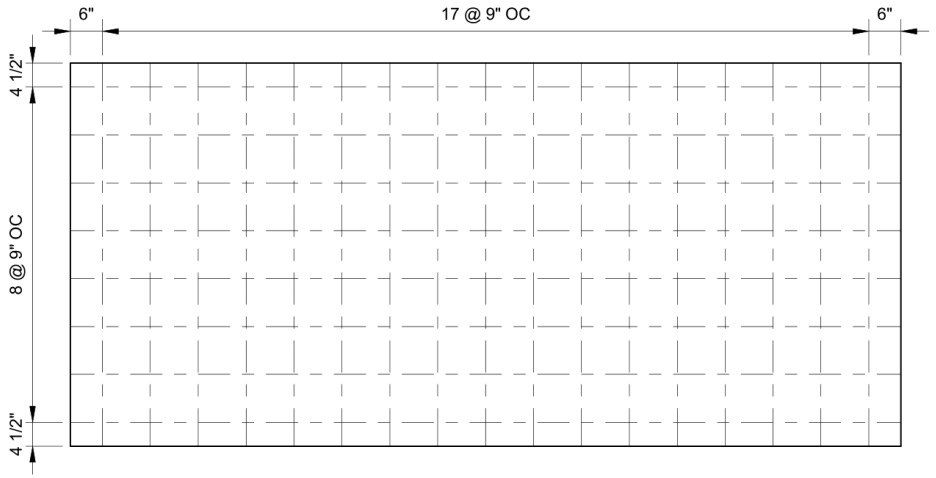

1 Slab Rebar Layout Top and Bottom
1/2" = 1'-0"

CIVIL & ENVIRONMENTAL ENGINEERING

University of Washington
Department of Civil and Environmental Engineering

NSF Secondary Evacuation Structures

Slab Rebar Layout Top and Bottom

Project Number	PTB_4.6_1_0
Date	5/1/2015
Drawn By	Author
Checked By	Checker

S.9

Scale 1/2" = 1'-0"

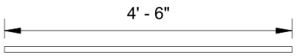

SHAPE 1: #9 Bar

2 Rebar SHAPE 1
1/2" = 1'-0"

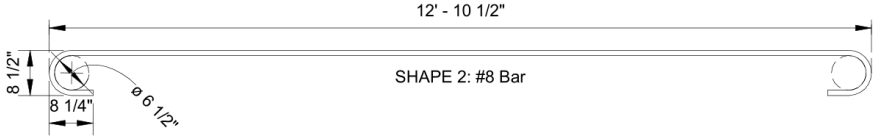

SHAPE 2: #8 Bar

1 Rebar SHAPE 2
1/2" = 1'-0"

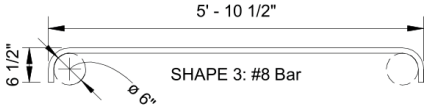

SHAPE 3: #8 Bar

3 Rebar SHAPE 3
1/2" = 1'-0"

CIVIL & ENVIRONMENTAL ENGINEERING

University of Washington
Department of Civil and Environmental Engineering

NSF Secondary Evacuation Structures

Rebar Details

Project Number	PTB_4.8_1_0
Date	5/1/2015
Drawn By	Author
Checked By	Checker

S.10

Scale 1/2" = 1'-0"

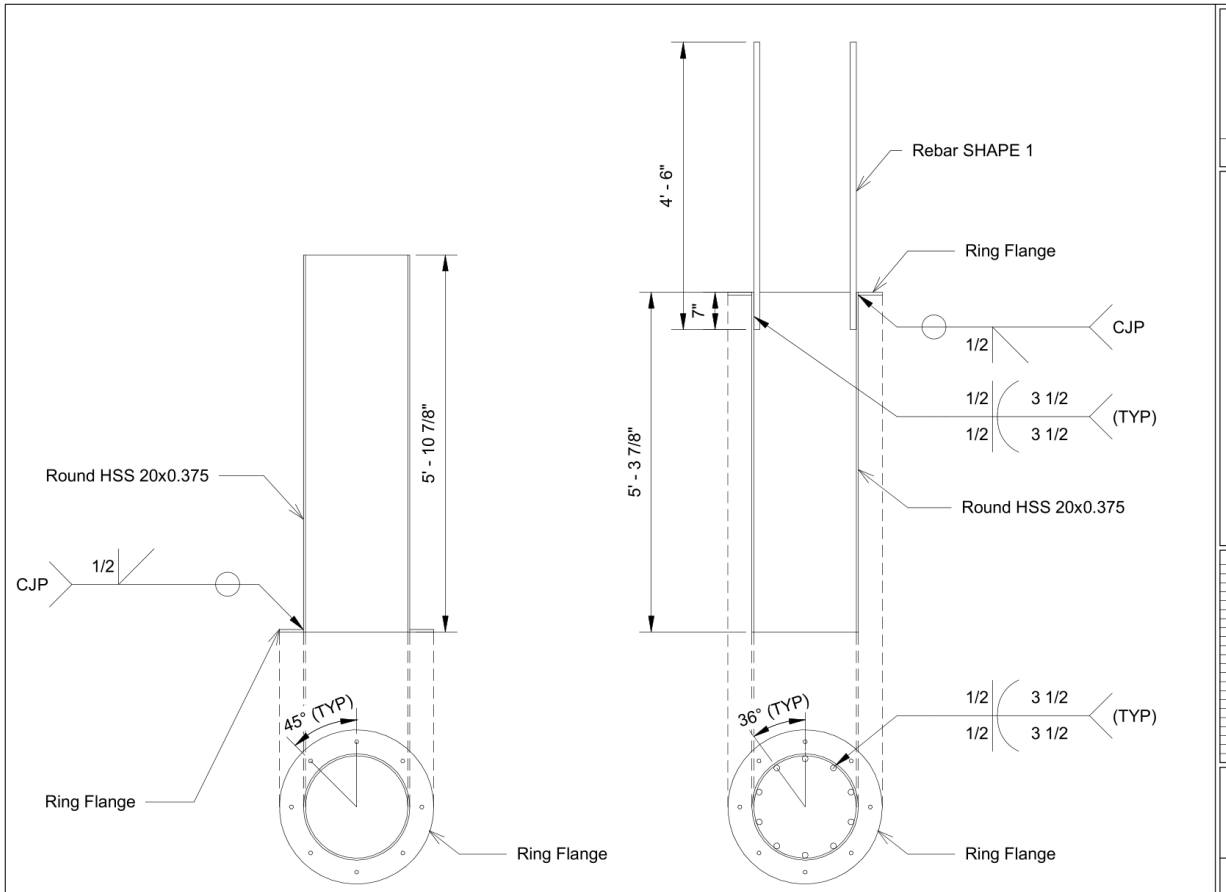

1 Collumn Fabrication Details
1/2" = 1'-0"

CIVIL & ENVIRONMENTAL ENGINEERING

University of Washington
Department of Civil and Environmental Engineering

NSF Secondary Evacuation Structures

Column Fabrication Details

Project Number	PTB_4.6_1_0
Date	5/1/2015
Drawn By	Alec Youtter
Checked By	Charles Roeder

S.11

Scale 1/2" = 1'-0"

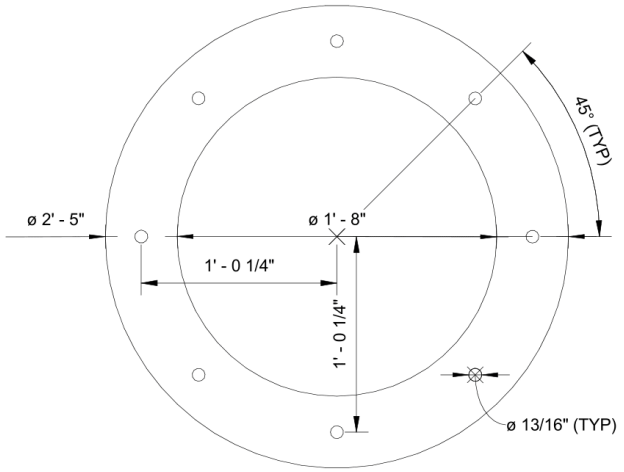

1 Ring Fabrication Detail
1 1/2" = 1'-0"

CIVIL & ENVIRONMENTAL ENGINEERING

University of Washington
Department of Civil and Environmental Engineering

NSF Secondary Evacuation Structures

Ring Fabrication Detail

Project Number	PTB_4.6_1_0
Date	5/1/2015
Drawn By	Author
Checked By	Checker

S.12

Scale 1 1/2" = 1'-0"

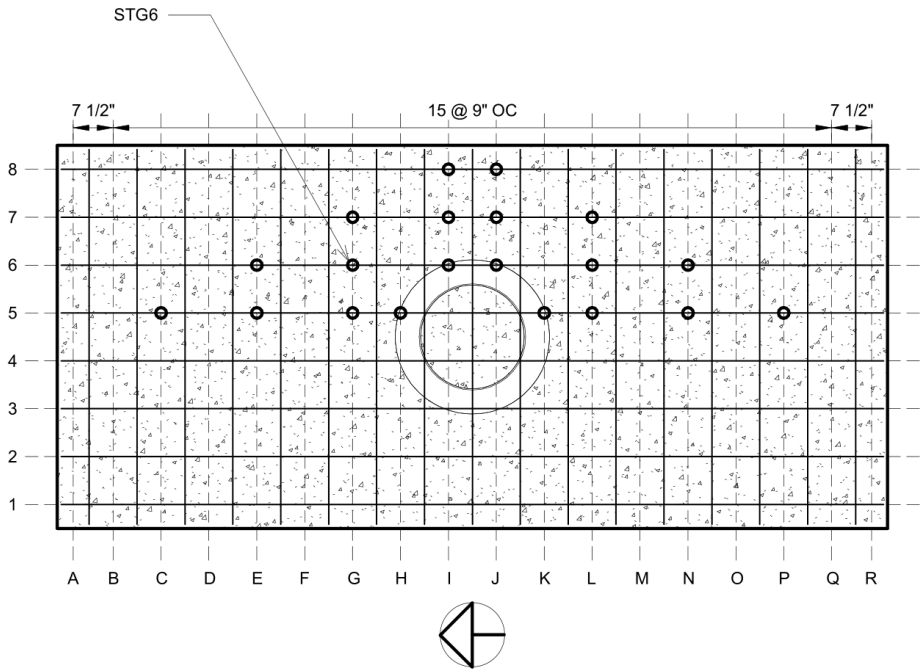

Naming Convention:
1. "S" for slab
2. "T" for top or "B" for Bottom
3. Column Letter
4. Row Number

Example: STG6 would be a strain gauge on a "Slab" "Top" bar in column "G" in row "6"

1 Slab Strain Gauge Layout
1/2" = 1'-0"

CIVIL & ENVIRONMENTAL ENGINEERING

University of Washington
Department of Civil and Environmental Engineering

NSF Secondary Evacuation Structures

Slab Strain Gauge Layout Top and Bottom

Project Number	PTB_4.6_1_0
Date	5/1/2015
Drawn By	Author
Checked By	Checker

S.13

Scale 1/2" = 1'-0"

Naming Convention:
1. "C" for Column
2. Rebar Letter
3. Level Number

Example: CI7 would be a strain gauge on "Column" bar "I" at level "7".

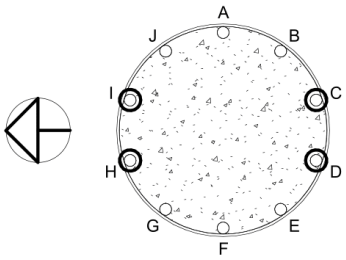

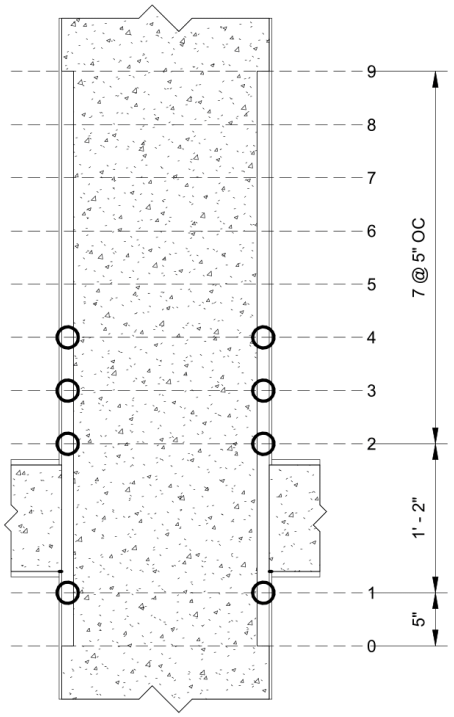

1 Column Strain Gauge Layout
1" = 1'-0"

CIVIL & ENVIRONMENTAL ENGINEERING

University of Washington
Department of Civil and Environmental Engineering

NSF Secondary Evacuation Structures

Column Strain Gauge Layout

Project Number	PTB_4.6_1_0
Date	5/1/2015
Drawn By	Author
Checked By	Checker

S.14

Scale 1" = 1'-0"

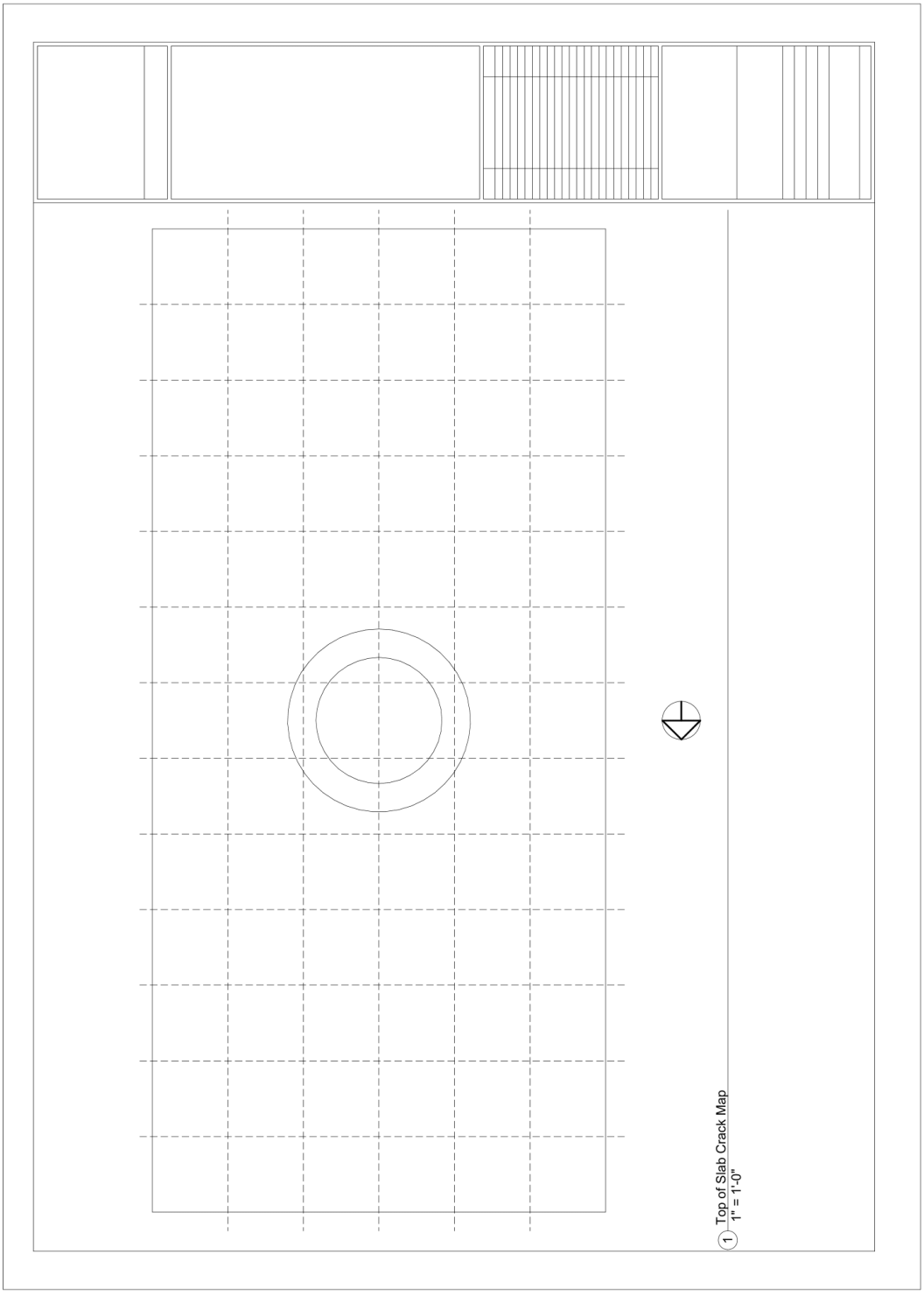
1 Top of Slab Crack Map
1" = 1'-0"

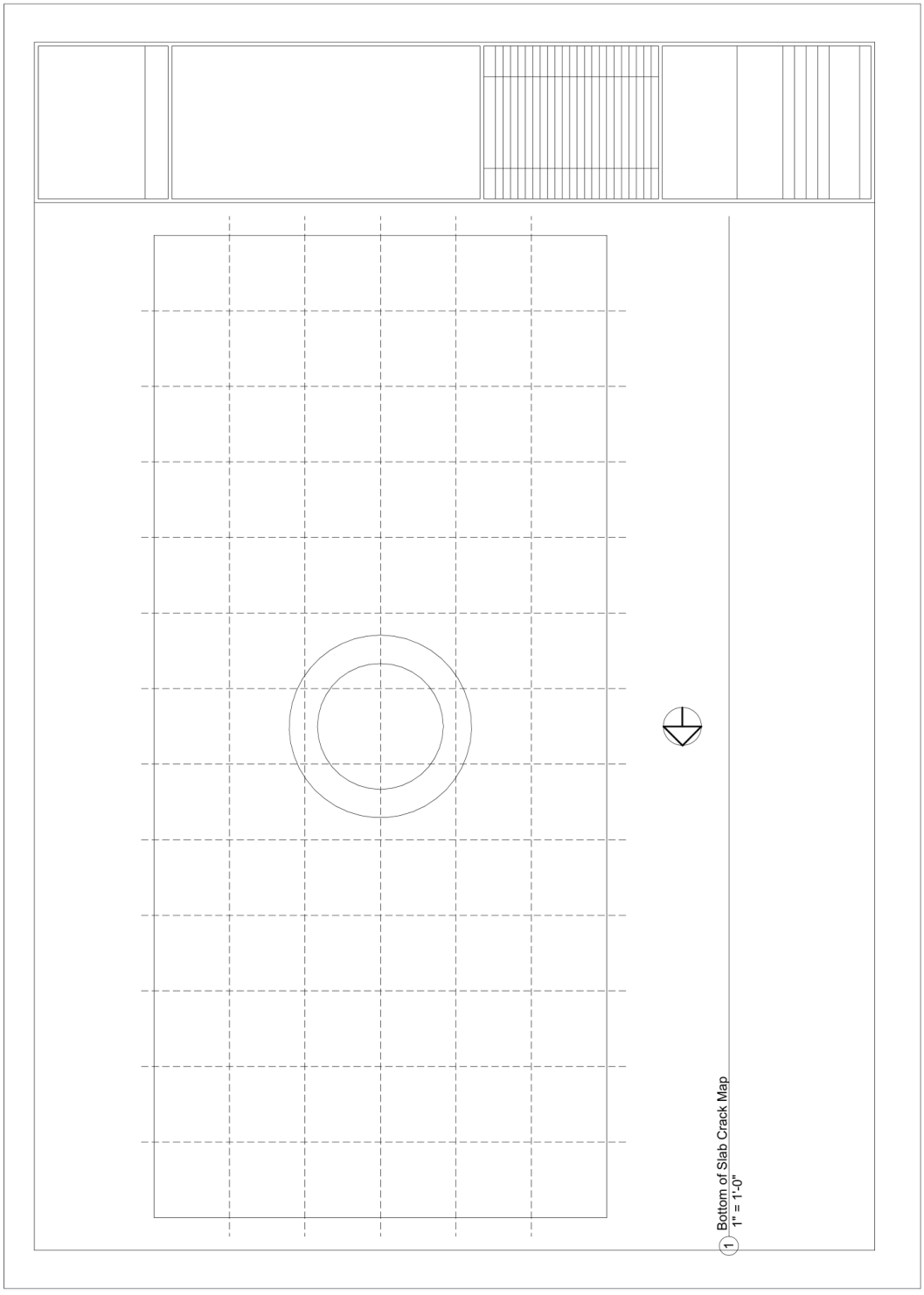
1
Bottom of Slab Crack Map
1" = 1'-0"

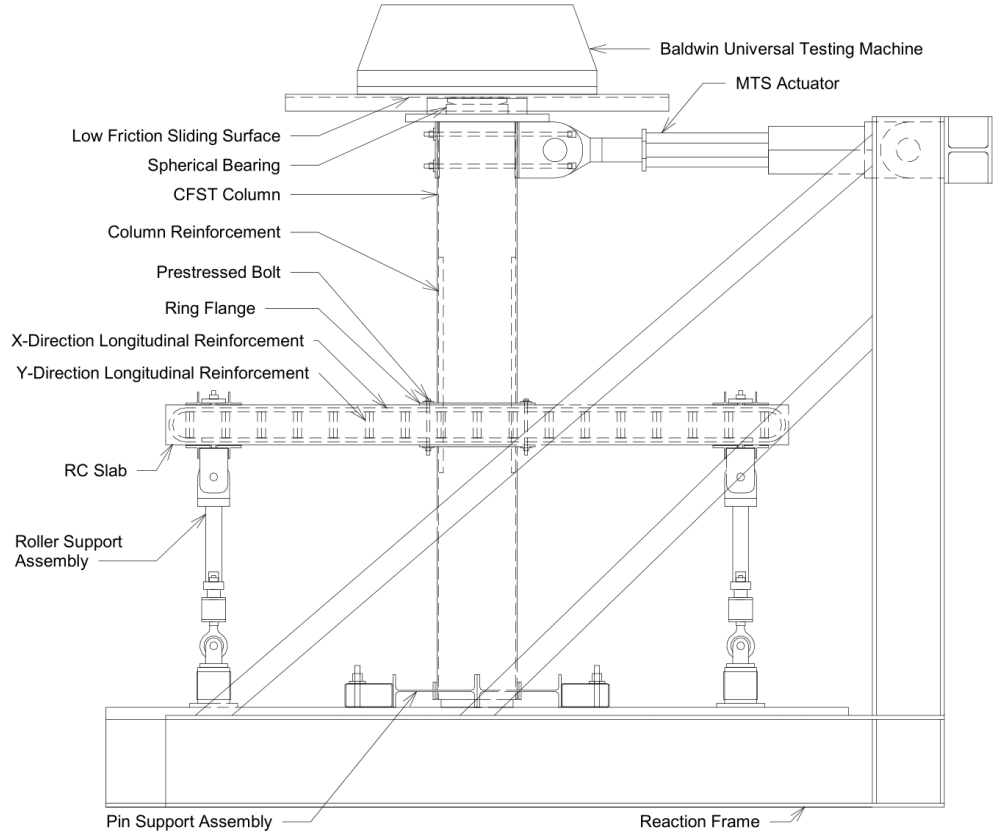

1 Setup Overview
3/8" = 1'-0"

CIVIL & ENVIRONMENTAL ENGINEERING

University of Washington
Department of Civil and Environmental Engineering

NSF Secondary Evacuation Structures

Setup Overview

Project Number	PTB_4.8_1_0
Date	5/1/2015
Drawn By	Alec Youtter
Checked By	Alec Youtter

S.17

Scale 3/8" = 1'-0"

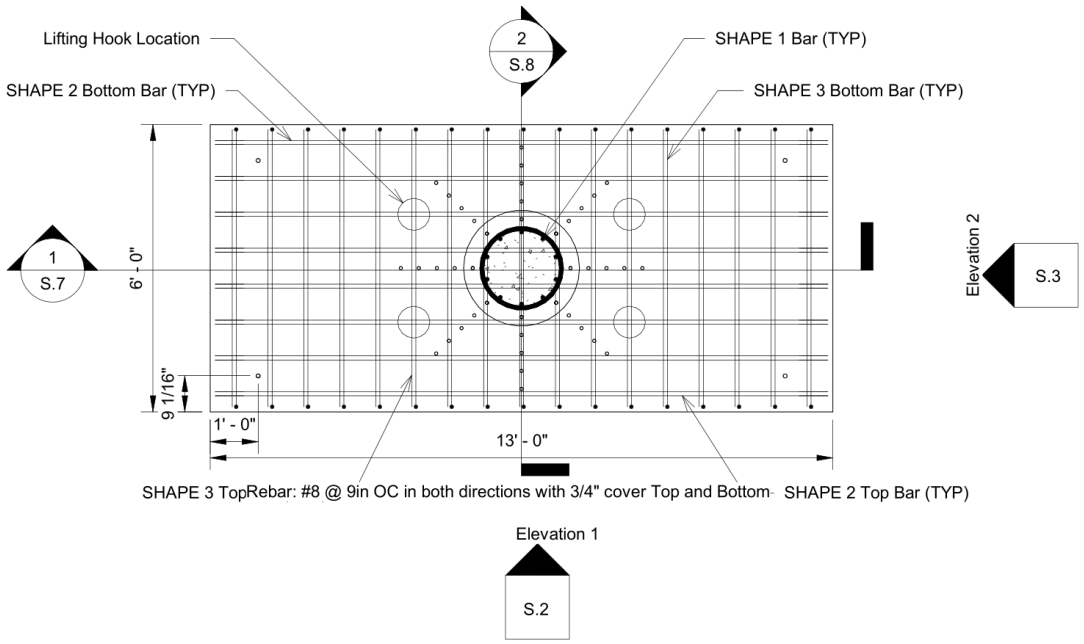

1 Level 2
3/8" = 1'-0"

CIVIL & ENVIRONMENTAL ENGINEERING

University of Washington
Department of Civil and Environmental Engineering

NSF Secondary Evacuation Structures

Plan View

Project Number	PTB_4.8_1_4
Date	5/1/2015
Drawn By	Alec Youtter
Checked By	Alec Youtter

S.1

Scale 3/8" = 1'-0"

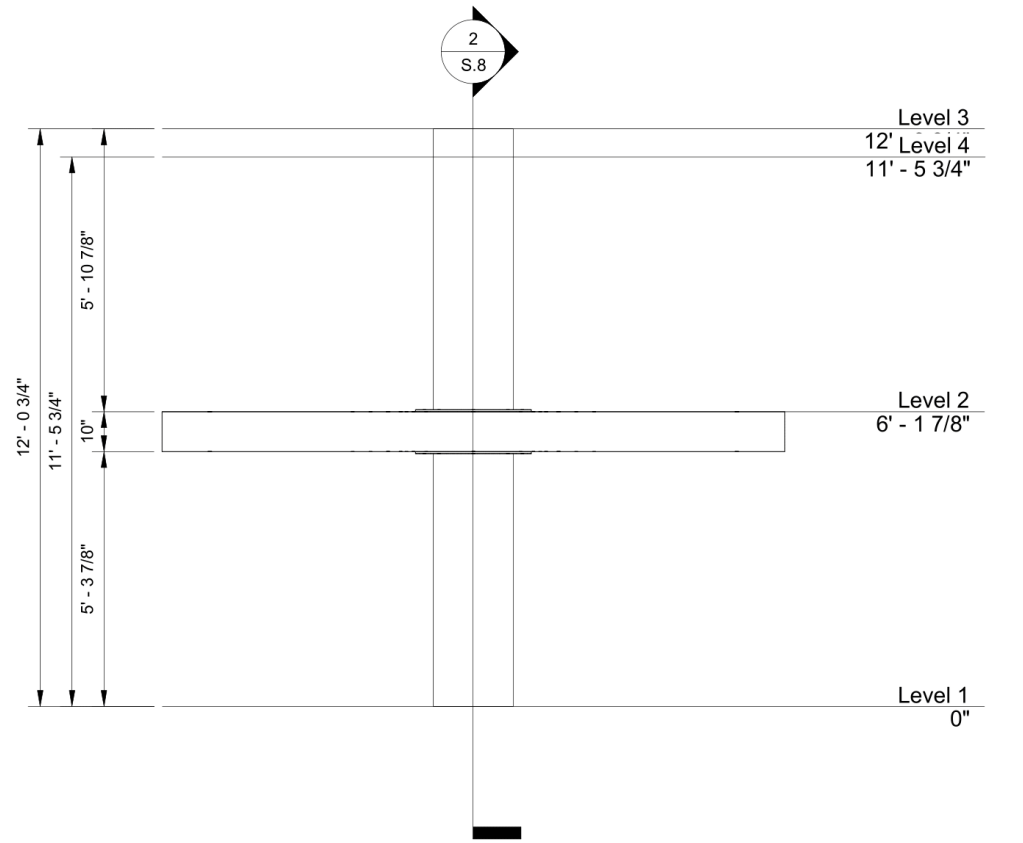

1 Elevation 1
3/8" = 1'-0"

CIVIL & ENVIRONMENTAL ENGINEERING

University of Washington
Department of Civil and Environmental Engineering

NSF Secondary Evacuation Structures

Elevation 1

Project Number	PTB_4.8_1_4
Date	5/1/2015
Drawn By	Alec Youtter
Checked By	Alec Youtter

S.2

Scale 3/8" = 1'-0"

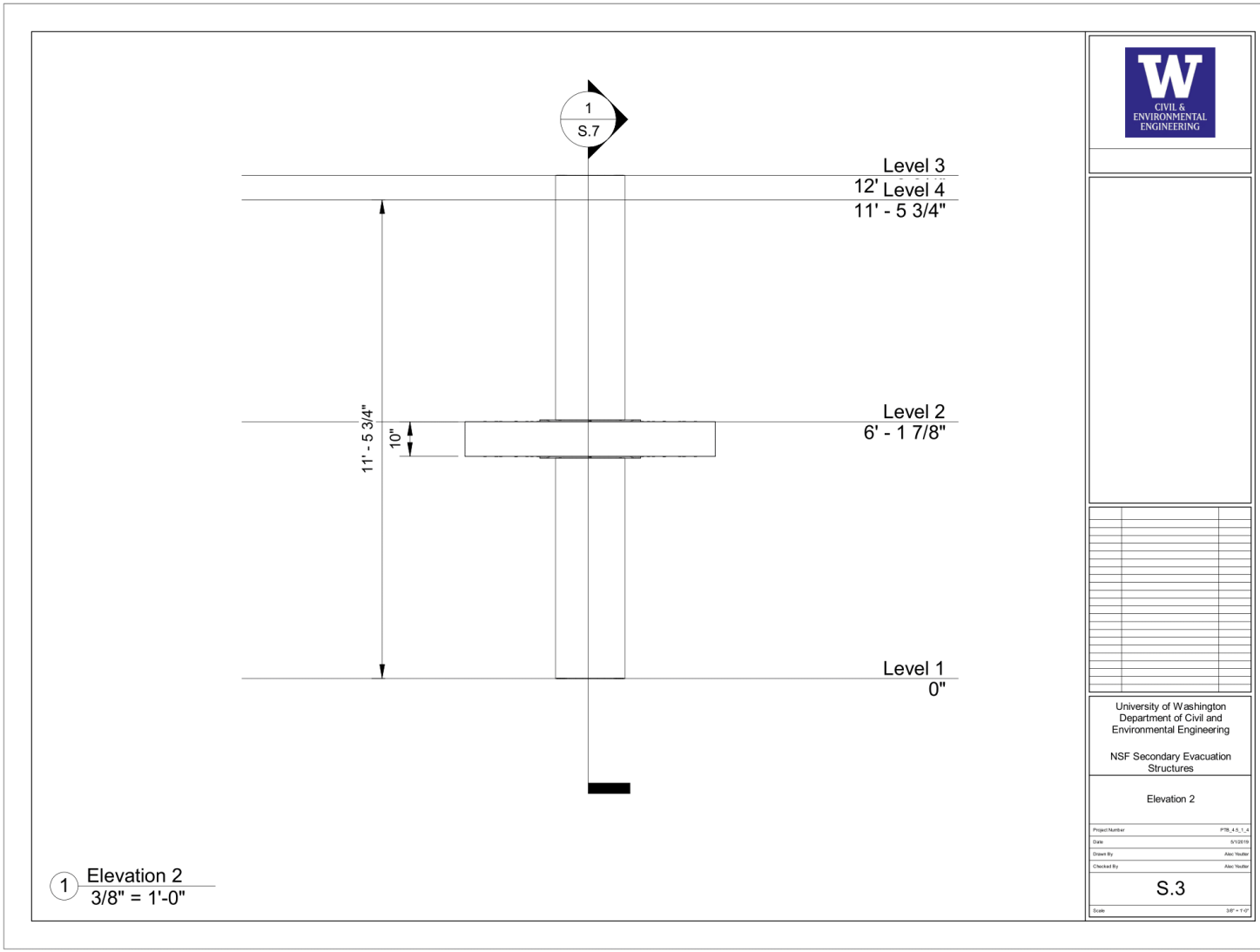
1
S.7
Level 3
12' Level 4
11' - 5 3/4"
Level 2
6' - 1 7/8"
Level 1
0"
11' - 5 3/4"
10"
1 Elevation 2
3/8" = 1'-0"
CIVIL & ENVIRONMENTAL ENGINEERING
University of Washington
Department of Civil and
Environmental Engineering
NSF Secondary Evacuation
Structures
Elevation 2
Project Number
PTB_4.8_1_4
Date
5/1/2015
Drawn By
Alec Youtter
Checked By
Alec Youtter
S.3
Scale
3/8" = 1'-0"

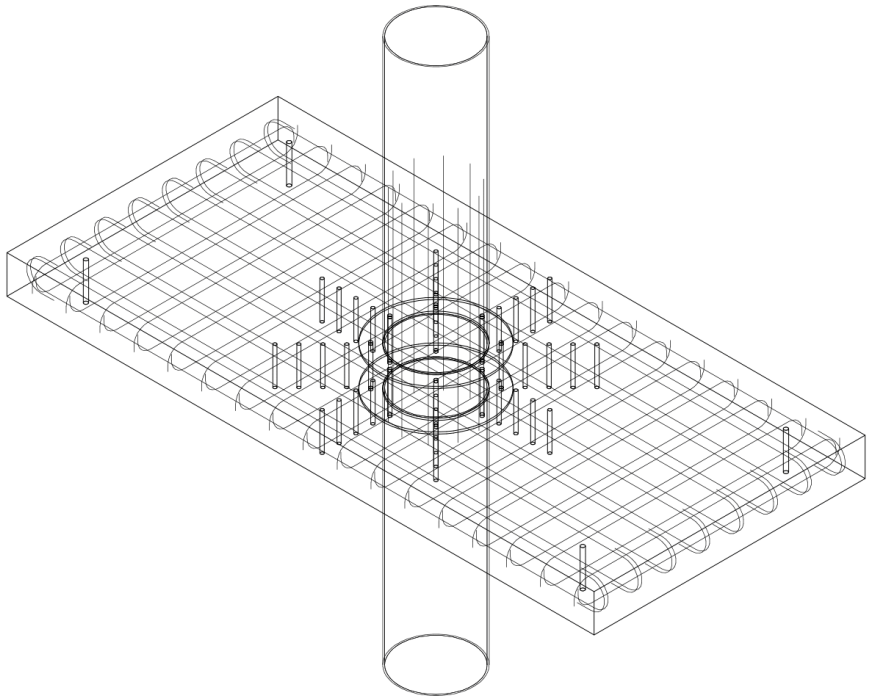

1 3D Isometric Wire Frame

CIVIL & ENVIRONMENTAL ENGINEERING

University of Washington
Department of Civil and Environmental Engineering

NSF Secondary Evacuation Structures

3D Isometric Wire Frame

Project Number	PTB_4.6_1_4
Date	5/1/2015
Drawn By	Alec Youtter
Checked By	Alec Youtter

S.4

Scale

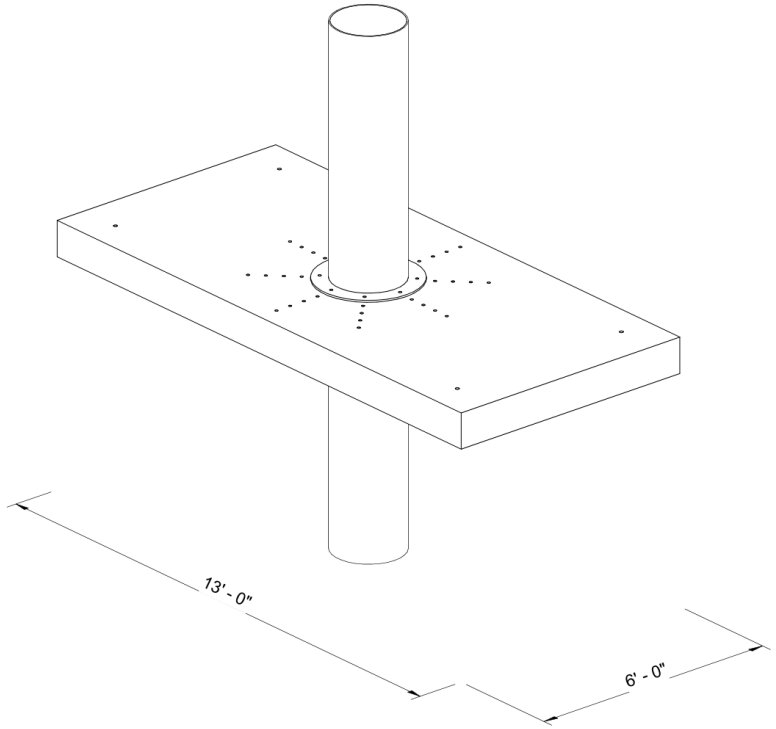

1 3D Solid Isometric View

CIVIL & ENVIRONMENTAL ENGINEERING

University of Washington
Department of Civil and Environmental Engineering

NSF Secondary Evacuation Structures

3D Solid Isometric View

Project Number	PTB_4.8_1_4
Date	5/1/2015
Drawn By	Alec Youtter
Checked By	Alec Youtter

S.5

Scale

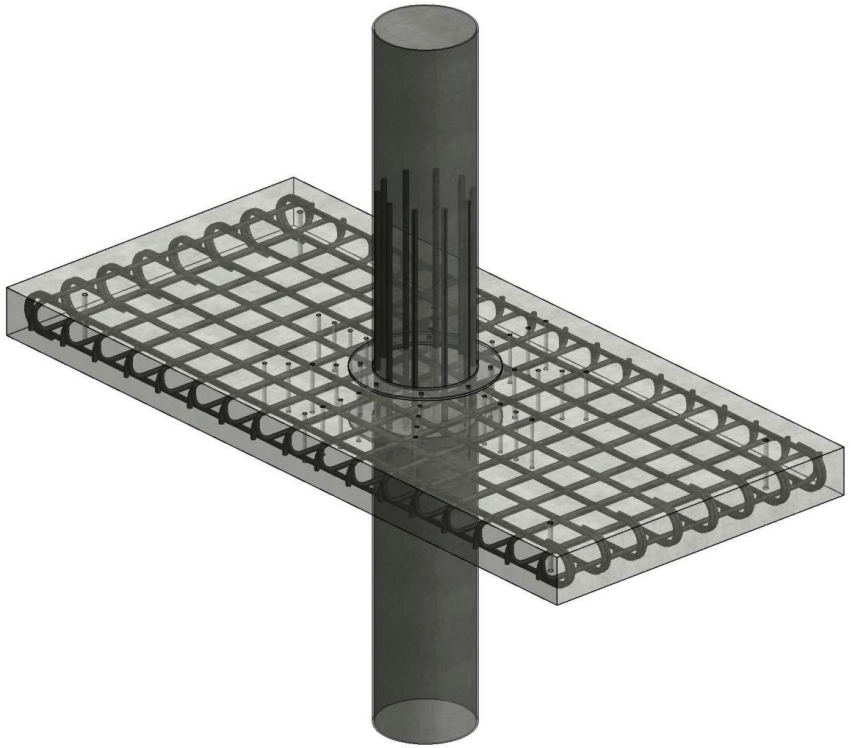

1 3D Semi-Transparent Render

CIVIL & ENVIRONMENTAL ENGINEERING

University of Washington
Department of Civil and Environmental Engineering

NSF Secondary Evacuation Structures

3D Semi-Transparent Render

Project Number	PTB_4.6_1_4
Date	5/1/2015
Drawn By	Alec Youtter
Checked By	Alec Youtter

S.6

Scale

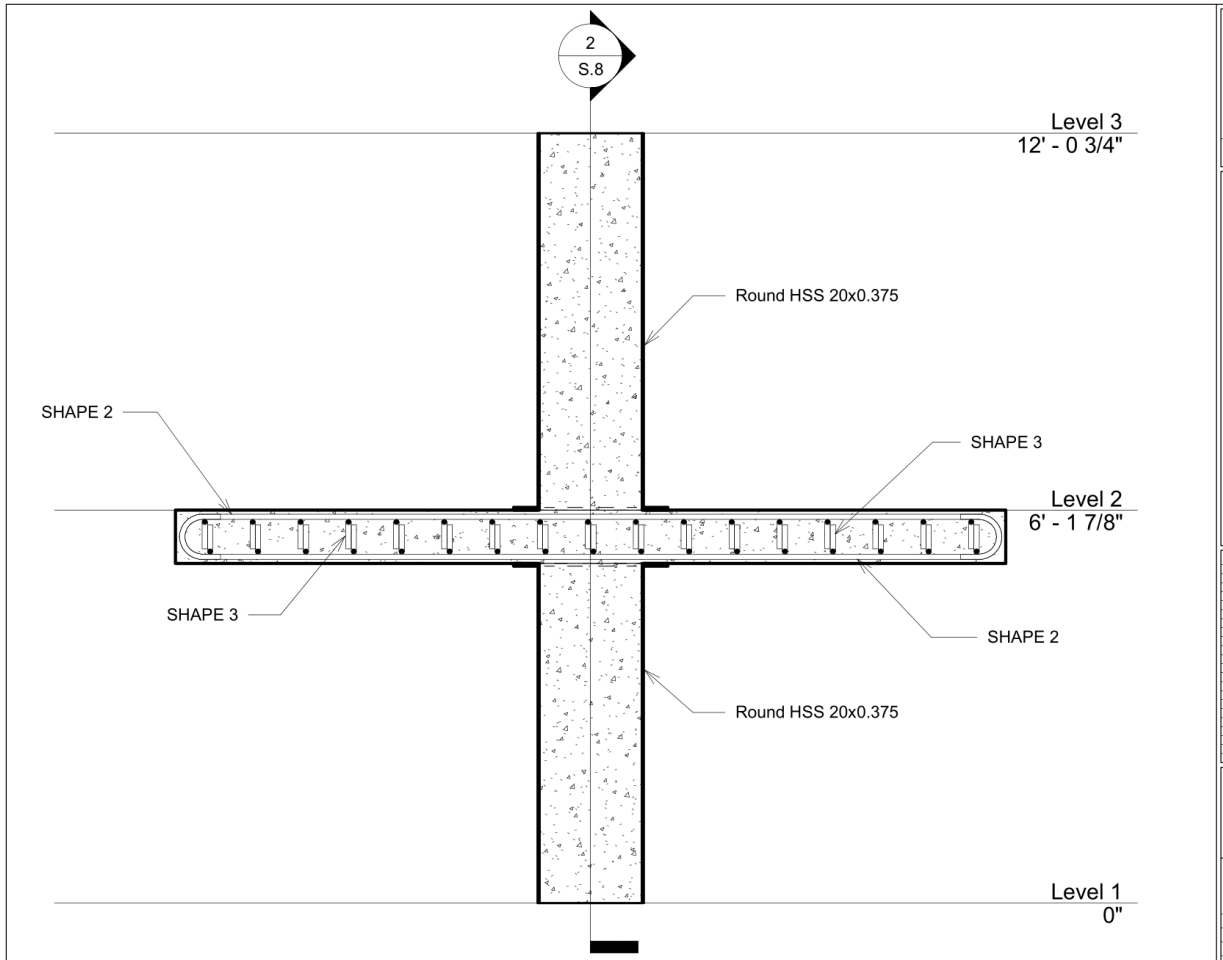

1 Section 1
1/2" = 1'-0"

CIVIL & ENVIRONMENTAL ENGINEERING

University of Washington
Department of Civil and Environmental Engineering

NSF Secondary Evacuation Structures

Section 1

Project Number	PTB_4.8_1_4
Date	5/1/2015
Drawn By	Alec Youtter
Checked By	Alec Youtter

S.7

Scale 1/2" = 1'-0"

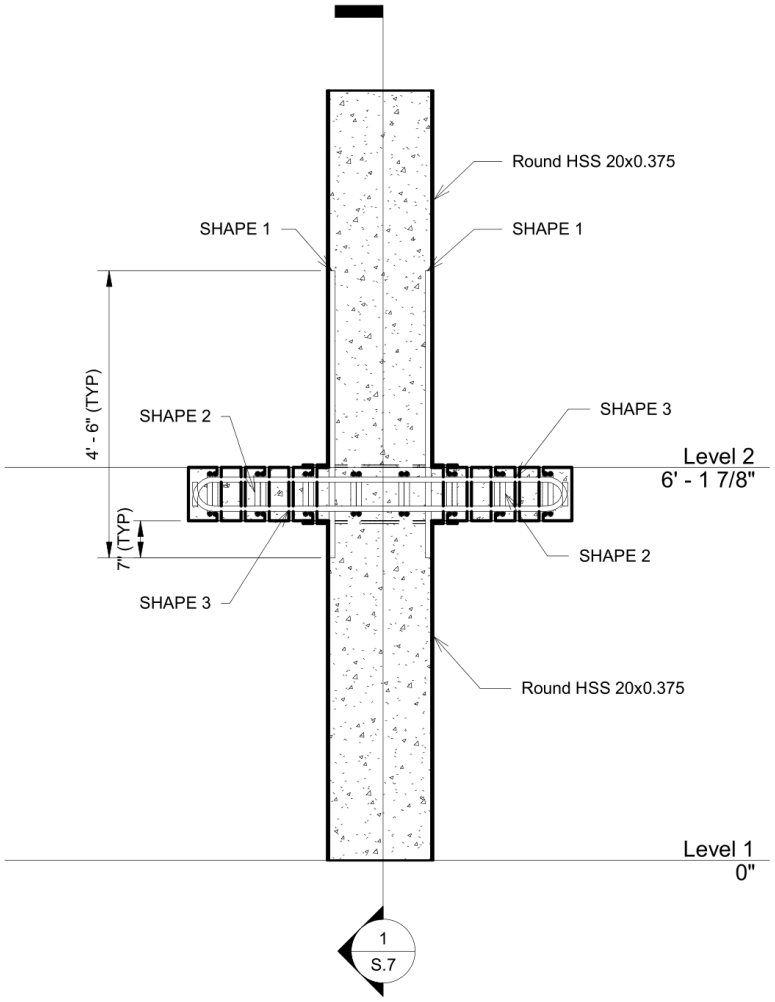

2 Section 2
1/2" = 1'-0"

CIVIL & ENVIRONMENTAL ENGINEERING

University of Washington
Department of Civil and Environmental Engineering

NSF Secondary Evacuation Structures

Section 2

Project Number	PTB_4.8_1_4
Date	5/1/2015
Drawn By	Alec Youtter
Checked By	Alec Youtter

S.8

Scale 1/2" = 1'-0"

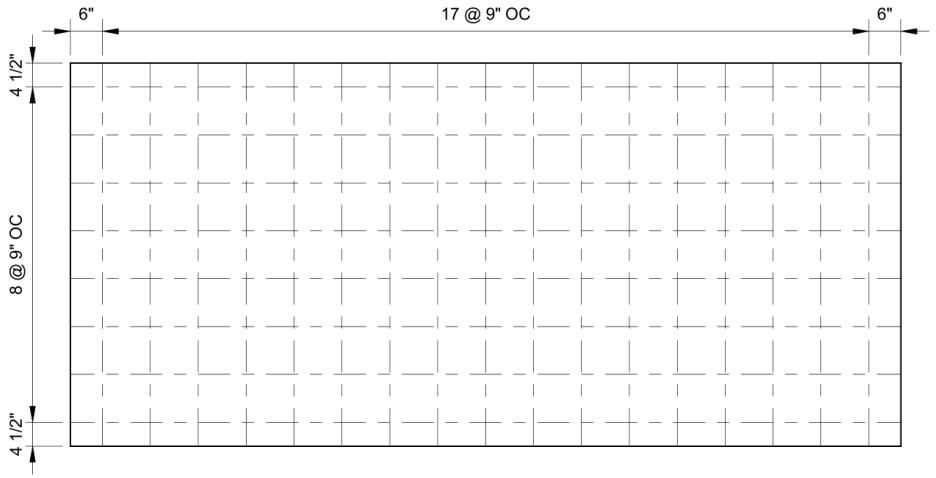

1 Slab Rebar Layout Top and Bottom
1/2" = 1'-0"

CIVIL & ENVIRONMENTAL ENGINEERING

University of Washington
Department of Civil and Environmental Engineering

NSF Secondary Evacuation Structures

Slab Rebar Layout Top and Bottom

Project Number	PTB_4.8_1_4
Date	5/1/2015
Drawn By	Author
Checked By	Checker

S.9

Scale 1/2" = 1'-0"

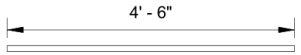

SHAPE 1: #9 Bar

1 Rebar SHAPE 1
1/2" = 1'-0"

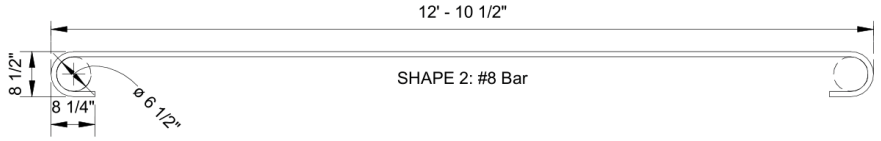

SHAPE 2: #8 Bar

2 Rebar SHAPE 2
1/2" = 1'-0"

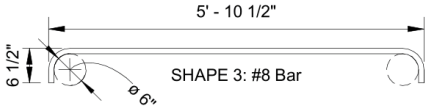

SHAPE 3: #8 Bar

3 Rebar SHAPE 3
1/2" = 1'-0"

CIVIL & ENVIRONMENTAL ENGINEERING

University of Washington
Department of Civil and Environmental Engineering

NSF Secondary Evacuation Structures

Rebar Details

Project Number	PTB_4.8_1_4
Date	5/1/2015
Drawn By	Author
Checked By	Checker

S.10

Scale 1/2" = 1'-0"

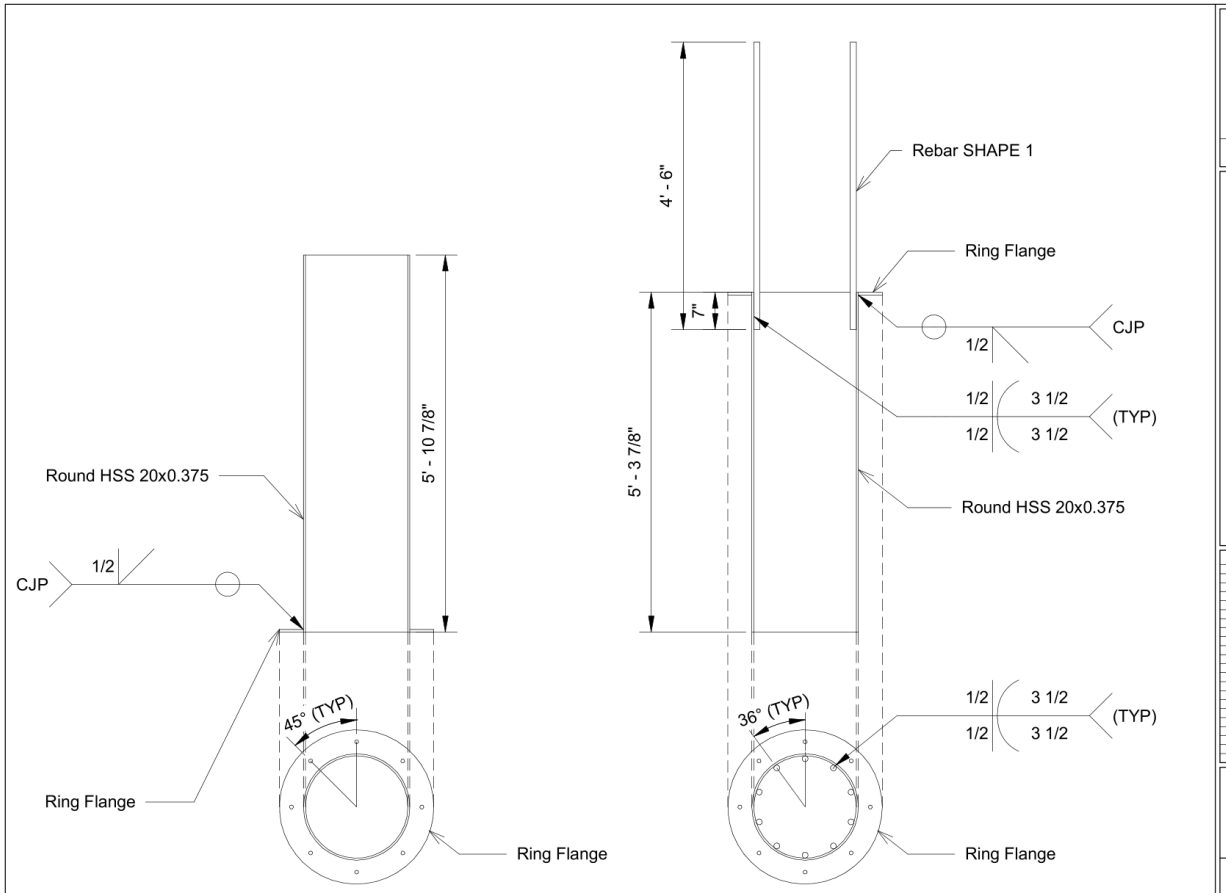

1 Collumn Fabrication Details
1/2" = 1'-0"

CIVIL & ENVIRONMENTAL ENGINEERING

University of Washington
Department of Civil and Environmental Engineering

NSF Secondary Evacuation Structures

Column Fabrication Details

Project Number	PTB_4.8_1_4
Date	5/1/2015
Drawn By	Alec Youtter
Checked By	Charles Roeder

S.11

Scale 1/2" = 1'-0"

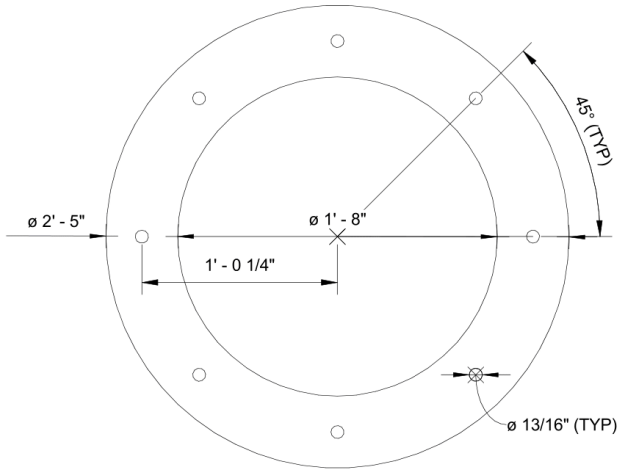

1 Ring Fabrication Detail
1 1/2" = 1'-0"

CIVIL & ENVIRONMENTAL ENGINEERING

University of Washington
Department of Civil and Environmental Engineering

NSF Secondary Evacuation Structures

Ring Fabrication Detail

Project Number	PTB_4.8_1_4
Date	5/1/2015
Drawn By	Author
Checked By	Checker

S.12

Scale 1 1/2" = 1'-0"

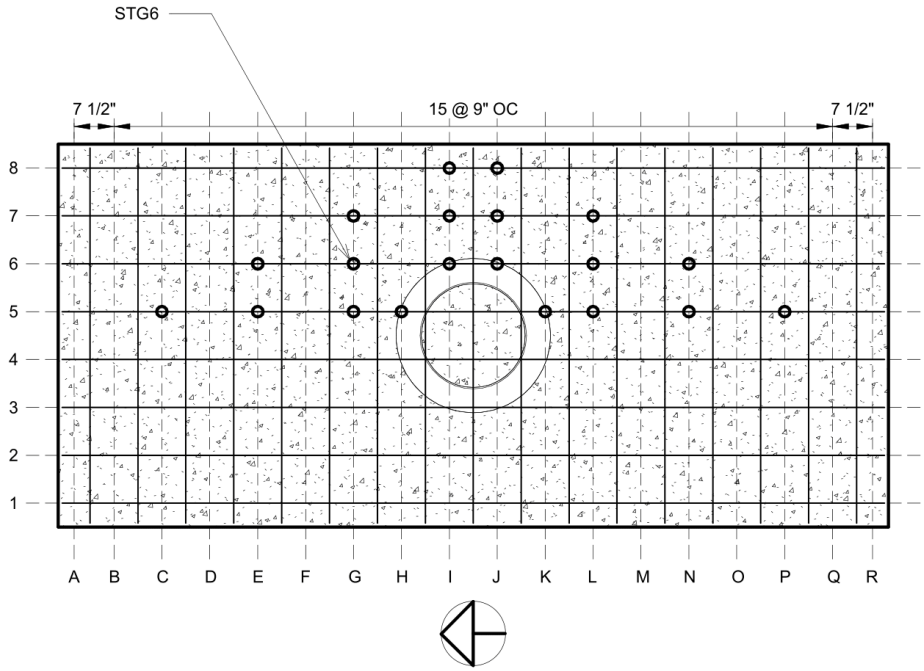

Naming Convention:
1. "S" for slab
2. "T" for top or "B" for Bottom
3. Column Letter
4. Row Number

Example: STG6 would be a strain gauge on a "Slab" "Top" bar in column "G" in row "6"

1 Slab Strain Gauge Layout
1/2" = 1'-0"

CIVIL & ENVIRONMENTAL ENGINEERING

University of Washington
Department of Civil and Environmental Engineering

NSF Secondary Evacuation Structures

Slab Strain Gauge Layout Top and Bottom

Project Number	PTB_4.8_1_4
Date	5/1/2015
Drawn By	Author
Checked By	Checker

S.13

Scale 1/2" = 1'-0"

Naming Convention:
1. "C" for Column
2. Rebar Letter
3. Level Number

Example: CI7 would be a strain gauge on "Column" bar "I" at level "7".

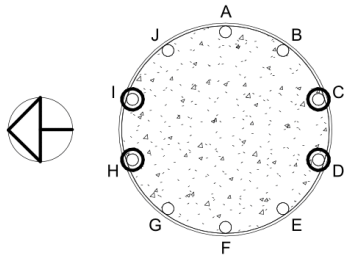

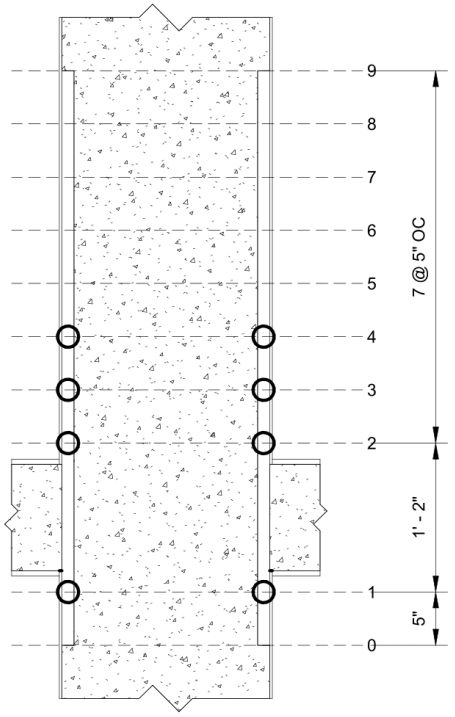

1 Column Strain Gauge Layout
1" = 1'-0"

CIVIL & ENVIRONMENTAL ENGINEERING

University of Washington
Department of Civil and Environmental Engineering

NSF Secondary Evacuation Structures

Column Strain Gauge Layout

Project Number	PTB_4.8_1_4
Date	5/1/2015
Drawn By	Author
Checked By	Checker

S.14

Scale 1" = 1'-0"

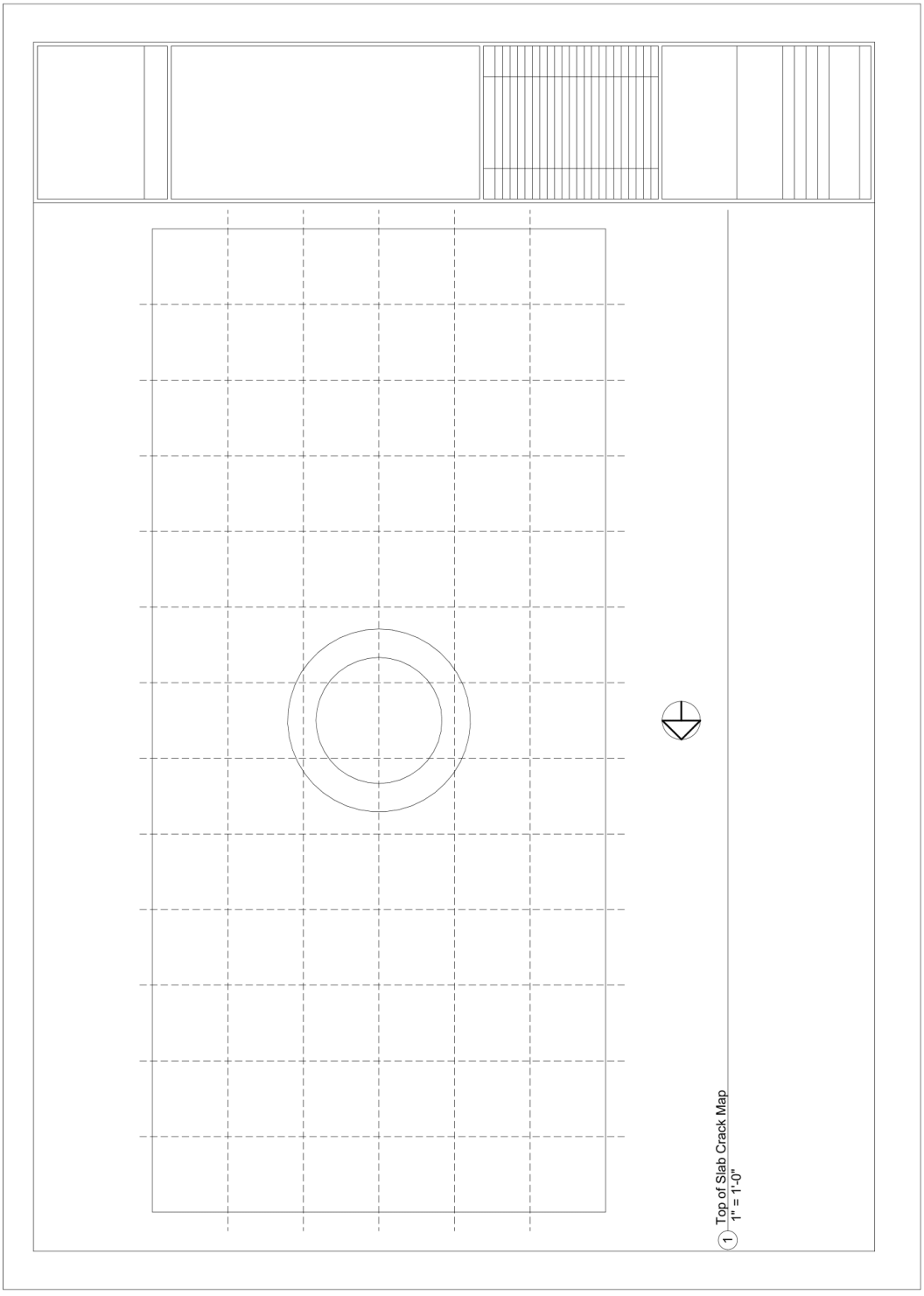
1 Top of Slab Crack Map
1" = 1'-0"

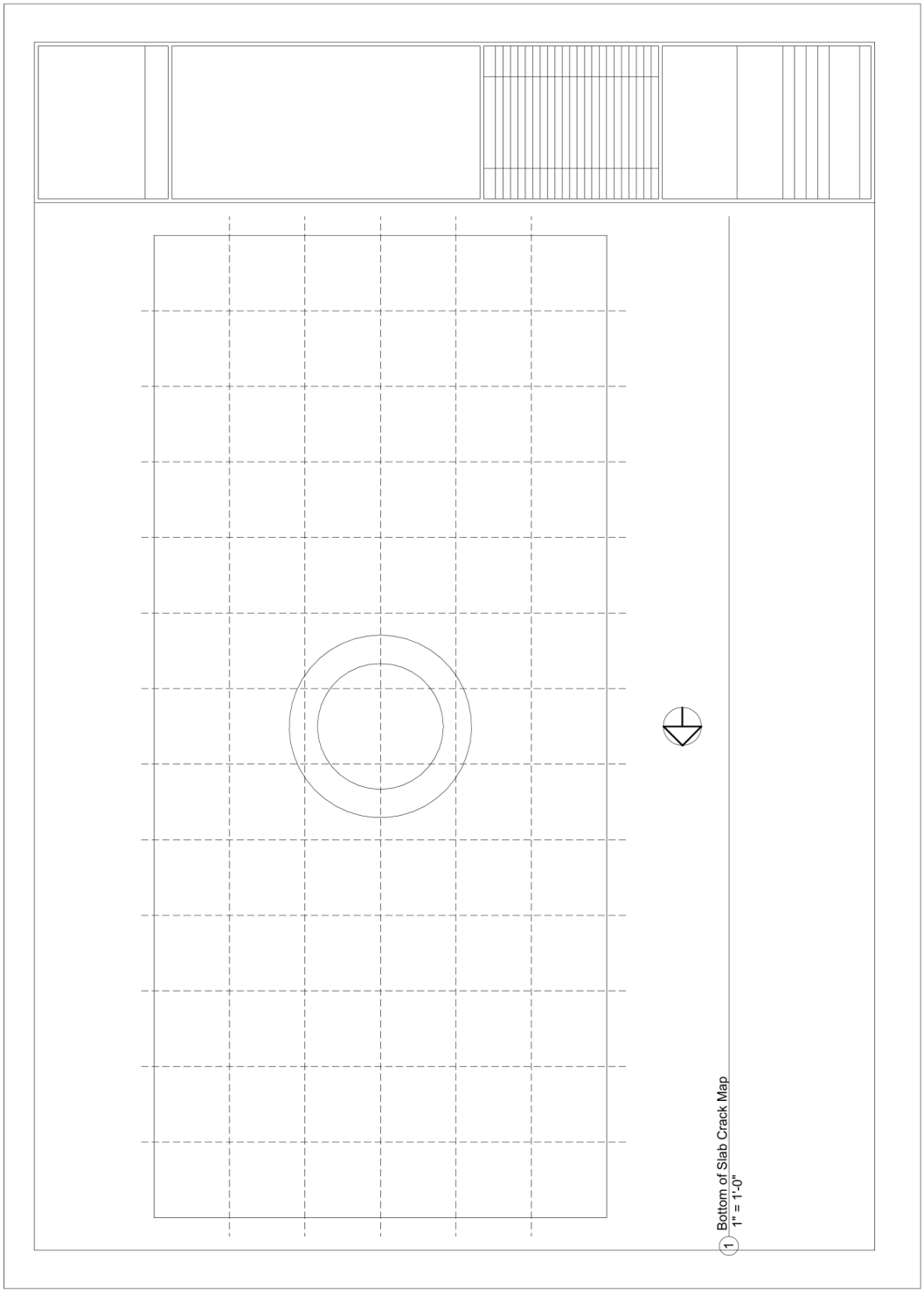
1
Bottom of Slab Crack Map
1" = 1'-0"

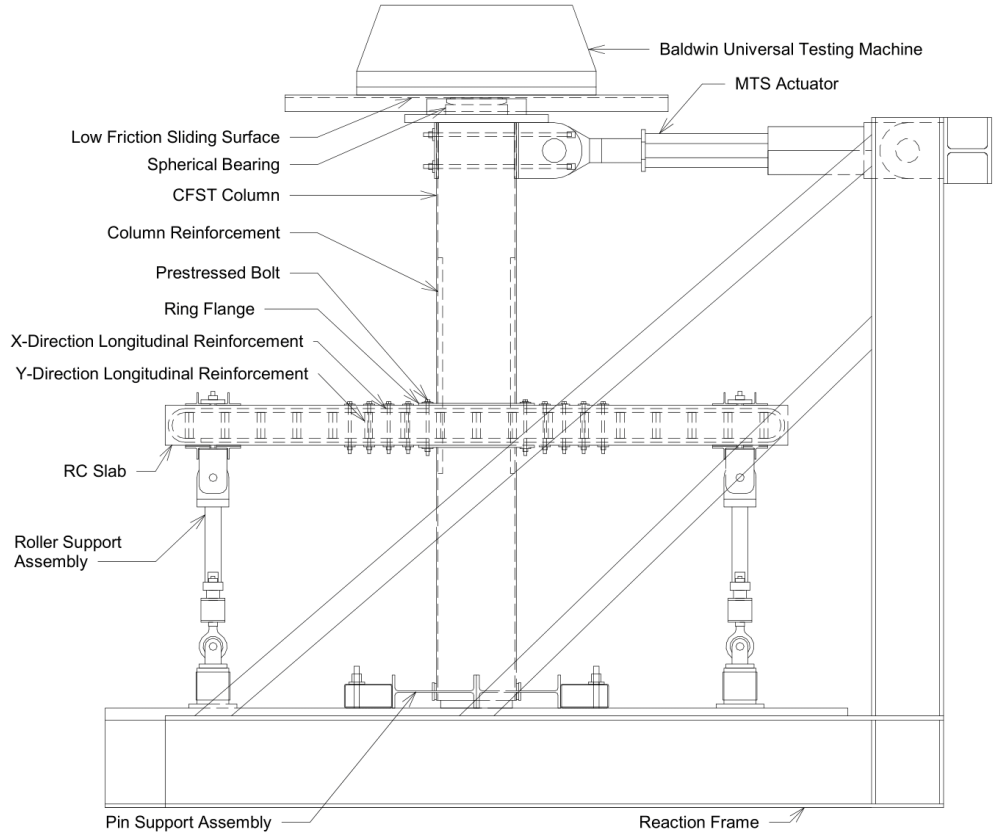

1 Setup Overview
3/8" = 1'-0"

CIVIL & ENVIRONMENTAL ENGINEERING

University of Washington
Department of Civil and Environmental Engineering

NSF Secondary Evacuation Structures

Setup Overview

Project Number	PTB_4.8_1_4
Date	5/1/2015
Drawn By	Alec Youtter
Checked By	Alec Youtter

S.17

Scale 3/8" = 1'-0"

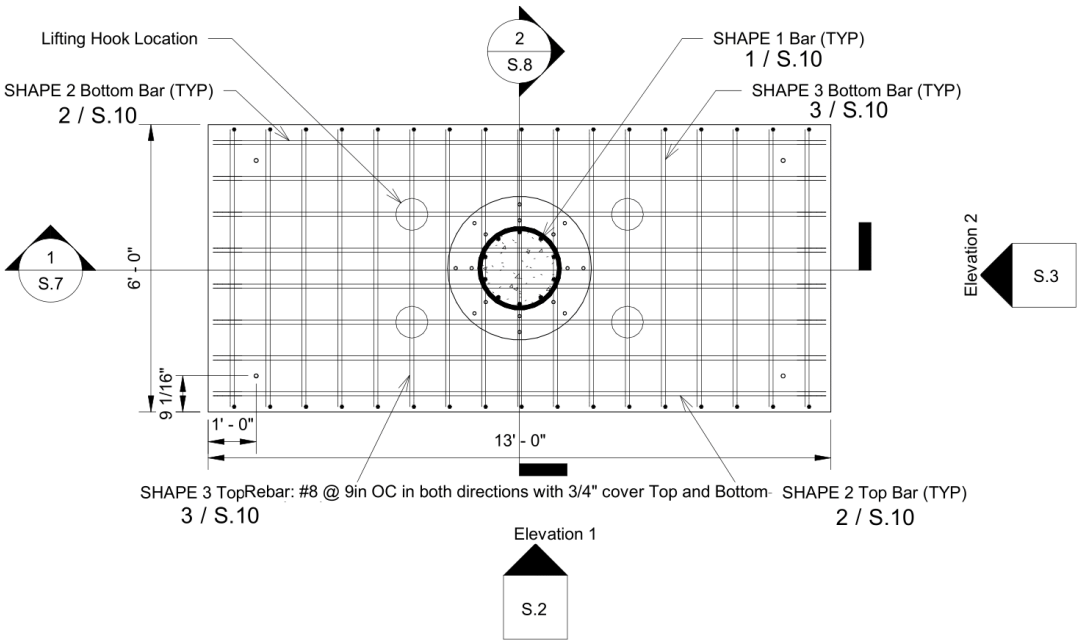

1 Level 2
3/8" = 1'-0"

CIVIL & ENVIRONMENTAL ENGINEERING

University of Washington
Department of Civil and Environmental Engineering

NSF Secondary Evacuation Structures

Plan View

Project Number	PTB_9_2_0
Date	5/1/2015
Drawn By	Alec Youtter
Checked By	Alec Youtter

S.1

Scale 3/8" = 1'-0"

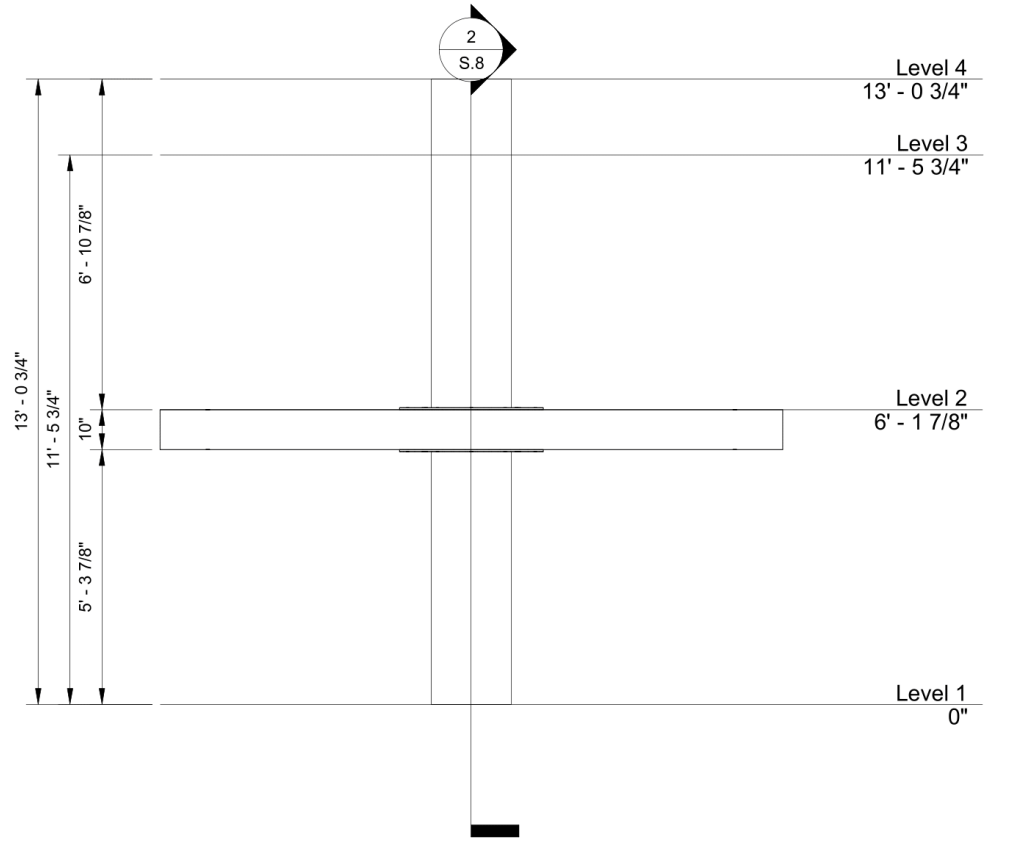

1 Elevation 1
3/8" = 1'-0"

CIVIL & ENVIRONMENTAL ENGINEERING

University of Washington
Department of Civil and Environmental Engineering

NSF Secondary Evacuation Structures

Elevation 1

Project Number	PTB_9_2_0
Date	5/1/2015
Drawn By	Alec Youtter
Checked By	Alec Youtter

S.2

Scale 3/8" = 1'-0"

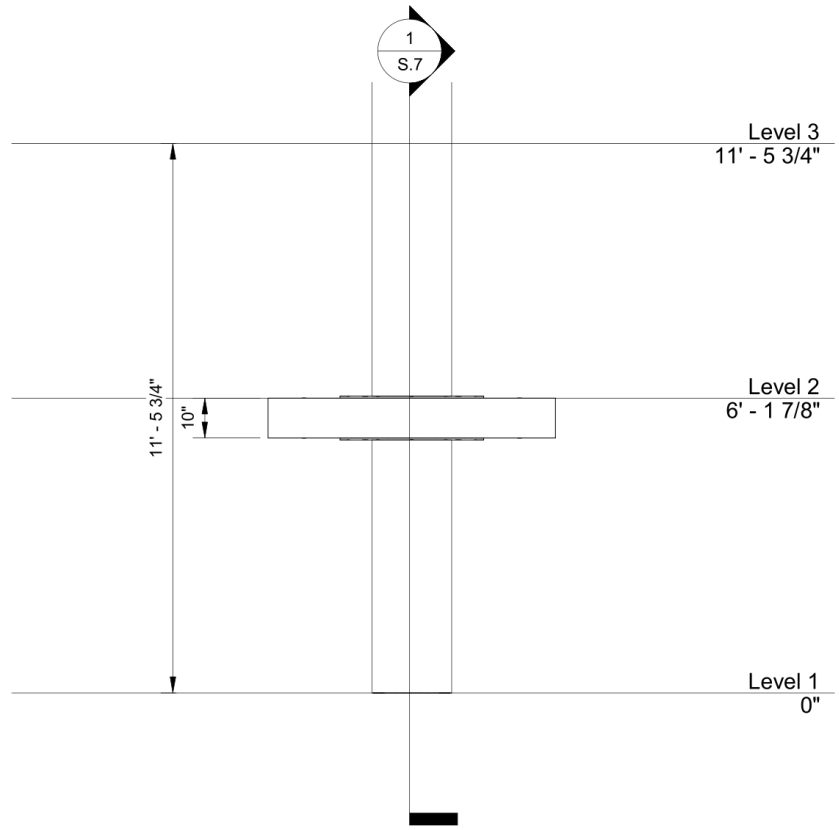

1 Elevation 2
3/8" = 1'-0"

CIVIL & ENVIRONMENTAL ENGINEERING

University of Washington
Department of Civil and Environmental Engineering

NSF Secondary Evacuation Structures

Elevation 2

Project Number	PTB_9_2_0
Date	5/1/2015
Drawn By	Alec Youtter
Checked By	Alec Youtter

S.3

Scale 3/8" = 1'-0"

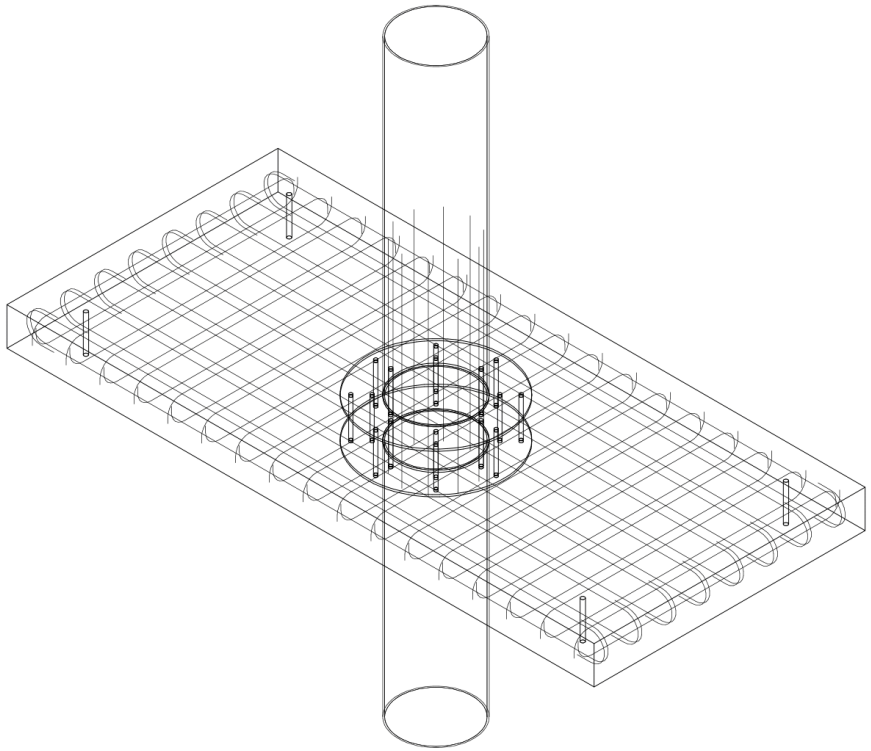

1 3D Isometric Wire Frame

CIVIL & ENVIRONMENTAL ENGINEERING

University of Washington
Department of Civil and Environmental Engineering

NSF Secondary Evacuation Structures

3D Isometric Wire Frame

Project Number	PTB_9_2_0
Date	5/1/2015
Drawn By	Alec Youtter
Checked By	Alec Youtter

S.4

Scale

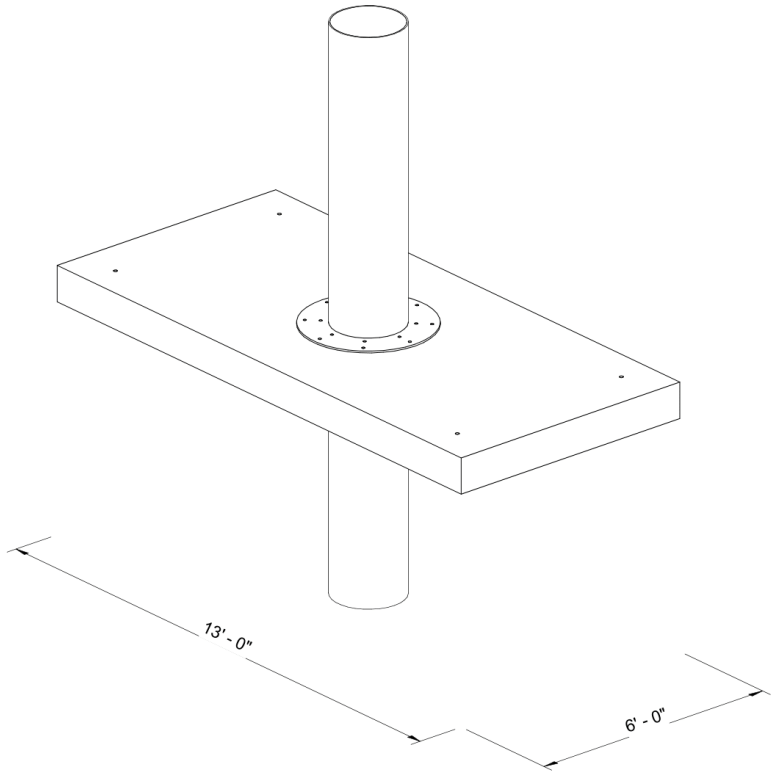

1 3D Solid Isometric View

CIVIL & ENVIRONMENTAL ENGINEERING

University of Washington
Department of Civil and Environmental Engineering

NSF Secondary Evacuation Structures

3D Solid Isometric View

Project Number	PTB_9_2_0
Date	5/1/2015
Drawn By	Alec Youtter
Checked By	Alec Youtter

S.5

Scale

1 3D Semi-Transparent Render

CIVIL & ENVIRONMENTAL ENGINEERING

University of Washington
Department of Civil and Environmental Engineering

NSF Secondary Evacuation Structures

3D Semi-Transparent Render

Project Number	PTB_9_2_0
Date	5/1/2015
Drawn By	Alec Youtter
Checked By	Alec Youtter

S.6

Scale

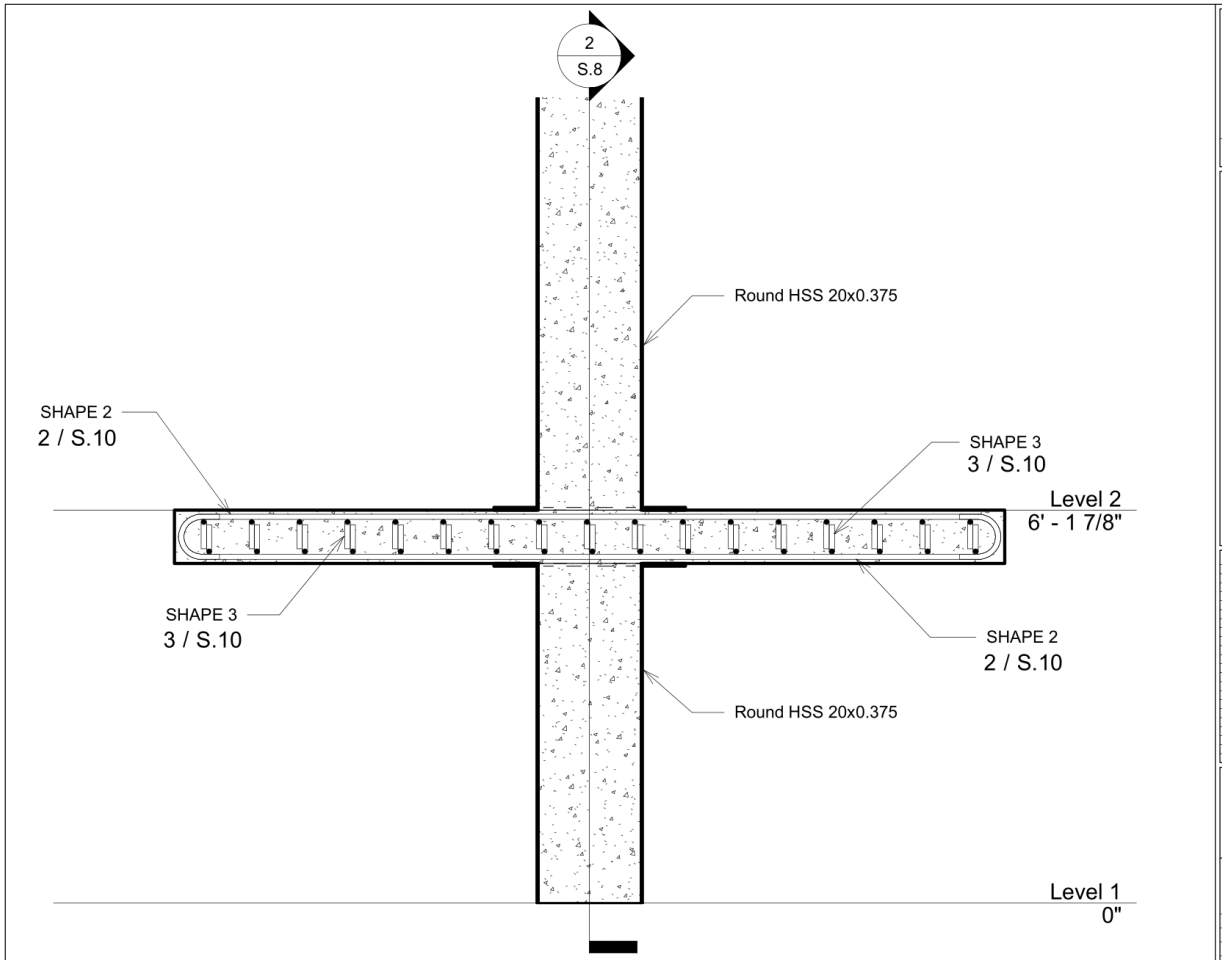

1 Section 1
1/2" = 1'-0"

CIVIL & ENVIRONMENTAL ENGINEERING

University of Washington
Department of Civil and Environmental Engineering

NSF Secondary Evacuation Structures

Section 1

Project Number	PTB_9_2_0
Date	5/1/2015
Drawn By	Alec Youtter
Checked By	Alec Youtter
Scale	1/2" = 1'-0"

S.7

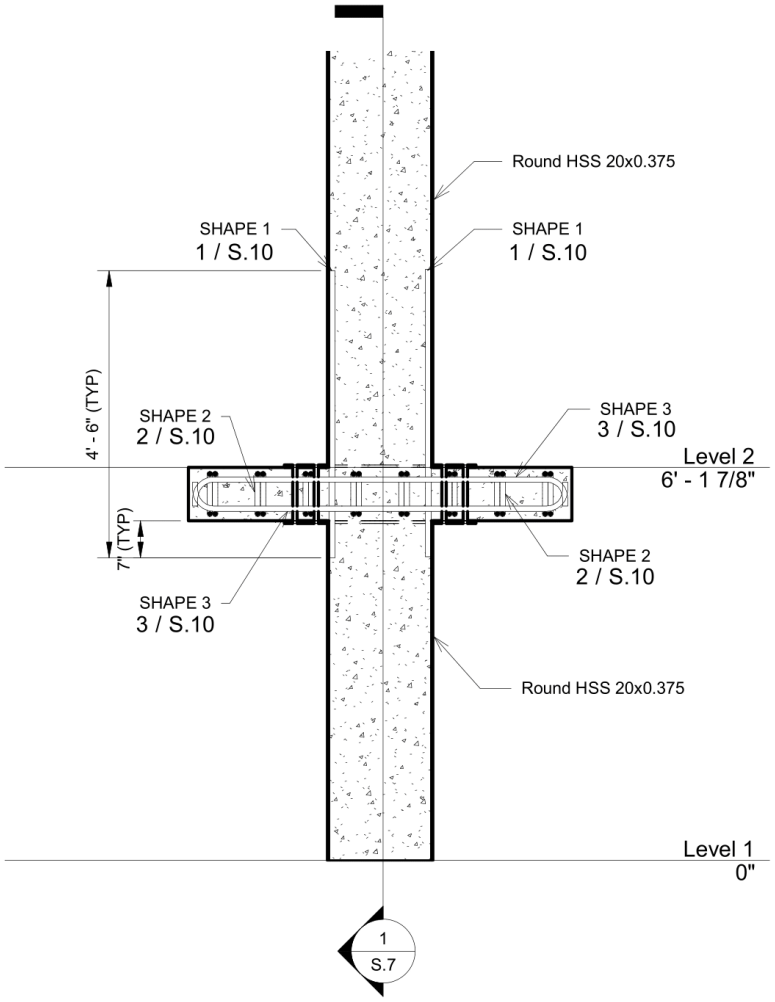

2 Section 2
1/2" = 1'-0"

CIVIL & ENVIRONMENTAL ENGINEERING

University of Washington
Department of Civil and Environmental Engineering

NSF Secondary Evacuation Structures

Section 2

Project Number	PTB_9_2_0
Date	5/1/2015
Drawn By	Alec Youtter
Checked By	Alec Youtter

S.8

Scale 1/2" = 1'-0"

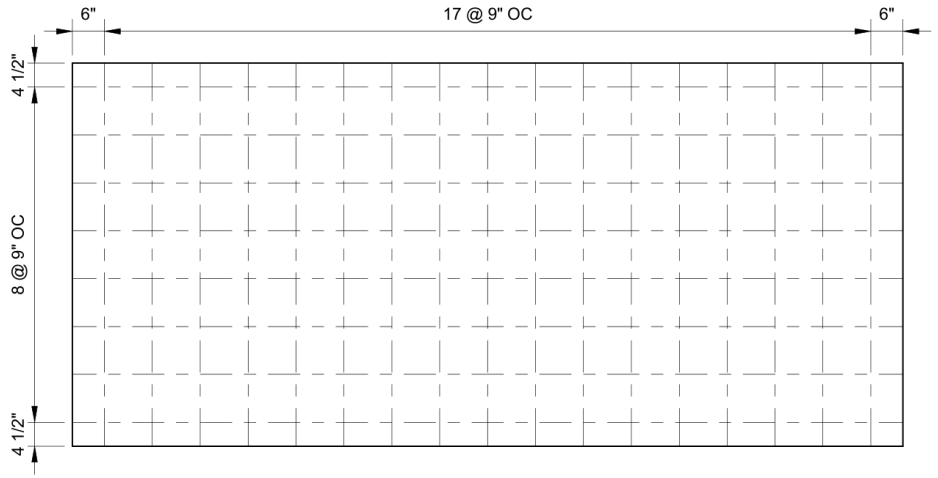

1 Slab Rebar Layout Top and Bottom
1/2" = 1'-0"

CIVIL & ENVIRONMENTAL ENGINEERING

University of Washington
Department of Civil and Environmental Engineering

NSF Secondary Evacuation Structures

Slab Rebar Layout Top and Bottom

Project Number	PTB_9_2_0
Date	5/1/2015
Drawn By	Author
Checked By	Checker

S.9

Scale 1/2" = 1'-0"

SHAPE 1: #9 Bar

1 Rebar SHAPE 1
1/2" = 1'-0"

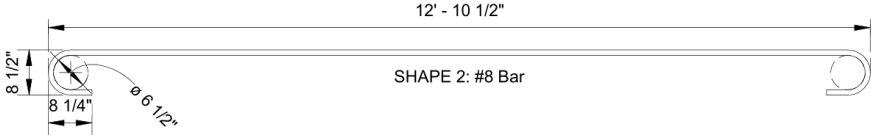

SHAPE 2: #8 Bar

2 Rebar SHAPE 2
1/2" = 1'-0"

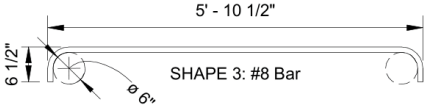

SHAPE 3: #8 Bar

3 Rebar SHAPE 3
1/2" = 1'-0"

CIVIL & ENVIRONMENTAL ENGINEERING

University of Washington
Department of Civil and Environmental Engineering

NSF Secondary Evacuation Structures

Rebar Details

Project Number	PTB_9_2_0
Date	5/1/2015
Drawn By	Author
Checked By	Checker

S.10

Scale 1/2" = 1'-0"

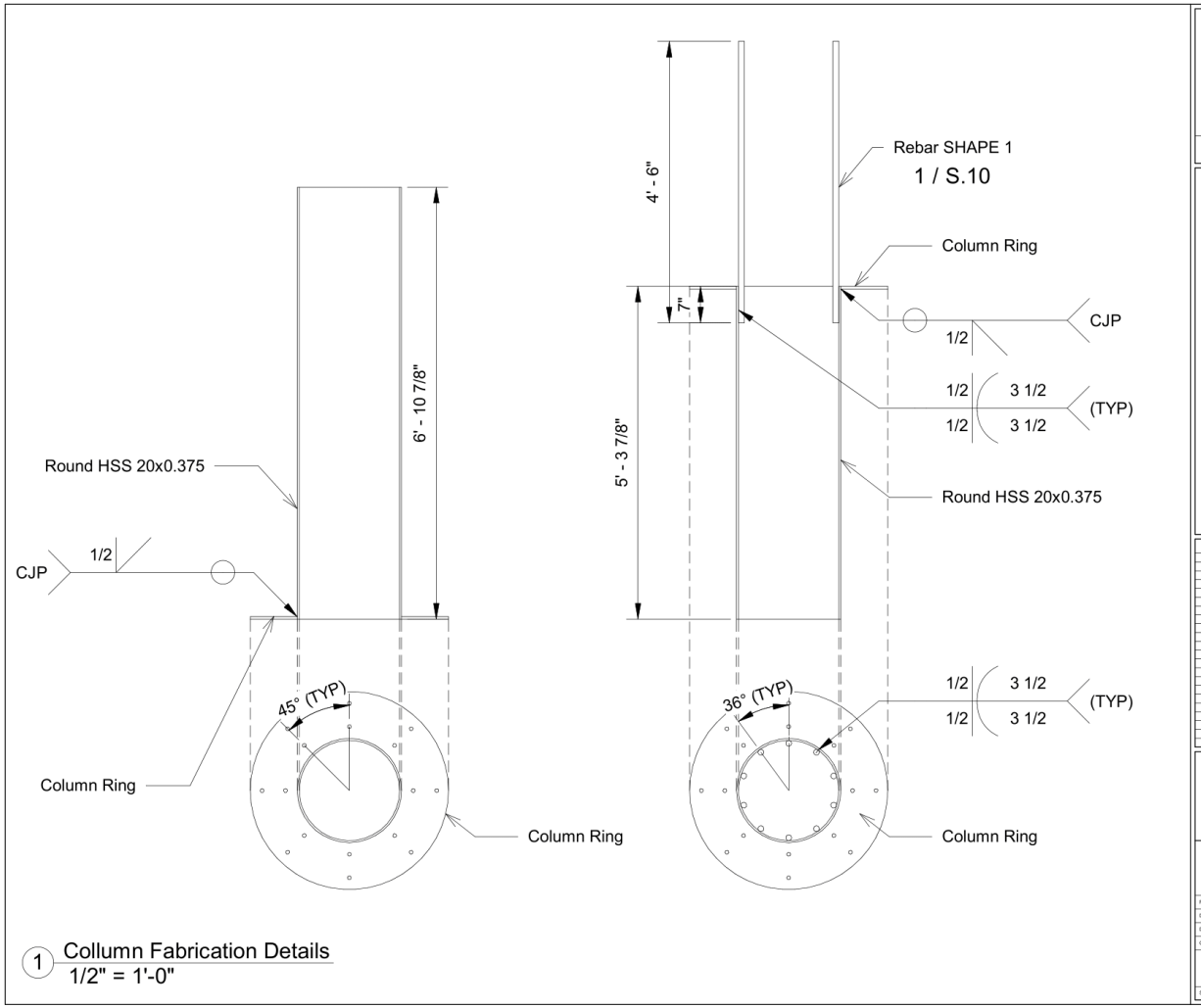

1 Collumn Fabrication Details
1/2" = 1'-0"

CIVIL & ENVIRONMENTAL ENGINEERING

University of Washington
Department of Civil and Environmental Engineering

NSF Secondary Evacuation Structures

Column Fabrication Details

Project Number	PTB_9_2_0
Date	5/1/2015
Drawn By	Alec Youtter
Checked By	Charles Roeder

S.11

Scale 1/2" = 1'-0"

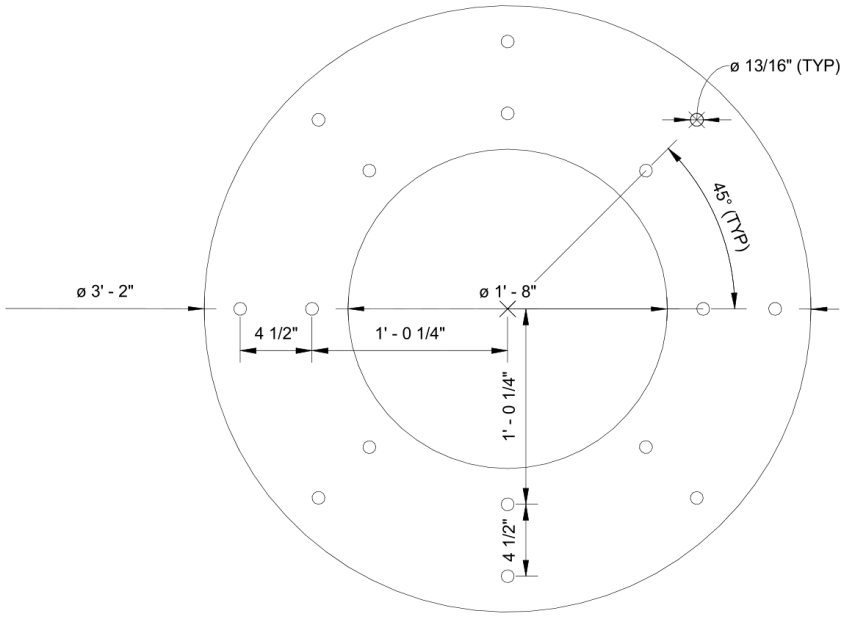

1 Ring Fabrication Detail
1 1/2" = 1'-0"

CIVIL & ENVIRONMENTAL ENGINEERING

University of Washington
Department of Civil and Environmental Engineering

NSF Secondary Evacuation Structures

Ring Fabrication Detail

Project Number	PTB_9_2_0
Date	5/1/2015
Drawn By	Author
Checked By	Checker

S.12

Scale 1 1/2" = 1'-0"

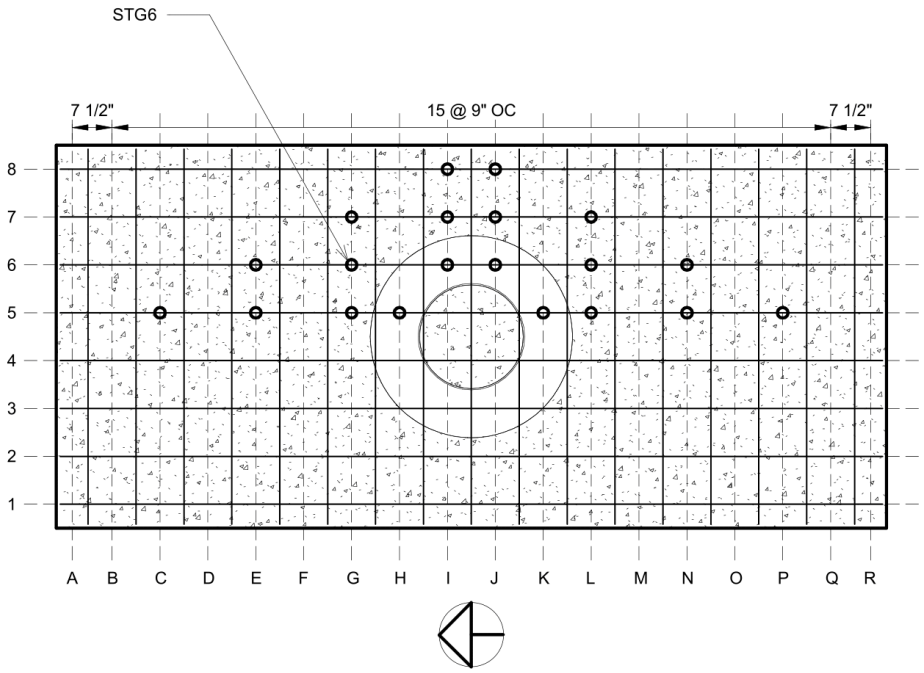

1 Slab Strain Gauge Layout
1/2" = 1'-0"

Naming Convention:
1. "S" for slab
2. "T" for top or "B" for Bottom
3. Column Letter
4. Row Number

Example: STG6 would be a strain gauge on a "Slab" "Top" bar in column "G" in row "6"

CIVIL & ENVIRONMENTAL ENGINEERING

University of Washington
Department of Civil and Environmental Engineering

NSF Secondary Evacuation Structures

Slab Strain Gauge Layout Top and Bottom

Project Number	PTB_9_2_0
Date	5/1/2015
Drawn By	Author
Checked By	Checker

S.13

Scale 1/2" = 1'-0"

Naming Convention:
1. "C" for Column
2. Rebar Letter
3. Level Number

Example: CI7 would be a strain gauge on "Column" bar "I" at level "7".

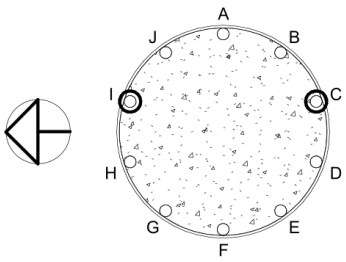

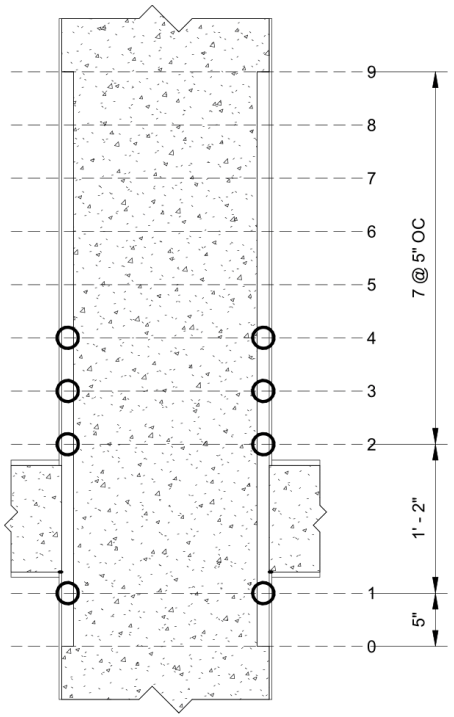

1 Column Strain Gauge Layout
1" = 1'-0"

CIVIL & ENVIRONMENTAL ENGINEERING

University of Washington
Department of Civil and Environmental Engineering

NSF Secondary Evacuation Structures

Column Strain Gauge Layout

Project Number	PTB_9_2_0
Date	5/1/2015
Drawn By	Author
Checked By	Checker

S.14

Scale 1" = 1'-0"

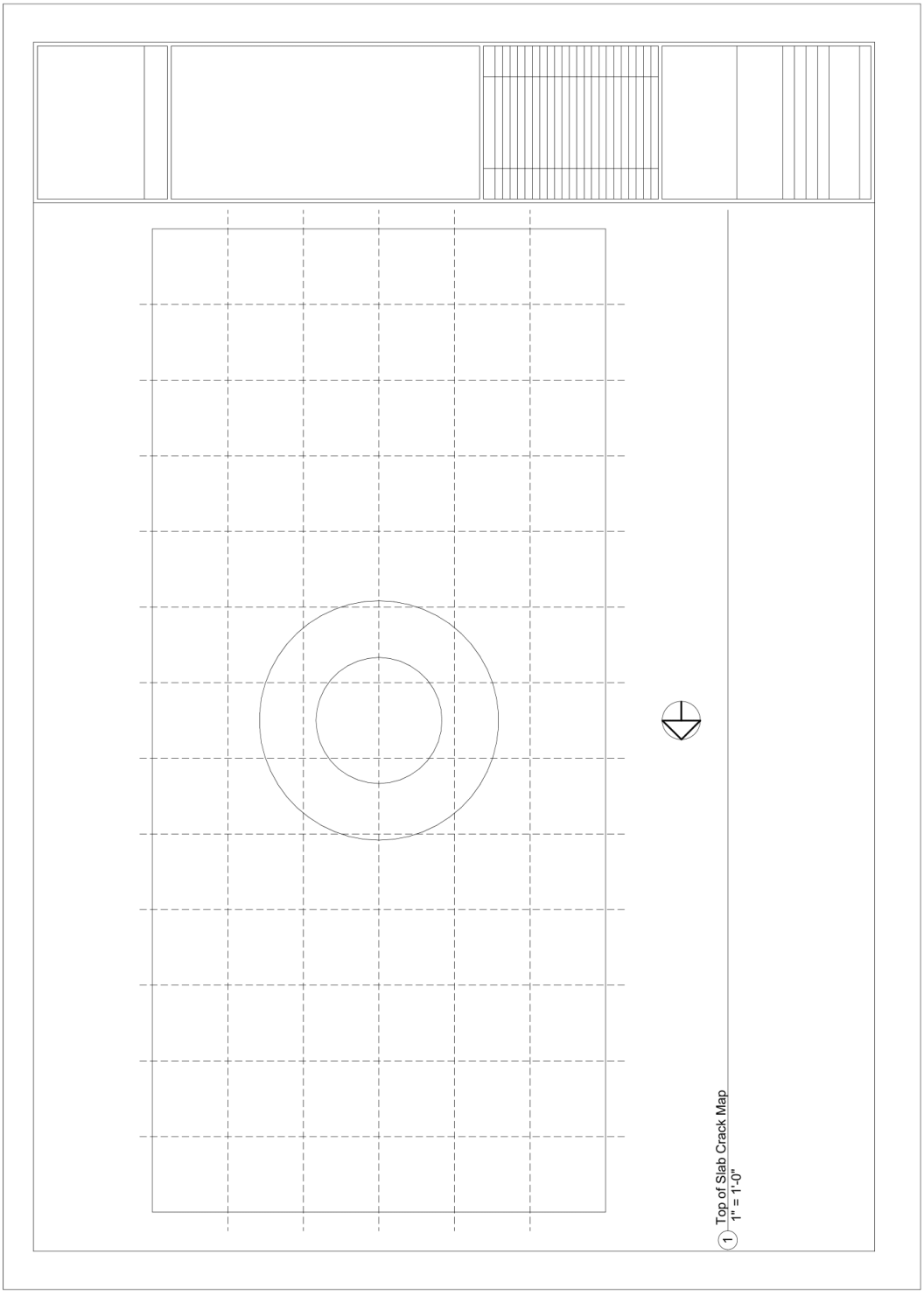
1 Top of Slab Crack Map
1" = 1'-0"

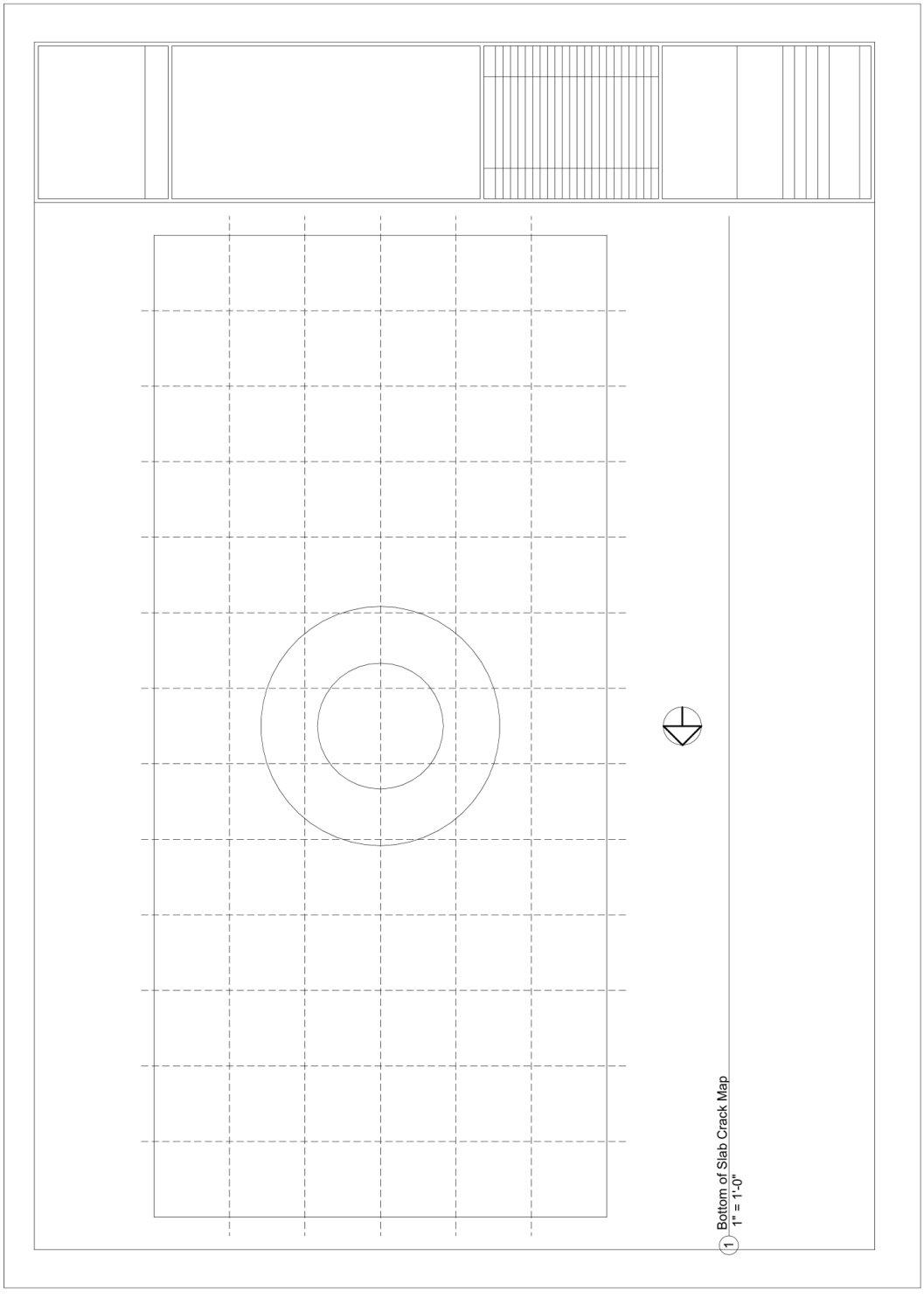
1
Bottom of Slab Crack Map
1" = 1'-0"

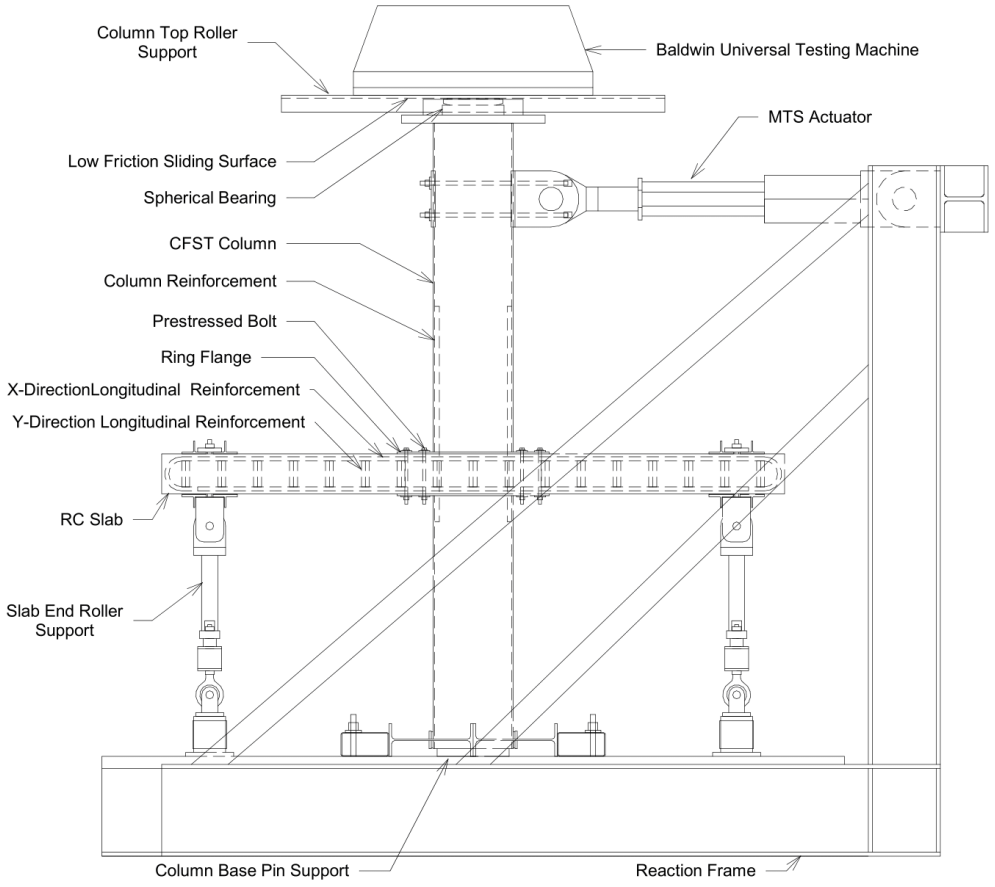

1 Setup Overview
3/8" = 1'-0"

CIVIL & ENVIRONMENTAL ENGINEERING

University of Washington
Department of Civil and Environmental Engineering

NSF Secondary Evacuation Structures

Setup Overview

Project Number	PTB_9_2_0
Date	5/1/2015
Drawn By	Alec Youtter
Checked By	Alec Youtter

S.17

Scale 3/8" = 1'-0"

	Ring Size 1: d/2 = 4.5"	Ring Size 2: d = 9"
Bolt Pattern 1	PTB_4.5_1_0 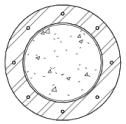	PTB_9_2_0 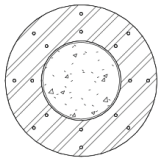
Bolt Pattern 2	PTB_4.5_1_4 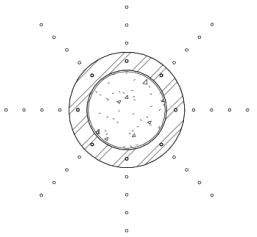	

Reference
SR_4_10_5 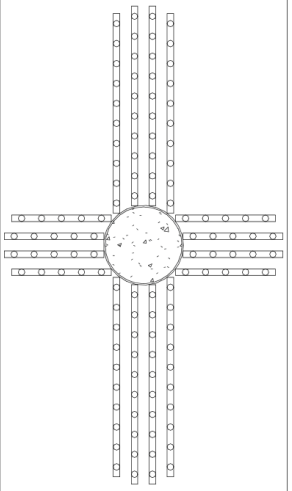

- Where "d" is the effective slab depth

1 Test Matrix
3/8" = 1'-0"

CIVIL & ENVIRONMENTAL ENGINEERING

University of Washington
Department of Civil and Environmental Engineering

NSF Secondary Evacuation Structures

Test Matrix

Project Number	Test Documents
Date	5/1/2015
Drawn By	Author
Checked By	Checker

S.1

Scale 3/8" = 1'-0"

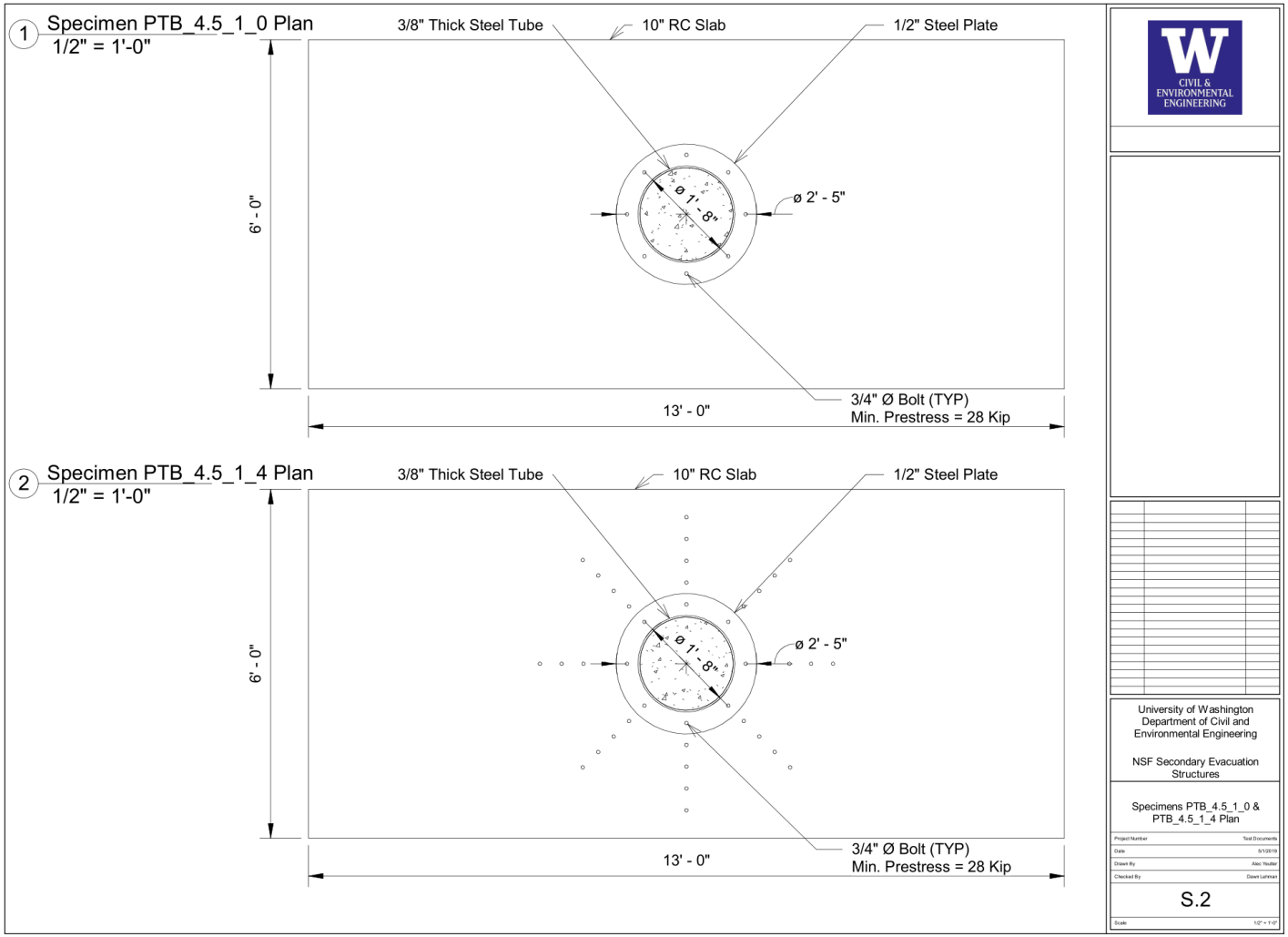
1
Specimen PTB_4.5_1_0 Plan
1/2" = 1'-0"
3/8" Thick Steel Tube
10" RC Slab
1/2" Steel Plate
ø 1' - 8"
ø 2' - 5"
6' - 0"
13' - 0"
3/4" Ø Bolt (TYP)
Min. Prestress = 28 Kip
2
Specimen PTB_4.5_1_4 Plan
1/2" = 1'-0"
3/8" Thick Steel Tube
10" RC Slab
1/2" Steel Plate
ø 1' - 8"
ø 2' - 5"
6' - 0"
13' - 0"
3/4" Ø Bolt (TYP)
Min. Prestress = 28 Kip
CIVIL & ENVIRONMENTAL ENGINEERING
University of Washington
Department of Civil and Environmental Engineering
NSF Secondary Evacuation Structures
Specimens PTB_4.5_1_0 & PTB_4.5_1_4 Plan
Project Number
Test Documents
Date
5/1/2015
Drawn By
Alec Youtter
Checked By
Dawn Lehman
S.2
Scale
1/2" = 1'-0"

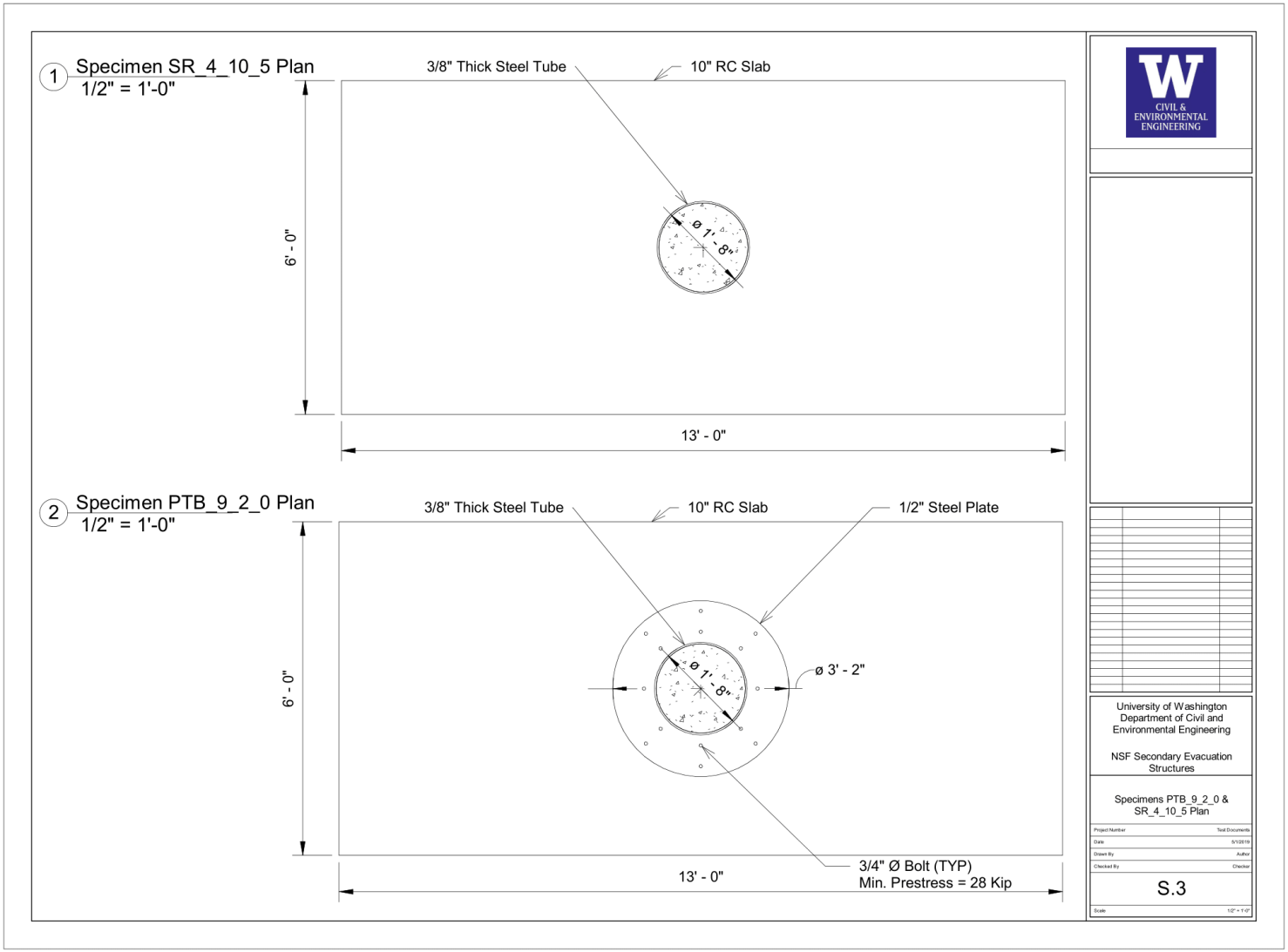
1
Specimen SR_4_10_5 Plan
1/2" = 1'-0"
3/8" Thick Steel Tube
10" RC Slab
Ø 1' - 8"
6' - 0"
13' - 0"
2
Specimen PTB_9_2_0 Plan
1/2" = 1'-0"
3/8" Thick Steel Tube
10" RC Slab
1/2" Steel Plate
Ø 1' - 8"
ø 3' - 2"
6' - 0"
13' - 0"
3/4" Ø Bolt (TYP)
Min. Prestress = 28 Kip
CIVIL & ENVIRONMENTAL ENGINEERING
University of Washington
Department of Civil and Environmental Engineering
NSF Secondary Evacuation Structures
Specimens PTB_9_2_0 & SR_4_10_5 Plan
Project Number
Test Documents
Date
5/1/2015
Drawn By
Author
Checked By
Checker
S.3
Scale
1/2" = 1'-0"

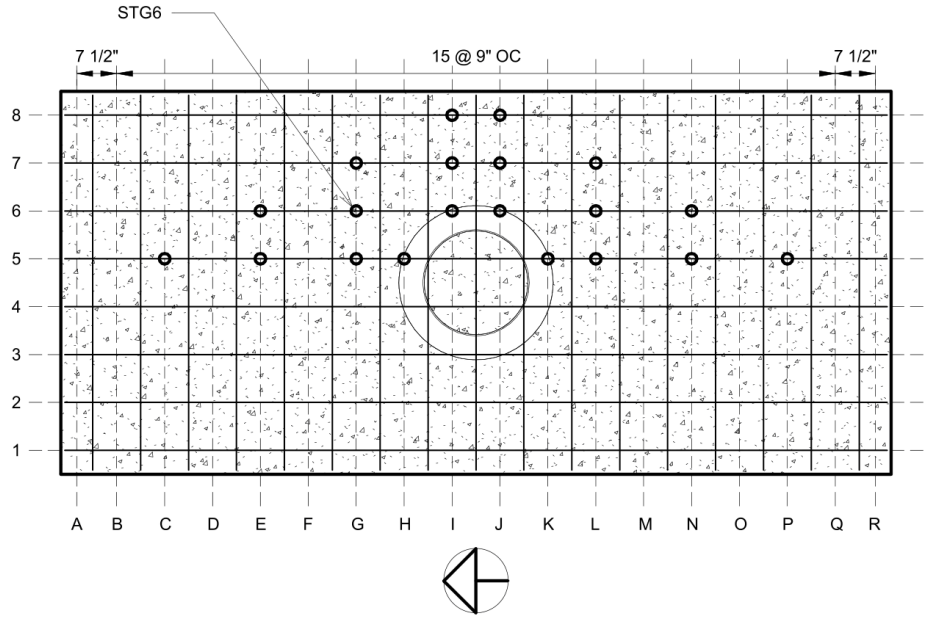

1 Slab Strain Gauge Layout
1/2" = 1'-0"

Naming Convention:
1. "S" for slab
2. "T" for top or "B" for Bottom
3. Column Letter
4. Row Number

Example: STG6 would be a strain gauge on a "Slab" "Top" bar in column "G" in row "6"

CIVIL & ENVIRONMENTAL ENGINEERING

University of Washington
Department of Civil and Environmental Engineering

NSF Secondary Evacuation Structures

Slab Strain Gauge Layout Top and Bottom

Project Number	Test Documents
Date	5/1/2015
Drawn By	Alec Youtter
Checked By	Alec Youtter

S.4

Scale 1/2" = 1'-0"

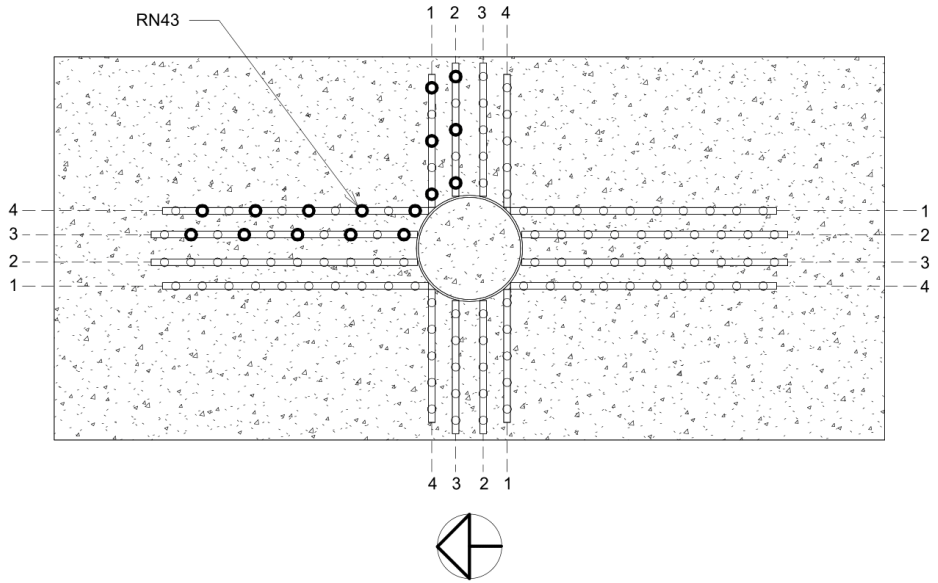

Naming Convention:
1. "R" for rail
2. "N" for North, "E" for East, "S" for South, or "W" for West of the column
3. Rail Number in the Clockwise Direction
4. Stud Number counting out from the column

Example: RN43 would be a strain gauge on the "Third" stud on the "Fourth" rail in the clockwise direction and is a "Rail" on the "North" side of the clolumn.

1 Stud Rail Strain Gauge Layout
1/2" = 1'-0"

CIVIL & ENVIRONMENTAL ENGINEERING

University of Washington
Department of Civil and Environmental Engineering

NSF Secondary Evacuation Structures

Stud Rail Strain Gauge Layout

Project Number	Test Documents
Date	5/1/2015
Drawn By	Alec
Checked By	Yeutter

S.5

Scale 1/2" = 1'-0"

Naming Convention:
1. "C" for Column
2. Rebar Letter
3. Level Number

Example: CI7 would be a strain gauge on "Column" bar "I" at level "7".

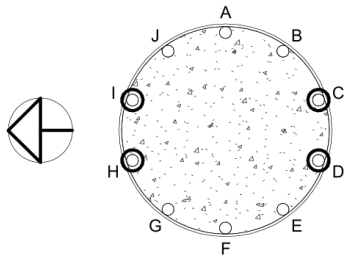

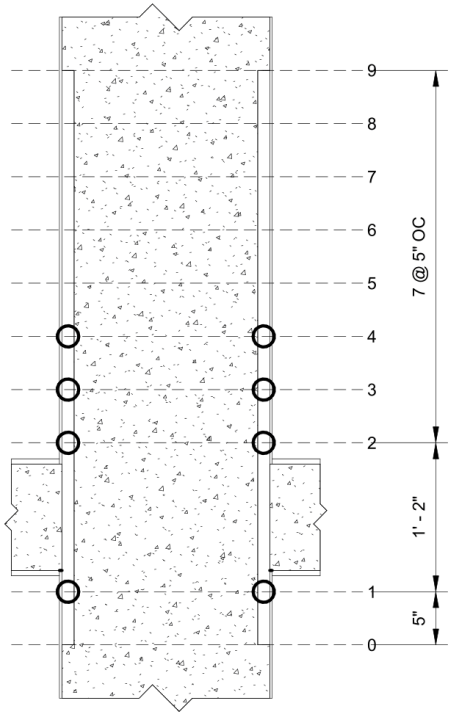

1 Column Strain Gauge Layout
1" = 1'-0"

CIVIL & ENVIRONMENTAL ENGINEERING

University of Washington
Department of Civil and Environmental Engineering

NSF Secondary Evacuation Structures

Column Strain Gauge Layout

Project Number	Test Documents
Date	5/1/2015
Drawn By	Alec Youtter
Checked By	Alec Youtter

S.6

Scale 1" = 1'-0"

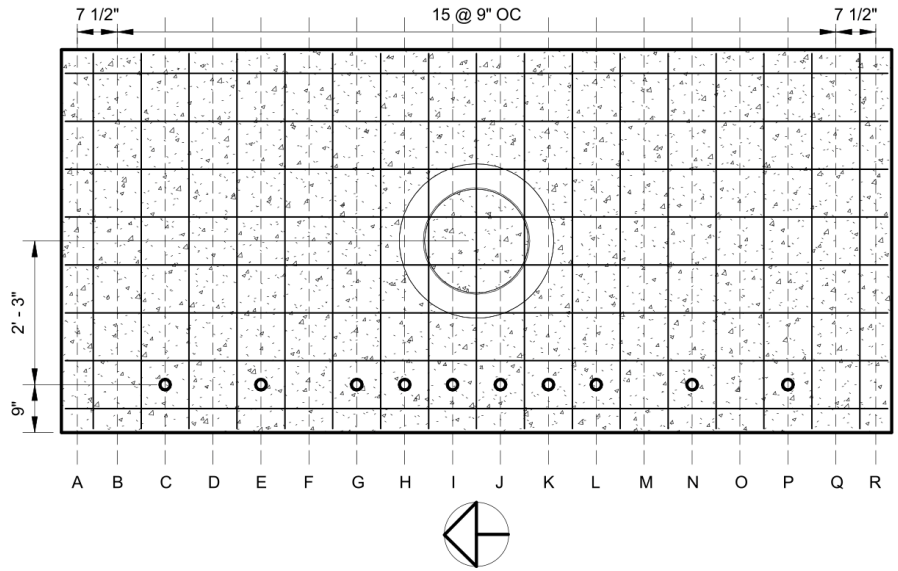

1 Slab Optotrac and String Pot. Layout
1/2" = 1'-0"

CIVIL & ENVIRONMENTAL ENGINEERING

University of Washington
Department of Civil and Environmental Engineering

NSF Secondary Evacuation Structures

Slab OptiTrack and String Pot. Layout

Project Number	Test Documents
Date	5/1/2015
Drawn By	Alec Youtter
Checked By	Alec Youtter

S.7

Scale 1/2" = 1'-0"

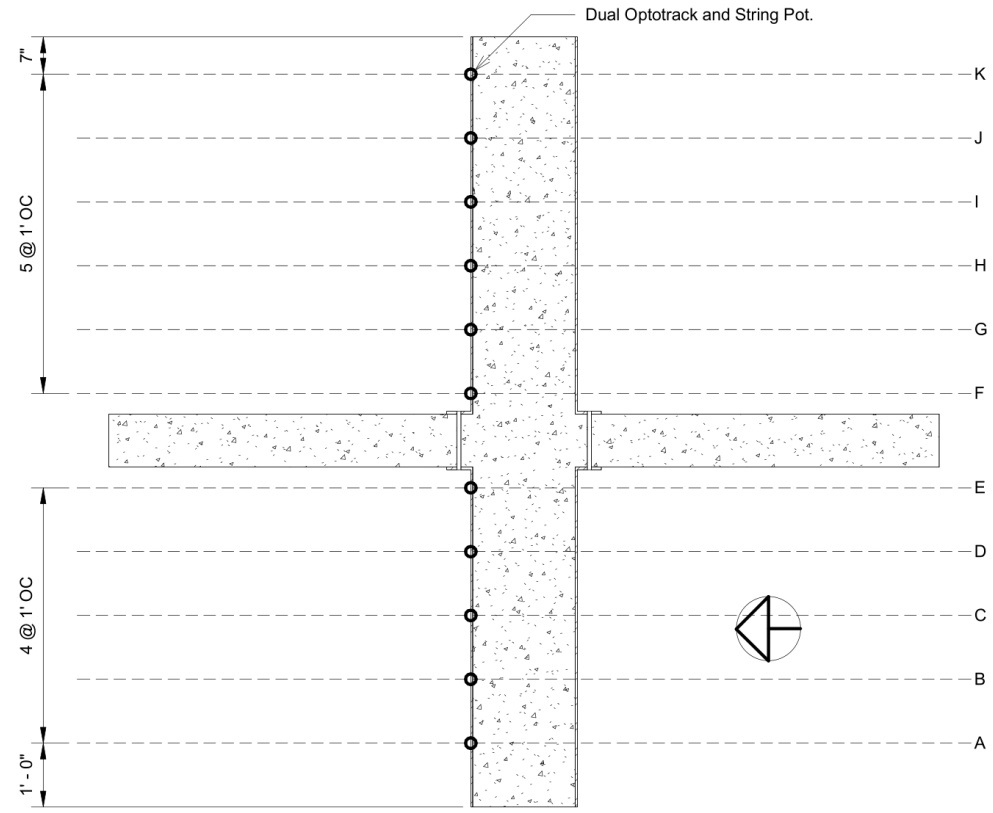

1 Column Optotrac and String Pot. Layout
1/2" = 1'-0"

CIVIL & ENVIRONMENTAL ENGINEERING

University of Washington
Department of Civil and Environmental Engineering

NSF Secondary Evacuation Structures

Column Optotrac and String Pot. Layout

Project Number	Test Documents
Date	5/1/2015
Drawn By	Alec Youtter
Checked By	Alec Youtter

S.8

Scale 1/2" = 1'-0"

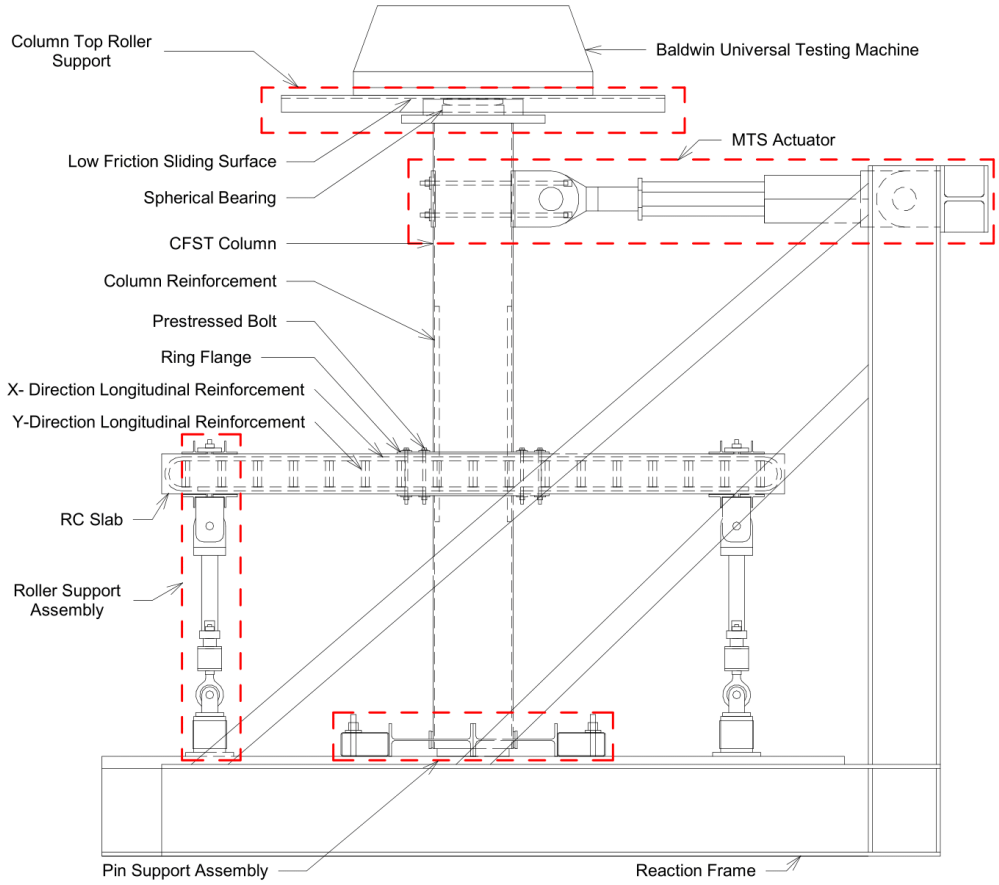

1 Setup Overview
3/8" = 1'-0"

CIVIL & ENVIRONMENTAL ENGINEERING

University of Washington
Department of Civil and Environmental Engineering

NSF Secondary Evacuation Structures

Setup Overview

Project Number	Test Documents
Date	5/1/2015
Drawn By	Alec Youtter
Checked By	Alec Youtter

S.9

Scale 3/8" = 1'-0"

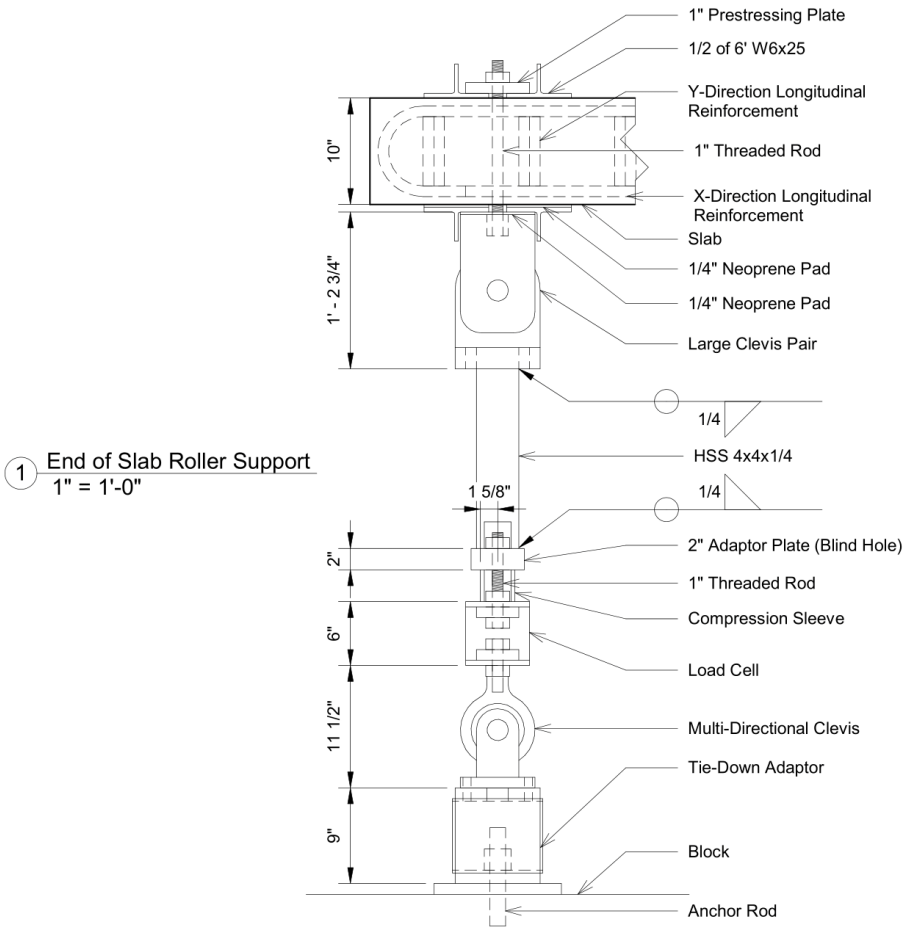

1 End of Slab Roller Support
1" = 1'-0"

CIVIL & ENVIRONMENTAL ENGINEERING

University of Washington
Department of Civil and Environmental Engineering

NSF Secondary Evacuation Structures

End of Slab Roller Support Detail

Project Number	Test Documents
Date	5/1/2015
Drawn By	Alec Youtter
Checked By	Alec Youtter

S.10

Scale 1" = 1'-0"

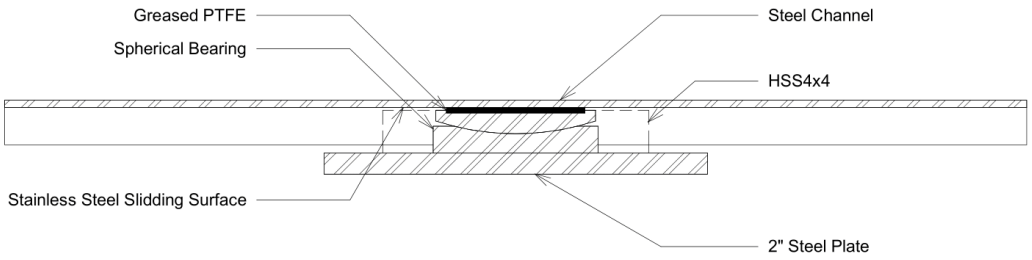

1 Column Top Roller Support West Section
1" = 1'-0"

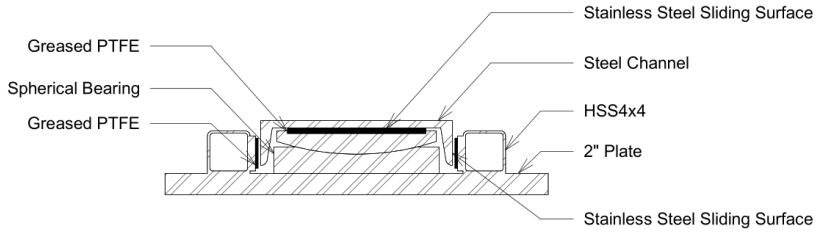

2 Column Top Roller Support North Section
1" = 1'-0"

CIVIL & ENVIRONMENTAL ENGINEERING

University of Washington
Department of Civil and Environmental Engineering

NSF Secondary Evacuation Structures

Column Top Roller Support

Project Number	Test Documents
Date	5/1/2015
Drawn By	Author
Checked By	Checker

S.11

Scale 1" = 1'-0"

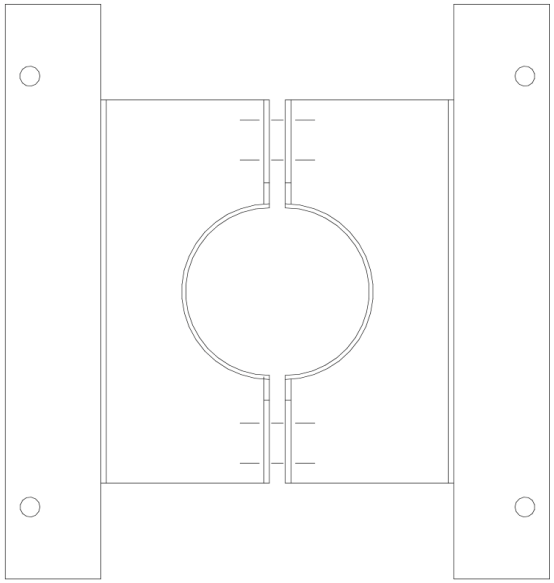

1 Column Base Pin Support Plan View
3/4" = 1'-0"

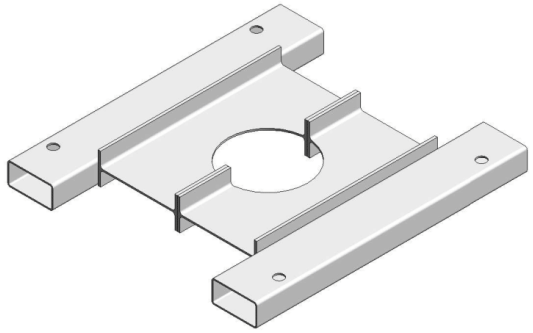

4 {3D}

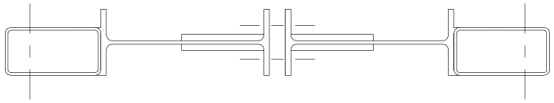

2 Column Base Pin Support West Elevation
3/4" = 1'-0"

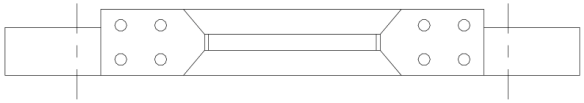

3 Column Base Pin Support North Elevation
3/4" = 1'-0"

CIVIL & ENVIRONMENTAL ENGINEERING

University of Washington
Department of Civil and Environmental Engineering

NSF Secondary Evacuation Structures

Column Base Pin Support

Project Number	Test Documents
Date	5/1/2015
Drawn By	Author
Checked By	Checker

S.12

Scale 3/4" = 1'-0"

APPENDIX C: FORMWORK DESIGN

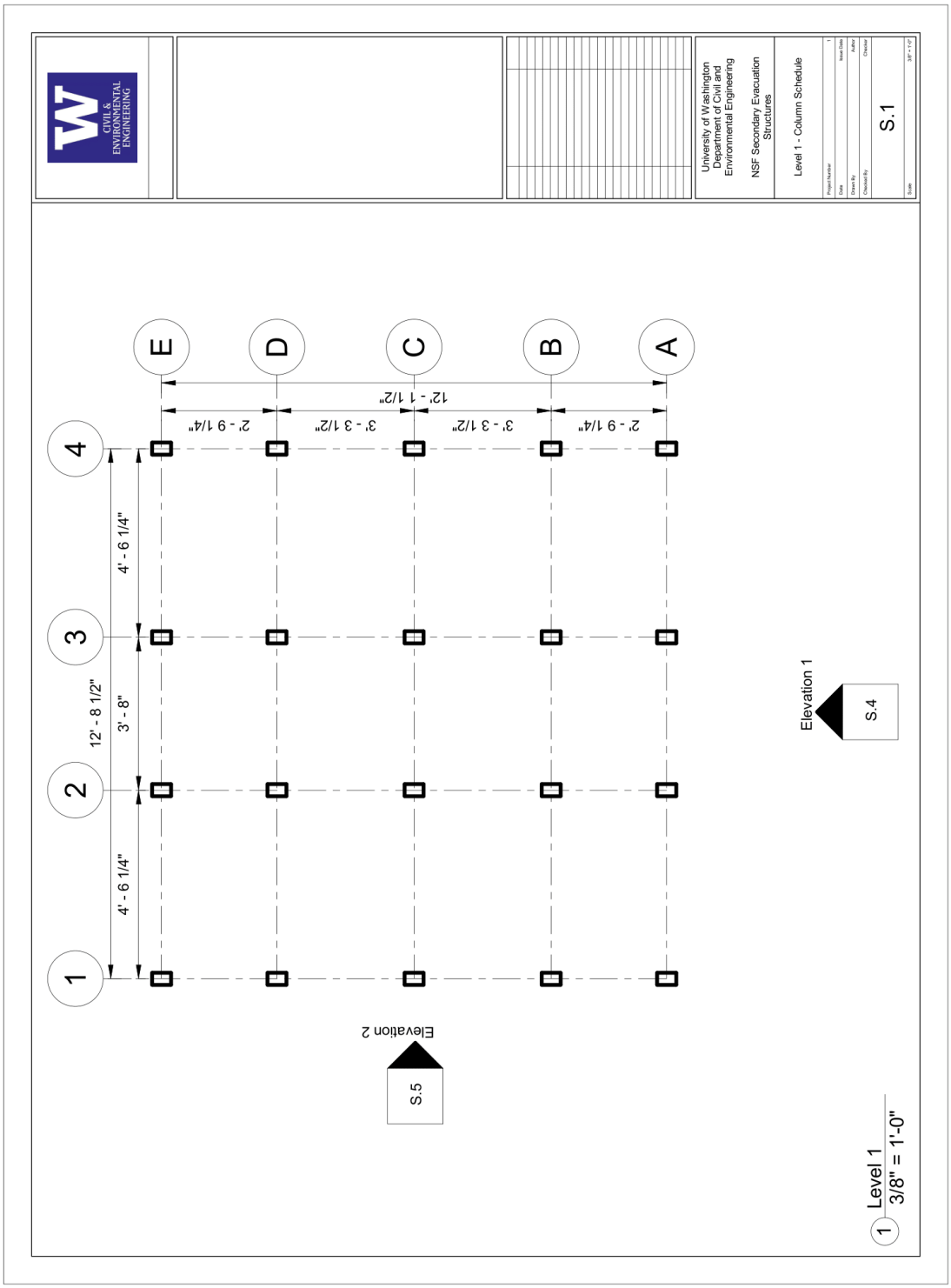

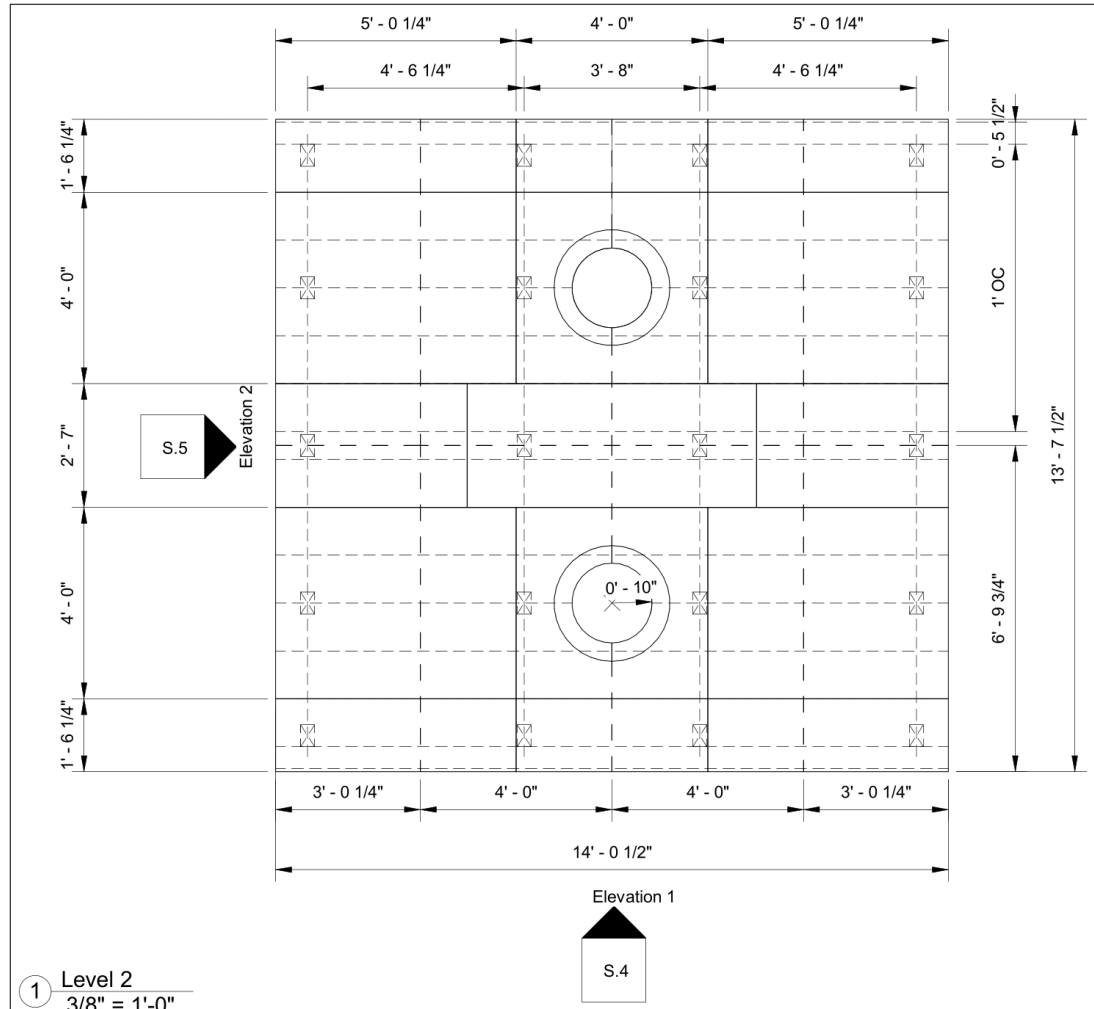

1 Level 2
3/8" = 1'-0"

CIVIL & ENVIRONMENTAL ENGINEERING

University of Washington
Department of Civil and Environmental Engineering

NSF Secondary Evacuation Structures

Level 2

Project Number	1
Date	Issue Date
Drawn By	Alec
Checked By	Checker

S.2

Scale 3/8" = 1'-0"

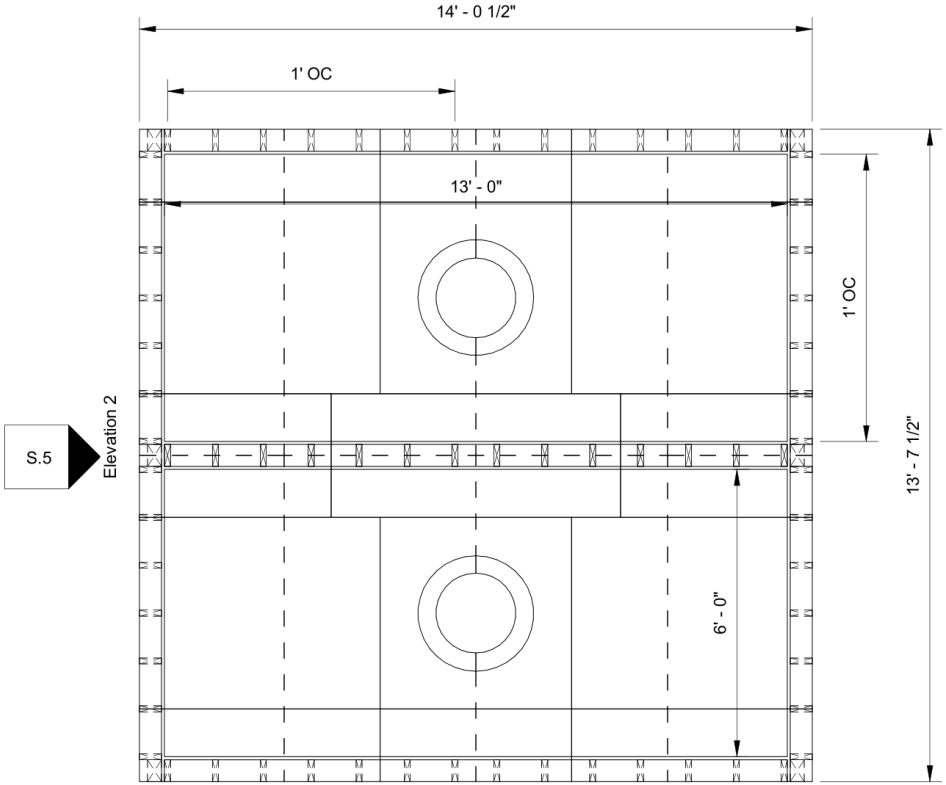

1 Level 3
3/8" = 1'-0"

CIVIL & ENVIRONMENTAL ENGINEERING

University of Washington
Department of Civil and Environmental Engineering

NSF Secondary Evacuation Structures

Level 3

Project Number	1
Date	Issue Date
Drawn By	Author
Checked By	Checker

S.3

Scale 3/8" = 1'-0"

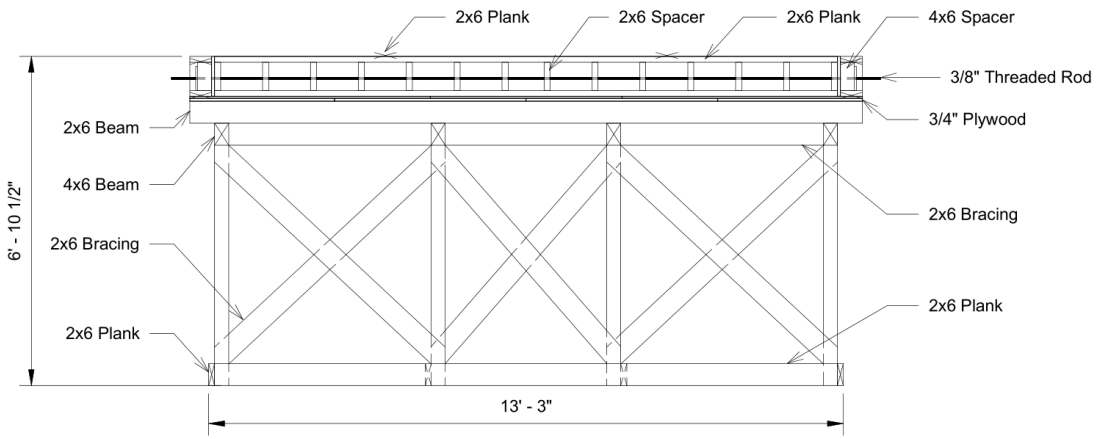

1 Elevation 1
3/8" = 1'-0"

CIVIL & ENVIRONMENTAL ENGINEERING

University of Washington
Department of Civil and Environmental Engineering

NSF Secondary Evacuation Structures

Elevation 1

Project Number	1
Date	Issue Date
Drawn By	Alec
Checked By	Checker

S.4

Scale 3/8" = 1'-0"

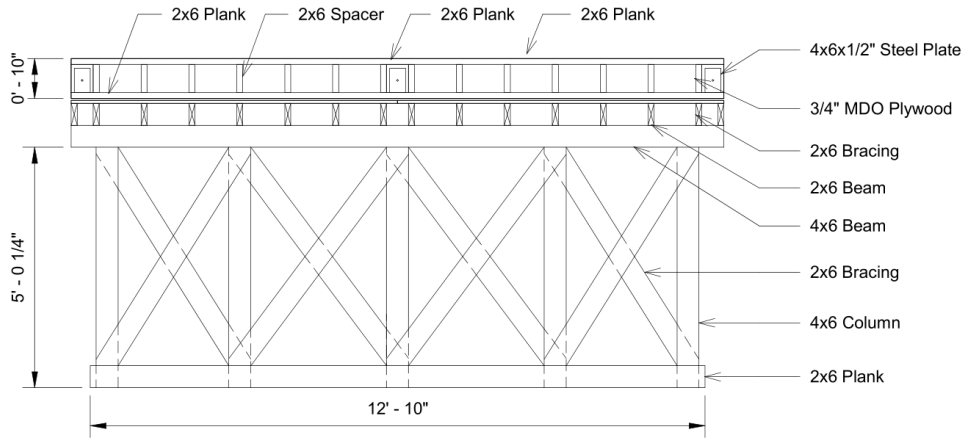

1 Elevation 2
3/8" = 1'-0"

CIVIL & ENVIRONMENTAL ENGINEERING

University of Washington
Department of Civil and Environmental Engineering

NSF Secondary Evacuation Structures

Elevation 2

Project Number	1
Date	Issue Date
Drawn By	Author
Checked By	Checker

S.5

Scale 3/8" = 1'-0"

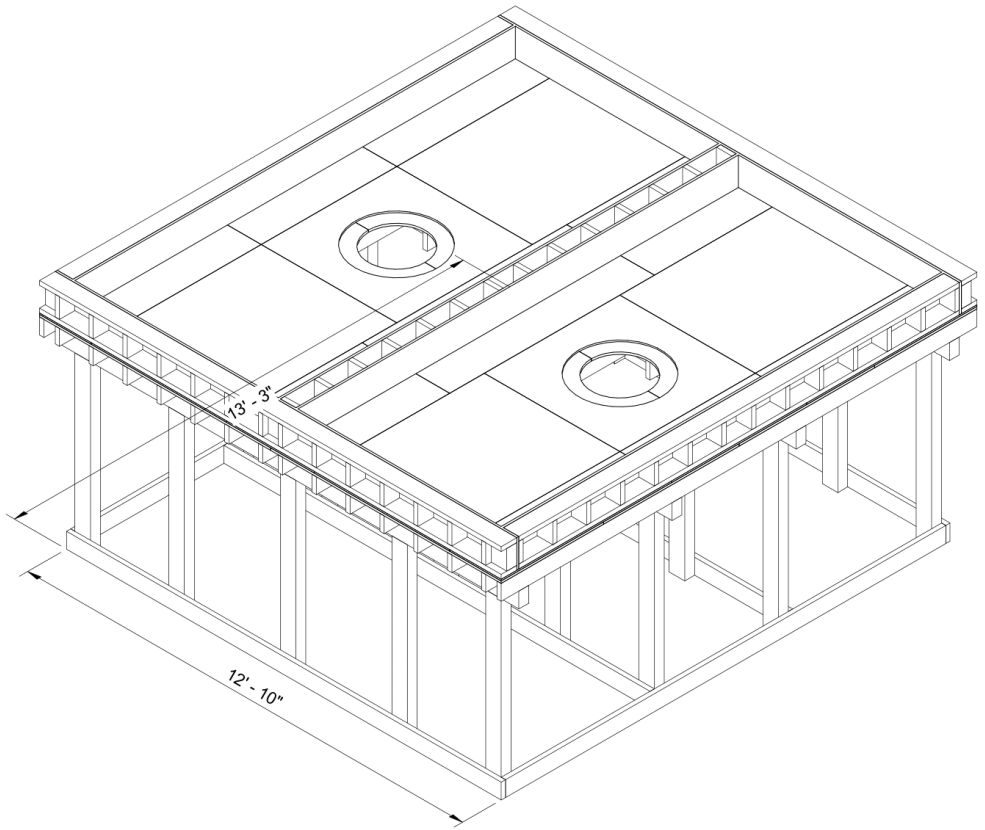

1 3D Isometric View

CIVIL & ENVIRONMENTAL ENGINEERING

University of Washington
Department of Civil and Environmental Engineering

NSF Secondary Evacuation Structures

3D View

Project Number	1
Date	Issue Date
Drawn By	Author
Checked By	Checker

S.6

Scale

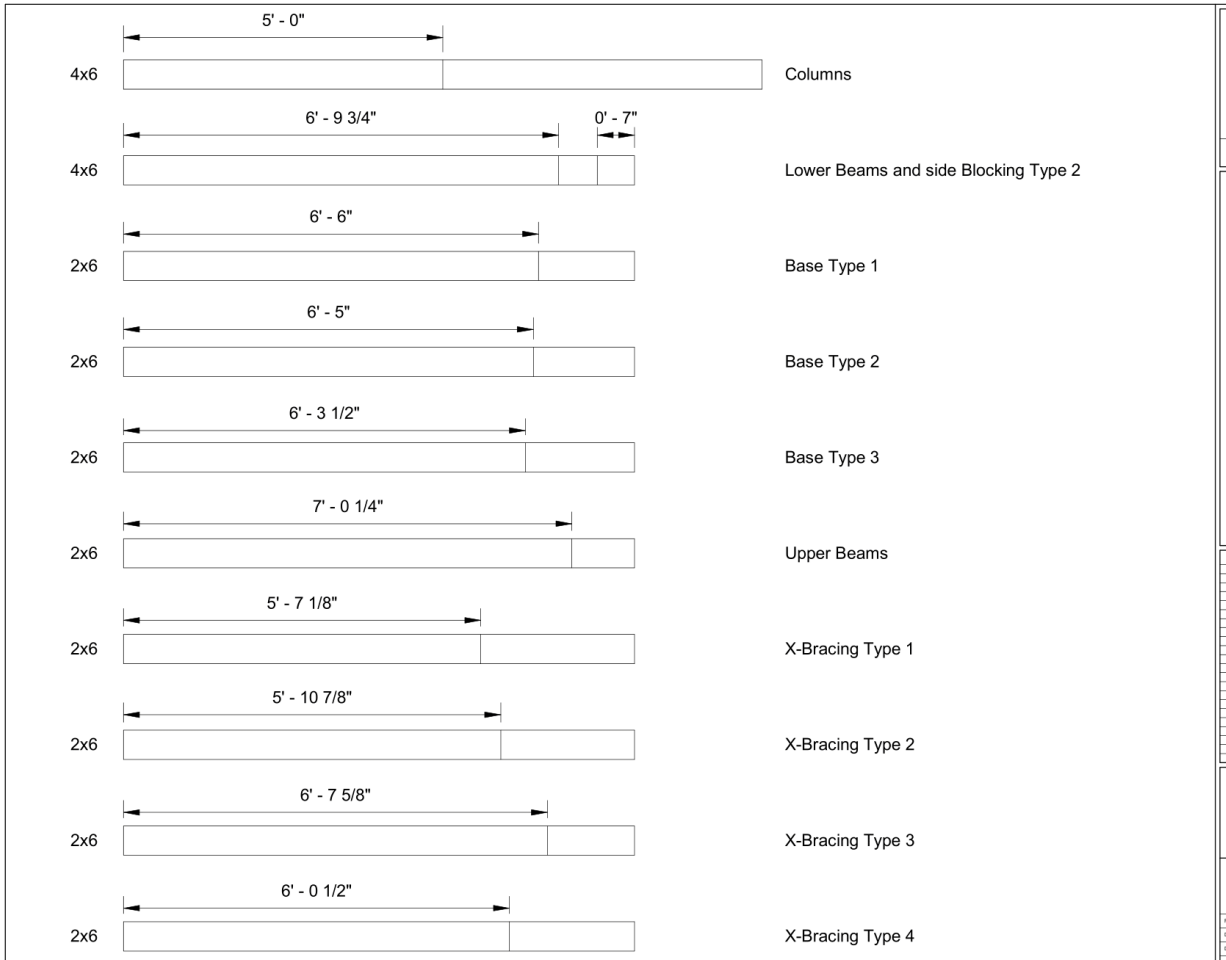

1 Parts 1
1/2" = 1'-0"

CIVIL & ENVIRONMENTAL ENGINEERING

University of Washington
Department of Civil and Environmental Engineering

NSF Secondary Evacuation Structures

Parts 1

Project Number 1
Date Issue Date
Drawn By Author
Checked By Checker

S.7

Scale 1/2" = 1'-0"

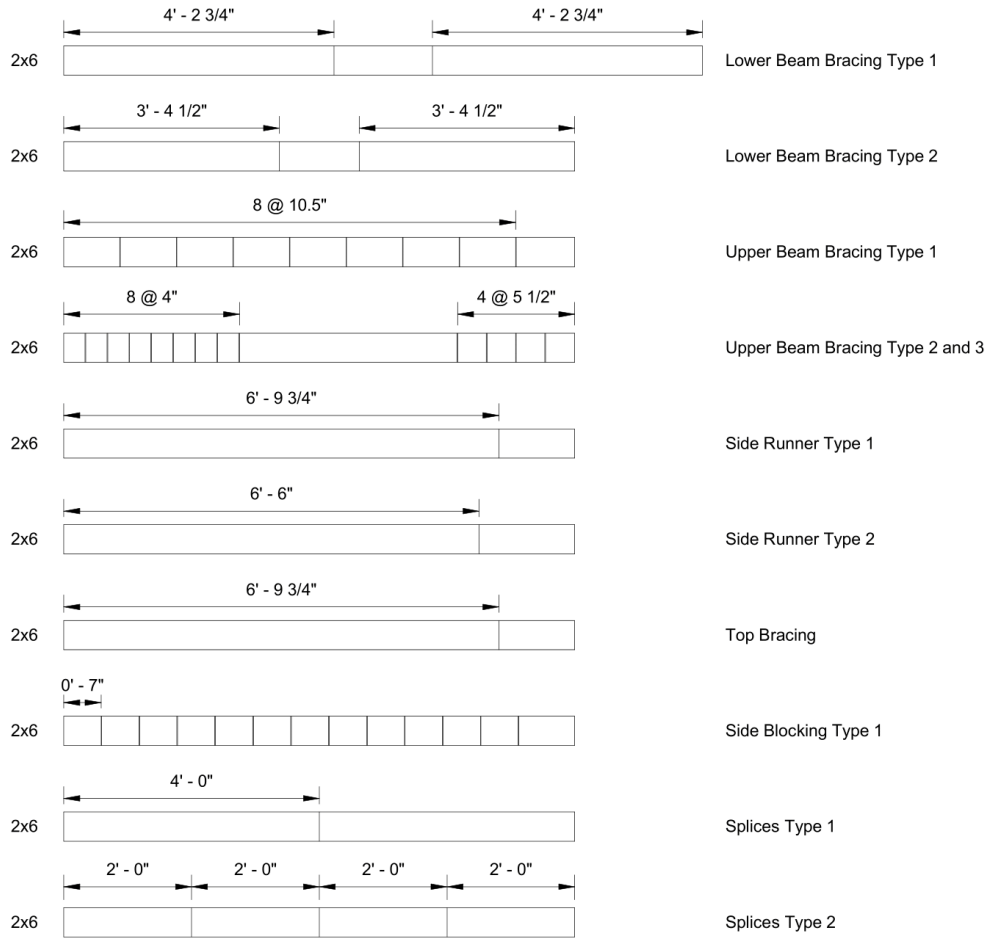

1 Parts 2
1/2" = 1'-0"

CIVIL & ENVIRONMENTAL ENGINEERING

University of Washington
Department of Civil and Environmental Engineering

NSF Secondary Evacuation Structures

Parts 2

Project Number 1
Date Issue Date
Drawn By Author
Checked By Checker

S.8

Scale 1/2" = 1'-0"

APPENDIX D: CRACK MAPS

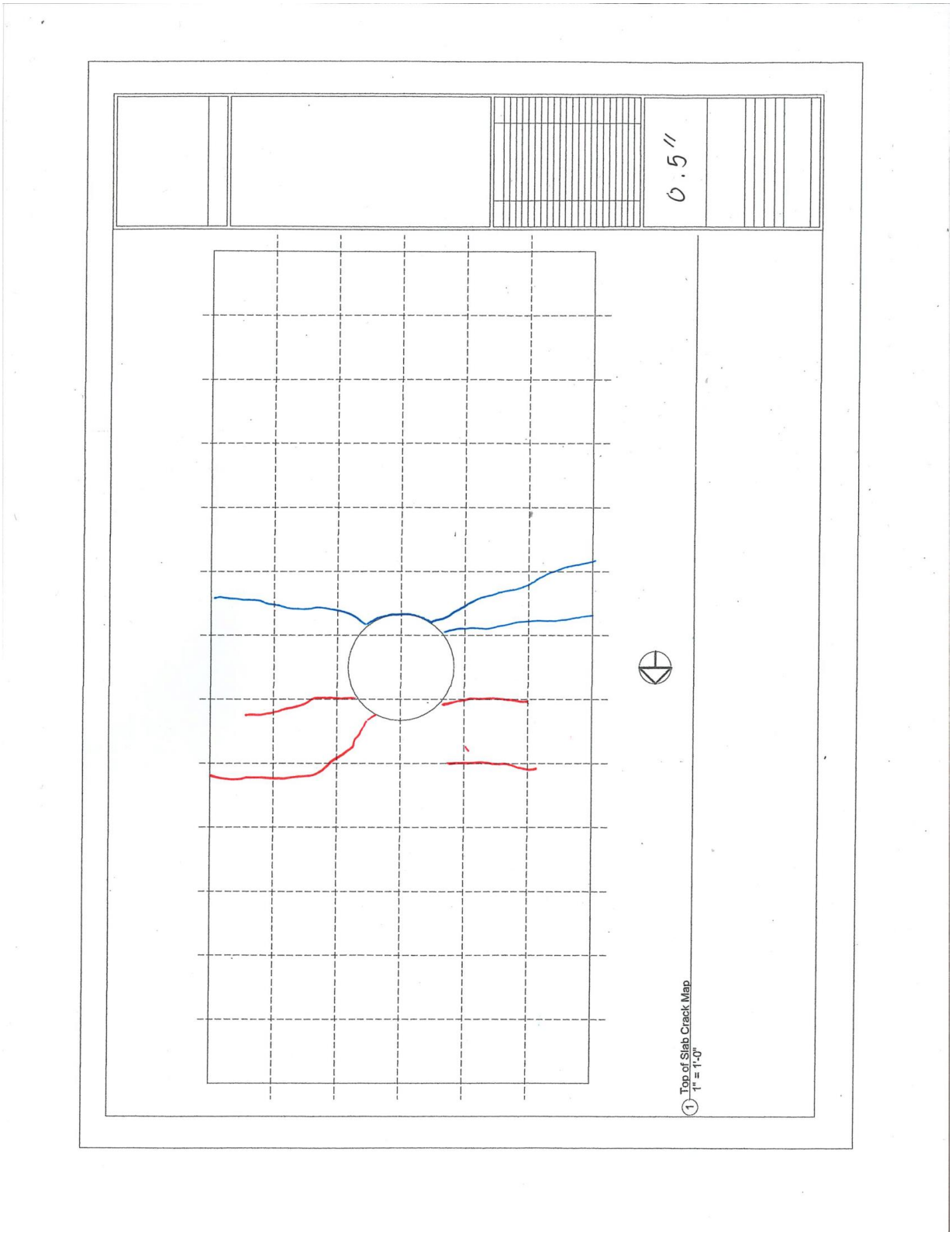

Figure 1: Top of Slab Crack Map– 0.21/-0.34% Drift (SR_4_10_5)

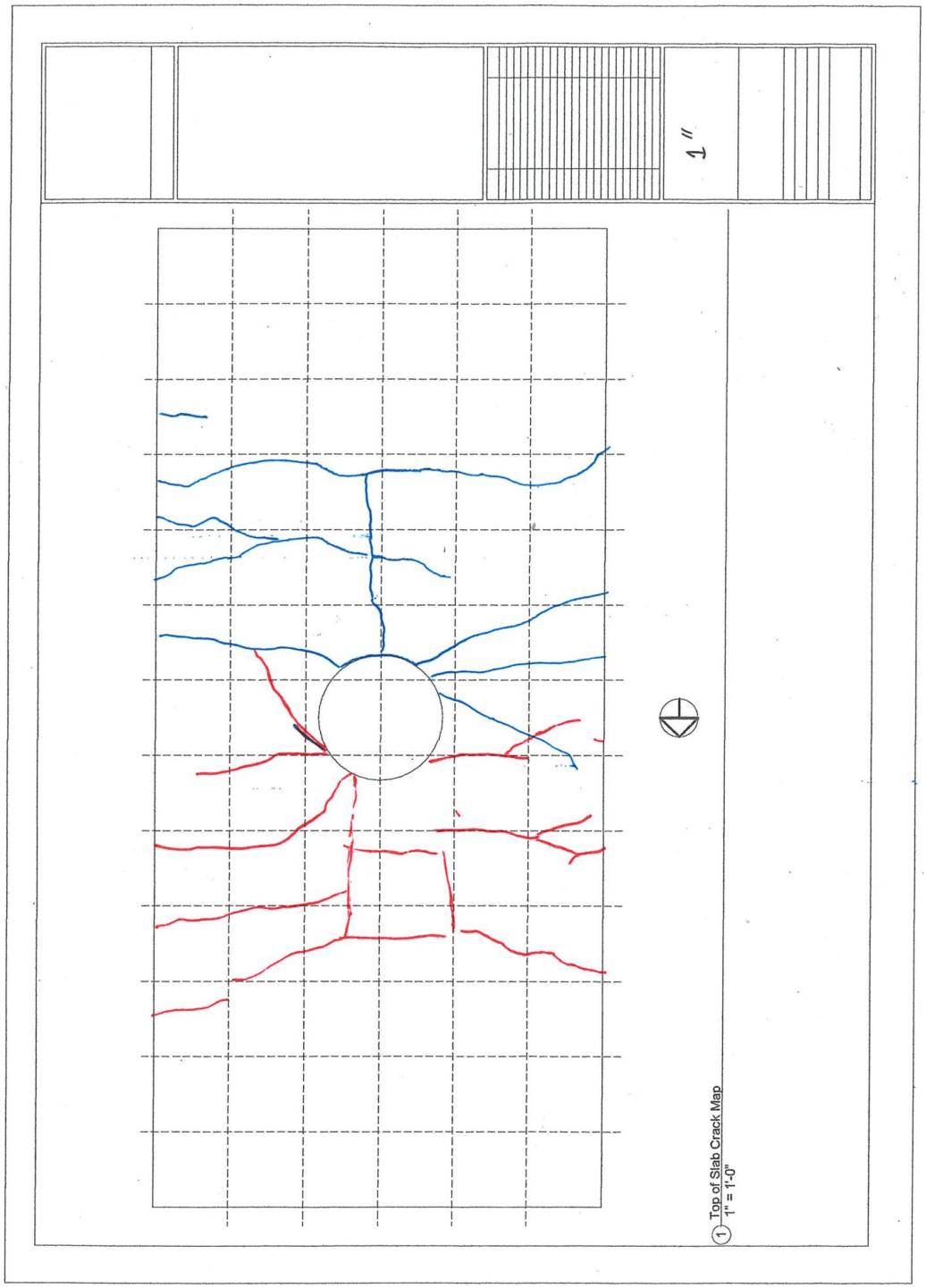

Figure 2: Top of Slab Crack Map– 0.56/-0.68% Drift (SR_4_10_5)

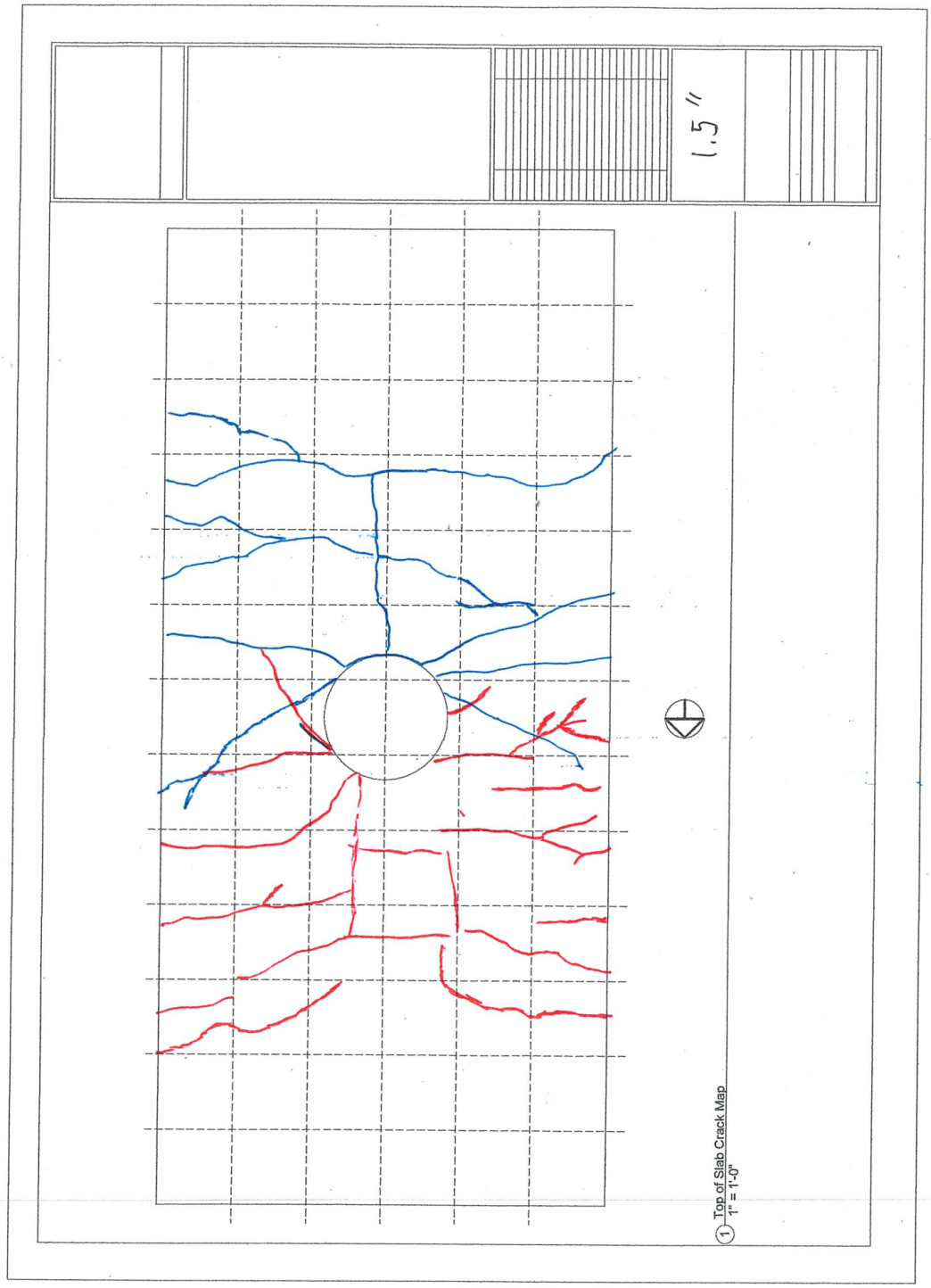

Figure 3: Top of Slab Crack Map– 0.91/-1.0% Drift (SR_4_10_5)

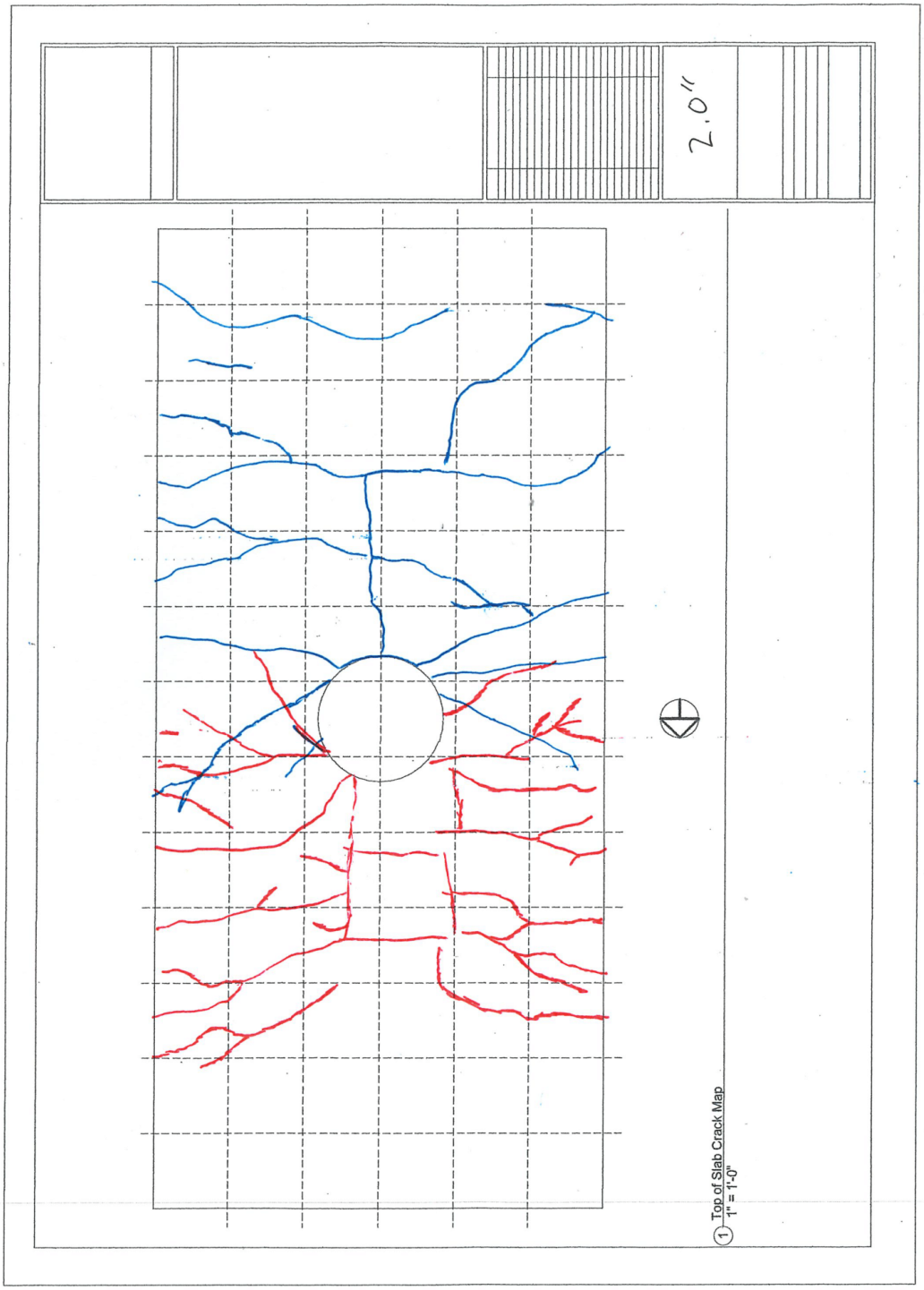

Figure 4: Top of Slab Crack Map– 1.3/-1.4% Drift (SR_4_10_5)

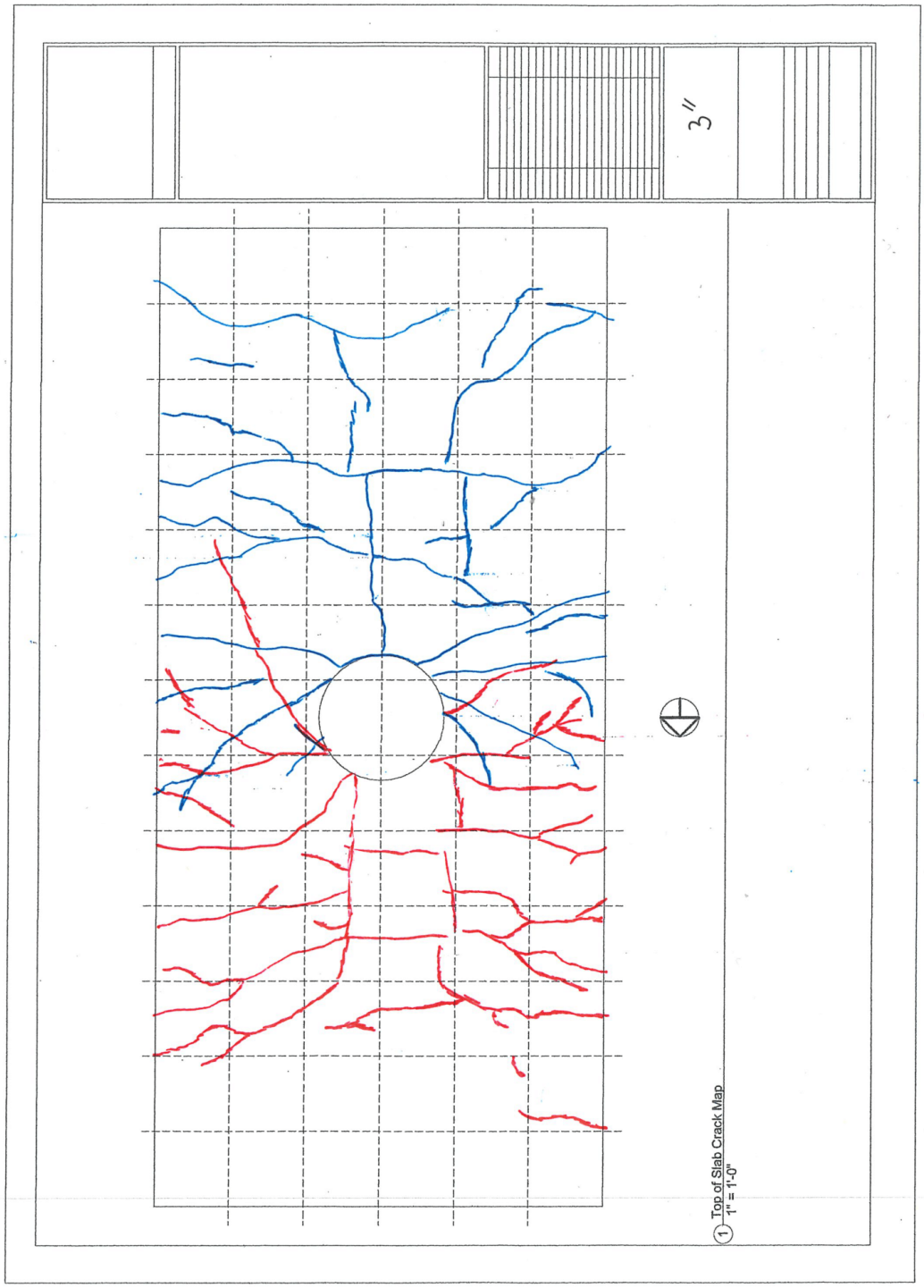

Figure 5: Top of Slab Crack Map– 2.0/-2.1% Drift (SR_4_10_5)

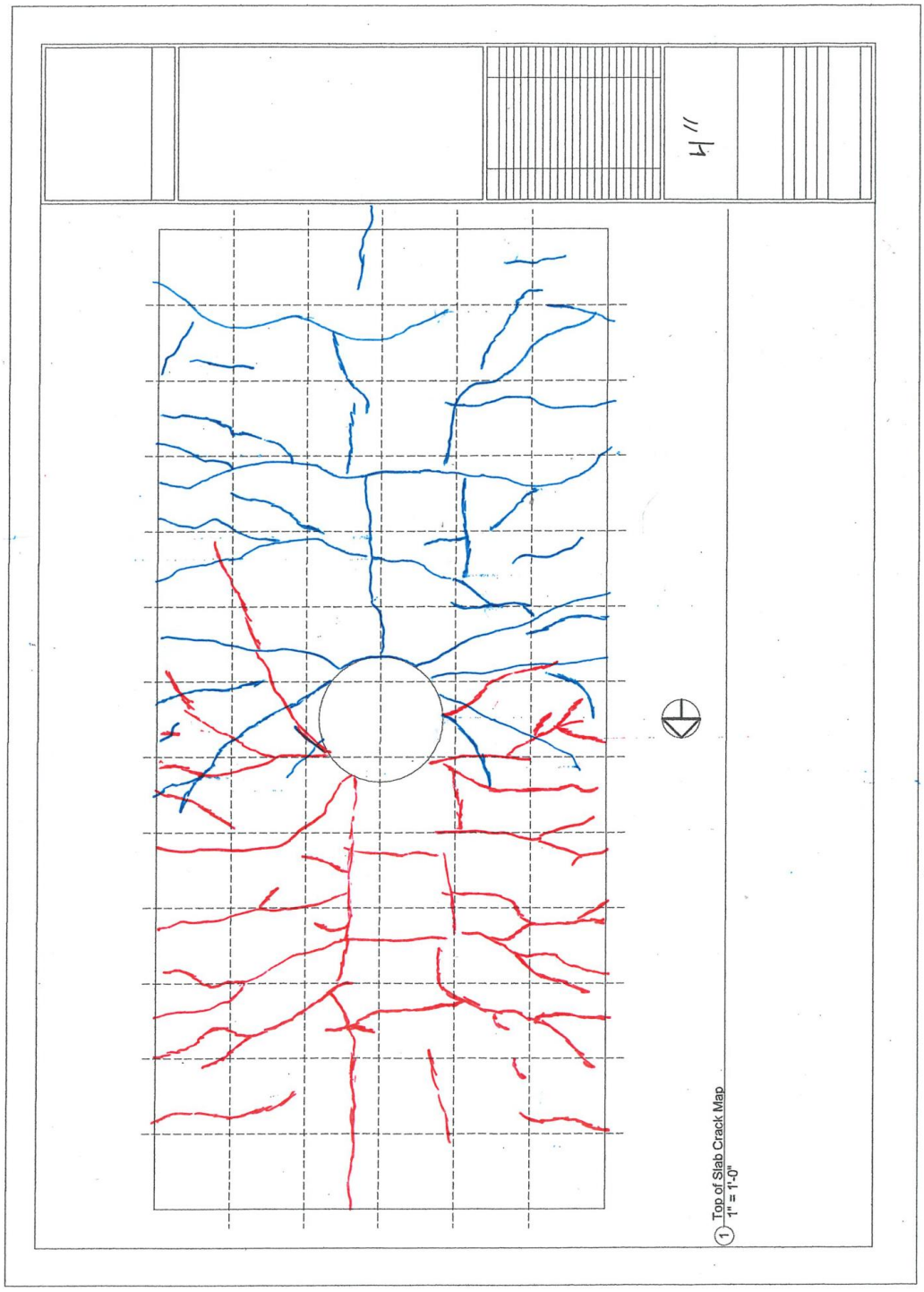

Figure 6: Top of Slab Crack Map– 2.7/-2.8% Drift (SR_4_10_5)

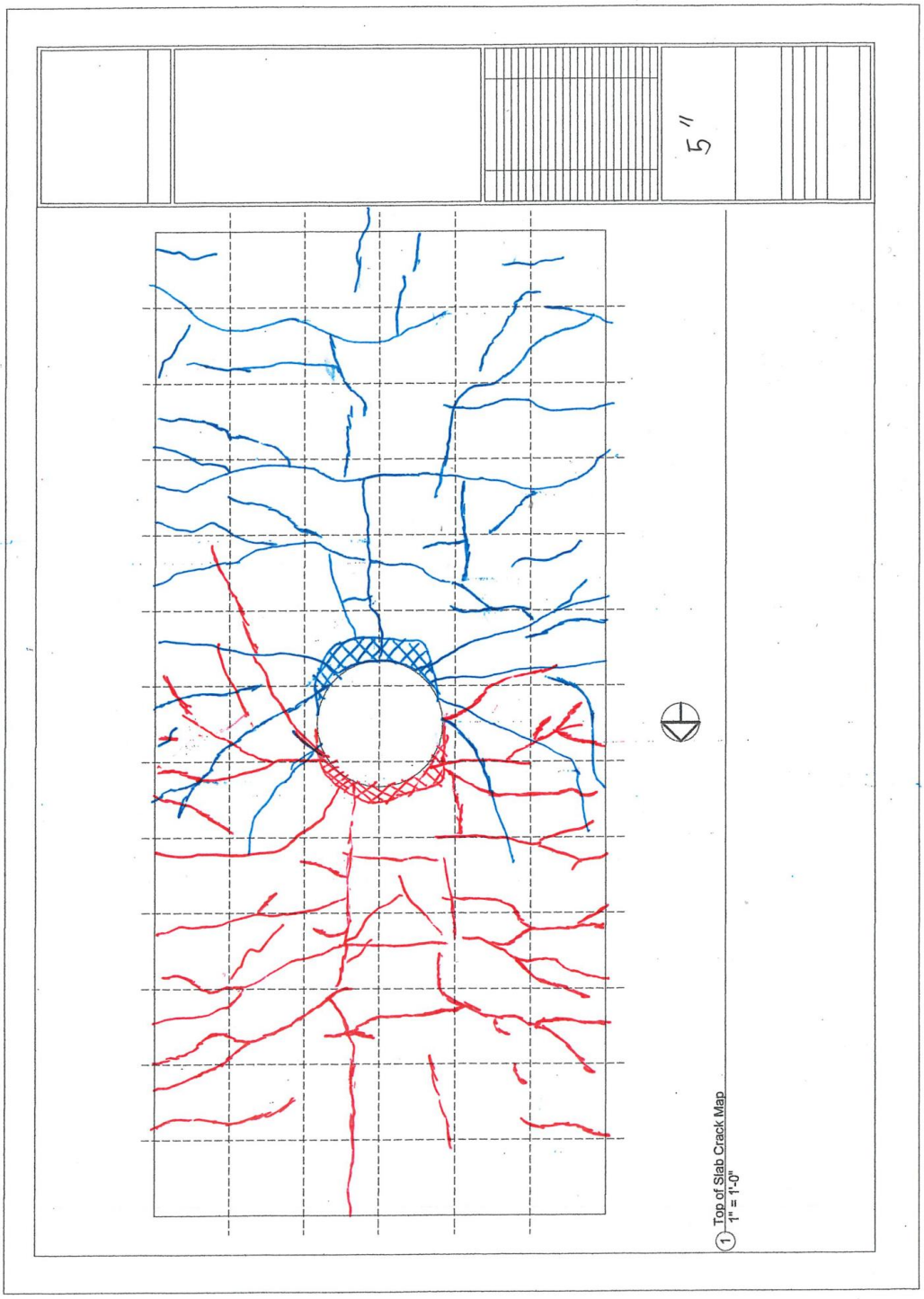

Figure 7: Top of Slab Crack Map– 3.4/-3.5% Drift (SR_4_10_5)

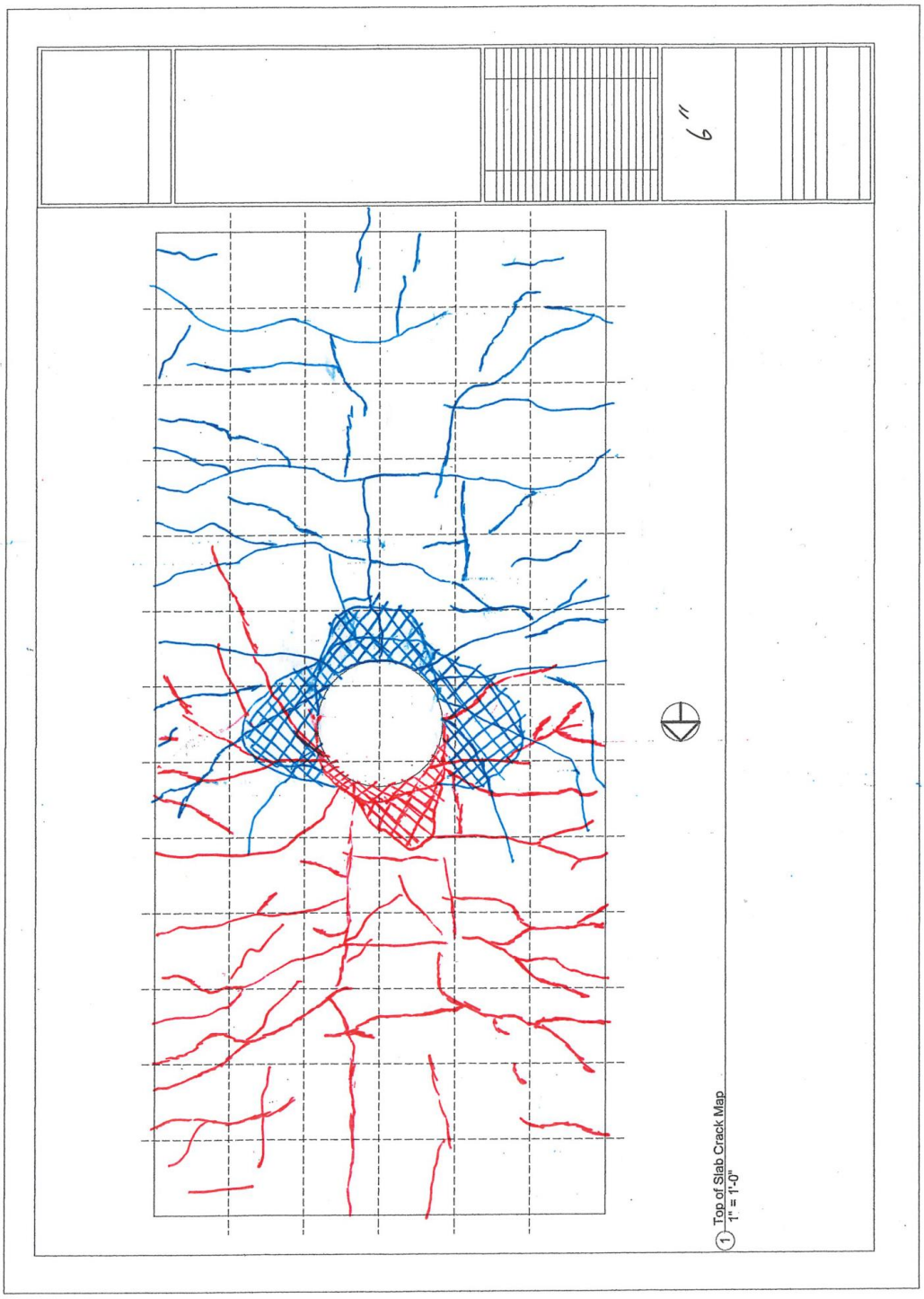

Figure 8: Top of Slab Crack Map– 4.2/-4.2% Drift (SR_4_10_5)

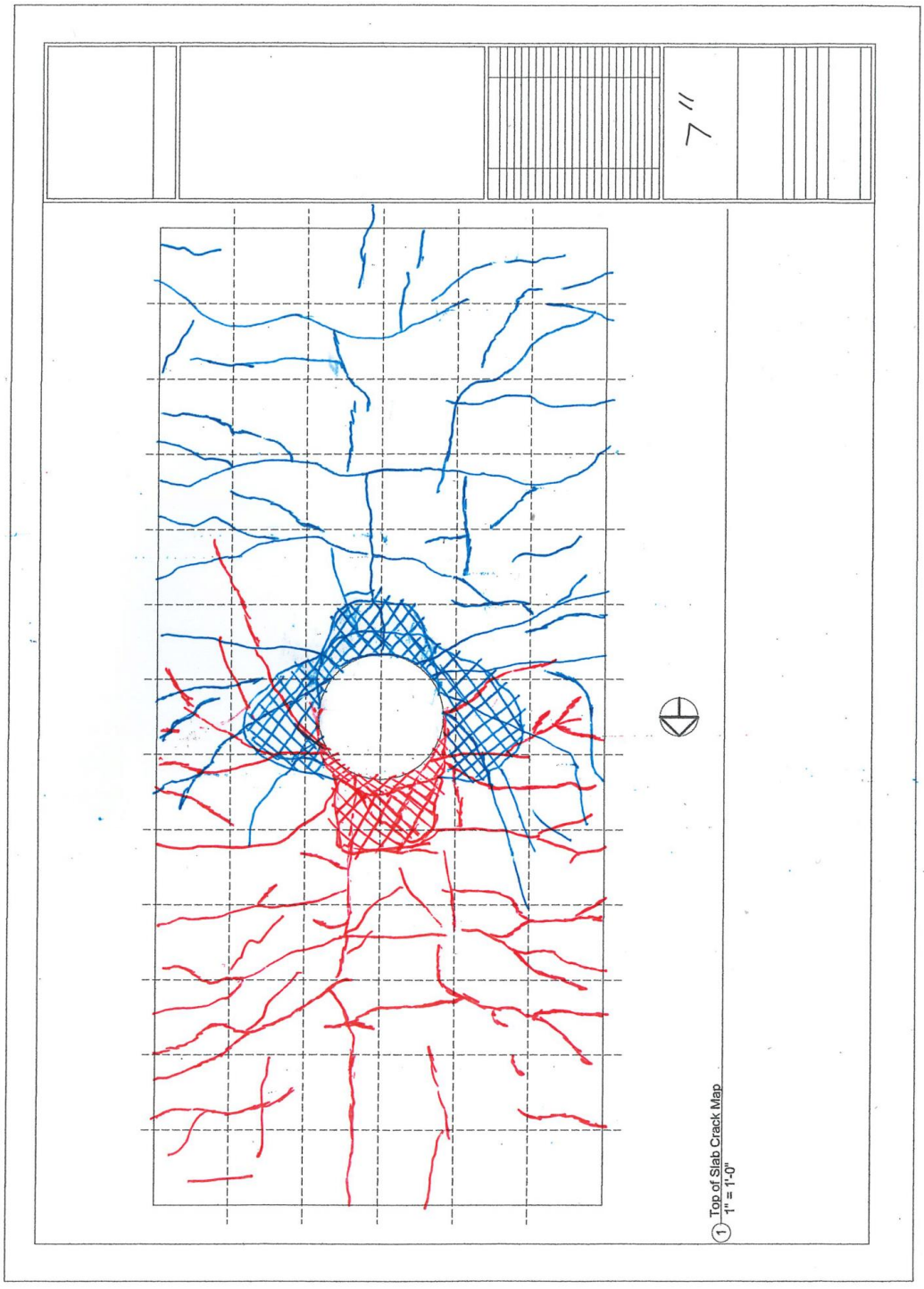

Figure 9: Top of Slab Crack Map– 4.9/-4.9% Drift (SR_4_10_5)

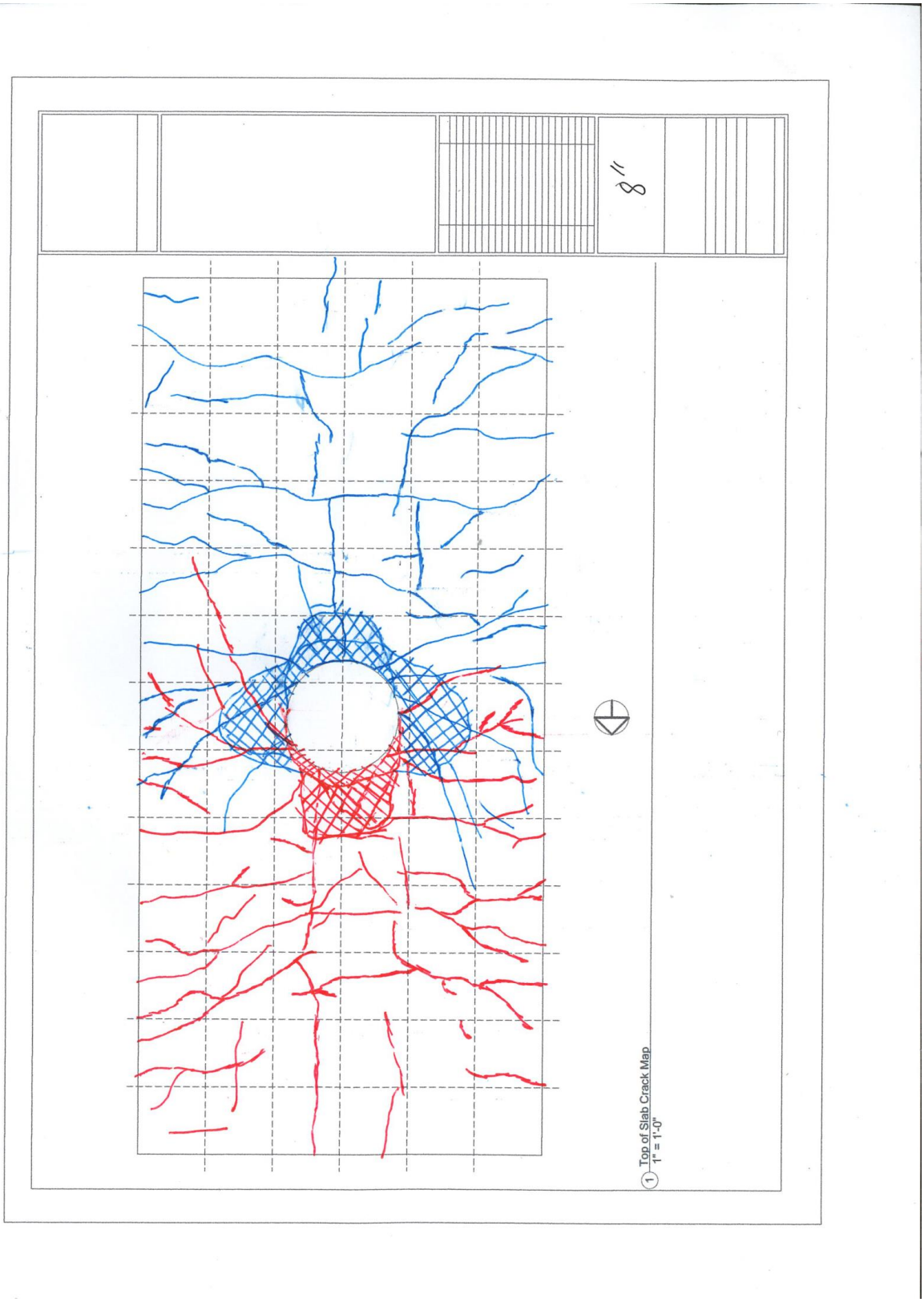

Figure 10: Top of Slab Crack Map– 5.6/-5.7% Drift (SR_4_10_5)

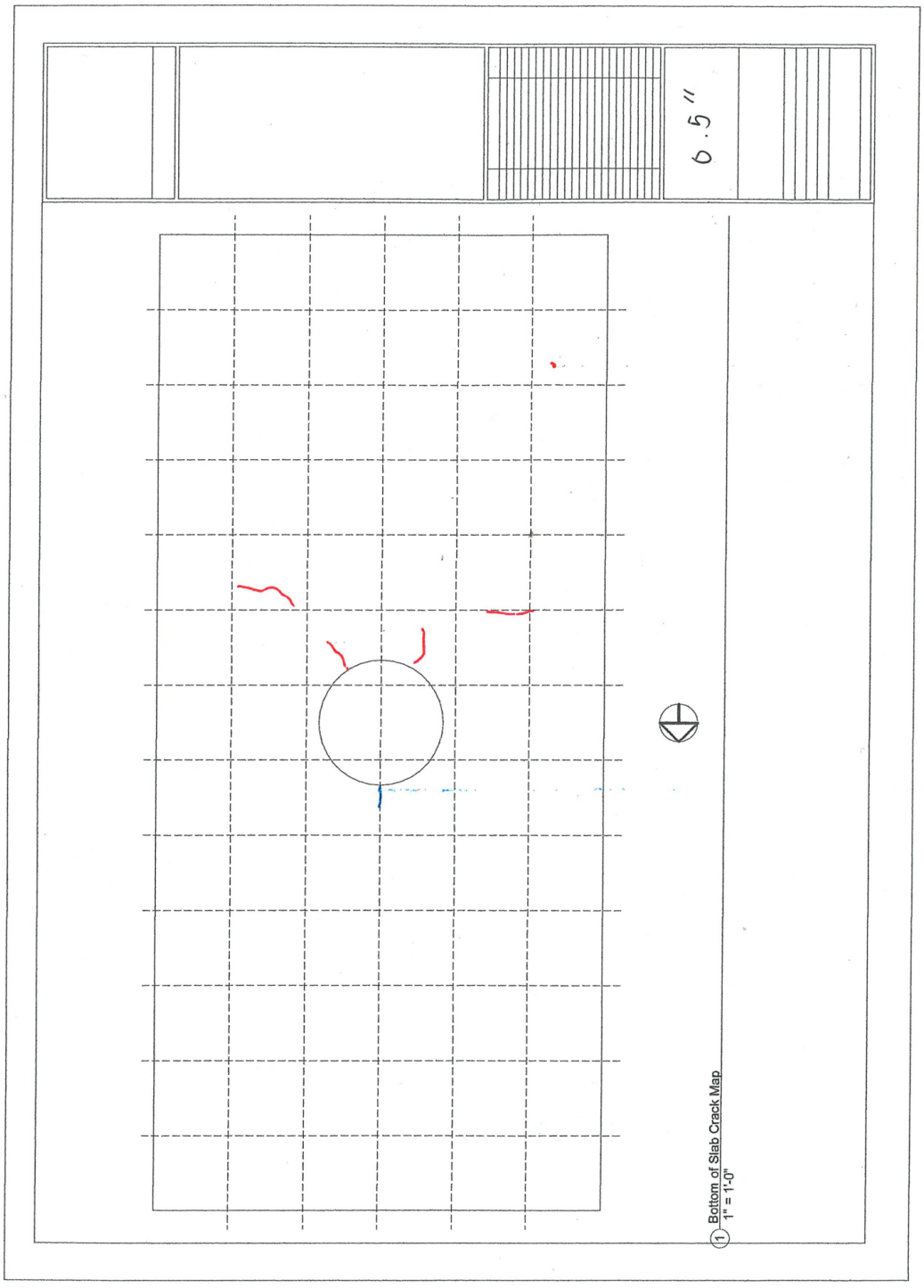

Figure 11: Bottom of Slab Crack Map– 0.21/-0.34% Drift (SR_4_10_5)

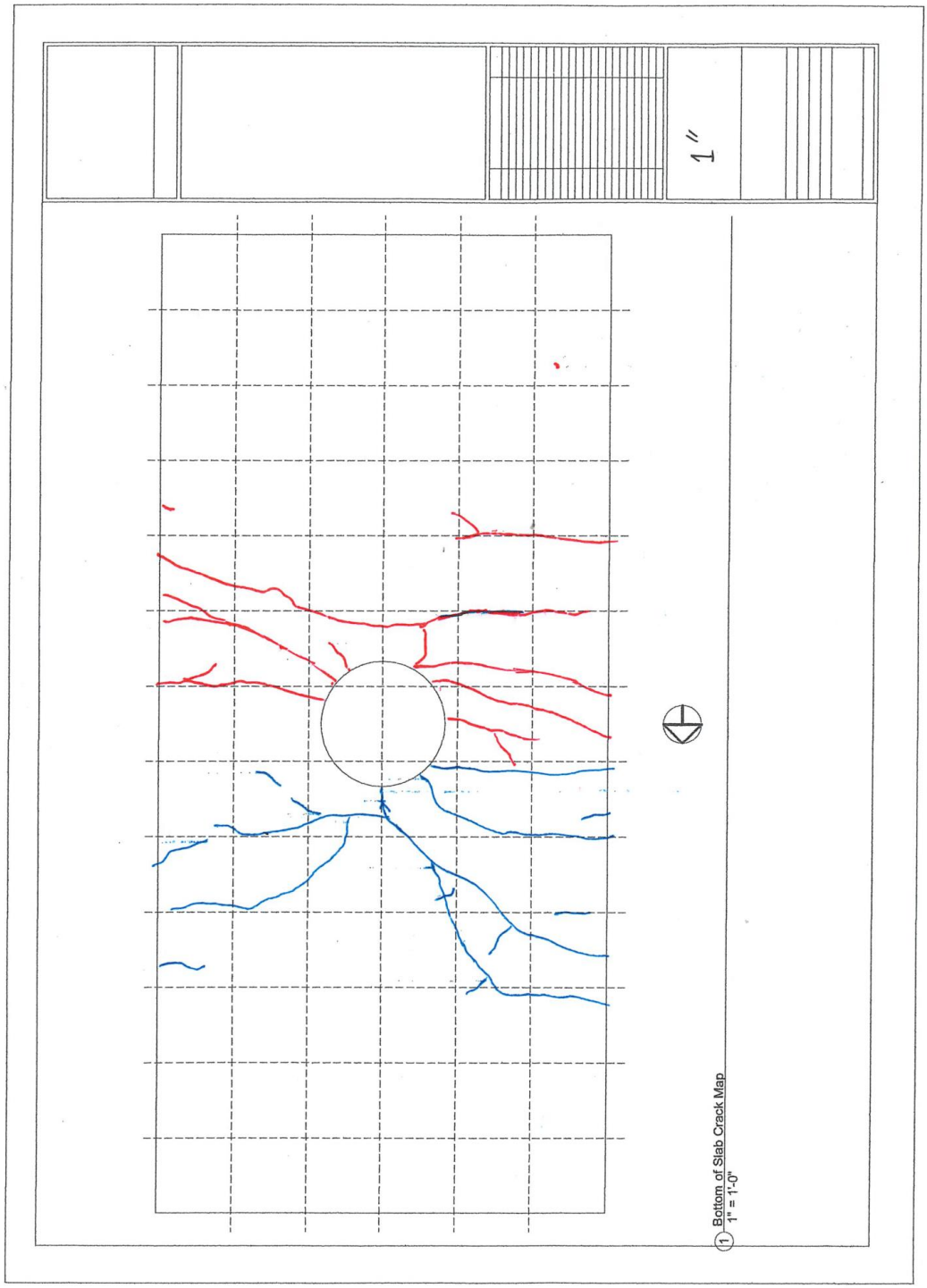

Figure 12: Bottom of Slab Crack Map– 0.56/-0.68% Drift (SR_4_10_5)

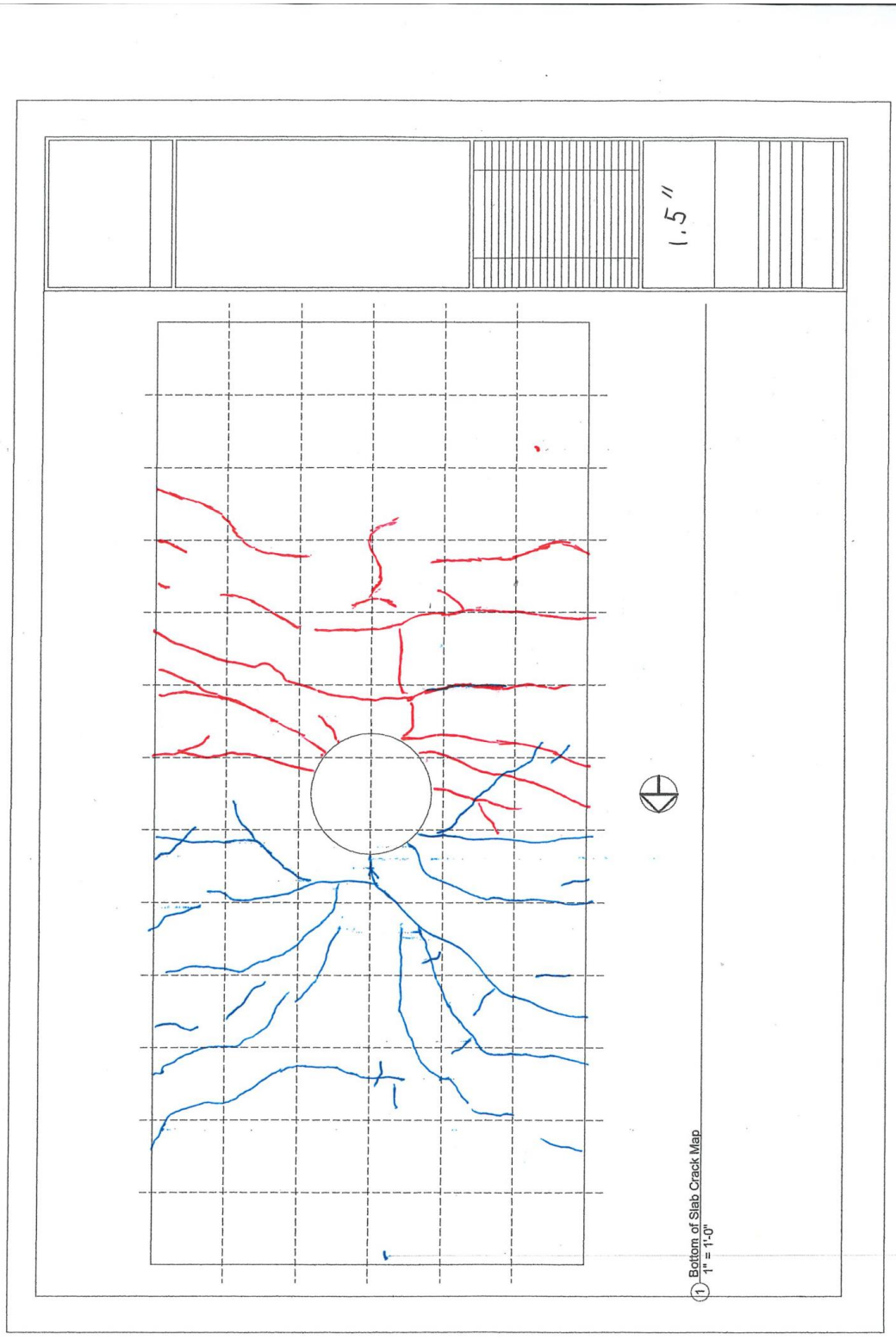

Figure 13: Bottom of Slab Crack Map– 0.91/-1.0% Drift (SR_4_10_5)

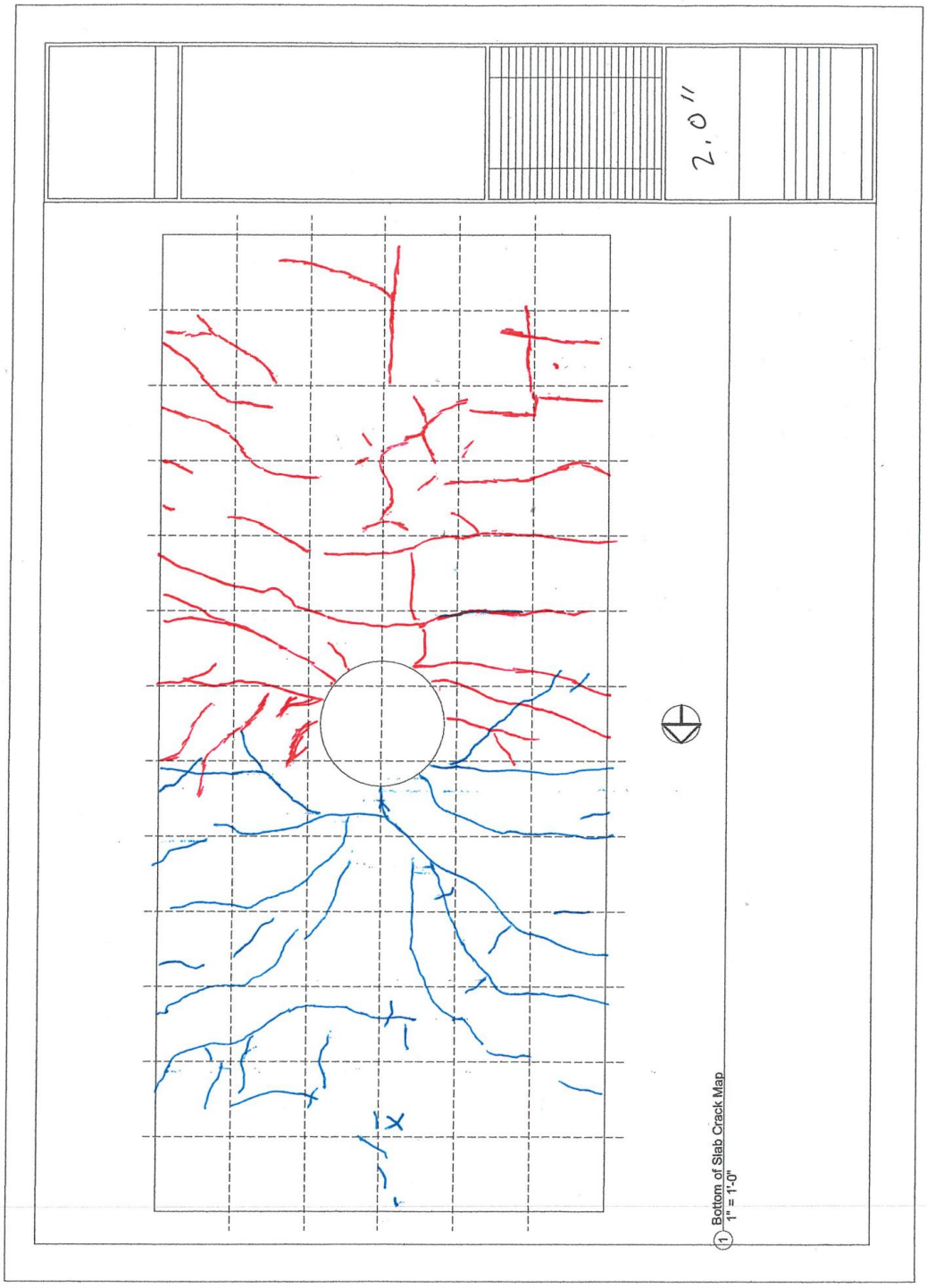

Figure 14: Bottom of Slab Crack Map– 1.3/-1.4% Drift (SR_4_10_5)

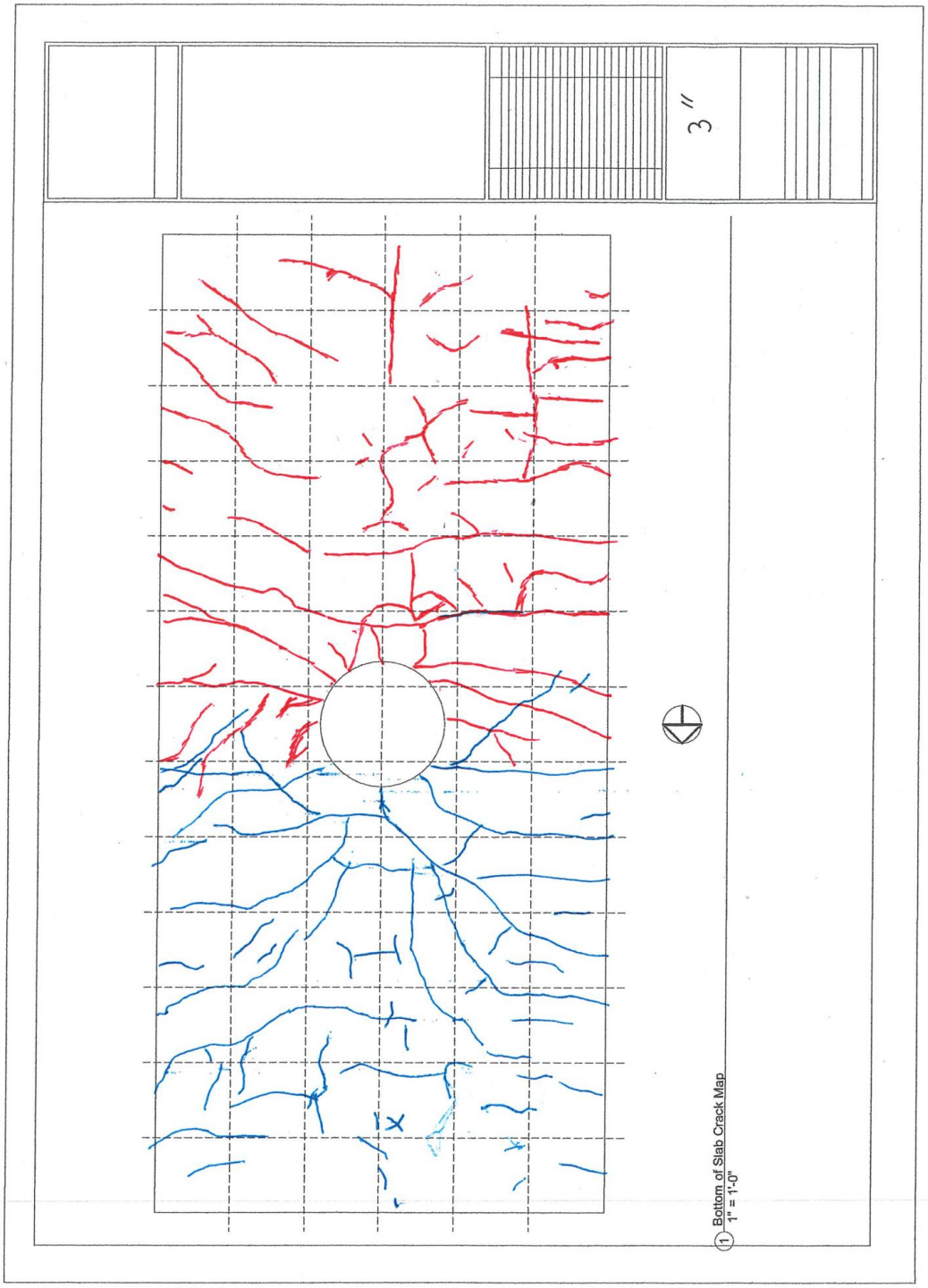

Figure 15: Bottom of Slab Crack Map– 2.0/-2.1% Drift (SR_4_10_5)

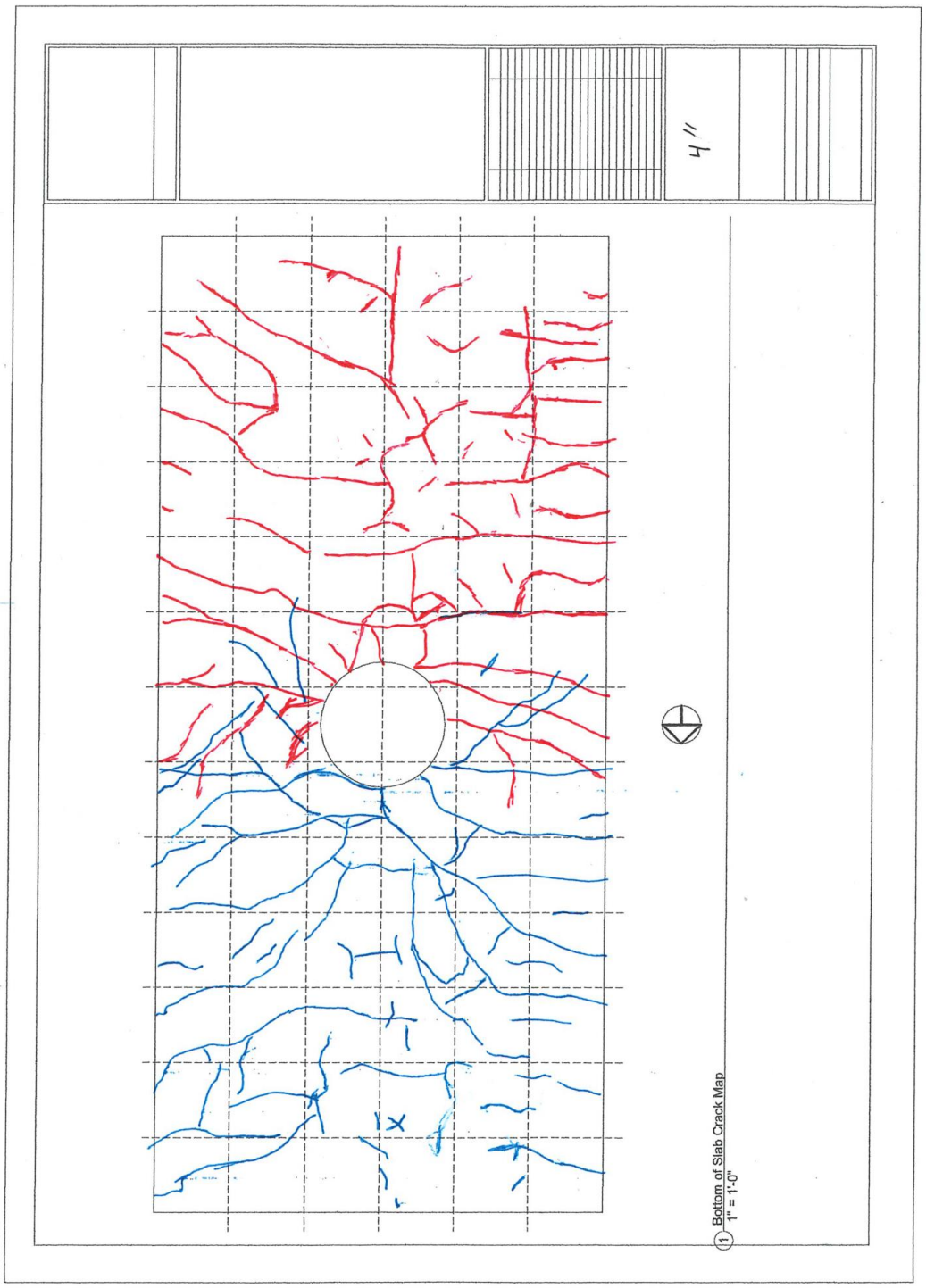

Figure 16: Bottom of Slab Crack Map– 2.7/-2.8% Drift (SR_4_10_5)

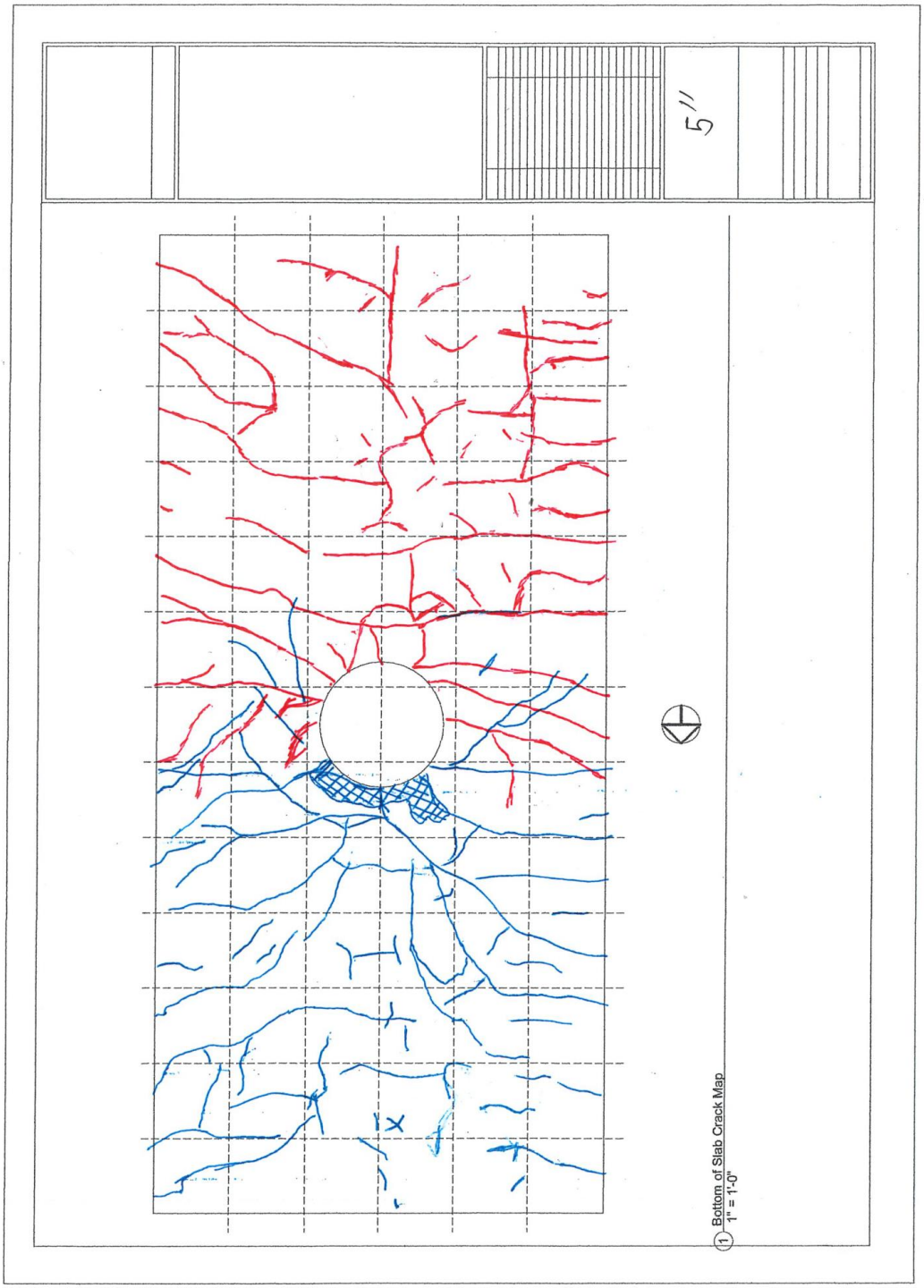

Figure 17: Bottom of Slab Crack Map– 3.4/-3.5% Drift (SR_4_10_5)

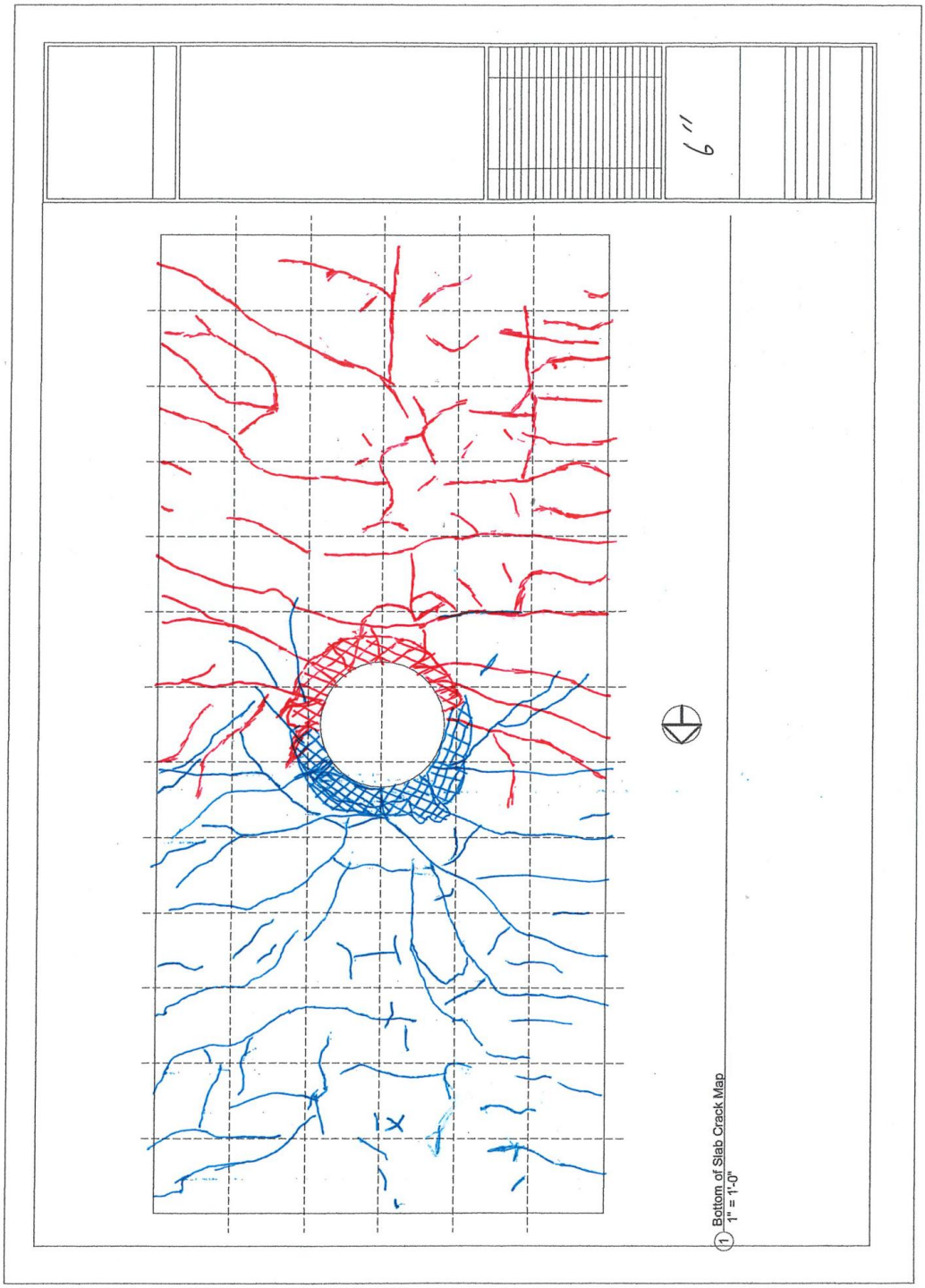

Figure 18: Bottom of Slab Crack Map– 4.2/-4.2% Drift (SR_4_10_5)

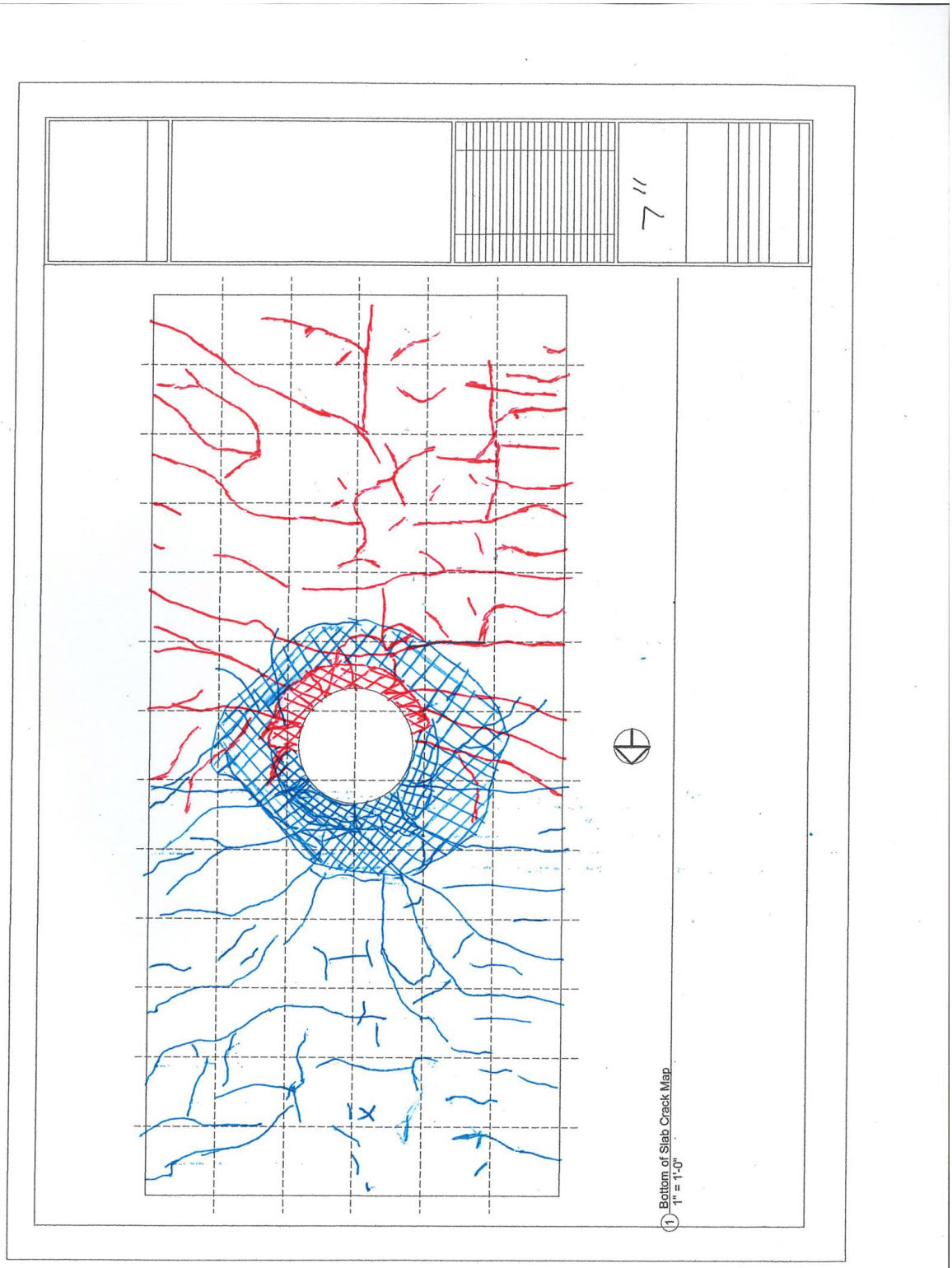

Figure 19: Bottom of Slab Crack Map– 4.9/-4.9% Drift (SR_4_10_5)

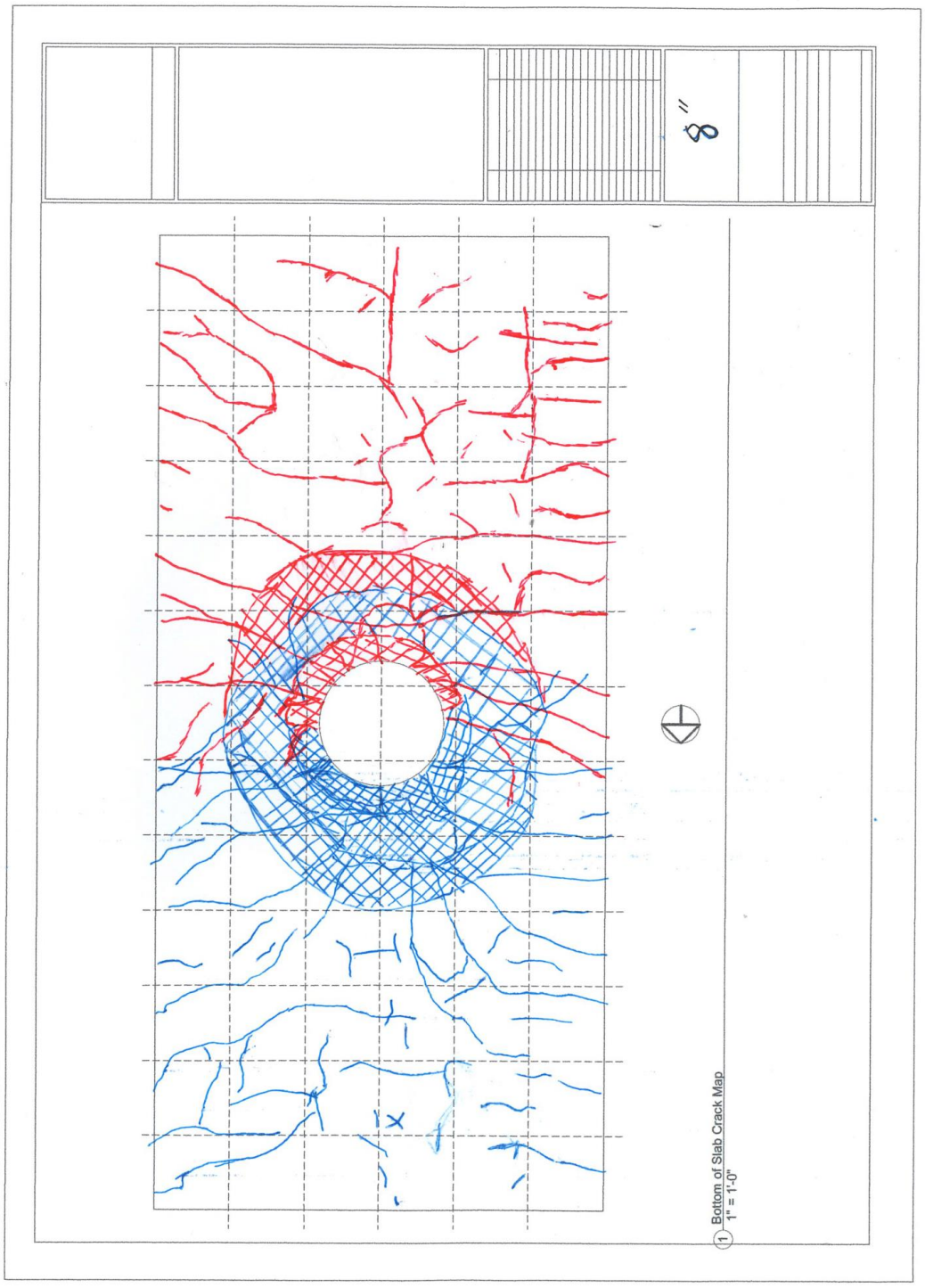

Figure 20: Bottom of Slab Crack Map– 5.6/-5.7% Drift (SR_4_10_5)

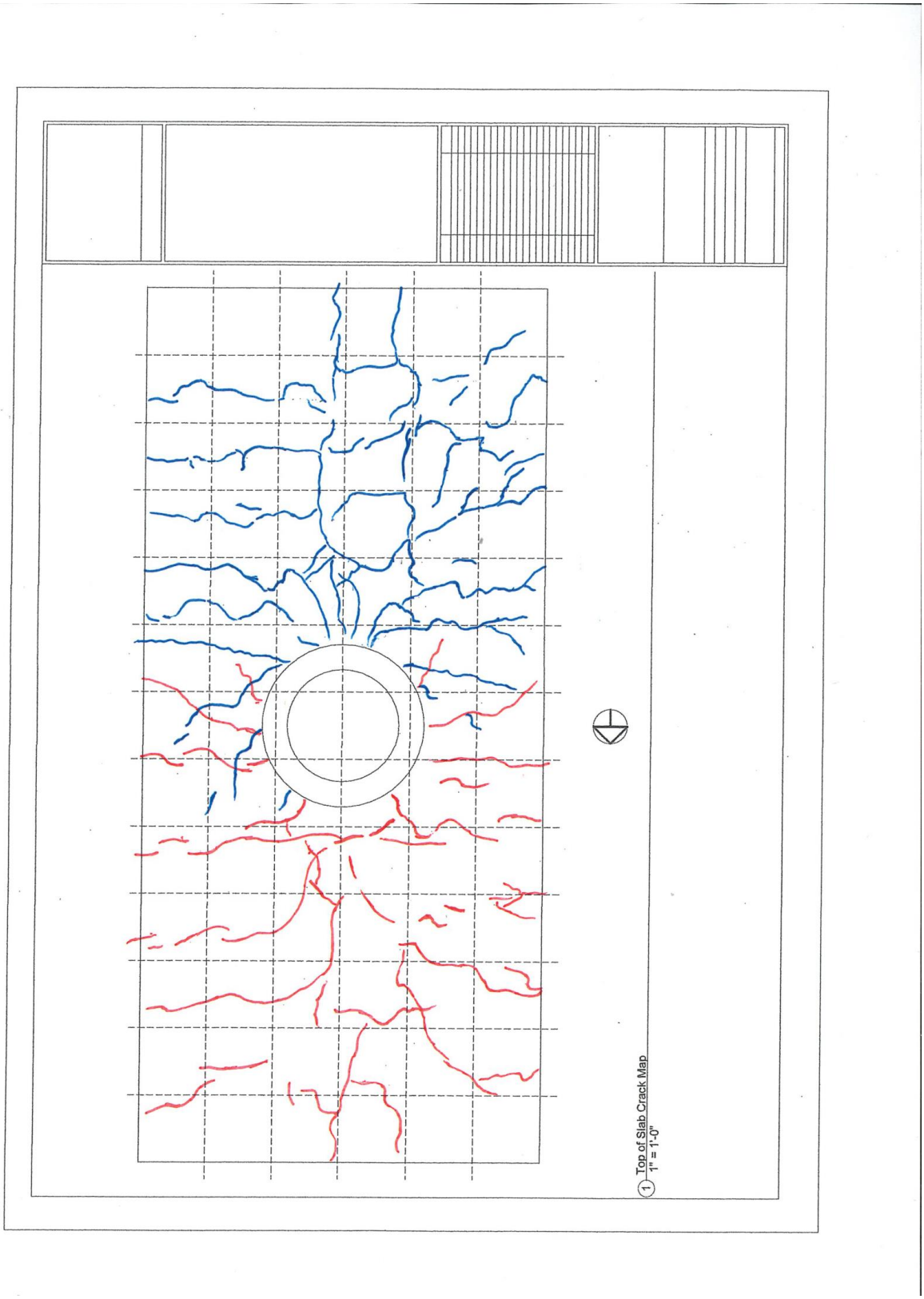

Figure 21: Top of Slab Crack Map– 1.3/-1.3% Drift (PTB_4.5_1_0)

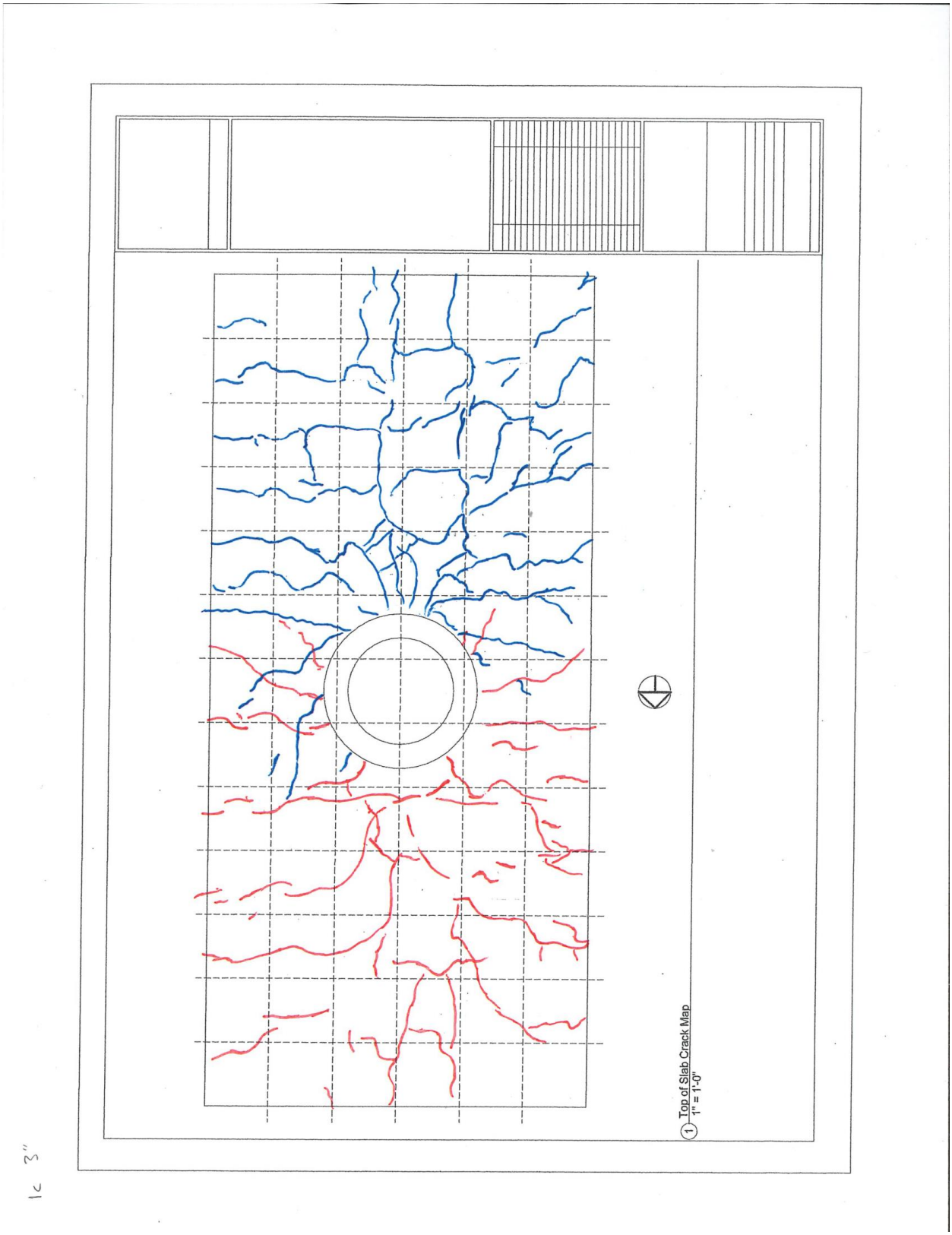

Figure 22: Top of Slab Crack Map– 2.0/-2.0% Drift (PTB_4.5_1_0)

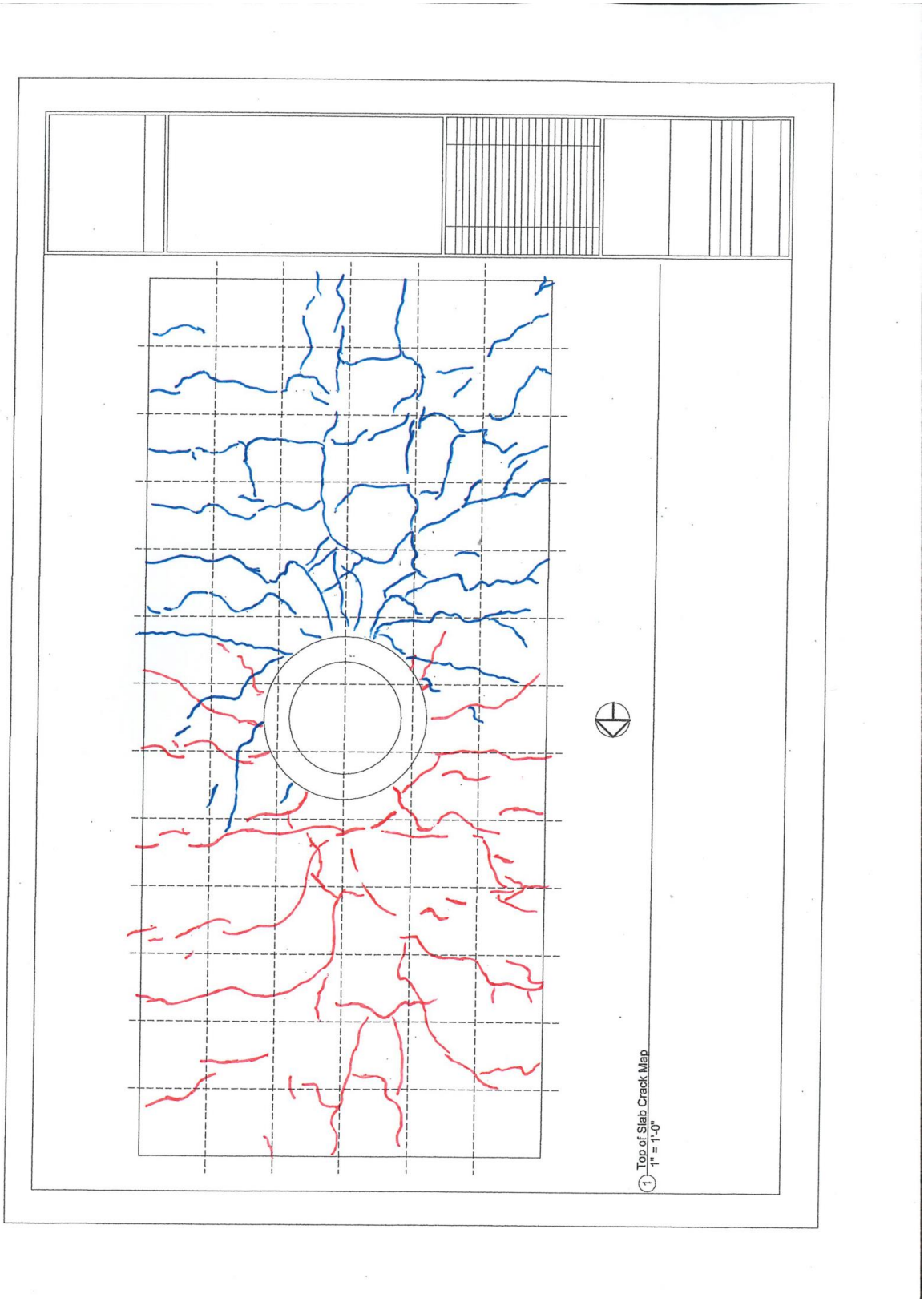

Figure 23: Top of Slab Crack Map– 2.6/-2.6% Drift (PTB_4.5_1_0)

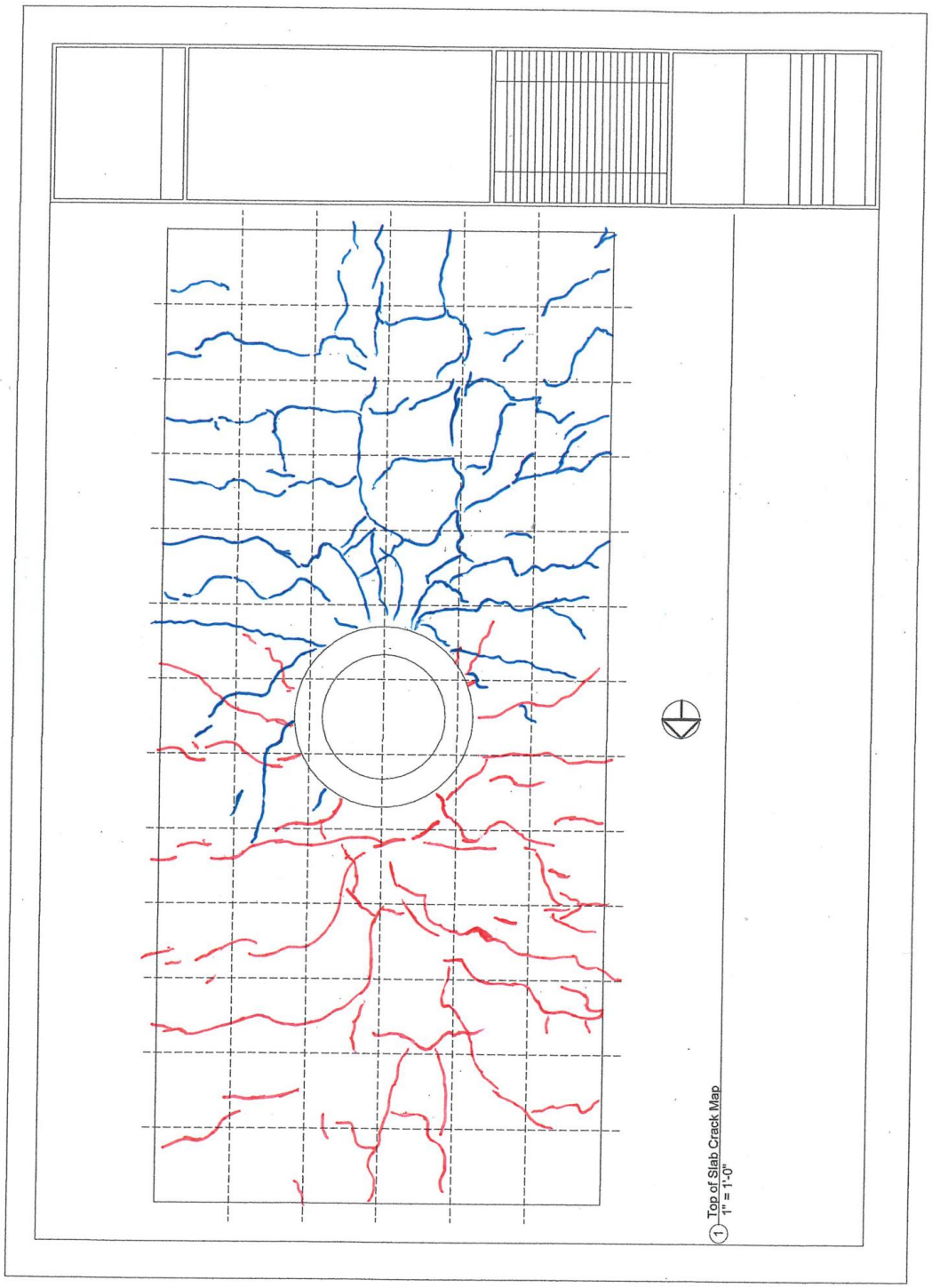

Figure 24: Top of Slab Crack Map– 3.4/-3.3% Drift (PTB_4.5_1_0)

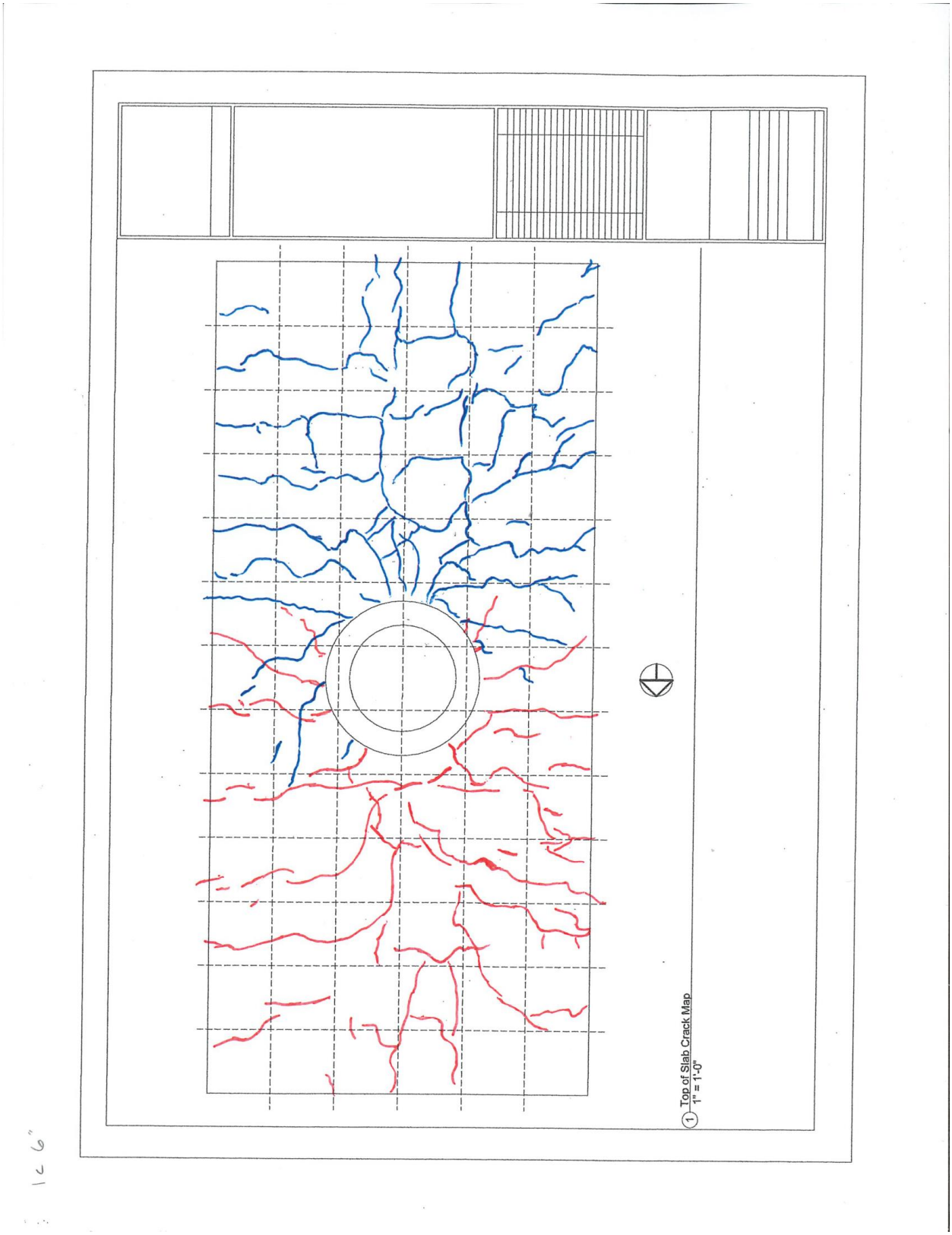

Figure 25: Top of Slab Crack Map– 4.1/-4.0% Drift (PTB_4.5_1_0)

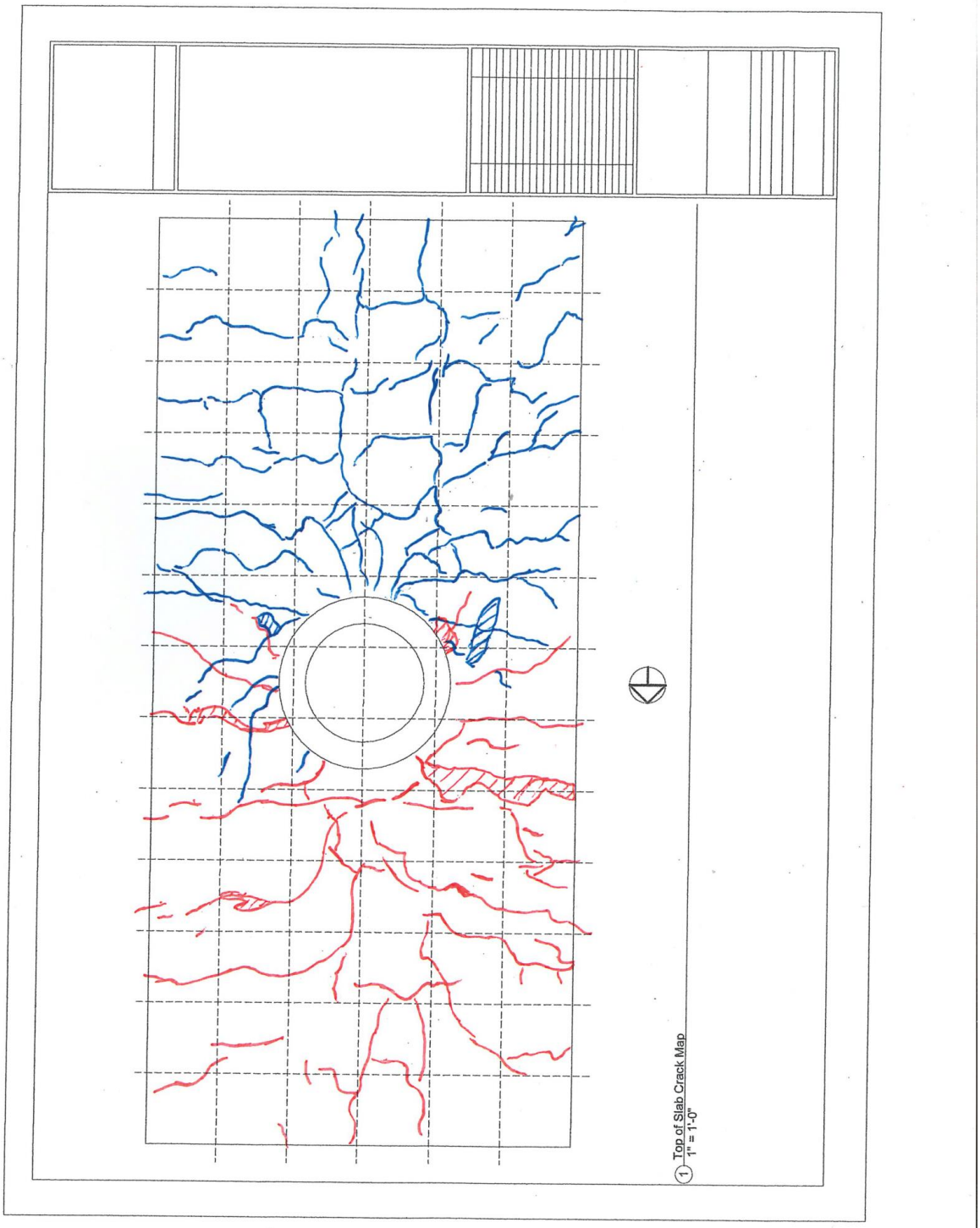

Figure 26: Top of Slab Crack Map– 4.8/-4.8% Drift (PTB_4.5_1_0)

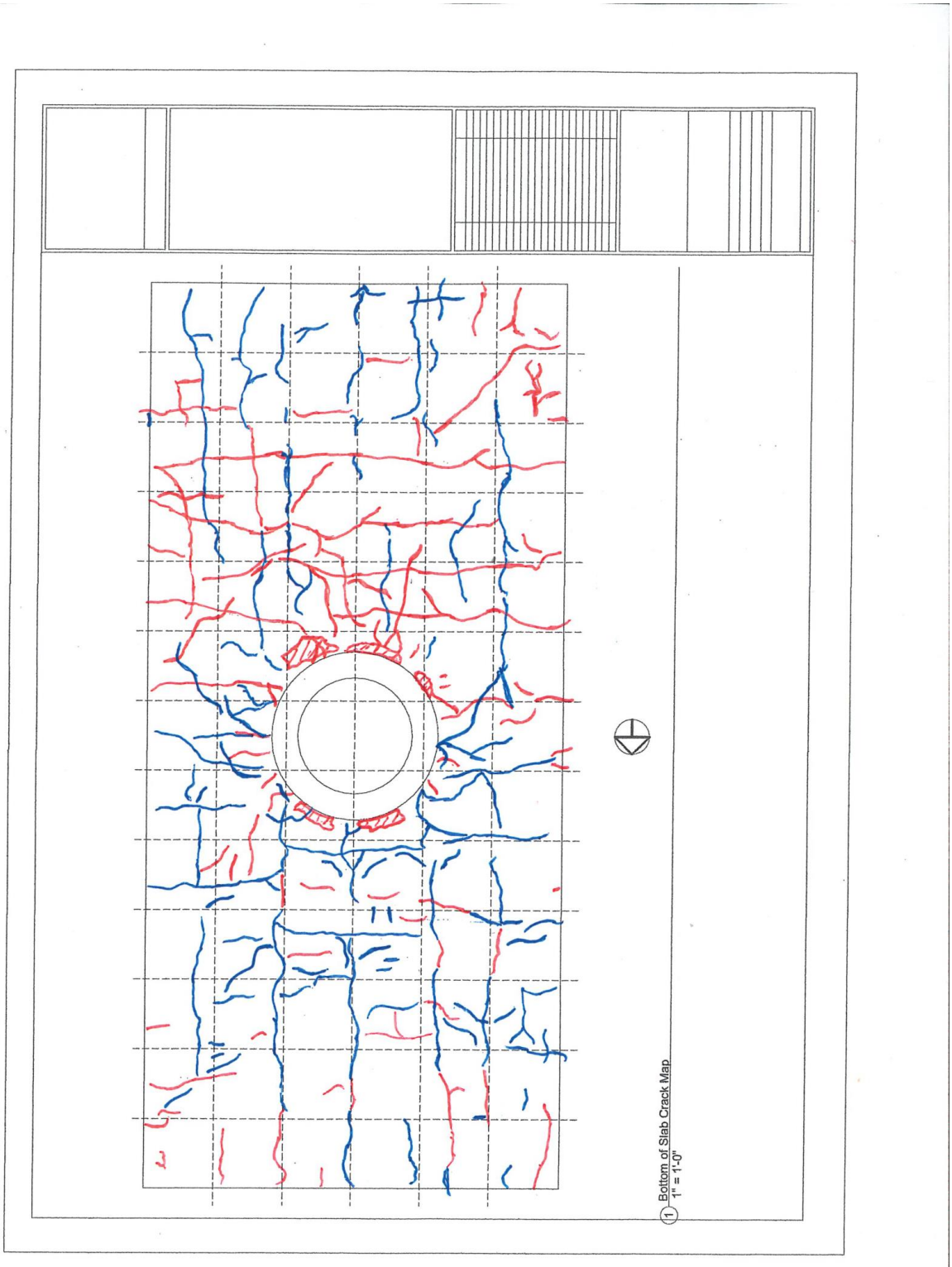

Figure 27: Bottom of Slab Crack Map– 1.3/-1.3% Drift (PTB_4.5_1_0)

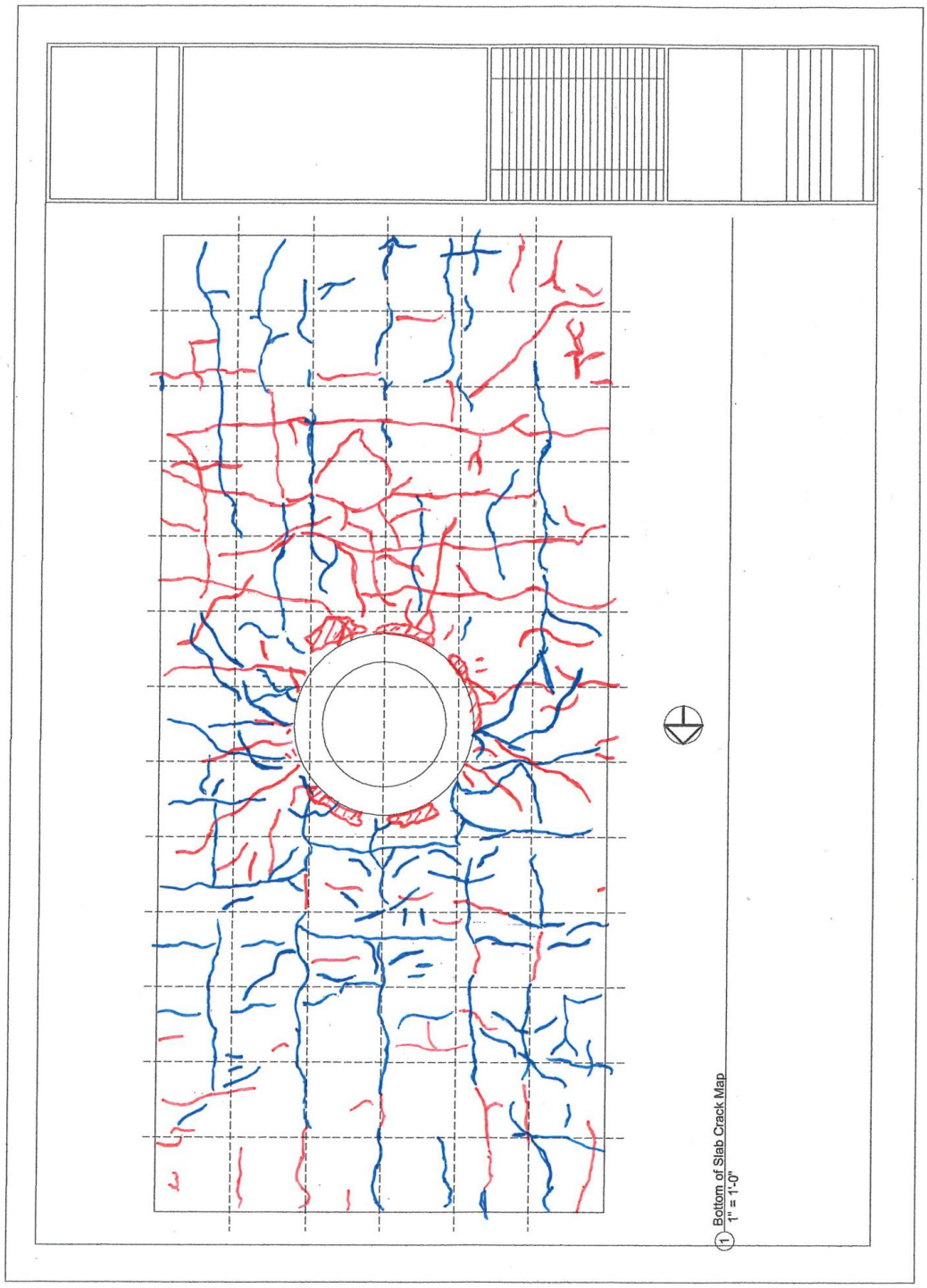

Figure 28: Bottom of Slab Crack Map– 2.0/-2.0% Drift (PTB_4.5_1_0)

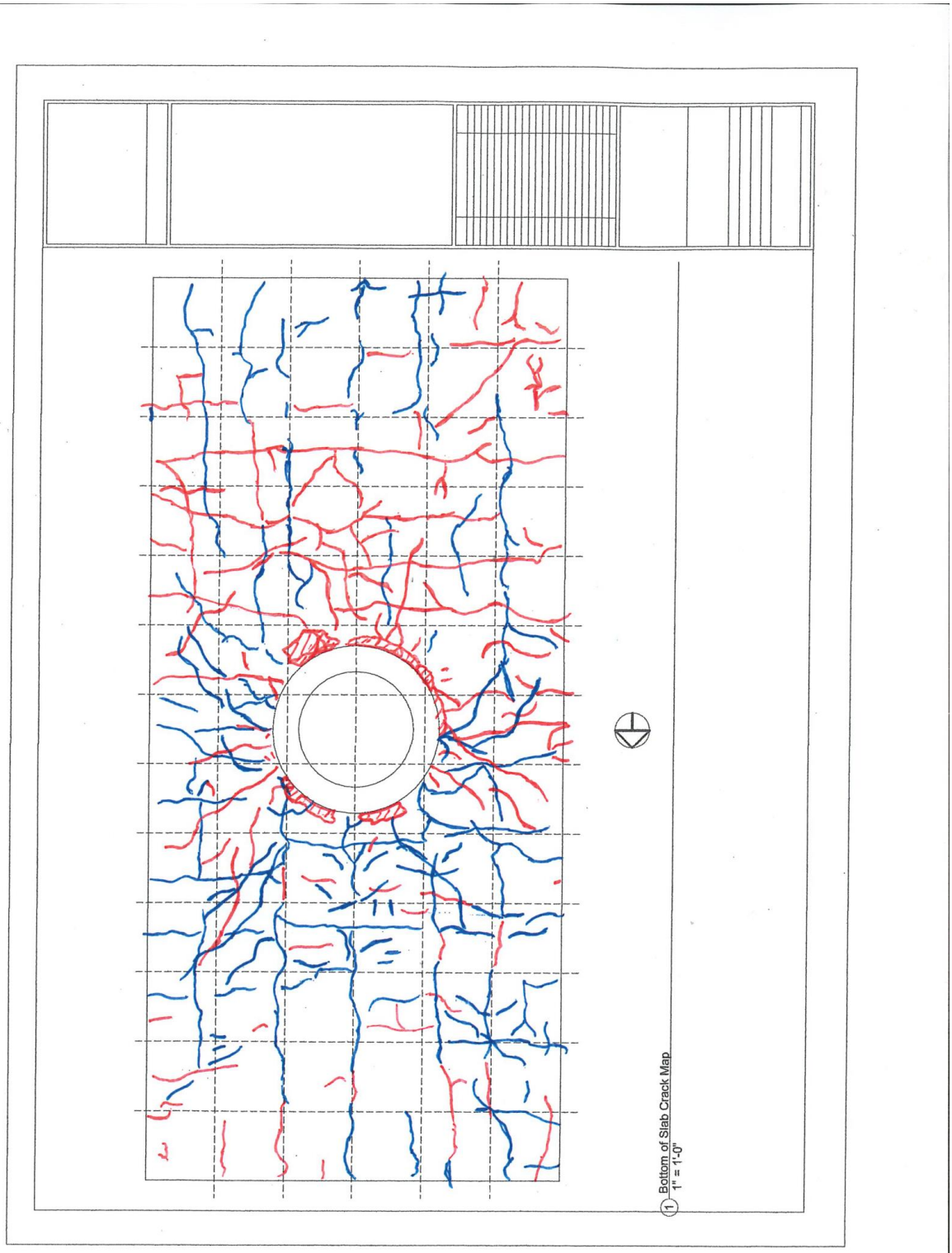

Figure 29: Bottom of Slab Crack Map– 2.6/-2.6% Drift (PTB_4.5_1_0)

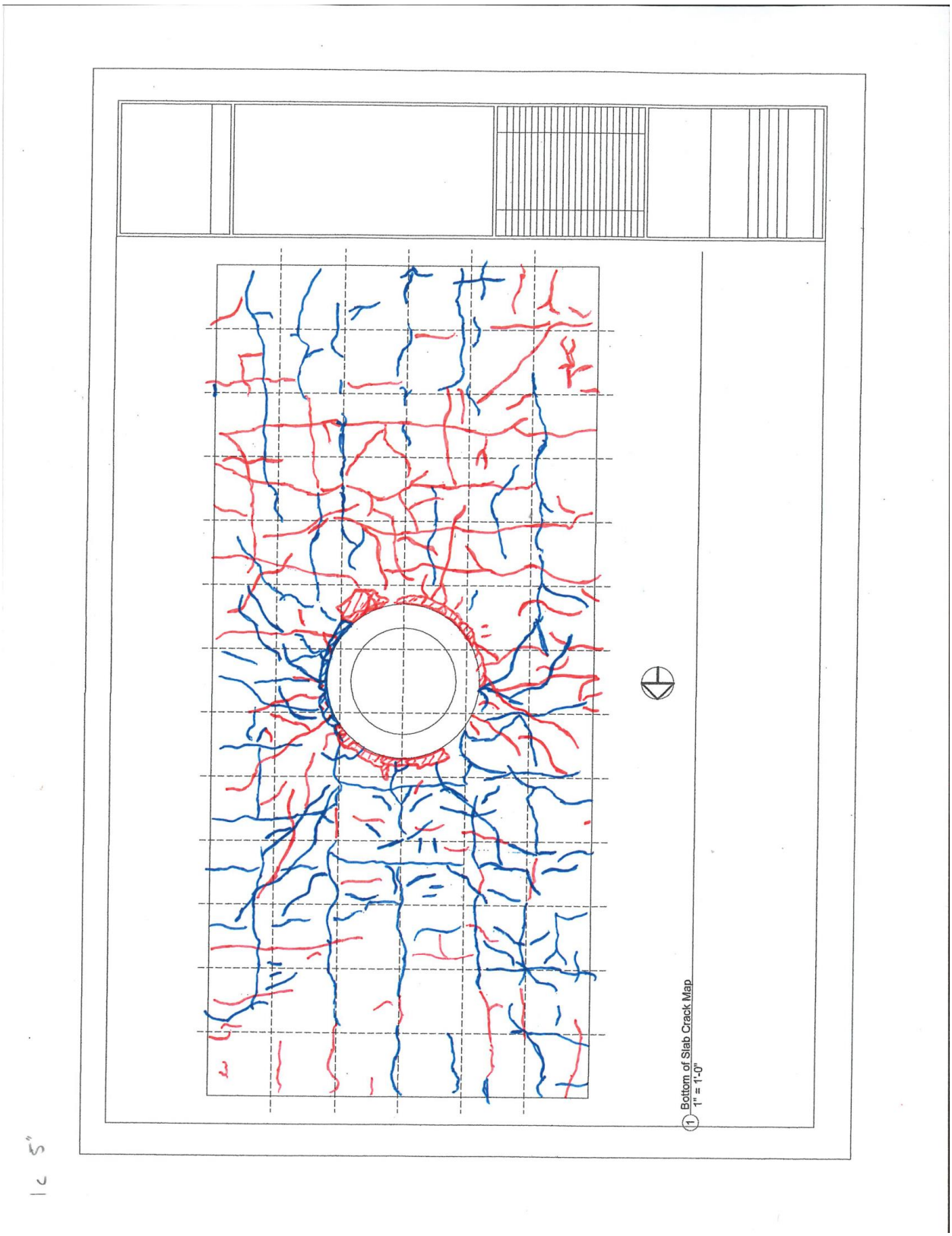

Figure 30: Bottom of Slab Crack Map– 3.4/-3.3% Drift (PTB_4.5_1_0)

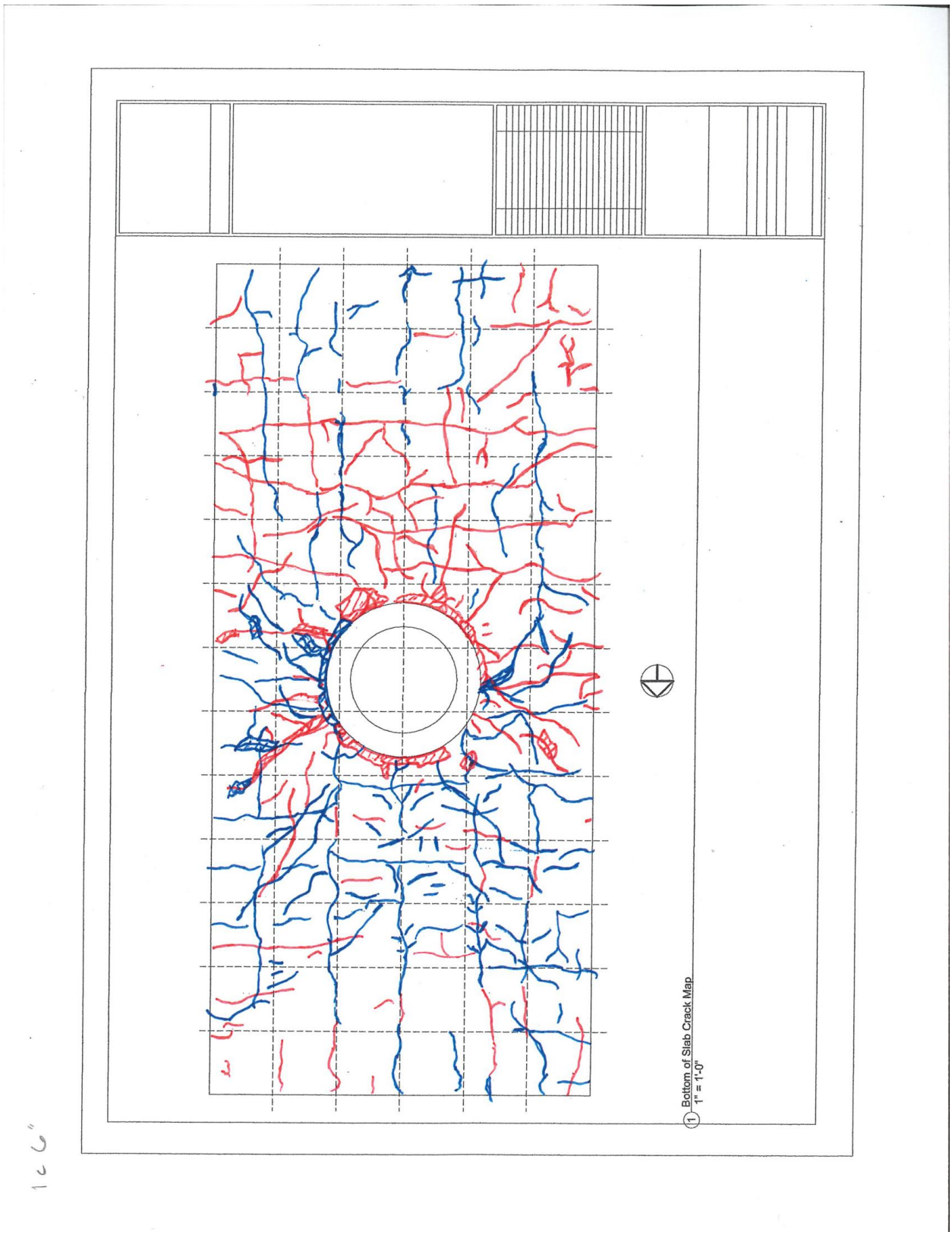

Figure 31: Bottom of Slab Crack Map– 4.1/-4.0% Drift (PTB_4.5_1_0)

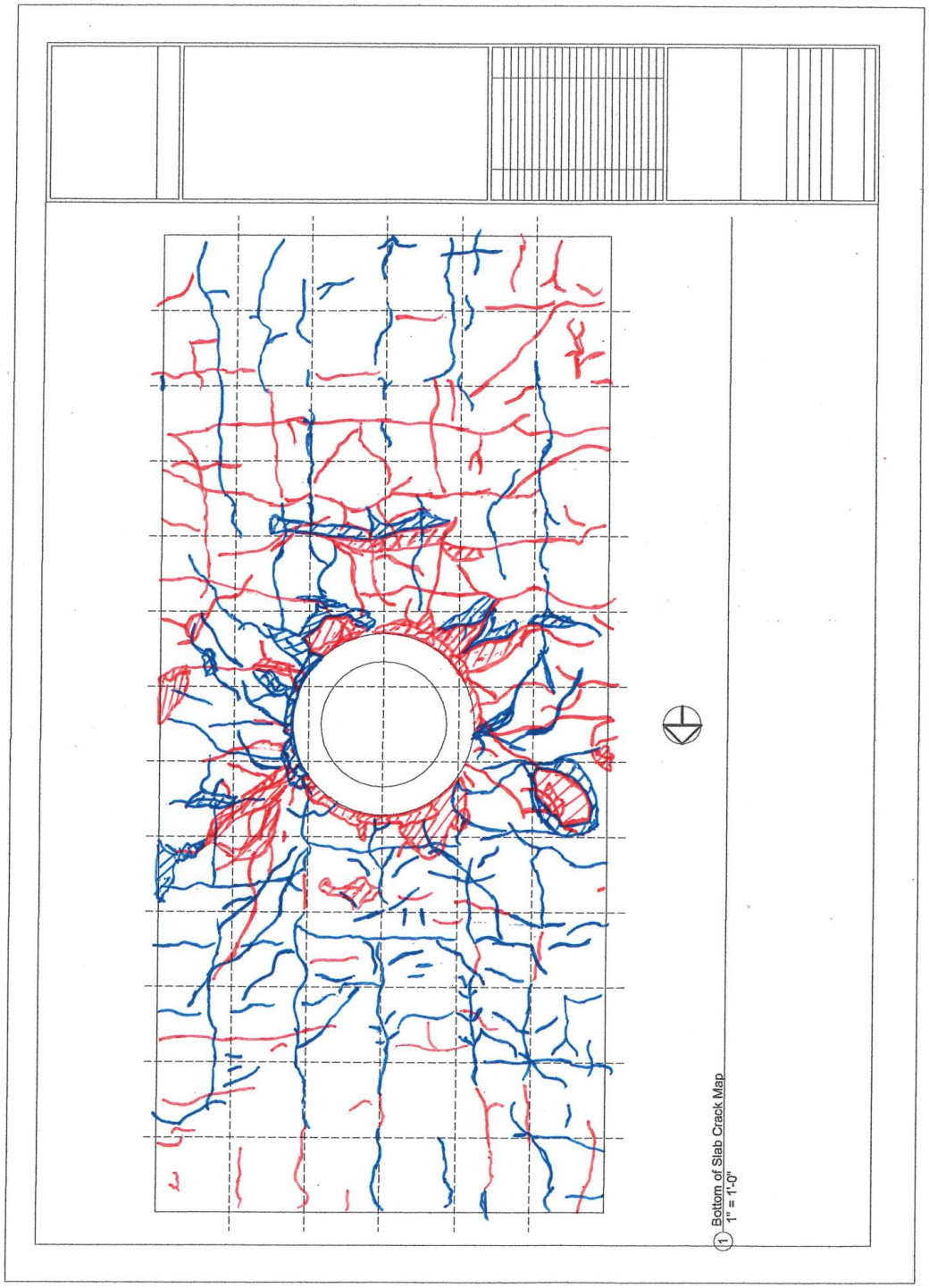

Figure 32: Bottom of Slab Crack Map– 4.8/-4.8% Drift (PTB_4.5_1_0)

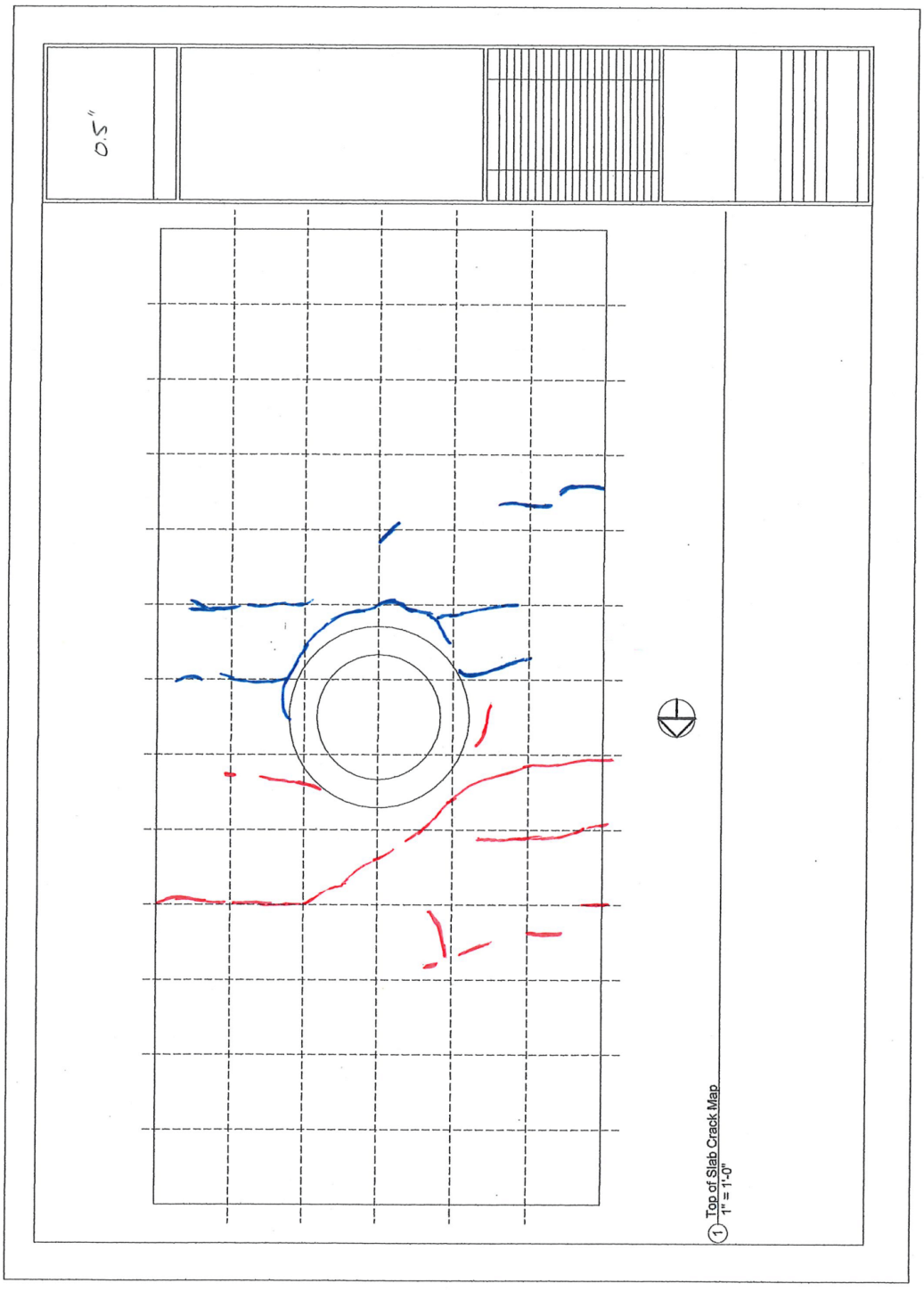

Figure 33: Top of Slab Crack Map– 0.34/-0.49% Drift (PTB_4.5_1_4)

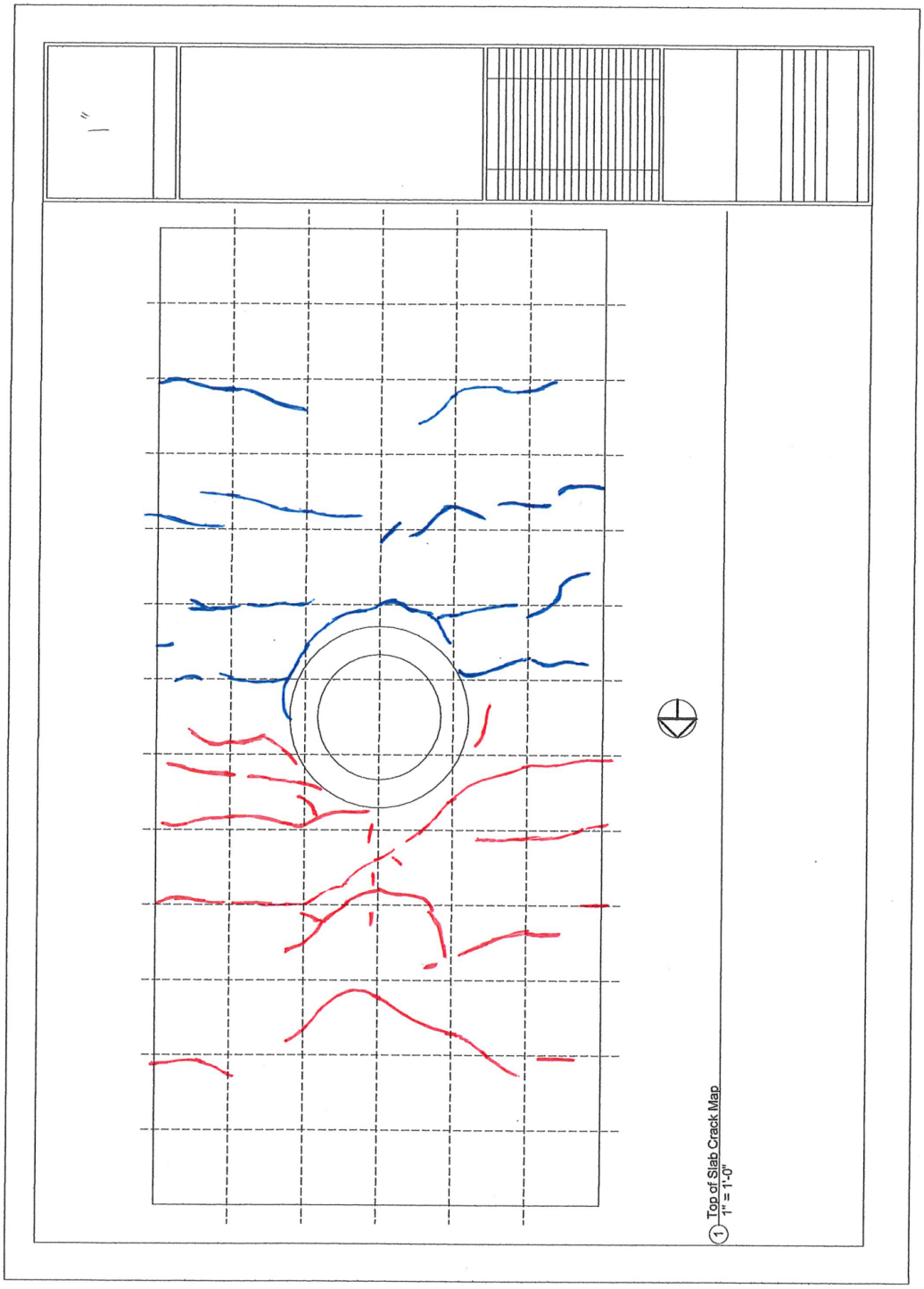

Figure 34: Top of Slab Crack Map– 0.56/-0.71% Drift (PTB_4.5_1_4)

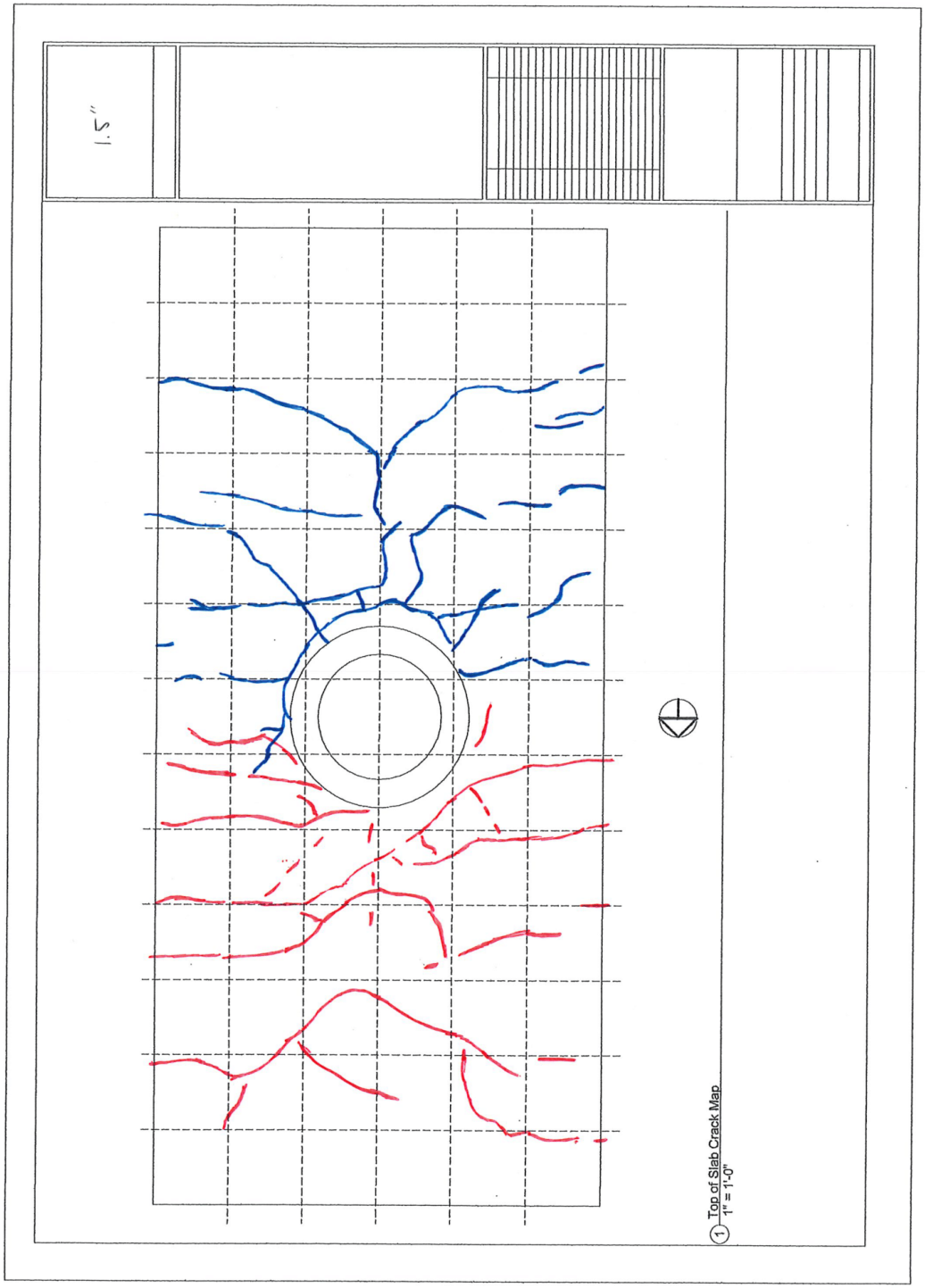

Figure 35: Top of Slab Crack Map– 0.91/-1.1% Drift (PTB_4.5_1_4)

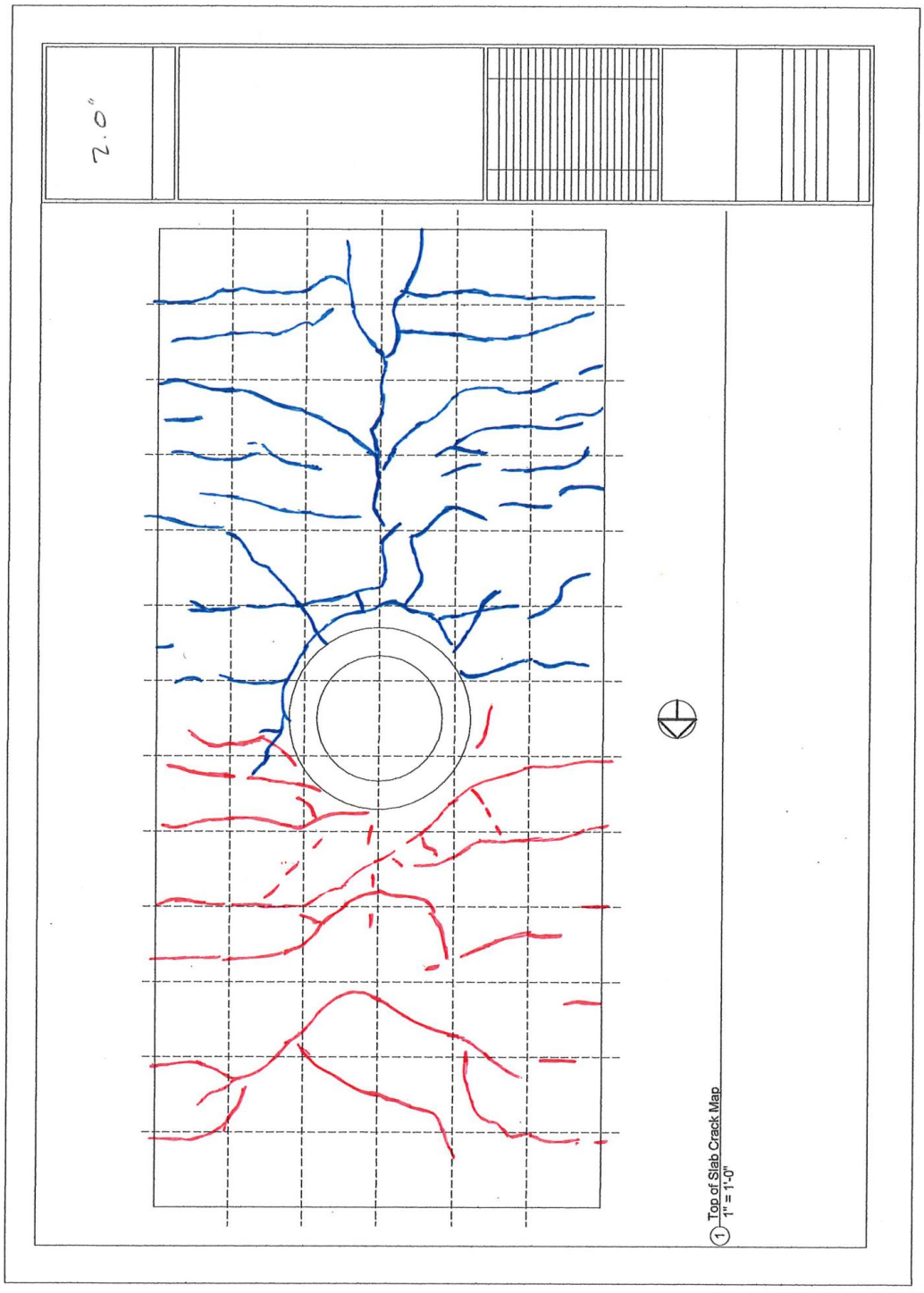

Figure 36: Top of Slab Crack Map– 1.2/-1.4% Drift (PTB_4.5_1_4)

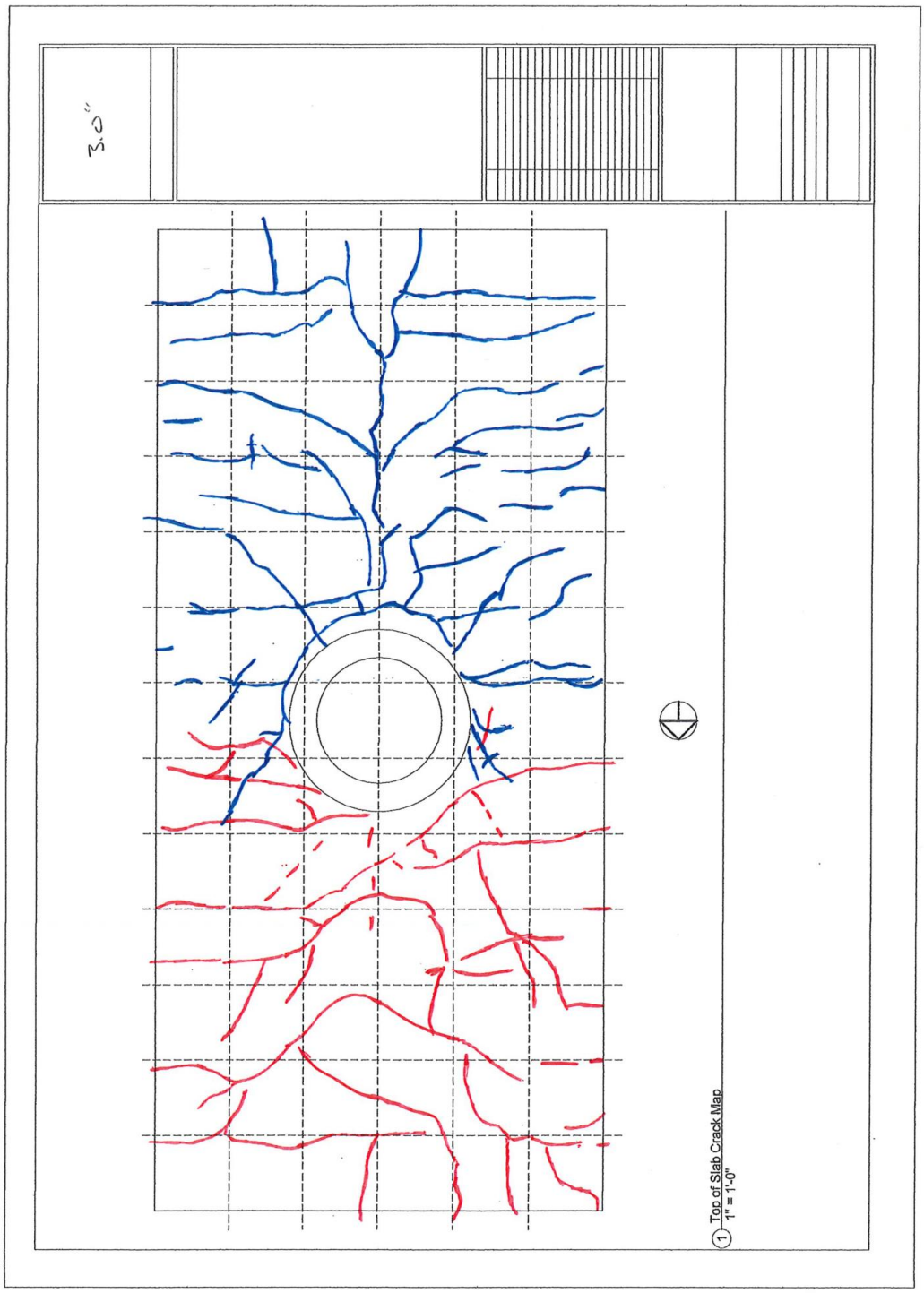

Figure 37: Top of Slab Crack Map– 1.9/-2.0% Drift (PTB_4.5_1_4)

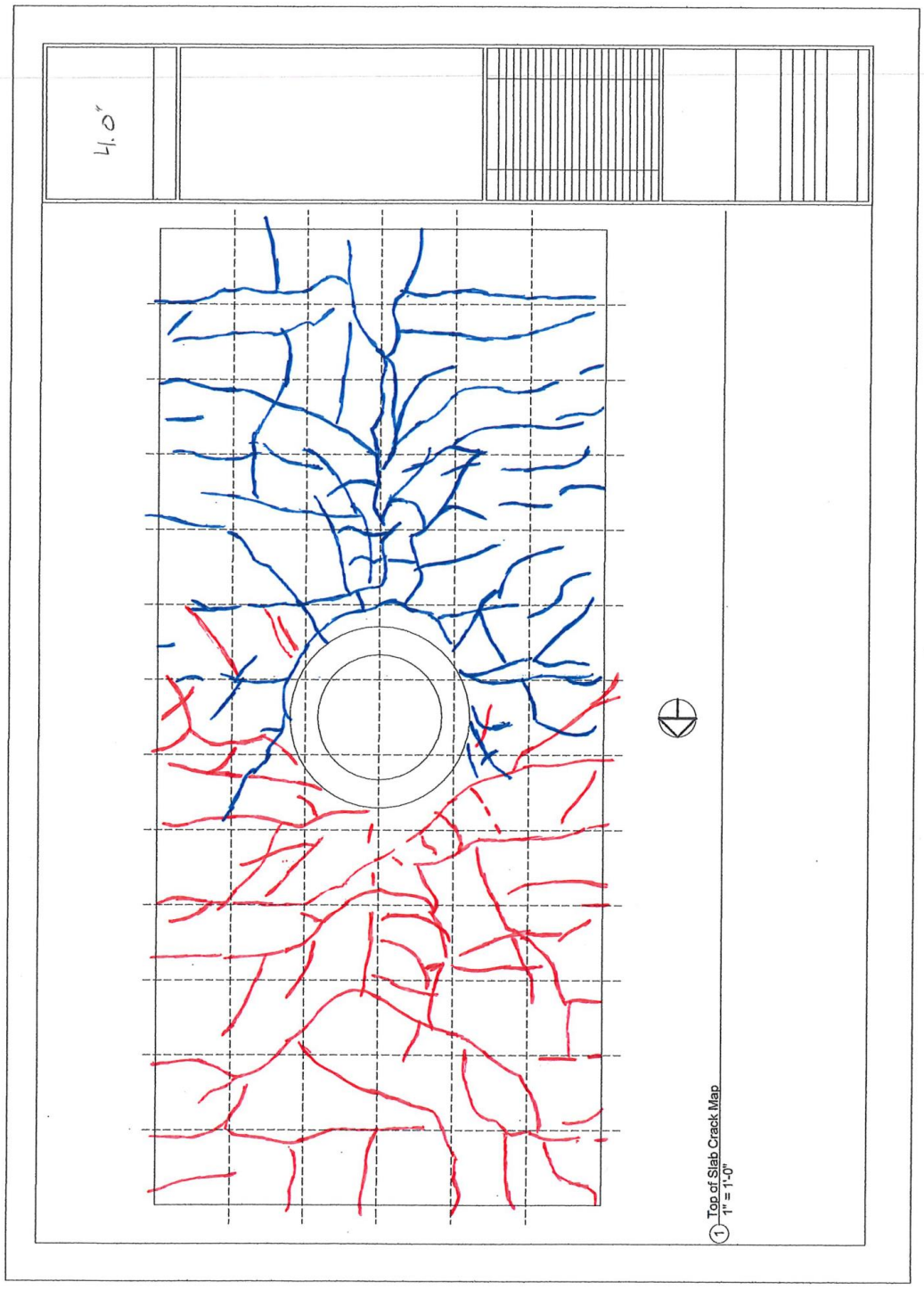

Figure 38: Top of Slab Crack Map– 2.6/-2.8% Drift (PTB_4.5_1_4)

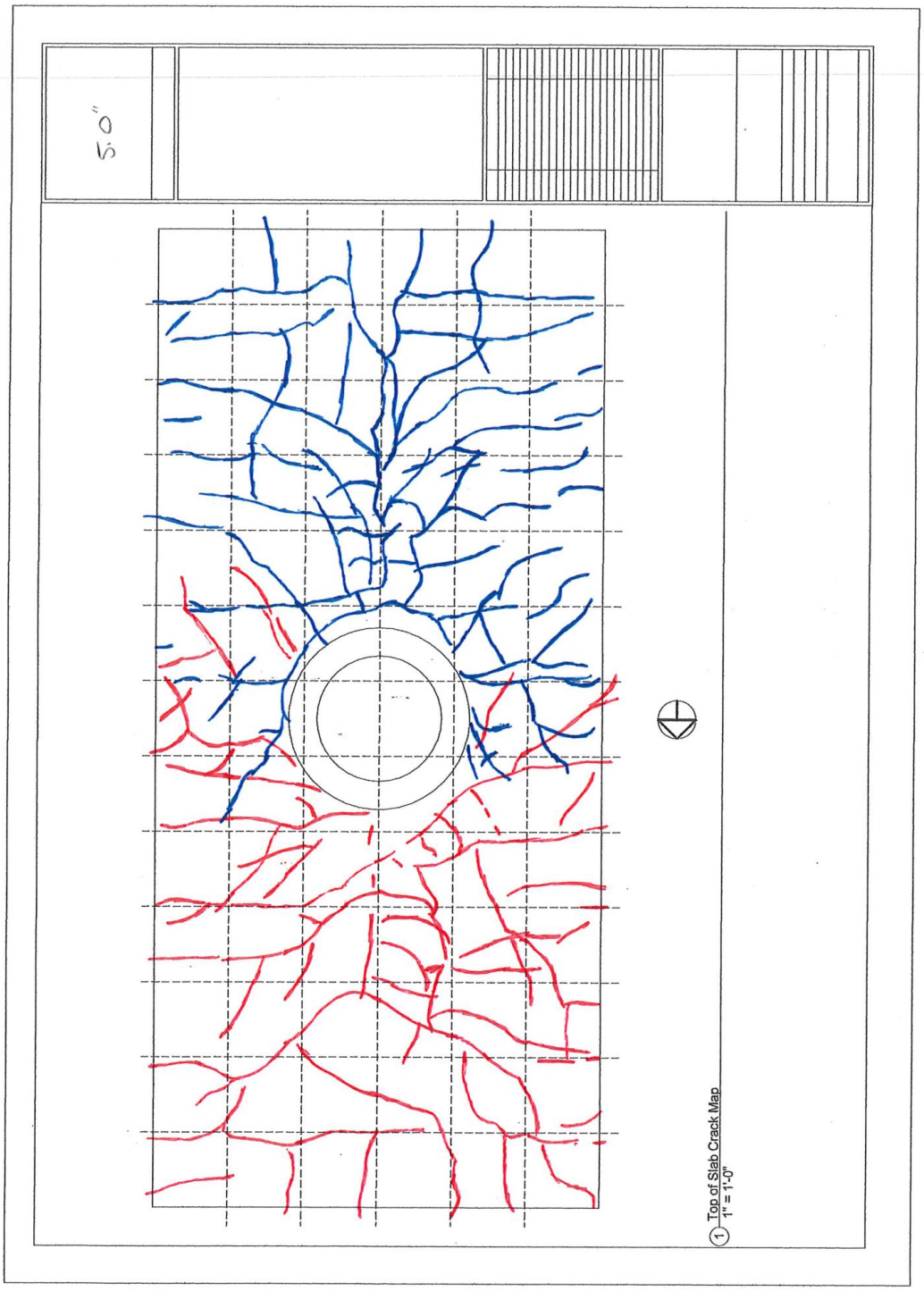

Figure 39: Top of Slab Crack Map– 3.4/-3.5% Drift (PTB_4.5_1_4)

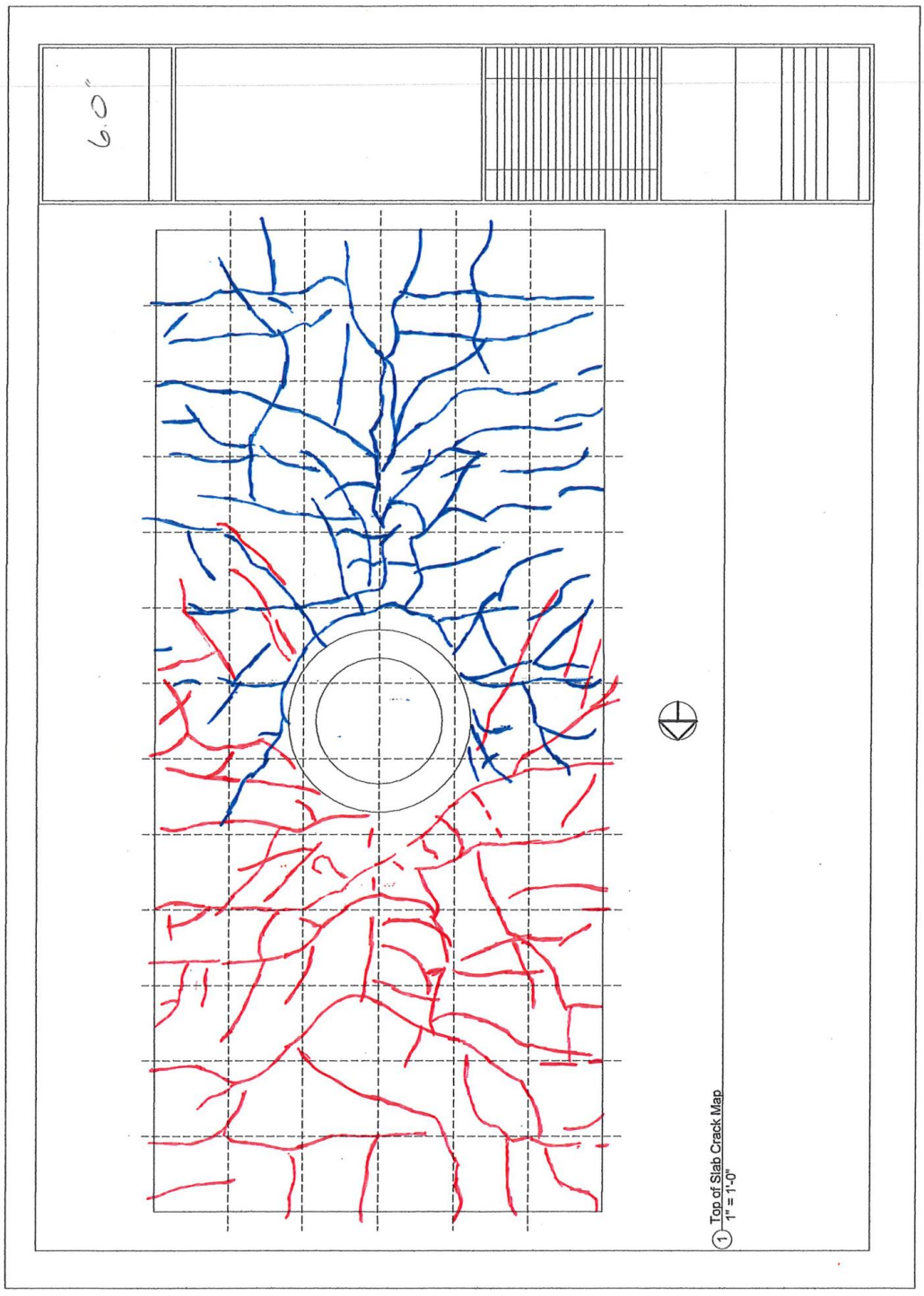

Figure 40: Top of Slab Crack Map– 4.1/-4.2% Drift (PTB_4.5_1_4)

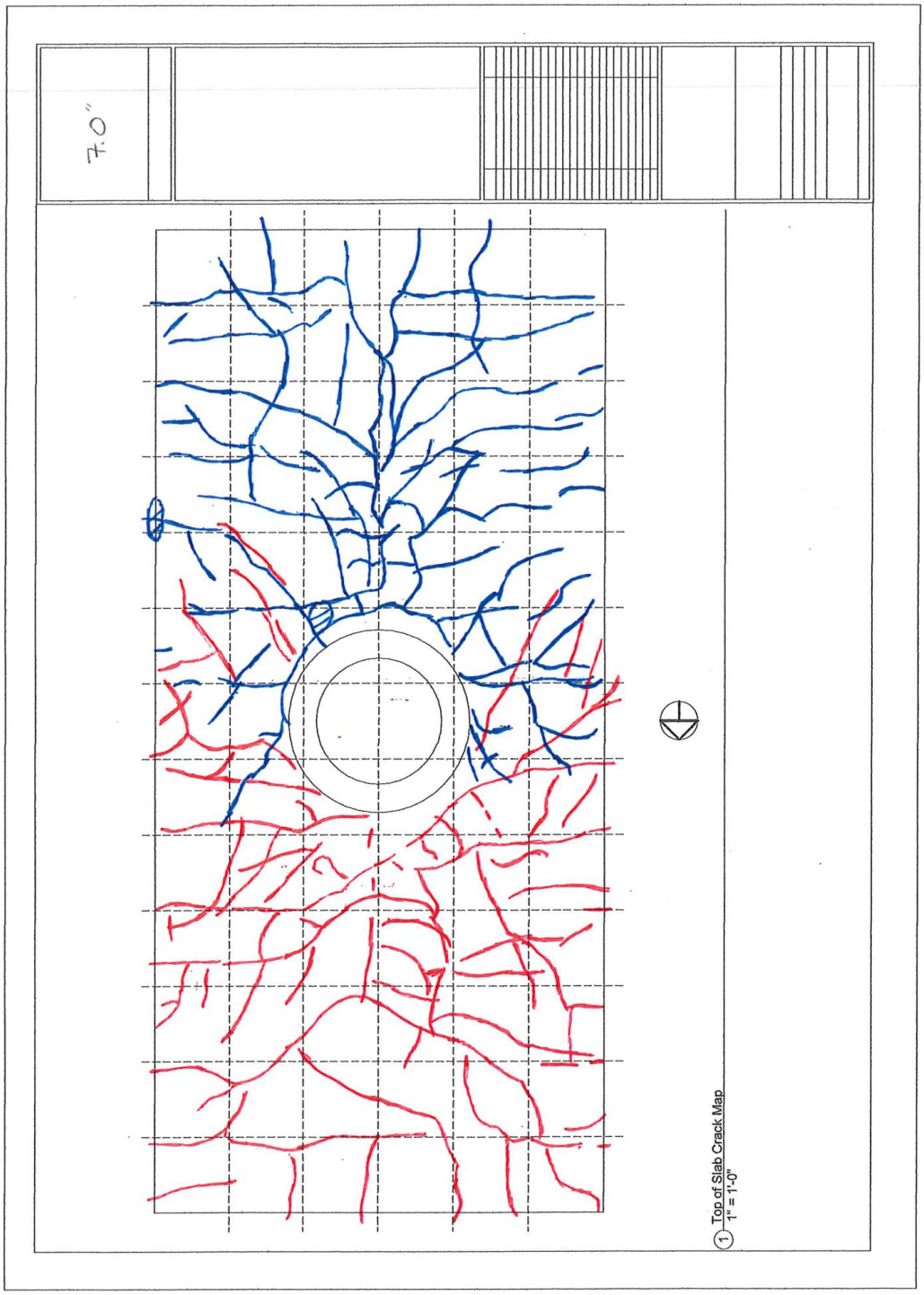

Figure 41: Top of Slab Crack Map– 4.8/-4.9% Drift (PTB_4.5_1_4)

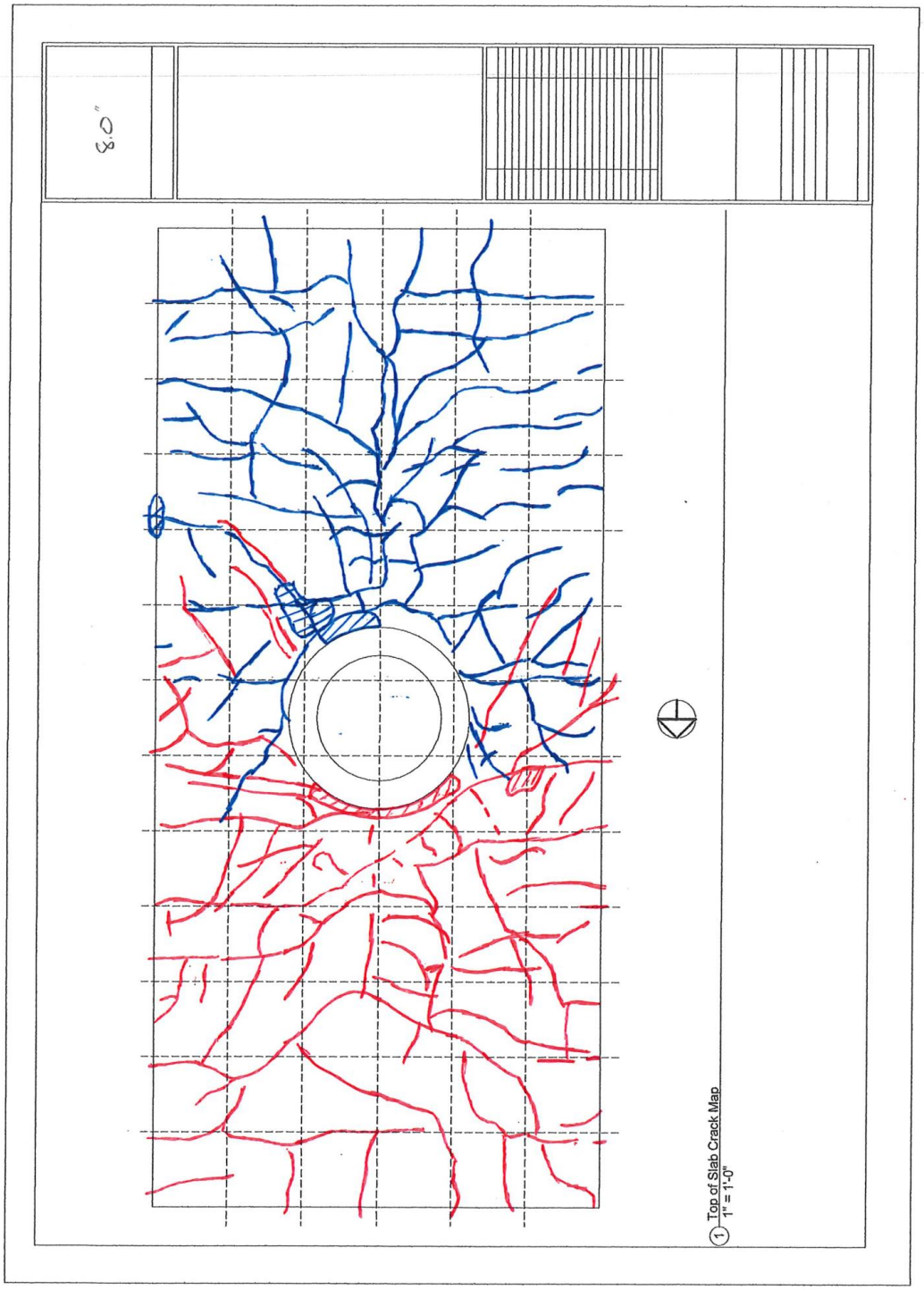

Figure 42: Top of Slab Crack Map– 5.5/-5.6% Drift (PTB_4.5_1_4)

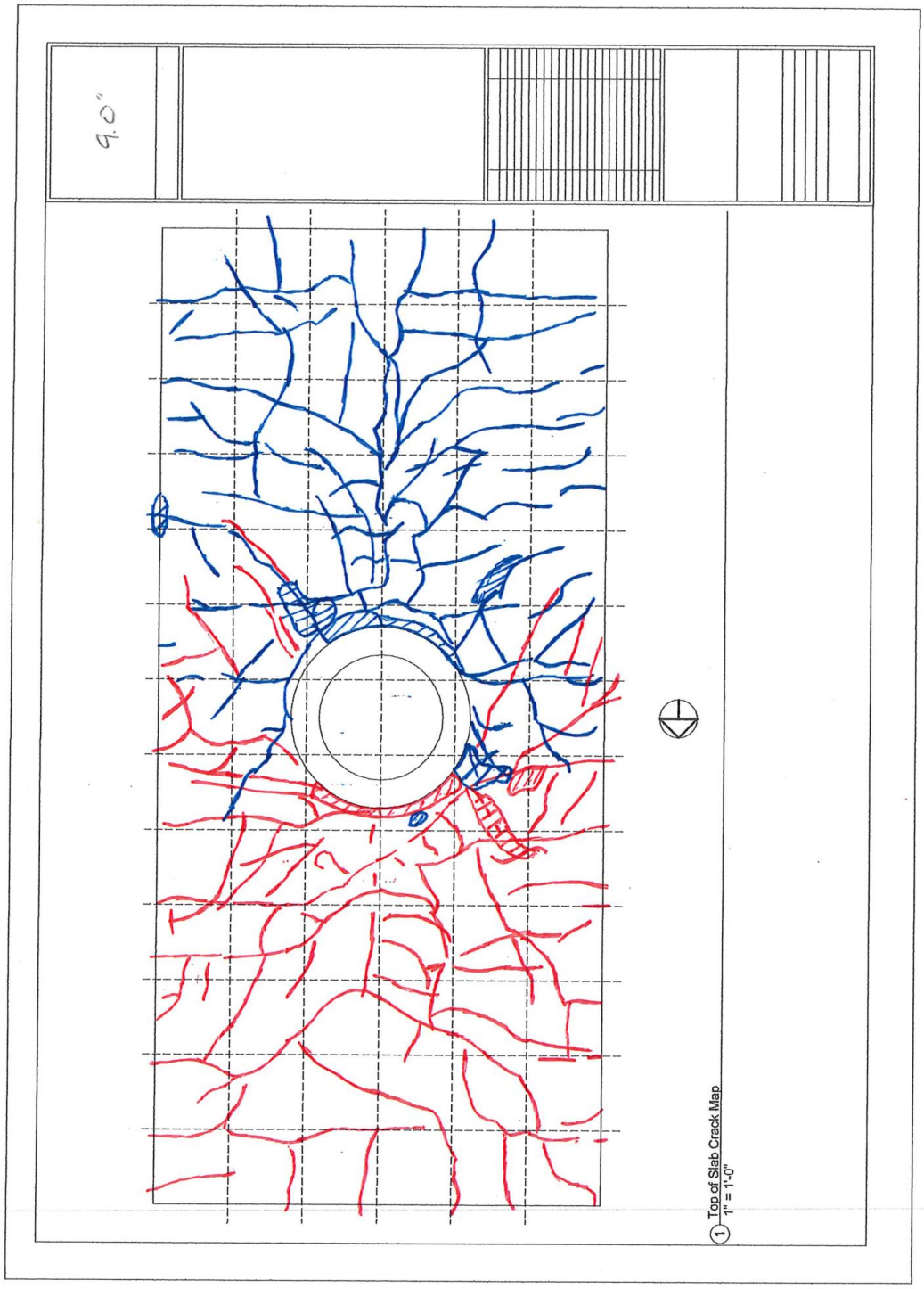

Figure 43: Top of Slab Crack Map– 6.3/-6.3% Drift (PTB_4.5_1_4)

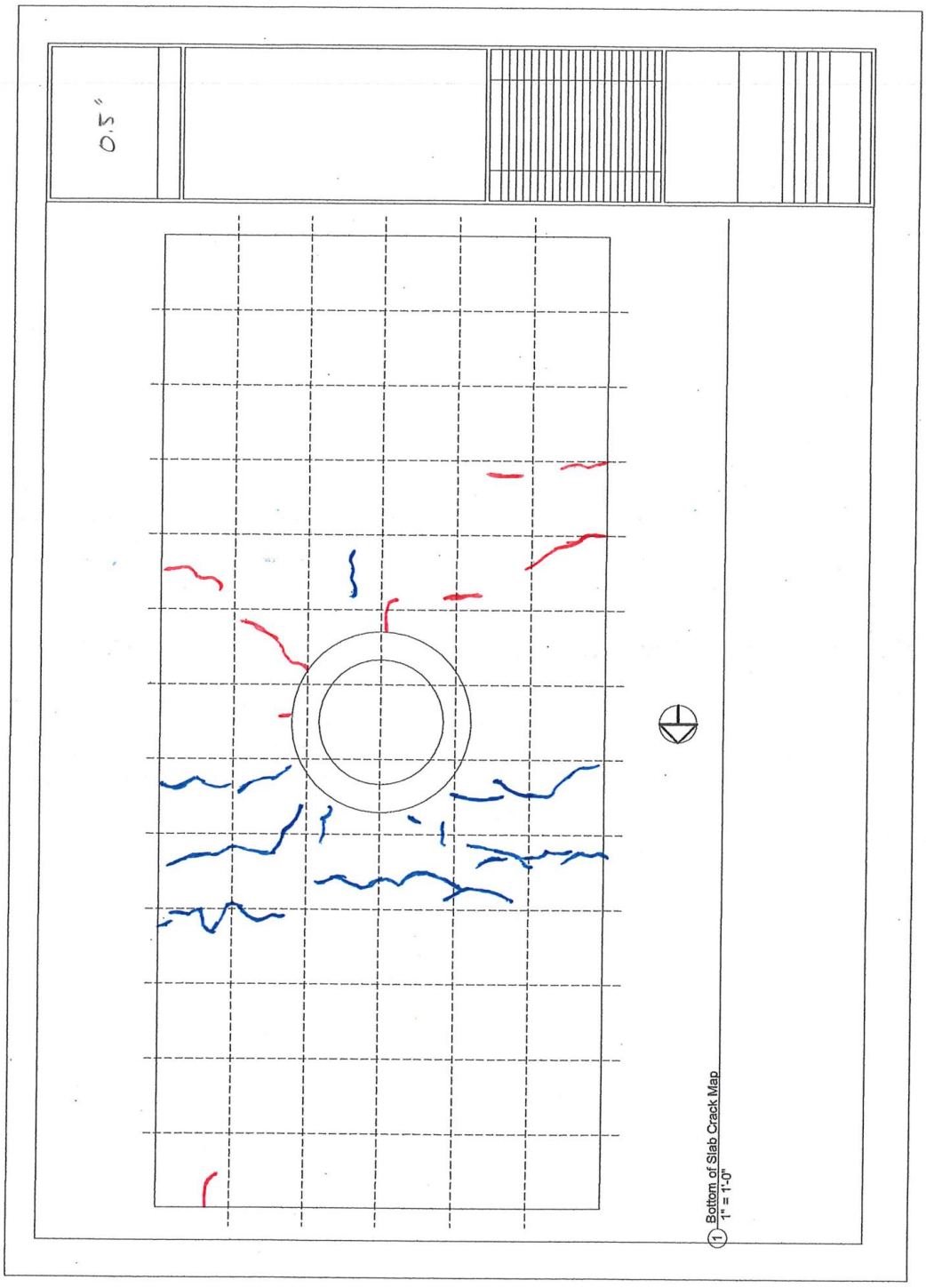

Figure 44: Bottom of Slab Crack Map– 0.34/-0.49% Drift (PTB_4.5_1_4)

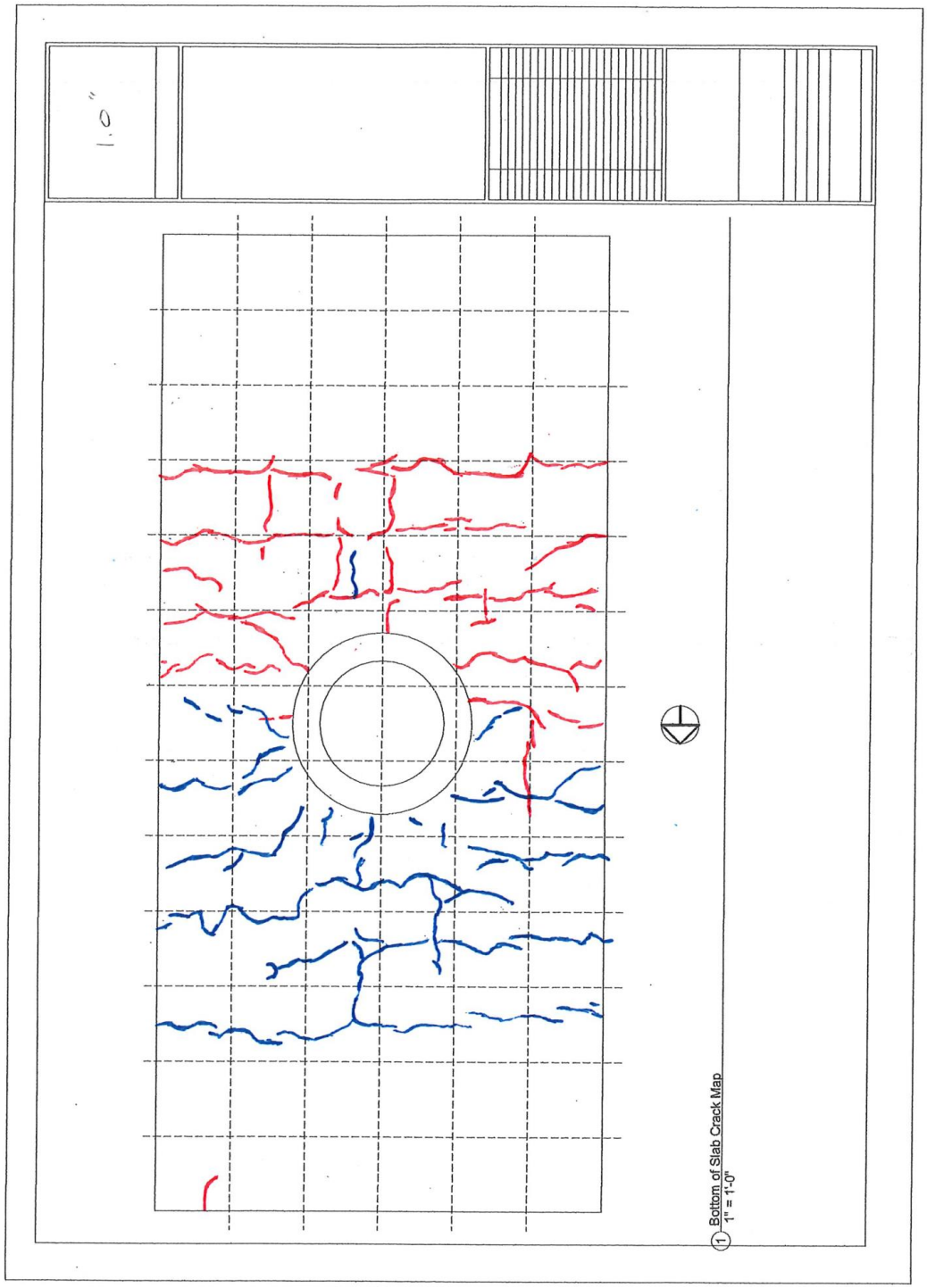

Figure 45: Bottom of Slab Crack Map– 0.56/-0.71% Drift (PTB_4.5_1_4)

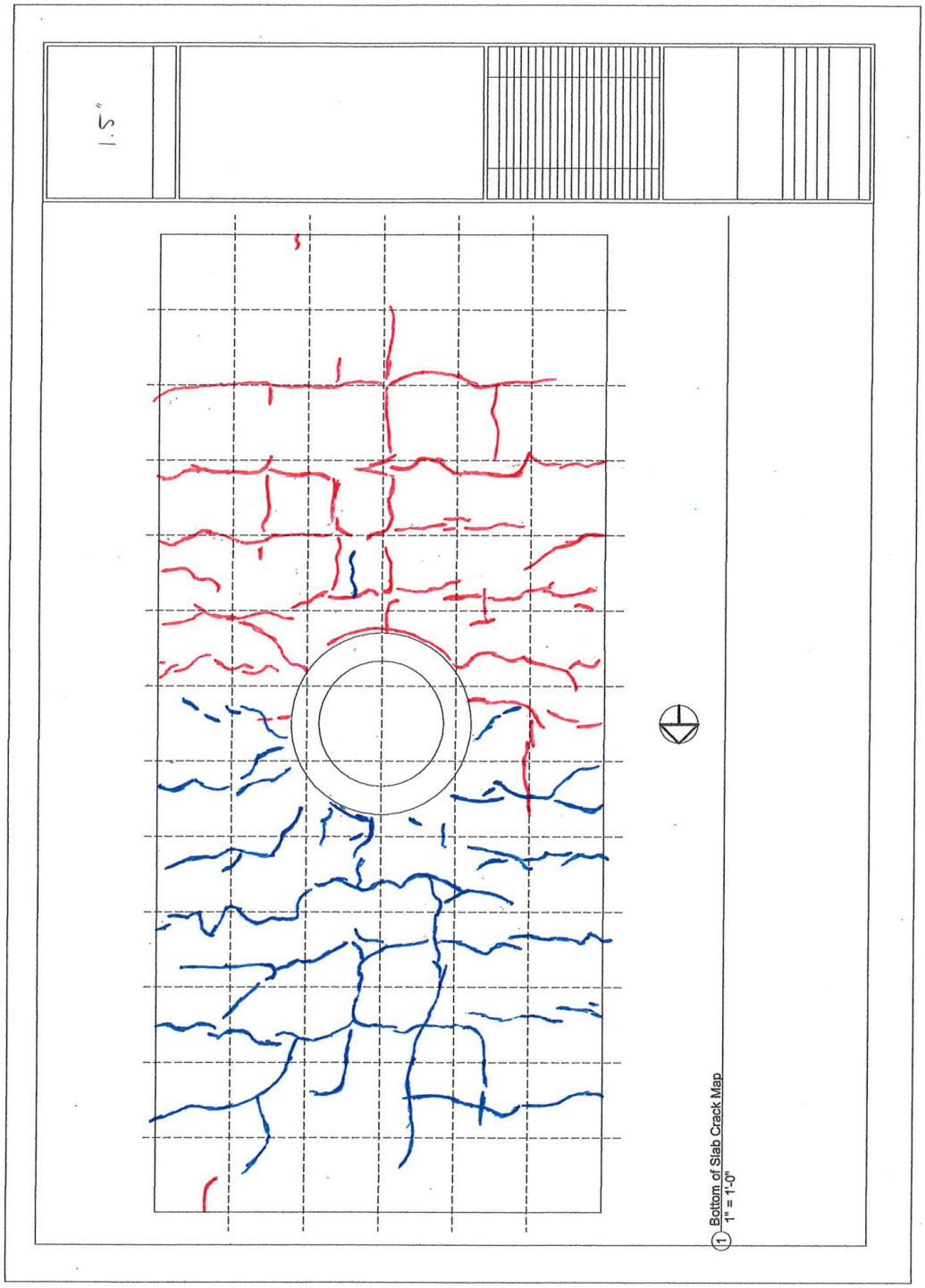

Figure 46: Bottom of Slab Crack Map– 0.91/-1.1% Drift (PTB_4.5_1_4)

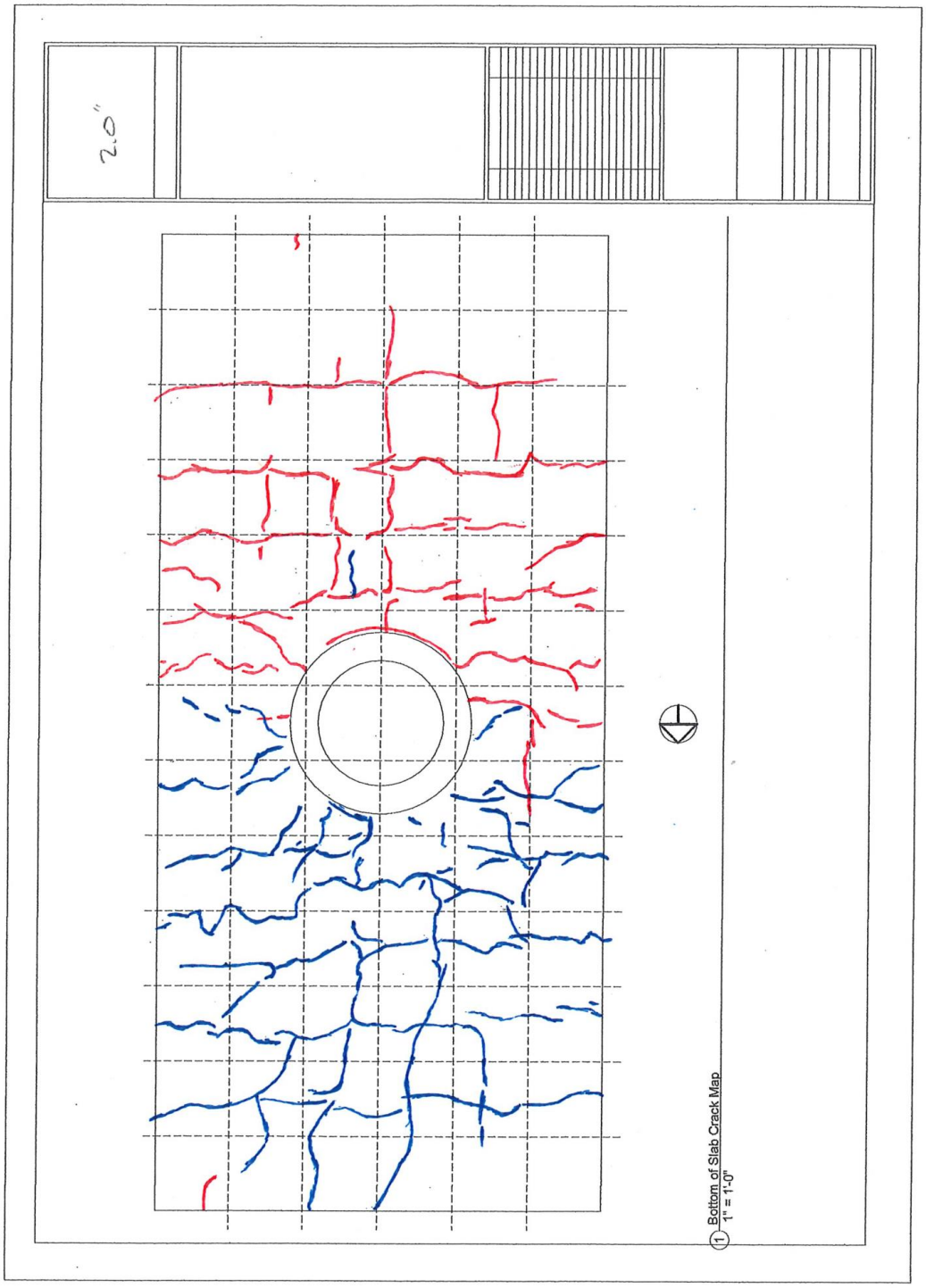

Figure 47: Bottom of Slab Crack Map– 1.2/-1.4% Drift (PTB_4.5_1_4)

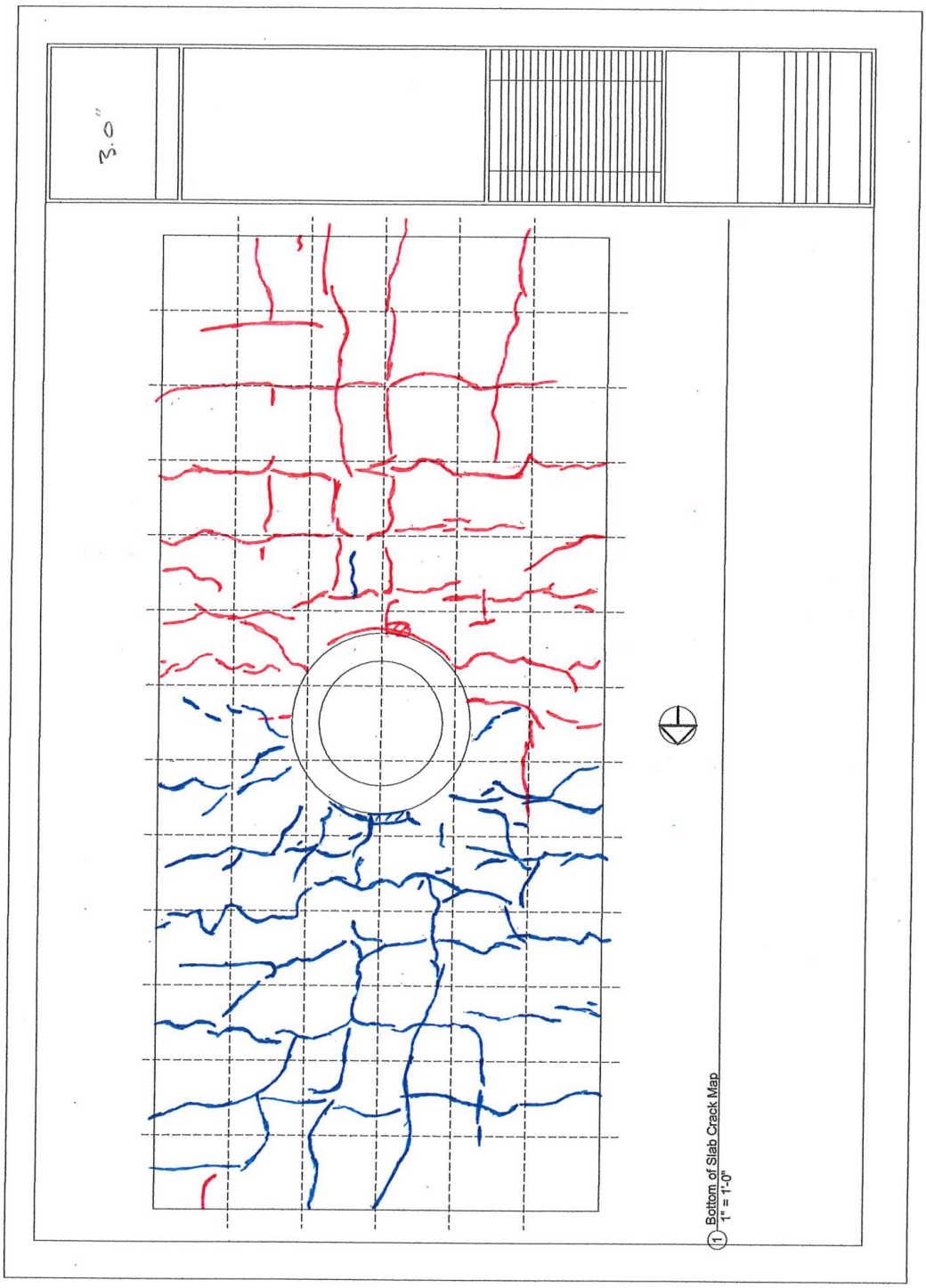

Figure 48: Bottom of Slab Crack Map– 1.9/-2.0% Drift (PTB_4.5_1_4)

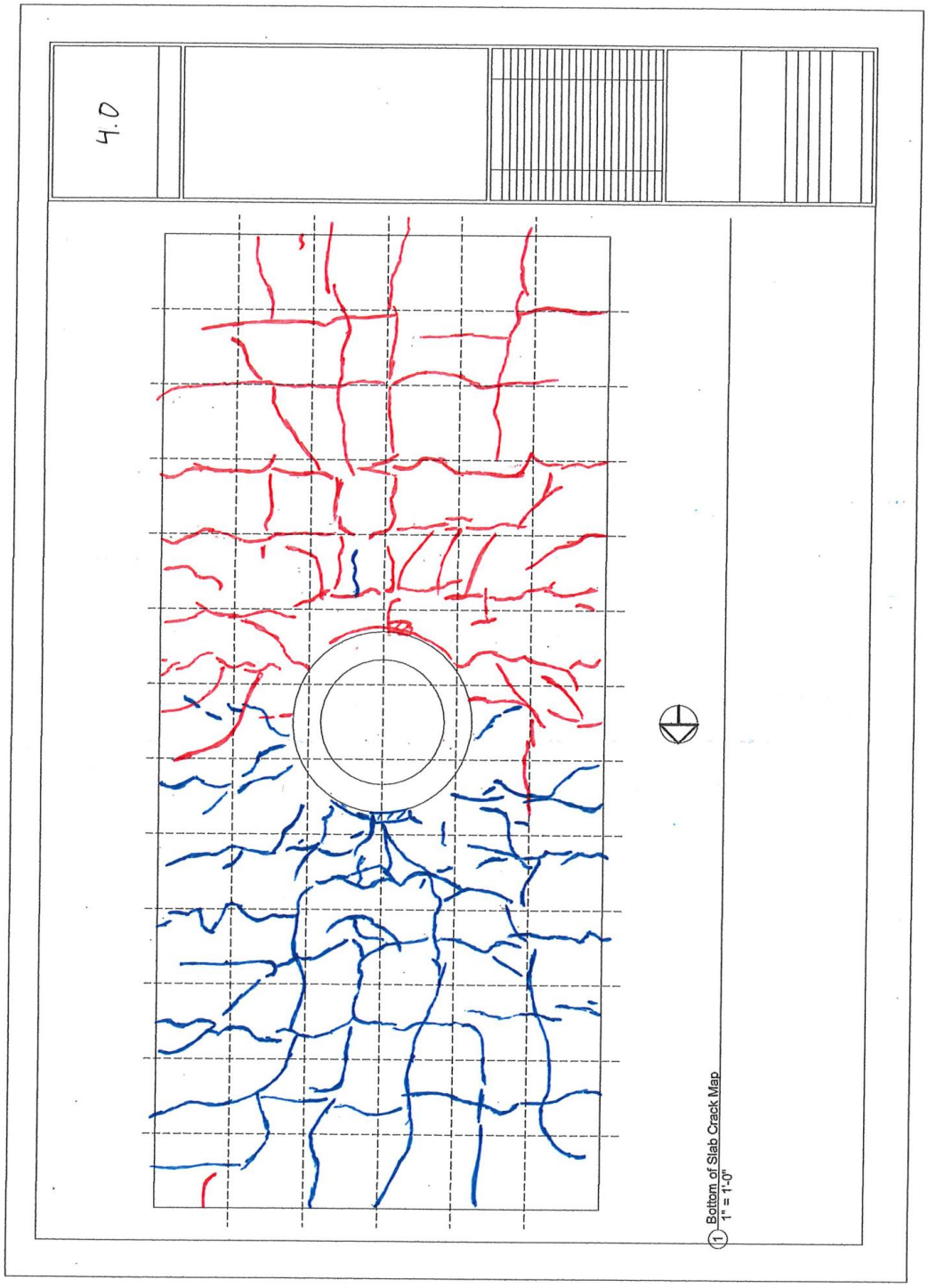

Figure 49: Bottom of Slab Crack Map– 2.6/-2.8% Drift (PTB_4.5_1_4)

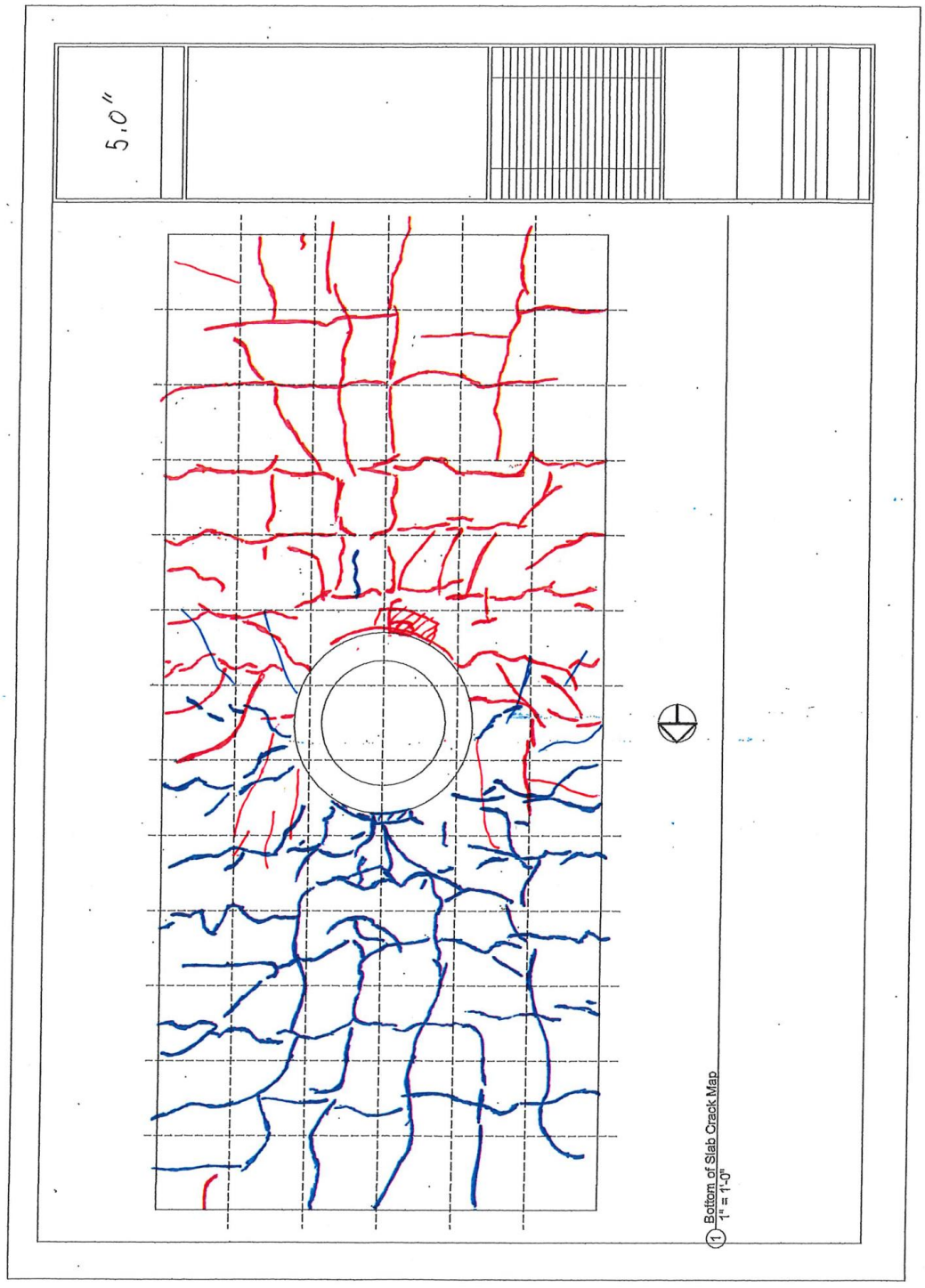

Figure 50: Bottom of Slab Crack Map– 3.4/-3.5% Drift (PTB_4.5_1_4)

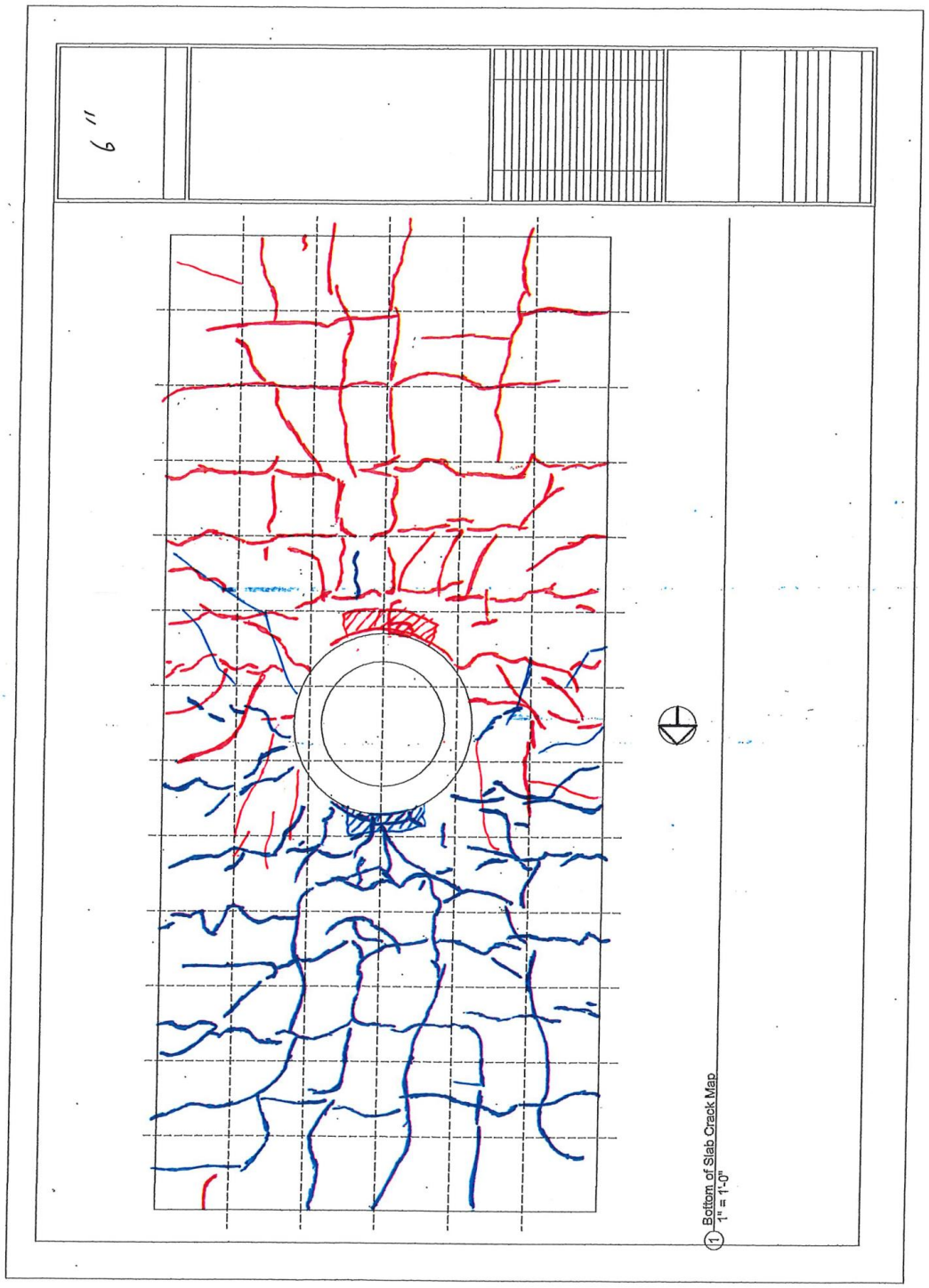

Figure 51: Bottom of Slab Crack Map– 4.1/-4.2% Drift (PTB_4.5_1_4)

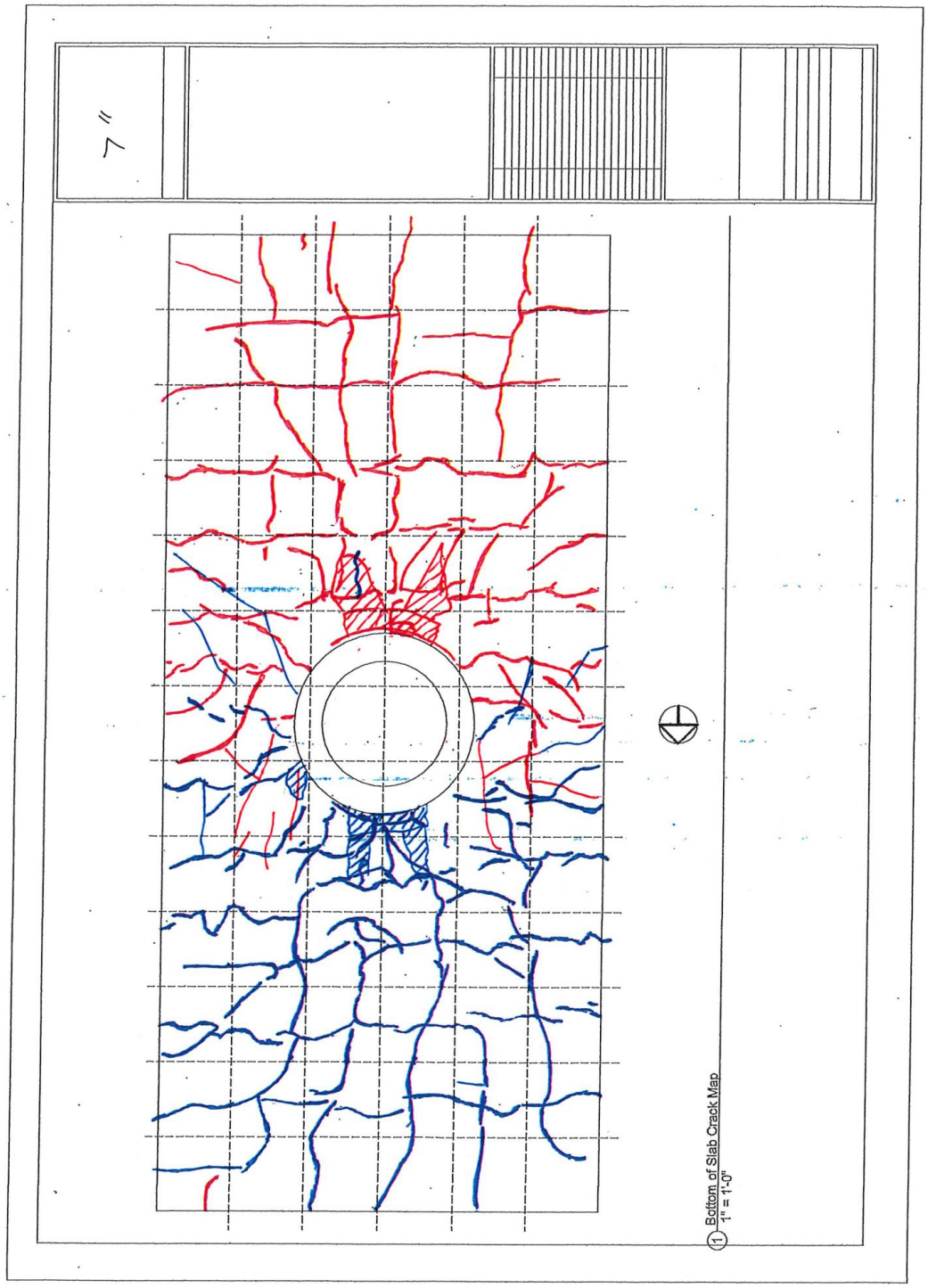

Figure 52: Bottom of Slab Crack Map– 4.8/-4.9% Drift (PTB_4.5_1_4)

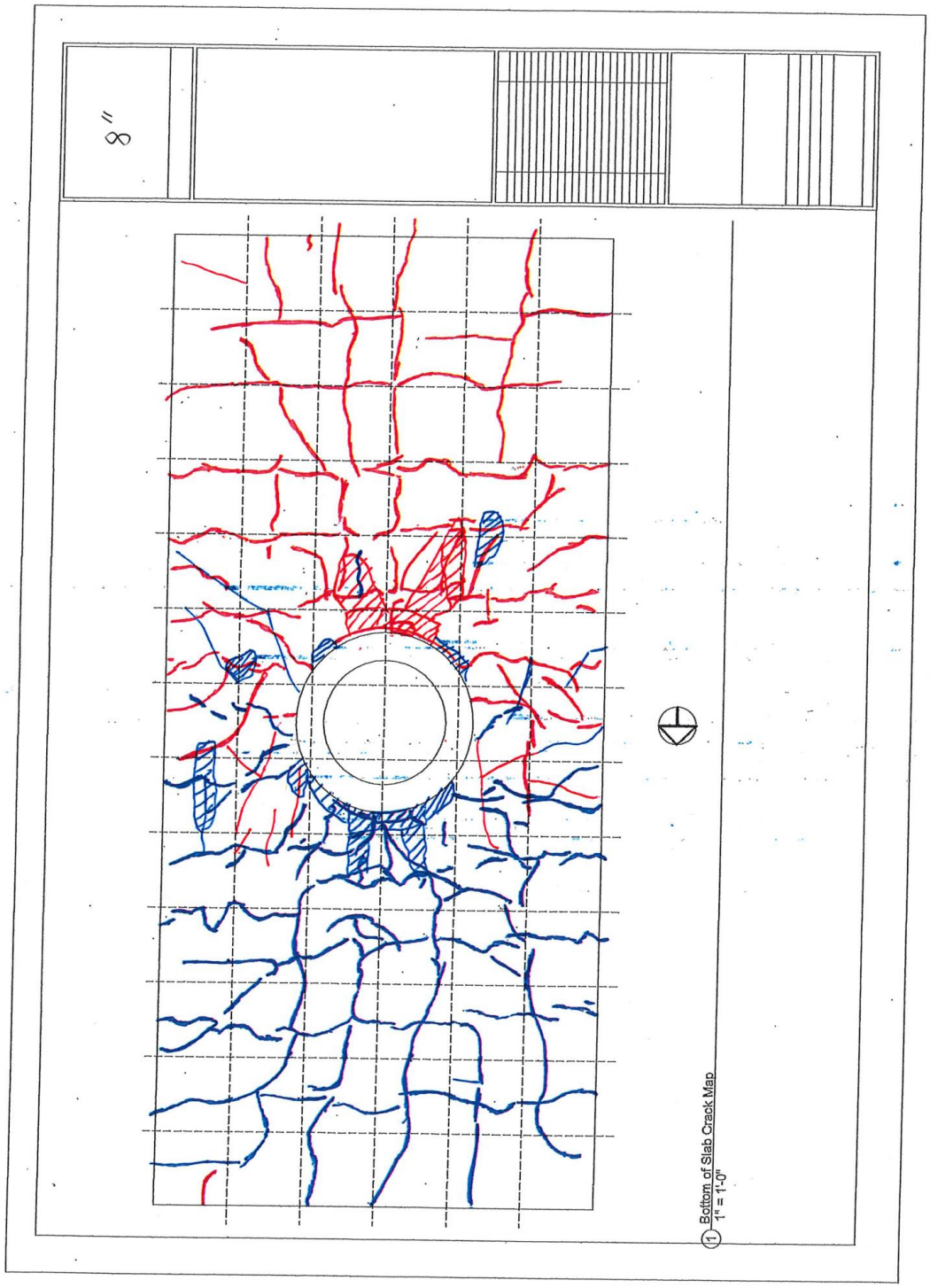

Figure 53: Bottom of Slab Crack Map– 5.5/-5.6% Drift (PTB_4.5_1_4)

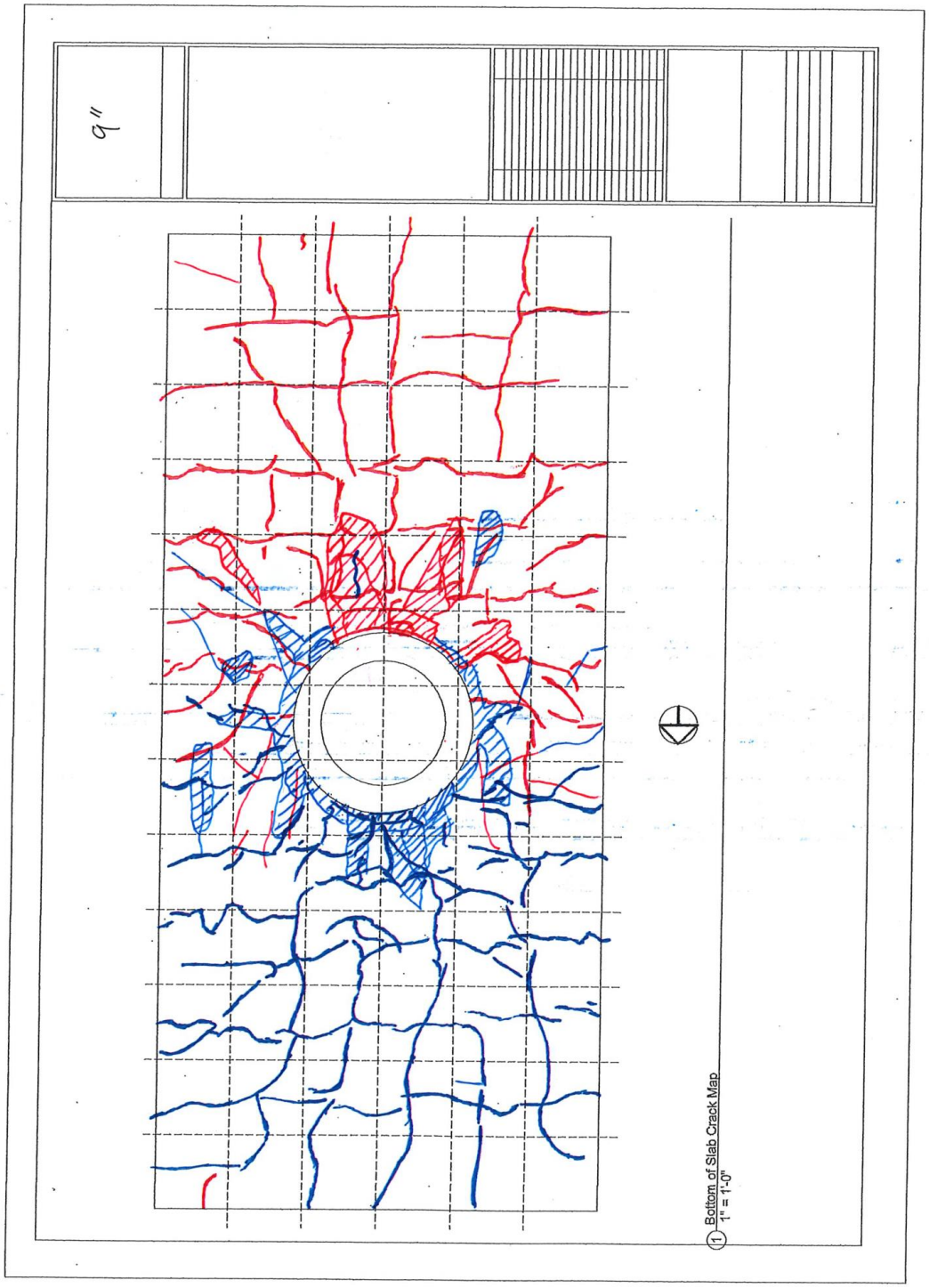

Figure 54: Bottom of Slab Crack Map– 6.3/-6.3% Drift (PTB_4.5_1_4)

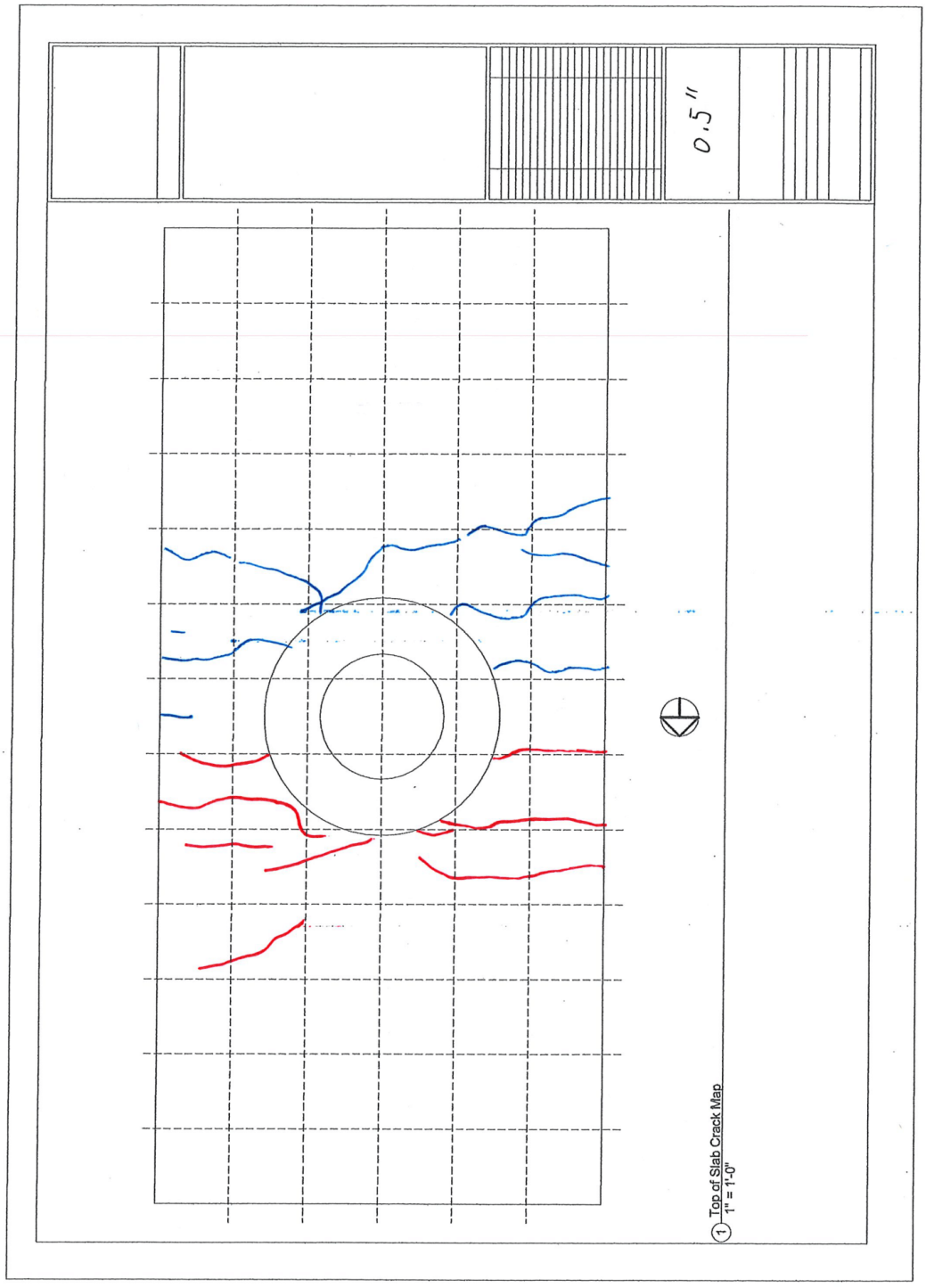

Figure 55: Top of Slab Crack Map– 0.30/-0.31% Drift (PTB_9_2_0)

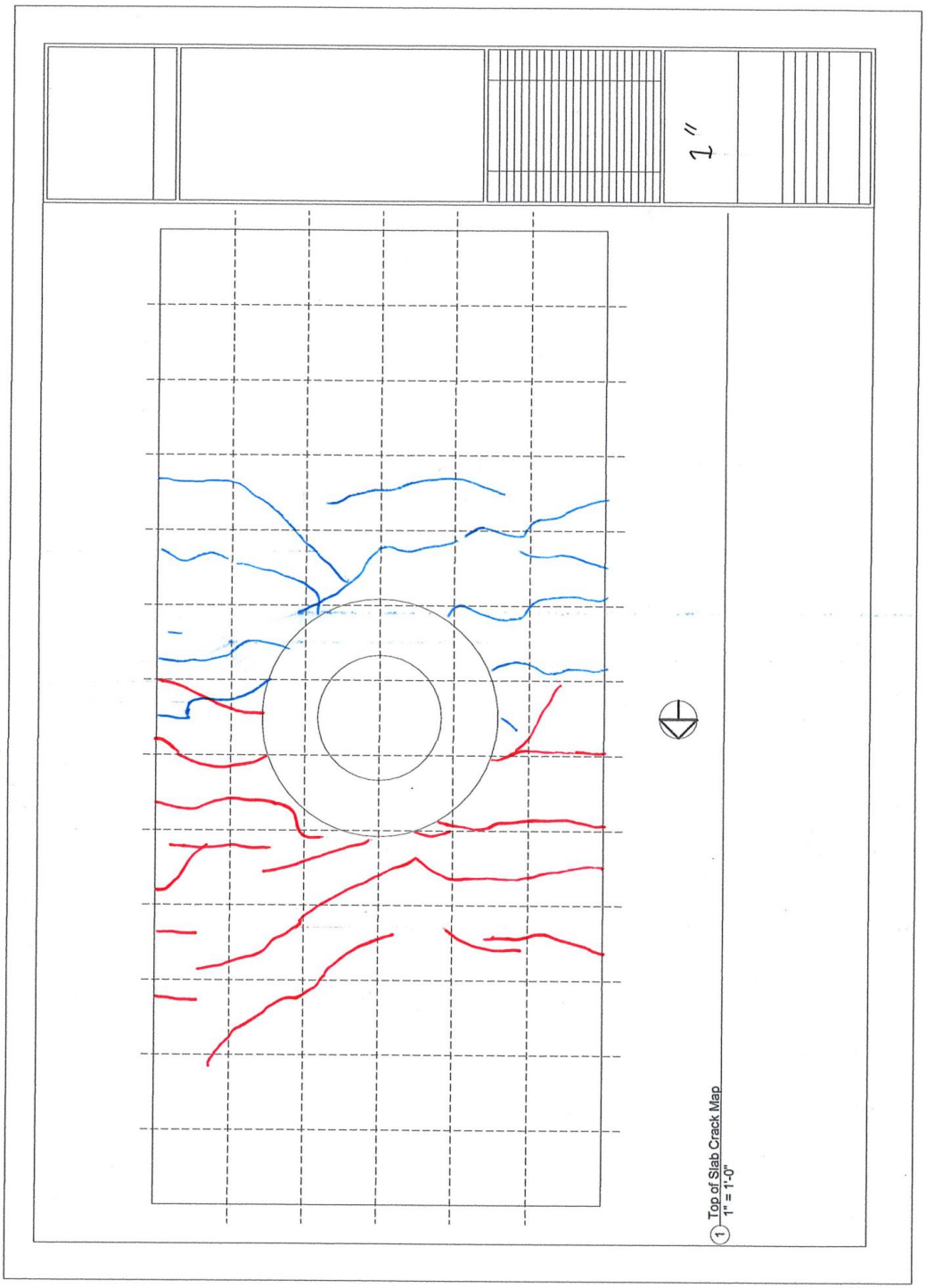

Figure 56: Top of Slab Crack Map– 0.63/-0.64% Drift (PTB_9_2_0)

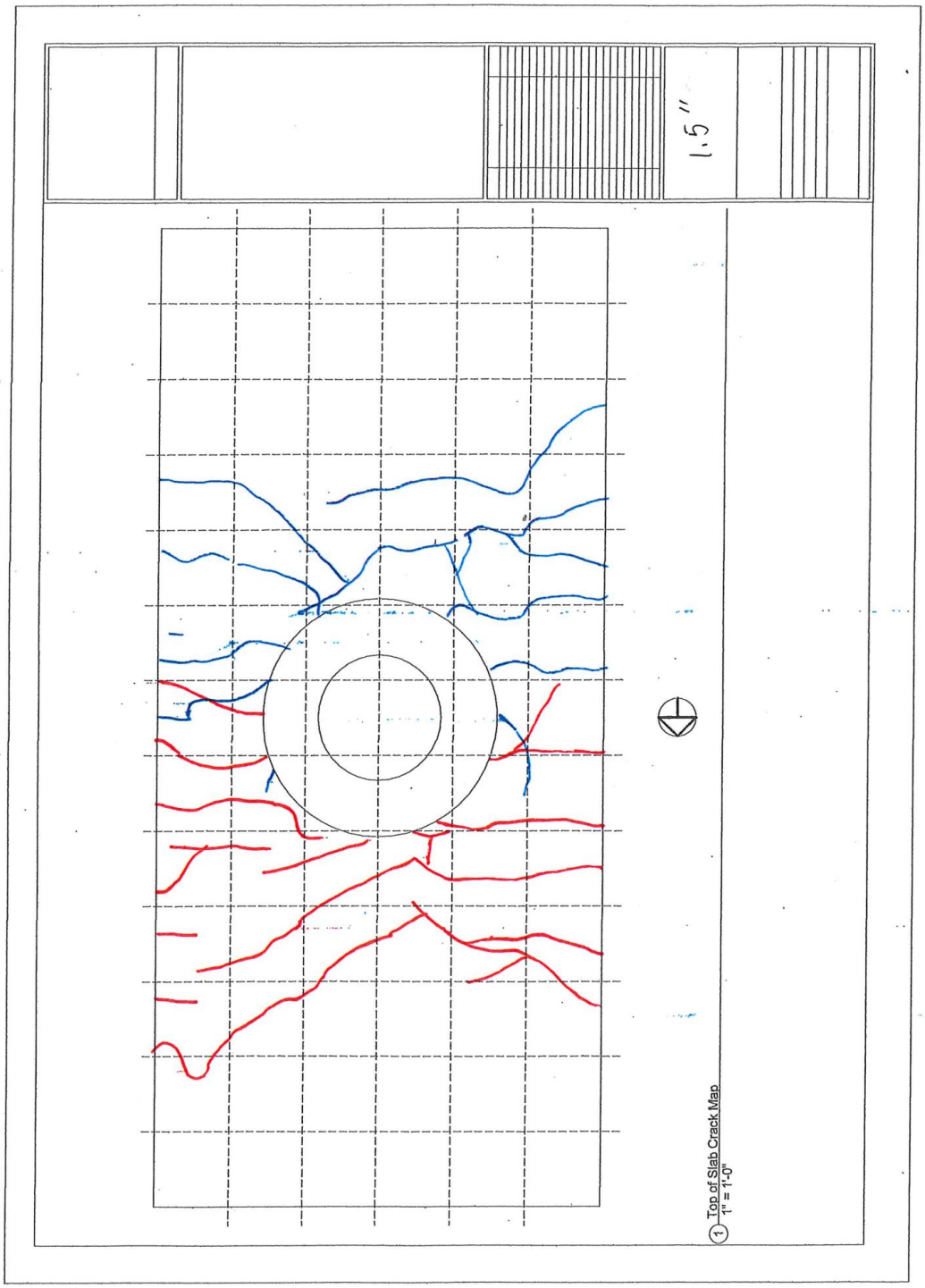

Figure 57: Top of Slab Crack Map– 0.96/-0.97% Drift (PTB_9_2_0)

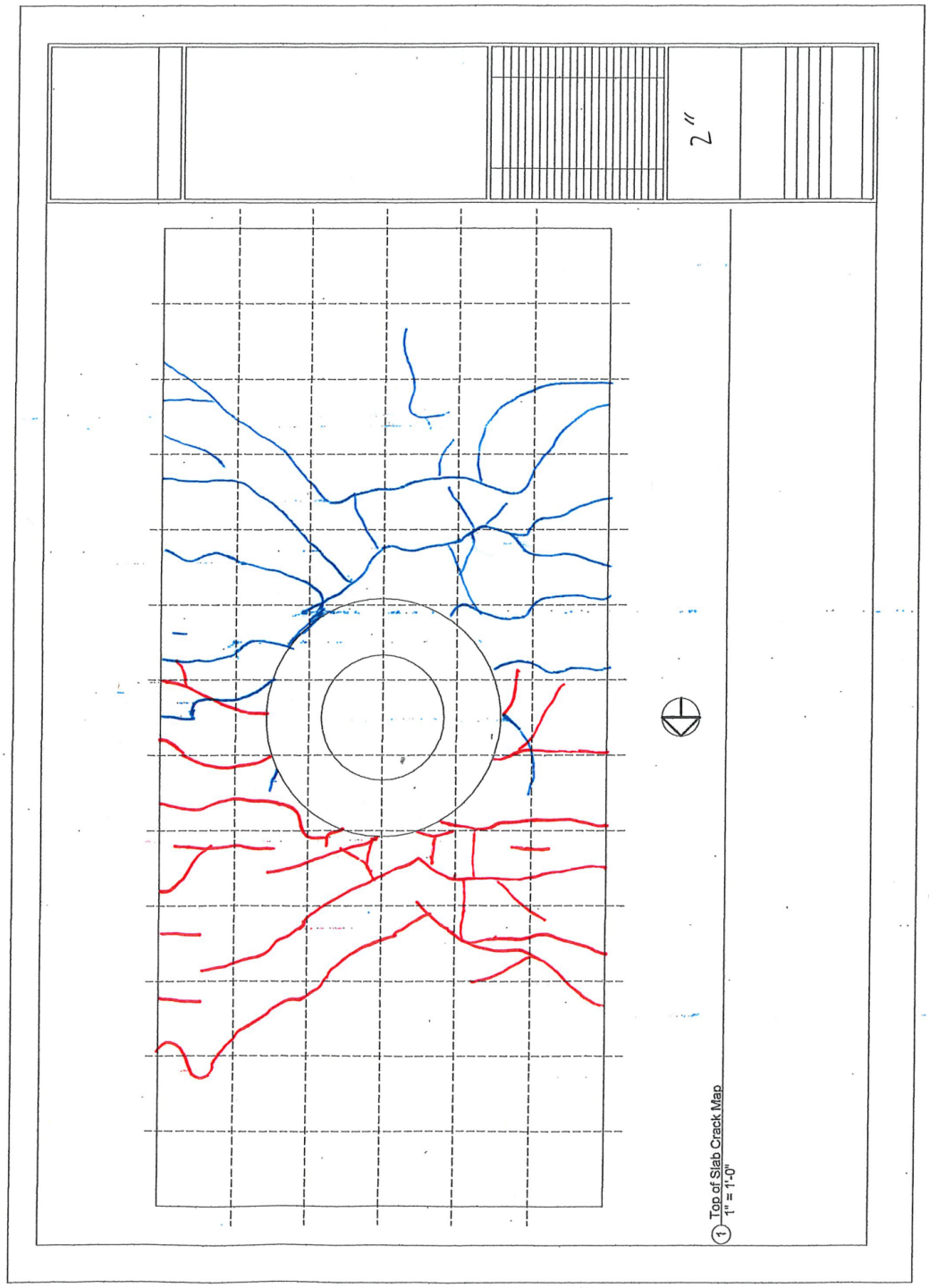

Figure 58: Top of Slab Crack Map– 1.3/-1.3% Drift (PTB_9_2_0)

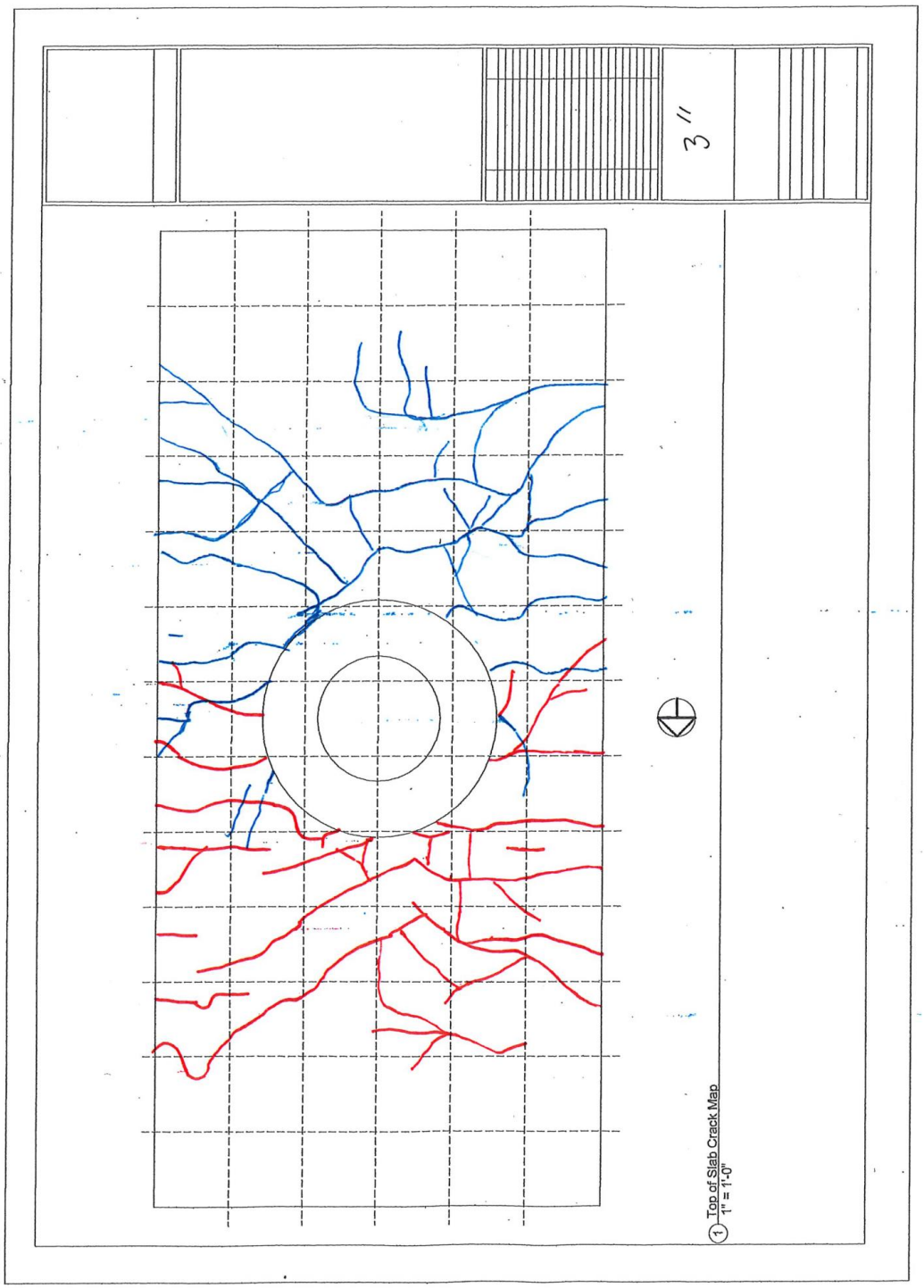

Figure 59: Top of Slab Crack Map– 2.0/-2.0% Drift (PTB_9_2_0)

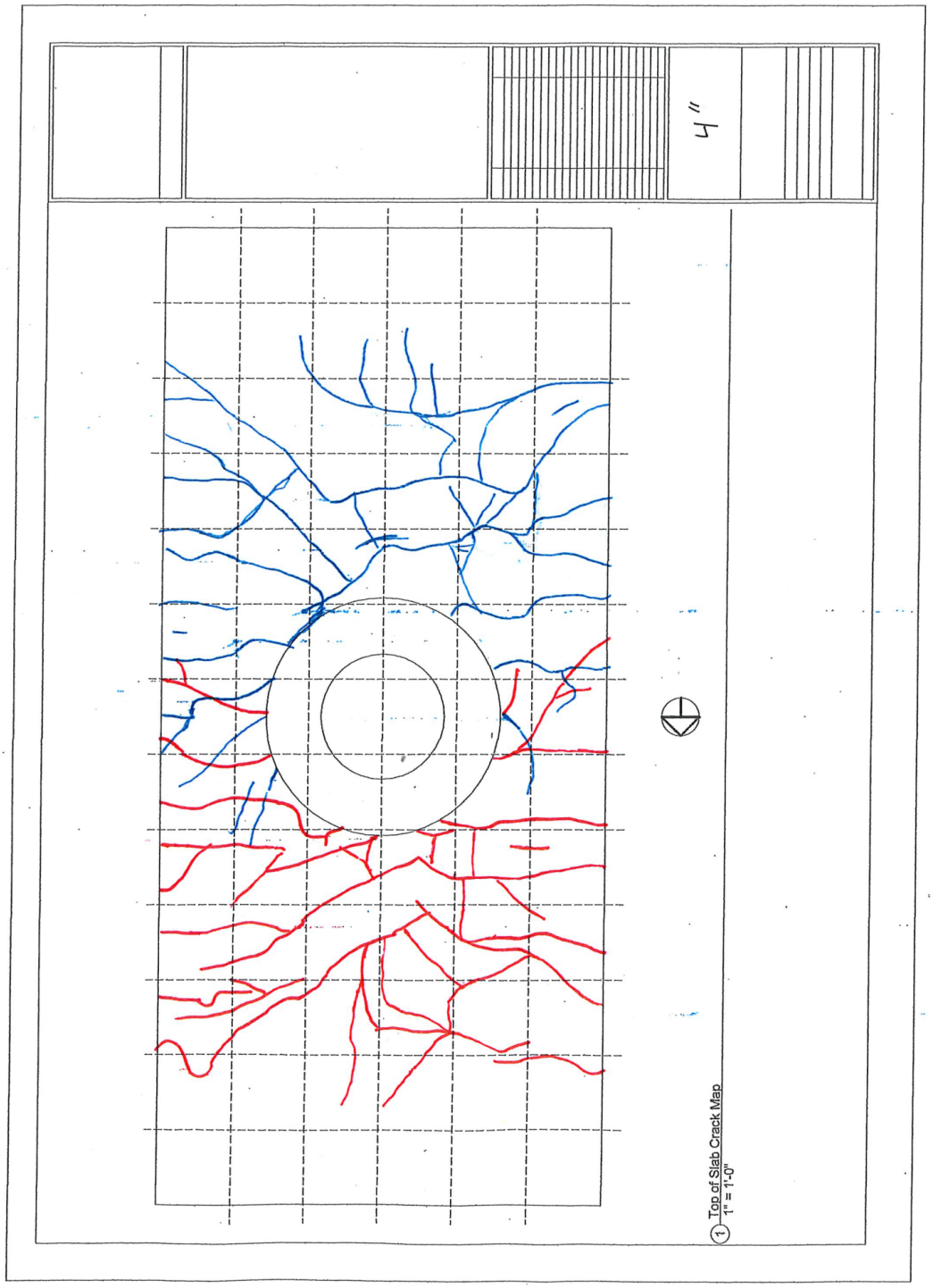

Figure 60: Top of Slab Crack Map– 2.7/-2.7% Drift (PTB_9_2_0)

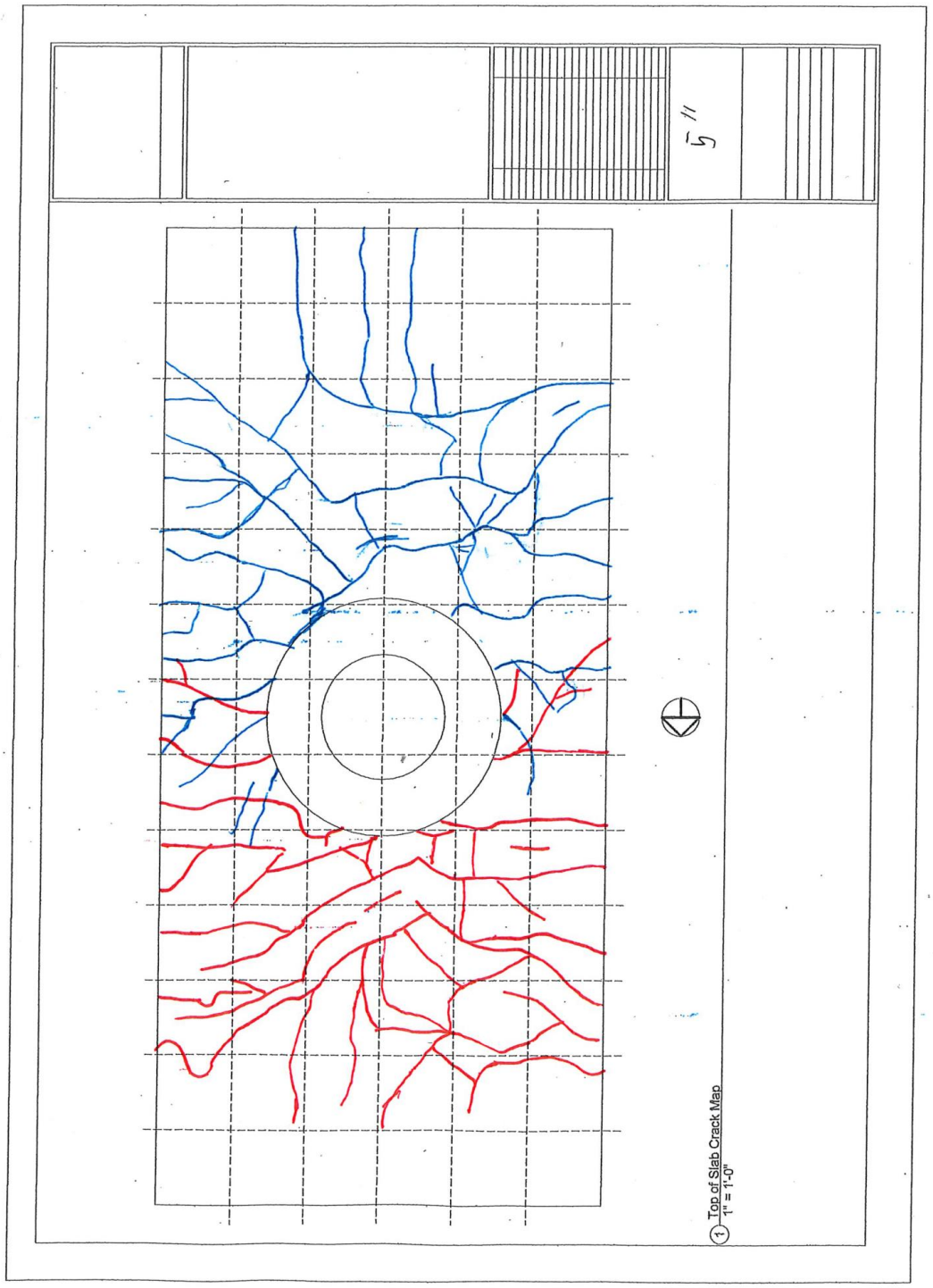

Figure 61: Top of Slab Crack Map– 3.4/-3.4% Drift (PTB_9_2_0)

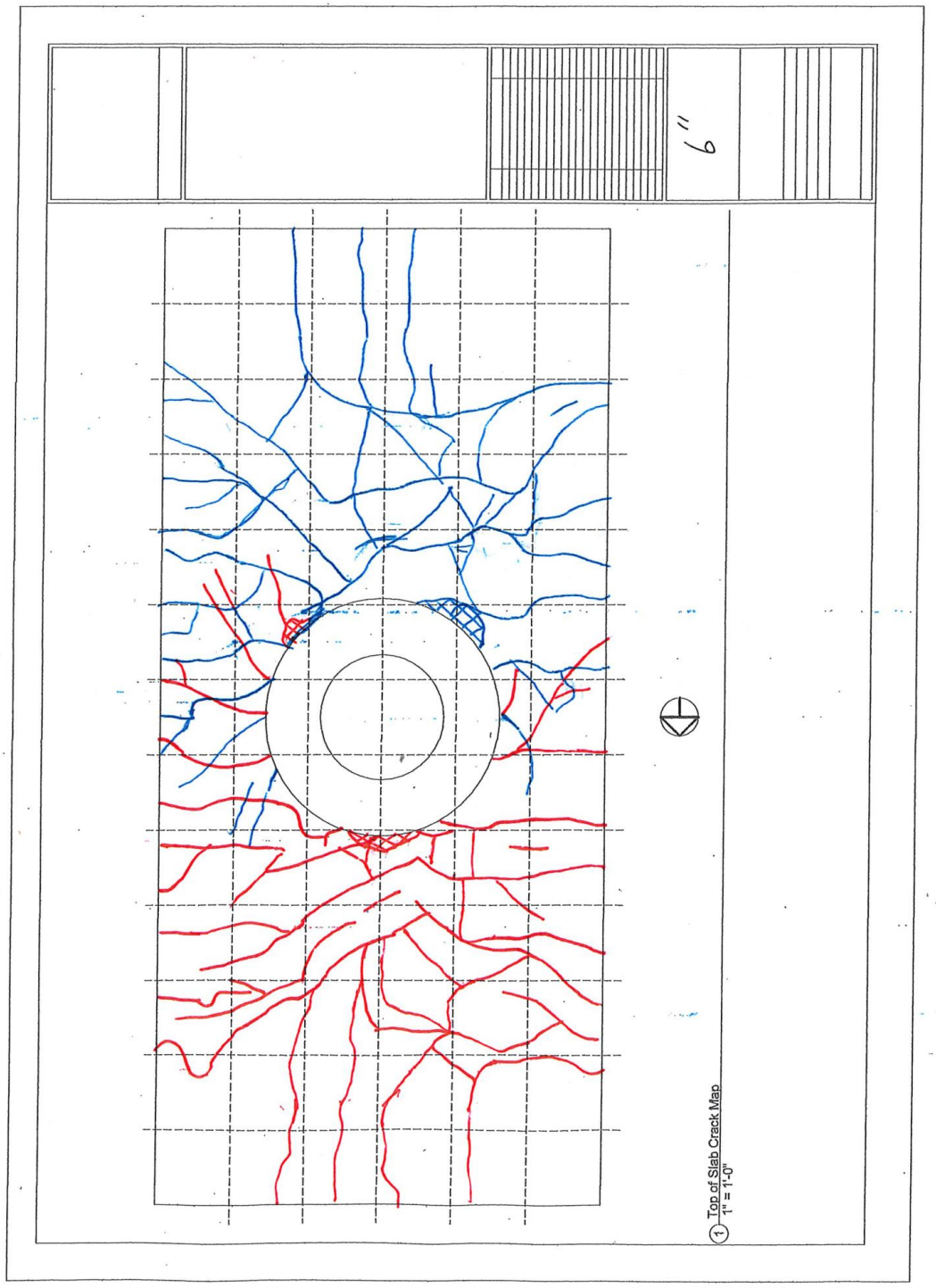

Figure 62: Top of Slab Crack Map– 4.1/-4.1% Drift (PTB_9_2_0)

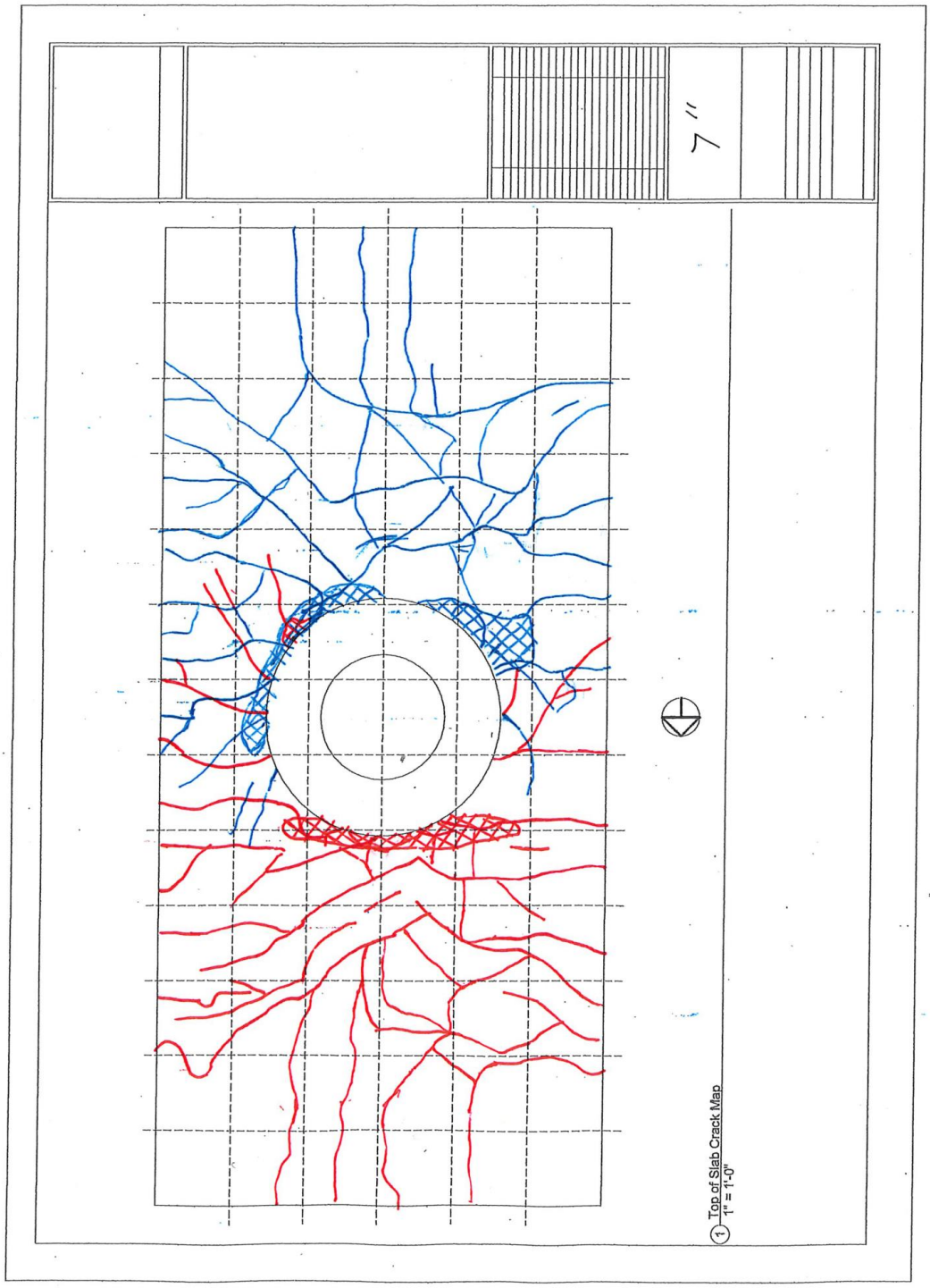

Figure 63: Top of Slab Crack Map– 4.9/-4.8% Drift (PTB_9_2_0)

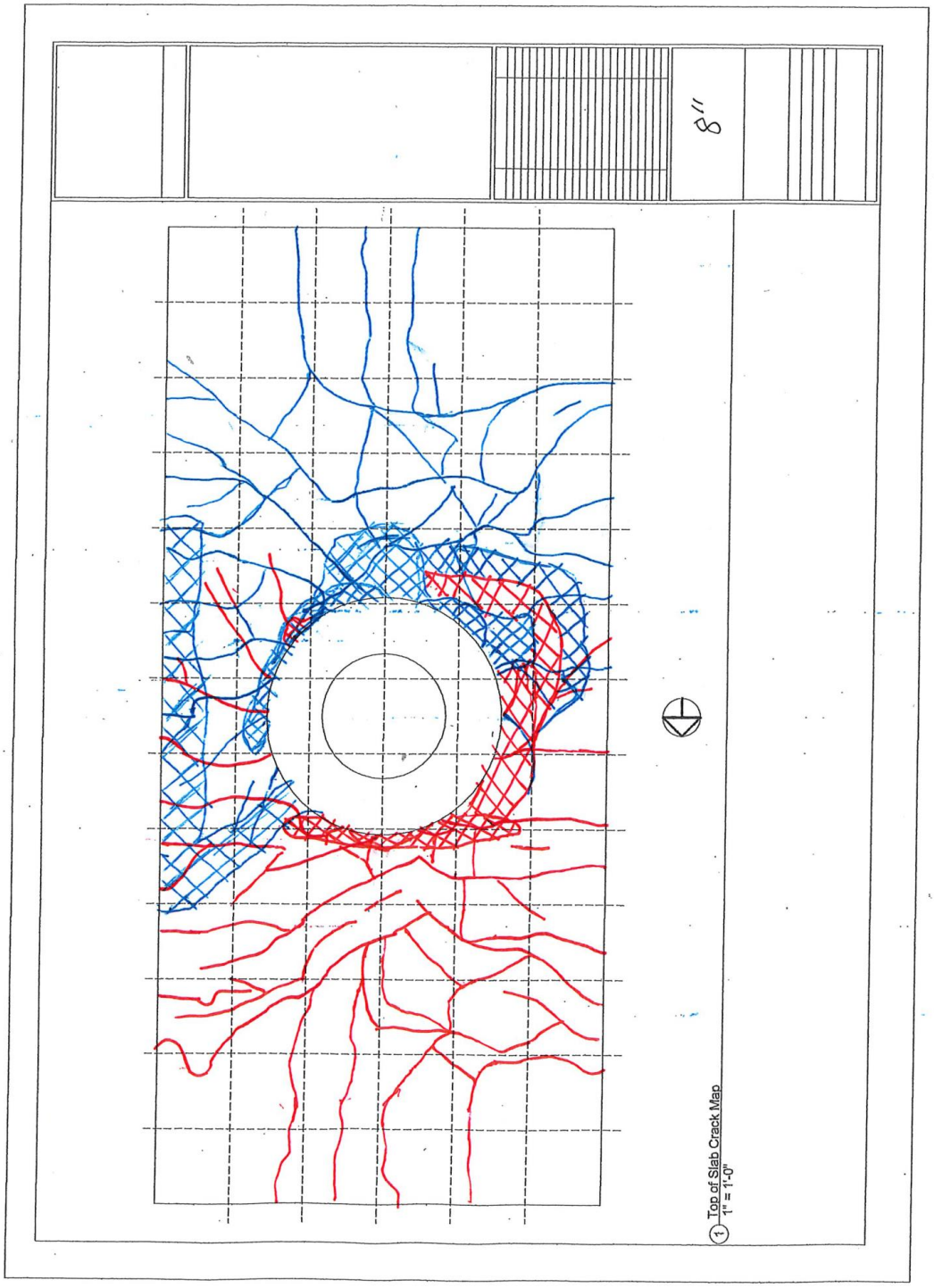

Figure 64: Top of Slab Crack Map– 5.6/-5.5% Drift (PTB_9_2_0)

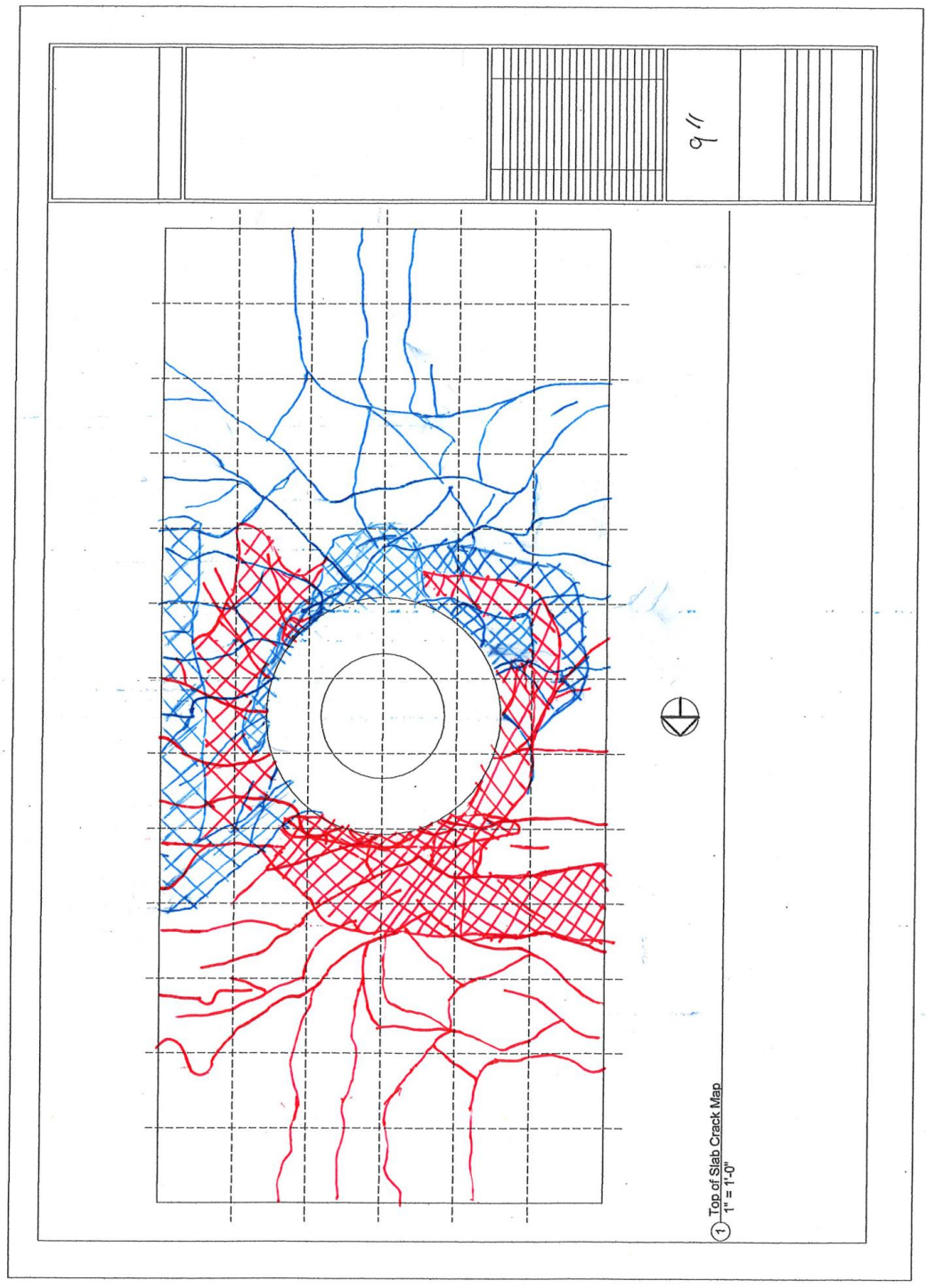

Figure 65: Top of Slab Crack Map– 6.4/-6.2% Drift (PTB_9_2_0)

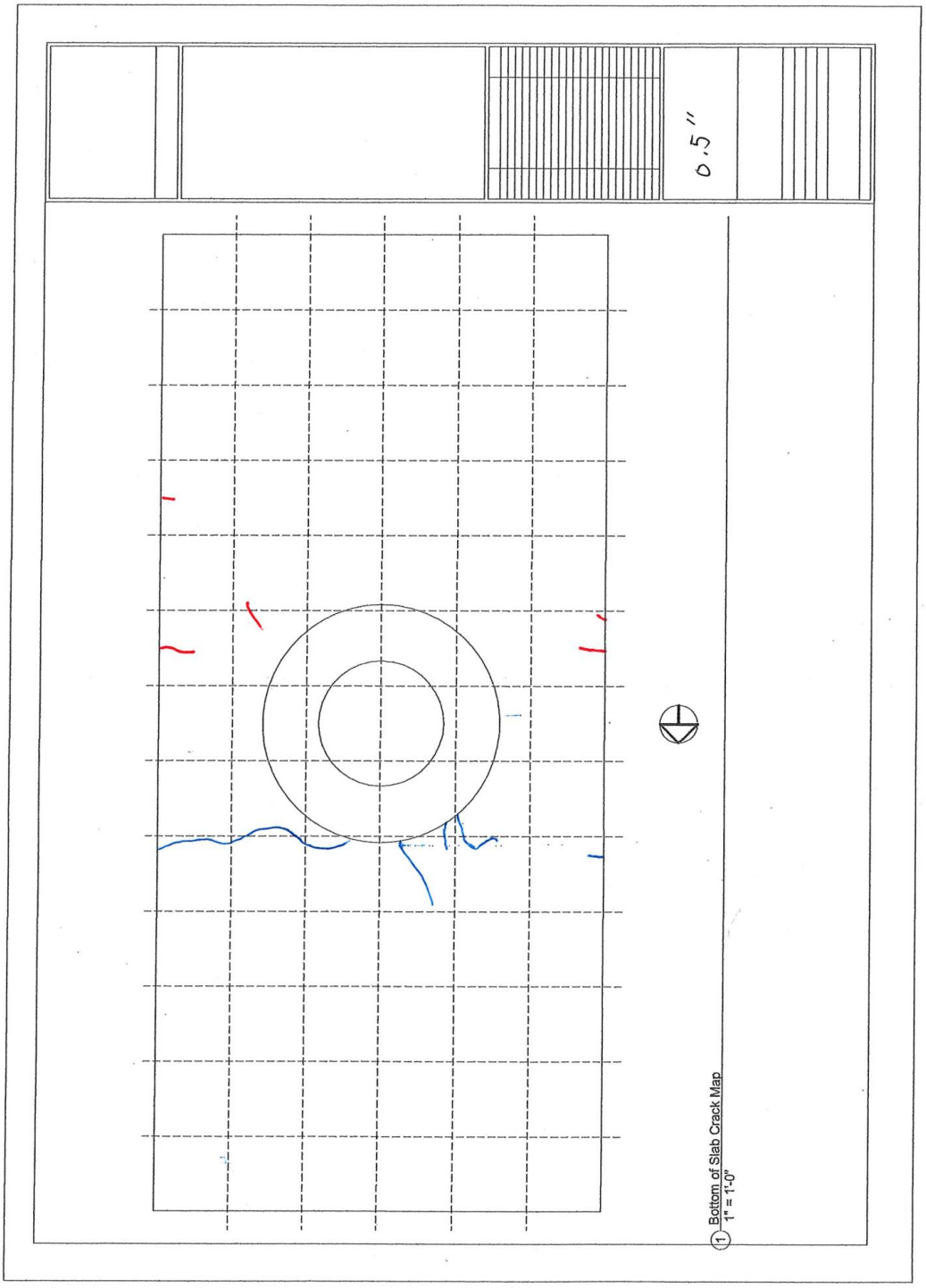

Figure 66: Bottom of Slab Crack Map– 0.30/-0.31% Drift (PTB_9_2_0)

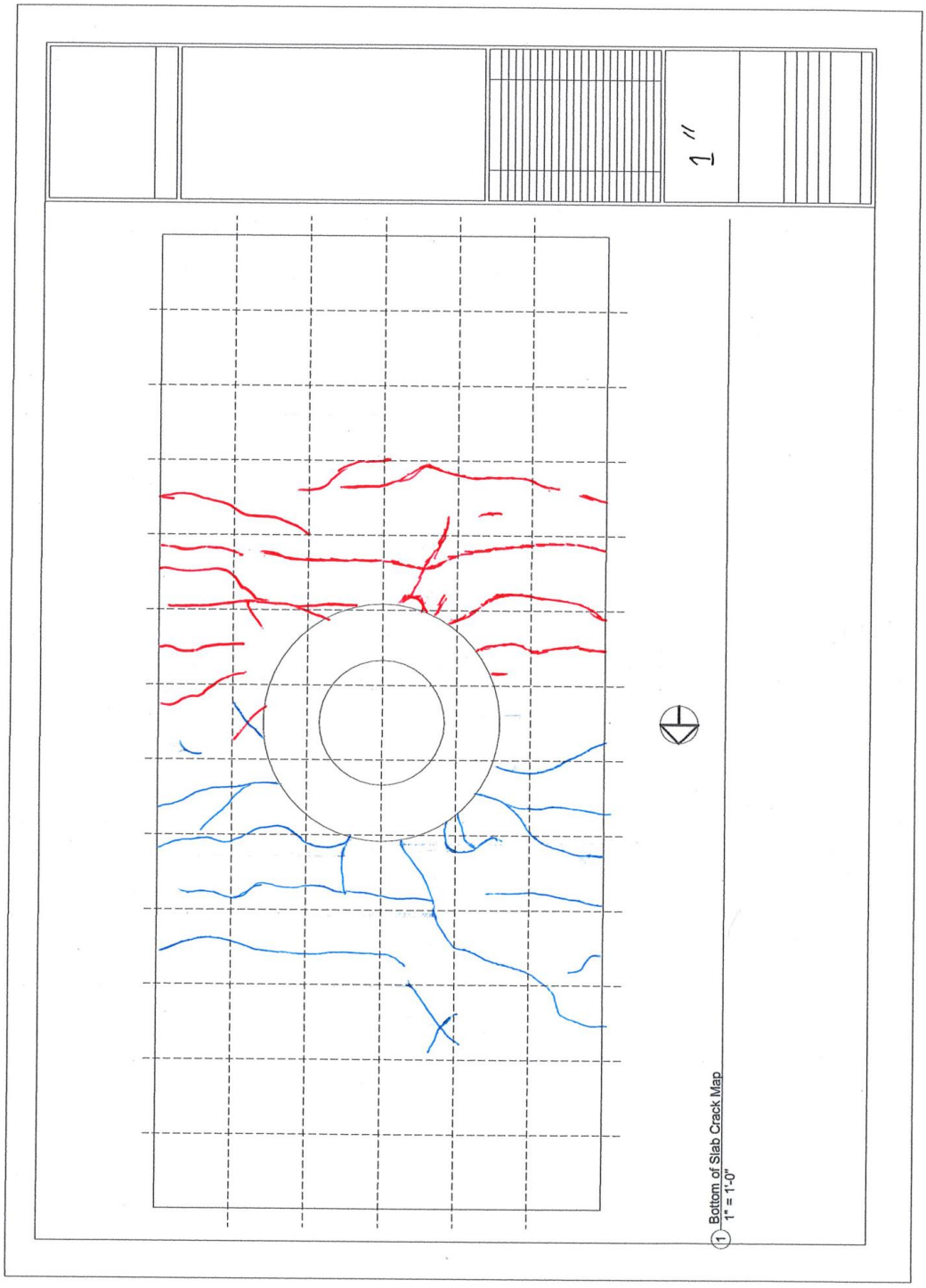

Figure 67: Bottom of Slab Crack Map– 0.63/-0.64% Drift (PTB_9_2_0)

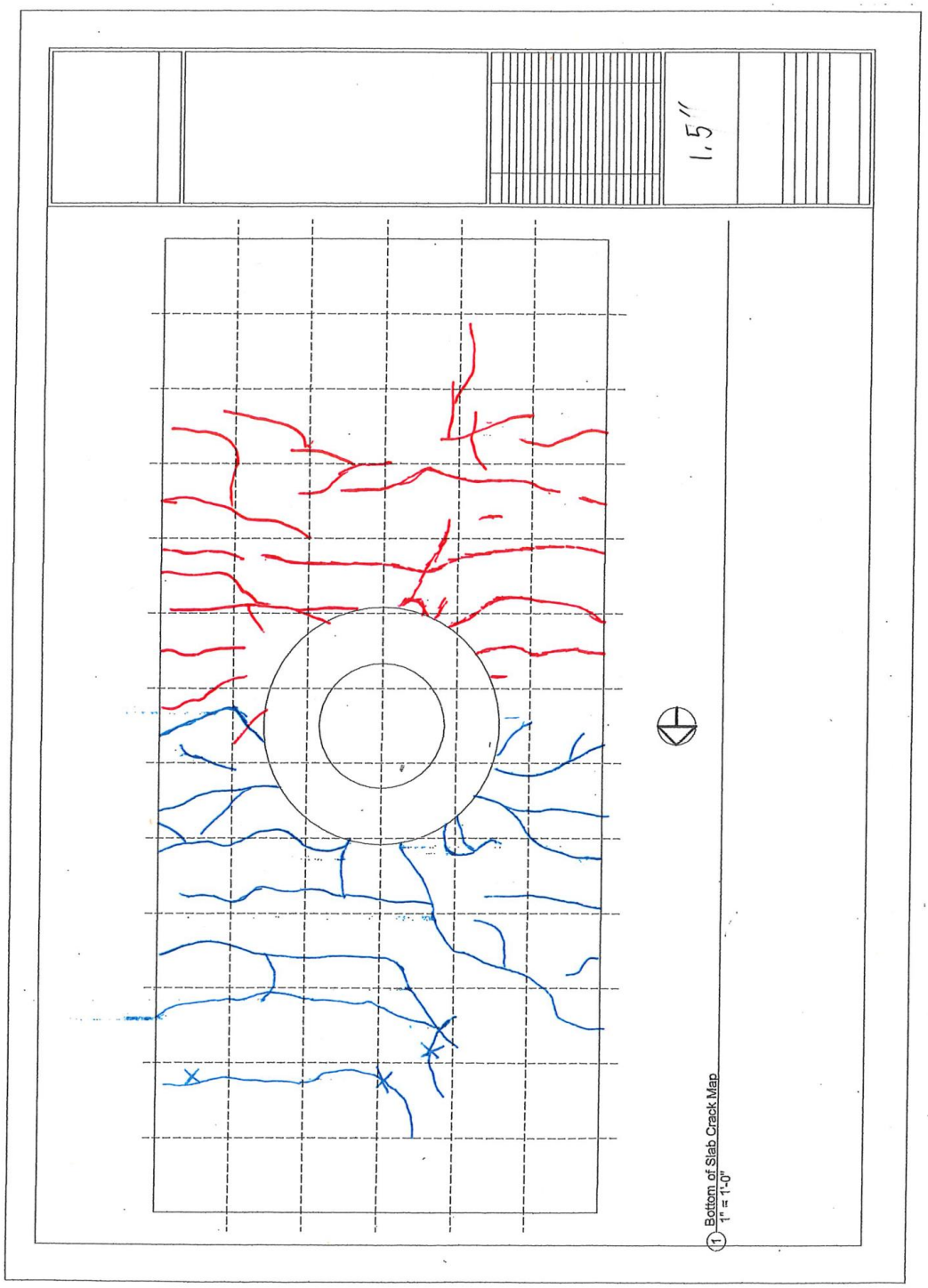

Figure 68: Bottom of Slab Crack Map– 0.96/-0.97% Drift (PTB_9_2_0)

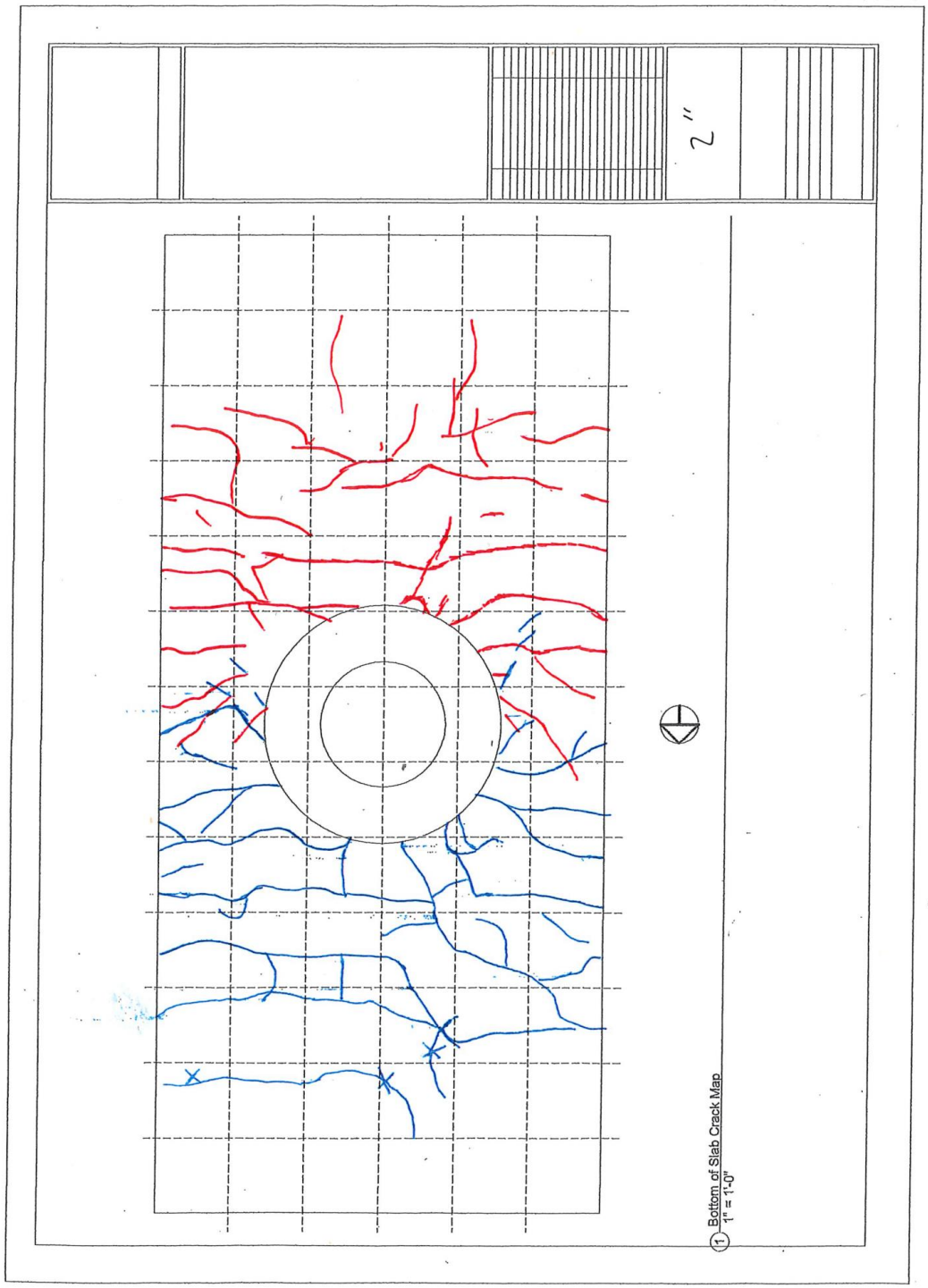

Figure 69: Bottom of Slab Crack Map– 1.3/-1.3% Drift (PTB_9_2_0)

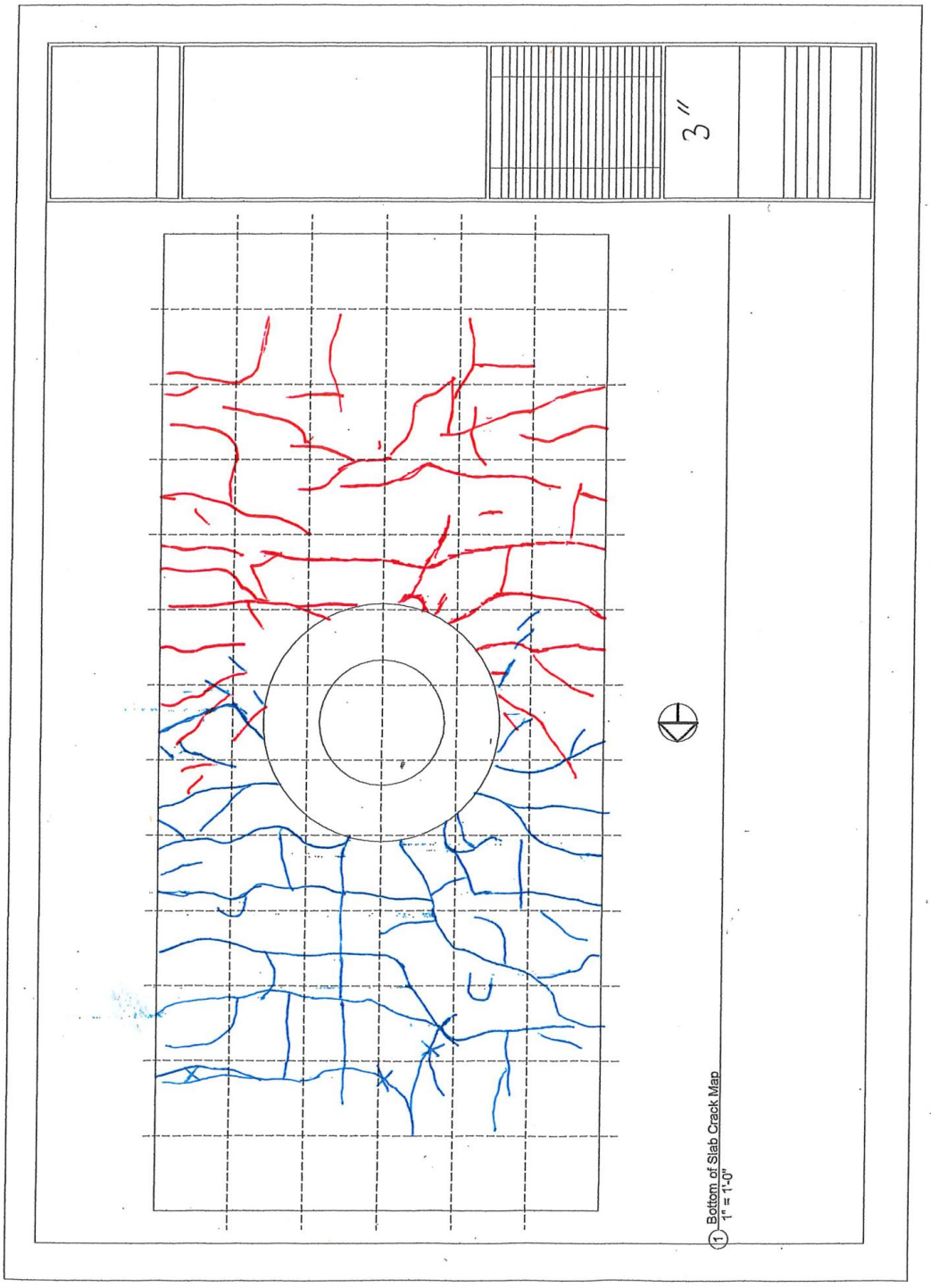

Figure 70: Bottom of Slab Crack Map– 2.0/-2.0% Drift (PTB_9_2_0)

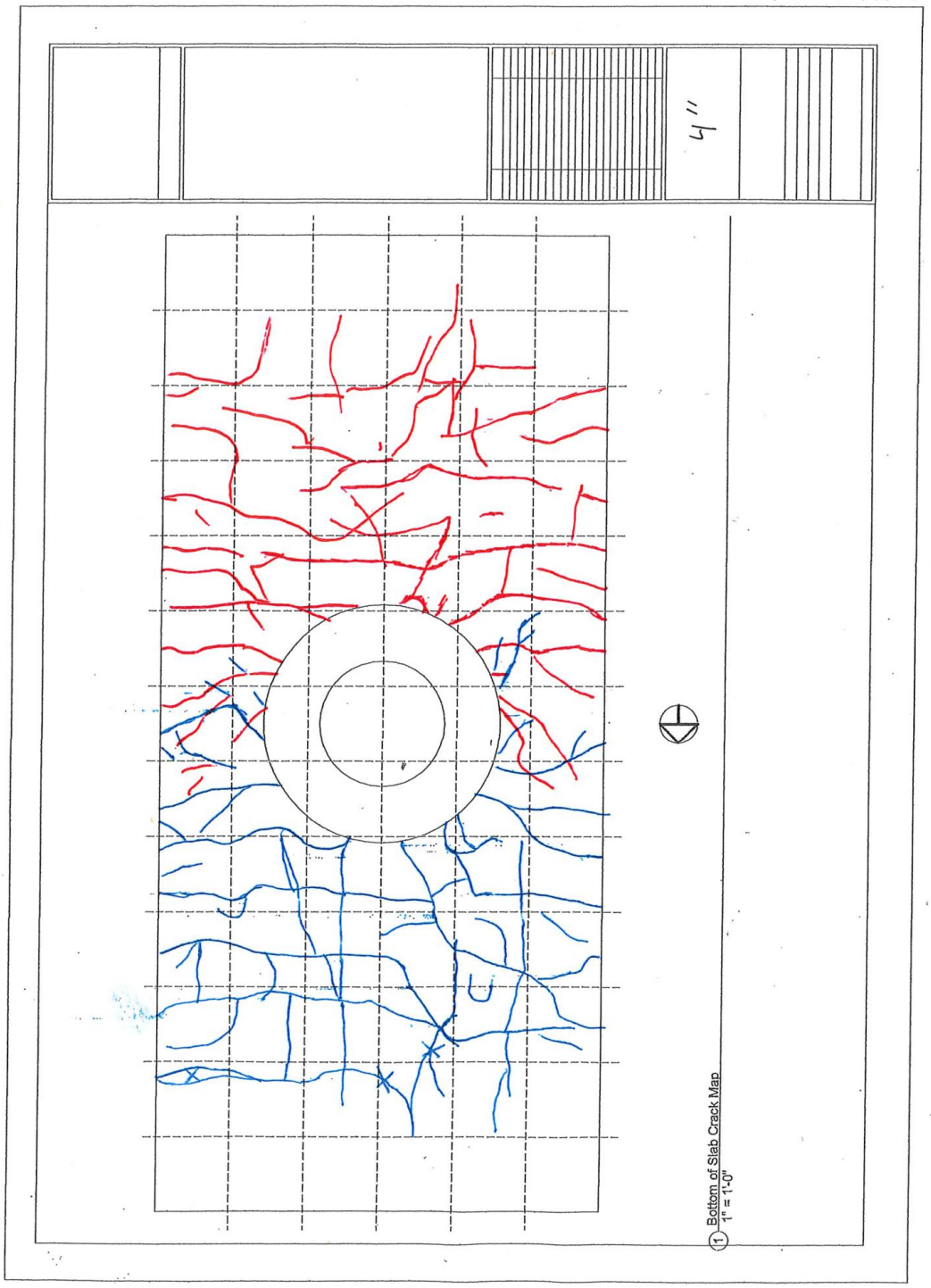

Figure 71: Bottom of Slab Crack Map– 2.7/-2.7% Drift (PTB_9_2_0)

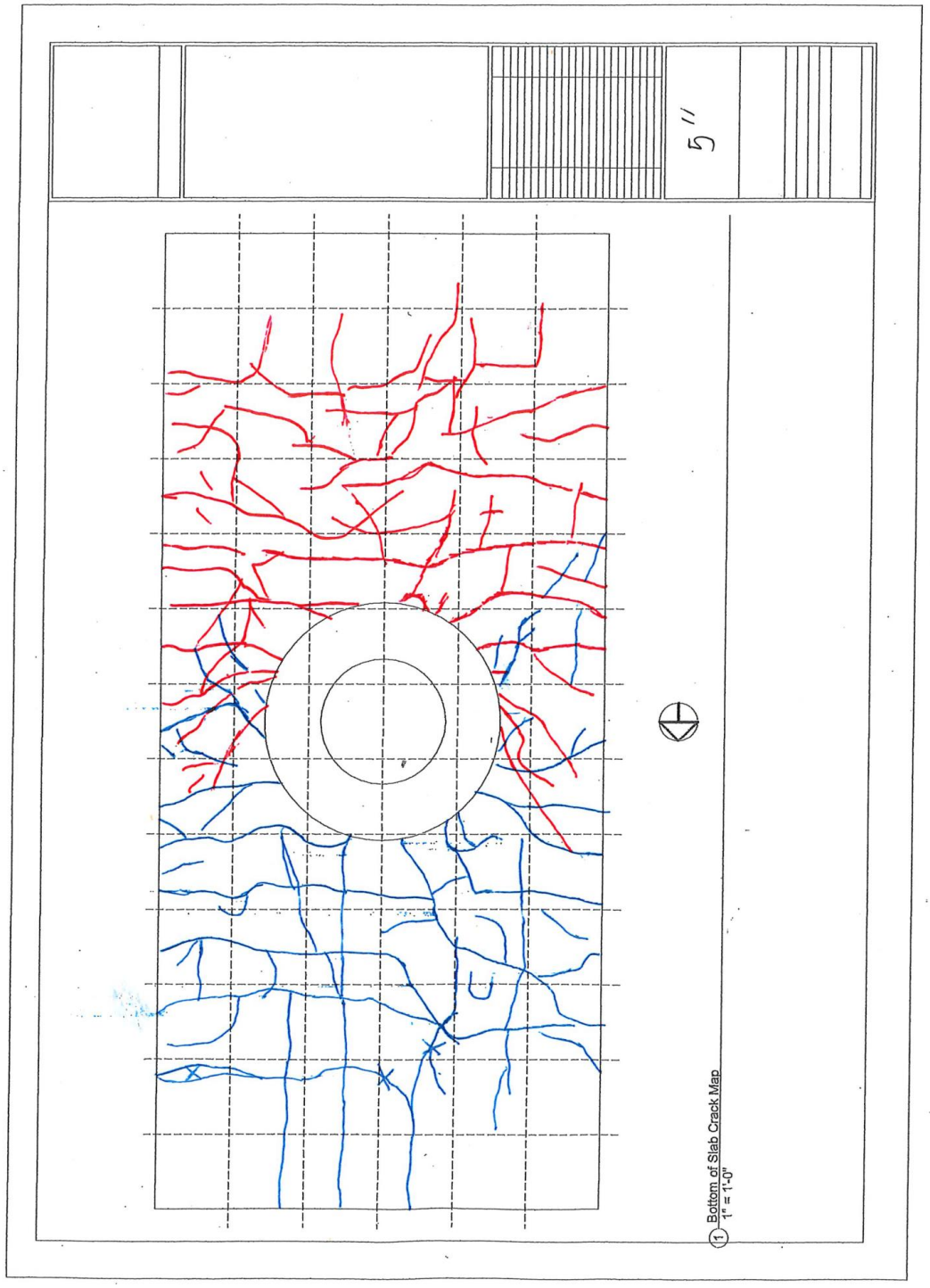

Figure 72: Bottom of Slab Crack Map– 3.4/-3.4% Drift (PTB_9_2_0)

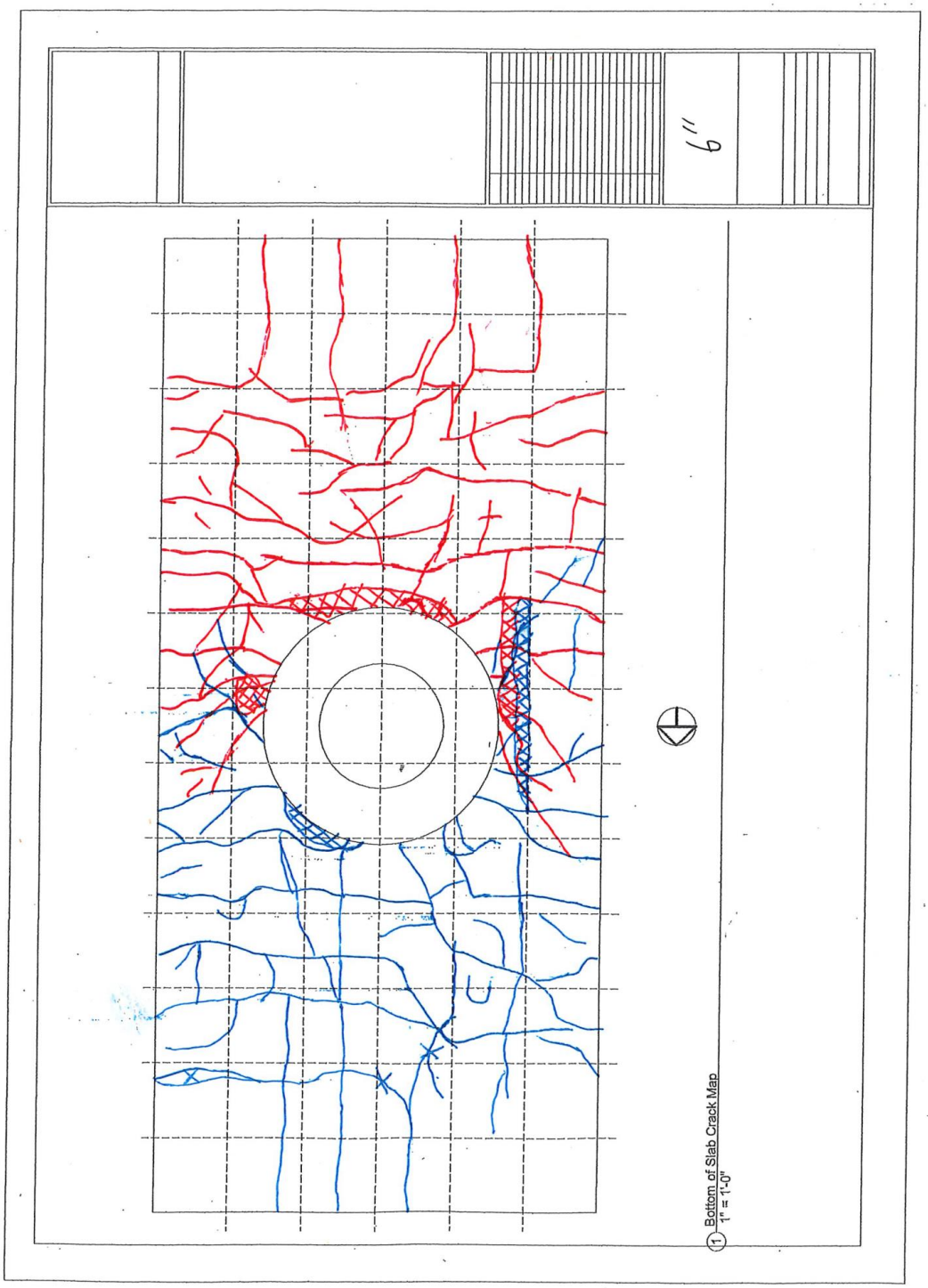

Figure 73: Bottom of Slab Crack Map– 4.1/-4.1% Drift (PTB_9_2_0)

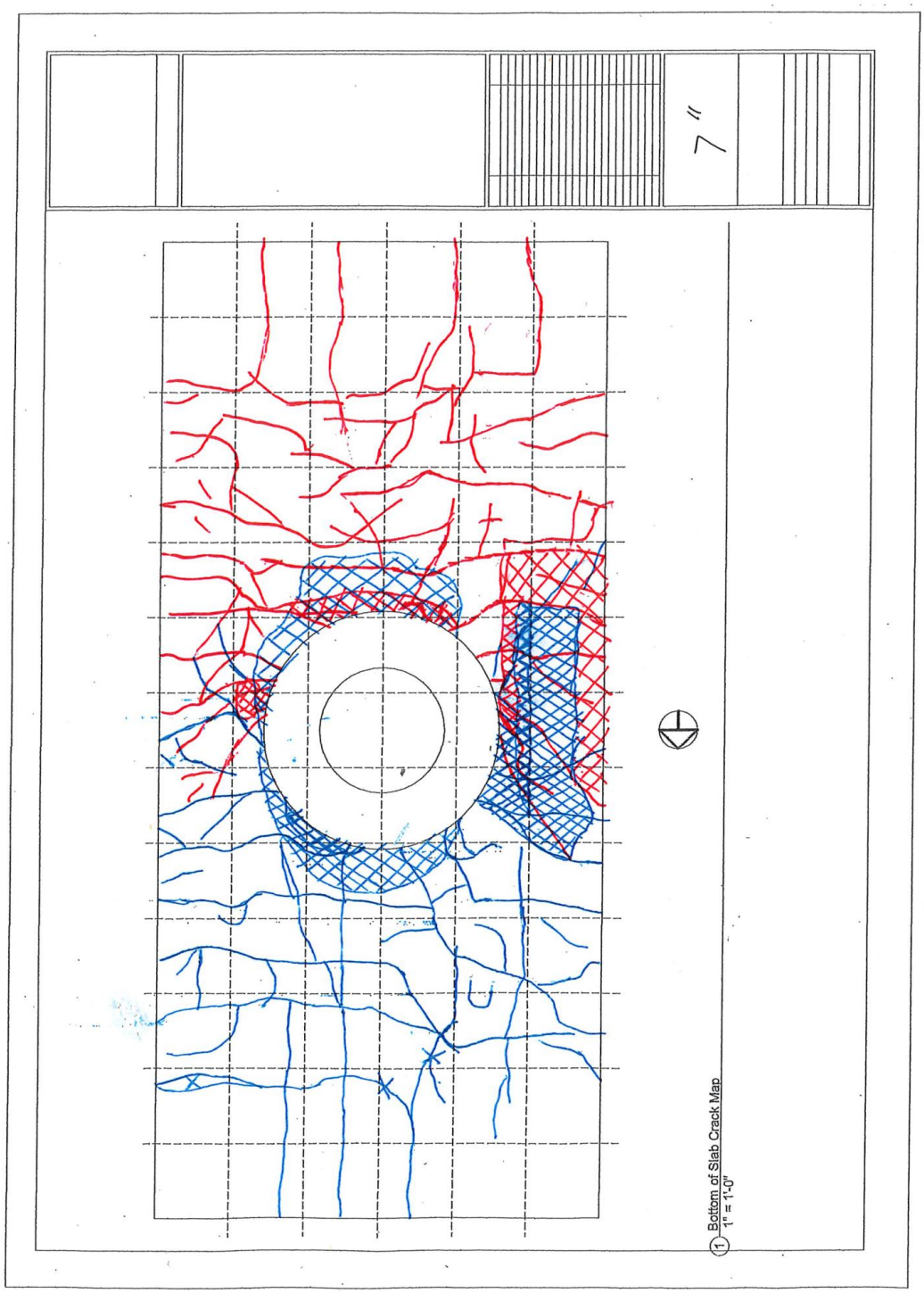

Figure 74: Bottom of Slab Crack Map– 4.9/-4.8% Drift (PTB_9_2_0)

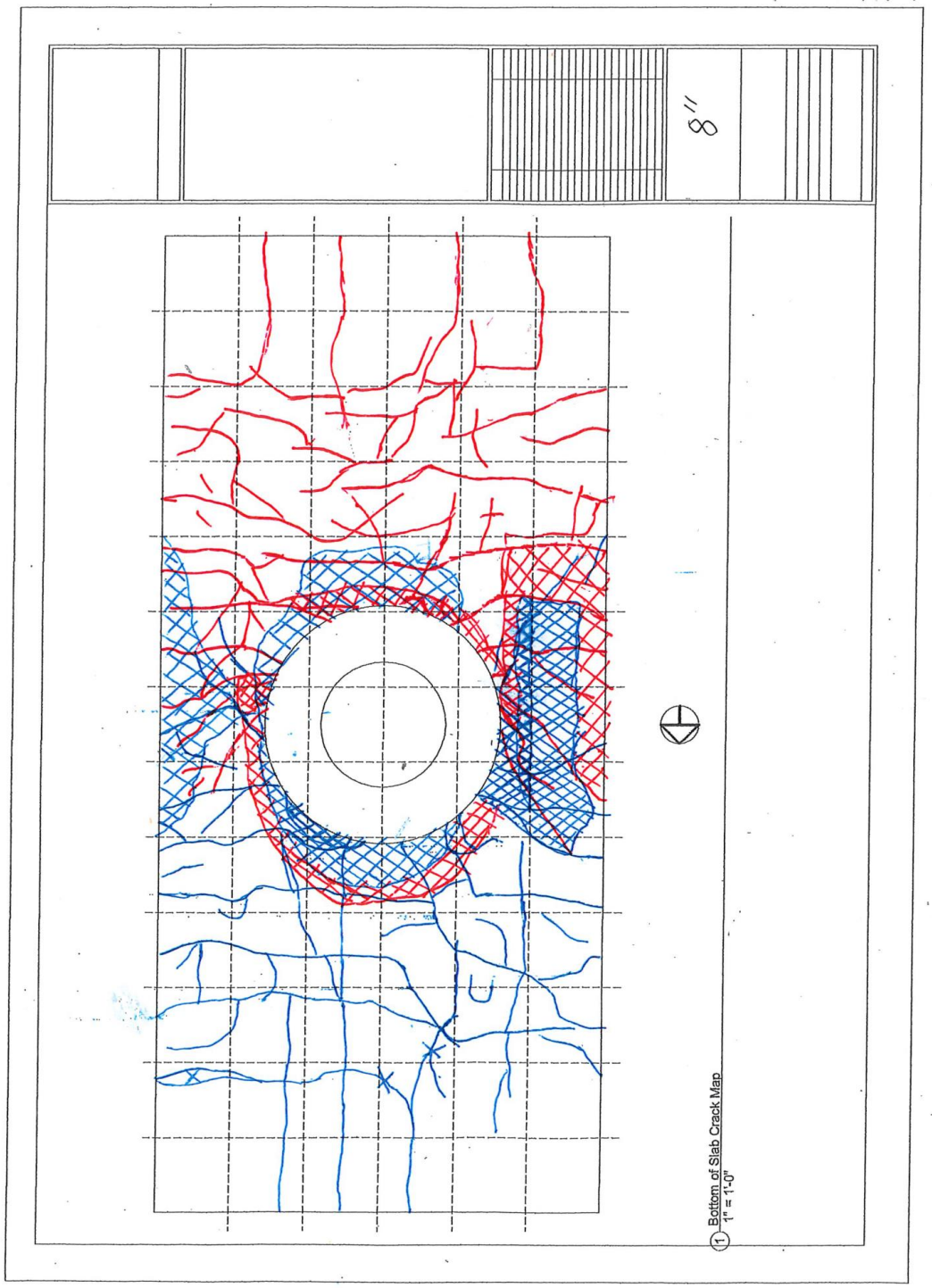

Figure 75: Bottom of Slab Crack Map– 5.6/-5.5% Drift (PTB_9_2_0)

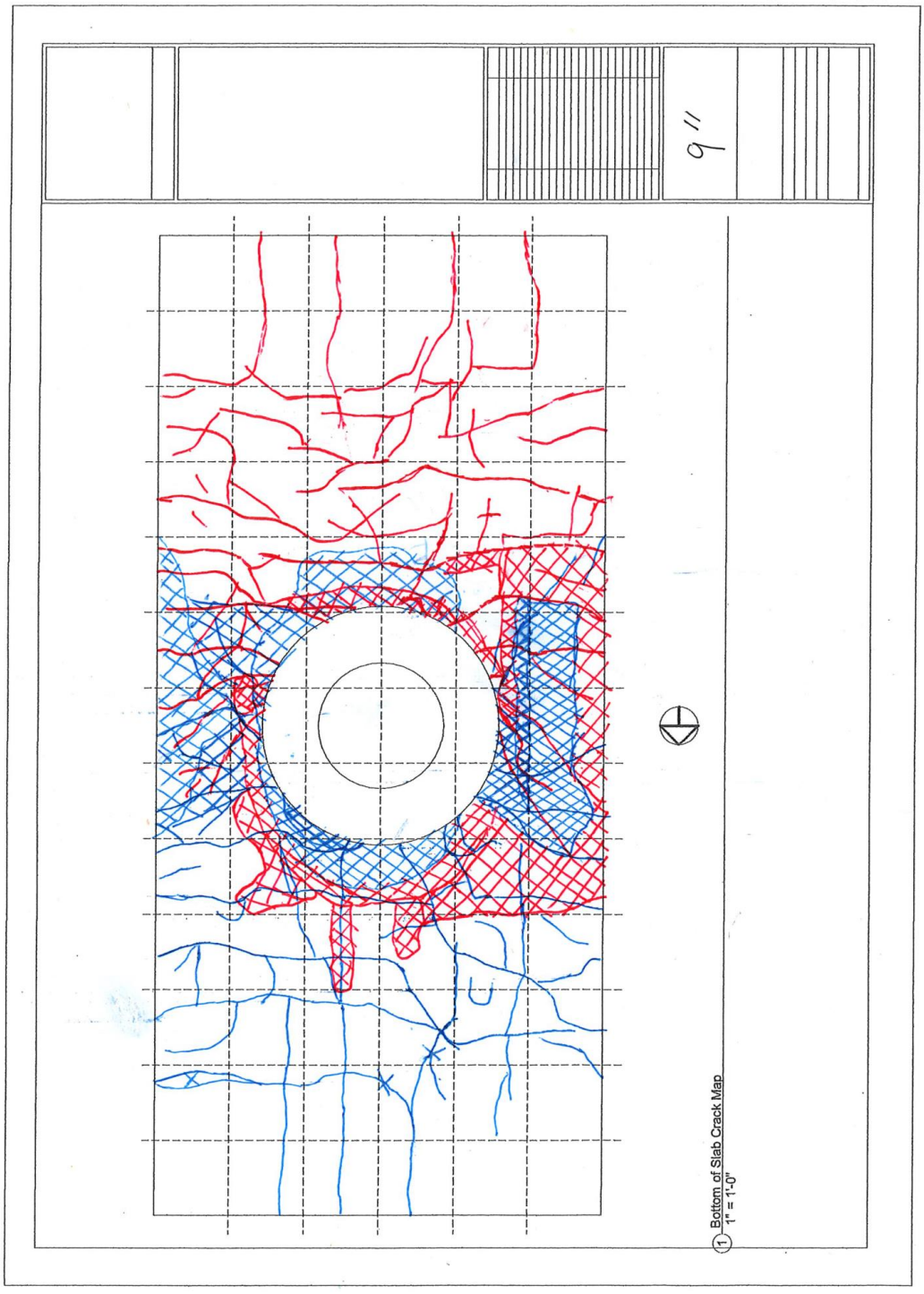

Figure 76: Bottom of Slab Crack Map– 6.4/-6.2% Drift (PTB_9_2_0)

APPENDIX E: STRAIN SUMMARY PLOTS

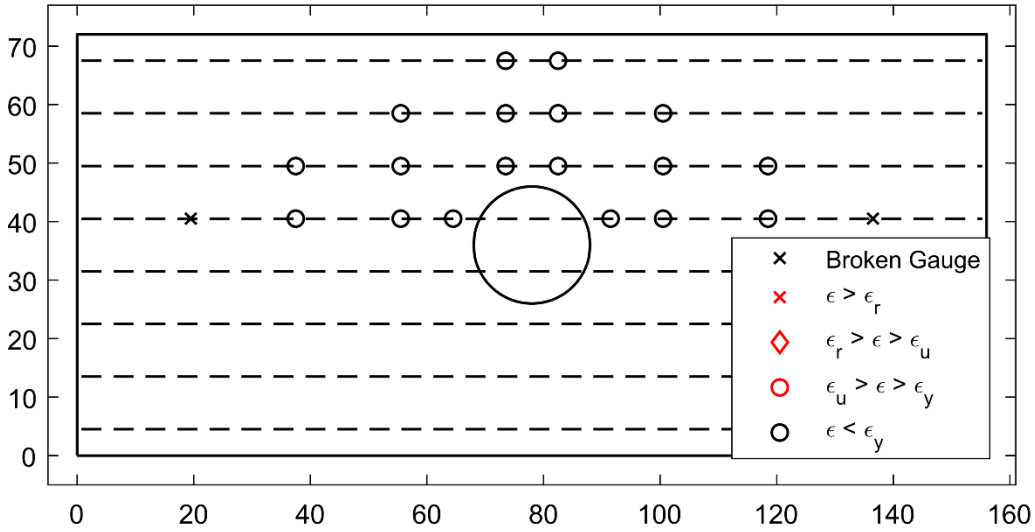

Figure 1: Top Reinforcement Strain Summary – 0.21% (SR_4_10_5)

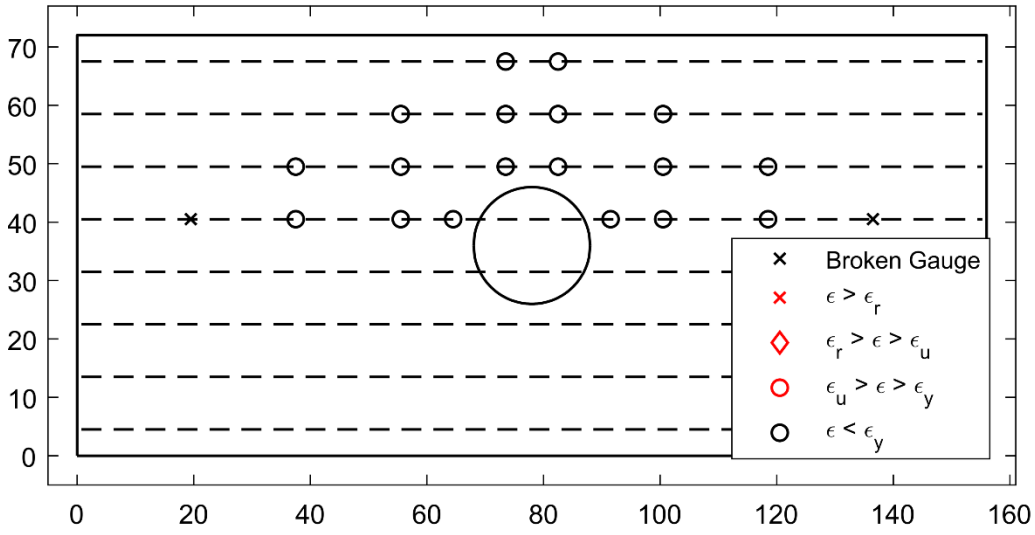

Figure 2: Top Reinforcement Strain Summary – 0.56% (SR_4_10_5)

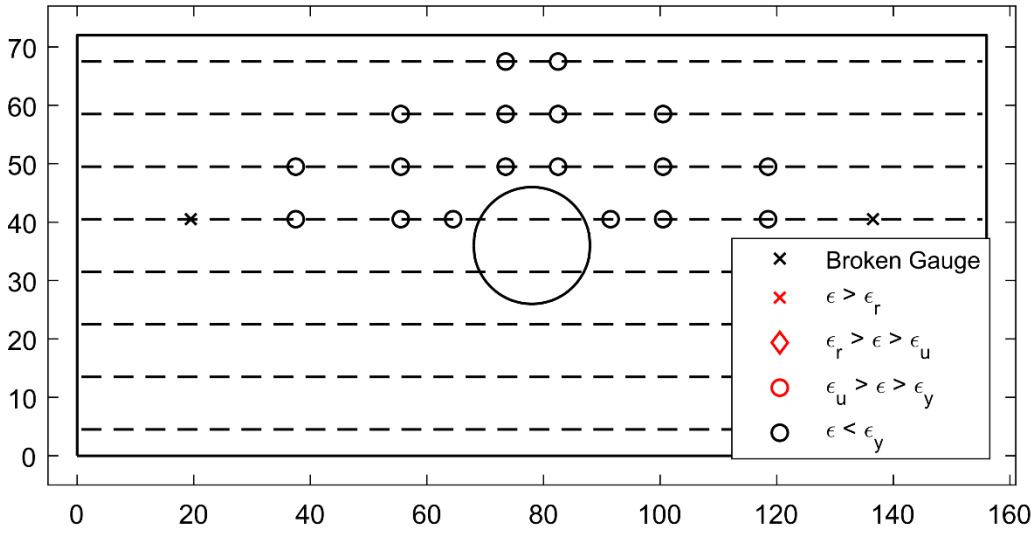

Figure 3: Top Reinforcement Strain Summary – 0.91% (SR_4_10_5)

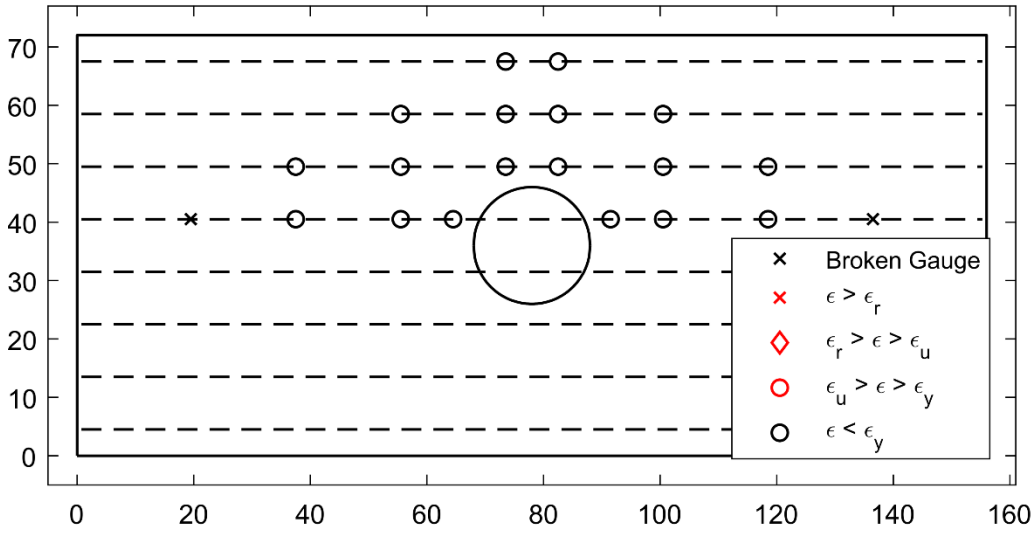

Figure 4: Top Reinforcement Strain Summary – 1.3% (SR_4_10_5)

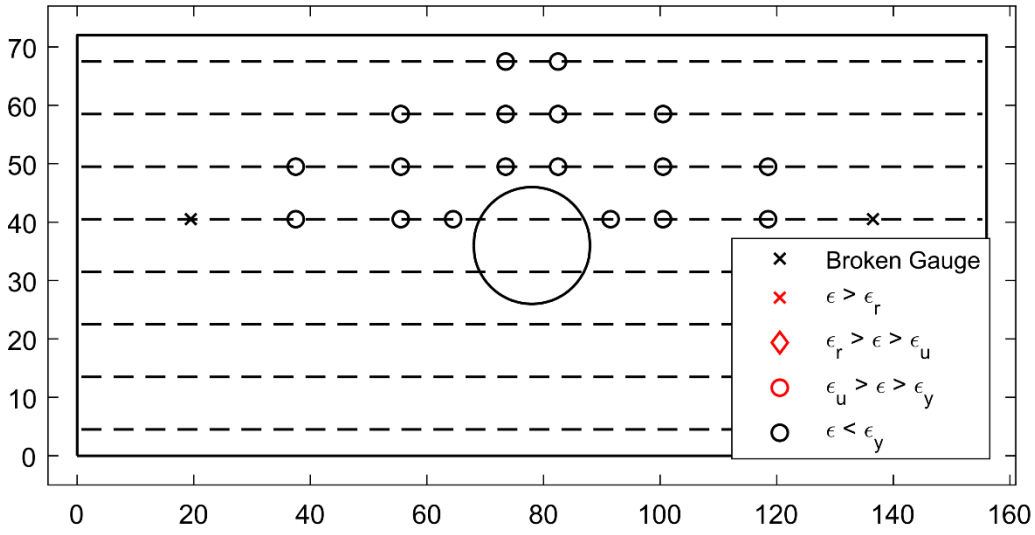

Figure 5: Top Reinforcement Strain Summary – 2.0% (SR_4_10_5)

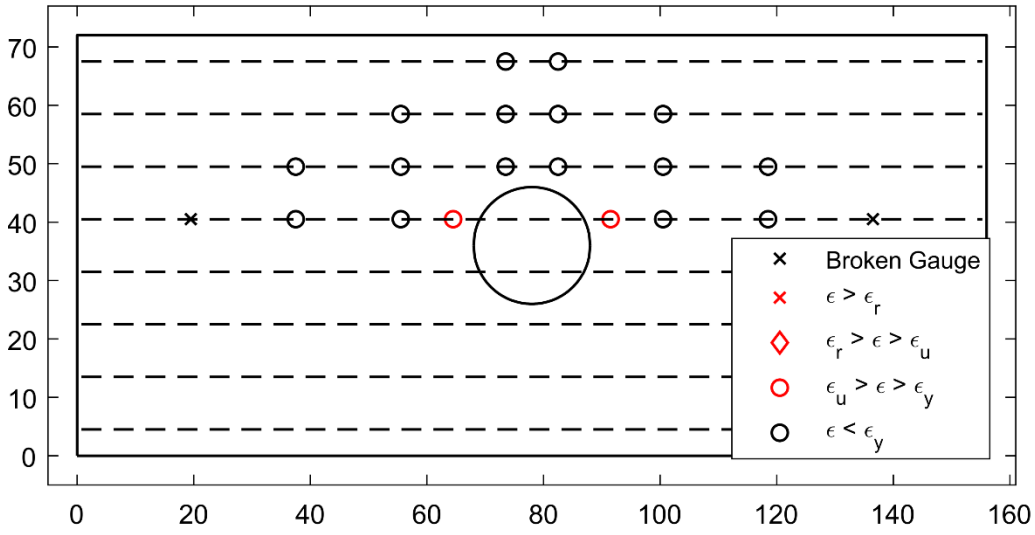

Figure 6: Top Reinforcement Strain Summary – 2.7% (SR_4_10_5)

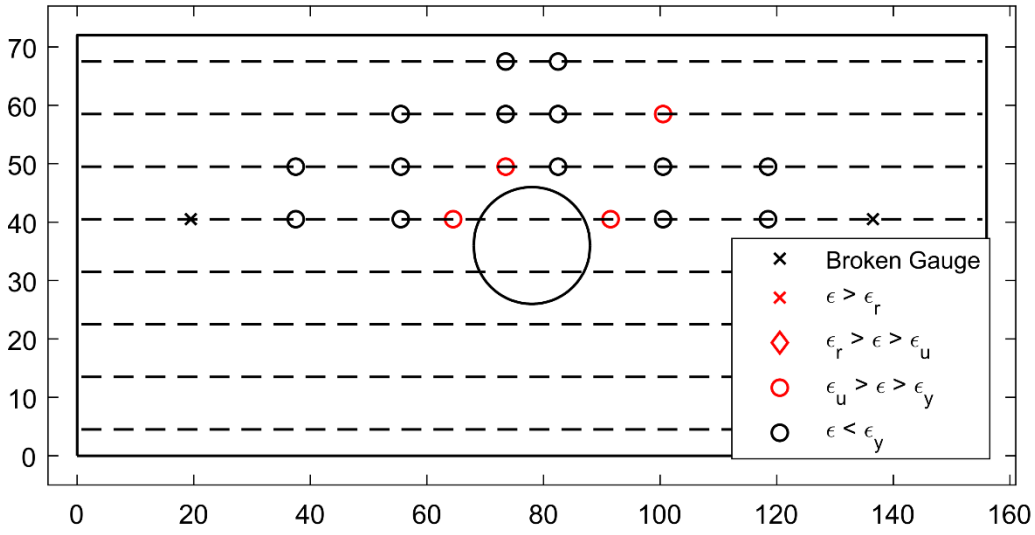

Figure 7: Top Reinforcement Strain Summary – 3.4% (SR_4_10_5)

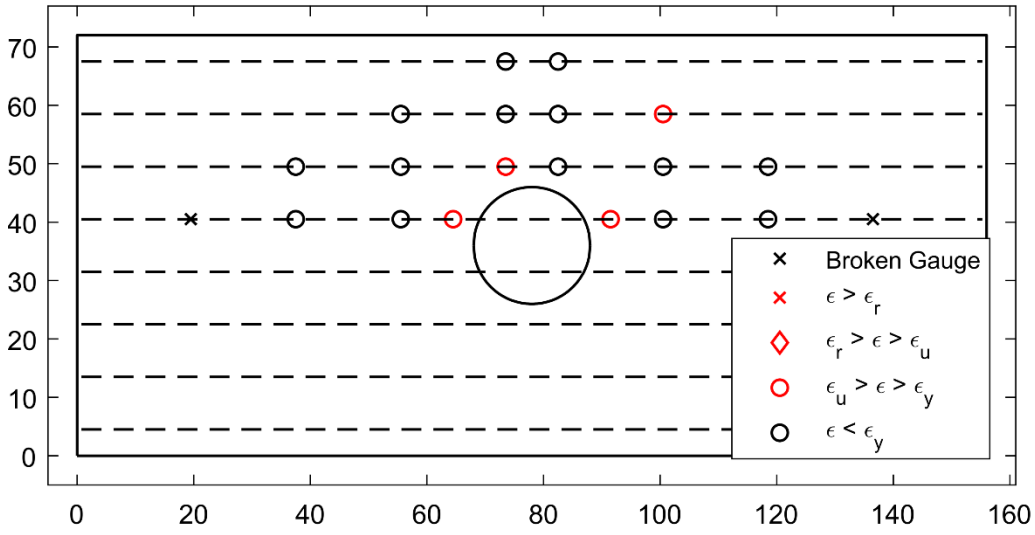

Figure 8: Top Reinforcement Strain Summary – 4.2% (SR_4_10_5)

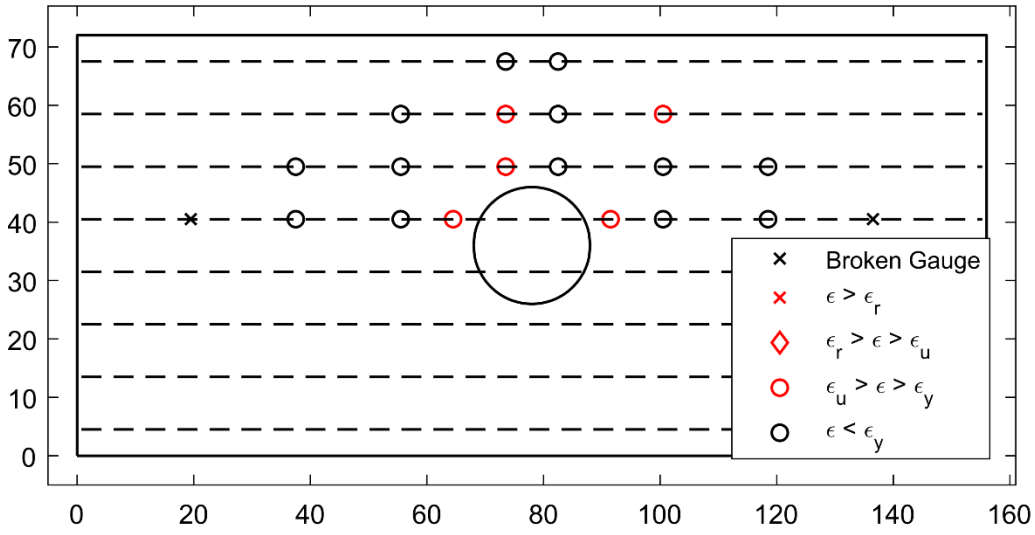

Figure 9: Top Reinforcement Strain Summary – 4.9% (SR_4_10_5)

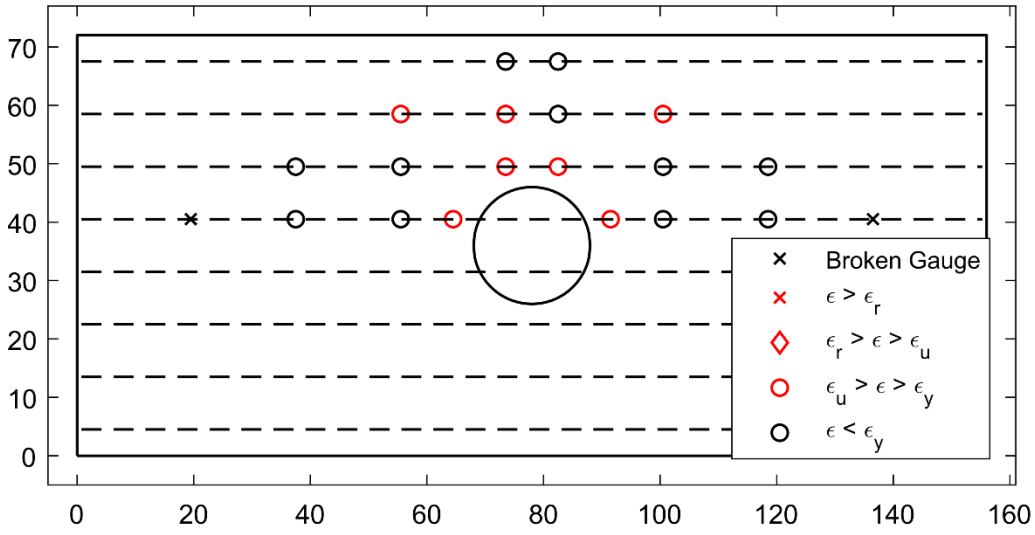

Figure 10: Top Reinforcement Strain Summary – 5.6% (SR_4_10_5)

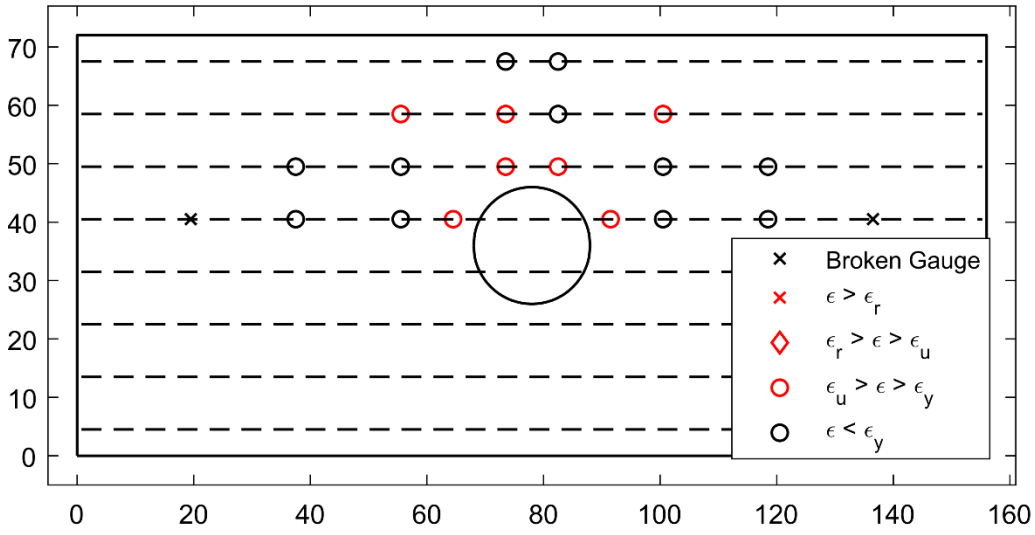

Figure 11: Top Reinforcement Strain Summary – 6.4% (SR_4_10_5)

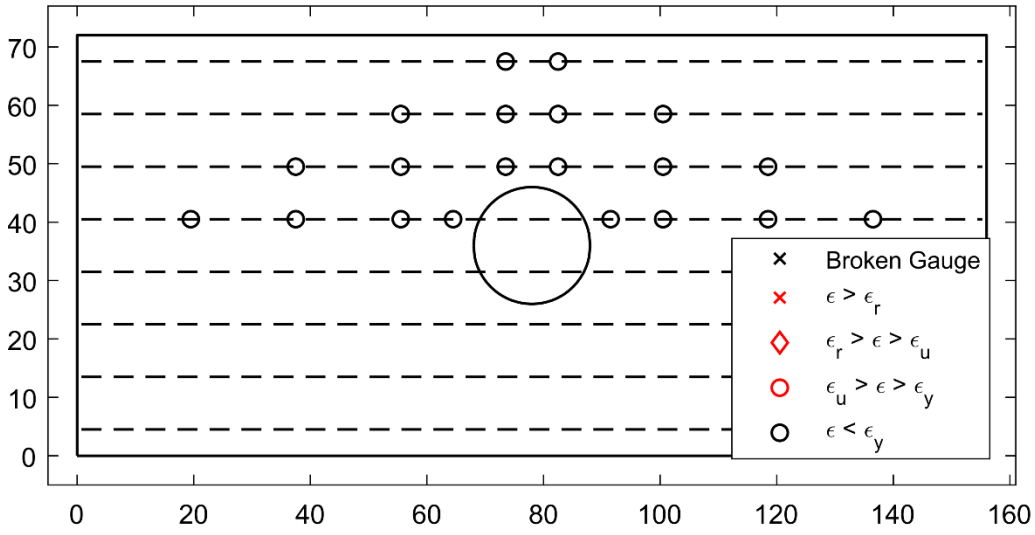

Figure 12: Bottom Reinforcement Strain Summary – 0.21% (SR_4_10_5)

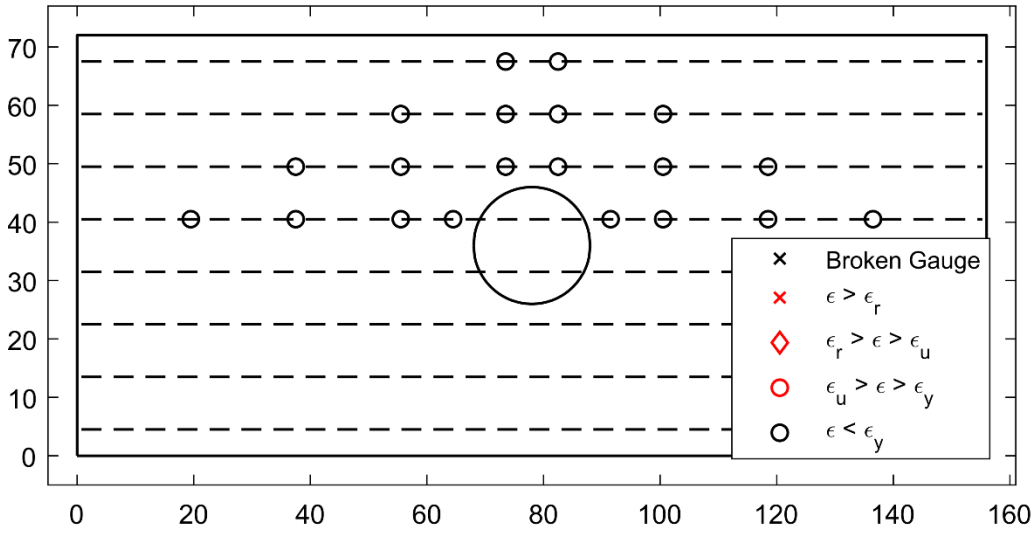

Figure 13: Bottom Reinforcement Strain Summary – 0.56% (SR_4_10_5)

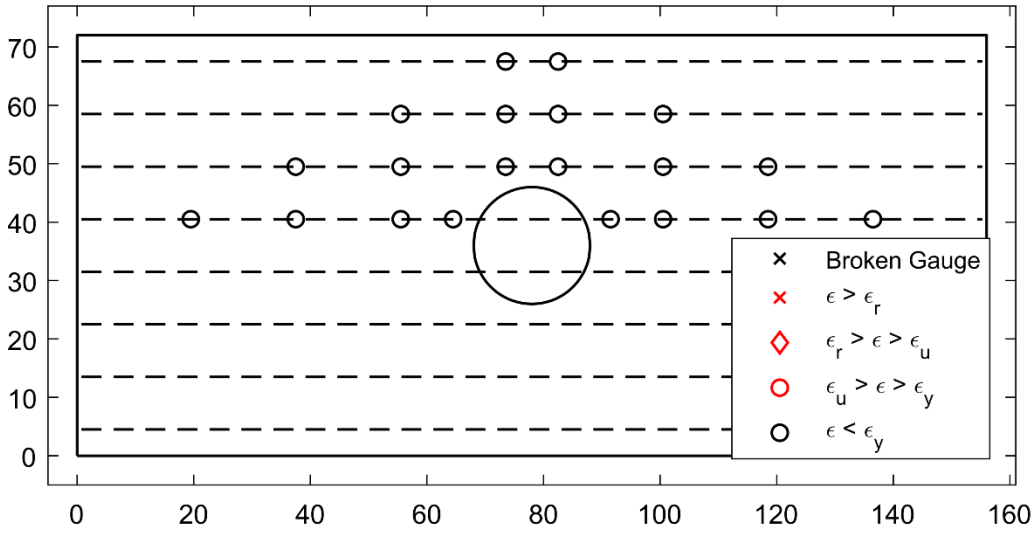

Figure 14: Bottom Reinforcement Strain Summary – 0.91% (SR_4_10_5)

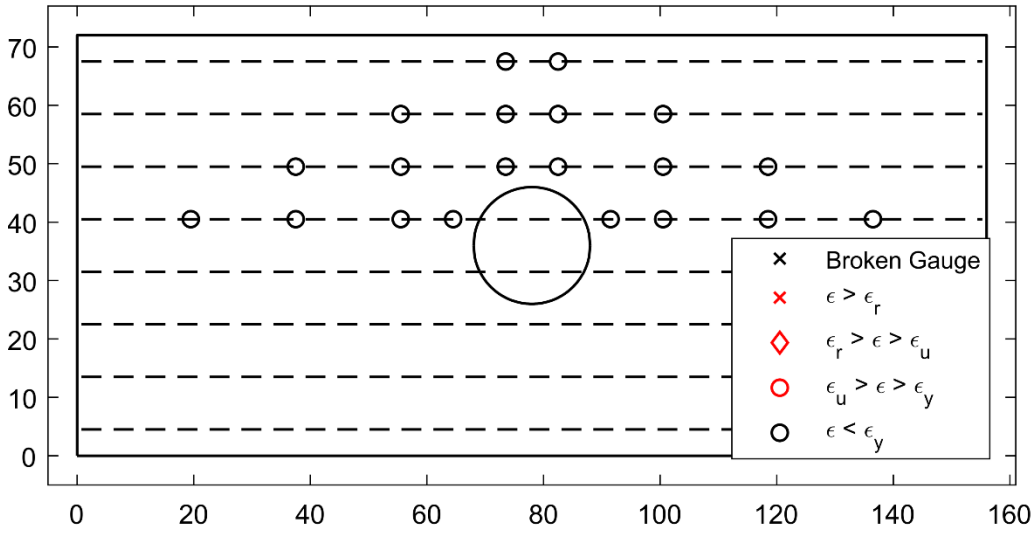

Figure 15: Bottom Reinforcement Strain Summary – 1.3% (SR_4_10_5)

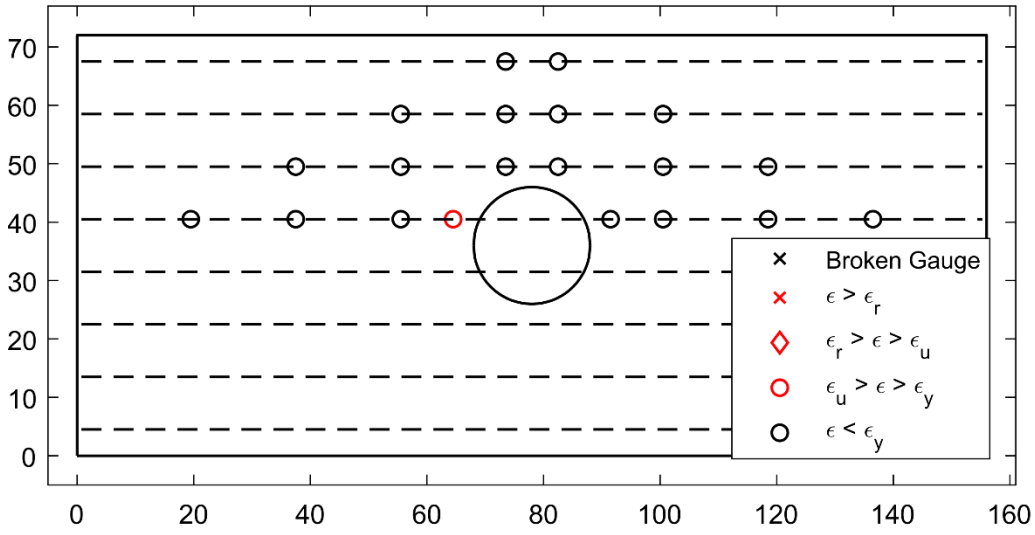

Figure 16: Bottom Reinforcement Strain Summary – 2.0% (SR_4_10_5)

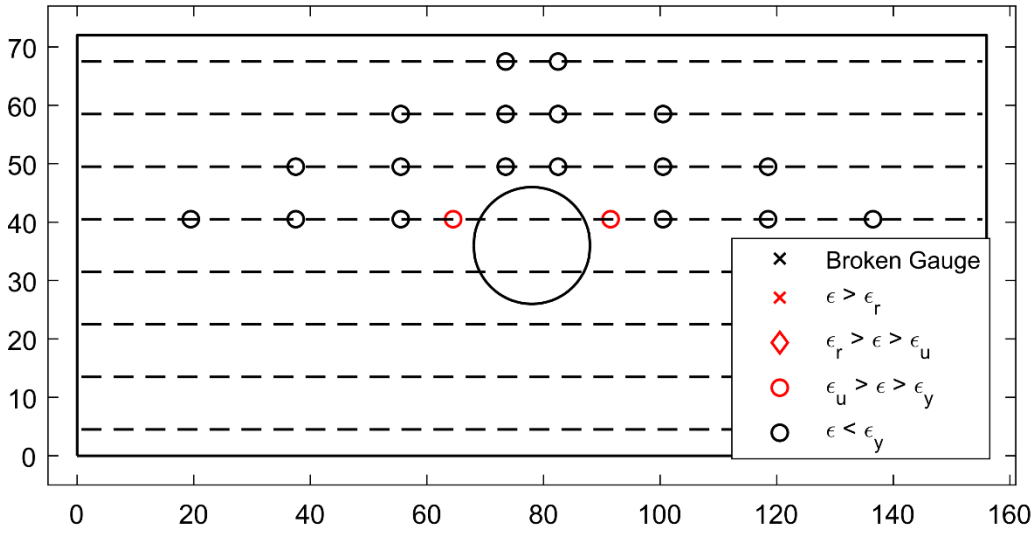

Figure 17: Bottom Reinforcement Strain Summary – 2.7% (SR_4_10_5)

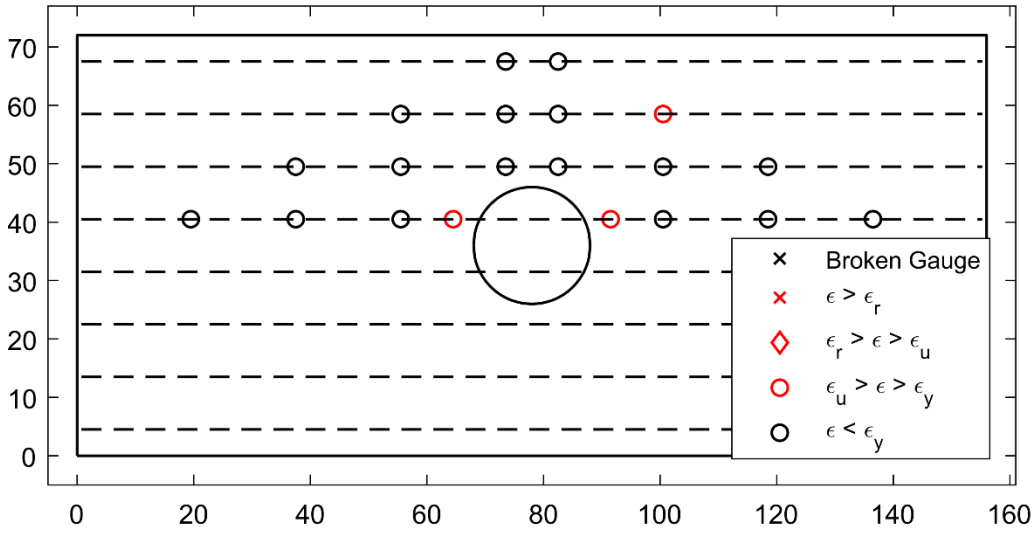

Figure 18: Bottom Reinforcement Strain Summary – 3.4% (SR_4_10_5)

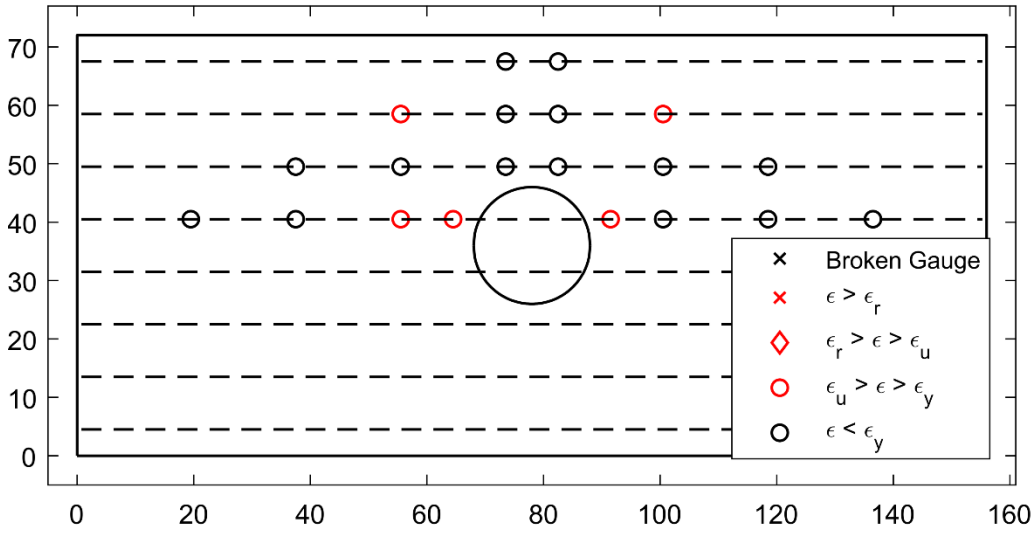

Figure 19: Bottom Reinforcement Strain Summary – 4.2% (SR_4_10_5)

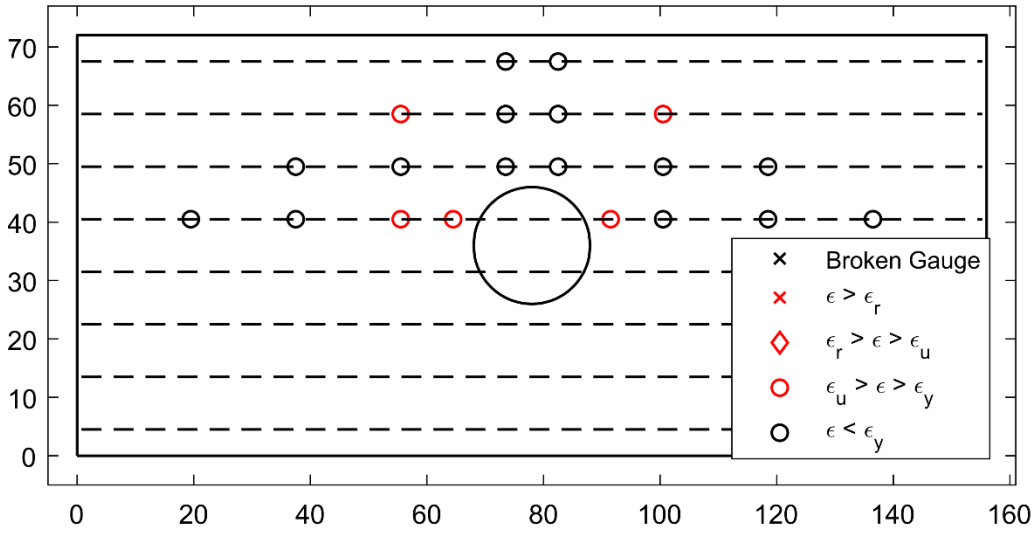

Figure 20: Bottom Reinforcement Strain Summary – 4.9% (SR_4_10_5)

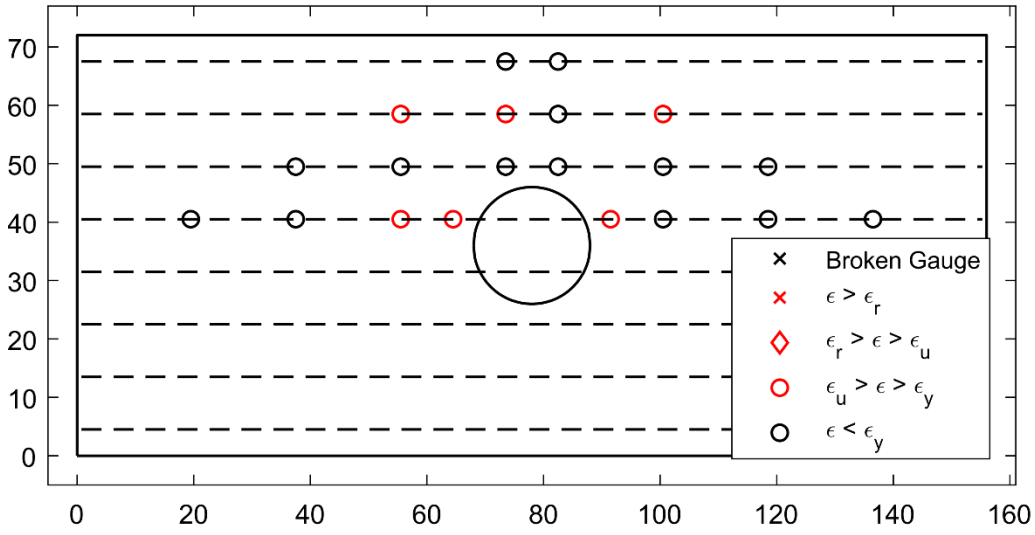

Figure 21: Bottom Reinforcement Strain Summary – 5.6% (SR_4_10_5)

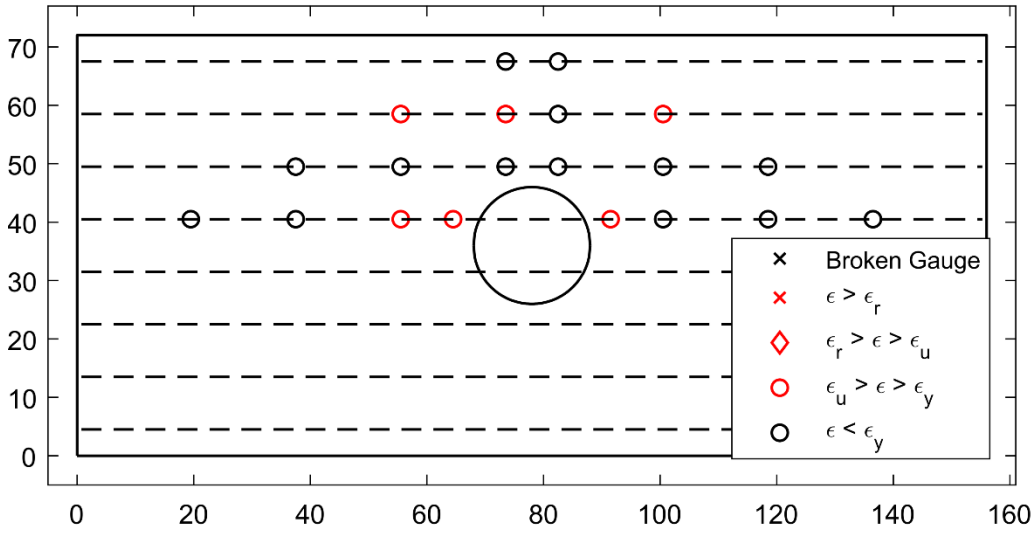

Figure 22: Bottom Reinforcement Strain Summary – 6.4% (SR_4_10_5)

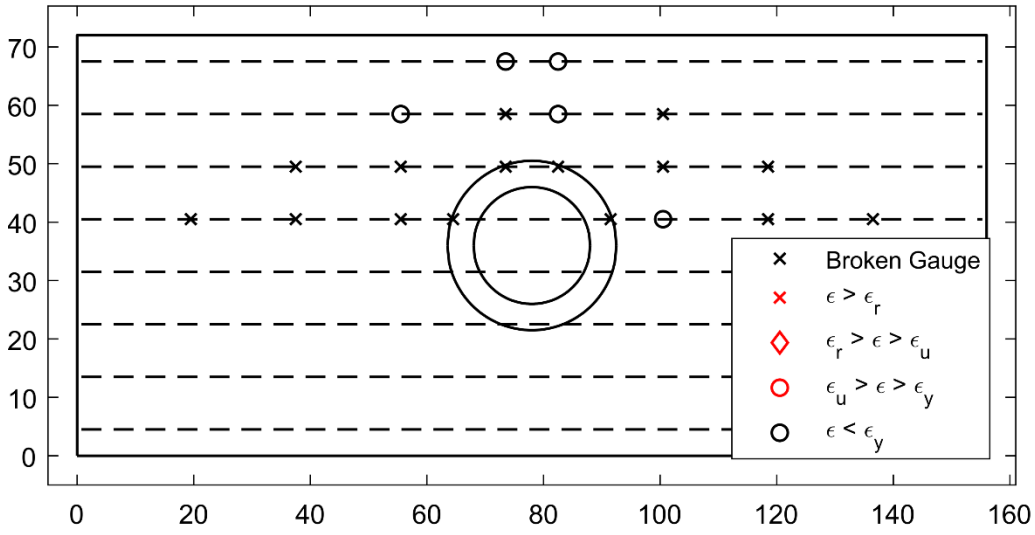

Figure 23: Top Reinforcement Strain Summary – 1.3% (PTB_4.5_1_0)

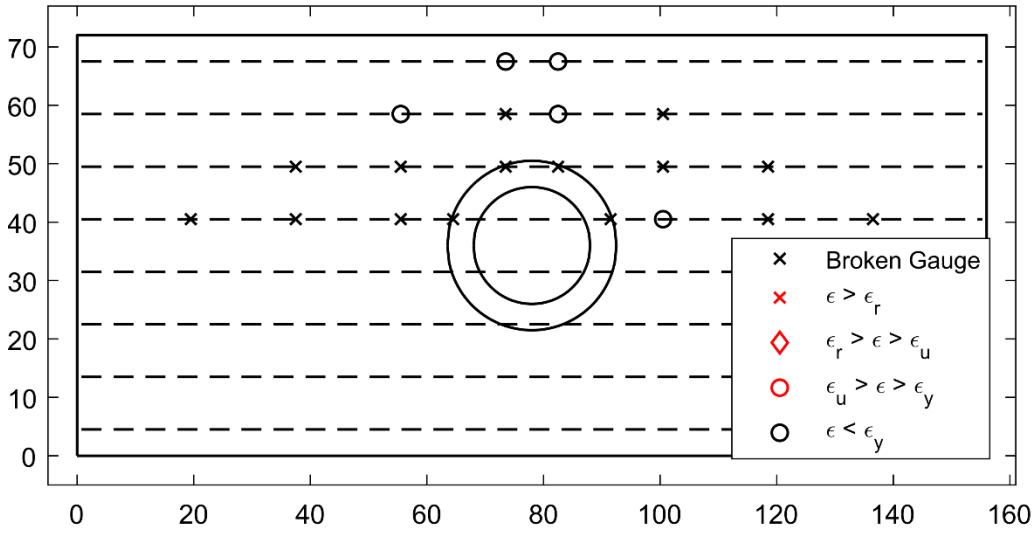

Figure 24: Top Reinforcement Strain Summary – 2.0% (PTB_4.5_1_0)

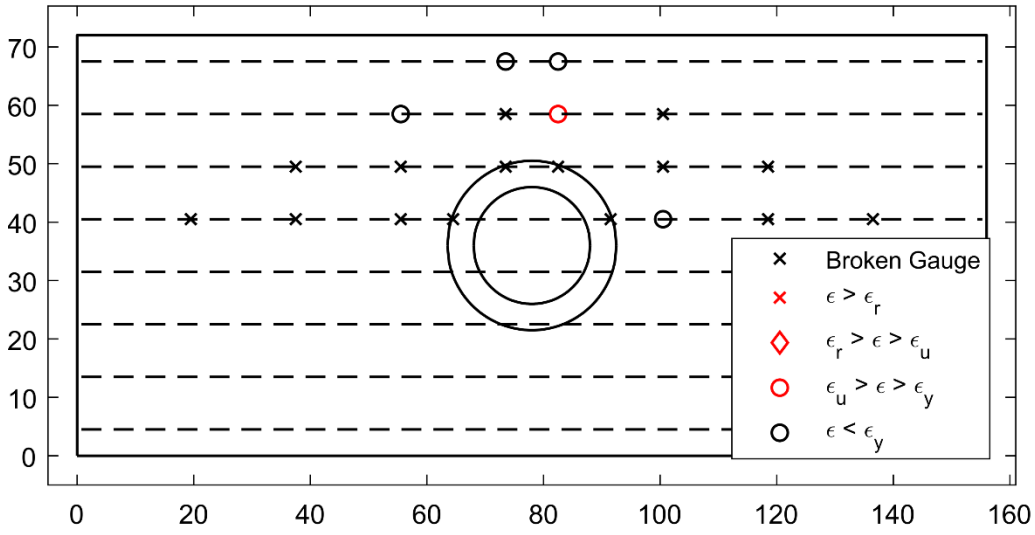

Figure 25: Top Reinforcement Strain Summary – 2.6% (PTB_4.5_1_0)

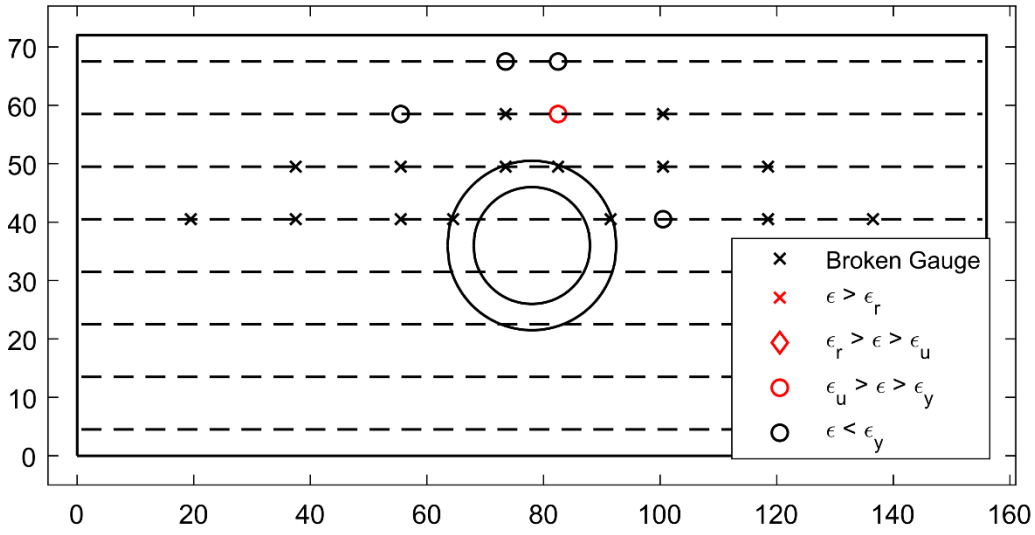

Figure 26: Top Reinforcement Strain Summary – 3.4% (PTB_4.5_1_0)

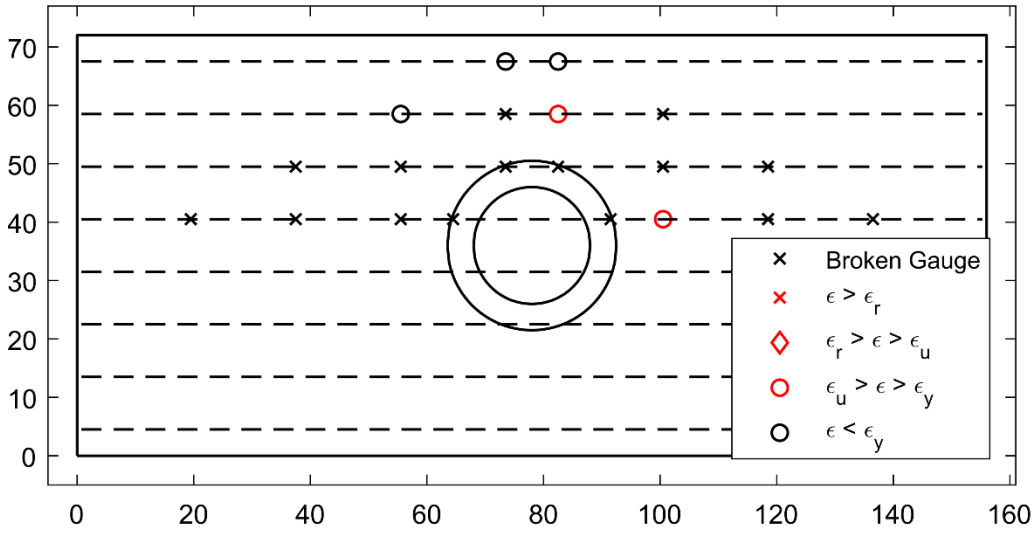

Figure 27: Top Reinforcement Strain Summary – 4.1% (PTB_4.5_1_0)

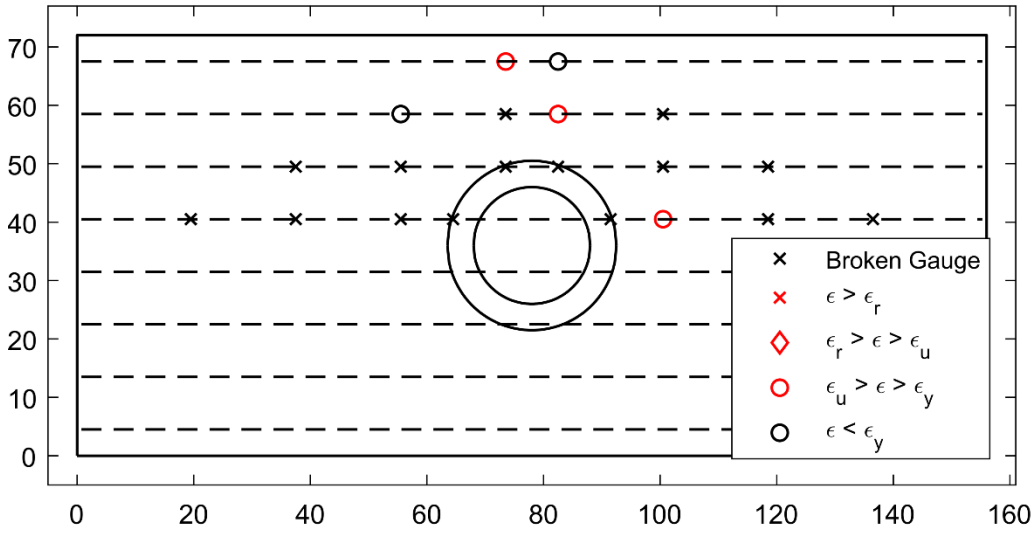

Figure 28: Top Reinforcement Strain Summary – 4.8% (PTB_4.5_1_0)

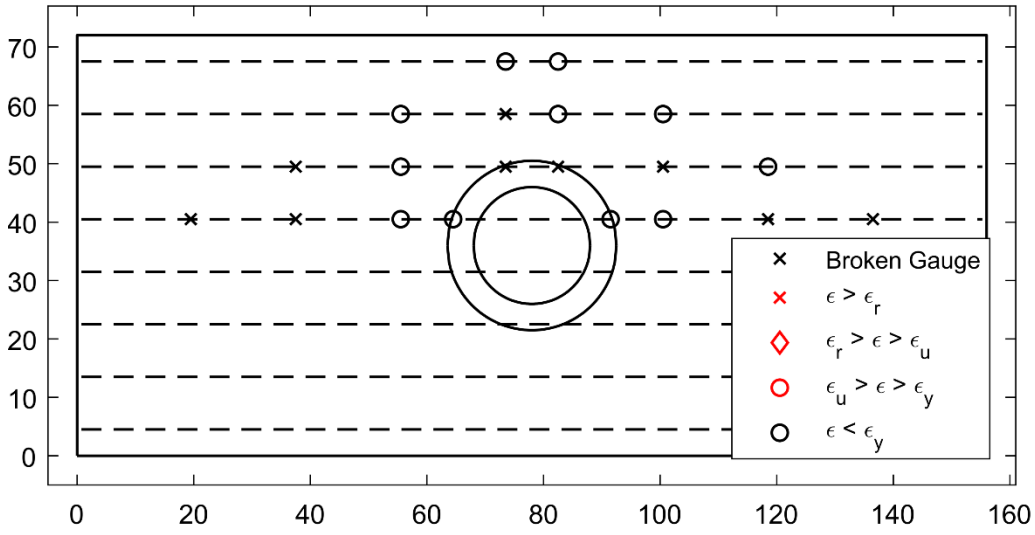

Figure 29: Bottom Reinforcement Strain Summary – 1.3% (PTB_4.5_1_0)

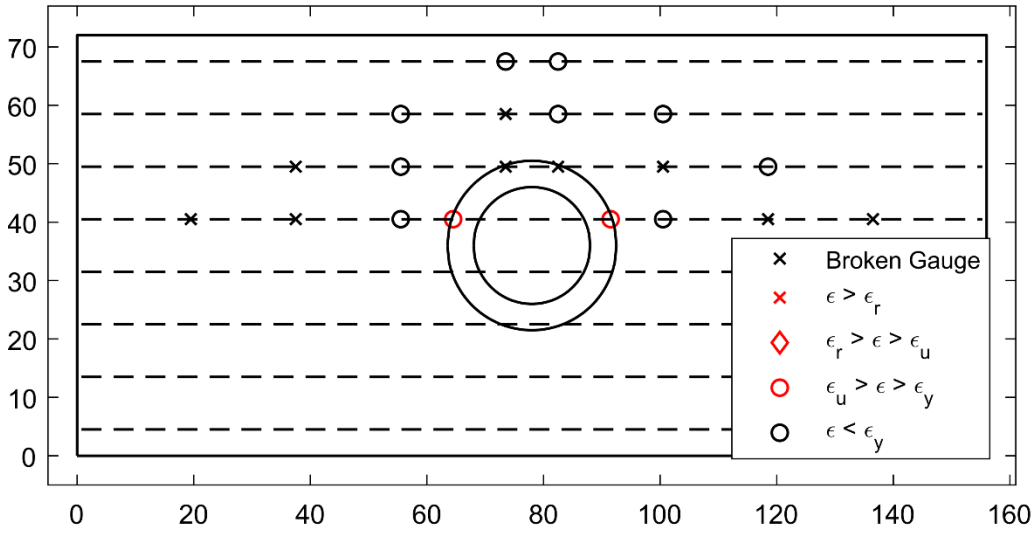

Figure 30: Bottom Reinforcement Strain Summary – 2.0% (PTB_4.5_1_0)

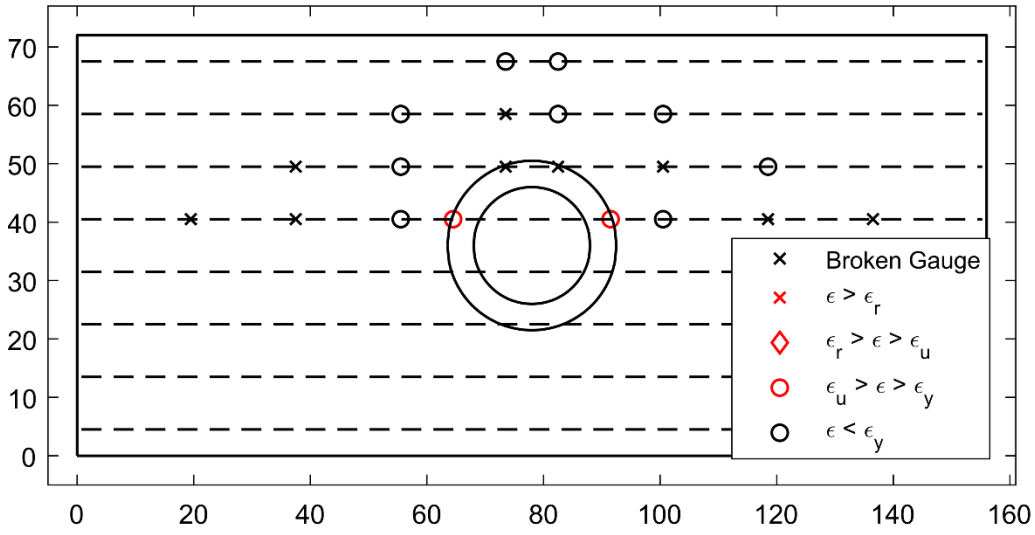

Figure 31: Bottom Reinforcement Strain Summary – 2.6% (PTB_4.5_1_0)

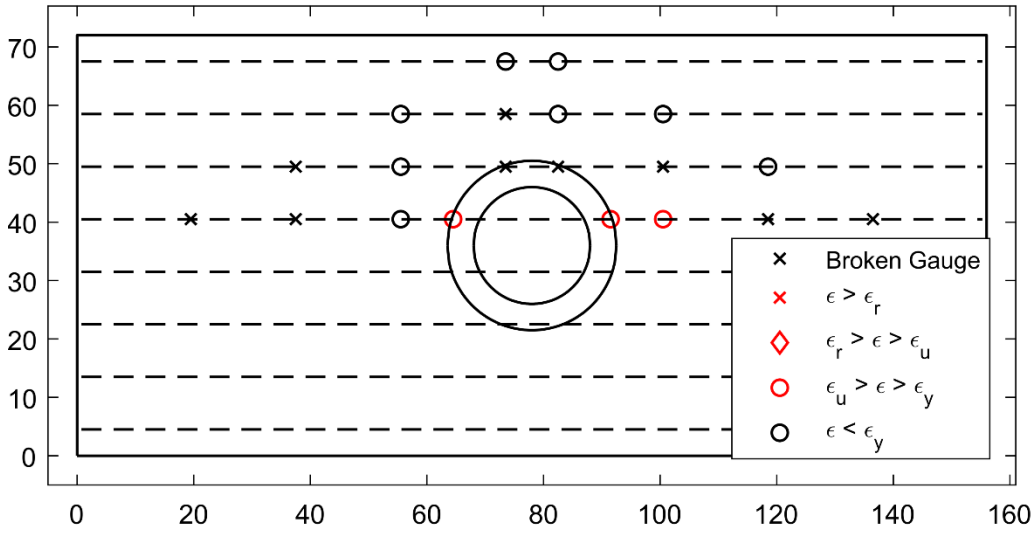

Figure 32: Bottom Reinforcement Strain Summary – 3.4% (PTB_4.5_1_0)

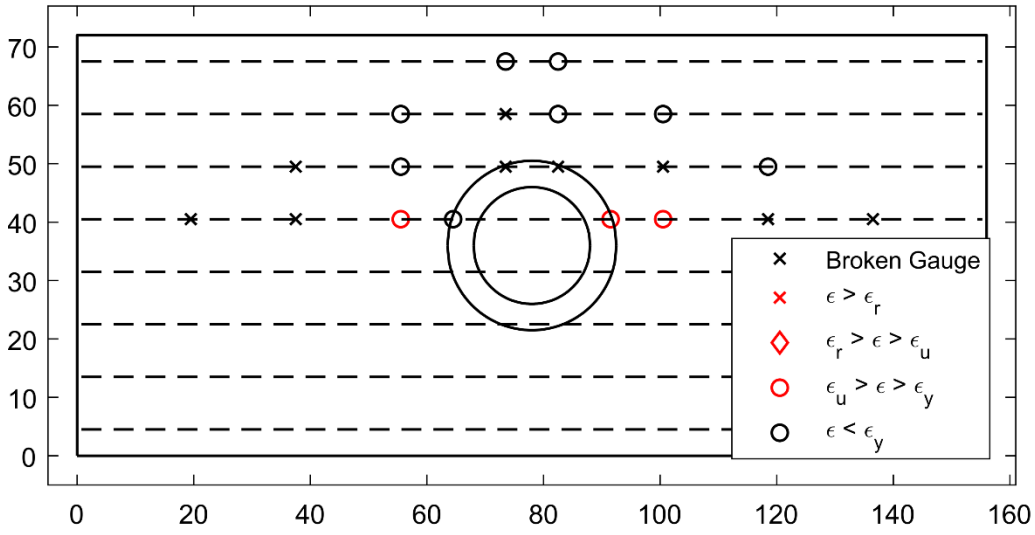

Figure 33: Bottom Reinforcement Strain Summary – 4.1% (PTB_4.5_1_0)

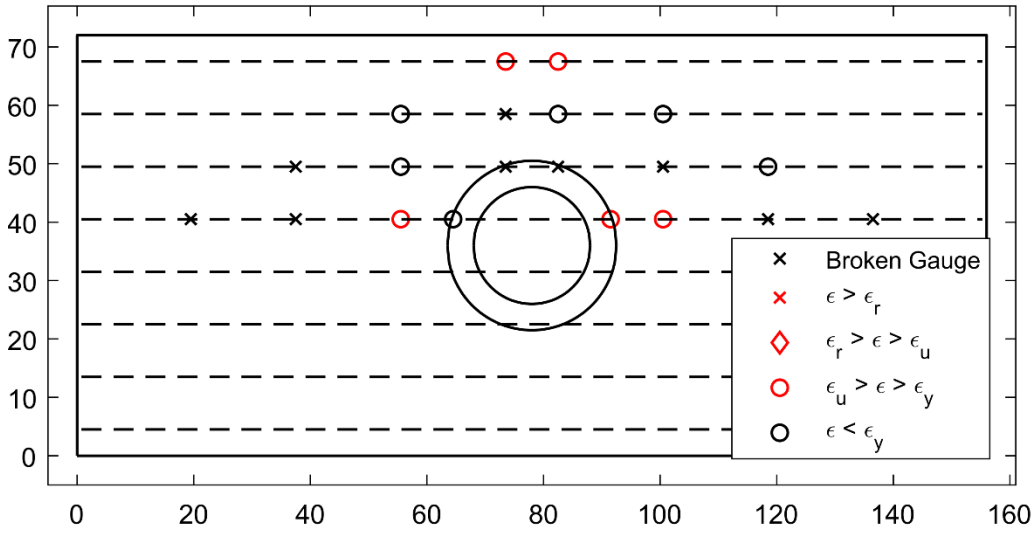

Figure 34: Bottom Reinforcement Strain Summary – 4.8% (PTB_4.5_1_0)

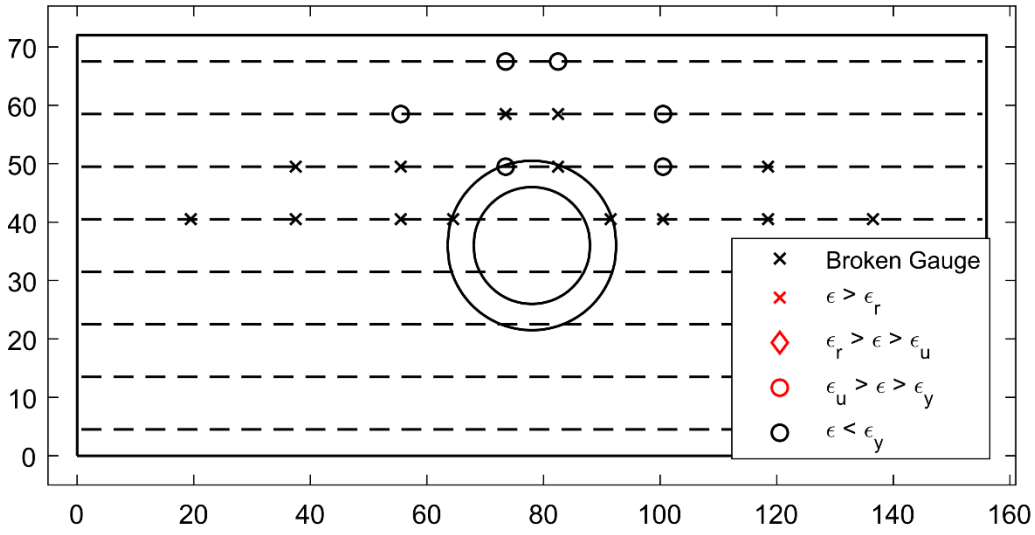

Figure 35: Top Reinforcement Strain Summary – 0.34% (PTB_4.5_1_4)

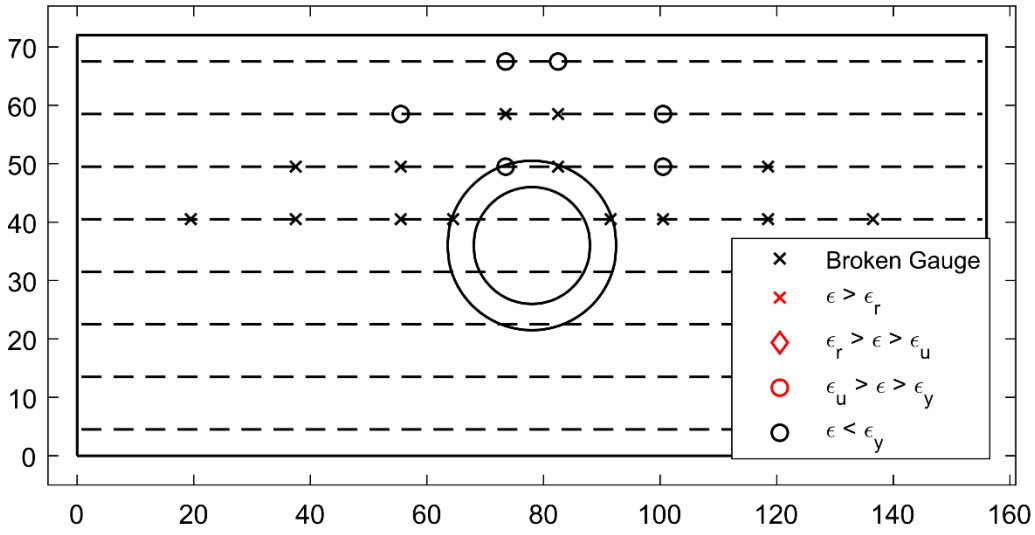

Figure 36: Top Reinforcement Strain Summary – 0.56% (PTB_4.5_1_4)

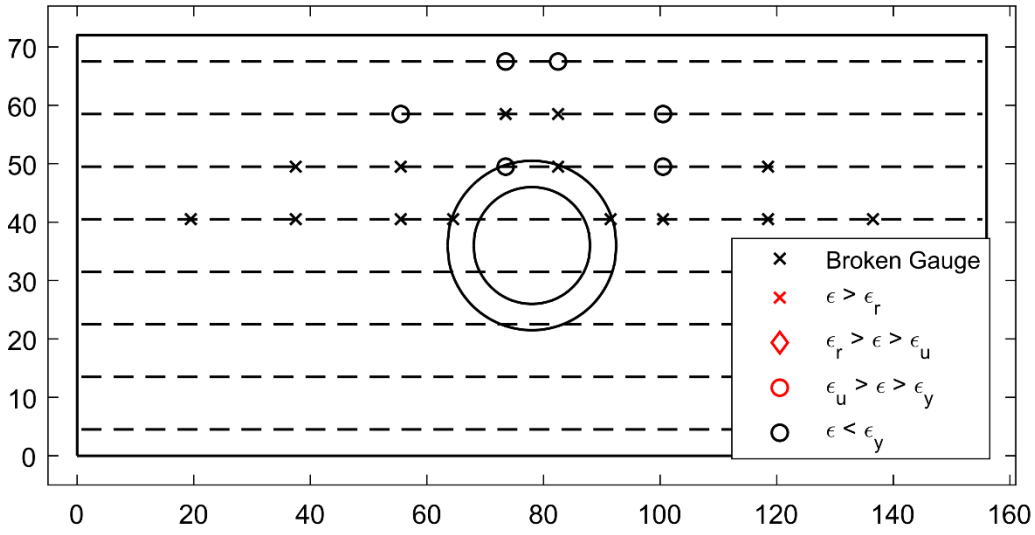

Figure 37: Top Reinforcement Strain Summary – 0.91% (PTB_4.5_1_4)

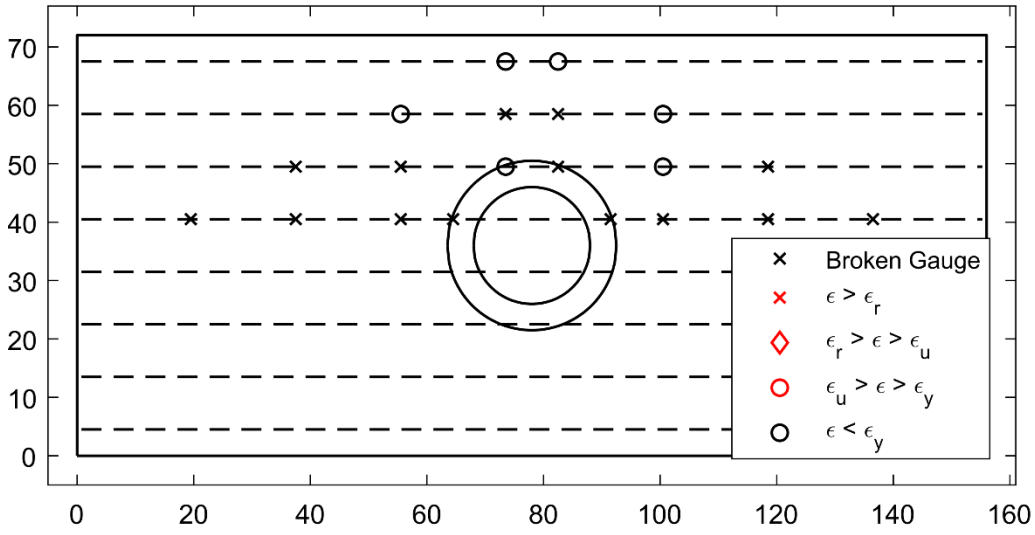

Figure 38: Top Reinforcement Strain Summary – 1.2% (PTB_4.5_1_4)

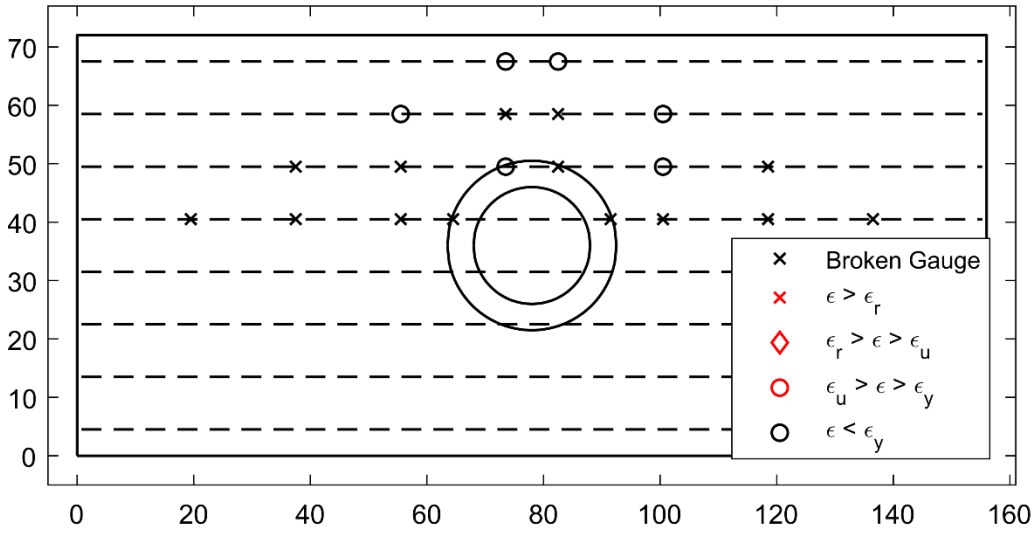

Figure 39: Top Reinforcement Strain Summary – 1.9% (PTB_4.5_1_4)

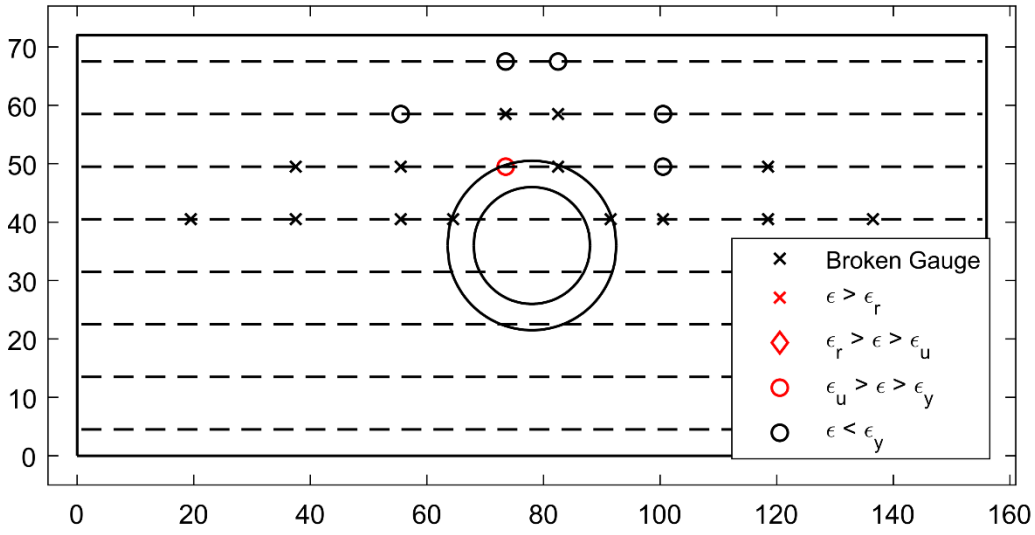

Figure 40: Top Reinforcement Strain Summary – 2.6% (PTB_4.5_1_4)

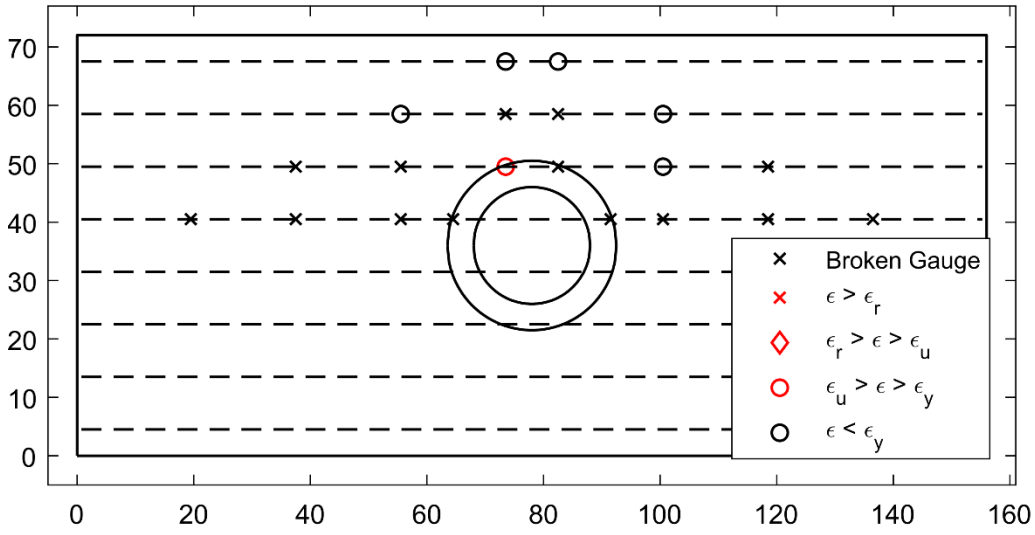

Figure 41: Top Reinforcement Strain Summary – 3.4% (PTB_4.5_1_4)

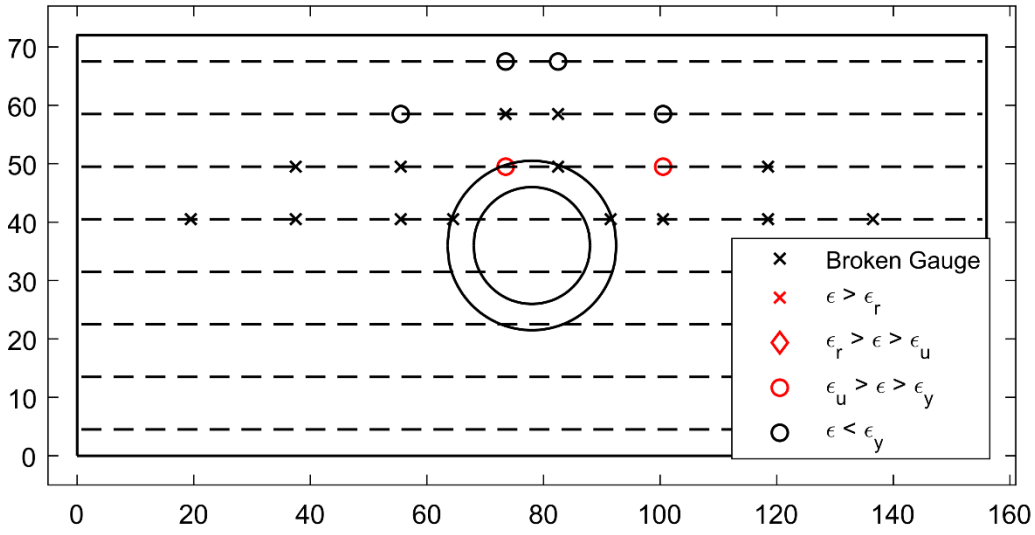

Figure 42: Top Reinforcement Strain Summary – 4.1% (PTB_4.5_1_4)

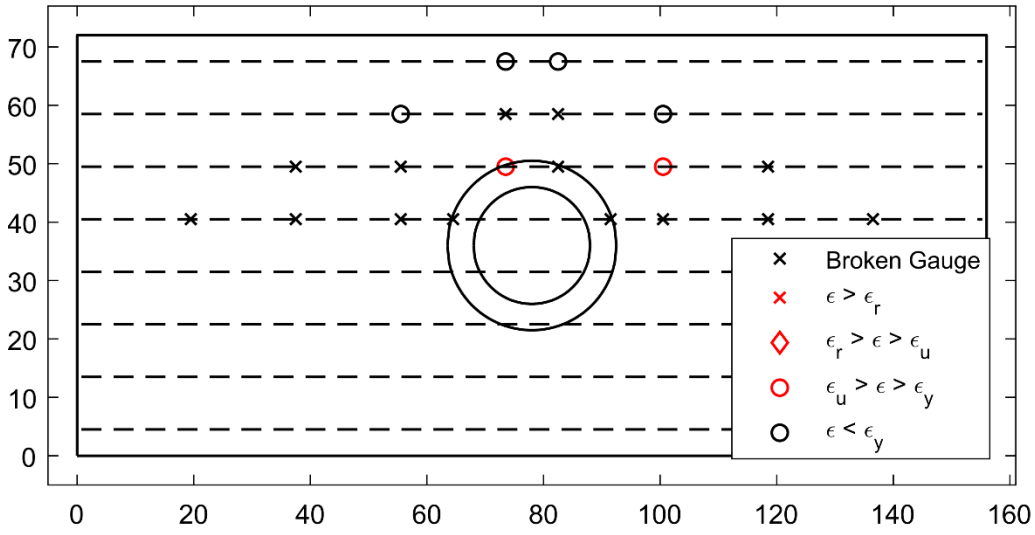

Figure 43: Top Reinforcement Strain Summary – 4.8% (PTB_4.5_1_4)

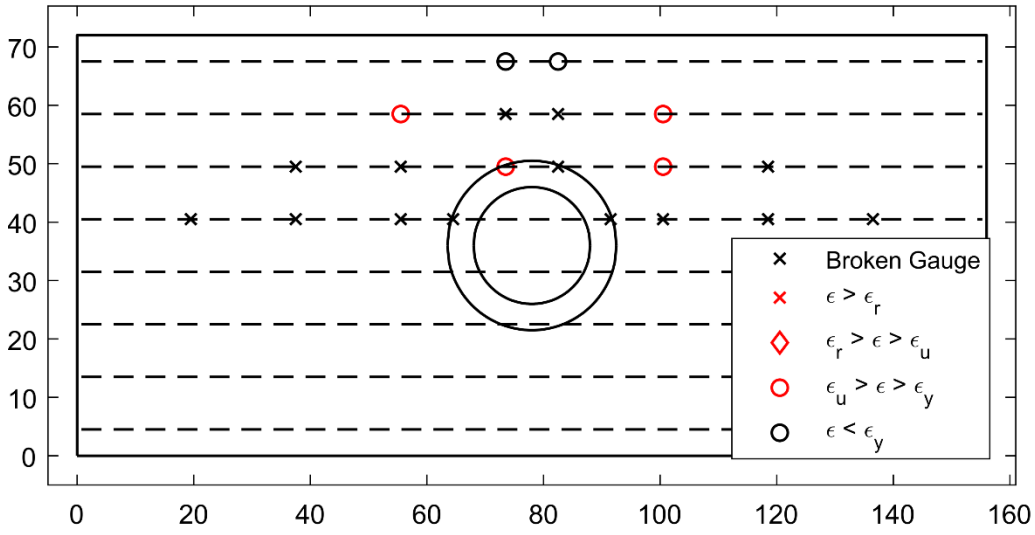

Figure 44: Top Reinforcement Strain Summary – 5.5% (PTB_4.5_1_4)

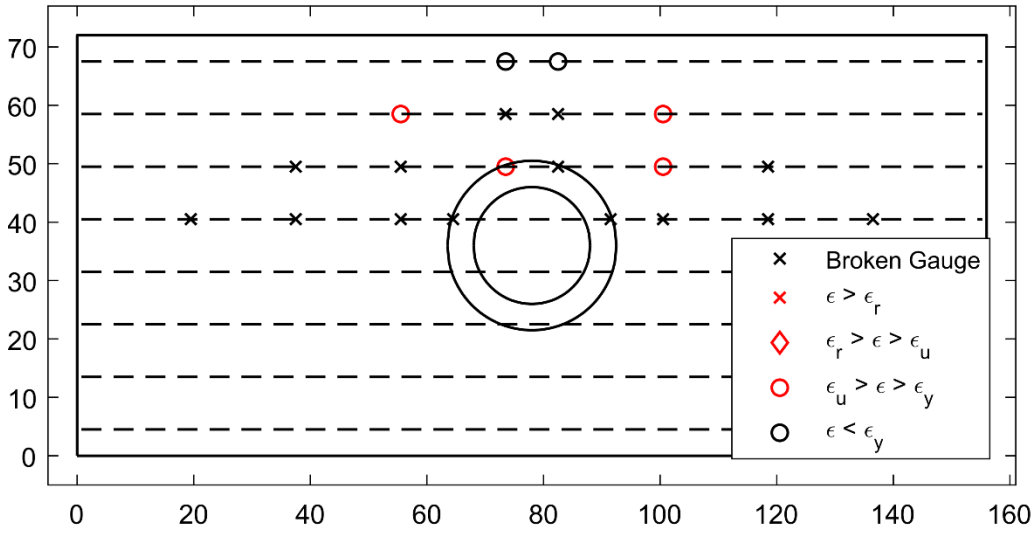

Figure 45: Top Reinforcement Strain Summary – 6.3% (PTB_4.5_1_4)

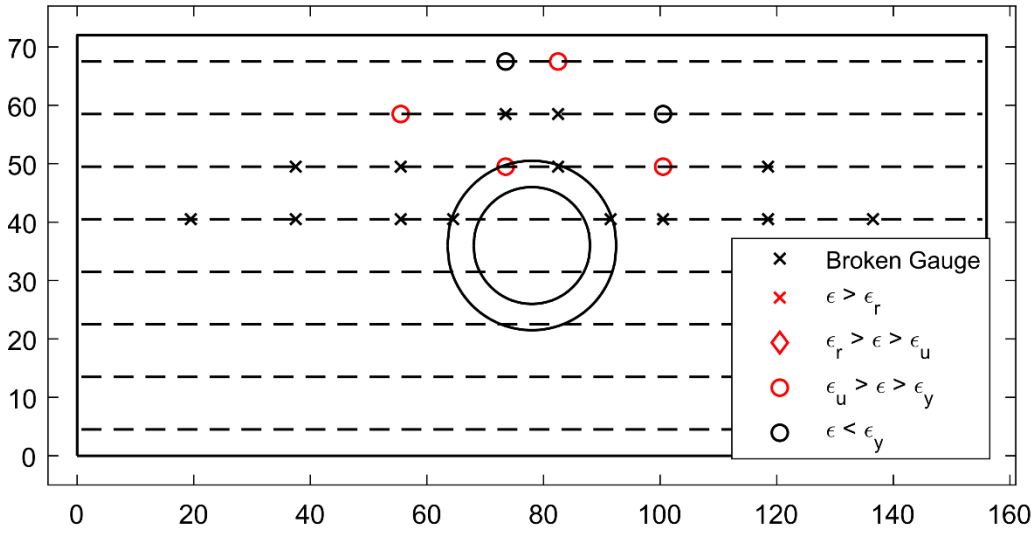

Figure 46: Top Reinforcement Strain Summary – 6.7% (PTB_4.5_1_4)

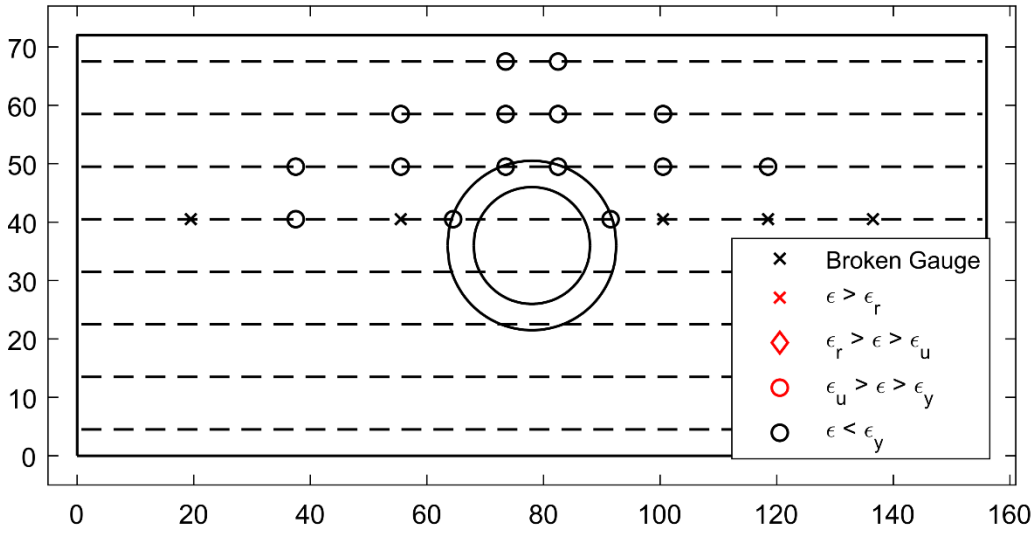

Figure 47: Bottom Reinforcement Strain Summary – 0.34% (PTB_4.5_1_4)

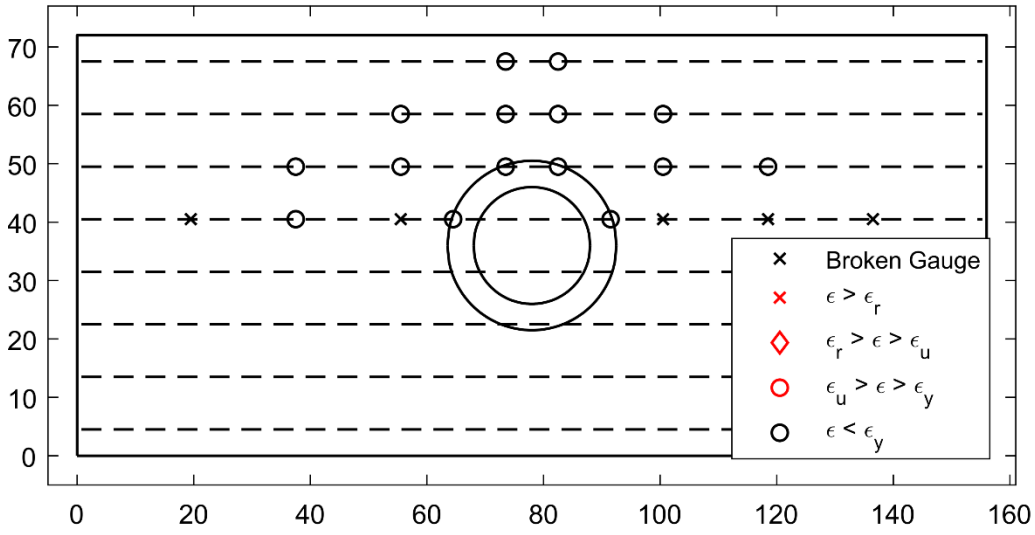

Figure 48: Bottom Reinforcement Strain Summary – 0.56% (PTB_4.5_1_4)

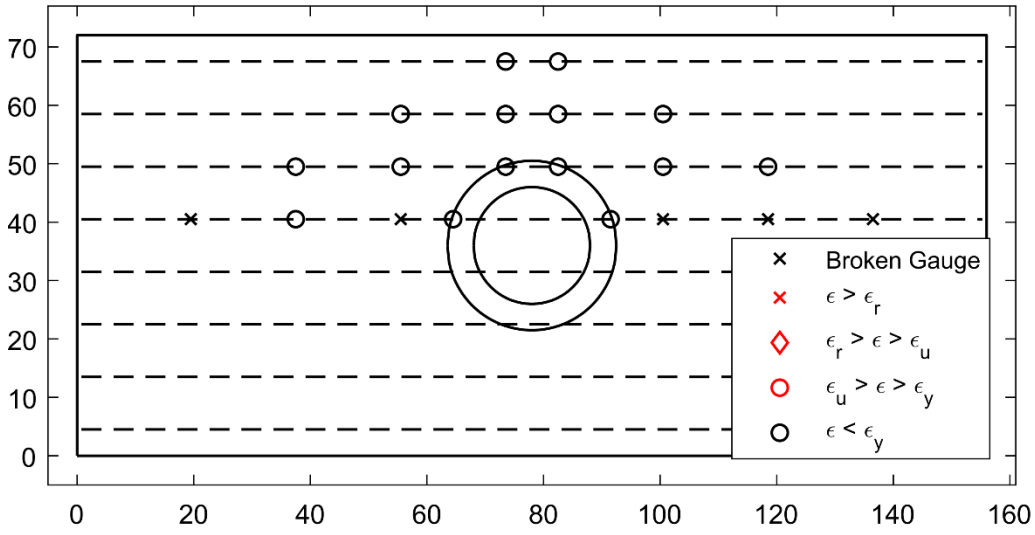

Figure 49: Bottom Reinforcement Strain Summary – 0.91% (PTB_4.5_1_4)

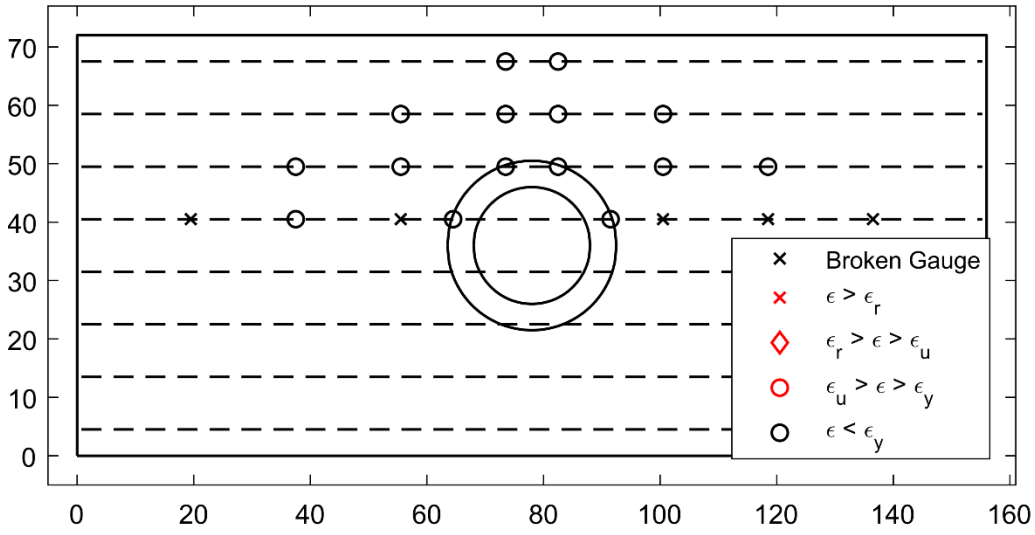

Figure 50: Bottom Reinforcement Strain Summary – 1.2% (PTB_4.5_1_4)

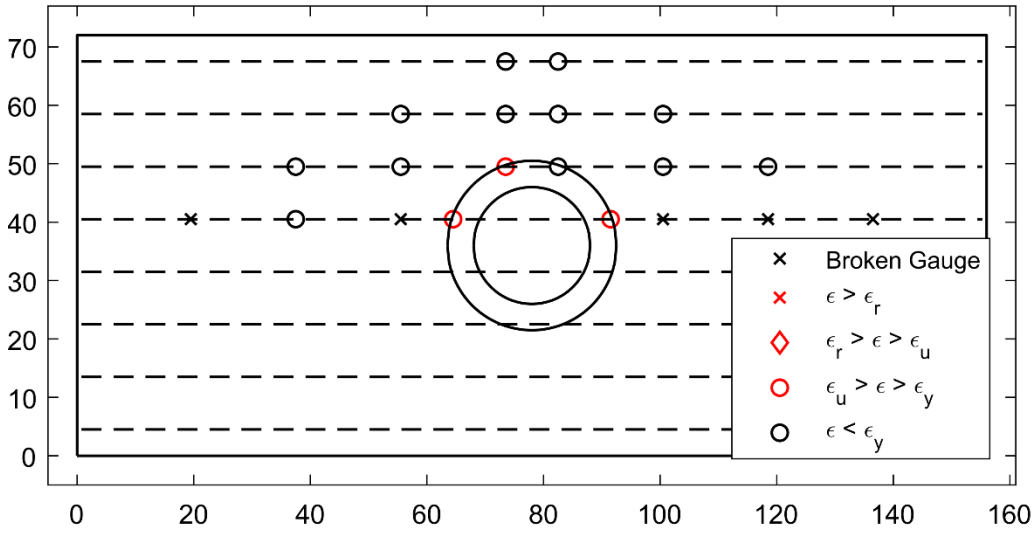

Figure 51: Bottom Reinforcement Strain Summary – 1.9% (PTB_4.5_1_4)

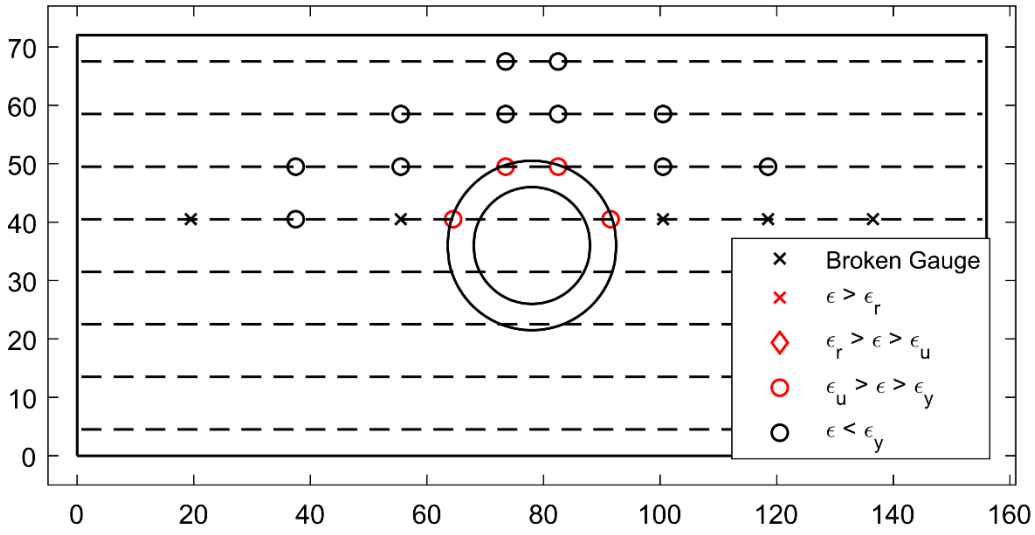

Figure 52: Bottom Reinforcement Strain Summary – 2.6% (PTB_4.5_1_4)

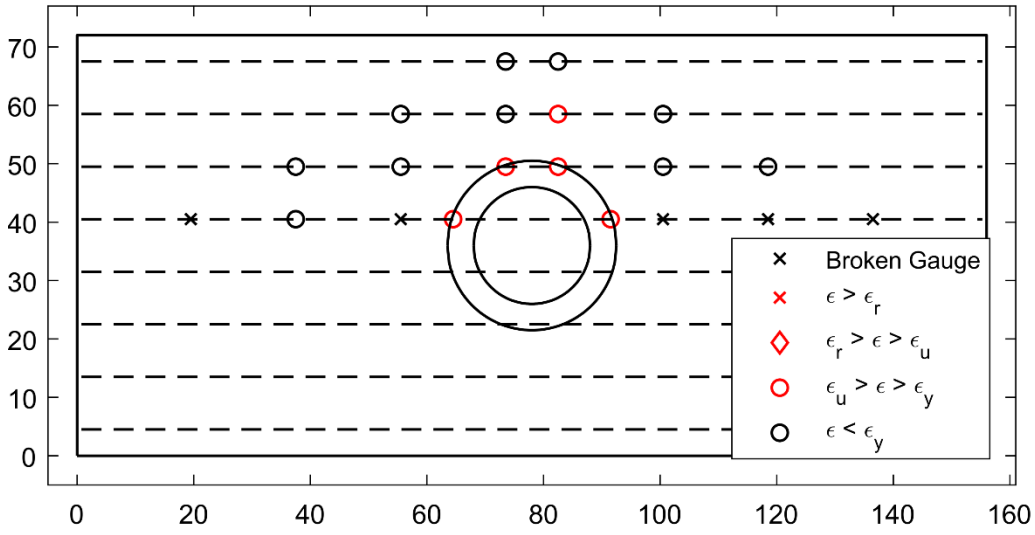

Figure 53: Bottom Reinforcement Strain Summary – 3.4% (PTB_4.5_1_4)

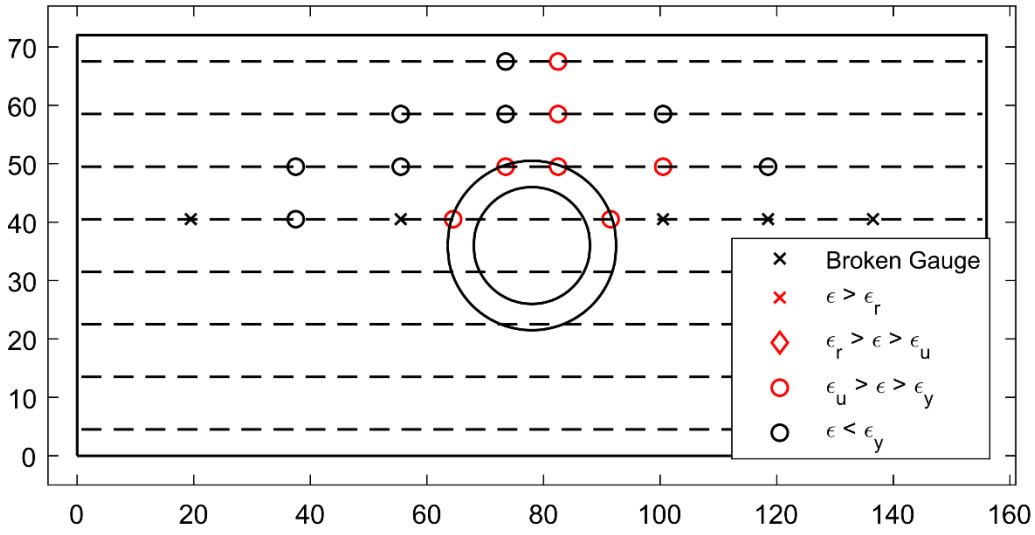

Figure 54: Bottom Reinforcement Strain Summary – 4.1% (PTB_4.5_1_4)

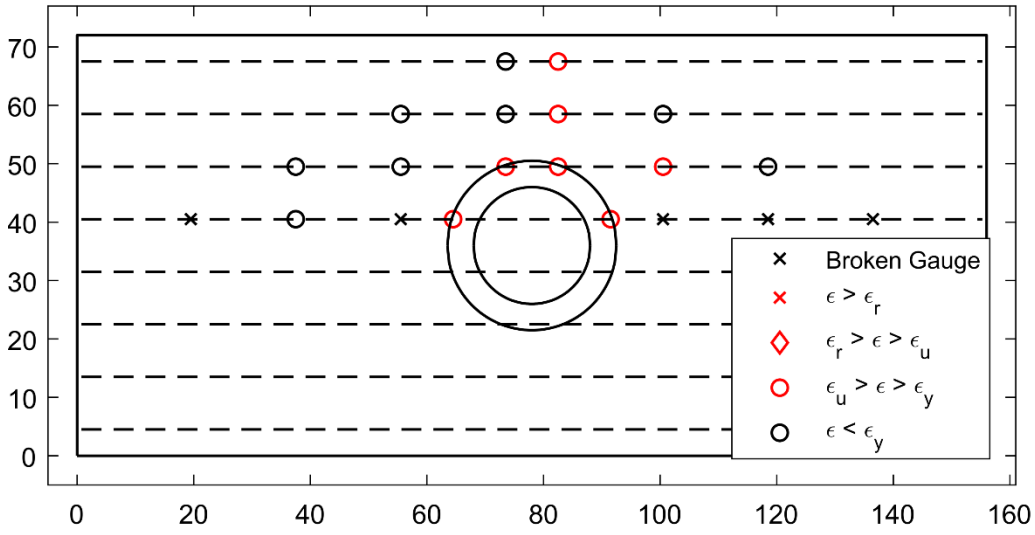

Figure 55: Bottom Reinforcement Strain Summary – 4.8% (PTB_4.5_1_4)

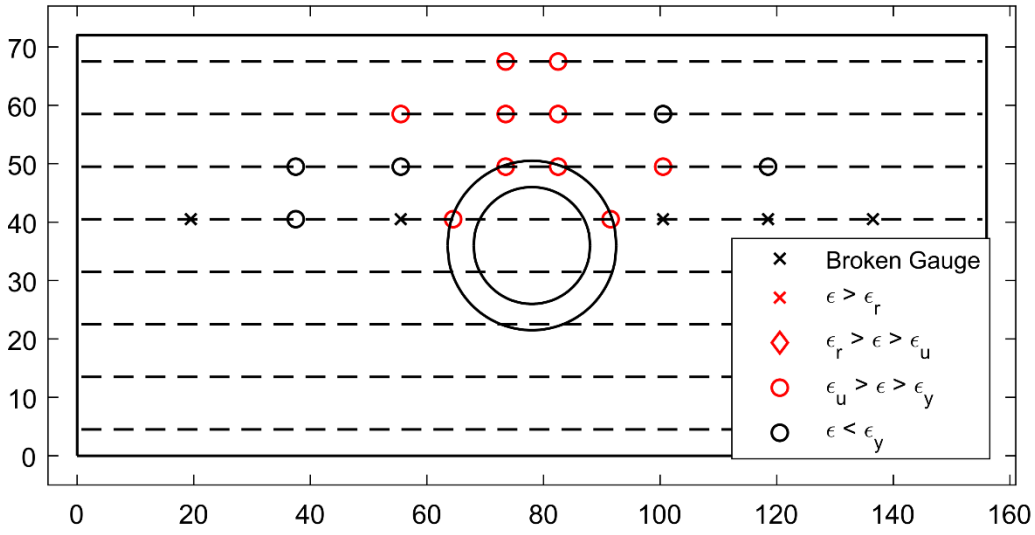

Figure 56: Bottom Reinforcement Strain Summary – 5.5% (PTB_4.5_1_4)

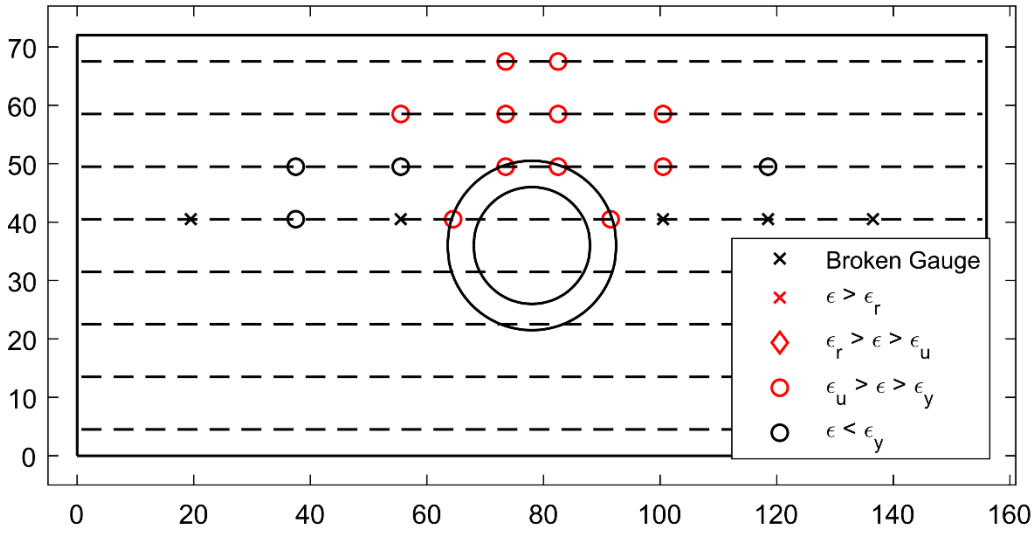

Figure 57: Bottom Reinforcement Strain Summary – 6.3% (PTB_4.5_1_4)

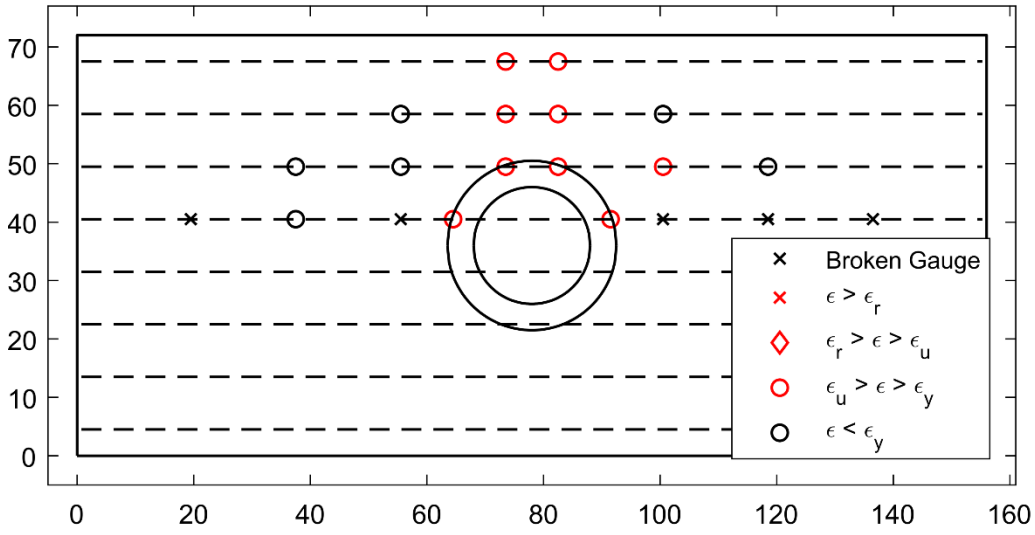

Figure 58: Bottom Reinforcement Strain Summary – 6.7% (PTB_4.5_1_4)

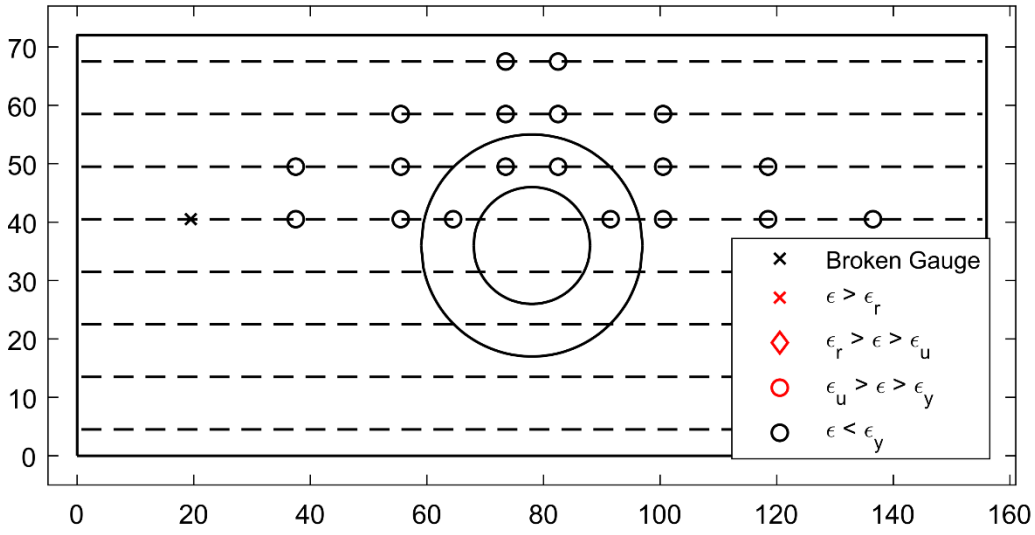

Figure 59: Top Reinforcement Strain Summary – 0.30% (PTB_9_2_0)

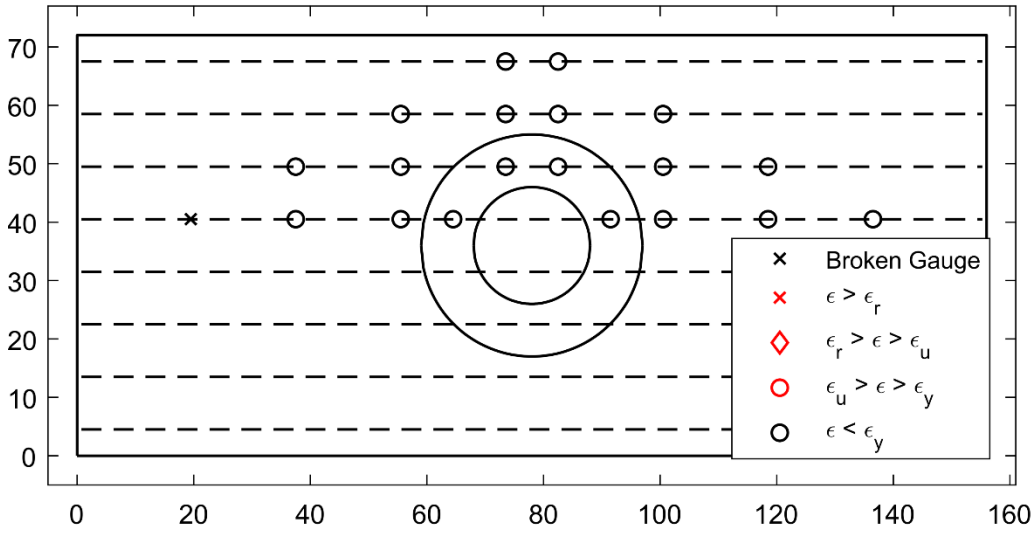

Figure 60: Top Reinforcement Strain Summary – 0.63% (PTB_9_2_0)

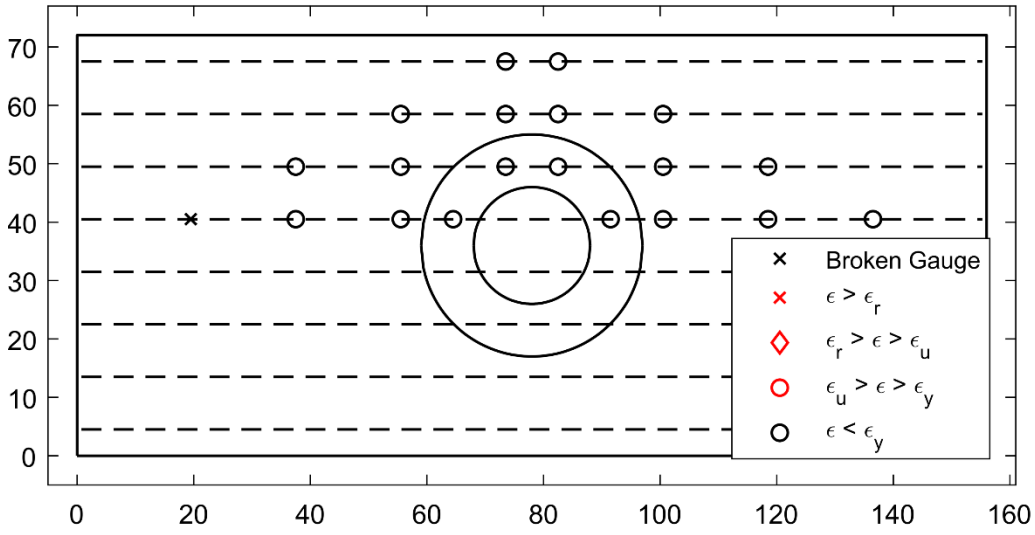

Figure 61: Top Reinforcement Strain Summary – 0.96% (PTB_9_2_0)

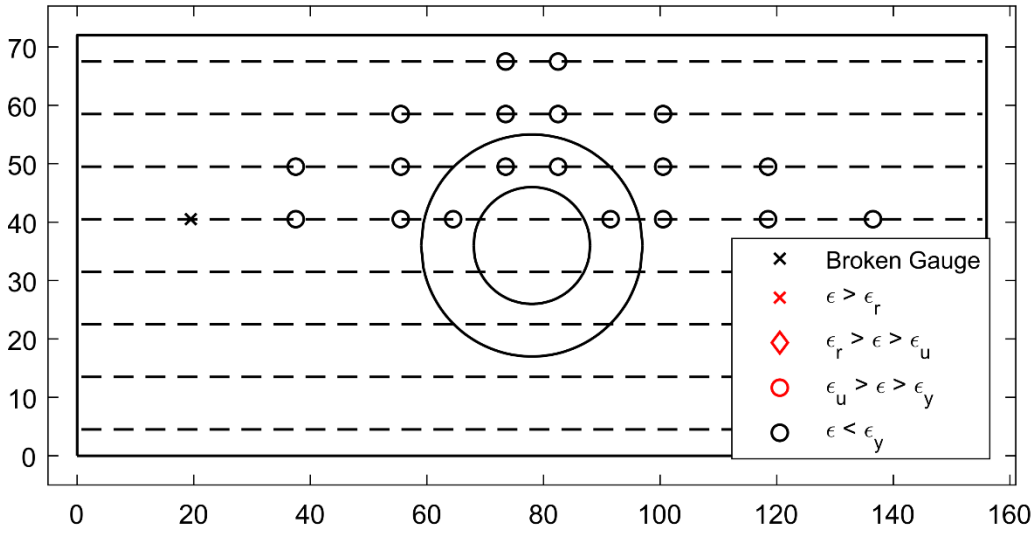

Figure 62: Top Reinforcement Strain Summary – 1.3% (PTB_9_2_0)

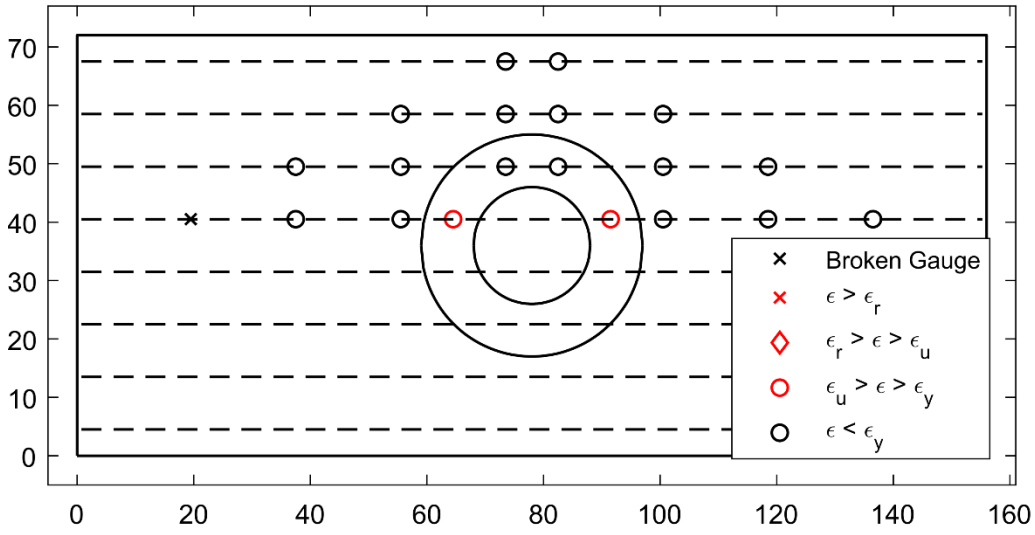

Figure 63: Top Reinforcement Strain Summary – 2.0% (PTB_9_2_0)

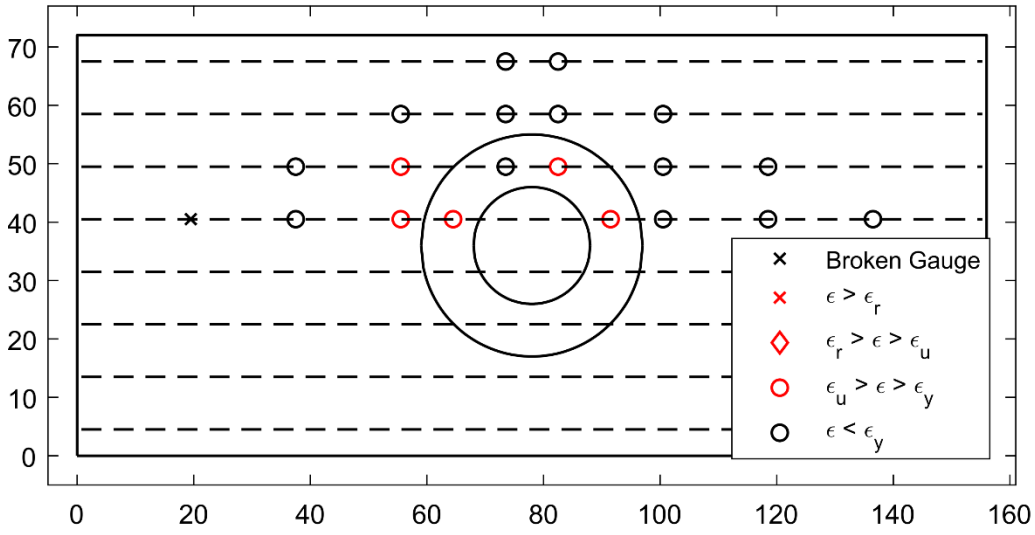

Figure 64: Top Reinforcement Strain Summary – 2.7% (PTB_9_2_0)

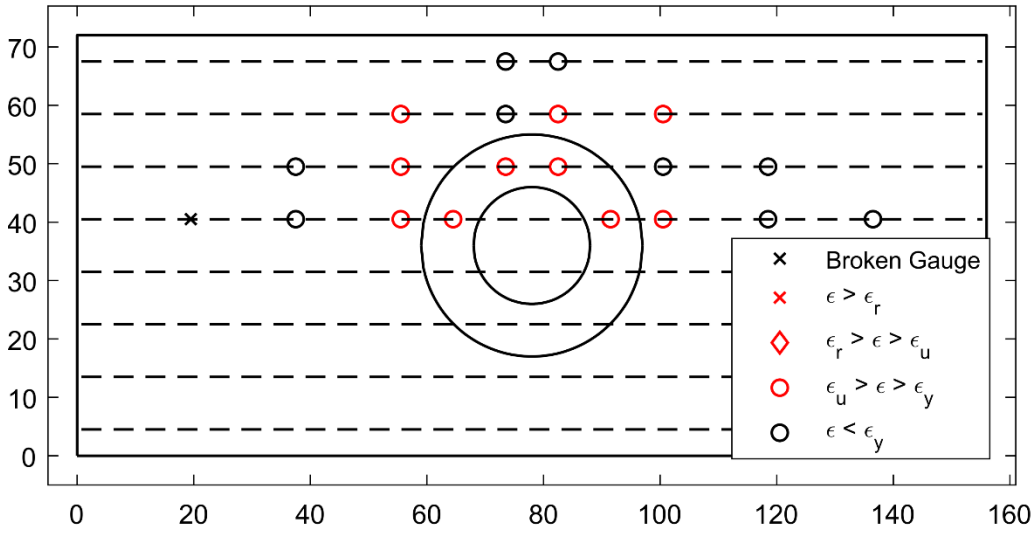

Figure 65: Top Reinforcement Strain Summary – 3.4% (PTB_9_2_0)

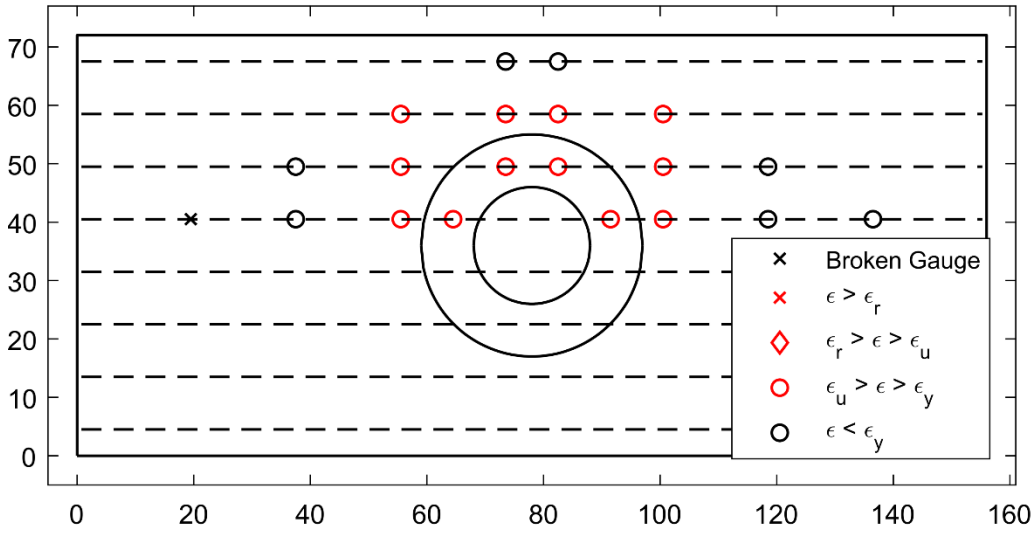

Figure 66: Top Reinforcement Strain Summary – 4.1% (PTB_9_2_0)

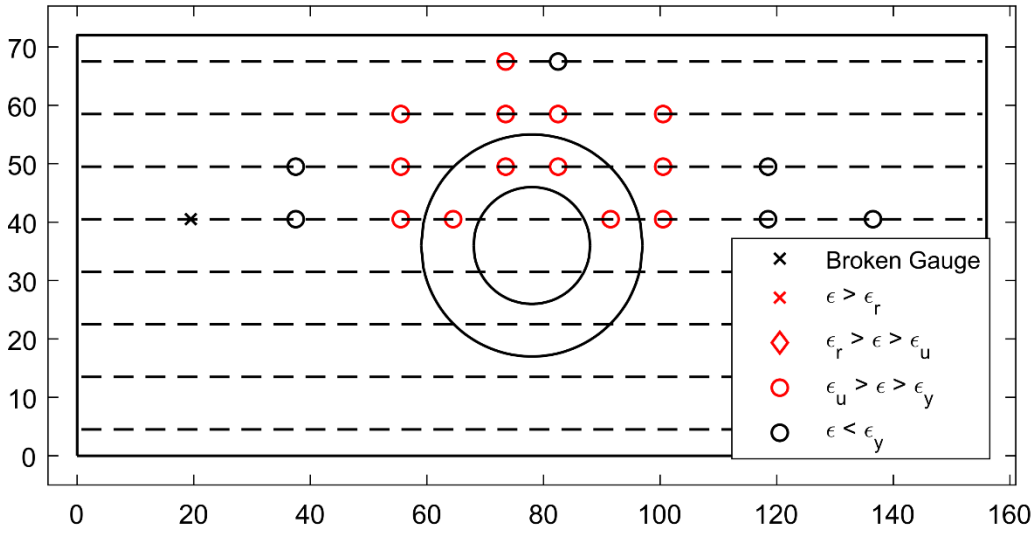

Figure 67: Top Reinforcement Strain Summary – 4.9% (PTB_9_2_0)

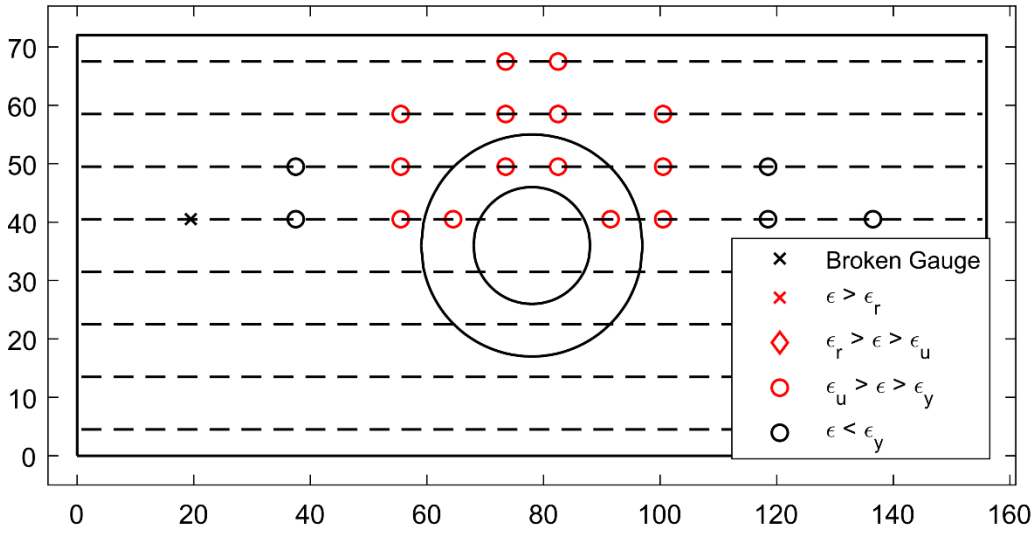

Figure 68: Top Reinforcement Strain Summary – 5.6% (PTB_9_2_0)

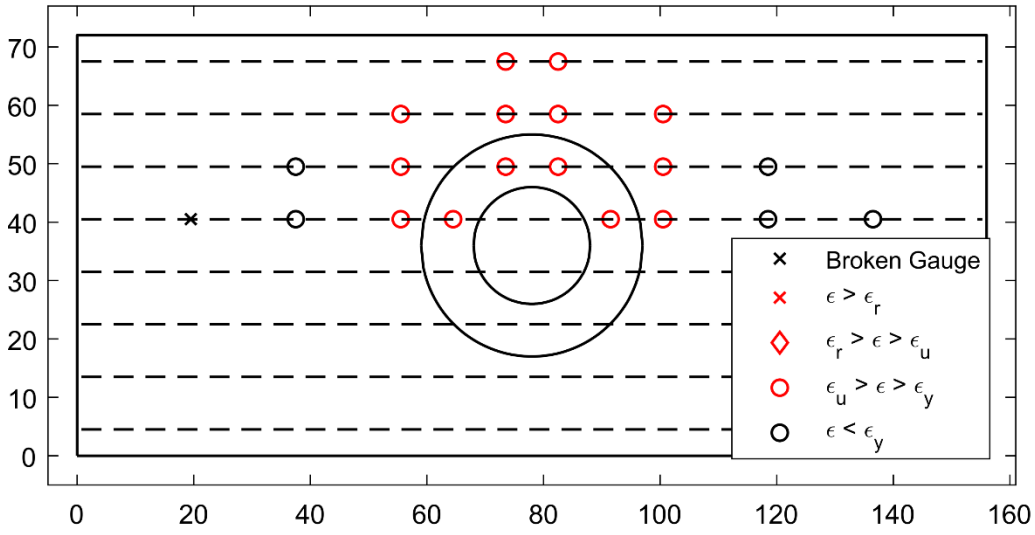

Figure 69: Top Reinforcement Strain Summary – 6.4% (PTB_9_2_0)

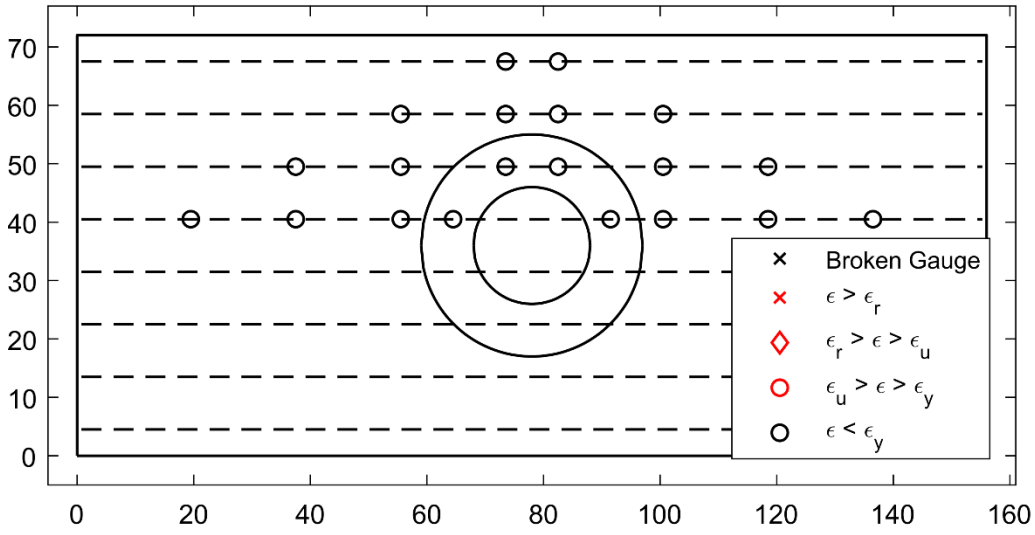

Figure 70: Bottom Reinforcement Strain Summary – 0.30% (PTB_9_2_0)

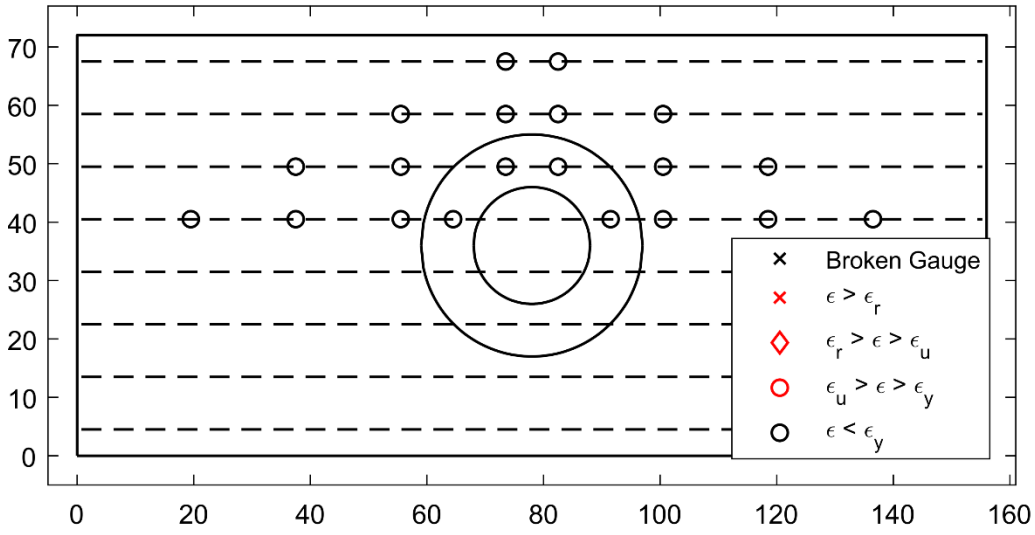

Figure 71: Bottom Reinforcement Strain Summary – 0.63% (PTB_9_2_0)

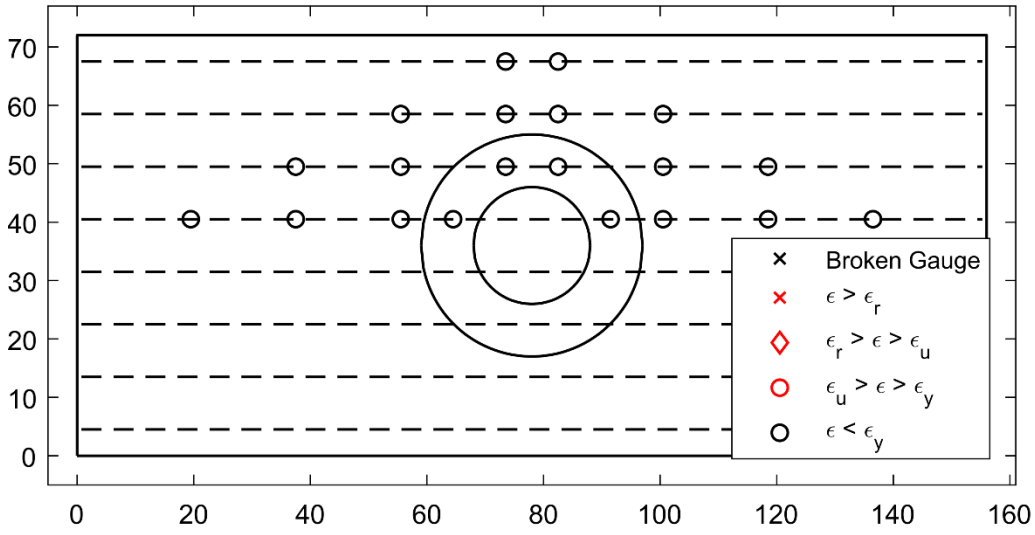

Figure 72: Bottom Reinforcement Strain Summary – 0.96% (PTB_9_2_0)

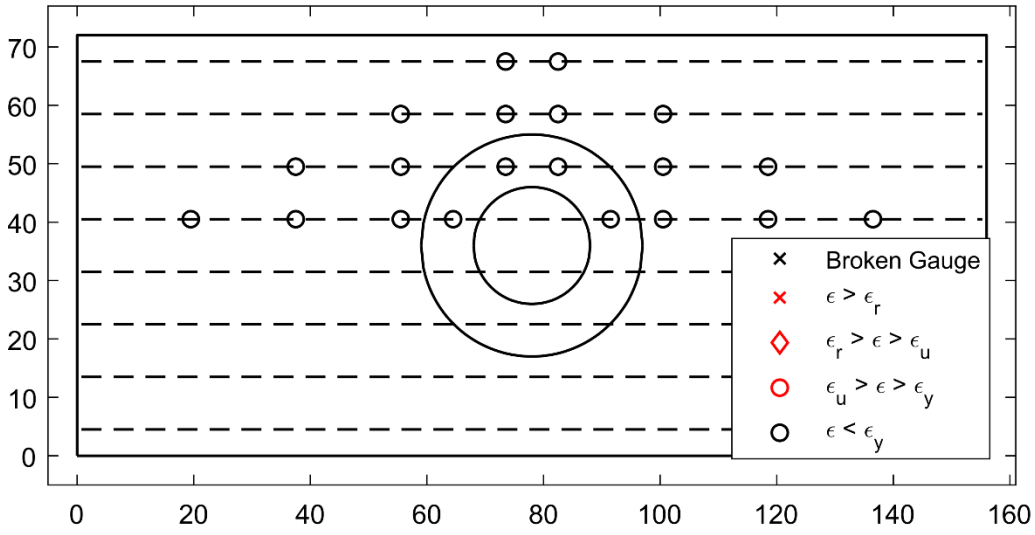

Figure 73: Bottom Reinforcement Strain Summary – 1.3% (PTB_9_2_0)

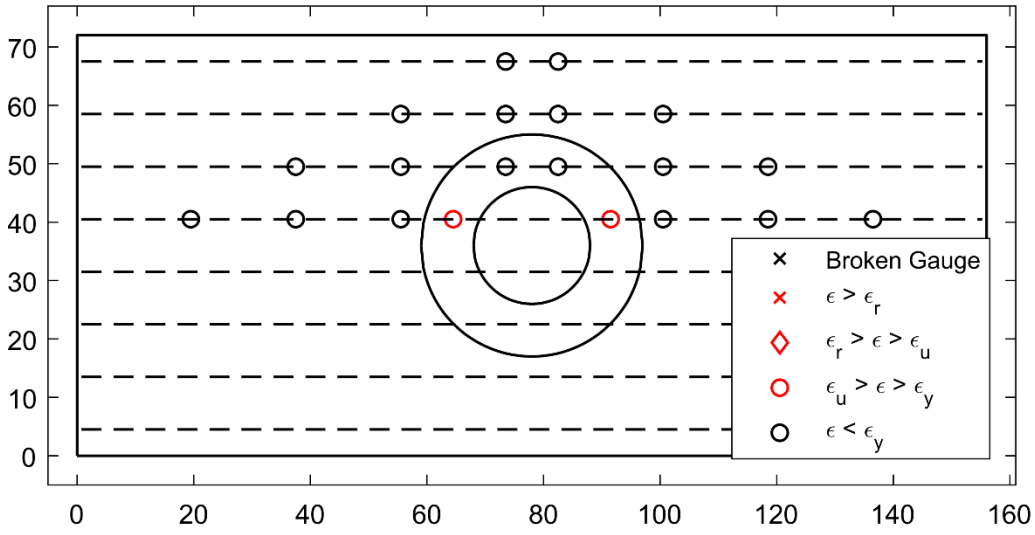

Figure 74: Bottom Reinforcement Strain Summary – 2.0% (PTB_9_2_0)

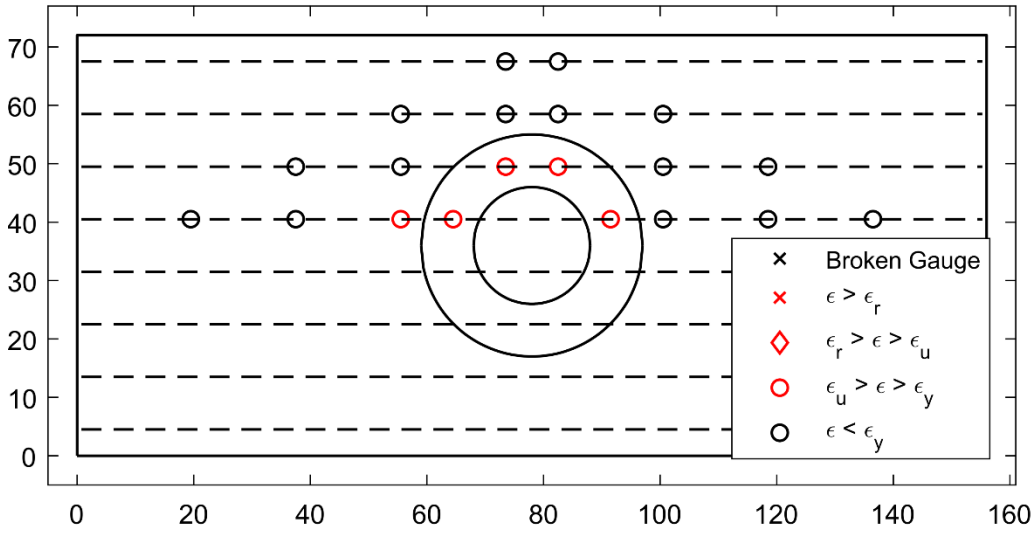

Figure 75: Bottom Reinforcement Strain Summary – 2.7% (PTB_9_2_0)

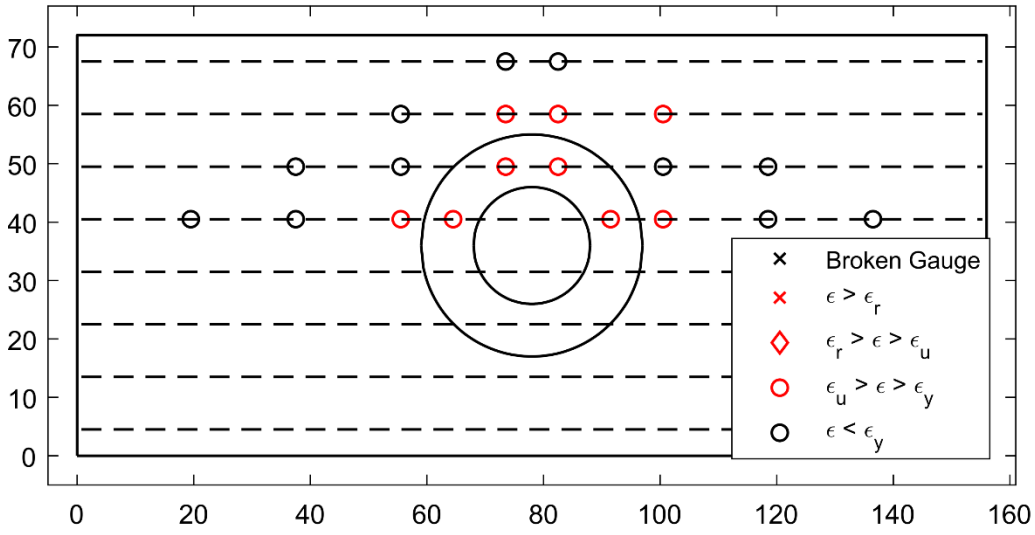

Figure 76: Bottom Reinforcement Strain Summary – 3.4% (PTB_9_2_0)

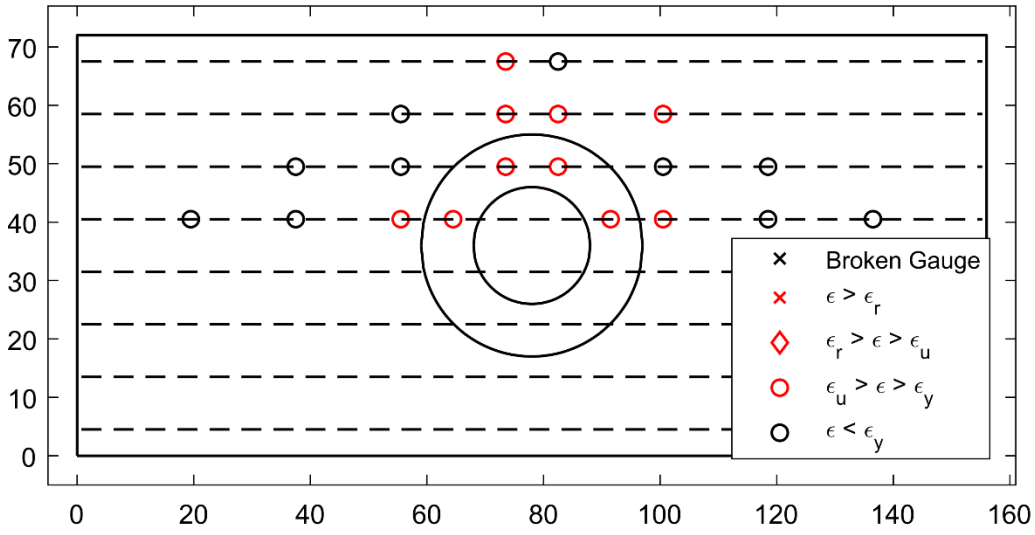

Figure 77: Bottom Reinforcement Strain Summary – 4.1% (PTB_9_2_0)

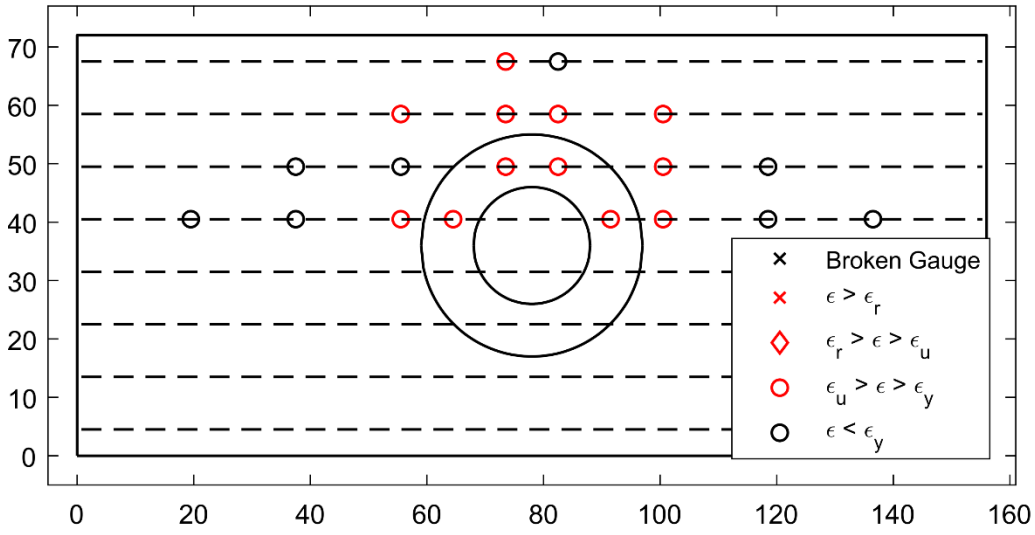

Figure 78: Bottom Reinforcement Strain Summary – 4.9% (PTB_9_2_0)

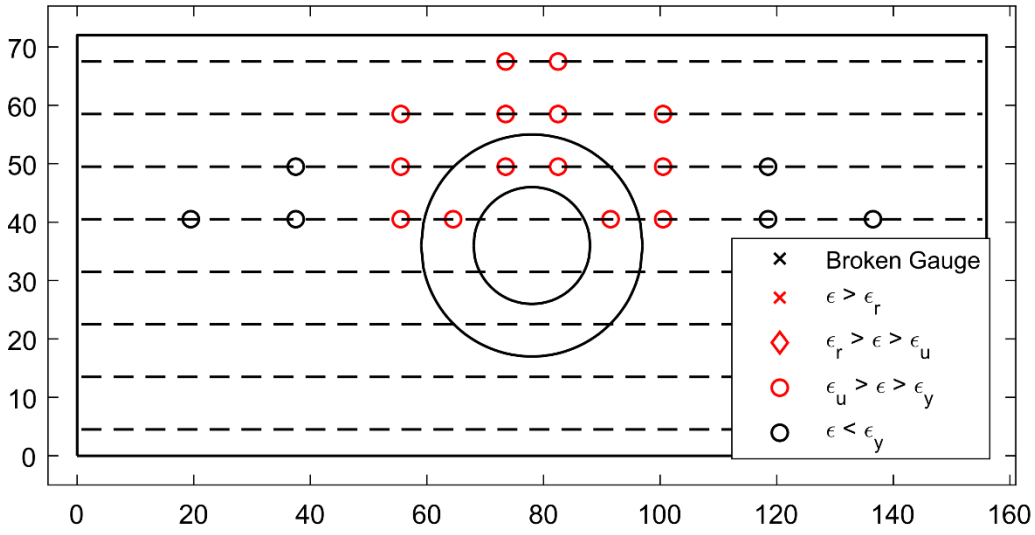

Figure 79: Bottom Reinforcement Strain Summary – 5.6% (PTB_9_2_0)

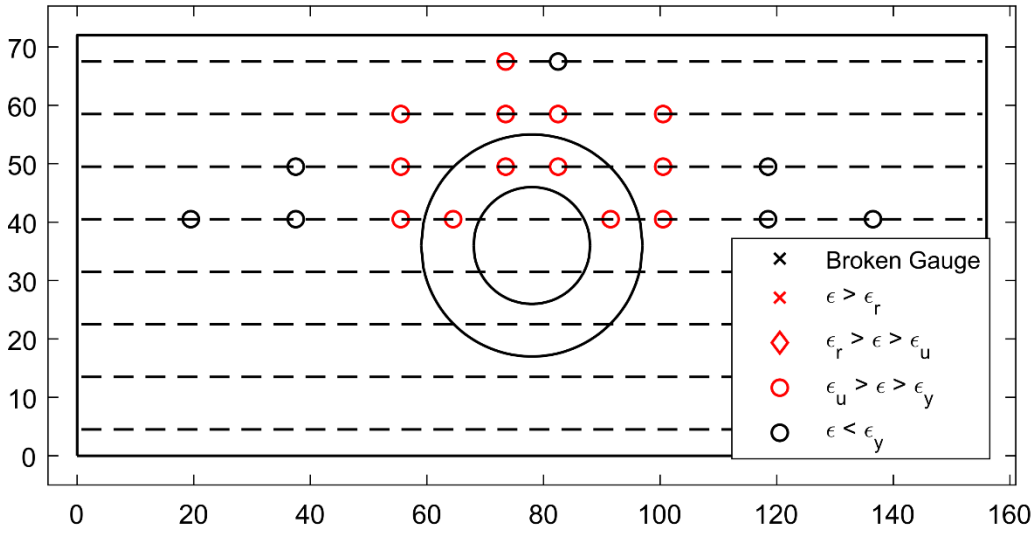

Figure 80: Bottom Reinforcement Strain Summary – 6.4% (PTB_9_2_0)

APPENDIX F: SLAB DISPLACED SHAPE

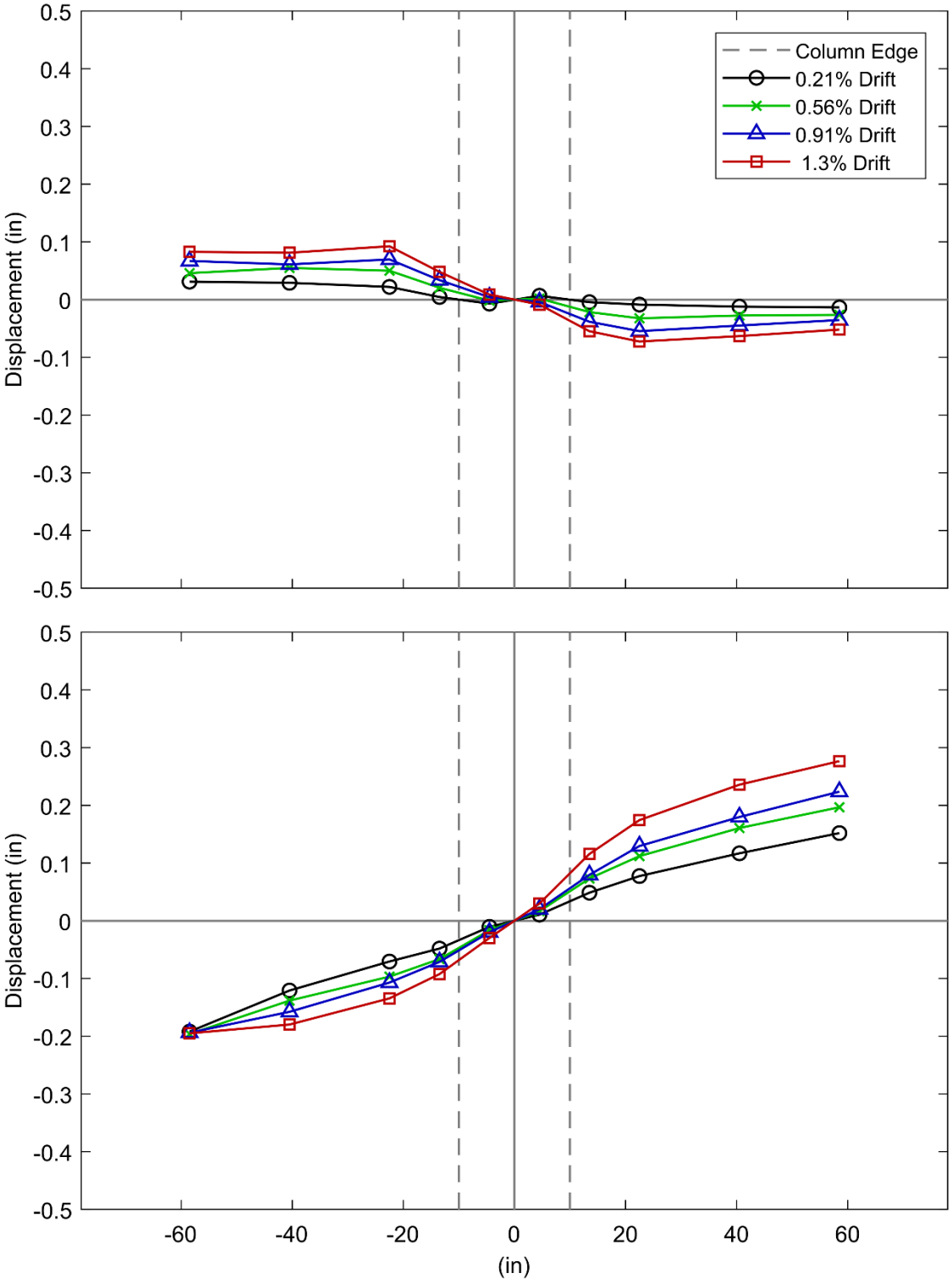

Figure 1: Low Drift Cycles Measured Slab Displaced Shape (SR_4_10_5)

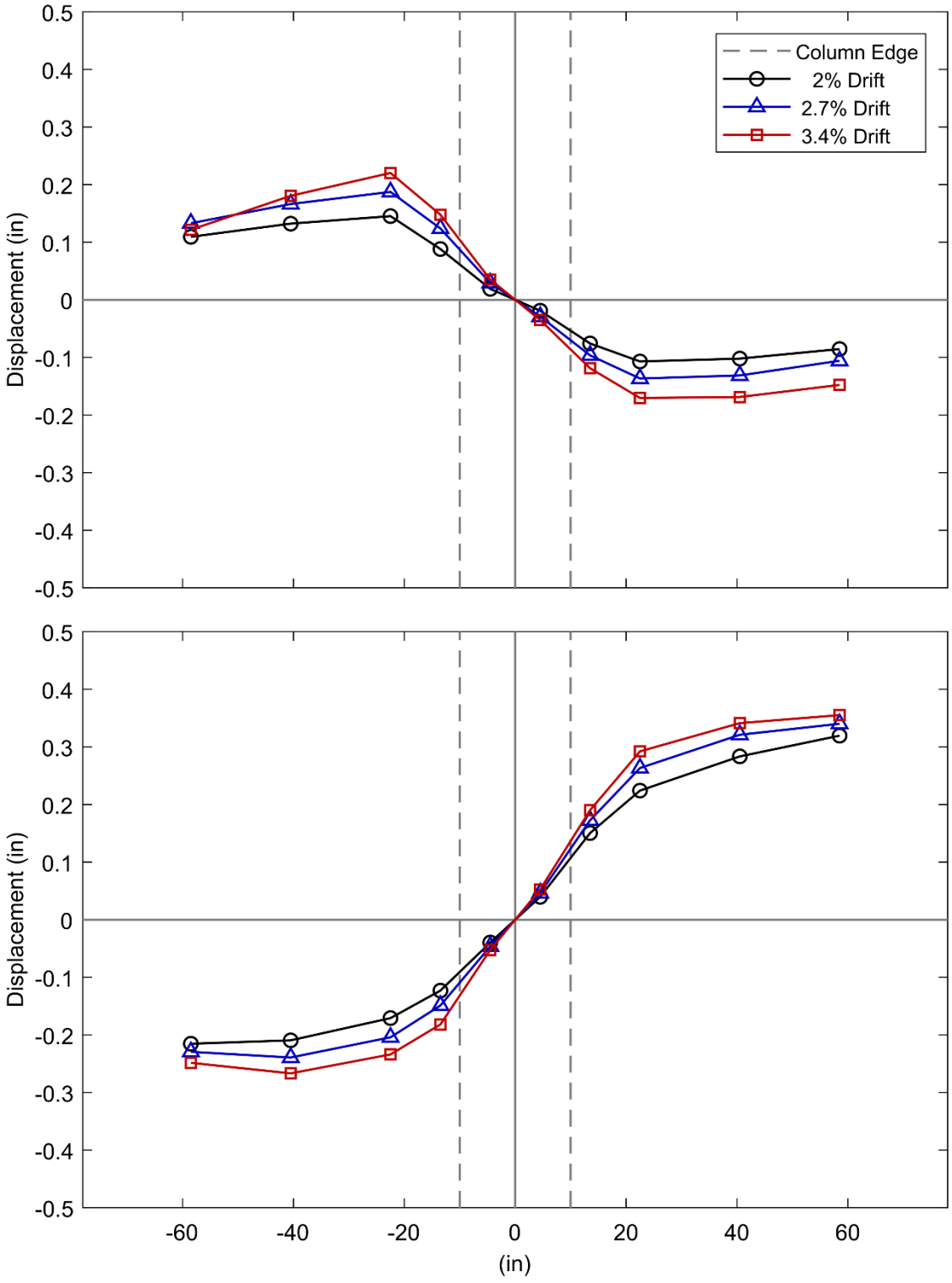

Figure 2: Moderate Drift Cycles Measured Slab Displaced Shape (SR_4_10_5)

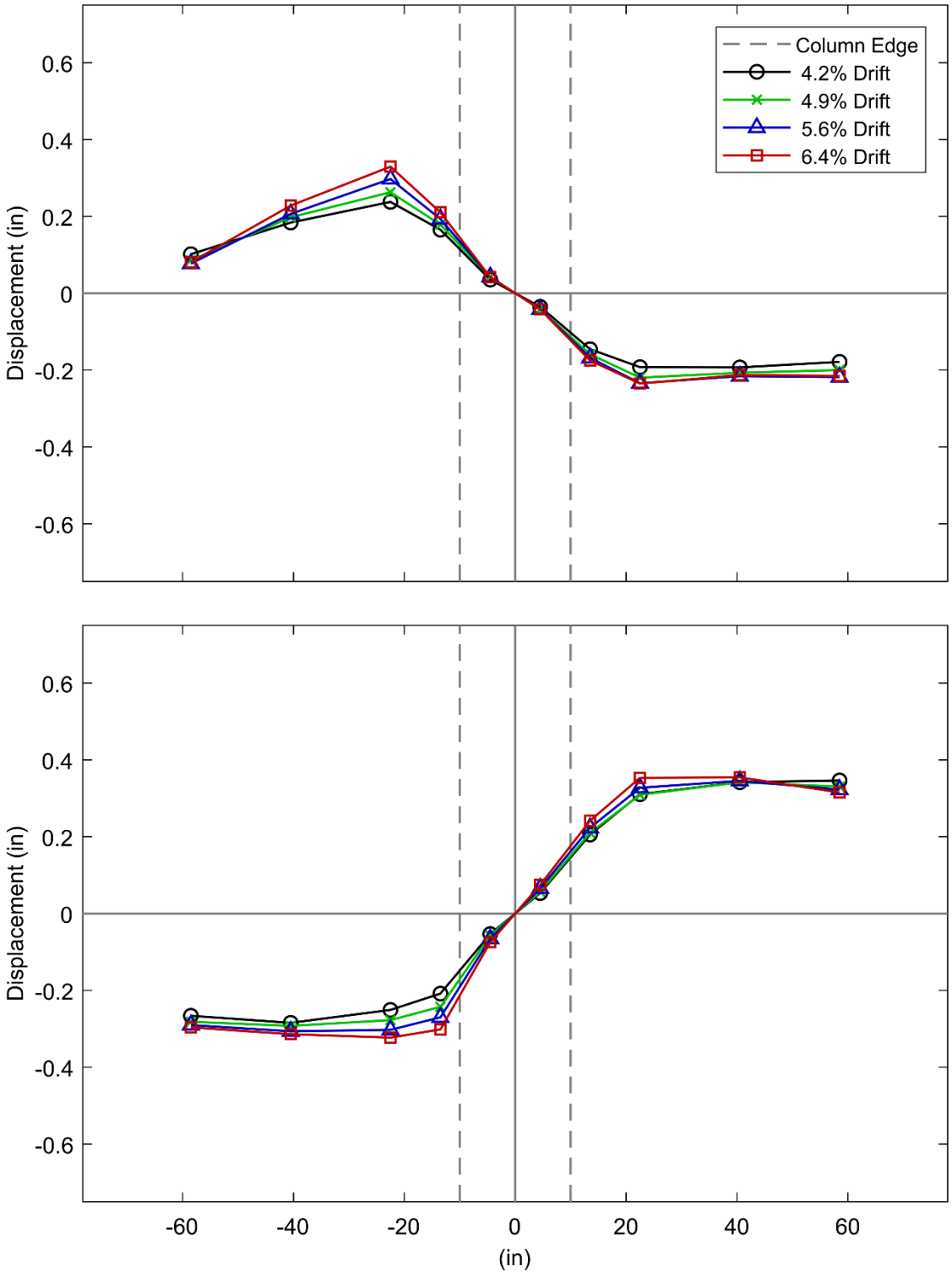

Figure 3: High Drift Cycles Measured Slab Displaced Shape (SR_4_10_5)

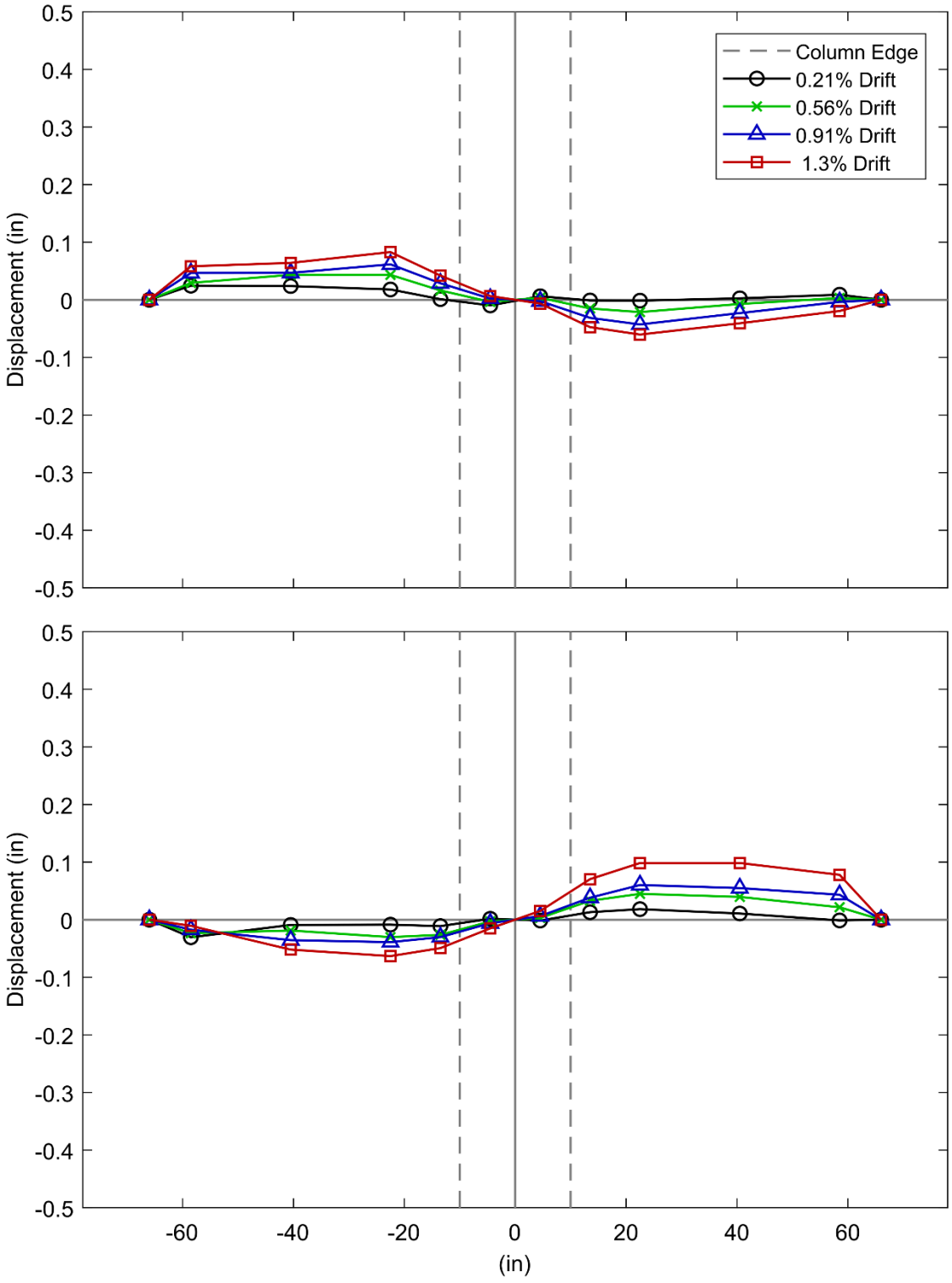

Figure 4: Low Drift Cycles Corrected Slab Displaced Shape (SR_4_10_5)

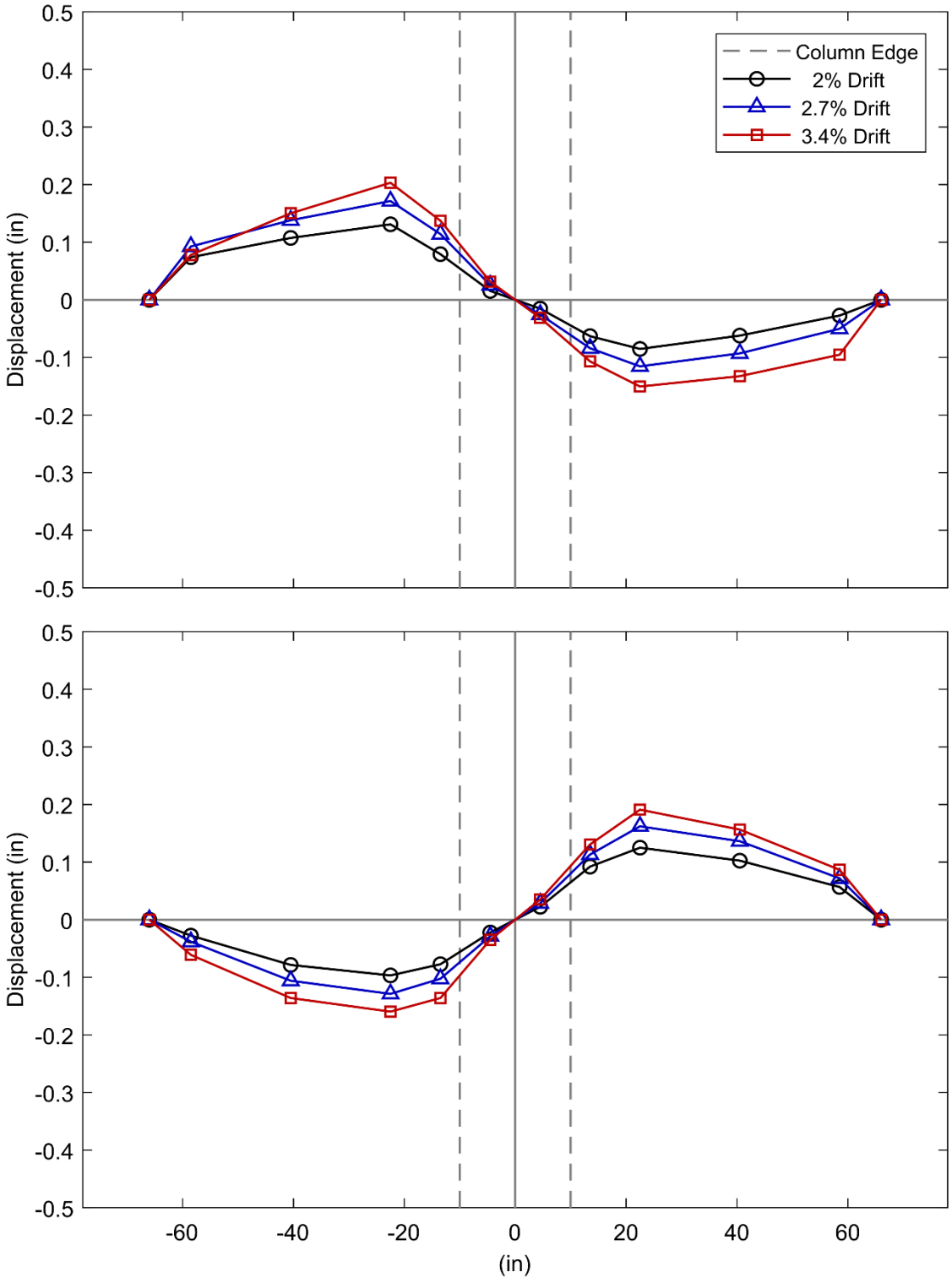

Figure 5: Moderate Drift Cycles Corrected Slab Displaced Shape (SR_4_10_5)

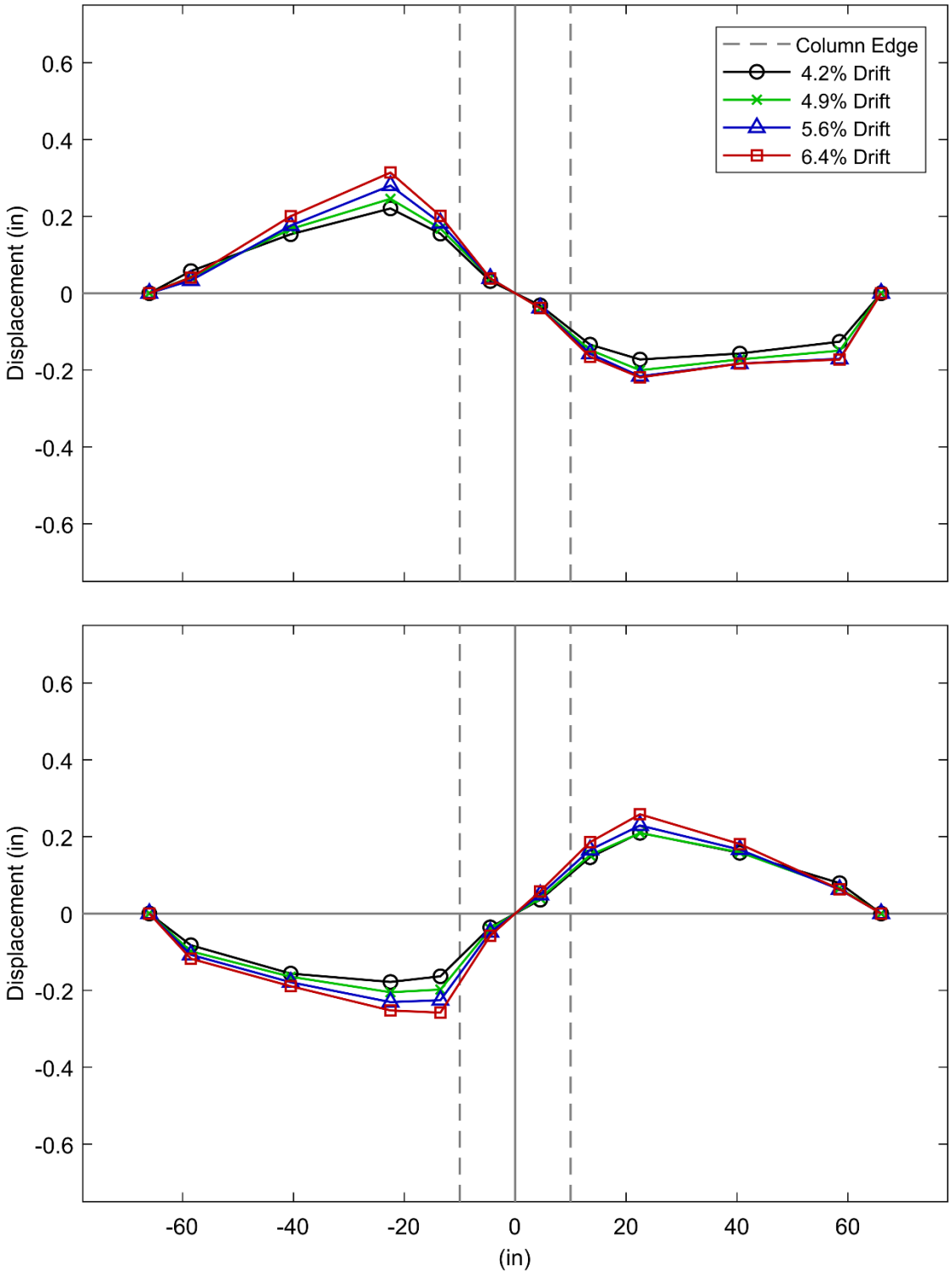

Figure 6: High Drift Cycles Corrected Slab Displaced Shape (SR_4_10_5)

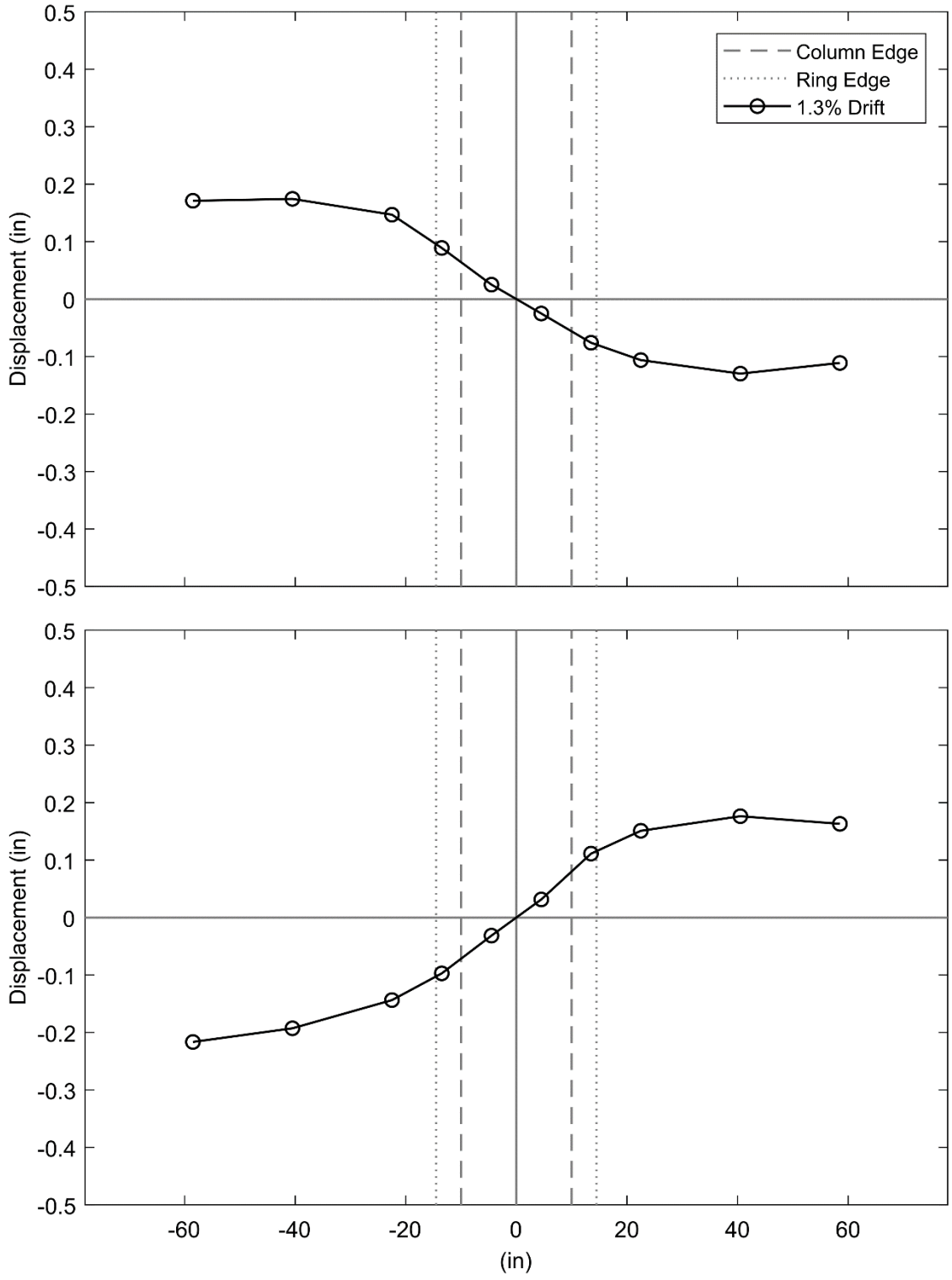

Figure 7: Low Drift Cycles Measured Slab Displaced Shape (PTB_4.5_1_0)

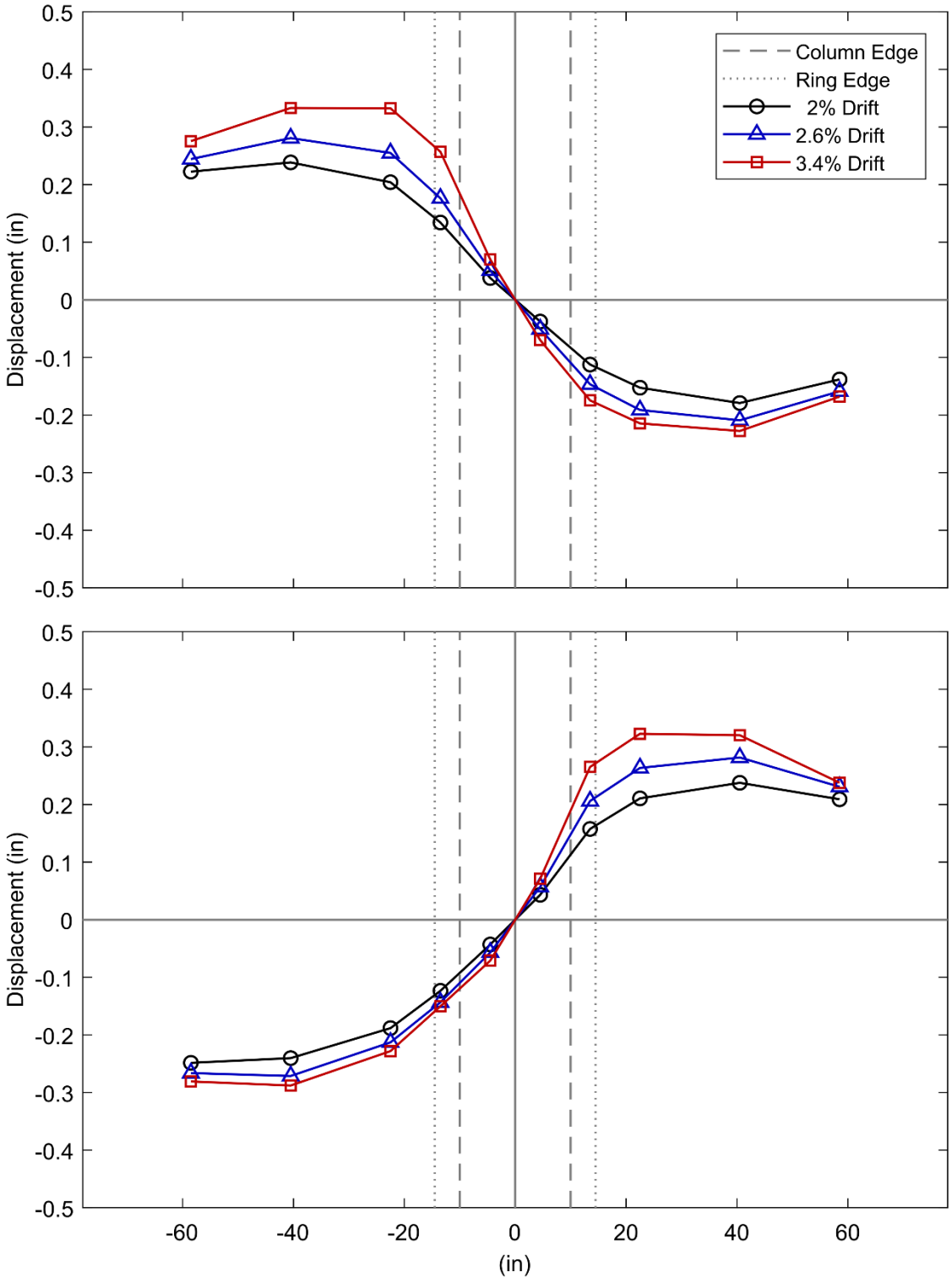

Figure 8: Moderate Drift Cycles Measured Slab Displaced Shape (PTB_4.5_1_0)

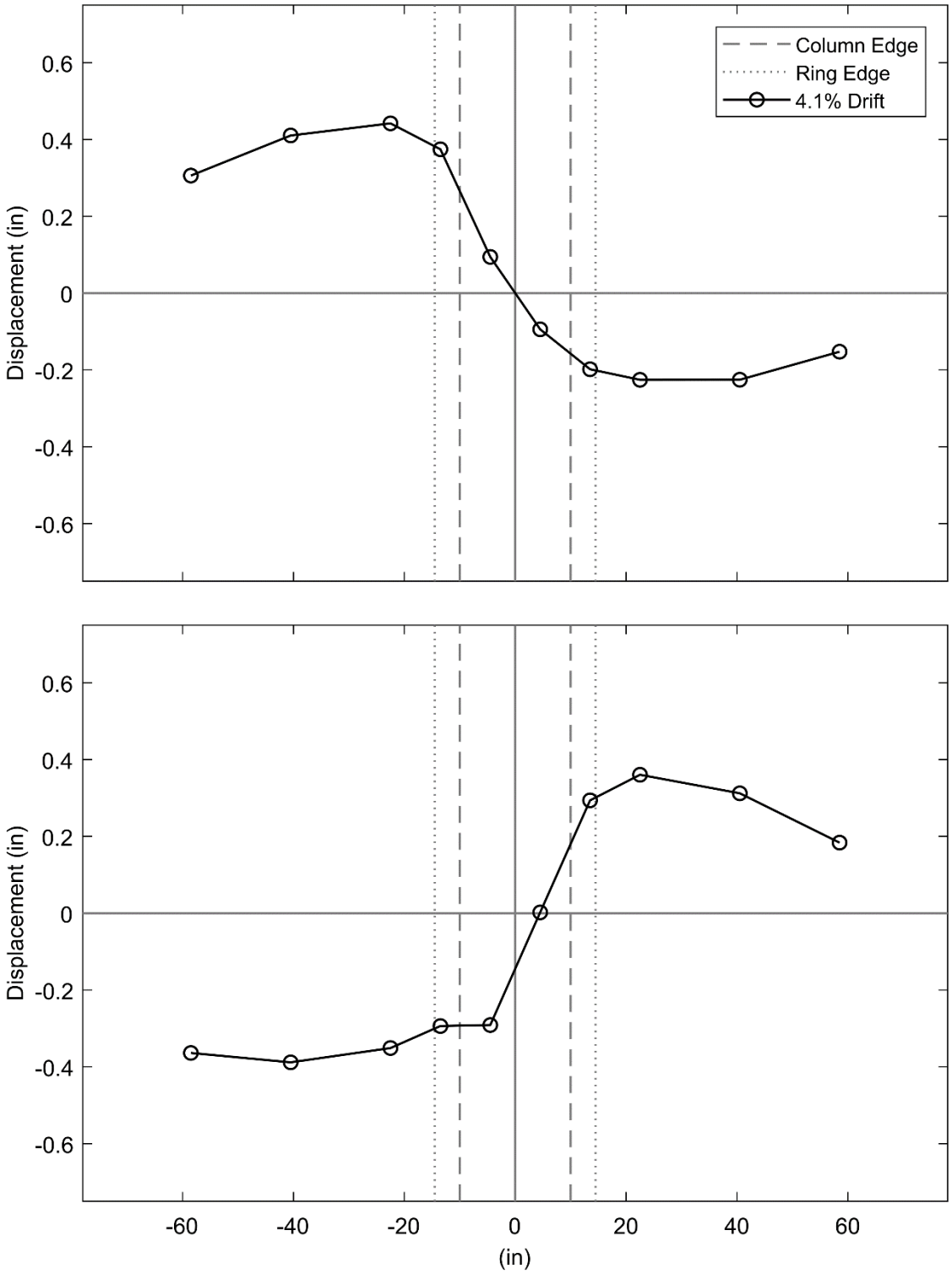

Figure 9: High Drift Cycles Measured Slab Displaced Shape (PTB_4.5_1_0)

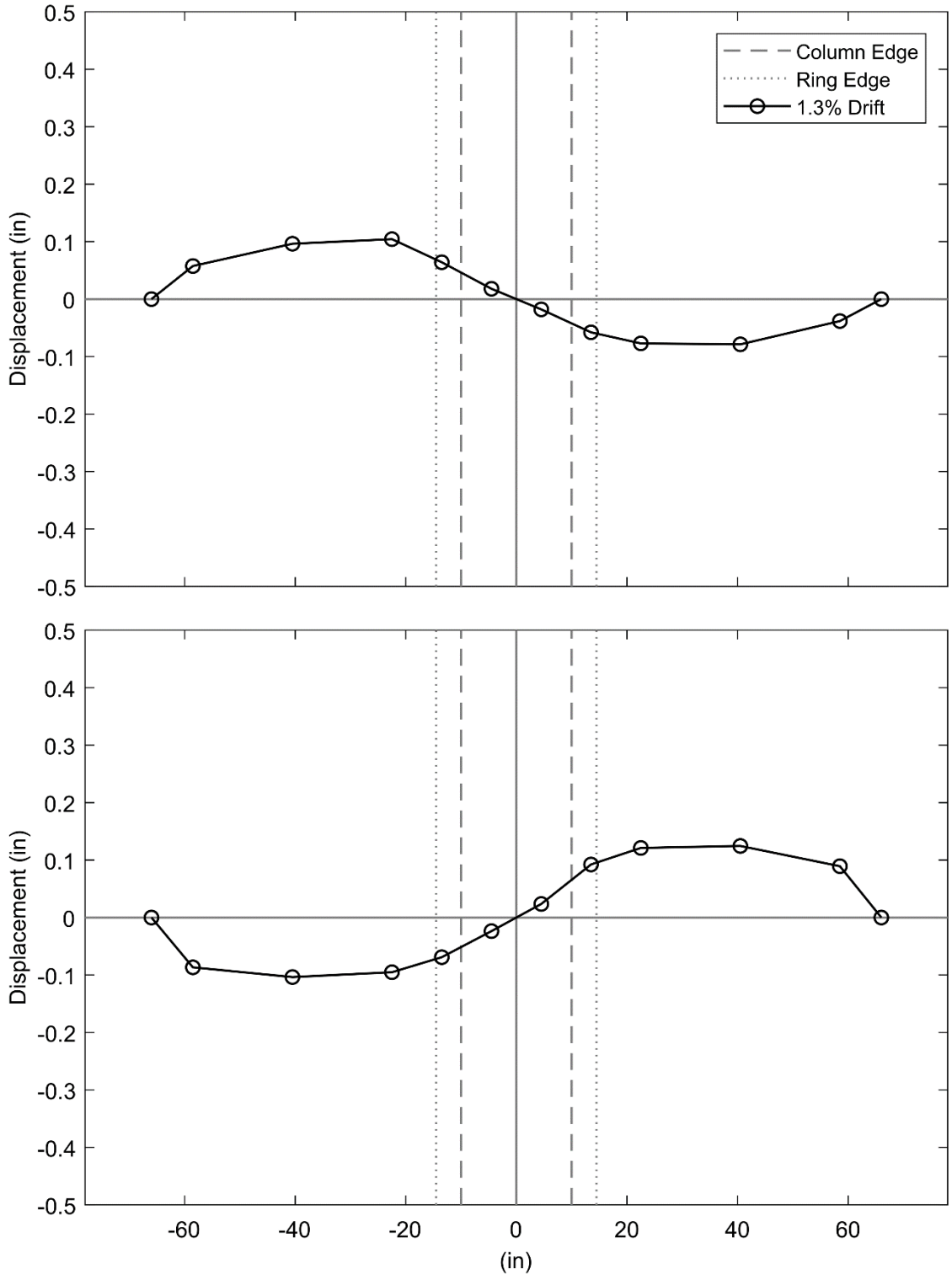

Figure 10: Low Drift Cycles Corrected Slab Displaced Shape (PTB_4.5_1_0)

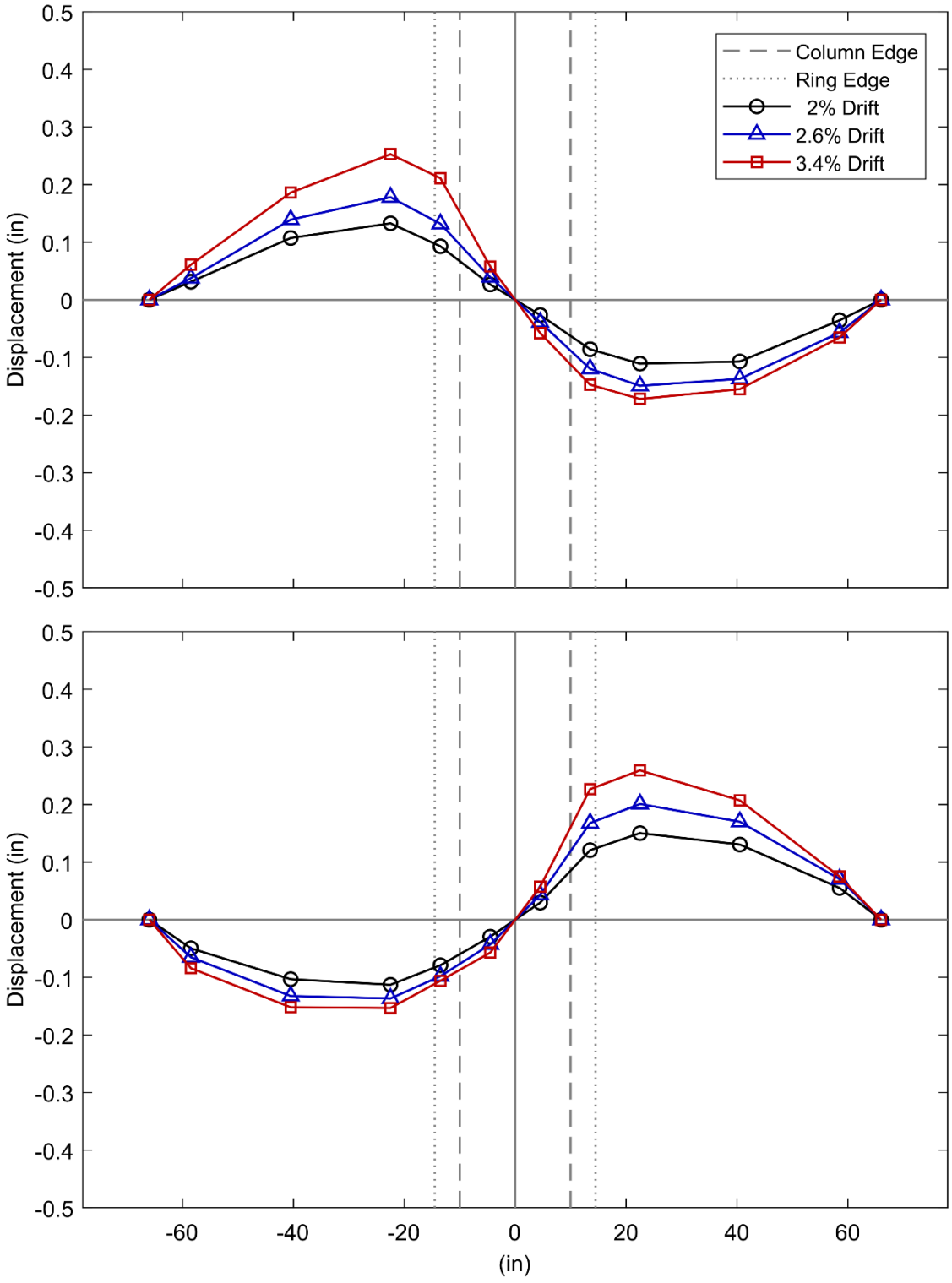

Figure 11: Moderate Drift Cycles Corrected Slab Displaced Shape (PTB_4.5_1_0)

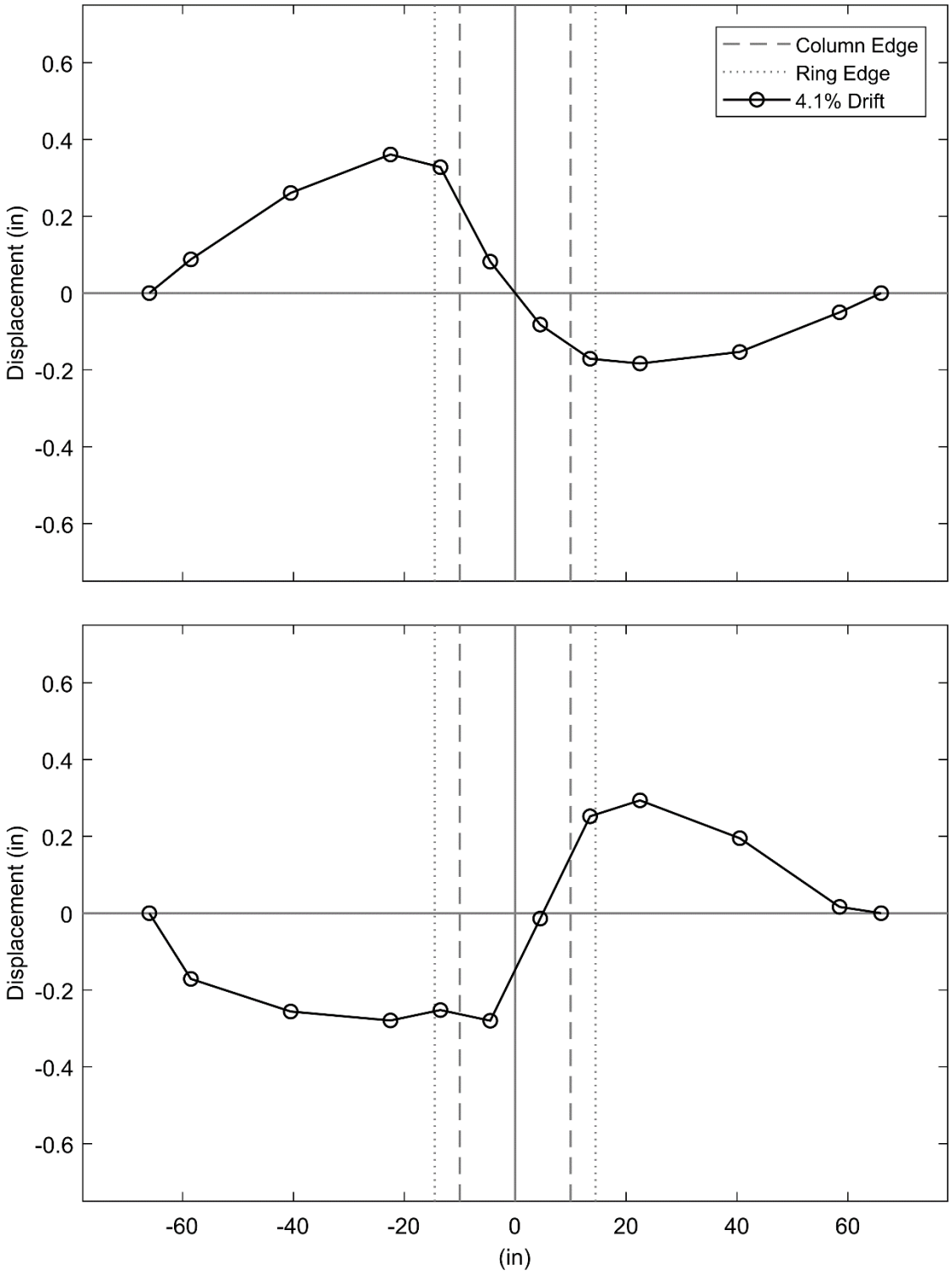

Figure 12: High Drift Cycles Corrected Slab Displaced Shape (PTB_4.5_1_0)

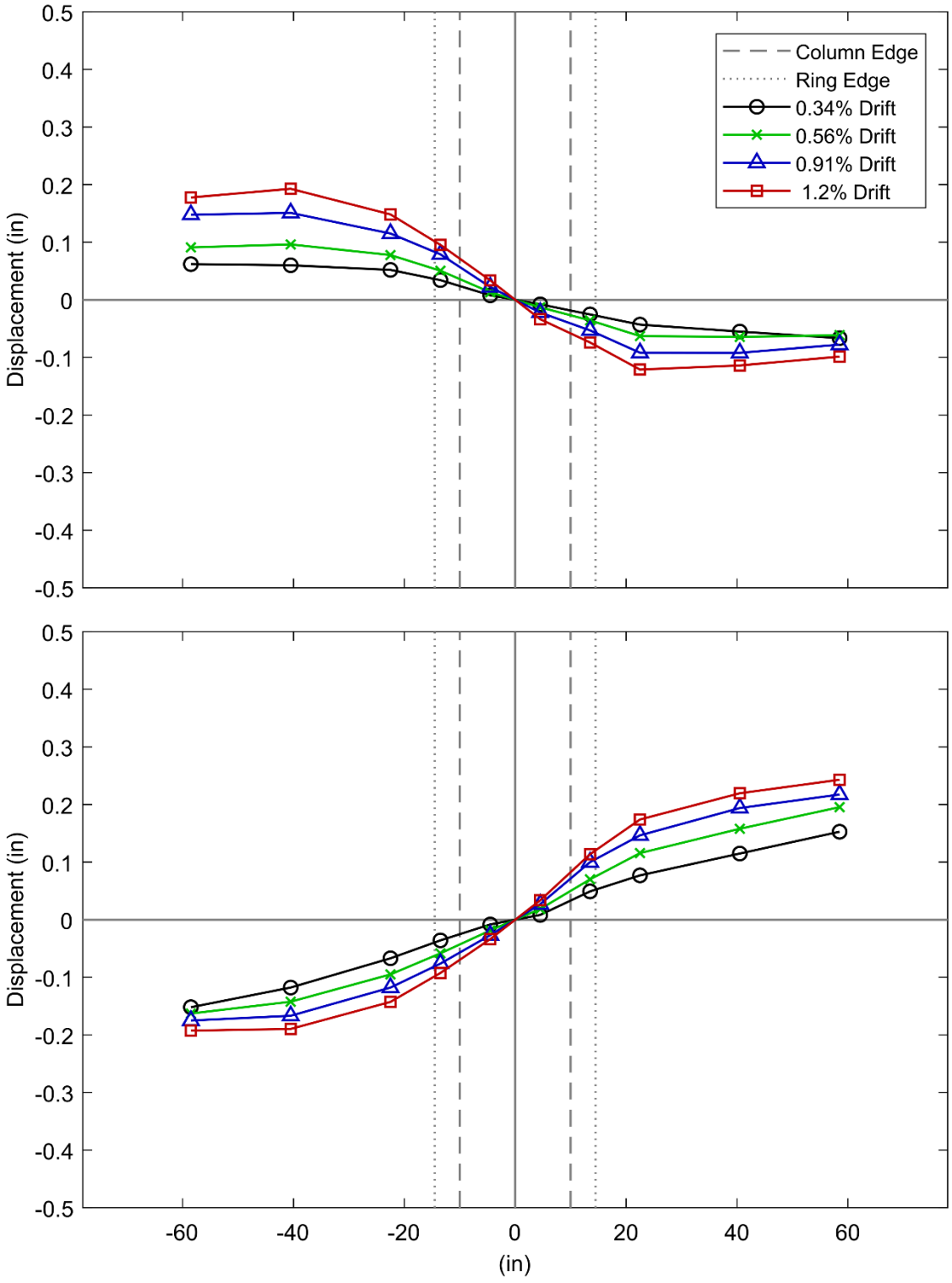

Figure 13: Low Drift Cycles Measured Slab Displaced Shape (PTB_4.5_1_4)

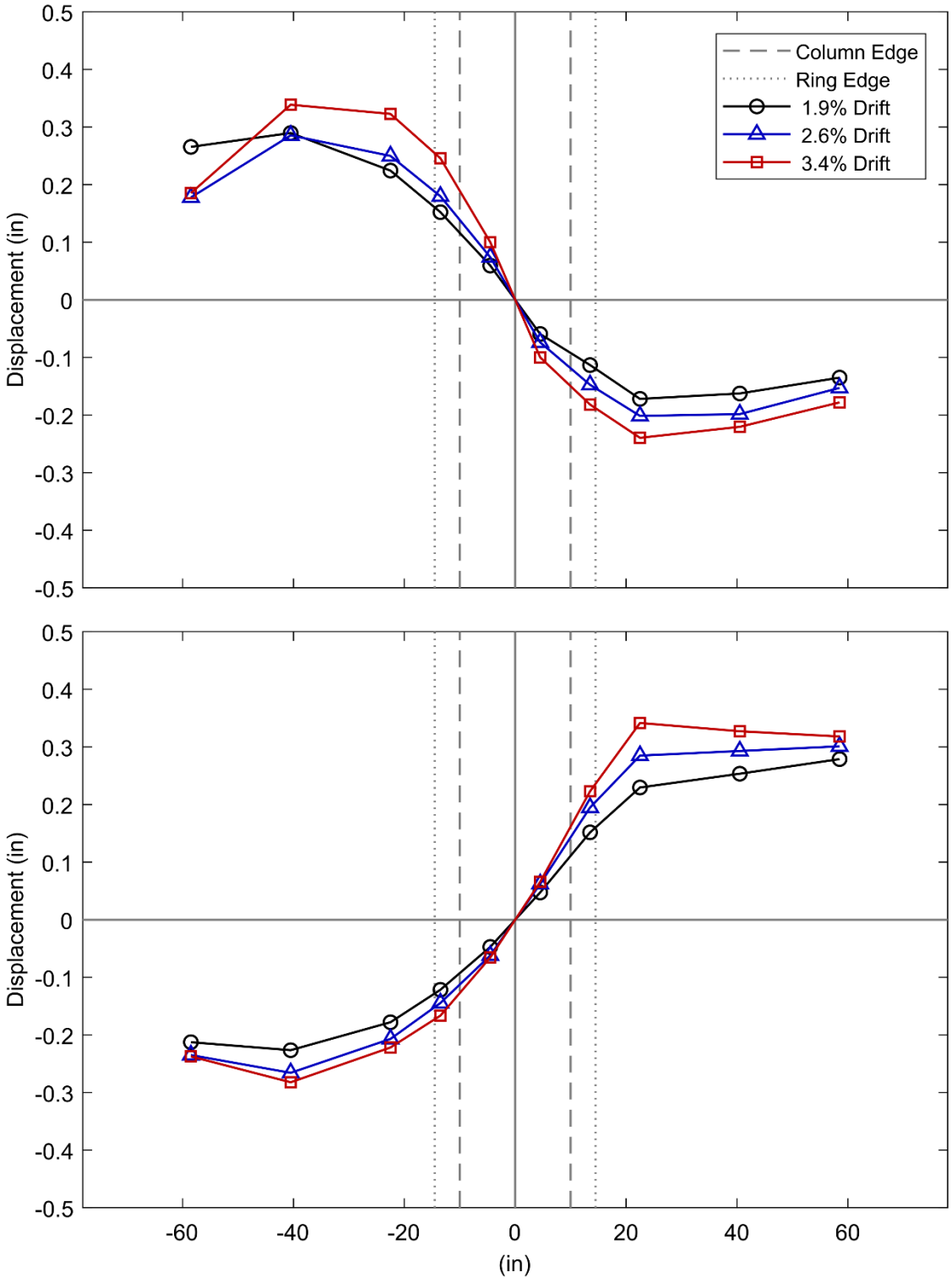

Figure 14: Moderate Drift Cycles Measured Slab Displaced Shape (PTB_4.5_1_4)

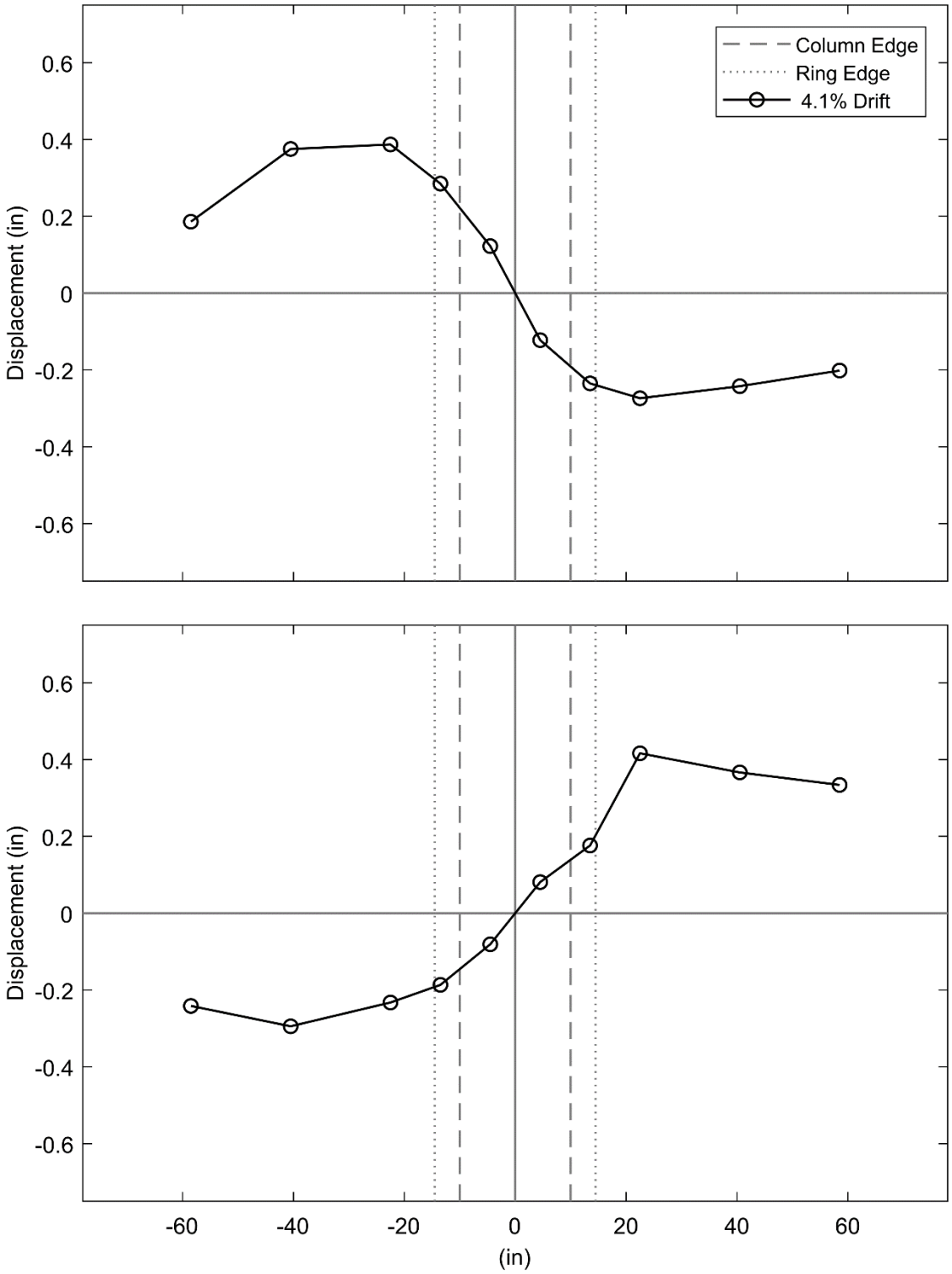

Figure 15: High Drift Cycles Measured Slab Displaced Shape (PTB_4.5_1_4)

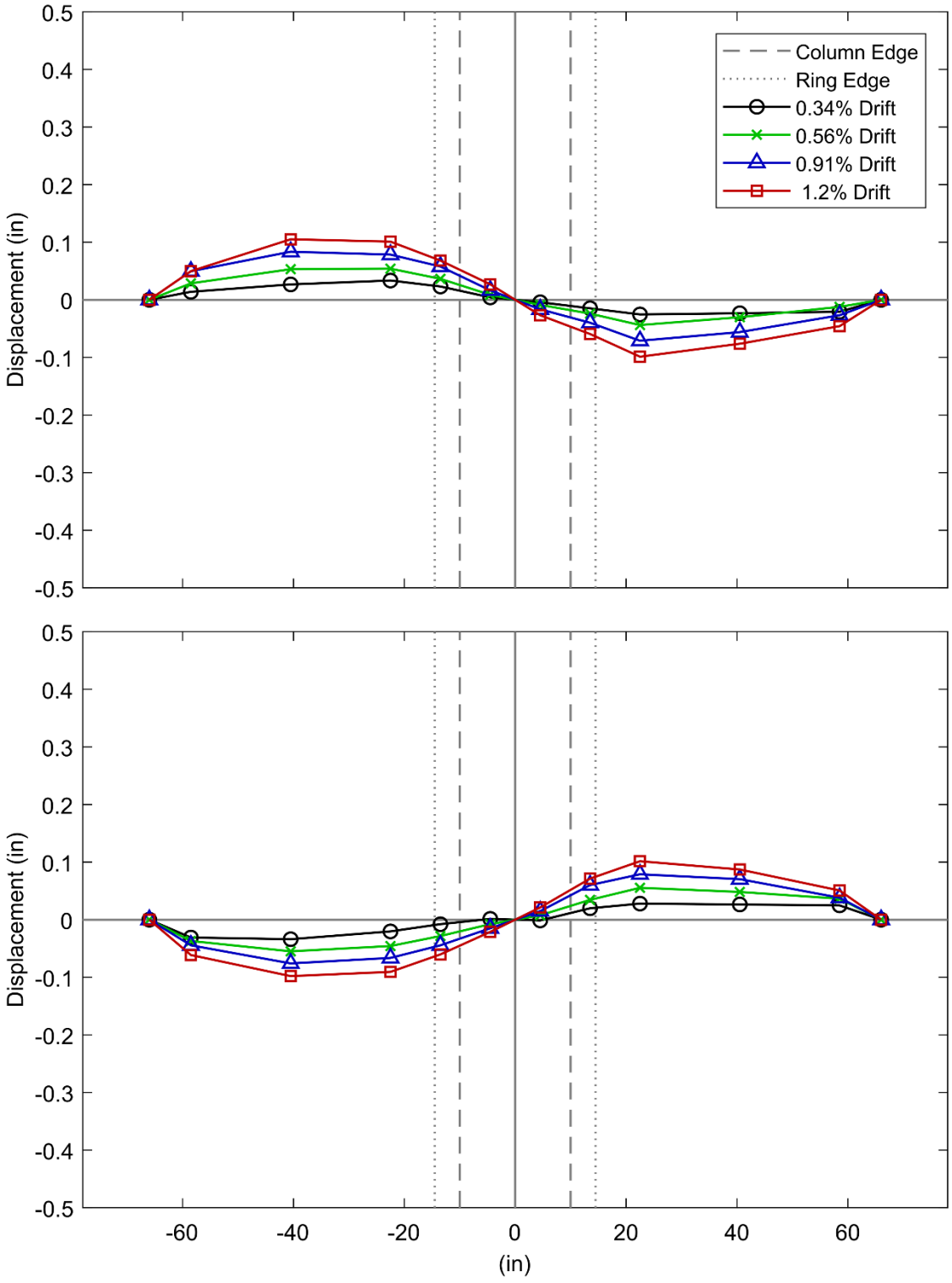

Figure 16: Low Drift Cycles Corrected Slab Displaced Shape (PTB_4.5_1_4)

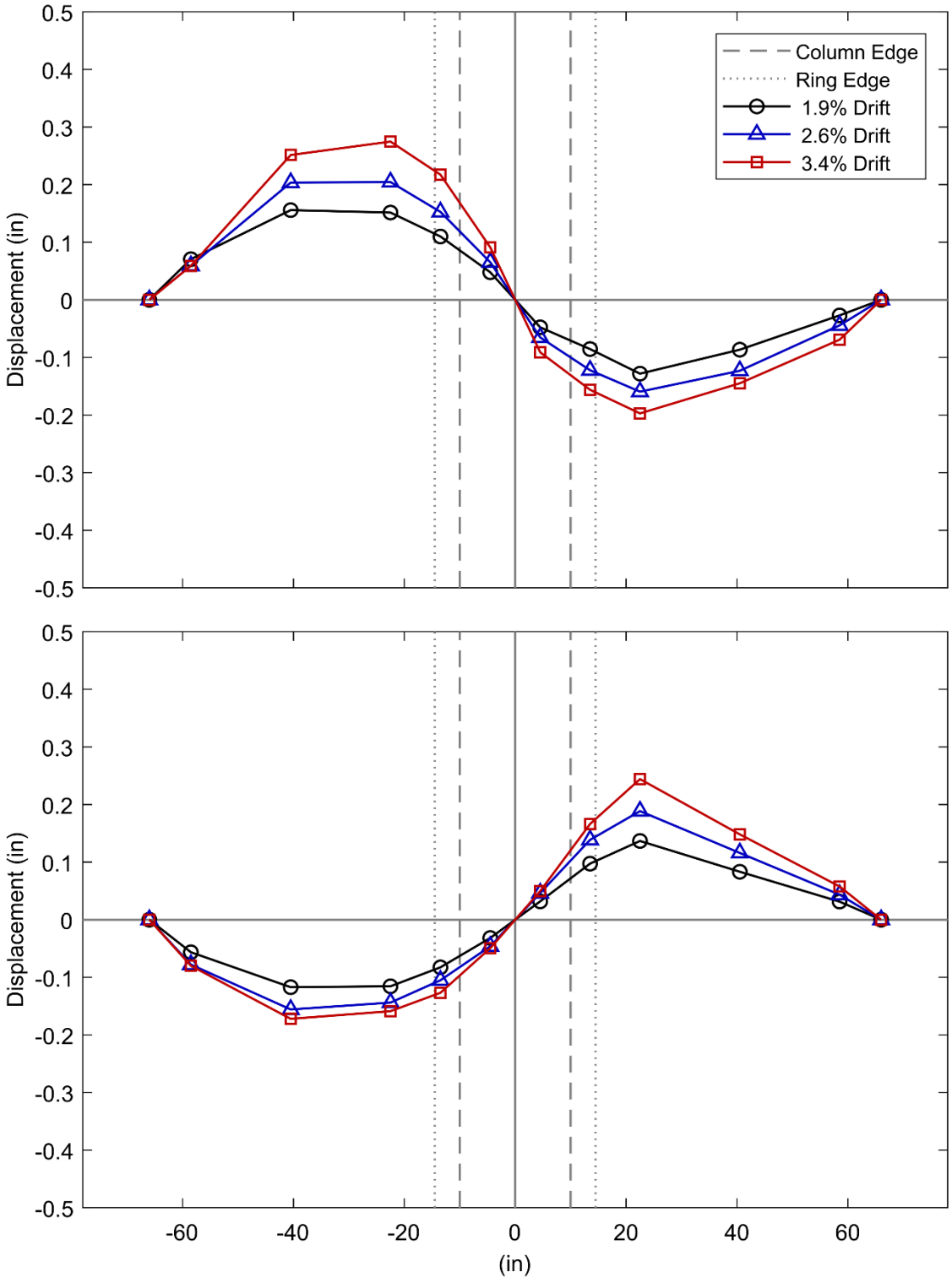

Figure 17: Moderate Drift Cycles Corrected Slab Displaced Shape (PTB_4.5_1_4)

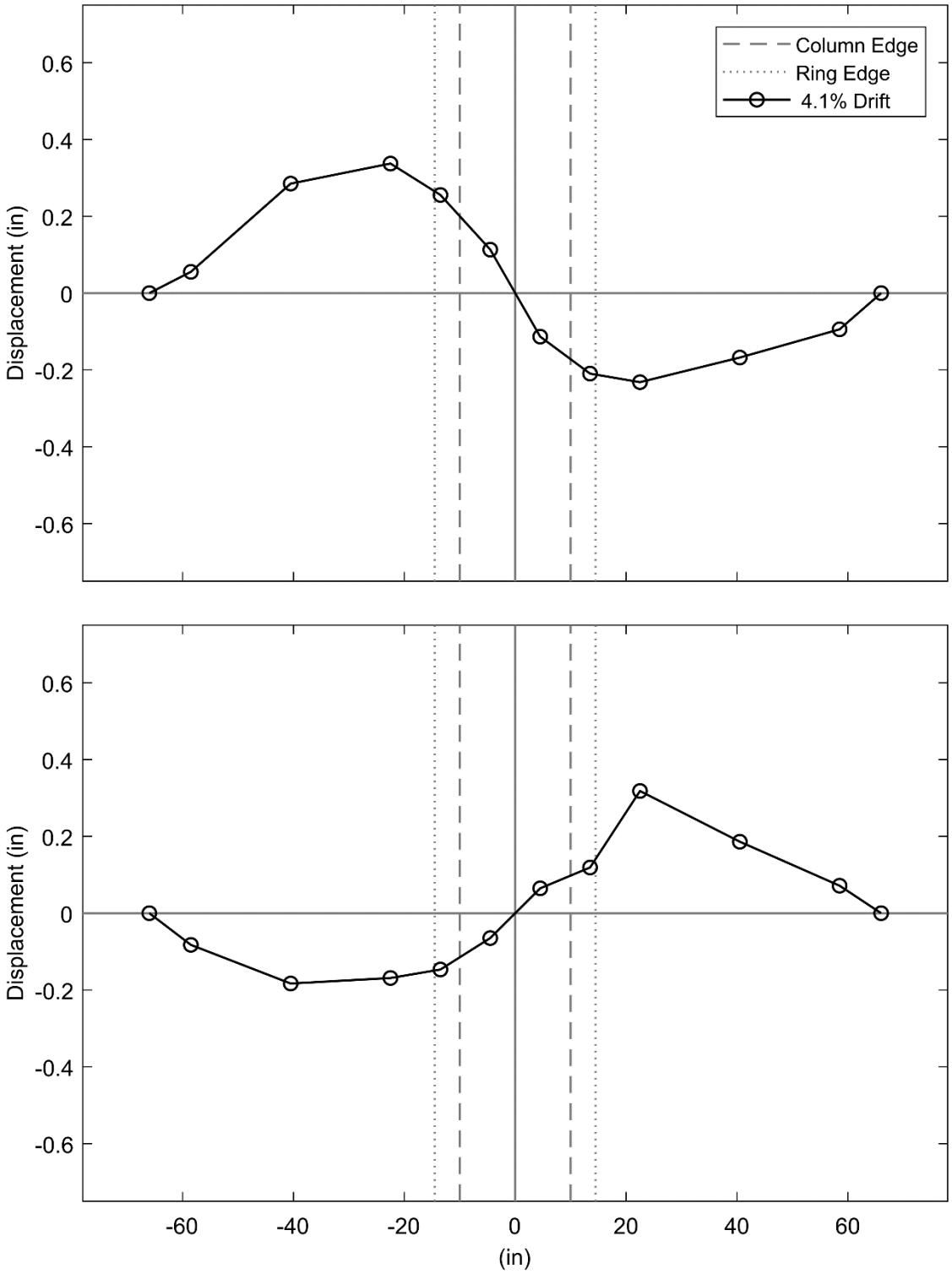

Figure 18: High Drift Cycles Corrected Slab Displaced Shape (PTB_4.5_1_4)

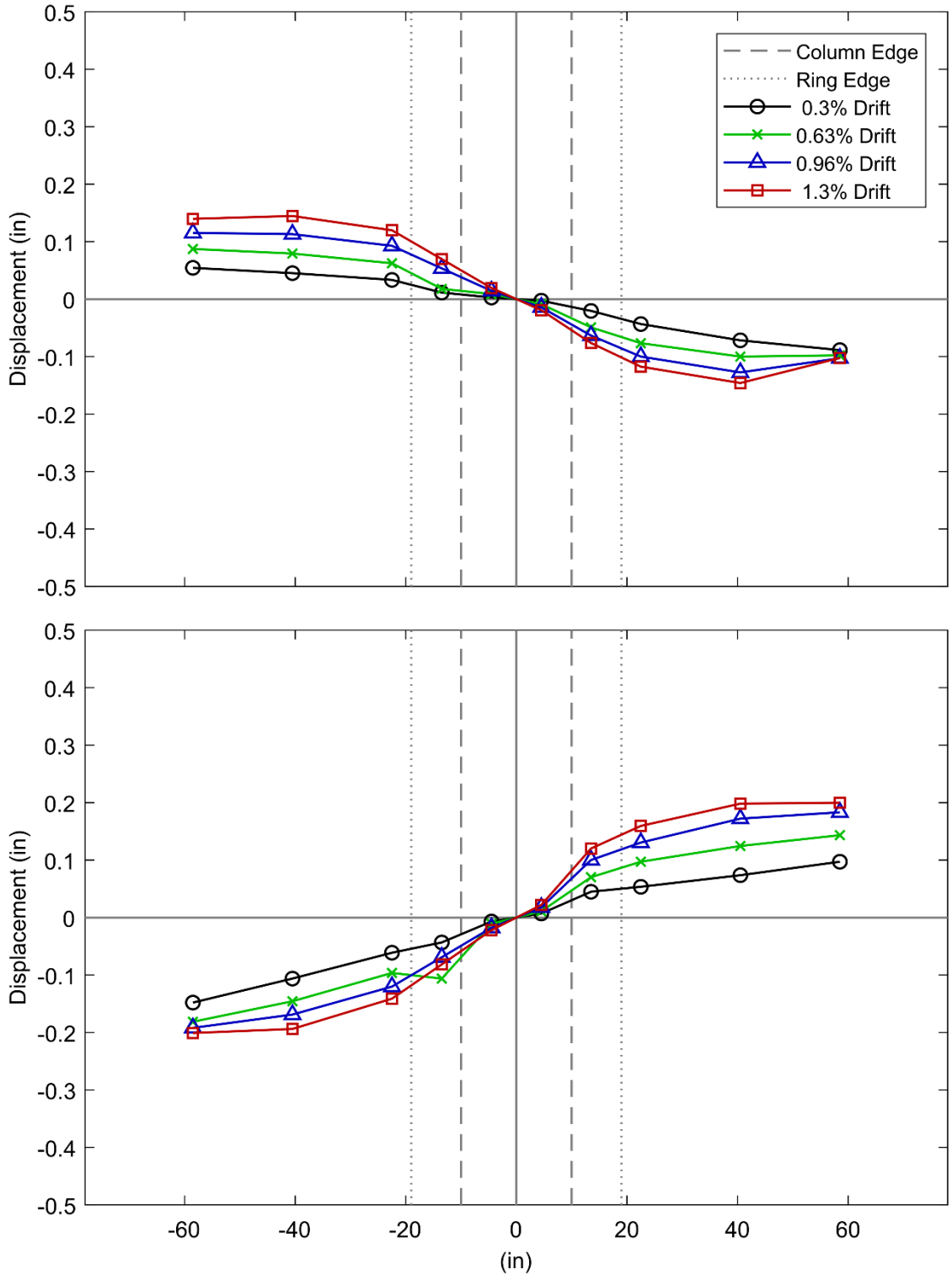

Figure 19: Low Drift Cycles Measured Slab Displaced Shape (PTB_9_2_0)

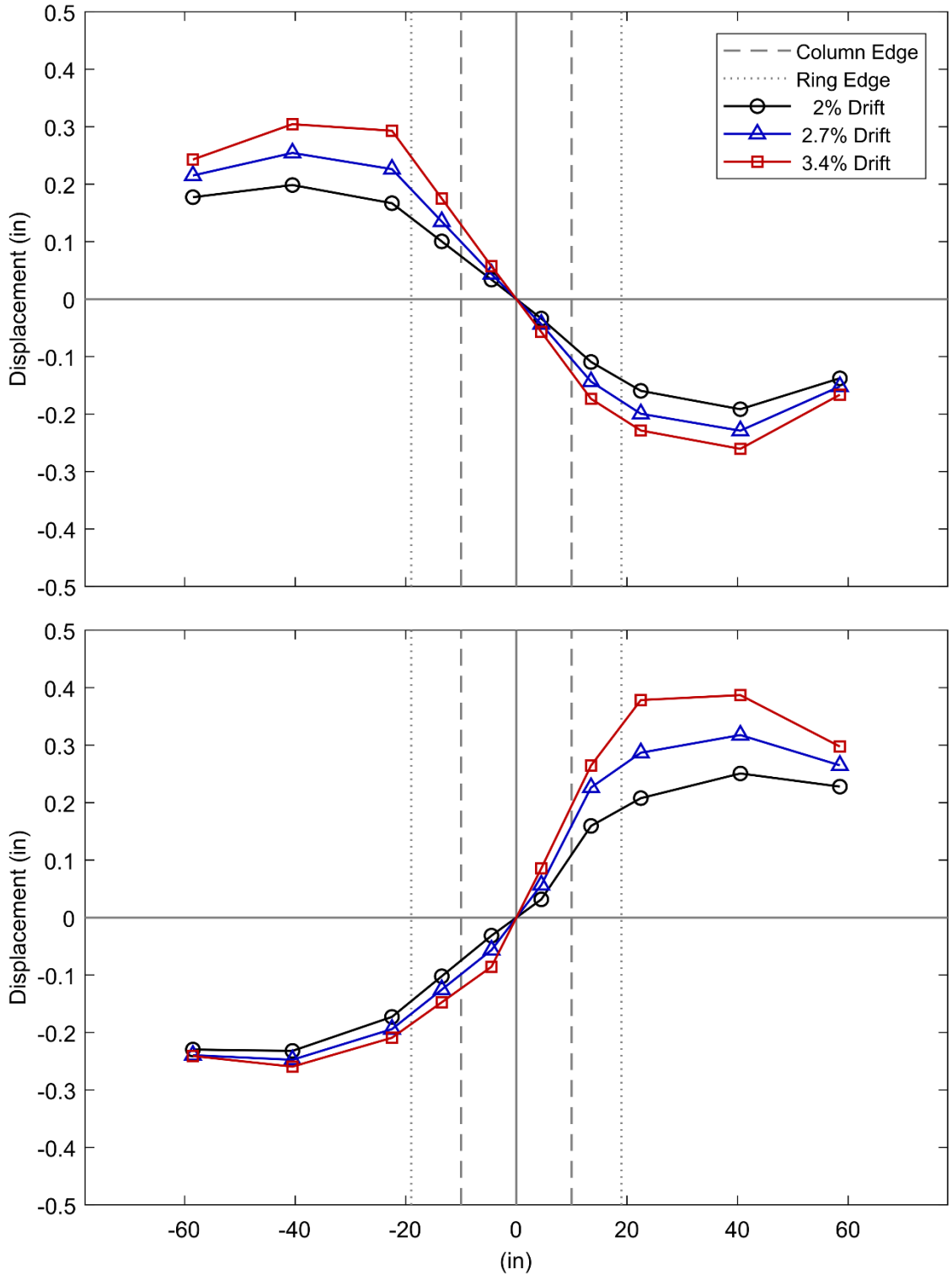

Figure 20: Moderate Drift Cycles Measured Slab Displaced Shape (PTB_9_2_0)

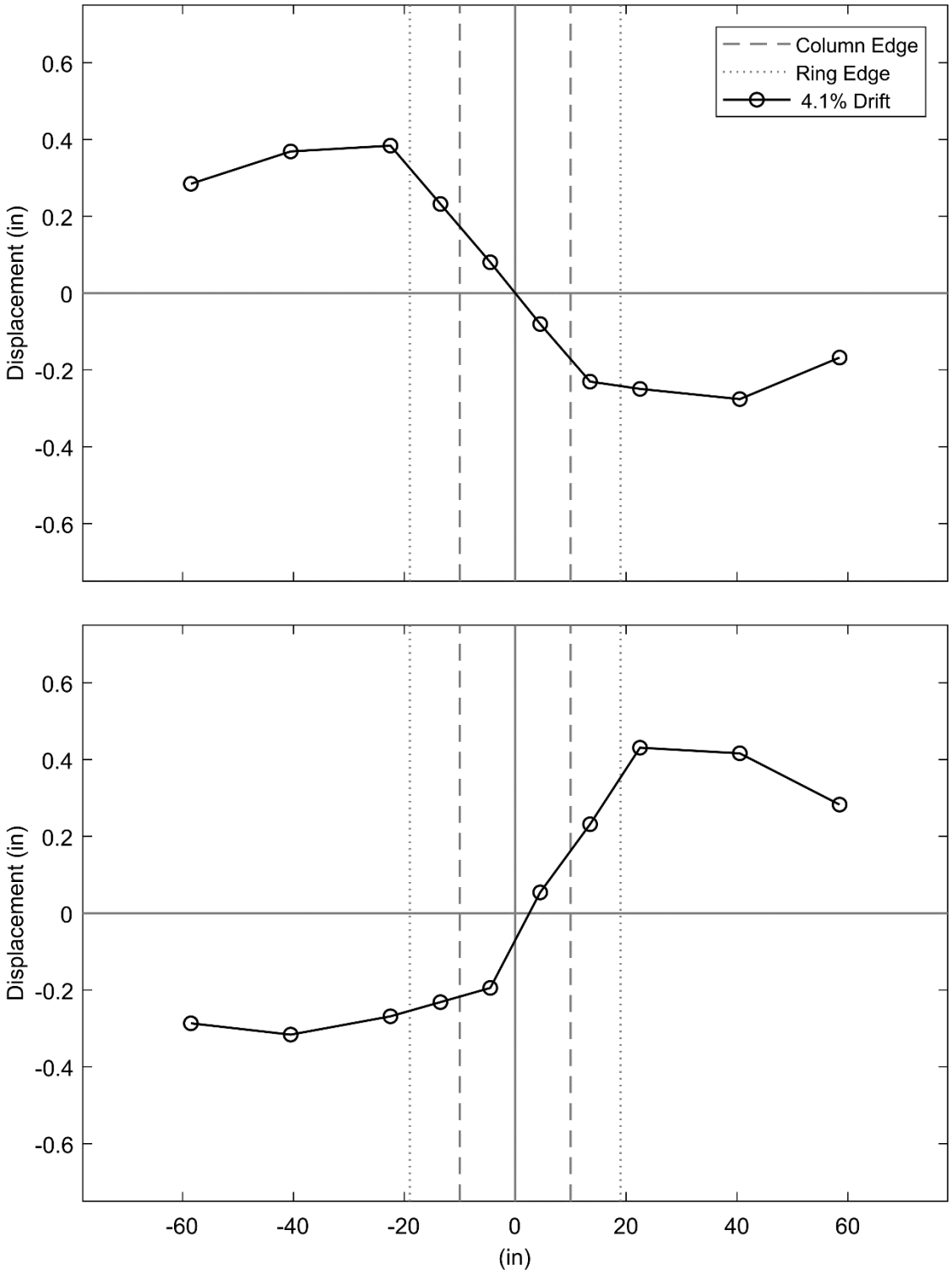

Figure 21: High Drift Cycles Measured Slab Displaced Shape (PTB_9_2_0)

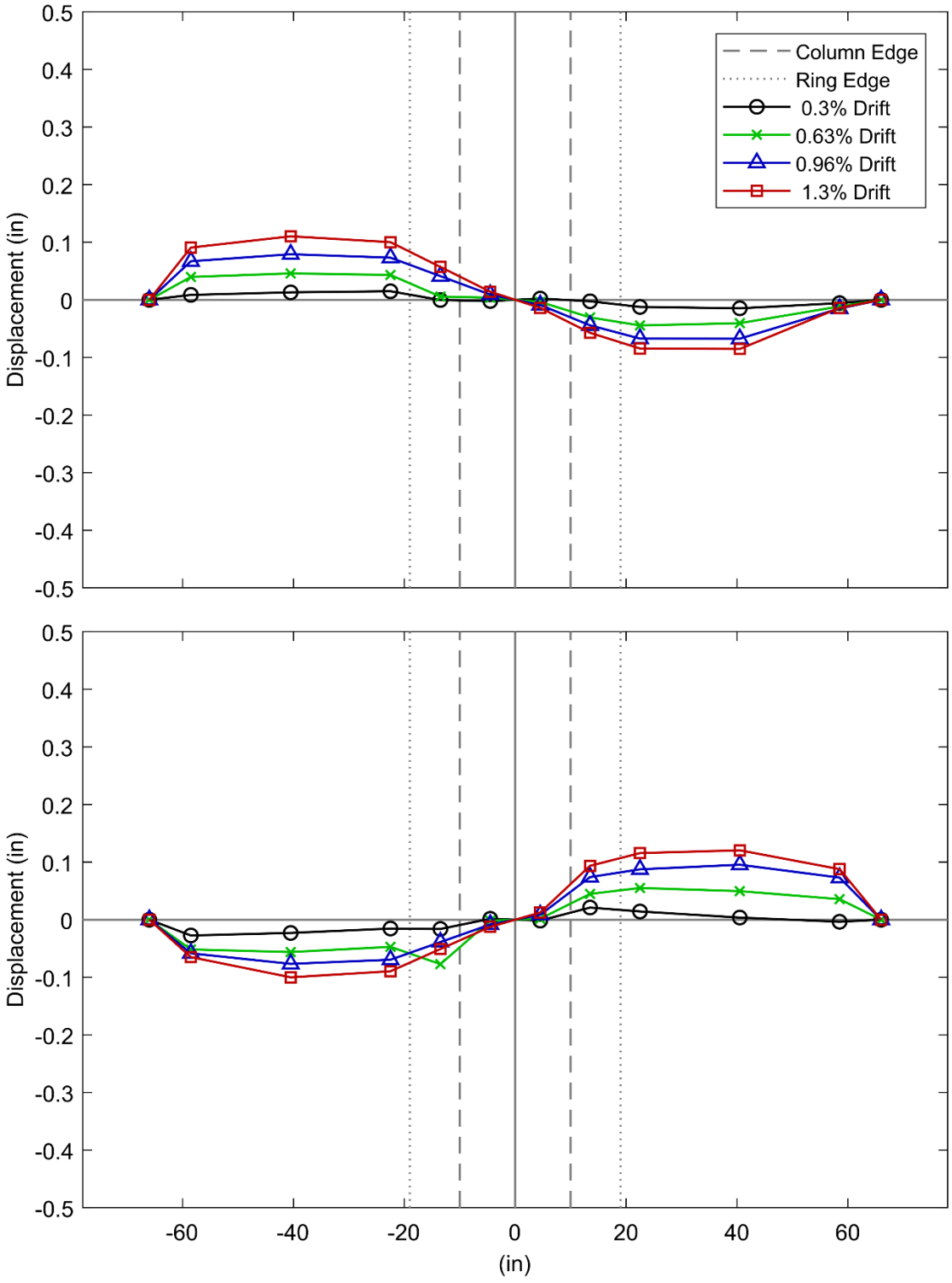

Figure 22: Low Drift Cycles Corrected Slab Displaced Shape (PTB_9_2_0)

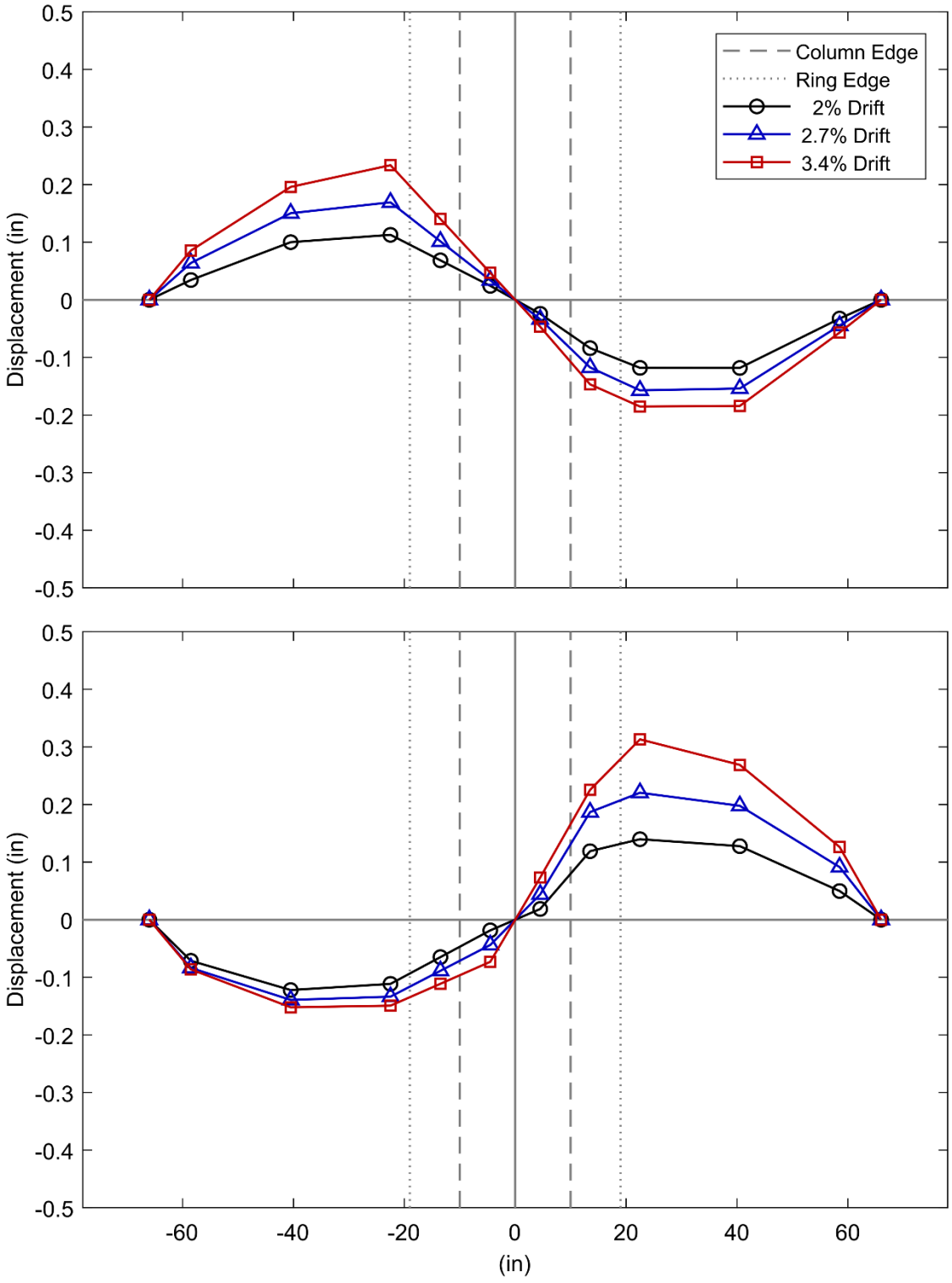

Figure 23: Moderate Drift Cycles Corrected Slab Displaced Shape (PTB_9_2_0)

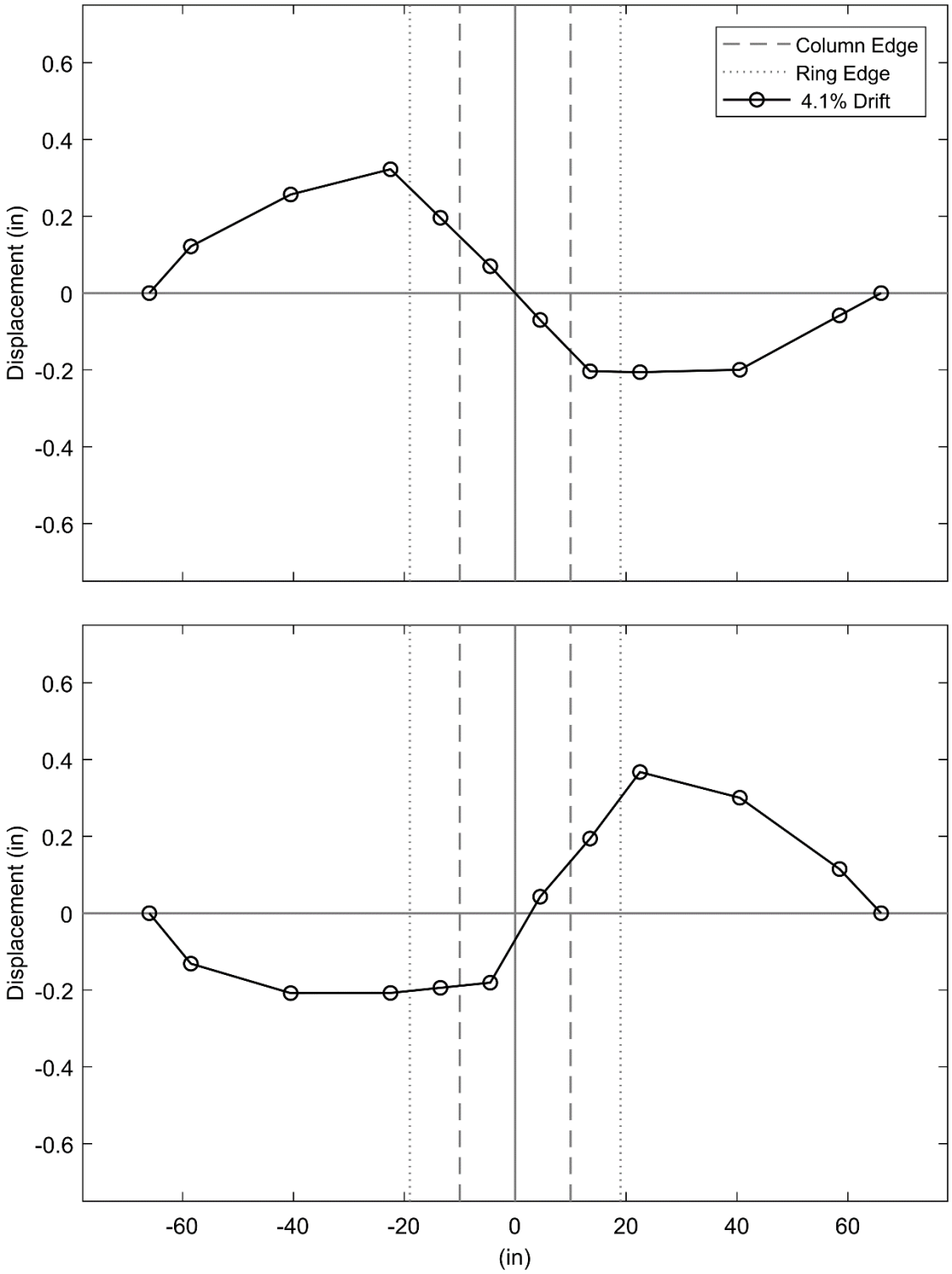

Figure 24: High Drift Cycles Corrected Slab Displaced Shape (PTB_9_2_0)

APPENDIX G: SLAB ROTATION PROFILE

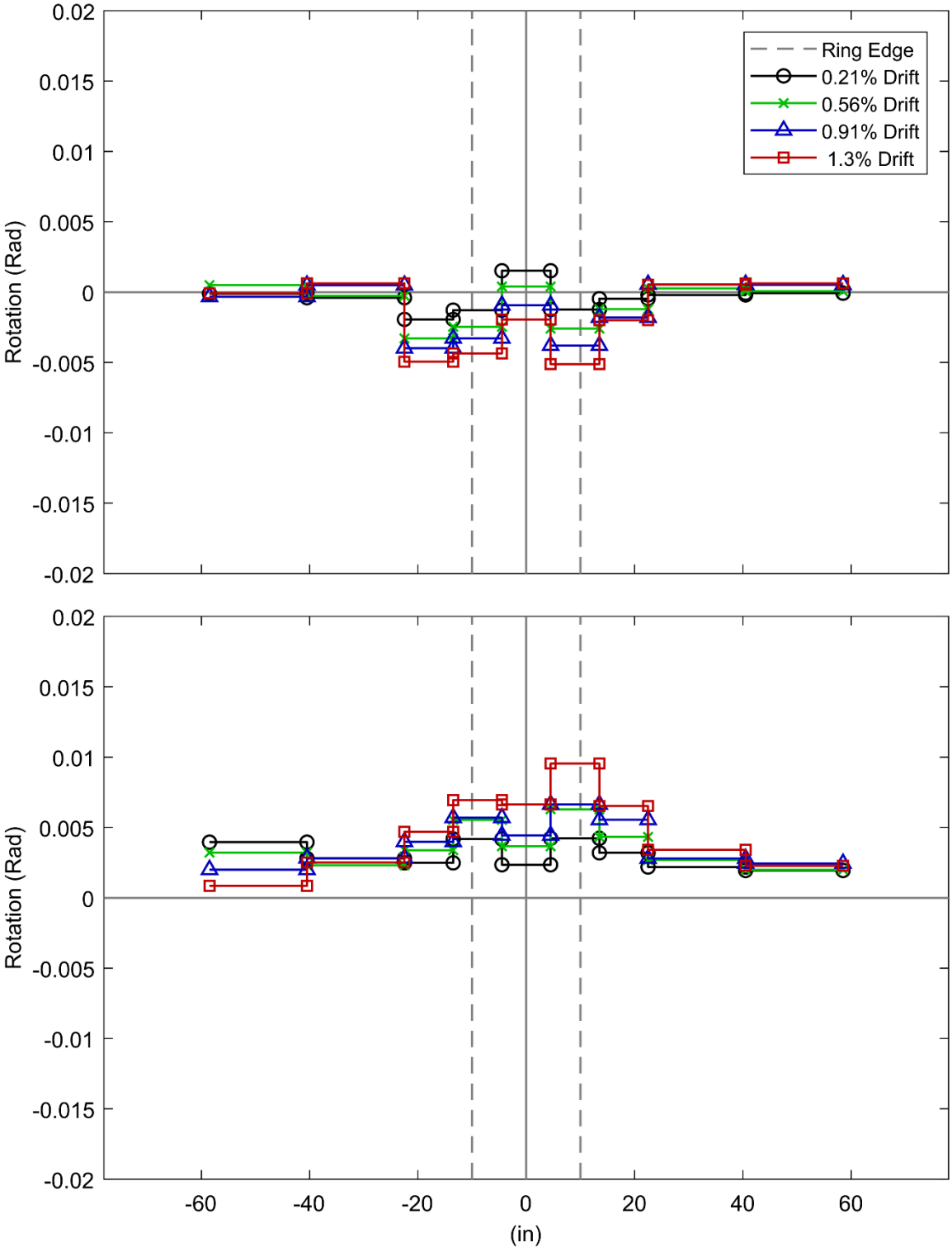

Figure 1: Low Drift Cycles Measured Slab Rotation Profile (SR_4_10_5)

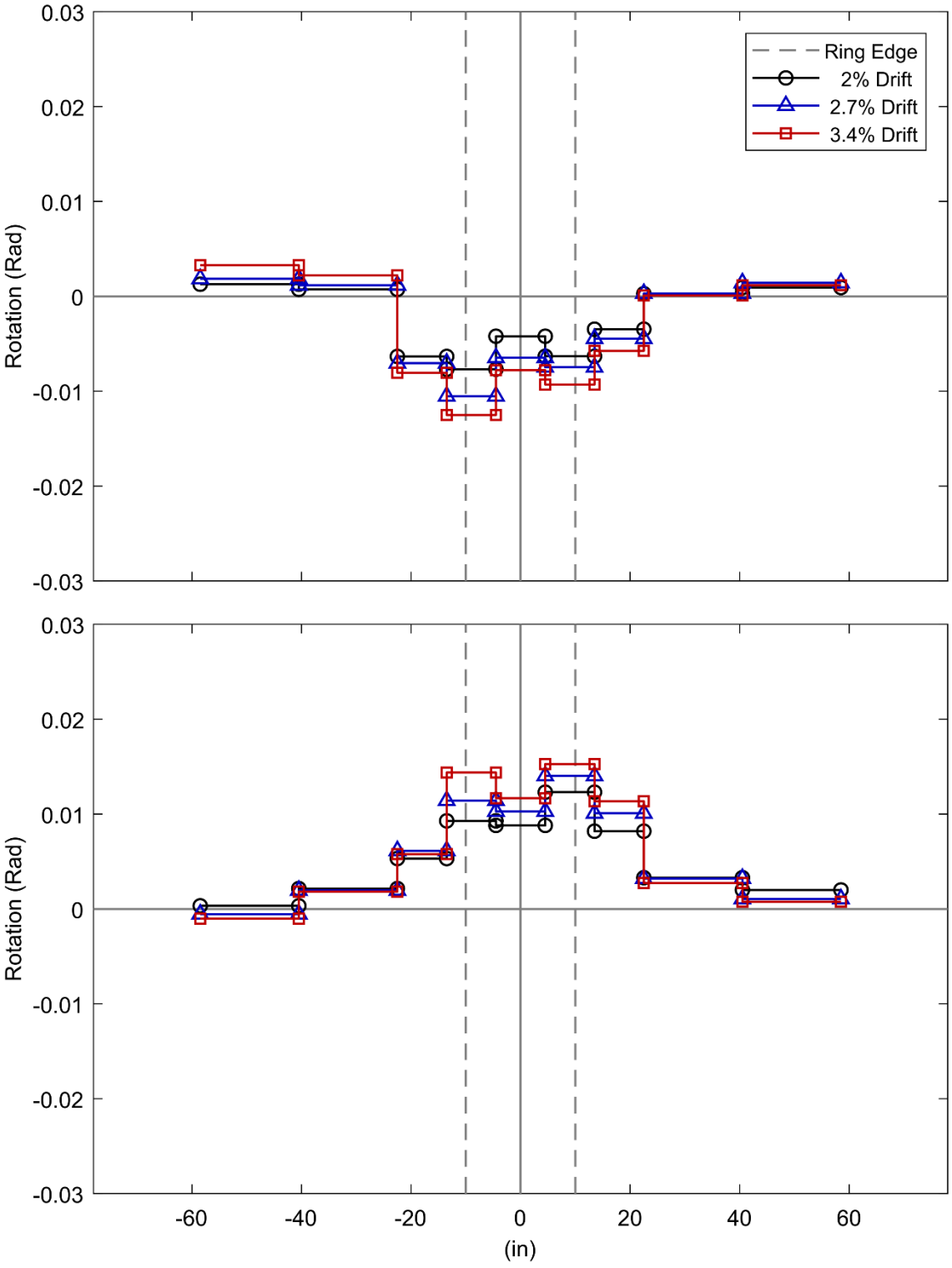

Figure 2: Moderate Drift Cycles Measured Slab Rotation Profile (SR_4_10_5)

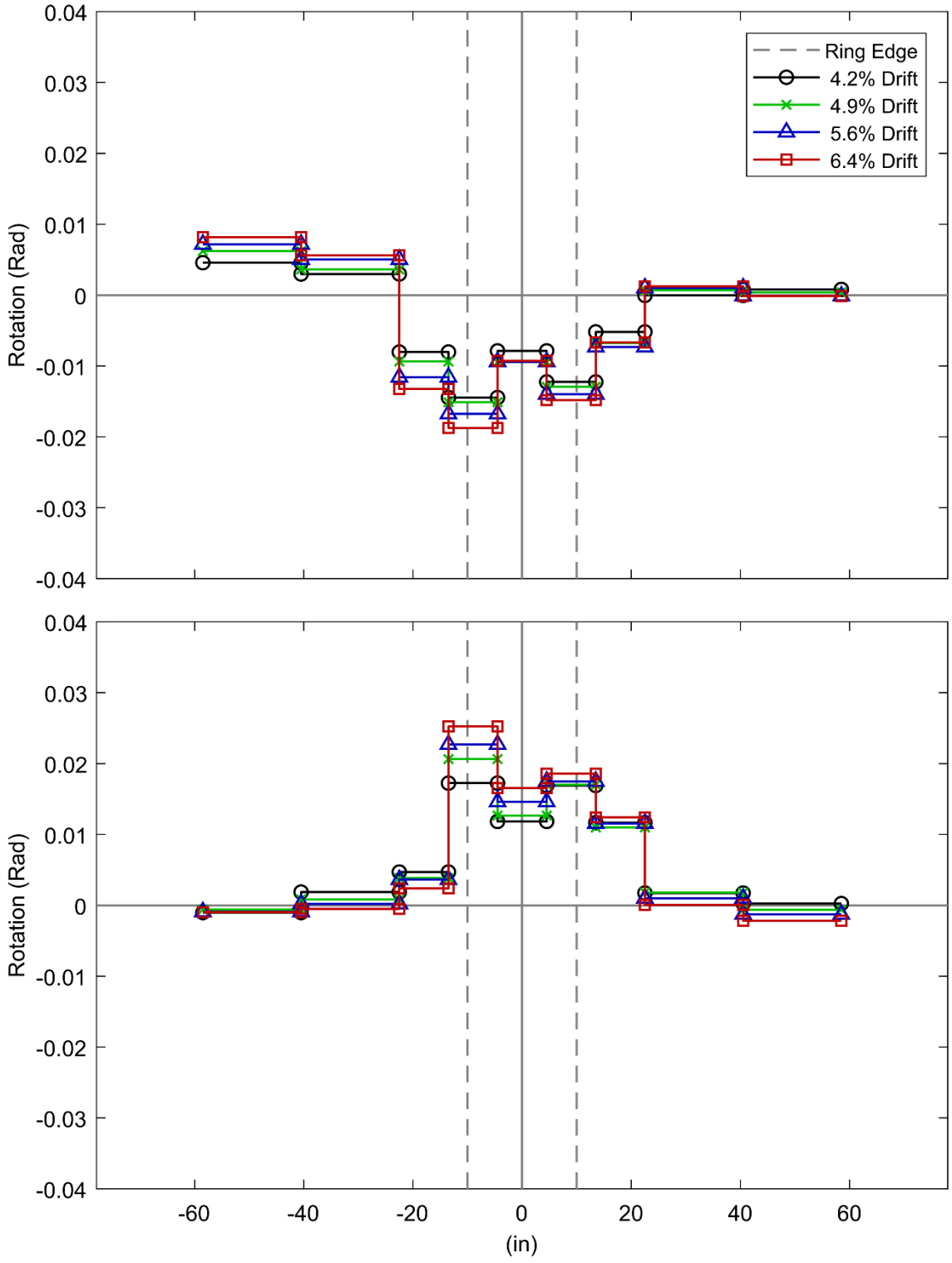

Figure 3: High Drift Cycles Measured Slab Rotation Profile (SR_4_10_5)

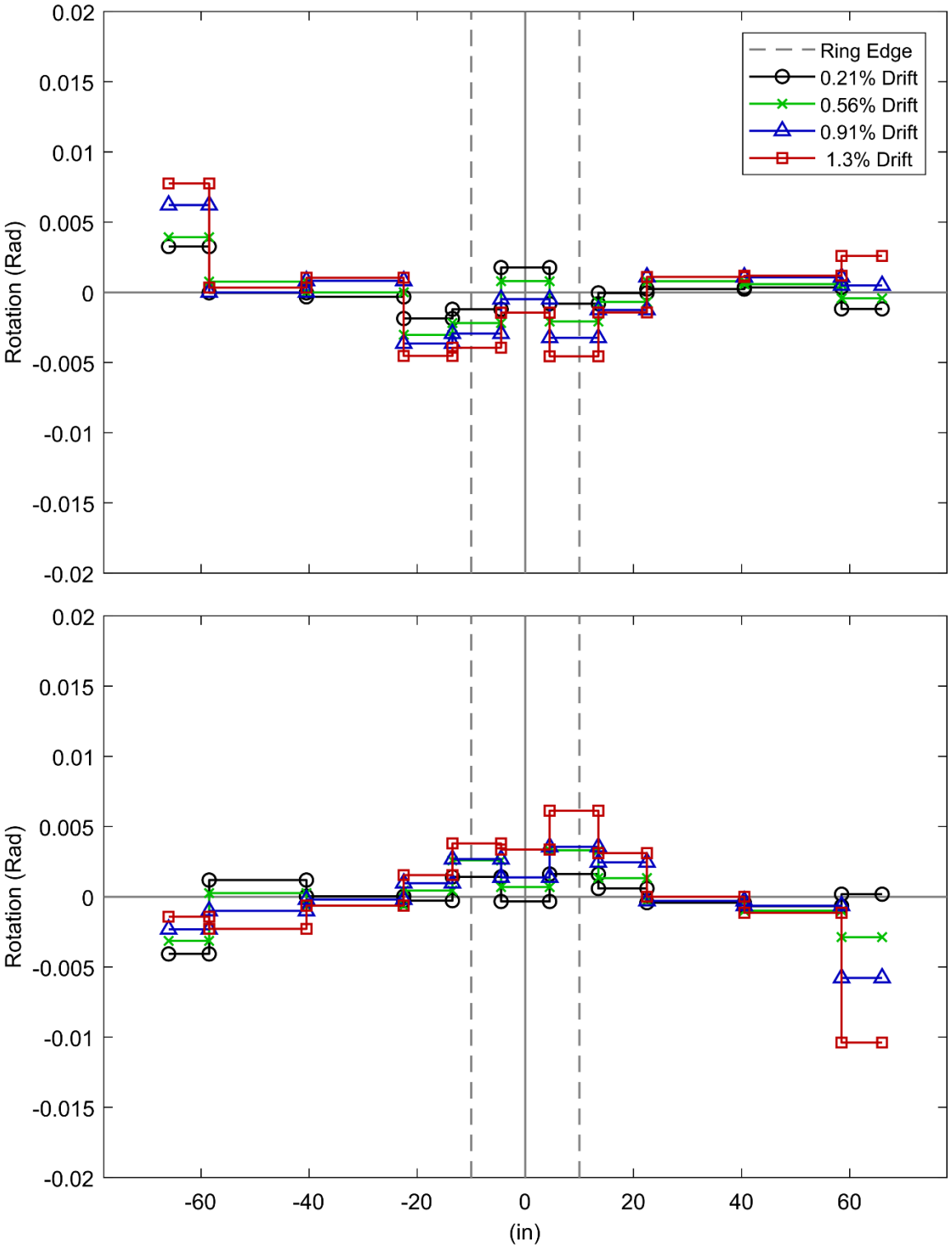

Figure 4: Low Drift Cycles Corrected Slab Rotation Profile (SR_4_10_5)

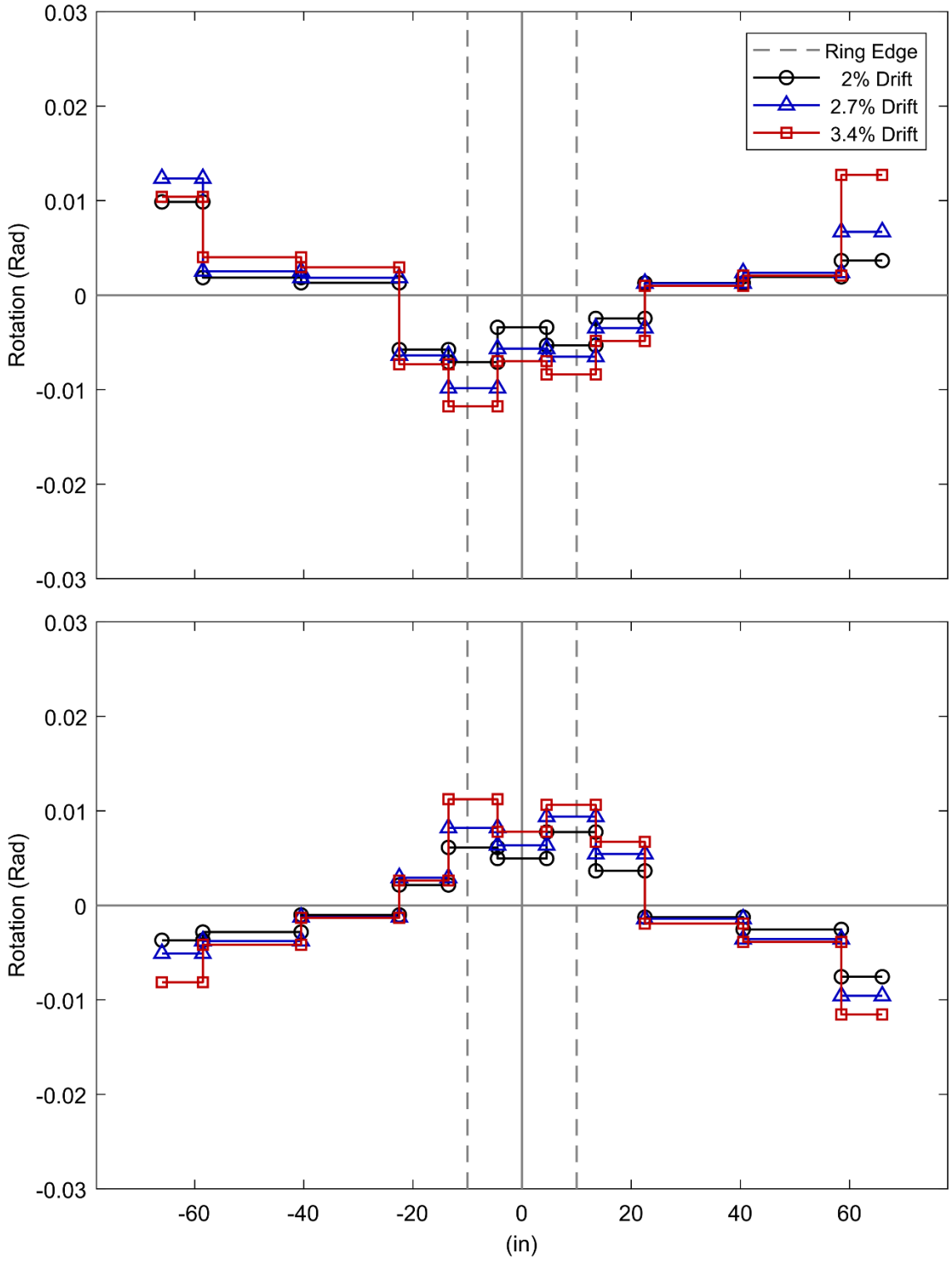

Figure 5: Moderate Drift Cycles Corrected Slab Rotation Profile (SR_4_10_5)

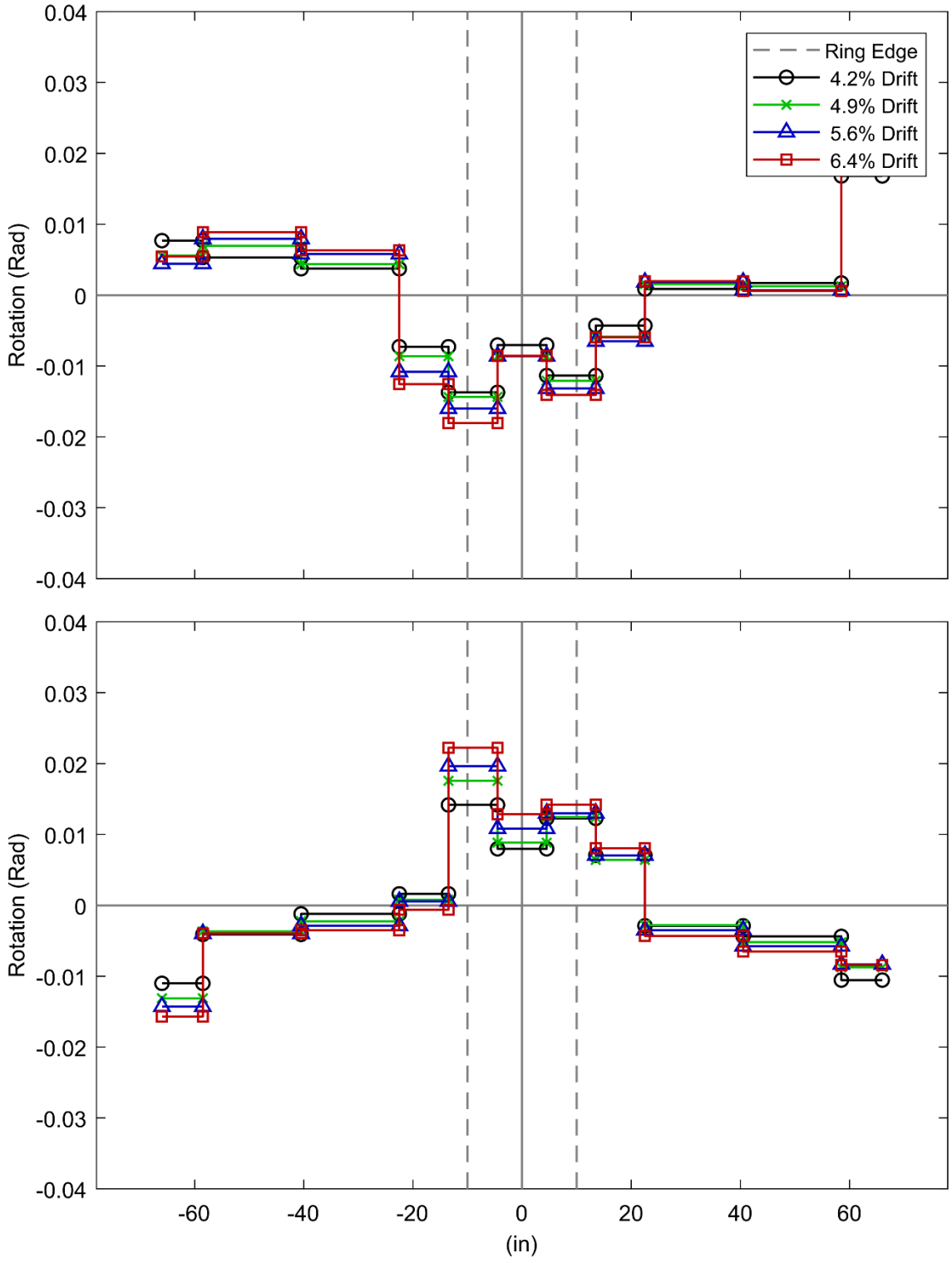

Figure 6: High Drift Cycles Corrected Slab Rotation Profile (SR_4_10_5)

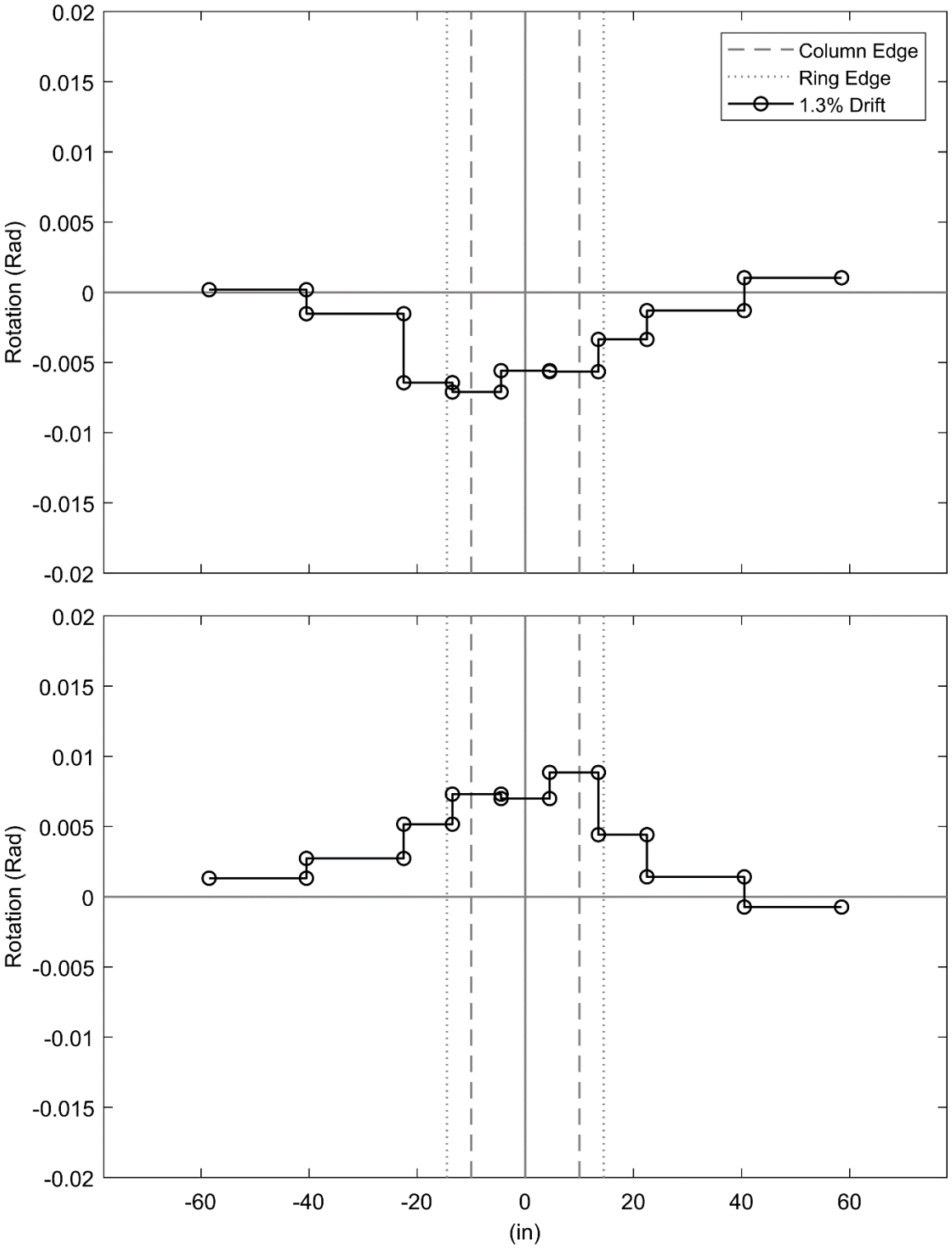

Figure 7: Low Drift Cycles Measured Slab Rotation Profile (PTB_4.5_1_0)

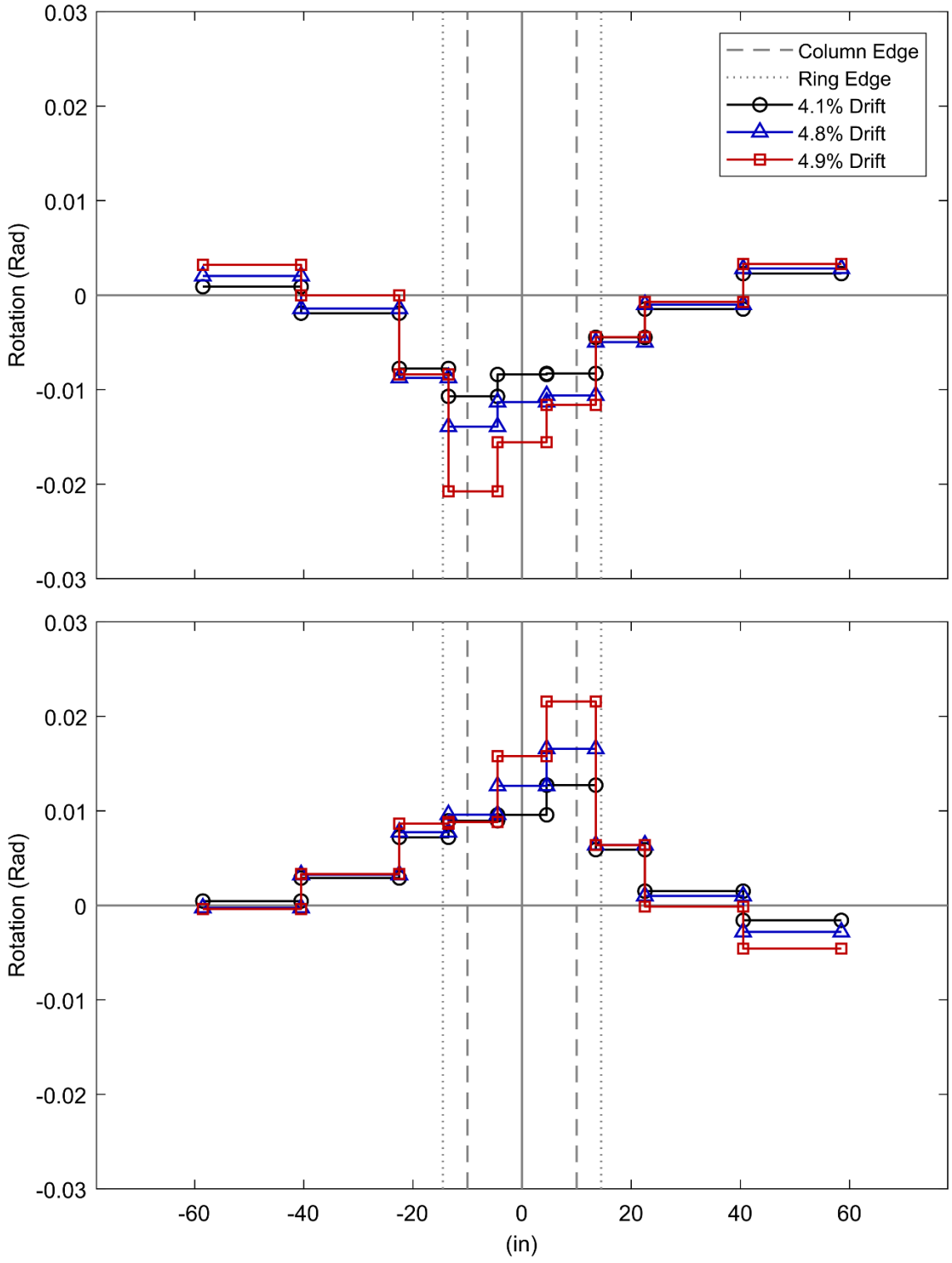

Figure 8: Moderate Drift Cycles Measured Slab Rotation Profile (PTB_4.5_1_0)

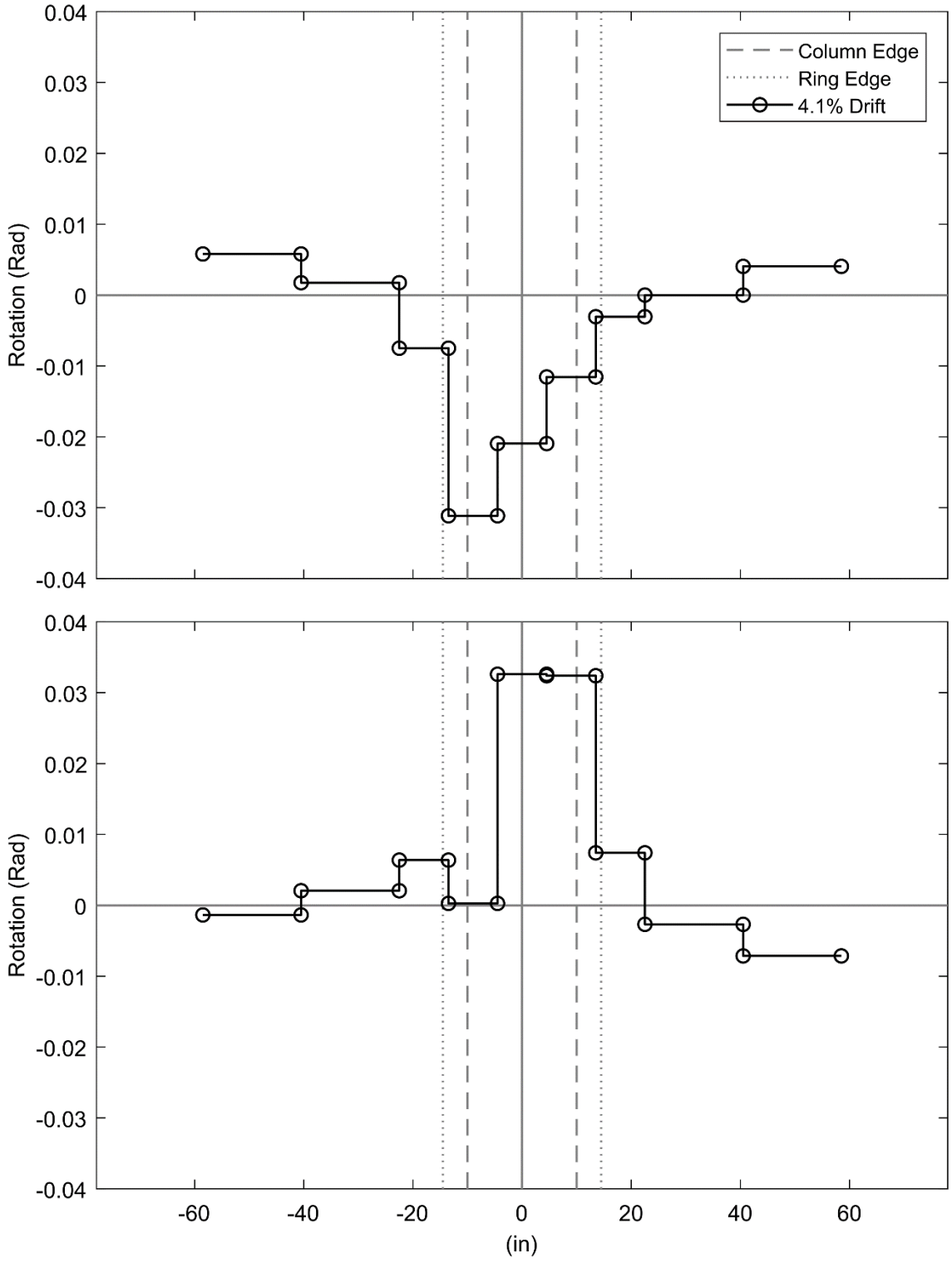

Figure 9: High Drift Cycles Measured Slab Rotation Profile (PTB_4.5_1_0)

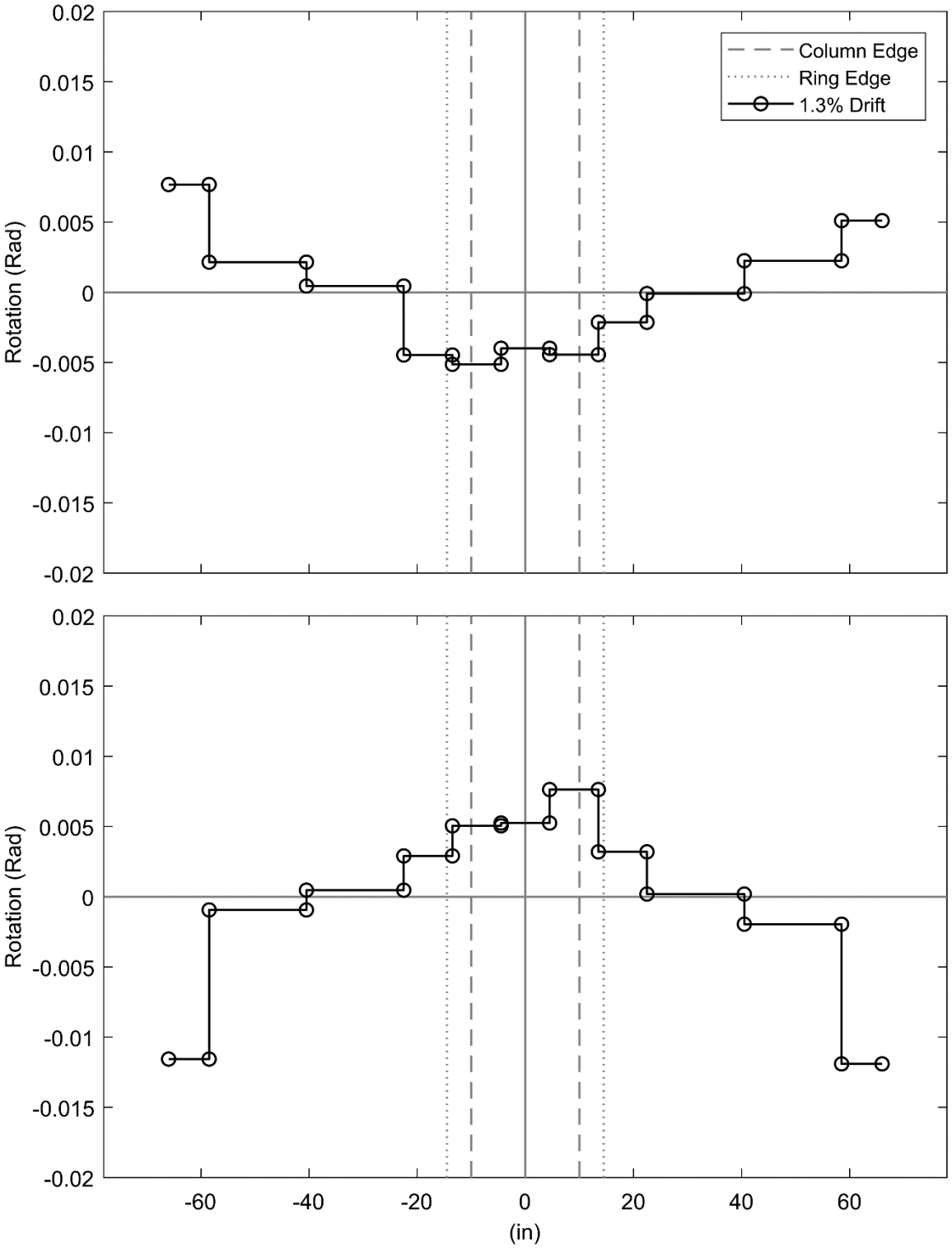

Figure 10: Low Drift Cycles Corrected Slab Rotation Profile (PTB_4.5_1_0)

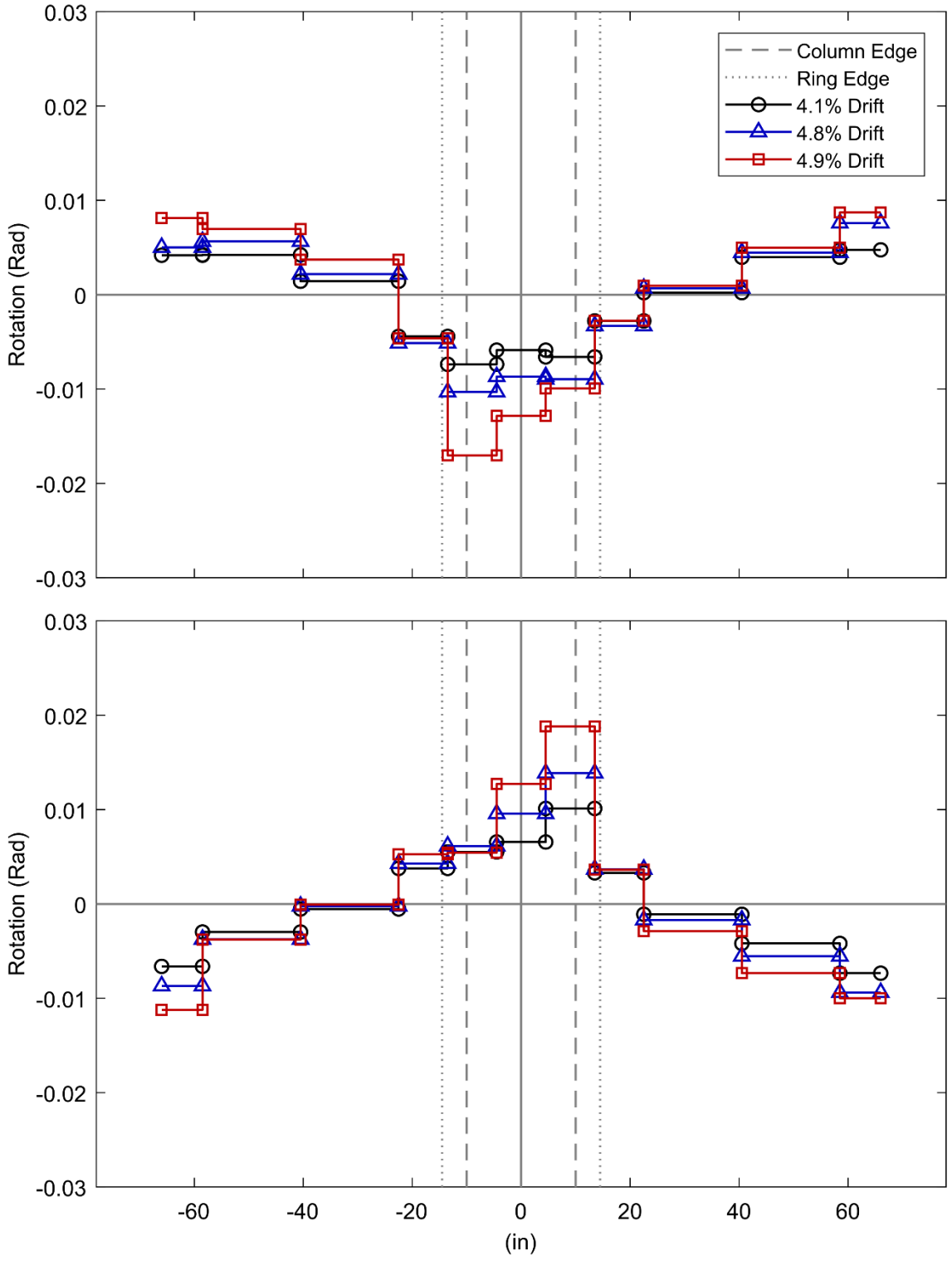

Figure 11: Moderate Drift Cycles Corrected Slab Rotation Profile (PTB_4.5_1_0)

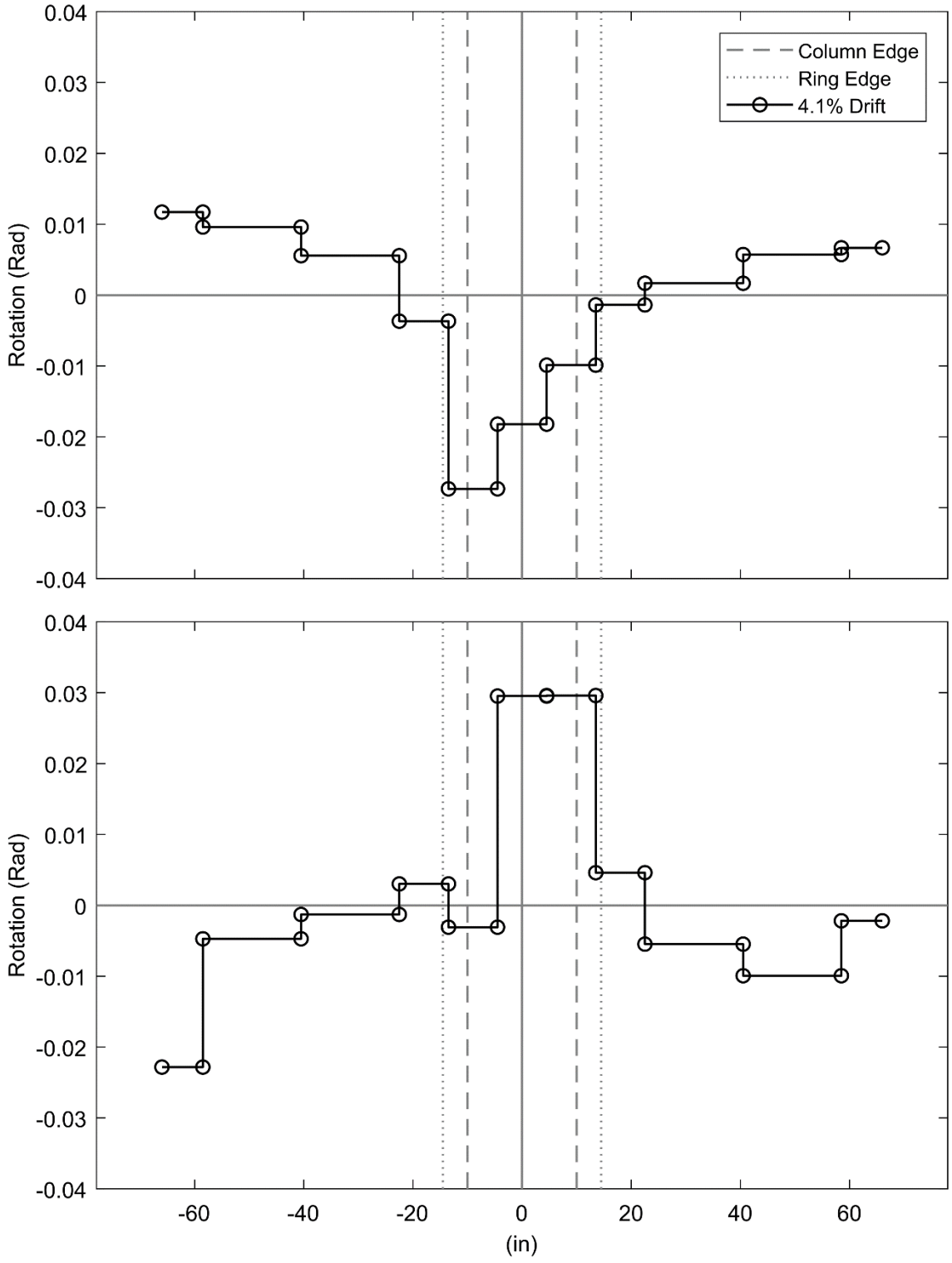

Figure 12: High Drift Cycles Corrected Slab Rotation Profile (PTB_4.5_1_0)

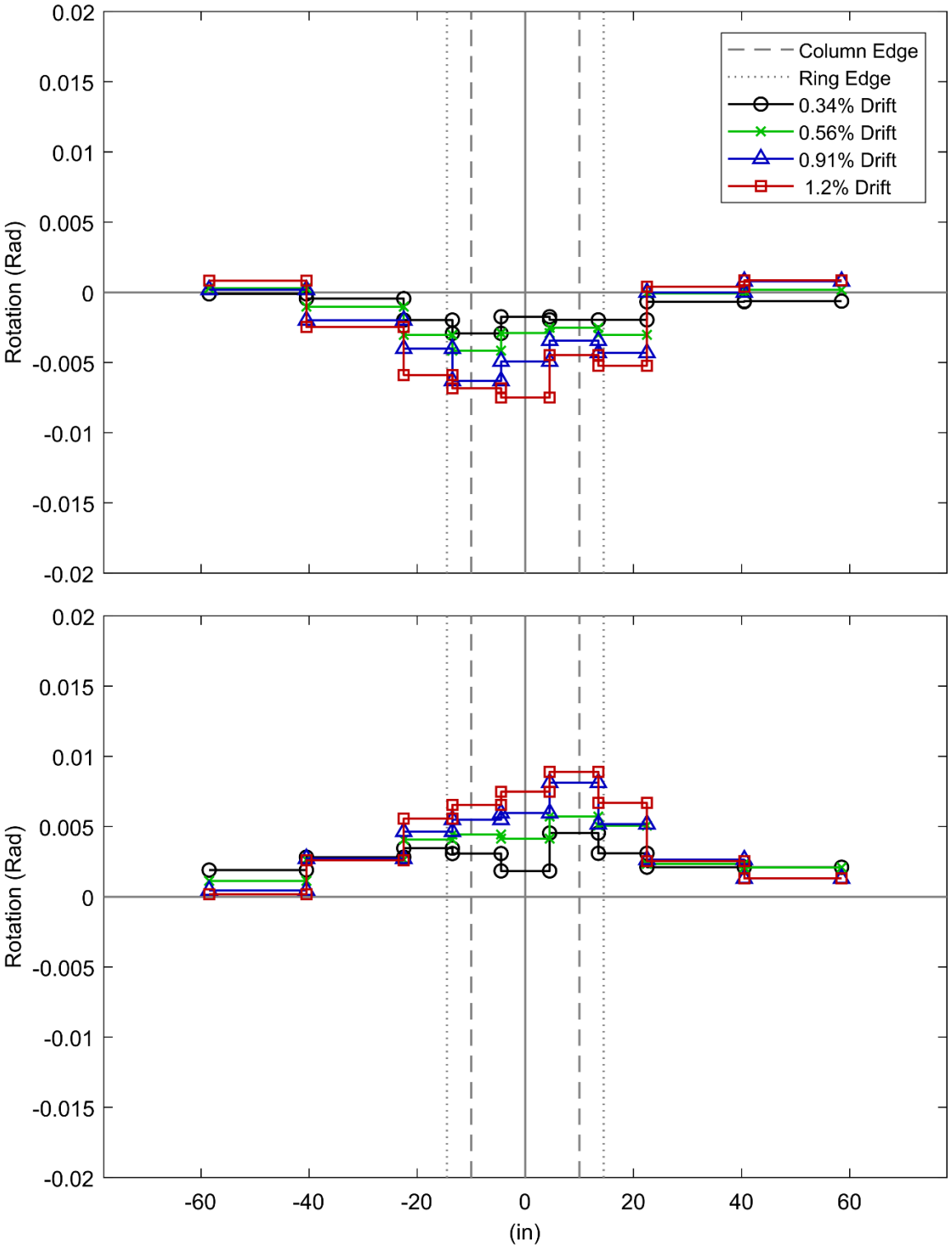

Figure 13: Low Drift Cycles Measured Slab Rotation Profile (PTB_4.5_1_4)

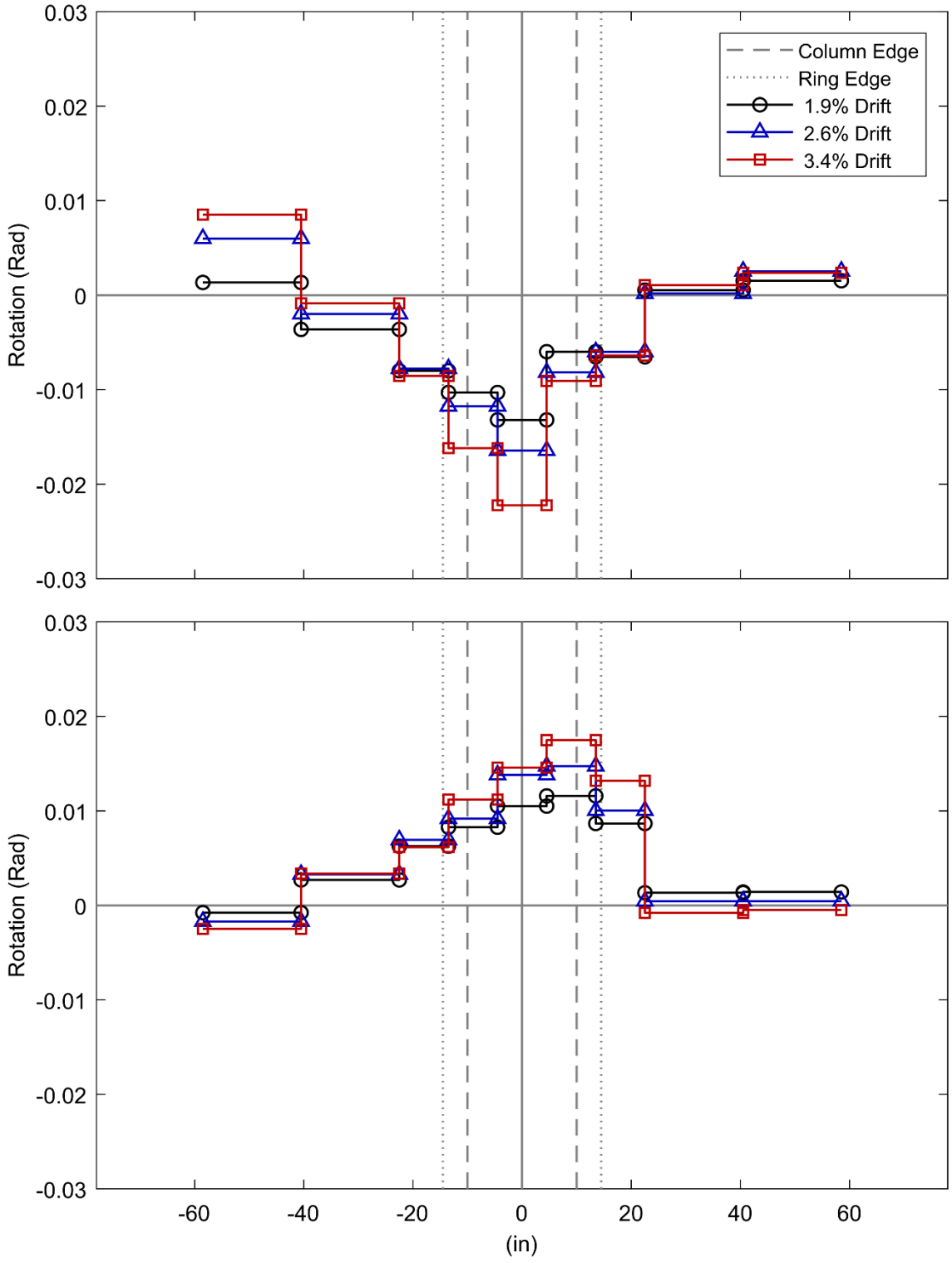

Figure 14: Moderate Drift Cycles Measured Slab Rotation Profile (PTB_4.5_1_4)

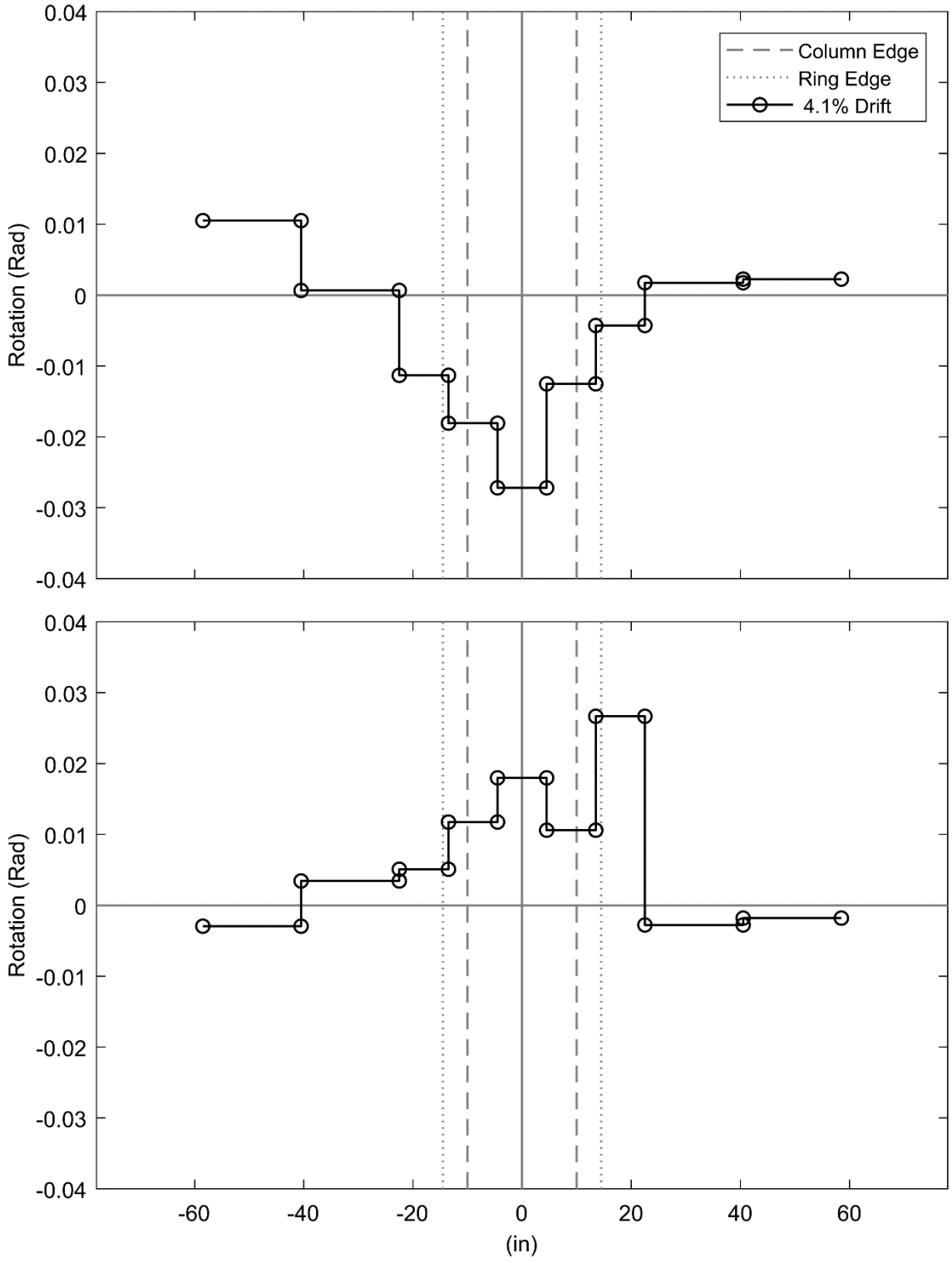

Figure 15: High Drift Cycles Measured Slab Rotation Profile (PTB_4.5_1_4)

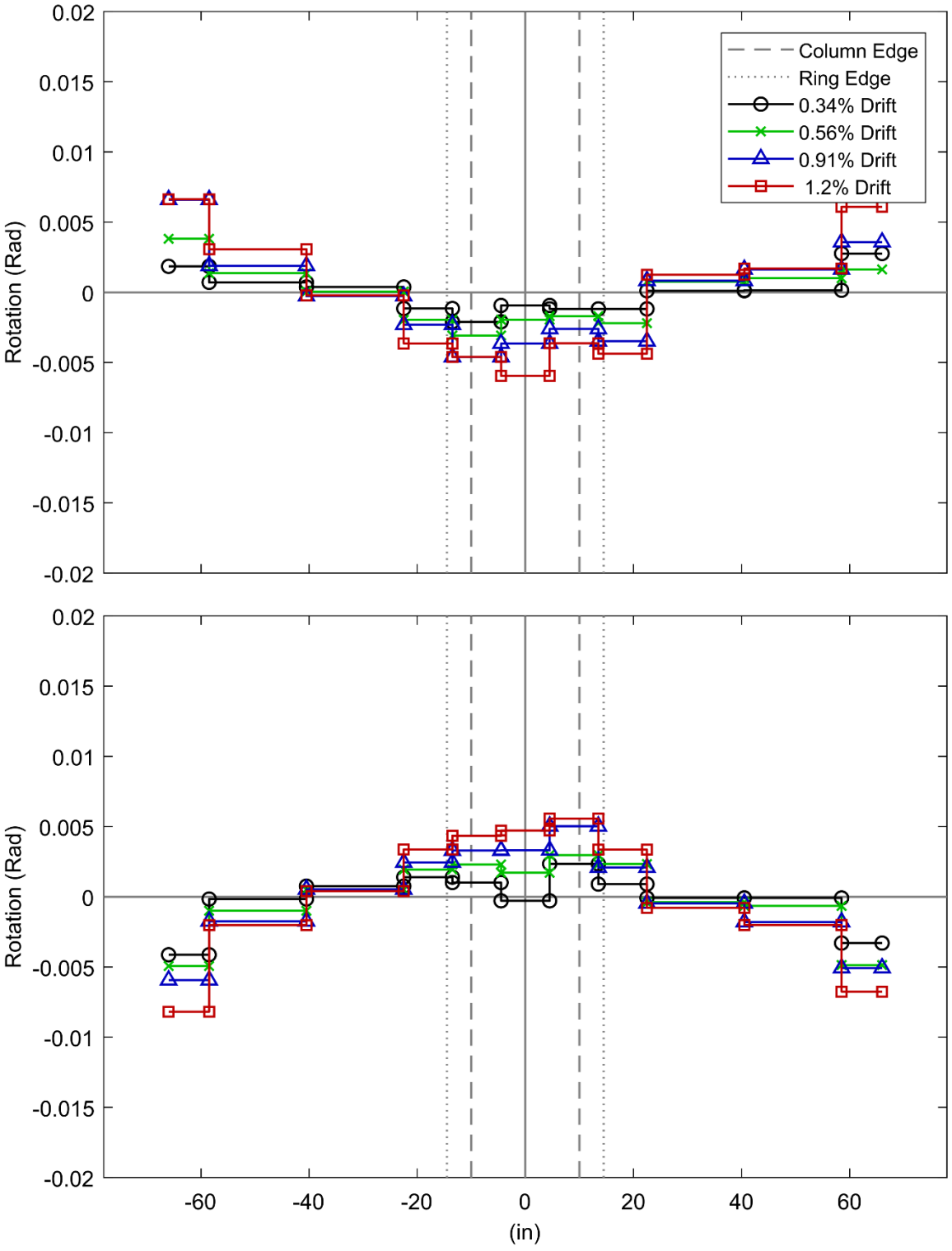

Figure 16: Low Drift Cycles Corrected Slab Rotation Profile (PTB_4.5_1_4)

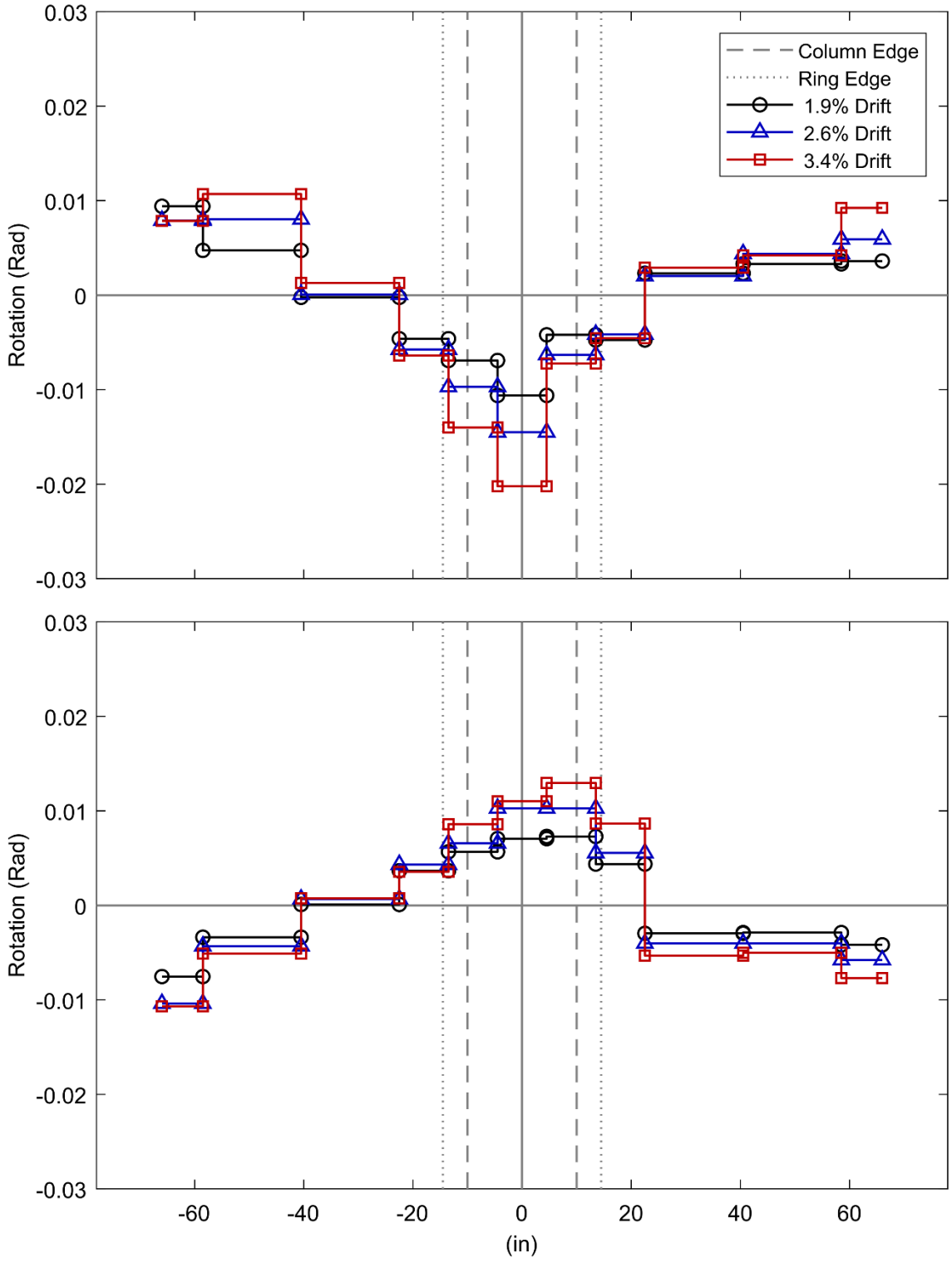

Figure 17: Moderate Drift Cycles Corrected Slab Rotation Profile (PTB_4.5_1_4)

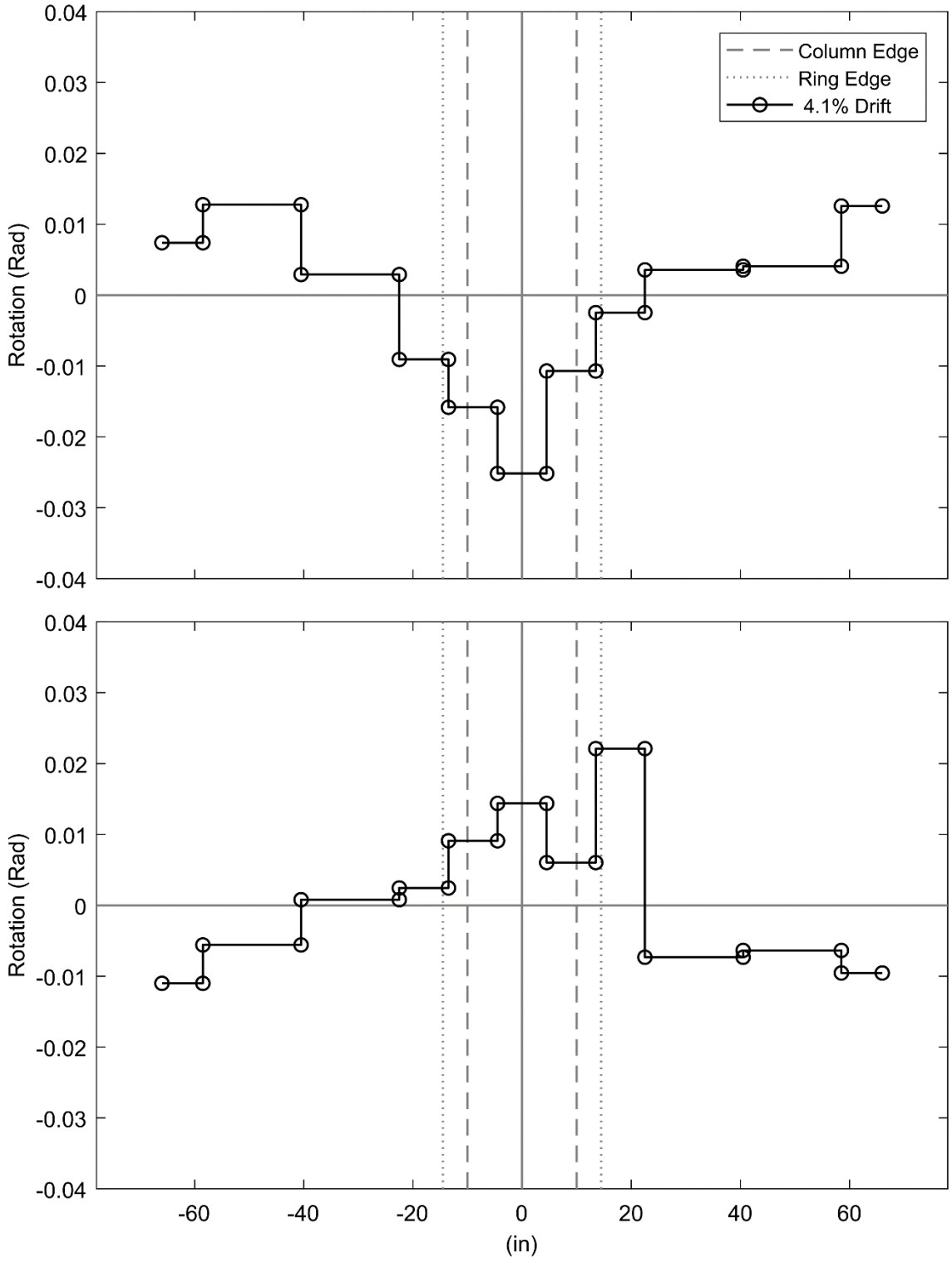

Figure 18: High Drift Cycles Corrected Slab Rotation Profile (PTB_4.5_1_4)

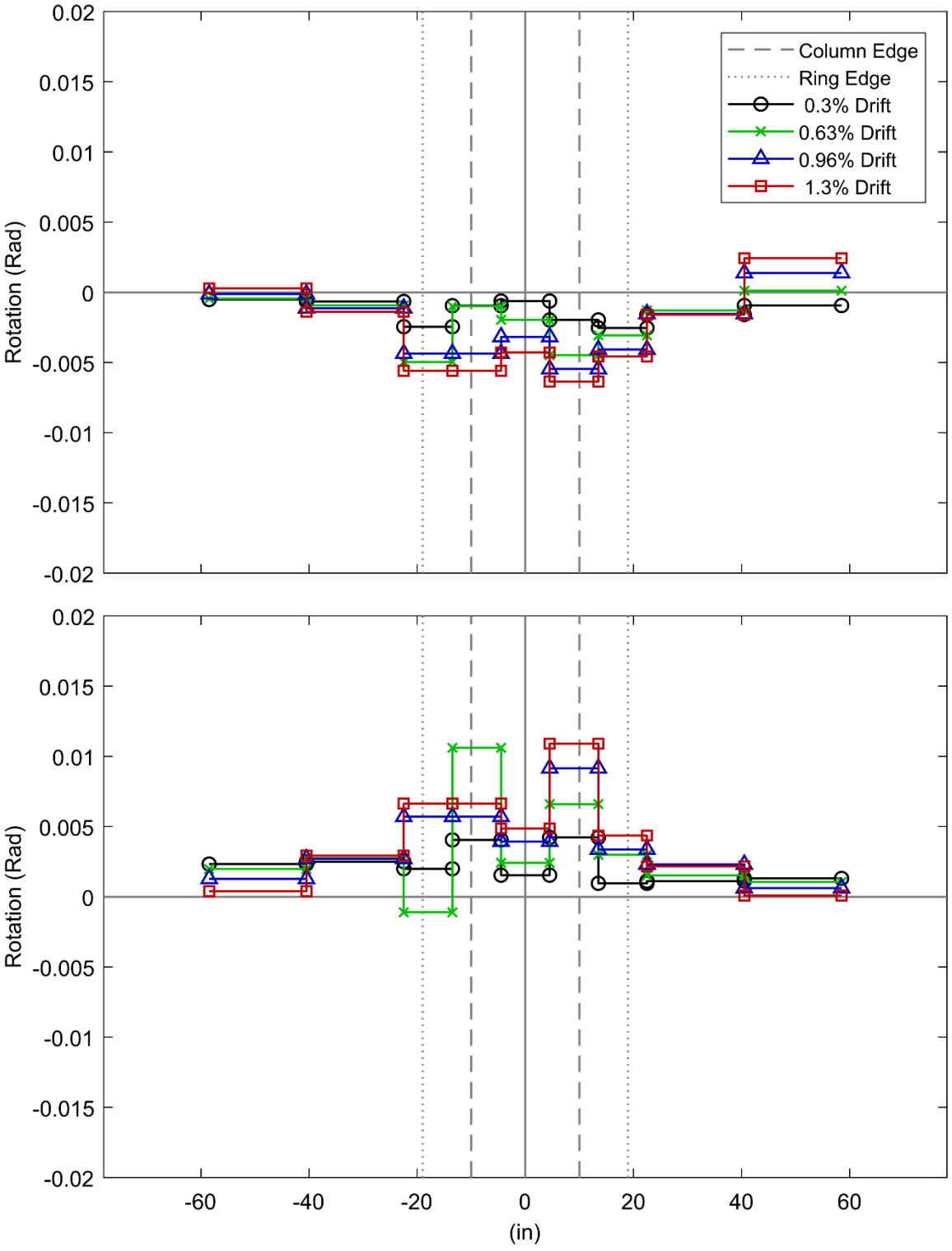

Figure 19: Low Drift Cycles Measured Slab Rotation Profile (PTB_9_2_0)

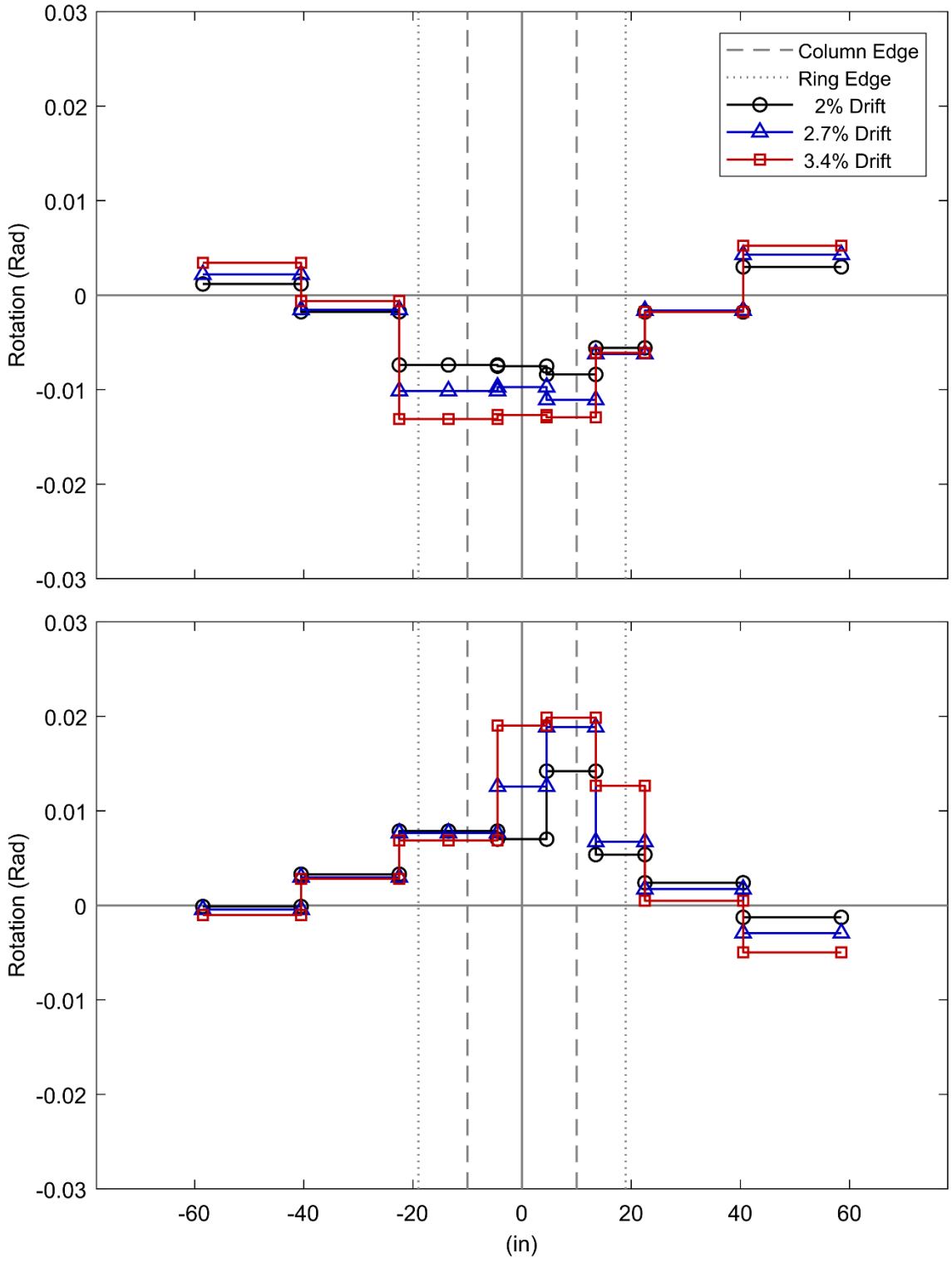

Figure 20: Moderate Drift Cycles Measured Slab Rotation Profile (PTB_9_2_0)

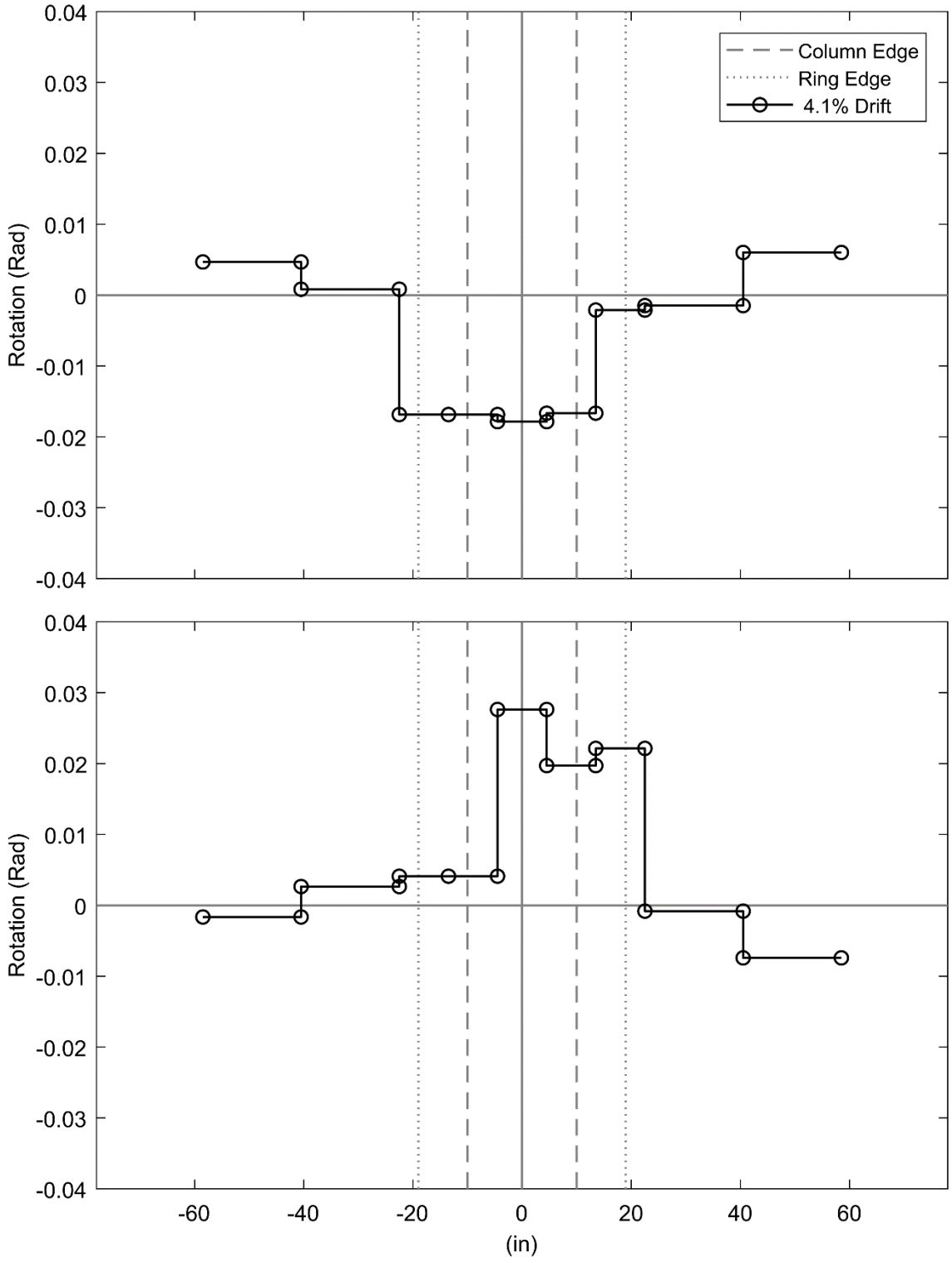

Figure 21: High Drift Cycles Measured Slab Rotation Profile (PTB_9_2_0)

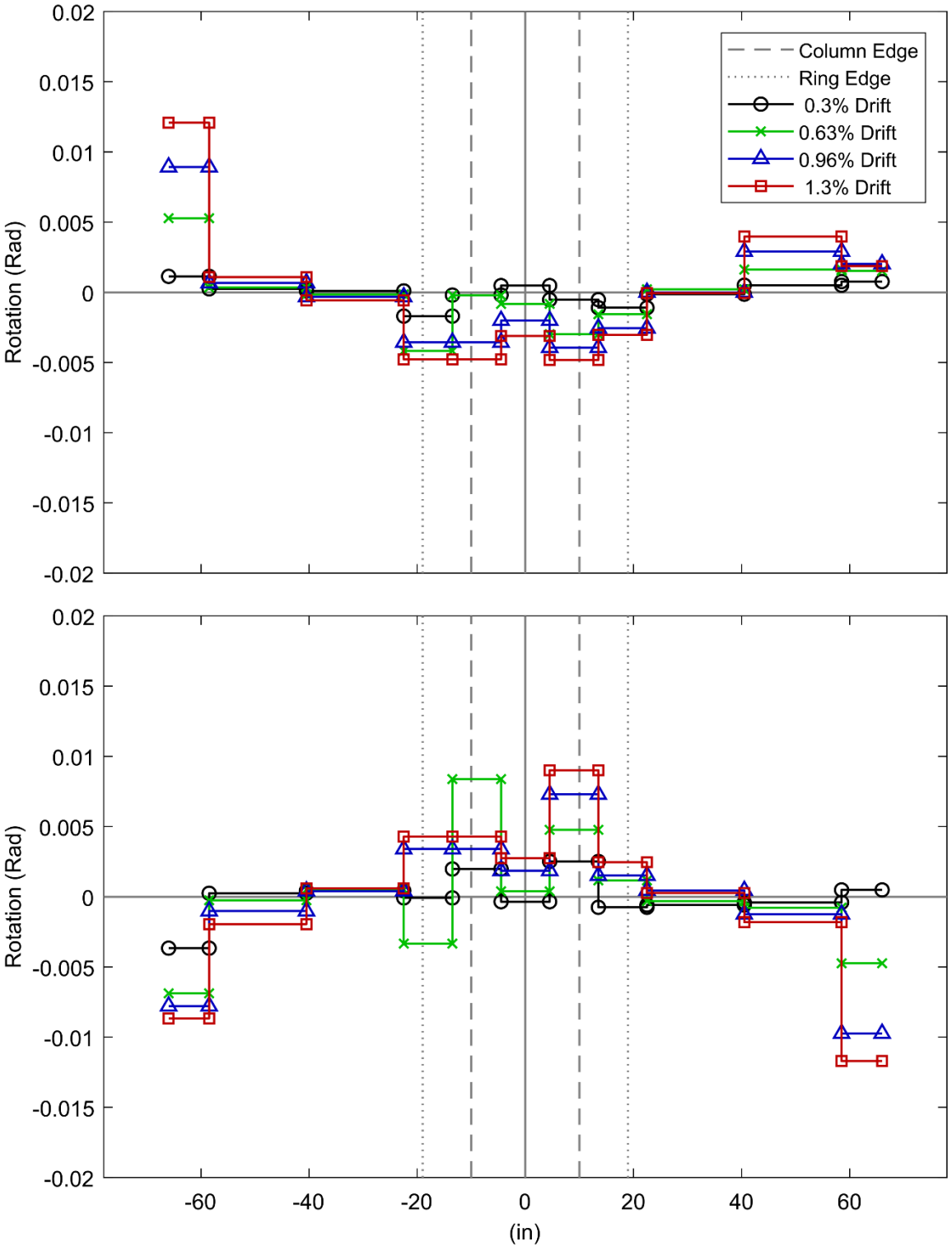

Figure 22: Low Drift Cycles Corrected Slab Rotation Profile (PTB_9_2_0)

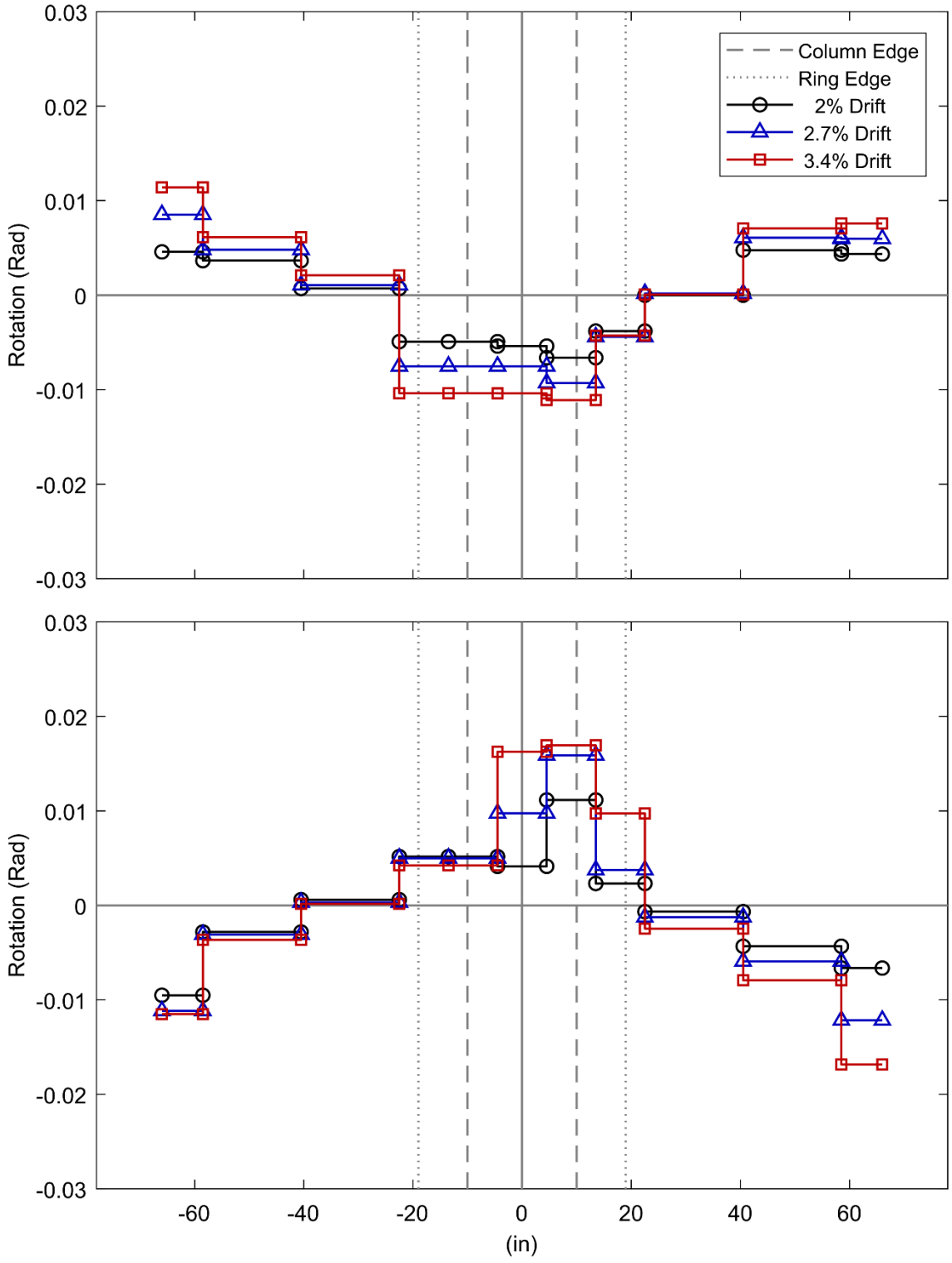

Figure 23: Moderate Drift Cycles Corrected Slab Rotation Profile (PTB_9_2_0)

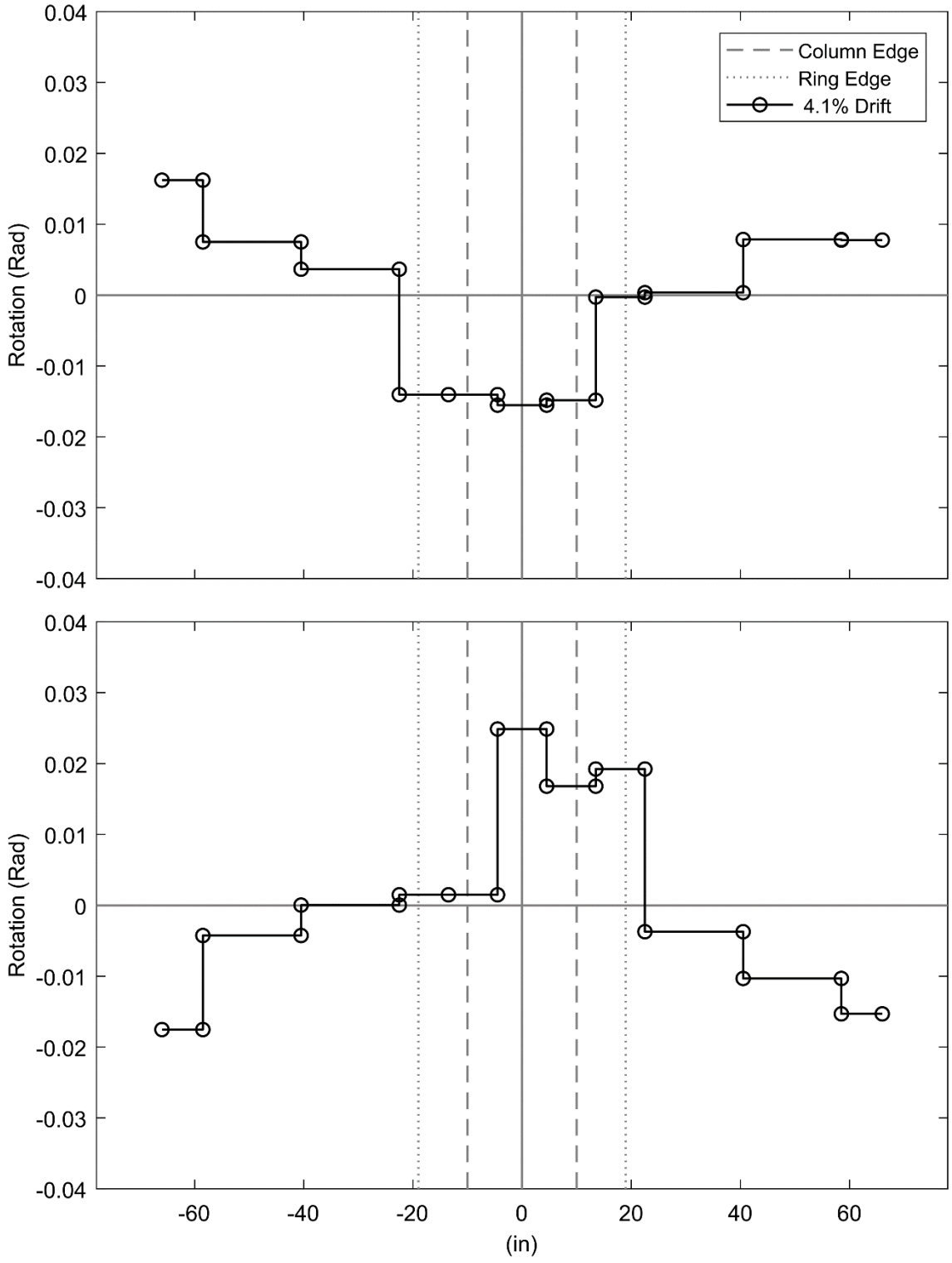

Figure 24: High Drift Cycles Corrected Slab Rotation Profile (PTB_9_2_0)

APPENDIX H: STRAIN VS. DRIFT

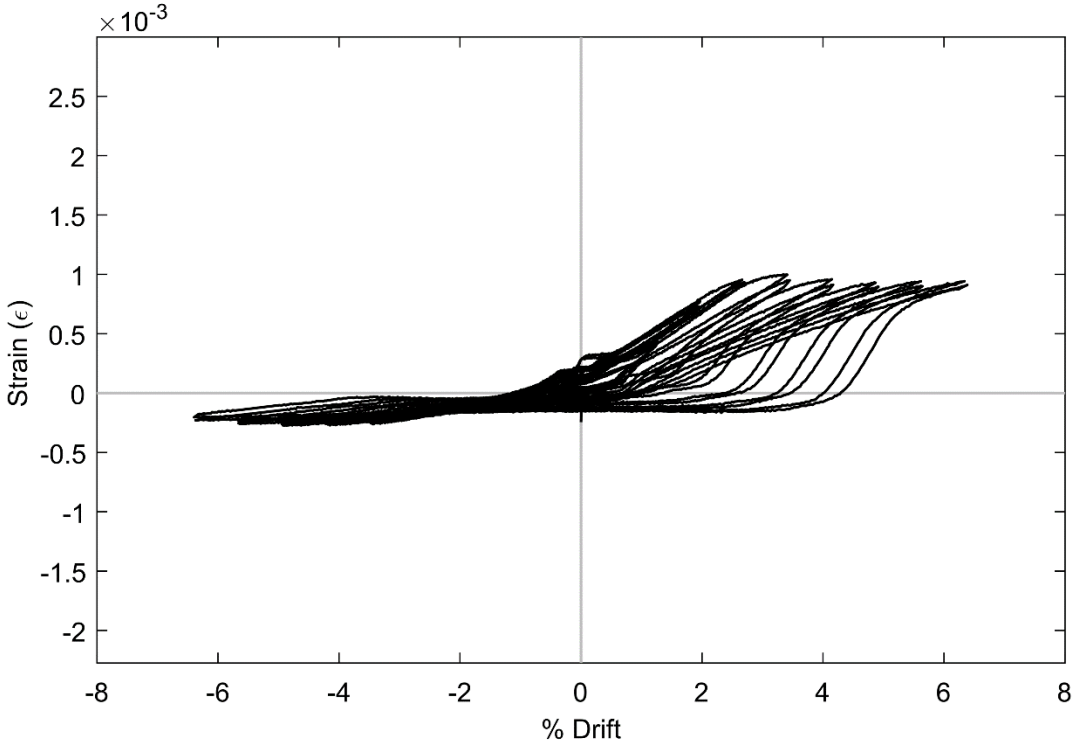

Figure 1: SG STE5 (SR_4_10_5)

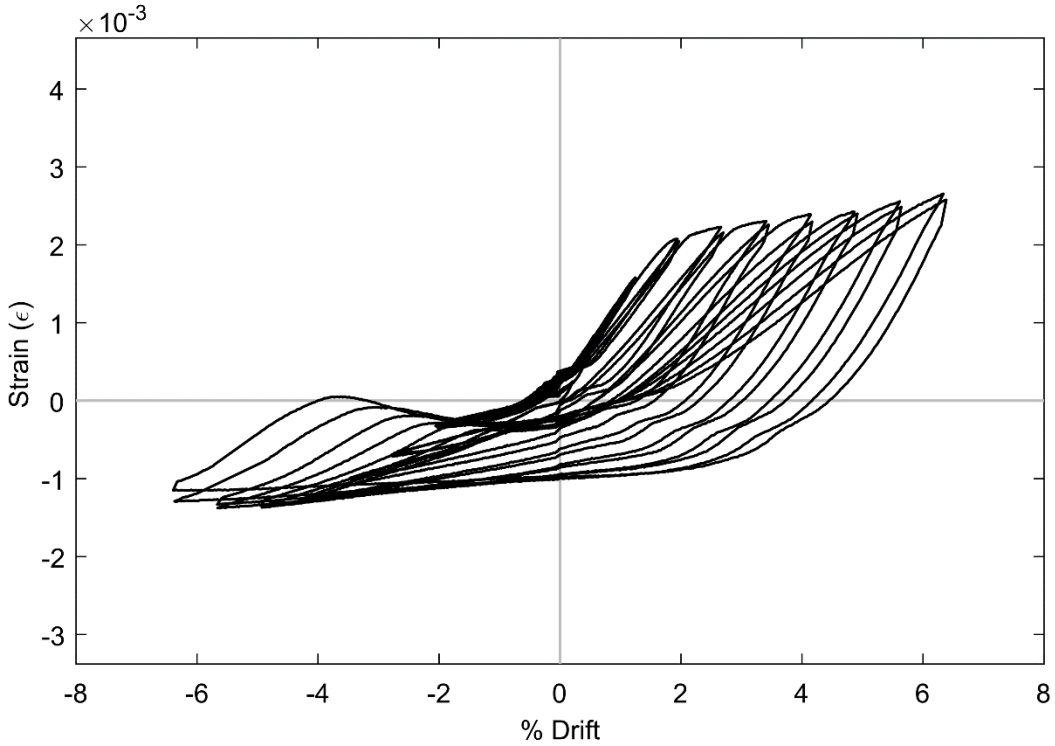

Figure 2: SG STG5 (SR_4_10_5)

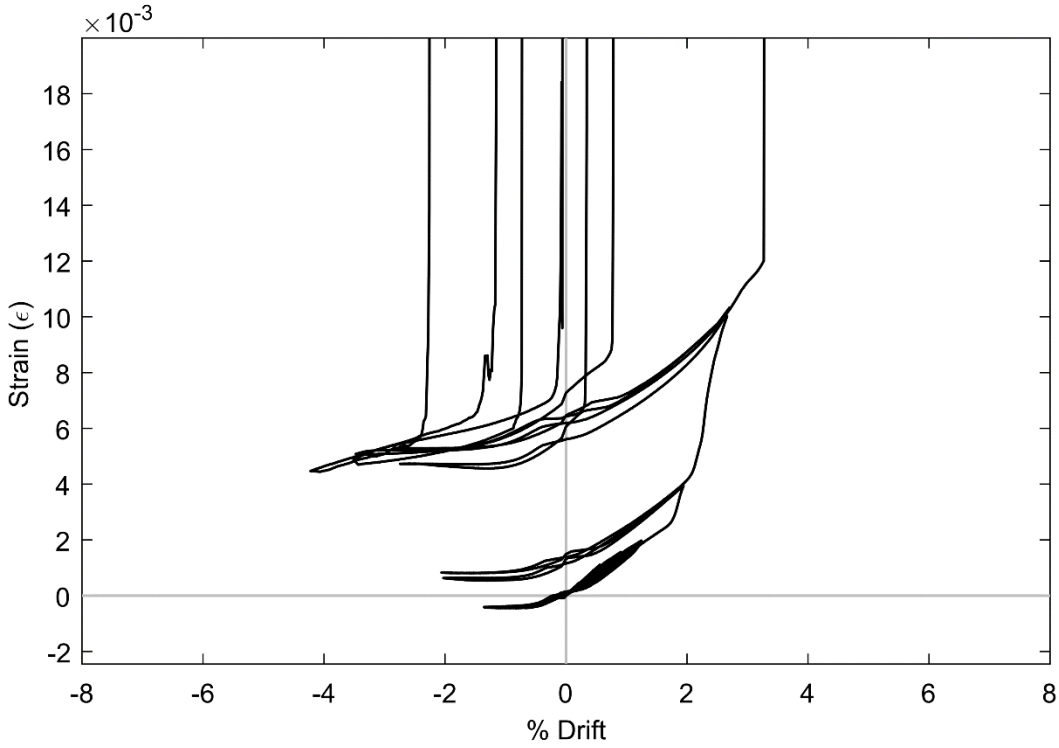

Figure 3: SG STH5 (SR_4_10_5)

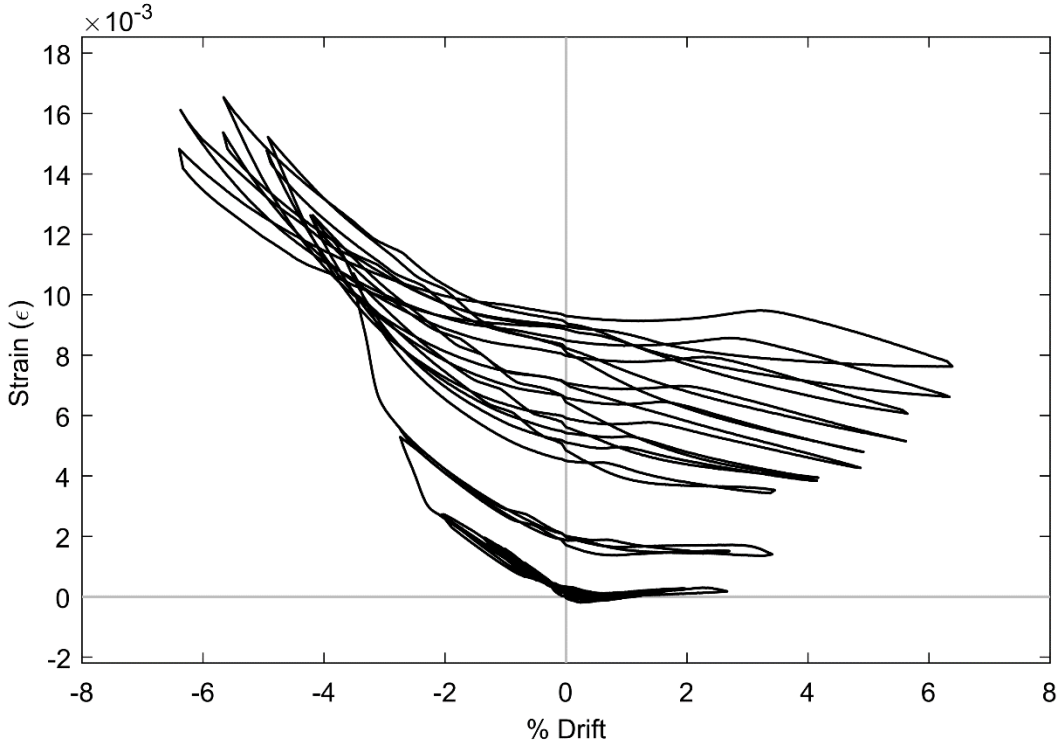

Figure 4: SG STK5 (SR_4_10_5)

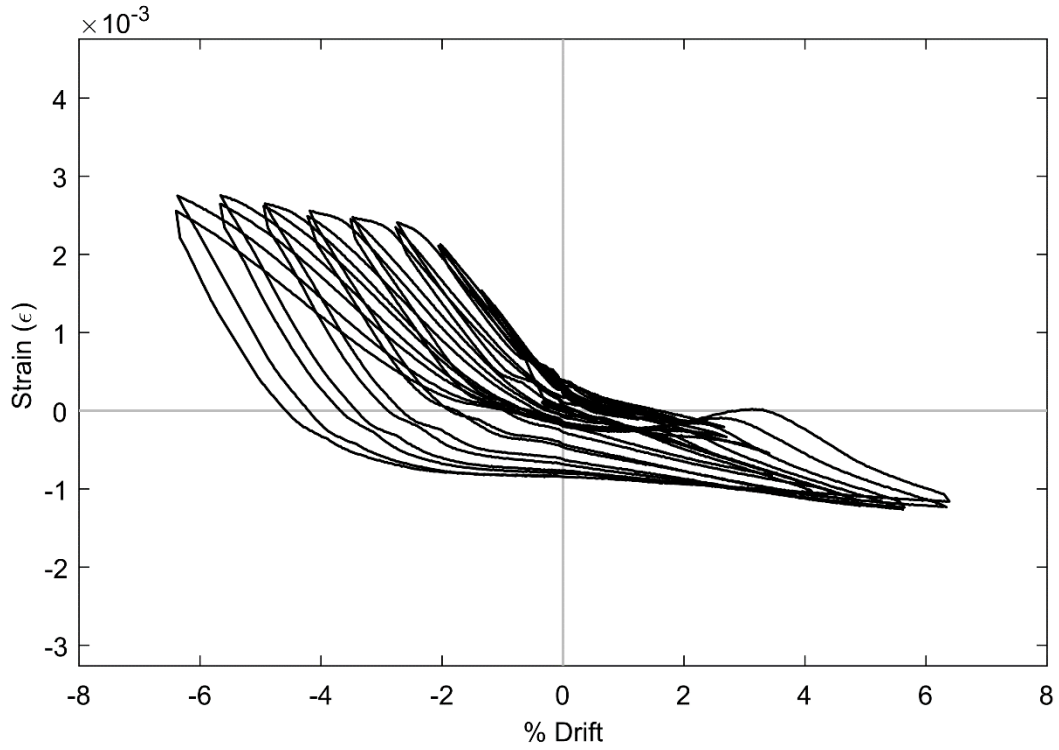

Figure 5: SG STL5 (SR_4_10_5)

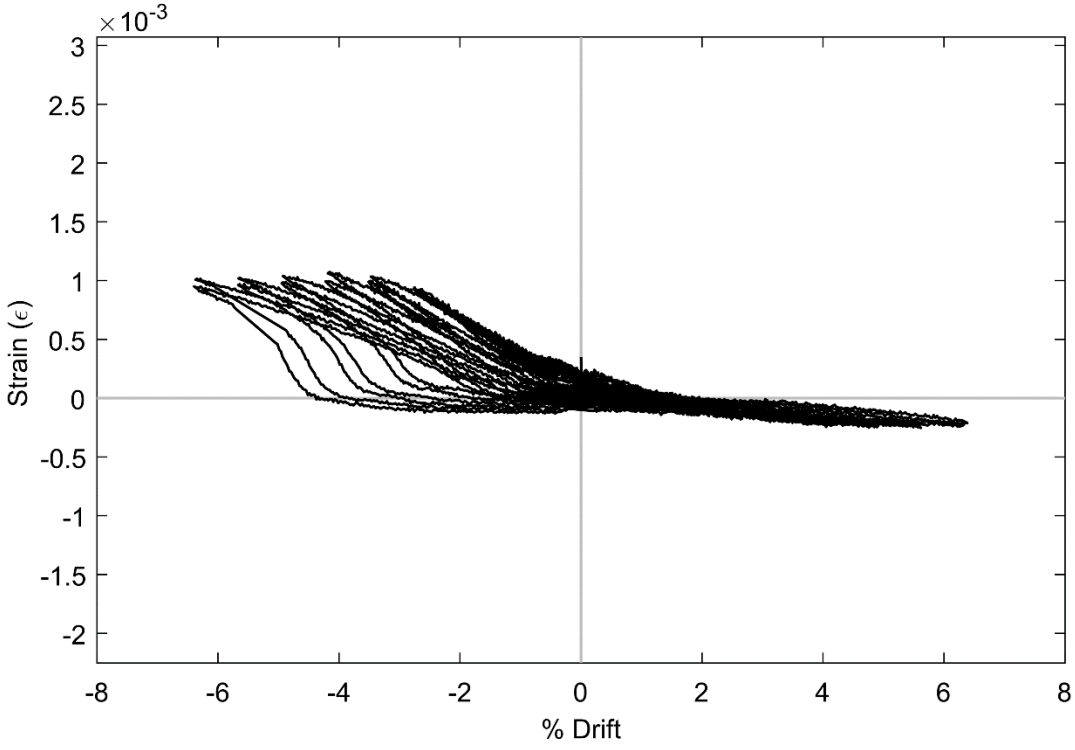

Figure 6: SG STN5 (SR_4_10_5)

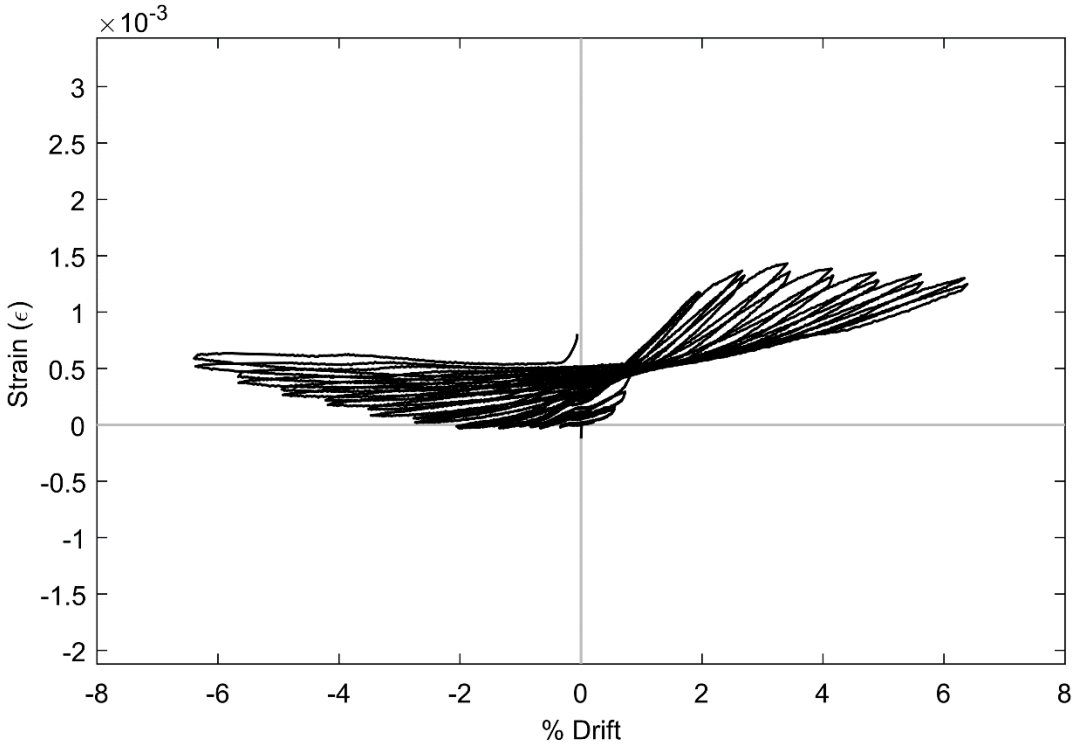

Figure 7: SG STE6 (SR_4_10_5)

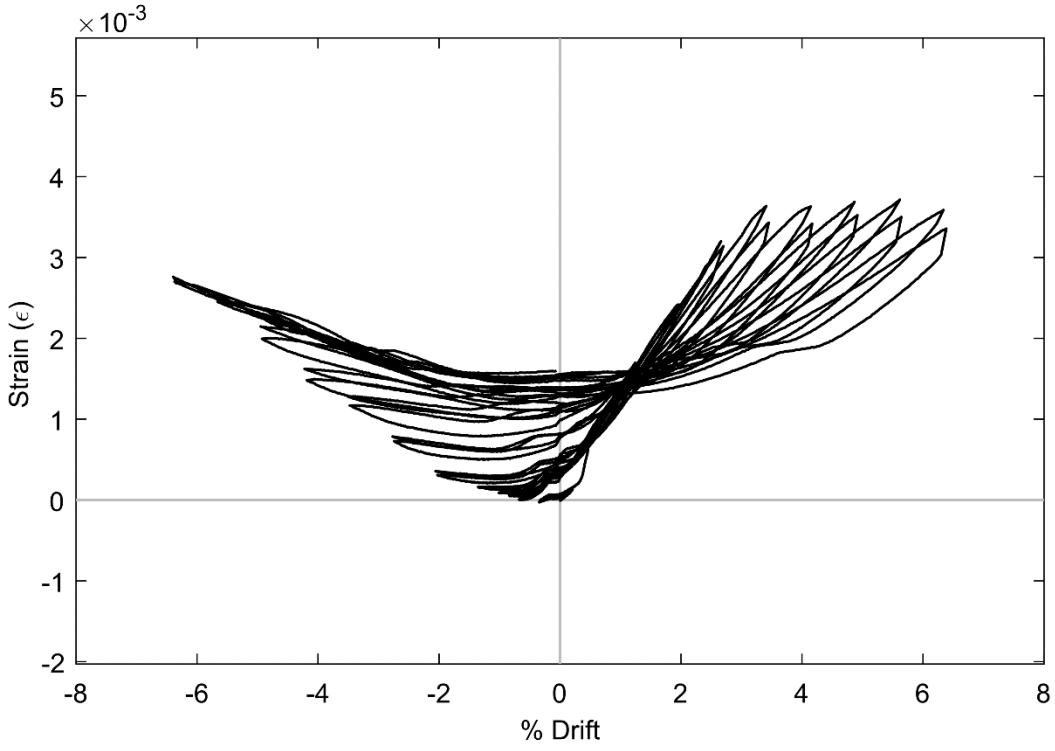

Figure 8: SG STG6 (SR_4_10_5)

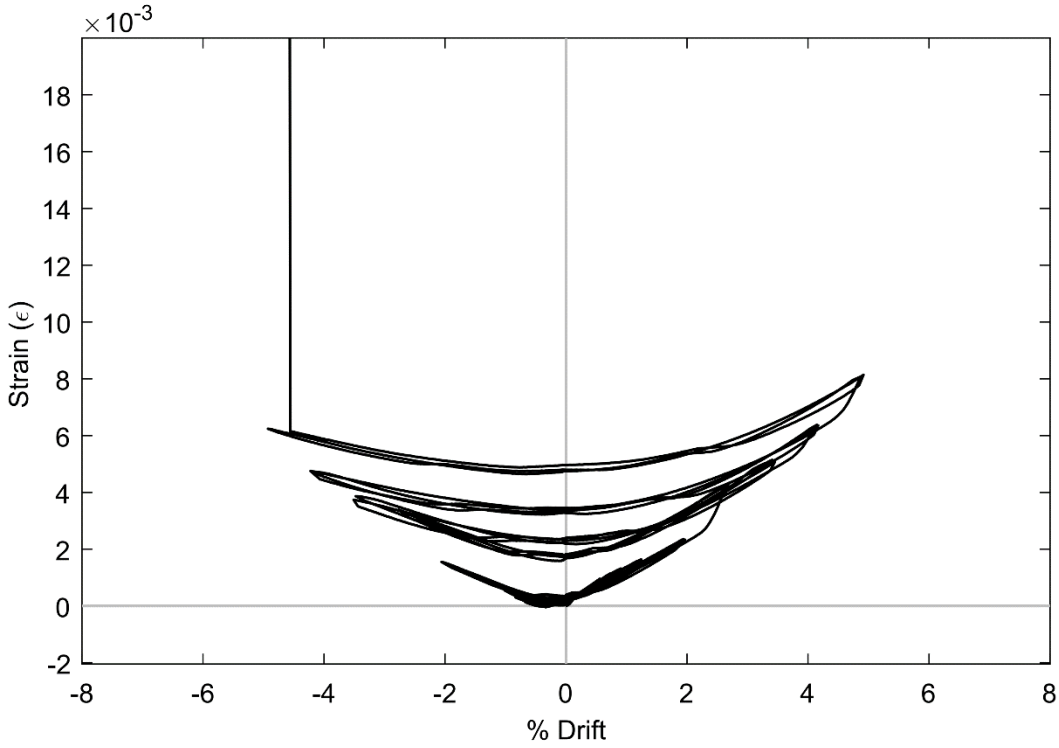

Figure 9: SG STI6 (SR_4_10_5)

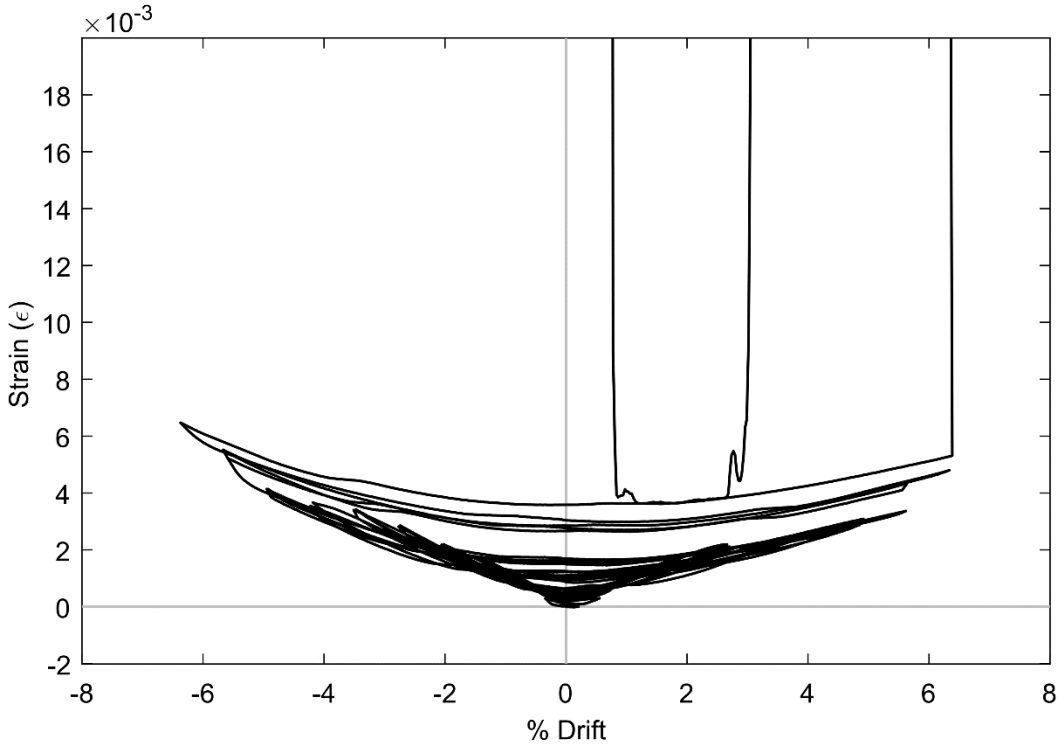

Figure 10: SG STJ6 (SR_4_10_5)

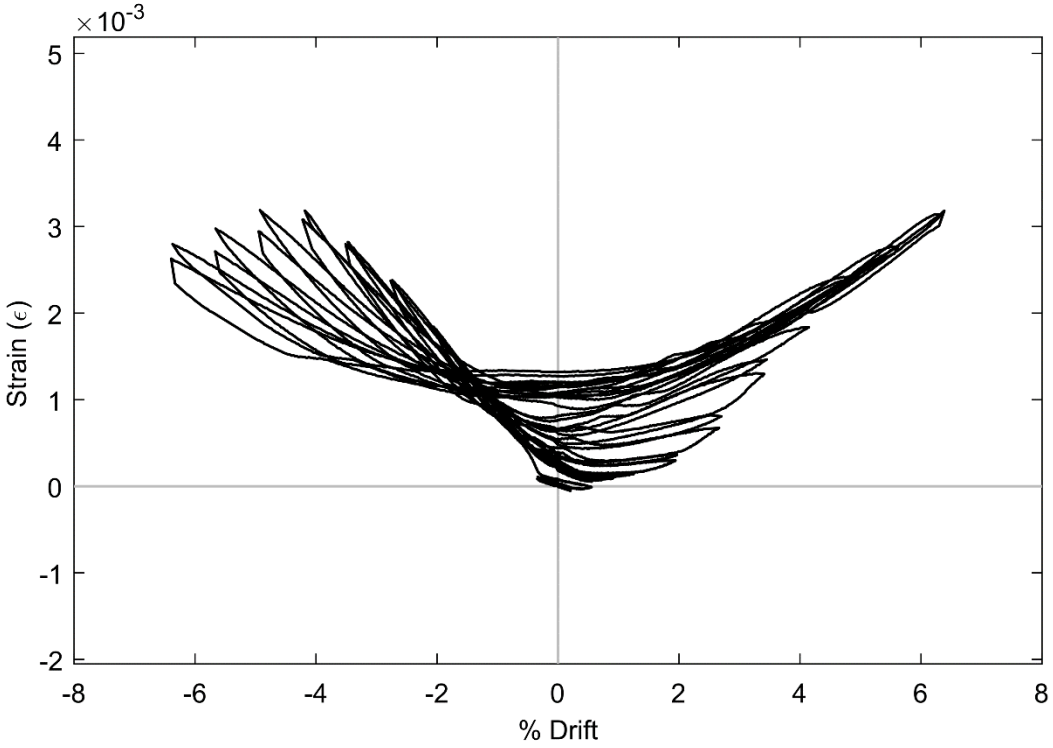

Figure 11: SG STL6 (SR_4_10_5)

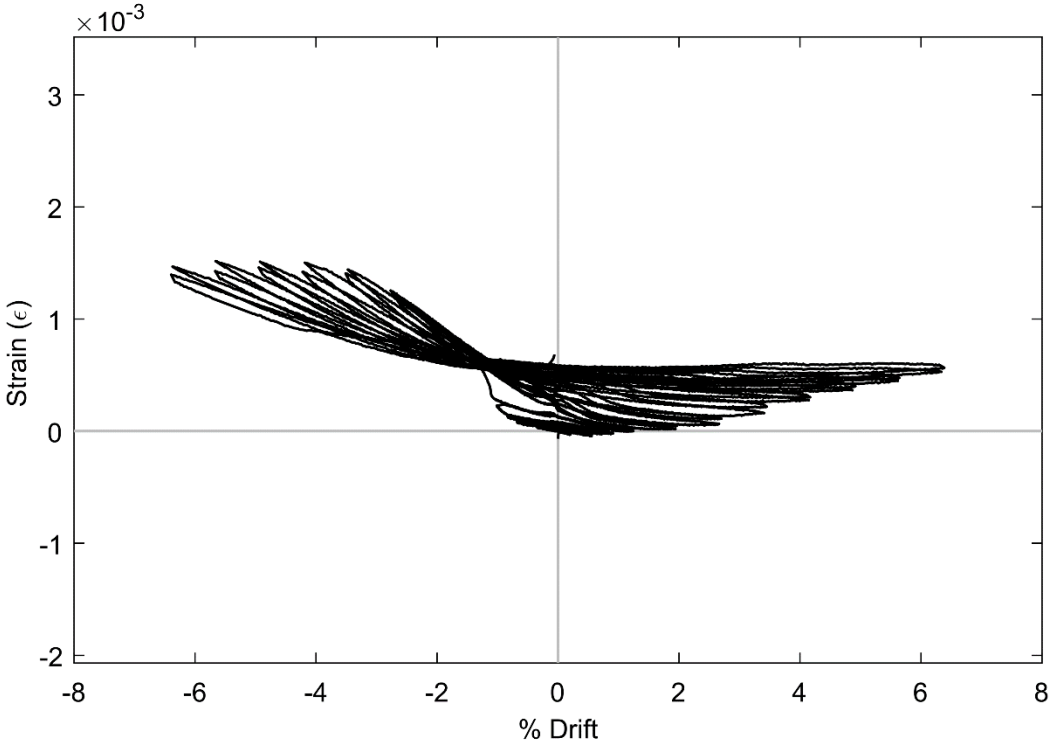

Figure 12: SG STN6 (SR_4_10_5)

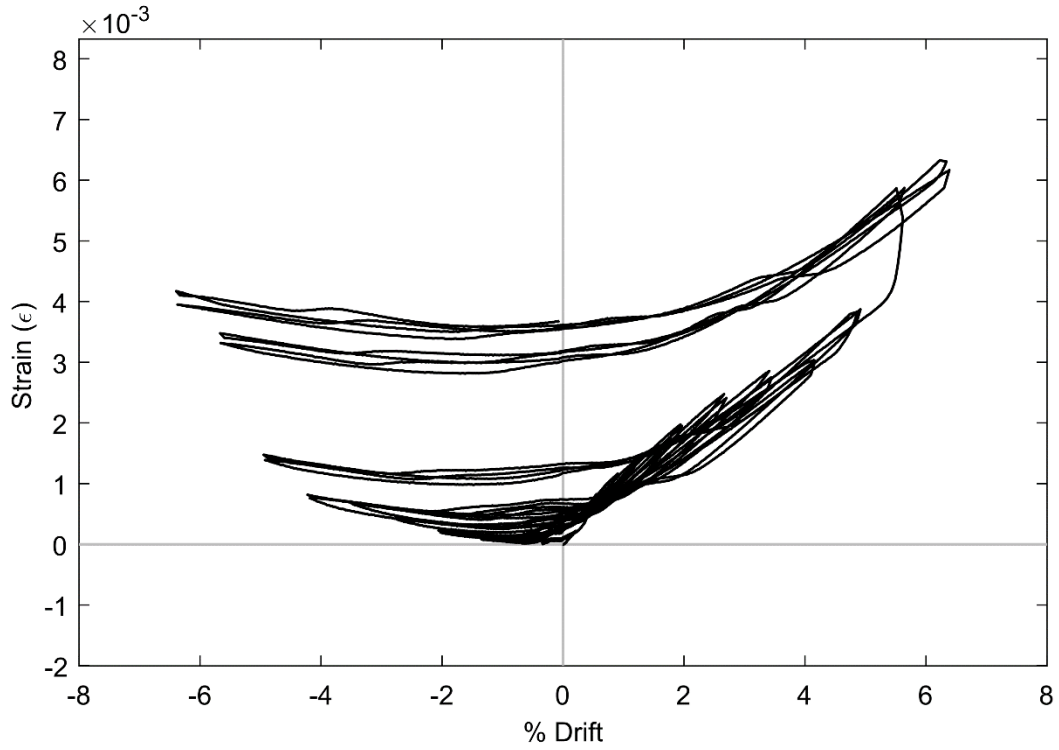

Figure 13: SG STG7 (SR_4_10_5)

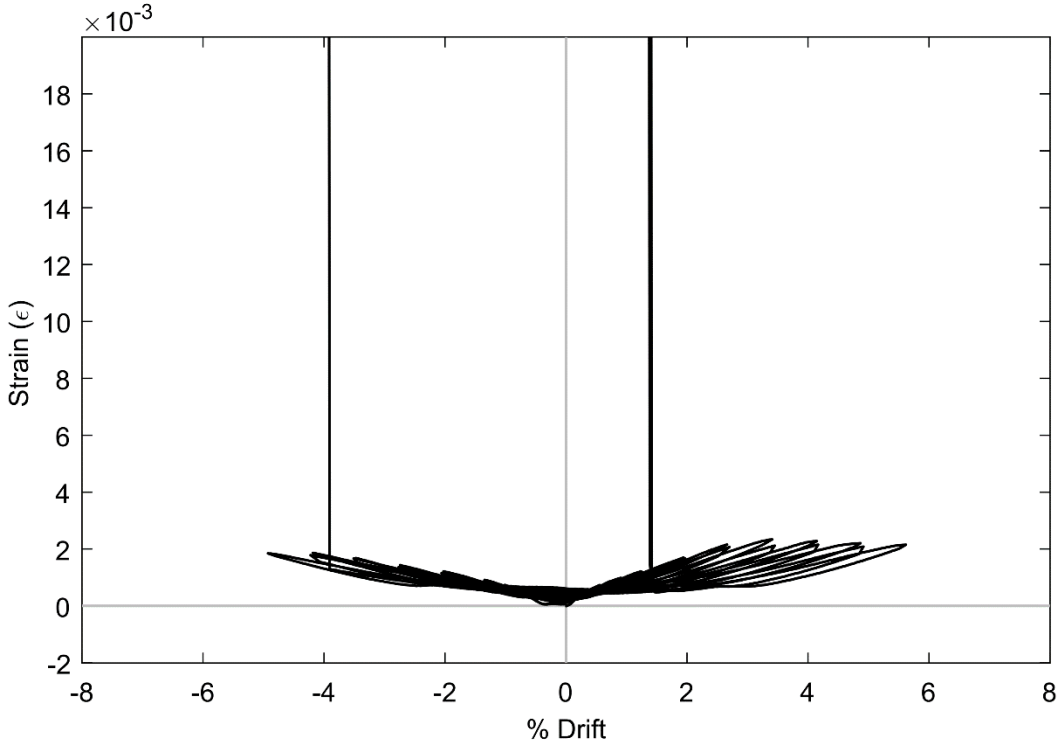

Figure 14: SG STI7 (SR_4_10_5)

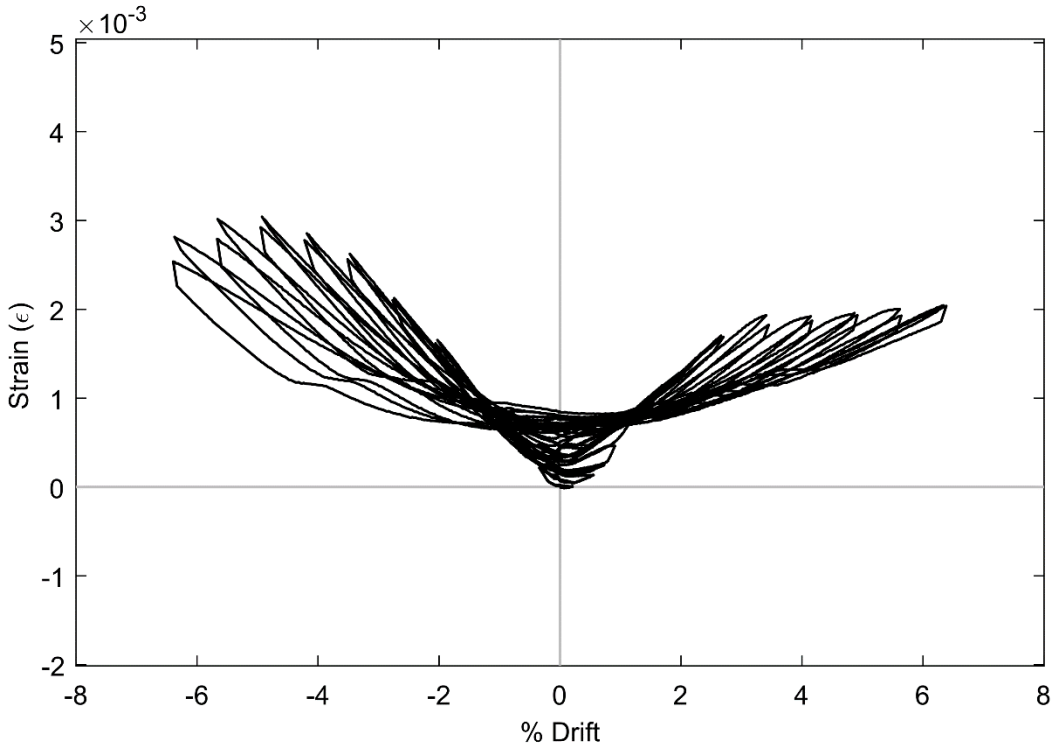

Figure 15: SG STJ7 (SR_4_10_5)

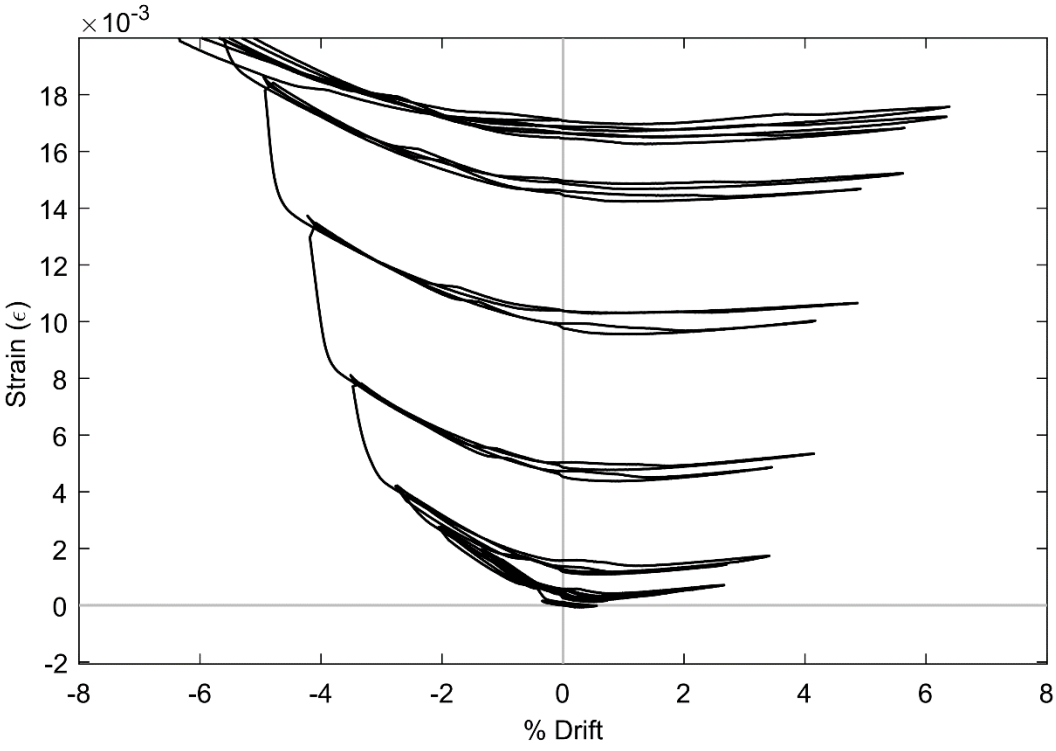

Figure 16: SG STL7 (SR_4_10_5)

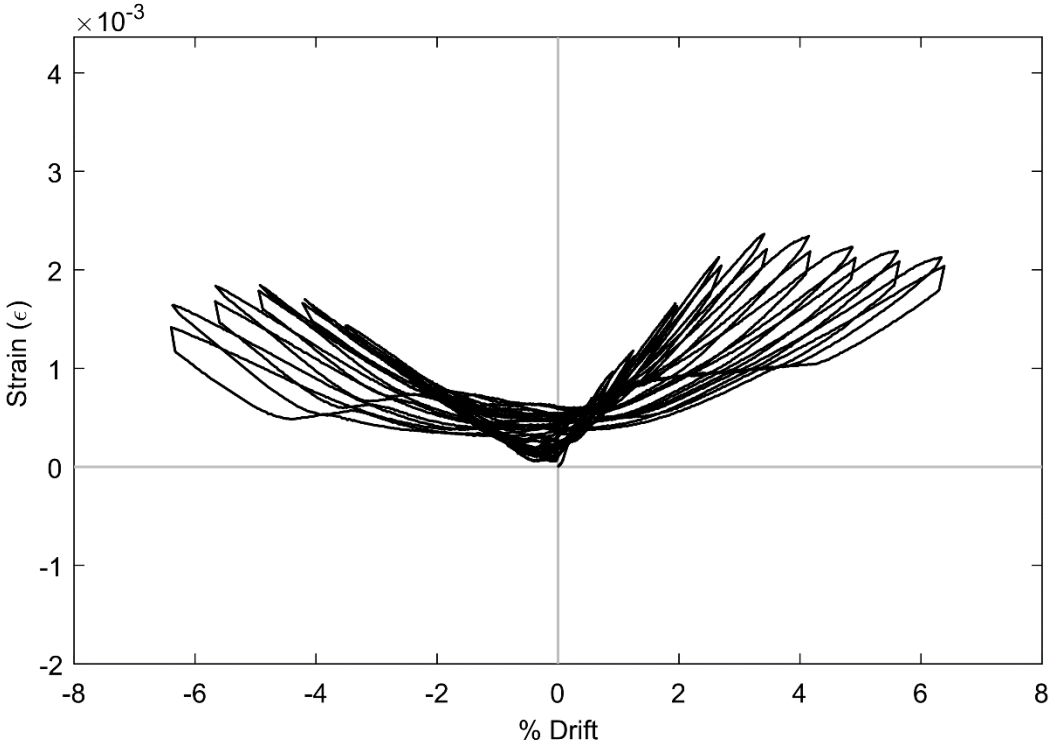

Figure 17: SG STI8 (SR_4_10_5)

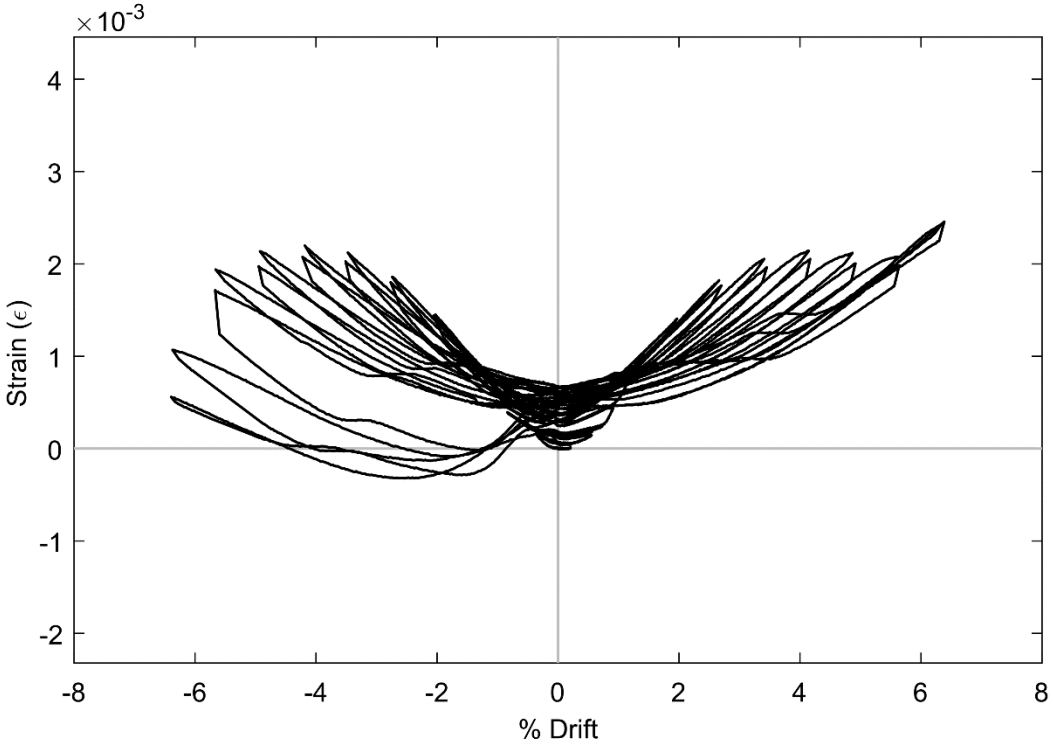

Figure 18: SG STJ8 (SR_4_10_5)

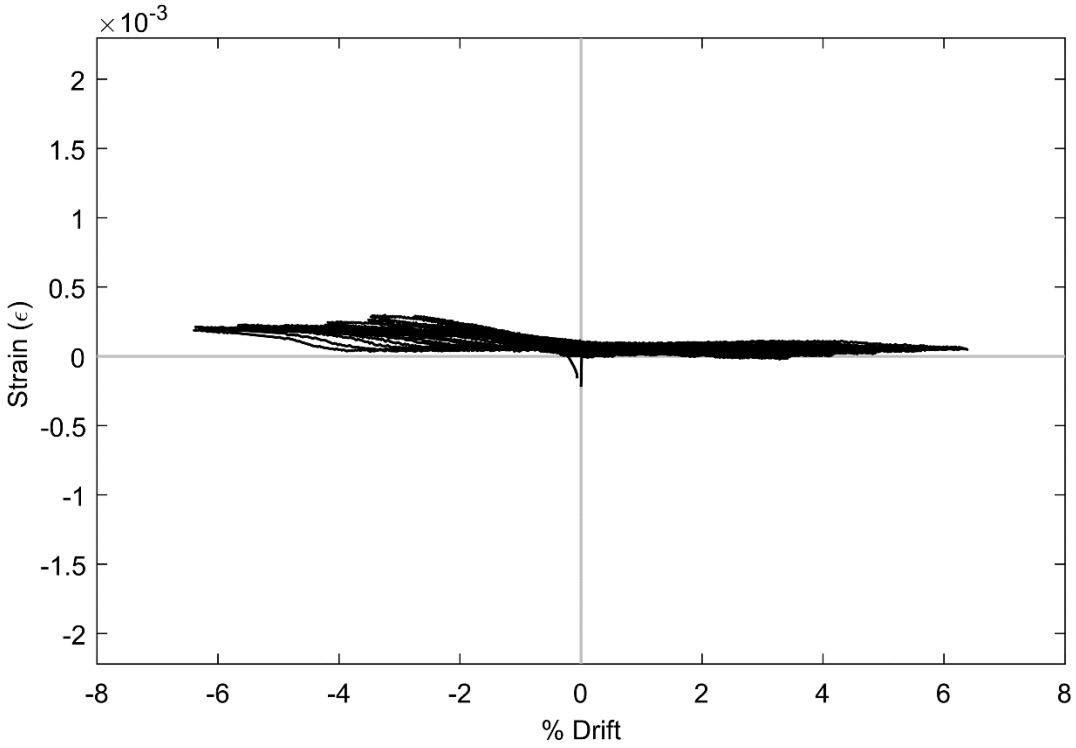

Figure 19: SG SBC5 (SR_4_10_5)

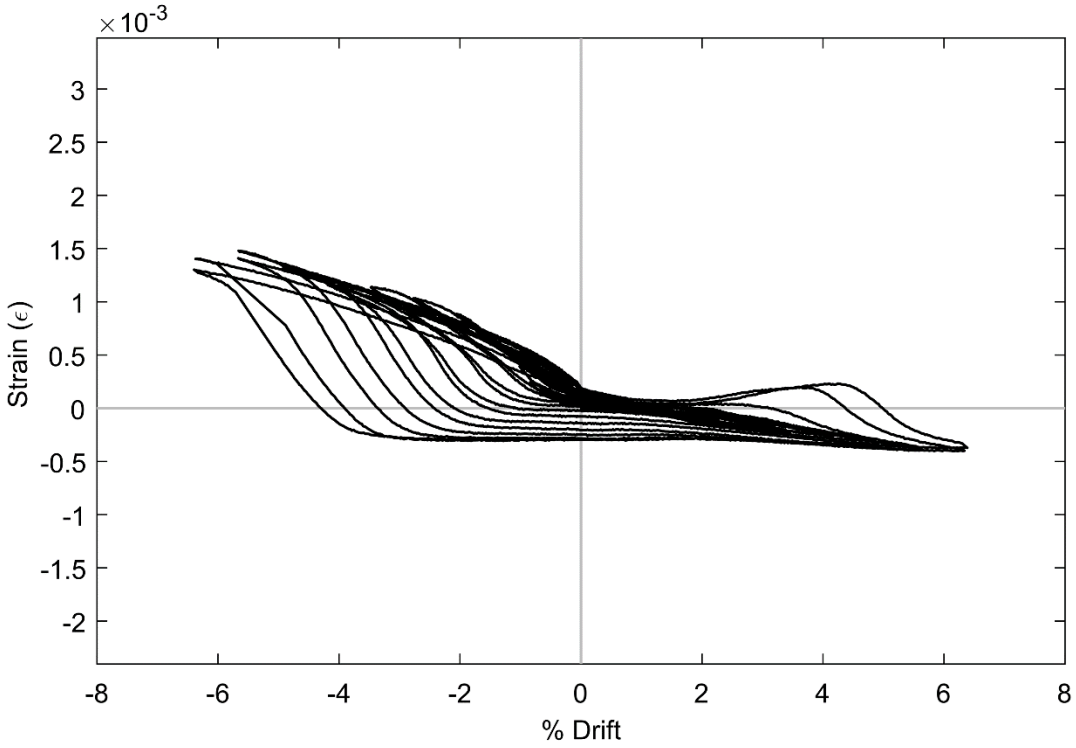

Figure 20: SG SBE5 (SR_4_10_5)

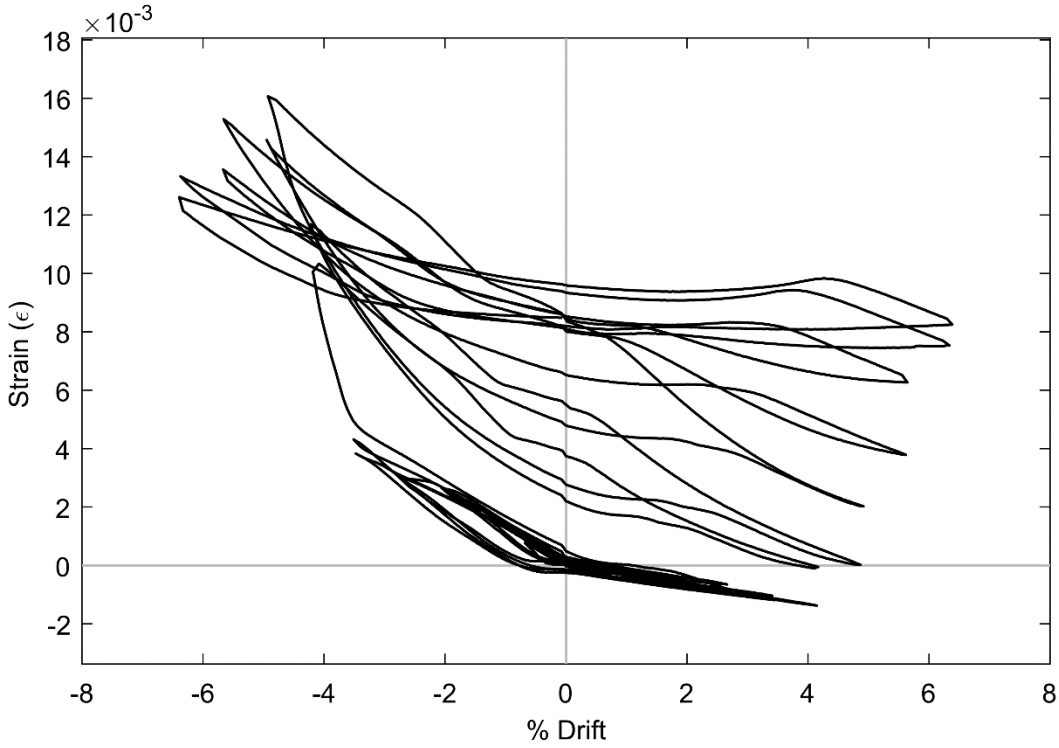

Figure 21: SG SBG5 (SR_4_10_5)

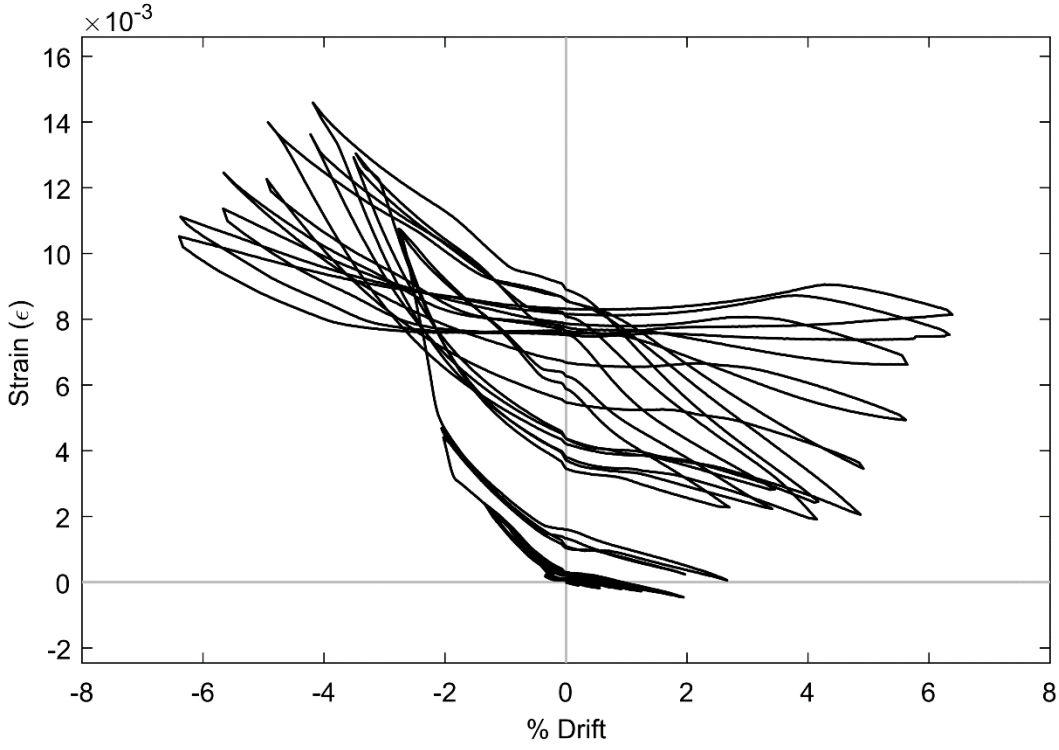

Figure 22: SG SBH5 (SR_4_10_5)

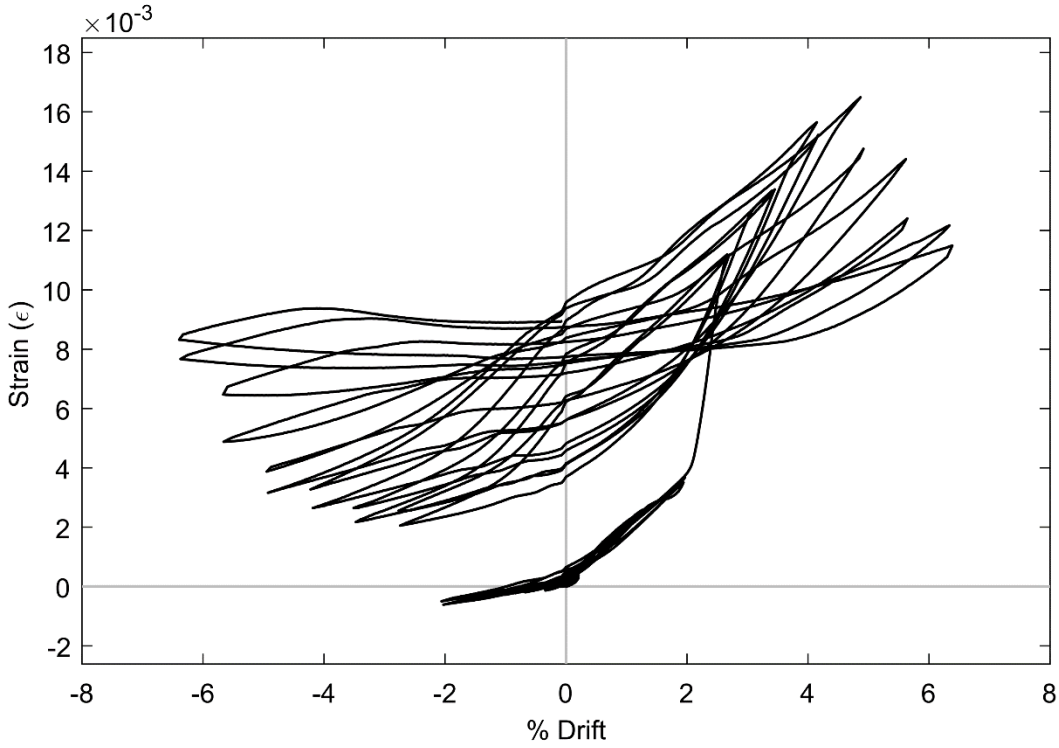

Figure 23: SG SBK5 (SR_4_10_5)

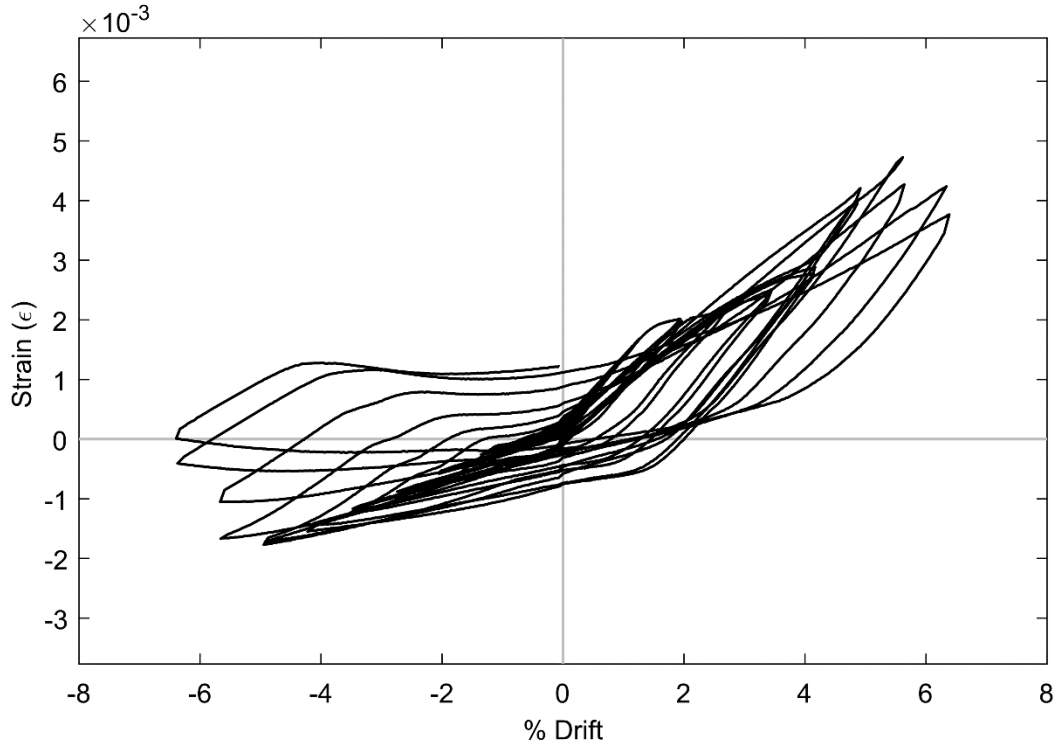

Figure 24: SG SBL5 (SR_4_10_5)

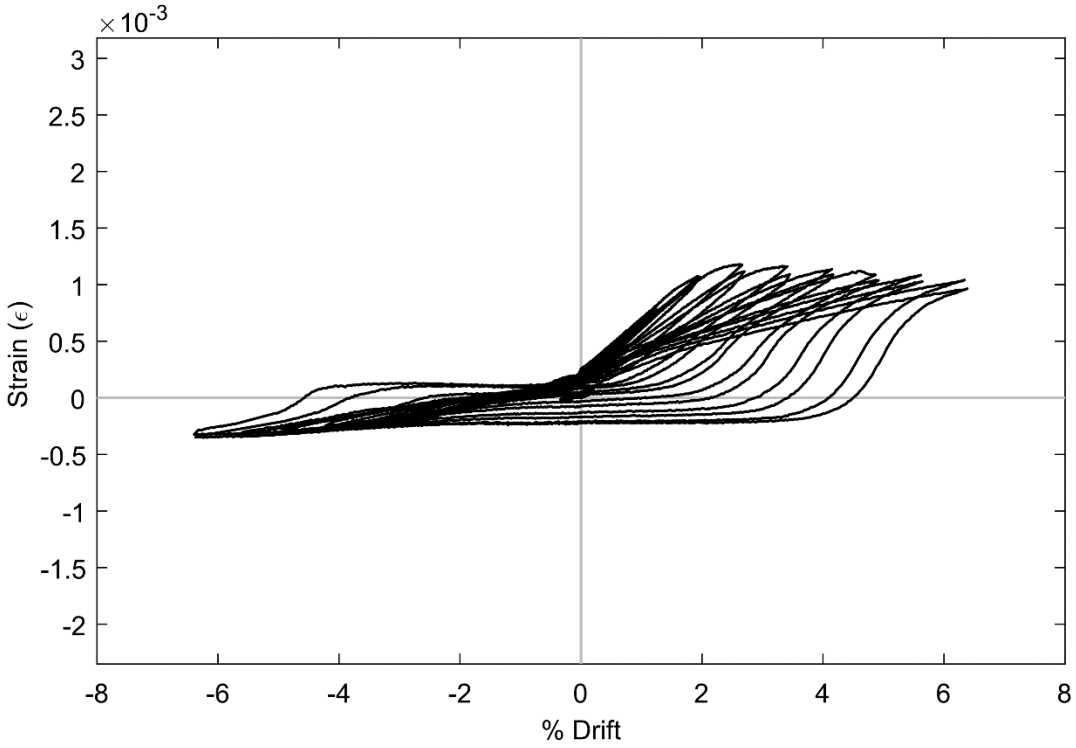

Figure 25: SG SBN5 (SR_4_10_5)

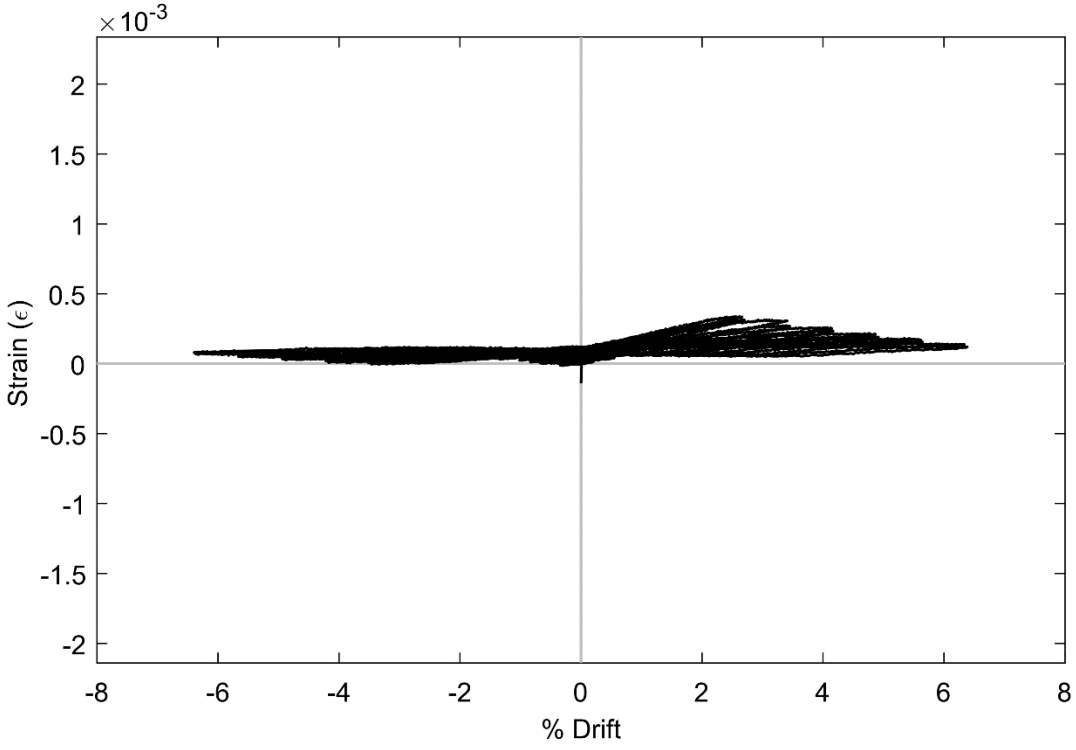

Figure 26: SG SBP5 (SR_4_10_5)

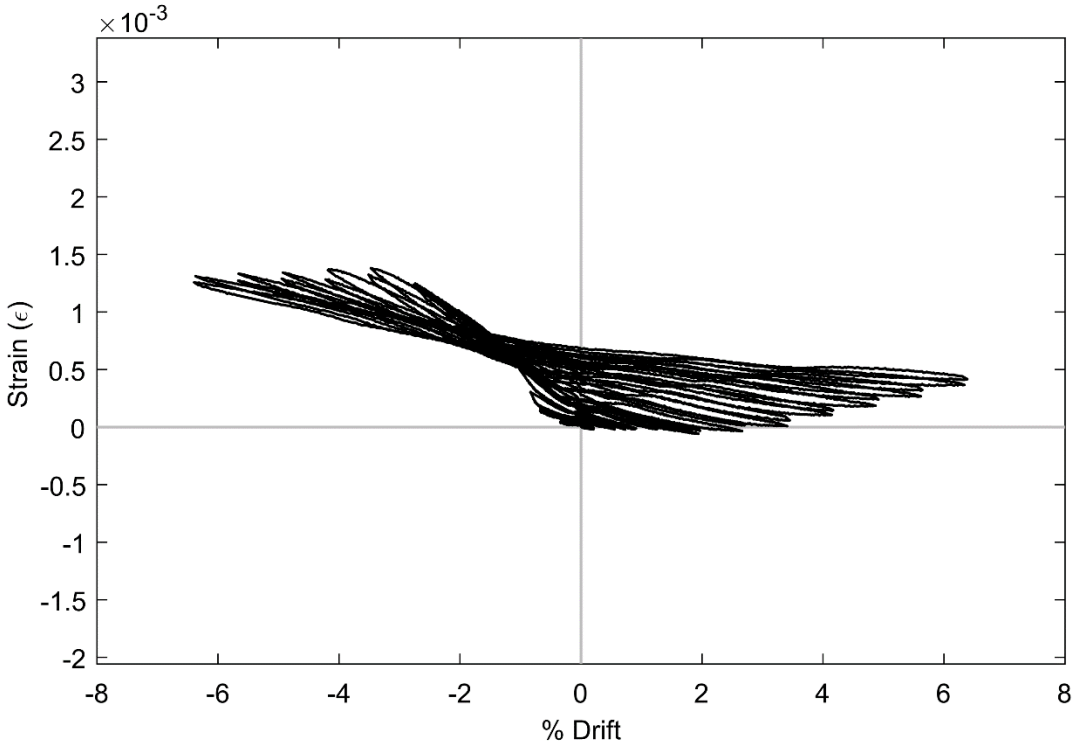

Figure 27: SG SBE6 (SR_4_10_5)

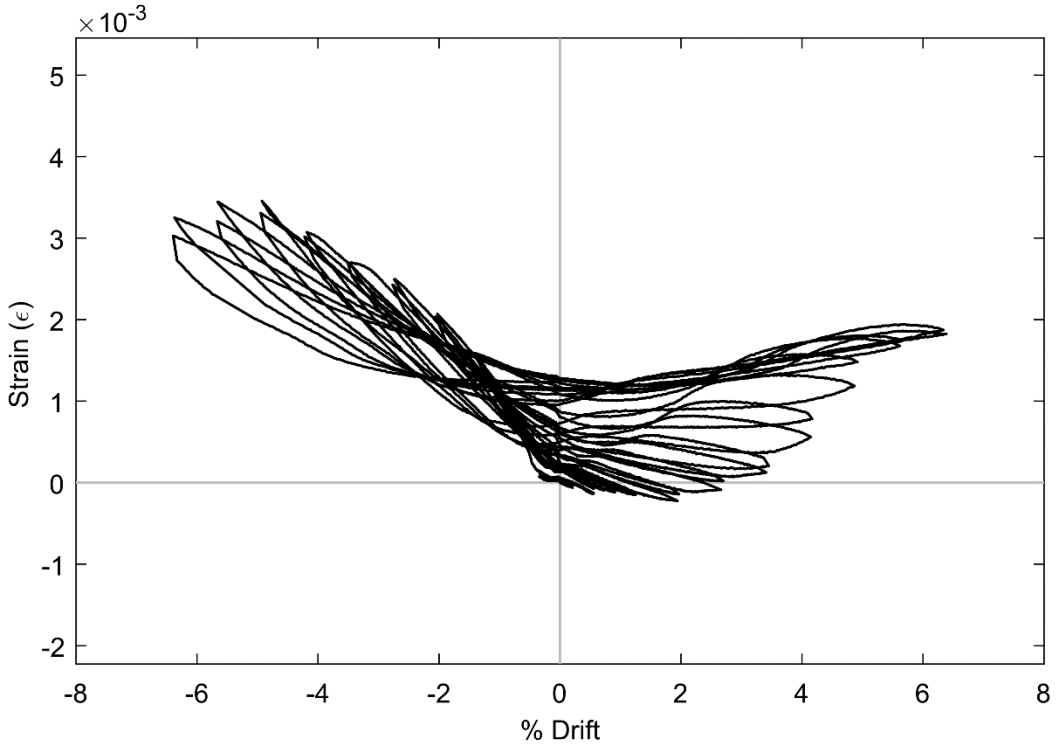

Figure 28: SG SBG6 (SR_4_10_5)

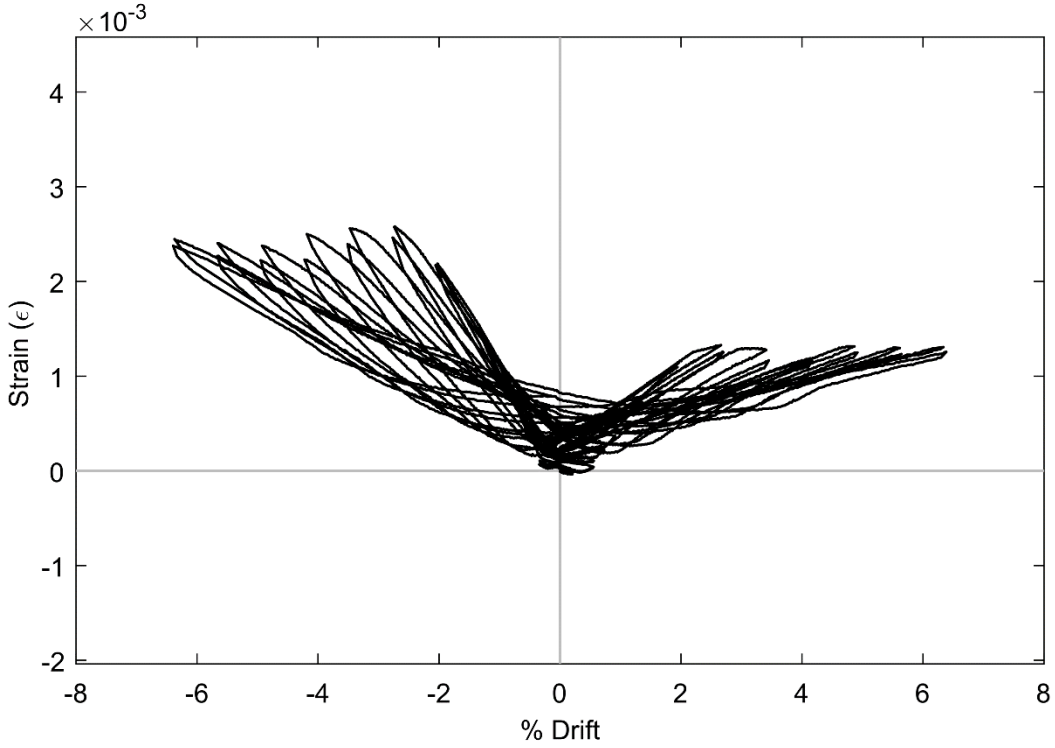

Figure 29: SG SBI6 (SR_4_10_5)

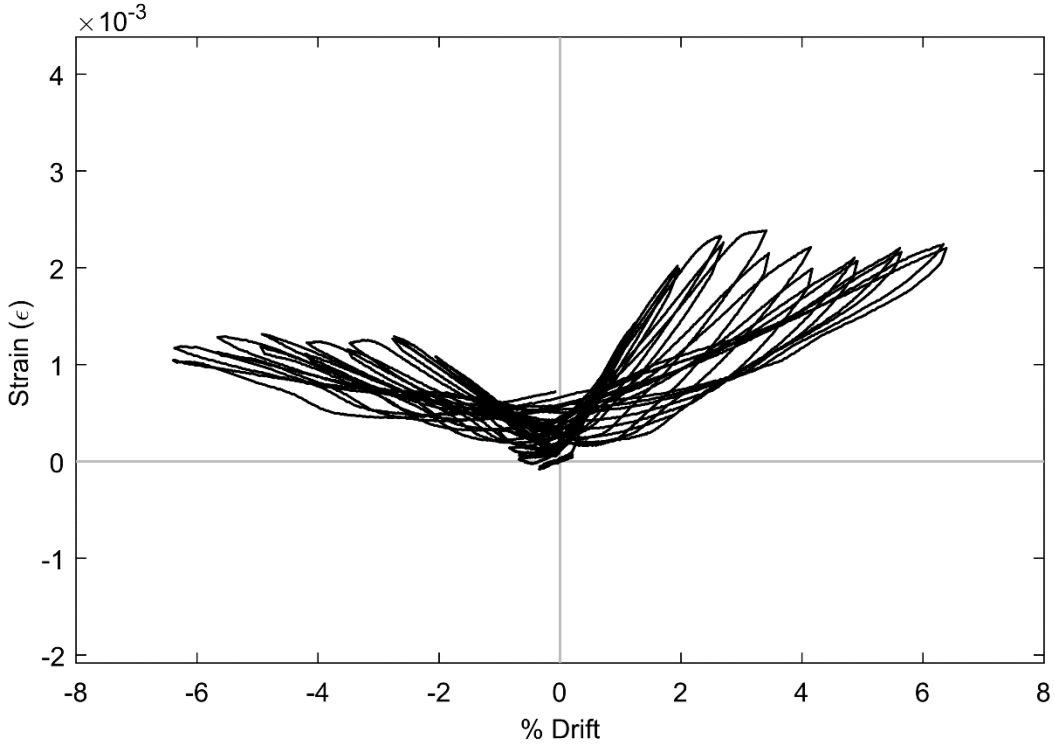

Figure 30: SG SBJ6 (SR_4_10_5)

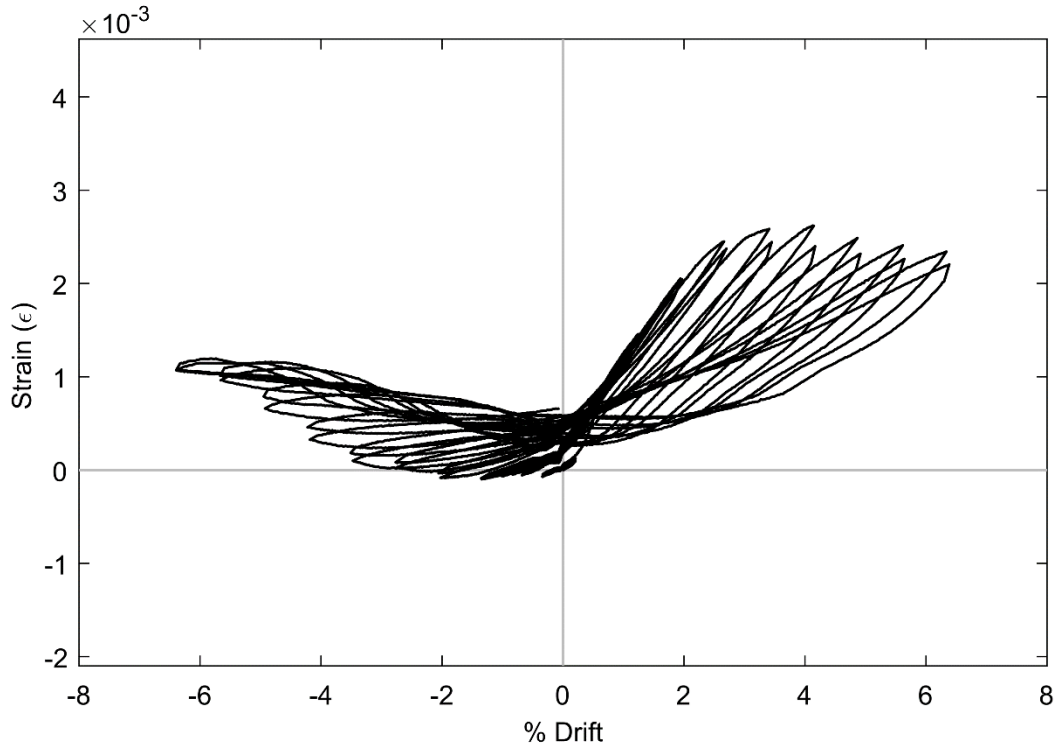

Figure 31: SG SBL6 (SR_4_10_5)

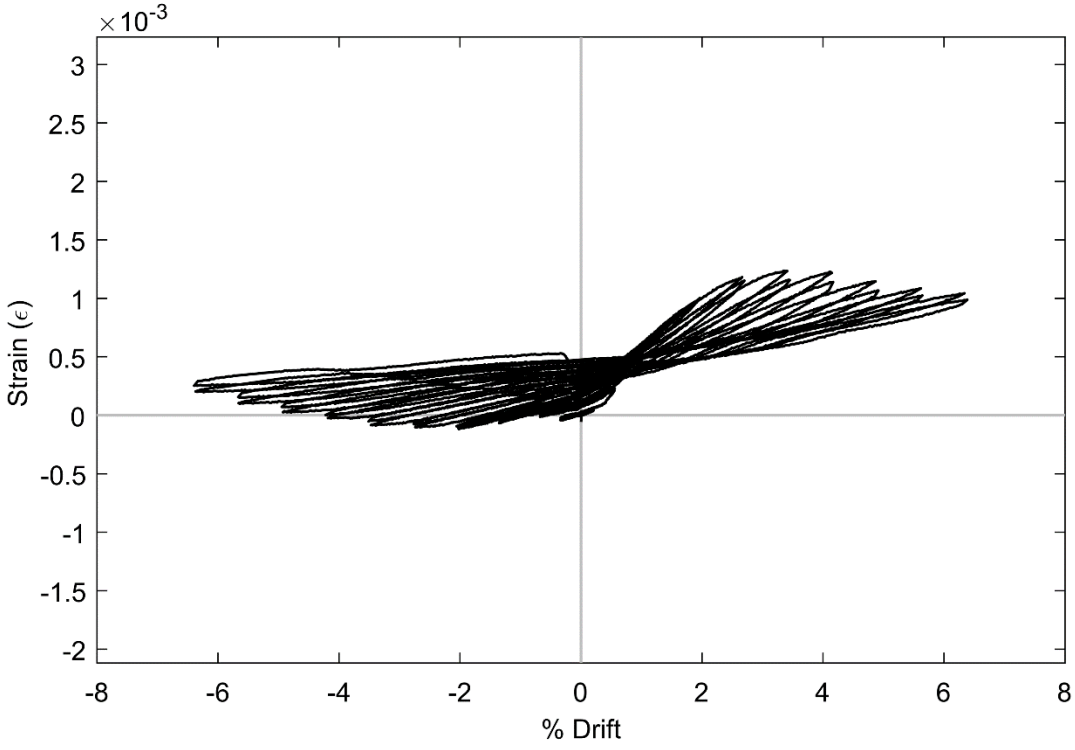

Figure 32: SG SBN6 (SR_4_10_5)

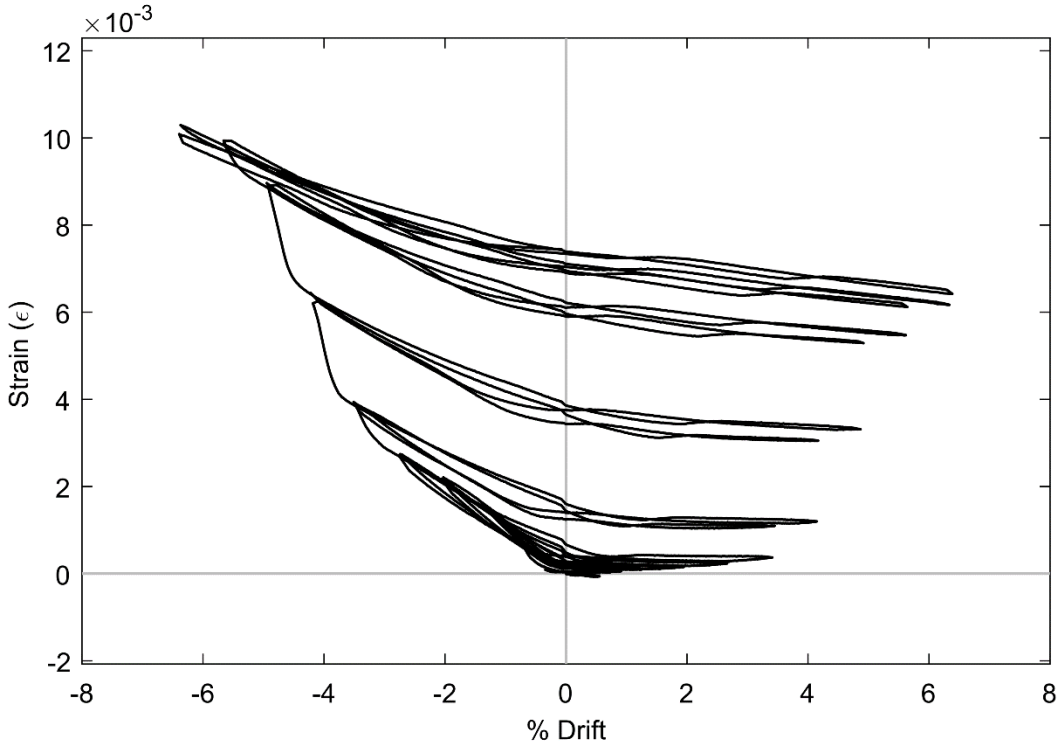

Figure 33: SG SBG7 (SR_4_10_5)

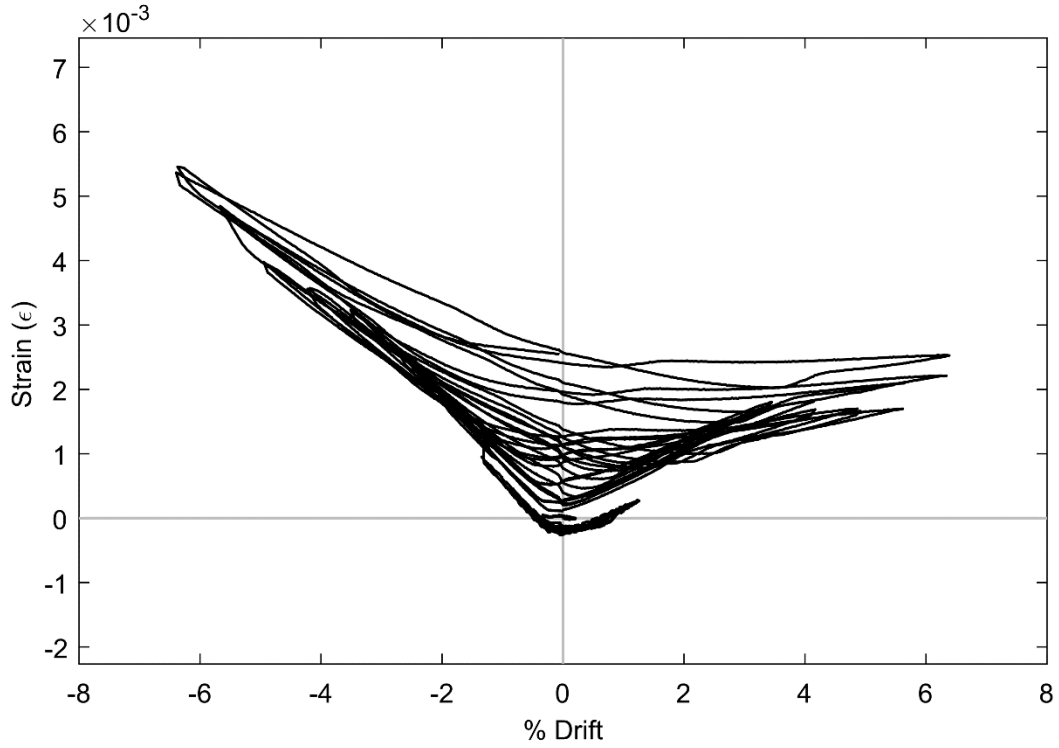

Figure 34: SG SBI7 (SR_4_10_5)

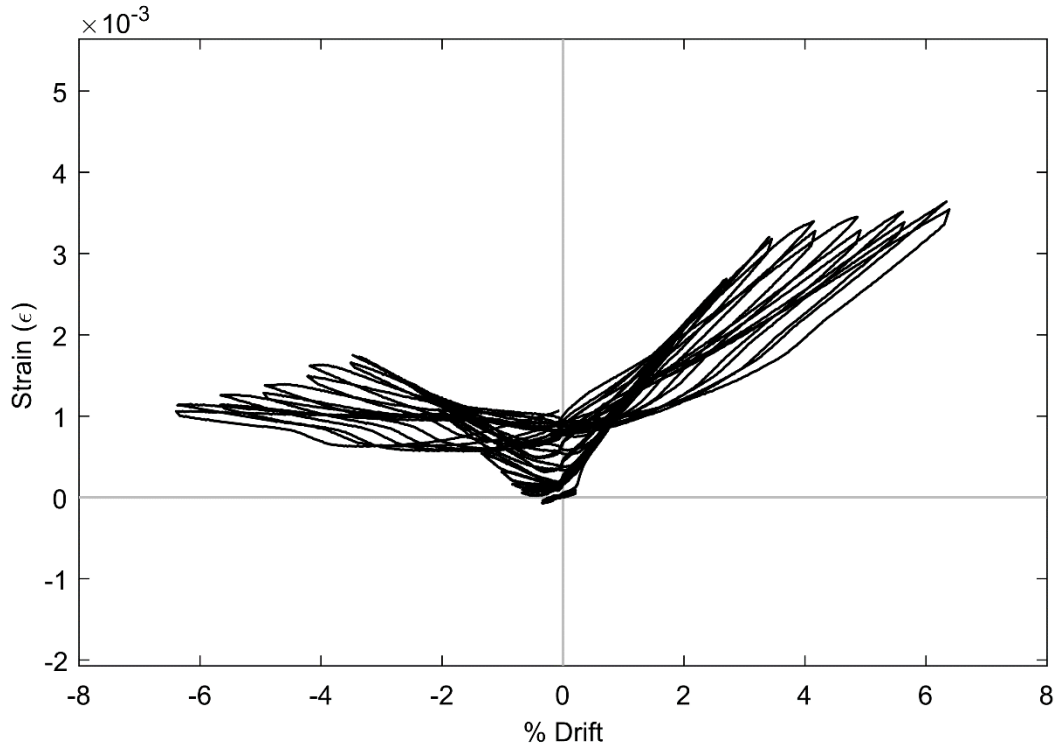

Figure 35: SG SBJ7 (SR_4_10_5)

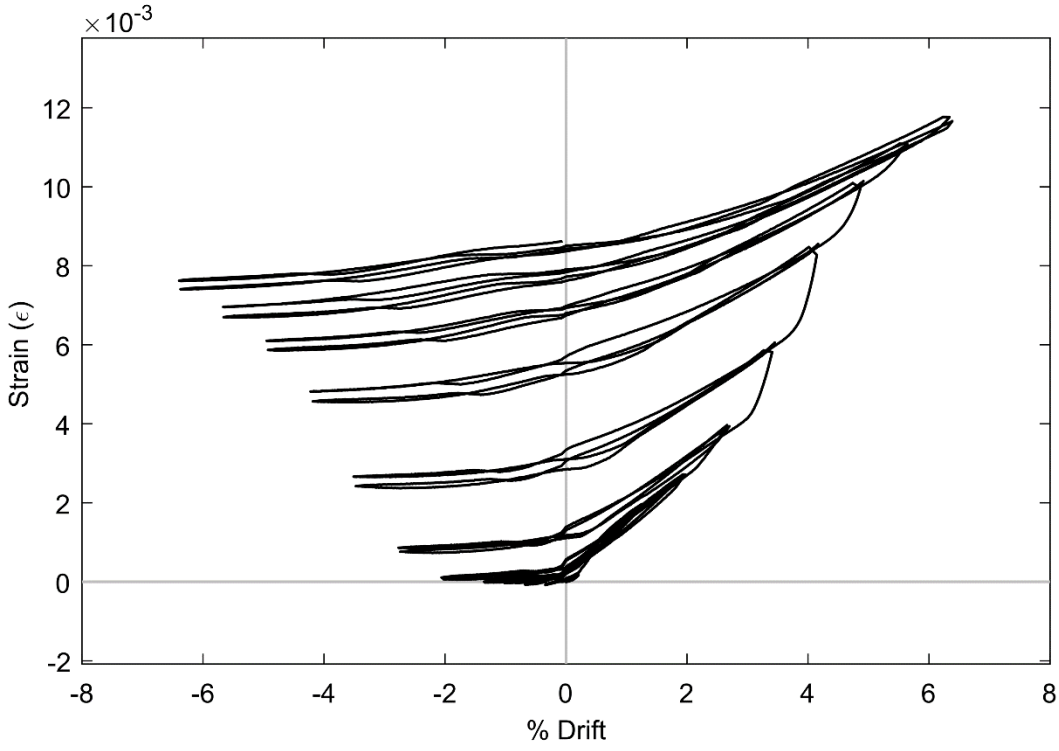

Figure 36: SG SBL7 (SR_4_10_5)

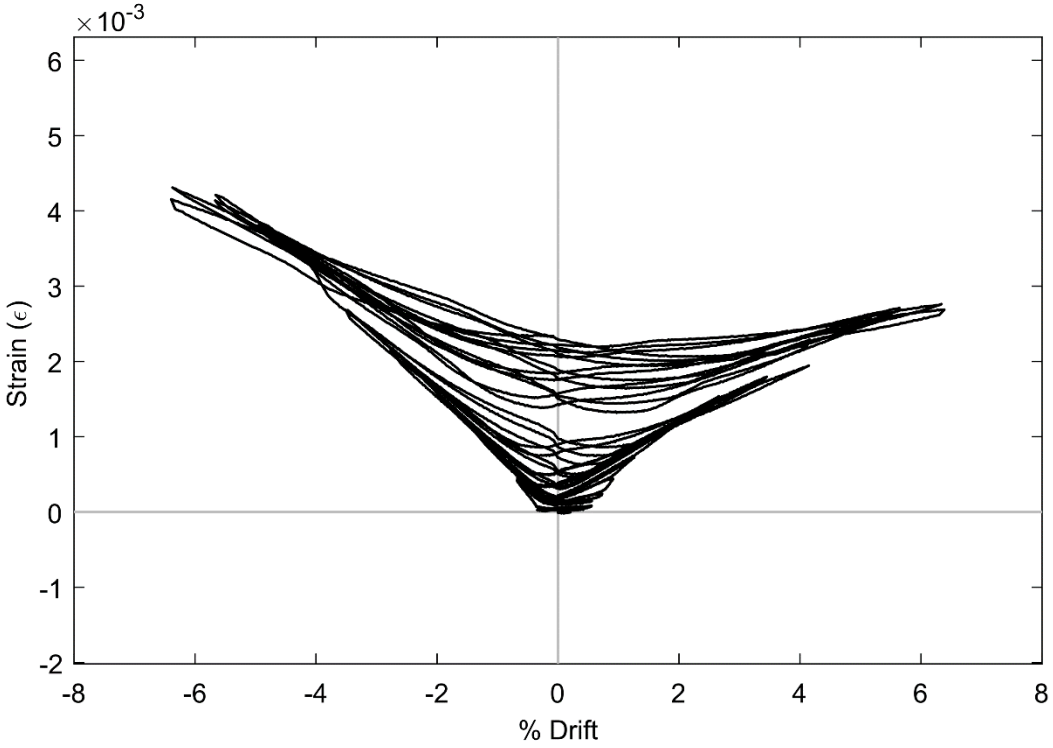

Figure 37: SG SBI8 (SR_4_10_5)

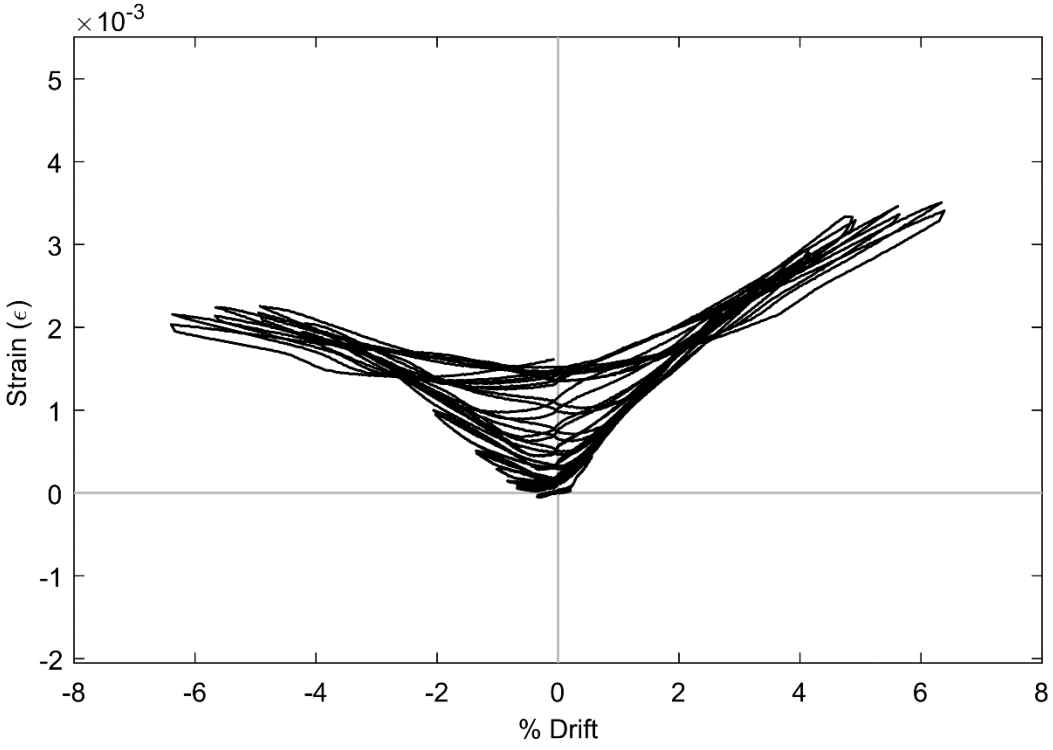

Figure 38: SG SBJ8 (SR_4_10_5)

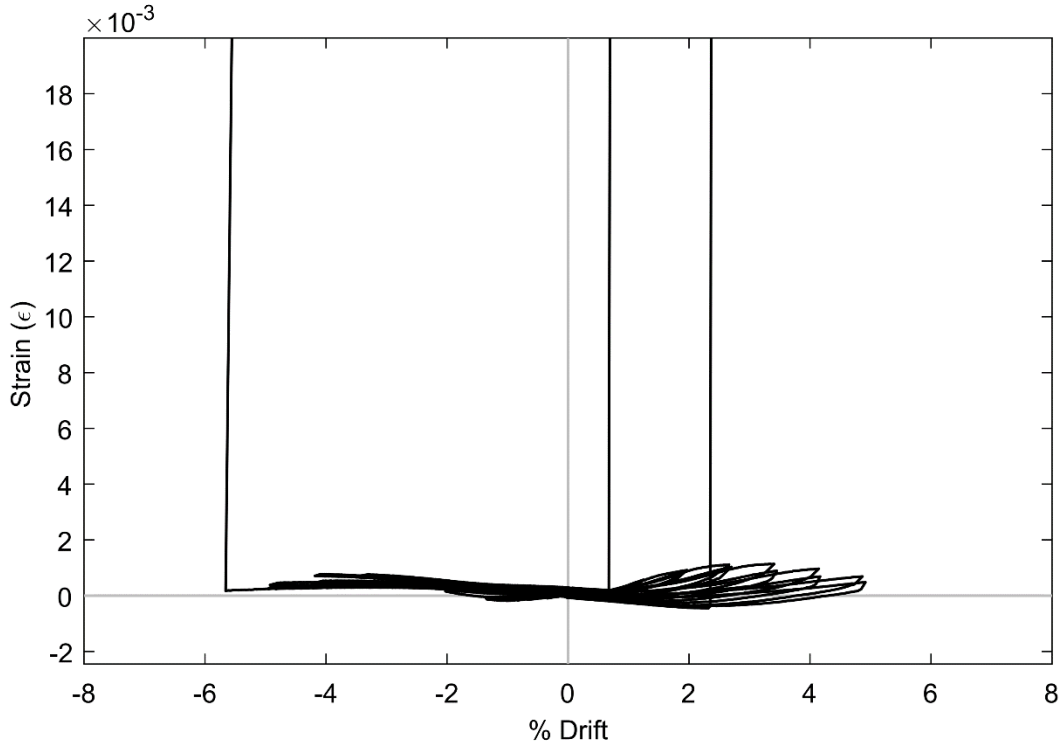

Figure 39: SG CC1 (SR_4_10_5)

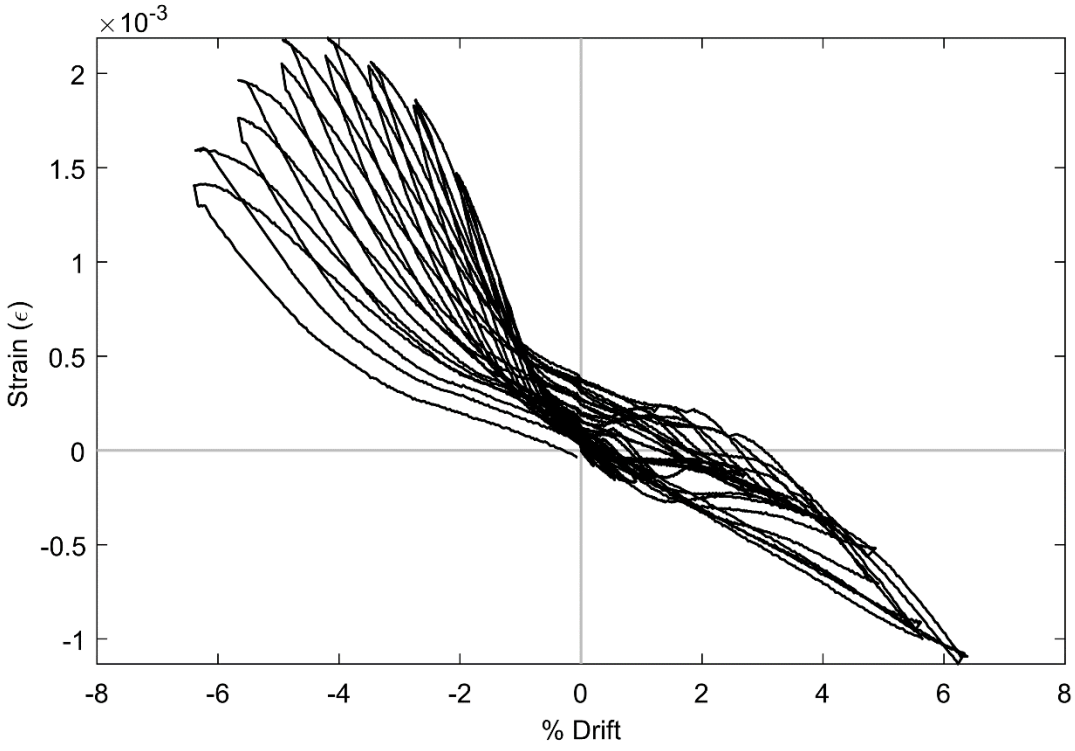

Figure 40: SG CC2 (SR_4_10_5)

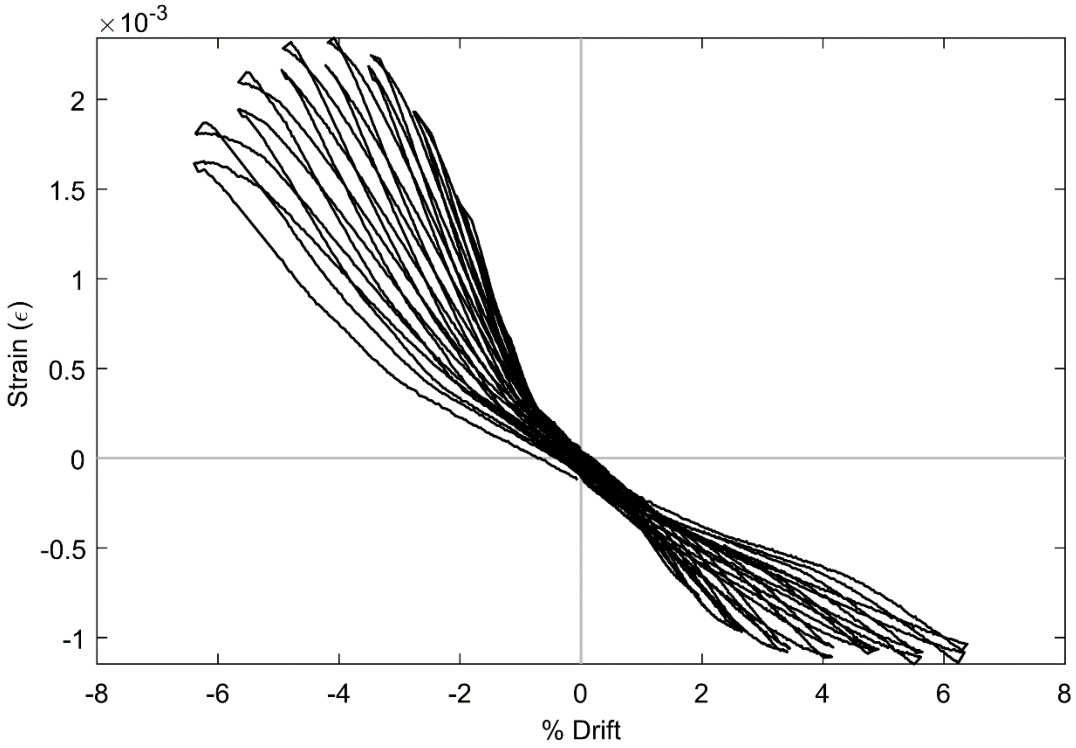

Figure 41: SG CC3 (SR_4_10_5)

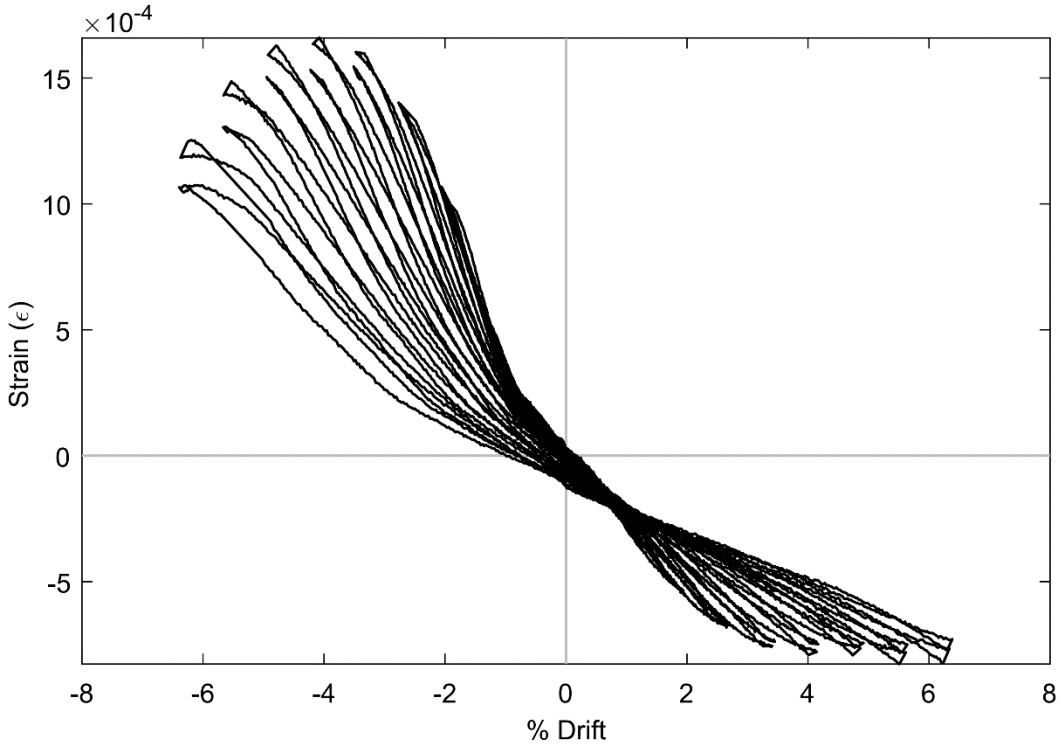

Figure 42: SG CC4 (SR_4_10_5)

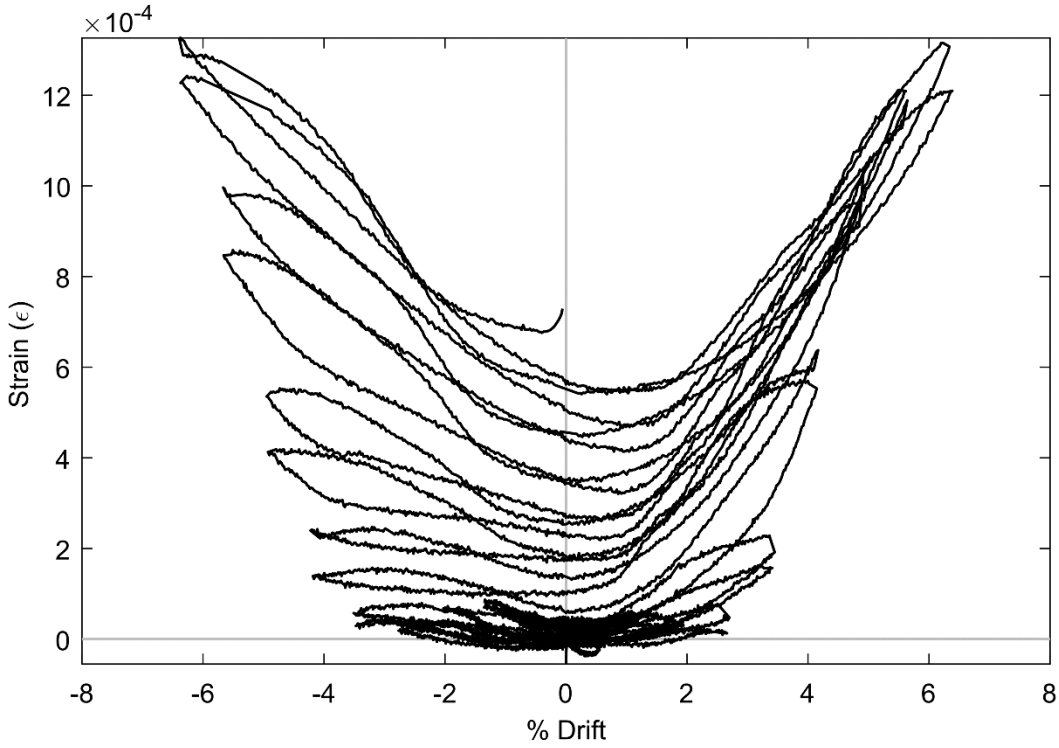

Figure 43: SG RN31 (SR_4_10_5)

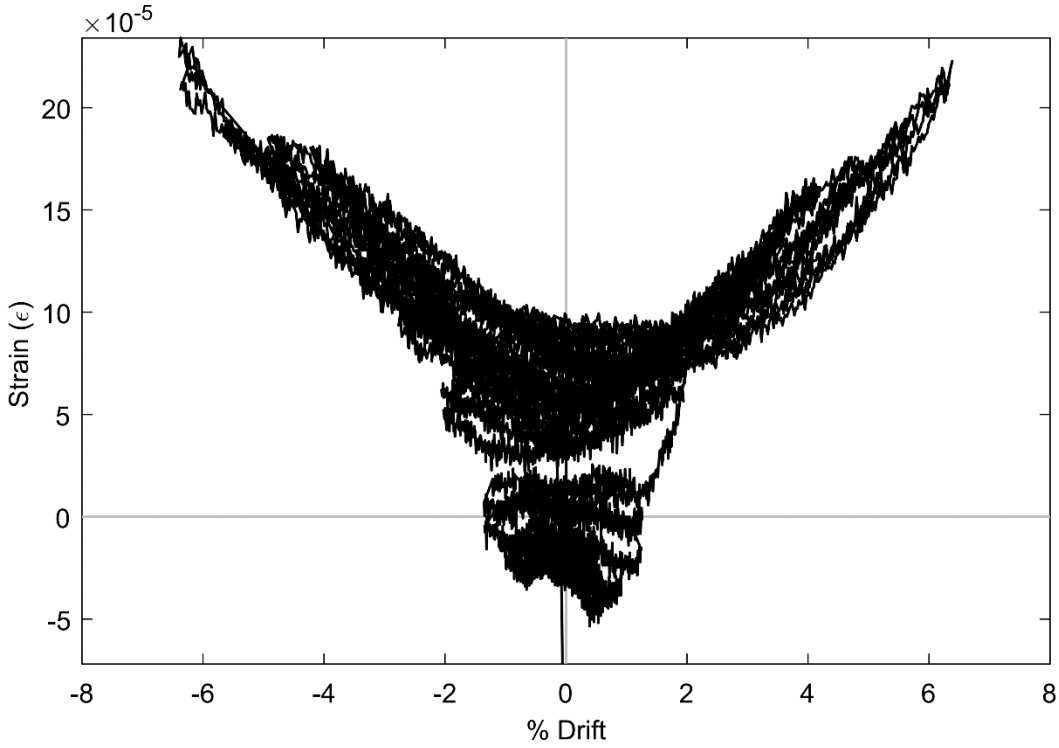

Figure 44: SG RN33 (SR_4_10_5)

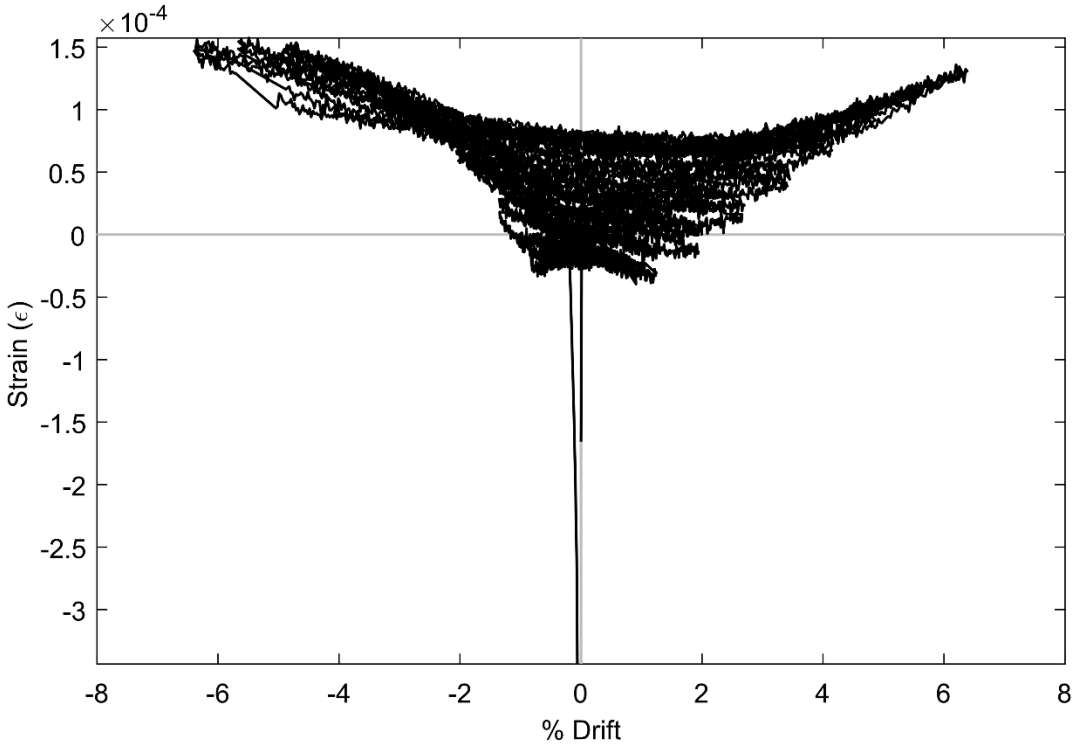

Figure 45: SG RN35 (SR_4_10_5)

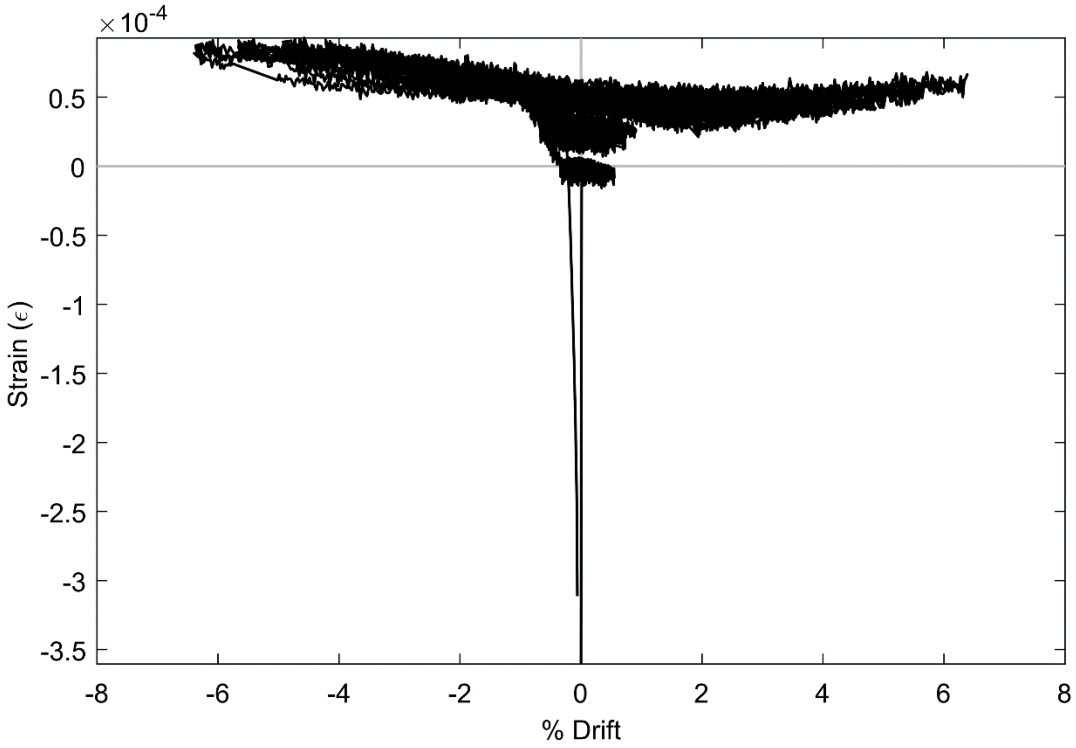

Figure 46: SG RN37 (SR_4_10_5)

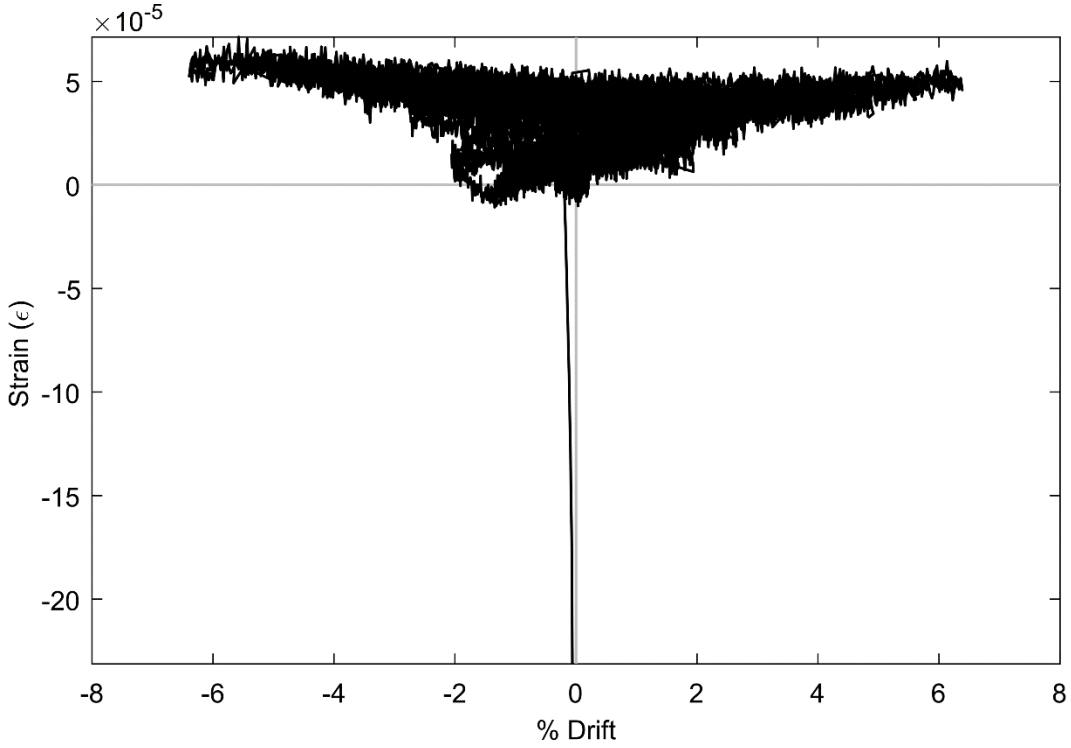

Figure 47: SG RN39 (SR_4_10_5)

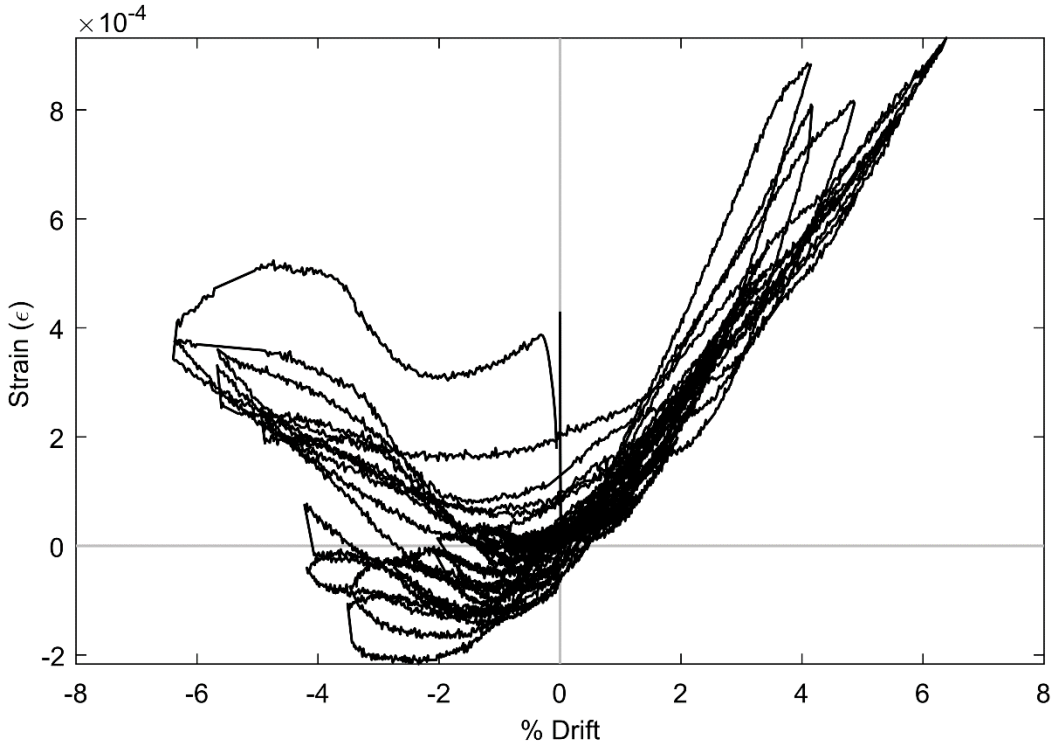

Figure 48: SG RN41 (SR_4_10_5)

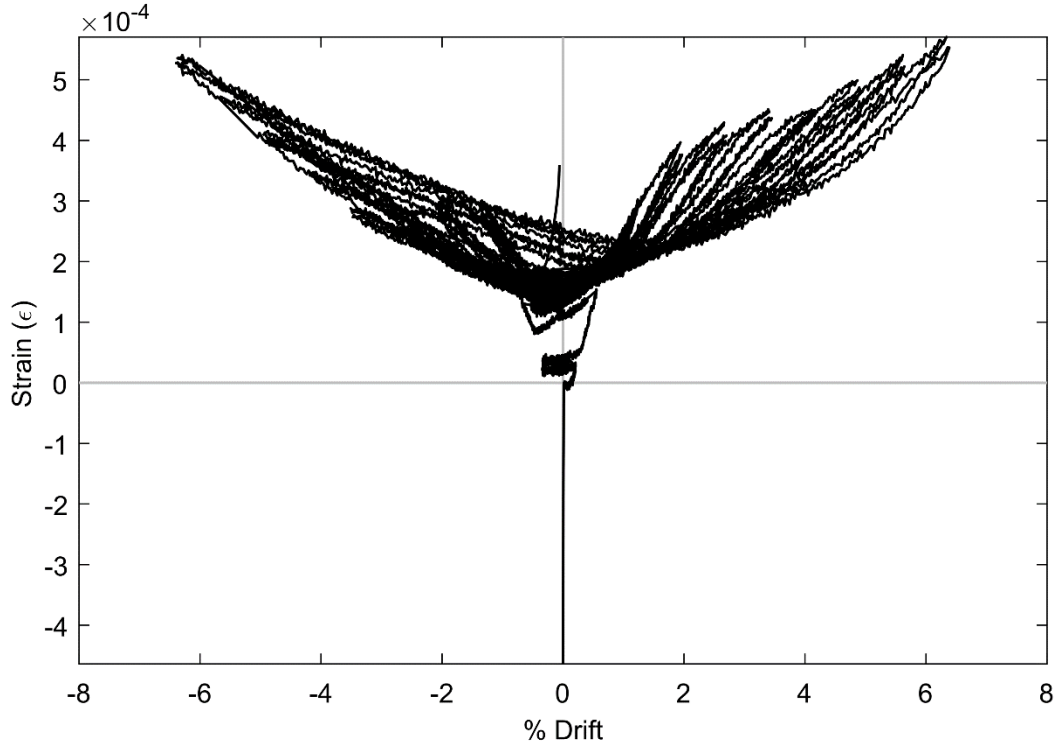

Figure 49: SG RN43 (SR_4_10_5)

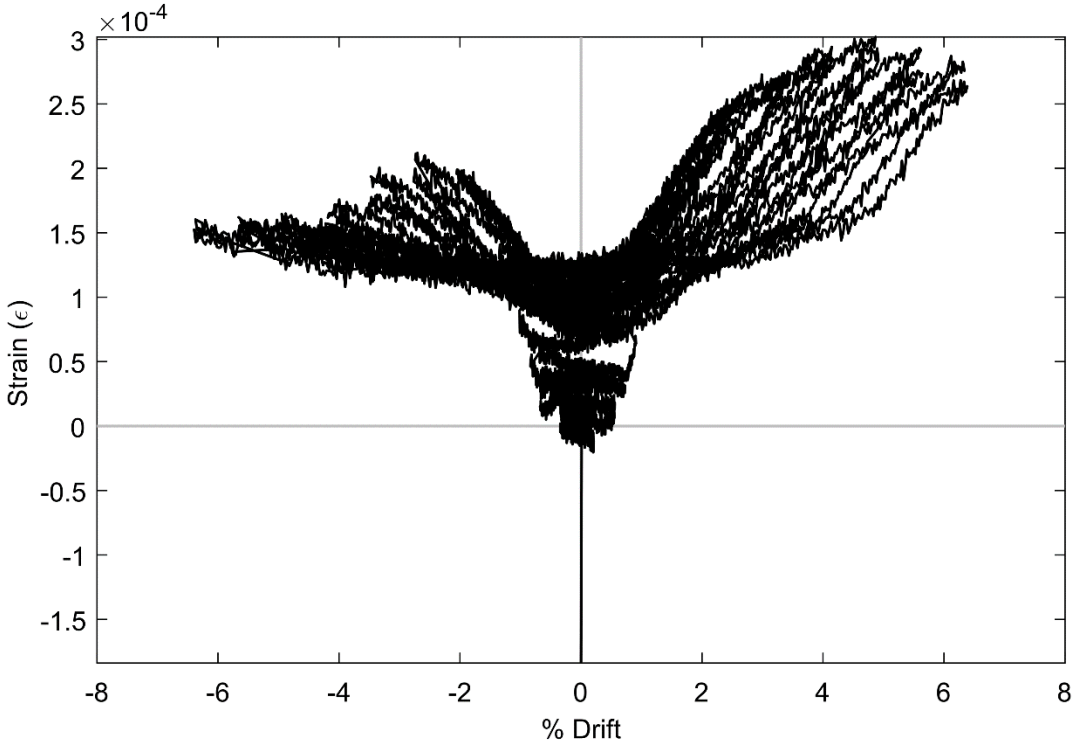

Figure 50: SG RN45 (SR_4_10_5)

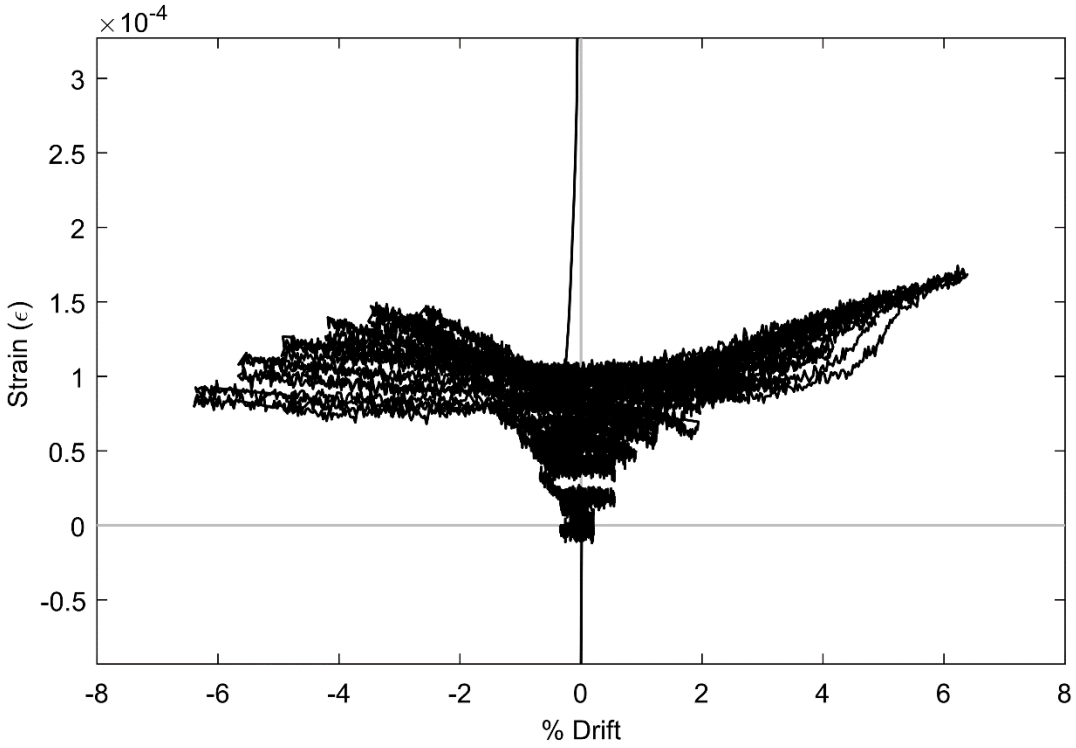

Figure 51: SG RN47 (SR_4_10_5)

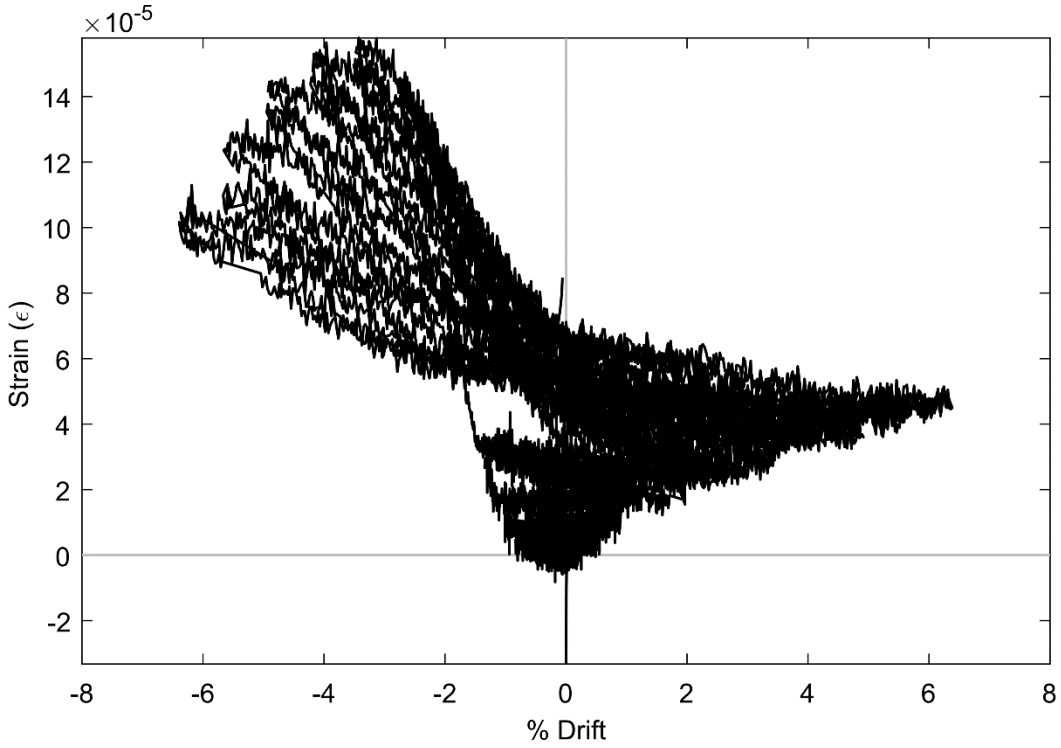

Figure 52: SG RN49 (SR_4_10_5)

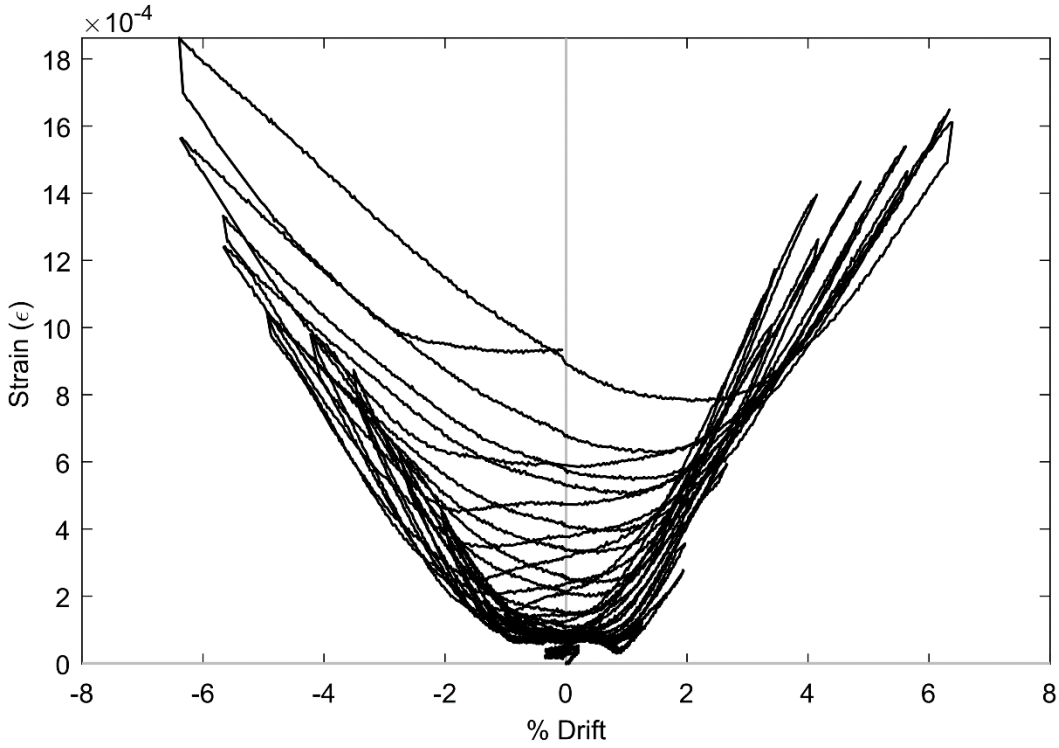

Figure 53: SG RE11 (SR_4_10_5)

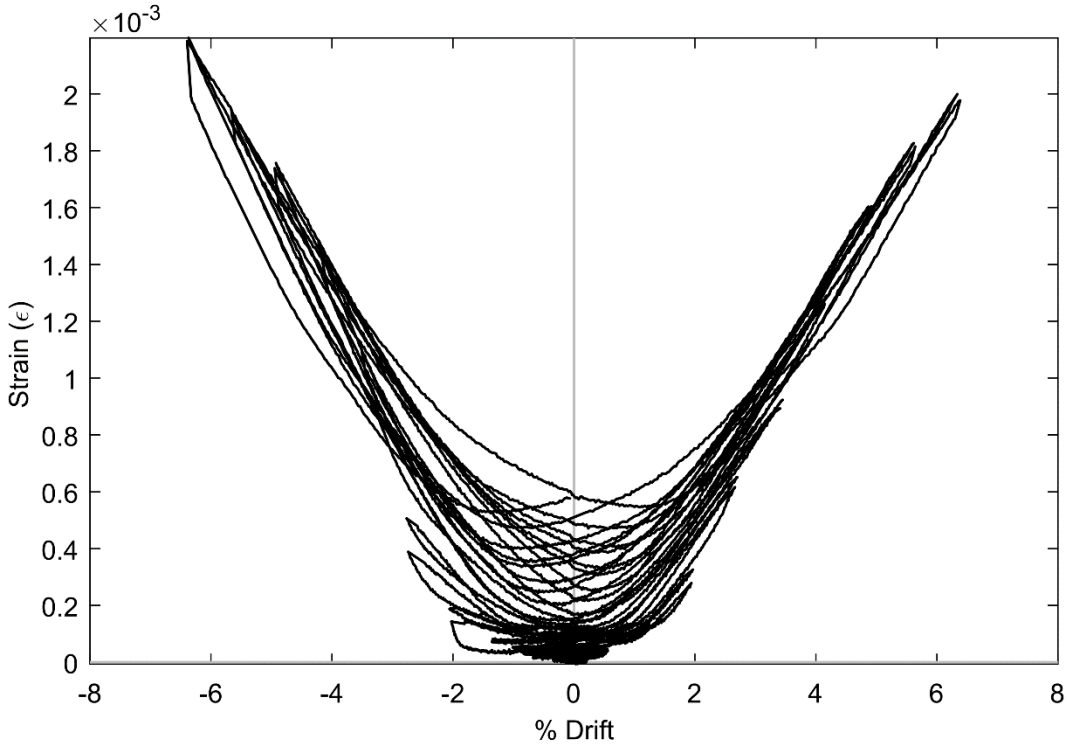

Figure 54: SG RE13 (SR_4_10_5)

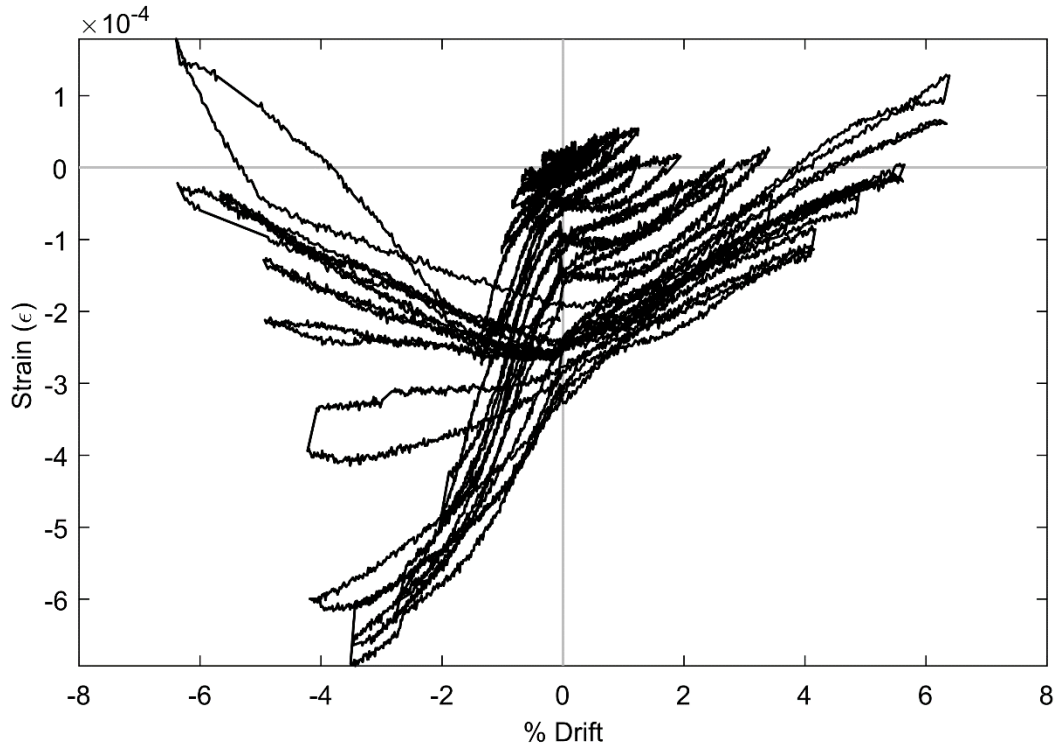

Figure 55: SG RE15 (SR_4_10_5)

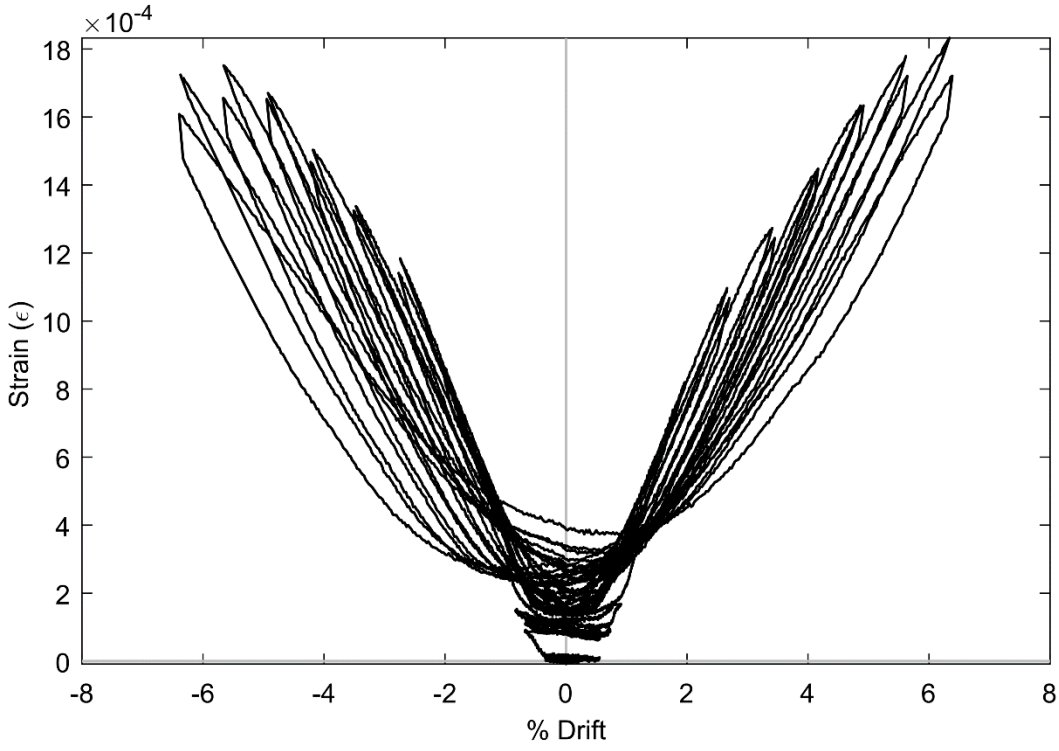

Figure 56: SG RE23 (SR_4_10_5)

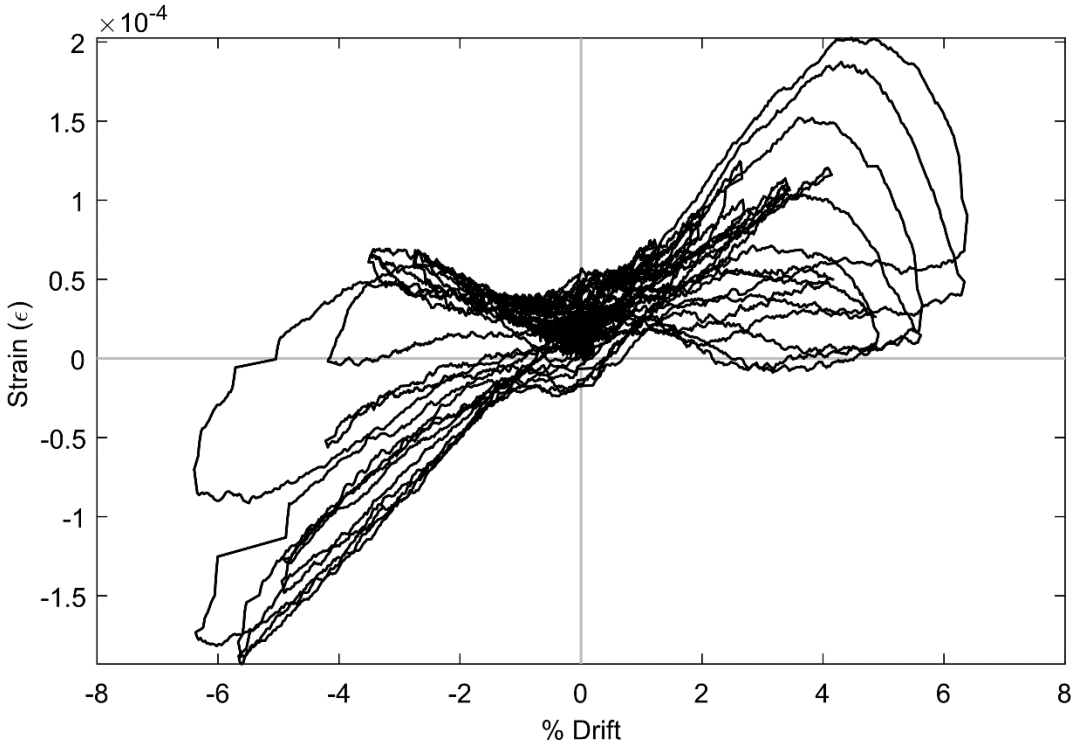

Figure 57: SG RE25 (SR_4_10_5)

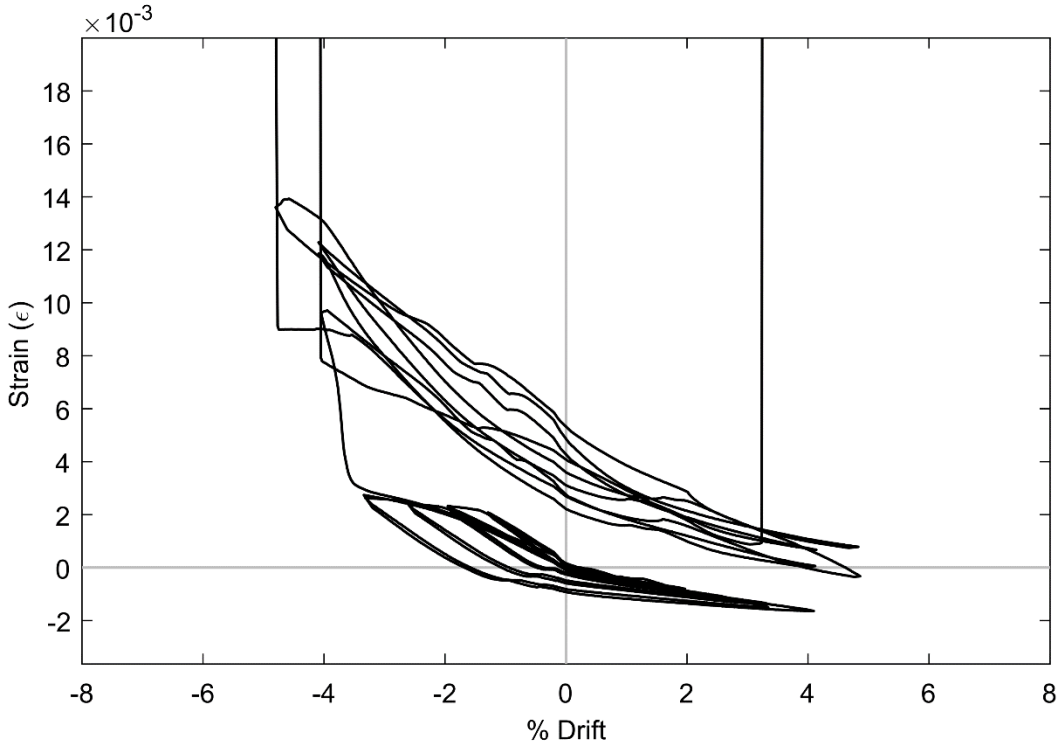

Figure 58: SG STL5 (PTB_4.5_1_0)

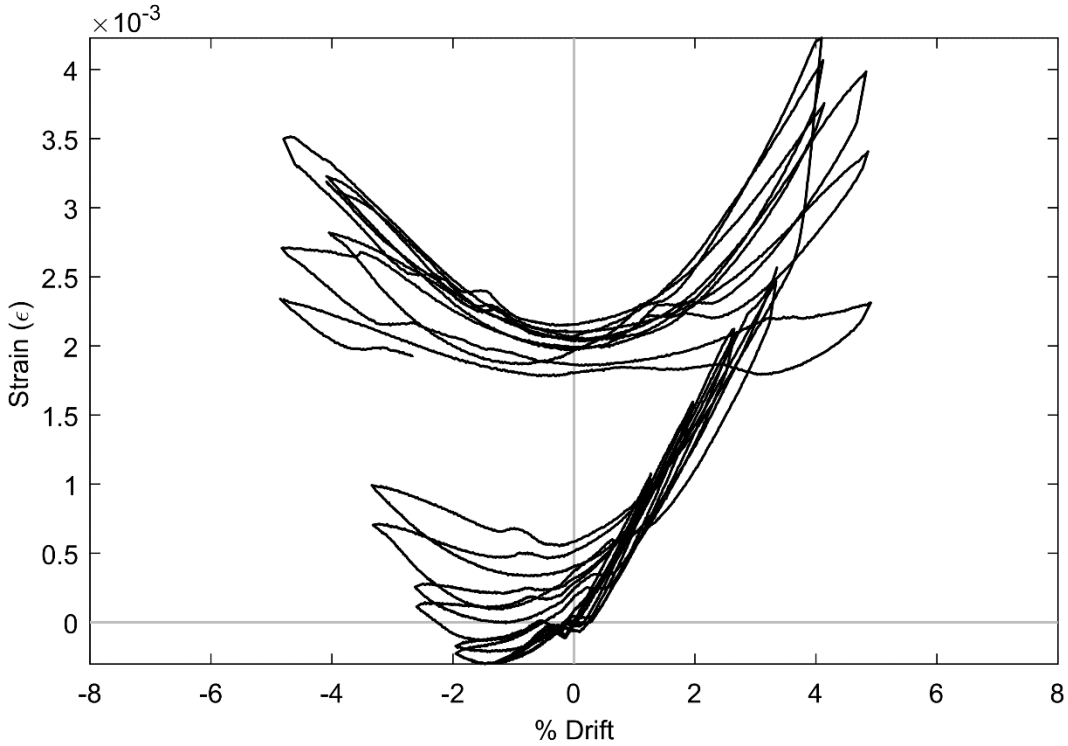

Figure 59: SG STG7 (PTB_4.5_1_0)

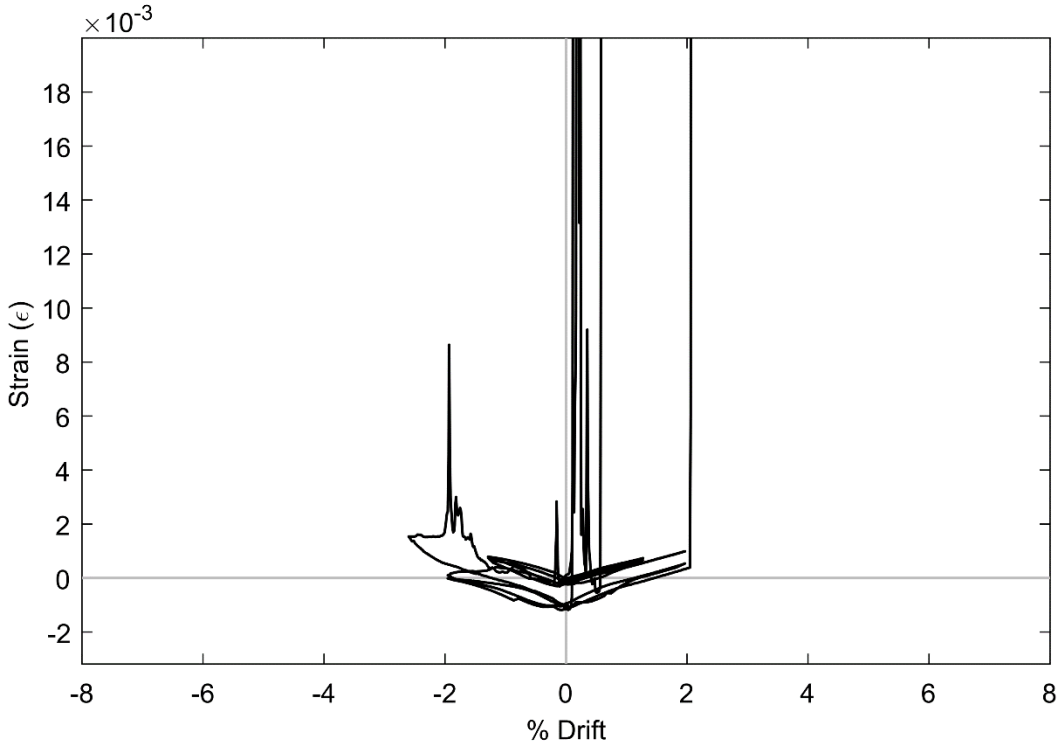

Figure 60: SG STJ7 (PTB_4.5_1_0)

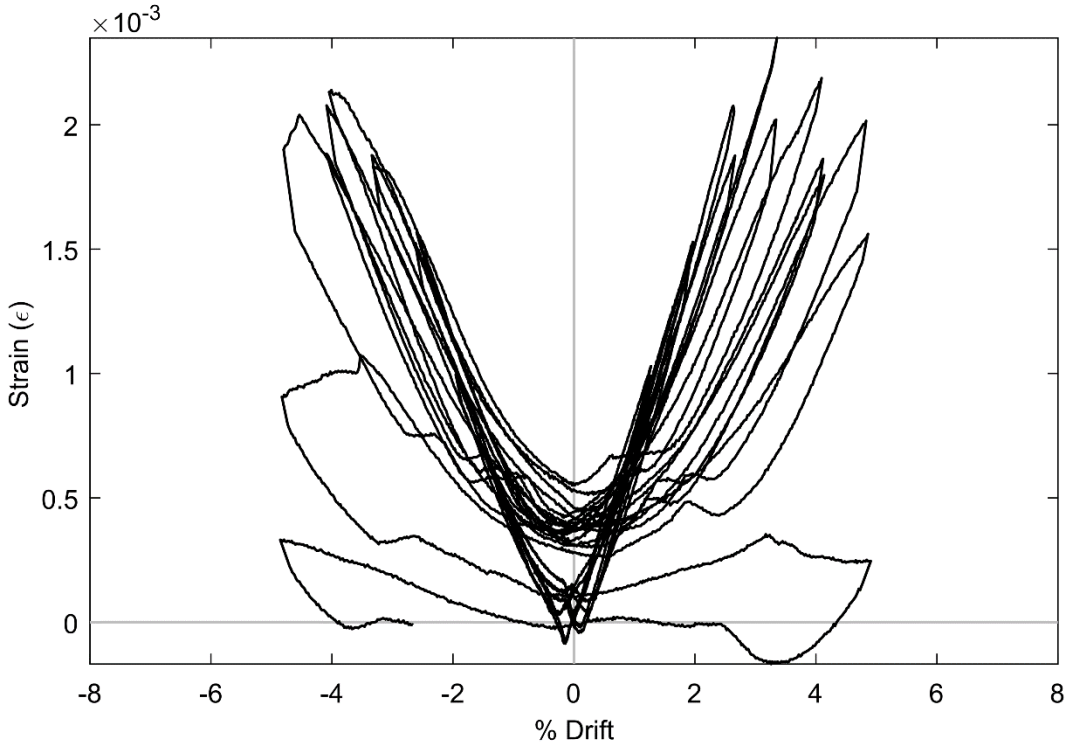

Figure 61: SG STI8 (PTB_4.5_1_0)

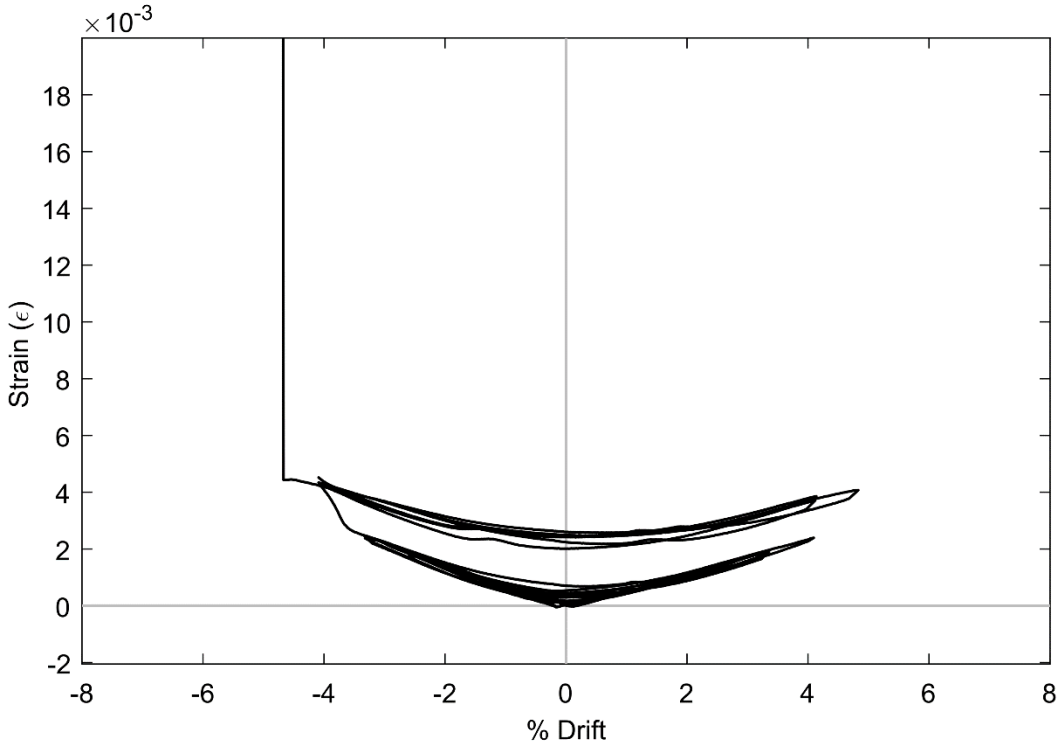

Figure 62: SG STJ8 (PTB_4.5_1_0)

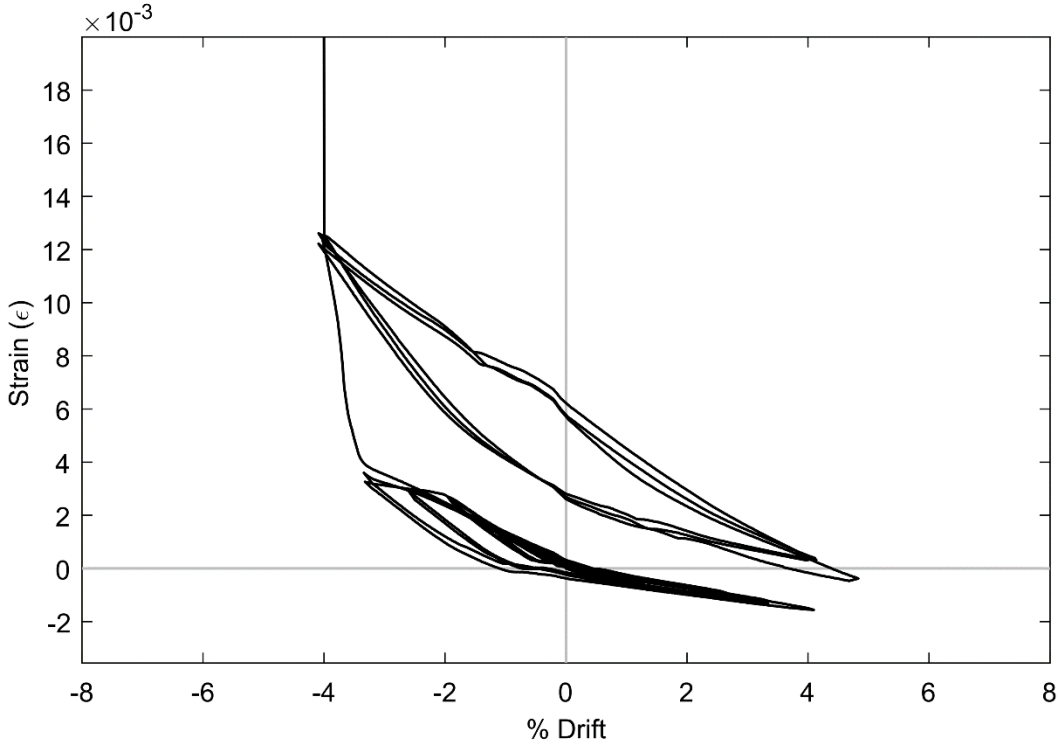

Figure 63: SG SBG5 (PTB_4.5_1_0)

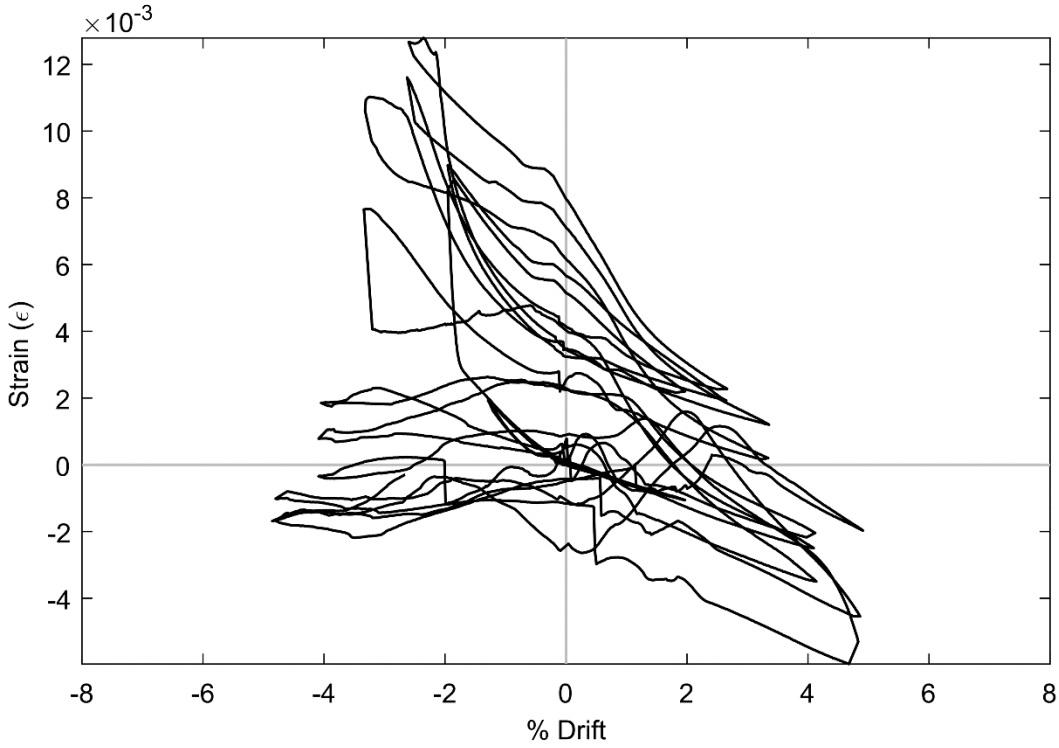

Figure 64: SG SBH5 (PTB_4.5_1_0)

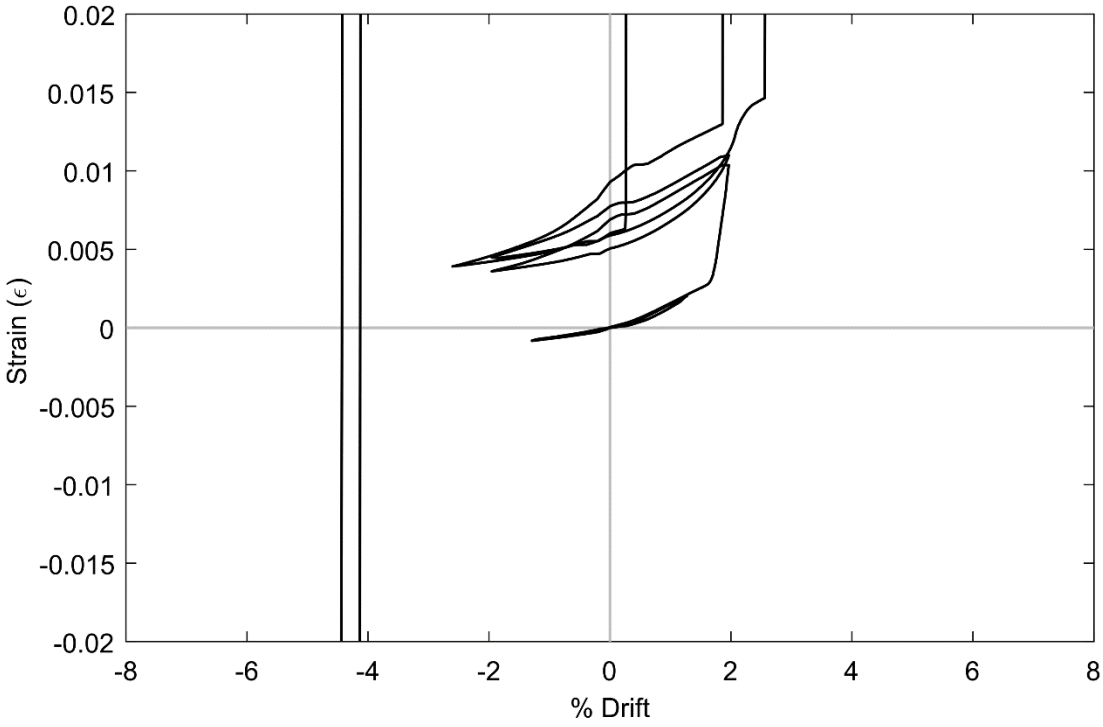

Figure 65: SG SBK5 (PTB_4.5_1_0)

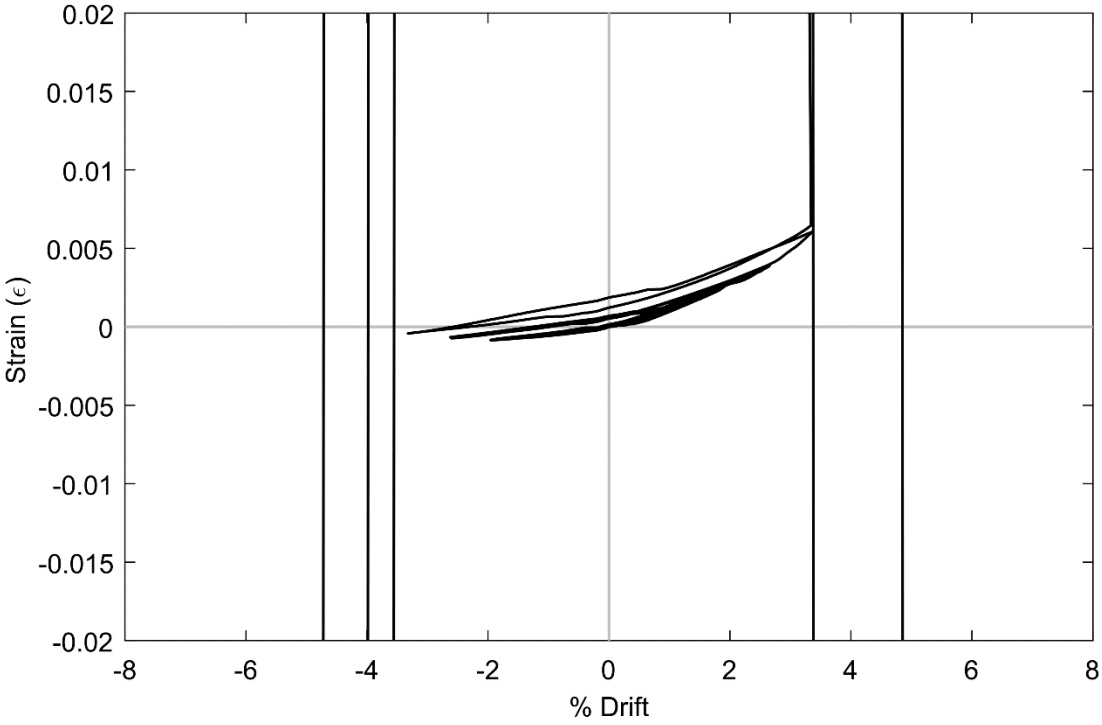

Figure 66: SG SBL5 (PTB_4.5_1_0)

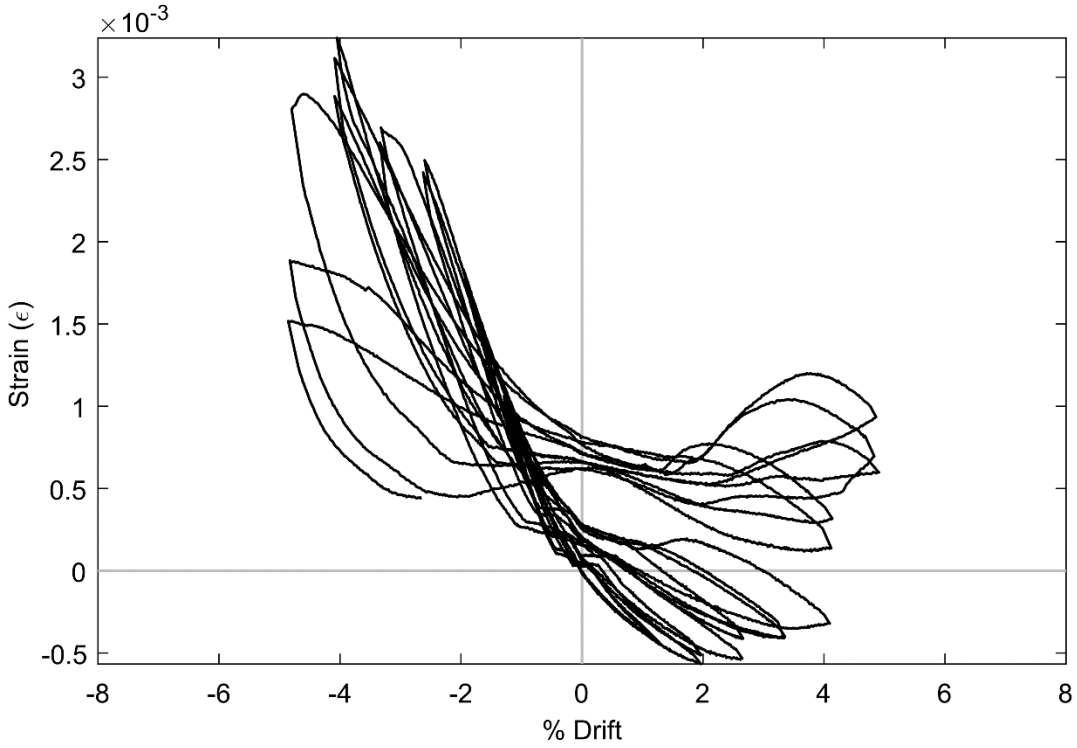

Figure 67: SG SBG6 (PTB_4.5_1_0)

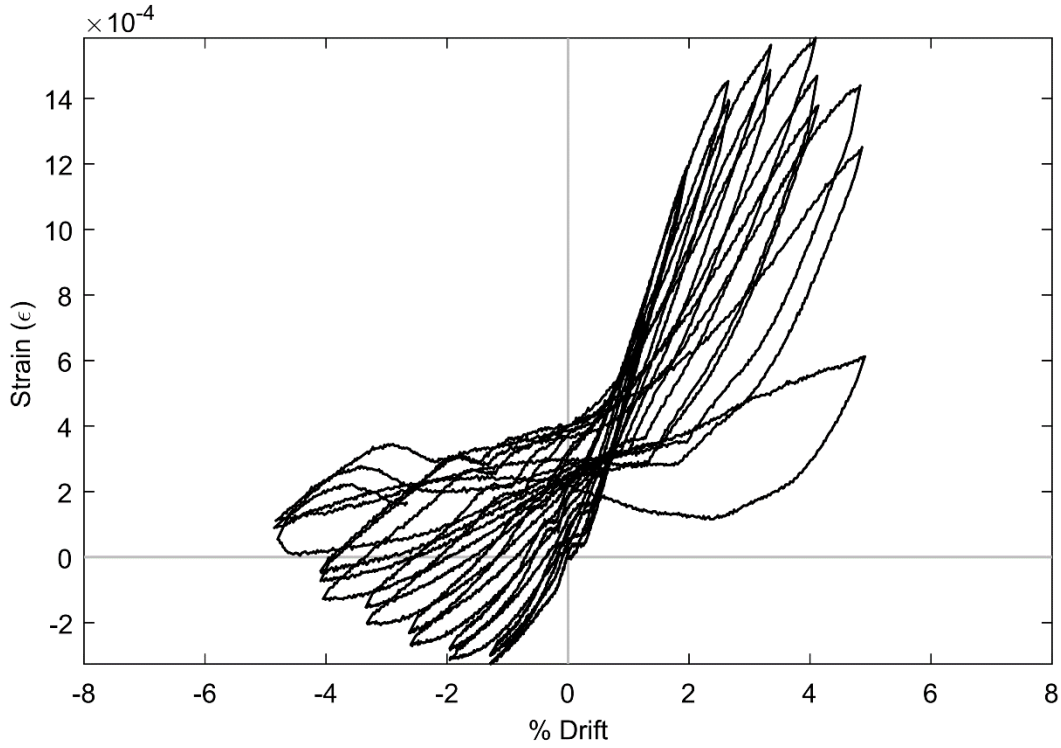

Figure 68: SG SBN6 (PTB_4.5_1_0)

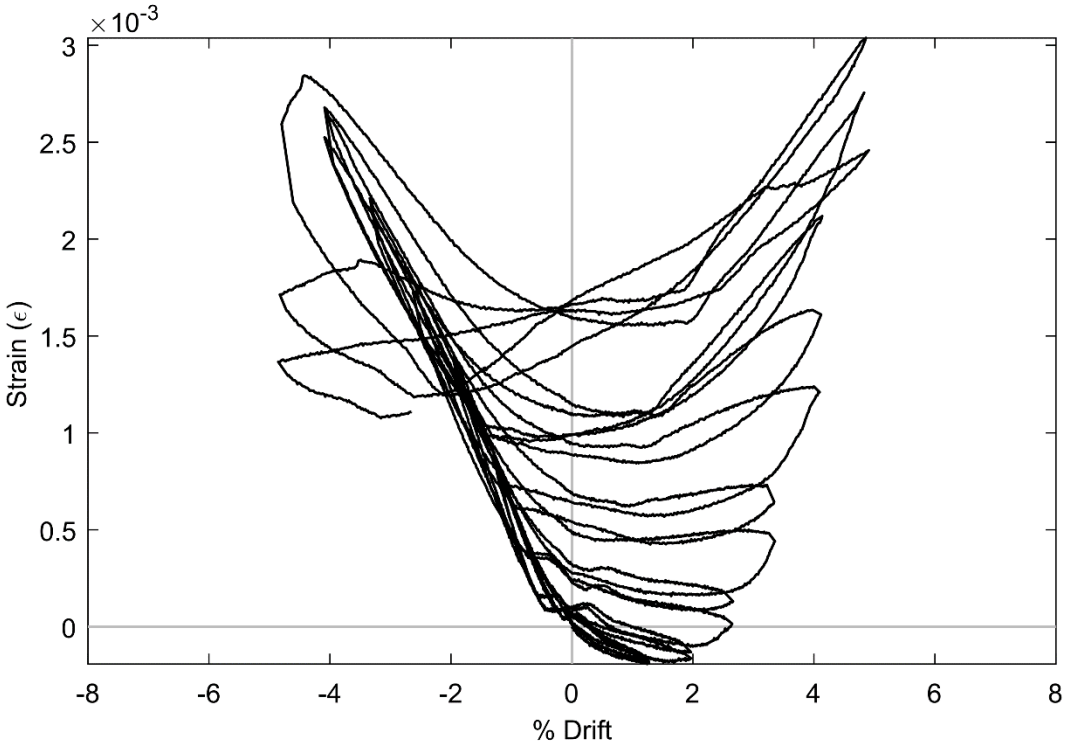

Figure 69: SG SBG7 (PTB_4.5_1_0)

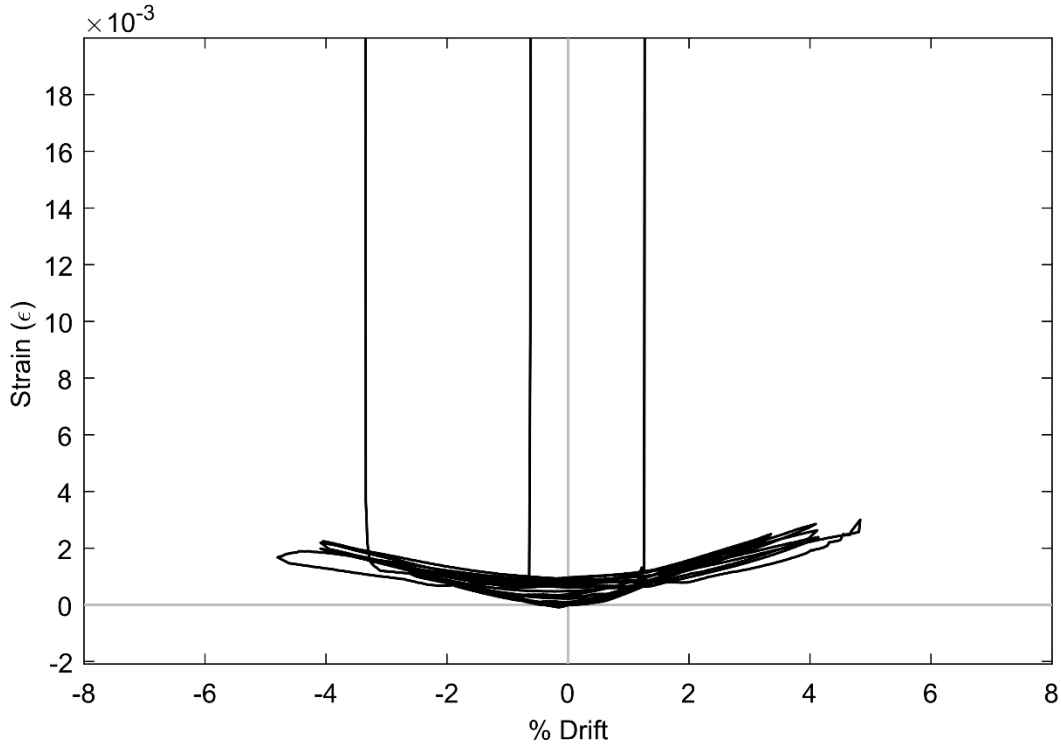

Figure 70: SG SBJ7 (PTB_4.5_1_0)

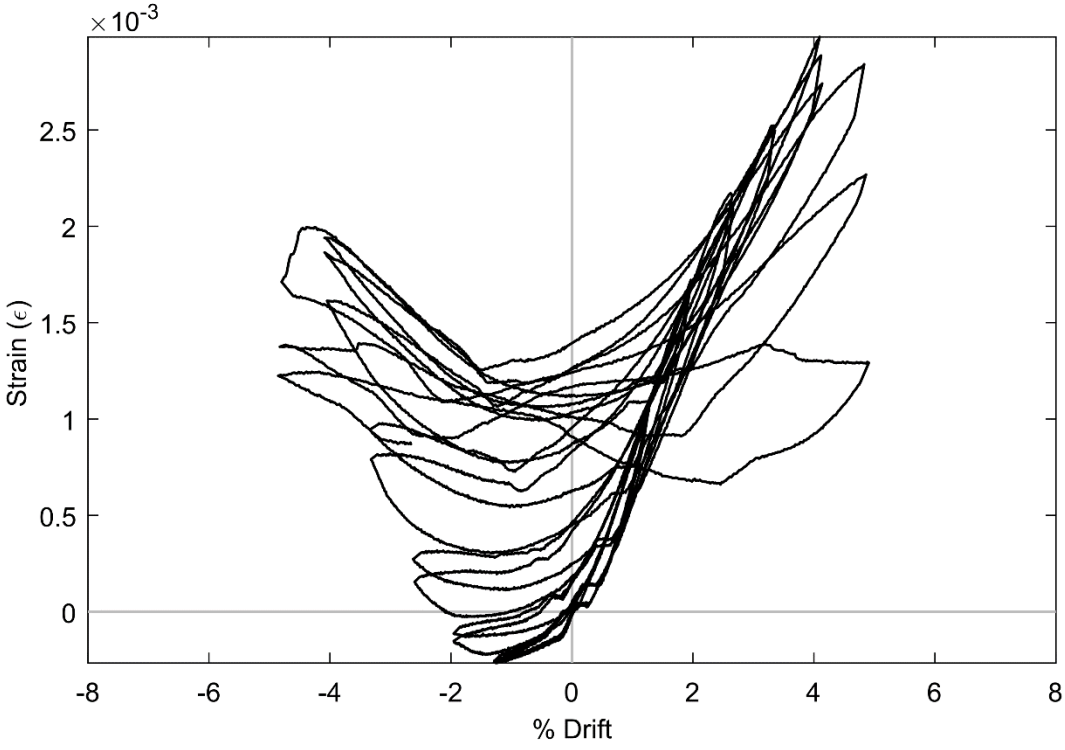

Figure 71: SG SBL7 (PTB_4.5_1_0)

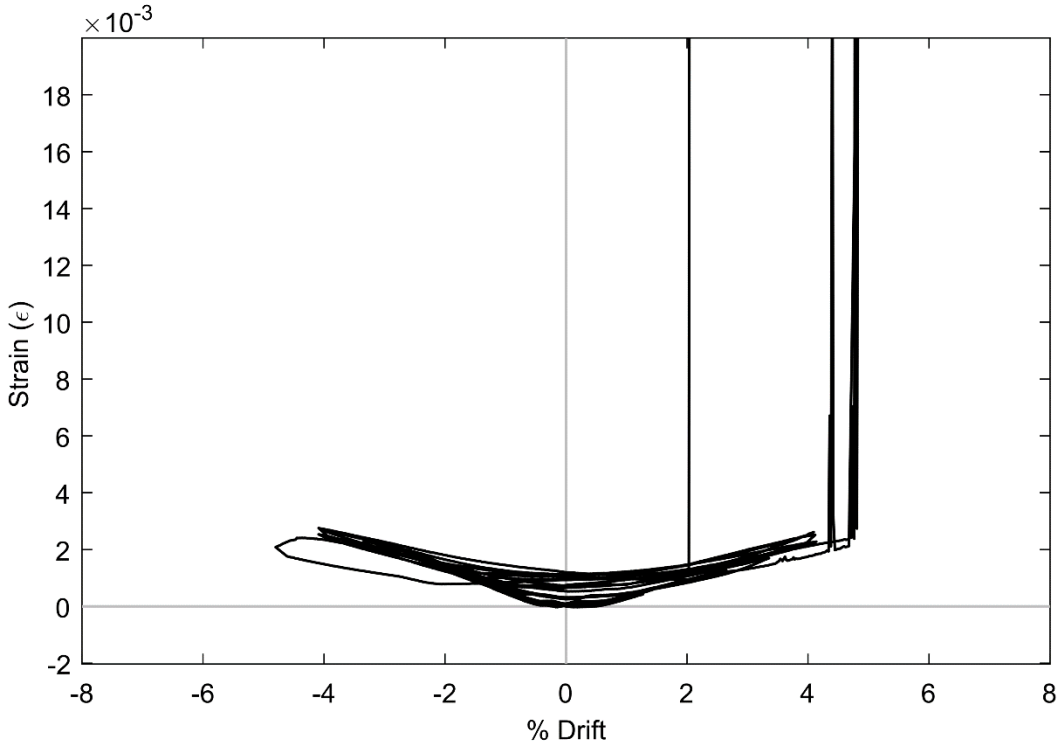

Figure 72: SG SBI8 (PTB_4.5_1_0)

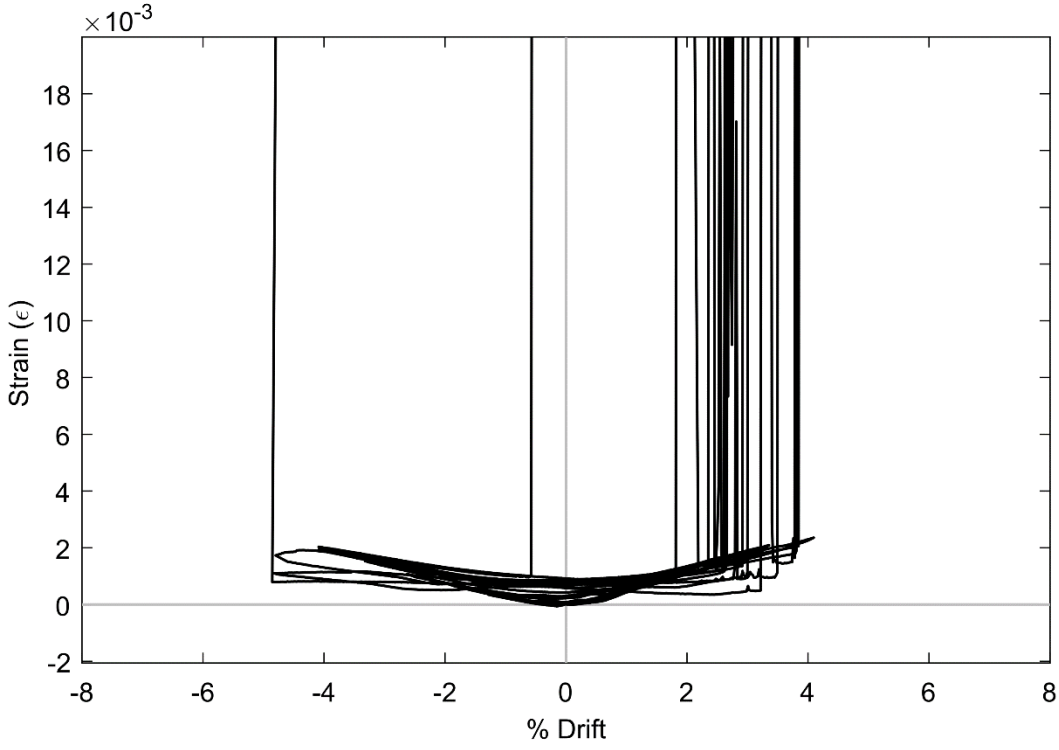

Figure 73: SG SBJ8 (PTB_4.5_1_0)

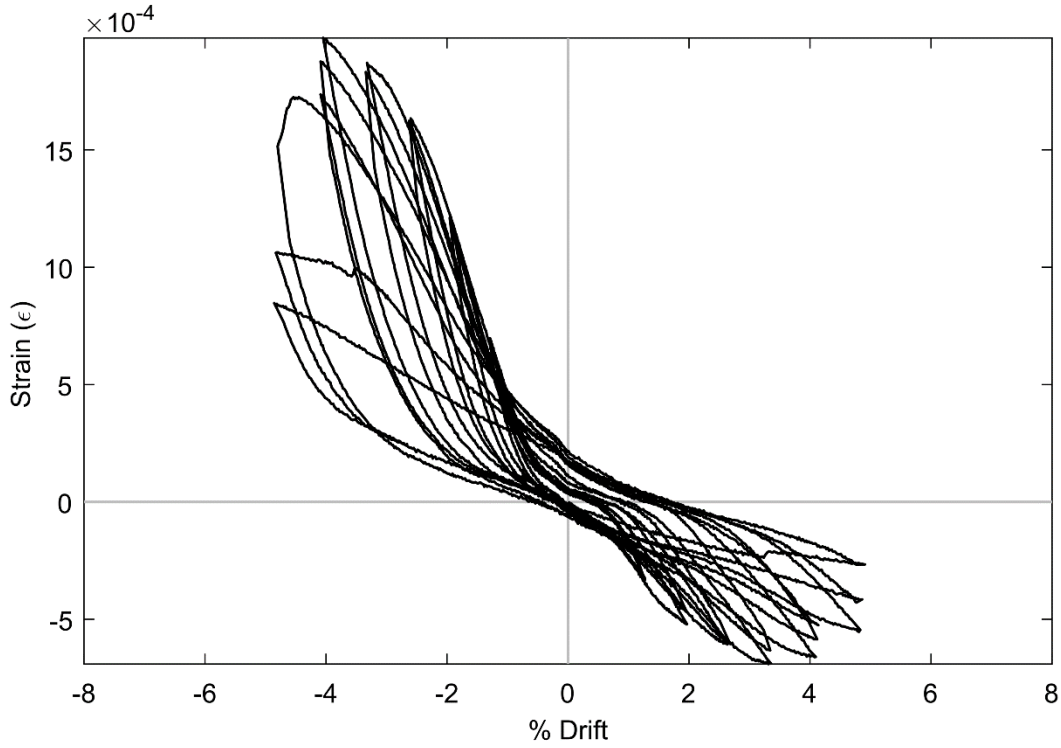

Figure 74: SG CC2 (PTB_4.5_1_0)

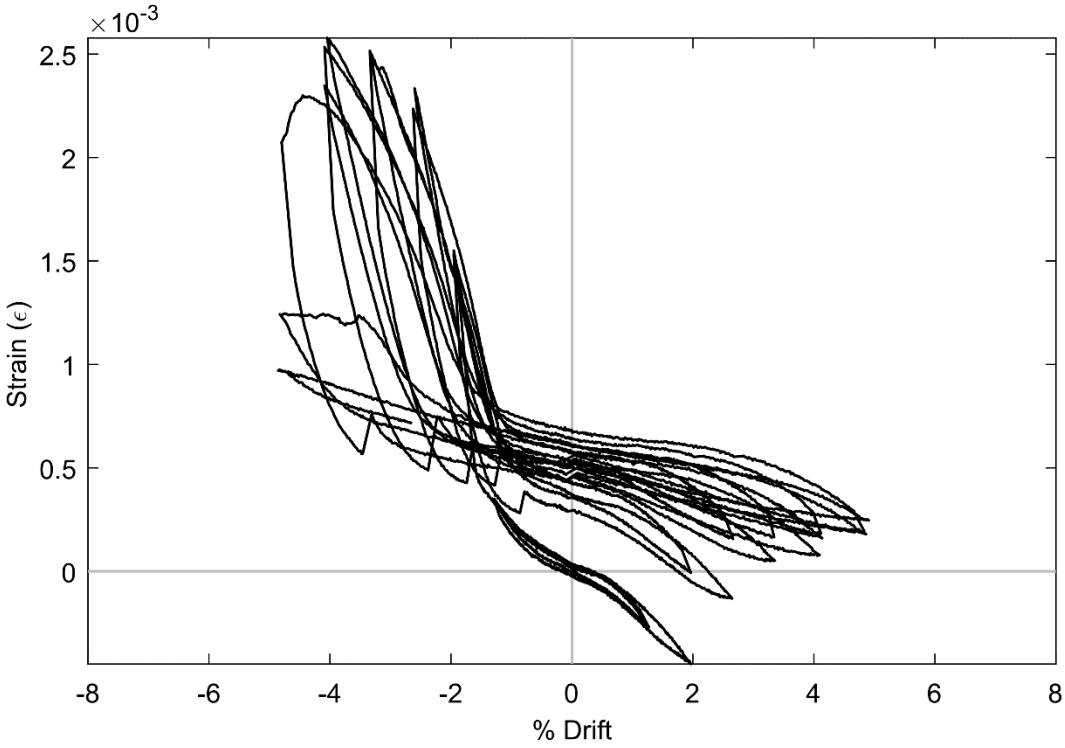

Figure 75: SG CC3 (PTB_4.5_1_0)

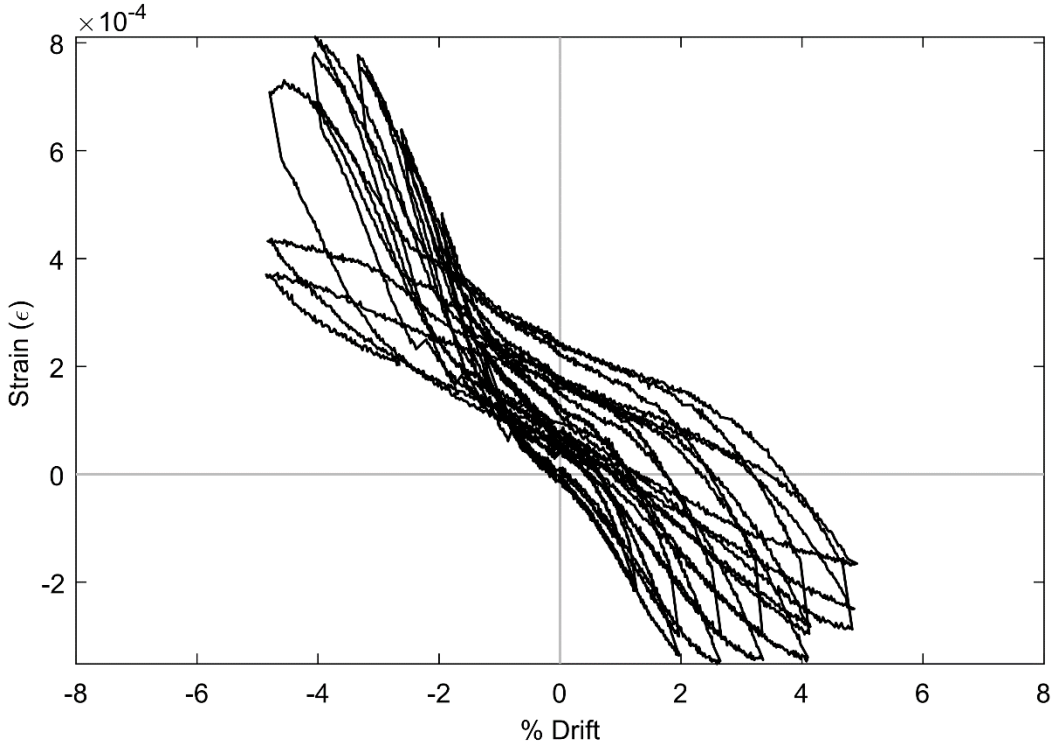

Figure 76: SG CC4 (PTB_4.5_1_0)

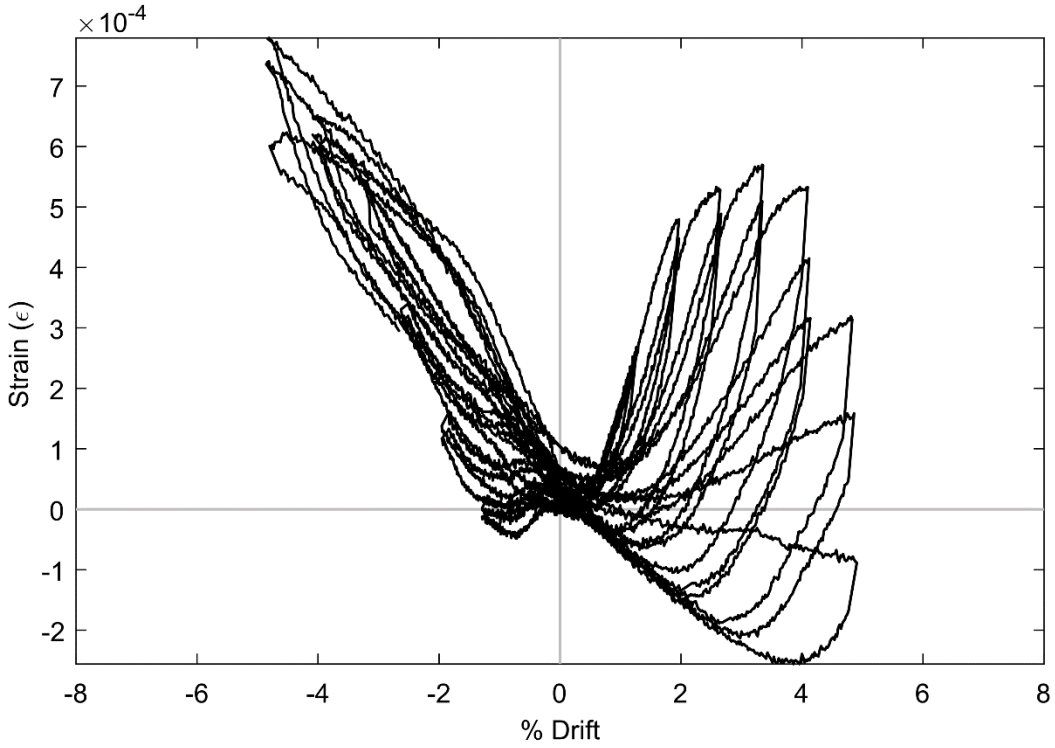

Figure 77: SG CD1 (PTB_4.5_1_0)

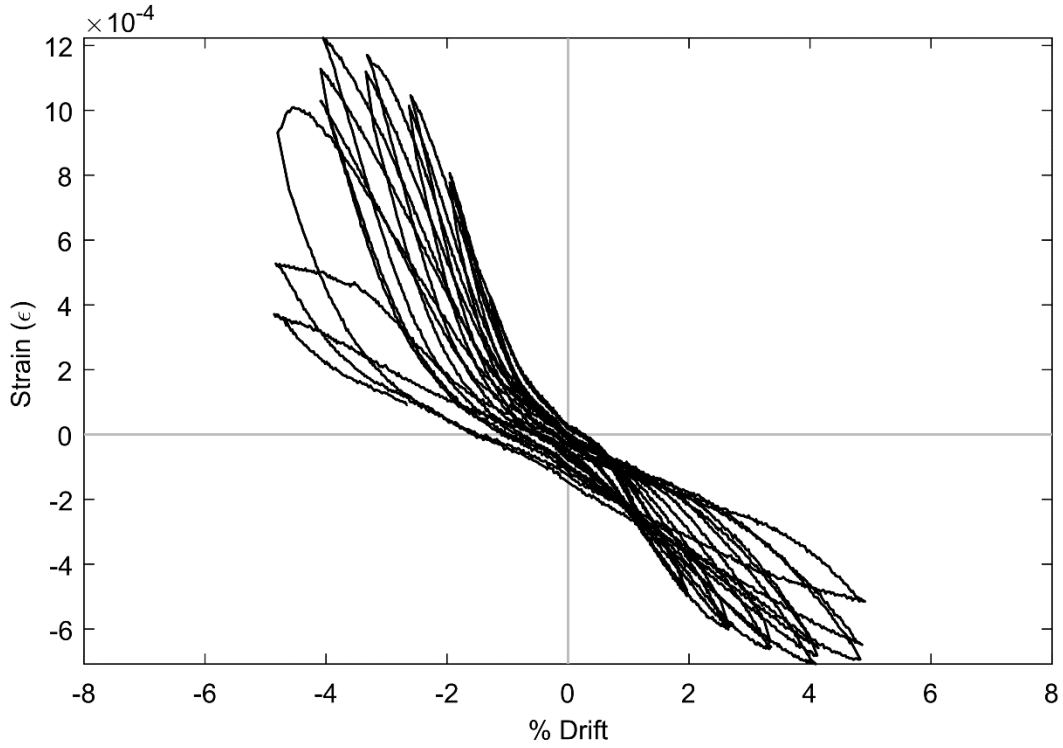

Figure 78: SG CD3 (PTB_4.5_1_0)

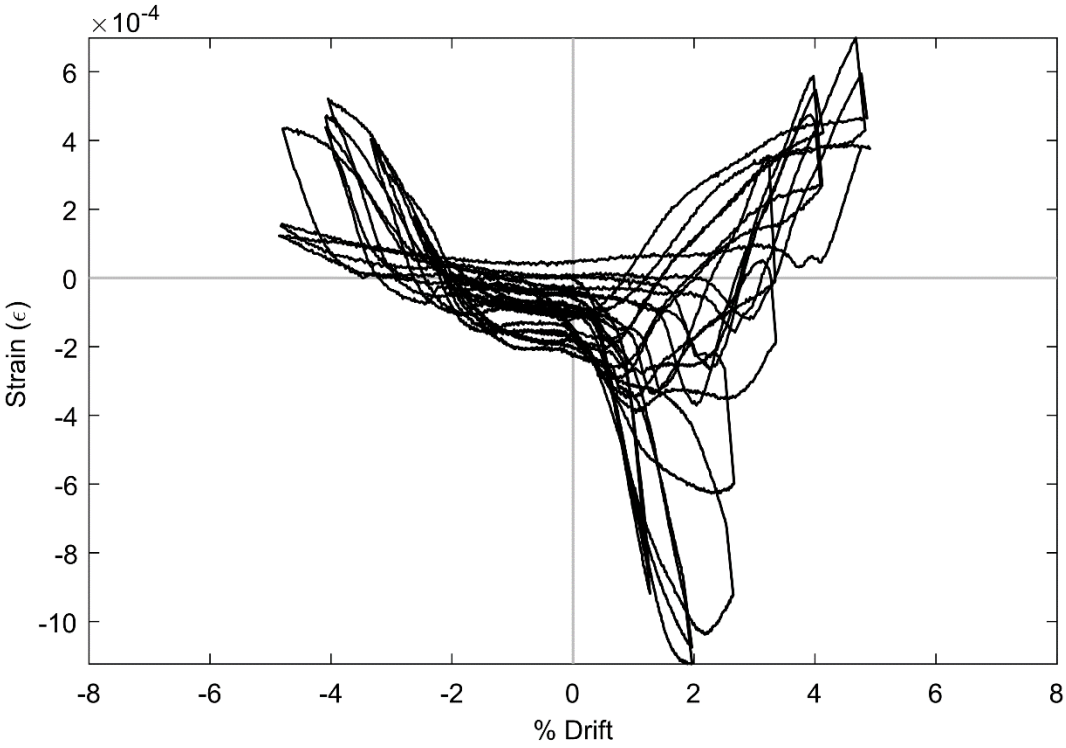

Figure 79: SG CI1 (PTB_4.5_1_0)

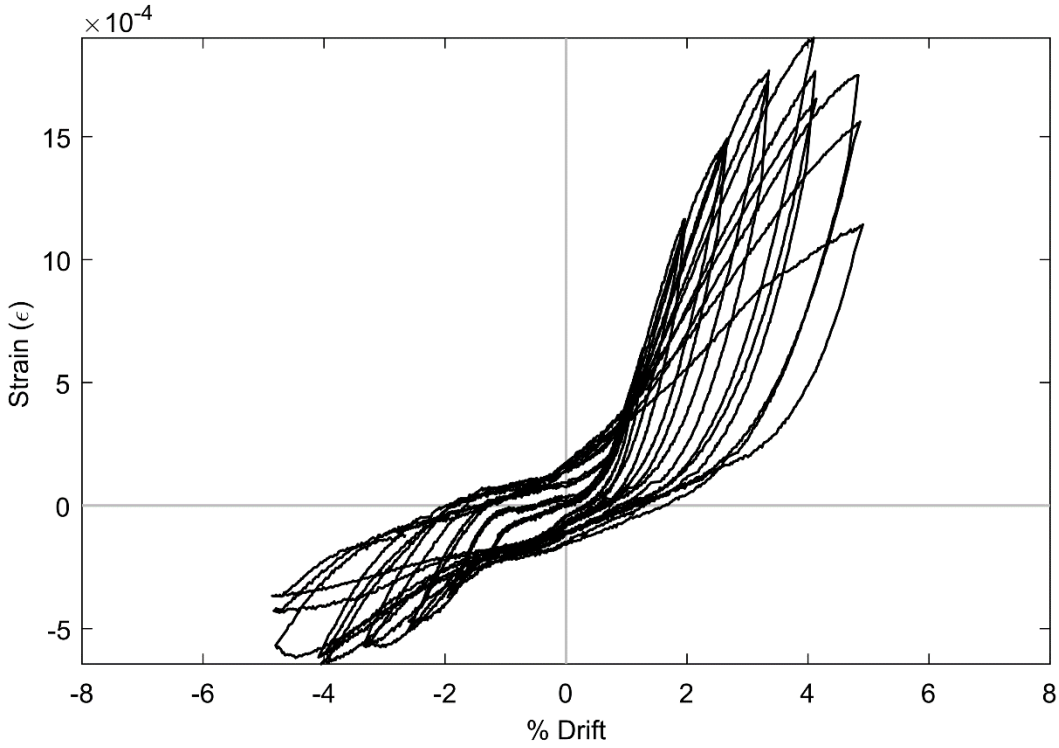

Figure 80: SG CI2 (PTB_4.5_1_0)

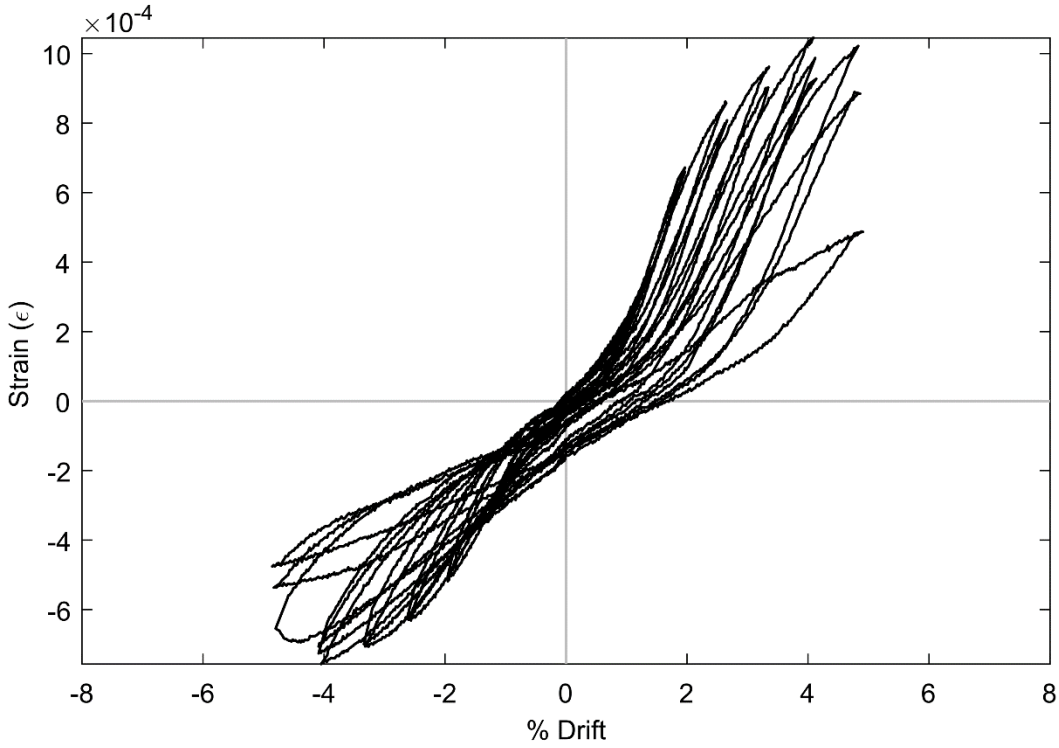

Figure 81: SG CI3 (PTB_4.5_1_0)

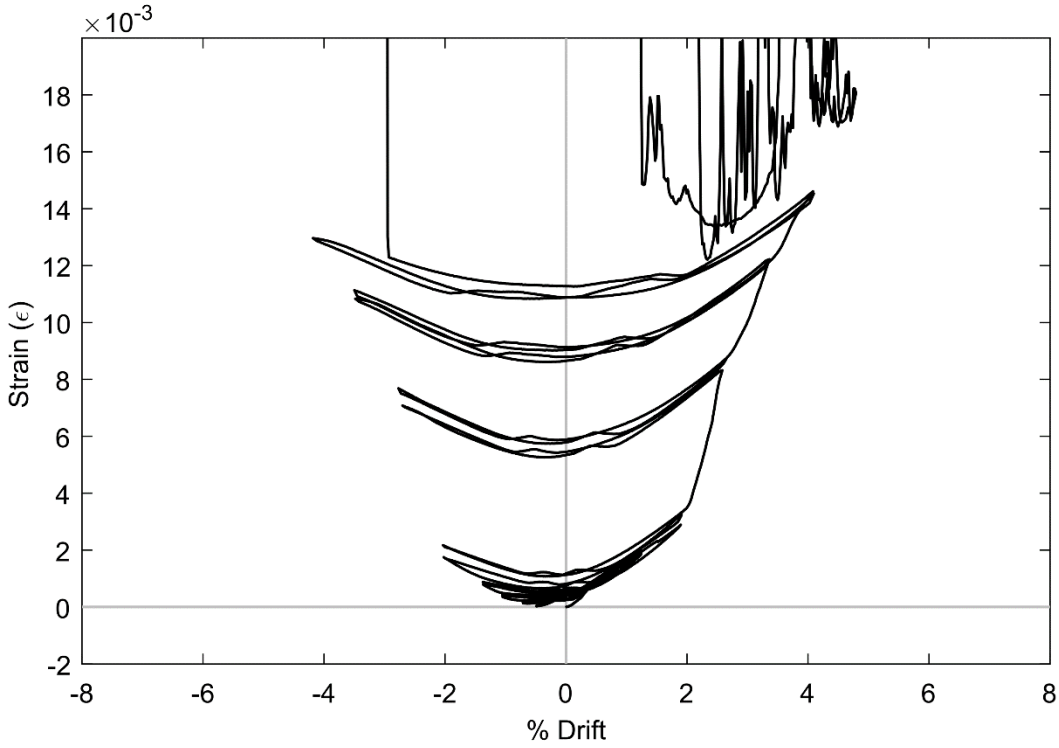

Figure 82: SG STI6 (PTB_4.5_1_4)

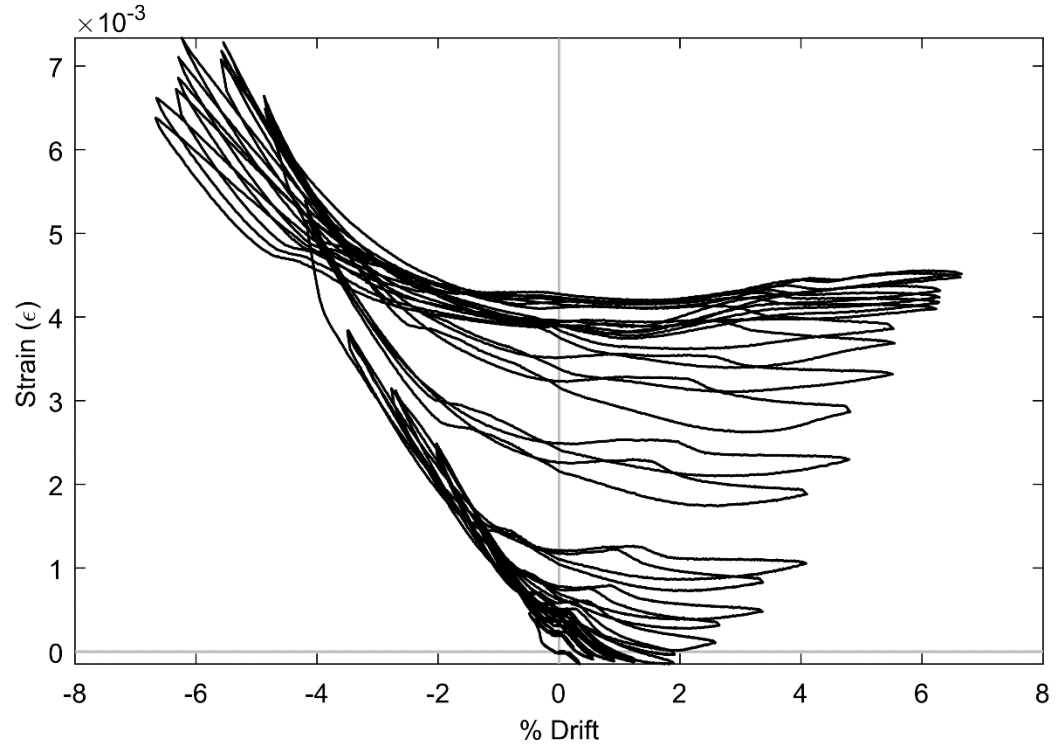

Figure 83: SG STL6 (PTB_4.5_1_4)

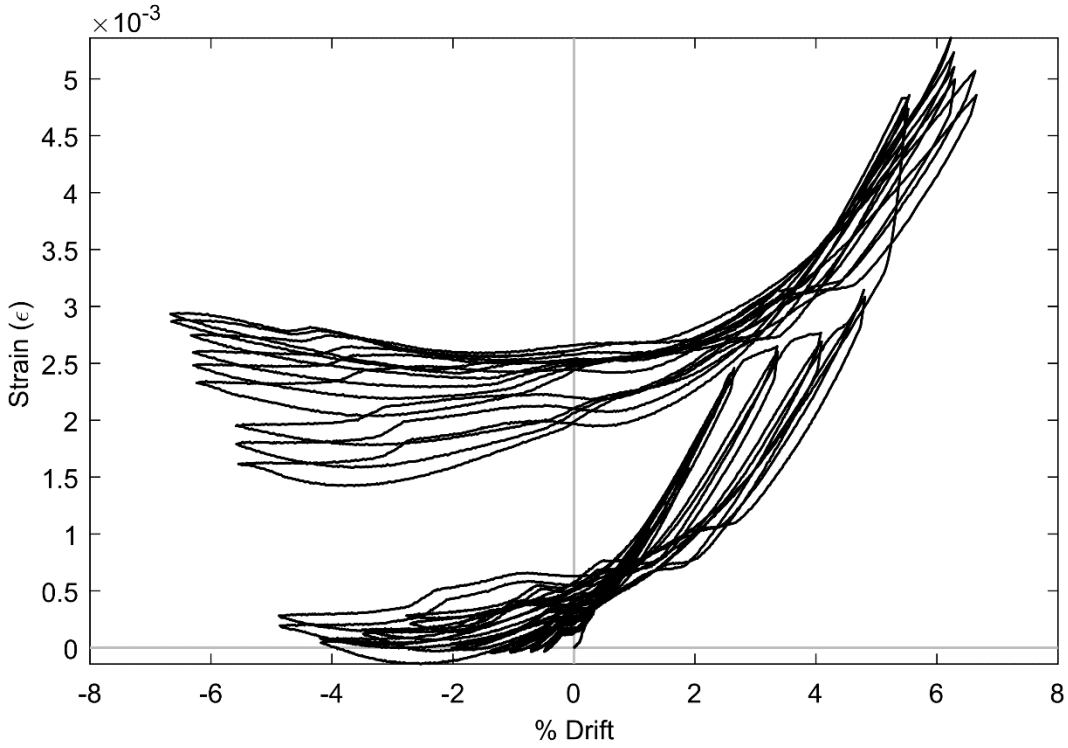

Figure 84: SG STG7 (PTB_4.5_1_4)

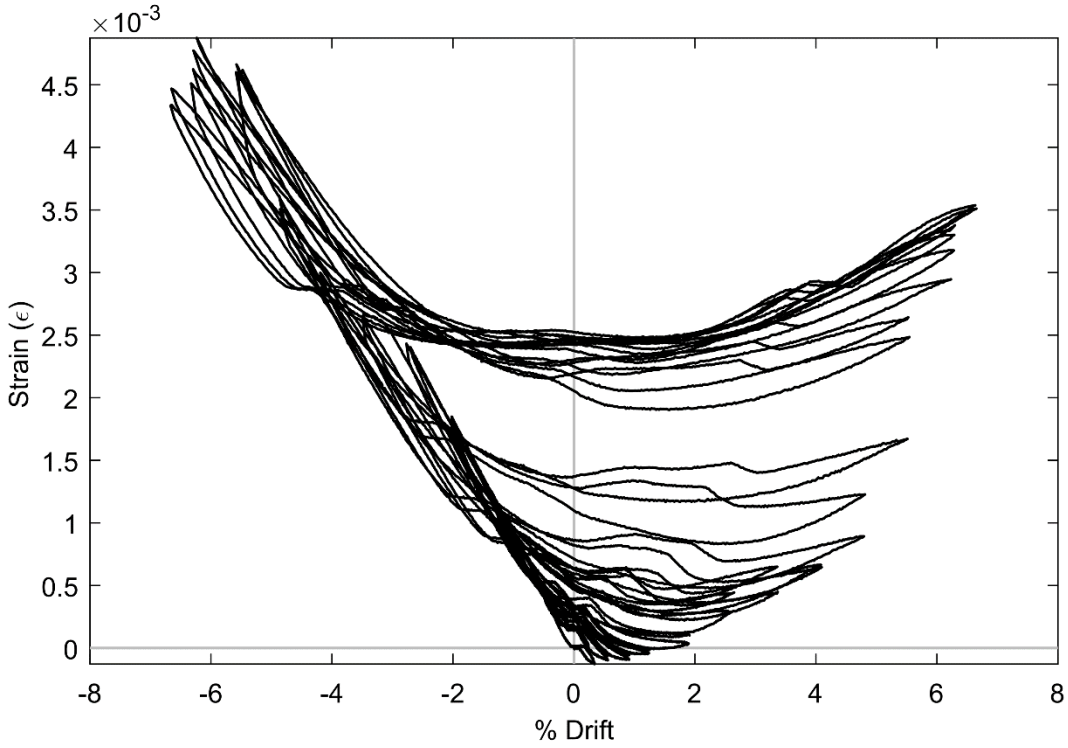

Figure 85: SG STL7 (PTB_4.5_1_4)

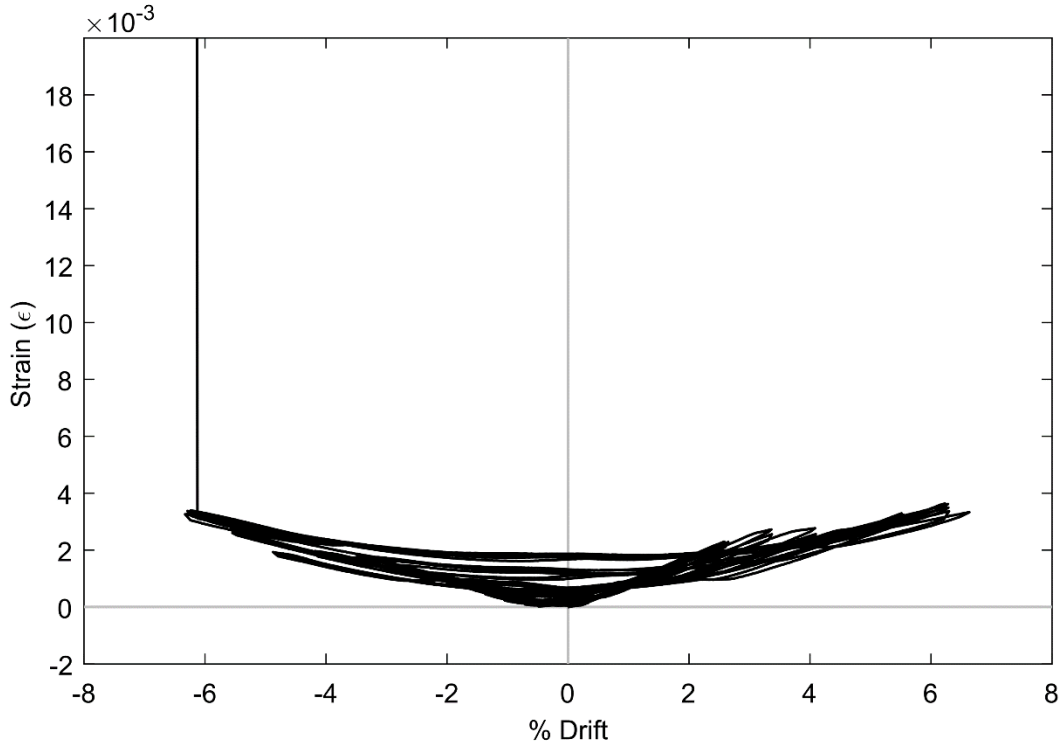

Figure 86: SG STI8 (PTB_4.5_1_4)

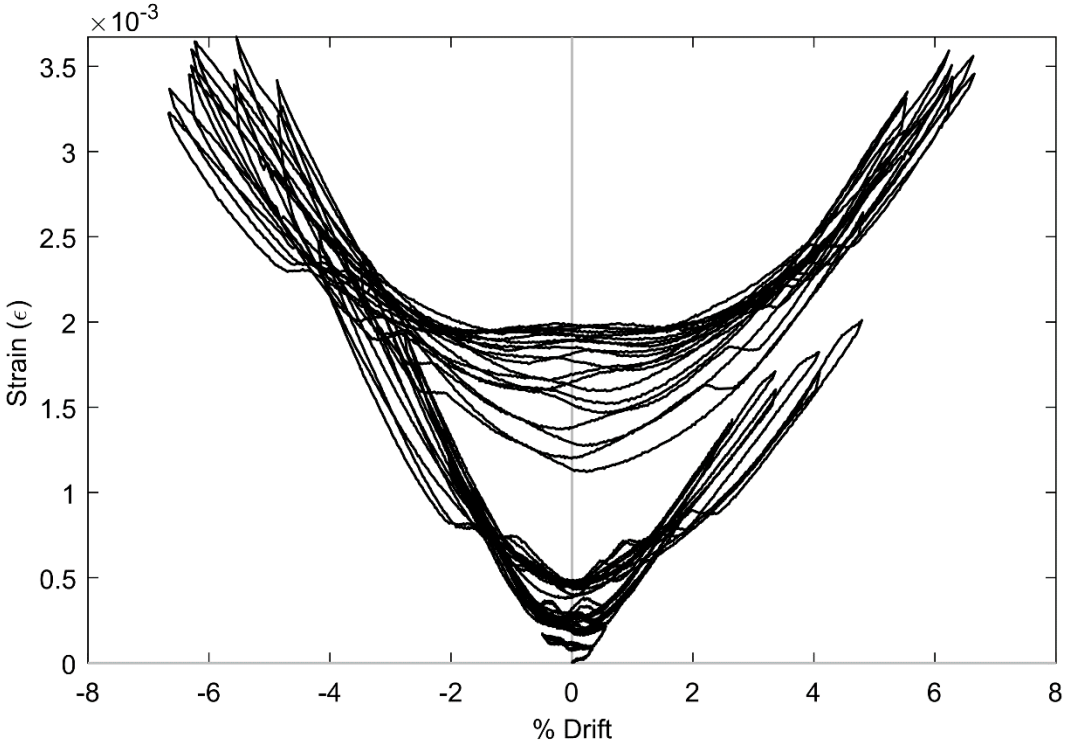

Figure 87: SG STJ8 (PTB_4.5_1_4)

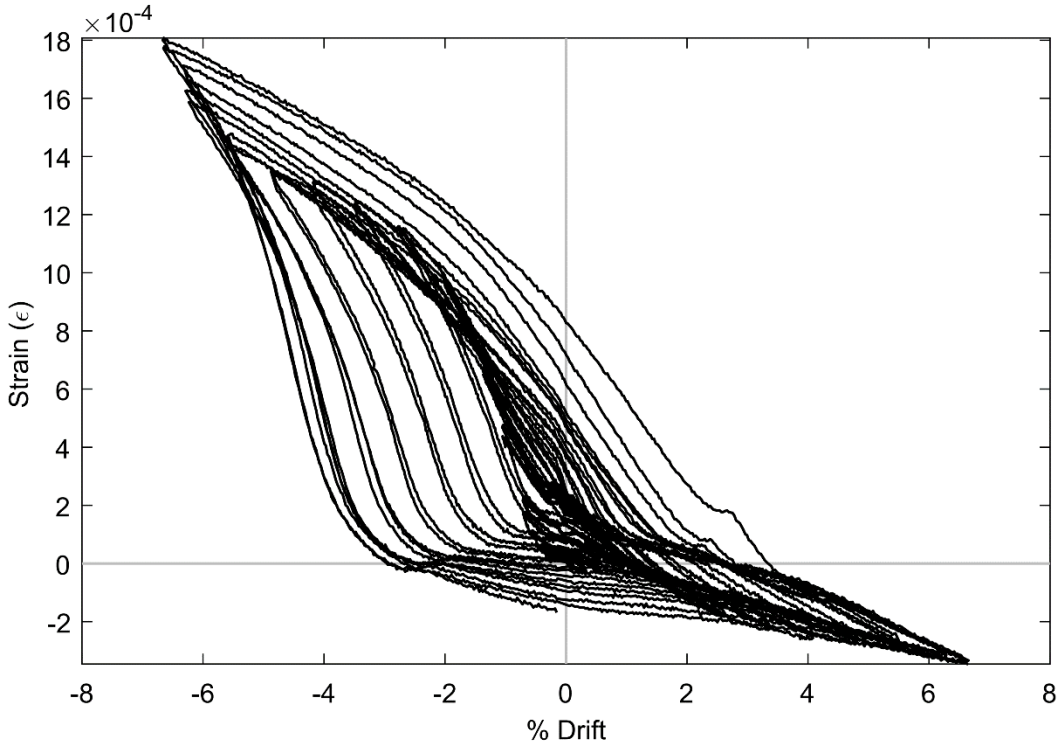

Figure 88: SG SBE5 (PTB_4.5_1_4)

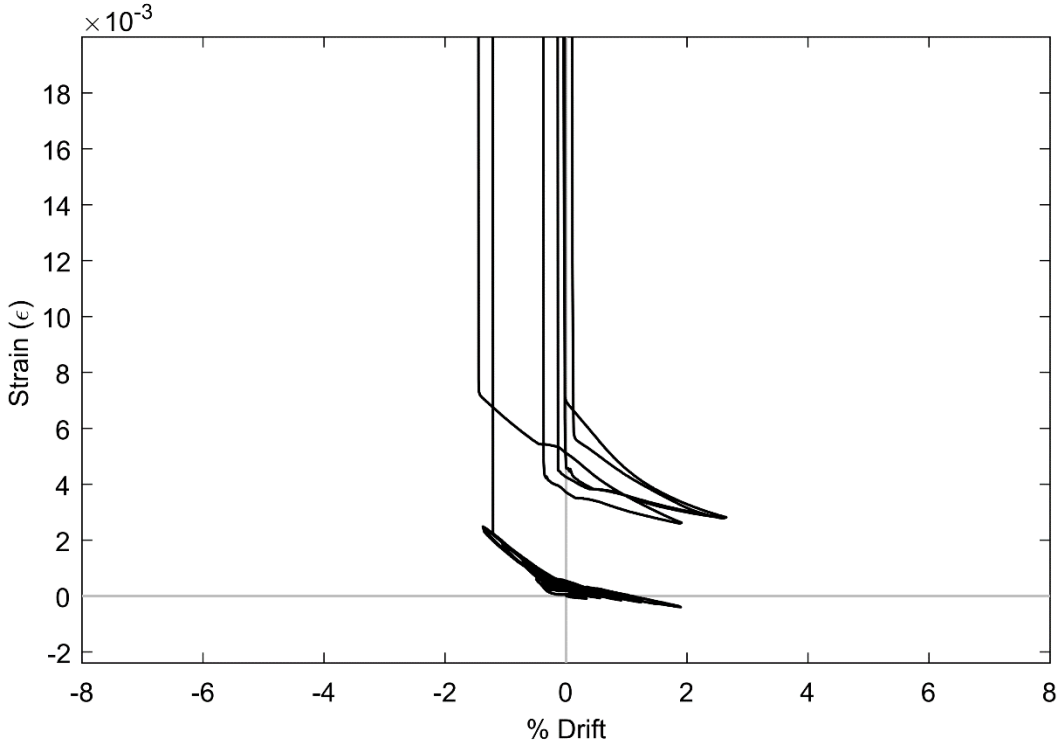

Figure 89: SG SBH5 (PTB_4.5_1_4)

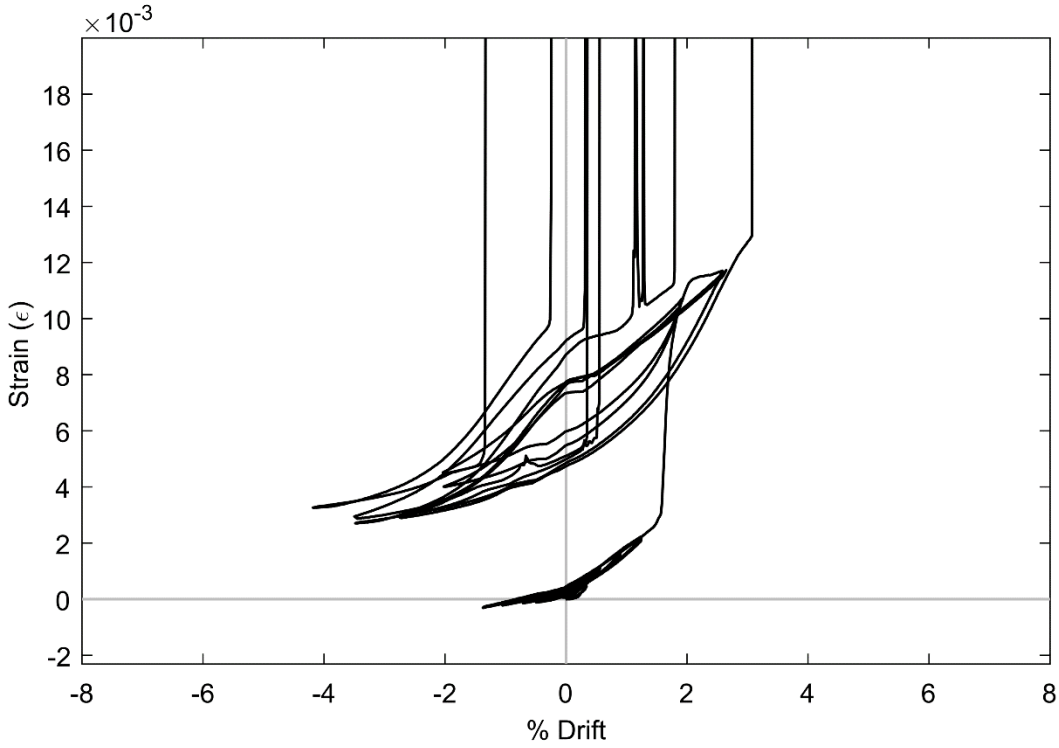

Figure 90: SG SBK5 (PTB_4.5_1_4)

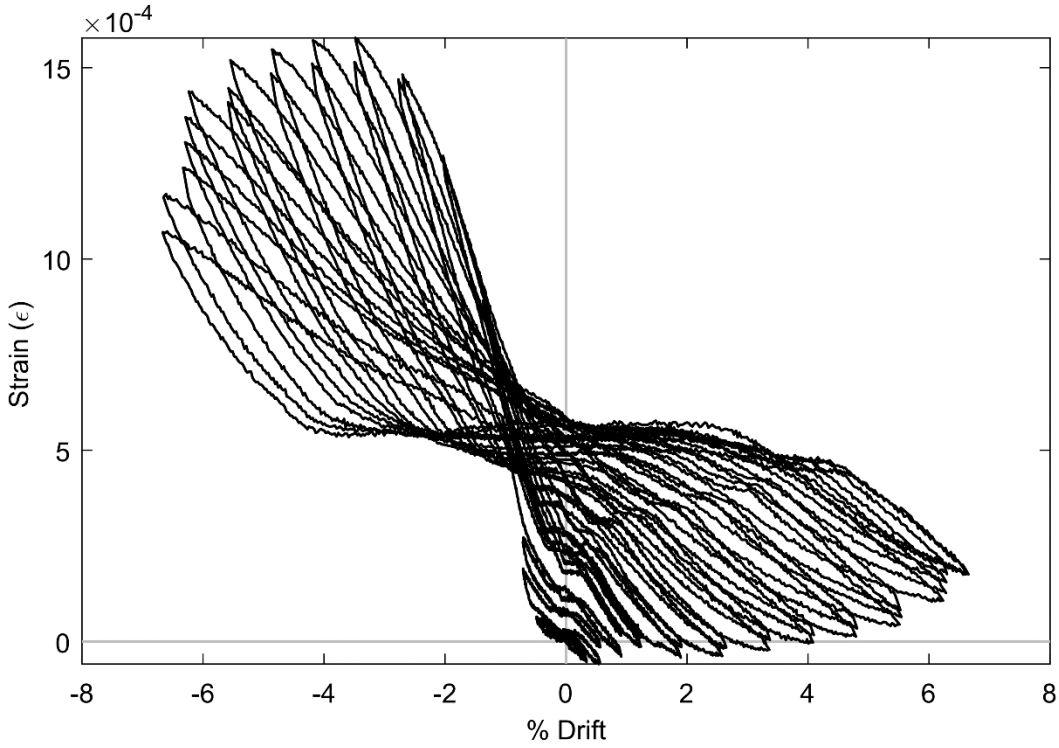

Figure 91: SG SBE6 (PTB_4.5_1_4)

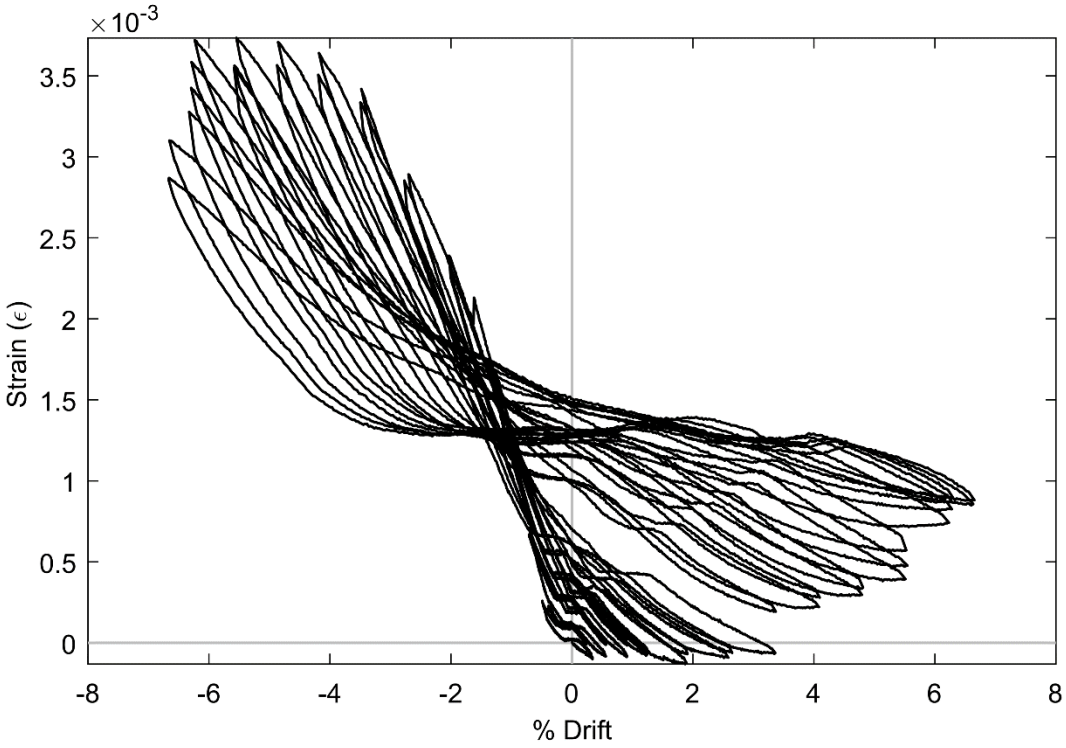

Figure 92: SG SBG6 (PTB_4.5_1_4)

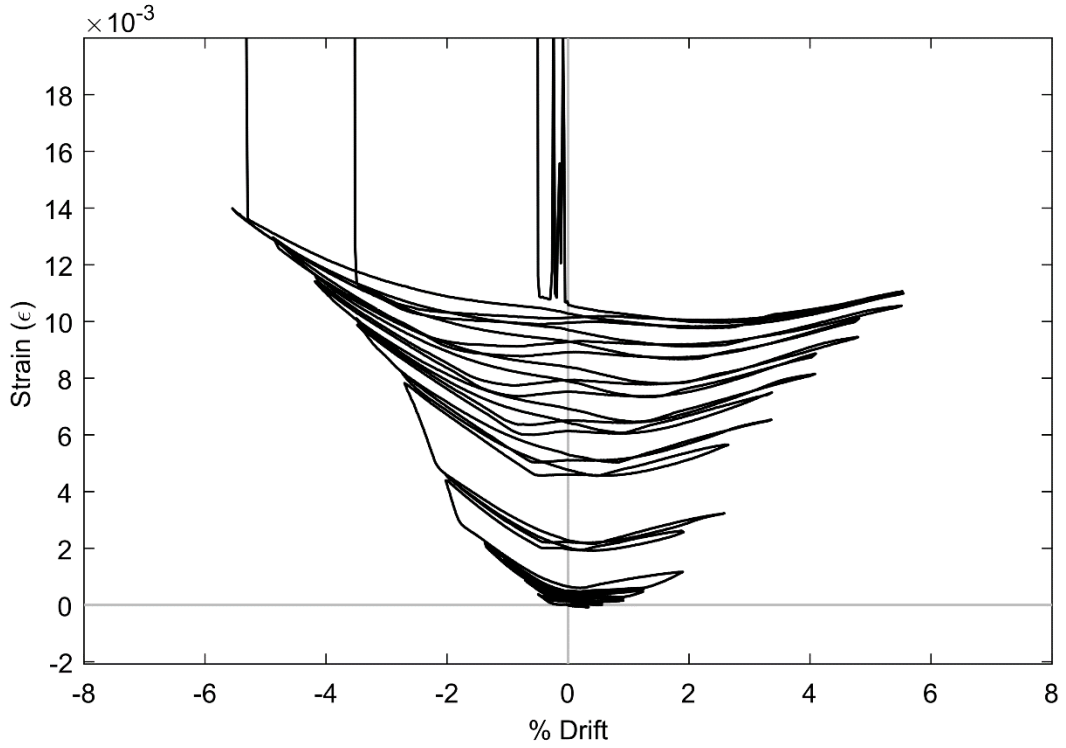

Figure 93: SG SBI6 (PTB_4.5_1_4)

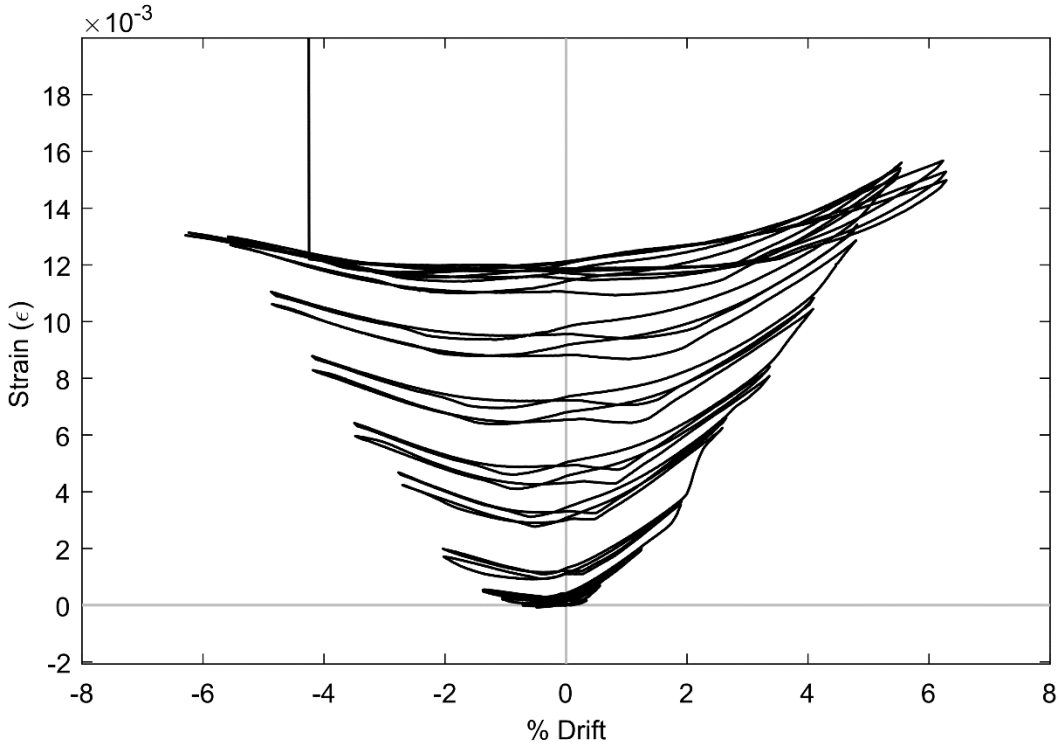

Figure 94: SG SBJ6 (PTB_4.5_1_4)

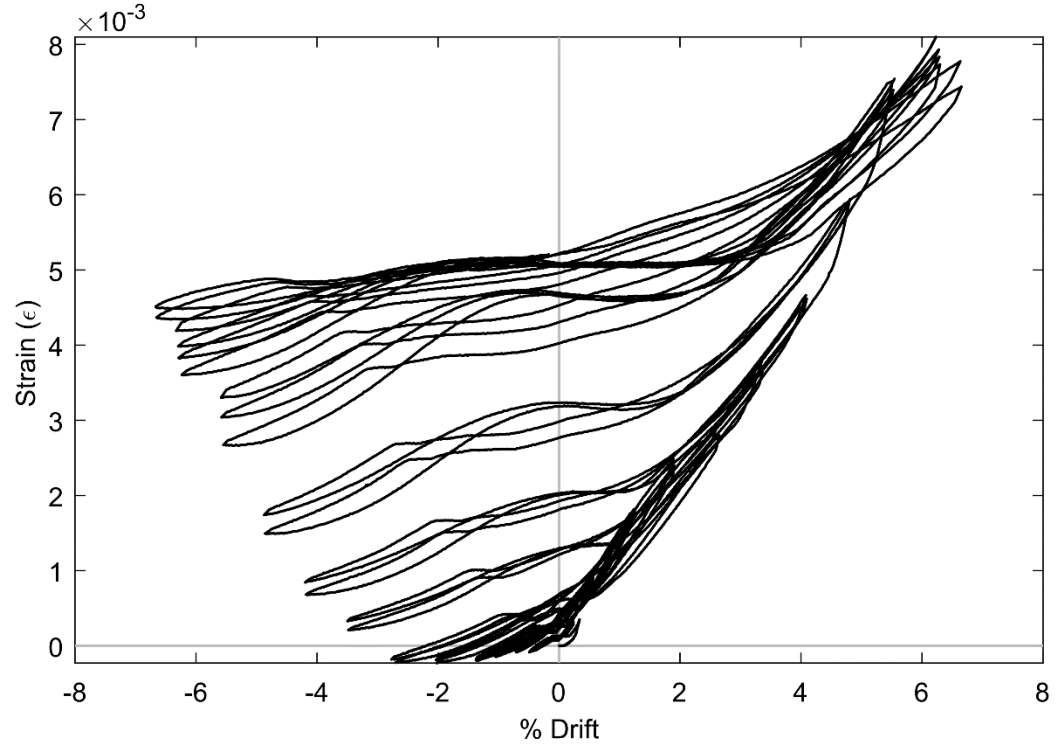

Figure 95: SG SBL6 (PTB_4.5_1_4)

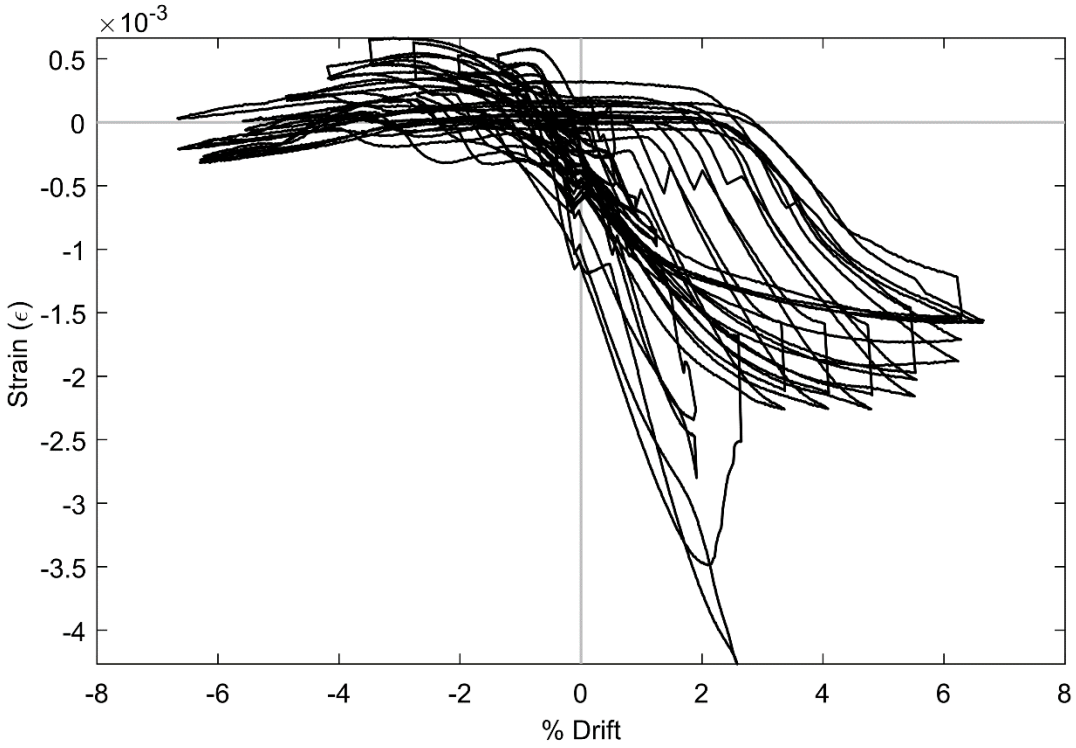

Figure 96: SG SBN6 (PTB_4.5_1_4)

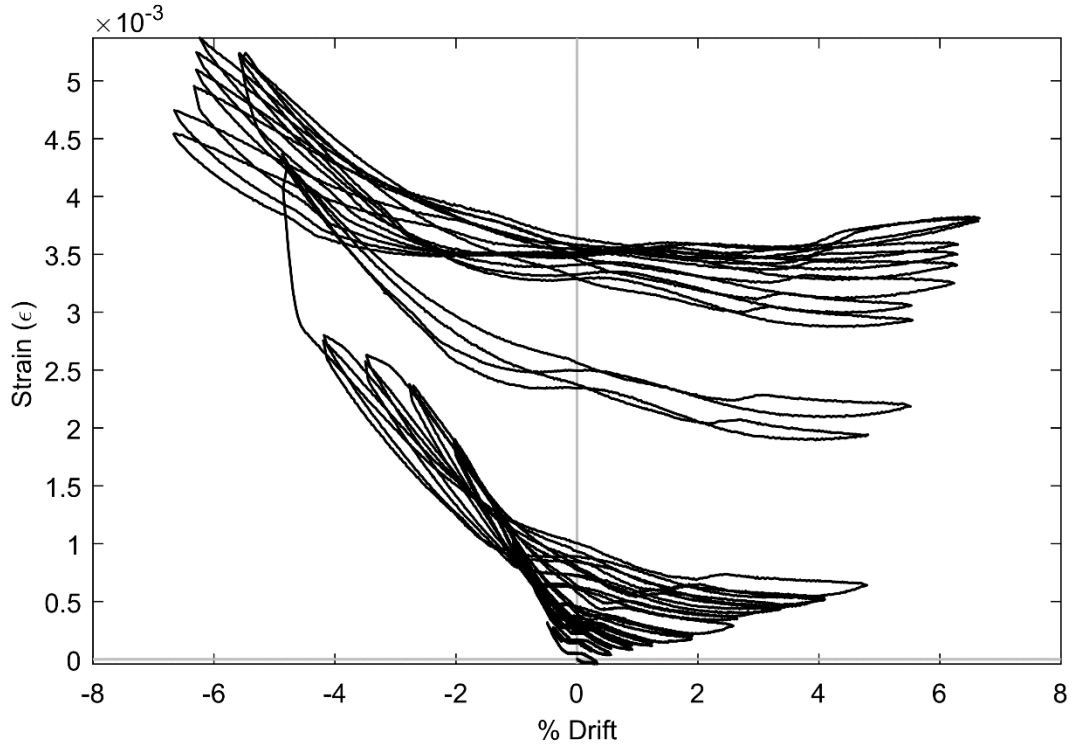

Figure 97: SG SBG7 (PTB_4.5_1_4)

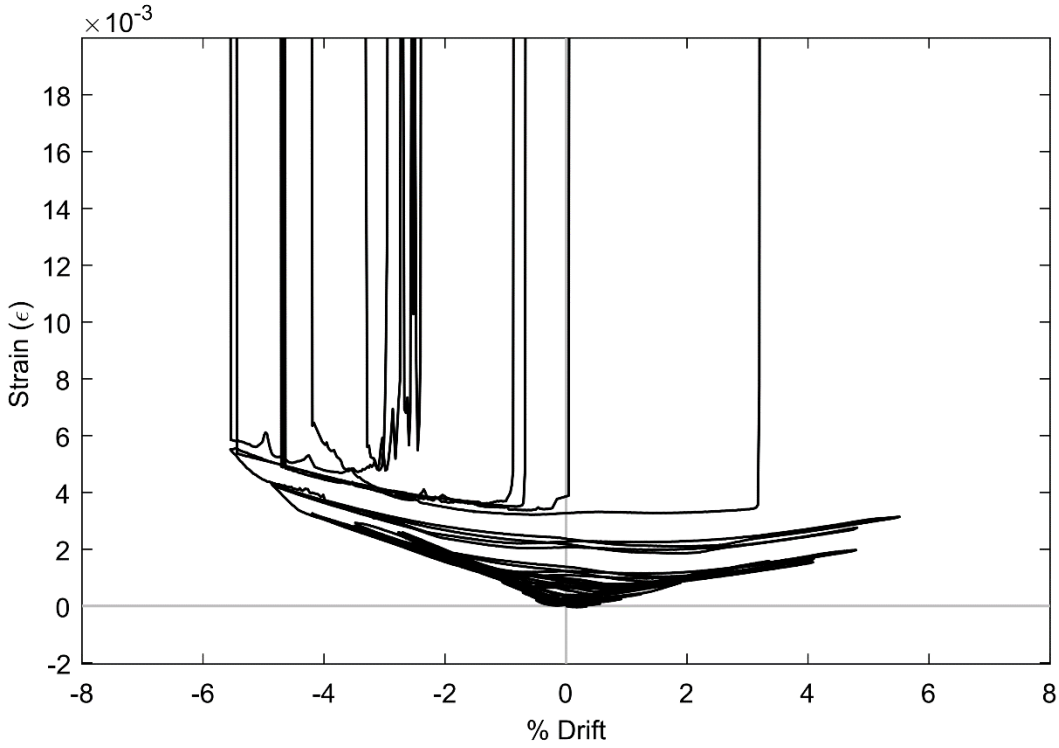

Figure 98: SG SBI7 (PTB_4.5_1_4)

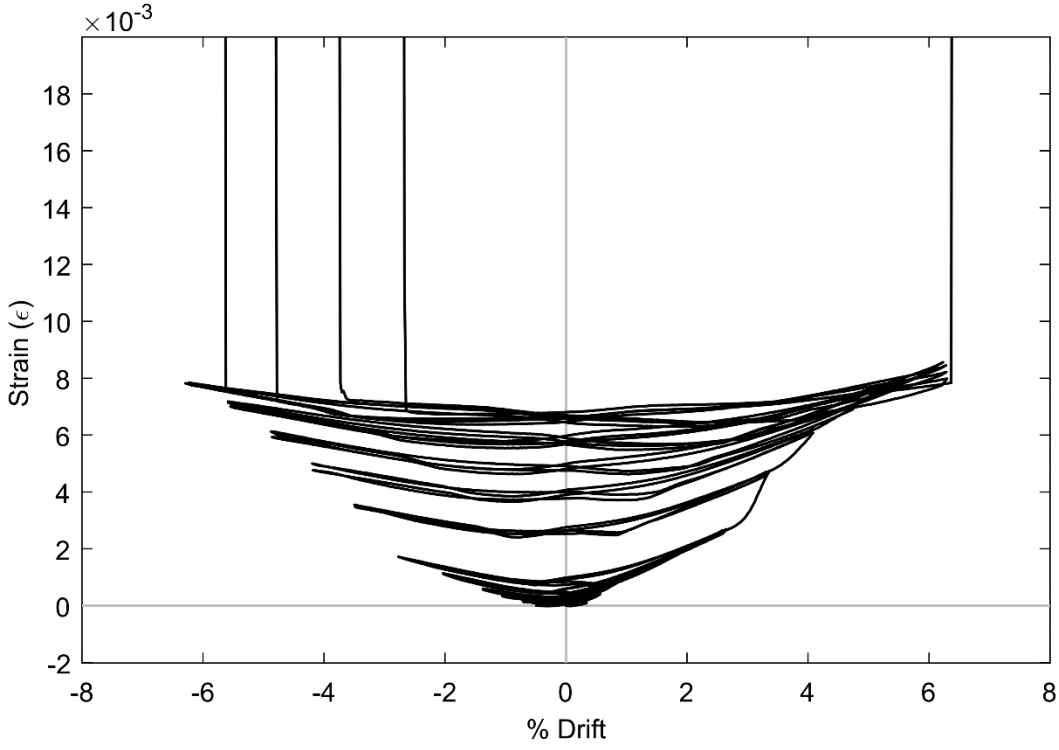

Figure 99: SG SBJ7 (PTB_4.5_1_4)

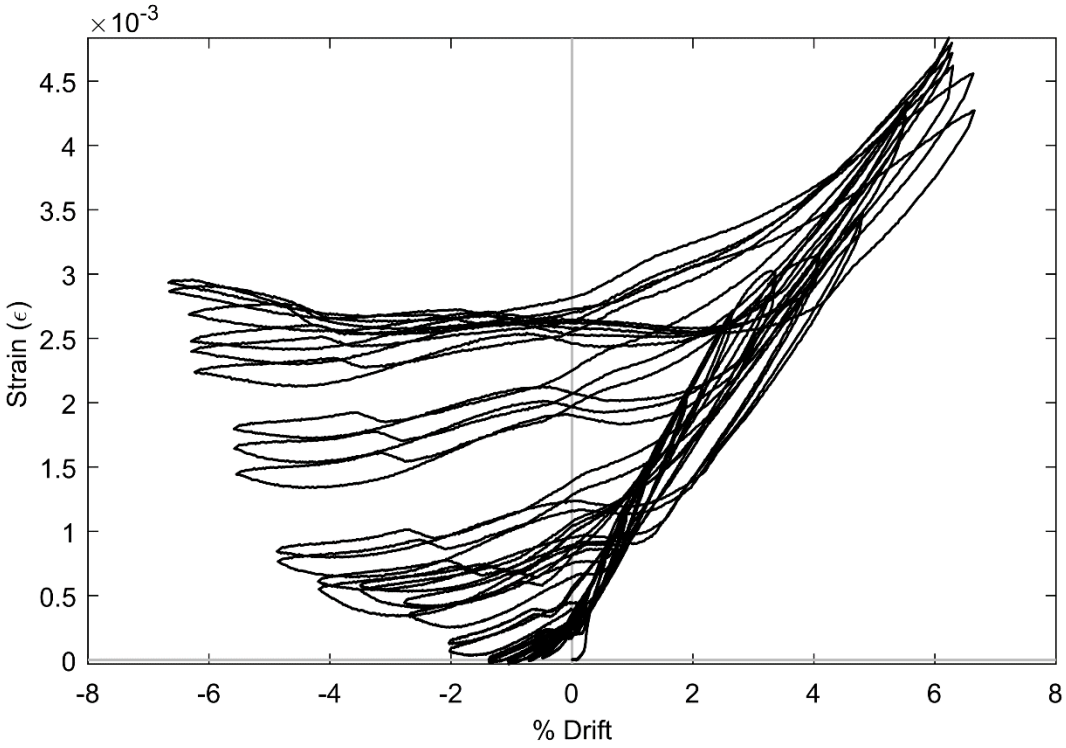

Figure 100: SG SBL7 (PTB_4.5_1_4)

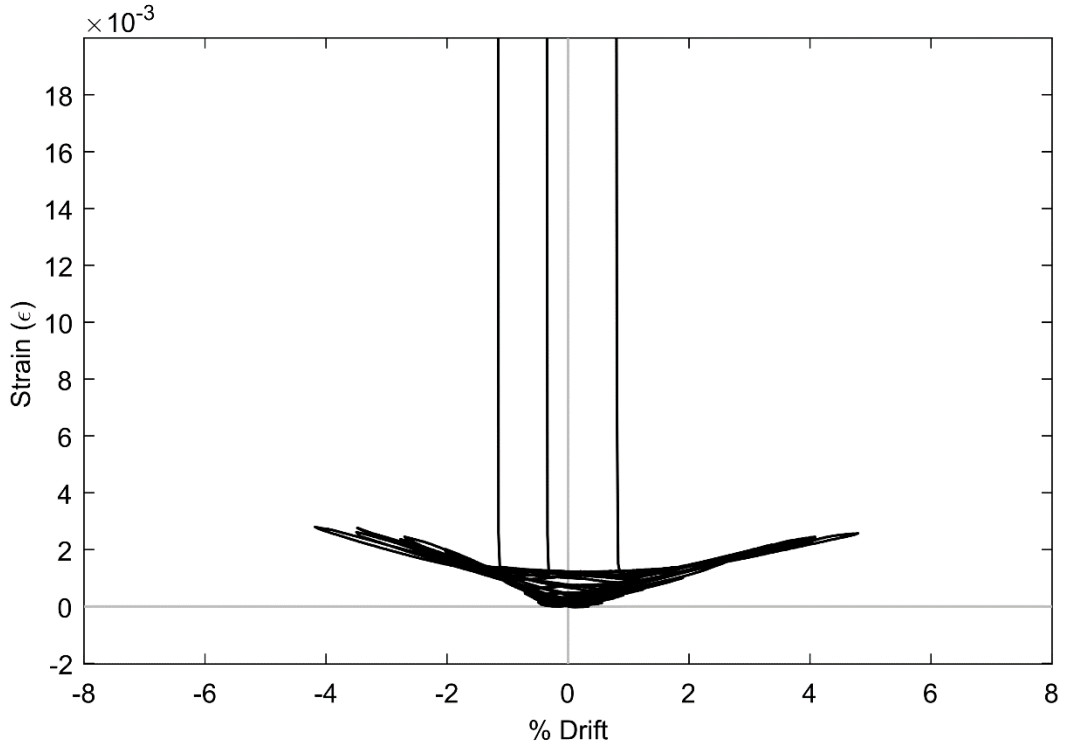

Figure 101: SG SBI8 (PTB_4.5_1_4)

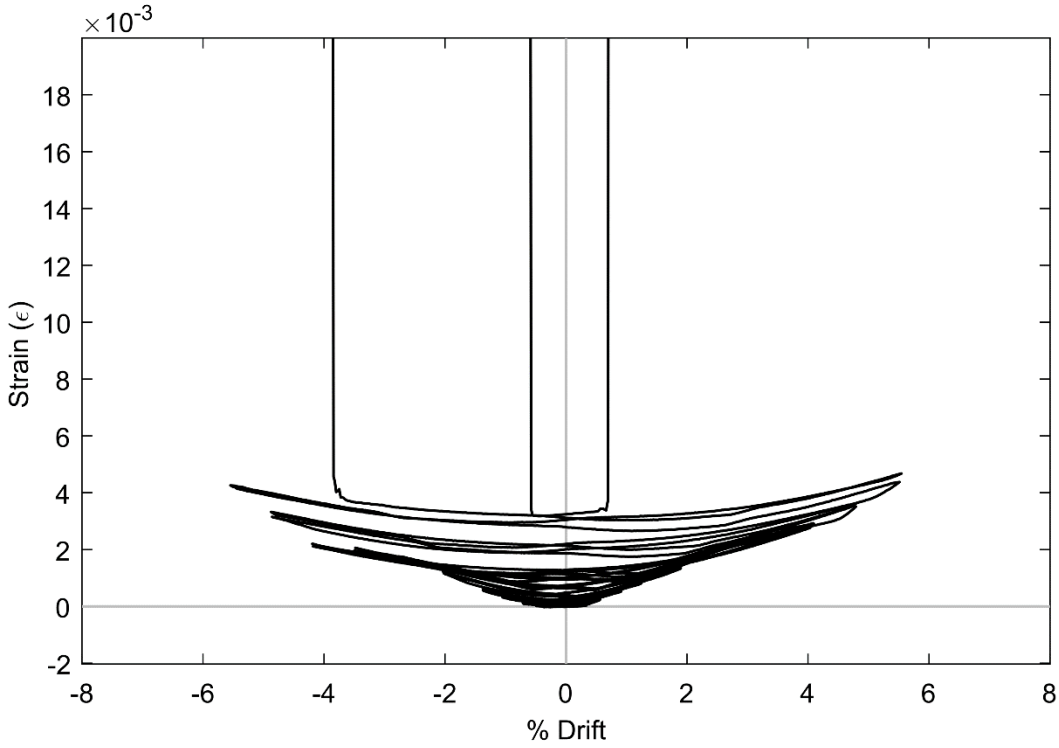

Figure 102: SG SBJ8 (PTB_4.5_1_4)

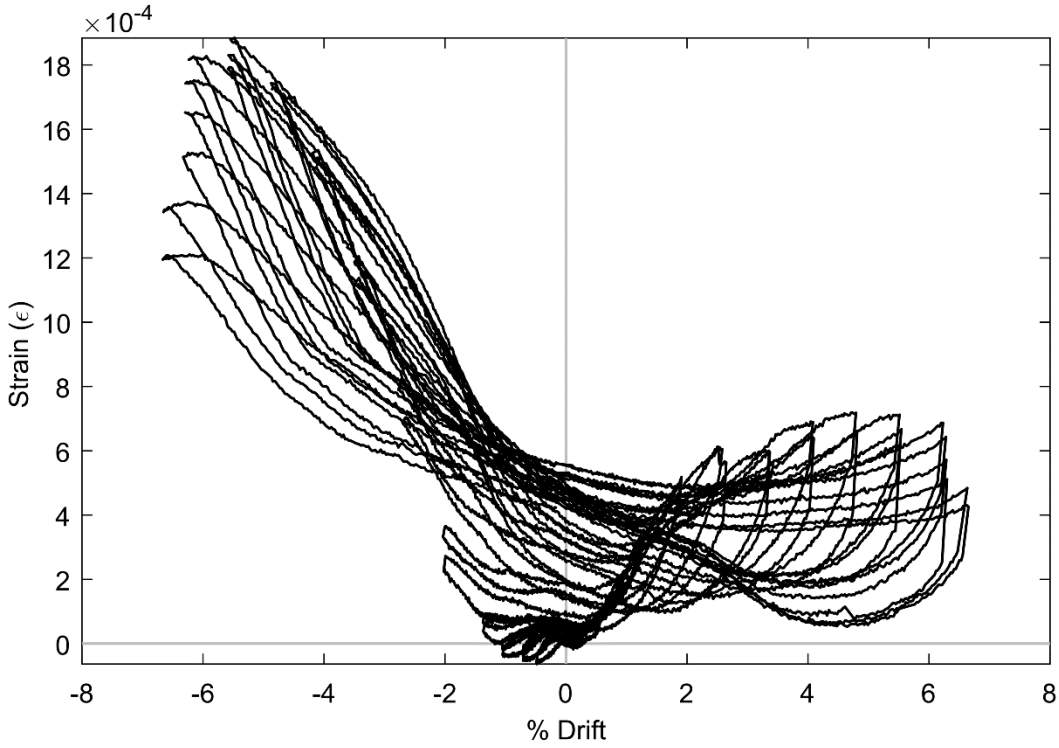

Figure 103: SG CC1 (PTB_4.5_1_4)

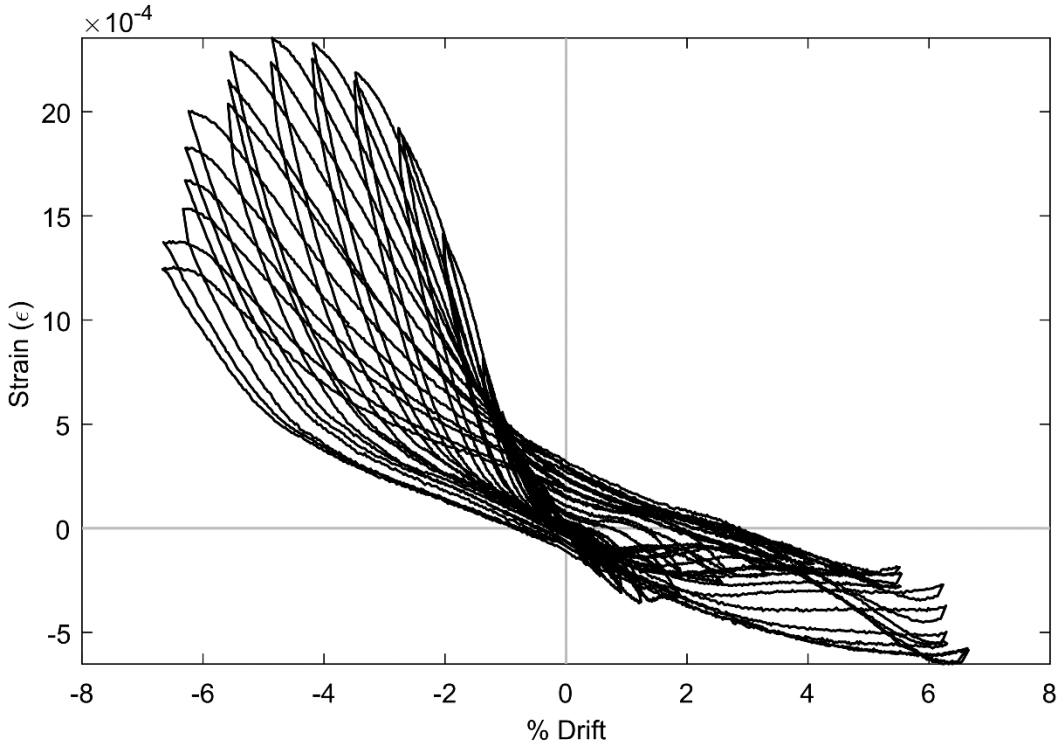

Figure 104: SG CC2 (PTB_4.5_1_4)

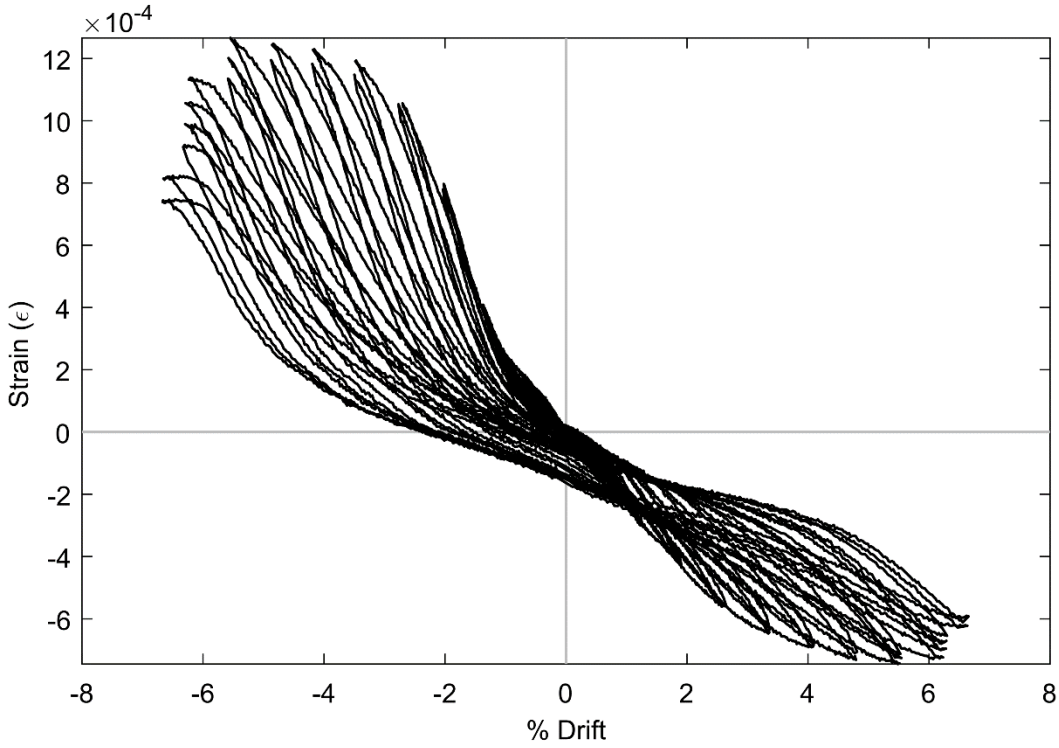

Figure 105: SG CC4 (PTB_4.5_1_4)

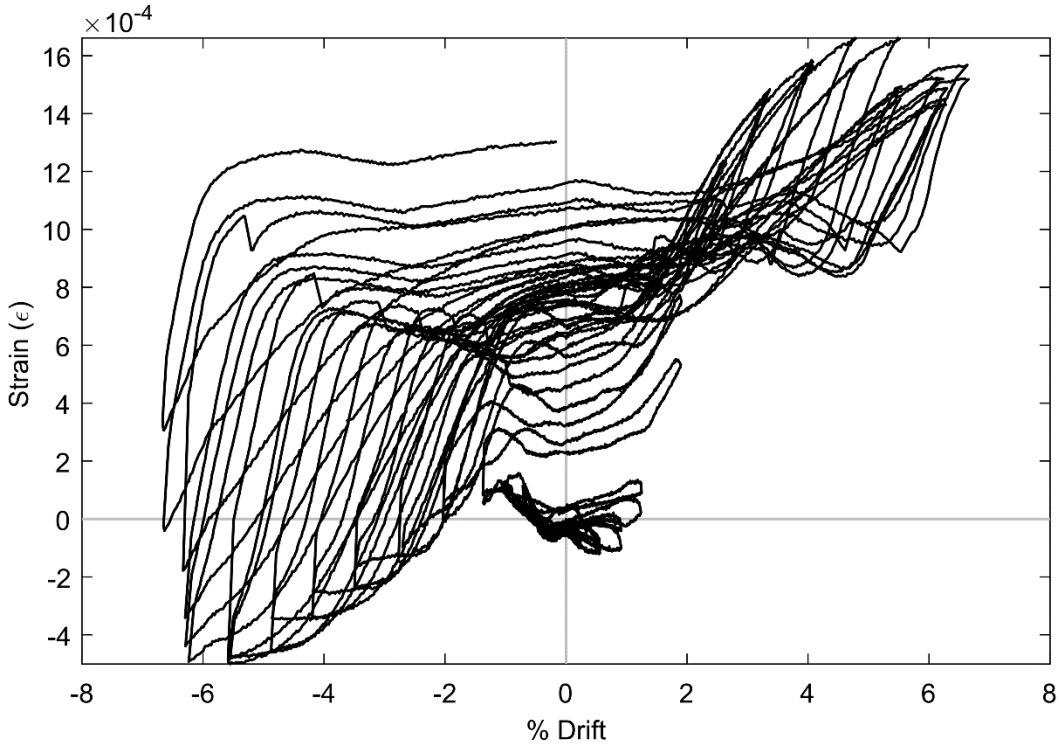

Figure 106: SG CH1 (PTB_4.5_1_4)

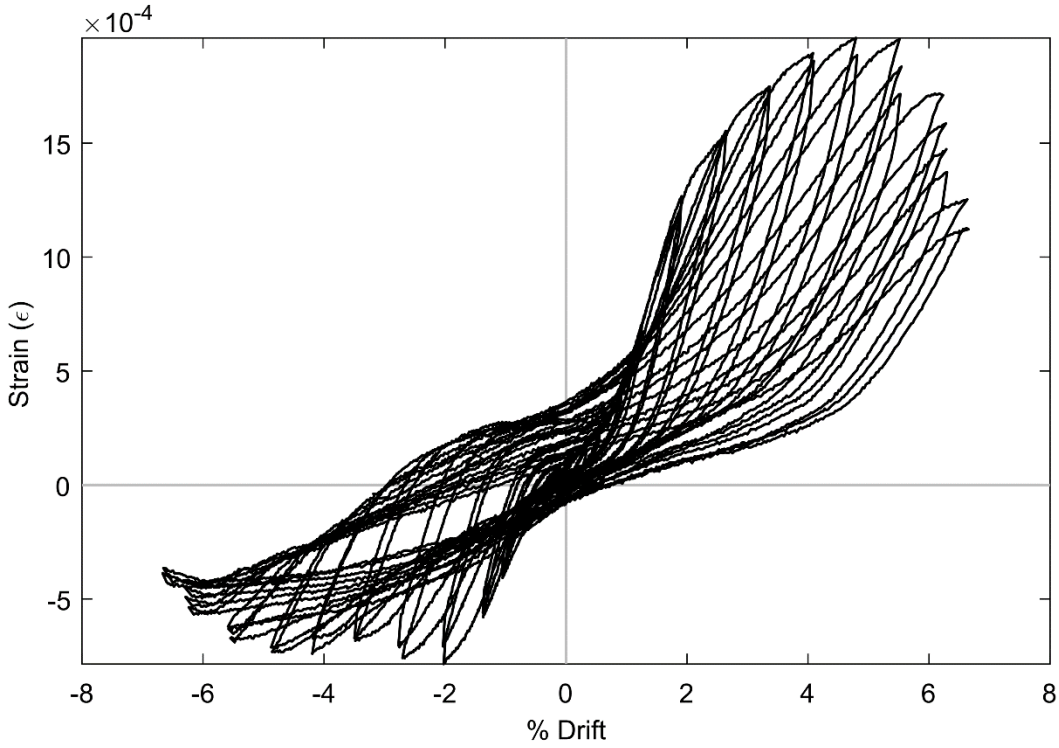

Figure 107: SG CH2 (PTB_4.5_1_4)

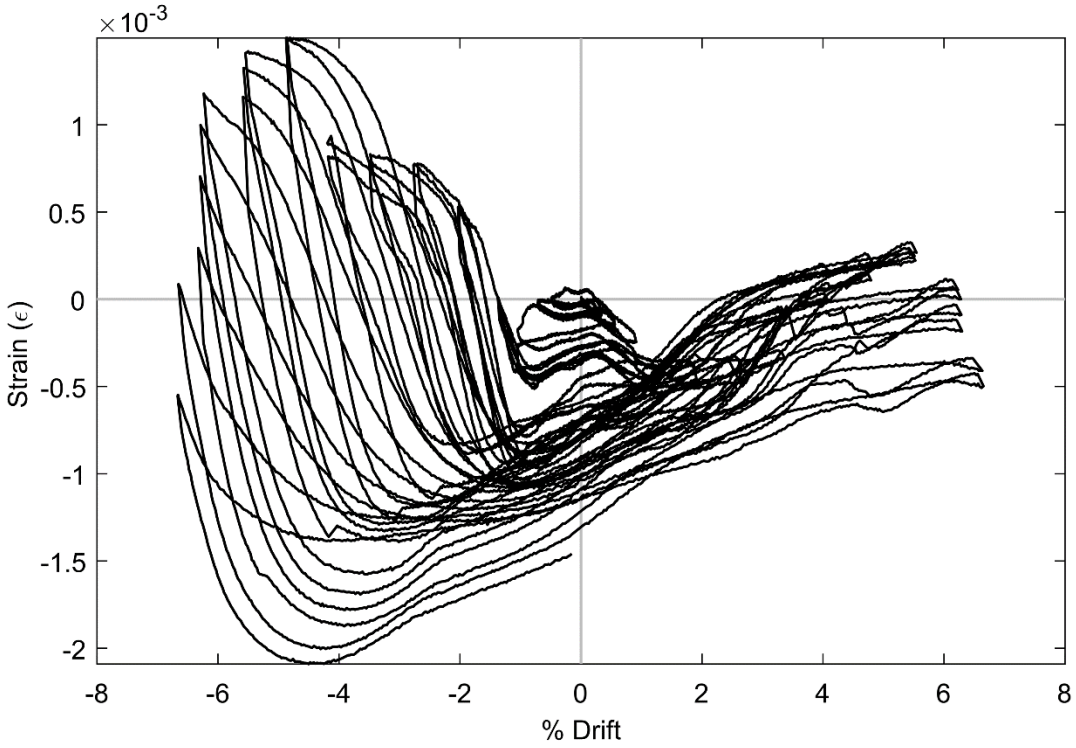

Figure 108: SG CI1 (PTB_4.5_1_4)

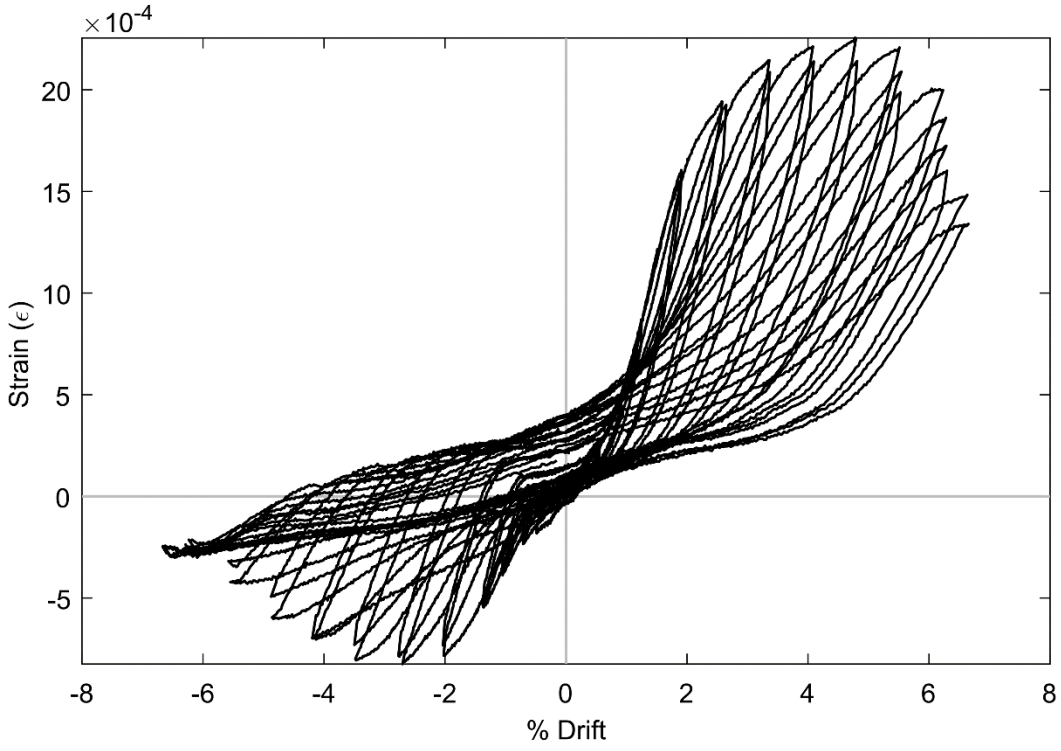

Figure 109: SG CI2 (PTB_4.5_1_4)

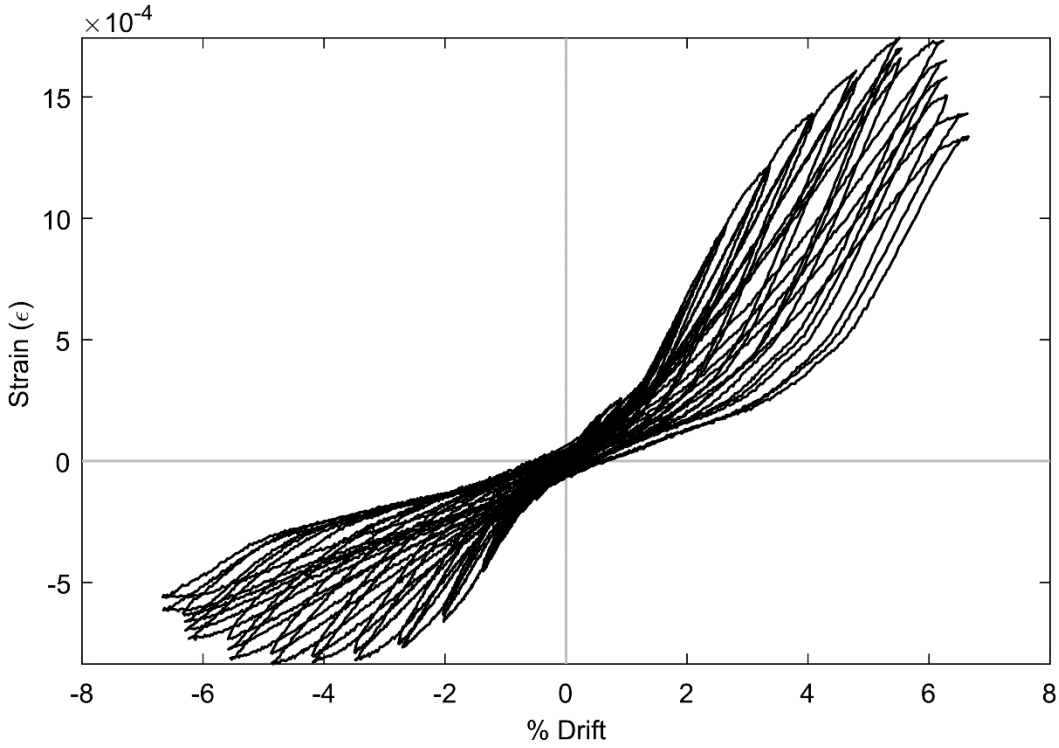

Figure 110: SG CI3 (PTB_4.5_1_4)

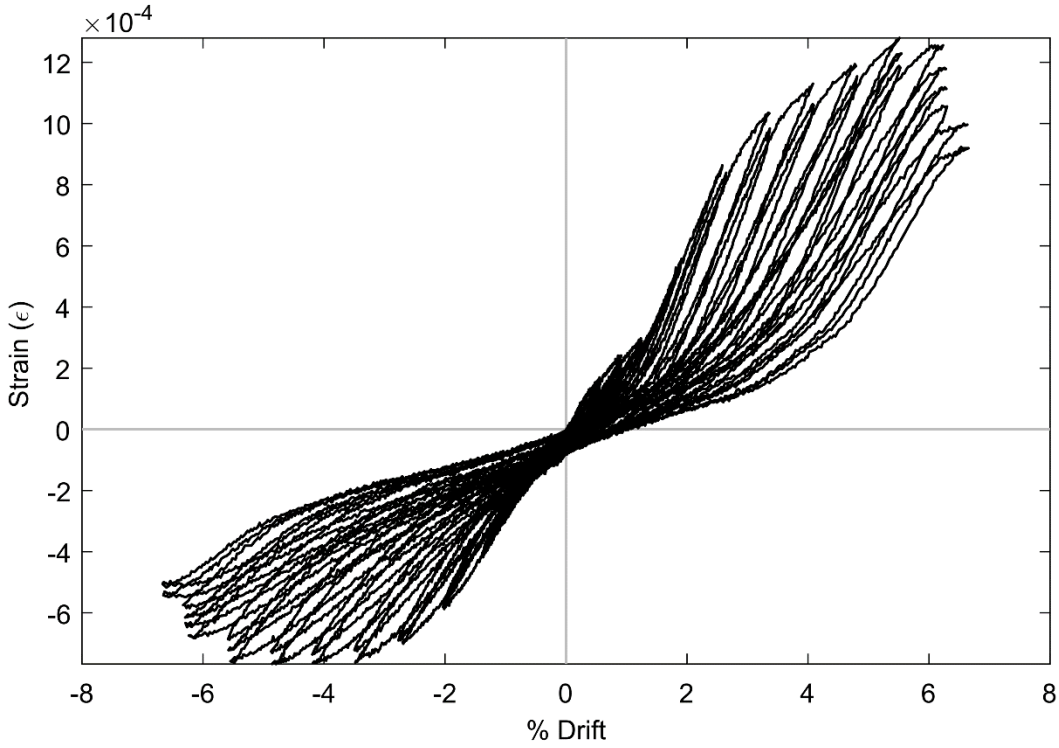

Figure 111: SG CI4 (PTB_4.5_1_4)

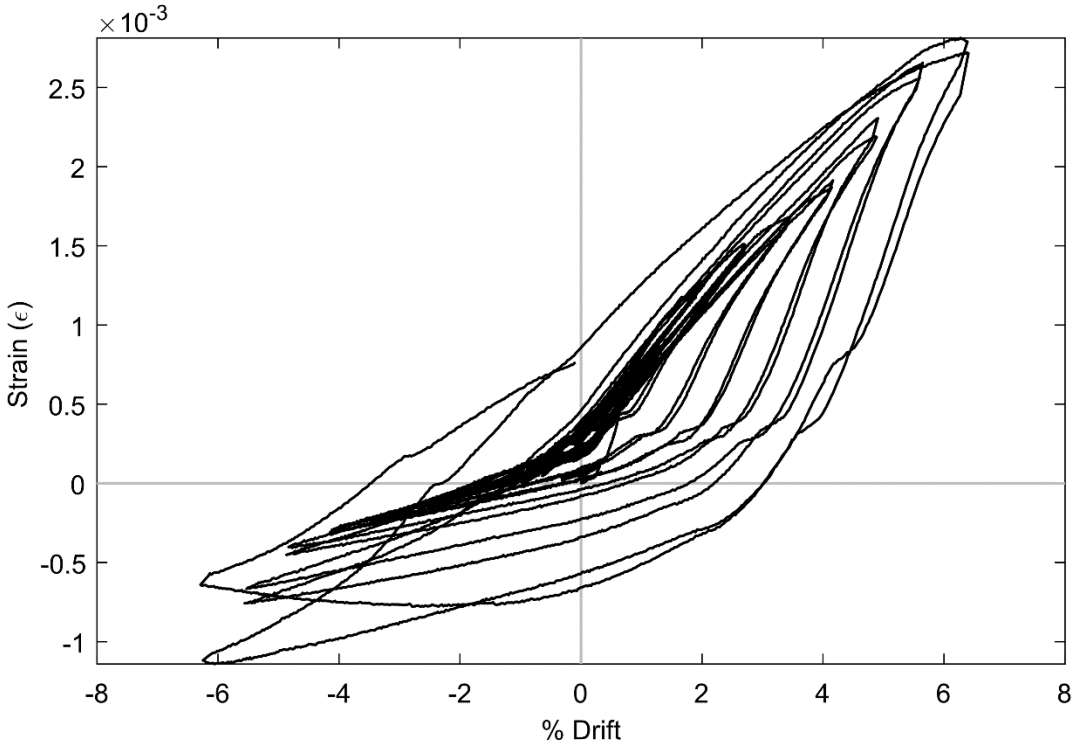

Figure 112: SG STE5 (PTB_9_2_0)

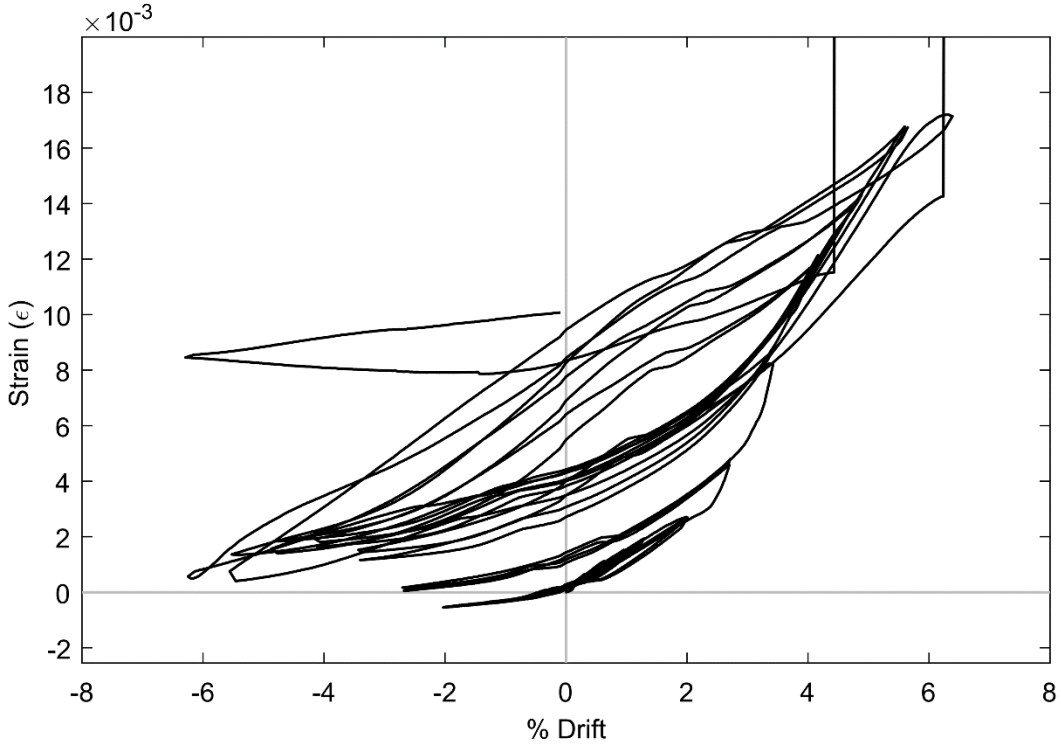

Figure 113: SG STG5 (PTB_9_2_0)

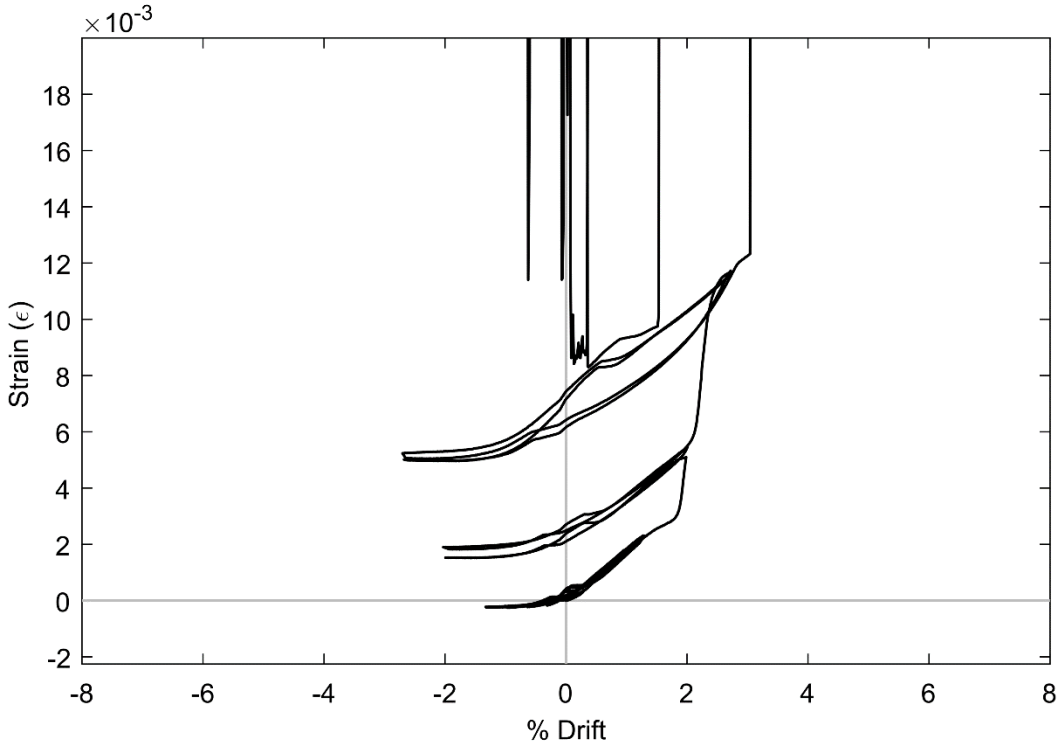

Figure 114: SG STH5 (PTB_9_2_0)

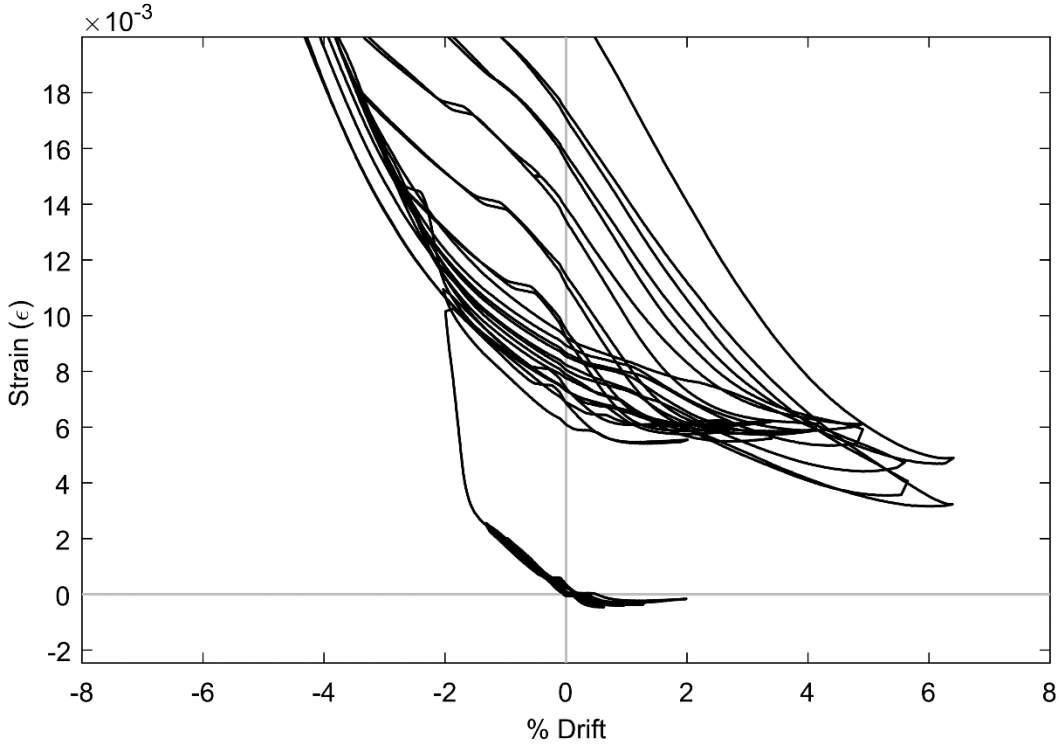

Figure 115: SG STK5 (PTB_9_2_0)

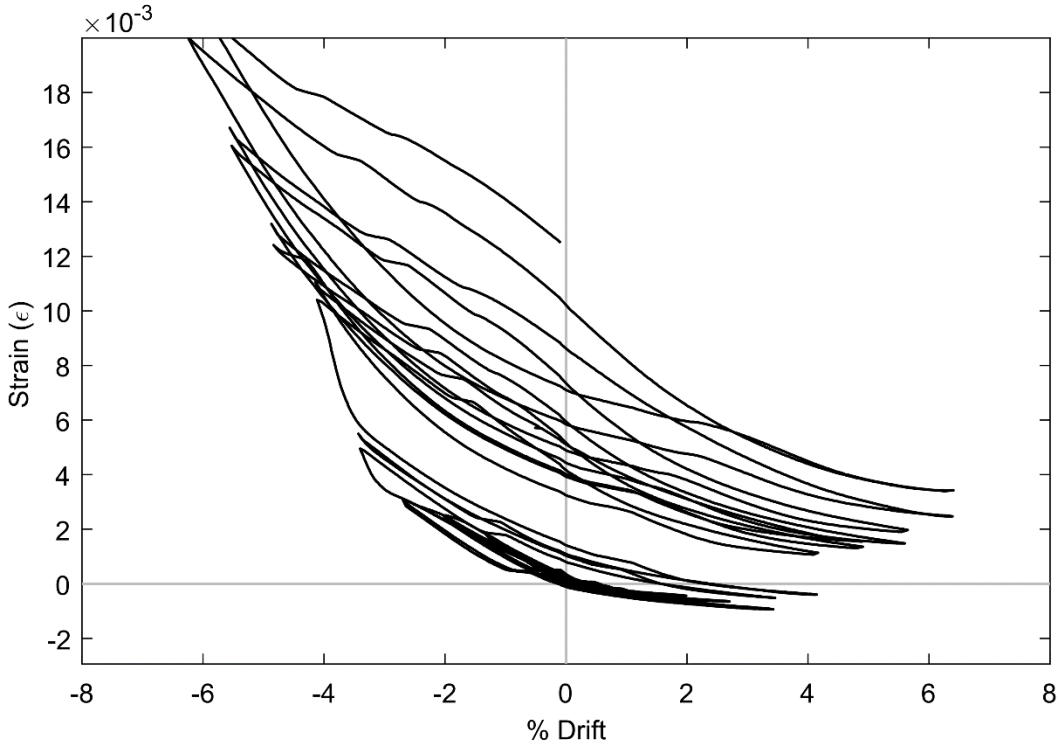

Figure 116: SG STL5 (PTB_9_2_0)

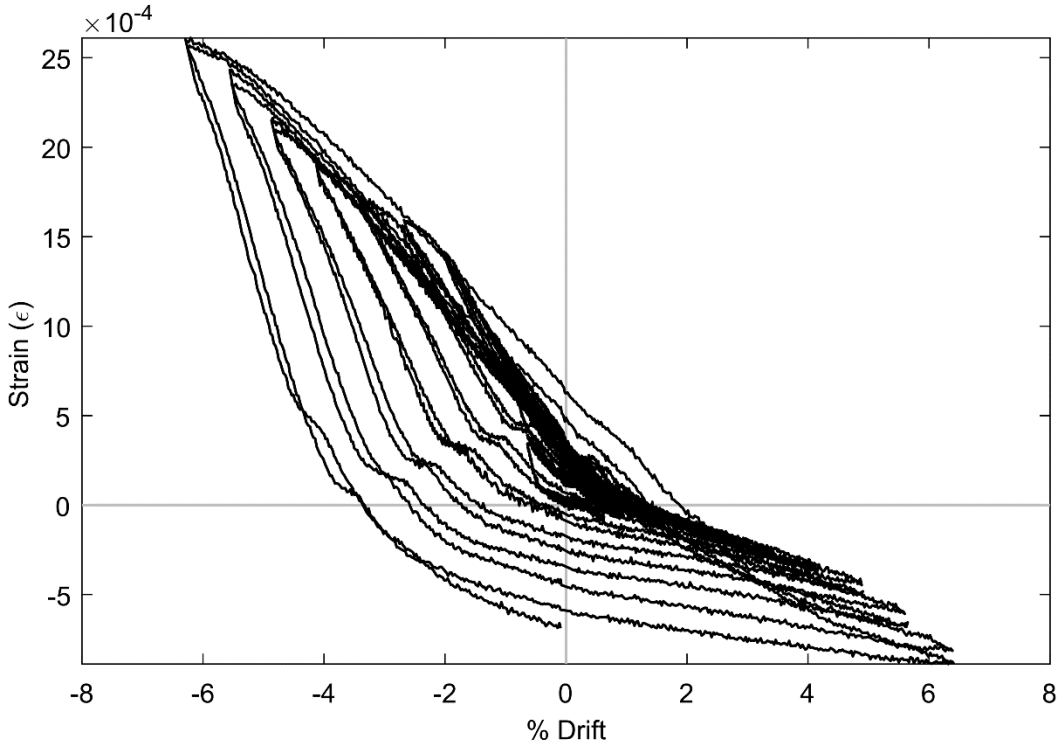

Figure 117: SG STN5 (PTB_9_2_0)

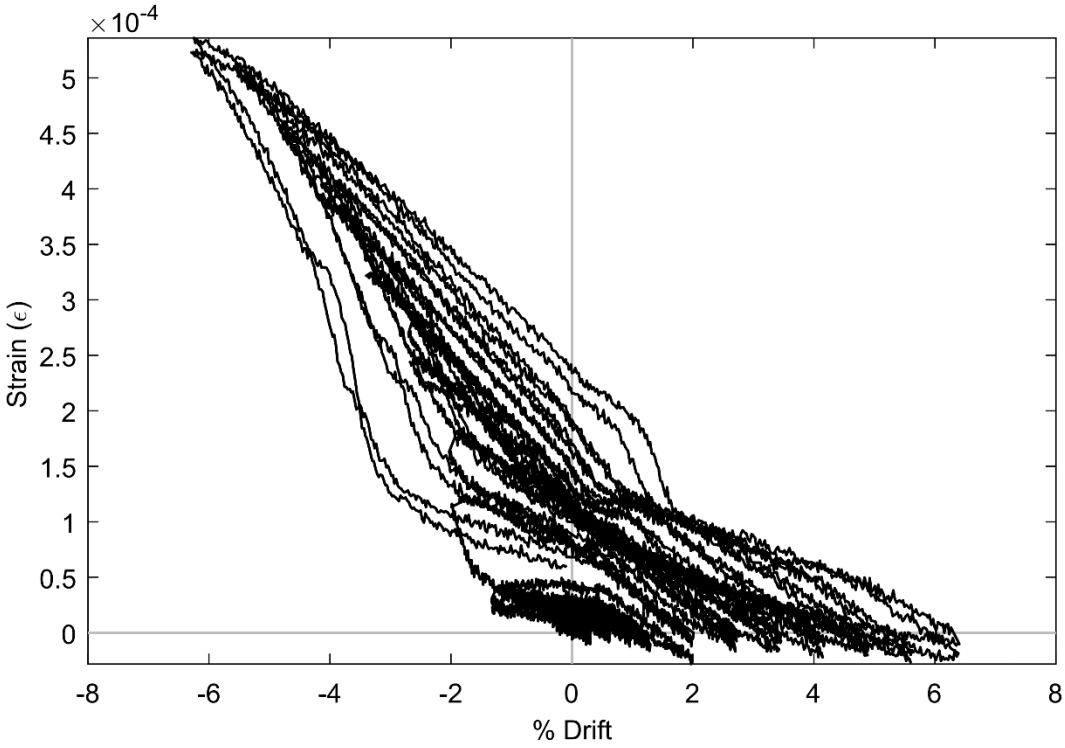

Figure 118: SG STP5 (PTB_9_2_0)

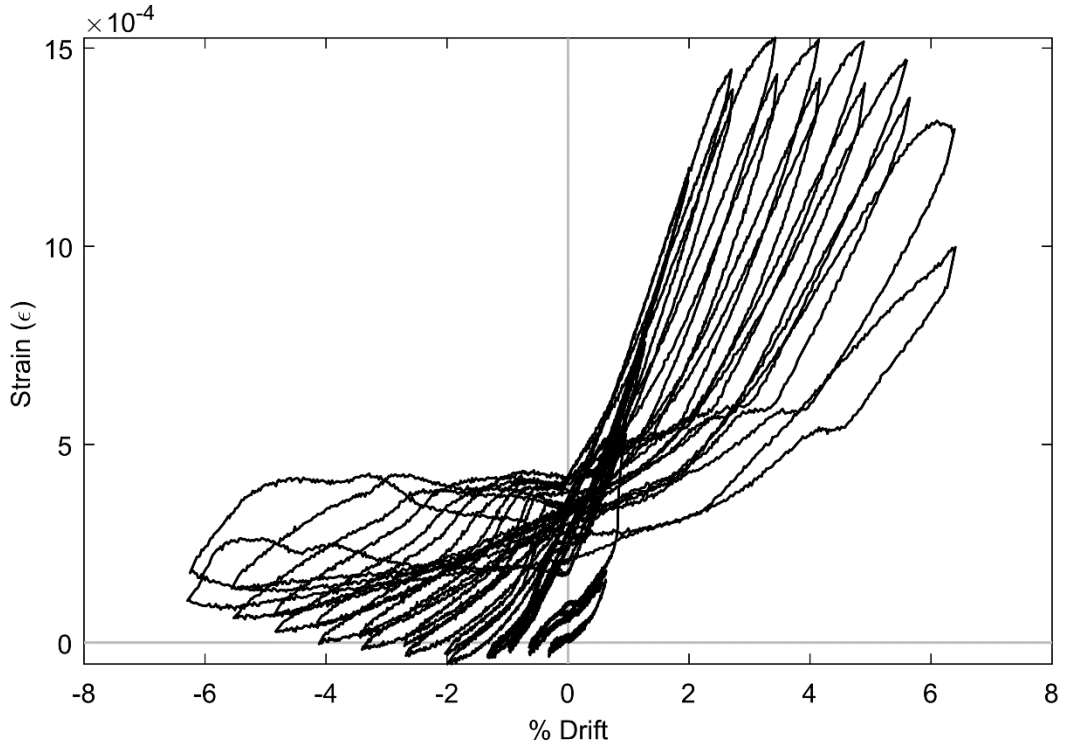

Figure 119: SG STE6 (PTB_9_2_0)

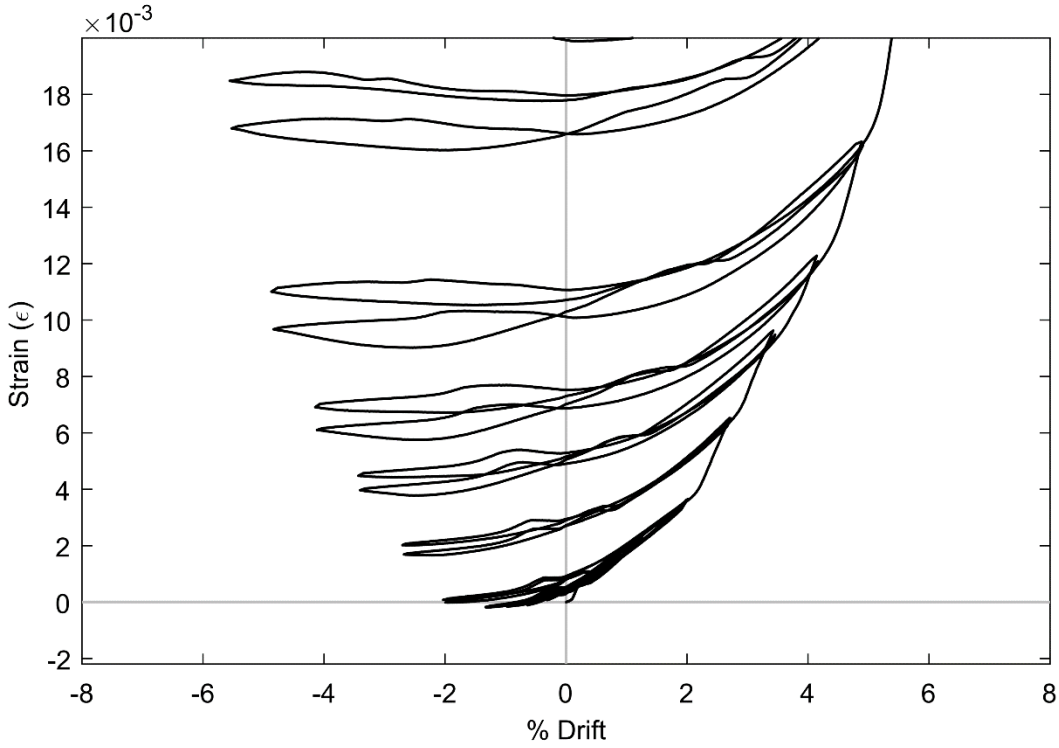

Figure 120: SG STG6 (PTB_9_2_0)

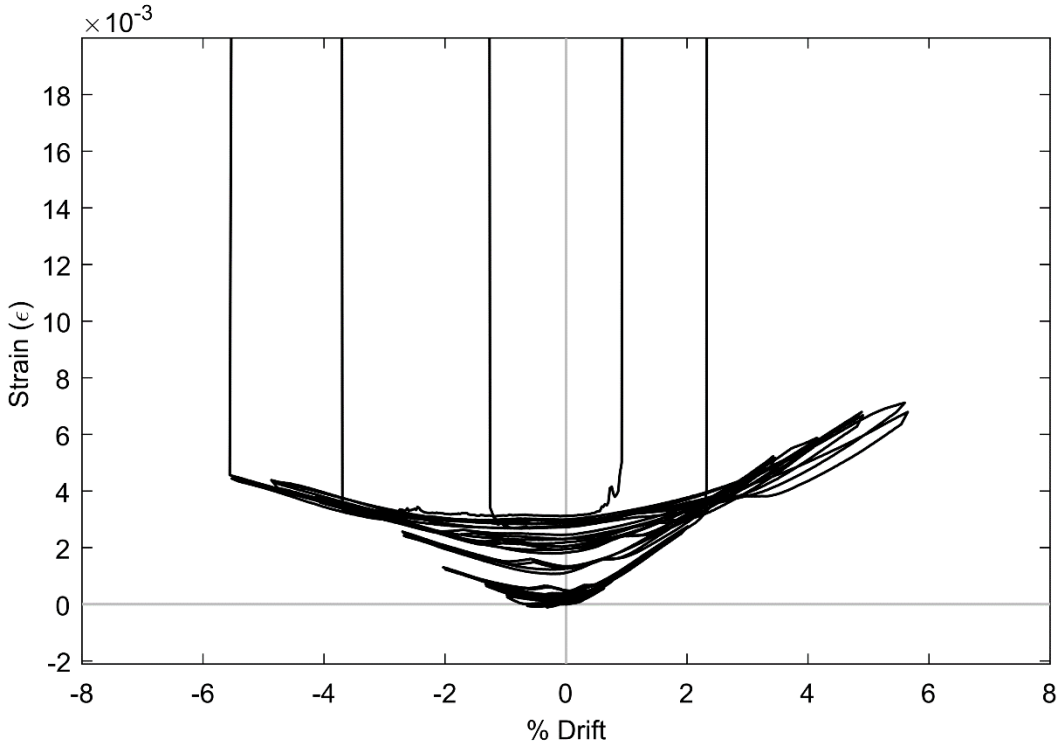

Figure 121: SG STI6 (PTB_9_2_0)

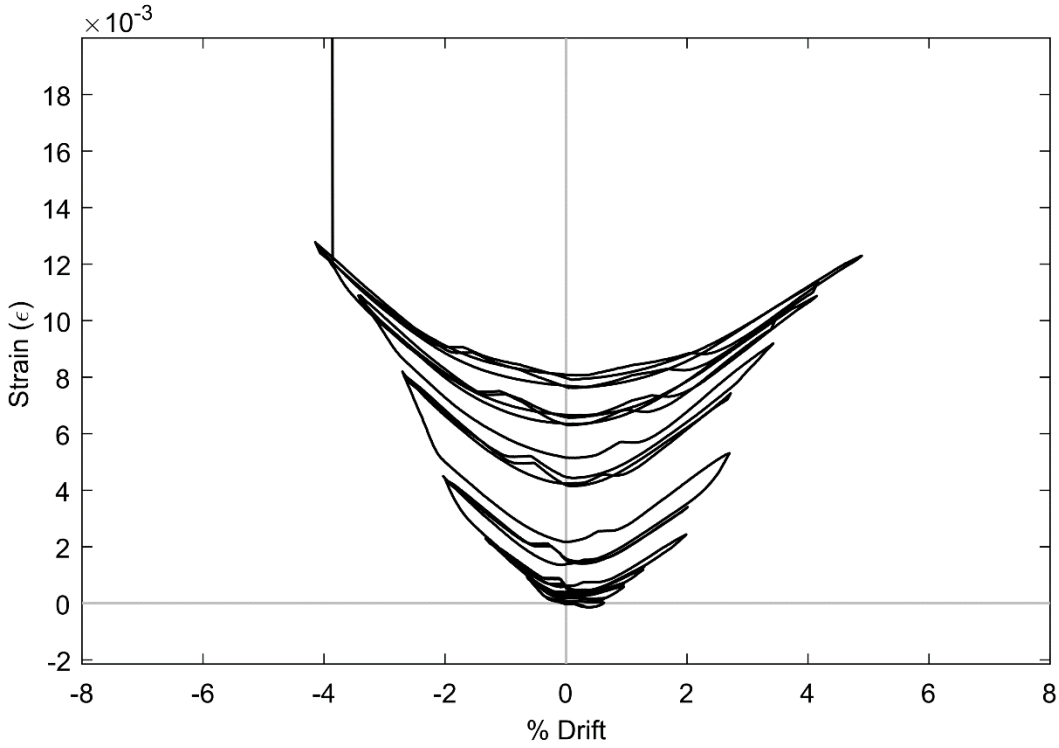

Figure 122: SG STJ6 (PTB_9_2_0)

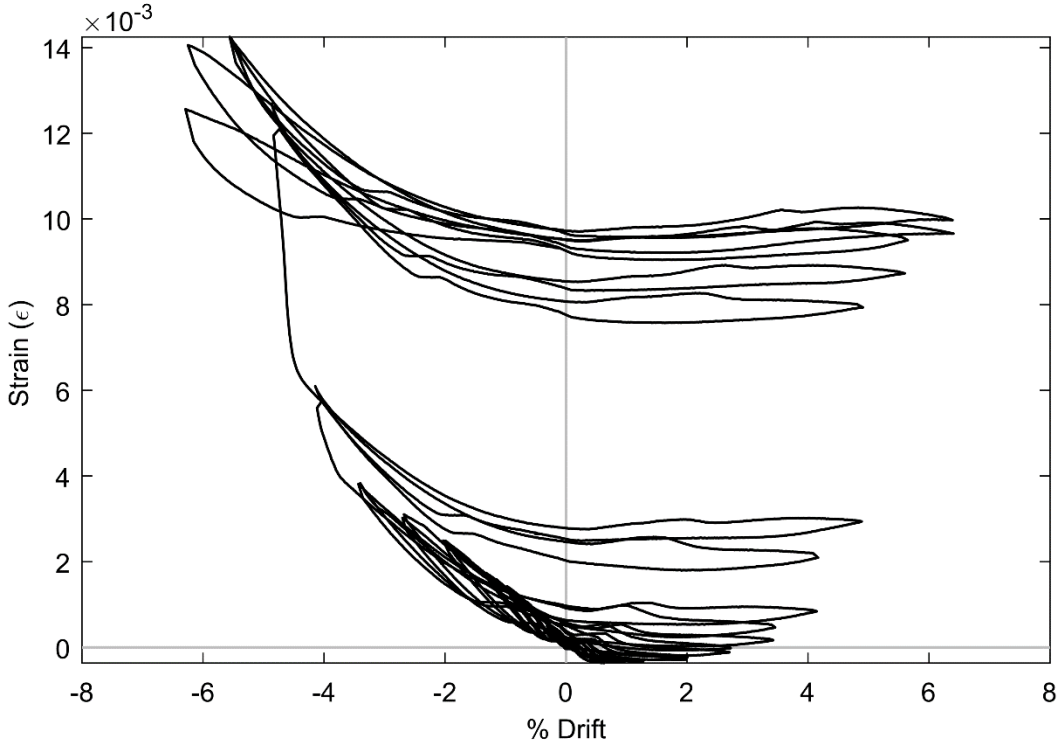

Figure 123: SG STL6 (PTB_9_2_0)

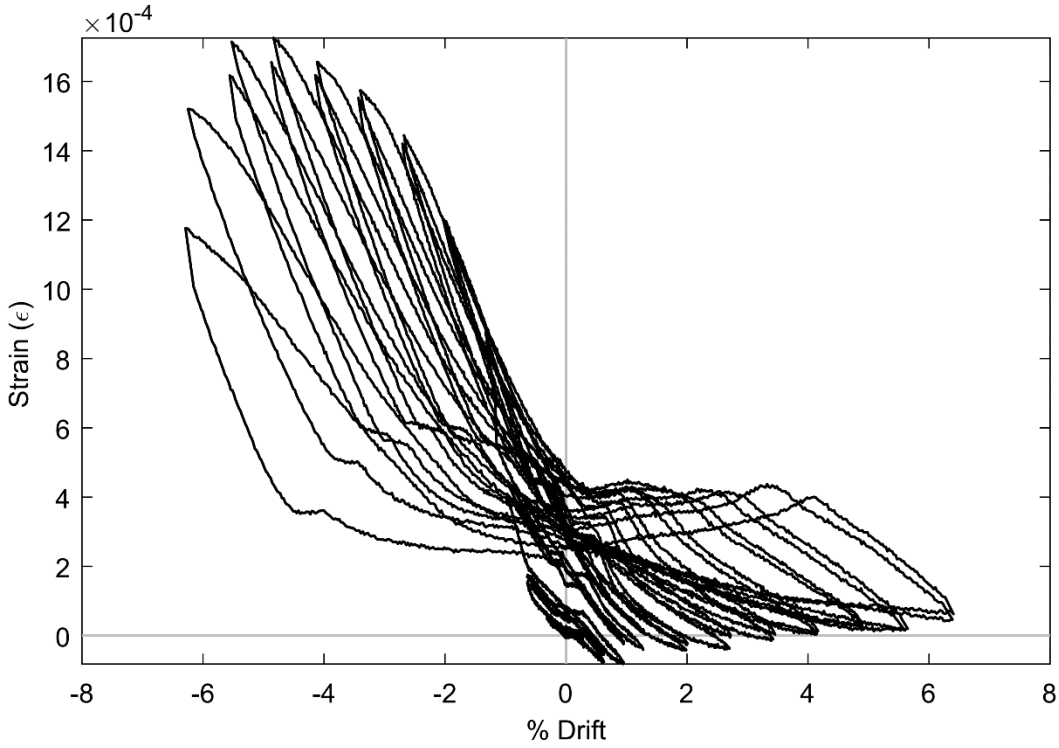

Figure 124: SG STN6 (PTB_9_2_0)

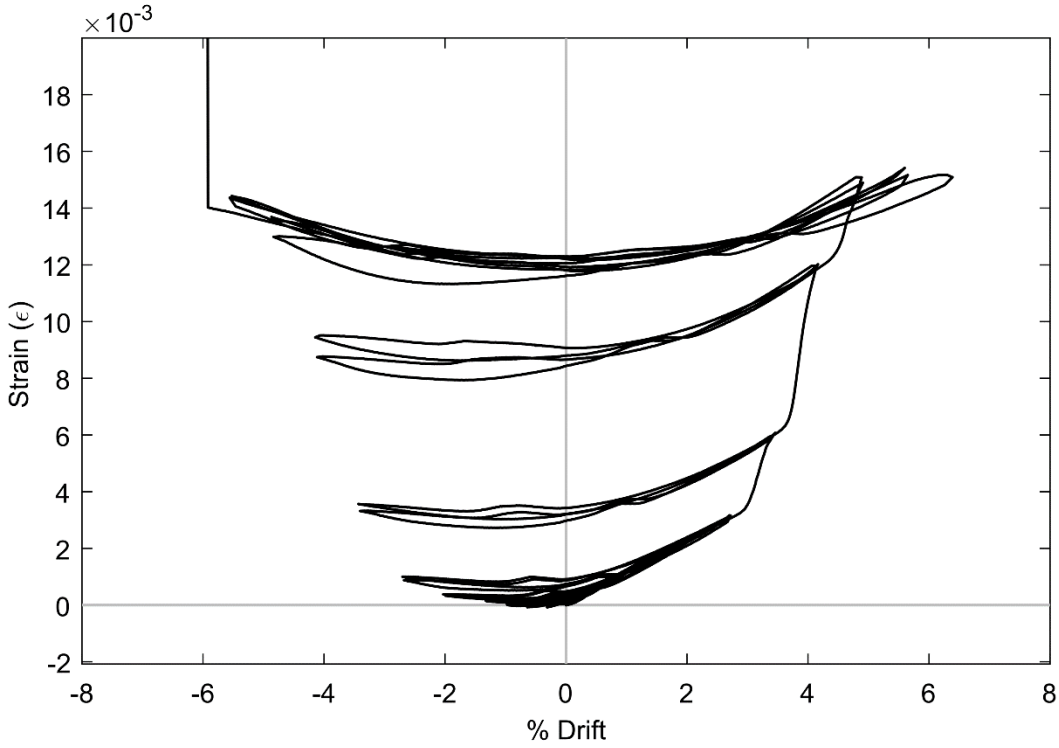

Figure 125: SG STG7 (PTB_9_2_0)

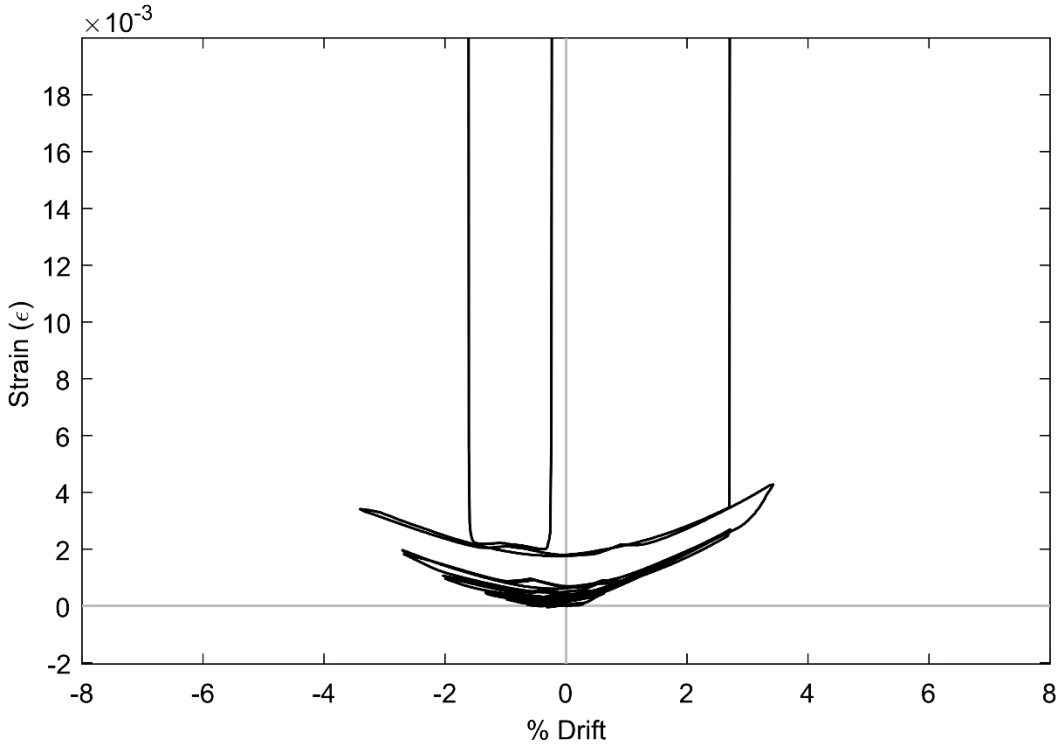

Figure 126: SG STI7 (PTB_9_2_0)

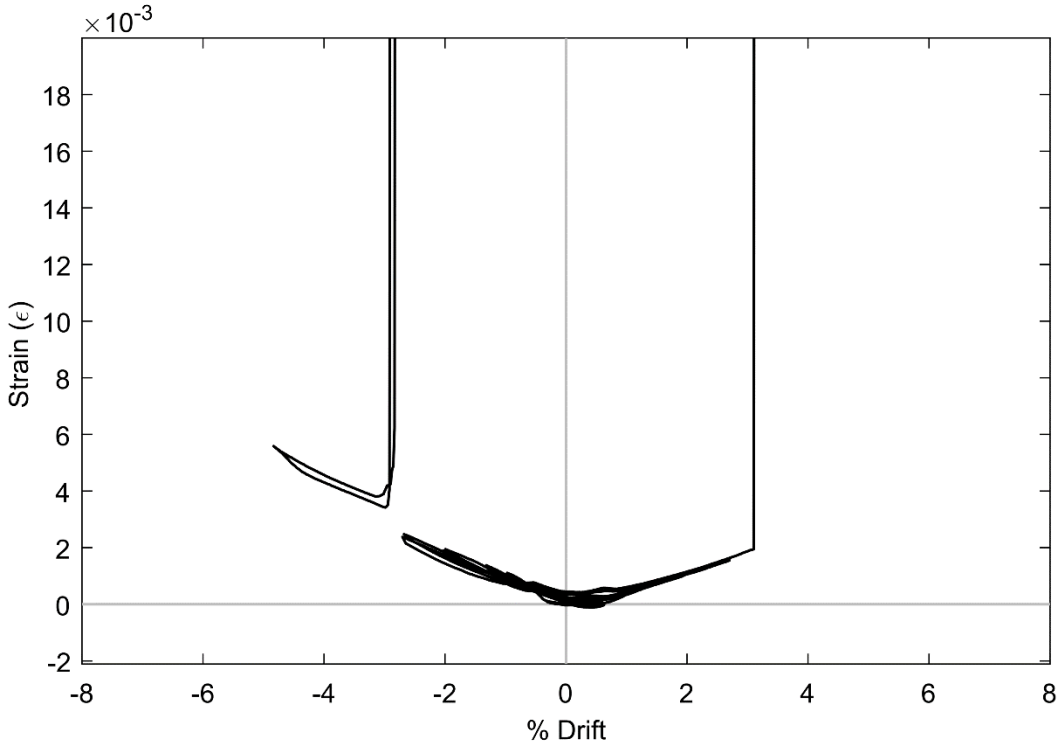

Figure 127: SG STJ7 (PTB_9_2_0)

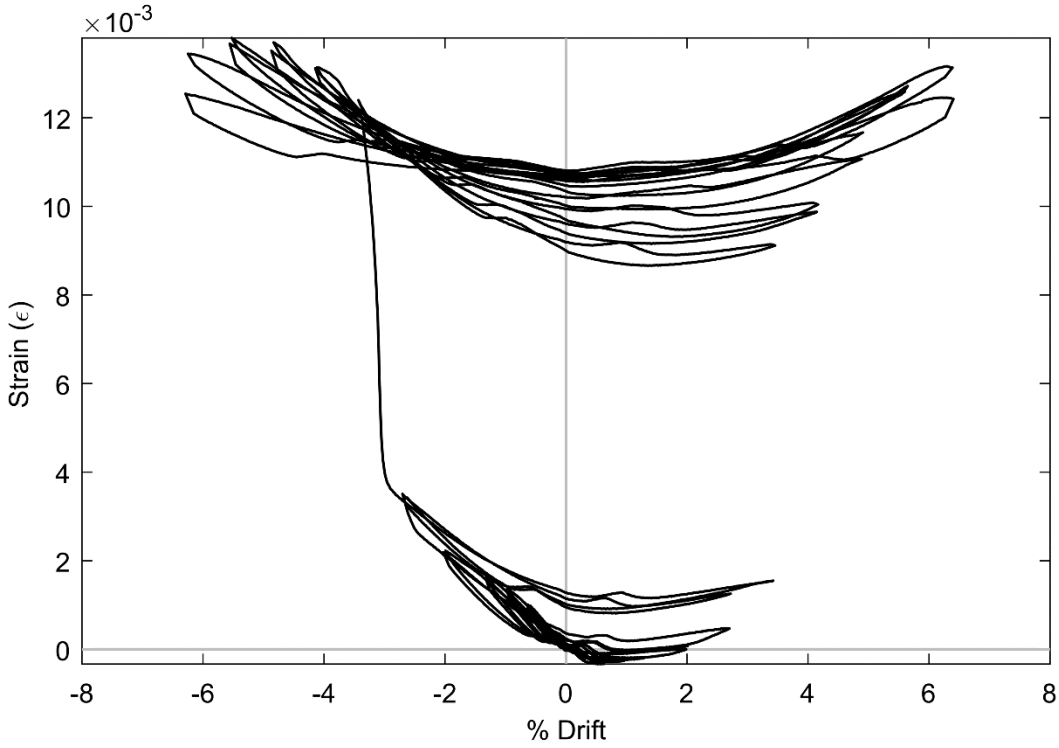

Figure 128: SG STL7 (PTB_9_2_0)

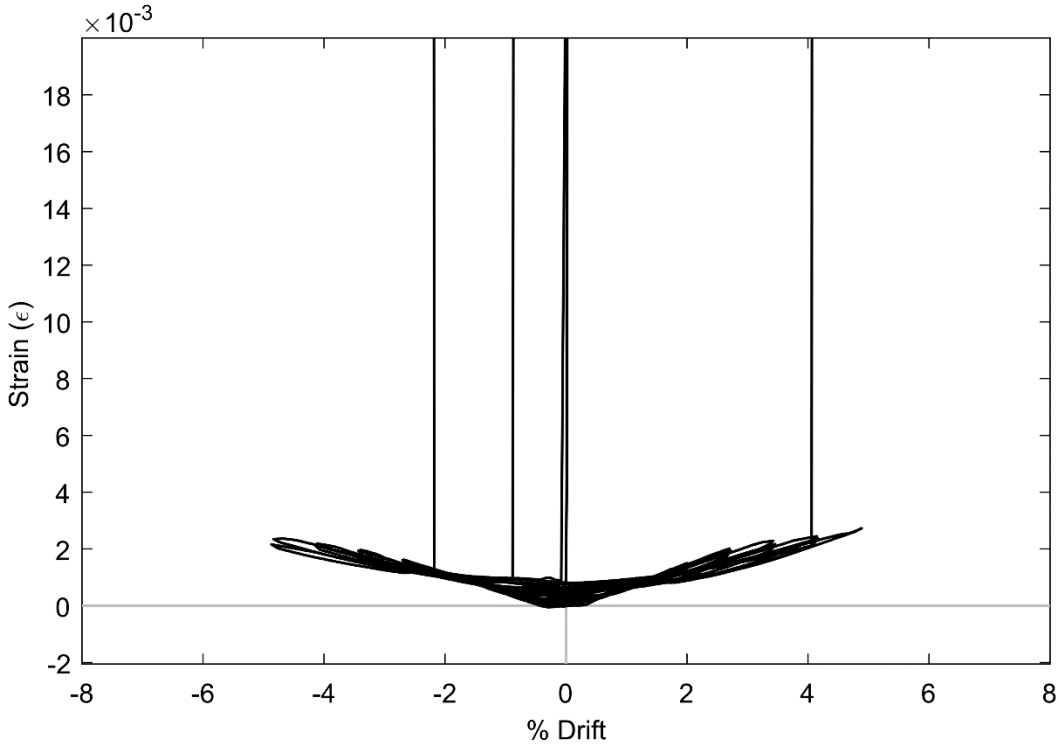

Figure 129: SG STI8 (PTB_9_2_0)

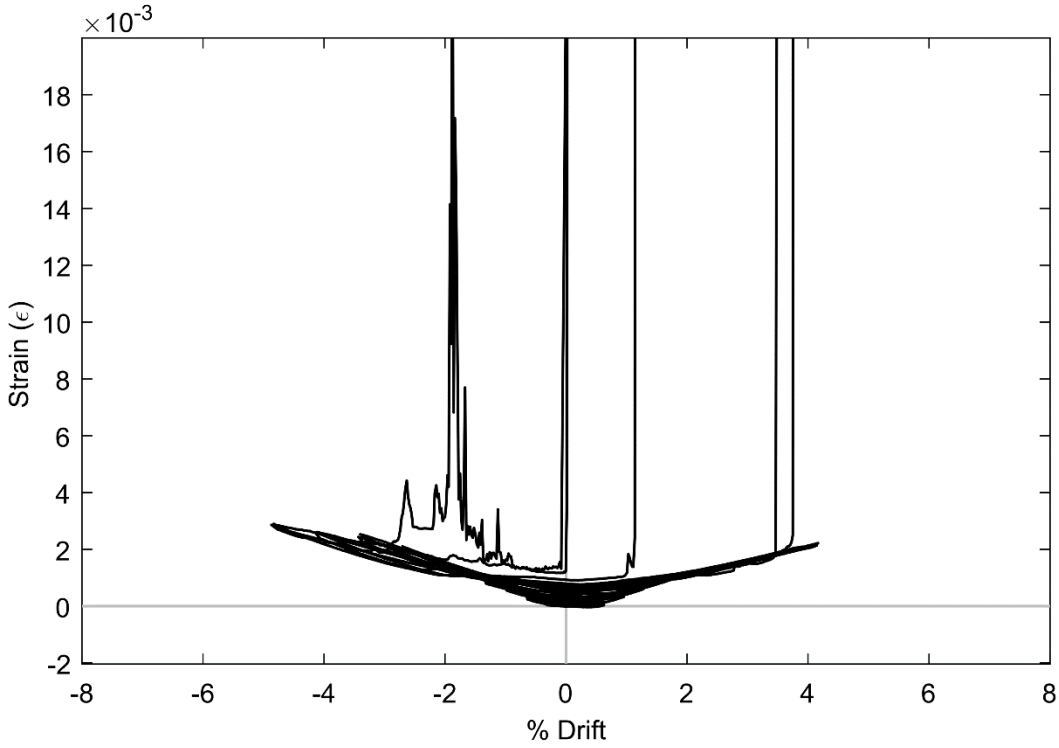

Figure 130: SG STJ8 (PTB_9_2_0)

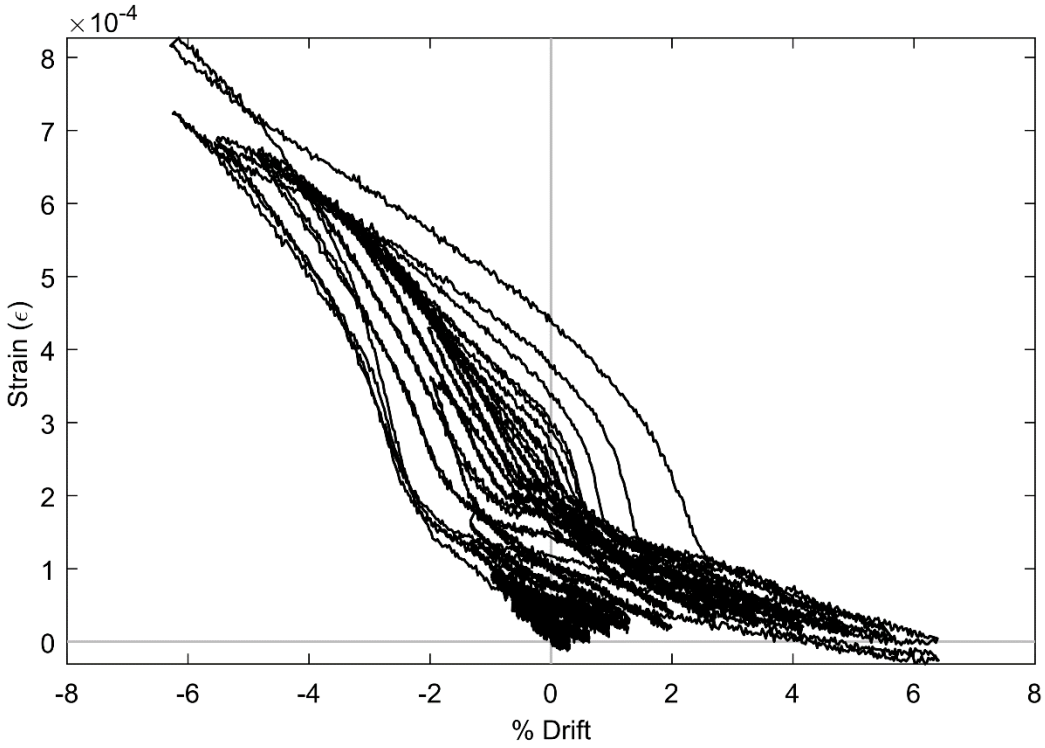

Figure 131: SG SBC5 (PTB_9_2_0)

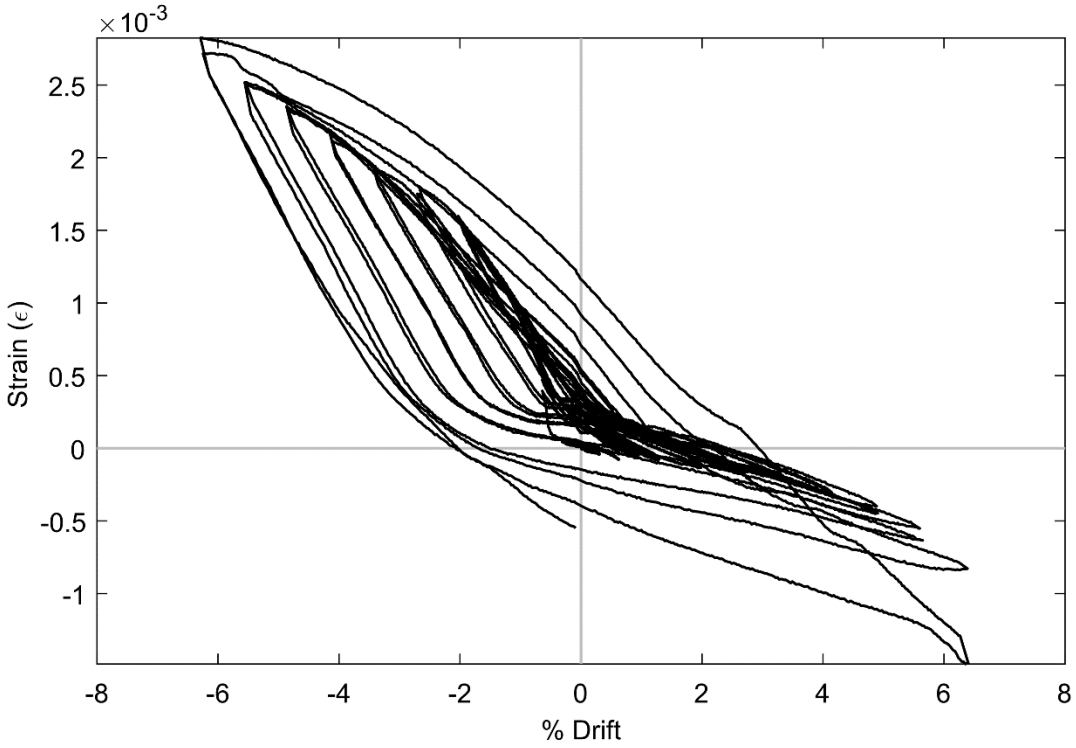

Figure 132: SG SBE5 (PTB_9_2_0)

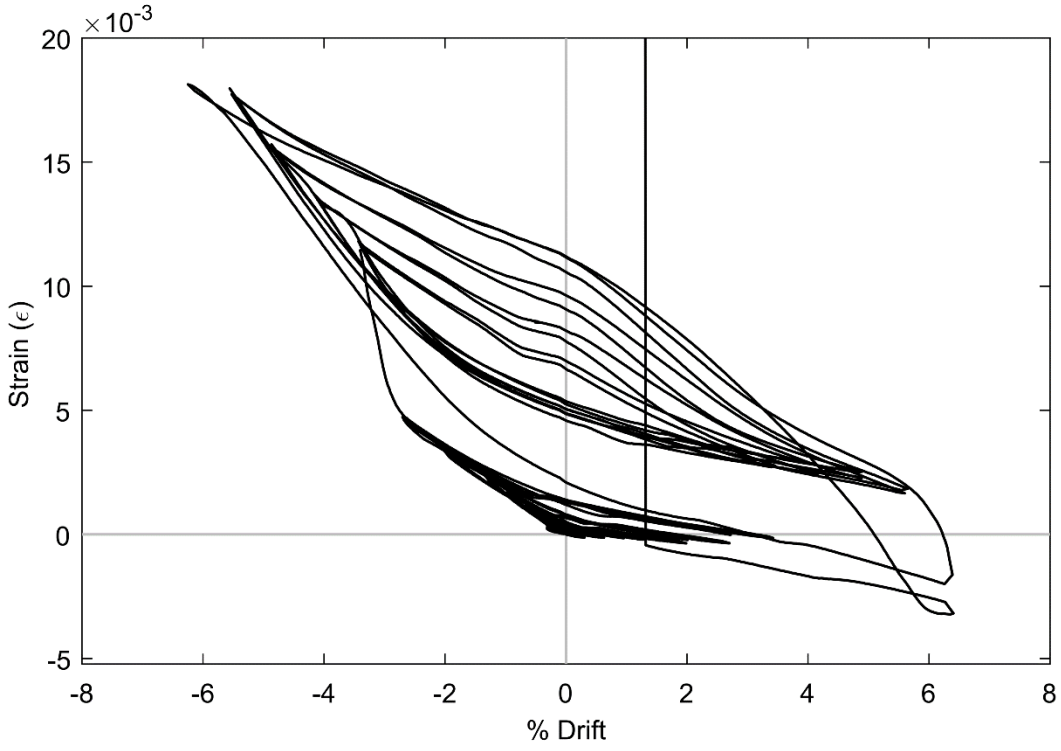

Figure 133: SG SBG5 (PTB_9_2_0)

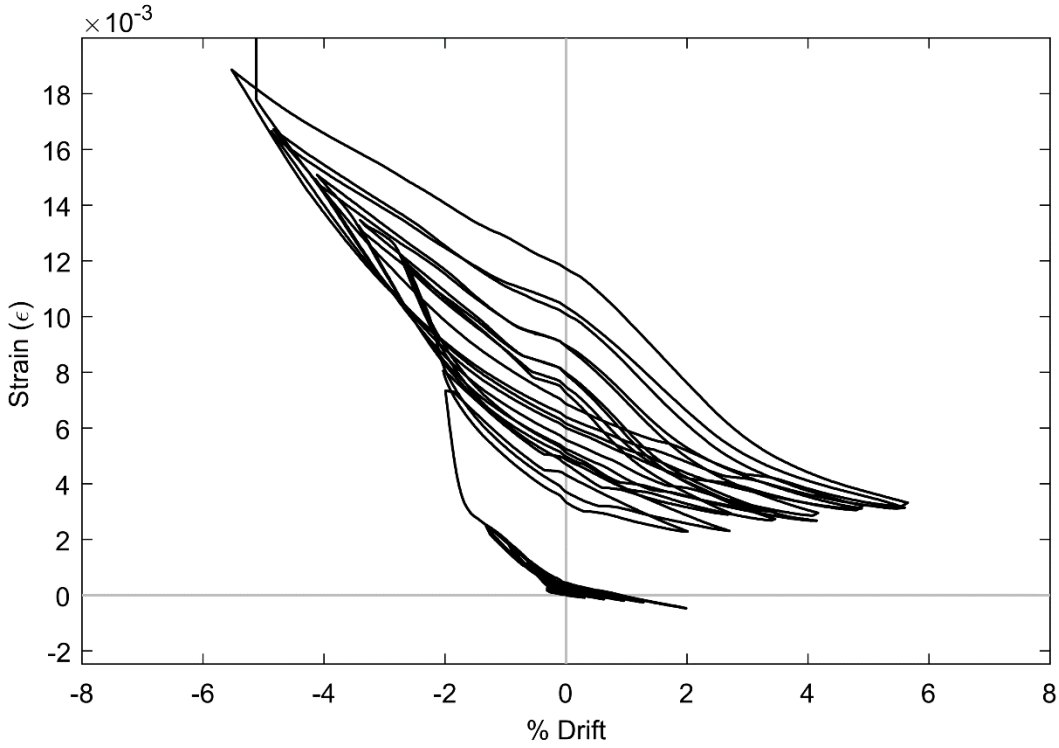

Figure 134: SG SBH5 (PTB_9_2_0)

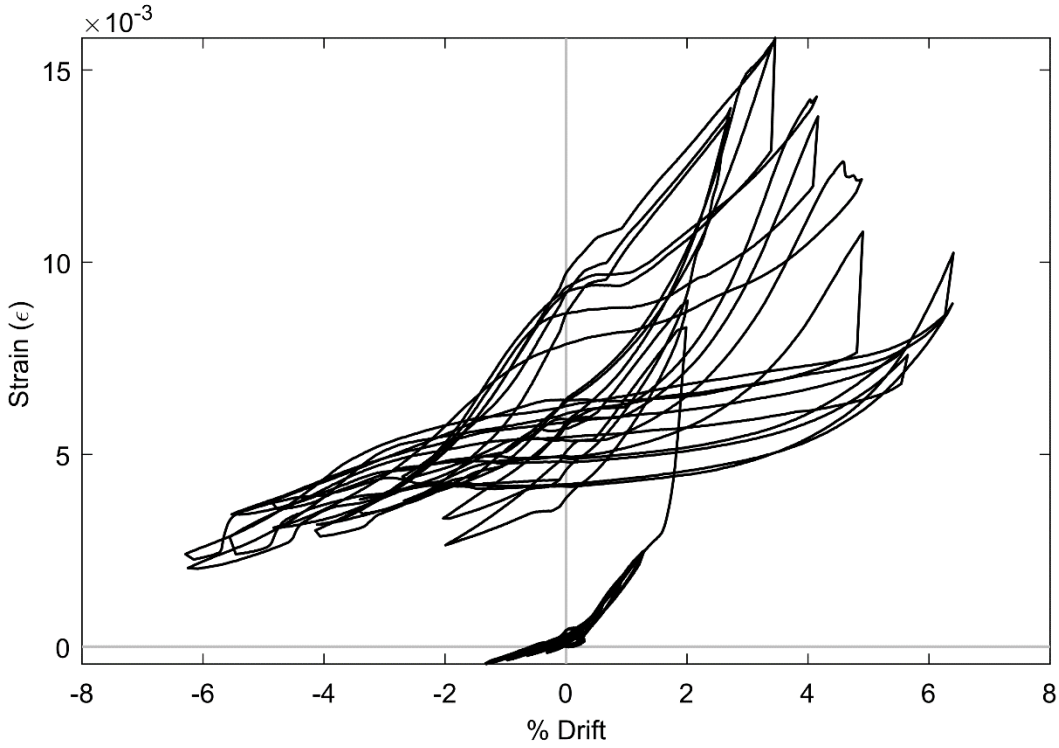

Figure 135: SG SBK5 (PTB_9_2_0)

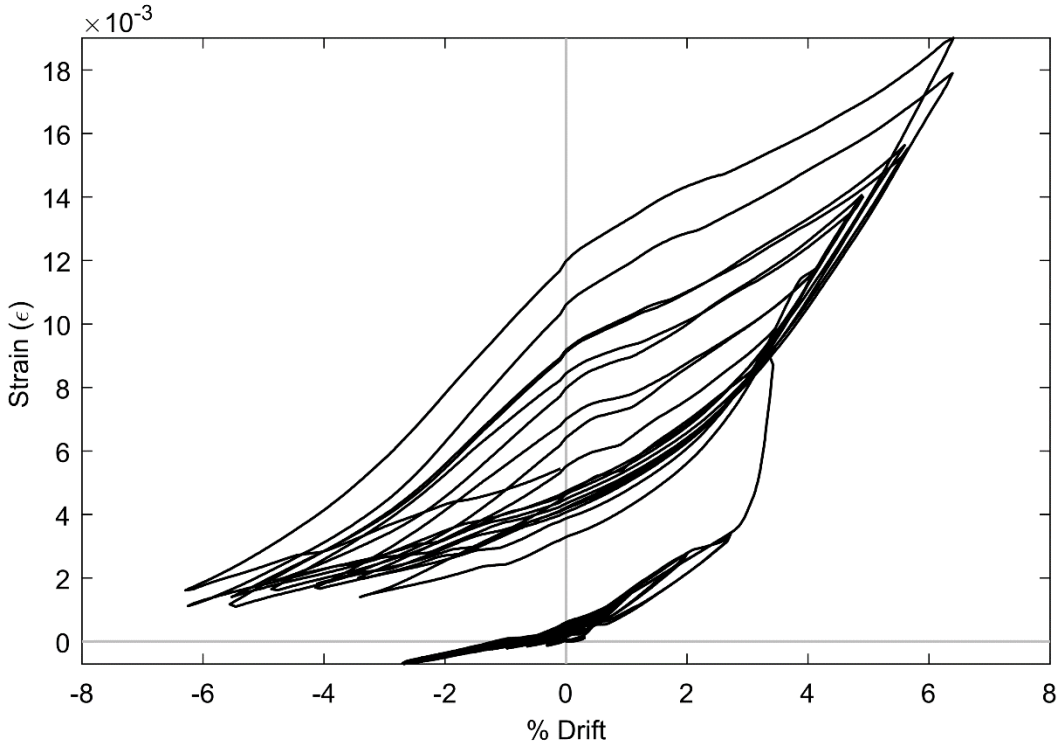

Figure 136: SG SBL5 (PTB_9_2_0)

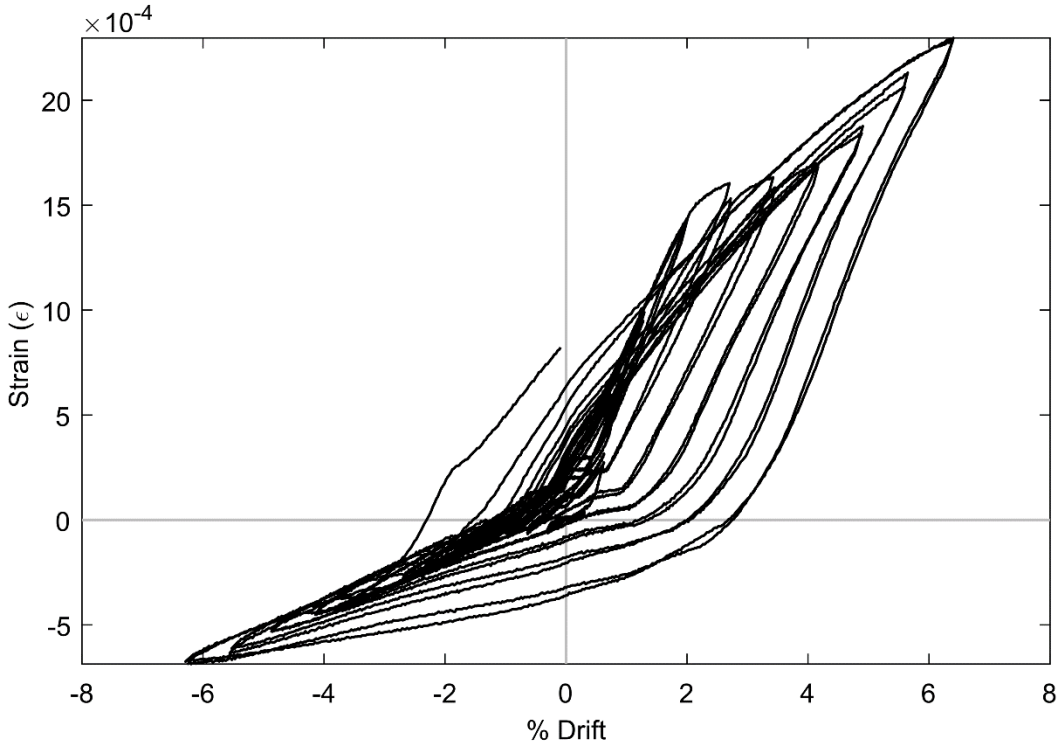

Figure 137: SG SBN5 (PTB_9_2_0)

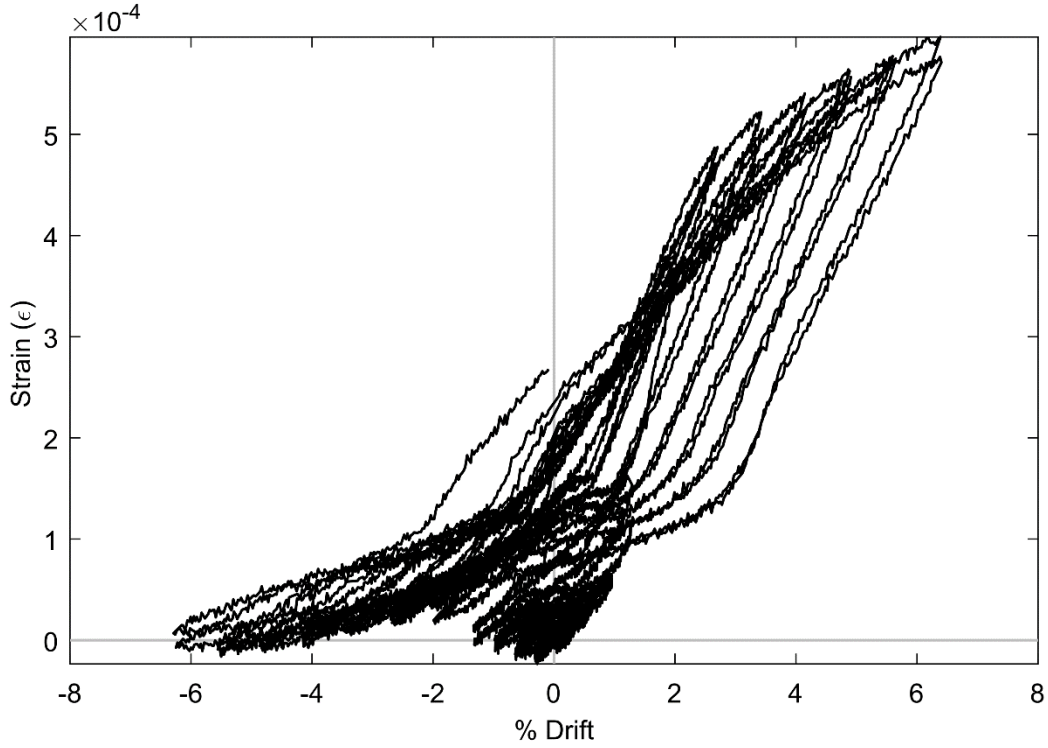

Figure 138: SG SBP5 (PTB_9_2_0)

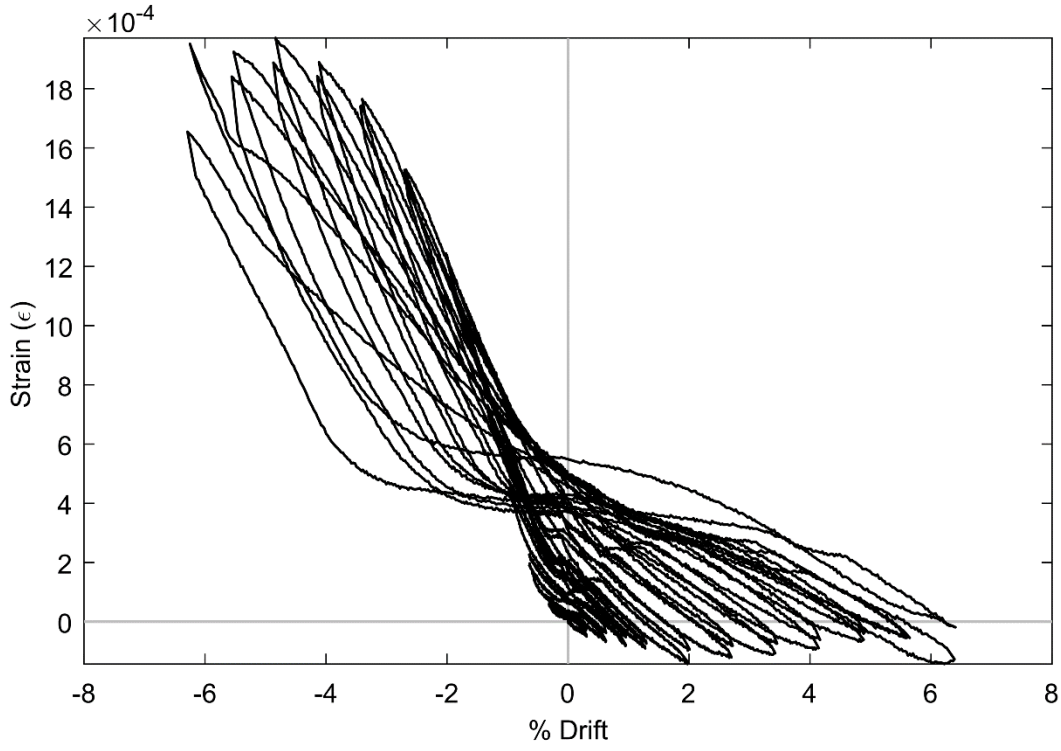

Figure 139: SG SBE6 (PTB_9_2_0)

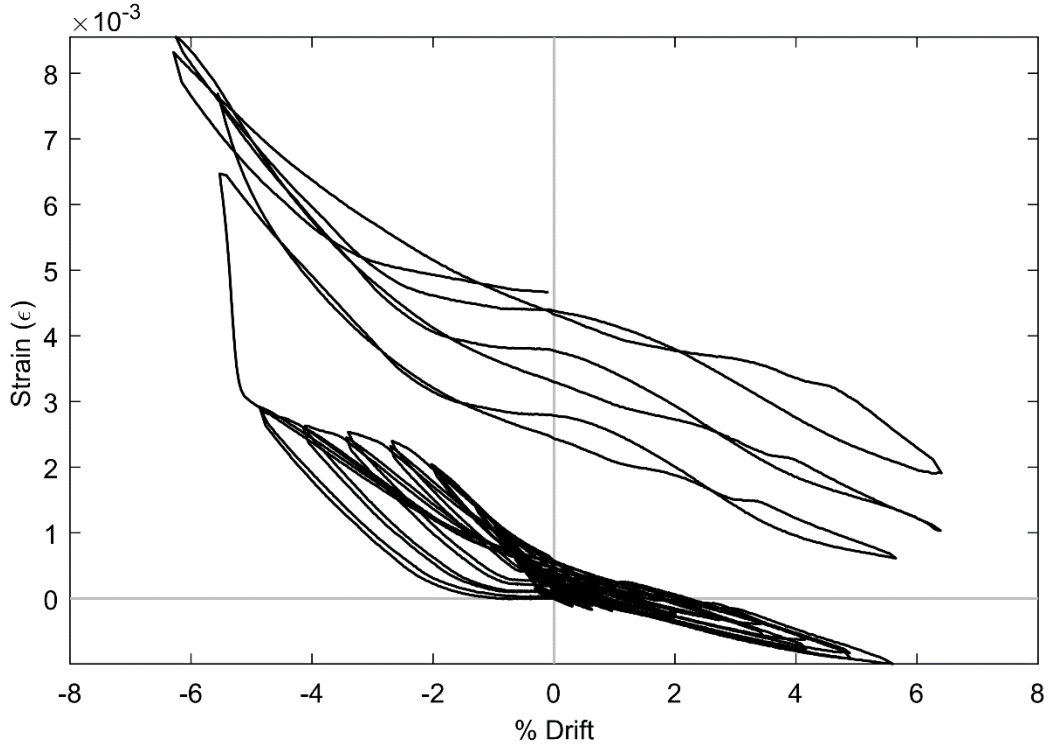

Figure 140: SG SBG6 (PTB_9_2_0)

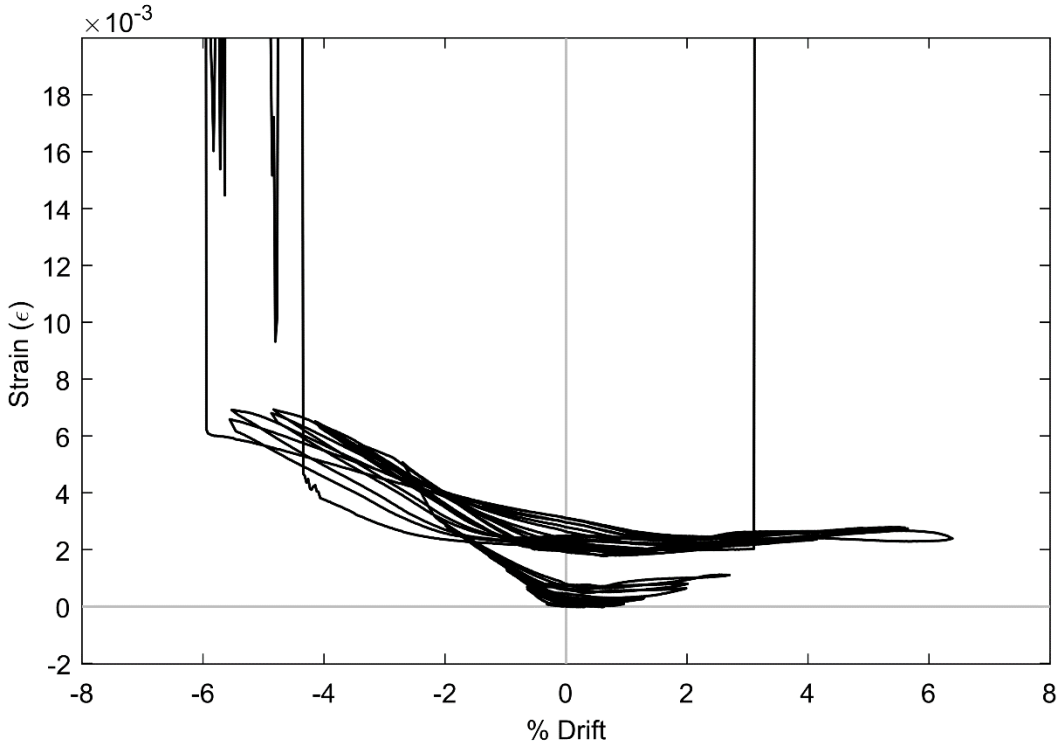

Figure 141: SG SBI6 (PTB_9_2_0)

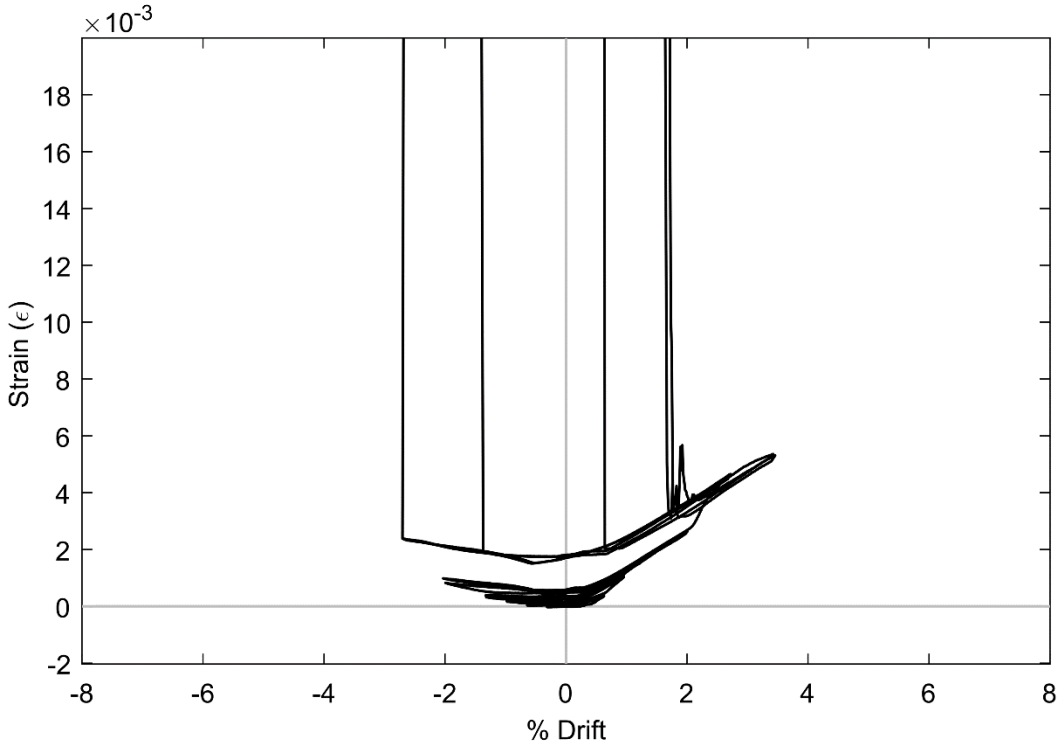

Figure 142: SG SBJ6 (PTB_9_2_0)

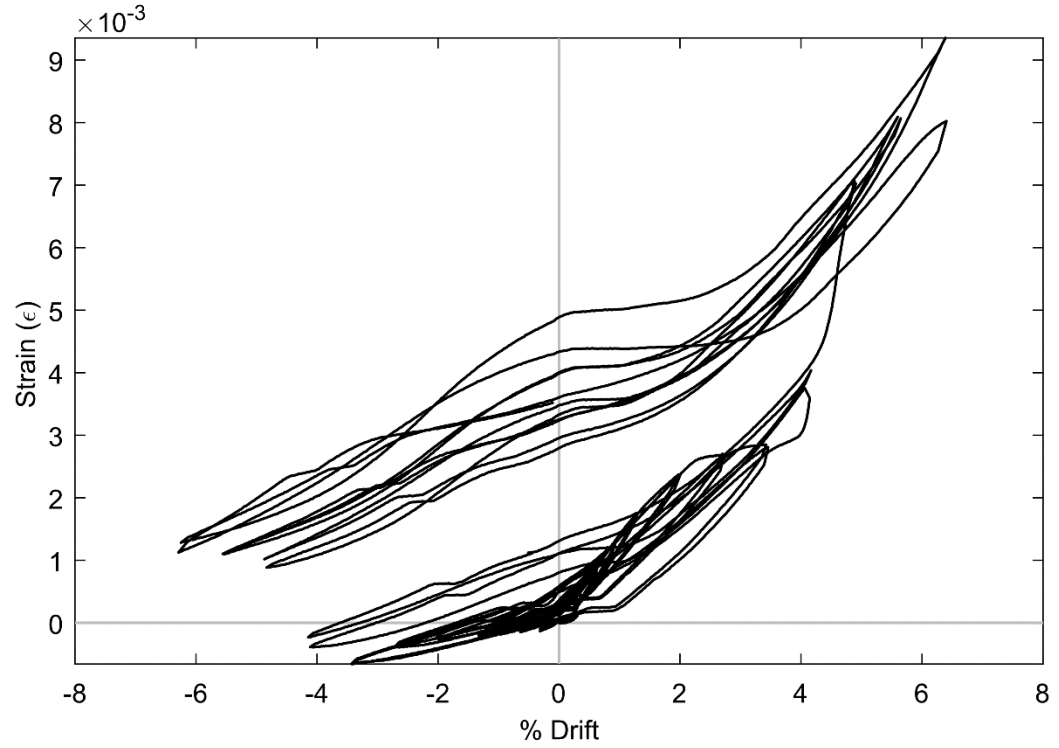

Figure 143: SG SBL6 (PTB_9_2_0)

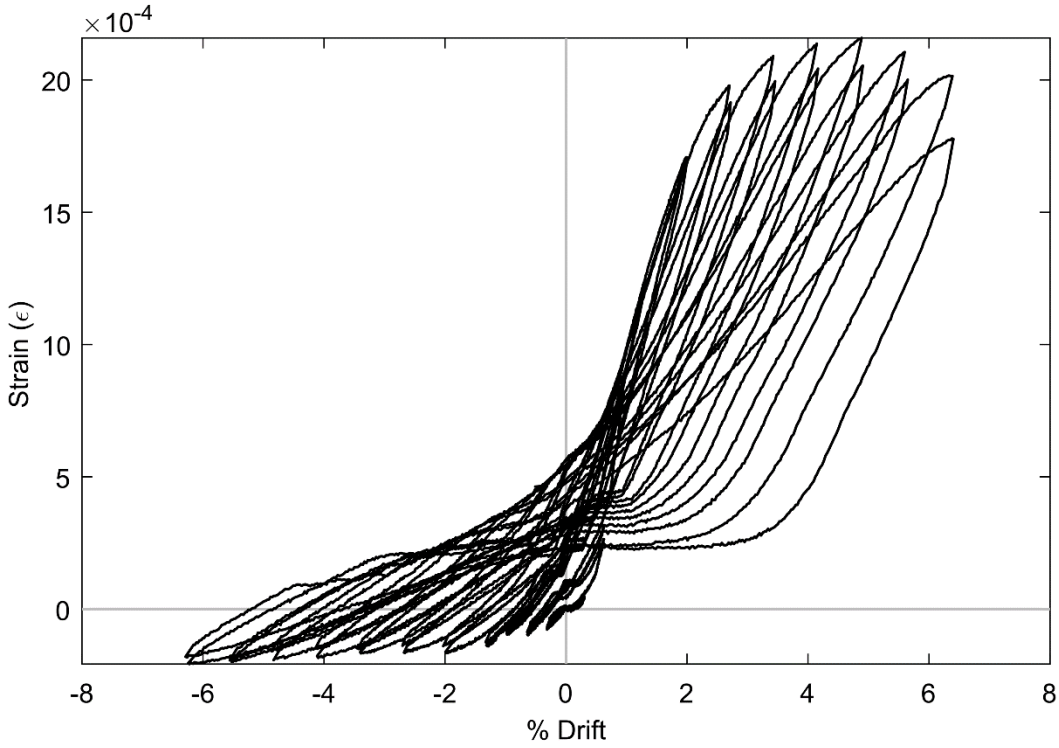

Figure 144: SG SBN6 (PTB_9_2_0)

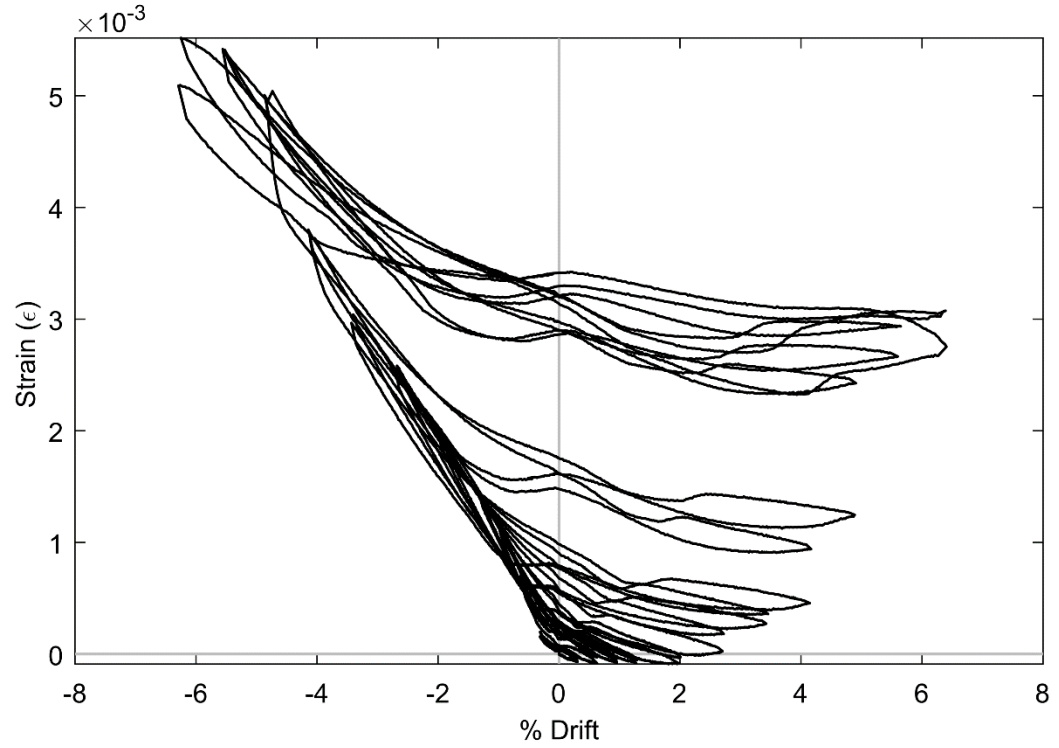

Figure 145: SG SBG7 (PTB_9_2_0)

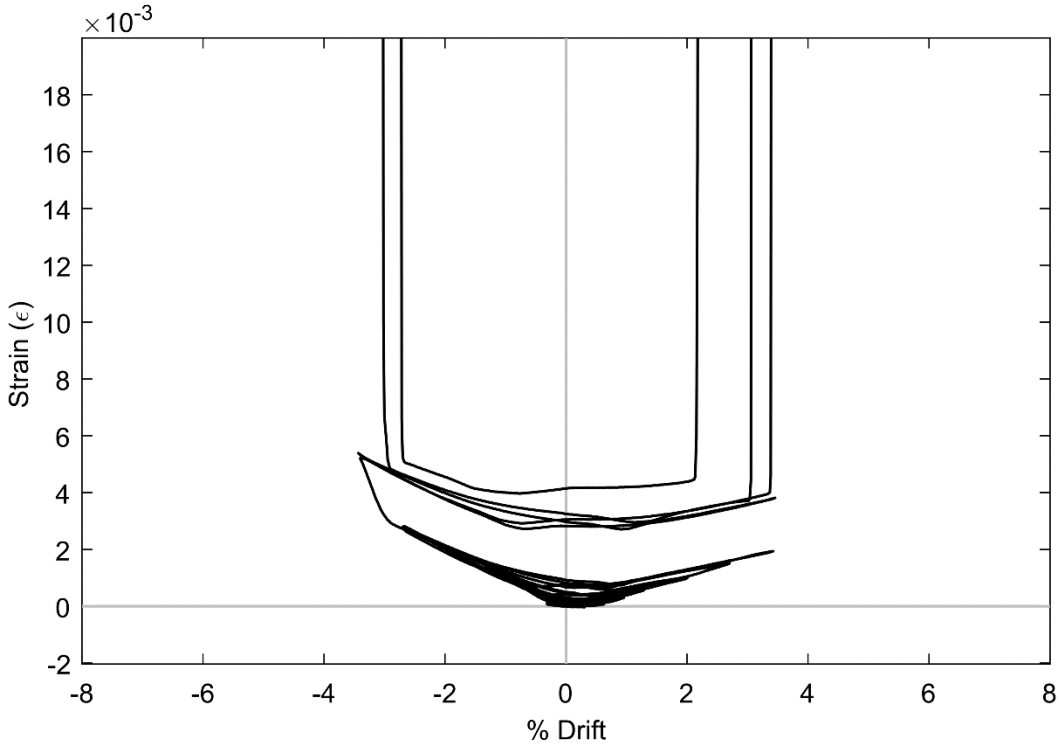

Figure 146: SG SBI7 (PTB_9_2_0)

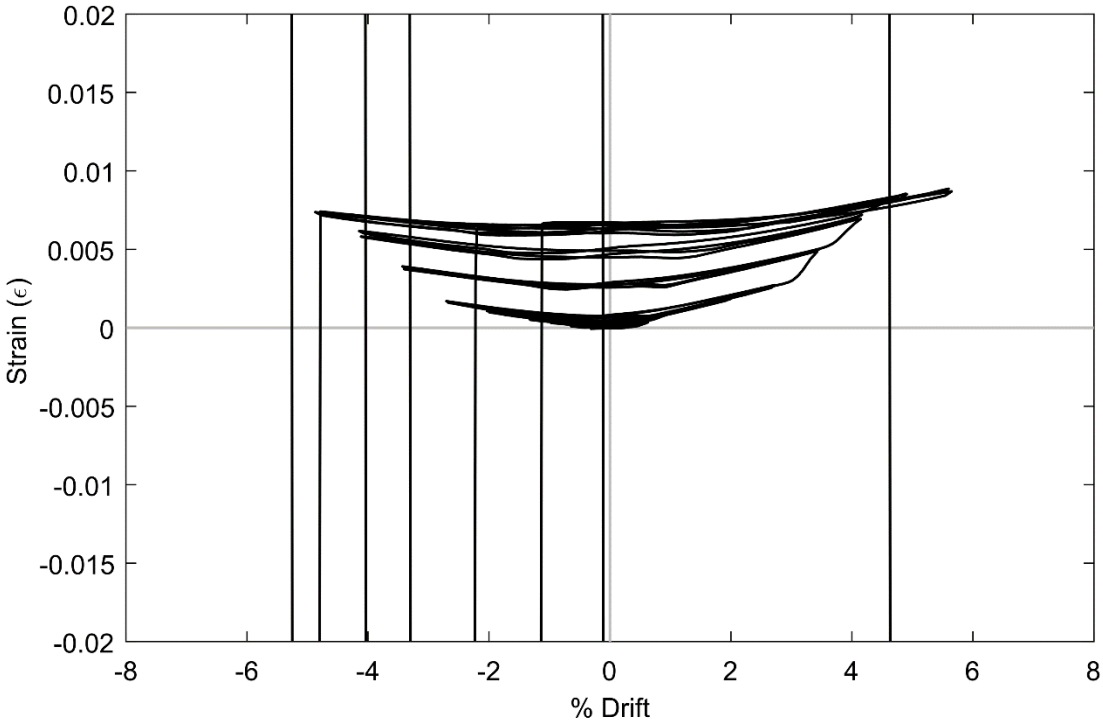

Figure 147: SG SBJ7 (PTB_9_2_0)

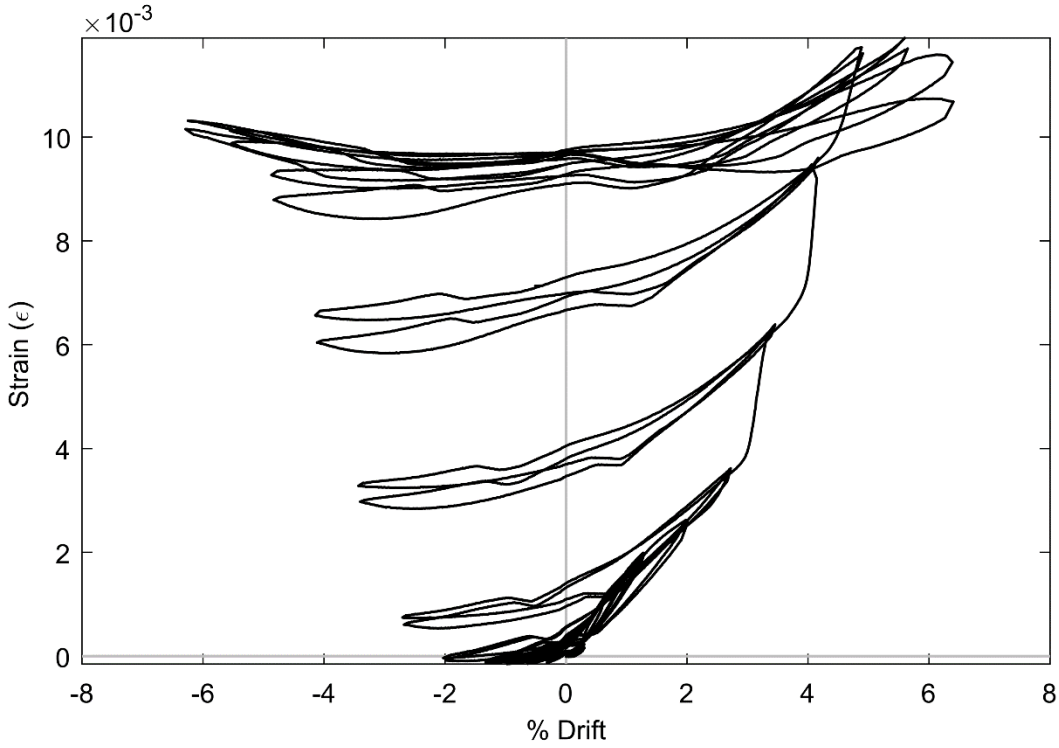

Figure 148: SG SBL7 (PTB_9_2_0)

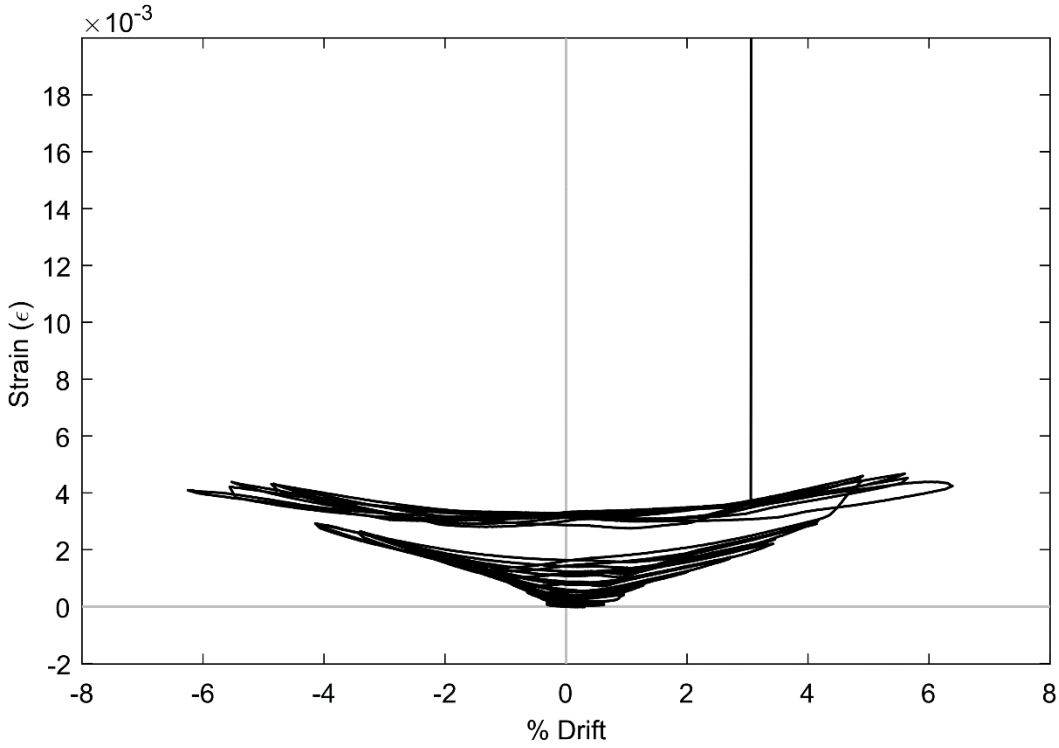

Figure 149: SG SBI8 (PTB_9_2_0)

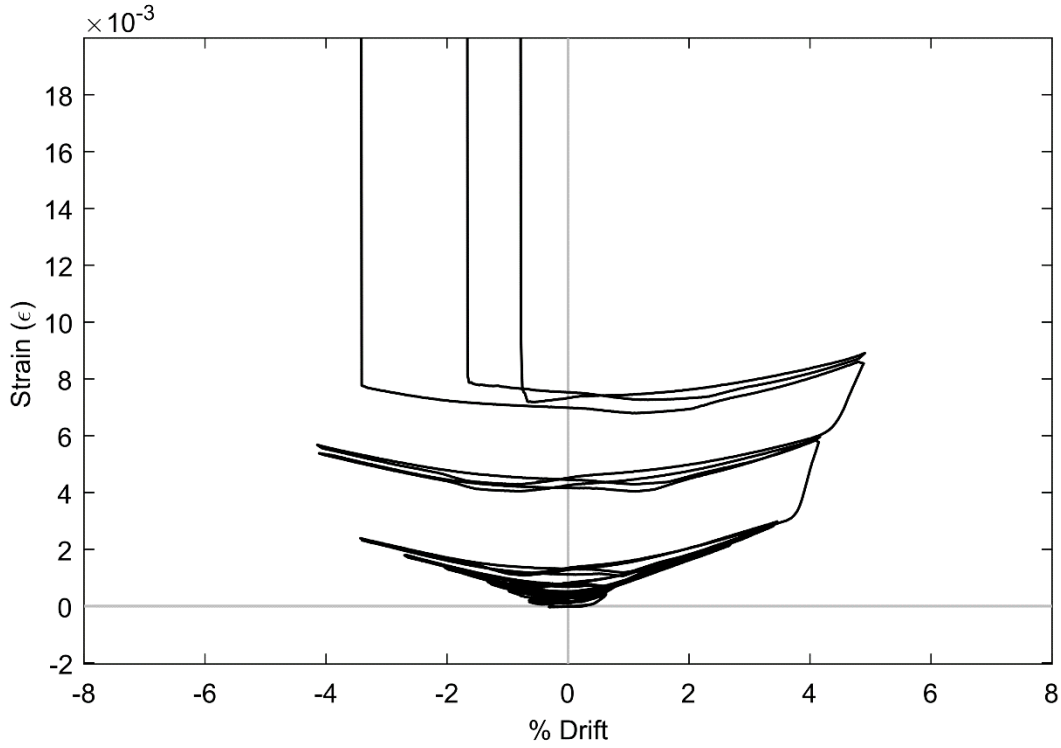

Figure 150: SG SBJ8 (PTB_9_2_0)

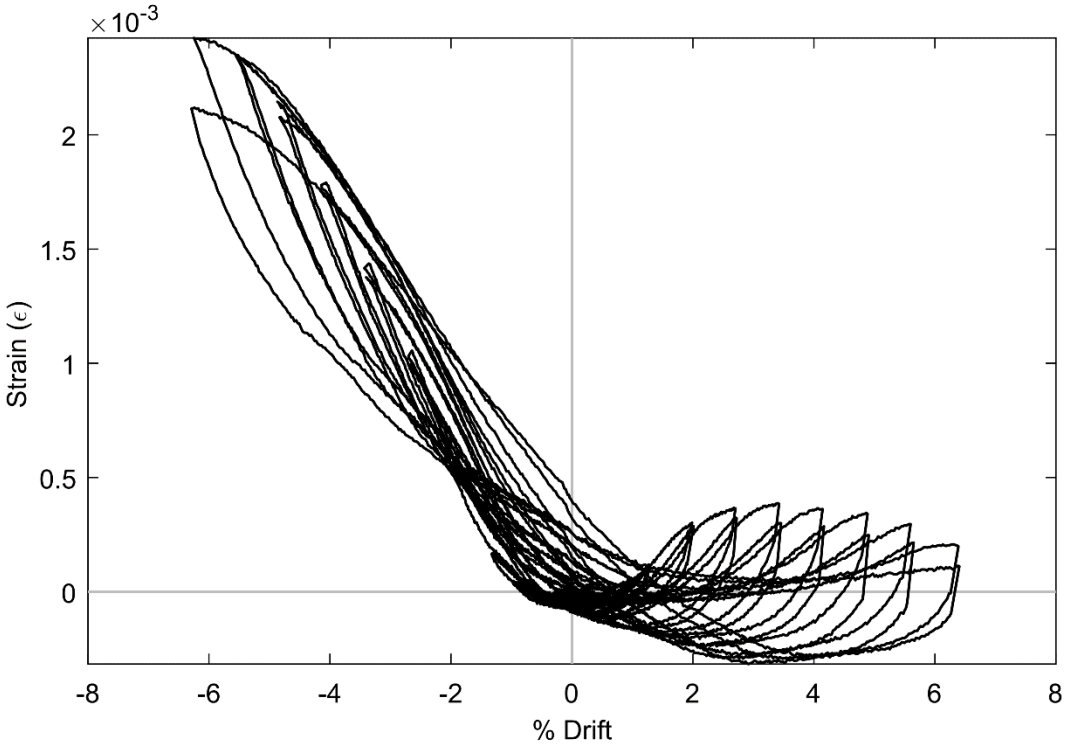

Figure 151: SG CC1 (PTB_9_2_0)

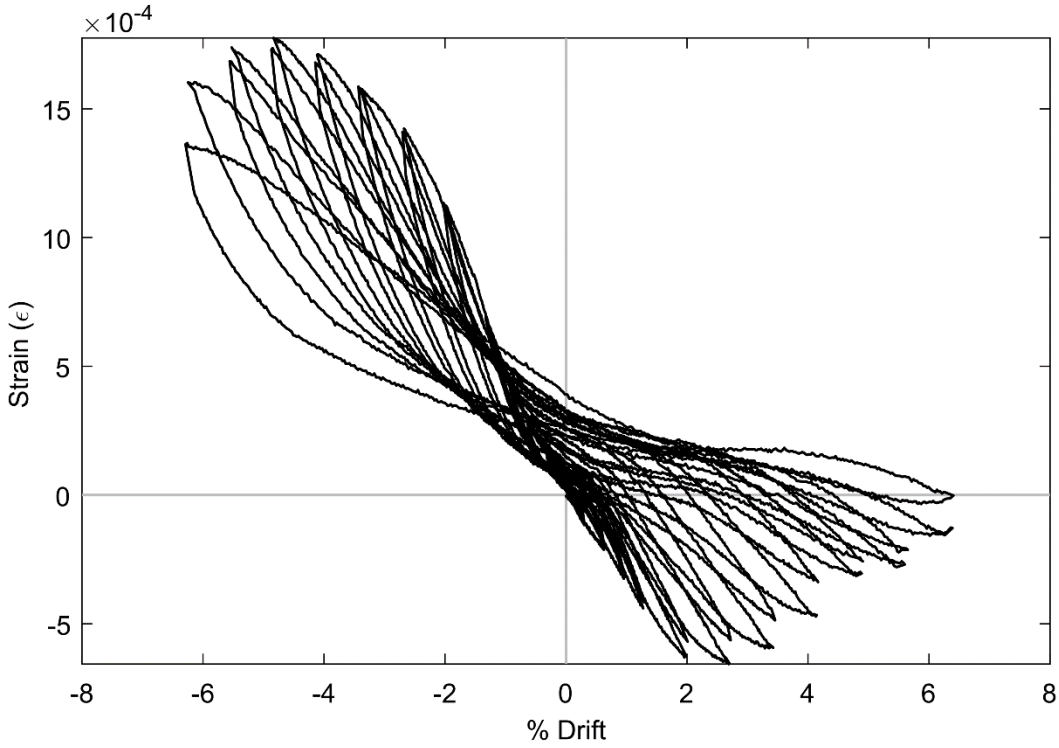

Figure 152: SG CC2 (PTB_9_2_0)

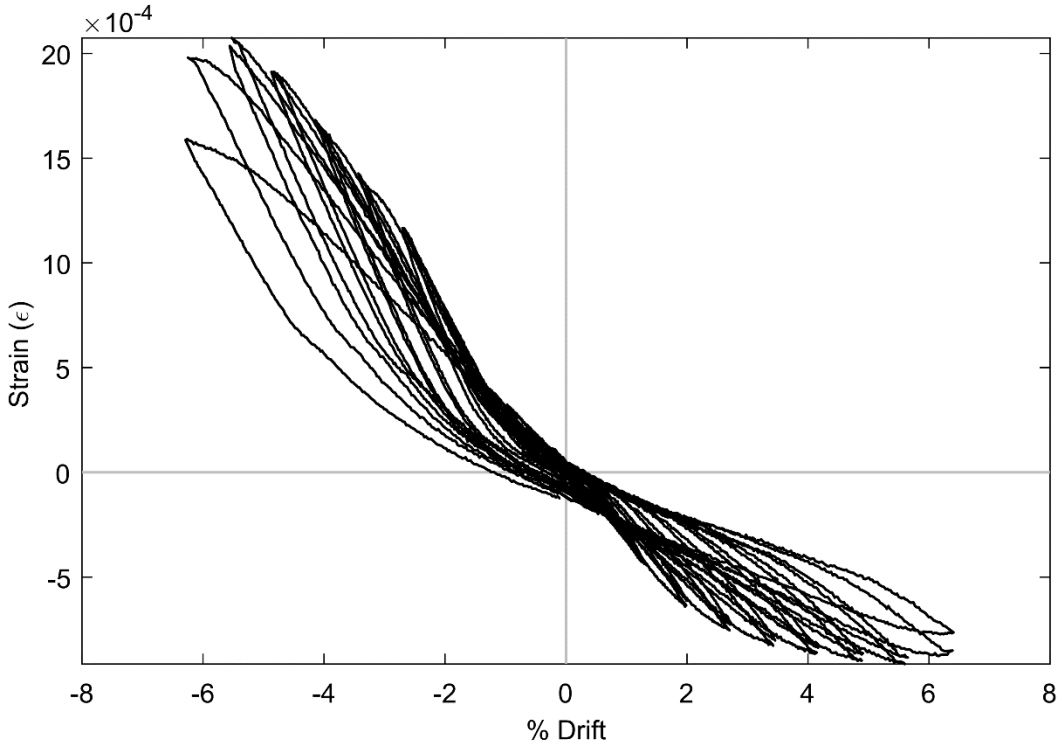

Figure 153: SG CC3 (PTB_9_2_0)

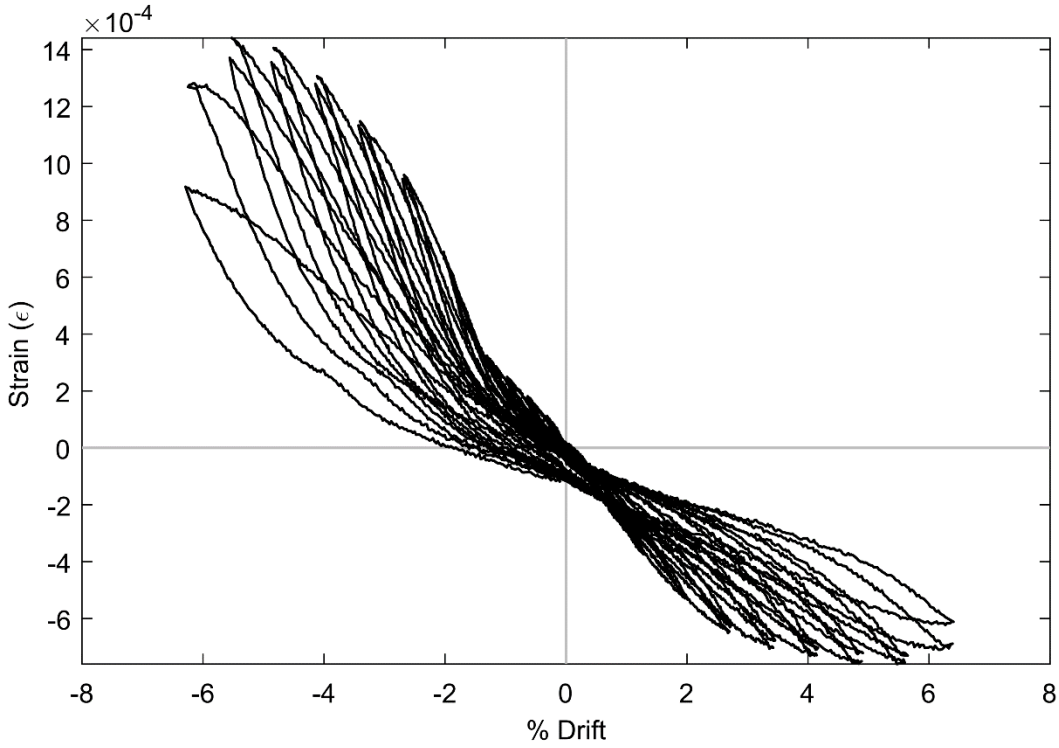

Figure 154: SG CC4 (PTB_9_2_0)

APPENDIX I: FEM MODELING

Performed by Junjie Wang

1. Test Program

The test specimens analyzed in this work were tested by Alec Yeutter. These were full-scale models representing interior slab-CFT column connections. The overall dimensions of slab and column are 3960 × 1830 × 254 mm and 3677 × 508 mm, respectively. The slab were supported at the slab ends and could slid along the horizontal direction. The column ends were pin supports, while the top end was applied a constant vertical load of 1470 kN.

The specimens were horizontally loaded at the top ends with a displacement-controlled load. The specimen in the test frame is shown in Figure (a). The slab reinforcement was #8 bars with spacing of 230 mm, while the column was reinforced by 10 #9 bars. The nominal cross-section area of #8 and #9 bars are 509 mm^2 and 645 mm^2, respectively.

(a) Experimental setup (b) Shear bolt arrangement

Figure 1: Slab-CFT Column Connection

The full test program consisted of four specimens. Test 1 had one row 19 mm shear bolt on the 114 mm wide tube ring, while the Test 2 were strengthen by another 4 row shear bolts

outside the tube ring (Figure 1 (b)). Test 4 had a 228 mm wide ring with 2 row bolts on it. Test 3 had no ring and shear bolt, but the shear studs were embedded in the joint area.

2. Modeling Scheme

This section describes the element types and material models used in the FEM of the slab-CFT column connection.

2.1. *Element Formulation and Material Model for Steel*

The steel tube, ring plate, and bolt washer are modeled with 4-node shell elements, which use the Belytschko-Lin-Tsay Shell formulation proposed by Belytschko, Lin, and Tsay (1984). Owing to its superior efficiency, the Belytschko-Lin-Tsay Shell is most commonly used in the explicit simulation. To expedite computational speed, the steel reinforcement is modeled with truss elements, which only carry the axial force. The shear bolts and horizontal supports are modeled using Hughes-Liu beam elements, which formulation is based on the Hughes-Liu shell (Hughes, & Liu, 1981a, 1981b). The advantages of Hughes-Liu beam element are computational efficiency, robustness, and compatibility with solid elements. The inelastic behaviors of the steel reinforcement, steel tube, and ring plate are modeled by the bilinear elastic-plastic model proposed by Krieg, and Key, (1976). The mechanical properties of steel are listed in Table 20.

Table 20: Mechanical Properteis of Steel Materials

Steel member	Yield Stress (MPa)	Ultimate Stress (MPa)	Ultimate Strain
Reinforcement	459	887	0.2
Steel tube	345	455	0.2
Ring plate	238	352	0.2
Shear bolt	900	1000	0.1

2.2. *Element Formulation and Material Model for Concrete*

The concrete is modeled with 8-node, reduced-integration solid elements (one integration point in each solid element), which can substantially reduce the computational time. The Flanagan-

Belytschko stiffness form with exact volume integration for the solid element method (Hallquist, 2016) is used to prevent the zero-energy deformation mode (hourglass deformation mode).

There are five material models can be used to simulate the plasticity and damage evolution of concrete. They are Concrete Damage Plastic Model (CDPM), Continuous Surface Cap Model (CSCM), Karagozian & Case (K&C) Concrete Model, RHT model and Winfrith model. The cyclic performance of these concrete models are compared with single element analysis (Figure 2, Figure 3, Figure 4, Figure 5, and Figure 6). The K&C model loads and unloads with a constant modulus, and the high strain portion of the curves are not captured. The softening behaviour of the RHT model is significantly higher than the expected concrete capacities at high strains. The Winfrith model does not have the capacity to model strength degradation and stiffness degradation under compression. The CSCM model has more reliable performance than the three models mentioned above, however the nonlinear behavior before the peak stress cannot be successfully captured. But, the CDPM model is capable of describing the realistic nonlinear behavior of the concrete, including stiffness degradation, irreversible displacements, confinement effect, and damage evolution.

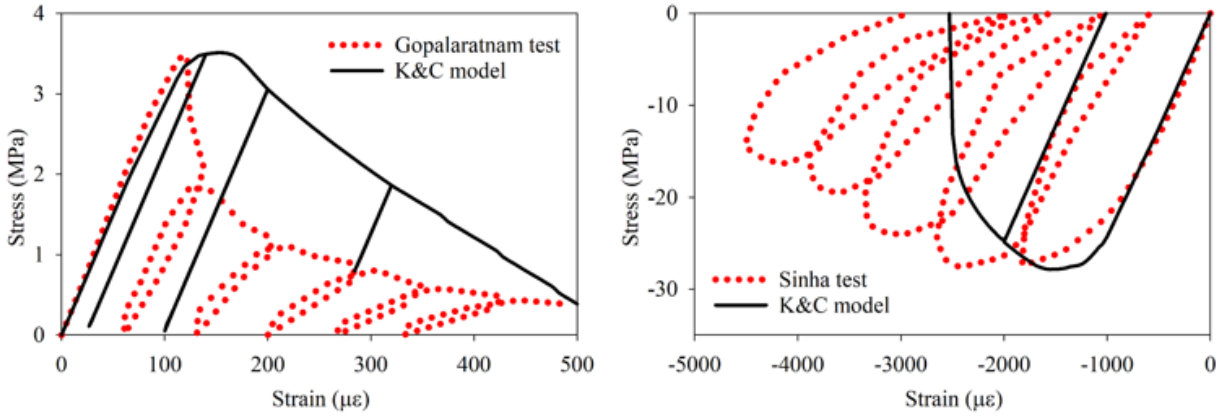

Figure 2: K&C Model

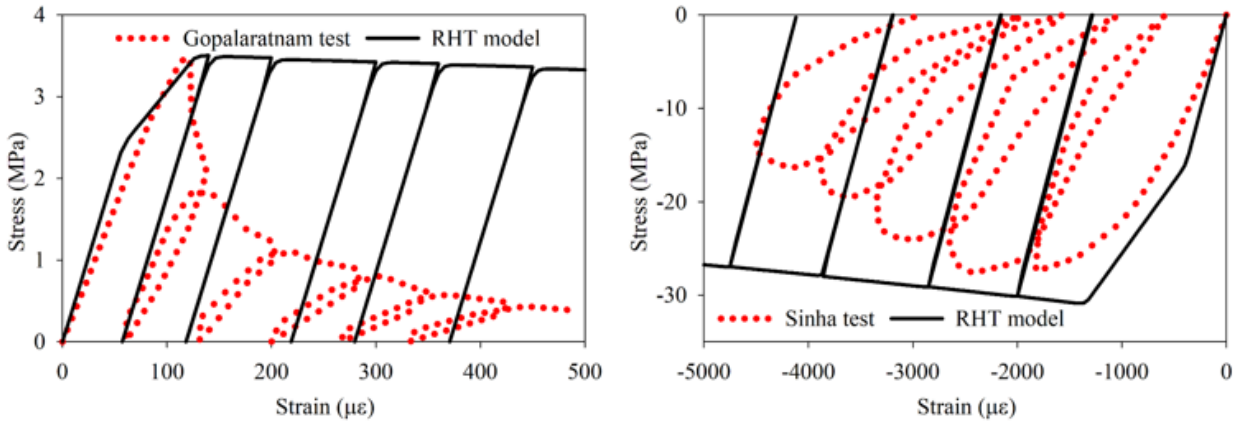

Figure 3: RHT Model

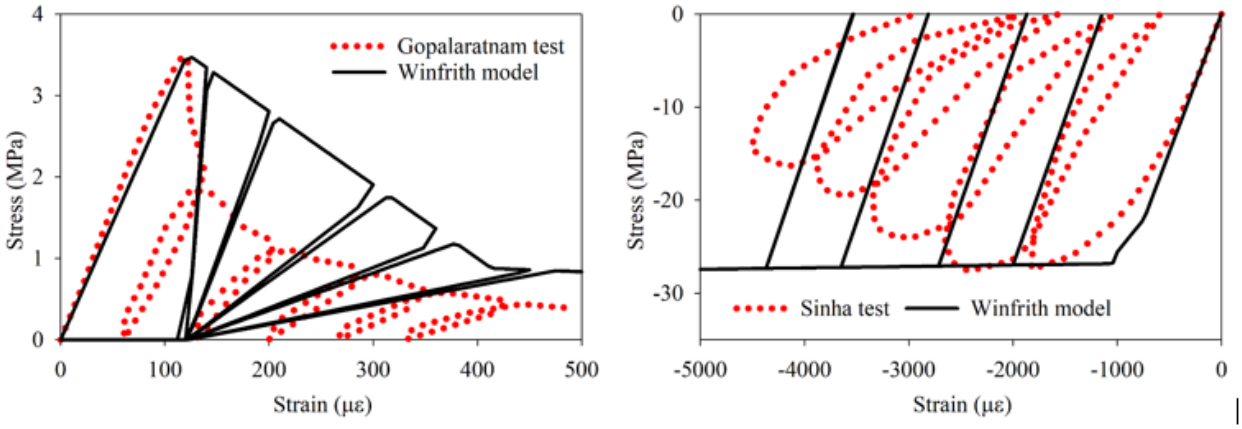

Figure 4: Winfrith Model

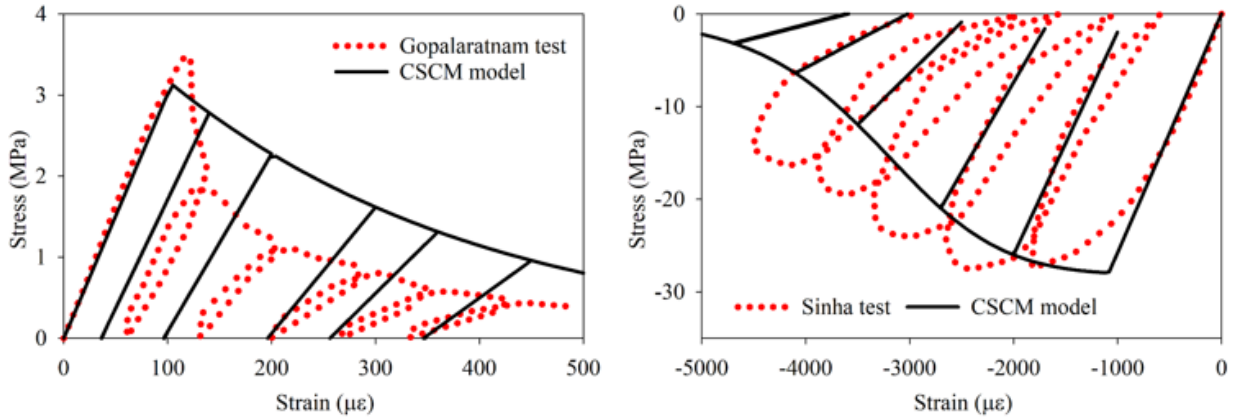

Figure 5: CSCM Model

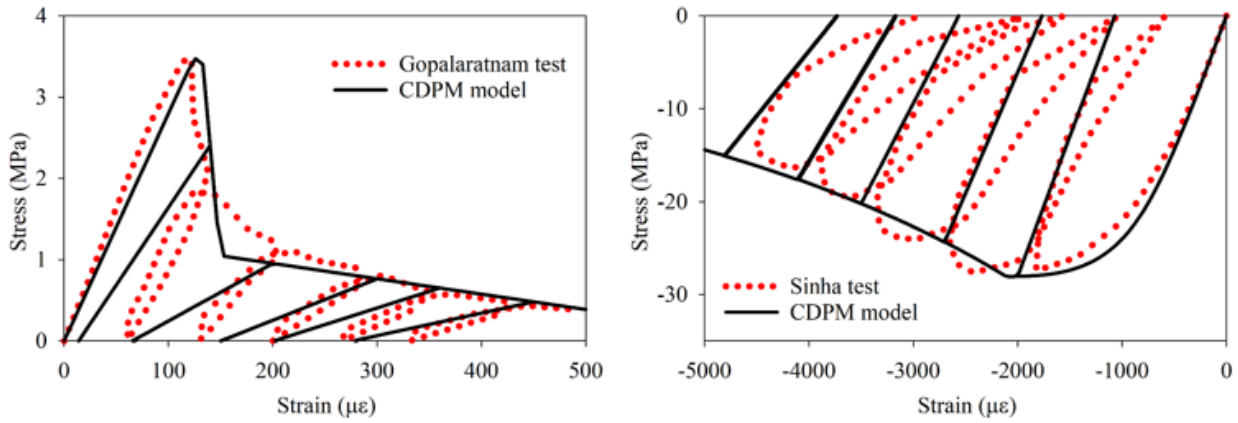

Figure 6: CDPM model

Therefore, the constitutive model used for the solid elements represented concrete is the CDPM model, which is proposed by Grassl, and Jirásek (2006), Grassl, Xenos, Nyström, Rempling, and Gylltoft (2013). As illustrated in Figure 7, the bilinear softening response is selected to represent the concrete damage evolution under tension. In Figure 7, f_t is the maximum tensile strength of concrete, and ω_f is the nonlinear displacement when the tensile stress of concrete reduces to zero. The stress-displacement response can be converted into stress-strain response via $\varepsilon_t = \omega_f / l_e$, where ε_t is the plastic strain when the tensile stress reduces to zero, l_e is the characteristic length of the element. The softening response of concrete is affected by the fracture energy of concrete (G_f), which can be obtained by Equation 60 (CEB-FIP, 2010). In Equation 1, f_c is the compressive strength of concrete (54.4 MPa). Based on Equation 60, the tensile strength, fracture energy, and elastic modulus are calculated as 4.3 MPa, 0.15 N/mm, and 34660 MPa, respectively.

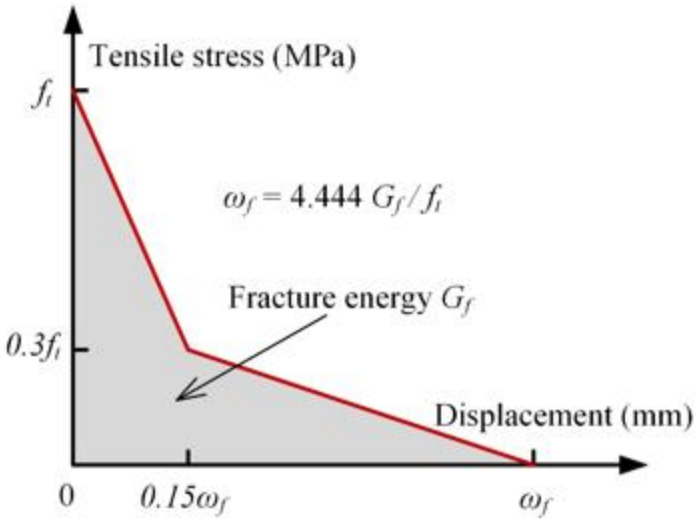

Figure 7: Uniaxial Tesnsile Softening Relationship for Concrete

$$G_f = 73 f_c^{0.18} \qquad 60$$

2.3. *Contact Properties*

The contacts between steel members and concrete are modeled using the automatic surface-to-surface contact algorithm with a friction coefficient of 0.5 (Tahmasebinia, Ranzi, & Zona, 2011). The steel reinforcements are perfectly bonded to the concrete, and the slips between these parts are neglected. The shear bolts are only constrained in the normal directions, while the shear bolts can slide along the axial direction.

3. FEM Validation

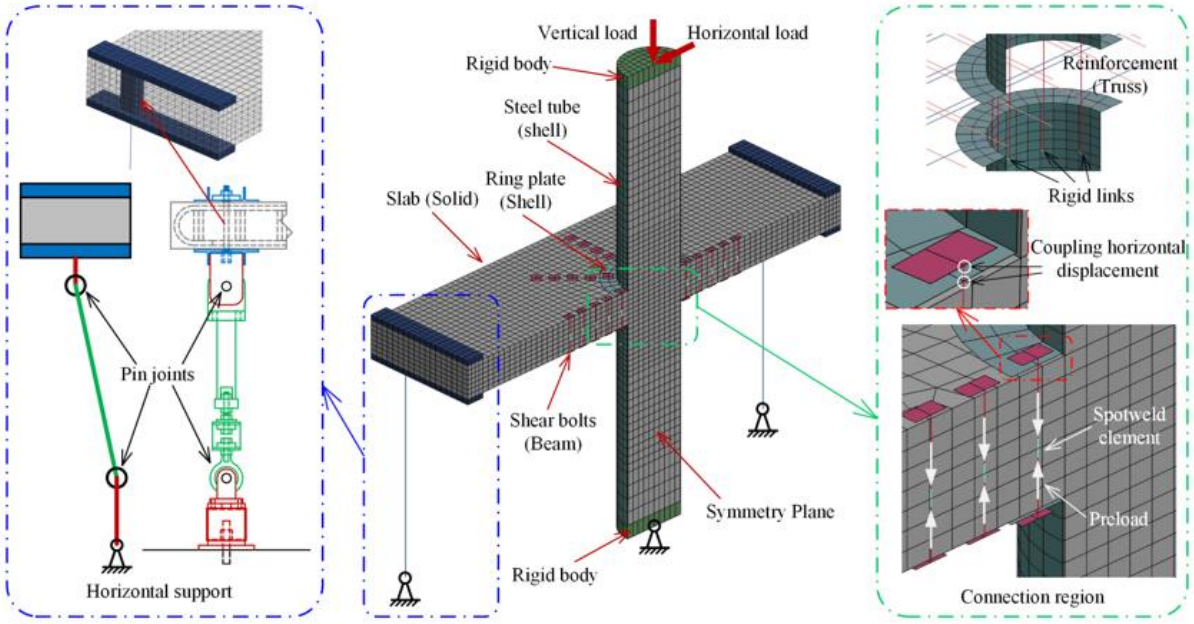

Figure 8: FEM Details

Figure 8shows the details of the FEM. Considering the symmetry, a half model is established. The mesh size used in the connection is about 40 mm. To overcome unnecessary stress concentration, both ends of the column are replaced by a rigid body. The bottom center node of the column is constrained by pin support. A constant vertical load is applied to the upper center node of the column, while a displacement-controlled horizontal load is also applied to this location. The horizontal support at the slab end is simplified as in Figure 8. The clamp devices are represented by two rectangular plates, while the vertical rods are simulated by beam elements. The rotation devices in the vertical rods are represented by pin joints. The preload in the shear bolt is applied through a spotweld element located in the center of the slab. The horizontal displacement of the bolt washer's center node is coupling to its neighboring ring plate node, while the vertical displacement is not constrained. Because the bottom ends of the column reinforcement are welded to the tube, a rigid link is established between reinforcement and tube to simulate this weld.

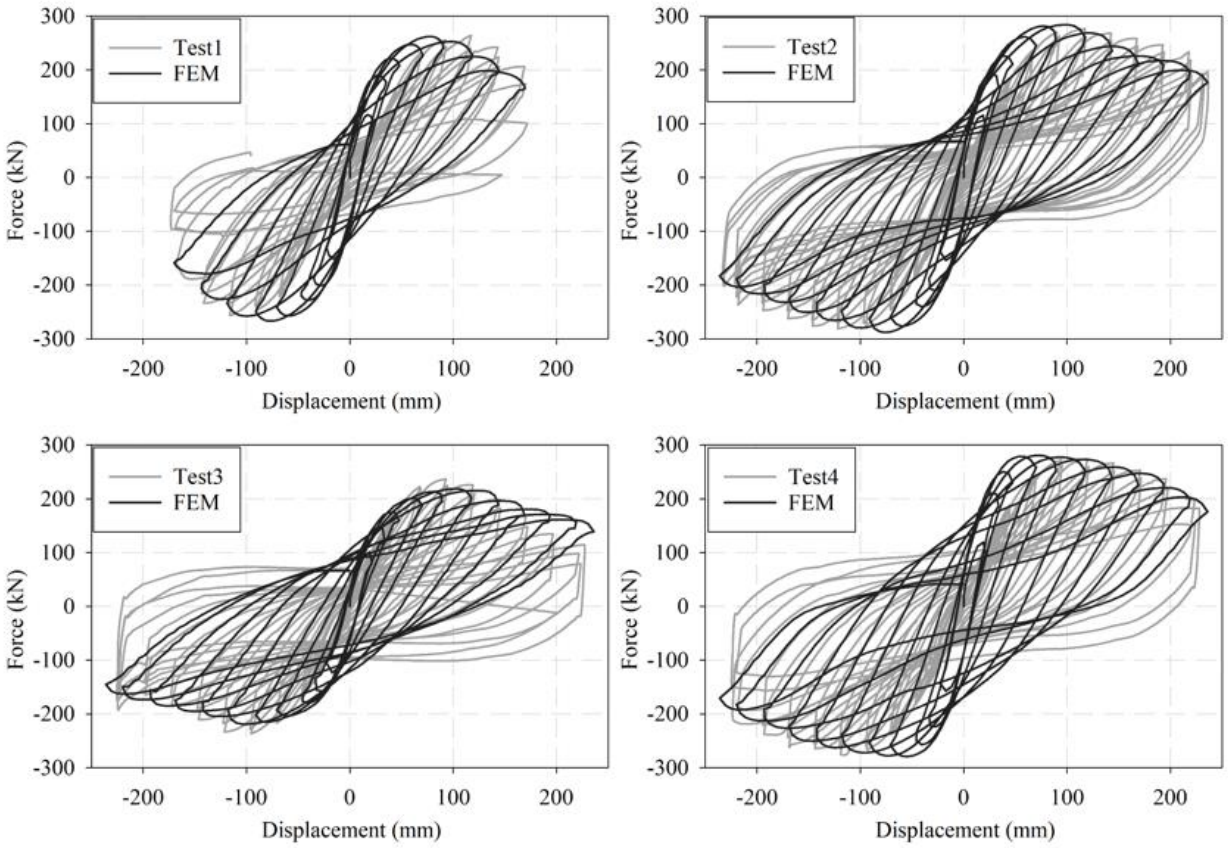

Figure 9: Comparison between FEM and Experimental Test

Figure 9 presents the comparison between the analytical observation and experimental result in terms of horizontal resistance versus horizontal displacement at the upper column end. The force measured by the built-in load cell in the actuator is taken as the lateral resistance of the test specimen. As shown in Figure 9, the presented FEM is capable of simulating the salient characteristics of the load-displacement curves, including the pinching effect and the resistance softening. The concrete crack development of all slabs from tests and FEA is presented in Figure 10. The simulated cracks match the experimentally observed cracks well.

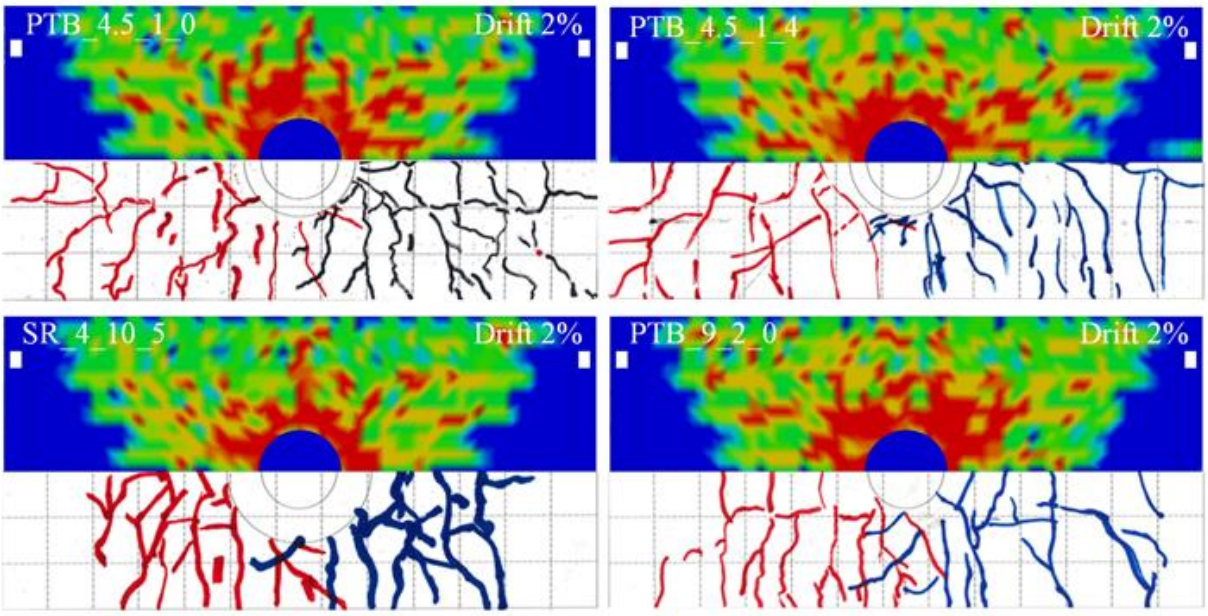

(a) Drift 2%

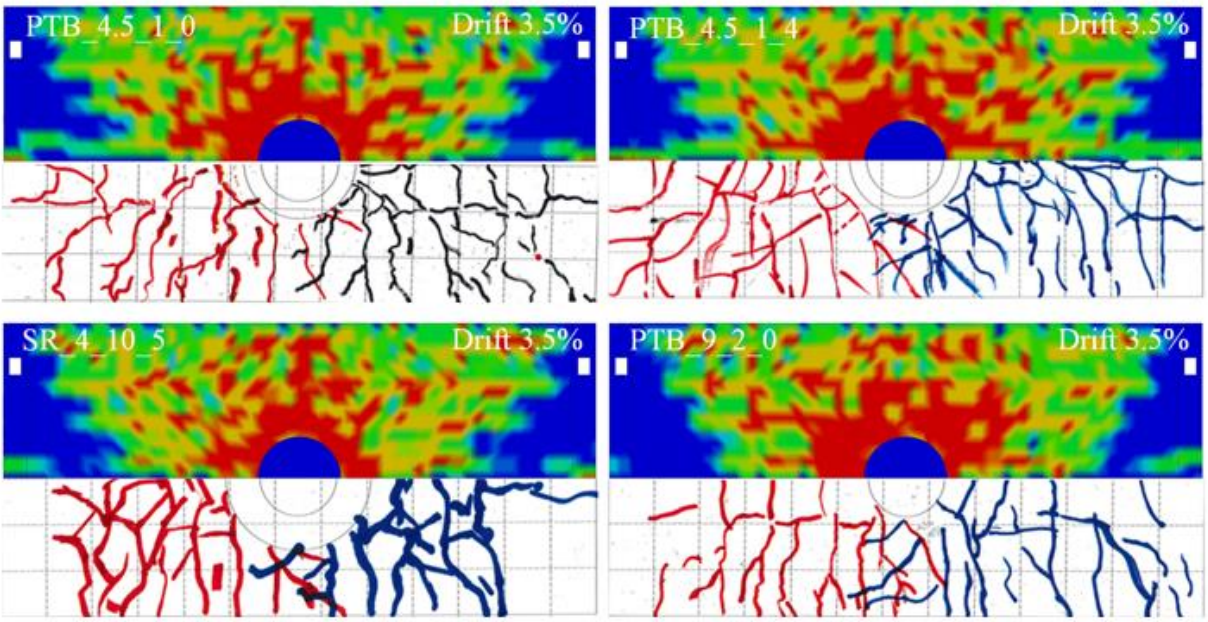

(b) Drift 3.5%

Figure 10: Top Joint Concrete Cracks

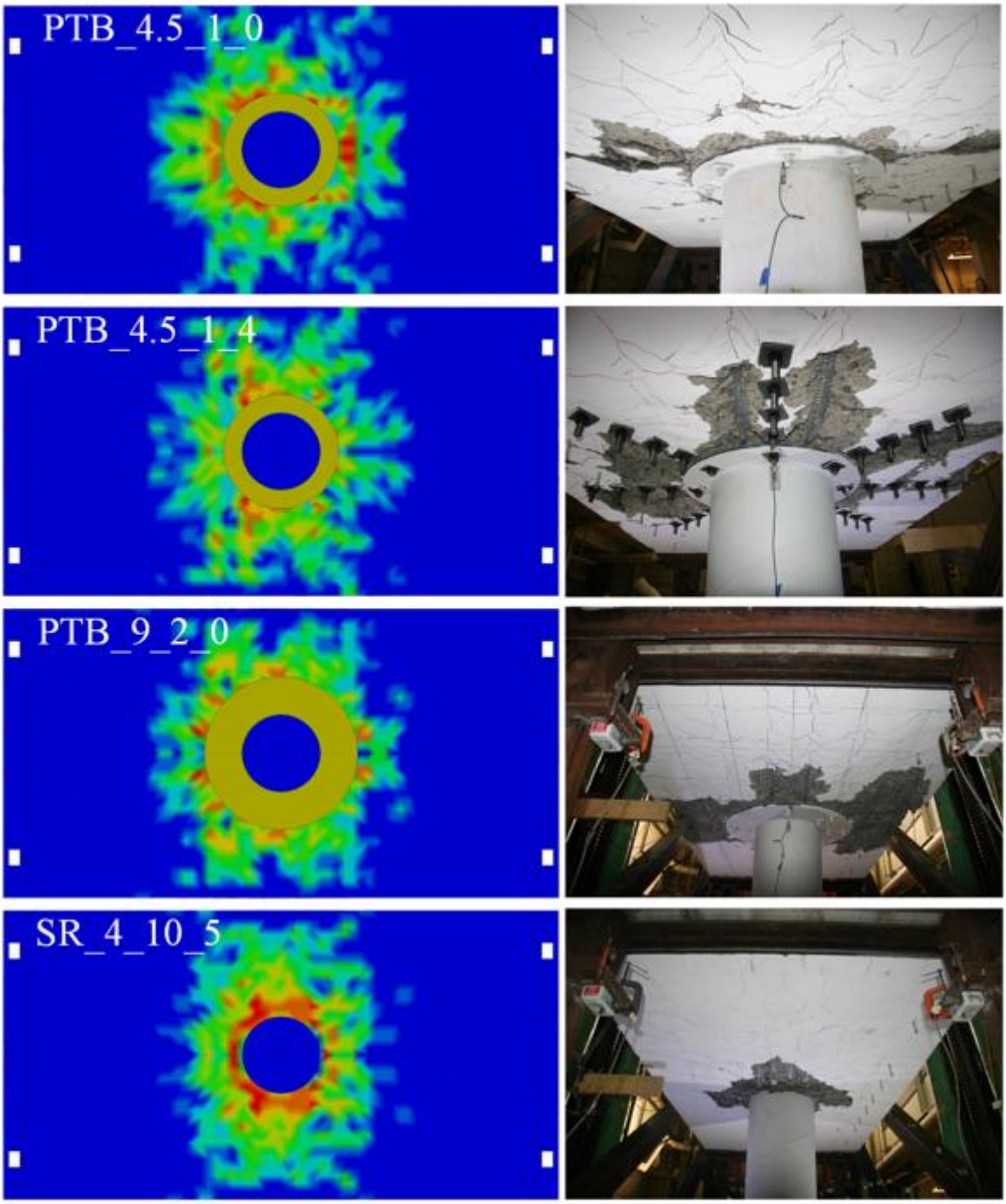

Figure 11: Bottom Joint Concrete Crushing

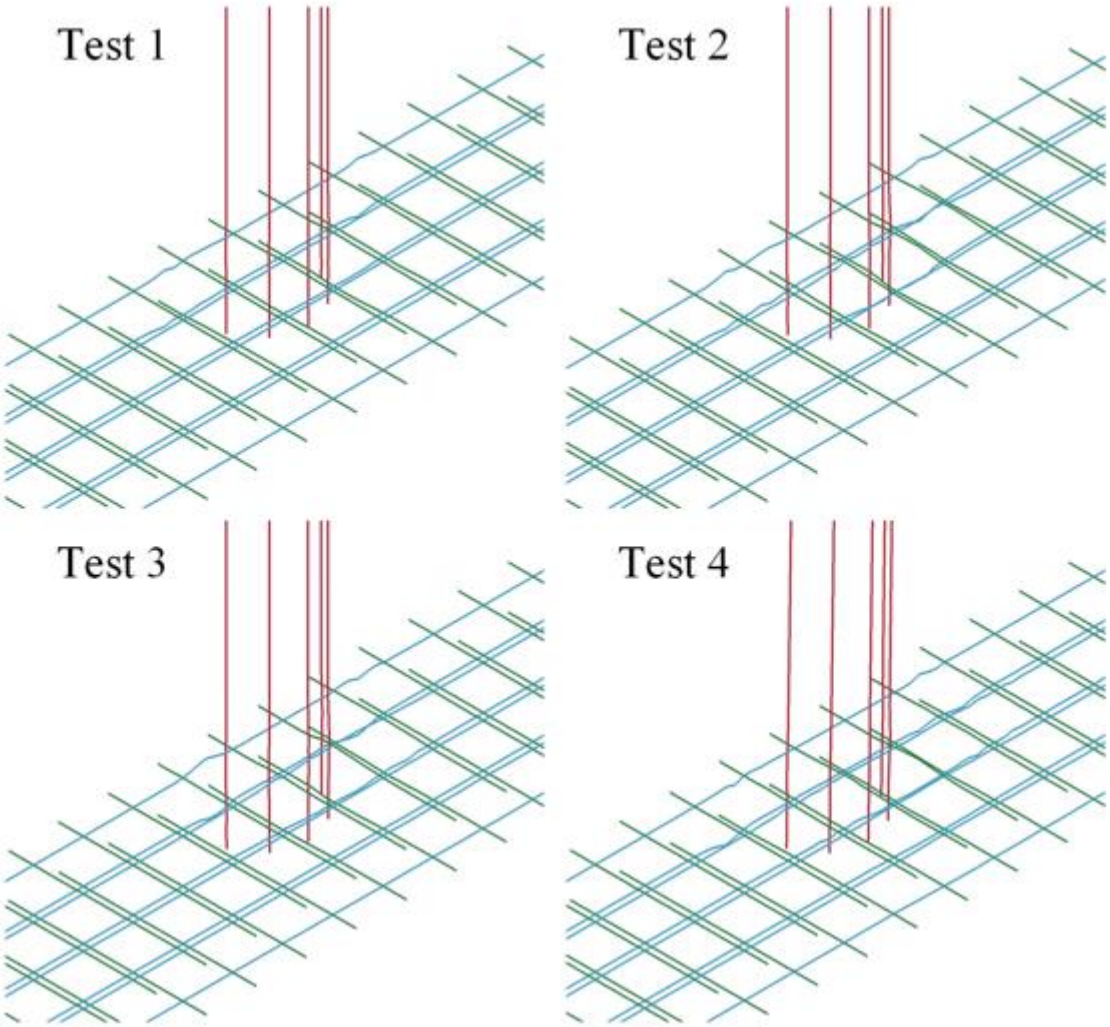

Figure 12: Reinforcement Buckling

Polak:

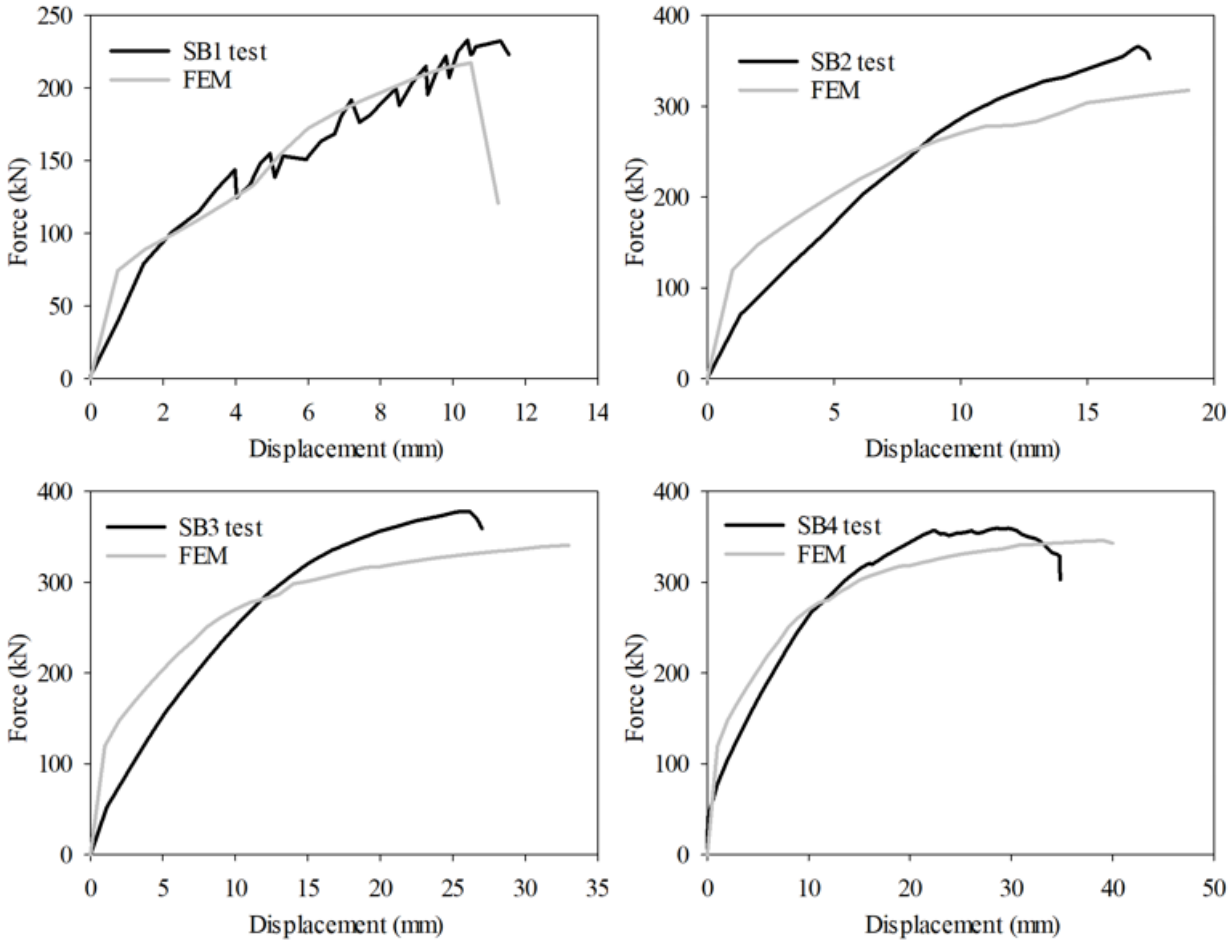

Figure 13: Polak Test Validation

4. FEM Investigation

4.1. *Effect of Bolt Preload*

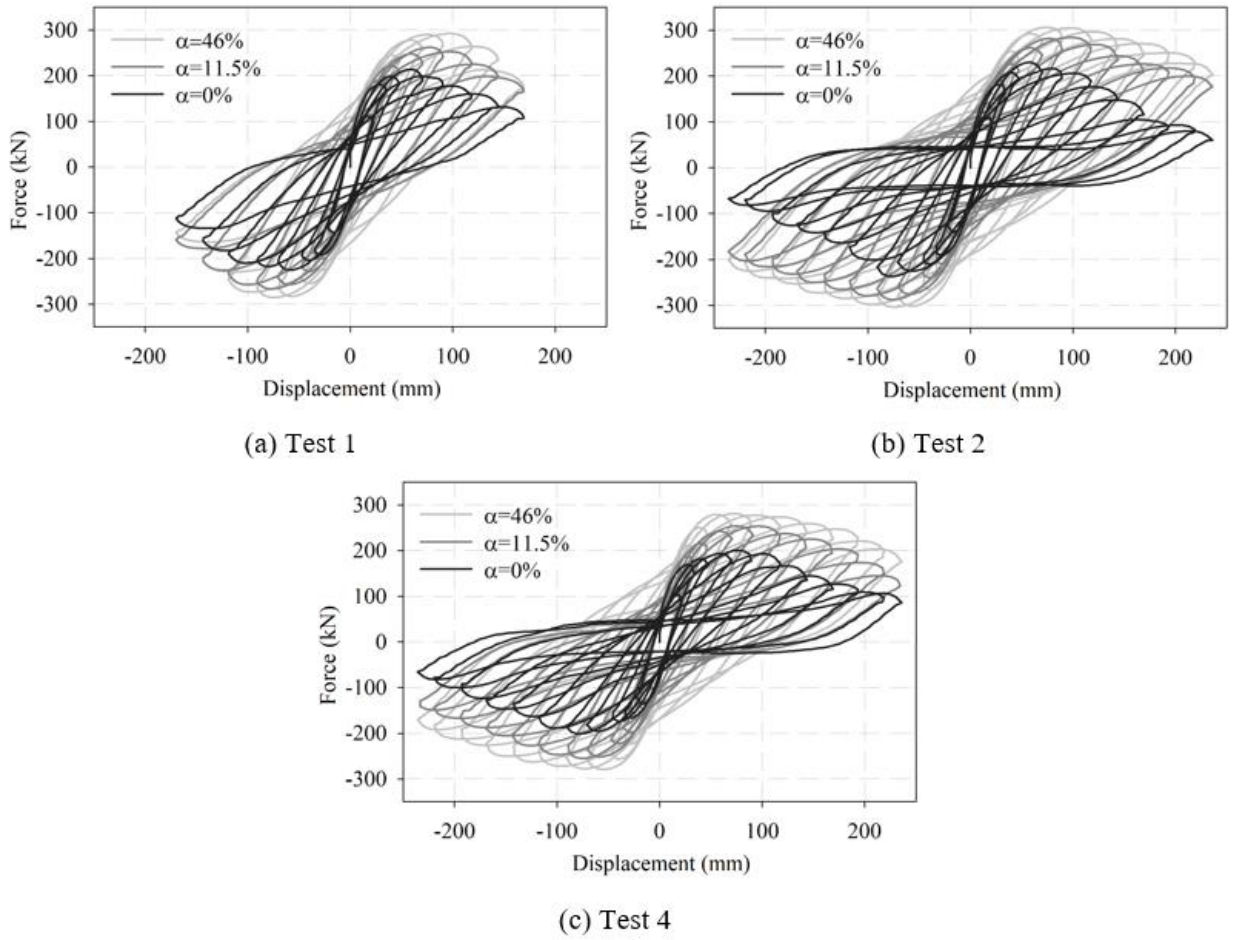

Figure 14: Effect of Bolt Preload

Table 21: Effects of Bolt Preload

Specimen	Preload ratio (%)	F_{peak} (kN)	Δ_{peak} (mm)	$0.8F_{peak}$ (kN)	$\Delta_{0.8peak}$ (mm)	β (%)
Test 1	46	292	98	234	145	137
	11.5	262	78	210	139	123
	0	214	60	171	110	-
Test 2	46	306	77	245	208	133
	11.5	284	101	227	166	123
	0	230	59	184	118	-
Test 4	46	281	71	225	194	140
	11.5	254	75	160	177	127
	0	200	77	160	135	-

4.2. *Effect of Ring Thickness*

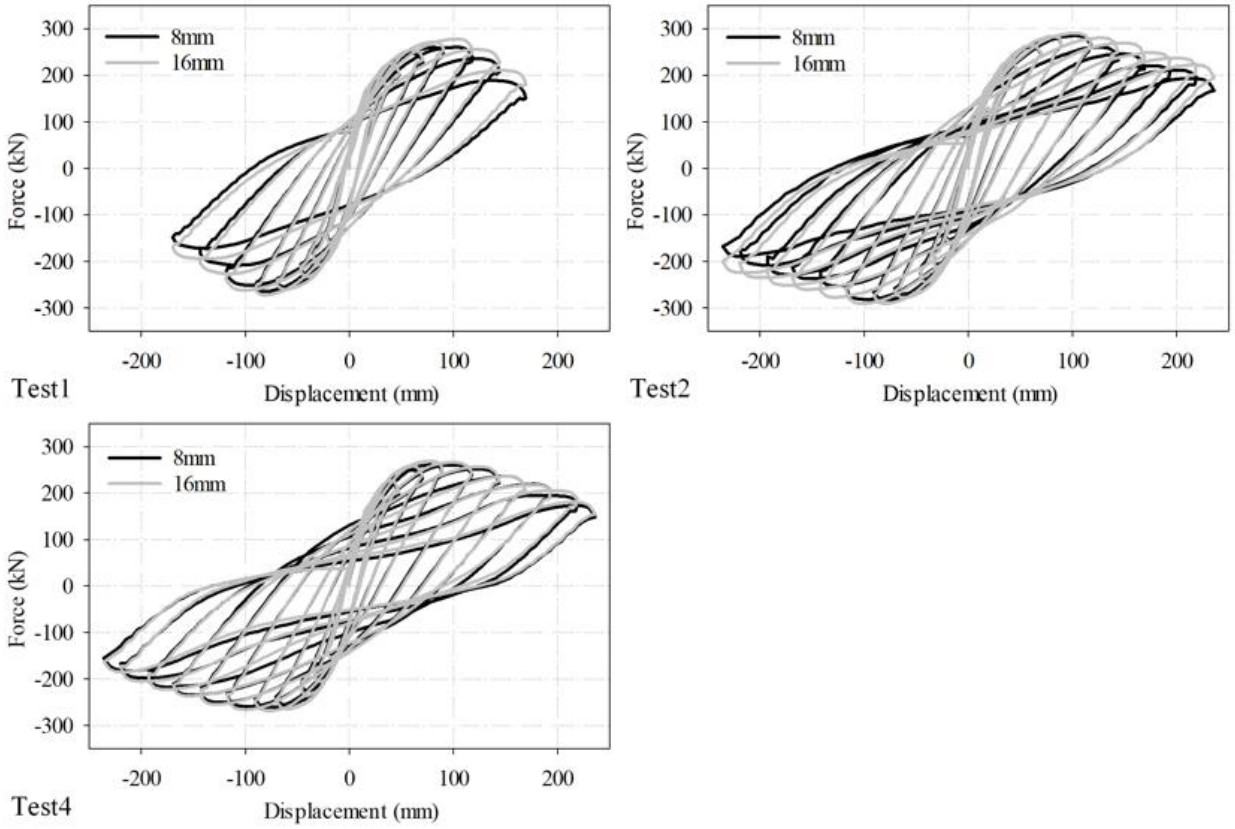

Figure 15: Effect of Ring Thickness

Table 22: Effects of Ring Thickness

Specimen	Ring thickness (mm)	F_{peak} (kN)	Δ_{peak} (mm)	$0.8F_{peak}$ (kN)	$\Delta_{0.8peak}$ (mm)	β (%)
Test 1	8	261	104	209	145	-
	16	278	110	222	145	107
Test 2	8	285	107	228	166	-
	16	290	107	232	213	102
Test 4	8	261	77	209	194	-
	16	269	77	215	188	103

4.3. *Effect of Bolt Number*

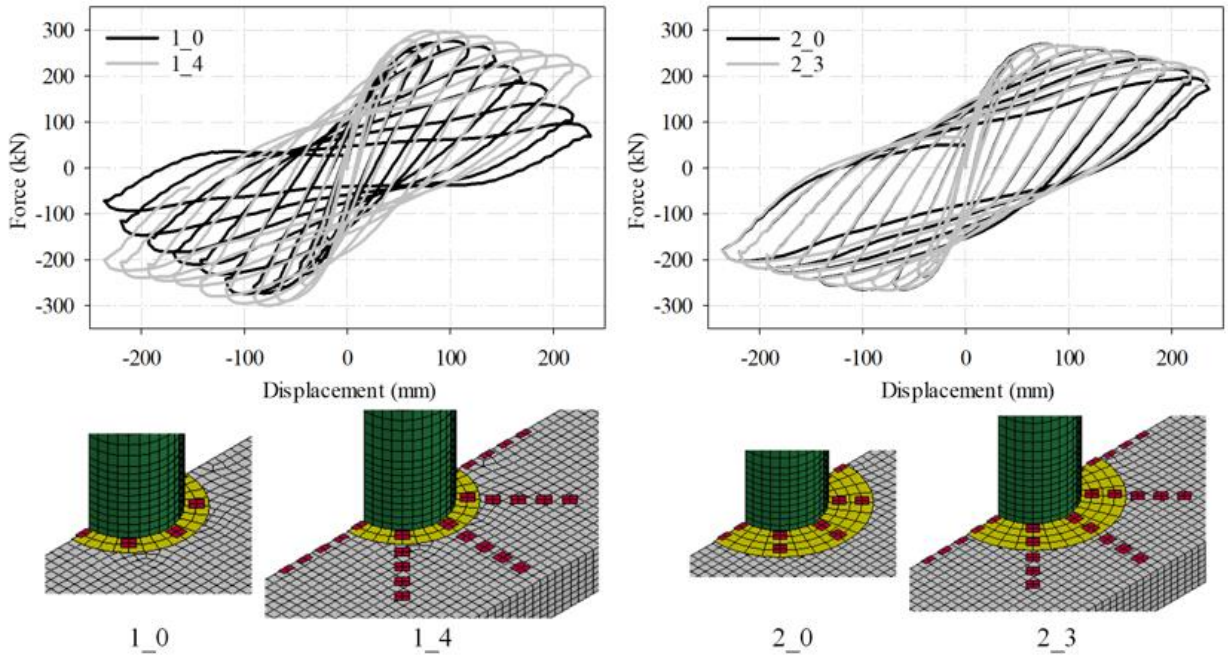

Figure 16: Effect of Bolt Number

Table 23: Effect of Bolt Number

Specimen	Bolt number (mm)	F_{peak} (kN)	Δ_{peak} (mm)	$0.8F_{peak}$ (kN)	$\Delta_{0.8peak}$ (mm)	β (%)
Test 1	1	277	96	222	155	-
	5	299	77	239	213	108
Test 4	2	270	77	216	208	-
	5	269	77	215	225	100

4.3. *Effect of Asymmetric Ring*

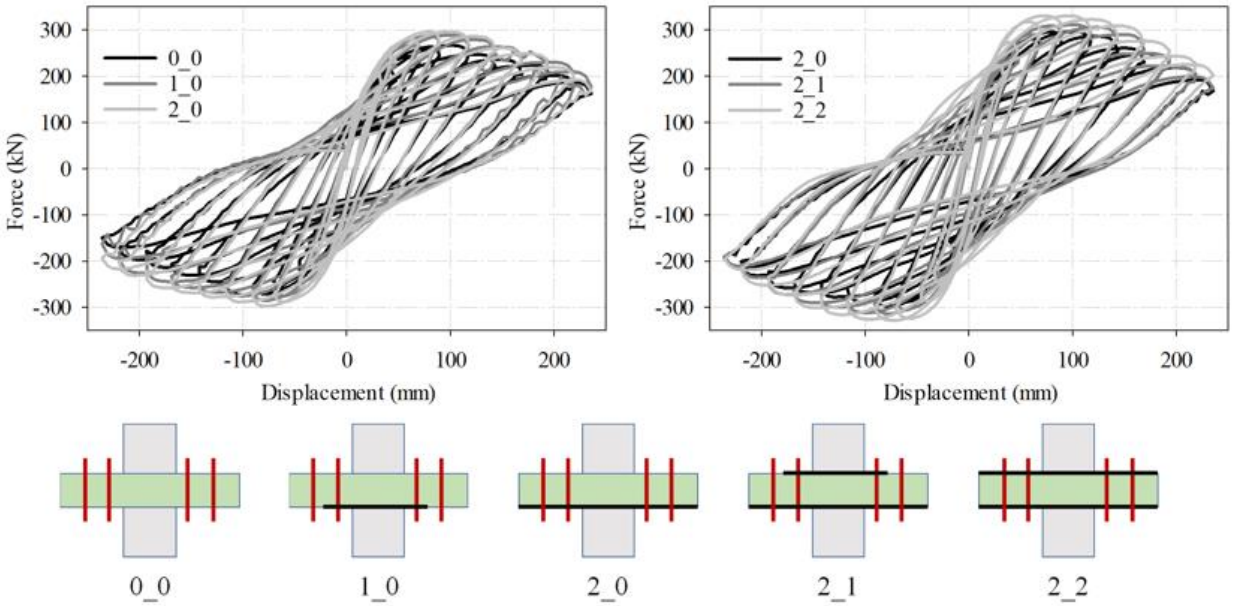

Figure 17: Effect of Asymmetric Ring

Table 24: Effect of Asymmetric Ring

Specimen	F_{peak} (kN)	Δ_{peak} (mm)	$0.8F_{peak}$ (kN)	$\Delta_{0.8peak}$ (mm)	β (%)
0_0	270	101	216	193	-
1_0	289	101	231	202	107
2_0	297	77	238	194	110
2_1	312	101	250	172	116
2_2	331	77	265	188	123

4.4. *Effect of Slab Thickness*

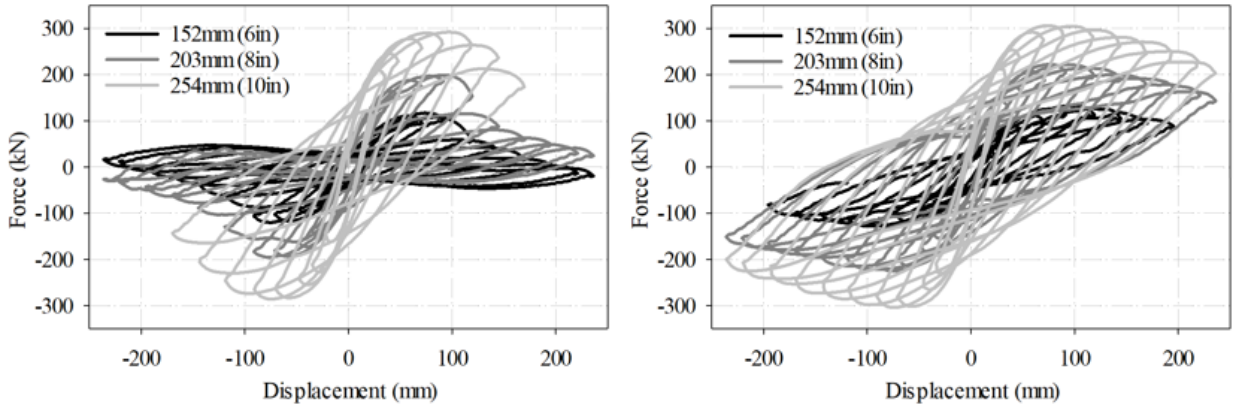

Figure 18: Effect of Slab Thickness

Table 25: Effect of Slab Thickness

Specimen	Slab thickness (mm)	F_{peak} (kN)	Δ_{peak} (mm)	$0.8F_{peak}$ (kN)	$\Delta_{0.8peak}$ (mm)	β (%)
Test 1	152	117	76	94	104	-
	203	199	91	159	117	170
	254	292	95	234	145	250
Test 2	152	133	97	106	163	-
	203	219	97	175	188	165
	254	306	71	245	208	230

4.5. *Effect of Ring Width*

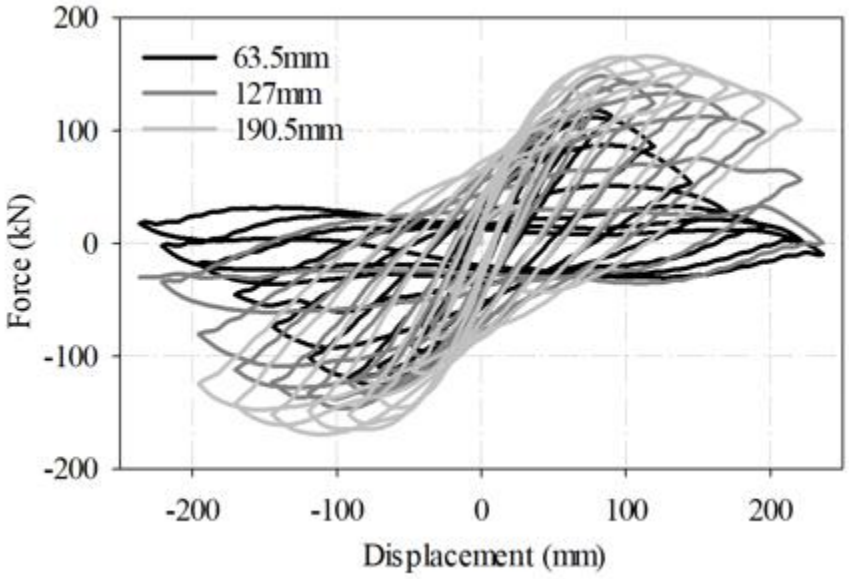

Figure 19: Effect of Ring Width

Table 26: Effect of Ring Width

Ring width (mm)	F_{peak} (kN)	Δ_{peak} (mm)	$0.8F_{peak}$ (kN)	$\Delta_{0.8peak}$ (mm)	β (%)
63.5	118	74	94	112	-
127	148	84	118	165	125
190.5	166	117	133	191	141

References:

Belytschko, T., Lin, J. I., & Chen-Shyh, T. (1984). Explicit algorithms for the nonlinear dynamics of shells. *Computer methods in applied mechanics and engineering*, *42*(2), 225-251.

CEB-FIP. (2010). *CEB-FIP model code 2010, design code.* Telford: Comité Euro-International du Béton-Fédération International de la Précontrainte.

Gopalaratnam, V. S., & Shah, S. P. (1985). Softening response of plain concrete in direct tension. *ACI Journal*, 82(3), 310-323.

Grassl, P., & Jirásek, M. (2006). Damage-plastic model for concrete failure. *International journal of solids and structures*, *43*(22-23), 7166-7196.

Grassl, P., Xenos, D., Nyström, U., Rempling, R., & Gylltoft, K. (2013). CDPM2: A damage-plasticity approach to modelling the failure of concrete. *International Journal of Solids and Structures*, *50*(24), 3805-3816.

Hallquist, J. O. (2016). *LS-DYNA keyword user's manual (Version R9.1).* Livermore, CA: Livermore Software Technology Corporation.

Hughes, T. J., & Liu, W. K. (1981a). Nonlinear finite element analysis of shells: Part I. Three-dimensional shells. *Computer methods in applied mechanics and engineering*, *26*(3), 331-362.

Hughes, T. J., & Liu, W. K. (1981b). Nonlinear finite element analysis of shells-part II. two-dimensional shells. *Computer Methods in Applied Mechanics and Engineering*, *27*(2), 167-181.

Krieg, R. D., & Key, S. W. (1976). Implementation of a time independent plasticity theory into structural computer programs. *Constitutive equations in viscoplasticity: Computational and engineering aspects*, 125-137.

Sinha, B. P., Gerstle, K. H., & Tulin, L. G. (1964). Stress-strain relations for concrete under cyclic loading. *ACI Journal*, 61(2), 195-212.

Tahmasebinia, F., Ranzi, G., & Zona, A. (2011). A probabilistic three-dimensional finite element study on simply-supported composite floor beams. *Australian Journal of Structural Engineering*, *12*(3), 251-262.